GEOSYNTHETICS '91

February 26-28, 1991 **Radisson Hotel, Atlanta, GA**

CONFERENCE PROCEEDINGS

Radisson Hotel
Atlanta, Georgia, U.S.A.
February 26-28, 1991

Volume 1

Sponsored by the North American Geosynthetics Society (NAGS)
and the Industrial Fabrics Association International (IFAI)
under the auspices of the International Geotextile Society (IGS)

SPONSORED BY

February 26-28, 1991 **Radisson Hotel, Atlanta, GA**

CONFERENCE PROCEEDINGS

Radisson Hotel
Atlanta, Georgia, U.S.A.
February 26-28, 1991

Volume 1

Sponsored by the North American Geosynthetics Society (NAGS)
and the Industrial Fabrics Association International (IFAI)
under the auspices of the International Geotextile Society (IGS)

Table of Contents

Volume I

Waste Containment Case Histories

Landfill Stabilization Through the Use of Geosynthetics ____ 1
Russell H. Fetrow
Russ Fetrow Engineering, Inc., USA
Maxwell M. Mick
ET AL
Russ Fetrow Engineering, Inc., USA

Geogrid Liner Support at Empire Sanitary Landfill ____ 15
Alan Stephens
Empire Sanitary Landfill, Inc., USA
Richard Bodner, P. E.
Martin & Martin, Inc., USA

Private Industry Maximum Security Landfill Case History ____ 23
Michel Marcotte
Solmers Internationale Consulting Engineers, Canada
Sophie Lagace
Solmers Internationale Consulting Engineers, Canada
Robert Denis
Solmers Internationale Consulting Engineers, Canada
Denis Faucher
PPG Canada Inc., Canada

The Evolution of Geosynthetics in a Landfill Lining System ____ 31
Jan Hutwelker
American Resource Consultants, USA
Thomas Pullar
American Resource Consultants, USA
Francis Taylor
Palco Linings Inc., USA

Application of Geosynthetics in the Design of Fully-Drained Mineral Waste Storage Facilities ____ 61
W. A. Cincilla
Knight Piesold and Co., Consulting Engineers, USA
G. A. Zagorski
Fluid Systems, Inc., USA

Geomembrane Applications in Australia ____ 77
Roger J. Parker
Golder Associates PTY LTD, Australia
Mike A. Sadlier
Polyfelt Geosynthetics PTY LTD, Australia

Waste Containment Interface Stability

Soil-Geosynthetics Interface Strength Characteristics: A Review of State-of-the-Art Testing Procedures ____ 87
Deanne L. Takasumi
CH2M Hill, Inc., USA
Kenneth R. Green
CH2M Hill, Inc., USA
Robert D. Holtz
University of Washington, USA

PVC Geocomposite for Improved Friction and Performance Properties ____ 101
David C. Lauwers
Occidental Chemical Corporation, USA

Landfill Liner Side Slope Design to Minimize Geomembrane Tensile Stress ____ 113
Michael Quinn
Barton & Loguidice, P. C., USA
Martin Chandler
Barton & Loguidice, P. C., USA

Structural Geogrids Used to Stabilize Soil Veneer Covers ____ 125
Vicky E. Chouery-Curtis
Tensar Environmental Systems Inc., USA
Stephen T. Butchko
Tensar Environmental Systems Inc., USA

Stability of High Refuse Slopes on Synthetic Lining Systems at the Bee Canyon Landfill ____ 145
Suji Somasundaram
The Earth Technology Corporation, USA
Kris Khilnani
The Earth Technology Corporation, USA

Shear Strength of Sand-Geomembrane Interfaces for Cover System and Lining Design ____ 159
S. J. Druschel
ABB Environmental Services Inc., USA
T. D. O'Rourke
Cornell University, USA

Geosynthetic Material Response to Landfill Cap Settlement and Subsidence ____ 175
Ronald K. Frobel, P. E.
R. K. Frobel & Associates, USA

Environmental Applications

Underwater Geomembrane Placement ____ 187
Fred P. Rohe
Environmental Protection, Inc., USA

Use of Geosynthetics in Lautaro Dam ____ 195
Luis Arrau
Ministry of Public Works, Chile
Donaldo Astorga
Ministry of Public Works, Chile

Witbank's 60Ml Floating Cover Reservoir: A Review of the First Five Years ____ 207
Richard B. Turner
Hawkins, Hawkins & Osborn, South Africa
Peter L. Davies
Aquatan, South Africa

Evaluation of Field Seams Quality by the Impact Test Procedure ____ 223
A. L. Rollin
Ecole Polytechnique, Canada
M. Lefebvre
Ecole Polytechnique, Canada
J. Lafleur
Ecole Polytechnique, Canada
M. Marcotte
Solmers Internationale, Canada

Analysis of Pinhole Seam Leaks Located in Geomembrane Liners Using the Electrical Leak Location Method: Case Histories ____ 239
Daren L. Laine
Southwest Research Institute, USA

Performance of Mount Elbert Forebay Reservoir Flexible Membrane Lining After 10 Years of Service ____ 255
W. R. Morrison
U. S. Department of the Interior, Bureau of Reclamation, USA
E.W. Gray, Jr.
U. S. Department of the Interior, Bureau of Reclamation, USA

Geosynthetic Durability

Puncture Resistance of Geomembranes Using a Truncated Cone Test ____ 273
Donald Hullings
EMCON Associates, USA
Robert Koerner
Drexel University, USA

Effects of Outdoor Exposure on a High Density Polyethylene Geomembrane ____ 287
Y. G. Hsuan
Geosynthetic Research Institute, Drexel University, USA
A. E. Lord Jr.
Geosynthetic Research Institute, Drexel University, USA
R. M. Koerner
Geosynthetic Research Institute, Drexel University, USA

The Resistance of Membranes in Cover Systems to Root Penetration by Grass and Trees ____ 303
Robert E. Landreth
U. S. Environmental Protection Agency, USA

The Chemical Resistance of Geotextiles to be Used in Secondary Containment Systems for Underground Storage Tanks ____ 311
Randy C. Pucetas
Hoechst Celanese Corp., USA
Karen L. Verschoor
Texas Research Institute Environmental Inc., USA
Sam R. Allen
Texas Research Institute Environmental Inc., USA
C. Joel Sprague
Nicolon Corporation, USA

Molecular and Rheological Changes in Polyethylene Occurring From Heat Seaming HDPE Liners ____ 317
Mark W. Cadwallader
Gundle Lining Systems Inc., USA
Jeffrey R. Burkinshaw
Phillips 66 Co., USA

Residual Stress Measurements in Geomembrane Sheets and Seams ____ 333
A. E. Lord Jr.
Geosynthetic Research Institute, Drexel University, USA
R. M. Koerner
Geosynthetic Research Institute, Drexel University, USA
M. H. Wayne
Geosynthetic Research Institute, Drexel University, USA

Determination of Long-Term Tensile Strength of Geosynthetics: A State-of-the-Art Review ____ 351
Tony M. Allen
Washington State Department of Transportation, USA

Technical Advances/Innovations

Eccentric Plate Loading Tests on Geogrid-Reinforced Subgrades ____ 381
Vito A. Guido
The Cooper Union, USA
Christopher H. Bakkala
Thornton-Tomasetti, P. C., USA
John J. Nocera
Malcolm Pirnie, Inc., USA

On the Design of Reinforced Embankments on Soft Brittle Clays ____ 395
B. L. J. Mylleville
The University of Western Ontario, Canada
R. K. Rowe
The University of Western Ontario, Canada

Using Geosynthetics to Reduce Earth Loads on Rigid Retaining Structures ____ 409
John S. Horvath
Manhattan College, USA

Electrical Methods of Seaming of Geomembrane Sheet ____ 425
E. O. Butts
Butts Consultants, Ltd., Canada
A. E. Lord, Jr.
Geosynthetic Research Institue, Drexel University, USA

Membrane Action in a Two-Layer Soil System Reinforced By Geotextile ____ 439
Philippe L. Bourdeau
Purdue University, USA

A Probabilistic Review of Geotextile Reinforced Slope Design ____ 455
Shi-Chieh Cheng
Drexel University, USA
Barry Christopher
Polyfelt, Inc., USA

Effect of Geotextiles on Water Migration in Freezing Soils and the Influence of Freezing on Performance ____ 469
Karen S. Henry
U. S. Army
Cold Regions Research and Engineering Laboratory, USA

Volume II

Failures and Solutions

Case History of a 9 m High Geogrid Reinforced Retaining Wall Backfilled with Cohesive Soil ____ 485
W. J. Burwash
Golder Associates Ltd., Canada
J. D. Frost
Purdue University, USA

A Shattered Geomembrane Liner Case History: Investigation And Remediation ____ 495
Ian D. Peggs
GeoSyntec Consultants, USA
Jules P. Winfree
GeoSyntec Consultants, USA

Geosynthetic Considerations in a Landfill on Compressible Clays ____ 507
Gregory Richardson
ENSCI, Corp., USA
Dick Reynolds
R. G. Gerber, USA

Technical Advancements/Testing & Research

Results of Laboratory Tests on a Geotextile/Bentonite Liner Material ____ 517
Hsin-Yu Shan
University of Texas - Austin, USA
David E. Daniel
University of Texas - Austin, USA

Load Test of a Large-Scale Geotextile-Reinforced Retaining Wall ____ 537
John W. Billiard
Canonie Environmental Services Corp., USA
J. T. H. Wu
University of Colorado at Denver, USA

Case History Comparison of Geosynthetic-Reinforced Soil Walls ____ 549
Alan F. Claybourn
Woodward-Clyde Federal Services, USA
Jonathan T. H. Wu
University of Colorado at Denver, USA

Creep Measurements on Polymeric Reinforcement ____ 561
R. J. Fannin
University of British Columbia, Canada
S. Hermann
Norwegian Geotechnical Institute, Norway

Comparative Behaviour of Metal and Tensar Geogrid Strips Under Static and Repeated Loading ____ 575
Thomas Hamilton Hanna
University of Sheffield, UK
Mabrouk Touahmia
University of Sheffield, UK

Short and Long Term Performance of Polymeric Geogrids ____ 587
I. Juran
Polytech University, USA
K. H. Farrag
Louisiana State University, USA
L. Richmond
Conwed Plastics, USA

Effectiveness of In-Membrane Test in Simulating Strength and Deformation Characteristics of a Nonwoven Geotextile Under Operational Conditions ____ 601
Hoe Ing Ling
University of Tokyo, Japan
Jonathan T. H. Wu
University of Colorado at Denver, USA
Fumio Tatsuoka
University of Tokyo, Japan

Large-Scale Pullout Tests: Assessment of Procedure and Results 615
G. E. Bauer
Carleton University, Canada
A. O. A. Halim
Carleton University, Canada
Q. Shang
University of Western Ontario, Canada

Effect of Pores Structure of Nonwoven Geotextiles on Their Clogging Behavior 629
Shobha K. Bhatia
Syracuse University, USA
Jacek Mlynarek
Ecole Polytechnique, Canada
Andre L. Rollin
Ecole Polytechnique, Canada
Jean Lafleur
Ecole Polytechnique, Canada

Load Distribution in Geogrids With Low Junction Efficiency 643
C. Bonczkiewicz
STS Consultants Ltd., USA
B. Christopher
Polyfelt Inc., USA
M. Simac
Intersol Engineering, USA

Comparative Hydraulic Performance of Resinated Geotextile Overwraps 653
R. Anne Gallup
GeoSyntec Consultants, USA
Robert C. Bachus
GeoSyntec Consultants, USA
Scott M. Luettich
GeoSyntec Consultants, USA

The Effect of Repeated Traffic Loading on Geosynthetic Reinforcement Anchorage Resistance 665
M. Nimmesgern
FMPA (Otto-Graf-Institut), Germany
David Bush
Netlon Limited, UK

Transportation Applications

Geogrid Reinforcement and Stabilization of a Highway Subgrade 673
Terry L. Yarger
Montana Department of Highways, USA
Francis E. Harrison, Jr.
Tensar Earth Technologies, USA
Earle William Mayberry
Tensar Earth Technologies, USA

Response of a Geogrid Earth Reinforced Retaining Wall With Full Height Precast Concrete Facing ____ 691
K. L. Fishman
State University of New York at Buffalo, USA
C. S. Desai
University of Arizona, USA

Geotextiles For Subgrade Stabilization in Permanent Roads and Highways ____ 701
Barry R. Christopher
Polyfelt, Inc., USA
Robert D. Holtz
University of Washington, USA

North Las Vegas: Reconstruction of Cheyenne Avenue Incorporating A High Geosynthetic Moisture Barrier ____ 715
Dave Guram
Phillips Fibers Corporation, USA
Mark Marienfeld
Phillips Fibers Corporation, USA
Dave Smiley
Phillips Fibers Corporation, USA
Dan Nesbitt
G. C. Wallace, Inc., USA

Raleigh Street Embankment-Orlando, Florida ____ 727
Robert L. Goehring, P. E.
Professional Services Industries, Inc., USA

Heavy Construction Applications

Utilization of Geotextile - Reinforced Retaining Wall for Stabilizing Weathered Mudstone Slope ____ 739
Dave Ta-Teh Chang
Chung-Yuan University, Taiwan, ROC
Tien - Chien Chen
Chung-Yuan University, Taiwan, ROC
Kuan-Hsien Su
Chung-Yuan University, Taiwan, ROC

Design and Construction of a Geotextile Wall ____ 775
Douglas Chandler
Shannon & Wilson, Inc., USA
Thomas Kirkland
Shannon & Wilson, Inc., USA

Geogrid Reinforced Soil Wall Bridge Replacement at Picnic Point, Snohomish County, Washington ____ 765
Roland D. Maynard, P. E.
Snohomish County Department of Public Works, USA
Steve E. Thomsen, P. E.
Snohomish County Department of Public Works, USA
Paul W. Grant, P. E.
Shannon & Wilson, Inc., USA

Design and Analysis of Three Reinforced Soil Retaining Walls ____ 781
Michael R. Simac
Intersol Engineering Inc., USA
Dr. Richard J. Bathurst
Royal Military College of Canada, Canada
Richard A. Goodrum
Mirafi, Inc., USA

High Clay Embankment Over Cannon Creek Constructed With Geogrid Reinforcement ____ 799
R. F. Hayden
Hayward Baker, Inc., USA
G. R. Schmertmann
University of California - Berkeley, USA
B. Q. Qedan
Arkansas Highway and Transportation Dept., USA
M. S. McGuire
Opterra, Inc., USA

A Case History of the Design and Construction of a Reinforced Soil Wall Using D. S. F. Fabric Geotextiles for the Purpose of Stabilizing a Major Landslip ____ 823
Peter Rankilor
Manstock Geotechnical Consultancy Services Ltd., United Kingdom

Reinforcement of a Failed Embankment Over Slough Mud ____ 839
Richard Barrows, P. E.
Oregon State Highway Division, USA
George Machan, P. E.
Oregon State Highway Division, USA

Commercial/Industrial Applications

Surcharge Embankments at Walt Disney World ____ 849
Ian Kinnear
Jammal & Associates, Inc., USA
Frank Wood
Disney Development Company, USA

Geogrid Reinforced Containment Dykes for Mountainside Oil Tank Farm in Seismic Zone ____ 861
Thomas T. Heike
SNC Inc., Canada
Michael A. Patterson
SNC Inc., Canada
John R. Kerr
Tensar Earth Technologies, Canada

A Simplified Design Method For Silt Fences ____ 879
Gregory N. Richardson
ENSCI, Corp., USA
Percy Middlebrooks
Georgia Department of Transportation, USA

Modular Block Faced Polymer Geogrid Reinforced Soil Walls U.S. Postal Service Combined Carrier Facility ____ 889
Robert B. Anderson
Tensar Earth Technologies, Inc., USA
Fred N. Boyd
U. S. Postal Service, USA
Larry Shaw
Gifford Hill, USA

Design and Construction of an 18 Foot High Geogrid Stayed Concrete Block Wall "A Case History" ____ 903
Douglas J. Yovaish
Michael D. Sims & Associates, USA
Stephen W. Berry
Michael D. Sims & Associates, USA

Geogrid Reinforced Soil-Cement Arch Over Accelerator Ring ____ 917
John P. Gnaedinger
STS Consultants Ltd., USA
Safdar A. Gill
STS Consultants Ltd., USA

Application of Geosynthetics to the W.H. Zimmer Generating Station Project ____ 935
Rudolph Bonaparte
GeoSyntec Consultants, USA
Joseph E. Fluet
GeoSyntec Consultants, USA
Ronald D. Johnson
Tensar Earth Technologies, Inc., USA
Vicky Chouery-Curtis
Tensar Earth Technologies, Inc., USA

Modular Concrete Retaining Wall and Geogrid Reinforcemnet Performance and Laboratory Modeling ____ 951
John C. Kliethermes
Service Engineering, USA
Kenneth Buttry
University of Wisconsin-Platteville, USA
Earl McCullough
University of Wisconsin-Platteville, USA
Richard Wetzel
University of Wisconsin-Platteville, USA

WASTE CONTAINMENT CASE HISTORIES

Landfill Stabilization Through the Use of Geosynthetics

Russell H. Fetrow
Russ Fetrow Engineering, Inc., USA
Maxwell M. Mick
ET AL
Russ Fetrow Engineering, Inc., USA

INTRODUCTION

Gas and odor problems at the Moonlight Rock Industrial Landfill in International Falls, Minnesota (see Figures 1 and 2), threatened future expansion of the site. The landfill was not covered and generated large quantities of methane and hydrogen sulfide gas. Residential neighbors demanded removal of the existing waste.

The 90 acre site, of which 45 acres received mixed wood and pulpmill waste, was steep and unstable. During preliminary site visits, gas was observed bubbling up through the waste. The instability of the site varied in different locations. In some areas it was impossible to walk due to the liquid or oatmeal like consistency. In other areas, the wastes might migrate up to 100 meters in a weeks' time. The surface of the landfill literally shook like a bowl of jelly.

Before any attempts could be made to correct the gas and odor problems, the site had to be stabilized. Conventional methods to dewater the site, such as wells and cutoff trenches, were not practical. The material acts like a sponge yet has a permeability in many areas that approaches that of bentonite clay. Also, because the construction season in Northern Minnesota is very short, any cover had to be placed within one year.

STABILIZATION

The landfill is situated on 13 meters of clay and rises 20 meters above the surrounding flat land. Bore hole tests showed that water had mounded to within a meter of the surface over half the site. The landfill itself was poorly shaped for handling a synthetic cover and would need to be regraded for proper surface drainage. One fourth of the landfill was virtually a liquid and could not support vehicular traffic of any kind and, in many areas, would not even support foot traffic. Removal of the water would be the conventional way to stabilize the landfill but in this situation it would not be cost effective or timely. Since, wells or cutoff trenches would have to be constructed across areas that would not support the necessary equipment and water removal would literally take years.

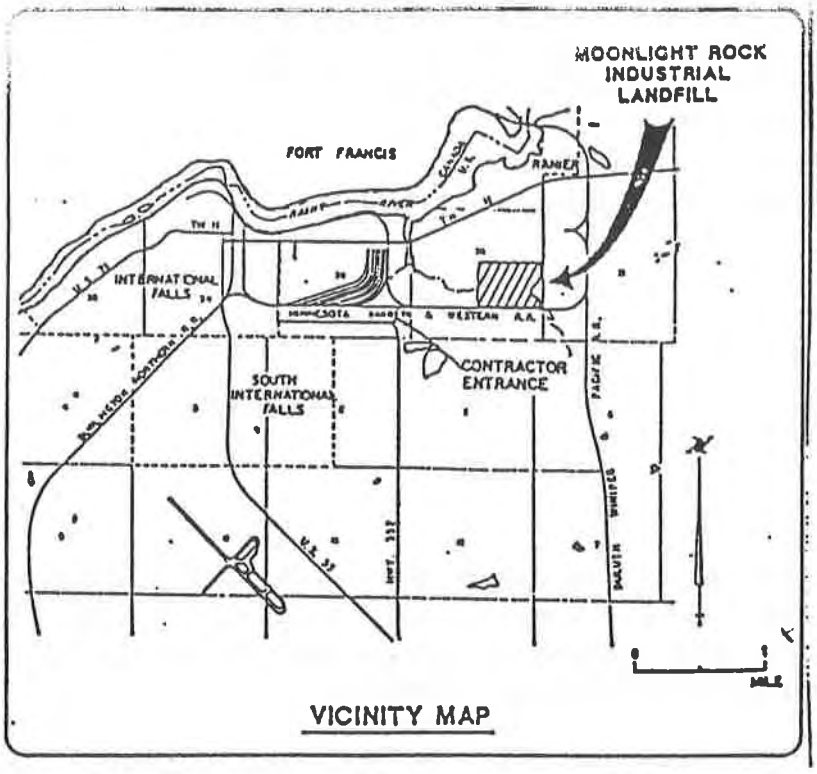

Figure 1

Figure 2

In the Southwest quarter of the landfill, where the wastes were slowly flowing and varied from 0 to 10 meters in depth, it was decided to use a biaxial geogrid over the area. This would allow a 0.6 meter layer of sand to be placed across the site. One concern was that the material could still move in the form of a giant mud wave under the final cover, so a rock berm was constructed diagonally across the southwest (worst) section of the landfill to divide the problem in half and reduce the potential degree of failure. This berm would also help to dewater the area by providing a conduit for water to reach the leachate lines. Upon completion of the cutoff berm, the biaxial geogrid was placed over the waste material and placement of a clean sharp sand over the grid was begun. It quickly became obvious that the material under the geogrid would not support the weight of the sand and the tracked dozer placing the material. As the sand was placed, it tended to sink out of sight pushing mud waves in all directions. A solution was quickly hit upon. Bark and old wood chips from the mill provided a light buoyant medium that literally floated the tracked dozers across the geogrid. This material was placed 1 to 1.5 meters thick in many areas but provided a way to place drainage material over the wastes without forming excessive mud waves. After the bark was placed, another layer of biaxial geogrid was placed over the bark and 0.6 meters of sand was then easily spread across this surface. Tears in the geogrid from logs floating to the surface were patched with layers of geogrid after the log had been removed or punched back down. These breaks resembled volcanoes as the material trapped under the geogrid found its way out through the fissure (see Figures 3, 4, and 5 for stabilization plans and details).

The entire site needed to be regraded for slope. As material was pushed to the ridge line of the landfill, some slopes that had been relatively stable, but too steep for liner placement, began to slide. This was always a potential problem, but the speed with which the instabilities developed was surprising. To prevent the material from sliding completely off the slope, a layer of biaxial geogrid was quickly placed over the slide areas and loaded with pit run sand and rock from the base up (see Figure 6). This locked in the toe of the slide and allowed the surface to be weighted, forcing water out and helping to stabilize the slide areas. Wherever possible rock drainage ditches were cut into the base of the slides to improve the long term stability of these areas by keeping the bases dewatered.

Several small rotational surface failures in the landfill were observed. To prevent the excessive surface movement that would eventually cause failures and tearing of the topcap, these areas were also covered with biaxial geogrid. A layer of bark was placed at the upper surface and sand at the lower surface to help prevent further rotation of the waste material.

All of the landfill surface was soft and this played havoc with the placement of rock and sand for the gas collection system and topcap. For this reason, a combination of biaxial geogrid with an 0.27 kg/m nonwoven geotextile as a filter medium was used. The geotextile prevented wastes from penetrating the gas collection blanket of rock, while allowing water to escape. This created a very tough surface, making placement of the rock a clean and easy operation. In a couple of small areas of the landfill, the surface could barely support the weight of the low ground pressure tracked dozers. By placing another layer of geogrid over the geotextile perpendicular to the original geogrid it was found that enough surface stability was developed to support the machinery with minimal surface deflection.

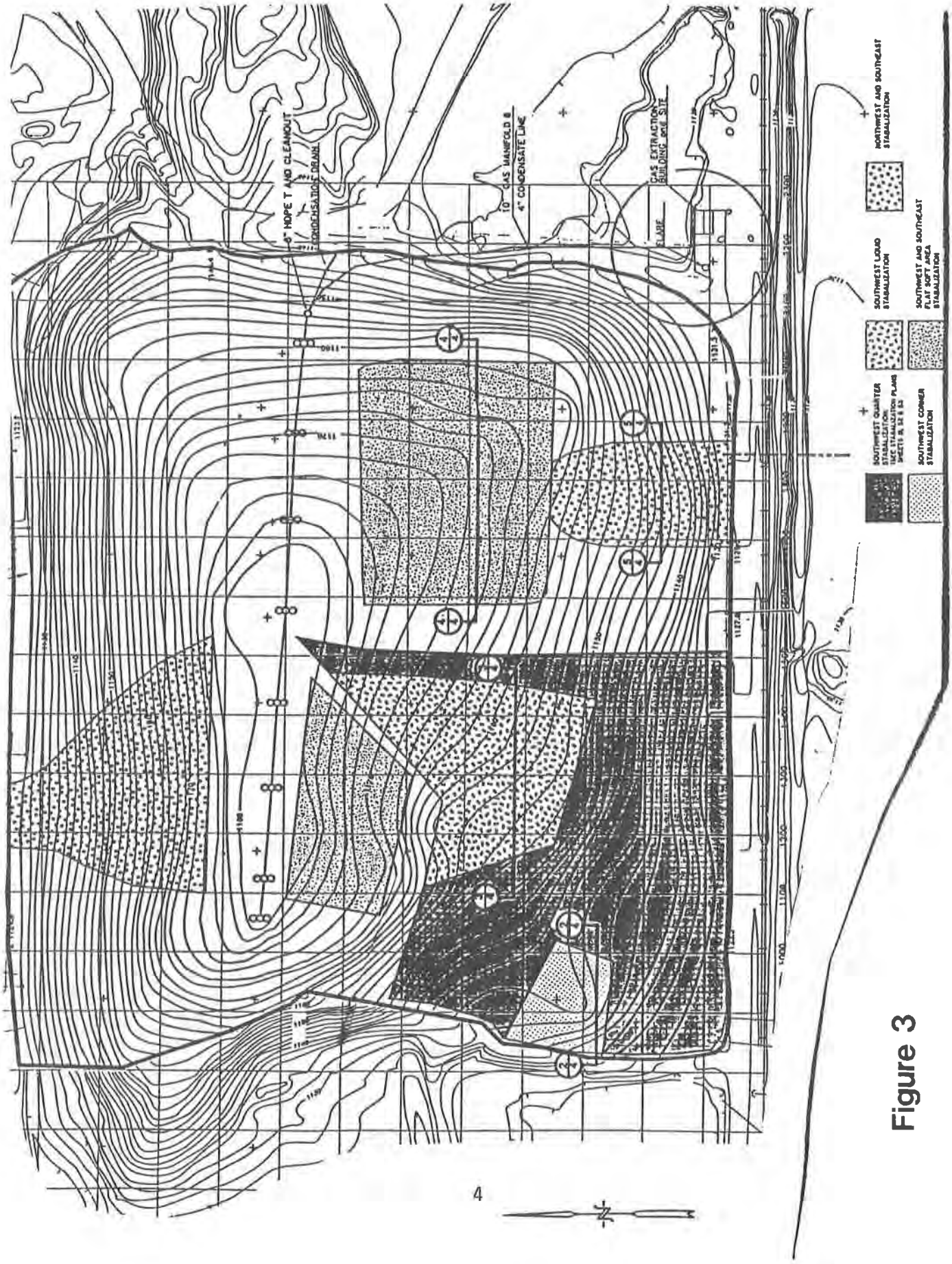
6" HDPE T AND CLEANOUT
CONDENSATE DRAIN
10" GAS MANIFOLD B
4" CONDENSATE LINE
GAS EXTRACTION BUILDING AND SITE
FLARE
NORTHWEST AND SOUTHEAST STABILIZATION
SOUTHWEST LIQUID STABILIZATION
SOUTHWEST AND SOUTHEAST FLAT SOFT AREA STABILIZATION
SOUTHWEST QUARTER STABILIZATION
SOUTHWEST CORNER STABILIZATION

Figure 3

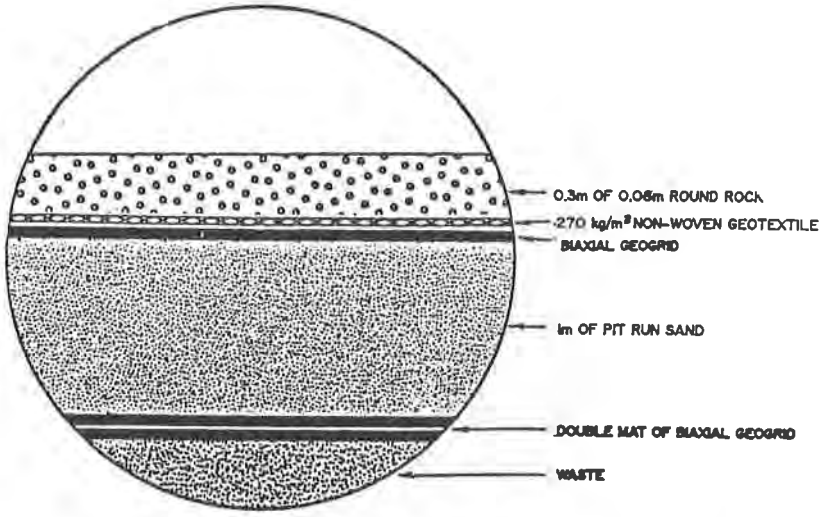

SOUTHWEST CORNER STABILIZATION 2/4

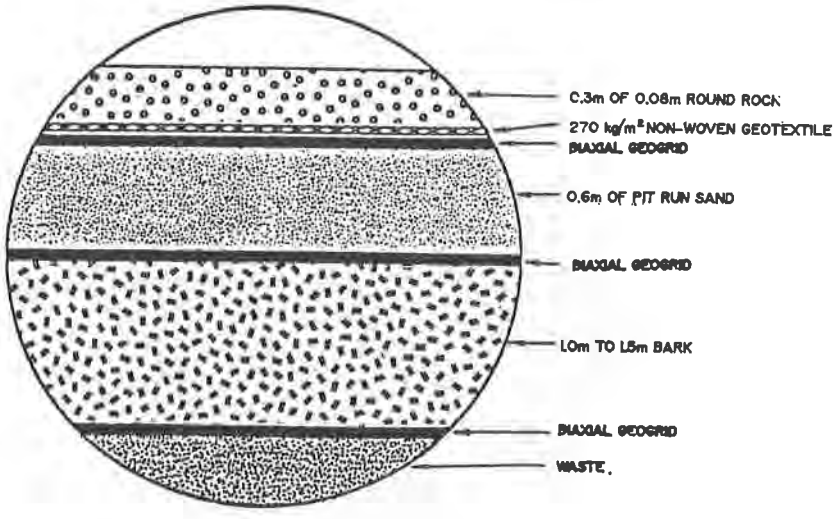

NOTE: BARK FLOATED ACROSS BIAXIAL GEOGRID TO SUPPORT "GENERIC TYPE OF EQUIPMENT". SAND CAUSED A MUD WAVE THAT COULDN'T BE DEALT WITH.

SOUTHWEST LIQUID STABILIZATION 3/4

Figure 4

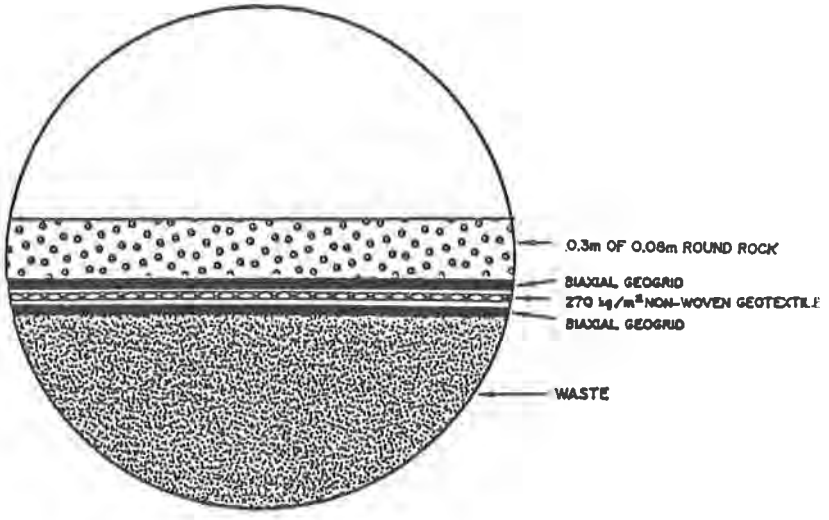

NOTE AREAS DOUBLED UP ON BIAXIAL GEOGRID FOR BETTER SUPPORT OF EQUIPMENT AND TO TIE BIAXIAL GEOGRID TOGETHER 90° OFFSET FOR MORE UNIFORM DISPLACEMENT.

SOUTHWEST AND SOUTHEAST FLAT SOFT AREA STABILIZATION

4/4

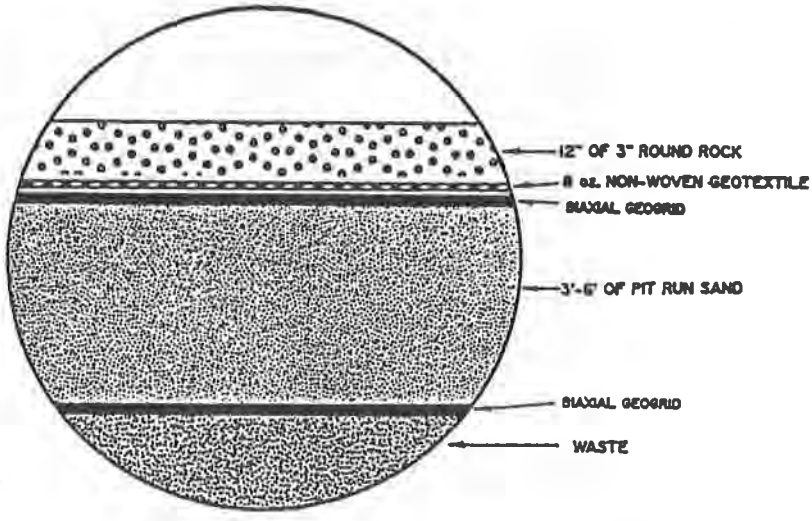

NOTE: THIS STABILIZATION WAS INSTALLED TO STOP THE SLIDING OF MATERIAL DOWNSLOPE.

NORTHWEST AND SOUTHEAST STABILIZATION

5/4

Figure 5

Figure 6

The use of geosynthetics for stabilizing the landfill at the surface has no counterpart in conventual engineering. Rip rap, a more common practice would have sunk to the bottom in many areas and the cost for placement would have been prohibitive. Settling of the landfill also would tend to cause fractures that could have torn the geomembrane cover. While this could still happen, the surface geotextile stresses have been distributed more uniformly over a larger area with the use of the biaxial geogrid and the nonwoven geotextile

GAS SYSTEM AND STARTUP

As the rock was installed over the geotextile material, HDPE perforated pipe has laid in for the gas collection system. These pipes were spaced every 45 meters across the landfill and connected to a series of HDPE vaults containing valves which connected the perforated pipes to the main gas manifold (see Figure 7).

To remove the gas from the landfill, a vacuum is created under the membrane top cap. This is accomplished through the use of a centrifugal blower. Landfill gases are pumped from the main collection header to a blower building and then to a totally enclosed ground flare. Gas quantity, quality and content are monitored at the building and adjustments to vacuum and flow rate are made accordingly. To insure that more than 98% of the hydrogen sulfide gas was converted to sulfur dioxide, the Minnesota Pollution Control Agency required that the flare maintain a temperature of 760 degrees C. with a retention time of one second.

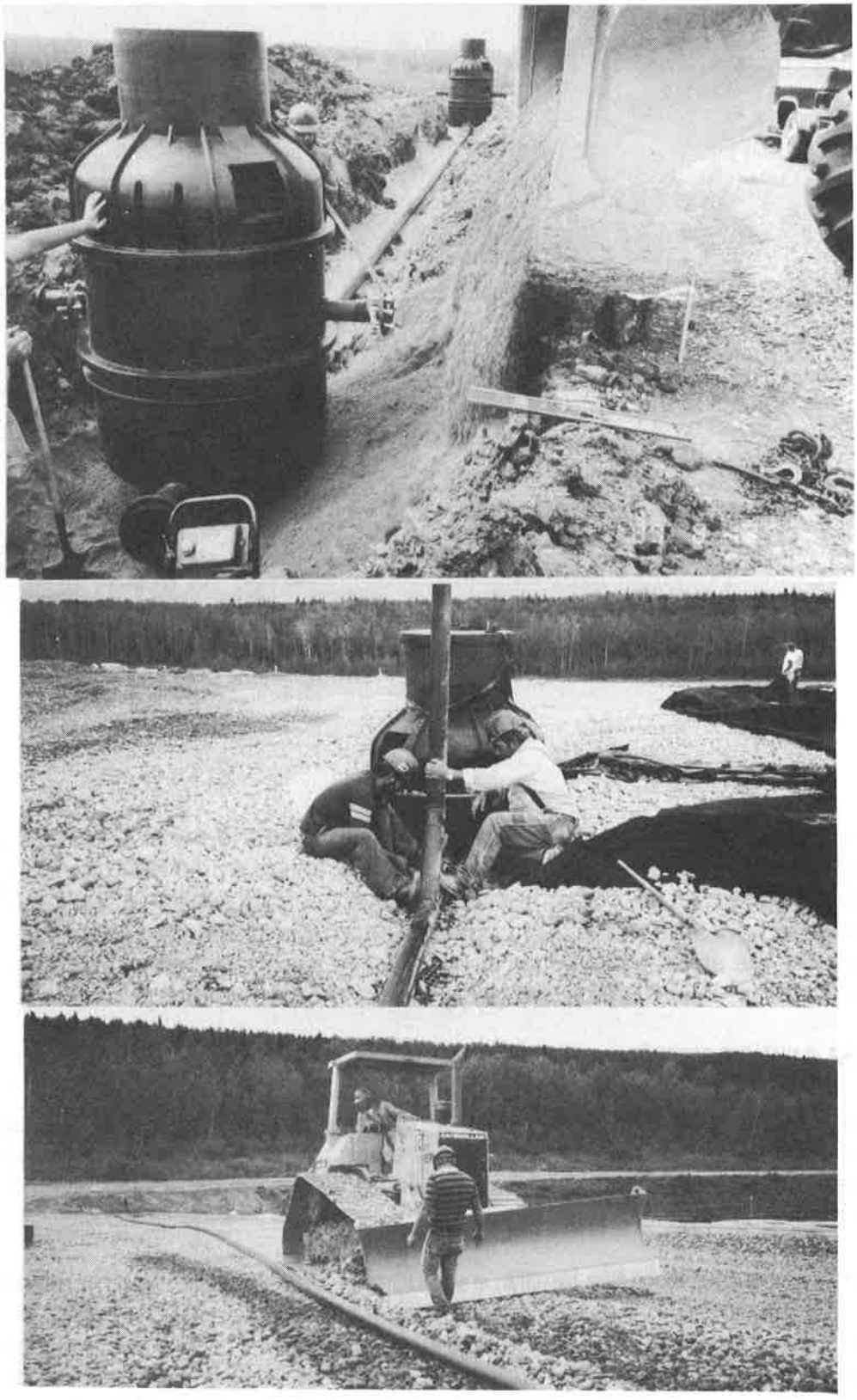

Figure 7

Upon startup of the flare the system appeared to be functioning very well but, as gas quality dropped from 55% to below 20%, it became very obvious that excessive air infiltration to the system was occurring. Upon inspection, piping inside the HDPE vaults was found to have cracked (see Figure 8). Repairs were made and the gas quality stabilized, but at levels of around 25% which is much less than the anticipated 40%. Tears in the liner around the HDPE vaults were suspected and in the spring three such tears were repaired. Settlement of the main gas manifold in the center of the landfill also caused problems as it filled with condensate and prevented an even vacuum over the landfill. This problem was also corrected and, with adjustments to the vacuum, a stable balance was achieved between air infiltration, suspected from around the edges of the 1.5 mm HDPE cover and the gas production rate of the landfill. At present, gas quality is averaging 40% methane by volume and 30% carbon dioxide.

GEOSYNTHETIC TOP CAP

The choice of materials to use for the top cap was one of the items considered. The landfill was mounded above the surrounding flatland and had side slopes of 2% to 25%. Clay, which was available in the area, was quickly eliminated because of the potential for erosion on steeper slopes and its inherent cracking when dried out. This made it a very poor barrier to escaping gasses and made it difficult, if not impossible, to achieve total recovery. Geosynthetics, specifically an (HDPE) geomembrane liner was determined to be the most practical solution for top-capping and maximum retention of the landfill gasses.

Figure 8a

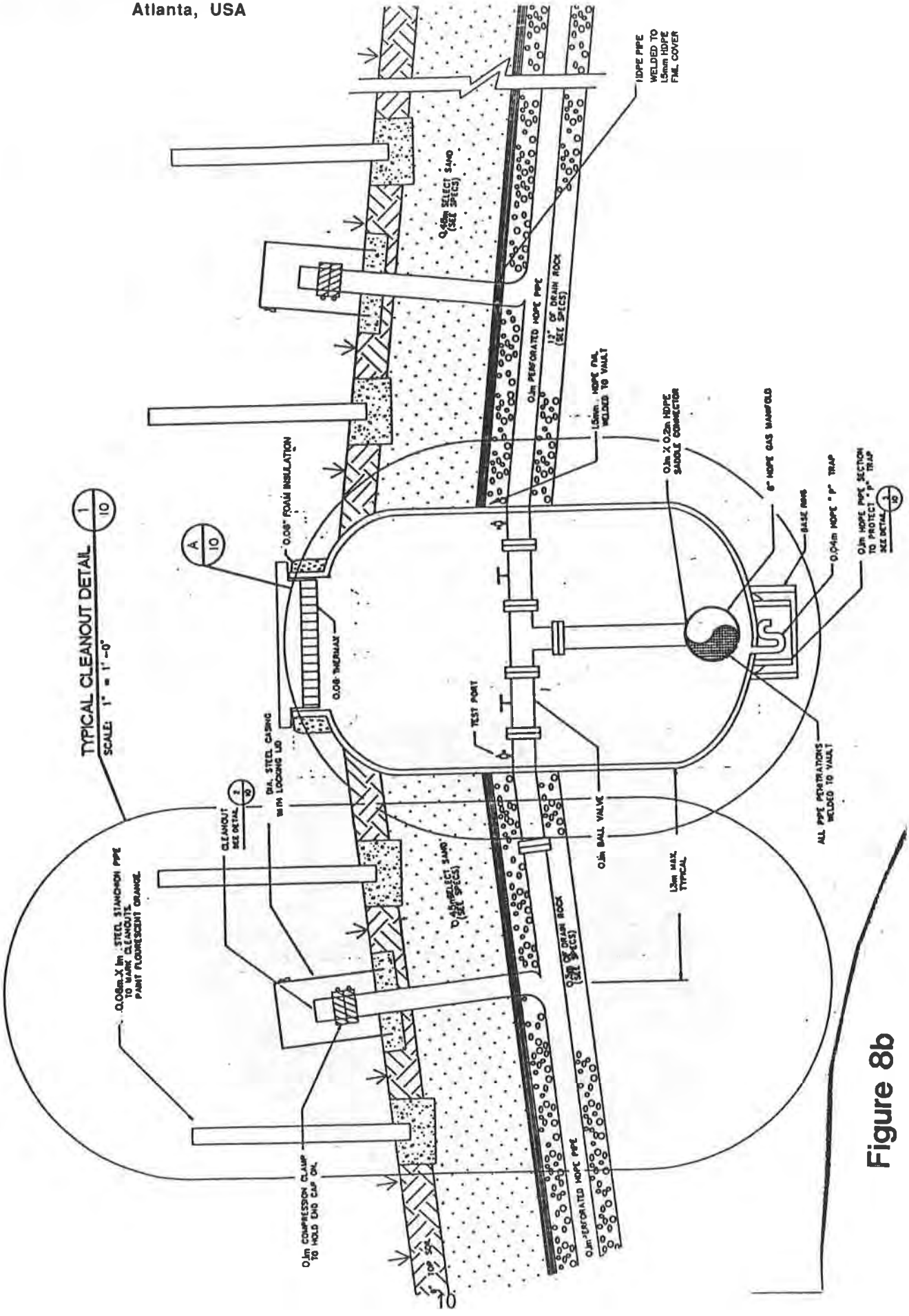
TYPICAL CLEANOUT DETAIL
SCALE: 1" = 1'-0"
0.06m X 1m STEEL STANCHION PIPE TO MARK CLEANOUTS PAINT FLOURESCENT ORANGE
CLEANOUT SEE DETAIL
DIA. STEEL CASING WITH LOCKING LID
0.06" FOAM INSULATION
0.06" THERMAX
TEST PORT
0.1m BALL VALVE
0.1m COMPRESSION CLAMP TO HOLD END CAP ON
0.1m PERFORATED HDPE PIPE
0.45m SELECT SAND (SEE SPECS)
12" OF DRAIN ROCK (SEE SPECS)
1.5mm HDPE FML WELDED TO VAULT
0.1m X 0.2m HDPE SADDLE CONNECTION
6" HDPE GAS MANIFOLD
BASE RING
0.04m HDPE "P" TRAP
0.1m HDPE PIPE SECTION TO PROTECT "P" TRAP SEE DETAIL
ALL PIPE PENETRATIONS WELDED TO VAULT
1.3m MAX. TYPICAL
10" SAG
10
A
10
1
10
2
10
3
10

Figure 8b

Once the landfill was regraded, stabilized, and covered with rock for the gas collection/retention layer, the synthetic cover was installed. This geosynthetic top cap was comprised of five layers: A nonwoven 0.27 kg/m geotextile for filter and cushion purposes; a geonet for aiding gas transmission, collecting freezing condensate under the liner, and for additional cushioning; 1.5 millimeter HDPE geomembrane, wedge welded; another layer of geonet on top for transmitting rainwater off the cover and preventing erosion; and finally a 0.27 kg/m nonwoven geotextile for filtration (see Figure 9). On top of these layers was placed 0.45 meters of a very clean sharp sand with permeabilities greater than 1 x 10-3 cm/sec. This is one of the most important aspects of a good cover, fast draining soil material that allows the geonet to remove the water before erosion can occur. This system proved out well during a 5 centimeter rain storm on the sand cover with no signs of erosion.

The final patches on the 1.5 millimeter geomembrane were being placed as the winter snows started to fall. The 0.45 meter cover of sand was finished just before temperatures dropped too low for placement, but the clay seal around the edge could not be placed in time to avoid the snows and extreme cold. In the spring of 1990, 0.15 meter of top soil was added and hydroseeded for the final cover.

Figure 9a

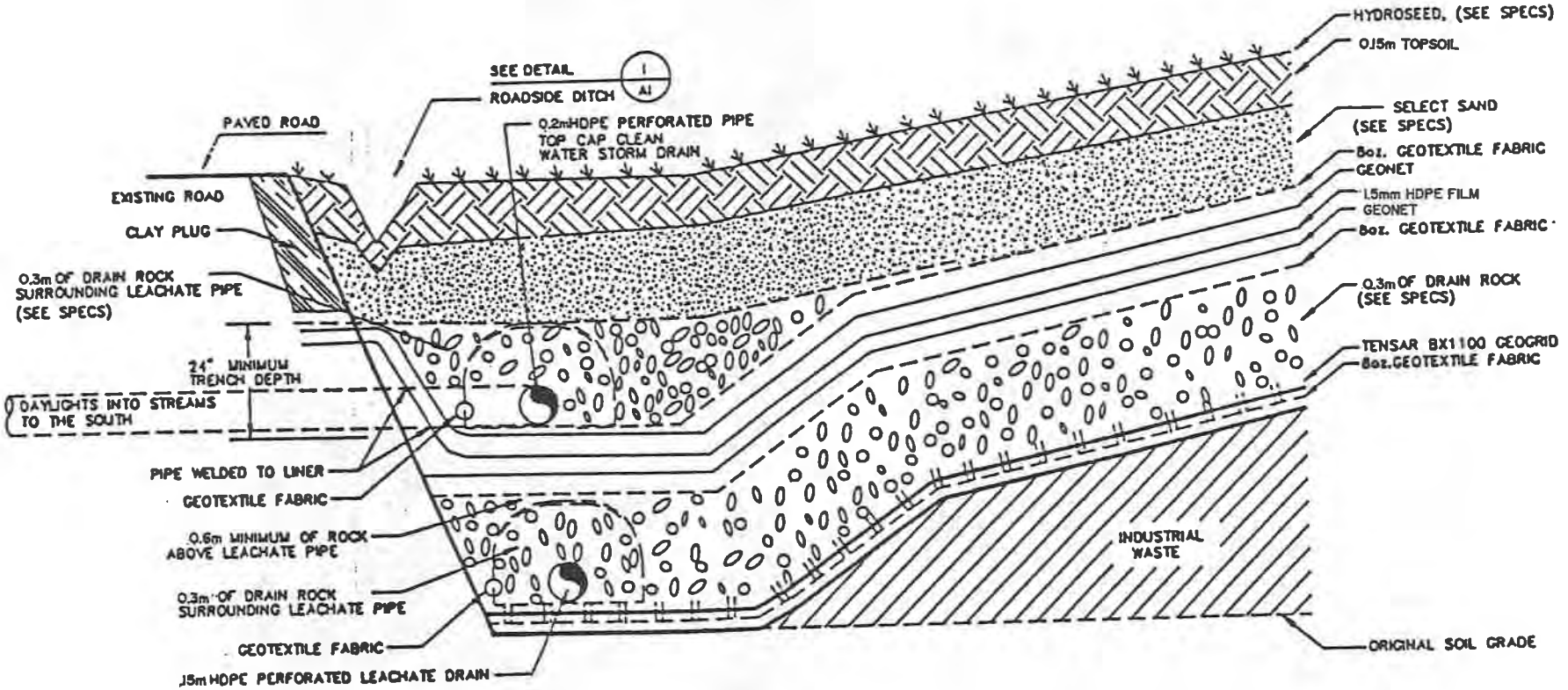

TOP CAP COVER DETAIL 1/6

N.T.S.

Figure 9b

CONCLUSIONS AND RECOMMENDATIONS

It is critical from our observations that the integrity of the liner be maintained in order to maximize the effectiveness of a geosynthetic cover in gas recovery. The odors from Moonlight Rock Landfill are now limited to the active area and no longer create adverse air quality for the surrounding residents. Changes in operation and future covers on the existing open waste site will further improve the quality of the air at the landfill.

Due to the nature of the waste material at the Moonlight Rock Landfill and its instability, it was recommended that any changes in the landfill surface be noted yearly and potential tearing investigated. Any drastic changes in gas quality should also cause a site investigation for potential liner tears. As it is, this landfill could not have been cleaned up, or the air quality improved so drastically without the use of geosynthetics.

ACKNOWLEDGEMENTS

Fetrow Engineering, Inc., would like to thank all the parties involved who made this project a success. First, Boise Cascade Corporation, as the project owner, and their concern for environmental issues helped move this project along. Mike Romslo, the Project Engineer for Boise Cascade, whose knowledge and practicality kept the project and the eventual operation running smoothly. Background information from Barr Engineering and testing by Braun Engineering testing labs were also important factors.

A special thanks to Gundle lining systems and Tensar who both sent technical representatives to the site on several occasions to help solve problems encountered in stabilizing the landfill and to insure the project was moving along smoothly.

The contractors who actually did the work; Ulland Brothers (the rock contractors) O'Leary Construction (building and mechanical) and Geo-Con (liner installation) also deserve recognition. I have never worked with a more conscientious group of contractors. They made the project happen under adverse conditions and time frames.

Geogrid Liner Support at Empire Sanitary Landfill

Alan Stephens
Empire Sanitary Landfill, Inc., USA
Richard Bodner, P. E.
Martin & Martin, Inc., USA

INTRODUCTION

The Empire Sanitary Landfill, Inc., located in Taylor Borough near Scranton in Northeastern Pennsylvania, is a 150 acre double lined municipal solid waste landfill situated on a 600 acre parcel which is accepting approximately 5,000 tons per day of municipal and residual/special handling waste. The facility design incorporates a double flexible membrane liner system to capture the leachate generated by the facility, and is predicated on the use of geosynthetics; including geofabric, geonet, geogrid, and geomembrane in order to adequately protect the environment.

HISTORY

The Empire Sanitary Landfill site is located on the east flank of a hillside overlooking the City of Scranton. The lower 60% of the site is underlain by 5 veins of anthracite coal which was subject to both deep mining and strip mining. Thus, prior to initiation of construction of the landfill, the site was characterized by approximately 350 acres of wooded strip pits and 250 acres of virgin wooded hillside.

In late 1985 and early 1986, engineering, geology, and hydrogeological consultants initiated the detailed studies of the site as necessary to prepare and submit an application to the Pennsylvania Department of Environmental Resources (DER) for a permit to construct and operate a double lined sanitary landfill. These studies included both surface and subsurface site characterization in order to define site characteristics and constraints as they related to designing the facility. The design plans were completed and submitted to DER in July of 1986, and following 10 months of DER review and communication between the regulators, owners, and Empire's consultants, the site was permitted in May of 1987. Construction began immediately, and operations commenced in November of 1987 on the initial 18 acre pad. Through 1987 to the present time, construction of subsequent pads continued as waste was delivered and the site began to fill.

SITE CONSTRAINTS

As noted, the lower 60% of the site is underlain by 5 seams of anthracite coal, which was subjected to both deep mining and surface stripping. Figure 1, Typical Geologic Cross Section, shows a general cross-section of the property. The coal seams ranged in thickness from a few feet to several feet. Initial deep mining took place in the late 1800's to early 1900's, with approximately 80% to 90% of the pillars being pulled by the mid 1900's. Strip mining of the crop coal then took over, with the recoverable coal being removed by conventional strip mining techniques by the 1960's.

As a part of the initial site study, over 30 deep borings were completed to confirm deep mine mapping and to characterize the subsurface conditions. The drilling program, augmented by seismic traverse surveys, and detailed field mapping of exposed highwalls, confirmed that the deep mines had essentially completely collapsed. As a precautionary measure, the design required that additional drilling and seismic surveys be completed on each pad underlain by deep mining, following excavation to design grades.

THE PROBLEM

During the excavation of Pad 3 of the 10 pads permitted, a slab of roof rock was exhumed which was bridging a void approximately 6 feet in diameter and 1 foot deep. This discovery prompted the initiation of the detailed area drilling program to reconfirm the maximum anticipated subsidence which the lining system may be subjected to. As a result of numerous core holes drilled through the deep mines, and an analysis of the data by Empire's site geology and engineering staff, engineering and geologic consultants, and representatives of Pennsylvania's DER and Bureau of Abandoned Mine Reclamation and the Bureau of Solid Waste Management, the maximum anticipated subsidence at the subbase grade was defined as a void with dimensions of 21 feet in diameter and 1 foot in depth.

While this size subsidence may not have resulted in the failure of the Flexible Membrane Liner System (FMLS) it was determined that a support system should be incorporated into the liner design to insure that subsidence would not compromise the liner or the piping systems associated therewith.

THE SOLUTION

After evaluating available options to provide for the necessary safety and security of the FMLS, Empire and its staff determined that a geogrid reinforcement was the best product to provide the necessary support of the approximately 150 feet of refuse to be placed on the liner while maintaining the ability of flex with potential limited subgrade settlement. Obviously, support of the liner system was essential; with cost, ease of installation, and long term product longevity being important also. The resulting Typical Liner

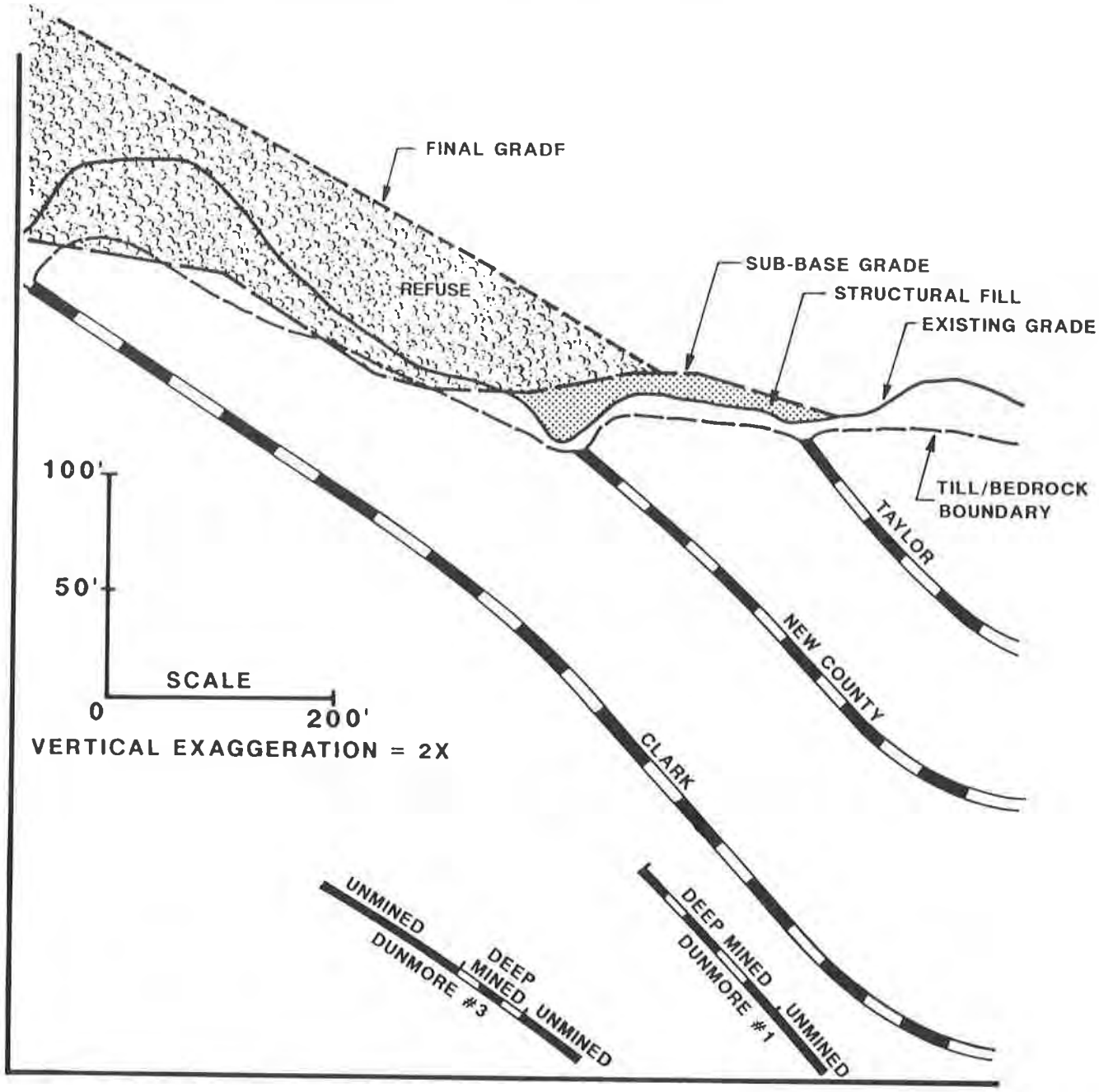

TYPICAL GEOLOGIC CROSS SECTION

- FIGURE 1 -

Section, Figure 2, indicates the ultimate liner at Empire which incorporates all of the earthen materials, piping system, and geosynthetic layers, including the geogrid. Because of the stage of construction on Pad 3 at the time the geogrid design was completed, the geogrid reinforcement was placed in the 12 inch witness zone material in Pad 3.

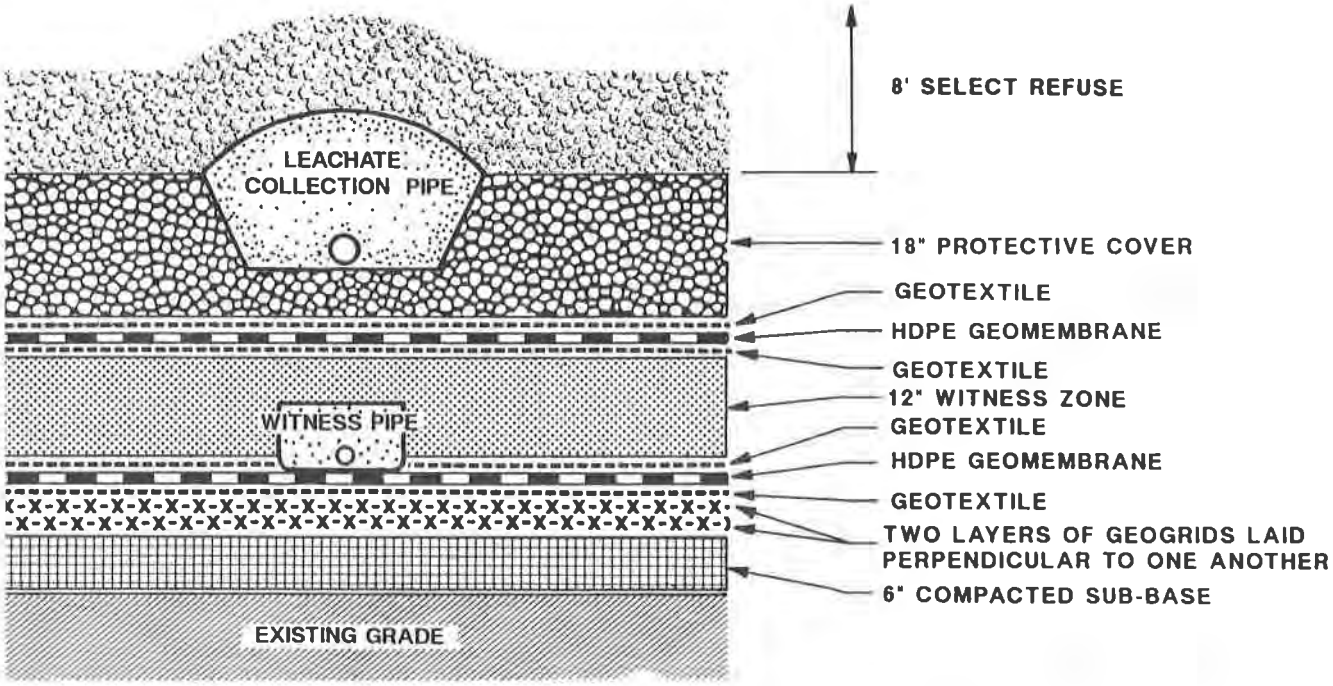

TYPICAL LINER SECTION

- FIGURE 2 -

Designing a structurally stable landfill requires preventing rupture and/or creep failure of the geomembrane and any other component of the lining system. The most economically feasible solution was the use of a geogrid reinforced soil support system specifically designed to prevent rupture and/or creep failure of the geomembranes, protect the integrity of the overall lining system and minimize bending and shear stresses on the piping system. The required geogrid tensile strength was determined based on maximum diameter and depth of a potential depression, the weight of the fill/waste material to be placed on top of the lining system, the maximum allowable strain of the system and the design life of the structure.

The design methodology used is based on the tensioned membrane theory (1) with the assumption that the geogrid spanning a void behaves as a tensile element able to transmit tensile stresses but not shear stresses (1,2). When a depression forms below the geogrid layer(s) supporting a landfill lining system, the geogrid deflects into the depression as tensile forces develop. This

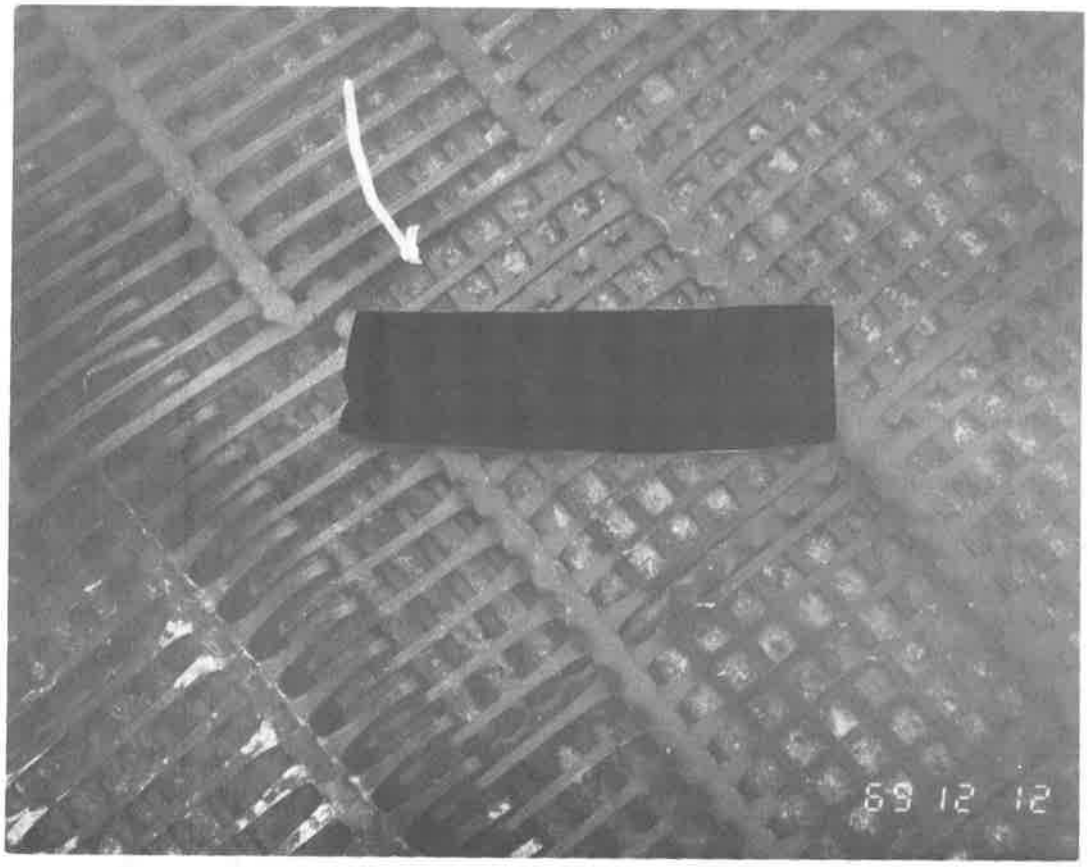
89 12 12

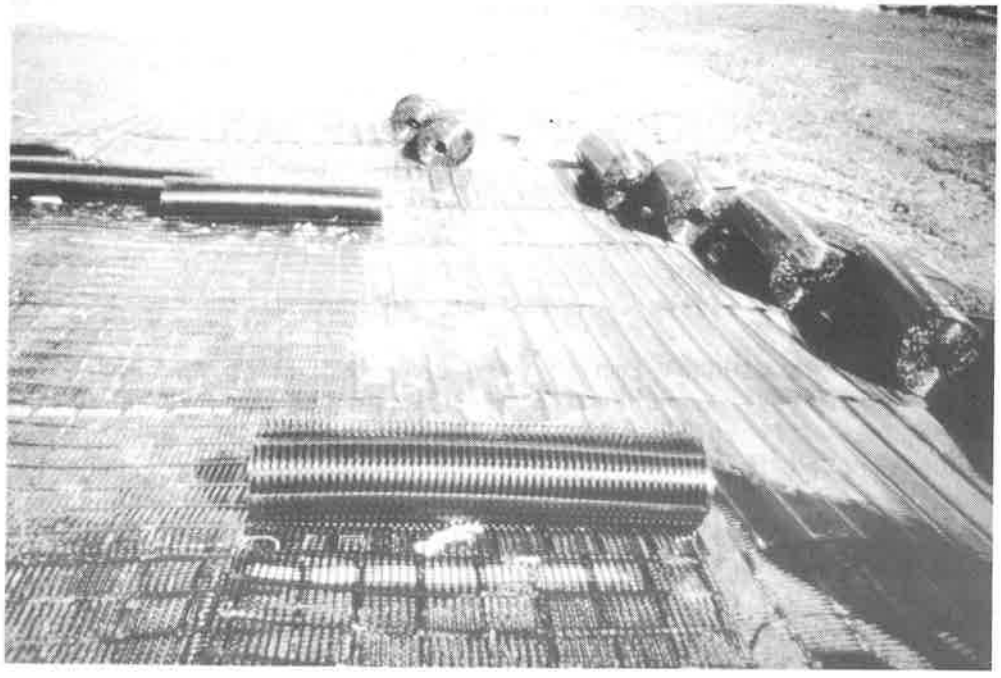

deflection has two effects: the material above the geogrid bends, which generates soil/waste arching; and the geogrid strains which mobilizes a portion of its tensile strength (3).

Two layers of structural geogrids were required to support and protect the integrity of the lining system. The geogrid layers were to be placed directly below the secondary geomembrane as illustrated in Figure 2, except in Pad 3, where they were placed in the witness zone. The two layers were laid perpendicular to one another and were placed directly on top of one another. Figure 3 illustrates the actual placement during field installation. Connection of subsequent roll ends was performed with the use of a 1.5 by 0.25 inch flat Bodkin HDPE bar, as illustrated in Figure 4, Bodkin Joint Detail. Adjacent rolls were secured with the use of white plastic ties. The geogrid layers were placed flat, free of slack or wrinkles. Figure 5 shows a partially completed geogrid installation.

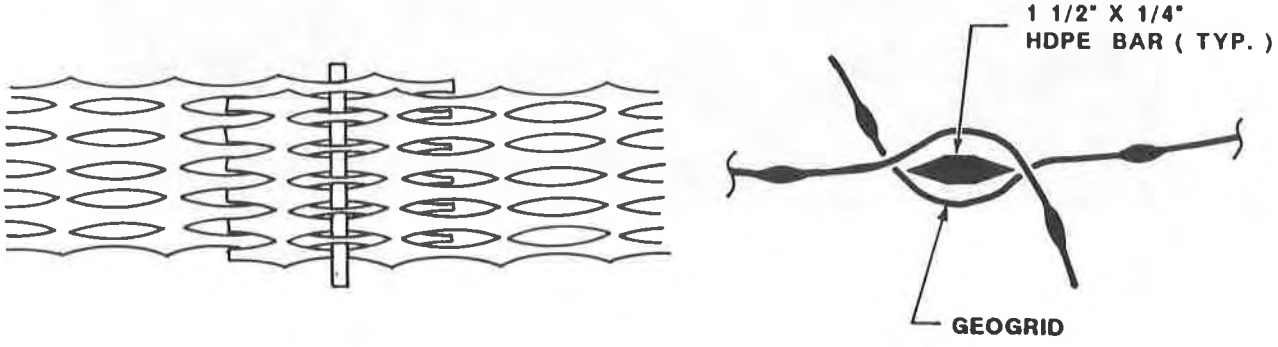

BODKIN JOINT DETAIL

- FIGURE 4 -

The geogrid layers used at Empire were selected based on several pertinent features and characteristics. Changing of some of the geogrid properties could alter the design significantly. Some of the most pertinent geogrid properties that were incorporated in the design are: i) allowable design strength defined based on a minimum of 10,000 hours of creep testing; ii) junction strength equal to or greater than 90%; iii) chemical compatibility; iv) high tensile strength and modulus at very low strains; and v) high flexural rigidity.

One of the major limiting design parameters is the maximum allowable strain of the lining system. At Empire Sanitary Landfill, the maximum allowable strain

was governed by the yield strain of the geomembrane which was equal to 10%. As determined by the Pennsylvania DER, a factor of safety equal to 2.0 was used to calculate the allowable strain; therefore 5% was the design strain limit.

It is important for the structural geogrid element supporting a landfill lining system to develop its working strength at strain levels that are consistent with the allowable strain of the lining system components. Thus a documented and well defined allowable design strength for the structural geogrid was essential in order to adequately determine the allowable design strength corresponding to a maximum allowable strain equal to 5% (4). It is vital for the geogrid to be able to retain its engineering properties over the design life of the structure. Potential causes of in-ground degradation for materials used in waste containment applications include attack by leachate, ultra-violet light and deterioration due to microbial attack. Another important consideration is the susceptibility of the geosynthetic materials to construction-induced damage by construction equipment during field installation. This potential for damage is a significant consideration which must be taken into account during design. The reduction in strength must be quantified through actual field trials (3, 5, 6, 7).

The final design package was reviewed by Empire and its staff professionals, consultants, geogrid manufacturer, and liner manufacturer and installer; then submitted to DER for review and approval. Figures 6 and 7 show the deployment of the geogrid at Empire, being laid perpendicular to one another in Figure 6; and the geogrid, geofabric, and secondary geomembrane being placed in Figure 7.

Geogrid reinforcement installation in the areas underlain by deep mine activity has continued with the construction of Pad 4 at Empire, and will be utilized again when Pads 7 and 10 are placed. The characteristics, availability, cost, and ease of installation of the geogrid have helped to maintain Empire Sanitary Landfill as an outstanding landfill facility in the northeast corridor.

ACKNOWLEDGEMENTS

Empire Sanitary Landfill, Inc. is appreciative of the support provided to it by Vicky E. Chouery-Curtis and TENSAR Environmental Systems, Inc.; as well as Ron Sturgeon, P.E.; Jerry Linski; and Rob Sochovka of its site staff; Martin and Marin, Inc., Design Engineering Consultants; Meiser and Earl, Inc., Hydrogeologic Consultants; Jeff Barnes, P.E., Geotechnical Consultant; SLT Lining System, the liner fabricator and installer; Norman T. Bryan, Jr., P.E., Plastics Pipe Institute; and the interest and technical review afforded Empire by the Pennsylvania Department of Environmental Resources - Wilkes-Barre Regional Office - Waste Management staff; the Bureau of Abandoned Mine Reclamation; and the Bureau of Solid Waste Management.

REFERENCES

1. ASCE Manuals and Reports on Engineering Practice No. 66. Structural Plastics Selection Manual.

2. ASCE Manuals and Reports on Engineering Practice No. 63. Structural Plastics Design Manual.

3. "Design of TENSAR Geogrid Reinforcement to Support Landfill and Cover Systems", Tensar Technical Note WM3, The Tensar Corporation, Morrow, Georgia, May 1989.

4. V. Chouery-Curtis, S.T. Butchko, "How to Economize & Optimize Land Use without Compromising the Landfill Structural Stability". Proceedings HMCRI's 7th National RCRA Superfund Conference, St. Louis, Missouri, May 1990, Pgs. 123-140.

5. Bonaparte, R. and Berg, R.R., "Long-Term Allowable Tension for Geosynthetic Reinforcement", Proceedings, Geosynthetics '87, Vol. 1, New Orleans, LA, February 1987, pgs. 181-192.

6. Wrigley, N.E., "The Durability and Aging of Geogrids", Proceedings, Durability and Aging of Geosynthetics, Geosynthetic Research Institute, Drexel University, Philadelphia, PA, December 1988.

7. Giroud, J.P., "Analysis of Stresses and Elongation in Geomembranes, Proceedings of Internal Conference on Geomembranes", Volume II, Denver, 1984, pgs. 481-484.

Private Industry Maximum Security Landfill Case History

Michel Marcotte
Solmers Internationale Consulting Engineers, Canada
Sophie Lagace
Solmers Internationale Consulting Engineers, Canada
Robert Denis
Solmers Internationale Consulting Engineers, Canada
Denis Faucher
PPG Canada Inc., Canada

INTRODUCTION

Ever since 1948, PPG Canada Inc. has been producing chlorine from brine electrolysis at its Beauharnois plant located on the south shore of Montreal (Qc, Canada). For this process, a film of mercury was used as the cathode electrodes. Forty years of continuous handling of liquid mercury inevitably brought about some level of soil contamination of the surroundings. Remedial actions were thus undertaken by the owner in 1987 as part of a five-year restoration and process modernization program towards an environmental friendly technology. On account of the sizeable volume of contaminated soils as confirmed from geostatistical analyses (125000 m3), on-site landfilling was preferred over alternate solutions. Conceptual design obviously called for a double-lined maximum security containment system designed to hold both sludges and construction debris in addition to contaminated soils.

PRELIMINARY CONSIDERATIONS

Siting was located on the owner's premises on a relatively flat plateau, fifteen meters above all neighboring streamflows. The area is characterized by the following stratigraphy (Figure 1); cambro-ordovician Potsdam sandstone, glacial moraine (up to five meters thick), Champlain marine clay (8 to 11 meters thick), and weathered silty clay (3,3 to 5,5 meters thick). On account of both depth and space restrictions imposed by a relatively shallow water table and sensitive clay deposits, existing roadways, county lines and surface water drainage paths, the optimized landfill shape came out as a relatively slender and asymmetric polygon (Figure 2) yielding an approximate projected area of 30000 m2, partially elevated (1,0 m) from the surrounding stripped groundlevel by its peripheric embankment.

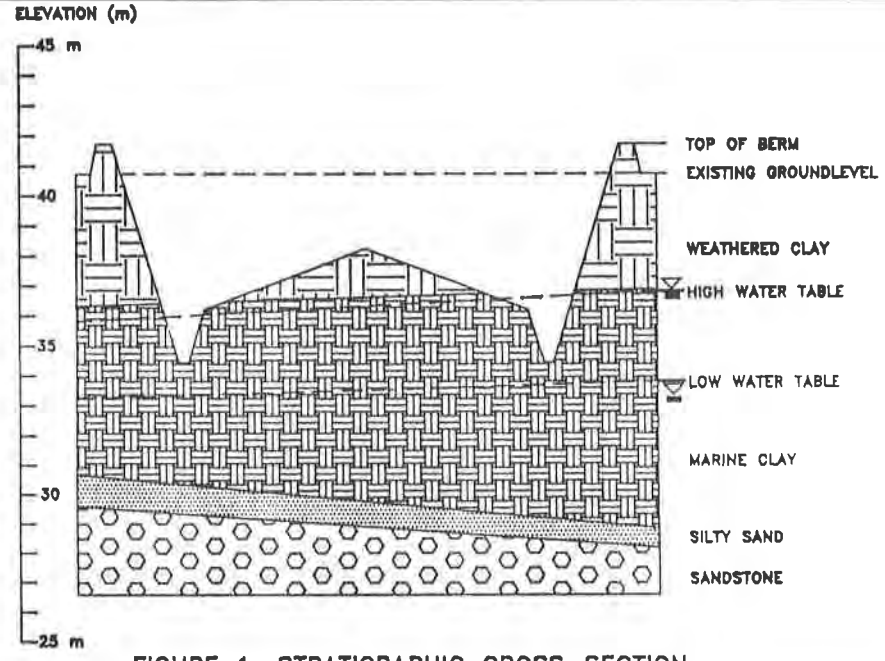

FIGURE 1. STRATIGRAPHIC CROSS-SECTION
(NO HORIZONTAL SCALE)

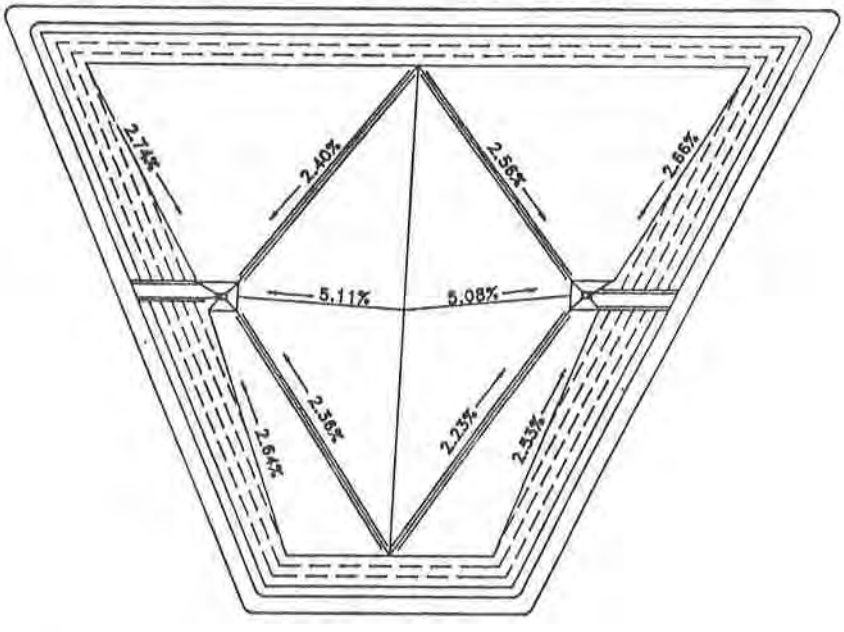

FIGURE 2. PLAN VIEW
(NOT TO SCALE)

DESIGN ELEMENTS

The most critical elements of this maximum security landfill were the various geosynthetics which were particularly preferred over natural materials on account of their inherent space saving advantages (see Figure 3). A thick non-woven geotextile (500 g/m2) connected to tertiary sumps was first incorporated over the excavated grade in order to essentially provide a clean working foundation along with longitudinal drainage during construction.

Furthermore, this tertiary drainage layer would also be closely monitored in order to provide data on the overall double-lined system long-term efficiency. The secondary hydraulic barrier, a 1,5 mm (60 mil) high density polyethylene geomembrane, was then incorporated over this tertiary drainage layer followed by its corresponding secondary drainage layer, a polyethylene geonet. The primary hydraulic barrier, a composite layer of clay/geomembrane, was then incorporated, followed by its corresponding primary drainage layer.

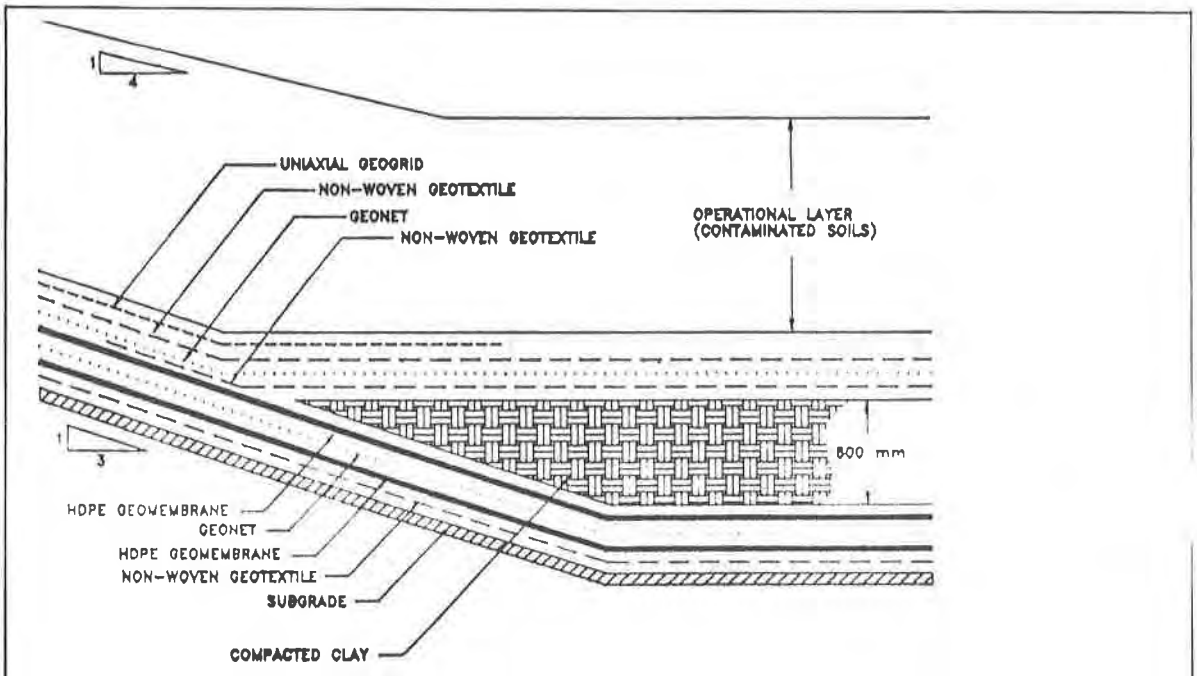

FIGURE 3. GEOSYNTHETIC CROSS-SECTION
(NOT TO SCALE)

This composite primary barrier was unique in that the 600 mm clay component was above its 2,5 mm (100 mil) high density polyethylene geomembrane component. This rather unorthodox pairing was preferred over the more classic approach (geosynthetic on top) in order to take full advantage of the clay's absorbency of the contaminants (1) which is expected to reduce the toxicity of the percolating leachate and ensuing treatment costs. This particular arrangement also greatly accelerated and simplified installation procedures since clay was never used as the geomembrane subgrade which traditionally impairs geosynthetic field assembly unless perfect field conditions govern. The primary drainage layer was composed of a geonet inserted between two separation/filtration non-woven geotextiles (500 g/m2).

Since the overall stability of the internal side slopes was deemed marginal at best under long term exposure, uniaxial geogrids were inserted under an operational clay layer reducing the original incline from 3H:1V to 4H:1V. All geosynthetic components were designed using USEPA's design and analysis methodology (2) complemented with extensive field experience.

PROJECT SPECIFICS

On account of the shallow sensitive clay deposit (in some places, less than a few meters below existing groundlevel), long-term drainage at the bottom of the cell following anticipated settlements required special attention. No less than eight triangular drainage planes were required (see Figure 2), each with its own three-dimensional orientation. At first glance, this scheme foretold complex construction and control procedures added to the fact that useful baselines could not be determined from the cell's irregular shape. But since the cell had been completely designed through computer assisted design software (CAD), an in-house subroutine was developped in order to generate a superimposed depth grid to which the earthwork contractor could easily refer by using laser beacons positioned at different space coordinates. The use of geosynthetics proved again beneficial since they would all ultimately conform to the original subgrade preparation without further earthwork or surveying.

The shallow excavation also necessitated tiered sumps with corresponding inclined high density polyethylene riser pipes (355 mm in diameter). For added protection against contingencies, the primary drainage systems were designed with back-up accesses: vertical riser pipes (630 mm in diameter) loosely encased in concrete man-holes in order to relieve down-drag (Figure 4).

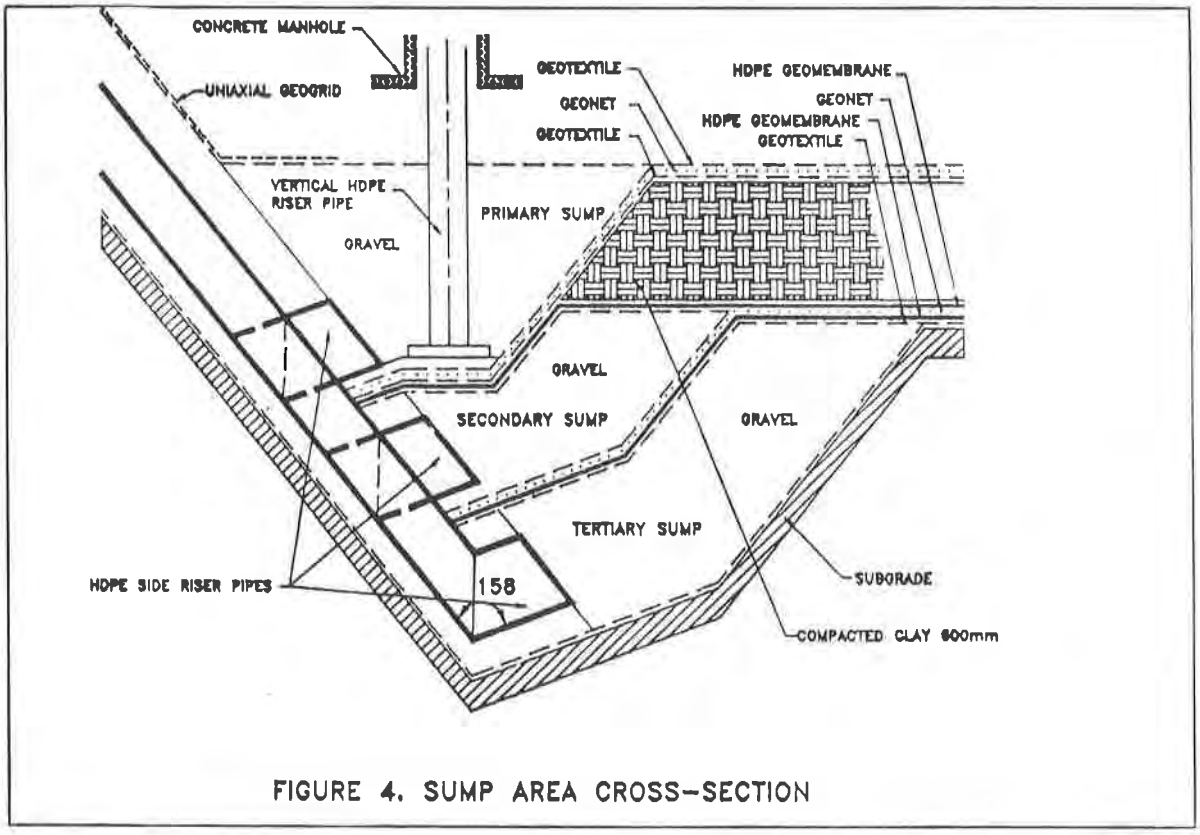

FIGURE 4. SUMP AREA CROSS-SECTION

All geosynthetics were closely examined for their chemical compatibility with a representative leachate sample which contained inorganic sulphurs and chlorides, Group I and II metallic compounds (Hg, Na, K, Mg, Ca & Ba) within a slightly basic solution (ph values between 7,9 and 9,1). This analysis was completed by the values yielded from a modified EPA 9090 accelerated testing program.

Excavation (70000 m3) and site preparation including clearing and banking (10000 m3) required eight weeks, while six weeks were needed to install all geosynthetics in accordance with an extensive quality assurance program (65000 m2 of geomembrane, 80000 m2 of geotextile, 65000 m2 of geonet, and 11000 m2 of geogrid). All in all, close to fifteen (15) kilometers of geomembrane seaming were required through three types of assembly; double hot wedge for most structural seams, double hot air and hand extrusion fillet for all repair work. In addition to various product conformance tests, 232 destructive tests samples were conducted on fusion seams samples for both peel and shear strengths yielding values of well over 90% of the parent material's stress at yield point (4).

OPERATIONAL PROCEDURES

In conformance with permitting regulations, operational procedures particularly addressed placement methodology of the different types of landfilled materials. A one meter thick operational layer of screened contaminated soils (free of any debris) would first be required prior to any heavy traffic. Sludges were to be thinly spread across the bottom of the cell provided that overall bearing capacity would not be reduced beyond practicality. Construction debris were to be placed in a single lift within layers of compacted soils, at least 1,6 m away from any geosynthetic. Those debris were to be scrutinized and prepared in accordance with the following guidelines: essentially bi-dimensional and free of any protrusions, height being limited to 60% of a standard lift thickness (1 m). Pieces were to rest on their side corresponding to the largest area which was limited to 1,5 m2 or 1,2 m x 1,2 m. All plastic debris were to be crushed prior to burying.

COST ANALYSIS

Project costs including permitting, engineering, construction, landfilling and closure (scheduled for late 1991) will average $25.77 (Cdn) per cubic meter of landfill space ($15.80/metric ton). These costs may roughly be broken down as per the following percentages: engineering and construction monitoring (12,4%), overall construction (77,9%) and backfilling (9,7%). These figures exclude all costs related to site restoration and post-closure monitoring

CONCLUSION

This specific project would likely have proven impracticable without the vast utilization of geosynthetics, since constructional aspects of conventional methods were quickly identified as major hindrances. Over-excavation into sensitive material in order to accomodate equivalent placement of both clay and granular materials would have been problematic. Limiting the excavation grades within workable conditions would have required for similar air space either a higher closure elevation conflicting with regulations (3), or a much larger projected area whereby related project costs would have at least doubled.

ACKOWLEDGEMENTS

The authors are grateful to PPG CANADA Inc., to LOISELLE EXCAVATION Inc. who was responsible for the earthwork on site and to the installer, CONSTRUCTION TECHNIQUES JACQUES COTE Inc., for their collaboration in the preparation of this paper.

REFERENCES

(1) "Etude Hydrogéologique du Site d'Enfouissement, Phase I", GEOS-TECSULT, Rapport no. 2428, May 1985.

(2) "Requirements for Hazardous Waste Landfill Design, Construction and Closure", US Environmental Protection Agency, CERI-88-33, June 1988.

(3) "Guide d'Implantation et de Gestion des Lieux d'Enfouissement des Sols Contaminés", Ministère de l'Environnement du Québec, Direction des substances Dangereuses, January 1988.

(4) "Rapport Final des Travaux de Contrôles de la Qualité Effectués par Construction Technique Jacques Côté Inc.", Robert Denis and Sophie Lagacé, Cellule d'Enfouissement à Sécurité Maximale #9, Usine de PPG Canada Inc., Internal report, October 1989.

The Evolution of Geosynthetics in a Landfill Lining System

Jan Hutwelker
American Resource Consultants, USA
Thomas Pullar
American Resource Consultants, USA
Francis Taylor
Palco Linings Inc., USA

ABSTRACT

This paper will detail the evolution of geosynthetic usage in sanitary waste landfill lining systems in the 80's by reviewing the case history of Grand Central Sanitary Landfill, located in Pen Argyl, Pennsylvania. Grand Central Landfill started operations in the 50's as a natural renovation fill. In 1978, plans were permitted to line future expansion areas with geomembranes. In 1984, the first lining system was constructed, with three more areas lined in the remaining portion of the decade. Each successive fill area involved additions and improvements to the geosynthetic system.

This paper will also discuss the change in design concept from leachate containment to leachate removal. The primary geomembrane was originallly the focus of both design and construction. The successive cells saw an increase in the efficiency of leachate removal as new materials and techniques were added. A H.E.L.P. model will be used in the paper to detail this improved efficiency.

A regulatory overview will be provided to demonstrate the effects of regulatory change on the design and use of geosynthetics. The paper will conclude with a discussion of recommendations based on the experience gained in multi cell landfill construction.

FACILITY OVERVIEW

Grand Central Sanitary Landfill, Inc. and Grand Central Sanitation, Inc. (both referred to as G.C.S.L.) have been family run business' for two generations. Owned and operated by the Perin family, G.C.S.L. is located in Plainfield Township, Northampton County, Pennsylvania.

The G.C.S.L. site is a 52 acre sanitary landfill that operates under a permit from the Pennsylvania Department of Environmental Resources (P.A. D.E.R.) (Figure 1). G.C.S.L. is permitted to receive municipal, commercial and residual waste. Landfilling began at the site in the early 50's using natural renovation techniques for Fill Areas 1 and 2 and continues today on a double synthetic lined portion of the site (Fill Areas 3 through 6).

Detailed landfill design plans were developed for the landfill in 1978 and permitted by P.A. D.E.R. in November, 1980. Current landfill operations follow these approved plans with permit amendments granted for new waste streams, groundwater monitoring improvements, double synthetic liners and construction of leachate treatment facilities.

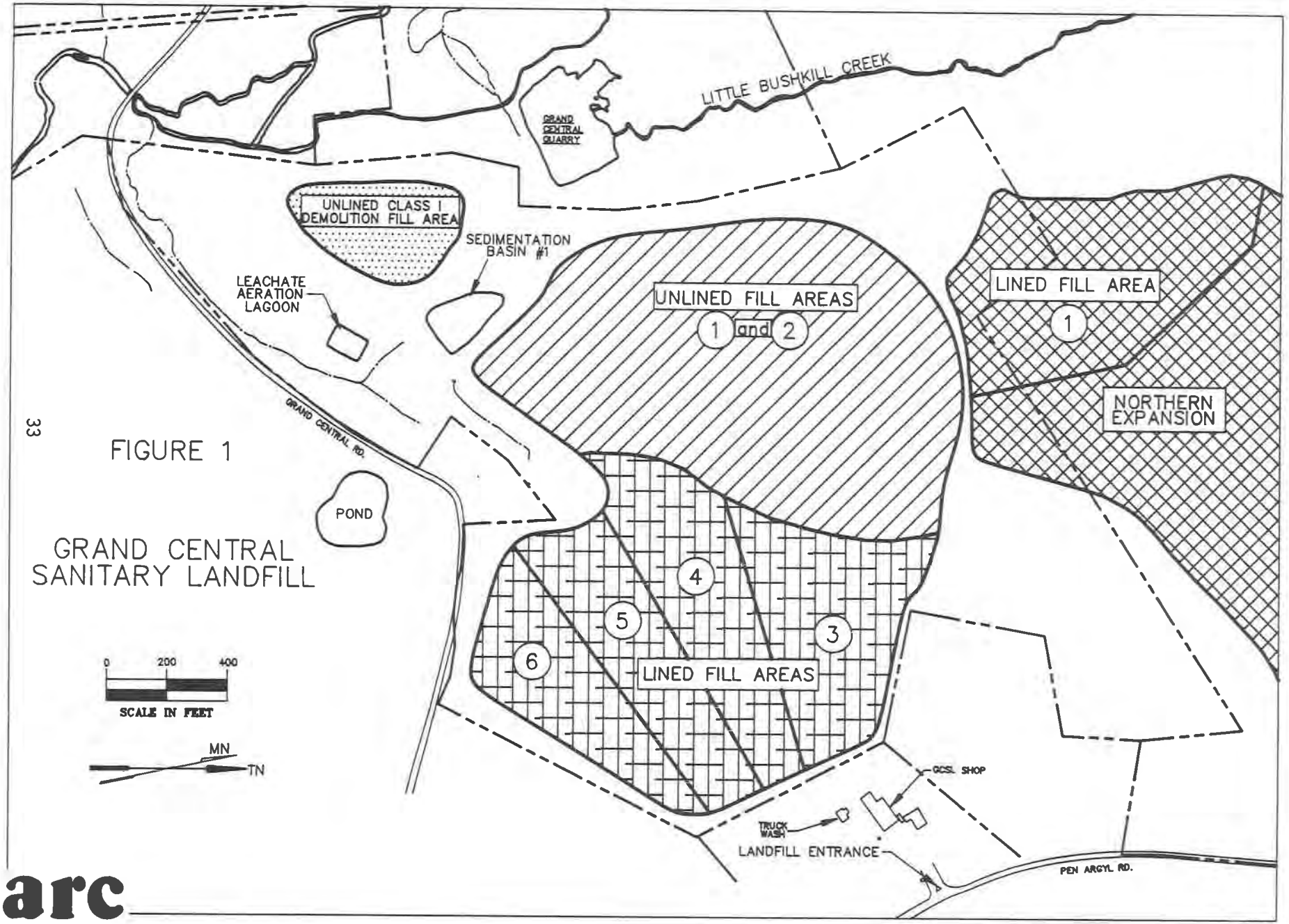

FIGURE 1

GRAND CENTRAL SANITARY LANDFILL

arc

CHRONOLOGICAL DEVELOPMENT OF GEOSYNTHETIC USAGE

FILL AREAS 3 AND 4 (1984 and 1985)

Secondary Liner

Subbase covered with 4" of compacted clay and sand. 3/8" sprayed asphalt MC-30 applied over subbase.

Secondary Collection Zone

Collection zone consisted of a 12" layer of sand (stone chips). Trenches wrapped with a 4 oz./S.Y. non-woven geotextile and 4" PVC pipe was set in place and backfilled with 2B stone.

Primary Liner

30 mil PVC primary liner installed (Note: No geotextile used above/below liner).

Liner Protective Cover

Cover consisted of 6" of select soil (no stones over 1/2") and 8" of fine shale and clay.

Leachate Collection Zone

Trenches wrapped with 4 oz./S.Y. non-woven geotextile and 4" PVC pipe was set in place and backfilled with 2B stone.

Initial Waste

Initial waste consisted of 2' of selected municipal waste. This was residental waste with no object larger than two feet in its greatest dimension.

Quality Control

Liner field seams air lance tested per ASTM D4437. Field

seam samples from tie-in seam between Areas 3 and 4 tested for peel and shear strength per NSF Standard 54. Note that seam specimens required "curing" time prior to testing. Material certifications provided.

NOTE: In April, 1987, American Resource Consultants, Inc. submitted a permit amendment application to replace the secondary asphalt liner with 30 mil PVC in Fill Areas 5 and 6. This amendment was approved in July, 1987. In July, 1988 a permit amendment was approved to replace the 30 mil PVC primary liner with 50 mil PVC in Fill Area 6.

FILL AREA 5 (1987)

Underdrains

4" and 6" PVC pipe placed 4' under subbase in trenches backfilled with #3 stone.

Secondary Liner

30 mil PVC secondary liner. Liner covered with a 12 oz./S.Y. non-woven geotextile.

Secondary Collection Zone

Collection zone consisted of a 12" layer of sand (stone and chips). Trenches lined with 4 oz./S.Y. non-woven geotextile and 4" PVC pipe was set in place and backfilled with #3 stone.

Primary Liner

Collection zone covered with a woven polypropylene

geotextile. 30 mil PVC primary liner. Liner covered with 12 oz./S.Y. non-woven geotextile.

Liner Protective Cover

Cover consisted of a 6" of sifted clay or sand and 8" of shaley clay.

Leachate Collection Zone

Trenches lined with 4 oz./S.Y. non-woven geotextile and 4" PVC pipe was set in place and backfilled with #3 stone.

Flow Zone

Flow zone consisted of several layers of whole tires to protect liner and convey leachate to collection system.

Initial Waste

Initial waste consisted of 2' of selected municipal waste.

Quality Control

Liner field seams air lance tested per ASTM D4437. Field seam samples tested from all field seams for peel and shear strength per NSF Standard 54. Material certifications provided. Full time inspector present during liner installation. Factory seam samples tested from all factory panels. Geotextiles overlapped, no sewing.

FILL AREA 6 (1988)

Underdrains

4" PVC pipe in 2' deep trenches backfilled with #3 stone. Trench covered with a woven polypropylene geotextile. Drain connected to 8" tie-in pipe to Fill Area 5 groundwater underdrain.

Secondary Liner

Subbase covered with a 12 oz./S.Y. non-woven geofabric. 30 mil PVC secondary liner. Liner covered with a 4 oz./S.Y. non-woven geotextile.

Secondary Collection Zone

Collection zone consisted of a 12" layer of sand (stone chips). Trenches lined with 4 oz./S.Y. non-woven geotextile and 4" PVC pipe was set in place and backfilled with #3 stone.

Primary Liner

Collection zone covered with 4 oz./S.Y. non-woven geotextile. 50 mil PVC primary liner. Liner covered with 12 oz./S.Y. non-woven geotextile.

Liner Protective Cover

Cover consisted of 6" of sifted clay or sand and 8" of shaley clay.

Leachate Collection Zone

Trenches lined with 4 oz./S.Y. non-woven geotextile and 4" PVC pipe was set in place and backfilled with #3 stone.

Flow Zone

Flow zone consisted of 2'-4' of whole tires to protect

liner and convey leachate to collection system.

Initial Waste

Initial waste consisted of 2' of selected waste.

Quality Control

Liner field seams air lance tested per ASTM D4437. Field seam samples tested from all field seams for peel and shear strength per NSF Standard 54. Material certifications provided. Full time inspector present during liner installation. Factory seam samples tested from all factory panels for peel and shear strength per NSF Standard 54. Geotextiles sewn.

NORTHERN EXPENSION CELL ONE (1990)

Subgrade

Minimum 6" prepared subbase compacted to +95% standard proctor. Permeability is less than or equal to 1 X 10 -5 c.m./sec.

Secondary Liner

30 mil Oil Resistant PVC. The landfill expansion was permitted for a PVC liner. In October, 1990, a permit amendment was given to replace the PVC liners with Oil-Resistant grade PVC. This change was made to allow the acceptance of individual residual wastes containing higher concentrations of oils, greases and volatile organic compounds than are normally considered acceptable for PVC liners. This covered worst case waste

streams although the leachate quality may still have been acceptable to standard PVC. This liner is underlain and covered with a 12 oz./S.Y. non-woven geotextile.

Secondary Collection Zone

Collection zone consisted of a 12" layer of sand with a permeability greater than or equal to 1 X 10 -2 c.m./sec. Trenches lined with 4 oz./S.Y. non-woven geotextile. 4" SDR 11 HDPE perforated pipe was set in place at 100' O.C. and backfilled with AASHTO #3 stone.

Primary Liner

50 mil Oil Resistant PVC liner. Liner underlain and covered with a 12 oz./S.Y. non-woven geotextile.

Leachate Collection Zone

Collection zone consisted of a 18" layer of sand with a permeability greater than or equal to 1 X 10 -2 c.m./sec. Trenches lined with 4 oz./S.Y. non-woven geotextile. 6" SDR 11 HDPE perforated pipe was set in place at 100' O.C. and backfilled with AASHTO #3 stone.

Flow Zone

Flow zone consisted of 2' - 4' of whole tires to protect liner and convey leachate to collection system.

Initial Waste

Initial layer of waste consisted of 8' of selected waste.

Quality Control

Liner field seams air lance tested per ASTM D4437. Field seam samples tested from all field seams for peel and

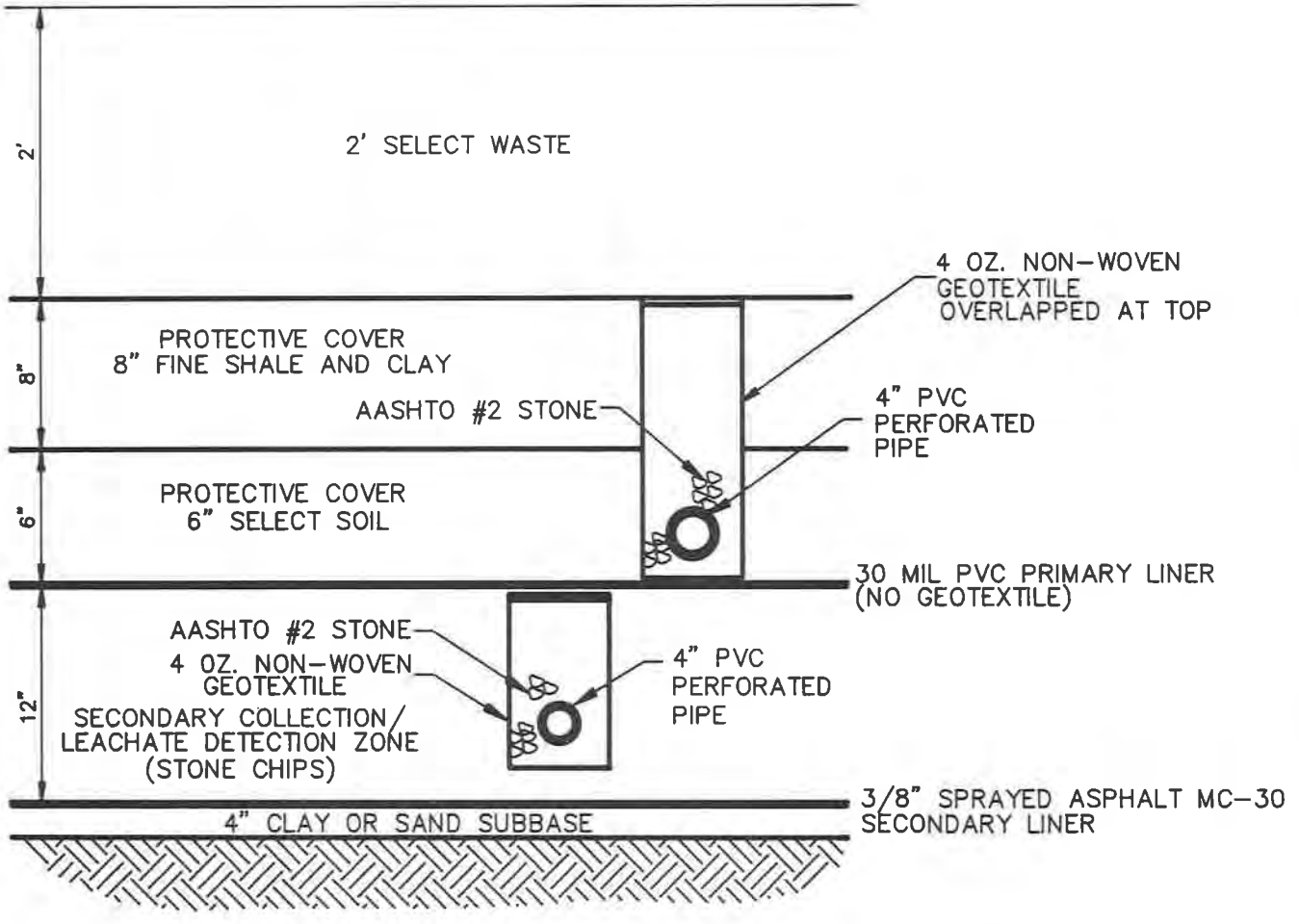

FILL AREAS 3 & 4 – (1984 & 1985)

TYPICAL LINER SYSTEM DETAIL

N.T.S.

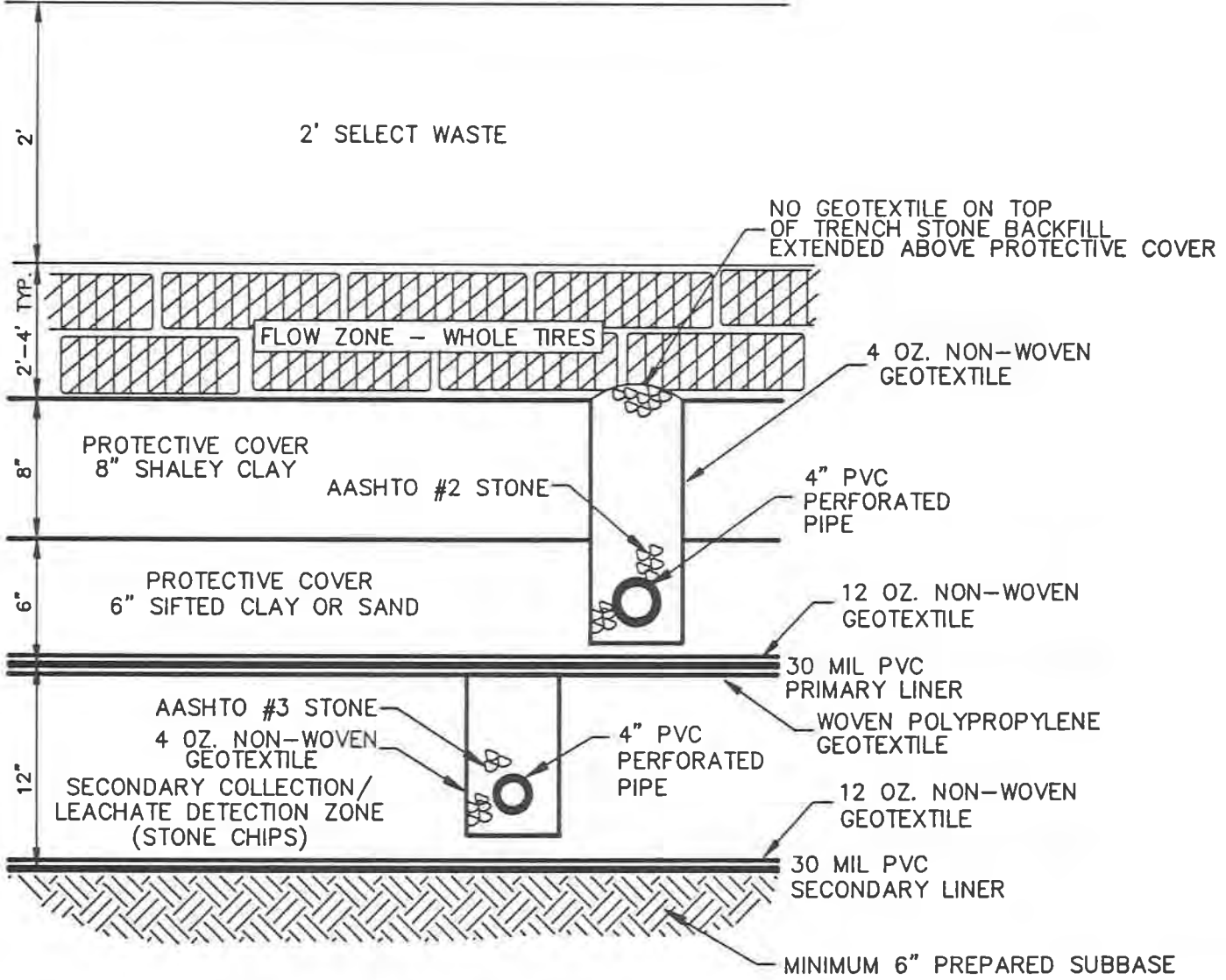

FILL AREA 5 - (1987)
TYPICAL LINER SYSTEM DETAIL

N.T.S.

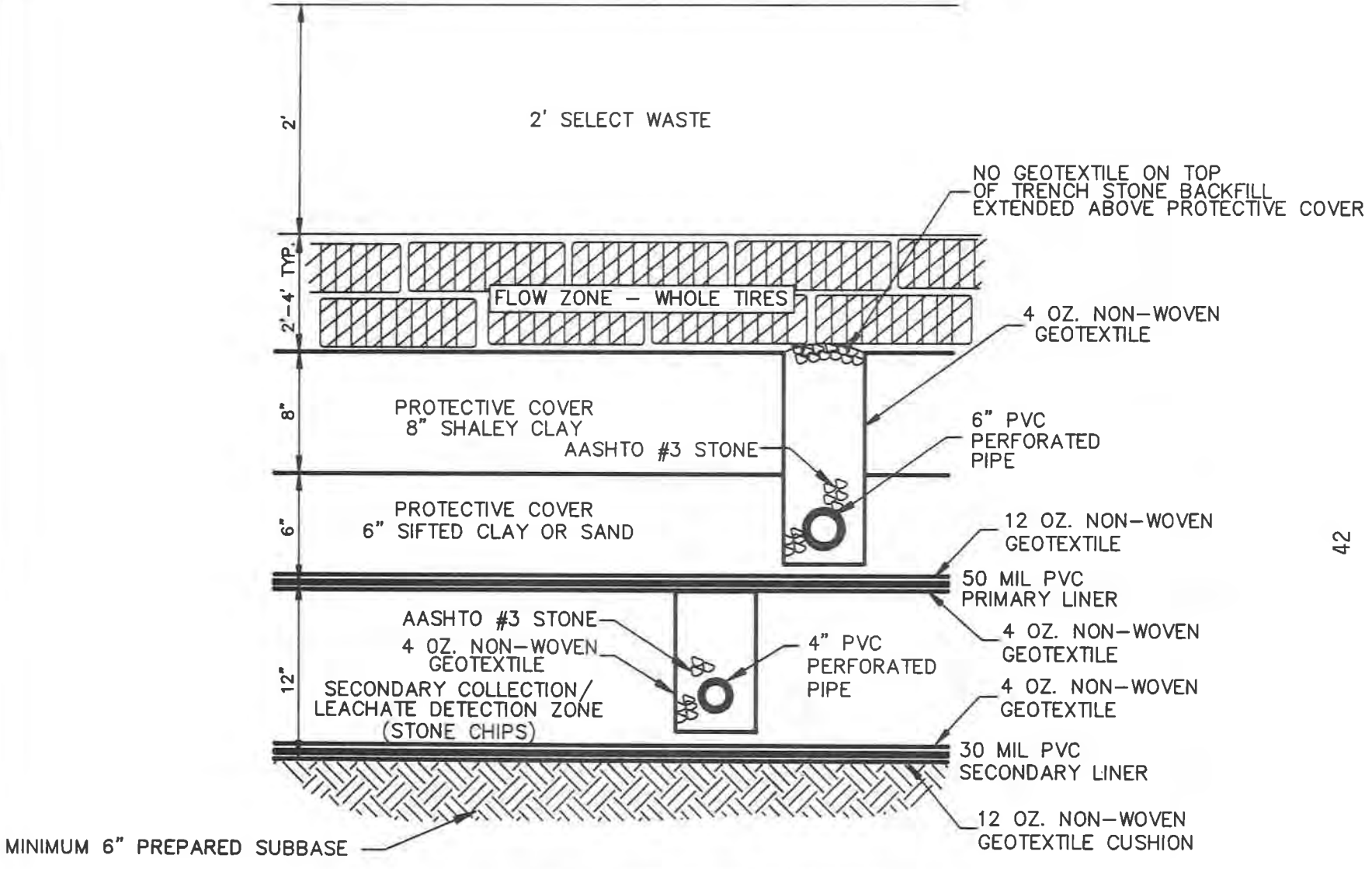

FILL AREA 6 - (1988)
TYPICAL LINER SYSTEM DETAIL
N.T.S.

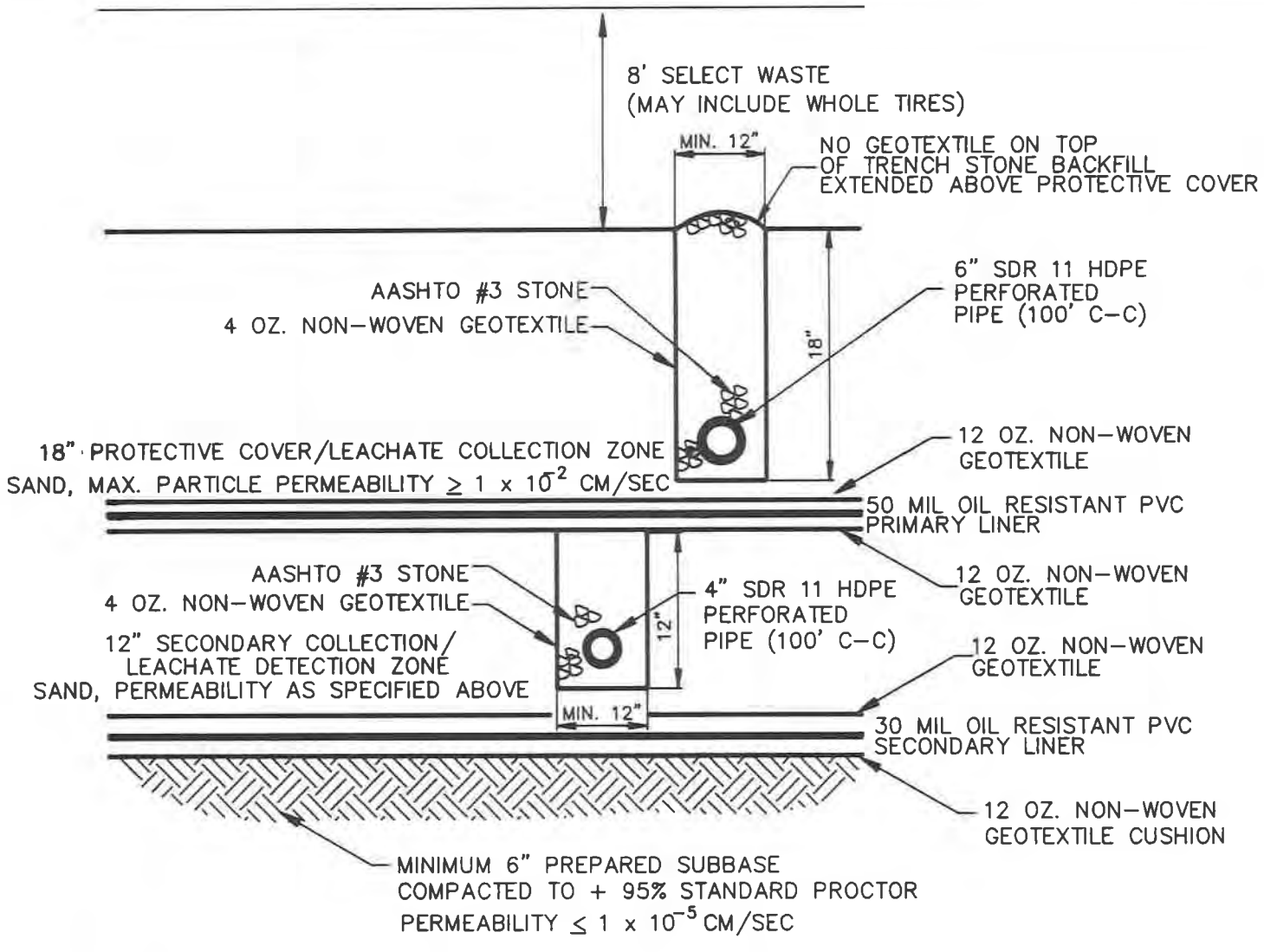

CELL 1 – NORTHERN EXPANSION (1990)

TYPICAL LINER SYSTEM DETAIL

N.T.S.

shear strength per NSF Standard 54. Material certifications provided. Full time inspector present during liner installation. Factory seam samples tested from all factory panels for peel and shear strength per NSF Standard 54. Geotextiles sewn.

FILL AREA 1 AND 2 CLOSURE (1990)

Geotextile

12 oz./S.Y. non-woven for geomembrane protection.

Geomembrane Cap

30 mil PVC.

Geotextile

4 oz./S.Y. non-woven for geomembrane protection.

Geonet

Extruded cross strand polyethylene net for drainage.

Geotextile

12 oz./S.Y. non-woven for filtration.

TECHNICAL DISCUSSION

Municipal sanitary landfill applications has been an area of tremendous growth in the design and construction usage of geosynthetic products, particularly geomembranes.

Geomembranes may offer significant advantages over liners of natural soils or clay. Geomembranes are several orders of magnitude less permeable to liquids than clay is. This allows a 30

to 50 mil thick PVC, for instance, to offer a more impermeable barrier than a three-foot thick layer of clay. Clay liners may also lose their natural barrier properties through reactions with chemicals found in the landfill leachates. Geomembranes are easily tested for chemical resistance to leachates. The consistency of geomembrane properties provides a high confidence level when making a determination of geomembrane chemical compatibility.

Geomembranes also provide a significant cost saving over clay liners. PVC geomembranes are available in panel sizes as wide as 100' and as long as 600'. PVC's large panel sizes makes for a fast, inexpensive installation. An additional cost savings is realized by saving the air space that a thick clay barrier would occupy. On a per acre basis, with a double liner system, PVC geomembranes save nearly 6,500 cubic yards of air space that would be needed for a 2' thick clay liner.

PVC GEOMEMBRANE

The PVC geomembrane was immersion tested for compatibility with the G.C.S.L. leachate in accordance with E.P.A. Method 9090. The immersion test showed no apparent changes or trends in the values of the material parameters tested. This indicates that the PVC material is apparently not reacting with the leachate and is compatible for use. Table 1 shows the results of the immersion test (1).

TABLE 1

30 MIL PVC GEOMEMBRANE/WASTE COMPATABILITY TEST

	Test Method	NSF Std. 54 Requirement	Unexposed Result	120 Day @ 30 C	120 Day @ 50 C
1. Breaking Factor (min) (Pounds/in width)	ASTM D882	69	81	80	75
2. Elongation @ Break (min) (Percent)	ASTM D882	300	304	315	325
3. Modulus (force) @ 100% (min) (Pounds/in width)	ASTM D882	27	50	47	43
4. Tear Resistance (min) (Pounds)	ASTM D1004	8	13	12	9
5. Hydrostatic Resistance (Lbs./sq. in min)	ASTM D751 Method A	82	121	112	106

50 MIL PVC GEOMEMBRANE/WASTE COMPATABILITY TEST (5)

	Test Method	NSF Std. 54 Requirement	Unexposed Result	120 Day @ 23 C	120 Day @ 50 C
1. Breaking Factor (min) (Pounds/in width)	ASTM D882	115	165	156	153
2. Elongation @ Break (min) (Percent)	ASTM D882	300	341	364	373
3. Modulus (force) @ 100% (min) (Pounds/in width)	ASTM D882	45	68	65	63
4. Tear Resistance (min) (Pounds)	ASTM D1004	12	25	21	20
5. Hydrostatic Resistance (Lbs./sq. in min)	ASTM D751 Method A	110	204	186	179

* Please note that ASTM D638 is used in testing for EPA 9090 specification. NSF Standard 54 is based on ASTM D882 which gives higher elongation values.

Several other materials were also considered chemically compatible with the waste and leachate to be contained. PVC was selected over other available materials because of its superior mechanical properties and over 30 years of proven in ground performance (2). PVC's ability to elongate three dimensionally provides a significant safety factor during installation and during the service life of the liner. The U.S. Bureau of Reclamation has studied various geomembranes for three-dimensional elongation performance in hydrostatic pressure testing. A Bureau study tested PVC liners and other materials for their relative puncture resistance over a simulated rock subbase (3). PVC demonstrated the best three dimensional elongation by elongating over plastic pyramids 1/2 inch, 1 inch and 1 1/2 inch without failure at 75 psi pressure. That is comparable to 165 feet of water head pressure. This elongation ability is more than is necessary to handle the stresses of installation or minor subgrade settlements.

PVC is manufactured through the calendering process. Calendering of PVC provides the strictest tolerances of material thickness and properties available. The manufacturer furnishes quality control certificates which list the test values measured for each lot of material tested.

Fabrication of the calendered rolls into the field sized panels is done by dielectric welding. Destructive samples of factory seams are taken from every four hours of production and tested for shear

and peel strengths. The test results are logged and identified per panel location. These tests are certified and provided to the project engineer.

The 30 mil PVC was furnished to the site in panels approximately 75' wide by 400' long. The 50 mil PVC was furnished to the site in panels approximately 60' wide by 300' long. Specific panel sizes were made to fit a specific site location. A panel layout drawing detailed these locations.

GEOMEMBRANE INSTALLATION

The PVC arrived at the site on pallets, accordian folded. The panels are spread into position with panel overlaps of six (6) to eight (8) inches. A three (3) inch seam is created by bodied chemical fusion. Great care needs to be taken during the seaming operation to ensure that the bonded area is clean and free of moisture.

The mechanical behavior of PVC is again beneficial when the critical area of field seams is examined. This can be seen in the stress-strain behavior of PVC. Figure 2 shows the relationship of stress (force) to strain (elongation) for PVC. At 13% strain PVC exhibits a stress of 3.9 ppi. This stress is a fraction of PVC's tensile strength. The benefit of this stress-strain behavior is that PVC field seams are unlikely to be stressed to their design limits. Unlike PVC, geomembranes that exhibit yield

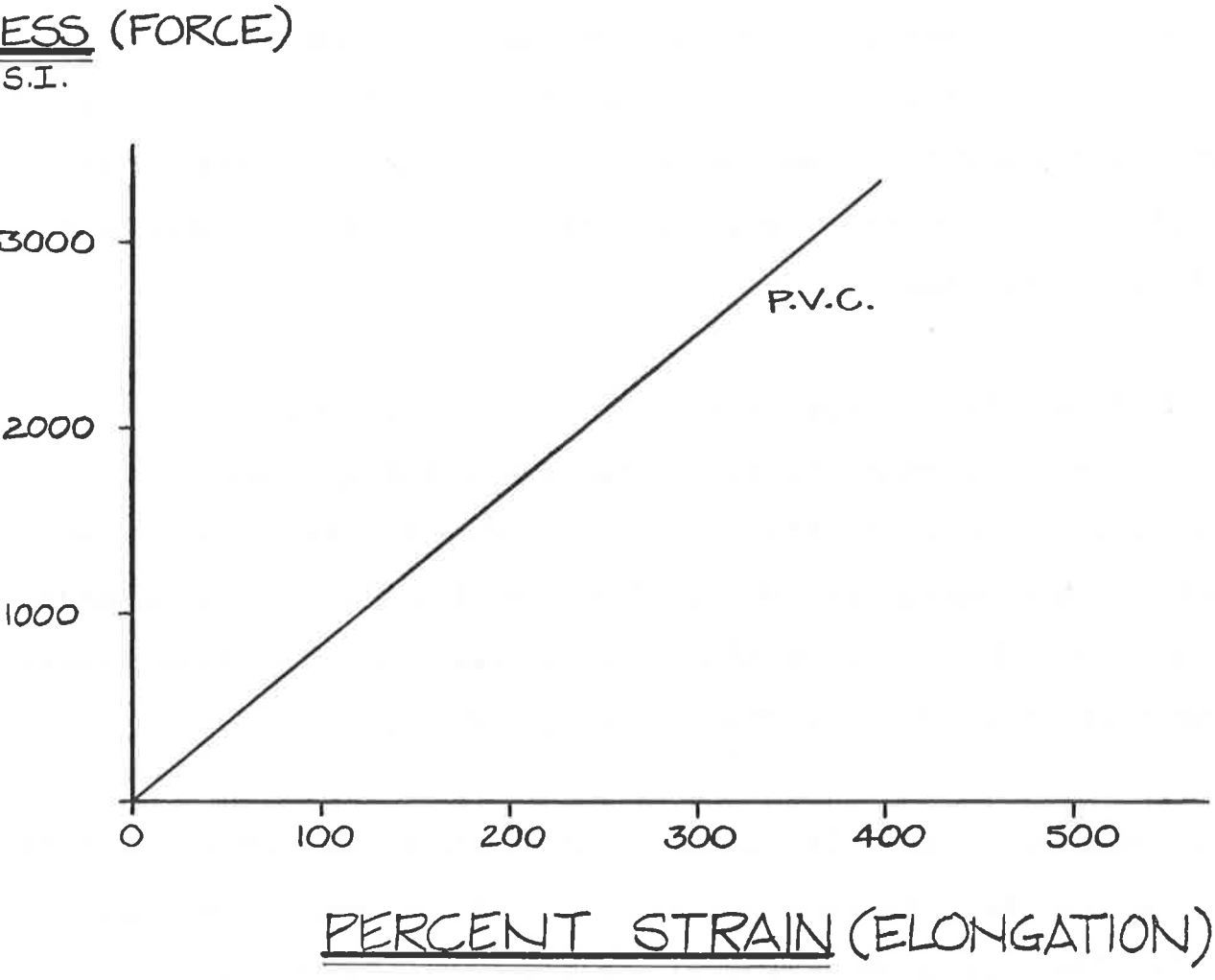
ESS (FORCE)
S.I.
3000
2000
1000
P.V.C.
0
100
200
300
400
500
PERCENT STRAIN (ELONGATION)

FIGURE 2

characteristics do not share this stress-strain relationship and will exhibit stress levels that meet or exceed their design tensile properties when elongated by 13%.

The first Fill Area at G.C.S.L. was designed in 1978 using asphalt as the primary liner. A permit amendment was granted in 1984 to substitute the 30 mil PVC liner for the asphalt. At the time of construction, G.C.S.L. was one of only six sites in the state of Pennsylvania which was lined and one of only three which had a double liner system.

The initial Fill Area construction at G.C.S.L. went well considering the newness of the technology being applied. This was due in large measure to the great care taken by the owner/operator to ensure the integrity of the liner system during construction process. The integrity of the liner system has since been proven by the lack of leachate in the secondary collection zone.

One problem that was discovered after landfilling began was that leachate removal efficiency in Fill Area 3 was poor. Attempts to improve the leachate removal efficiency began with minor modifications to the leachate collection trenches in Fill Area 4. The trench was extended above the 14" protective soil layer into the first layer of waste. This allowed the collection trenches to intercept leachate flowing over the protective soil layer. A more significant improvement in leachate removal was realized in Fill

LUTION OF GEOSYNTHETICS AT GRAND CENTRAL SANITARY LANDFILL						
T DATA AND RESULTS SUMMARY OF H.E.L.P. MODEL RUNS						
EMBER 28, 1990						
VARIABLES	FILL AREA	FILL AREA	FILL AREA	NORTHERN		
	3&4	5	6	EXPANSION		
H THICKNESS	720"	720"	720"	720"		
	C=.000199cm/s	C=.000199cm/s	C=.000199cm/s	C=.000199cm/s		
ARY DRAINAGE	8" SHALE/CLAY	2' TIRES	2'-4' TIRES	8'TIRES		
R SUMMARY	C=.000064cm/s	C=11.22cm/s	C=34.5cm/s	C=7.8cm/s		
	6" SELECT	8" CLAY	8"CLAY	18"SAND		
	SOIL	C=.000064cm/s	C=.000064cm/s	C=.00999cm/s		
	C=.0000001cm/s	6"CLAY/SAND	6"CLAY/SAND			
		C=.000025cm/s	C=.000025cm/s			
ARY LINER						
ERIAL	PVC	PVC	PVC	PVC		
KNESS	30 MIL	30 MIL	50 MIL	50 MIL		
K FRACTION	0.00001	0.00001	0.00001	0.00001		
DETECTION	12" SAND	12" SAND	12" SAND	12" SAND		
R SUMMARY	C=.0017cm/s	C=.0017cm/s	C=.0017cm/s	C=.00999cm/s		
NDARY LINER						
ERIAL	MC-30 ASPHALT	PVC	PVC	PVC		
KNESS	3/8"	30 MIL	30 MIL	30 MIL		
K FRACTION	N/A	0.00001	0.00001	0.00001		
ARY						
ECTION PIPES						
PE (min.)	0.063	0.051	0.105	0.02		
CING	700'	400'	200'	100'		
NDARY						
ECTION PIPES						
PE	0.063	0.051	0.105	0.02		
CING	700'	200'	200'	100'		
RESULTS						
ON	151.2 INCHES	14.6 INCHES	14.5 INCHES	7.3 INCHES		
ARY LINER						
ON	2.7 INCHES	0.4 INCHES	0.2 INCHES	0.8 INCHES		
NDARY LINER						
TURATED HYDRAULIC CONDUCTIVITY						

Area 5 by installing a layer of whole tires above the lined protective cover. This tire layer thickness was increased for Fill Area 6. The improvement in leachate removal efficiency is shown in Chart A. An added benefit of the tire layer was the increased protection of the liner system during initial landfilling operations.

H.E.L.P. MODEL SUMMARY

In order to help quantify the effectiveness of the upgrades to landfill liner system configurations at Grand Central, four different cross sections were modeled using the H.E.L.P. computer model (4). The first liner system cross section evaluated was the liner configuration for Fill Areas 3 and 4, the second cross section represented fill Area 5, the third cross section represented fill Area 6, and finally, cross section 4 represented Cell 1 of the Northern Expansion.

Included in the output from the H.E.L.P. model is a value hydraulic head on the liner system. This value can be used as a gauge in predicting how well a given leachate collection system design will convey leachate away from the liner system thereby minimizing hydraulic head on the geomembrane. Results of the model runs indicate that the hydraulic head decreases significantly as liner and liner drainage improvements were made at Grand Central. As shown on the results summary, the hydraulic head on the primary liner was predicted to be 151.2 inches for the liner configuration

in Fill Area 3 and 4, compared to a predicted 7.3 inches on the primary liner in the Northern Expansion.

In conclusion, the design modifications which appear to have had the greatest impact on leachate removal are the use of whole tires as protective cover in the drainage layer, and decreasing the spacing between the leachate collection pipes. As shown on the attached summary, the hydraulic head decreases from 151.2 inches to 14.6 inches with the addition of the tires and the closer spacing of the collection pipes. It should be noted that a liner leak fraction of 0.00001 was used in the model input for the primary liners in each case. This conservative value was chosen to produce a relatively high hydraulic head value on the primary liner, as leakage of leachate to the secondary collection zone is minimized.

CONSTRUCTION TECHNIQUES

The G.C.S. landfill case history is an example of not only advances in geosynthetic usage but also improvements in construction through the use of geosynthetics.

The use of geotextiles increased with each successive cell primarily as a means of protecting the geomembrane from damage during earth covering operations. Geotextiles were used first over the geomembrane in Fill Area 5, then both under and over the geomembrane in Fill Area 6 and in Cell One. Even with the most thorough of precautions taken during earthwork operations,

irregularities may be unavoidable. Irrregularities such as oversized particles in the subgrade or cover materials and traffic damage to the subgrade may be harmful to the long-term success of a geomembrane. Geotextiles correct minor subgrade irregularities that could damage a geomembrane as well as insure a clean surface for field seaming operations. Geotextiles also help to reduce washouts from occuring during rainy periods.

One part of landfill construction that has produced problems in the past is tying-in new lined areas to existing lined areas. Potential problems may include: overfilling of disposal areas, leachate seeps and surface run-off over the edges of lined areas and difficulties in unearthing existing liner for attachment to the new liner. G.C.S.L. had experienced all of these problems to some degree and continually improved their approach to handling them with the construction of each successive Fill Area.

The leading edge (tie-in edge) of Fill Area 3 was covered with roofing felt paper prior to being covered with soil. While this was an improvement, the felt paper was not durable or strong enough to withstand abuse during unearthing. A non-woven geotextile was used to cover the leading edges of Fill Area 4 and 5. The non-woven geotextile was able to be pulled back by hand after excavating most of the soil cover. This exposed a sufficient quantity of the clean, undamaged PVC geomembrane for attachment to the new PVC geomembrane.

Controlling leachate seeps and landfill surface run-off was accomplished by building a berm between the Fill Areas. The initial berm was 2' high. This was successful in containing most of the leachate seeps and surface run-off. However, greater success was achieved by building the berm to a height of 5' with a 3H to 1V slope ratio. This created a natural set back for the landfilling operation as well as keeping run-off out of the next Fill Area. The geomembrane covers the berm and is easily accessed on the clean side for continuation of the landfill construction.

REGULATORY OVERVIEW

Landfills in Pennsylvania have been regulated by the Pennsylvania Department of Environmental Resources since 1970 using the various rules and regulations enacted to provide design criteria and performance standards to operators and engineers. Until 1988, landfill regulations were contained in Chapter 75 of the regulations. In April 1988, new solid waste regulations went into effect in Pennsylvania covering every aspect of waste handling from generation, storage, and transportation, to recycling and disposal. The following summary compares the regulations that governed the design and construction of Grand Central Sanitary Landfill.

FEATURE	CHAPTER 75	CHAPTER 273
Natural Renovation	Allowed	Not Allowed
Secondary Liner	Optional 33% interior slope max 1% slope min Asphalt or soil 10 -4 cm/sec	Mandatory 25% interior slope max 2% slope min 30 mil or clay 10 -7 cm/sec
Leak Detection Zone	sand perm. contrast 175' pipe spacing	0.25 inch part. 10 -2 cm/sec 100' pipe spac.
Primary Liner	20 mil or 10 -7 cm/sec 33% slope max 1% slope min	50 mil 10 -7 cm/sec 25% slope max 2% slope min
Protective Cover	14 in. 2" max part. N/A leach. collection	18 in. 0.25" max part 10 -2 cm/sec
Allowable Leach. Head	N/A	1' max.
Liner Comp. Testing	N/A	E.P.A. Method 9090

Note that while regulations do not address geotextiles, it is D.E.R.'s policy to require geotextiles for liner cushioning, pipe trench lining, road base construction, drainage ditch lining and erosion control purposes.

CONCLUSION AND RECOMMENDATIONS

A successful geosynthetic installation is a combination of proper design and installation. A critical part of installation quality is the foresight that can only be gained by experience. The experience gained at the G.C.S.L. site can be attributed to the

owner's intense commitment to quality as well as to the fact that the same cast of players was involved in the construction of each Fill Area.

In conclusion, the following recommendations are made based on the experience gained at the G.C.S.L. site:

- Allow sufficient scheduling time for delivery and installation of the entire liner system including protective cover before the onset of cold weather. This means starting the job in the spring or summer. Cold weather not only hinders the liner installation but also causes difficulties with the associated earthwork.

- Install markers to maintain a setback of the landfilling operation from the liner edge.

- Install a berm (temporary, if necessary) to facilitate runoff containment.

- Provide close coordination of liner installation and associated earthwork. Scheduling is critical to avoid duplication of efforts in fine grading and compaction operations.

- Utilize geotextiles to improve performance of the liner system as well as improve installation efficiency.

ACKNOWLEDGEMENTS

The authors would like to thank the Perin family for their cooperation in writing this paper.

CONVERSION TABLE

WEIGHTS

1 ounce	28.35 grams
1 pound	0.4536 kilogram
1 English ton	0.9072 metric ton

SQUARE MEASURE

1 sq. inch	6.452 sq. centimeters
1 square foot	9.2903 sq. decimeters

LINEAR MEASURE

1 inch	2.54 centimeters
1 foot	3.048 decimeters

MEASURE OF VOLUME

1 cubic foot	28.347 cubic decimeters
1 quart liquid	0.9463 liter
1 gallon	0.3785 decaliter

OTHERS

O.C.	On Center

REFERENCES

1. E.P.A. Method 9090 Immersion Test; October, 1988, May, 1989, and October, 1989. Precision Laboratories, Inc., Orange, California.

2. Morrison and Starbuck. "Performance of Plastic Canal Linings"; United States Department of the Interior, Bureau of Reclamation; Engineering and Research Center. January, 1984.

3. Frobel, Ronald K. "A Micro Computer-Based Test Facility for Hydrostatic Stress Testing of Flexible Membrane Linings", United States Bureau of Reclamation. Denver, Colorado. 1983.

4. Schroeder, Paul R. "The Hydrologic Evaluation of Landfill Performance (H.E.L.P.) Version 2". Waterways Experiment Station, Corps of Engineers. Vicksburg, Mississippi.

Application of Geosynthetics in the Design of Fully-Drained Mineral Waste Storage Facilities

W. A. Cincilla
Knight Piesold and Co., Consulting Engineers, USA
G. A. Zagorski
Fluid Systems, Inc., USA

INTRODUCTION

The mineral industries in the United States generate substantial volumes of processing wastes each year. The milling of gold ores alone produces an estimated 100 million tons of tailings (spent ore) which may contain a variety of heavy metals, residual process reagents and toxic liquids. Since these wastes can vary dramatically from the perspectives of both physical and geochemical properties, storage technologies and the potential for environmental impact are likewise largely site specific. Fortunately, the design and construction of these facilities have been allowed to evolve with an emphasis on performance rather than prescriptive compliance, in contrast to that of the hazardous waste field. The result of such an evolution has been the fostering of innovative engineered alternatives to meet the required environmental performance goals.

The techniques which have been historically employed for mineral waste storage ranged from direct dumping into nearby rivers and streams, to impoundment in water-retaining-type reservoirs. In the 1960's, however, environmental pressures and disasters such as the one which occurred in Buffalo Creek, West Virginia (Volpe, 1972) provided a new emphasis on design procedures and resulted in the formulation of the first federal legislation to regulate the impact of mineral waste storage on the environment.Partly due to the increase in awareness of mining companies, government regulation, and economics, waste storage practice has more recently developed as a geotechnical and mineral engineering function which is generally carried out by specialist firms. This paper describes an innovative methodology for mineral waste management which has proven highly successful in a number of facilities operating in environmentally sensitive areas of the western U.S.A. and Canada. The key to the approach is a combination of controlled waste deposition and, more importantly, drainage, the capacity for which has been greatly enhanced in recent years through the development of durable and cost effective geosynthetics. Also included in the paper is a brief review of mineral waste storage design and construction practice along with a selected case history of a project where geosynthetics have been successfully applied to meet strict performance and cost criteria.

While the base of experience for the information provided in this paper centers on the storage of milled gold tailings, the general concepts described are equally applicable to a variety of industrial particulate wastes generated as slurries including fly ash, fine coal refuse and refinery sludges.

WASTE MANAGEMENT PRACTICE AND GEOSYNTHETICS

Applications. The application of geosynthetics in mineral waste management can be divided into four basic categories:

1) Hydraulic barriers (liners).

2) Hydraulic breaks (leak detection and drainage).

3) Soil separation (for drains etc).

4) Soil reinforcement (embankments, pads, foundations etc.).

The general use of geosynthetics as alternatives to natural materials in construction related to mineral waste management has increased drastically over the past decade, with the greatest increase being in geomembranes for pad, ditch, and leach pad liners. Due to the broad scope of application of these products in the mineral industries, further discussions will be limited to innovative applications for hydraulic breaks and soil separation. In order to provide a technical basis for the discussion to follow, an overview of waste management practice is given below.

Overview of Waste Management Practice. In general, most waste products produced during mineral processing have a significant liquid component at some point in the process flowsheet. Even where solid particles can be screened or filtered effectively, the resulting waste "cake" contains up to 30% moisture and is transported in this semi-solid form by means of conventional bulk-materials equipment such as conveyors or trucks from a stockpile area. More commonly, however, the soil-sized waste particles are transported in pipelines in slurry form, the solids content of which may vary from a few percent by weight to the pumpable limits of the particular slurry (near 70%). Waste slurries are then transported via pipeline and deposited in an impoundment where the liquid fraction is allowed to separate and is collected and, where possible, returned to the process. At this point in the depositional process, the water fraction becomes the most significant factor in maintaining a stable, environmentally-acceptable containment for the waste. Drainage, therefore becomes the most important design parameter to be considered by the engineer.

Fully-saturated waste deposits present particular problems from the point of view of seepage since the hydraulic heads, and hence gradients, rise continuously as the facility is filled, due to the fine-grained nature of the waste particles. Simply, material is being added faster than its ability to dissipate excess pore pressure. Since seepage is directly related to head, higher and higher volumes of seepage enter

through the liner system and into the foundation soils and local groundwater as filling proceeds. Since all types of liner systems, including geomembranes, have some finite "installed" permittivity, this concept is equally valid for all cases.

The stability of the embankments also becomes an important design element due to the fact that large volumes of saturated waste are being impounded. Designs must include drains and monitoring schemes consistent with water-dam practice. Figure 1 illustrates the relationship between head (h), hydraulic gradient (i) and time for wastes deposited in a conventional water-retaining type facility. These conventional types of storage facilities are difficult to reclaim due to the fact that working surfaces for light earth-moving equipment are costly to establish. As well, continued consolidation of the saturated deposit may result in the formation of low areas which tend to collect runoff and further contribute to long-term seepage and instability.

Figure 1
Conventional Water Retaining Facility

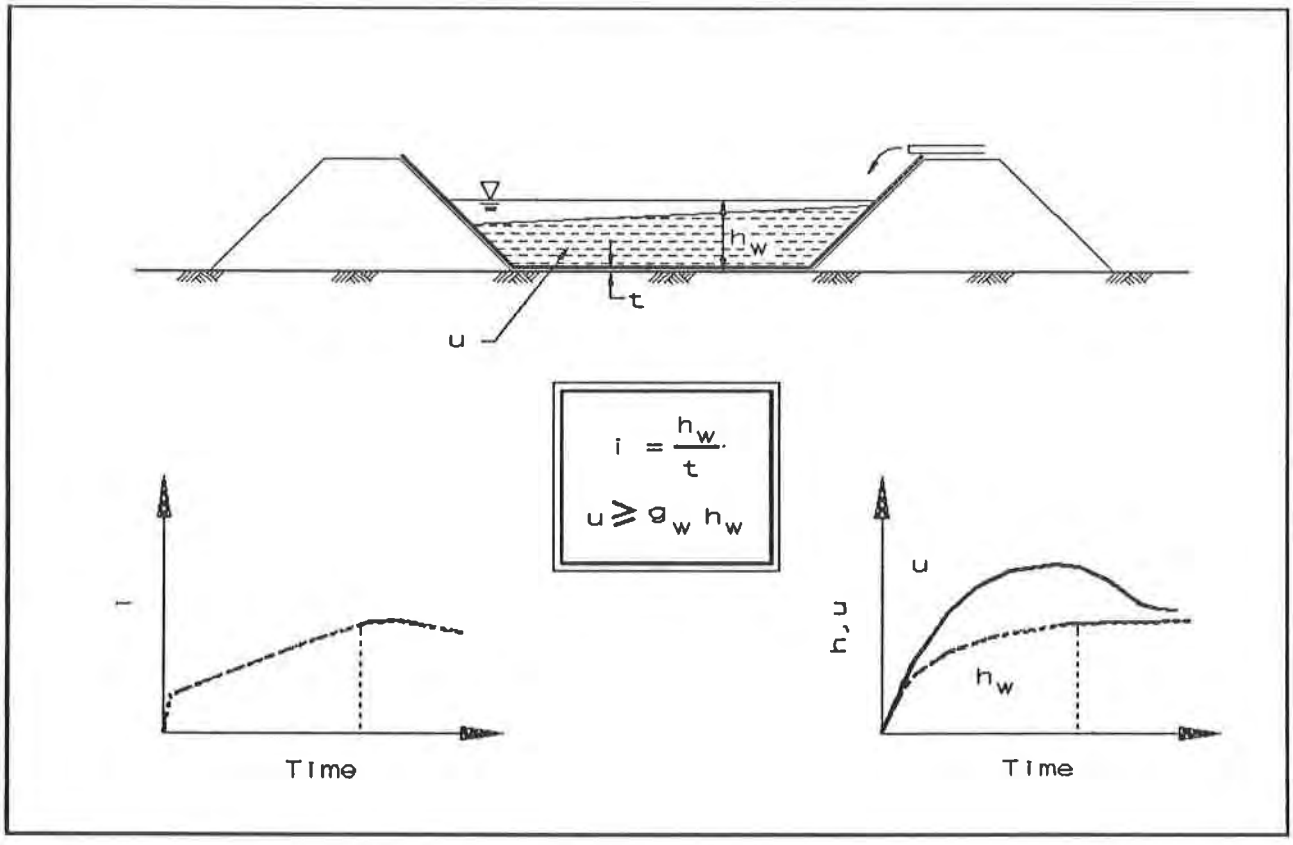

It is apparent that by reduction of pore pressure within the deposit, via underdrainage and continuous removal of surface flows, superior performance could be achieved. However, the practical cost constraints make the solution to the potential problems of fluid collection and transport more difficult. The concept of a "fully-

drained" waste storage facility is by no means novel. Engineers have for many years recognized that the removal of water from soils provides some definite advantages but, until recently, this had not been applied in a systematic manner to the storage of mineral wastes.

DESIGN ISSUES AND PHILOSOPHY

General. The design engineer is faced with numerous issues during the preliminary stages of a mineral waste storage project, with facility siting, the cost and availability of both natural and synthetic construction materials, and regulatory requirements and permitting schedules heading the list. In terms of overall facility performance, one of the most important factors, and one that is often overlooked to some degree when more "conventional" design concepts are being applied, are the properties of the waste itself. These are not limited to physical, but include geochemical and rheological properties as well. From the perspective of drainage and selection of drainage media, the waste properties demand close analysis, the results of which may strongly influence the viability of the design methodology.

Figure 2
Typical Mineral Waste Sieve Analysis

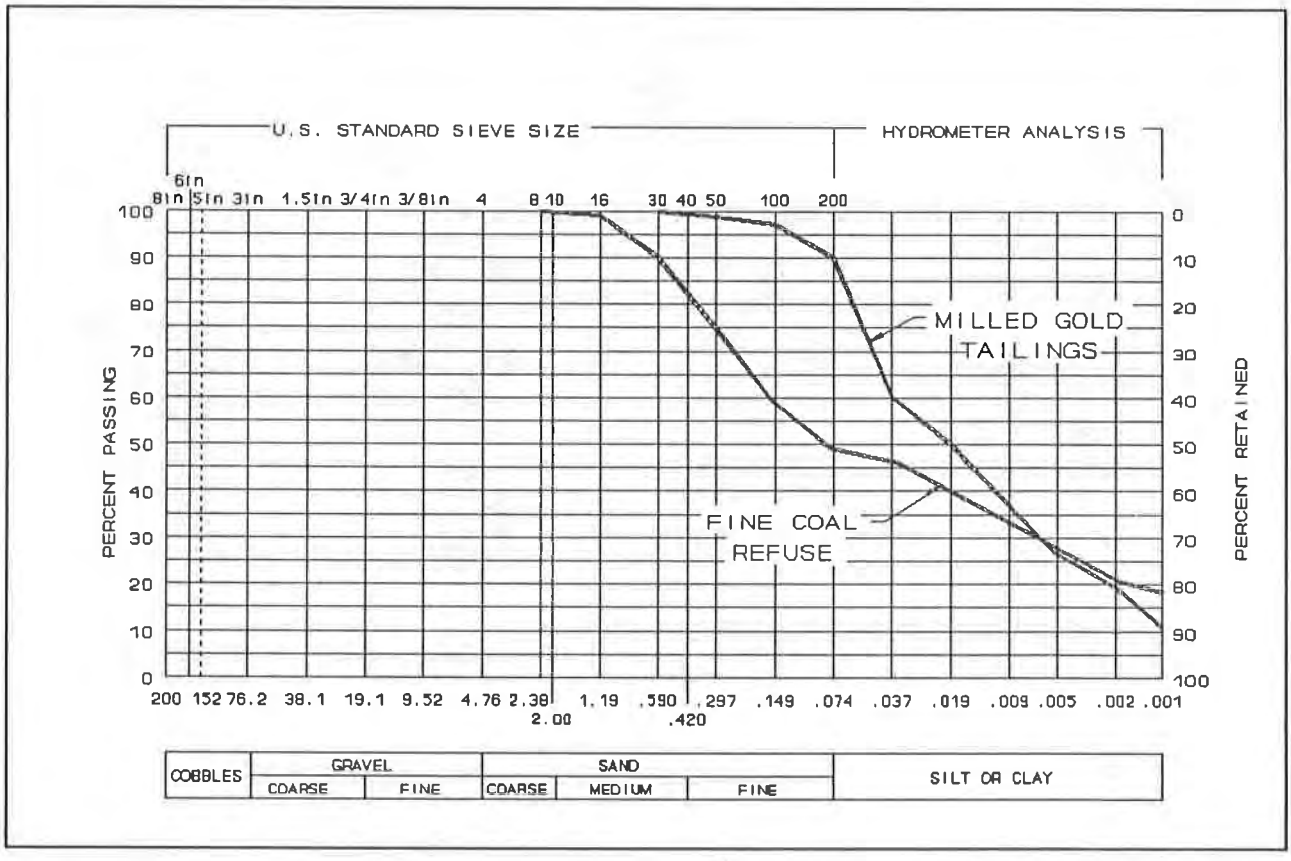

Influence of Waste Properties. The drainage and rheological properties of a waste slurry are the primary factors which influence the design of effective drainage and deposition systems. Typical particle-size distributions for selected samples of milled gold tailings samples and fine coal refuse are shown on Figure 2.

Slurries produced in gold ore processing may vary generally between 35% and 50% solids by weight and have soil particle specific gravities between 2.6 and 3.5. Coal refuse is highly variable with broad variations in both top and bottom particle sizes. From the pipeline to its ultimate destination in a consolidated waste deposit, the waste slurry undergoes several stages of particle segregation which are illustrated on Figure 3. The following description of the depositional process is reproduced from Cincilla and East (1989) and is included for completeness.

In Stage 1, the slurry is in a super-saturated condition with solid particles completely suspended in the fluid. There is minimal intergranular contact and a hydrostatic pore pressure distribution is present, resulting in an unstable condition which requires agitation for particles to remain in suspension.

Figure 3
State of Solids During Deposition and Consolidation

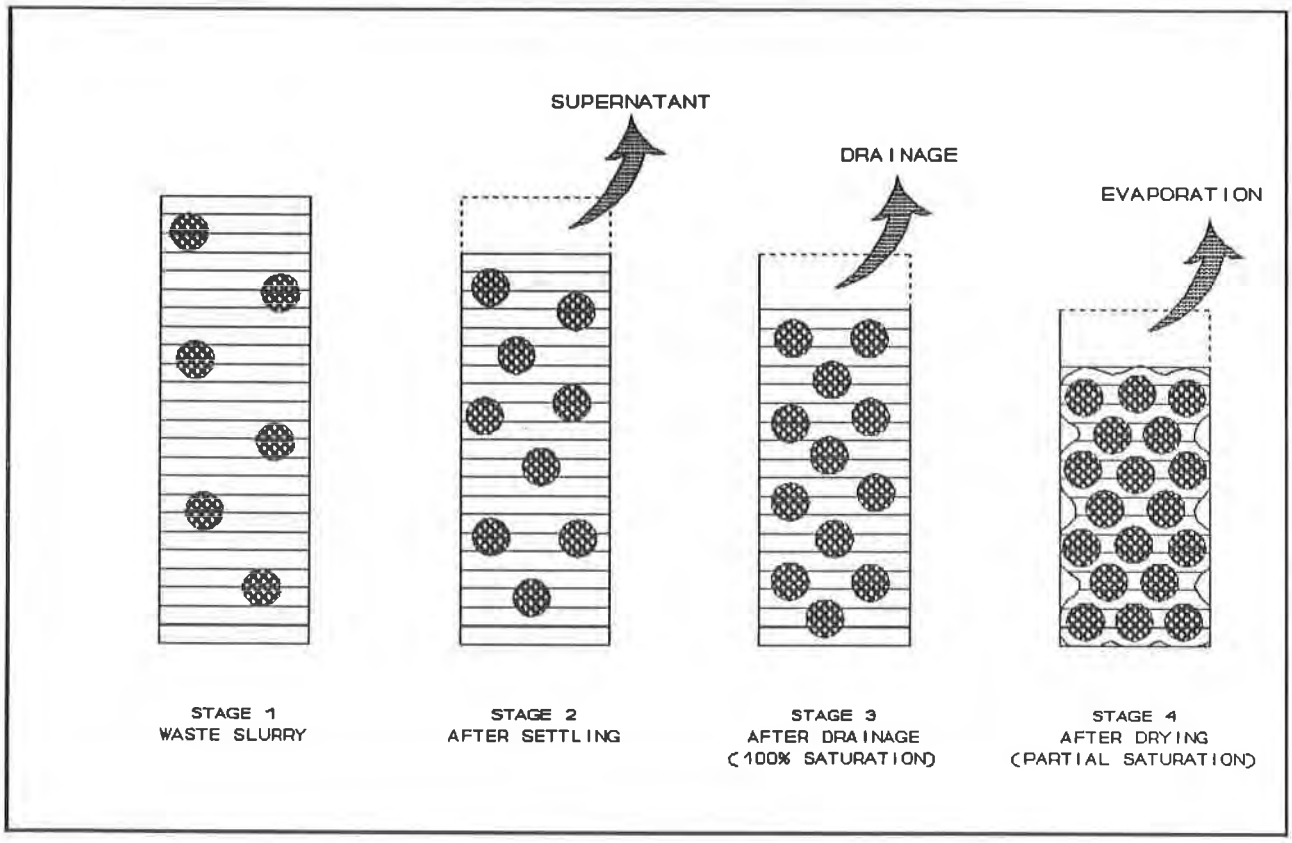

Stage 2 begins where the slurry has been initially deposited in a super-saturated plastic condition under water. As the solid particles settle, low intergranular contact is established and bleeding of surface water has started, with further release of liquid induced by drainage and/or evaporation. Loading of the settled deposit will result in formation of excess pore pressures which will slowly dissipate with seepage.

Stage 3 is characterized by increased in-place density by means of application of underdrainage, which causes further consolidation and dissipation of positive pore pressures.

Stage 4 develops as the drained deposit is allowed to air-dry and consolidate. This consolidation is significant and results from the development of negative or suction pressures in the deposit as air is entrained within the soil structure. The resultant layer of air-dried waste is a stable, partially-saturated mass which has a lower permeability and greatly increased resistance to liquefaction under seismic loading. The most significant attribute of the slurry's transformation from Stage 1 to Stage 4 is the increase in the dry density of solids as shown on Figure 4, which illustrates actual test results on samples of milled gold tailings from Nevada and fine coal refuse from Western Kentucky. A gold slurry initially at a solids content of 42% increases in dry solid density from approximately 900 kg/m³ (52 pcf) to nearly 1600 kg/m³ (100 pcf) merely by allowing settlement, drainage and air-drying in

Figure 4
Dry Density of Solids for Different Deposition Methods

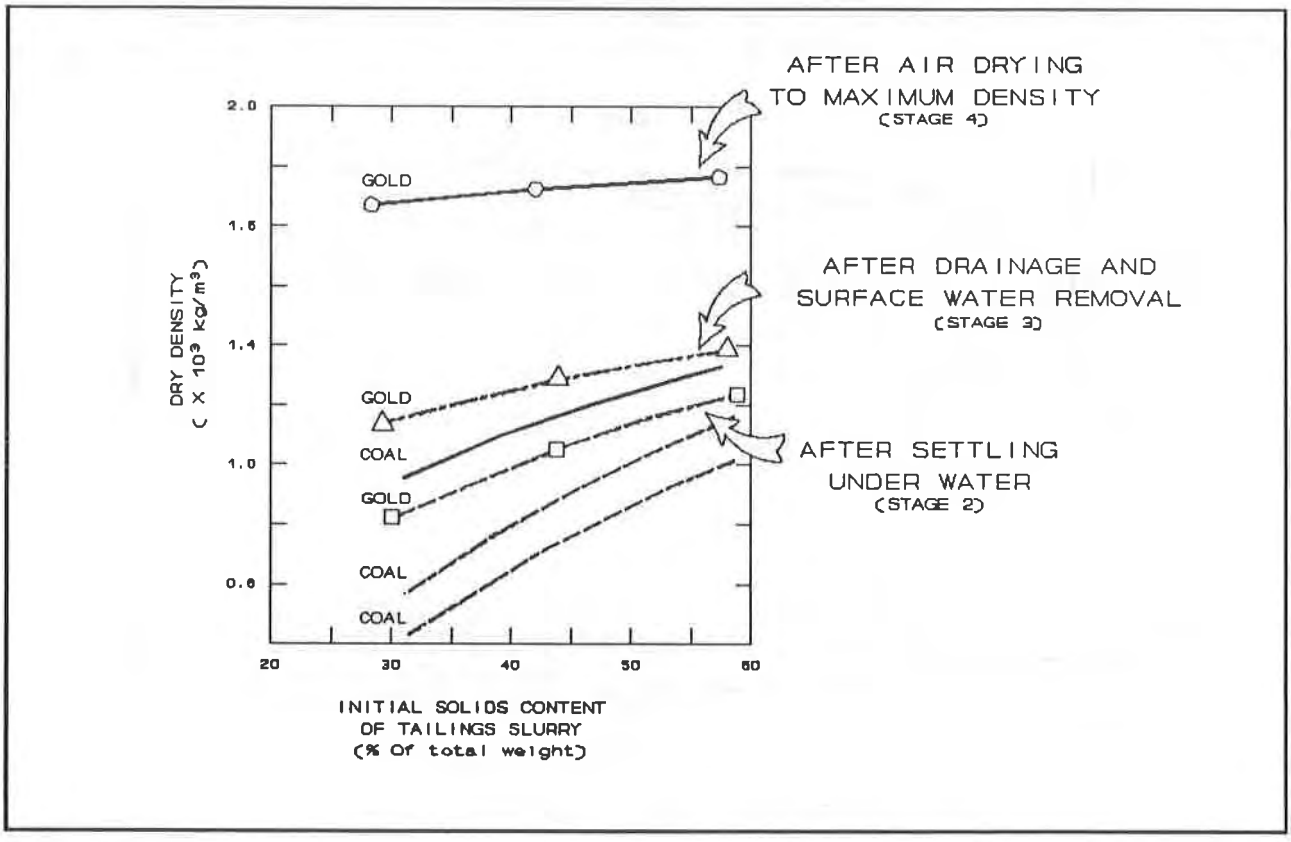

relatively thin layers prior to deposition of a fresh layer of waste. Thus, by allowing the waste slurry to achieve Stage 4 conditions, available storage volume has been doubled due to the increased density.

In order to achieve Stage 4 conditions, a sufficient level of air-drying of the thinly-deposited (100 to 150 mm) layer of waste must be allowed for through a systematic rotational waste discharge strategy. This strategy must take into account the local climatic conditions relative to the rate of waste production and an overall rheological properties of the slurry. Figure 5 illustrates the dry density volume, saturation and moisture conditions within the layers of waste slurry as it progresses from a fully-saturated to partially-saturated state by drainage and drying. The bottom scale (evaporation) is essentially a time scale which varies based on the local climate.

In the illustration, once the moisture content has been reduced to approximately 20%, the dry density shows little increase with continued drying. In practice, once this point has been reached, a new layer of waste is added and the cycle begins again.

This general depositional concept was described initially by Knight and Haile (Knight and Haile, 1983), who used the term "sub-aerial" to describe deposition above water as opposed to sub-aqueous, or under-water deposition.

Figure 5
Relationship Between Shrinkage, Dry Density, Moisture and Saturation for Tailings Slurry of 48% Initial Solids Content (By Weight)

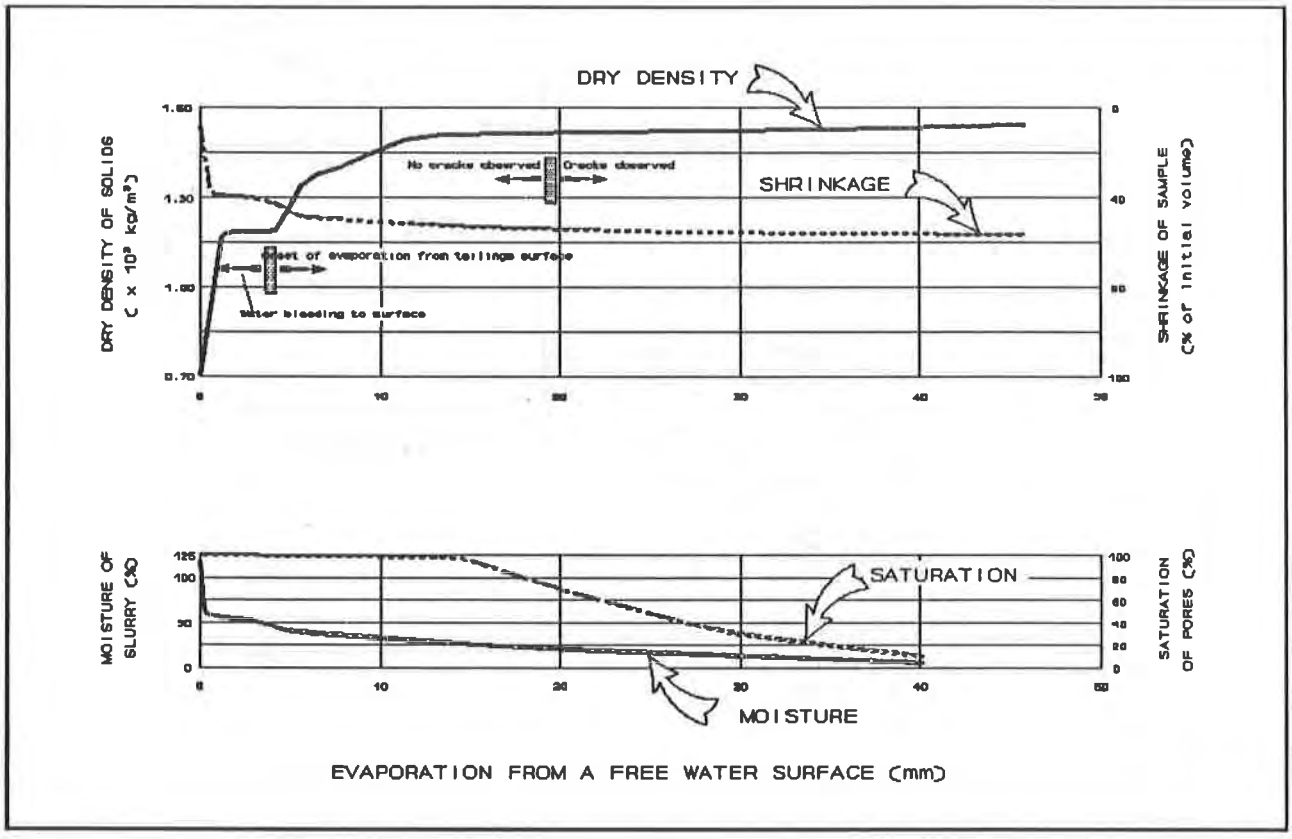

DESIGN OF FLUID COLLECTION AND REMOVAL SYSTEMS

Fluid collection and removal in a fully-drained mineral waste disposal facility is divided into three main categories: underdrainage, supernatant or surface water, and internal embankment seepage. Underdrainage and supernatant fluid account for more than 95% of the total fluid collected within the facility. Based on the results of laboratory studies as well as field measurements of flows, approximately 50 to 70% of the total slurry water content is liberated as supernatant runoff as the slurry undergoes natural settling. Underdrainage may contribute an additional 10 to 20%, with the balance either permanently locked into the soil structure or lost by evaporation or sub-surface seepage. In arid areas where water conservation is a key issue,water recovery by underdrainage alone offers a cost savings over the facility lifetime greatly in excess of the initial construction cost.

The design of underdrains ranges from a simple system of finger drains to a complete blanket having internal collection pipework constructed on the entire base of the facility. Depending on the cost and availability of sands and gravels, the materials employed in the construction of the underdrainage systems vary greatly. Geotextile and geonet sandwiches have also proven effective where the cost of natural high-permeability soils has been prohibitive. Since the basic objective of the

drainage system is to reduce the head on the liners and/or native soils, the integrity of the drains must be maintained by design since, in most cases, the deposited waste is very fine-grained and therefore subject to mass infiltration into the drains. For this reason, a filter relationship must be established for natural drains. This relationship can also be maintained through the use of a geotextile for soil separation.

Supernatant removal is undertaken by means of various methods including: continuous decanting via towers or sloping filter drains, or by means of pumping from limited pond areas within the storage basin. Figure 6 illustrates schematically one type of collection system which includes a separate lined pond for the storage of collected process water. Note the relationship between pore pressure, hydraulic gradient and time which are in great contrast to those illustrated in Figure 2 for a conventional design.

Figure 6
Fully Drained Waste Management System

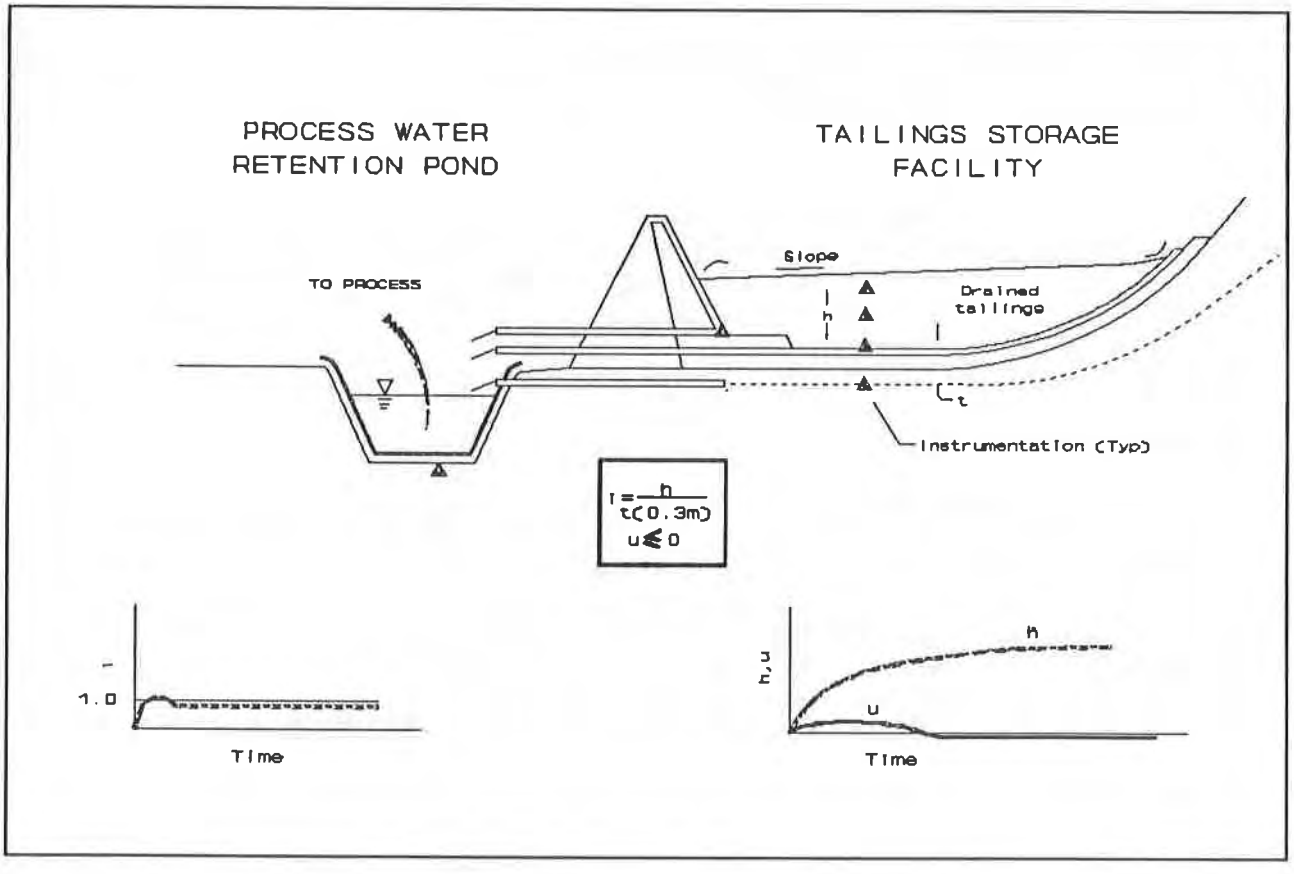

Where the liner system for the facility is a critical design element, as in the case of gold wastes produced via cyanidation processes, the design and performance of the underdrainage becomes increasingly more important. Some States have adopted prescriptive liner standards for different classifications for mineral wastes which are similar in form to those in force for hazardous waste storage. Common practice is to require an LCRS (leachate collection and recovery system) between an inner and outer liner. This two-liner requirement, while effective, is cost-prohibitive in most mineral waste applications and a technical alternative which has been accepted in several states, particularly California, is the idea of using complete underdrainage, which functions as an LCRS, and the deposited waste as an actual "inner" liner. The drained waste, due to its fine-grained nature, can function as a liner so long as surface water is continuously removed and as along as sequential deposition can be used to cause formation of a laminated structure. This laminated soil structure produces horizontal permeability components which are as much as 50 to 100 times greater than the vertical component with the overall result of near order of magnitude reductions in effective permeability merely through a change to a systematic rotational "sub-aerial" depositional strategy.

Figure 7 illustrates an example of prescriptive standards for LCRS inflow for a Group B waste classification in the State of California in contrast to an alternative design employing only a single outer soil liner.

Another factor which provides further decreases in the permeability of the deposited waste is the effect of partial saturation. Negative pore pressures induced by induction of air into the voids during air-drying act to effect a decrease in permeability, which may approach one order of magnitude.

In summary, underdrainage and supernatant removal are simple concepts which can yield impressive results both in terms of facility construction cost as well as environmental performance.

A key factor in maintaining a rotational waste discharge pattern is the mechanism and logistics of waste distribution. By reducing the velocity of the discharged slurry to permit laminar flow conditions to develop, particle segregation is enhanced, resulting in coarser fractions being deposited closer to the point of discharge. Additionally, the intergranular "scrubbing" which occurs under laminar flow conditions yields clearer water. Distribution of slurry flow is accomplished through a variety of means including multiple spigots and spraybars, which have been employed successfully under a range of operational and climatic conditions.

The positive effects which are accrued due to favorable depositional patterns are the first step in providing an overall disposal system which is centered around the efficient removal of excess pore fluid through continuous drainage and surface water removal.

Figure 7
Comparison of Inflow to LCRS

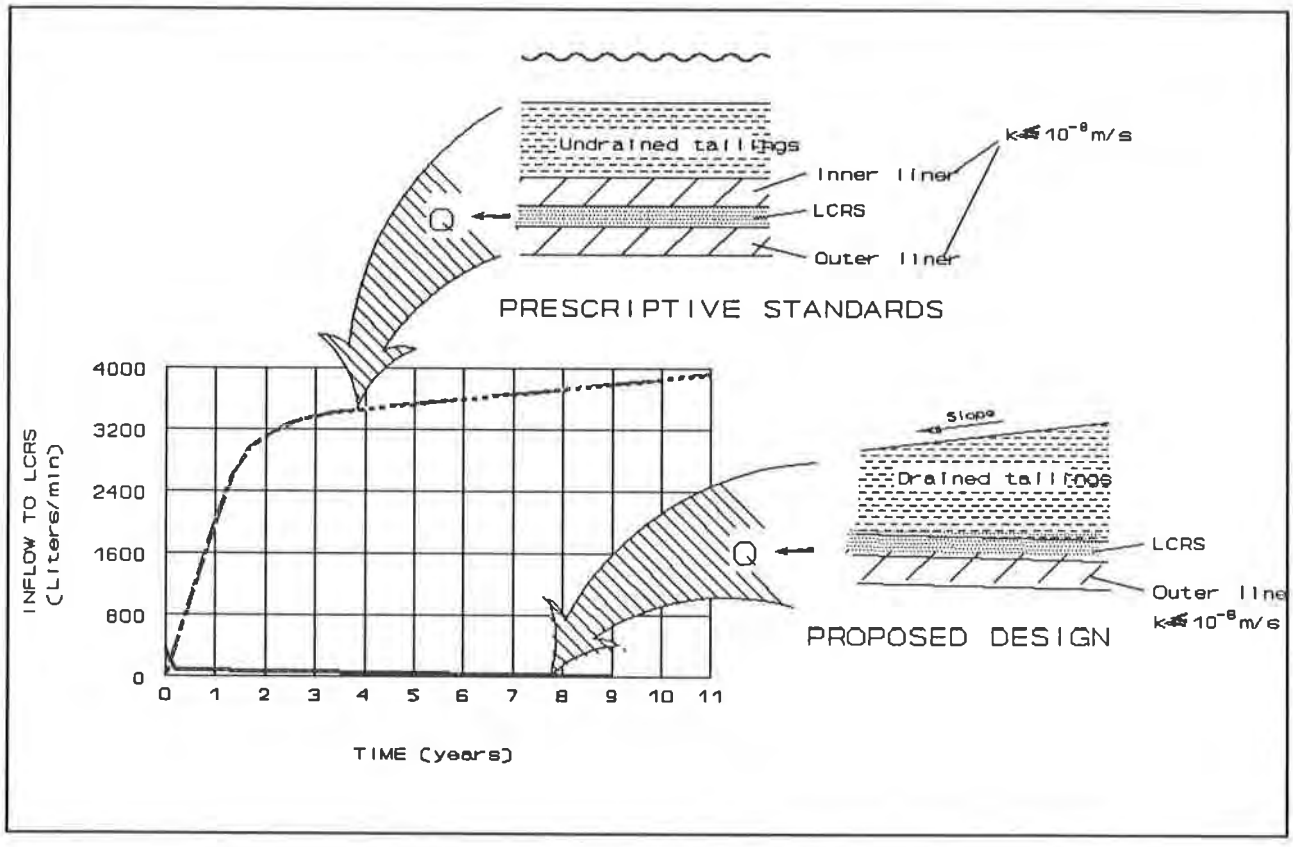

CASE HISTORY

General. The following sections provide a basin description of a tailings storage facility which was commissioned in the fall of 1988. The design of the fluid collection systems incorporated a geotextile/geonet sandwich for the sloping gravity drainage system which is used to continuously decant process solution which separates from the tailings slurry during deposition. The fluid removal system was the first of its kind in North America in which a geosynthetic product was used as a substitute for costly screened gravels. The facility has operated under adverse climatic conditions for over 2 years and is meeting or exceeding design goals for low hydraulic heads on liners.

Project Overview. The project is located in northern Nevada and includes a cyanidation mill with nominal daily throughput of approximately 4.4 x 10^6 kg/day (1000 tons) at an average solids content of 35% by weight. The site selected for waste disposal was a gently-sloping area requiring the construction of a four-sided earthfill embankment for containment of solids. The primary liner consists of 0.5 meters (1.5 feet) of compacted low-permeability silty soils with permeabilities in the range of 1 x 10^{-9} m/sec. The natural soil liner was selected based on superior performance for attenuation of cyanide and arsenic. Underdrainage is collected by

means of a complete 0.3-m-thick (1-ft.) sandy gravel blanket which was constructed on top of the liner. Internal collection pipework consists of 100 and 150-mm-diameter (4 and 6-in.) corrugated polyethylene tubing (CPT) which collects at the low end of the basin and passes beneath the embankment in a 0.3-m-diameter (12-in.) high density polyethylene (HDPE) pipeline encased in reinforced concrete and terminates in a double-lined process water pond.

Waste slurry is deposited along the west embankment and supernatant fluid and surface runoff flow down a gently-sloping surface to the east embankment where they are continuously decanted via a sloping drainage system. The sloping drainage system is composed of a sandwich of HDPE geonet covered by a layer of high-permeability woven monofilament geotextile and a protective .15-m (6-in.) cover of sand. The sandwich was constructed as shown on Figure 8, which illustrates the double geonet and bonded geotextile methodology. The bottom layer of geonet which had a needle-punched non-woven polyester geotextile bonded to its base, was laid on the preface interior surface of the "collection" embankment face. Geonet from each successive panel were tied together and the top layer of geonet, which had a woven monofilament geotextile bonded to one side, was added. Both layers of geonet and geotextile were anchored on the embankment crest in a common anchor trench. The sand filter was then placed over the surface of exposed woven geotextile to complete the installation. Collected fluids travel down the sloping decant and are collected in a slotted HDPE header pipe and passed into the process pond via the reinforced-concrete-encased pipeline. Figure 9 is a photograph of the geonet decant during installation. Figure 10 shows an aerial view of the facility after completion of the first planned expansion.

The 5.7 x 10^6 liter (1.5 x 10^6 gallon) process pond is equipped with an inner 60-mil HDPE geomembrane and an outer 0.3-m-thick (12-in.) soil liner with a geonet LCRS between the two liners. External sumps collect process water and LCRS flows, which are returned via a submersible pump to the mill for reuse on a continuous basis.

Tailings are distributed over a 300-m-wide (1000-ft.) beach area by means of 14 spraybars, each of which is operated individually for a 24-hour period to deposit a 100 to 150-mm (4 to 6-in.) layer of waste. Flow to the spraybars is controlled by valving located at each spraybar offtake. This arrangement allows for a cycle time of 14 days prior to the deposition of a fresh layer of tailings.

As designed, the facility has an ultimate capacity of 2.7 x 10^9 kg (3.0 x 10^6 tons) of waste solids at an average in-place dry density of 1.36 x 10^3 kg/m^3 (85 pcf). Expansion of the facility to ultimate capacity will be achieved through staged embankment construction. This construction is by downstream methods on the fluid collection side, and by upstream methods on the waste deposition side, utilizing the drained and consolidated coarse waste fraction as the foundation for the upstream raises.

The design of the double geonet drain was influenced by three major factors:

1) permeability and clogging potential of the outer geotextile;

Figure 8
Double Geonet Fluid Decant Design

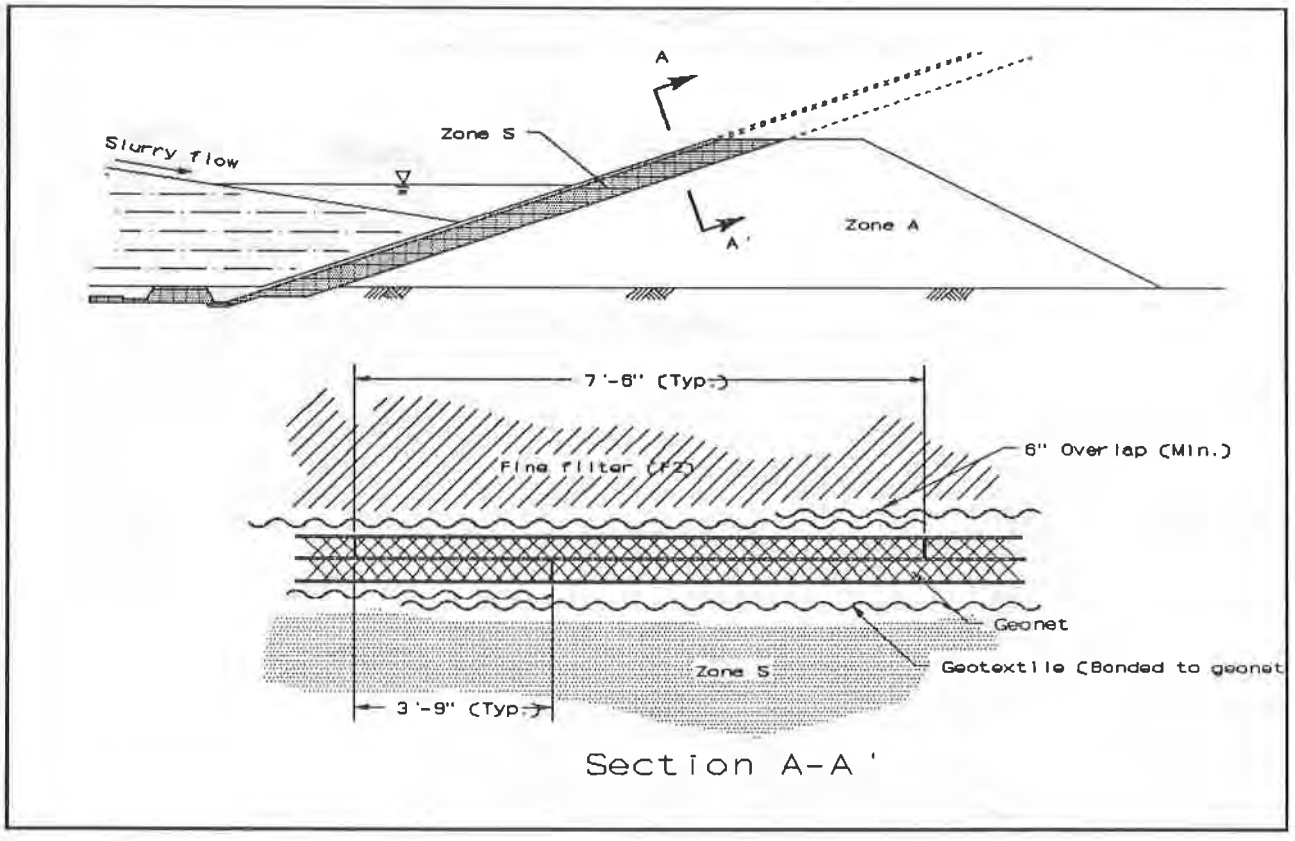

2) performance of the geonet under anticipated design loads; and

3) the cost and constructibility of the system.

Due to the nature of the application, and the fact that (at that time) no established criteria existed for analysis of clogging potential for the boundary conditions expected on the woven geotextile, a testing device identical to that which was under testing by the ASTM (Suits et al, 1987) was constructed. The results of a small-scale testing program on several types of candidate materials using the device indicated that a woven, monofilament geotextile was the logical choice. The sand layer was added for UV protection and filtration capacity.

Double geonets were employed in various applications at that time, however, no published data like that presented by Koerner (1989) was available. It is interesting to note that the issue of reduced transmissivity caused by bridging of the geotextile was one of the primary factors in the design process on this project.

Figure 9
Construction of the Geonet Decant

CONCLUSION

Over the past five years, over 15 facilities for storage of mineral wastes have been designed and constructed using the general principles outlined in this paper. Of these projects, there have been several in which the application of geosynthetics, in particular, geonets, geotextiles and geomembranes, has provided low-cost alternatives to more-traditional earth materials. The experience gained on these projects has lead to continued optimization of construction techniques and to further innovative application of geosynthetic products.

Figure 10
Aerial View of the Facility After the First Expansion

REFERENCES

1. Cincilla, W. A. and D. R. East, "The Design and Construction of Fully-Drained Systems in Storage of Mineral Wastes", in Proceedings of the 21st Mid-Atlantic Industrial Waste Conference, Harrisburg, Pennsylvania, June 1989.

2. Knight, R. B. and J. P. Haile, "Sub-Aerial Tailings Deposition", in Proceedings of the 7th Pan American Conference on Soil Mechanics and Foundation Engineering, Vancouver, British Columbia, Canada, June 1983.

3. Koerner, Robert M., "Behavior of Double Geonet Drainage Systems", Geotechnical Fabrics Report, Sept.-Oct. 1989, pp. 39-44.

4. Suites, L. David, et al, "ASTM Geotextile Committee Testing Update", in Geotextile Testing and the Design Engineer, ASTM STP 952, ASTM, Philadelphia, PA, 1987, pp. 161-175.

5. Volpe, Richard L., "Engineering Aspects of the 1972 Buffalo Creek Dam Failure", in Proceedings of the 1st International Symposium on Stability in Coal Mining, Vancouver, British Columbia, Canada, C. O. Brawner and Ian P. F. Dorling, Eds. (San Francisco, CA: Miller Freeman Publications, 1978.)

Geomembrane Applications in Australia

Roger J. Parker
Golder Associates PTY LTD, Australia
Mike A. Sadlier
Polyfelt Geosynthetics PTY LTD, Australia

ABSTRACT

This paper provides an overview of the application of geomembranes in Australia and relates the current trends in use to the environmental regulatory control now applicable. The paper presents examples of geomembrane use in Australia which effectively provides a history of usage and some indication of where future trends may lie.

INTRODUCTION

There has only been limited use of geomembranes in Australia and the current regulatory framework allows considerable flexibility in approach to disposal of wastes. Where there has been a requirement to contain waste, compacted clay has generally been the favoured choice for formation of low permeability barriers.

During the 1980's there was increased use of geomembranes in Australia for lining of waste and other containment structures. However, the extent of use of geomembranes is considerably less than in the USA even taking account of population differences. Nevertheless, the use is increasing and will continue to increase as the regulatory authorities require increased application and improved performance of waste containment systems.

This paper has been prepared to provide an outline of the regulatory environment which currently exists in Australia and the impact that this has had on the use of lining systems for waste containment. In addition the paper documents the likely future directions for lining requirements in Australia.

REGULATORY FRAMEWORK

In discussing the use of geomembranes in Australia it is important to understand the regulatory framework within the country and the factors which influence environmental control of wastes. Although Australia is considered to be an arid country, there is only limited reliance on use of groundwater for domestic purposes and this is mainly in rural areas. In many areas the groundwater is brackish to saline, thus limiting the use of the water.

The limited use of groundwater for domestic purposes, the limited manufacturing industry and the sparse population of Australia combine to produce an environmental regulatory framework very different to North America and Europe. Up until very recently, the approach to disposal of industrial, mining and domestic waste has been based on the principle of "dilute and disperse". As long as the waste was placed in a confined area and was ultimately out of sight, limited control was placed on the disposal process. This attitude is now changing rapidly and we are seeing the development of a regulatory framework that will impose much greater control over the disposal of all forms of waste.

In Australia, environmental legislation and regulation is largely a state matter. Federal government can only control environmental matters through the use of financial controls on the states, although consideration is being given to formation of a national Environment Protection Authority. Each state within Australia has developed separate approaches to environmental legislation and regulation so that there has been a diversity in control measures required for waste disposal. In particular, there is seen to be a significant difference in environmental controls between so-called "manufacturing states" and the "mining states".

As environmental awareness changes within the community and attitudes to environmental responsibility and liability change within industry and government, we are seeing rapid changes in environmental regulatory control. Although there is still a diversity between the states, evidence of change in the approach to control of waste disposal and concern over contamination is seen in the following:

Engineered containment systems have been constructed or are proposed for several landfills in at least three states.

Most states are now requiring consideration to be given to closure of waste disposal sites in the initial planning phase. Greater attention is being given to issues such as appropriate capping measures and gas control.

Most states are now concerned with the issue of contamination of soil and groundwater and at least three states have published guidelines for assessment of contaminated land and one is establishing a formal system of auditing of contaminated land.

GENERAL APPROACH

Australian use of geomembranes has largely been in applications for mining, industrial and public health areas and it has only been in recent times that lining has been considered in waste disposal. Some of the reasons for this are the relatively low population densities, the lack of dependence on groundwater for public supplies and a record with early liner types of poor ultra violet (UV) light exposure performance in a country where high UV light exposures occur.

Until the advent of heap leach mineral extraction most geomembrane applications were for water or waste water containment. Heap leaching became widespread during the 1980's and helped to develop confidence in liner performance as installations intended for short term service proved to have longer service capacity. The attention has now shifted more to environmental

protection in a broader sense as well as solid or liquid waste containment and treatment including capping of existing waste deposits and covers for anaerobic processes.

Since there is limited regulatory control, the geomembrane option for lining is still chosen or not chosen on the basis of an economic life cost appraisal after comparison with other options that are considered viable. These other options may include recycling or processing, cartage to remote sites or conventional clay soil or concrete construction. As experience develops and confidence grows, the geomembrane option is being accorded a longer service life and is tending to compare more favourably, particularly, in areas where there are limited supplies of clay soil.

The following sections describe examples of geomembrane use in Australia. These examples are discussed partly in chronological order and thus provide a "potted history" of Australian geomembrane use.

RED MUD STORAGE AREAS, WESTERN AUSTRALIA

One of the first large scale uses of geomembranes in Australia was at Alcoa of Australia's alumina works in Western Australia. Of the three refineries operated by Alcoa, the Kwinana Works, just to the south of Perth, was the first to use geomembranes on a large scale for a Cooling Pond and then a red mud storage site known as Area H.

The near surface geology of the Kwinana area comprises dunal sand overlying variable limestone (calcarenite). Shallow groundwater in the area is used for industrial and agricultural purposes. Early use of thin (less than 0.4 m thick) clay liners (for Red Mud Storage Areas A, B, C and F) resulted in some leakage of caustic liquor to the groundwater. The adoption of such thin clay lining was largely dictated by the significant cost of transporting clay some 20 km from the nearest substantial borrow area. Specific problems with the clay liners were attributed to the difficulty of ensuring the integrity of a thin clay layer over large areas (the surface area of each pond varies between 20 and 100 ha) and the occurrence of shrinkage cracks between construction and filling.

As a result of problems with the early storage areas it was decided that future containment systems should use a composite liner system comprising compacted clay and geomembrane. It was considered that such an approach would be more economical than construction of a thicker compacted clay liner.

The adopted liner design for the Cooling Pond (area of about 15 ha) and Residue Storage Area H (area of 45 ha) was as follows, in ascending sequence:

- 0.5 m of compacted clay, placed at or wet of optimum moisture content
- 0.76 mm thick PVC geomembrane, field welded and tested by air-lance
- 1 m of sand to provide an underdrain to the red mud and as a protective layer from traffic.

A pipe network was constructed in the sand layer to facilitate liquor collection. The underdrain was required to assist with consolidation and hence densification and as a measure to reduce liquor head on the liner system.

Subsequent to the construction of the Kwinana facilities in 1980 and 1981, Alcoa constructed similar lining systems for other red mud storage areas in Western Australia and in recent years they have constructed several facilities using HDPE geomembranes. Alcoa's early use of PVC enabled a fabrication industry to be established in Western Australia and considerable use was made of PVC lining systems for water retention structures and in the resurgent Australian gold industry in the early 1980's.

PERSEVERANCE GOLD HEAP LEACH PAD, VICTORIA

Following the large scale use of geomembranes by Alcoa, the next major development with geomembranes has been use for lining systems for heap leach pads. With the introduction of HDPE membranes into Australia, the gold industry quickly changed from use of PVC to HDPE. There has now been considerable use of HDPE for heap leach pads throughout the gold mining areas of Western Australia, Northern Territory and Queensland. The following example of geomembrane use for a heap leach pad is from the State of Victoria. This site is used as an example of heap leach pad construction since it is one of the few in Australia that has close engineering control during construction.

The Perseverance Gold Mine is at Nagambie about 120 km north of Melbourne in an area of traditional mixed farming and wine production. It is an open pit mine with the ore being crushed and treated by cyanide leaching in a heap leach up to 30 m high with an area of some 80,000 m^2 with ancillary pondage.

The immediate subsoil conditions comprise high plasticity clays and the 1.0 mm thick HDPE geomembrane liner was installed directly over the prepared and compacted clay base. Delays in the issue of mining and environmental permits pushed the liner installation window from the dry, hot summer of 1989 into the winter which arrived with plenty of early rain.

Conditions for deployment and field welding of the 6.86 m wide HDPE sheet became extremely difficult with wind damage to some of the liner and an unworkable wet clay surface. Non-woven polypropylene geotextile fabric was used extensively to improve working conditions and the liner was deployed largely by winching from fixed locations. This demanded new operator skills in weather watching to predict wind shifts and to take protective action. The majority of the welding was carried out using fusion welding plant with some extrusion welding.

The installation of the geomembrane was under the direction of mine staff with independent quality control being provided by a consulting engineer approved by the Victorian Environment Protection Authority. All work was inspected by the quality control engineer and welding was fully tested by non-destructive methods and some destructive testing.

Gold leaching operations commenced in September 1989 and proceeded satisfactorily with a second stage pad liner being installed in early 1990 under relatively good conditions in the preferred summer period.

HENDERSON LANDFILL, WESTERN AUSTRALIA

This is the first use of a synthetic liner for a landfill in Australia. The Henderson Landfill site is located near Perth in Western Australia within the City of Cockburn (just north of Alcoa's red mud storage areas at Kwinana). The near surface geology comprises dunal sand over limestone with shallow groundwater used for industrial, agricultural and limited domestic purposes. The general area is heavily industrialised and the general waste stream includes many potential pollutants from industry as well as the normal domestic waste.

Planners were essentially left with two choices for this facility. The first was to establish a transfer station within the municipality and consolidate and cart the waste to a remote, geologically secure (and less sensitive) site. The second was to establish a landfill within the municipality which was required to incorporate an adequate liner and leachate collection system. Costing comparisons put the cost of the first option at about A$30 per tonne with about 40 km of haulage and the second at about A$16 per tonne including the premium for lining which was estimated at A$4 per tonne.

The site itself is an old limestone quarry with high permeability base and the water table is normally about 3 m below the quarry floor. Site preparation involved little more than trimming the site into two initial cells, as indicated on Figure 1 (Halpern Glick Maunsell, 1990a). A clay liner was installed over those parts of the site where the base was less than 3 m above the water table; a requirement of the local EPA.

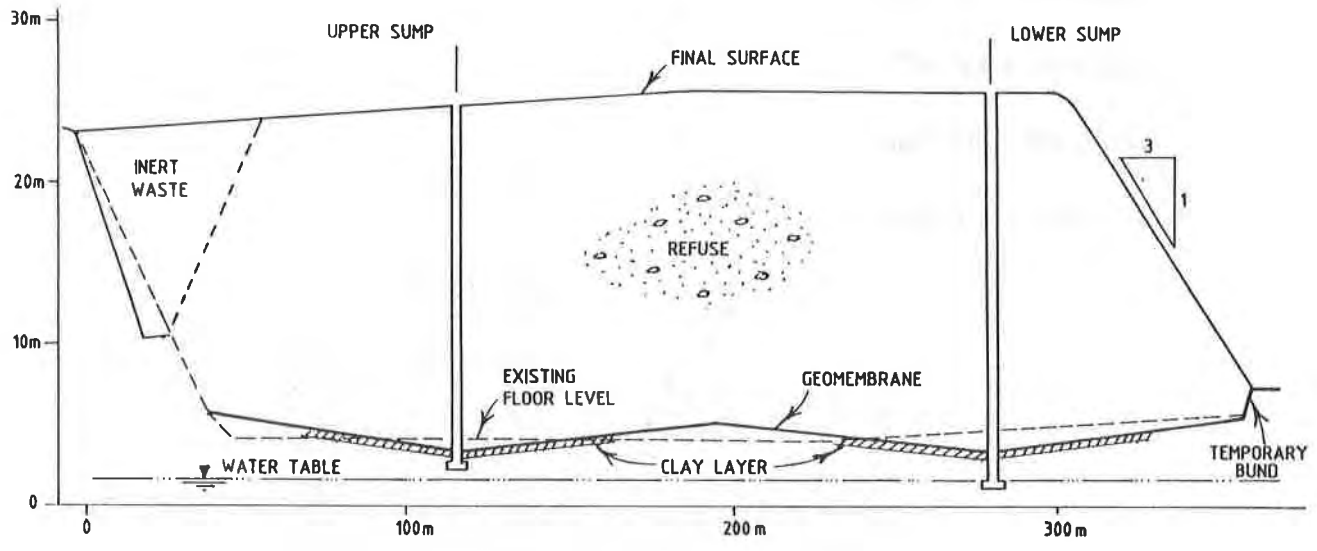

Figure 1. Cross-section - Henderson Landfill

The liner itself is 2.0 mm thick HDPE liner in 6.86 mm wide seamless rolls. It was welded together on site with a combination of fusion and extrusion welding techniques supplemented by a program of non-destructive and destructive testing. Total area is about 60,000 m^2 and the complete installation took about six weeks.

The liner was covered with a protective cover of 300 mm of sand and a further 300 mm of crushed limestone which combine to provide a drainage layer with collection pipes and an operational surface. Leachate is collected via sumps for recirculation and eventual treatment.

GOSNELLS LANDFILL, WESTERN AUSTRALIA

This facility is in the City of Gosnells near Perth in Western Australia and it started life as an industrial liquid waste collection pit and has since been topped up with domestic waste prior to the installation of a HDPE cover.

The original pit came into service around 1979 and was constructed with a liner using a mix of local clay and bentonite in an area of generally clay soils. There has been some evidence of local soil contamination and several incidents of stormwater overtopping occurred around 1987 and 1988. The liquid waste comprised a mixture of hydrocarbons and had formed a heavy sludge at the base of the pond. As a preparation to final capping the pit has been receiving solid domestic waste as landfill to a depth of about 3 metres. The surface has since become relatively firm and was able to support D7 bulldozer (with a track bearing pressure of about 10 kPa) operations without difficulty.

The cap has the following layers, as illustrated in Figure 2 (Halpern Glick Maunsell, 1990b):

- Sandy Loam - Soil Cover - 300 mm
- Clean Sand - 100 mm
- 1.0 mm thick HDPE
- Clean Sand - 100 mm
- Clay Cover - 300 mm

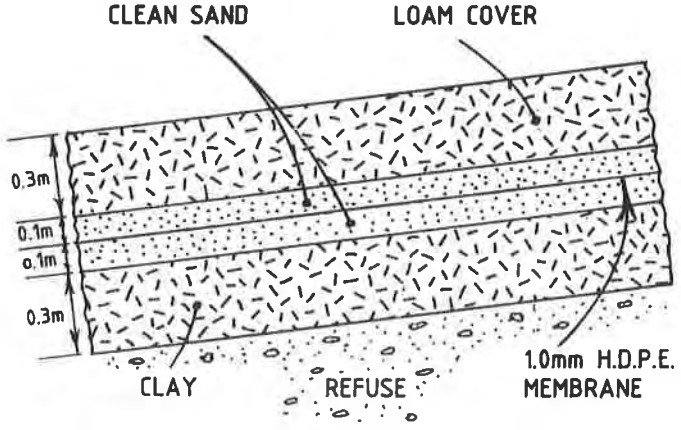

Figure 2. Capping Design - Gosnells Landfill

The plan dimensions are 132 m by 58 m and the cover crown is superelevated by about 3.5 m relative to the perimeter which is restrained by anchor trenches. Gas vents are fitted across the crown and around the edges.

The cover is to be constructed from 1.0 mm thick HDPE liner material supplied in 6.86 m wide seamless rolls and welded using a combination of fusion and extrusion welding supported by non-destructive and destructive testing.

To the knowledge of the authors, the Gosnells site will be the first use of geomembranes in Australia for capping of waste. However, there are at least two other sites in the design phase which will involve capping using composite liner systems. These are a refinery tailings pond near Perth and a acid/oil sludge disposal site in Brisbane (Queensland).

BRISBANE CITY COUNCIL WASTE DISPOSAL CONTRACT, QUEENSLAND

The City of Brisbane is a municipality serving a population of about 1 million people. Tenders were called early in 1990 for a contract for waste collection and disposal of the entire Brisbane municipality for the next 30 years. Tendering for the contract attracted several bids, although at the time of writing these have been narrowed down to two remaining bids both of which involve use of geomembranes in combination with other lining materials. The following sections describe the proposed lining systems for each of the landfills, using information obtained from publicly available information (References 3 and 4).

Proposed Rochedale Landfill. The proposed Rochedale site (Pacific Waste Management, 1990) is located in a former brick clay pit located to the south of the Brisbane CBD. The floor of the pit is in clayey soil and is generally above the water table although there is evidence of spring activity in parts of the site.

The proposed liner design is illustrated in Figure 3 and comprises the following elements:

- prepared subgrade (including sub-liner groundwater drainage system)
- 0.9 m of compacted local clay soil to have in situ permeability of not less than 1×10^{-9} m/s
- 1.5 mm HDPE geomembrane
- leachate collection system comprising geonet (where required), geotextile and selected porous fill.

Subgrade preparation will involve levelling of the base and preparation of batters. Final capping of the site will involve a 1 m thickness of compacted clay covered by topsoil.

Proposed Swanbank Landfill The proposed Swanbank Landfill (Railwaste Technology, 1990) is to be located in the Shire of Moreton located on the western boundary of the City of Brisbane. The site is a former open cut coal mine used to supply coal to the Swanbank Power Station. A cross-section of the proposed liner system is illustrated as Figure 4.

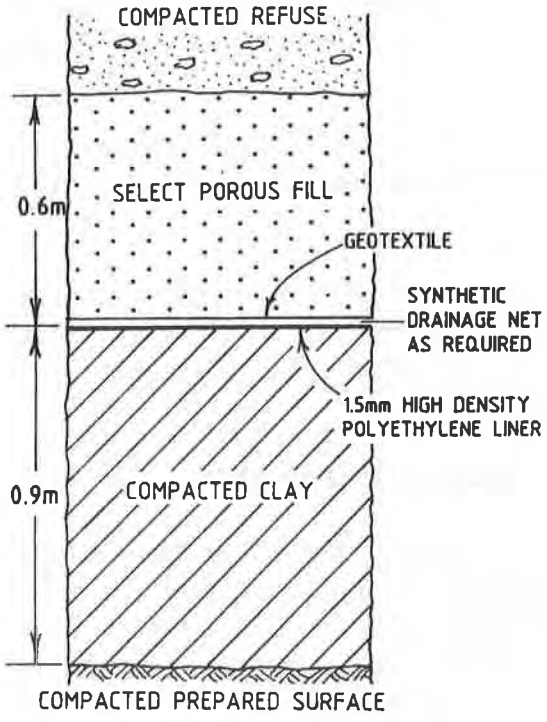

Figure 3. Proposed Base Liner Rochedale Landfill

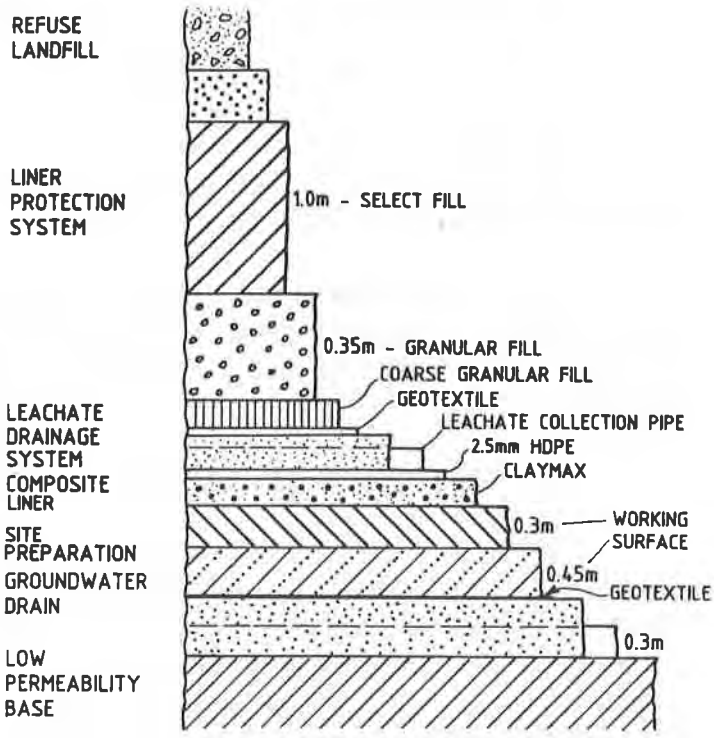

Figure 4. Proposed Base Liner Swanbank Landfill

Once the site has been shaped and prepared, a system of groundwater drains will be installed at the base of each landfill cell. These drains will consist of a trench of granular material excavated into the shaped, compacted low permeability base. Overlying the groundwater drainage system will be a geotextile and a bedding layer of non-carbonaceous material placed to provide a bedding for construction of the composite liner.

The composite liner proposed will consist of a 2.5 mm thick HDPE liner underlain by a bentonite/geotextile composite liner. The bentonite liner is proposed to protect the HDPE from protrusions and to provide a back-up liner to the HDPE.

The leachate collection system above the liner will comprise ascending layers of geonet, geotextile, 0.15 m fine granular layer (-25 mm) and 0.35 m coarse granular layer (-150 mm). The leachate drainage system will be overlain be 1.0 m of compacted waste to provide a working platform which in turn will be overlain by a non-combustible layer of waste as a final protection over the lining system.

Because of concern over the potential for combustion of the underlying coal strata, provision will be made for monitoring of temperature in the groundwater drainage system. If excessive temperature is monitored water will be recycled through the groundwater drain to reduce temperature.

AQUACULTURE

There are many innovative uses for geomembranes being considered in Australia, some of which are following overseas trends. These include geomembranes for sludge digesters, cut-offs for existing dams, and aquaculture. The use of geomembranes for lining of aquaculture ponds is described below as an example of one of these innovative uses.

In Australian coastal regions interest is growing in the use of membrane liners in the establishment of efficient environments for the farming of high protein and gourmet food sources such as fish, prawns, and crayfish. The major requirements are relatively warm, stable water temperatures, clean water and lagoons shaped to permit rapid harvest. Nutrition requirements are supplemented at controlled levels as cultivation proceeds.

Many early ventures used polyvinylchloride and modified polyethylene liners and suffered from UV light degradation or animal penetration. HDPE contains no plasticisers or additives and provides excellent UV light performance without attracting animals or insects in search of food. Wide roll widths allow for operator installation without welding (narrow pond widths are chosen so that only one width of HDPE is required to avoid need for welding).

There are now several successful farms in northern New South Wales producing fresh water crayfish for gourmet markets and there are proposals in hand to use spent sea water from power station cooling to cultivate seasonal tropical fish.

FUTURE DIRECTIONS

The mining industry in Australia has enjoyed a buoyant period which is now slowing down as commodity prices subside and new taxation measures on gold production take effect. Geomembrane use is likely to continue for pondages and heap leach pads in the mining industry but at a reduced level of activity.

It can be expected that there will be increasing environmental awareness and greater regulatory control for the disposal of waste in Australia. This is likely to lead to increased requirements for containment of waste disposal systems where natural geological containment is not an option. If current trends continue it is likely that regulatory authorities will assess each individual sites on its merits with both natural and artificial lining systems being accepted where appropriate.

Where artificial lining systems are required, it can be expected that compacted clay, geomembranes or composite systems will be selected depending in the cost effectiveness of each system. Traditionally, compacted clay soil has been used as the usual medium when lining for waste containment is considered. However, geomembranes are gaining acceptance as an alternative to clay for use in composite systems. It can be expected that a conservative view will apply to the further introduction of geomembranes so it will be a matter of establishing performance records in existing applications and demonstrating that geomembranes provide an effective alternative or adjunct to clay liners.

In this environment it can be expected that geomembrane use will grow in Australia but on a basis of continual enhancement of performance and cost effectiveness. If there is to be growth in the use of geomembranes in a relatively unregulated environment it will be necessary to encourage a quality image based on material performance and selection, proper design and detailing, appropriate installation and quality assurance programs. It will be necessary to educate owners that quality lining systems will only be achieved if all of these aspects are handled appropriately by experienced engineers, suppliers and fabricators.

CONCLUSIONS

Geomembrane use in Australia is increasing at a significant rate but does not have the impetus provided by centralised regulations and technical guidance which would give rise to extensive environmental applications. There are geographical and hydrogeological reasons for the less regulated approach to environmental matters in Australia. However, geomembrane use will continue to increase on the basis of economic appraisal of control measures and provided that performance standards are maintained.

REFERENCES

Halpern Glick Maunsell, (1990a), personal communication with Mr. J. Scott

Halpern Glick Maunsell, (1990b), Drawing No. 8695/C202, Kelvin Road Landfill

Railwaste Technology Pty Ltd, (1990), Environmental Impact Study, Brisbane City Council Waste Collection Tender

Pacific Waste Management Pty Ltd, (1990), Environmental Impact Study, Brisbane City Council Tender

0226rjp

WASTE CONTAINMENT INTERFACE STABILITY

Soil-Geosynthetics Interface Strength Characteristics: A Review of State-of-the-Art Testing Procedures

Deanne L. Takasumi
CH2M Hill, Inc., USA
Kenneth R. Green
CH2M Hill, Inc., USA
Robert D. Holtz
University of Washington, USA

ABSTRACT

Selection of appropriate geosynthetic materials for use in leachate collection and liner systems for solid and hazardous waste landfills requires a knowledge of the strength characteristics of the soil-geosynthetic interface. Because there are several direct shear test procedures currently being used to evaluate soil-geosynthetic interface strength characteristics, these test procedures were reviewed and evaluated with respect to the effects of the test procedures themselves on test results. The review revealed that there is a wide range of interface strength characteristics reported and that there are significant variations in how interface testing is done. The range of test results is a result not only of variation in the materials being tested but also of variation in the soil samples used, the procedures selected for testing, and the methods of calculating contact efficiencies. On the basis of the review findings, additional research with respect to appropriate test procedures for determining interface strength characteristics is recommended. There is the need to 1) develop a better understanding of the test conditions affecting design interface strength characteristics and 2) to develop, if possible, a consistent approach to testing.

INTRODUCTION

Regulatory requirements for solid and hazardous waste landfills require the installation of a leachate collection system and liner to reduce discharges of landfill leachate into the environment. The leachate collection system and liner typically consist of a combination of geosynthetic materials and natural or processed soil. A critical element in designing these systems is determining the maximum slope in order to obtain maximum disposal volume. Evaluation of slope stability requires knowledge of the strength characteristics of the interfaces of the soil and geosynthetic materials.

Collios et al. (1980) and Ingold (1982) suggest that the direct shear test is the appropriate test for evaluating strength characteristics of the soil-geosynthetic interface if the extensibility of the geosynthetic does not affect its field performance. This paper summarizes a review prepared by Takasumi (1990) of state-of-the-art direct shear interface testing procedures and the effects these procedures have on the test results. The test conditions thought to affect the test results are described in some detail. On the basis of the findings of this review, a procedure is suggested for testing interface strength and recommendations are made for future research.

Materials Tested. In order to compare direct shear interface test results, the properties of the soil material that will be in contact with the geosynthetic as well as the properties of the geosynthetic material itself must be identified. A wide variety of both cohesionless and cohesive soils have been tested, although not consistently with the same apparatus or at the same compaction conditions and densities. Cohesionless soils have ranged from fine sands to gravels; cohesive soils have included gravelly silts, lean and fat clays, Ottawa sand-bentonite mixtures, and almost everything in between. For purposes of this review, the soil materials were grouped into two broad classifications, cohesionless materials and cohesive materials, to reflect different strength characteristics.

Geosynthetic materials were divided into two groups for purposes of this review: geotextiles and geomembranes. Geotextile materials include wovens and needle-punched or heat-bonded non-wovens. Geomembrane materials include high density polyethylene (HDPE), polyvinyl chloride (PVC), chlorosulfonated polyethylene (CSPE), ethylene propylene diene monomer (EPDM), and chlorinated polyethylene (CPE). Both textured and smooth geomembranes were tested.

Efficiency. Interface strength test results have been reported both as a friction angle and as an adhesion value. Collios et al. (1980) introduced the concept of contact efficiency, E, which is the ratio of the soil's friction angle or cohesion to the soil-geosynthetic interface friction angle or cohesion. Cohesion efficiency, E_c, is defined as

$$E_c = c_a/c \qquad (1)$$

and friction angle efficiency, E_ϕ, is

$$E_\phi = \tan \delta/\tan \phi \qquad (2)$$

where c_a = adhesion of soil to geosynthetic, c = cohesion of soil alone, δ = soil to geosynthetic friction angle, and ϕ = soil friction angle.

Contact efficiency calculations were based on soil strength alone as determined from direct shear or triaxial shear tests and on the soil-geosynthetic strength as a peak and/or residual friction angle.

Generally, the interface strength, or contact efficiency, of a soil-geotextile interface appears to be affected by the following:

- Geotextile opening size. If the openings in the geotextile are similar in size to the soil particles, the soil interlocks with the geotextile, resulting in a relatively high efficiency.
- Geotextile deformability. Geotextiles that deform around soil grains result in relatively high contact efficiencies.
- Soil type, particle size, particle size distribution, and particle angularity.

The interface strength, or contact efficiency, of a soil and geomembrane interface appears to be affected by the following:

- Geosynthetic surface roughness. Rough surfaces have higher efficiencies than do smooth surfaces; therefore, textured HDPE and reinforced CSPE have higher efficiencies than do smooth HDPE and plain CSPE.

- Geosynthetic polymer surface hardness. Soft surfaces have higher efficiencies than do hard surfaces; therefore, PVC, EPDM, plain CSPE, and CPE (lower surface hardness) have higher efficiencies than do smooth HDPE.

On the basis of a review of the available literature, a wide range of efficiencies was reported and are probably a result of variation in (1) test procedures, (2) moisture content and density for identical soil types, (3) type of geosynthetic materials evaluated, and (4) method of calculating contact efficiencies. The significant variation in interface test results suggests the need for a better understanding of which test conditions affect interface strength characteristics. A discussion of these test conditions follows.

TYPE OF TEST APPARATUS

Richards and Scott (1985) describe three types of direct shear apparatus: fixed shear, partially fixed shear, and free shear (see Fig. 1 below) and the advantages and disadvantages of each. Table 1 summarizes the test conditions for each type of test apparatus. A brief description of each test apparatus and its effects on test results follows below.

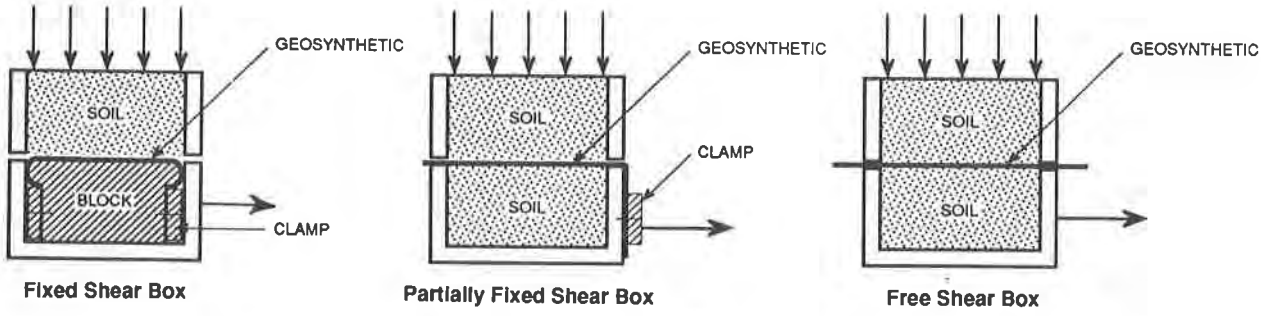

Figure 1. Direct shear interface test apparatus types.
(Adapted from Richards and Scott, 1985, p. 15.)

- Fixed shear test: The geosynthetic is either glued or clamped to the rigid base of the lower shear box. The major disadvantage of fixed shear tests is that they do not allow the geosynthetic to strain or elongate.

- Partially fixed shear test: The upper and lower boxes are filled with soil and the geosynthetic attached to one end of the lower box. One of the disadvantages of this test is that the geosynthetic may deform into the lower box.

- Free shear test: The upper and lower boxes are filled with soil, but the geosynthetic is not attached to either of the boxes. The geosynthetic may slide during the test and it may deform into the lower box.

Collios et al. (1980), Ingold (1982), and Richards and Scott (1985) conducted interface tests on cohesionless soil in contact with geotextiles to evaluate the

Table 1. Summary of test conditions for cohesionless soil.

Test Apparatus Type	Approx. Test Apparatus Size (cm)	Approx. Sample Thickness (cm)	Approx. Strain Rate (mm/min)	Degree of Saturation	Approx. Normal Stress (kPa)	Reference
COHESIONLESS SOIL						
Fixed shear, Partially fixed shear	25	10	6	Dry	Up to 300	Collios et al. (1980)
Fixed shear	20[a]	18	3	Dry	5 to 50	Eigenbrod and Locker (1987)
Partially fixed shear	6	6	3	Dry and saturated	5 to 50	Eigenbrod and Locker (1987)
Fixed shear, Partially fixed shear	30	NR	1	Saturated	Up to 200	Ingold (1982)
Fixed shear	6	NR	1	Saturated	Up to 200	Ingold (1982)
Fixed shear	10	2	0.127	Saturated	14 to 100	Martin et al. (1984)
Fixed shear	32	10	10, 25, 75	Dry	50, 115, 180	Myles (1982)
Fixed shear	32	12	0.5	Dry, saturated	50, 100, 150, 200	Miyamori (1982)
Fixed shear, Free shear	2[b]	3	NR	Dry	50 to 1,000	Negussey et al. (1989)
Fixed shear	6	NR	0.4 to 0.6	Dry	3.5 to 35	O'Rourke et al. (1990)
Fixed shear, Free shear	5	NR	NR	Dry	75, 150, 300	Richards and Scott (1985)
Partially fixed shear, Free shear	30	NR	0.3	Dry	Up to 100	Williams and Houlihan (1987)
COHESIVE SOIL						
Partially fixed shear	6	6	0.24	Saturated	5 to 50	Eigenbrod and Locker (1987)
Not reported	6	2	0.0033 and 0.9	As compacted	50, 100, 150, 250, 350	Fourie and Fabian (1987)
Fixed shear	10	2	0.06	As compacted	72, 1,44, 216, 288	Koerner et al. (1986)
Fixed shear	5	<1	0.6	As compacted Pre-soaked	240 and 480	Seed (1989)
Partially fixed shear	30	NR	0.3	Dry	Up to 100	Williams and Houlihan (1987)

[a]Circular shear box.
[b]Ringshear box.
NR = Not reported.

effects of test apparatus type. Collios et al. found that a partially fixed shear box with the same soil on both sides of the box had a higher friction angle than a fixed shear box. Ingold found that similar strength values were obtained for a fixed shear box and a partially fixed shear box. Finally, Richards and Scott found that a fixed shear box produced higher strength values than did a free shear box.

SIZE OF TEST APPARATUS

The shear box test apparatus varies in size from a conventional 5- or 6-cm-square (about 2- to 2.4-in.) box to a 46-cm-square (about 18-in.) box (see Table 1). The ASTM D 3080 standard for conducting direct shear tests on soil recommends a minimum box length of about 12 times the maximum particle size. Jewell and Wroth (1987) recommend a minimum box length of 50 times the mean grain size (D_{50}).

The majority of shear boxes in the United States have upper and lower boxes of the same size. Myles (1982), Miyamori et al. (1986), and Eigenbrod and Locker (1987), however, have designed shear boxes in which the lower box is larger than the upper box. This allows high strains to be achieved without loss of shear area; therefore, no area correction is required.

Most of the recent testing was focused on tests of interface strength characteristics in an apparatus larger than the conventional soil shear box, typically in the range of about 15- to 30-cm-square (about 6- to 12-in.). Ingold (1982) conducted interface tests on cohesionless soil to evaluate box size effects. On the basis of the literature reviewed, no researchers have commented on the effects of apparatus size on cohesive soil.

Cohesionless Soil in Contact With a Geotextile at Low to Moderate Normal Stresses. Ingold (1982) found that at normal stresses higher than about 80 kPa (1,670 psf), both the large (30-cm) and small (6-cm) boxes gave similar results for a fine to medium sand in contact with a non-woven geotextile. However, he found that at normal stresses lower than about 65 kPa (1,360 psf), the large box produced lower strength values. Ingold attributes this variation to the magnitude of relative movement between the geotextile and the soil caused by normal stress effects (see under Normal Stress below). In both large and small boxes the peak shear stress occurred at about 5 percent strain in the shear box, which corresponds to a relative movement of 1.5 cm and 0.3 cm in the large and small boxes, respectively.

The results of Eigenbrod and Locker (1987) and Williams and Houlihan (1987) were compared. For concrete sand in contact with a non-woven geotextile at normal stresses up to about 100 kPa (about 2,000 psf), both large boxes produced similar friction angle efficiencies. For concrete sand in contact with a woven geotextile under similar test conditions, Williams and Houlihan's (1987) large box produced higher friction angle efficiencies than did Eigenbrod and Locker's (1987) large box.

Cohesionless Soil in Contact With a Geomembrane at Low to High Normal Stresses. O'Rourke et al. (1990) compared the results from various researchers for Ottawa sand in contact with a smooth HDPE geomembrane. They found that the friction angle for a 6-cm, 7-cm, 10-cm, 28-cm, and 30-cm-square (about 2.4-, 2.8-, 4-, 11-, and 12-in.) box were similar. Results from Williams and Houlihan (1987) and Seed (1989) for concrete sand in contact with smooth HDPE geomembrane were compared. For concrete sand with similar coefficients of uniformity, the large (30-cm) and small (5-cm) boxes produced similar friction efficiencies.

SAMPLE THICKNESS

The upper soil sample thickness ranged from less than 1 cm to 18 cm (about less than 0.4 to 7 in.) (see Table 1). The 6-cm conventional direct shear box typically has 2.54-cm-thick (1.0-in.) upper and lower boxes to meet the minimum length to thickness ratio of 2 to 1. In addition, the ASTM D 3080 standard for the direct shear test recommends a minimum thickness of six times the maximum particle size.

SAMPLE DENSITY AND MOISTURE CONTENT

Moisture and density conditions varied for the testing that was reviewed. Cohesionless soil samples had remolded densities ranging from loose to dense, based on standard Proctor, modified Proctor, or relative density. Cohesive soil samples were typically remolded to at least 90% of modified or standard Proctor and either at optimum or wet of optimum moisture content.

Cohesionless Soil. Eigenbrod and Locker (1987) reported peak and residual strength values for both concrete sand alone and concrete sand in contact with geotextiles and plain CSPE. They found that similar friction angles were obtained for loose and for dense sand at residual values in contact with geosynthetics. The lowest efficiencies were typically for peak sand in conjunction with peak soil-geosynthetic interface friction angles.

Miyamori et al. (1986) reported peak and residual strength values for a fine to medium sand in contact with geotextiles. They also found that similar friction angles were obtained for loose and for dense sand at residual values in contact with geotextiles.

Cohesive Soil. Fourie and Fabian (1987) conducted tests on silty clay compacted at various moisture contents in contact with a geotextile. They found that silty clay in contact with a woven geotextile resulted in the apparent adhesion decreasing with increasing moisture content.

Seed (1989) conducted tests on soil-bentonite in contact with a smooth and textured HDPE geomembrane. The soil-bentonite samples were compacted to various dry densities and moisture contents. He found that contours of strength values could be drawn in zones roughly parallel to the zero air voids curve.

CONSOLIDATION AND STRAIN RATE

Soil samples usually were consolidated at normal stress before applying shear stress. Shear stress was applied, in general, at a constant strain rate that varied from 0.0033 to 1,200 mm/min (about 0.00013 to 47 in./min) (see Table 1). Most researchers did not specify whether the tests were conducted in drained or undrained conditions. In some tests, to represent an unconsolidated condition, soil samples were not allowed to consolidate under the normal stress and were sheared immediately after applying normal stress.

The ASTM D 3080 standard for conducting a direct shear test requires that the soil sample be consolidated under normal pressure before shearing. After consolidation is complete, the sample is to be sheared slowly enough to allow for dissipation of excess pore pressure. A total elapsed time to failure $\geq$ 50 times t_{50} under the normal stress is recommended.

Cohesionless Soil. Martin et al. (1984), Saxena and Budiman (1985), and Saxena and Wong (1984) reported that their tests were conducted on cohesionless soil at strain rates representing a drained condition. Martin et al. (1984) conducted tests on Ottawa and concrete sand in contact with non-woven and woven geotextiles or with various geomembranes at a strain rate of 0.127 mm/min (0.005 in./min). Saxena and Budiman (1985) and Saxena and Wong (1984) conducted tests on ballast in contact with woven and non-woven geotextiles or with HDPE geomembrane at a strain rate of 0.76 mm/min (0.03 in./min).

Williams and Houlihan (1987) commented that tests conducted on Ottawa and concrete sand in contact with non-woven and woven geotextiles or with various geomembranes were relatively insensitive to strain rates in the range of 0.003 to 3 mm/min (0.0001 to 0.1 in./min). Myles (1982) tests on medium sand in contact with non-woven and woven geotextiles were relatively insensitive to strain rates in the range of 5 to 100 mm/min (0.2 to 3.9 in./min).

Cohesive Soil. Fourie and Fabian (1987) conducted tests on a silty clay in contact with a needle-punched, non-woven and a woven geotextile at strain rates of 0.0033 and 0.9 mm/min (about 0.00013 and 0.035 in./min). They found that the drained strength envelope for the silty clay in contact with a geotextile was "friction-like" and had a zero cohesion intercept; the woven geotextile had higher friction angles than did the non-woven geotextile.

For the undrained condition, Fourie and Fabian (1987) found that the bond strength develops differently for non-woven and woven geotextiles. For a non-woven geotextile, the envelope is "friction-like." For a woven geotextile, the envelope is "friction-like" at normal stresses less than about 100 kPa (about 2,000 psf) and has an undrained (friction angle equal to zero) envelope at normal stresses higher than about 100 kPa. Fourie and Fabian report that the difference in bond strength behavior can be attributed to drainage occurring at the clay-geotextile interface because of the high permeability and the high transmissivity of the non-woven geotextile. For the woven geotextile, the clay-geotextile interface is probably drained at lower normal stresses and undrained at higher normal stresses because of reduced transmissivity. They also found that the non-woven geotextile produced higher strength values than did the woven geotextile. For both the non-woven and woven geotextiles, the undrained condition produced lower strength values than did the drained condition.

Koerner et al. (1986), Lafleur et al. (1987), Saxena and Budiman (1985), and Saxena and Wong (1984) reported that their tests on cohesive soil were conducted at strain rates slow enough to dissipate excess pore pressure and represent a drained condition. Koerner et al. conducted tests on a variety of low-permeability cohesive soils in contact with various geomembranes at a strain rate of 0.06 mm/min (about 0.0024 in./min). Lafleur et al. conducted tests on remolded plastic clay in contact with non-woven and woven geotextiles at a strain rate of 0.024 mm/min (about 0.006 in./min). Saxena and Budiman and Saxena and Wong conducted tests on a fine sandy clay in contact with non-woven and woven geotextiles at a strain rate of 0.76 mm/min (about 0.03 in./min).

DEGREE OF SATURATION

Tests were conducted both dry and at saturated conditions for cohesionless soil samples (see Table 1). Tests were typically conducted on as-compacted cohesive

soil samples. Only a few tests on saturated cohesive soil samples have been reported (Eigenbrod and Locker, 1987; Saxena and Budiman, 1985; Seed, 1989; and Seed et al., 1988). Relatively few tests have been conducted on saturation effects, probably because it is difficult to adapt equipment to enable full saturation of the samples and the degree of saturation at the shear interface cannot be verified.

Cohesionless Soil. Eigenbrod and Locker (1987), Degoutte and Mathieu (1986), and Seed (1989) reported that cohesionless soil in contact with geotextiles or geomembranes produced similar strength values for both the dry and saturated (wet) condition. Miyamori et al. (1986); Saxena and Wong (1984); and Geotek, Inc. (1987) reported that for cohesionless soil in contact with geotextiles or geomembranes, the dry condition produced higher strength values than did the saturated condition.

Cohesive Soil. The results of Seed et al. (1988) showed that, for a cohesive soil in contact with an HDPE geomembrane, the as-compacted condition produced a "friction-like" strength envelope and the saturated condition produced an undrained (friction angle equal to zero) strength envelope. When compared to results for the "as-compacted" tests, Seed (1989) found strengths to be substantially lower for the saturated undrained (or partially-drained) conditions.

NORMAL STRESS

The normal stress range varies from 3.5 to 1,200 kPa (about 73 to 25,000 psf) (see Table 1). The 6-cm conventional direct shear apparatus typically has a capacity up to about 150 kPa (about 3,000 psf). Modifications of conventional equipment can be made to allow testing at normal stresses up to about 500 kPa (about 10,000 psf). The large shear boxes typically are designed to conduct tests at normal stresses of less than about 200 kPa (about 4,000 psf). The large shear boxes of Collios et al. (1980) and Geotek, Inc. (1987) have a high normal stress range of 200 to 1,200 kPa (about 4,000 to 25,000 psf).

Collios et al. (1980), Ingold (1982), Akber et al. (1985), O'Rourke et al. (1990), and Degoutte and Mathieu (1986) have reported the effects of normal stresses on cohesionless soil. Fourie and Fabian (1987) commented on the effects of normal stress on cohesive soil.

Cohesionless Soil. Collios et al. (1980) and Ingold (1982) reported that at normal stresses less than about 100 kPa (about 2,000 psf), the strength values are lower than at normal stresses above about 100 kPa for a sand in contact with a non-woven geotextile. They attribute the lower values to the fact that the geotextile has not deformed to the shape of the support material. Collios et al. also recommended that values presented in their paper should not be used for normal stresses less than about 100 kPa (about 2,000 psf). Ingold attributed lower strength values to an apparent rougher surface of the geotextile at high normal stresses. He found that at low normal stresses, the condition of the exposed geotextile surface was similar to when it was installed, but that at high normal stresses, the geotextile was very raveled.

In contrast, for a fine gravel in contact with a non-woven geotextile and various geomembranes, Akber et al. (1985) found that the strength was higher at normal stresses less than about 100 kPa (about 2,000 psf) and that it stabilized at normal stresses above 100 kPa.

O'Rourke et al. (1988) conducted tests at normal stresses in the range of 3.5 to 35.0 kPa (about 73 to 730 psf) on Ottawa sand in contact with a smooth HDPE and PVC geomembranes. They found that there was no apparent curvature of the strength envelope in the low normal stress range. Negussey et al. (1989) conducted tests at normal stresses in the range of 50 to 1,000 kPa (about 1,000 to 20,000 psf) on Ottawa sand in contact with a smooth HDPE geomembrane. They found that there was no apparent curvature of the strength envelope in the low to high normal stress range. In addition, Seed (1989) conducted tests at about 150, 300, and 500 kPa (3,300, 6,600 and 10,000 psf) on concrete sand in contact with a smooth HDPE geomembrane. He also found that there was no apparent curvature of the strength envelope in the low to high normal stress range.

Degoutte and Mathieu (1986) conducted tests on fine sand in contact with a geotextile and PVC geomembrane at normal stresses up to 1,200 kPa (about 25,000 psf). They found that at normal stresses less than about 800 kPa (about 17,000 psf), higher friction values were obtained than at the normal stresses above 800 kPa.

Cohesive Soil. Fourie and Fabian (1987) reported that at normal stresses higher than about 150 kPa (about 3,000 psf), the strength values were higher than at normal stresses lower than about 150 kPa for a silty clay in contact with a nonwoven geotextile. They attributed the higher strength to the fact that either the geotextile has deformed to the shape of the soil particles, a rougher surface of the geotextile has occurred at high normal stresses, or the geotextile has small material stiffness.

SUMMARY AND CONCLUSIONS

Table 2 is a summary of the effects of testing conditions on contact efficiency of geosynthetic materials. The very wide range of contact efficiencies presented in the literature for the soil and geosynthetic interface is a result of variation in materials tested, test procedures, and methods of calculation of contact efficiency.

The following conclusions can be made on the basis of the review of the literature:

- The test apparatus type affects friction angle efficiency for cohesionless soil in contact with geotextiles. The partially fixed shear box with the same soil on both sides of the box had a higher friction angle than a fixed shear box; the fixed shear test produces higher friction angle efficiencies than does a free shear test. If large displacements can occur at the soil-geosynthetic interface in the field, a fixed shear test may give unconservatively high friction angle efficiencies.

- There are not enough data to compare the effects of test apparatus type for cohesive soil in contact with geosynthetics and for cohesionless soil in contact with geomembranes.

- For the range of equipment currently used for testing, apparatus size does not appear to affect significantly the efficiency for cohesionless sands in contact with geosynthetics. The size of the apparatus is likely to affect the efficiency for cohesionless material containing gravels; however, additional testing is necessary to confirm this.

Table 2. Effects of Testing Conditions on Contact Efficiencies of Geosynthetic Materials.

Material or Test Procedure	Clean Cohesionless Soil	Cohesive Soil
Geotextile Opening Size	Efficiency is higher for geotextile opening size similar to or larger than soil grain size than for geotextile opening size smaller than soil grain size.	Efficiency is higher for geotextile opening size similar to or larger than soil grain size than for geotextile opening size smaller than soil grain size.
Geotextile Deformability	Efficiency is higher for a flexible geotextile than for a stiff geotextile.	No data reported.
Geomembrane Surface Roughness	Efficiency is higher for a textured surface than for a smooth surface.	Efficiency is higher for a textured surface than for a smooth surface.
Geomembrane Polymer	Efficiency is higher for a soft polymer (e.g., PVC) than a hard polymer (e.g., HDPE).	Efficiency is higher for a soft polymer (e.g., PVC) than a hard polymer (e.g., HDPE).
Apparatus Type		
Geotextile	Efficiency may be higher for a partially fixed condition than a fixed condition.	No data reported.
Geomembrane	Insufficient data to draw conclusion.	No data reported.
Apparatus Size	Test apparatus size does not significantly affect efficiency.	No data reported.
Sample Density and Moisture Content	Efficiency is similar for varying density and moisture content when evaluated on the basis of residual values.	Insufficient data to draw conclusion.
Consolidation and Strain Rate	Efficiency is similar for drained and undrained conditions.	Insufficient data to draw conclusion.
Degree of Saturation	Efficiency is similar for dry and saturated conditions.	Insufficient data to draw conclusion.
Normal Stress		
Geotextile	Efficiency is lower at low normal stresses (<100 kPa) than at high normal stresses.	Efficiency is lower at low normal stresses (<100 kPa) than at high normal stresses.
Geomembrane	Insufficient data to draw conclusion.	No data reported.

- There are not enough data to determine the effects of test apparatus size for cohesive soil in contact with geosynthetics.

- The compacted soil density for cohesionless soil does not significantly affect the contact efficiency for soil friction and soil-geosynthetic friction reported as residual values.

- The compacted soil density and moisture content affect the contact efficiency for cohesive soil. Additional research should be conducted to verify the trend developed by Seed (1989) that contours of strength values could be drawn in approximately parallel lines to the zero air voids line.

- The strain rate, 0.003 to 3 mm/min (0.001 to 0.1 in./min), used to conduct the tests does not significantly affect the results for clean cohesionless soil.

- The strain rate affects the results of cohesive soil. If tests are performed slowly enough to dissipate pore water pressures (0.0033 mm/min or about 0.0013 in./min for a silty clay), a "friction-like" failure envelope develops. If tests are performed relatively fast (0.9 mm/min or about 0.035 in./min for a silty clay), an undrained envelope develops. At rates in between, a combination envelope develops. It is not known to what extent an undrained condition exists because pore pressures cannot be monitored.

- For clean cohesionless material in contact with geosynthetics, the saturated condition may produce slightly lower friction angles than for the dry condition. It appears that saturation may substantially affect the results of cohesive soil; however, there are not enough data to determine the effects of saturation on the efficiency.

- Low normal stresses (< about 100 KPa) appear to affect the contact efficiency of soil in contact with geotextiles. It appears that this could be attributed to the fact that the geotextile has not deformed. In addition, high normal stresses may affect the contact efficiency of soil in contact with geomembrane because of penetration of soil particles into the membrane surface.

RECOMMENDATIONS FOR INTERFACE STRENGTH TESTING

In order to get comparable test results, testing should be performed using similar test conditions and variations should be reported. The recommended test program first should involve performing laboratory tests on proposed soil samples to determine material properties. Then it should include direct shear interface tests conducted at the interface between the soil and the geosynthetic material.

Soil Material Property Testing. Laboratory tests performed on soil samples collected from proposed construction sources should include the following:

- A particle size analysis to determine the particle size distribution and maximum particle size of the soil

- Atterberg limits tests to classify the fine-grained portion of the sample

- Moisture-density tests to determine field placement conditions

- Consolidation tests, if appropriate, to estimate the rate of pore pressure dissipation

- Direct shear tests to determine soil strength. Tests should be conducted to represent field conditions; however, to develop correlations, it is recommended that tests be conducted consolidated-drained.

In addition, the angularity or roundness of the soil samples should be noted.

Direct Shear Interface Testing. Direct shear interface test conditions should include the following:

- Selection of test apparatus size that is appropriate for soil sample particle size and geosynthetic opening size. Fine-grained soil in contact with most geotextiles and geomembranes can be tested in a 5-cm (about 2 in.) or larger box. Coarse-grained sand in contact with most geotextiles and geomembranes should be tested in at least a 10-cm box (about 4 in.). Gravel should be tested in a box at least 12 times the maximum grain diameter. For purposes of consistency, however, it is recommended that testing be done in a minimum 30-cm box (about 12 in.) as recommended in the proposed ASTM standard test for direct shear interface tests (ASTM draft designation 01.81.07).

- Soil sample thicknesses that are a minimum of six times the maximum grain diameter, as recommended by ASTM D 3080.

- Soil samples compacted to a moisture content and density similar to expected field conditions. If saturation is a design condition, the samples should be tested in a saturated condition.

- Consolidated conditions and a strain rate that represent expected field conditions. However, to develop correlations, it should be run at a strain rate slow enough to allow for dissipation of pore pressure and achieve a drained condition.

- A normal stress range representing possible field conditions from during construction of the liner to interim and final site configurations. This includes low stresses for short-term and either drained or undrained conditions, with possibly high normal stresses for operation and long-term conditions.

RESEARCH NEEDS

This review of the literature pointed to the need for additional research in order to better assess and predict the strength of materials for design purposes. Additional research is recommended for cohesive and cohesionless soils in contact with geosynthetics to evaluate the following:

- Type of test apparatus (for both types of soils)
- Size of test apparatus (for both types of soils)
- Contours of strength at varying sample densities and moisture contents (for cohesive soils)
- Measures to monitor pore pressure (for cohesive soils)
- Methods to control degree of saturation (for cohesive soils)
- High normal stresses to evaluate penetration into membrane surface (for both types of soils)

REFERENCES

Akber, S. Z., Y. Hammamji, and J. Lafleur, (1985) "Frictional Characteristics of Geomembranes, Geotextiles, and Geomembrane/Geotextile Composites," Proceedings of the Second Canadian Symposium on Geotextiles and Geomembranes, Edmonton, Alberta, pp. 209-217.

Collios, A., P. Delmas, J. P. Gourc, and J. P. Giroud, (1980) "Experiments on Soil Reinforcement With Geotextiles," The Use of Geotextiles for Soil Improvement, 80-177, ASCE National Convention, Portland, Oregon, pp. 53-73.

Degoutte, G., and G. Mathieu, (1986) "Experimental Research of Friction Between Soil and Geomembranes or Geotextiles Using a Thirty by Thirty Square Centimeter Shearbox," Proceedings of the Third International Conference on Geotextiles, Vienna, Austria, pp. 1251-1256.

Eigenbrod, K. D., and J. G. Locker, (1987) "Determination of Friction Values for the Design of Side Slopes Lined or Protected With Geosynthetics," Canadian Geotechnical Journal, Vol. 24, No. 4, pp. 509-519.

Fourie, A. B., and K. J. Fabian, (1987) "Laboratory Determination of Clay-Geotextile Interaction," Geotextiles and Geomembranes, Vol. 6, No. 4, pp. 275-294.

Geotek Inc., (1987) Direct Shear Testing of Friction Liner Material, Prepared for Gundle Lining Systems, Inc.

Ingold, T. S., (1982) "Some Observations on the Laboratory Measurement of Soil-Geotextile Bond," Geotechnical Testing Journal, Vol. 5, No. 3/4, pp. 57-67.

Jewell, R. A., and C. P. Wroth, (1987) "Direct Shear Tests and Reinforced Sand," Geotechnique, Vol. 37, No. 1, pp. 53-68.

Koerner, R. M., J. P. Martin, and G. R. Koerner, (1986) "Shear Strength Parameters Between Geomembranes and Cohesive Soils," Geotextiles and Geomembranes, Vol. 44, No. 1, pp. 21-30.

Lafleur, J., M. S. Sall, and A. Ducharme, (1987) "Frictional Characteristics of Geotextiles With Compacted Lateritic Gravels and Clays," Proceedings of the Geosynthetics '87 Conference, New Orleans, Louisiana, pp. 205-215.

Martin, J. P., R. M. Koerner, and J. E. Whitty, (1984) "Experimental Friction Evaluation of Slippage Between Geomembranes, Geotextiles and Soils,"

Proceedings of the International Conference on Geomembranes, Denver, Colorado, pp. 191-196.

Miyamori, T., S. Iwai, and K. Makiuchi, (1986) "Frictional Characteristics of Non-Woven Fabrics," Proceedings of the Third International Conference on Geotextiles, Vienna, Austria, pp. 701-705.

Myles, B., (1982) "Assessment of Soil Fabric Friction by Means of Shear Evaluation," Proceedings of the Second International Conference on Geotextiles, Las Vegas, Nevada, pp. 787-791.

Negussey, D., W. K. D. Wijewickreme, and Y. P. Vaid, (1989) "Geomembrane Interface Friction," Canadian Geotechnical Journal, Vol. 26, No. 1, pp. 165-169.

O'Rourke, T. D., S. J. Druschel, and A. N. Netravali, (1990) "Shear Strength Characteristics of Sand Polymer Interfaces," Journal of Geotechnical Engineering, Vol. 116, No. 3, pp. 451-469.

Richards, E. A., and J. D. Scott, (1985) "Soil Geotextile Frictional Properties," Proceedings of the Second Canadian Symposium on Geotextiles and Geomembranes, Edmonton, Alberta, pp. 13-24.

Saxena, S. K., and J. S. Budiman, (1985) "Interface Response of Geotextiles," Proceedings of the Eleventh International Conference on Soil Mechanics and Foundation Engineering, San Francisco, California, pp. 1801-1804.

Saxena, S. K., and Y. T. Wong, (1984) "Frictional Characteristics of a Geomembrane," Proceedings of the International Conference on Geomembranes, Denver, Colorado, pp. 187-190.

Seed, R. B., (April 1989) Final Results of Direct Shear Tests; Liner Interface Strength, Cedar Hills Regional Landfill, Prepared for CH2M HILL.

Seed, R. B., J. K. Mitchell, and H. B. Seed, (1988) Slope Stability Failure Investigation: Landfill Unit B-19, Phase I-A, Kettleman Hills, California, Report No. UCB/GT/88-01.

Takasumi, D. L., (1990) "Interface Strength Characteristics Between Soil and Geosynthetics: A State of the Art Review," Project prepared in partial fulfillment of Masters of Science in Civil Engineering.

Williams, N. D., and M. F. Houlihan, (1987) "Evaluation of Interface Friction Properties Between Geosynthetics and Soils," Proceedings of the '87 Geosynthetics Conference, New Orleans, Vol. 2, pp. 616-627.

PVC Geocomposite for Improved Friction and Performance Properties

David C. Lauwers
Occidental Chemical Corporation, USA

With the emphasis of waste containment being placed upon improving the stability of the various interfaces uses in their construction, geocomposites with improved coefficient of friction properties provide possible solutions. The geocomposite which is addressed in this paper, not only offers improved slope stability properties, but also other improvements over geomembranes presently used. The geocomposite consists of a PVC geomembrane laminated to a nonwoven polyester fabric. This combination offers, along with the improved friction properties, greater puncture resistance and higher tear resistance than flexible geomemebranes. It also is not susceptible to the stress cracking associated with the more crystalline geoemembranes.

In this paper, this geocomposite was compared to a PVC geomembrane using various index tests. The purpose was to determine what benefits the geocomposite offers over the present practice of placing a geomembrane along with a geotextile in containment applications. This paper also summarizes several case studies in which this geocomposite worked successfully, and some planned future commercial uses of this material.

The index tests that were conducted in this study are as follows:

1. Coefficient of Friction testing according to proposed ASTM draft for "Determining the Coefficient of Geosynthetic/Geosynthetic and Soil/Geosynthetic Friction by Direct Shear Method".

2. Puncture resistance testing according to GRI GS1 standard test entitled "CBR Puncture Strength".

3. Physical testing according to NSF 54 Standard for Geomembranes.

Coefficient of Friction Testing

The purpose of the coefficient of friction testing was to develop comparative data under controlled laboratory conditions using a wide range of soils used in waste containment applications. These materials included Ottawa sand, glacial till, lean clay and fresh concrete. This test data should not be used as a table to determine design parameters. Recent papers presented on friction testing recommend that specific friction testing be conducted using the design parameters, materials and conditions expected for specific projects.

The interface shearing resistances were determined for each of the three previously described normal stresses. The test data were plotted on a graph of shear stress versus normal stress. A best fit straight line was drawn through the data points to obtain a total stress interface friction angle and adhesion. The data points correspond to the peak shear stress generated for each normal stress. The coefficient of friction, interface friction angle and adhesion, derived from the test results are summarized in Table 1.

The reported adhesion is the shear stress intercept of the best fit straight line drawn through the test data. This value may not be the "true adhesion" of the interface and caution should be exercised in using this adhesion value for applications involving normal stresses outside the range covered by the test.

The testing program involved thirteen (13) direct shear interface strength tests. The configuration (from top to bottom) for each direct shear interface was as follows:

- selected soil compacted to a specific dry density and water content;
- selected geosynthetic material (i.e., PVC geomembrane, or selected geocomposite); and
- concrete sand.

It should be noted that for the three (3) direct shear interface tests of the geotextile and PVC geomembrane, a selected soil was compacted above the geotextile during each test. However, in each test, the actual interface which was tested was between the geotextile and the PVC geomembrane. It should also be noted that in all of the tests which involved the various geocomposites, the geotextile side of the geocomposite was always selected as the shearing surface. The test was conducted in this manner so that comparative results could be obtained of the geotextile in contact with the geomembrane versus the geocomposite with best friction surface facing the soil being tested.

In the coefficient of friction testing, the following geosynthetic materials were used:

1. A 4.2 oz. nonwoven polyester geosynthetic
2. A 30 mil PVC flexible geomembrane.
3. A geocomposite of 30 mil PVC flexible geomembrane and 4.2 oz. polyester geosynthetic.
4. A geocomposite of 30 mil PVC flexible geomembrane and 6.0 oz. polyester geosynthetic.
5. A geocomposite of 30 mil PVC flexible geomembrane and 3.6 oz. polyester geosynthetic.

The soils used for the testing program, provided by GeoServices, were the ollowing:

1. A commercially available Ottawa sand referred to as Ottawa sand in this report;

2. A glacial till common to the Northwestern United States referred to as glacial till;

3. A lean clay common to the Northeastern United States referred to as clay in this report; and

4. A concrete sand was used as a bedding layer during all of the direct shear interface tests, referred to as dense sand in this report.

5. A commercial freshly-cast concrete tested within one hour of preparation.

For detail of the specific parameters used in conducting the friction testing, onsults that section titled **"Specific Coefficient of Friction Tests Parameters"**, at he end of this paper.

riction Test Results Summary

The results of the friction testing in Table 1 show, a substantial increase in the oefficient of friction properties of the geocomposite versus the geomembrane to soil nterface or the geotextile to geomembrane interface. The weakest interface is between he geotextile and the geomembrane. This has been the failure mechanism seen in everal sideslope failures. By laminating the geotextile to the geomembrane, this weak nterface is eliminated.

In the case of the Ottawa sand and glacial till, the interface friction angle ncreases by 10 degrees by using the geocomposite. This allow for the design of steeper lopes for both landfill cover and liners than is possible using present designs.

TABLE 1

DIRECT SHEAR TEST RESULTS

TEST NUMBER	INTERFACE TESTED (1)	COEFFICIENT OF FRICTION	INTERFACE FRICTION ANGLE	ADHESION(2)
1	**Ottawa sand**/30 mil PVC/4.2 oz. fabric	0.61	31.2°	171 psf
2	**Ottawa sand**/30 mil PVC/6.0 oz. fabric	0.62	31.6°	187 psf
3	**Ottawa sand**/30 mil PVC	0.45	24.1°	0 psf
4	**Ottawa sand 4.2 oz. fabric**/30 mil PVC	0.38	20.7°	43 psf
5	**Glacial till**/30 mil PVC/4.2 oz. fabric	0.54	28.4°	131 psf
6	**Glacial till**/30 mil PVC/6.0 oz. fabric	0.59	30.5°	121 psf
7	**Glacial till**/30 mil PVC	0.38	20.9°	154 psf
8	**Glacial till 4.2 oz. fabric**/30 mil PVC	0.46	24.7°	50 psf
9	**Clay**/30 mil PVC/4.2 oz. fabric	0.50	26.7°	167 psf
10	**Clay**/30 mil PVC/6.0 oz. fabric	0.50	26.4°	156 psf
11	**Clay**/30 mil PVC	0.41	22.4°	71 psf
12	**Clay 4.2 oz. fabric** /30 mil PVC	0.43	23.5°	36 psf
13	**Fresh Concrete**/30 mil PVC/3.6 oz. fabric	0.48	30.1°	237 psf

NOTES: (1) The material named in bold face before the slash denotes the upper component of the tested interface. The geocomposites were all tested having the geotextile side of the geocomposite as the shearing surface.

(2) The reported value of adhesion may not be the "true adhesion" of the interface and caution should be exercised in using this adhesion value for applications involving normal stresses outside the range covered by the test.

BR Puncture Strength Test

The CBR Puncture Strength test is a modification of ASTM D3787 where the size of he plunger is increased from 5/16" to 2.0". The CBR mold has an inside diameter of .0". The specimen, contained in the mold, is placed under the plunger which is ttached to the crosshead of a constant rate of extension testing machine. After the pecimen is given a preload of 2 pounds, the test begins as the plunger moves down at constant rate of 2"/minute.

The composite tested in this case was a 30 mil PVC geomembrane laminated to a 3.6 z. nonwoven polyester. The geocomposite was tested both with the fabric facing the lunger and the geomembrane facing the plunger. This was compared to the 30 mil PVC eomembrane. The results of the testing are summarized in Table 2.

TABLE 2

CBR PUNCTURE DATA FOR PVC VERSUS GEOCOMPOSITE

	GEOCOMPOSITE TEXTILE FACING PLUNGER	PVC FACING PLUNGER	30 MIL PVC
LOAD	459 458 436 429 441	456 500 507 510 506	292 294 284
AVERAGE LOAD	445	496	290
EXTENSION	1.83 1.86 1.90 1.81 1.86	1.99 1.96 2.03 1.95 2.02	4.14 4.20 4.41
AVERAGE EXTENSION	1.85	1.99	4.25

uncture Test Results Summary

The results of the puncture testing show a 50% increase in the puncture resistance f the geocomposite compared to the geomembrane. In applications where settling and ossible protrusions sharp objects, this gives a margin of safety in design. This also llows for bridging of settlement areas in applications such as landfill covers. The eight of the fabric and geomembrane in the geocomposite can be chosen to meet the equired puncture resistance for specific applications.

NSF Standard 54 Testing

Standard physical properties including tensile, elongation 100% modulus, hydrostatic resistance, and graves tear were tested using the appropriate ASTM test methods specified in the NSF 54 Standard for geomembranes. In this testing a 20 mil PVC geomembrane/ 4.2 oz fabric and a 30 mil PVC geomembrane/3.6 oz fabric composites were compared to corresponding gauges of PVC geomembrane. The actual test methods and the results of the testing are summarized in Table 3.

TABLE 3

PHYSICAL PROPERTIES OF GEOCOMPOSITE

PROPERTY		20 MIL PVC 4.2 OZ FABRIC	20 MIL PVC	30 MIL PVC 3.6 OZ FABRIC	30 MIL PVC
MD/TD					
TENSILE LB/INCH	ASTM D882	69/60	50/55	96/90	90/85
ELONGATION %	ASTM D882	455/453	444/447	458/492	500/560
100% MODULUS LB/INCH	ASTM D882	38/47	30/25	59/63	45/42
HYDROSTATIC PSI	ASTM D751 METHOD A	200+	75	200+	110
GRAVES TEAR LBS	ASTM D1004 DIE C	16.5/16.9	6.3/6.5	19.6/18.7	10.0/10.2

Physical Property Test Results Summary

As evident by the results of the test, substantial improvements are made in all physical properties. Tear resistance can easily be increased by 100%. The modulus, hydrostatic resistance and tensile are all improved. Again all properties can be designed for specific applications by varying either the thickness of the PVC geomembrane or the weight of the geotextile.

ase Study Summaries

The following are short case studies of applications where this geocomposite was sed because of its unique properties.

il Well Drilling Site Containment

Michigan environmental regulations require that there is complete cleanup of any pilled contaminants on an oil well drilling site. In order to accomplish this, many rilling operators use a geomembrane under all the equipment used at a site. This auses safety issues in wet and snowy weather since the geomembrane becomes very lippery, leading to falls and possible injury. Since the PVC geocomposite can still e fabricated into large panels at the factory, the panel can be designed to cover the ntire drilling site, and no further fabrication is required at the site.

At Duell #36 drilling site, a geocomposite of 20 mil PVC geomembrane with a 4.2 unce nonwoven geotextile was used to provide containment under site equipment. The se of the fabric backed geocomposite, with the fabric side facing up, because of its igh coefficient of friction, provided good footing even in the worst weather onditions. It provides the added benefit of increased protection to puncture due to eavy equipment traffic and uneven subgrade. In actual usage, the incidents of slips nd falls have been significantly reduced.

aira Rado Golf Course

Applications which are designed with steep slopes has not been possible with past eomembranes. This geocomposite now can be used for these applications. It's possible o apply a topsoil to the liner and maintain a stable slope in the application.

At Tiara Rado Golf Course, a liner was needed for a pond on the course designed o be used for irrigation. Conventional geomembrane could not be used due to the steep lopes of the pond. A 30 PVC geomembrane/4.2 ounce fabric geocomposite was used with he fabric facing up. The whole pond which involved 21,500 square feet was able to be ined using two prefabricated panels. This greatly minimized the field seams required nd required less than a day to install. The pond is now functioning well supporting he topsoil applied for astectic purposes.

Other applications are planned for the geocomposite. These include the lining of he Coachella Canal and several landfill caps.

oachella Canal

This geocomposite was originally developed with the Coachella canal in mind. This roject involves lining the canal with a geomembrane and then covering it with concrete ile there is water in the canal. The PVC geomembrane did not have the coefficient f friction required to hold the specially formulated concrete in place until it set . A geotextile was adhered to the PVC geomembrane to provide the coefficient of riction needed to hold the concrete. The geocomposite provides the coefficient of riction required without the necessity of adhering the geotextile. A panel of the eocomposite, fabricated for this project, will be used in the near future.

Landfill Caps

This PVC geocomposite has been specified into several landfill caps. The increased coefficient of friction allows for steeper slopes to be used in the design of the caps. This allows for more useful volume in the same amount of area. It has the added advantage of providing far greater resistance to puncture from settling and tear due to the stresses of the steeper slopes.

Summary

The data from this study shows that there is a definite improvement in the friction, puncture and physical properties of this geocomposite over the geomembrane. As seen in Graph 1 as much as a 10 degree improvement was seen in friction angle. Graph 2 shows a puncture resistance improvement of 50%. This offers an opportunity to explore othwe designs in the construction for landfills, canals, waste water treatment inclosures and other applications. Further work is necessary to understand all the performance parameters of this geocomposite. Long term testing is still underway with initial results after a year of testing showing very little change in physical properties.

This study was limited in nature in both the materials chosen and the test conducted on the goetextiles. A wide range of weight of the geotextile can be prepared using PVC geomembrane from 10 to 60 mils depending upon the applications. Further work will be conducted as the applications for this geocomposite are expanded.

Acknowledgements

I wish to thank to following people for their assistance in this study.

Dan Campbell - Hoechst Celanese Corporation
Robert Koerner - Geosynthetic Research Institute
Robert Swan - GeoServices Inc.
Fred P. Rohe - Environmental Protection Inc.
William R. Morrison - U. S. Department of Interior

Graph 2

CBR PUNCTURE DATA

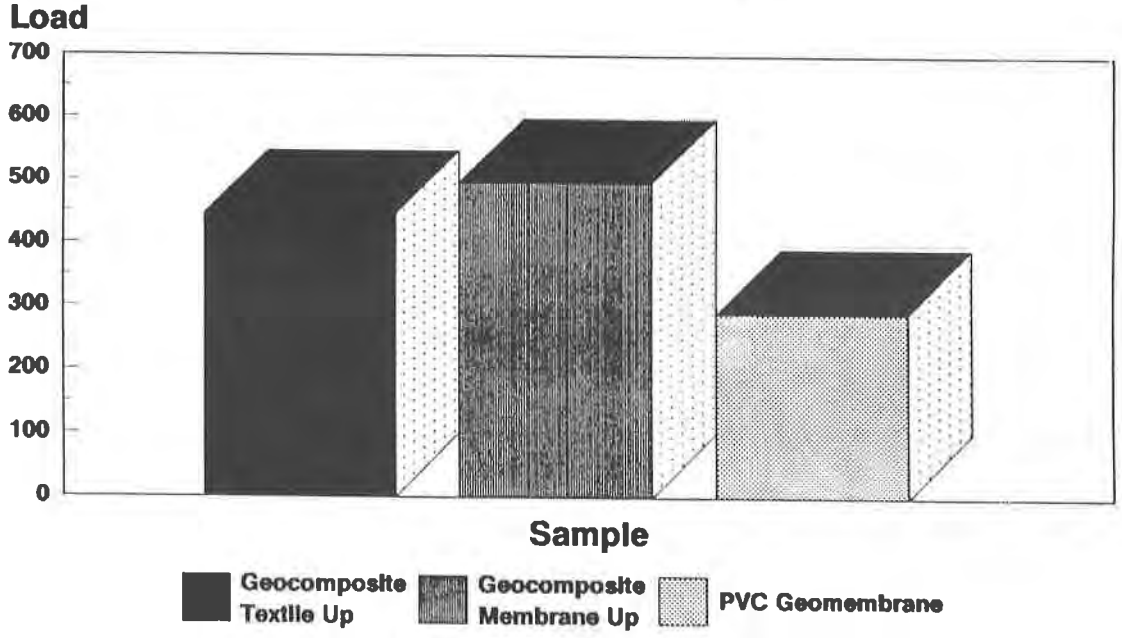

Graph 1

INTERFACE FRICTION ANGLE RESULTS

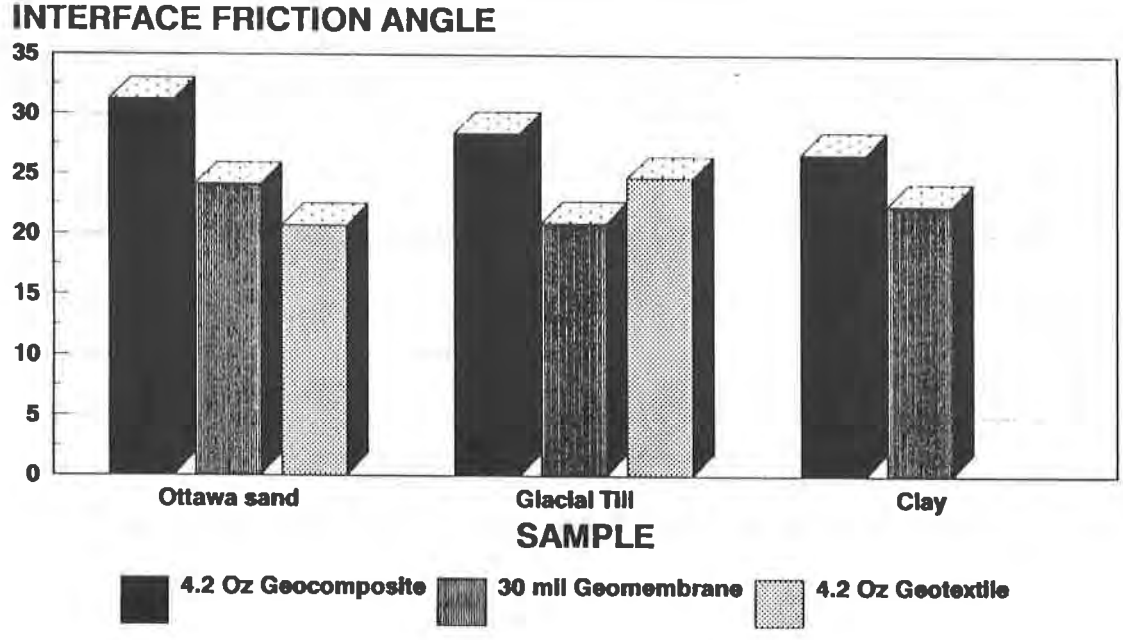

Specific Coefficient of Friction Test Parameters

The soil property testing to determine soil index properties and compaction are summarized below:

TEST METHOD	SOIL TYPE
Particle size analysis (ASTM D 422)	Ottawa sand, glacial till, and clay
Hydrometer analysis (ASTM D 422)	glacial till and clay
Atterberg Limits (ASTM D 4318)	glacial till and clay
Standard Proctor Compaction (ASTM D 698)	glacial till and clay
Maximum index dry density (ASTM D 4253)	Ottawa sand
Minimum index dry density (ASTM D 4254)	Ottawa sand

The soils used in each interface test were compacted as follows:

- Ottawa sand, compacted under dry conditions between 95 and 100 percent of its maximum dry density as determined in the maximum index dry density determination (ASTM D 4253);
- glacial till, compacted between 95 and 100 percent of its maximum dry density and between optimum moisture content and 3 percent wet of the optimum moisture content as determined in the standard Proctor compaction test (ASTM D 698); and
- clay, compacted between 95 and 100 percent of its maximum dry density and between optimum moisture content and 3 percent wet of the optimum moisture content as determined in the standard Proctor compaction test (ASTM D 698).

Specific details regarding the direct shear interface testing program are summarized below:

- Shear box dimensions: 12 in. by 12 in. (305 mm by 305 mm).
- Shear box depth: 4 in. (100 mm) above and below the interface tested.
- Normal stresses applied to the soil in the box: 1.5, 2.5, and 4.0 psi (10, 17, and 27 kPa).

- Shear displacement rates:
  - Test Numbers 4, 8, 12, and 13: 0.2 in./min (5 mm/min) for the upper half of the shear box;
  - in all of the other tests: 0.04 in./min (1 mm/min) for the upper half of the shear box; and
  - in all tests, the lower half of the shear box is fixed.
- Soil placement:
  - Test Numbers 1 through 4: Ottawa sand compacted to a dry density of 110 to 112 lb/ft^3 (17.4 to 17.7 kN/m^3) under dry conditions;
  - Test Numbers 5 through 8: glacial till compacted to a dry density of 130 to 134 lb/ft^3 (20.6 to 21.2 kN/m^3) at a moisture content of 7.6 to 8.5 percent; and
  - Test Numbers 9 through 12: clay compacted to a dry density of 98 to 101 lb/ft^3 (15.5 to 16 kN/m^3) at a moisture content of 23.5 to 24.2 percent.
  - Test Number 13: freshly-cast concrete (tested within an hour of preparation).
- All of the geosynthetic materials used during this study were tested in the machine direction.
- Since the lower box was larger than the upper box, all of the tests were conducted using a constant effective sample area. Therefore, an area correction was not required.
- All of the tests were run until a constant load was recorded.

TEST RESULTS

Soil Index Property and Compaction Testing

- Ottawa sand:
  - selected particle sizes (D_{10} - 0.40 mm, D_{30} = 1.00 mm, and D_{60} = 1.5 mm) (see Figure A-1),
  - coefficient of uniformity (C_u): 3.8,
  - coefficient of curvature (C_c): 1.7,
  - particle shape: subrounded to rounded,
  - soil type as determined by the Unified Soil Classification System (USCS): SP (poorly graded sand),

- maximum index dry density: 116 lb/ft^3 (18.4 kN/m^3), and
- minimum index dry density: 95 lb/ft^3 (15.1 kN/m^3).

- glacial till:
  - Percent finer for selected sieve sizes: U.S. Standard Sieve No. 4 = 69%, U.S. Standard Sieve No. 40 = 54%, and U.S. Standard Sieve No. 200 = 29% (see Figure A-2),
  - Atterberg limits: liquid limit (LL) = 23.2%, plastic limit (PL) = 19.9%, and plasticity index (PL) = 3.3 (see Figure A-2).
  - soil type as determined by the Unified Soil Classification System (USCS): SM (silty sand with gravel), and
  - Standard Proctor compaction: maximum dry density = 134.5 lb/ft^3 (21.3 kN/m^3) and optimum moisture content = 7.5% (see Figure A-3).

- clay
  - Percent finer for selected sieve sizes: U.S. Standard Sieve No. 4 = 0%; U.S. Standard Sieve No. 40 = 0%; and U.S. Standard Sieve No. 200 = 98% (see Figure A-4),
  - Atterberg limits: liquid limit (LL) = 43.6%; plastic limit (PL) = 26.4%; and plasticity index (PI) = 17.2 (see Figure A-4),
  - soil type as determined by the Unified Soil Classification System (USCS): CL (lean clay); and
  - Standard Proctor compaction: maximum dry density = 101.4 lb/ft^3 (16.1 kN/m^3) and optimum moisture content = 23% (see Figure A-5).

Landfill Liner Side Slope Design to Minimize Geomembrane Tensile Stress

Michael Quinn
Barton & Loguidice, P. C., USA
Martin Chandler
Barton & Loguidice, P. C., USA

ABSTRACT

The establishment of State regulations requiring all new solid waste landfill facilities to integrate soil barrier and drainage layers with geosynthetic barrier layers presented the Design Engineers with the task of assuring slope stability of a multi-layered composite liner system on steep landfill side slopes. The slope design utilized addresses both the stability of soil layers placed above the primary geomembrane liner as well as the short and long term integrity of the geomembrane liner when exposed to tensile stresses of construction and "active block" slope support.

This paper presents the design considerations of two landfill liner side slopes for which the design effort was to minimize the tensile stresses in the geomembrane and thereby reduce the probability of tensile stress failure in sheet material and in liner seams. Both designs depart from the current trend towards increasing the frictional resistance of geomembranes, and rely instead upon geosynthetic materials specifically designed for tensile strength and slope stabilization. A geogrid and geotextile are provided to maintain the stability of overlying soil layers and to cushion the geomembranes from mechanical tensile stress. In addition, the design concept allows for acceptable displacements to occur to the interface of the primary geomembrane liner and an overlying nonwoven geotextile. This interface will accommodate the potential for yielding of overlying geosynthetic materials and soils as a result of refuse placement and subsequent settlement. Liner system construction in this manner will help to ensure the long term integrity of the primary geomembrane liner as an effective and efficient barrier to vertical leachate flow.

INTRODUCTION

Current New York State regulations require municipal solid waste containment facilities to incorporate a liner system comprised of two double composite liners interlayered with two leachate collection and removal systems (LCRS). The required construction of the composite liners includes two components; a 60 mil geomembrane and a compacted soil liner with a maximum permeability of 1.0×10^{-7} cm/sec. Separating and overlying the composite liners are the primary and secondary LCRS.

The primary and secondary LCRS must be constructed of natural or geosynthetic materials having minimum permeabilities equal to 1.0×10^{-3} cm/sec and 1.0×10^{-2} cm/sec respectively. A liner system configured in this manner provides a highly efficient barrier against vertical leachate flow.

The liner system, as described above, requires the Design Engineer to consider the stability, constructability and survivability of the geomembrane and other geosynthetic liner components. These concerns become particularly critical where the liner system is to be placed on landfill side slopes. It is on liner system side slopes that a multitude of design concerns inherently develop including:

- soil layer stability,
- soil layer compactibility,
- geomembrane liner tensile stress,
- geomembrane liner puncture, and
- construction equipment performance and safety.

In recognition of the above listed design concerns, the State regulations modify the required liner system configuration on side slopes while still affording the maximum environmental protection. The State regulations allow the Design Engineer to eliminate the compacted soil liner component of the primary composite liner; therefore, the primary geomembrane directly overlies the primary LCRS on side slopes with grades in excess of 25 percent. The elimination of the primary soil liner component reduces the amount of tensile stress applied to the secondary geomembrane liner through the elimination of added liner system weight and compactive effort required to meet the soil liner permeability requirements.

The exclusion of the primary soil liner component, however, does reduce the hydraulic barrier efficiency of the primary liner to a single geomembrane liner. The loss of primary liner efficiency, although potentially significant, is far outweighed by the gains associated with reducing the amount of mechanical stress and construction activity above the secondary composite liner. Furthermore, through the use of geosynthetic design, the Design Engineer may minimize the stresses applied to construct the mandated liner system on landfill side slopes. It is these aspects of the liner system design and the concept of geomembrane stress minimization which are presented in this paper.

LINER SYSTEM DESCRIPTION

Two municipal solid waste facilities have provided the Design Engineer with the opportunity to develop and implement a geosynthetic system that minimizes geomembrane tensile stresses. Both facilities and liner system designs have been endorsed by the New York State Department of Environmental Conservation (NYSDEC), one facility is currently under construction. The liner system designs incorporate the use of geomembrane, geotextile, geonet, geogrid and natural barrier and drainage layers. Figure 1 illustrates the various liner system components. The critical aspect of each liner system design was the stability of the geosynthetic and natural materials on side slopes. The following paragraphs briefly discuss the primary function of each liner system component illustrated by Figure 1 and its relation to liner system slope stability.

- Secondary Soil Liner is a two foot thick compacted soil barrier layer with a maximum permeability of 1×10^{-7} cm/sec. Both projects will utilize on site SM-SC type (Unified Soil Classification System symbol) soils to construct this layer. This soil liner is stable on the 3 horizontal and 1 vertical liner side slopes.

- Secondary Geomembrane Liner is a 60 mil high density polyethylene (HDPE) liner placed in direct contact with the secondary soil liner. These two materials form the secondary composite liner. A 12 oz. per square yard geotextile is used to cushion the secondary geomembrane liner from mechanical tensile stress. The geomembrane will be anchored and support itself on liner system side slopes.

- Secondary LCRS is composed of a 1 foot thick 1×10^{-2} cm/sec permeability granular drainage layer on the landfill base grade, and a 200 mil HDPE geonet on landfill side slopes. Both of these drainage materials are overlain by a 6 oz. per square yard geotextile separation and filtration fabric. The granular drainage material does not present slope stability concerns since it is absent from side slopes. The geonet is used in place of the granular fill and is self supporting within an anchor trench.

- Primary Soil Liner is an eighteen inch compacted soil barrier layer compacted in two distinct lifts. The first lift of soil is placed to obtain a 12 inch soil layer with a maximum permeability of 1×10^{-5} cm/sec. The second lift of soil is placed to obtain a 6 inch soil layer with a maximum permeability of 1×10^{-7} cm/sec. The specified compaction of the initial 12 inch lift is minimized to alleviate concerns of damaging the underlying geosynthetic materials. Placement of the primary soil liner is limited to the landfill base grade; therefore, this layer does not pose any slope stability concerns.

- Primary Geomembrane Liner is a 60 mil HDPE liner placed in direct contact with either the primary soil liner (landfill base grades) or the secondary LCRS (landfill side slopes). On liner system side slopes the primary geomembrane liner completes a geosynthetic "sandwich" comprised of two 60 mil geomembranes, a geotextile layer and a geonet layer. The stability of these geosynthetic materials is maintained during deployment by securing them within a geomembrane anchor trench as shown on Figure No. 1.

- Primary LCRS is a two foot thick granular soil layer with a minimum permeability of 1×10^{-3} cm/sec. The primary function of this layer is to promote rapid lateral drainage. On side slopes this layer overlies the previously deployed geosynthetic materials. The placement of this layer requires slope stabilization measures which will ensure that effective drainage and protection is maintained and geomembrane liners are not excessively stressed in an area of the landfill where double composite protection is absent.

- Protective Soil Liner is a six inch thick SM type soil layer placed above and separated from the primary LCRS by a 6 oz. per square yard geotextile fabric. This soil layer promotes runoff, liner system protection, slope stabilization and reduces leachate collection quantities by reducing the percolation (prior to waste placement) into the primary LCRS.

Collectively, all liner system components described above comprise a containment system which is 7.5 feet thick over landfill base grades and 4.5 feet thick on landfill side slopes. This system will serve as a highly efficient hydraulic barrier, but requires the Design Engineer to thoroughly analyze side slopes for cover soil stability and geomembrane liner tensile stresses. The techniques used to evaluate these side slope concerns are discussed in the subsequent sections of this paper.

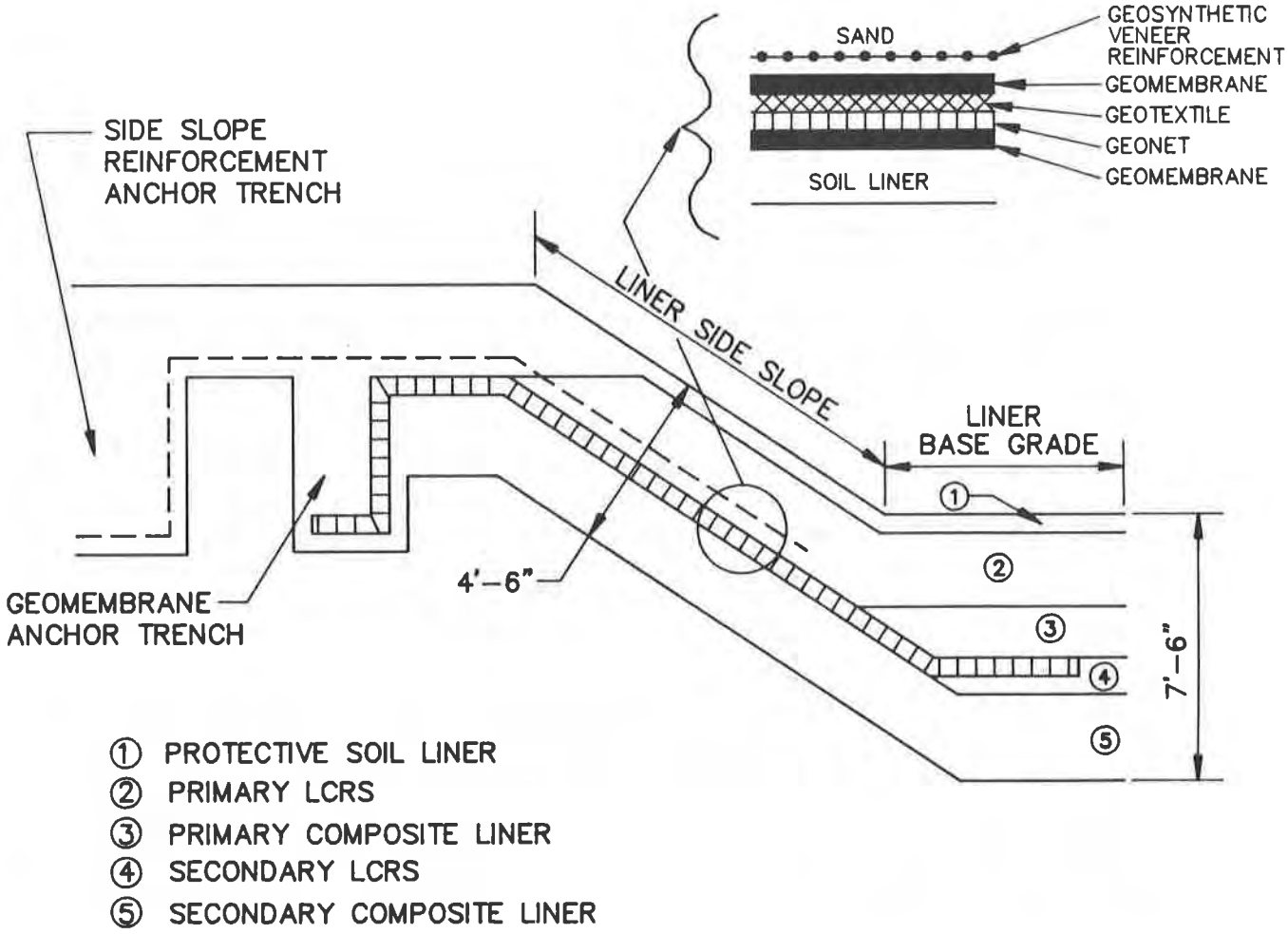

Fig.1 Landfill Liner System

PRELIMINARY SLOPE STABILITY EVALUATION

A preliminary evaluation of slope stability was performed for the multi-layered liner system described above. The evaluation involved computing the factor of safety for each soil-to-geosynthetic and geosynthetic-to-geosynthetic interface based on an infinite slope analysis. Table 1 shows the various possible slope material interfaces for the specific side slope design interface friction angles, and resultant factors of safety. The factors of safety were computed using the equation below.

$$F.S. = \tan \phi_i / \tan \beta \qquad (1)$$

Where: F.S. = the Factor of Safety
ϕ_i = the interface friction angle
β = the landfill side slope angle

TABLE 1

Factors of Safety for Selected Landfill Side Slope Interfaces
Based on a 3 Horizontal to 1 Vertical Slope Angle

Side Slope Interface	Interface Friction Angle	Factor of Safety
Compacted Soil/Geomembrane	15	0.80
Geomembrane/Geonet	10	0.53
Geonet/Geotextile	14	0.75
Geotextile/Geomembrane	9	0.48
Geotextile/Sand	>25	>1.40
Geomembrane/Sand	18	0.97

Review of Table 1 and the computed factors of safety shows that concerns for slope stability are warranted if slope stability is based entirely on interface friction and slope inclination. More importantly, however, this simple analysis identifies that a critical slope interface lies between the primary geomembrane and an underlying nonwoven geotextile. The side slope configured in this manner induces an unfavorable shear stress condition where shear stress below the liner (T_B) is lower than shear stress above the liner (T_A). This shear stress condition creates geomembrane tensile stress, and effectively forces the geomembrane to perform as a structural component of the liner system. Although a stable liner system could be designed under this shear stress condition, it would require the imposition of an unacceptable slope geometry. Therefore, an alternate design solution using additional geosynthetic materials was implemented.

The design requirement was a side slope liner system which provided the following shear stress condition:

$$T_A \leq T_B \qquad (2)$$

Where: $T_A = C_{aA} + (W \cos \beta) \tan \phi_{iA}$
$T_B = C_{aB} + (W \cos \beta) \tan \phi_{iB}$
$W = \delta hL$
δ = cover soil unit weight
h = cover soil thickness
L = slope length
β = slope angle
C_a = liner adhesion, in lbs/ft (assumed, 0 for design purposes)
ϕ_i = interface friction angle

One approach which appeared very attractive was to use textured high density polyethylene (Textured HDPE) geomembrane. The frictional resistance of this material against a nonwoven geotextile will exceed that of the overlying primary LCRS sand; therefore, the expression above (Equation 2) would be satisfied. In addition, Textured HDPE would provide a factor of safety at the primary LCRS sand interface of approximately 1.5 using Equation (1). However, the ability of the Texture HDPE to "lock" with the underlying nonwoven geotextile only results in the movement of the shear plane downward to the next geosynthetic interface. The interface friction angle between nonwoven geotextile and geonet has been shown to be approximately equal to the geomembrane and nonwoven geotextile interface friction angle. In fact, this interface friction resistance can be carried one step further through the use of a heat laminated geocomposite where nonwoven geotextile is bonded to geonet. This effort would only move the shear plane from the geotextile and geonet interface to the geonet and secondary geomembrane interface. Again, a T_A greater than T_B condition would develop.

Clearly there was a need to support the liner system cover soils in a manner which would effectively limit any structural support from the primary geomembrane liner. With the design problem defined in this manner, the landfill side slope design presented in the subsequent section has been utilized.

LINER SYSTEM SIDE SLOPE DESIGN

To resolve geomembrane tension concerns, a nonwoven geotextile was placed above the primary geomembrane as shown in Figure 2A. The inclusion of this material serves two functions. First, the geotextile creates a T_A less than or equal to T_B shear stress condition, and second, it provides a cushion which will buffer the geomembrane liner from mechanical tensile stress during construction.

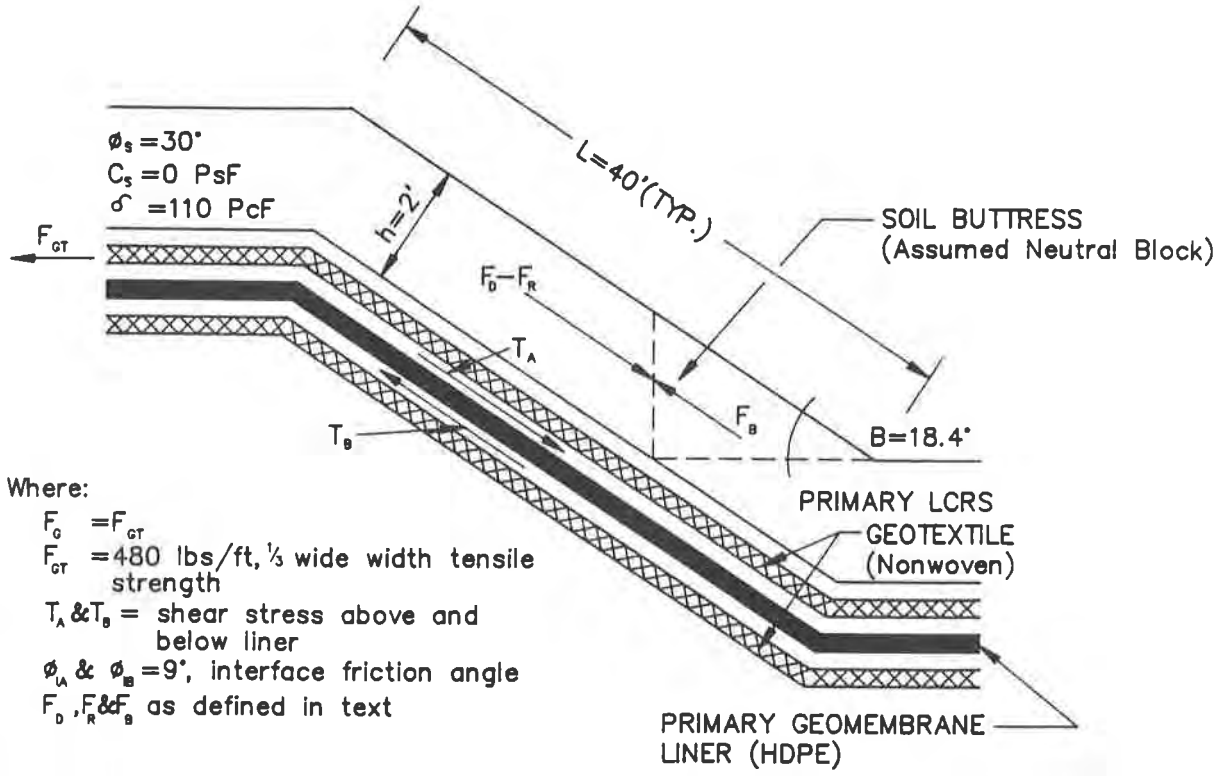

Fig. 2A Engineering Design Parameters and Acting Forces – Unreinforced Side Slope

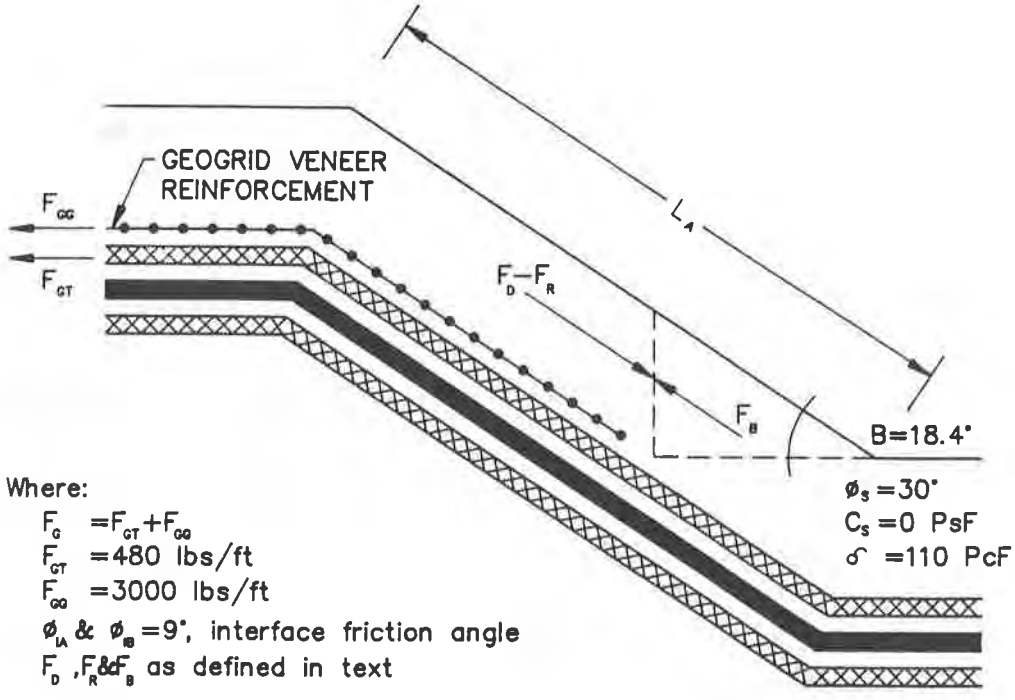

Fig. 2B Engineering Design Parameters and Acting Forces – Geogrid Reinforced Side Slope

It is the primary function of the geotextile which effectively minimizes the tensile stress in the primary geomembrane. An examination of the equilibrium equation presented below serves to demonstrate this effectiveness. All design parameters are shown in Figure 2A.

$$F_D = \frac{F_R + F_G + F_B}{F.S.} \qquad (3)$$

Where: F.S. = Factor of Safety
F_D = $\delta hL \sin \beta$, which is the driving force
F_R = $\delta hL \cos \beta \tan \phi_i$, which is the frictional resisting force to sliding or upper shear stress (T_A)
F_G = allowable wide width tensile strength of the structural geosynthetic liner system component(s)
F_B = $\cos \phi_S / \cos(\phi_S + \beta)\ [(h/\cos \beta)C_S + (\delta h^2/\sin 2\beta)\tan \phi_S)]$, which is the buttress force of the cover soil (2)
C_S, ϕ_S = soil strength parameters

The term F_R is the value which must be balanced with the shear stress below the liner (T_B) to alleviate geomembrane tensile stress for the given side slope design. By inspection of this term as defined, it is intuitively obvious, for a given slope angle and cover soil layer, that the shear stress above the liner is controlled by the interface friction angle (ϕ_i). By lowering the interface friction angle the frictional resistance is reduced which results in the minimizing of tensile stress in the primary geomembrane.

Table 2 below compares geomembrane tensile stresses developed between smooth and textural HDPE geomembrane for several selected interface friction surfaces. Review of the values computed shows that geomembrane tensile stress may be alleviated for the liner system previously detailed by placing a nonwoven geotextile above the primary geomembrane liner.

TABLE 2
Geomembrane Tensile Stress Comparison as a Function of Boundary Interface Friction Angles

Geomembrane Type	Overlying Material	Overlying Interface Friction Angle (ϕ_{iA})	Underlying Interface Friction Angle (ϕ_{iB})	Geomembrane Tensile Stress (lbs./ft.)
Textured HDPE	Sand	30°(1)	9°	6,857
Textured HDPE	Sand/GT	25°(1)	9°	5,040
Smooth HDPE	Sand	18°	9°	2,726
Smooth HDPE	Sand/GT	9°	9°	0

(1)Effective ϕ_{iA}, interface friction limited by overlying materials

Geomembrane tensile stress values presented in Table 2 were computed using the equation given below after Koerner (2).

$$G_T = [\delta\ h \cos\beta\ (\tan\phi_{iA} - \tan\phi_{iB})]L \qquad (4)$$

Where: G_T = geomembrane liner tension in lbs./ft.
δ = unit weight of cover soil material in lbs./ft.^{3}
h = cover soil thickness in feet
β = slope angle
$\phi_{iA,B}$ = interface friction angle above and below geomembrane
L = length of liner system slope

The inclusion of the nonwoven geotextile promotes a favorable geomembrane shear stress condition, but it also places greater demands on the two other slope support terms F_G and F_B from Equation 3. To demonstrate liner side slopes stability, it was necessary to first analyze the slope conditions illustrated by Figure 2A and determine the factor of safety when support is provided by the optimized shearing resistance (F_R), nonwoven geotextile wide width tensile strength (F_G) and soil buttressing (F_B). Using Equation 3 and inserting the definitions for the various terms the factor of safety may be expressed as:

$$F.S. = \frac{(\delta hL \cos\beta \tan\phi_i) + F_G}{\delta hL \sin\beta} + \frac{\cos\phi_S/\cos(\phi_S+\beta)[(h/\cos\beta)C_S + (\delta h^2/\sin 2\beta)\tan\phi_S]}{\delta hL \sin\beta} \qquad (5)$$

Using the design and engineering parameters as defined in Figure 2A and a wide width geotextile tensile strength of 120 pounds per inch a factor of safety of only 0.84 is calculated. Since a minimum factor of safety greater than unity is desired, additional slope reinforcement was required.

A uniaxial HDPE geogrid was selected, and the following design calculation utilized in determining the amount of obtainable slope reinforcement from one layer of material. Again, utilizing Equation 3, the terms as defined, were inserted and the equation was solved for slope length (L) yielding the following equation:

$$L_a = \frac{F_B + F_G}{h\delta\ [(F.S. \sin\beta) - (\cos\beta \tan\phi_i)]} \qquad (6)$$

Where: L_a = allowable slope length
$F_G = F_{GG} + F_{GT}$
F_{GG} = geogrid wide width long term tensile strength
F_{GT} = 1/3 geotextile wide width tensile strength
All other variables previously defined

Computing L_a from this equation gives the allowable slope length which may be supported by the specified geogrid. Using a factor of safety of 1.25, a geogrid long term tensile strength of 3,000 pounds per foot at less than 10 percent strain, and the design parameters as defined in Figure 2B, an allowable slope length of approximately 75 feet may be computed using Equation (6). Actual side slope lengths at each landfill facility are less than the above computed allowable length.

A final component of the landfill liner system is a nominal six inch thick protective soil liner placed above the primary LCRS. This soil layer serves as an effective operations layer as well as a slope stabilization layer. The glacial till soil specified develops significant shear strength with minimal compactive effort, (i.e., tracked in by dozer and smooth drum rolled) and placement above the primary LCRS ensures that drained soil conditions are maintained. The addition of this layer also minimizes the amount of incident rainfall that enters the primary LCRS which may, under intense storm conditions, cause seepage failure of the sands and/or gravel which comprise the primary LCRS. A stability analysis using Morgenstern and Price's method gives a factor of safety equal to 1.77 for a maximum allowable slope of 75 feet (4). This is an increase of 0.52 in the factor of safety by virtue of placing the protective soil liner component.

The geogrid and nonwoven geotextile veneer reinforcement system as designed will have additional benefits during the operational life of the landfill. Both of these materials will reduce geomembrane stresses resulting from waste placement and subsequent settlement since shear stress relaxation will occur above the primary geomembrane. Shear stress induced by waste settlement will be released either by yielding of the geogrid and geotextile or shearing within the primary LCRS and/or protective soil liner. Shear stress relaxation in these materials will not result in any reduction in liner system efficiency and is therefore acceptable.
Effectively, veneer reinforcement materials become sacrificial tensile stress release materials upon waste placement, assuming proper waste placement sequences are specified by the Designer Engineer and observed by the Owner/Operator of the landfill facility.

SUMMARY

This paper illustrates the "design by function" concept whereby the Design Engineer focuses on the primary function of each particular liner system component and assures that this function is not compromised by other design concerns. Landfill liner side slopes present the Design Engineer with the formidable problem of providing stable slope conditions without jeopardizing hydraulic efficiency of the liner system. It has been shown that the design by function concept applied directly in rendering an appropriate solution to the side slope problem presented.

The specific design presented emphasizes the importance of evaluating shear stress conditions above and below geosynthetic liners. It has been shown how a favorable shear stress above the liner, less than or equal to the shear stress below the liner, condition may be achieved, thereby minimizing geomembrane tensile stress. The minimization of geomembrane tensile stress is likely to have far reaching advantages including long term sheet and seam service life, and enhanced prevention of unacceptable liner system leakage rates, which could result in premature landfill cell closure.

The design by function concept was then utilized to establish a slope stability analysis for the selection of a reinforcement material for support of specific cover soil conditions. The calculations presented result in the selection of a geogrid with a long term wide width tensile strength of 3,000 pounds per foot at less than 10 percent strain. The geogrid tensile strength plus the tensile strength of a heavy nonwoven geotextile and the shear strength of the cover soils (buttress effect) were shown capable of supporting a 75 foot slope length and maintain a 1.77 factor of safety.

Lastly, with ample cover soil support provided and an acceptable geomembrane shear stress condition established, the Design Engineer has successfully produced a liner system where the critical geomembrane component of the liner system functions as it is intended, which is as a hydraulic barrier and not as a structural support material.

REFERENCES

1. Koerner, R. M., Designing with Geosynthetics, 2nd Edition, Prentice Hall Publ. Co., Englewood Cliffs, NJ, 1990.

2. Koerner, R. M., Hwu, B., "Stability and Tension Considerations Regarding Cover Soils on Geomembrane Lined Slopes", Design Seminar sponsored by NYSDEC, SUNY Albany and USEPA at Univ. at Albany, August 8-10, 1990.

3. Martin, J. P., Koerner, R. M. and Whitty, J. E., "Experimental Friction Evaluation of Slippage Between Geomembranes, Geotextiles and Soils", Proc. Inlt. Conf. on Geomembranes, IFAI, Denver, CO, 1984.

4. Morgenstern, N. R. and Price, V. E., "The Analysis of Stability of General Slip Surfaces", Geotechnique, Vol. 15, No. 1, 1965.

5. Williams, N.D., Houlihan, M., "Evaluation of Friction Coefficients Between Geomembranes, Geotextiles and Related Products", Proc. Inlt. Conf. on Geotextiles, Vienna, Austria, 1986.

Structural Geogrids Used to Stabilize Soil Veneer Covers

Vicky E. Chouery-Curtis
Tensar Environmental Systems Inc., USA
Stephen T. Butchko
Tensar Environmental Systems Inc., USA

ABSTRACT

When geosynthetics are utilized for containment, drainage and filtration, a protective soil veneer cover is required on top of the lining or cover system to reduce the potential of construction, down drag effect, and weather induced damages. The stability of the soil veneer cover and thus, the steepness of the sides slopes can be controlled by the critical interface friction angles between the different geosynthetics and various soil layers.

Steeper sides slopes can be realized, without compromising stability by using structural geogrids to support the weight of the soil veneer cover and lower the total load on the underlying critical geosynthetic plane. The paper will summarize the advantages of a geogrid reinforced soil veneer cover, and will briefly discuss the simplified method of analysis, and some construction related problems. A brief case study will be presented.

INTRODUCTION

Over the past couple of years, several sliding failures occurred at various waste containment facilities throughout the United States. One of the factors common to most of the sliding failures was the low interface friction angle between the various geosynthetic components of the lining system. The excessive number of failures prompted the engineering community to further evaluate the potential and causes of sliding failures.

To meet the new regulations, most waste containment facilities are being lined with a double or a composite lining system. Final caps typically consist of a single lining system. A thin layer of soil approximately 18 to 36 inches thick is placed along the sides slopes of a cell or a final cap to protect the underlying lining system against weather and/or construction induced damage. However, when two different materials (soil/geosynthetic or geosynthetic/geosynthetic) are placed next to each other, the analysis and performance of interface friction is critical and should be carefully assessed. Most sides slopes and final covers are typically built

at approximately 4H:1V (14.3^0) to 3H:1V (18.4^0) slope angles. Fig. 1 shows typical cross-section of lining and cap systems.

The interface friction angle between all the different components of a lining system should be compared to the proposed slope angle. The interface friction angle can be as low as 7 or 8 degrees. Yet, we are trying to construct our side slopes up to 14^0 or steeper. If the component interface friction is less than the slope angle, there is a potential for a sliding failure to occur along the critical interface which can result in rupture and/or creep failure of one or more components of the lining system.

POTENTIAL STABILITY PROBLEMS

Stability is one of the primary issues for lining and cap systems where the slope angle often range from 4H:1V up to 2.5H:1V. Interface angle between adjacent geosynthetics or between soil layers and geosynthetics typically range from 8 to 25 degrees. The combination of low interface friction angle and steep side slopes creates potential slip surfaces that can cause instability of the cover system. If the component interface friction is less than the slope angle, there is a potential for a sliding failure along the critical interface. Slippage within the lining system will result in excessive tensile stresses in the geosynthetic components above the critical plane. This may result in unacceptable straining or creep failure of one or more components of the lining system.

If the soil veneer cover placed along the side slopes of a cell begins to slide down the slope, there is a potential for rupturing of the underlying geosynthetic layers. Fig. 2 illustrates an example of downslope movement that resulted in rupturing of the underlying Flexible Membrane Liner (FML). Depending on the sequence of construction and waste placement, a more severe or excessive sliding failure can occur along the sides slopes of a partially filled cell.

If the soil cover layer placed along the sides of a final cap begins to slide downslope, there is potential for tension cracks to develop. Formation of tension cracks will increase percolation through the soil veneer cover. A significant increase in the flow can result in build-up of hydrostatic pressure which will exacerbate the instability of the soil veneer cover leading to a progressive failure.

REINFORCED SOIL VENEER COVER

A reinforced soil veneer cover is one that is stabilized using high-strength, low deformation structural tensile element that is capable to interlock with the surrounding material developing a composite system. The tensile element which is a structural geogrid is required to support the weight of the soil veneer cover layer and prevent potential downslope movement. By interlocking with the surrounding soil,

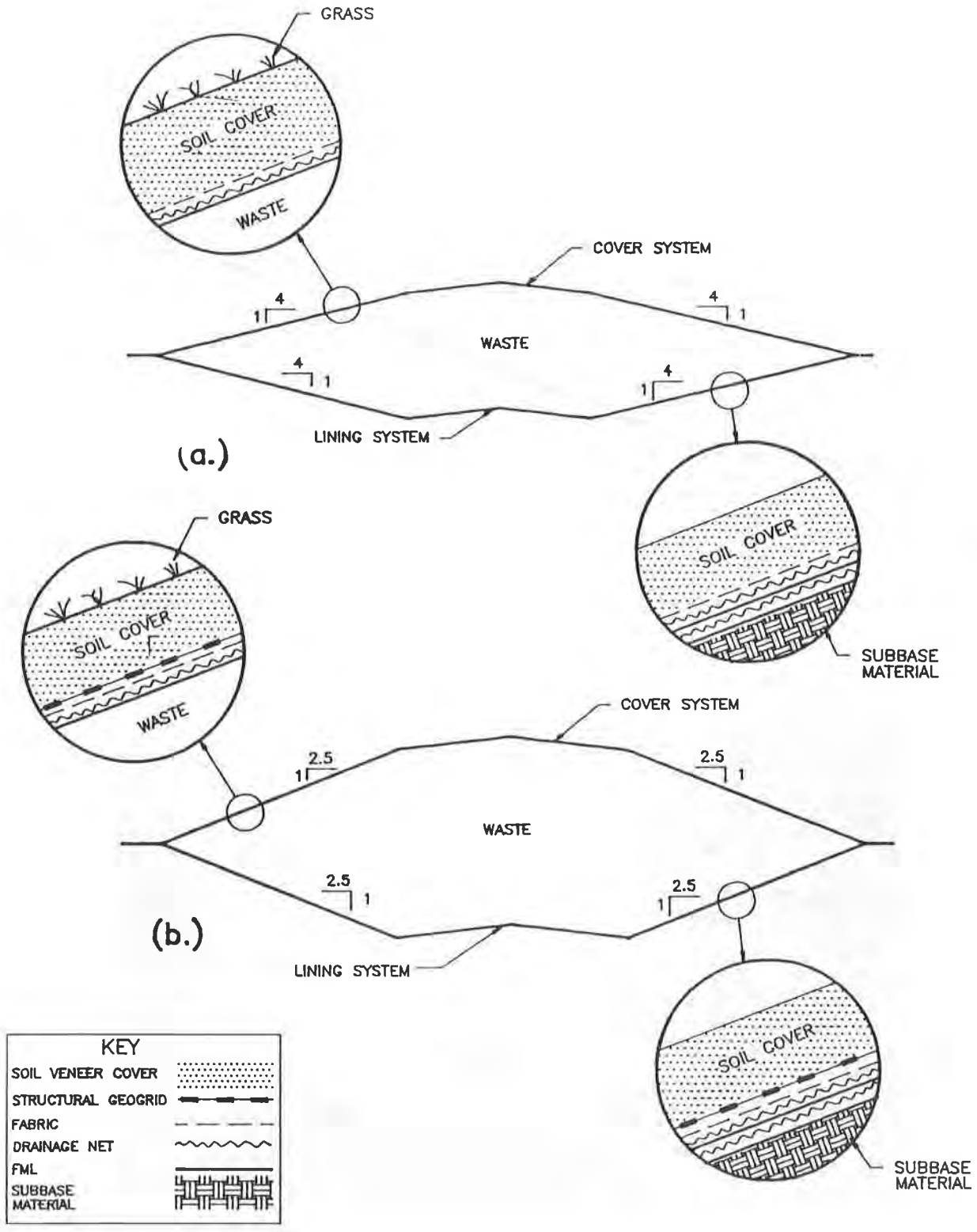

FIGURE 1: COMPONENTS OF LINING AND CAP SYSTEMS

(a) Unreinforced Alternative
(b) Reinforced Soil Veneer Covers

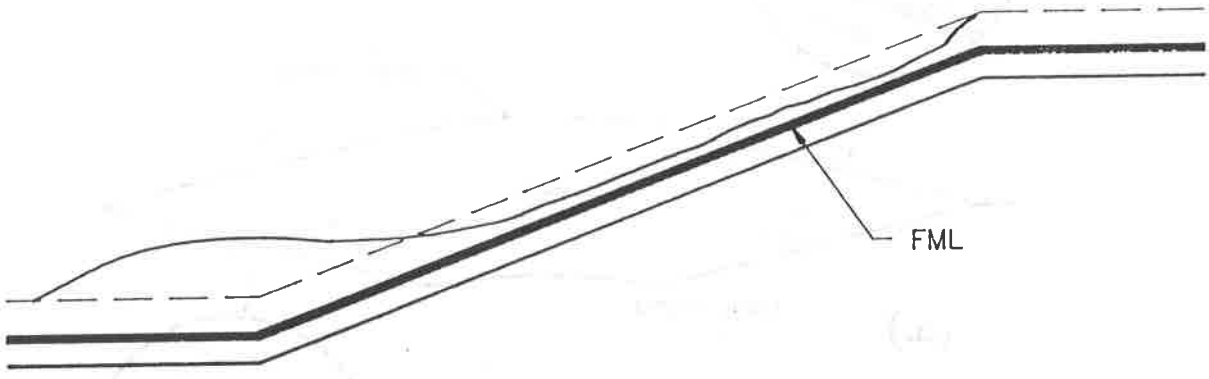

(a.)

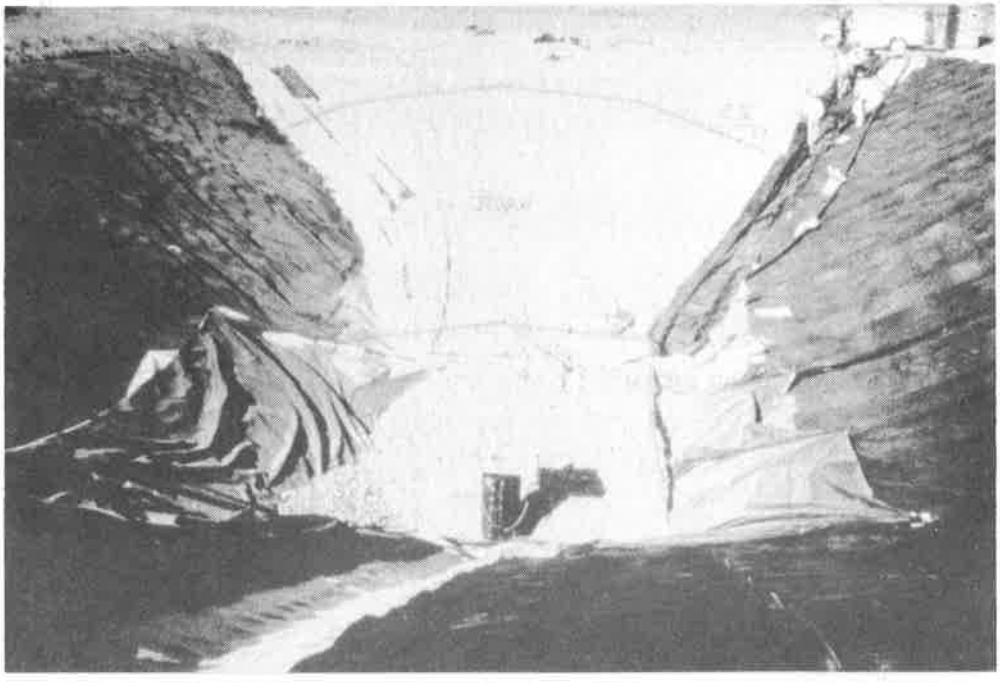

(b.)

FIGURE 2: EXAMPLE OF SLIDING FAILURES

(a) Typical Cross-section
(b) Actual Sliding Failure and Rupturing of Underlying FML

the structural geogrid will provide the additional resisting force required to minimize the potential for sliding failures. Downslope movements can result in overstressing of the geomembrane and/or the leachate collection layers. Overstressing of any of the geosynthetic components can lead to an eventual failure of the lining system. The use of a structural geogrid can increase the factor of safety against potential sliding failures and most importantly can protect the long-term integrity of the lining or cap systems.

COMPONENTS OF GEOGRID REINFORCED SOIL VENEER COVER.

Figure 1 illustrates the different components of typical unreinforced and reinforced lining and cover systems. For cell construction, a composite or a double lining system can be specified. A typical lining system may consist (from the bottom up) of a compacted subbase layer, a secondary FML, a leak detection drainage net, a primary FML, a leachate collection drainage composite, a structural geogrid and a protective soil veneer layer. Final caps may consist of a single lining system where a FML, a drainage composite, a structural geogrid and a protective soil veneer layer are used. A permanent soil veneer cover is an integral part of the cap system as it provides protection against frost, construction and weather induced damages, and promotes adequate runoff of surface water.

MATERIAL PROPERTIES

Soil: The parameters of the soil cover and subbase material are determined using standard geotechnical engineering procedures. Specifically, the moist unit weight and the effective-stress friction angle should be measured to better determine the critical failure planes. The saturated unit weight should be determined when analyzing saturated conditions.

Critical Interface Angle: The critical interface friction angle between the various geosynthetics materials and/or the soil layers can be estimated for conceptual design purposes, using published data. However the interface angles are product dependent and should be verified based on testing of the proposed materials prior to final design or issue of final specifications. Care should be taken to adequately interpret the test results and understand the difference in the parameters generated. Differences in test results could be due to several reason some of which are as follows: (i) differences in confining pressures applied during the tests, (ii) Saturated vs dry conditions, (iii) test methods and apparatus used, (iv) and interpretations of the test results (i.e) how do test conditions compare to actual field conditions and what is effect of various variables. Designers need to realize that interpretation of the data is crucial for adequate selection of the appropriate design parameters. Table I indicate certain range of values of interface angles between various materials (4, 12, 15). The numbers outlined in Table I can only be used for conceptual assessment of a project.

TABLE I
RANGE OF VALUES OF INTERFACE FRICTION ANGLES*

INTERFACES	FRICTION ANGLE
Geosynthetic/Soil	
Stiff Geogrid/Sand	23^0 to 34^0
HDPE FML (smooth)/Sand	18^0 to 26^0
PVC FML/Sand	20^0 to 28^0
Nonwoven Fabric/Sand	21^0 to 29^0
HDPE FML (smooth)/Clay	12^0 to 19^0
PVC FML/Clay	13^0 to 20^0
Nonwoven Fabric/Clay	14^0 to 22^0
Geosynthetic/Geosynthetic	
Nonwoven Fabric/HDPE FML (smooth)	9^0 to 16^0
Nonwoven Fabric/PVC FML	12^0 to 18^0
Nonwoven Fabric/Drainage Net	10^0 to 16^0
HDPE FML (smooth)/Drainage Net	8^0 to 15^0

*NOTE: The value of interface friction angles are product dependent. Testing is recommended based on project specifics and final intended use of the various geosynthetic products.

Geosynthetic Components: As noted above, a variety of planar, polymer based synthetic materials are commonly utilized in construction of municipal and hazardous waste facilities. These materials are FMLs, fabrics, drainage nets, and geogrids. Although all are polymer based materials, the manufacturing processes and selected resins can vary widely between and within each category. The desired, manufactured properties of the geosynthetics are dictated by their respective functions.

The four categories of geosynthetics commonly used in waste facilities and their primary function are summarized below. All geosynthetics must be resistant to chemical and biological degradation for utilization in waste containment. A FML is used for containment and must have a very low permeability, so as to provide adequate leachate containment for the design life of the structure. A fabric is used for separation and must be capable of passing fluid through it while retaining soil above it. A drainage net is used for drainage and must be able to transmit large flow under high compressive loading. A geogrid is used to provide tensile reinforcement. This function classifies geogrids as structural elements, which is a unique classification, in comparison to the other planar geosynthetics.

Within this paper, the category of geogrids is reviewed in detail. The physical properties of geogrids required for performance in their applications are defined. Comparisons are made on how these functions vary and complement the functions of other geosynthetic material used in waste containment applications.

Geogrids: Geogrids were first introduced into North America in the early 1980's. According to ASTM definition, a geogrid is any planar structure formed by a regular network of tensile elements with apertures of sufficient size to allow interlocking with surrounding soil, rock, earth or any geotechnical material to perform the functions of reinforcement and/or segregation. Geogrids are produced in biaxial and uniaxial load carrying configuration, and were specifically developed for long-term reinforcement of critical soil structures.

Uniaxial geogrids are manufactured from high density polyethylene (HDPE) resins. Even within the families of HDPE resins, there are many differences among their key characteristics which can dramatically affect the performance of the end-products, when used in critical load bearing applications (3, 14). There are several resin characteristics that will affect processing, end-use properties, and performance of a finished product. These resin parameters are: density, melt index, molecular weight, molecular weight distribution, degree of orientation, and chain branching or entanglement (14). Tensile properties and creep strain are significantly affected by the type and composition of the various resins. Testing of various HDPE resins with similar melt indices and densities indicated variations of up to 100% greater creep strain at designated loads after only 1000 hours of creep testing. This is important when critical structures are designed assuming a particular creep strain. The molecular weight and its distribution, as well as the number of chain branches control the creep characteristics. As recognized by polymer chemists, ten thousand (10,000) hour creep testing is the only reliable way to assure that long-term performance is acceptable (1, 2, 14). Figure 3 illustrates typical stress-strain response of structural geogrids.

As a structural element used to reinforce soil veneer cover layers, there are two primary design properties that need accurate definition. Those properties are: i) long-term stress-strain behavior; and ii) junction efficiency. The key word here is long-term. Geosynthetics are polymer based materials which means that they are viscoelastic, i.e. their stress-strain characteristics are time and temperature sensitive.

This structural classification means that the long-term physical properties of geogrids must be accurately defined. The long-term stress-strain relationship should account for time or creep, temperature, installation damage, biological durability, chemical durability, and structural connections. Table II outlines typical chemical compatibility test results performed, per EPA 9090 test method, on an HDPE geogrid immersed in what was classified as the most severe leachate environment encountered in municipal solid waste facilities. Test methods and a standard of practice have been established by the Geosynthetic Research Institute (GRI) at Drexel University to define long-term load carrying capacity of a geosynthetic.

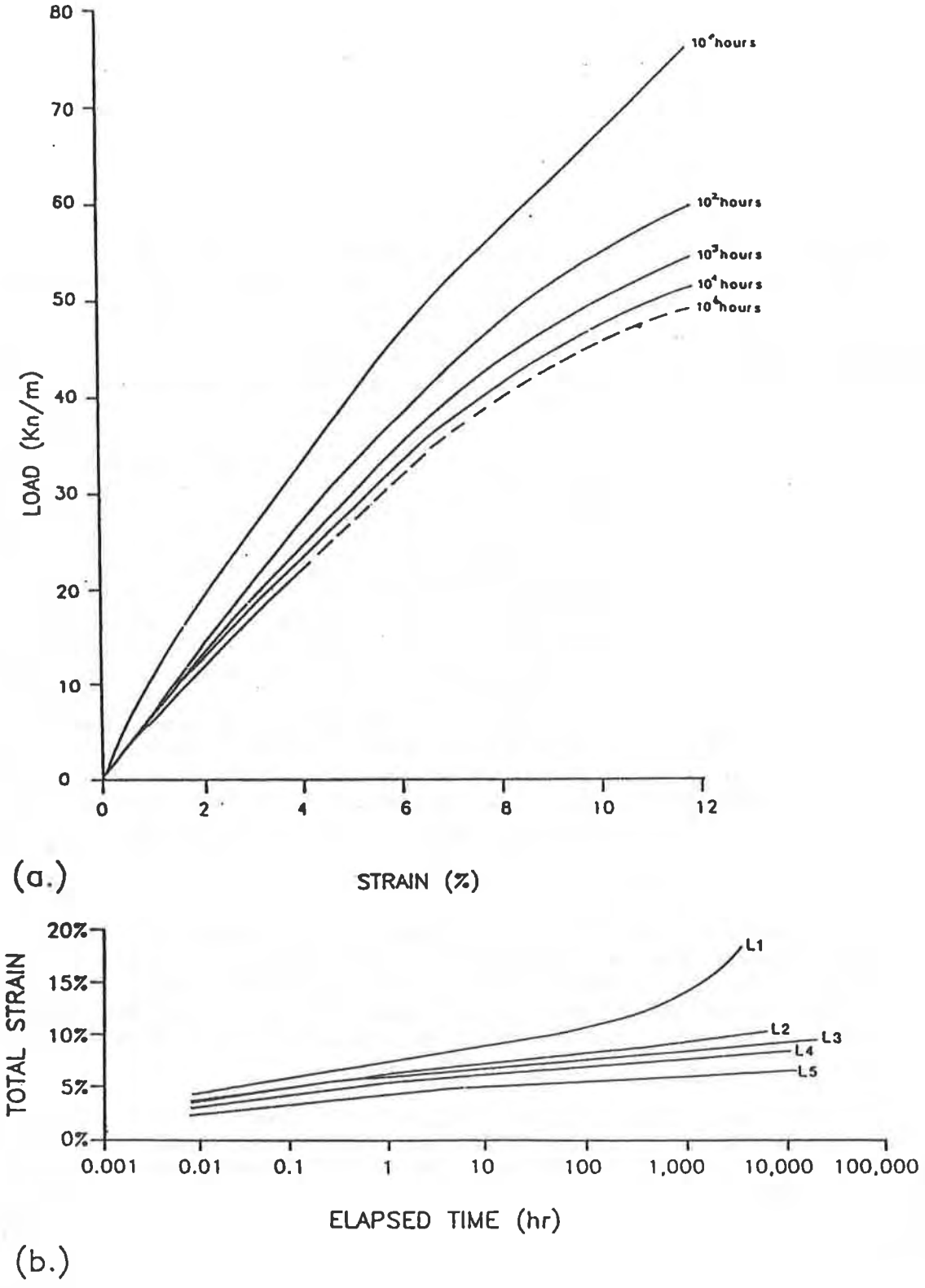

FIGURE 3: TYPICAL STRUCTURAL GEOGRID RESPONSE (4, 5, 6)

(a) Isochronous Load-Strain Curve
(b) Creep Strain vs Time

TABLE II
SUMMARY OF TYPICAL LABORATORY TEST DATA PERFORMED
ON STRUCTURAL HDPE GEOGRID USING EPA TEST METHOD 9090

MECHANICAL PROPERTY	IMMERS. TEMP.	UNITS	INITIAL VALUE	30-DAY VALUE	30-DAY % CHANGE	120-DAY VALUE	120-DAY % CHANGE Initial	120-DAY % CHANGE Prev.
WIDE WIDTH	23	lbs.	2468	2579	4.50	2440	-1.13	-5.65
TENSILE	50		2468	2455	-0.53	2677	8.47	4.86
RIB	23	lbs.	303.7	323.5	6.52	316.8	4.31	0.73
STRENGTH	50		303.7	318.8	4.97	322.3	6.12	2.06
NODE	23	lbs.	268.6	293.5	9.27	288.3	7.33	-5.29
STRENGTH	50		268.6	283.5	5.55	284.5	5.92	-6.04

PHYSICAL PROPERTY	IMMERS. TEMP.	UNITS	INITIAL VALUE	30-DAY VALUE	30-DAY % CHANGE	120-DAY VALUE	120-DAY % CHANGE Initial	120-DAY % CHANGE Prev.
DIMENSIONS (Ave. both dir)	23				0.00		0.00	
	50				0.00		0.00	
THICKNESS	23				0.00		0.00	
	50				0.00		0.00	
MASS	23				0.17		-0.12	
	50				-0.44		-0.13	
SPEC.GRAVITY	23		0.9658	0.9719	0.63	0.9727	0.71	
	50		0.9658	0.9731	0.76	0.9689	0.32	
DENSITY	23		0.9634	0.9695	0.63	0.9715	0.84	
	50		0.9634	0.9707	0.76	0.9665	0.32	
VOLATILES	23		0.32	0.23		0.74		
	50		0.32	0.20		0.23		

Creep behavior of geosynthetics is a complex phenomena that is a function of specific resin type, polymer composition, manufacturing process, geometric configuration and temperature (1, 2). However creep tests are the only reliable criteria for determining allowable geosynthetics tensile strength (1, 2). It has been shown that short-term tensile tests do not, and thus should not be used to, predict long-term rupture performance (1, 2, 9).

Figure 4 (a & b) illustrates the potential of creep failures after only 1000 hours of creep testing of an HDPE geomembrane and a high strength woven geotextile, respectively. The maximum applied constant load was approximately only 40% of the ultimate tensile load for all geosynthetics considered. In contrast creep testing

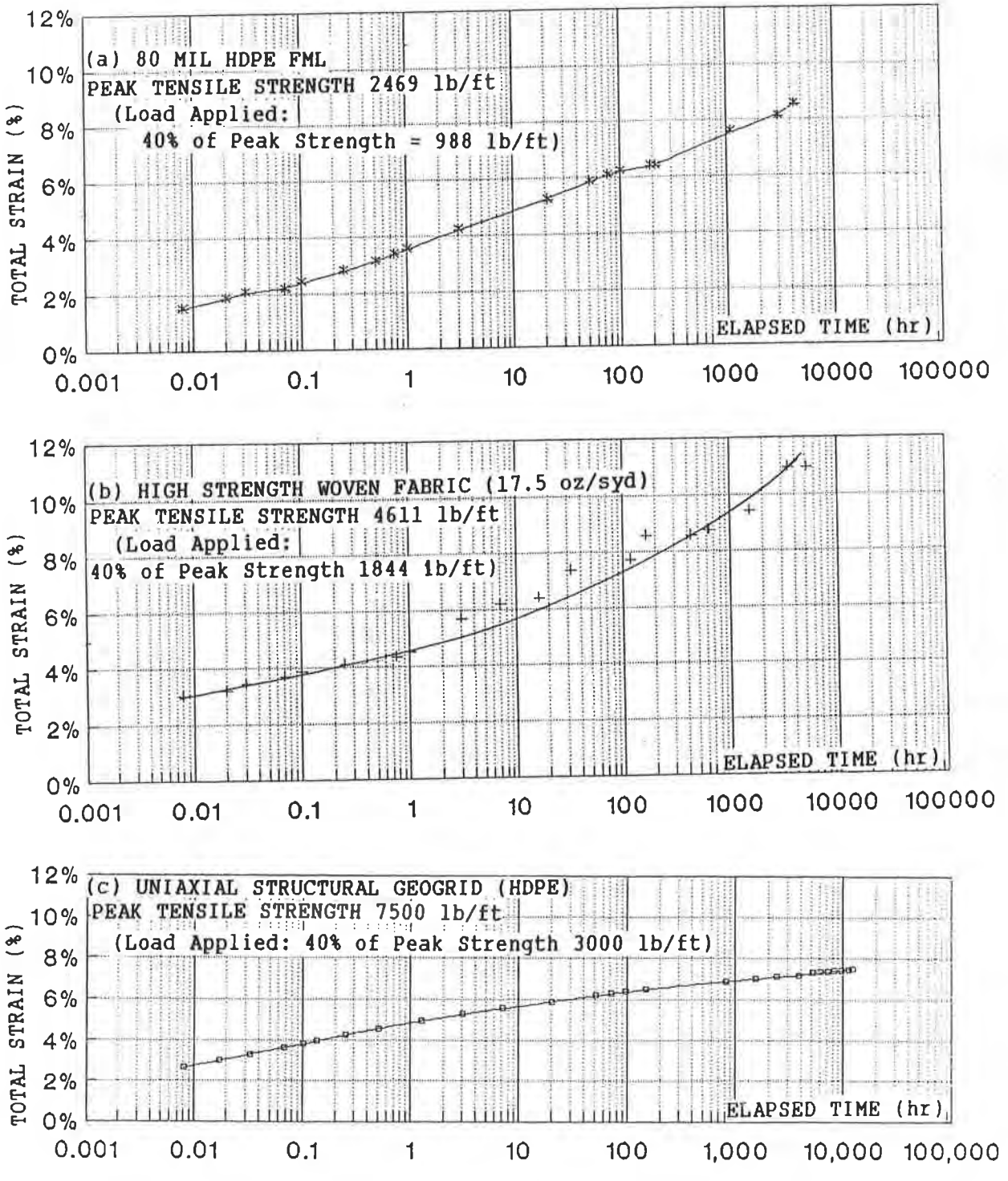

FIGURE 4: CREEP DATA FOR (a) HDPE FML (b) HIGH STRENGTH WOVEN FABRIC AND (c) HDPE STRUCTURAL GEOGRID

of HDPE structural geogrid (see Figure 4c) shows adequate response even after 10,000 hour testing. Notice the total strain variation between the structural geogrid (4c) and the other geosynthetic (4 a & b).

The GRI Standard of Practice GG4 "Determination of the Long-Term Design Strength of Stiff Geogrids" addresses all the above noted variables which should be accounted for in determining long-term load carrying capacity (9). Furthermore, it references specific test methods or provides procedures for definition of these variables. Minimum creep testing of 10,000 hours is required, per GRI:GG3 "Tension Creep Testing of Stiff Geogrids" (8). The 10,000 hrs. creep testing should be performed through the junctions as opposed to the ribs only. This data may be extrapolated one order of magnitude, per polymer engineering rule of thumb (reference ASCE manual 63), to a design-life of approximately 10 years. Creep performance for longer design lives may be defined with accepted polymer extrapolation techniques such as time-temperature superposition for up to two orders of magnitude shift from actual test data (3, 16).

The junction efficiency of structural geogrids ensure adequate load transfer from the ribs through the junction to the adjacent ribs (10). It is crucial to ensure full tensile strength transfer from the ribs through the junctions to the adjacent ribs. Failure to do so will require reduction of the allowable long-term tensile strength as specified in GRI-GG4.

Connections in geosynthetics could be the weak link in the chain. Uniformity of the geogrid structure is essential to prevent stress concentration and provide continuity of the geogrid's tensile strength through the connections utilized at roll ends. A mechanical joint referred to as Bodkin connection (5), is normally used to connect structural geogrids at roll ends. Failure to ensure adequate connections will require further reduction of the allowable tensile strength used for final design.

APPLICATIONS

A protective soil veneer cover layer is required on top of lining systems placed along the side slopes of a cell or along the sides slopes of a final cap. Using a structural geogrid to reinforce soil veneer covers provide several benefits. The construction of stable steep side slopes (2.5H:1V) present an economical solution. By steepening the side slopes, the useful volume of a cell is increased within the permitted boundaries. At the same time, the volume of fill required to construct the side slope is significantly decreased resulting in additional cost savings. And finally the integrity and long-term performance of the lining system can be improved and protected.

Cell Construction: Eighteen to 24 inches thick soil veneer cover layer are typically specified to be placed along the side slopes of a cell. The soil veneer layer is necessary to protect the lining system against construction and weather induced damages. Placement and compaction of the veneer cover is directly related to the soil type used and the final slope angle. To reduce potential sliding failure a structural geogrid is used to reinforce the soil veneer cover layer thus minimizing

transfer of undue stresses and strains to the underlying geosynthetics layers. In addition to improving the long term integrity of the lining system, the use of a geogrid layer permit placement of the soil veneer layer over the full length of the slope, thus minimizing potential construction and weather induced damages to the lining system.

Final Caps: A soil veneer cover layer is an integral component of the final cap. Based on various state regulations a soil veneer layer 18 to 36 inches thick is specified to protect the underlying lining system. A minimum of six inches of topsoil is specified to promote a vegetative cover, prevent erosion and ensure adequate run-off. Depending on the slope angle, maximum slope length, type and thickness of the soil cover and the critical interface angle, the final cap may be unstable. Structural geogrids are used to provide an additional resisting force and thus minimize potential sliding problems.

Containment Berms: With the new regulations (New York State Mandate 27, December 1990), existing and new tank farms should have a contained area around each tank that has a capacity equal to 1.5 times the capacity of the tank. However some of the existing tanks have limited space constraints. To meet the new regulations, several containment berms have to be constructed with very steep side slopes. To minimize potential sliding problems a structural geogrid is used to reinforce the soil veneer cover placed along the sides slope of containment berms and dikes.

DESIGN OF REINFORCED SOIL VENEER COVERS

It is advantageous to construct steep slopes to maximize the storage volume within the permitted land area. However, the interface friction angle between adjacent geosynthetics and/or between a geosynthetic and the surrounding soil is often lower (8^0 to 16^0) than the proposed conventional slope angle (14.3^0 TO 18.4^0). The interface angle between the various components of the lining system should be compared to the friction angle of the cover soil and to the proposed slope angle. If the component interface angle is less than the slope angle, there is a potential for a sliding failure along the critical interface. Typically, the frictional resistance between the drainage net and the FML controls the analysis. Slippage within the lining system, will result in excessive tensile stresses in the geosynthetic components placed above the critical plane. This may result in unacceptable strain or even creep failure of one or more components of the lining system.

These tensile forces can be minimized by flattening the side slopes, or by decreasing the driving force, which is related to the weight of the soil veneer cover. Flattening the slope angle is not a desirable option, particularly since the primary goal is to increase capacity of disposal facilities. Furthermore, it is not always possible to flatten the side slopes or decrease the thickness of the protective soil

veneer cover layer. Design requirements are typically mandated by State Regulatory Agencies (13). It is essential to prevent potential downslope movement of the soil veneer cover layer. Slippage will result in excessive tensile stresses and unacceptable strain in the various lining system components. Overstressing of any of the geosynthetic components can lead to an eventual failure of the lining system.

Slopes steeper than 2.5H:1V can be realized without compromising stability by using a structural geogrid layer to carry the weight of the soil veneer cover layer. The geogrid is typically placed at the bottom of the soil layer. The geogrid will help carry the weight of the soil veneer layer and provide the required tensile strength necessary to minimize potential slippage. Using a structural element will thereby minimize transfer of the excessive tensile stresses to the underlying components of the lining system. By providing the required tensile strength to resist the driving force, the geogrid will reduce the potential for rupture or creep failure of the various geosynthetic components and will improve the long-term integrity of the lining system.

The most simplified and commonly used design method is based on the rigid block analysis, where the soil layer is assumed to behave as a sliding block (7). Fig. 5 shows the forces and outline the assumptions that are used in the analysis of a reinforced soil veneer cover. Additional forces due to construction loading and snow loads can be easily incorporated in the design. The structural geogrid used to stabilize a soil veneer cover, must have a continuous structure, must provide high tensile strength at low deformation, must fully interlock with the surrounding soil, and must have high junction strength. Particles of soil locked into the grid apertures bear against the transverse bars forming a passive wedge. The effect of the passive wedge is to shift the shear failure plane up into the overlying soil layer. Interlocking and the formation of the passive wedge will result in a series of "mini-tie-backs" (6, 7, 11). Fig. 6 illustrates the formation of passive wedges. Thus the imposed excess stresses are transferred upslope to the anchor zone as opposed to the underlying geosynthetic layers.

Long-term properties must be based on a comprehensive test program of sufficient duration which can be extrapolated to required design lives (>100 years) based on accepted polymer principles. The structural geogrid must provide the required tension at extremely low strain levels. Significant strains would cause unacceptable elongation of the geosynthetics located above the critical interface where slippage would occur. the geogrid can provide the required tensile strength to: (1) resist the imposed stresses, (2) minimize slippage of the soil veneer cover and (3) reduce the potential for creep failure or rupture of the various geosynthetic components.

It is important for a reinforcement material to develop its working strength without significant movements at strain levels that are close to the strain levels at which the soils develop peak strength. The tensile element should be dimensionally stable and posses a high flexural rigidity. The geogrid should be placed fold-free. The uniaxial geogrid should be unrolled with the strong direction along the slope face. Adjacent layers of geogrid can be butted one to another and secured using plastic ties. To prevent pullout failure, the geogrid layer should be secured at the

ASSUMPTIONS:

1– ZERO COHESION AT CRITICAL SLIDING PLANE

2– RIGID BODY ANALYSIS (i.e. ASSUME SOIL COVER BEHAVES AS A SLIDING BLOCK)

3– TOTAL NORMAL FORCES IS RESISTED ON SIDE SLOPES (NEGLECT EFFECT OF RESISTING WEDGE AT TOE OF SLOPE, IF ANY)

4– THERE ARE NO SEEPAGE PRESSURES IN THE PROTECTIVE SOIL COVER LAYER

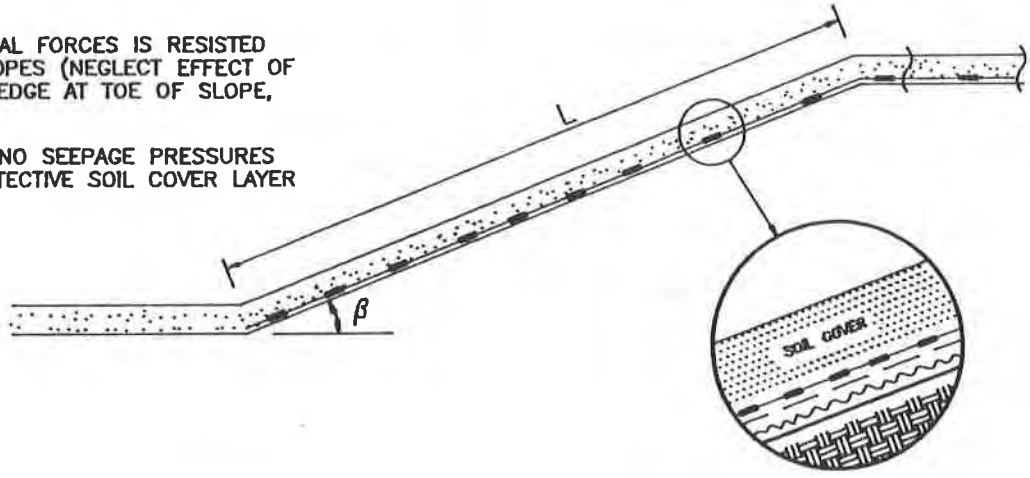

(a.)

T = REQUIRED TENSILE STRENGTH
L = TOTAL SLOPE LENGTH
F_D = DRIVING FORCE
W = WEIGHT OF SOIL COVER
F_F = RESISTING FORCE
β = SLOPE ANGLE
Z = THICKNESS OF SOIL COVER
$F_D = W \sin\beta$
$F_F = W \cos\beta \tan \phi'_c$
$F_R = F_F + T$
ϕ'_c = CRITICAL INTERFACE FRICTION ANGLE

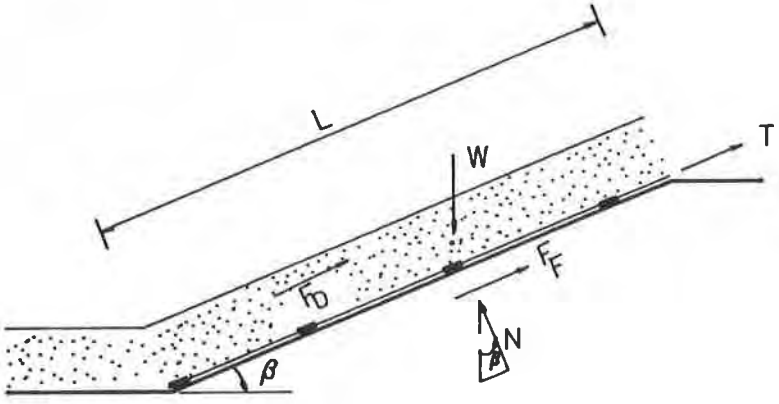

(b.)

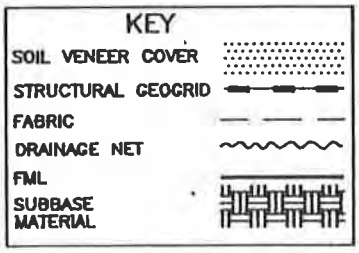

FIGURE 5: ASSUMPTIONS AND EQUATIONS USED WITH THE STATIC BLOCK ANALYSES (7)

(a) Assumptions
(b) Equations

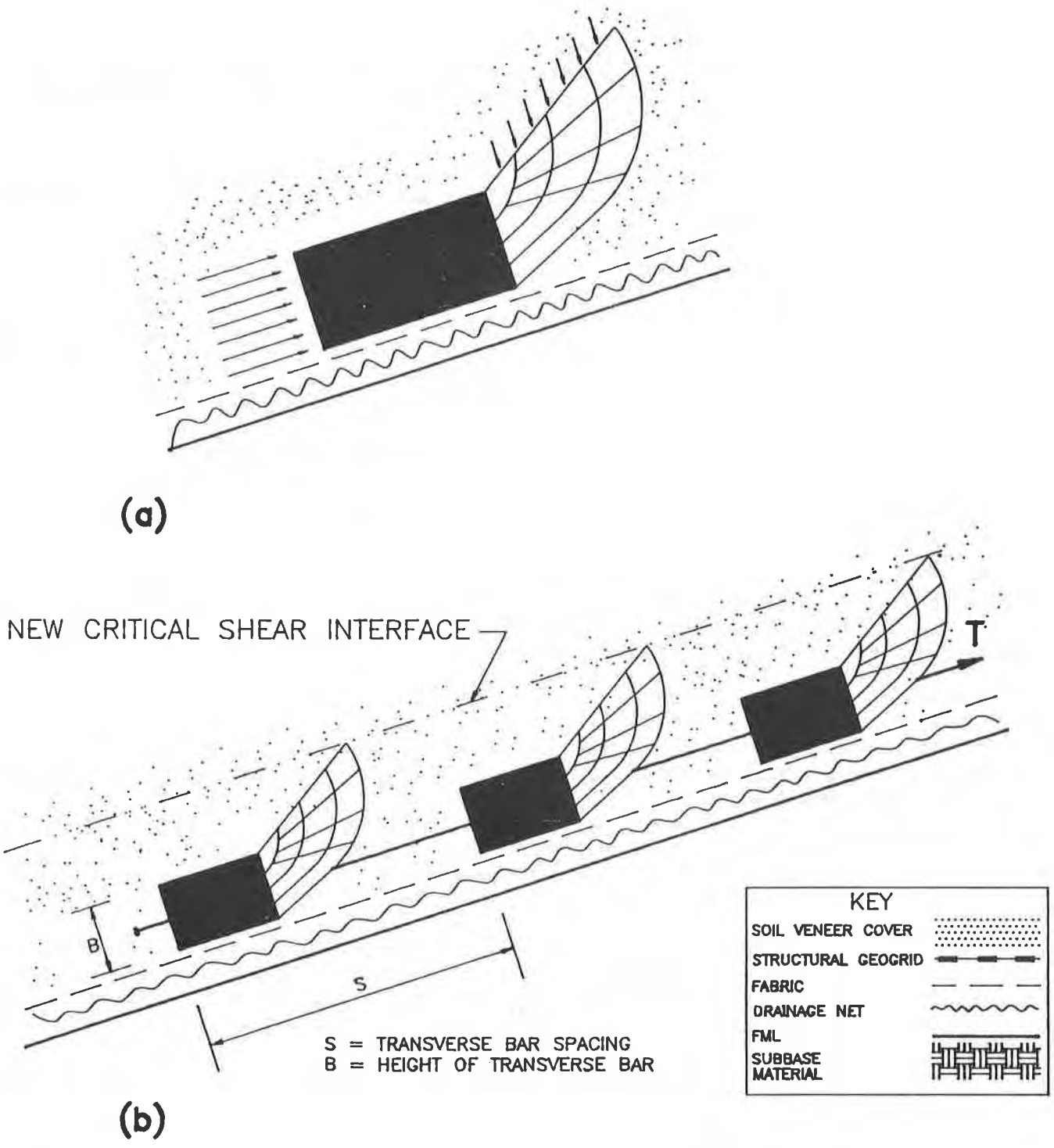

FIGURE 6: TIEBACK EFFECT WITH STRUCTURAL GEOGRIDS

(a) Formation of Passive Wedge
(b) Series of Geogrid Bars (After Jewell 1984)

top of the slope. Anchoring of the geogrid can be accomplished by either embedding the geogrid in a layer of soil or using an anchor trench. Care should be taken to adequately determine the required thickness of the soil cover layer to be placed on top of the anchored area.

A brief case history is presented to best illustrate the use of structural geogrid to support the weight of a protective soil veneer cover layer and minimize potential sliding problems.

A composite double lining system was proposed and built for a Solid Waste Landfill in New York State. The final cross-section consisted (from bottom up) of a 2 foot thick subbase layer, a textured HDPE FML, a drainage composite, a primary textured HDPE FML and a two foot thick protective soil veneer cover layer. The maximum slope angle was equal to 18.4^0 (3H:1V) and the most critical interface angle was equal to 18^0. The maximum slope length was equal to 285 feet.

To improve the stability of the soil veneer cover and help protect the long-term integrity of the new lining system, a layer of structural geogrid was placed at the bottom of the soil veneer cover layer. Fig. 7 shows the actual placement of the geogrid along the side slopes. The geogrid layer was anchored in an anchor trench located at a certain horizontal distance from the top of the slope. On several sections of the sites, the geogrid was embedded in a horizontal soil layer to prevent pullout failure. Fig. 8 illustrates the placement of the protective soil veneer layer placed on top of the geogrid. Notice that the soil veneer cover layer was first placed on top of the anchored area, then along the sides slopes.

CONCLUSION

To evaluate the long-term stability of a protective soil veneer cover layer and prevent potential sliding problems, the design engineer should carefully determine the following parameters:

(i) Determine the most critical interface friction angle based on actual testing. Note that interpretation of the test results is crucial to determining the values to be used in final design.

(ii) The allowable design strength of the structural geogrid should be adequately defined and should account for creep, temperature, construction induced damages, chemical compatibility and structural connections. The minimum 10,000 hour creep testing is a must if a structural element is to be used to improve the long-term integrity of a lining or cap system.

(iii) Designing of the appropriate anchor trench and/or determining the required embedment length to minimize potential for pullout failure are important steps in the design and should be carefully assessed.

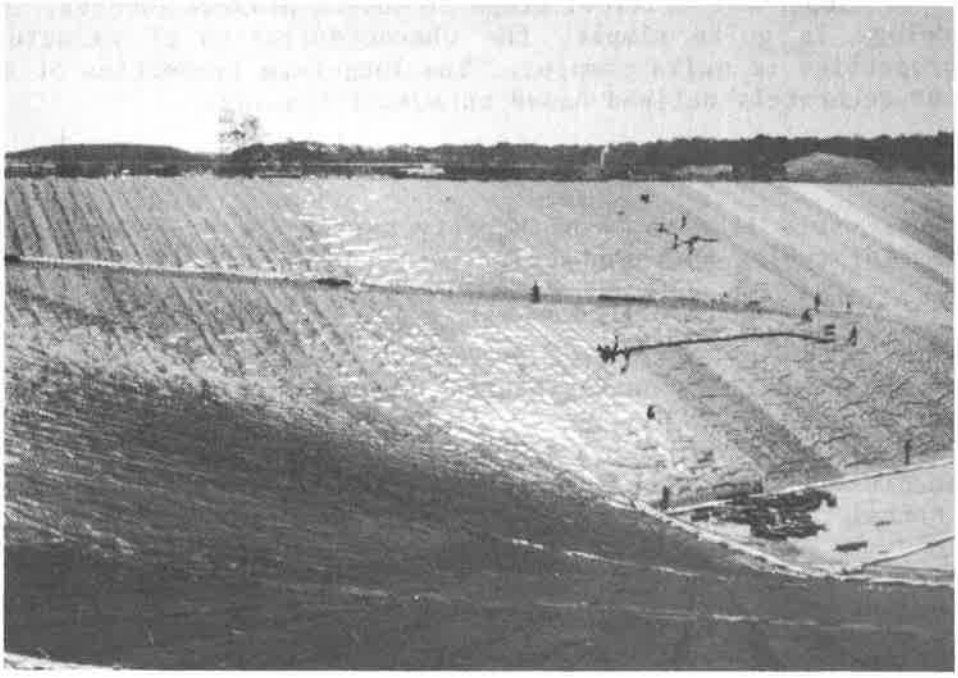

FIGURE 7: PLACEMENT OF GEOGRID LAYER AT BOTTOM OF COVER SOIL
(Municipal Solid Waste Landfill in New York State)

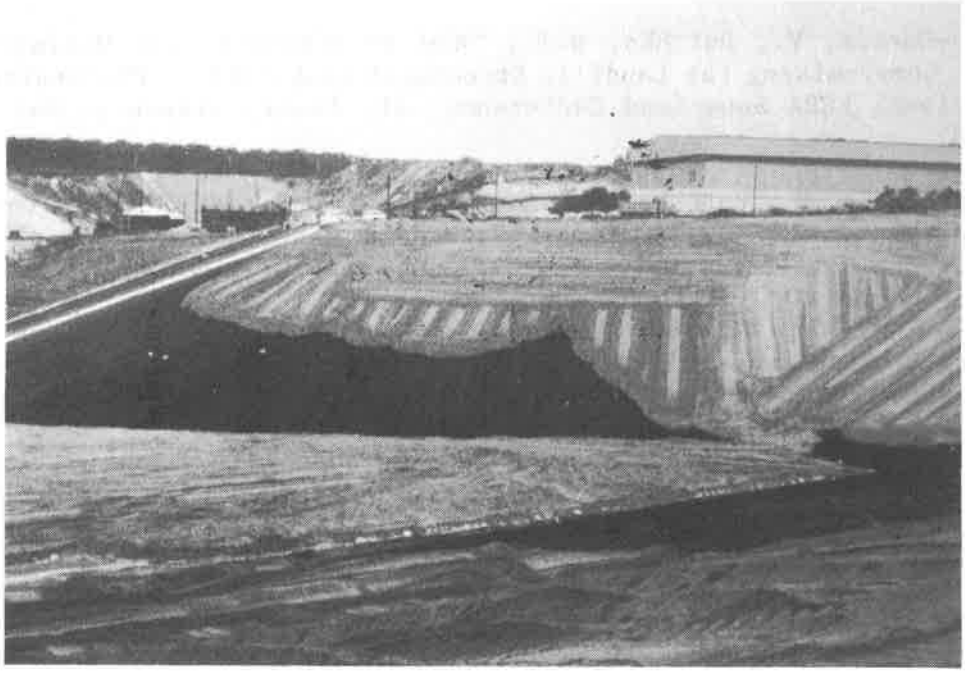

FIGURE 8: COVER SOIL PLACED FROM TOP DOWN THE SLOPE FACE.
(Municipal Solid Waste Landfill in New York State)

Structural testing, data interpretation, design and appropriate installation techniques are all important critical steps to ensure project success. Although the design methodology is quite simple, the characterization of structural geogrid performance properties is quite complex. The long-term properties of a structural geogrid must be accurately defined based on actual testing.

ACKNOWLEDGEMENTS

The authors would like to thank Beverly Martin for drafting the figures and Constance Adams for typing this manuscript.

REFERENCES

1. ASCE Manuals and reports on Engineering Practice No. 66. Structural Plastics Selection Manual.

2. ASCE Manuals and reports on Engineering Practice No. 63. Structural Plastics Design Manual.

3. Bonaparte, R. and Berg, R.R., "Long-Term Allowable Tension for Geosynthetic Reinforcement", PROCEEDINGS, GEOSYNTHETICS '87, Vol. 1, New Orleans, LA, February 1987, pp.181-192.

4. Carroll Jr., R.G. and Chouery-Curtis, V., "Geogrid Reinforcement in Landfill Closures". Proceedings of the 4th GRI Seminar on the Topic of Landfill Closures, Philadelphia, PA, December 13-14, 1990.

5. Chouery-Curtis, V., Butchko, S.T., "How to Economize and Optimize Land Use without Compromising the Landfill Structural Stability". Proceedings HM CRI's 7th National RCRA Superfund Conference, St. Louis, Missouri, May 1990, Pgs. 123-140.

6. Chouery-Curtis, V., Butchko, S.T., "Structural Geogrids in Waste Containment". Proceedings of the Eighth Annual Hazardous Materials Management Conference International, Atlantic City, New Jersey, June 5-7, 1990.

7. Design of Tensar Geogrid Reinforcement of Soil Veneer Covers for Waste Containment Structures - Tensar Technical Note: WM2, The Tensar Corporation, Morrow, GA, June 1989.

8. Geosynthetic Research Institute GRI Test Methods GG3: "Tension Creep Testing of Stiff Geogrids", Drexel University, Philadelphia, PA, January 1990.

9. Geosynthetic Research Institute, GRI Test Method GG4 - "Determination of the Long-Term Design Strength of Stiff Geogrids", (Revised), Drexel University, Philadelphia, PA, January 1990.

10. Geosynthetic Research Institute (GRI) Test Method GG-5 Geogrid Pullout Behavior (Draft), Drexel University, Philadelphia, PA, 1990.

11. Jewell, R.A. Milligan, G.W.E., Sarsby, R.W. and DuBois, D., "Interaction Between Soil and Geogrids," Proc. of Polymer Grid Reinforcement Conference, London, pp. 18-30, March 1984.

12. Martin, J.P., Koerner, R.M., and Whitly, J.E., Experimental Friction Evaluation of Slippage Between Geomembranes, Geotextiles and Soils, Proceeding of the International Conference on Geomembranes, Denver, CO, June 1984.

13. New York State, Department of Environmental Conservation, GNYCRR Part 360 Solid Waste Management Facilities, 31 December 1988, (Pp. 2-39, 360-2.13).

14. Tensar Technical Note: PT13.0, October 1987, "High Density Polyethylene Resin Characteristics Which Affect Performance of Products Bearing High Sustained Loads in Soil Reinforcement Application".

15. Williams, N.D., and Houlihan, M.F., Evaluation of Interface Friction Properties Between Geosynthetics and Soils, Proceedings of the Geosynthetics '87 Conferences, New Orleans, LA, February 1987.

16. Wrigley, N.E., "The Durability and Aging of Geogrids", PROCEEDINGS, DURABILITY AND AGING OF GEOSYNTHETICS, Geosynthetic Research Institute, Drexel University, Philadelphia, PA, December 1988.

Stability of High Refuse Slopes on Synthetic Lining Systems at the Bee Canyon Landfill

Suji Somasundaram
The Earth Technology Corporation, USA
Kris Khilnani
The Earth Technology Corporation, USA

ABSTRACT

The 360-acre, Class III Bee Canyon Landfill in Orange County California is lined with a composite high density polyethylene (HDPE) and clay lining system on canyon bottoms and a single HDPE lining system on canyon side slopes. Special design consideration was given to the stability of a 440-foot high final refuse slope at the down canyon face of the landfill. Preliminary stability analyses of this refuse slope indicated that the most critical potential failure modes consisted of block type failures occurring along the interfaces within the lining system on the bottom and sides of the canyon. Site-specific interface shear strength properties between various components of the lining system were determined for clay lining materials, smooth and textured HDPE and non-woven geotextiles. Two-dimensional stability analyses indicated that the interface shear strength between various components of the lining system, i.e., HDPE/clay, HDPE/geotextile, were of critical importance for the overall stability. To incorporate the adverse effects of the canyon geometry, three-demensional stability analyses were performed on potential failure blocks bound by the canyon floor and side slopes. Use of smooth HDPE lining gave unacceptably low factors of safety. Based on the results of these analyses, an overall 3:1 (horizontal:vertical) refuse slope configuration with textured HDPE along the canyon bottoms and lower portions of the canyon side slopes for some distance from the toe of the landfill was selected. The lining for the canyon side slopes away from the toe of the landfill slope was designed to consist of smooth HDPE.

INTRODUCTION

Bee Canyon Landfill, a Class III Landfill operated by the Integrated Waste Management Department (IWMD), County of Orange California, started accepting refuse in January 1990. The landfill, with a total capacity of 110 million cubic yards and an estimated life of 25 to 30 years, will cover an area of about 360 acres.

The site consists of a main canyon (Bee Canyon) and several tributary canyons. It is underlain by sedimentary rocks consisting mostly of sandstone, siltstone and claystone, and features 65 mapped ancient landslides covering 30 to 40 percent of the landfill area. The canyon bottoms contain variable thicknesses of alluvium ranging up to 60 feet. The site preparation for refuse containment system includes stabilizing/removing the landslides, removing relatively compressible alluvium and weathered bedrock, fine grading the sides and bottoms of the canyons, installing subdrains in canyons, and constructing a lining and leachate control and recovery system (LCRS). When completed, the landfill will have a 440-foot high refuse slope face at the mouth of the main canyon. This paper addresses the slope stability considerations and the impact of the lining system on the stability of final and interim landfill slopes for the Bee Canyon Landfill.

LINING SYSTEM

The as-graded topography of the canyon bottoms and side slopes near the mouth of the main canyon, for the first phase of landfill development is shown on Figure 1. The canyon bottoms were designed to have slopes ranging from 3 to 6 percent while the canyon side slopes range from 2:1 (horizontal:vertical) to 4:1.

Typical lining systems as presented in Figure 2, consist of composite lining (clay and HDPE) in the canyon bottoms and single HDPE on the side slopes. The approximate limits of the composite lining system within the first phase of landfill development are shown on Figure 1. The composite lining system consists of 80 mil HDPE on 1 to 2-foot thick compacted clay obtained from on-site sources. The clay lining material is processed to a maximum size of 1-inch and compacted to a minimum of 90 percent of Modified Proctor dry density (as per ASTM D1557) at moisture content from 2 to 5 percent above optimum. The single lining on side slopes consists of 80 mil HDPE on 16 oz. geotextile on prepared side slope surfaces.

SLOPE GEOMETRY AND POTENTIAL FAILURE MECHANISMS

At the final closure of the landfill, the maximum height of the front face of the landfill refuse slope, including a final cover system, is expected to be approximately 440 feet. The toe of this southwestern facing slope will be located at the mouth of the main canyon at the southwestern corner of the site. A slope and bench configuration is proposed for this slope face.

The stability analyses for this final slope was carried out with the following main objectives.

- Evaluation of a safe slope for the 440-foot high final landfill face that would have acceptable factors of safety against potential failure. Potential circular failure surfaces through the refuse and block failures along the various lining system interfaces were considered.

- Selection of a suitable lining system (smooth and/or textured HDPE) for the canyon floor and side slopes that would provide acceptable factors of safety against sliding.

Design criteria required minimum factors of safety of 1.5 and 1.1 under static and pseudostatic (for the maximum probable earthquake) conditions respectively. The latest California Waste Management Board regulations, however, require a minimum factor of safety of 1.5 under dynamic conditions for the critical slope. In lieu of achieving a factor of safety of 1.5 under dynamic conditions, a demonstration that the estimated seismically induced deformations computed by rigorous analytical methods are acceptable, needs to be provided.

In order to investigate various potential failure mechanisms and evaluate minimum factors of safety, several two-dimensional cross-sections and three-dimensional sliding blocks were considered.

Three two-dimensional cross-sections, Sections A-A', B-B' and C-C', were selected to characterize the final slope face configuration. The locations of these sections are shown on Figure 1. The sections were selected on the basis of one or more of the following factors: height of refuse; configuration of slope; geometry of the bottom and side slopes; and the lining system details. Section A-A' runs along the axis of the main canyon (running roughly northeast to southwest) through the maximum height of the refuse slope (440 feet). Since this cross section is located through the highest portion of the slope, it represents a critical section for potential circular failures that may occur

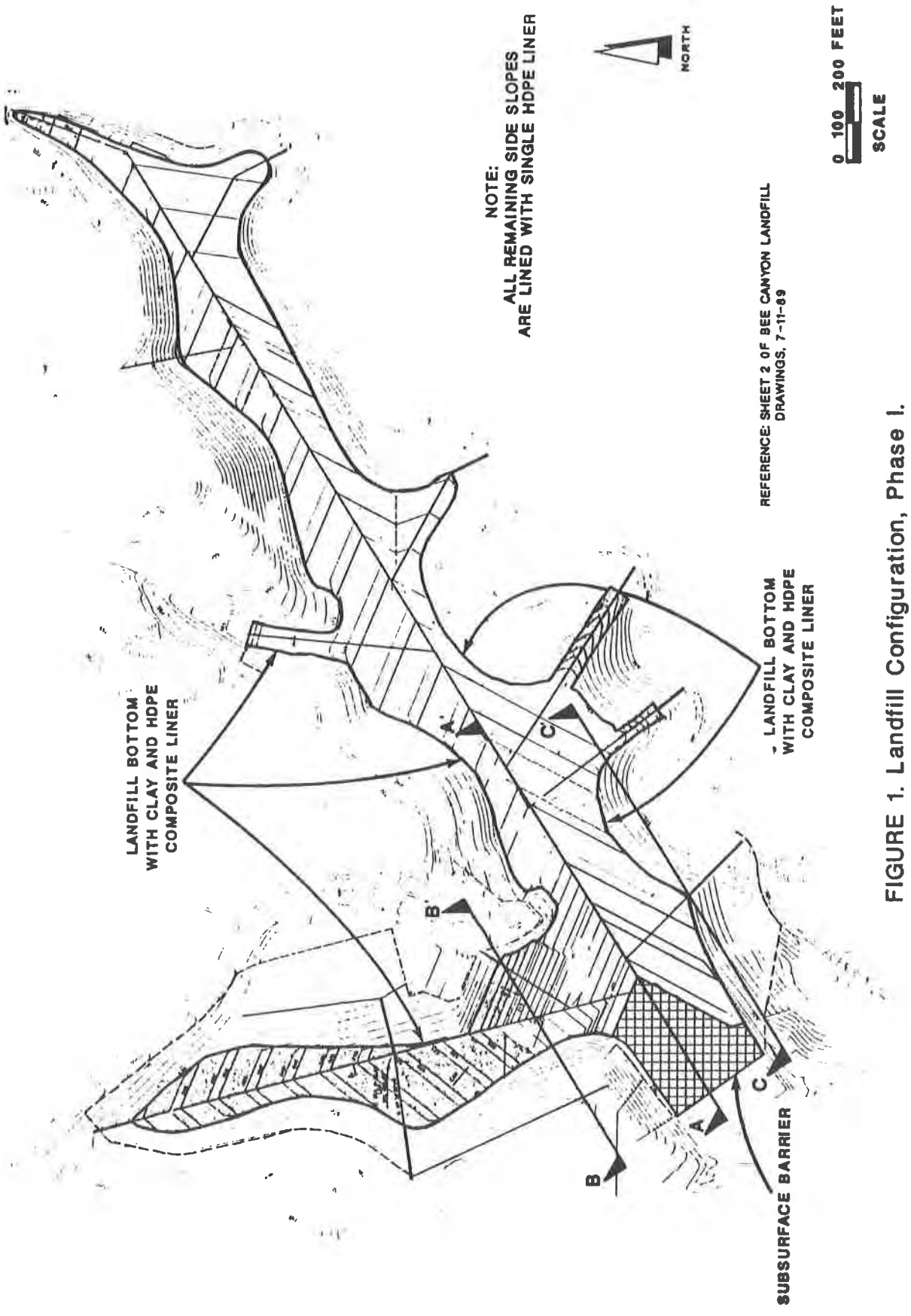

FIGURE 1. Landfill Configuration, Phase I.

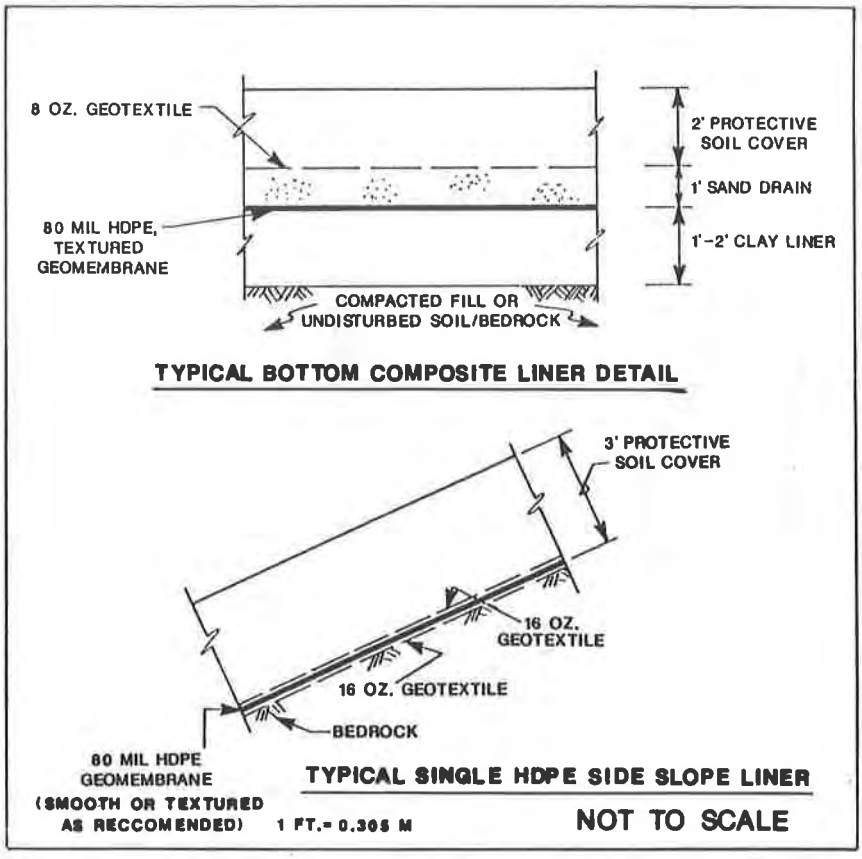

FIGURE 2. TYPICAL LINER SYSTEM DETAILS

through the refuse mass and potential block failures through the weakest interface of the composite lining system at the bottom of the landfill. Sections B-B' and C-C' were located parallel to Section A-A'. The height of the landfill slope at Sections B-B' and C-C' is approximately 300 feet and 400 feet, respectively. These two sections are representative of potential block failure mechanisms along the weakest interface of the canyon side slope HDPE lining system.

Stability analyses along circular and non-circular failure surfaces were performed using the Modified Bishop and Simplified Janbu Methods, respectively. For potential circular failure surfaces through the refuse, several trial failure surfaces were randomly generated from a number of different initiation points near the toe of the landfill slope, to obtain the minimum factor of safety. For potential block failures, failure planes were assumed to run along the weakest material or interface in the lining system. The minimum factor of safety was obtained by varying the initiation and exit points.

In addition to the two-dimensional slope stability analyses of the above cross-sections, a three-dimensional stability analysis of the final landfill slope configuration was also performed to incorporate the effects of the complex canyon geometry on the overall stability. The Computer Code 'CLARA' (Hungr, 1988) which extends the Modified Bishop and the Simplified Janbu Methods to three-dimensional configurations, was used for the three-dimensional stability analysis. The three-dimensional analysis considered the stability of a massive wedge of refuse at the mouth of the canyon, bounded by the composite lining system on the canyon floor and the single HDPE lining system along the canyon side slopes. The sliding surfaces at the bottom and sides of the canyon were assumed to

be along the weakest interface in the lining system. The floor of the canyon was modeled as a plane inclined down-canyon at 6 percent. The main canyon side slope facing southeast was modeled as a plane dipping 8 degrees SE and striking at an angle of 5 degrees with the axis of the canyon (diverging towards the mouth of the canyon). The northwest facing side slope was modeled as a plane dipping 14 degrees NW and striking at an angle of 5 degrees with the axis of the canyon (diverging towards the mouth of the canyon). The fourth failure plane of the block (back of the block) was assumed to run through the refuse. With three of the failure planes (floor and sides of the canyon) fixed, the fourth plane through the refuse mass was varied in order to determine minimum factor of safety.

MATERIAL PROPERTIES AND INTERFACE SHEAR STRENGTH PARAMETERS

Preliminary stability analyses of the final refuse slope indicated that the most critical potential failure modes consisted of block type failures occurring along interfaces within the lining system on the bottom and sides of the canyon. Therefore, a site-specific laboratory testing program was undertaken to evaluate the shear strength properties of the key components and interfaces of the lining system.

Interface shear strength properties between the various components of the lining system were determined for on-site clay liner materials, smooth and textured HDPE geomembranes and non-woven geotextiles. The properties for the refuse materials were obtained from existing data bases on other Class III landfills in the area.

Clay Lining Soil Properties Representative samples of the clay lining soil from the site were obtained and remolded at the density and moisture conditions specified for field placement, i.e., at least 90 percent of Modified Proctor dry density (ASTM D1557) at moisture contents of 2 to 5 percent above optimum moisture. The specimens were then saturated, consolidated and tested by direct shear and consolidated undrained triaxial compression tests. The results are summarized in Table 1.

Interface Shear Strength Parameters. Interface shear strength parameters between HDPE and the clay lining, and HDPE and geotextile were obtained from a direct shear test program conducted at the University of Alberta, Edmonton, Canada. The tests were carried out in a 12-inch x 12-inch shear box under normal stresses of approximately 6,000, 12,000 and 24,000 psf. The peak shear stress and the shear stress at a maximum displacement of 50mm were taken as the peak and residual shear strength, respectively.

TABLE 1

SUMMARY OF CLAY LINER SOIL SHEAR STRENGTH PARAMETERS

1 PSF = 0.0479 KN/M^2

TYPE OF TEST	TOTAL STRESS PARAMETERS		EFFECTIVE STRESS PARAMETERS	
	Cohesion C (psf)	Friction Angle (degrees)	Cohesion C (psf)	Friction Angle (degrees)
Direct Shear Test	1600	26	-	-
Consolidated Undrained Triaxial Compression Test	1500	15	0	35

Direct shear tests between clay and geomembranes were conducted under saturated, consolidated undrained conditions. The clay lining material was compacted in the test mold to the density and moisture content specified for field construction, prior to consolidation and shearing. Direct shear tests were performed on 80 mil HDPE textured lining from Gundle, SLT and Nilex, and 80-mil smooth HDPE lining from Gundle. The textured lining from the three manufacturers have different grades of textured surface due to different manufacturing processes and are likely to exhibit different interface shear strength properties. The smooth HDPE lining, on the other hand, is not expected to vary from manufacturer to manufacturer and should exhibit similar interface shear strength properties. Interfacial friction tests were also performed between SLT textured HDPE and Trevira 1155 needle-punched, nonwoven, 16-ounce geotextile. The results of the tests are presented in Table 2.

TABLE 2

SUMMARY OF INTERFACE SHEAR STRENGTH PARAMETERS
FROM LABORATORY TESTING PROGRAM

BEE CANYON CLAY LINING AND HDPE INTERFACE

1 PSF = 0.0479 KN/M^2

	PEAK		RESIDUAL	
HDPE (80 mil thick)	Interface Friction ø (Degrees)	Adhesion, a (psf)	Interface Friction ø (Degrees)	Adhesion, a (psf)
Gundle Smooth	13	1100	7	1100
Gundle Textured	21	2000	-	-
SLT - DRS Textured	19	2300	-	-
Nilex 'G' Spiked	7	4550	-	-

TREVIRA 1155 GEOTEXTILE (NONWOVEN, NEEDLE PUNCHED, 16 OZ.)
AND HDPE INTERFACE

	PEAK		RESIDUAL	
HDPE (80 mil thick)	Interface Friction ø (Degrees)	Adhesion, a (psf)	Interface Friction ø (Degrees)	Adhesion, a (psf)
SLT - Textured	30	0	18	0

The test results indicate that interface shear strength parameters (adhesion and friction angle) between the clay and the textured HDPE from Gundle and SLT are very similar while the textured (spiked) Nilex membrane exhibited a lower friction angle and a higher adhesion. The results of the site-specific laboratory test program were also compared to results on similar materials presented in the literature (Bonaparte, Williams and Giroud, 1985; Eigenbrod and Locker, 1987, Georgia Institute of Technology, 1987; Koerner, 1986; Seed, Mitchell and Seed, 1988; Soil and Material Engineers, Inc., 1987; University of Alberta, 1988). The comparison indicated that the measured friction angles were similar to those reported, but the values of interface adhesion measured during the site-specific testing were significantly higher.

Based on the test program and the review of available literature, suitable interface strength parameters were chosen for the stability analyses and are presented in Table 3. For the clay/HDPE interface, friction angles of 7 and 19 degrees were used for the smooth and textured HDPE, respectively. Adhesion was assumed to be negligible for smooth HDPE. For the textured HDPE, a nominal adhesion value of 200 psf (in line with values reported in the literature) was used. The values of adhesion used in the analysis are substantially lower than the values obtained from the testing program. The principal reasons for using lower values of adhesion are as follows:

a. Test data reported by others consistently indicates that adhesion between clay and HDPE is small to negligible, particularly in the case of smooth HDPE.

b. The clay lining itself has shear strength properties (1500 psf cohesion and 15° friction angle) which are lower than the measured shear strength properties of the clay/textured HDPE interface (2000-2300 psf adhesion and 19°-21° friction angle). Therefore, failure would occur through the clay material before the full measured strength of the interface materials is mobilized, and the use of high adhesion values measured for the clay/textured HDPE interface cannot be justified. The assumed design interface shear strength and shear strength of the clay lining are relatively close to each other particularly at higher pressures (deeper refuse depths). The measured interface strength of textured HDPE against clay is significantly higher. Thus the assumed design interface strength is more in line with the actual minimum shear strength of the lining system as a whole.

TABLE 3

SUMMARY OF UNDRAINED STRENGTH PARAMETERS
USED IN THE STABILITY ANALYSIS

1 PSF = 0.0479 KN/M^2

INTERFACE	Adhesion a (psf)	Interface Friction, ø (degrees)
Smooth HDPE/Geotextile Fabric	0	10
Textured HDPE/Geotextile Fabric	0	18
Smooth HDPE/Clay Lining	0	7
Textured HDPE/Clay Lining	200	19
Geotextile Fabric/Cover Soil	0	20
Clay Lining Material	1500	15

Note: Strength Properties for Landfill Refuse are presented in Figure 3.

c. The laboratory testing program was conducted under consolidated undrained conditions. The degree of saturation measured on samples after consolidation indicated that a significant number of samples were not completely saturated. The high values of adhesion obtained from tests may have been partly due to development of negative pore pressures during shearing. Actual pore pressure conditions during potential slip of the landfill slope may be different (increase or no change in pore pressures).

d. The presence of a film of moisture along the clay/HDPE interface (due to 'sweating' effect) could significantly reduce the adhesion. Also, over the long term, possible leakage through any defects in HDPE lining could result in a fluid at the interface between the HDPE and clay, and could reduce the adhesion.

For smooth HDPE/clay and textured HDPE/geotextile interfaces, the residual (rather than peak) friction angles obtained from site-specific tests were used in the stability analyses (Table 3). Test results indicated that the peak shear strengths for the smooth HDPE/clay and textured HDPE/geotextile interfaces occur at approximate relative displacements of 5mm and 15 mm, respectively. The residual friction angles were used in the analyses since sufficient relative movement along the interfaces and consequent mobilization of residual shear strength values could occur during construction, fill placement operations, and long term refuse fill settlement. For the textured HDPE/clay interface tested, the residual values were not different from the peak values.

Other interface shear strength parameters input in the stability analyses include: smooth HDPE against geotextile fabric; textured HDPE against cover soil; and geotextile fabric against cover soil. These interface shear strength parameters were chosen from the results reported in the literature cited above and are presented in Table 3. The design strength values indicate that for the canyon bottom where a composite lining system is used, the weakest interface exists between the HDPE (either smooth or textured) and the clay lining. For the side slopes where a single HDPE lining is used, the weakest interface exists between the HDPE (smooth or textured) and the geotextile fabric.

Waste Material Properties. The landfill waste material properties were based on a data base which consists of results of laboratory (direct shear, triaxial) and field testing (cone penetration tests, geophysics, field vane, blow counts) programs on waste material from other municipal waste landfills (Earth Technology Corporation, 1988 a, b). A review of available results from this data base indicates that the shear strength properties and the unit weight of refuse vary with depth and also exhibit scatter over a wide range of values. Based on the available data, lower bound and "best estimate" shear strength envelopes were selected for the stability analyses. The variation of strength and density with depth used in the analyses is presented in Figure 3.

RESULTS OF STABILITY ANALYSES

Two-dimensional stability analysis for Sections A-A', B-B' and C-C' and three-dimensional stability analyses for the entire landfill refuse slope were carried out to determine the slope of the final landfill front face and to determine the type of HDPE lining (smooth or textured) to be used on the canyon bottom and sideslopes.

Two-dimensional stability analysis sections are shown on Figure 4 and the results of the analyses are summarized in Table 4. Potential circular and block failure mechanisms were considered for Cross-Section A-A'. Results indicate that block failures along the lining interfaces are more critical and govern design. Results also indicate that a 3:1 average refuse slope configuration and textured liner along the canyon bottom are required to maintain a minimum static factor of safety of 1.5 for Section A-A'. Results of stability analyses of Sections B-B' and C-C' indicate that for a 3:1

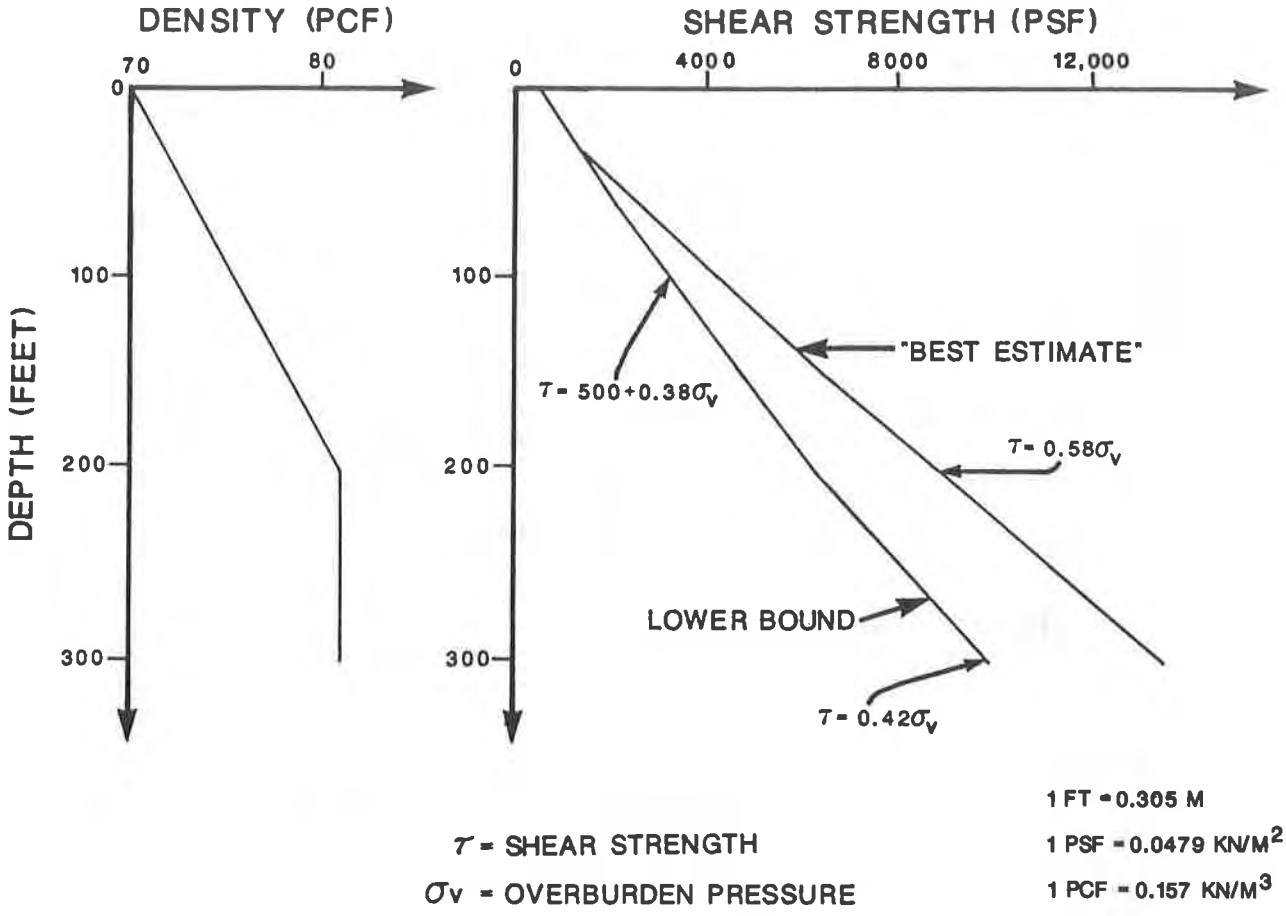

FIGURE 3. Material Properties–Depth Relationship for Refuse

refuse slope configuration, the use of smooth HDPE on the canyon side slopes would result in unacceptably low factors of safety (1.2 and 1.0 respectively), within portions of the final refuse slope. By using textured HDPE on the side slopes, the factors of safety increase to 1.4 for both sections. In summary, the two dimensional stability analyses indicate that an overall 3:1 refuse slope geometry with textured HDPE in the lining system would result in static factors of safety ranging from 1.4 to 1.5.

The site configuration suggests that a two-dimensional analysis may not provide an accurate evaluation of stability since it does not account for canyon side slope geometry. In order to incorporate the canyon geometry into the overall factor of safety, three-dimensional stability analyses of the slope were carried out. A typical potential failure block used for the three-dimensional stability analyses is illustrated in Figure 5. Results indicate that an overall 3:1 refuse slope would have a factor of safety of 1.8 if textured HDPE is used along the bottom and sides of the canyon. If smooth HDPE is used along the canyon side slopes the factor of safety drops to 1.4.

LIMITS OF SIDE SLOPES LINED WITH TEXTURED HDPE

As discussed above, textured HDPE lining was considered necessary for the canyon side slopes to provide an adequate static factor of safety. However, textured lining would be required only in those portions of the side slopes near the mouth of the canyon that are affected by potential instability due to height of refuse slope. Sensitivity studies were conducted by analyzing the stability of the two-dimensional Sections B-B' and C-C', and the three-dimensional block for varying lengths of

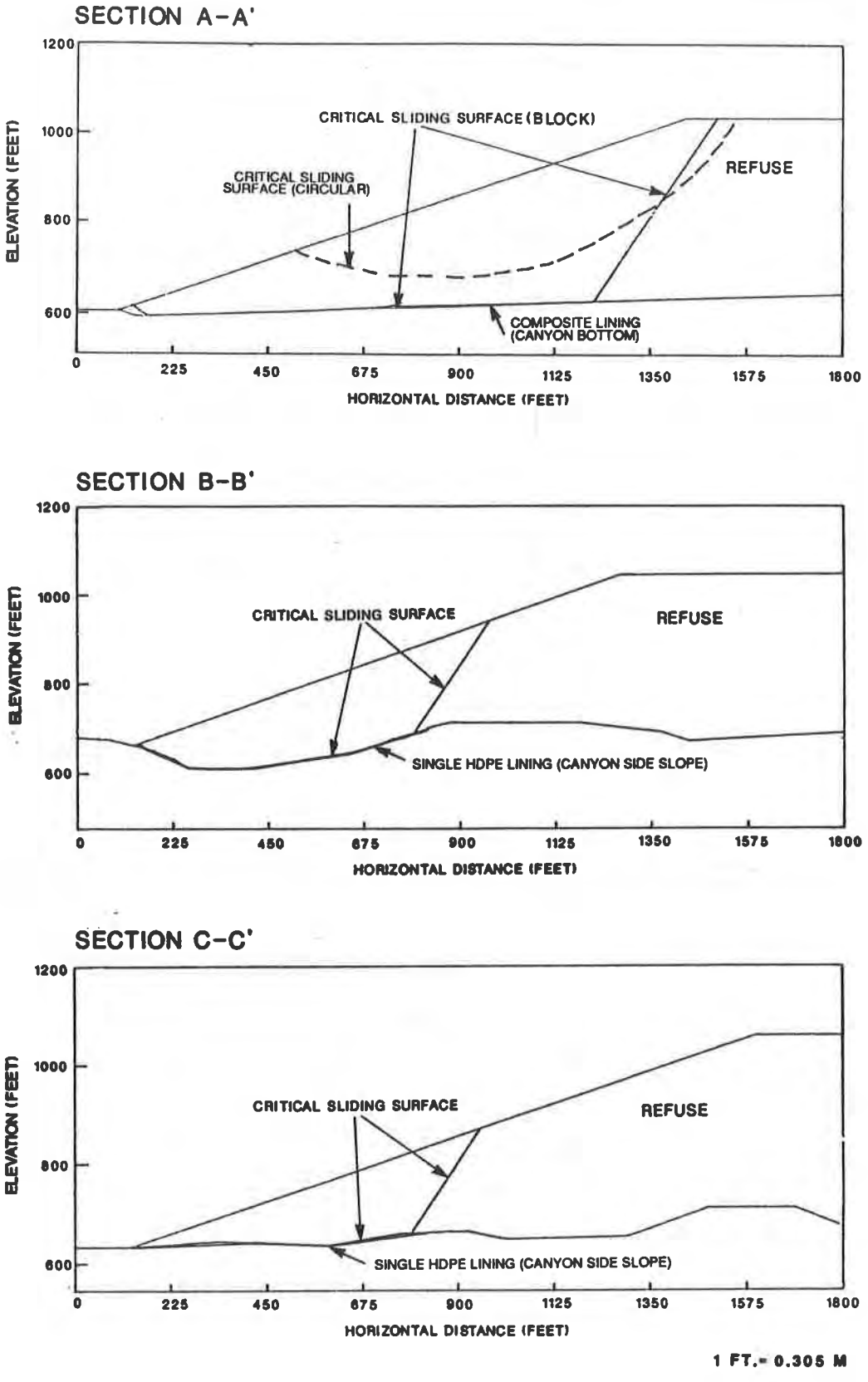

FIGURE 4. 2-Dimensional Stability Sections.

TABLE 4

RESULTS OF STATIC TWO-DIMENSIONAL
SLOPE STABILITY ANALYSIS ON FINAL LANDFILL SLOPE CONFIGURATION

Cross Section	Average Landfill Slope (H:V)	Critical Sliding Surface	Factor of Safety
A-A'		A. Circular Failure Mechanism (best estimate shear strength envelope for refuse).	
	2.5:1	Circular arc through refuse	1.6
	3:1	Circular arc through refuse	1.9
		B. Block Failure Mechanism (lower bound shear strength envelope for refuse).	
	3:1	Along smooth HDPE/clay liner interface on canyon floor; through refuse at back of sliding block.	0.8
	3:1	Along textured HDPE/clay liner interface on canyon floor; through refuse at back of sliding block.	1.5
B-B'	3:1	Case 1: smooth HDPE on side slopes; along smooth HDPE/geotextile interface on bottom of sliding block; through refuse at back of sliding block.	1.2
	3:1	Case 2: textured HDPE on side slopes; along geotextile/textured HDPE interface on bottom of sliding block; through refuse at back of sliding block.	1.4
C-C'	3:1	Case 1: smooth HDPE on side slopes; along smooth HDPE/geotextile interface on bottom of sliding block.	1.0
	3:1	Case 2: textured HDPE on side slopes; along geotextile/textured HDPE interface on bottom of sliding block; through refuse at back of sliding block.	1.4

canyon (from the toe of landfill slope), lined with textured HDPE. Based on the results of this analysis, textured HDPE was found to be necessary for side slopes for a minimum distance of 1,200 feet from the toe of the final slope, to maintain the minimum required factors of safety.

Smooth HDPE was found to be adequate for the canyon side slopes greater than 1200 feet away from the final slope face. Due to the high side slope inclinations and very low friction angles along the HDPE/geotextile interfaces, operational constraints were introduced to minimize the potential for failures during refuse placement operations. Recommended constraints included sequencing of landfilling operations such that any uneven filling of refuse, against canyon side slopes, if carried out, had a minimum width-to-height ratio of 2.5:1 and did not exceed 40 feet in height.

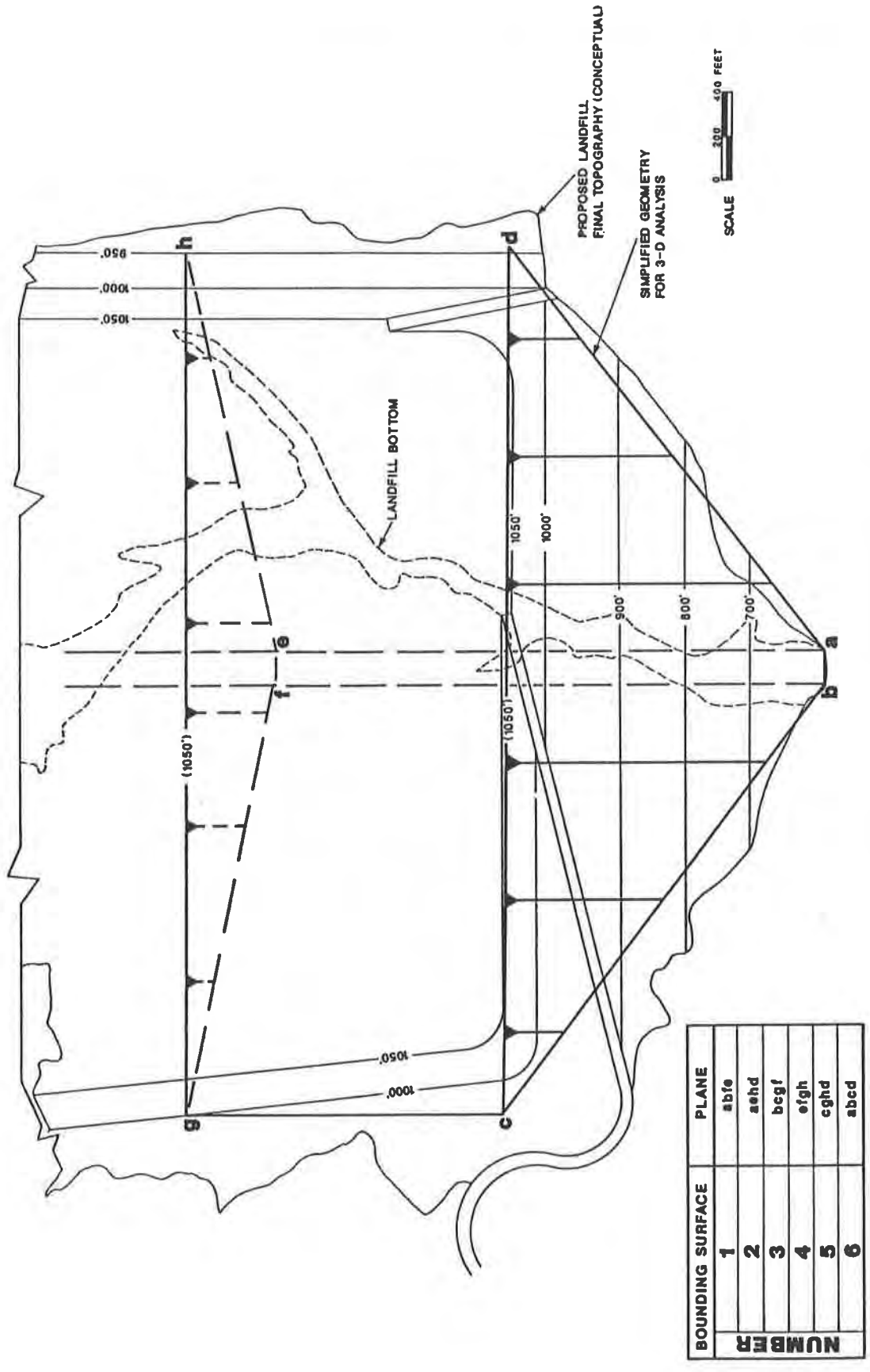

FIGURE 5. 3-Dimensional Sliding Block.

EFFECTS OF EARTHQUAKE LOADING ON SLOPE STABILITY

Based on a site-specific probabilistic evaluation of seismicity (Earth Technology Corporation, 1988c), the peak ground acceleration at the site, with an average return period of 100 years, was estimated at 0.22g for an earthquake on the Whittier-Elsinore fault.

Pseudostatic stability analyses were carried out on the two-dimensional sections A-A', B-B', C-C', and the three-dimensional block for an average design horizontal acceleration of 0.15g (approximately 2/3 of the 100-year peak ground acceleration of 0.22g). Results of the analysis, indicated minimum pseudostatic factors of safety of 0.9, 1.0, 0.9, and 1.0 for sections A-A', B-B', C-C', and the three-dimensional block, respectively.

During earthquake loading, the factor of safety is a time-dependent parameter, depending upon the seismically induced stresses at any particular instant. A pseudostatic factor of safety of less than 1.0 under an average design acceleration does not imply slope failure in a conventional sense, but rather some earthquake-induced displacement. The order of magnitude of the earthquake-induced displacements may be estimated approximately through integration of incremental displacements during a given time history of earthquake loading. In the case of the final landfill slope configuration, a simplified Newmark-type deformation analysis was performed to estimate the potential deformations that may be caused by the design seismic event. The analysis was performed assuming that section A-A' is a suitable two-dimensional representation of the landfill slope.

The yield acceleration for section A-A' was evaluated to be 0.1g based on a pseudostatic stability analyses. The dynamic characteristics of the refuse slopes and the resulting permanent deformations under the design seismic event were evaluated using guidelines provided by Makdisi and Seed (1978). Results of the analyses indicated anticipated permanent deformations ranging from 2 to 15 inches for a peak ground acceleration of 0.22g at the site.

CONCLUSIONS

The following conclusions and recommendations were made based on the stability evaluations.

- The maximum overall inclination of the 440-foot high final slope face should be no steeper than 3:1. This configuration may be achieved by a combination of 2.5:1 slopes between benches.

- To provide adequate static stability, textured HDPE lining was found to be necessary on the canyon floor and a portion of the canyon side slopes, (minimum distance of 1,200 feet from toe of landfill slope), influenced by the 440-foot high front face.

- Permanent deformation of the landfill slope could occur under the maximum probable earthquake. Based on the Newmark approach, such deformations would be on the order of 2 to 15 inches. These are not considered excessive in comparison to the deformations that occur due to settlement of refuse materials in the landfill.

ACKNOWLEDGEMENT

The authors wish to thank Frank Bowerman, Director and Chief Engineer, Integrated Waste Management Department for his review and permission to publish this paper. Other Earth Technology professionals who contributed to the analysis reported in the paper include Michael Raub, Daya Bettadapura and Saroj Weeraratne. Their contributions are greatly acknowledged.

REFERENCES

Bonaparte, R., Williams, N., and Giroud, J.P., 1985, Innovative Leachate Collection Systems for Hazardous Waste Containment Facilities, Prepared for HAZPRO 85, Baltimore.

Earth Technology Corporation, 1988a, "In-place Stability of Landfill Slopes, Puente Hills Landfills," Report Submitted to County Sanitation District, Los Angeles, California.

Earth Technology Corporation, 1988b, "Report for Synthetic Liner System Evaluation, Canyon 9 Area, Puente Hills Landfill," Report Submitted to County Sanitation District, Los Angeles, California.

Earth Technology Corporation, 1988c, "Site Characterization, Hydrogeological/Geotechnical Study, Bee Canyon, California," Report Submitted to the County of Orange, G.S.A. Waste Management Program, Santa Ana, California.

Eigenbrod, K.D. and Locker, J.G., 1987, Determination of Friction Values for the Design of Side-Slopes Lined or Protected with Geosynthetics, Canadian Geotechnical Journal, No. 24.

Georgia Institute of Technology, 1987, Interface Friction Analyses, Schlegal Lining Technologies, Inc., Report prepared for Schlegal Lining Technology, Inc., The Woodlands, Texas.

Hungr, O., 1988, "CLARA User's Manual," O. Hungr Geotechnical Research, Inc., 95 East 20th Avenue, Vancouver, B.C., Canada.

Koerner, Robert M., 1986, Designing with Geosynthetics, Prentice-Hall, Englewood Cliffs, NY.

Makdisi, F.I. and Seed, H.B., 1978, "Simplified Procedure for Estimating Dam and Embankment Earthquake-Induced Deformations," Journal of GT Division, ASCE, Vol. 104, No. GT7.

Seed, R.B., Mitchell, J.K. and Seed, H.B., 1988. Slope Stability Failure Investigation, Landfill Unit B-19, Phase I-A. Kettleman Hills, California, Report No. UCB/GT/88-01, University of California, Berkeley, California.

University of Alberta, Department of Civil Engineering, 1988, Reports 1 through 4, Testing Program for Puente Hills Landfill, Reports Submitted to Emcon Associates, San Jose, California.

Shear Strength of Sand-Geomembrane Interfaces for Cover System and Lining Design

S. J. Druschel
ABB Environmental Services Inc., USA
T. D. O'Rourke
Cornell University, USA

ABSTRACT

The stability of cover systems and linings on side slopes of waste impoundments is highly dependent upon the magnitude of the shear stress developed at the soil-geomembrane interface. While maximizing side slope angles will increase both the capacity and expected revenues of a waste facility, a stability failure of the containment barriers would be very costly and may force the immediate shutdown of the facility. Although considerable experimental work has been devoted to the shear properties of soil-geomembrane interfaces, fundamental questions remain about the influence of soil state, plastic type, and loading conditions.

An experimental program involving over 450 direct shear tests is discussed in which values were developed for the design of soil-geomembrane cover systems and linings. Interface shear strength parameters are reported as a function of soil type and unit weight, polymer type, normal stress, repeated loadings, and physical features of the surfaces. Recommendations are given for choosing interface shear strength parameters and applying them to design of geomembrane-based containment systems for waste impoundments.

Application of appropriate shear strength parameters is illustrated in two design examples. Minimum stability requirements may contribute to stricter design specifications for the drainage layer soils, or may dictate the necessary polymer hardness during geomembrane selection. Finally, the potential effects on stability of geomembrane degradation with time or chemical exposure, and the influences of forces derived from equipment operation, internal seepage, and placement of wastes are discussed.

BACKGROUND

Current practice in solid and hazardous waste disposal involves the isolation of the wastes from the surrounding environment through the use of low permeability geomembranes, designed to be a barrier to any leachate or groundwater flow. Cover systems function to limit infiltration of precipitation through the waste materials, reducing leachate formation, while liner systems act to collect leachate and minimize leakage to the environment. Frequently, a cover or liner system will contain a drainage layer of uniform or poorly-graded sand with interspaced piping, placed next to a geomembrane to reduce the likelihood of fluid head buildup which would encourage

flow through the barrier. However, a potential sliding plane may be created inadvertently within such a system because the friction at the sand-geomembrane interface can be relatively low.

Stability of the materials adjacent to a geomembrane barrier is critical to the construction, operation, and maintenance of a waste facility. First, as many landfills and other waste impoundments are several acres in size or larger, heavy equipment is used to move and grade the soil materials. The sand-geomembrane interface must be stable to support the equipment and maintain the safety of the construction work force. Second, waste above a liner system must not slide, or the barrier and the leachate collection piping will likely be disrupted, creating a functional failure of the facility. Third, should the soil materials above a geomembrane in a cover system slide, the geomembrane may tear or become exposed to sunlight and ultraviolet light degradation. It is ironic that, when in the presence of a hole or tear in the geomembrane, a cover system designed to minimize precipitation inflow serves very well to collect and concentrate the same precipitation, thereby encouraging passage of flow.

INTERFACE FRICTION

An experimental program involving over 450 direct shear tests was performed to characterize the friction that exists at the sand-geomembrane interface. The testing apparatus consisted of a 60-mm square shear box with a strain-controlled displacement system operating at 0.4 - 0.6 mm/min. Because of the low normal stress typical of most covers and of linings during construction, applied normal stresses ranged between 3.5 and 35 Kpa. An electronically instrumented proving ring measured the shear forces, and direct current displacement transducers measured the horizontal and vertical displacements. A complete description of the experimental program is given in O'Rourke et al. (1990), including comparisons of the results obtained in this program with results obtained in earlier studies.

Four sands were used in this study, three natural and one man-made, representative of sands that may be used for drainage or bedding purposes typically placed adjacent to a geomembrane in a lining or cover system. The grain size distributions of the three natural sands are shown in Figure 1. Ottawa sand was a uniform sand composed almost entirely of subrounded quartz particles with a mean grain size, D_{50}, equal to 0.4 mm. The fluvioglacial sand consisted of a heterogeneous mixture of quartz, limestone, siltstone, and quartzite particles with subangular shape and a D_{50} = 0.5 mm. The calcareous sand was composed entirely of rounded coral and shell fragments, and had a D_{50} = 0.6 mm. The manmade sand consisted of uniformly graded glass spheres with a D_{50} = 0.5 mm, and was used to discern the limiting conditions of interface shear behavior. The uniform grading was created by selecting only those glass spheres which would pass a No. 30 sieve but would be retained on a No. 40 sieve.

A total of 12 materials were used in the testing program, listed in Table 1. The materials were selected to provide a range of hardness by which to evaluate interface shear conditions.

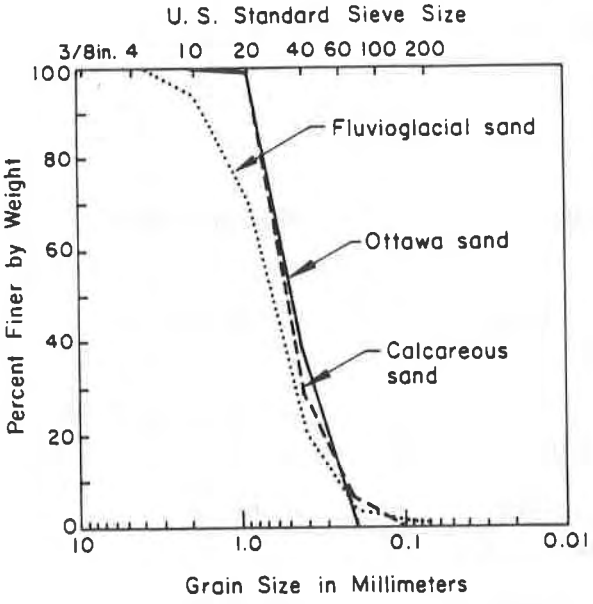

Figure 1. Grain Size Distribution Plots of Sands Used Used in Direct Shear Tests

Direct Shear Characteristics. Figure 2 contains typical results of seven direct shear tests of an Ottawa sand and HDPE geomembrane interface, and of Ottawa sand alone. Each test was performed with a normal stress equal to 20.7 kPa. The sand-only tests display shear stress peaks and vertical displacements that increase with increasing soil density. In contrast, there is no shear stress peak formed when the sand-HDPE interface is sheared, and vertical displacement is relatively quite small. Results of this form are typical of interfaces composed of sands and HDPE, MDPE, and non-plasticized PVC polymers.

Results of direct shear tests performed on Ottawa sand-plasticized PVC interfaces are shown in Figure 3, along with the Ottawa sand-only tests results. Levels of vertical displacement, while not equal to those measured in the sand only tests, are much larger than those of the sand-HDPE tests, and peaks have formed in the shear stress-versus-horizontal displacement plots. Note that for densities above approximately 17.0 kN/m^3, no further increase in the peak stress was realized, even with significant increase in soil density.

Effect of Repeated Loading. Repeated loading appeared to have no significant effect upon the shear strength characteristics of sand-HDPE interfaces, based on the results of 20 shear tests conducted with Ottawa sand on a single HDPE specimen. Sand densities ranged between 16.5 and 17.0 kN/m^3, and a normal stress of 20.7 kPa was used for all tests in this series. Figure 4 is a graph of the peak shear stress measured in each test plotted against repetition number. No appreciable trend of shear strength either increasing or decreasing may be seen.

TABLE 1 - LIST OF POLYMERS USED IN TESTING PROGRAM

COMPOSITION	SOURCE	PRODUCT NAME	MANUFACTURING PROCESS
HDPE	Gundle Lining Systems, Inc.	Gundline HD	extruded
HDPE[a]	Philips Drisco-pipe, Inc.	Driscopipe 8000	compression molded
MDPE[a]	E. I. DuPont DeNemours & Co.	Aldyl A	compression molded
PVC[b]	Dayton Plastics, Inc.	PVC pipe material	extruded
Plasticized[c] PVC	Palco Linings, Inc.	PVC liner	extruded
Plasticized[c] PVC	Staff Industries, Inc.	PVC liner	extruded
Plasticized[c] PVC	Watersaver Co., Inc.	PVC liner	extruded
Acrylic[d]	Rohm & Haas Co., Inc.	Acrylic sheet (plexiglass)	extruded
Epoxy[e]	Cornell Lab.	Epoxy A	molded
Epoxy[e]	Cornell Lab.	Epoxy B	molded
Epoxy[e]	Cornell Lab.	Epoxy C	molded

[a] High and medium density polyethylene samples specially prepared by compression molding for this study

[b] Polyvinyl chloride used in PVC pipe

[c] Plasticized PVC refers to polyvinyl chlorides with which plasticizers and solvent additives have been combined

[d] Polymethyl meta acrylic

[e] Epoxies specially mixed and cased at Cornell University

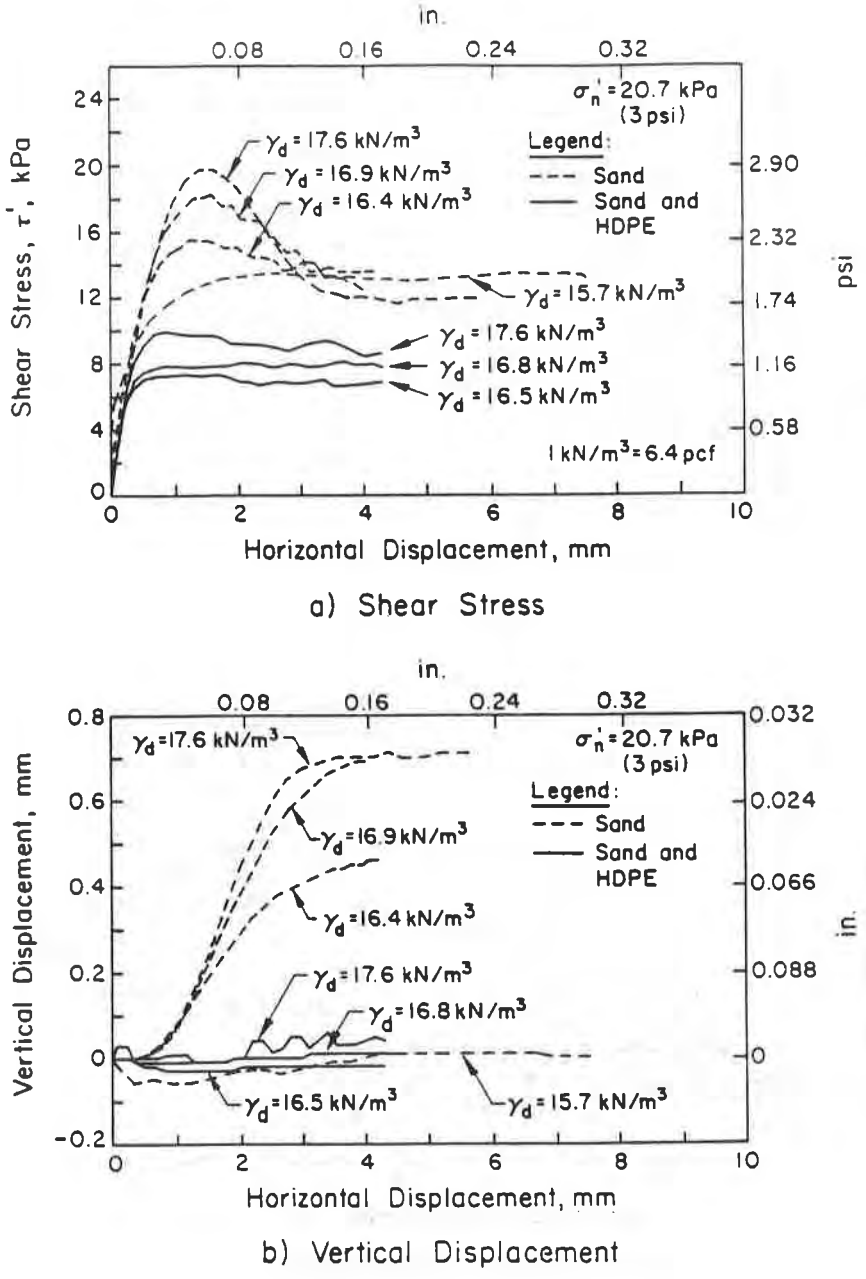

Figure 2. Direct Shear Test Data for Ottawa Sand on HDPE

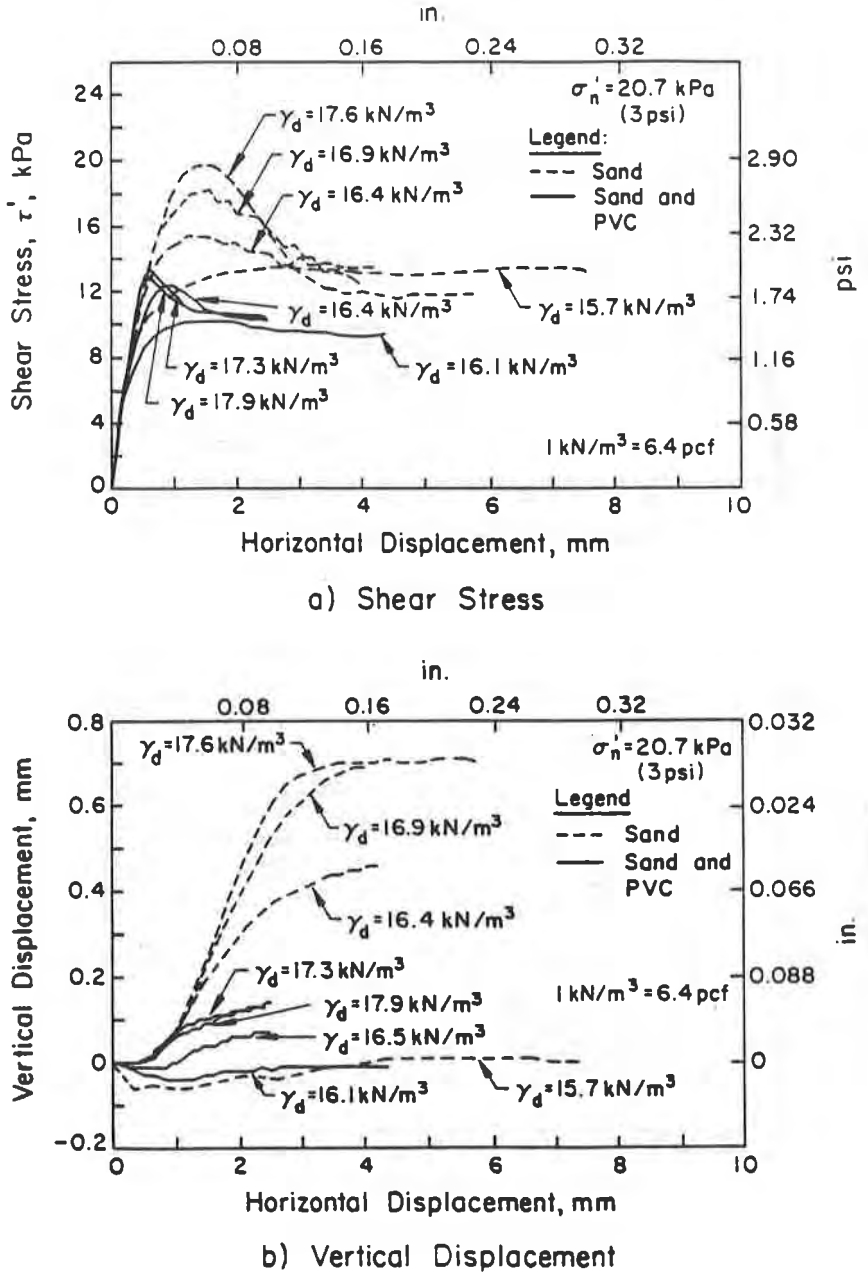

Figure 3. Direct Shear Test Data for Ottawa Sand on PVC Lining

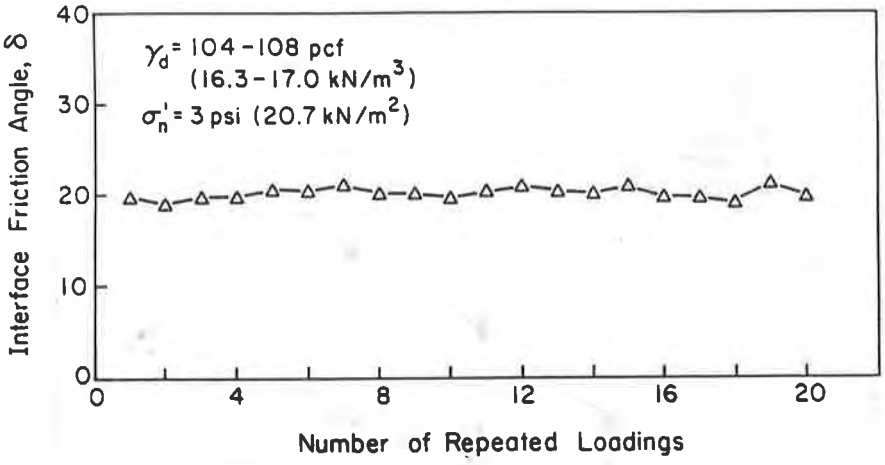

Figure 4. Interface Friction Angle, δ, as a Function of Number of Repeated Loadings for Ottawa Sand on HDPE

Effect of Normal Stress. The level of normal stress was varied in a series of tests on Ottawa sand and four different polymer surfaces to determine interface friction angles. For all tests, the Ottawa sand was prepared to a density within a relatively narrow range of between 16.5 and 17.0 kN/m^3. Figure 5 shows the peak direct shear stress plotted as a function of the normal stress for Ottawa sand alone and against each of two HDPE interfaces, while Figure 6 shows similar results for Ottawa sand and two types of PVC. The two HDPE samples gave virtually the same results, while the results from the rigid PVC pipe sample (H_d = 85) plotted substantially lower than the results for the softer PVC geomembrane (H_d = 35-45), which contains plasticizers to enhance its flexibility. For all four polymer samples, a linear relationship between peak shear stress and normal stress was found, and no significant adhesion amount was determined.

Influence of Soil Density and Type. The influence of soil type and unit weight was evaluated by performing direct shear tests using four different sands placed at a range of unit weights, against separate specimens from a single sample of MDPE, at the constant normal stress of 20.7 kPa. For comparison, tests were also run on the four sands alone over a similar range of unit weights. Figure 7 contains the results for each of the four sands, plotted as peak angles of direct shear resistance (ϕ'_{ds}) and maximum angles of interface shear resistance (δ) against soil dry unit weight (γ_d). The best straight-line fits for ϕ'_{ds} and δ versus γ_d, determined by means of linear regression analyses, are also shown for each series of tests. Although ϕ'_{ds} and δ vary significantly among the sands, the ratio of δ/ϕ'_{ds} displays relatively little variation. In the range of dry unit weights between 16-17 kN/m^3, δ/ϕ'_{ds} varies principally from 0.55 to 0.65, the lowest for the calcareous sand and the highest for the fluvioglacial sand.

Effect of Plastic Type. The effect of plastic type was first evaluated by performing direct shear tests on Ottawa sand against six different polymers over a range of soil densities but at a constant normal stress of 20.7 kPa. The results for two MDPE, two HDPE, and two PVC samples are shown in Figures 7a, 8, and 9 respectively. The

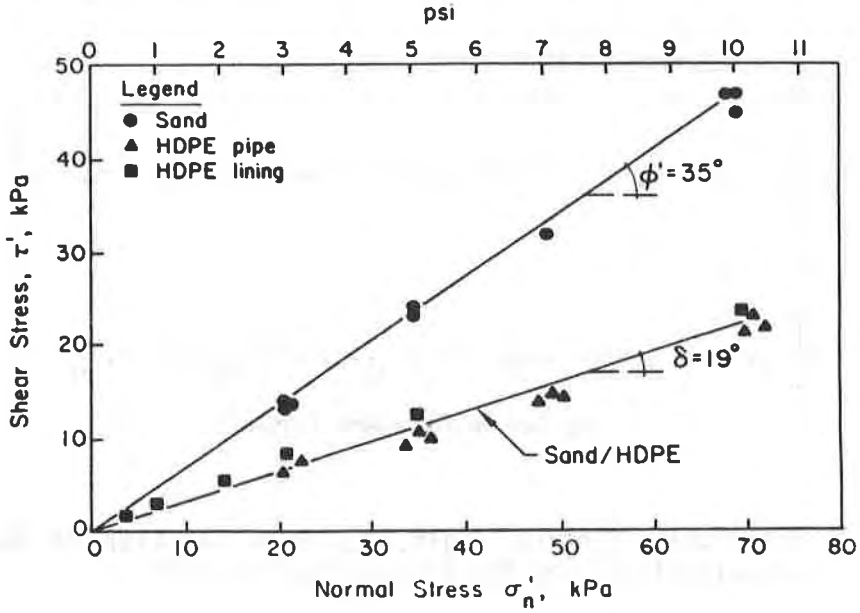

Figure 5. Shear vs. Normal Stress for Direct Shear Tests of Ottawa Sand on HDPE

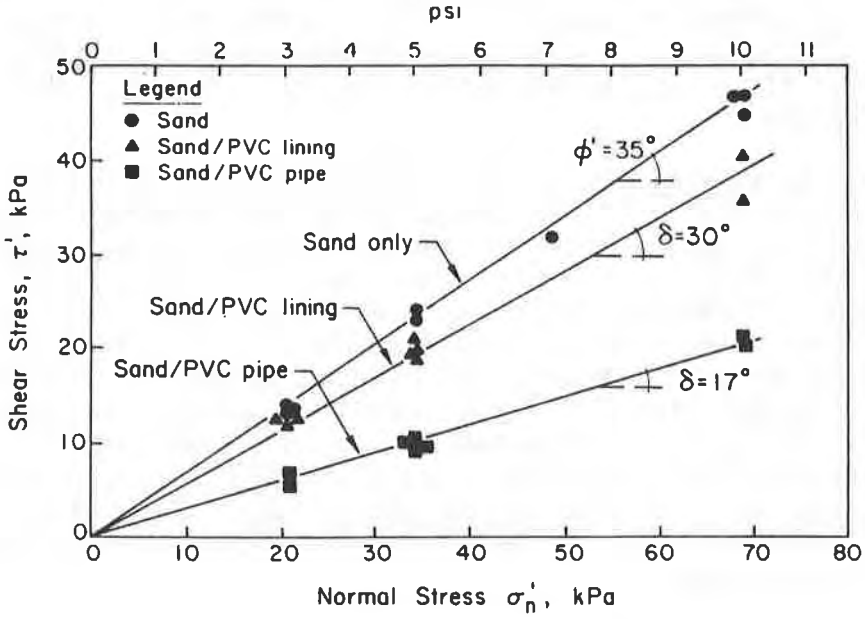

Figure 6. Shear vs. Normal Stress for Direct Shear Tests of Ottawa Sand on PVC Pipe and Lining Specimens

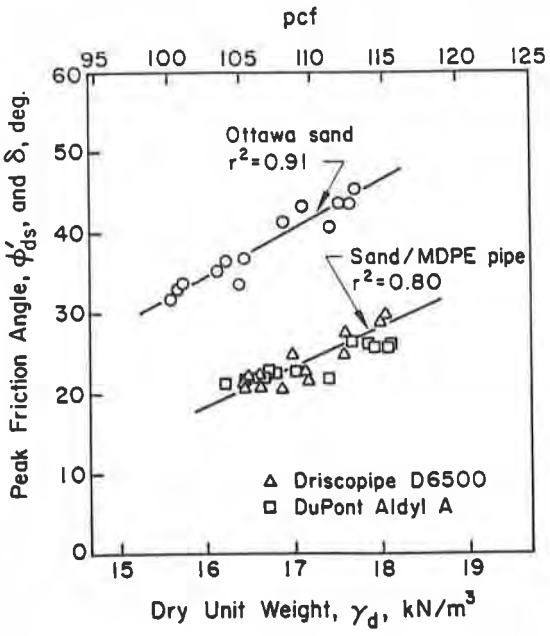

a. Ottawa Sand

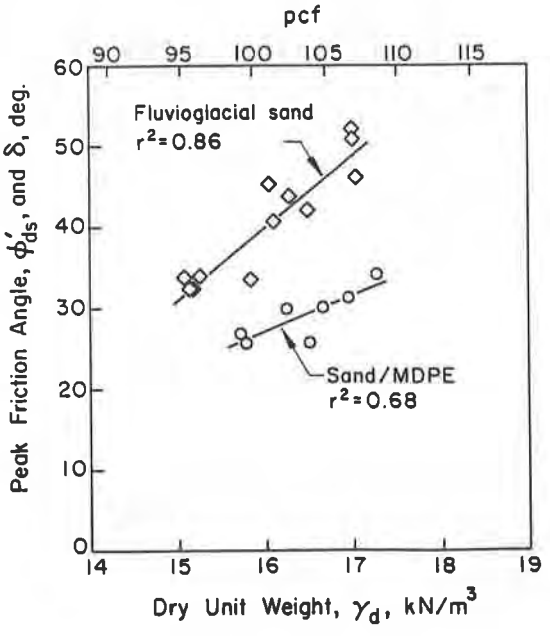

b. Fluvioglacial Sand

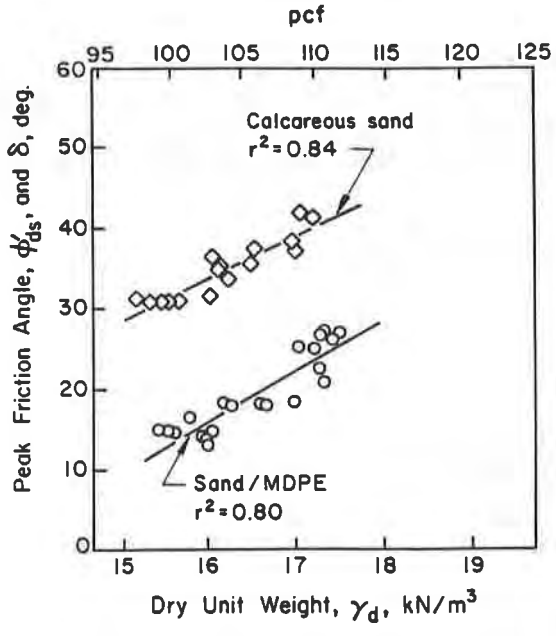

c. Calcareous Sand

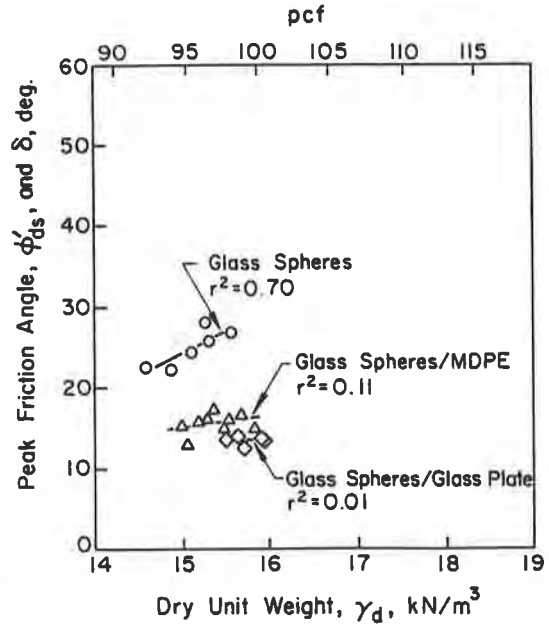

d. Glass Spheres

Figure 7. Peak ϕ'_{ds} and δ Plotted as Function of γ_d for Various Sands and Glass Spheres in Contact with MDPE

HDPE lining sample was sheared both parallel and perpendicular to the machine direction of the sample, and both sets of results are plotted in Figure 8. No significant difference was observed in either the MDPE or the HDPE comparisons, but a substantial variation was found for the PVC comparison, both in value and behavior. As noted in the evaluation of normal stress, the rigid PVC pipe sample gave results that were much lower than those of the flexible PVC geomembrane. Additionally, the peak friction angle determined for the PVC geomembrane reached a limiting value of about 30° when tested with Ottawa sand above a density of 16.5 kN/m^3. This limiting value is believed to be related to the critical state angle of shear resistance of the sand by the following equation:

$$\tan \delta_{max} = \sin \phi'_{cv}$$

A detailed discussion of this behavior may be found in O'Rourke, et al. (1990).

The difference between interface shear strength in various polymers may be accounted for by the relationship between the ratio of δ/ϕ'_{ds} and Shore D hardness, H_d (Figure 10). By knowing the H_d and ϕ'_{ds} for a particular sand at a minimum density, a designer may estimate the interface shear strength of a given sand-geomembrane combination. An evaluation of several sand-geomembrane combinations may quickly be made, providing flexibility and the ability to optimize the design of a cover or liming system to meet project-specific geometric and safety requirements.

APPLICATIONS

The use of the interface shear parameters in stability analyses may be best illustrated by two design examples that follow. Economic incentives drive most waste facility designs to provide a maximum capacity at the lowest cost, which often means attaining but not exceeding a minimum factor of safety as well as complying with any

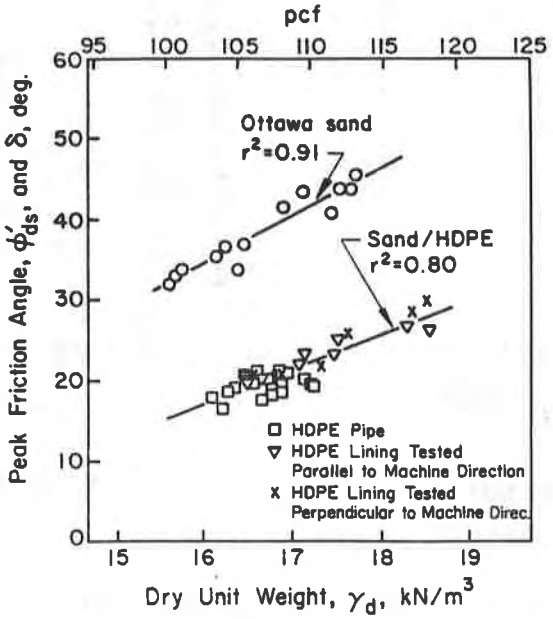

Figure 8. Peak ϕ'_{ds} and δ Plotted as a Function of γ_d for Ottawa Sand and Ottawa Sand on PVC Pipe and Lining

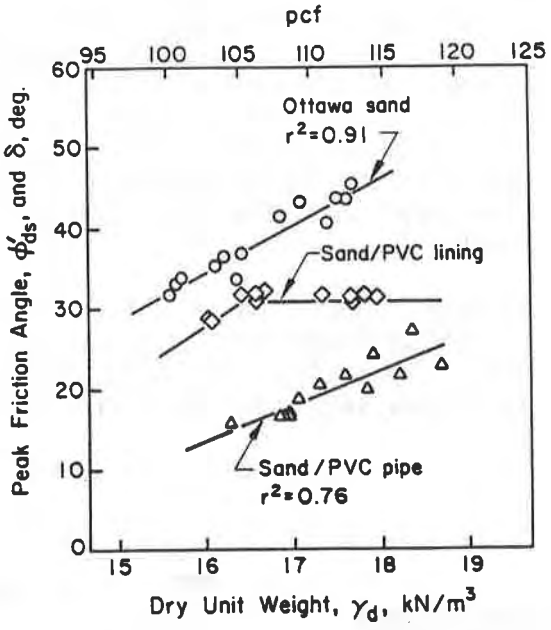

Figure 9. Peak ϕ'_{ds} and δ as a Function of γ_d for Ottawa Sand and Ottawa Sand on PVC Pipe and Lining

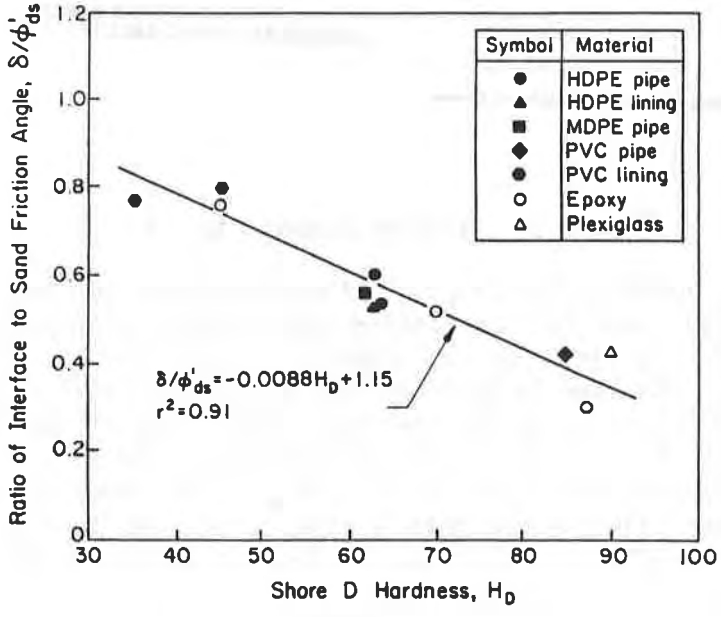

Figure 10. Ratio of Interface to Soil Friction Angles, δ/ϕ'_{ds}, vs. Shore D Hardness, H_D

technical requirements of the applicable regulations. Operational flexibility can also be important, because changes in the waste stream often occur over the projected life of the facility. Design Example #1 concerns a situation where the drainage sand specification of a cover system design is manipulated so a minimum required factor of safety may be met without the use of tensile reinforcement. In Design Example #2, an evaluation is made of the effects to facility operation caused by the potential use of an alternative geomembrane material in the liner system. Two different methods of analyses are used in the examples.

Design Example #1. A cover system, consisting of a 0.5m vegetative layer above a 0.3m sand drainage layer and a HDPE geomembrane, is being designed for an 8m high, 3H:1V exterior face of a landfill (Figure 11). The sand specified for this facility has characteristics similar to Ottawa sand described in this paper. A 1.2 minimum factor of safety is required.

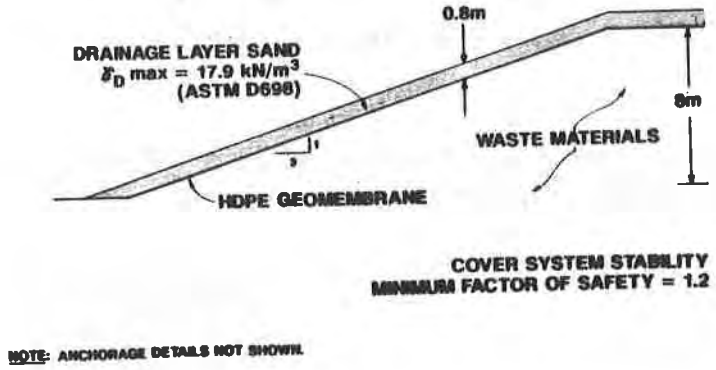

Figure 11. Design Example No. 1

For preliminary analysis the simplified wedge method is used, as discussed in Giroud and Beech (1989), and the assumption made that the shear and unit weight properties of the sand also apply to the vegetative cover soil. The initial design specifications call for the sand to be installed at a dry density equal to 90 percent of the maximum dry density, γ_{dmax}, as determined by ASTM D-698 (Standard Proctor Test), which testing has shown to be 17.9 kN/m^3. Direct shear testing of the sand at the 90 percent density level of 16.1 kN/m^3 shows a $\phi'_{ds} = 35°$, and a $\delta = 17°$ for the HDPE interface. In the simplified wedge method, the factor of safety is applied as a reduction of the shear strength angles by the following equations:

$$\phi'_m = \tan^{-1}\left(\frac{\tan \phi'_{ds}}{FS}\right)$$

$$\delta_m = \tan^{-1}\left(\frac{\tan \delta}{FS}\right)$$

in which ϕ'_m and δ_m are the mobilized angle of shearing resistance and the mobilized interface friction angle, respectively. For the materials used in this problem, $\phi'_m = 30.3°$ and $\delta_m = 14.3°$. The slope is then checked for stability by determining if any tensile reinforcement is needed for equilibrium, using the following equation:

$$a = \frac{\gamma_c T_c^2}{\sin 2\beta}\left[\left(\frac{2H\cos\beta}{T_c} - 1\right)\frac{\sin(\beta-\delta_m)}{\cos\delta_m} - \frac{\sin\phi_m}{\cos(\beta+ft_m)}\right]$$

where a = tensile reinforcement (kN/m or lb/ft)
γ_c = unit weight of cover soil (kN/m^3 or lb/ft^3)
T_c = thickness of cover soils (m or ft)
β = slope angle
H = height of slope (m or ft)

For the conditions of this problem, a minimum tensile reinforcement of 9.8 kN/m is needed to attain the 1.2 factor of safety requirement.

A second solution may be provided if an increase in the sand density can be achieved in the field. By specifying a dry density of 16.5 kN/m^3, equal to 92 percent of the maximum dry density, ϕ' may be taken as 37°, δ = 19°, ϕ'_m and δ_m as 32.1° and 16.0°, respectively, and the calculation shows that no tensile reinforcement is necessary. However, the designer must be very sure that the specified density level can actually be constructed, as this calculation also points out the sensitivity of the cover system stability to small changes in ϕ'_{ds} and δ. Perhaps a full scale field trial is necessary, consisting of a test pad constructed on the landfill side slopes, to test the effectiveness of the compaction method against the potentially less-than-firm waste slope.

Design Example #2. A new landfill cell is being piggybacked against the 3H:1V exterior face of an existing cell (Figure 12). The regulations require a liner system under all waste material to be placed in the new cell, including wastes placed above existing wastes. The liner system, which consists of a 0.6m layer of drainage sand (similar to Ottawa sand described herein) above a single geomembrane layer, will use two different types of geomembranes in separate sections of the landfill. HDPE will be placed on the cell bottom, because it has the best chemical compatibility with the probable leachate; while a plasticized PVC has been suggested for placement on the interior slope, to provide greater tolerance to the differential settlements which may occur. A preliminary design has been developed for a waste height of 30m, a 3H:1V exterior face, and top and bottom slope of 2 percent; in which a minimum factor of safety of 1.61 was obtained for interface stability using infinite slope calculations (FS = tanδ/tanβ).

However, an alternative geomembrane has been suggested for the interior slope, one which provides greater chemical compatibility than the PVC while still being able to withstand the probable differential settlements. No interface direct shear testing has yet been done with this alternative geomembrane, although Shore D hardness tests on manufacturer-supplied samples shows that it has a H_d of 54. Because of setback requirements, it is important to estimate a cell width required to meet the minimum 1.50 interface stability factor of safety caused by use of the alternative geomembrane.

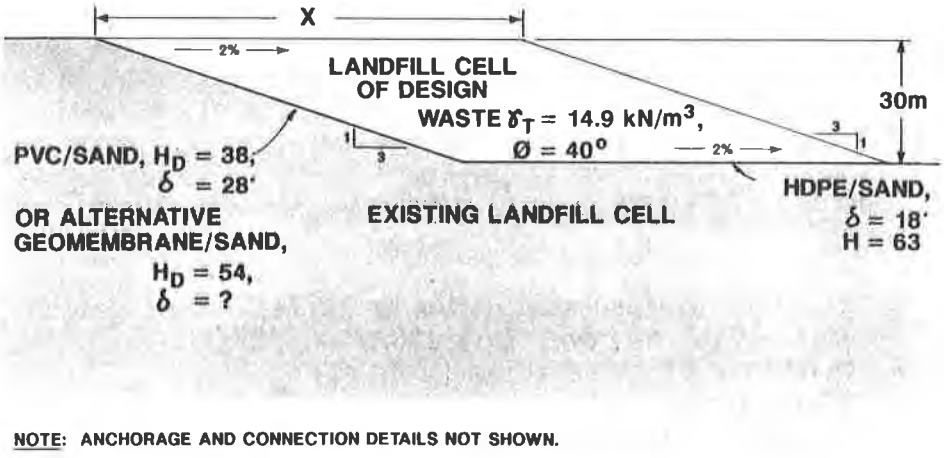

NOTE: ANCHORAGE AND CONNECTION DETAILS NOT SHOWN.

Figure 12. Design Example No. 2

The design specifications state that the Ottawa sand in the drainage layer must be placed at a minimum density of 16.2 kN/m^3. Direct shear testing has shown that at this density, ϕ'_{ds} = 35°, δ = 19° for the HDPE, and δ = 28° for the PVC. From Figure 10, a H_d = 54 has a δ/ϕ'_{ds} = 0.66. The interface friction angle of the alternative geomembrane may then be estimated at 23°, which provides a 1.28 factor of safety by infinite slope calculations. However, by optimizing the cell width, a 1.50 factor of safety against sliding is obtained for a cell width of 32m, using wedge analysis with a computerized limit equilibrium model (Morgenstern-Price method of slices).

ADDITIONAL CONSIDERATIONS

Landfill designs must evaluate several different loading combinations and possible durations when analyzing the stability of cover systems and linings. The weight of construction equipment is often modeled as an equivalent soil load on the slope, while it has been suggested by Richardson & Koerner (1987) that equipment braking force be approximated by 30 percent of the equipment weight applied at the surface and orientated parallel to the slope. Earthquake forces are frequently treated as a disturbing force located at the center of gravity of the potential sliding mass and orientated either horizontal or parallel to the slope face (U.S. Navy, 1986). If not properly controlled, seepage can be a major cause of instability, because the combination of a drainage layer above a geomembrane will direct seepage parallel to the slope face, which may create substantial driving forces. Seepage must be controlled, either by use of a tight vegetative cover and surface drainage to limit infiltration, or through use of internal collection drains to limit head buildup.

Should a given liner or cover system be less stable than desired for the various loading conditions, a change in slope geometry may be necessary. The slope angle may simply be flattened, or a stepped or benched face may be adopted to reduce the length of the interface weak plane. The width of the bench should be large enough to fully disrupt any potential linear failure plane, at a minimum equal to the horizontal width of the cover soils. Wedge analysis methods may be used to determine the stability of each step independently.

Although difficult to quantify, the effect of polymer aging or chemical degradation should be considered when analyzing long-term stability. While the softening of a polymer, due to long-term waste exposure for example, would actually

improve the interface shear strength; any increase in a polymer's hardness, such as from the volatilization of the plasticizers in a PVC geomembrane for example, would cause a decrease in the interface strength. Such time and exposure-dependent behavior is extremely difficult to predict, and may be best dealt with by the selection of a reasonable factor of safety.

CONCLUSIONS

The shear strength developed at a sand-geomembrane interface is critical to the stability of cover systems and linings used in waste containment structures. Based upon the results of an extensive testing program, a method to characterize the sand-geomembrane interface strength has been presented herein. Effects of variations in soil type and unit weight, polymer type, normal stress, repeated loading, and physical features of the polymer surface have been evaluated. Considerations have been made of design applications, illustrated in two sample problems.

ACKNOWLEDGMENTS

The research, on the basis of which this paper was written, was sponsored in part by the New York Gas Group (NYGAS) under a contract with Cornell University, entitled "Improved Anchoring Practices for Plastic Gas Distribution Piping." The research results do not necessarily represent the views of NYGAS, or imply any warranty on its part regarding authenticity. Research on polymer characteristics was supported by the New York State Water Resources Institute at Cornell University.

Special thanks are extended to Professor Anil Netravali of the New York State College of Human Ecology at Cornell University for his contributions regarding polymer hardness. Our gratitude also is extended to Dr. C.H. Trautmann of Cornell University and Mr. G. Pellerin of ABB Environmental Services, Inc., for their assistance during the testing program, and to Mr. D. Hunt, Mr. R. Koster, and Mr. S. Mitchell of ABB Environmental Services, Inc., for their discussion regarding applications in waste containment. Ms. Marie Peoples prepared the manuscript, and Mr. Ali Avcisoy and Ms. Dawne Gilpatrick prepared the drawings.

REFERENCES

Giroud, J.P. and Beech, J.F. (1989). "Stability of Soil Layers on Geosynthetic Lining Systems," Proceedings, Geosynthetics '89 Conference, IFAI, San Diego, California, pp 35 - 46.

O'Rourke, T.D., Druschel, S.J., and Netravali, A.N. (1990). "Shear Characteristics of Sand-Polymer Interfaces," Journal of Geotechnical Engineering, ASCE, Vol. 116, No. 3, March, pp 451-469.

Richardson, G.N. and Koerner, R.M. (1987). Geosynthetic Design Guidance for Hazardous Waste Landfill Cells and Surface Impoundments, Geosynthetic Research Institute, Drexel University, Philadelphia, Pennsylvania.

U.S. Navy (1986). Design Manual - Soil Mechanics, Foundations and Earth Structures," NAVFAC DM-7, Department of the Navy, Washington, D.C.

Geosynthetic Material Response to Landfill Cap Settlement and Subsidence

Ronald K. Frobel, P. E.
R.K. Frobel & Associates, USA

ABSTRACT

Once it has been determined that a landfill (hazardous or municipal) has reached the end of its useful life, it will become necessary to construct a final closure or cap which then must be maintained for many years (certainly in excess of the recommended 30 years). Stabilization may or may not be required before final closure begins. Settlement may be uniformly distributed and as is the case with old municipal landfills, will probably occur before closure. Subsidence, however, is not uniform and will occur after closure in an unevenly distributed manner for many years. In any event, the cap must be designed to settle or deflect and must retain original designed integrity (drainage, moisture barrier, gas collection, etc.) as much as possible.

This paper will review current design methodology for localized subsidence within a landfill cap after closure. Geosynthetic (geomembrane and/or geocomposite) barrier materials and their response to laboratory simulated subsidence were evaluated using large scale multiaxial stress-strain testing. It is shown that test results can be compared to theoretical subsidence values that could be used for either interim or final closure design.

This paper will review current EPA recommended landfill cap design and the subsidence mechanism under a cap due to waste decomposition. This multiaxial test will be described and test results will be given for several current geomembrane products used in cap design.

INTRODUCTION

Geosynthetics are now an accepted material for use in the design of solid and hazardous waste landfills. The design engineer is faced with the proper selection of geosynthetics based on design parameters such as puncture resistance, friction characteristics, seam strength, etc. Many geosynthetic properties are index test properties commonly used in manufacturing quality control and thus are a quick "reference" test method for comparison of products. Performance test methods, however are methods which simulate in the laboratory as closely as practical selected conditions experienced in the field and which can be used in design. One such performance test

conditions experienced in the field and which can be used in design. One such performance test method is the multiaxial stress rupture test currently under development in ASTM. This type of test could be used to evaluate a geosynthetic subjected to gradual or even sudden subsidence under a landfill cap.

CURRENT LANDFILL CAP MINIMUM REQUIREMENTS

RCRA Technical Guidance Documents present design and operating parameters and evaluation techniques that generally comply with Design and Operating Requirements for the Closure/Post Closure Requirements of Title 40 Code of Federal Regulations (40 CFR) part 264 (permitted) and part 265 (interim status) for treatment, storage and disposal facilities. Current Technical Resource Documents (TRD) present summaries of the state-of-the-art techniques determined by the U.S. Environmental Protection Agency to be acceptable engineering designs or procedures. Guidance currently available for landfill covers recommends as a minimum a multilayer final cover design that includes the following elements, from top to bottom (USEPA, 1989):

- A top layer consisting of two components: (1) a vegetated or armored surface component, selected to minimize erosion and promote surface drainage (2) a soil component with a minimum thickness of 60 cm (24 in.) comprised of top soil and/or fill soil as appropriate.

- A soil drainage layer (and protective bedding for a geomembrane) with minimum thickness of 30 cm (12 in.) (minimum hydraulic conductivity of 1×10^{-2} cm/sec) that will have a final slope of at least 3 percent after settlement and subsidence; or a drainage layer consisting of a geosynthetic with equivalent drainage performance characteristics.

- a two component, low permeability soil layer, lying wholly below the frost zone, that provides long term minimization of water infiltration into the underlying wastes consisting of (1) a 20 mil (0.5 mm) minimum thickness geomembrane and (2) a compacted soil component with minimum thickness of at least 60 cm (24 in.) and saturated hydraulic conductivity of 1×10^{-7} cm/sec., or less.

Depending on the region and climatic factors, the EPA recommended cover design can have optional layers to provide rodent/animal protection, frost protection, biotic barrier and gas venting. Figures 1 and 2 are the EPA recommended cover designs showing the location of the various layers.

The geomembrane component is required to have a minimum thickness of 20 mil (0.5 mm), however current caps are being constructed with 30 mil (0.75 mm) and thicker materials. The selected geomembrane must withstand stresses encountered both during installation and after closure. Site specific design factors include material compatibility with adjacent layers, installation stress, slope stability (surface friction), climate, normal stresses and settlement/subsidence.

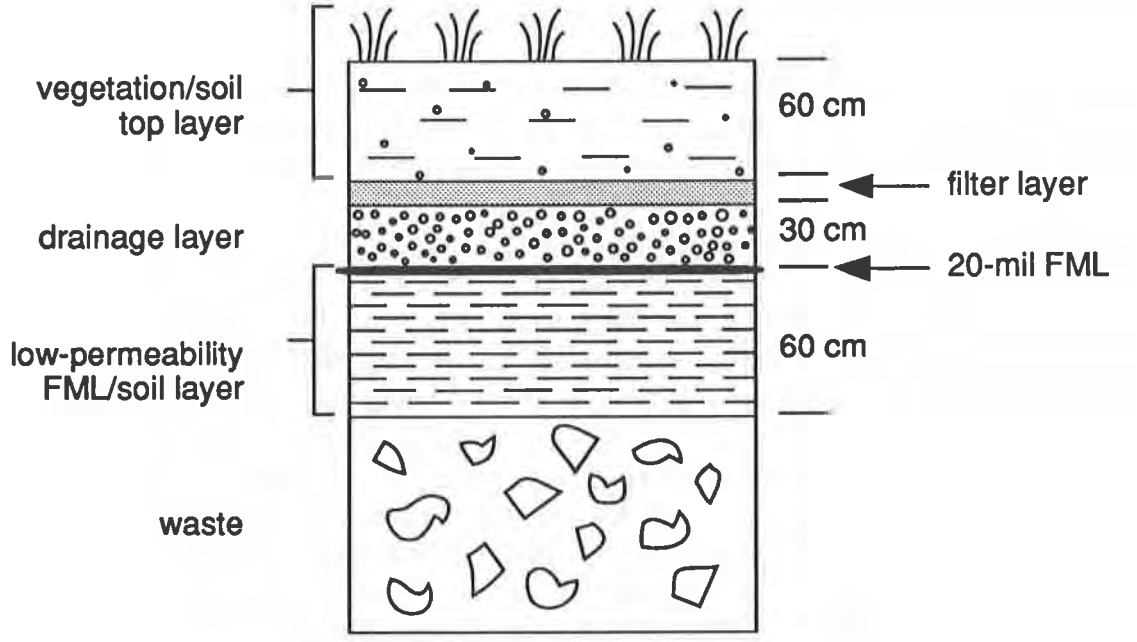

Figure 1. EPA Recommended Cover Design (USEPA, 1989)

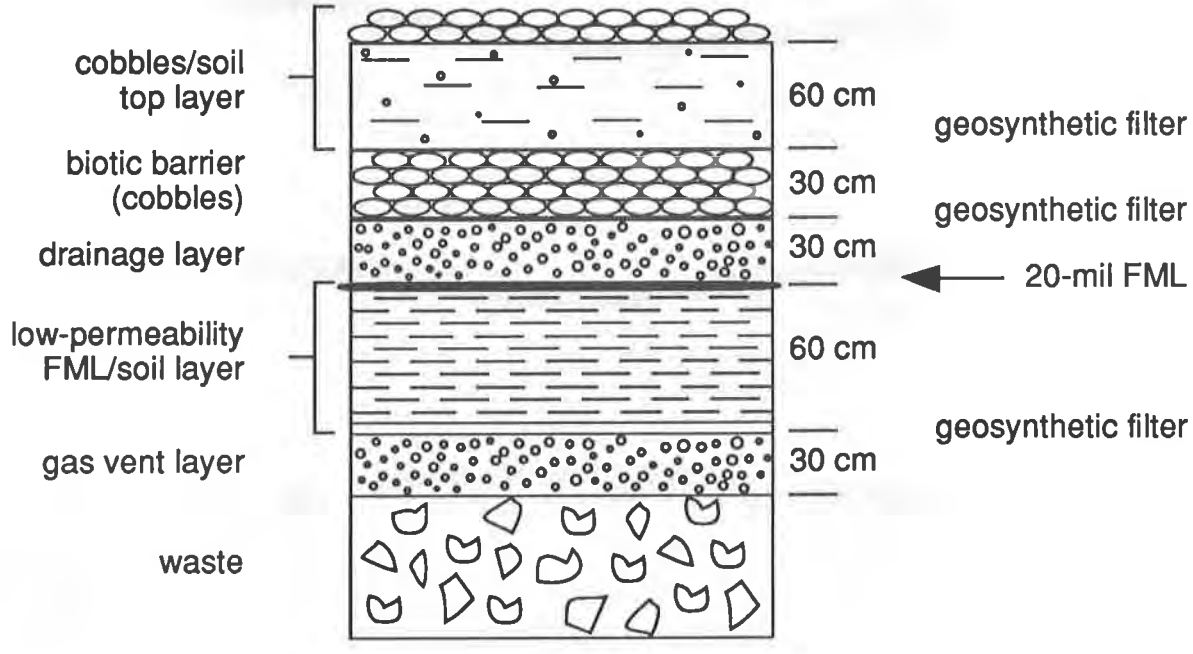

Figure 2. EPA Cover Design with Optional Layers (USEPA, 1989)

SUBSIDENCE RELATED PROBLEMS AFFECTING CAP DESIGNS

Settlements and subsidence of cover systems over municipal sanitary landfills and hazardous waste landfills are recognized and documented occurrences. Differential or localized subsidence will cause stress in the geosynthetics component of the cover system.

Classical techniques in evaluating the affects of subsidence can be found in many geotechnical areas of reference including foundation investigations, mining, tunneling, landfilling, thermo Karsts and Karst terrain and ground water withdrawal. Murphy and Gilbert (USEPA 1985, 1987) conducted studies to determine the potential for settlement of waste fill and subsequent cover system damage on hazardous waste landfills and to develop a numerical (FEM) model. Their studies identified three major settlement or subsidence related problems shown schematically in figure 3. The first is related to global or large area settlements within the waste pile causing tension cracks at the surface and disrupting any surface drainage. The second, also related to large area subsidence results in ponding of surface water. The third and most damaging to a geosynthetic in a cover system is localized cavity subsidence caused by a point source decomposition of material or sudden failure/deterioration of a container such as a metal barrel.

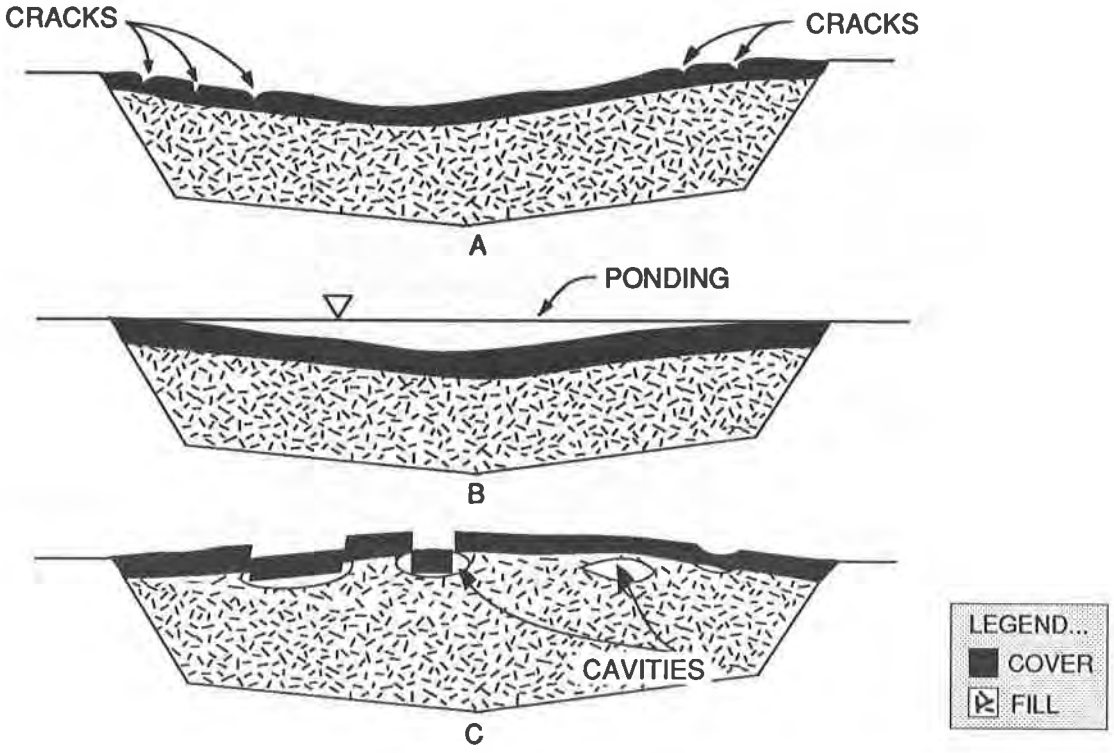

Figure 3. Subsidence Related Cover Problems
(USEPA, 1985)

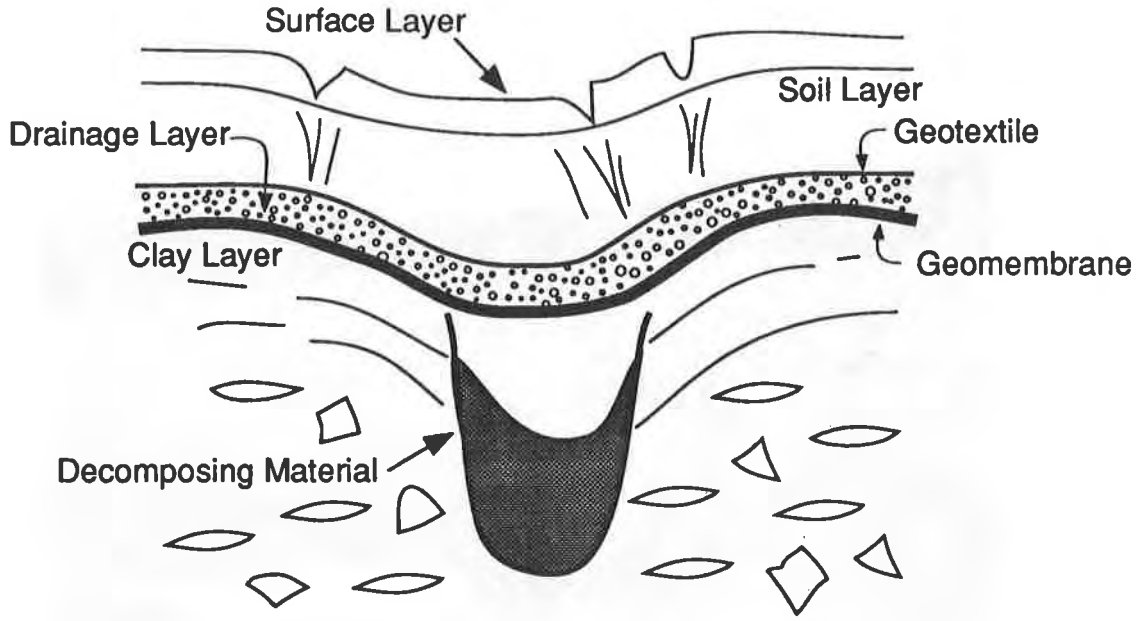

Figure 4. Localized Subsidence Effects on Cover Profiles

The third cover problem area of localized subsidence is the subject area of this discussion due to the potential for damage to the cover system geosynthetics. A schematic of localized subsidence due to post closure waste decomposition is shown in figure 4. Figure 5 is a photo showing the results of localized subsidence under a soil covered geomembrane cap. According to Gilbert and Murphy, 92 percent of cap subsidence is caused by collapse of voids in waste (USEPA, 1985). The larger waste facilities where wastes are buried in metal drums are potentially the worst case situations producing the greatest amounts of settlement. According to Gilbert and Murphy (USEPA, 1985) the maximum amount of cover subsidence for a worst case (drums, deep fill, loose waste) is estimated to be 11.5 percent.

The numerical models using equations for linearly elastic deformation and the use of finite element (FEM) analysis for predicting this amount of landfill settlement is described by Gilbert and Murphy (USEPA, 1985, 1987). The value of such analytical solutions is very limited and only as good as the numerous assumptions concerning waste placement methods. The analyses do not account sufficiently for construction methods and procedures and apply generally to hazardous waste drum placement and carefully placed soil layers.

The older landfills where air space was not important and thus compaction of waste layers was less critical will produce excessive settlements over the years. Due to the cost of landfilling operations today, air space is costly and waste layer compaction has increased to the point where densities within commercial landfills are ranging between 65 and 88 lb/ft^3 (10 - 13.8 kN/m^3). Thus, subsidence in the newer landfills may not be as much of a problem as in older landfills due to the filling of voids during compaction and the elimination of large waste drums and containers.

Figure 5. Results of Localized Subsidence of a Cap.

A simulation of the geometry of subsidence within a landfill can be extracted from the work done on coal mine subsidence and tunneling subsidence predictions. In general, allowable subsidence strains will be governed by the clay component in the cover (which should not exceed 1 percent maximum tensile strain), whereas the geomembrane component of the cap will generally be unaffected by strains up to 10 percent (USEPA, 1987). For landfills, the void volume will be approximately equal to the volume of the surface depression at the point of subsidence. Looking at the geometry of subsidence, the geomembrane or geosynthetic component can approximate a segment of a sphere (geometrical assumption) as the material expands to the void.

As the void opens up and the geosynthetic conforms to the subsidence created, stress is developed in the geosynthetic by the weight of the overburden soil and rock materials in the cap profile. The spherical radius of curvature of the geosynthetic material is related to the change in length of the portion of the material spanning the void. The stress on the geosynthetic is assumed to be normal to the material and soil interaction with the geomembrane is assumed to be negligible for layered soil materials used in a cap cover. This may not be the case when considering soil arching theory and interaction with a reinforcing geosynthetic such as a biaxial geogrid or woven geotextile (see Giroud, et al., 1988). A further assumption for the purposes of considering a circular opening (spherical deflection) is that the geosynthetic has isotropic tensile characteristics (this is of course not always the case). Figure 6 illustrates the deformed geosynthetic over the void area.

An estimate of the design strength of the geosynthetic when subjected to a gradual subsidence and normal loading can be obtained based on figure 6 using the following equation (USEPA, 1990):

$$\sigma_d = \frac{2 z r^2 \gamma_c H_c}{3t (r^2 + z^2)}$$

where: σ_d = Design stress in the geomembrane
z = Vertical deflection
r = Depression radius
γ_c = Average soil cover density
H_c = Average soil cover height
t = Geomembrane thickness

The soil cover density and thickness over the geomembrane will be known and the void dimensions z and r can be estimated from the type of waste, density of waste layers and age of landfill. The thickness (t) of the type of geomembrane selected for a cover material can then be chosen by trial and error beginning with 30 mil (0.75 mm) thickness. Once the stress is estimated for design purposes, a comparison can be made with multiaxial stress rupture results to determine a factor of safety for that particular product.

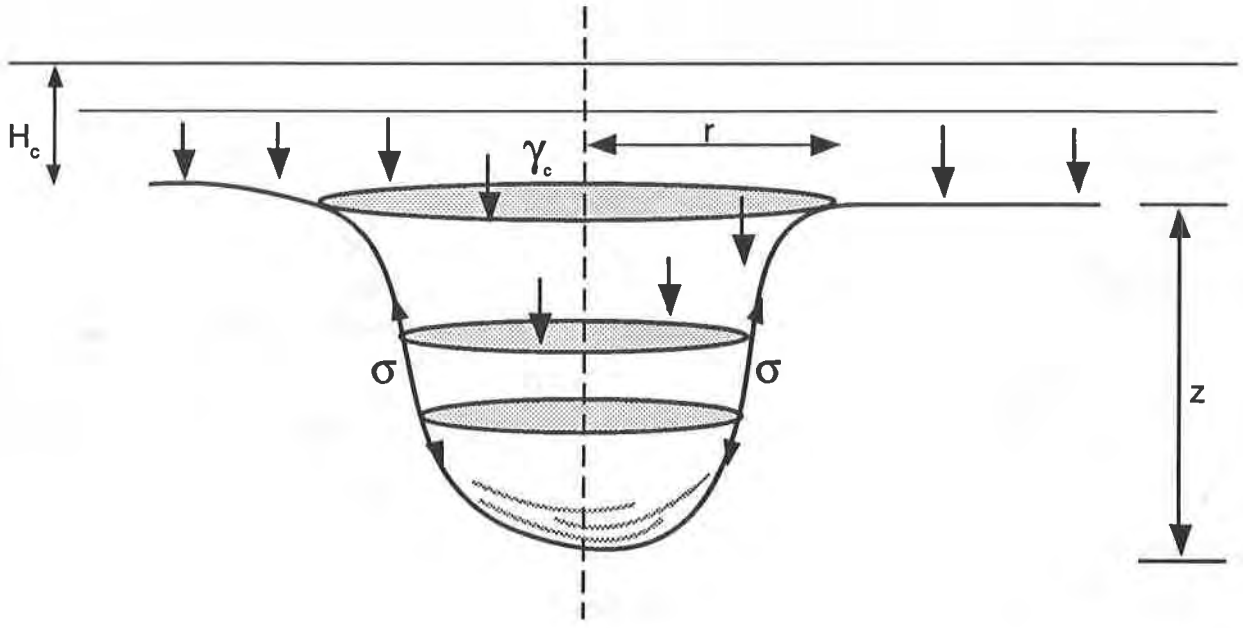

Figure 6. Spherical Segment Formed by Geosynthetic Conforming to a Void

where: σ = Stress in the geosynthetic
r = Radius of depression
z = Vertical Deflection
γ_c = Soil Cover Density
H_c = Soil Cover Height

MULTIAXIAL STRESS/STRAIN TESTING

Large scale "performance" test methods are becoming more and more popular as test methods which attempt to simulate stresses or loading occurring in the field. One such test method currently in draft form in ASTM (ASTM Committee D35 on Geosynthetics) and a GRI standard (GM-4) is the Multiaxial Stress Rupture test. In this test a geosynthetic is placed in a pressure apparatus approximately 20 inches (500 mm) in diameter and subjected to increasing pressure (air or air on water) until failure. The test is designed to evaluate a materials response to out-of-plane loading as would occur during sudden or uneven subsidence of supporting soils as in a landfill cover.

Figure 7 illustrates a multiaxial upward burst loading frame used for this type of testing. The top ring has a 500 mm inside diameter with smooth radius edge, 'o'-ring seals and bolted connection to the bottom plate. Pressure inlet/outlet ports as well as pressure measurement is located on the bottom plate. The top frame is for central deflection measurement via mechanical, optical or LVDT. This type of load frame allows for 360 degree observation of the specimen under test.

Based on current thinking and draft procedures, once the test specimen is placed in the loading frame and secured by the flanges, a seating (initial) pressure of 1 psi is maintained on the specimen for 20 minutes, after which pressure is raised incrementally, 1 psi/min until failure. Fail pressure, displacement measurements at pressure increments, mode of failure and time to failure are all recorded from which stress vs. strain curves can be generated based on the following formulations (ASTM, 1989 and GRI, 1989):

STRAIN CALCULATIONS

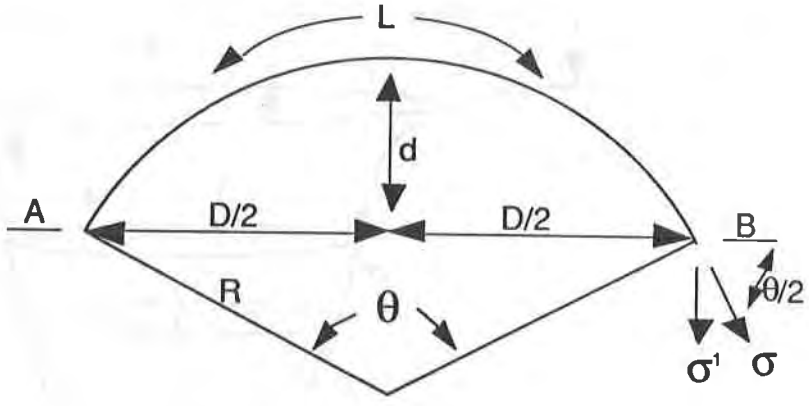

For d<D/2:

$$R = \frac{D^2 + 4d^2}{8d}$$

$$\theta = 2\tan^{-1}\frac{4(D)d}{D^2 - 4d^2}$$

$$L = R * \theta$$

$$\varepsilon = \frac{L - D}{D}(100)\ \text{in}\%$$

For d>D/2:

$$L = \pi\sqrt{\frac{D^2 + 4d^2}{8}}$$

$$\varepsilon = \frac{L - D}{D}(100)\ \text{in}\%$$

Where:

- R = Sphere radius
- L = Length of Segment A - B
- D = Specimen diameter
- d = Vertical deflection
- P = Internal Pressure
- t = Specimen thickness
- ε = Strain (%)
- σ = Stress kPa or psi

STRESS CALCULATIONS

For d<D/2:

$$\sigma = \frac{(D^2 + 4d^2)P}{4d\,t\,\sin(\theta/2)}$$

For d ≥D/2: $(\sigma = \sigma^1)$

$$\sigma = \frac{dP}{t}$$

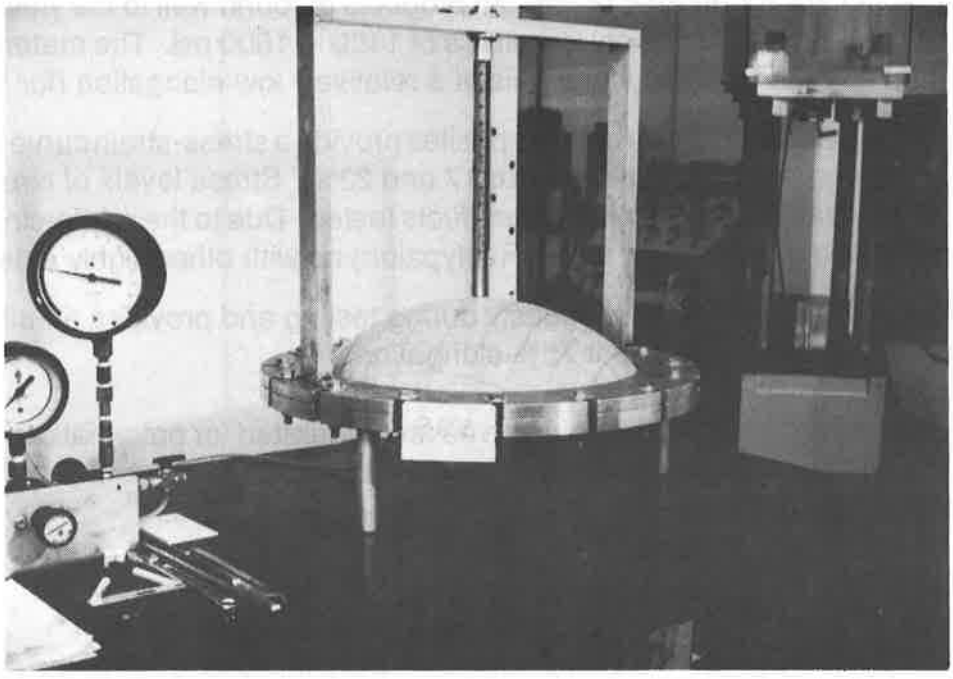

Figure 7. Photo Showing a Multiaxial Upward Burst Loading Frame With Specimen in Place.

Using the apparatus shown in figure 7, several types of geomembrane materials were tested. The geomembrane materials chosen were consistent with the types that could be specified in a cover design where a layered system is used. The types of geomembranes were as follows:

60 mil (1.5 mm) HDPE textured
40 mil (1.0 mm) VLDPE textured
40 mil (1.0 mm) VLDPE smooth
30 mil (0.75 mm) PVC
36 mil (0.90 mm) CSPER (Hypalon)/geotextile composite

All of the above products differ in polymer type and thickness. Three were developed for capping of steep slopes (60 mil textured HDPE, VLDPE textured and 30 mil Hypalon/geotextile). The HDPE products are semi-crystalline polymer materials and thus behave very differently under

stress as compared to the flexible thermoplastics such as PVC. All were tested using the procedure described previously. A summary of the stress vs. strain results are illustrated in the graph of figure 8. Referring to figure 8, the following general observations can be drawn.

- The HDPE textured sheet yields at approximately 11% and 2500 psi, after which the material creeps to failure, usually at a thin cross section of the textured material. Total elongation is approximately 16%.
- The VLDPE roughened or smooth products respond well to the yield point which occurs at 14 to 18% but at relatively low stress of 1400 to 1600 psi. The material creeps rapidly after yield and the textured sheet fails at a relatively low elongation (for VLDPE) of 42%
- The Hypalon/geotextile geocomposites provide a stress-strain curve with a sharp yield (also ultimate stress) point of between 17 and 23%. Stress levels of over 6500 psi at yield are substantially higher than other products tested. Due to the reinforcing scrim creep is not as much of a problem with CSPER (Hypalon) as with other highly extensible products
- PVC tends to creep continuously during testing and provides an ultimate stress of approximately 1800 psi at 75% elongation.

Once a series of stress-strain curves are generated for potential cap materials and seams, actual design stresses can be compared to these values to determine if the allowable or actual material stresses are exceeded.

CONCLUSIONS

The potential problems of cap subsidence are obvious, even to the casual observer. Aside from distorting a cap design intended to shed precipitation and minimize infiltration, subsidence will induce stress and strain on any geosynthetics placed in a landfill cap as part of the overall designs. Creep of the geosynthetic materials must be considered and evaluated and those that are highly creep sensitive should be avoided in some designs.

There is still much to be learned as to the waste characteristics and thus the mechanical properties of fill material at a specific waste site. As the newer "engineered" waste disposal landfills are constructed with known waste types and controlled placement methods, accurate engineering properties of the waste such as density (γ), internal angle of friction (ϕ) and subsidence angle (α) will be documented. Thus an accurate engineering analysis of subsidence within the waste pile and cap profile will be available which will provide the needed design values. Performance tests such as the multiaxial stress rupture can be used as a model to determine the adaptability of geosynthetic to known subsidence, not only in landfill caps but any other application where a geosynthetic may be required to conform to or bridge a void area. From this type of test, a family of stress vs. strain curves can be developed for various products (similar to figure 8) including seam areas thus providing an allowable stress/strain value. Comparing the allowable value to the design value will give the design engineer a needed factor of safety (FS) that the allowable value will not be exceeded.

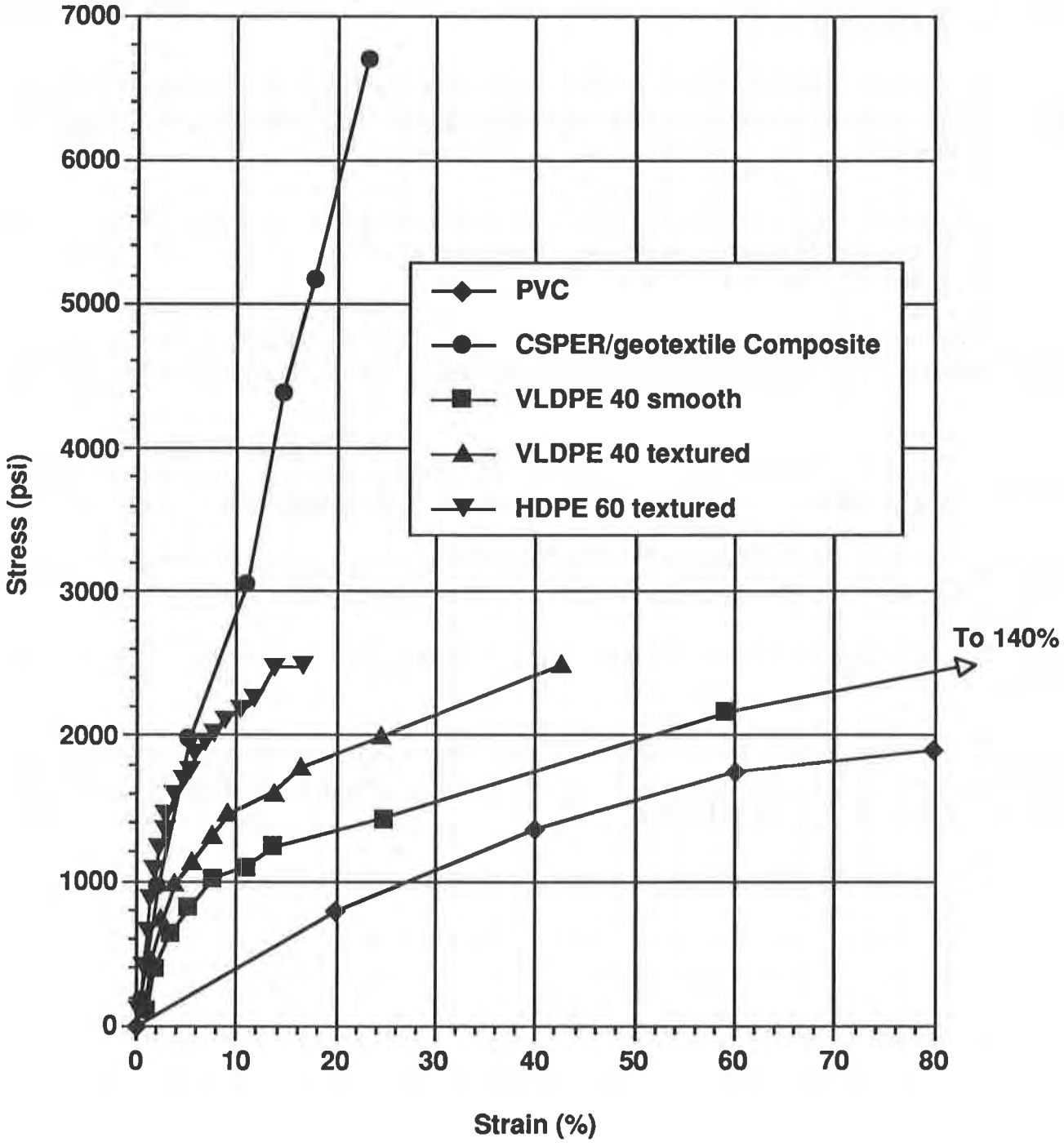

Figure 8. Multiaxial Stress vs. Strain For Five Geomembrane Materials

REFERENCES

U.S. Environmental Protection Agency. 1985. Final Covers on Hazardous Waste Landfills and Surface Impoundments, Report No. EPA/530-SW-89-047, Office of Solid Waste and Emergency Response, Washington, D.C.

U.S. Environmental Protection Agency. 1989. Settlement and Cover Subsidence of Hazardous Waste Landfills, Report No. EPA/600/2-85-035, Municipal Environmental Research Laboratory, Cincinnati, Ohio.

U.S. Environmental Protection Agency. 1987. Prediction, Mitigation of Subsidence Damage to Hazardous Waste Landfill Covers, Report No. EPA/600/2-87-025, Hazardous Waste Engineering Research Laboratory, Cincinnati, Ohio.

U.S. Environmental Protection Agency. 1990. Seminar Proceedings–Design and Construction of RCRA/CERCLA Final Covers, CERI 90-50, Office of Research and Development, Washington, D.C.

American Society for Testing and Materials (ASTM). 1989. Large Scale Hydrostatic Pressure Testing of Geosynthetics–Draft Method D35.10.88.01, ASTM, Philadelphia, Pennsylvania.

Geosynthetics Research Institute (GRI). 1989. Three Dimensional Geomembrane Tension Test, GRI Test Method GM 4, Geosynthetic Research Institute, Philadelphia, Pennsylvania.

Holzer, T.L.. 1984. Man-Induced Land Subsidence, Geological Society of America, Inc. Boulder, Colorado.

Giroud, J.P., R. Bonaparte, J. Beech and B.A. Gross. 1988. Load Carrying Capacity of a Soil Layer Supported by a Geosynthetic Overlying a Void. Proceedings International Geotechnical Symposium on Theory and Practice of Earth Reinforcement, Fukuoka, Japan, pp. 185-190.

ENVIRONMENTAL APPLICATIONS

Underwater Geomembrane Placement

Fred P. Rohe
Environmental Protection, Inc., USA

ABSTRACT

Environmental Protection, Inc. (EPI) participated in the design and development of a prototype system to install a 30 mil PVC liner and 3 inches of concrete underwater in the Coachella Canal located in Southern California. This project, under the direction of the U.S. Bureau of Reclamation, is the first of its kind anywhere in the world. The development of this technology required the cooperation of many different suppliers, including EPI, under the coordination of the prime contractor, Kiewit Pacific Company. The development and implementation of a unique solution to liner placement underwater is the beginning of a significant effort to conserve water resources and to reduce canal maintenance and construction costs.

INTRODUCTION

In the spring of 1988, EPI was one of several suppliers to bid on providing a 30 mil PVC geomembrane liner to the U.S. Bureau of Reclamation for canal improvement. The project, titled "Coachella Canal Inplace Lining Prototype, All American Canal Relocation, California," is the first of its kind anywhere. After completion of the bidding process, the Bureau of Reclamation determined that Kiewit Pacific Company (Kiewit), of Santa Fe Springs, California, should be awarded the contract. In the Fall of 1988, EPI was contacted by Mr. Bill Giroux, Design Engineer for Kiewit, regarding the supplying of the PVC geomembrane liner. Over the next several months, much research was done in order to develop methods of handling the PVC liner during the inplace lining process. Since the project was being done on a fast track schedule, actual fabrication of much of the equipment was being undertaken while other development was being done regarding the handing of the liner material. Fabrication of the geomembrane was undertaken during February and March of 1989 with shipment to California and actual placement of liner in the canal beginning in May of 1989.

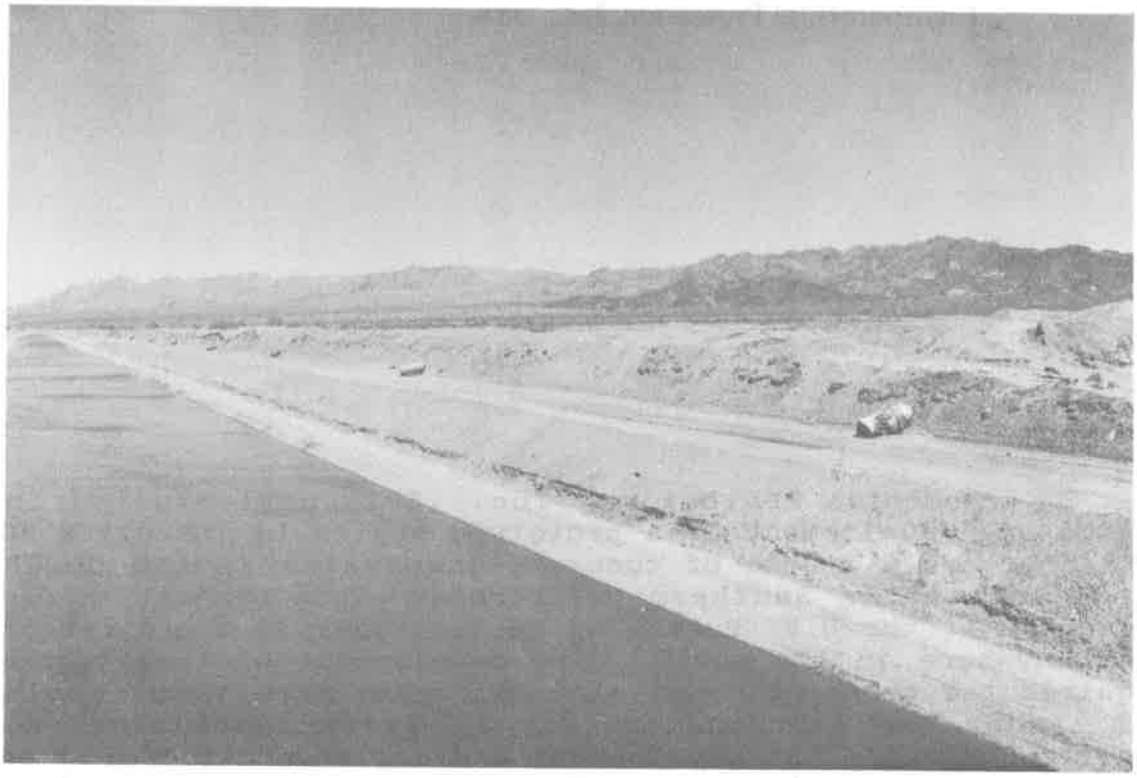

FIGURE 1. The Coachella Canal Prepared Grade and Geomembrane Rolls staged for Installation

MATERIAL

Polyvinyl Chloride (PVC) geomembrane was selected as the membrane lining material for the underwater application at the Coachella Canal. The Bureau's selection of PVC geomembrane was based on many factors, including:

1. The availability of large panels. PVC was fabricated into panels 58.6' x 200'.

2. The PVC geomembrane is highly flexible and retains its properties over a wide temperature range. This permits the liner to conform to the subgrade better than other available geomembrane materials.

3. The PVC geomembrane is easily field spliced with solvent welding. The PVC also has very good puncture, abrasive, and tear resistance properties, which are important in minimizing damage during installation.

4. PVC has a proven history of use in canal lining for more than 30 years by the Bureau of Reclamation.

Since the lining of the canal was to be done in two passes requiring a longitudinal seam in the PVC liner down the center of the canal, it was necessary to use a geomembrane that could be sealed underwater. Since an unbonded longitudinal seam would not provide the necessary seepage control, laboratory studies concluded that a vinyl swimming pool adhesive used to repair pool liners would be a suitable adhesive for this seam. Laboratory test results of seam strengths for the underwater seam proved comparable with normally fabricated field seams.

There was also a concern that the freshly placed concrete would have a tendency to slough down the 2.5 to 1 slope of the canal sidewalls over the geomembrane. Initial design requirements called for the application of a 3.4 ounce per square yard non-woven, needle-punched, geotextile fabric on the side slopes on top of the PVC. The final solution involved the contractor gluing this geotextile to the PVC liner at their facility in Santa Fe Springs. The liner panels were then refolded and rolled prior to installation at the project site. It is anticipated that a factory laminated product, which will provide both the 30 mil PVC and a non-woven geotextile bonded to one side of the liner, will be available for future projects.

This product will save considerable time and manpower in the placement of the two materials at the same time. Currently, a new GeoLam product, consisting of Trivera non-woven geotextile laminated to a PVC geomembrane, is being introduced by Occidental Chemical Corporation. This composite material has evolved from the research and development on this canal project.

The preliminary design concept, proposed by Mr. Giroux, involved holding the PVC in a manner much like a garage door track supports the sides of an overhead garage door. The track design called for the inclusion of a hem in the liner material along both sides of the panel. This hem was to be filled with a rope to provide body and hold the liner securely in the guide track. Since PVC geomembrane had never been installed underwater in an operating canal, there was no data available as to how the geomembrane would behave using this new procedure.

The development involved the use of a PVC jacketed nylon rope. In order to develop data as to the behavior of the liner during this installation procedure, EPI fabricated for Kiewit Pacific, several full size samples of the PVC liner. In addition, EPI fabricated a small section of liner 60 feet wide, which was furnished to Mr. Giroux at his office in Omaha, Nebraska. Mr. Giroux proceed to do full scale testing with this liner at the YMCA pool in Omaha. From the data generated in these tests, it was determined that support of the liner on the two outside edges would not be sufficient to control the final placement of

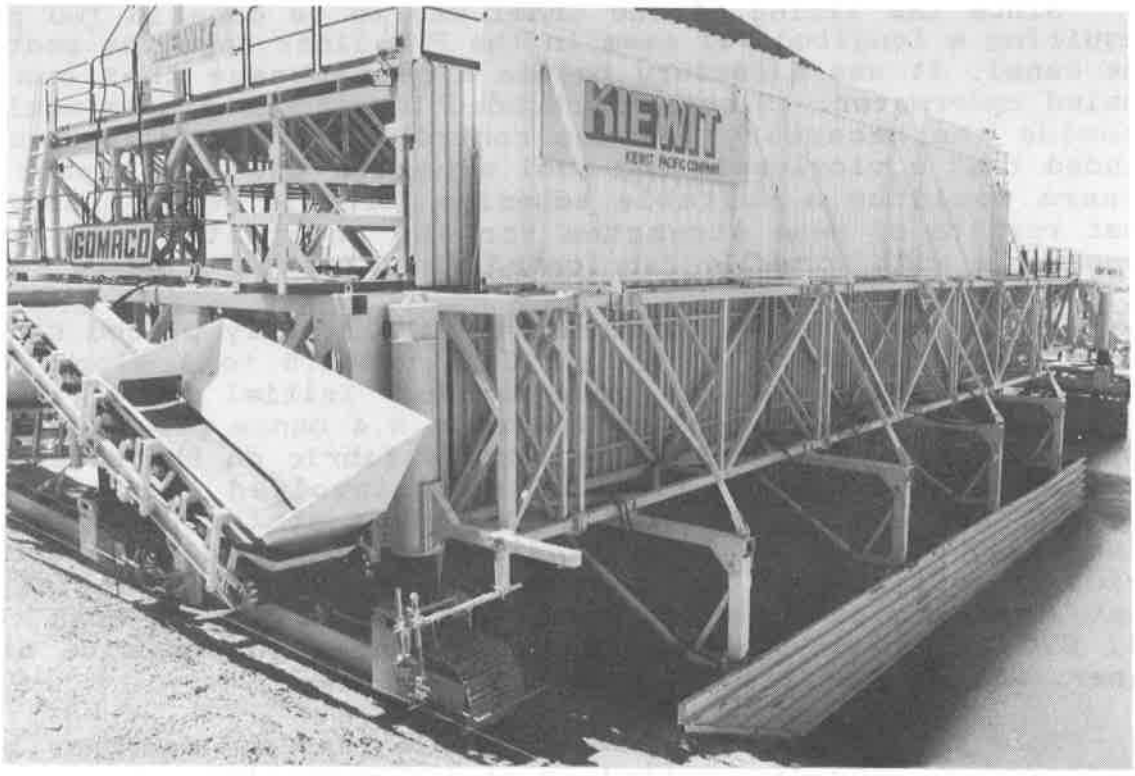

FIGURE 2. Paving Machine
PVC Geomembrane was deployed and
field welding performed on the top deck.

the liner. The design was then modified to have two center guide tracks, one at the toe of the slope, and one at the centerline of the canal. The outside guides would be at the top of the slope, and at the outside edge of the three foot overlap in the canal bottom. The center guides posed a problem in that a hem type seam would be subjected to forces which would exceed the normal peel strength of the seams.

The challenge for EPI was to develop a fabrication process which was both effective and cost competitive to provide the liner panels for this project. EPI developed a system whereby the ropes could be anchored into the PVC liner, and seams made with sufficient strength to resist the forces that would be placed on the liner during the underwater placement of the geomembrane. The final fabrication techniques are a proprietary process of EPI. The process was inspected in operation by the U.S. Bureau of Reclamation. All fabricated panels were tested for bonded seam strength and peel adhesion of the factory seams and a sample of each roll of material was supplied to the U.S. Bureau of Reclamation for physical property testing. In addi-

tion, all material that was supplied for the project by Occidental Chemical Corporation was also tested for compliance with the project specifications, which were consistent with NSF Standard #54.

DISCUSSION

The prototype project was to line 1.5 miles of the Coachella Canal near Niland, California. The canal at this section was approximately 110 feet wide and 9 feet deep. The side slopes of the canal were approximately 2.5:1. Since the canal was built 49 years ago in the sandy desert soil, it was necessary to reshape the canal prior to the placement of liner and concrete. A machine to dredge the canal and place a new sub-base of crushed aggregate was also designed and built by Kiewit. This machine precedes the paving unit and reshapes the sides and bottom of the canal to line and grade.

After shaping is completed, the paving unit proceeds along the canal, placing the PVC/geotextile composite inplace directly in front of a slipform paving unit designed and constructed by Gomaco, of Ida Grove, Nebraska (See figure 3).

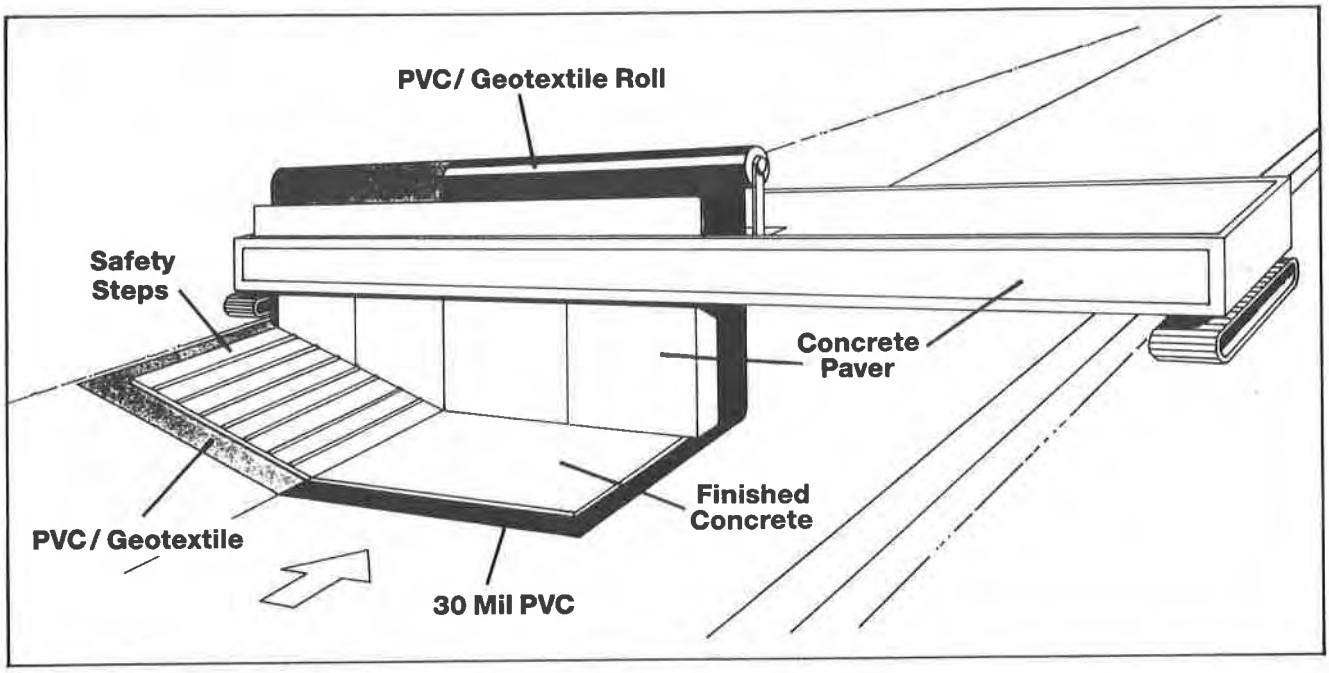

FIGURE 3. Skematic drawing of material placement.

After paving one half of the canal, the machine is turned around, and proceeds to pave the second half of the canal from

the performance during installation of the liner and geotextile combination for this project has shown itself to be very satisfactory. After completion of the lining of this section of the canal, the Bureau of Reclamation will monitor the performance to determine whether additional section should be lined and completed at a future date. Evaluation will include monitoring wells to determine seepage, and underwater inspection. Sections of the All-American Canal, which feeds the Coachella Canal, are being surveyed for potential relining efforts. The need to maintain water quality for environmental reasons prompted an environmental impact study before the project was started.

Extensive monitoring of the water quality is occurring during the placement of concrete and liner in the canal. No adverse effects to the environment have occurred or are anticipated. Since the canal supports a fishery with 16 different species, as well as the irrigation water to the Coachella Valley, the environmental priorities are very important.

EPI provided on site training for the placement and seaming of the PVC geomembrane. The Bureau of Reclamation also provided onsite inspection and quality assurance for the project. In addition, EPI provided actual random factory welded samples from every PVC panel for physical testing by the Bureau of Reclamation. EPI also provided in house testing of factory seams from every geomembrane panel. The geomembrane material was tested by the Bureau of Reclamation on a random basis prior to shipment to the project site. Occidental Chemical Corporation, the manufacturer of the PVC geomembrane, also coordinated their quality control testing in their lab with the Quality Control testing by the Bureau of Reclamation and EPI. This combination of efforts ensures that the final product installed for this prototype is as required by the Bureau's specifications.

It is estimated that by relining this canal, up to 115,000 acre feet annually (enough fresh water for up to 150,000 households) will be conserved. User fees generated from the water saved will offset the cost of the relining of the canal. The 5.2 million dollar contract is being shared by the Bureau of Reclamation (40%) as well as the Metropolitan Water District (54%) and the Imperial Irrigation District (6%), both of which serve the end users of the canal. The estimated cost to line the rest of the Coachella and the All-American Canals is estimated at $170 million. If initial estimated hold true, this figure is about 40% less than the alternative of constructing new sections of canal.

CONCLUSIONS

The development of a prototype lining system will eventually produce a new method to conserve water resources and to provide a

the opposite direction. Based on the design, speed of the paving unit, availability of concrete, and working 24 hours per day, it was estimated that the paving of 1.5 miles in one direction could be accomplished in approximately 3 days.

The initial paving operation was started in May of 1989. At that time, the water usage requirements in Southern California were reaching their peak. It was necessary to be able to regulate the flow of water so that the many adjustments to all of the various operating systems of the paving unit could be accomplished in reasonable fashion. Initially, about 1,200 feet of liner was placed during early May. The balance of the paving will be completed after modifications are made to the equipment to accommodate the soft substrate that underlies the canal bottom.

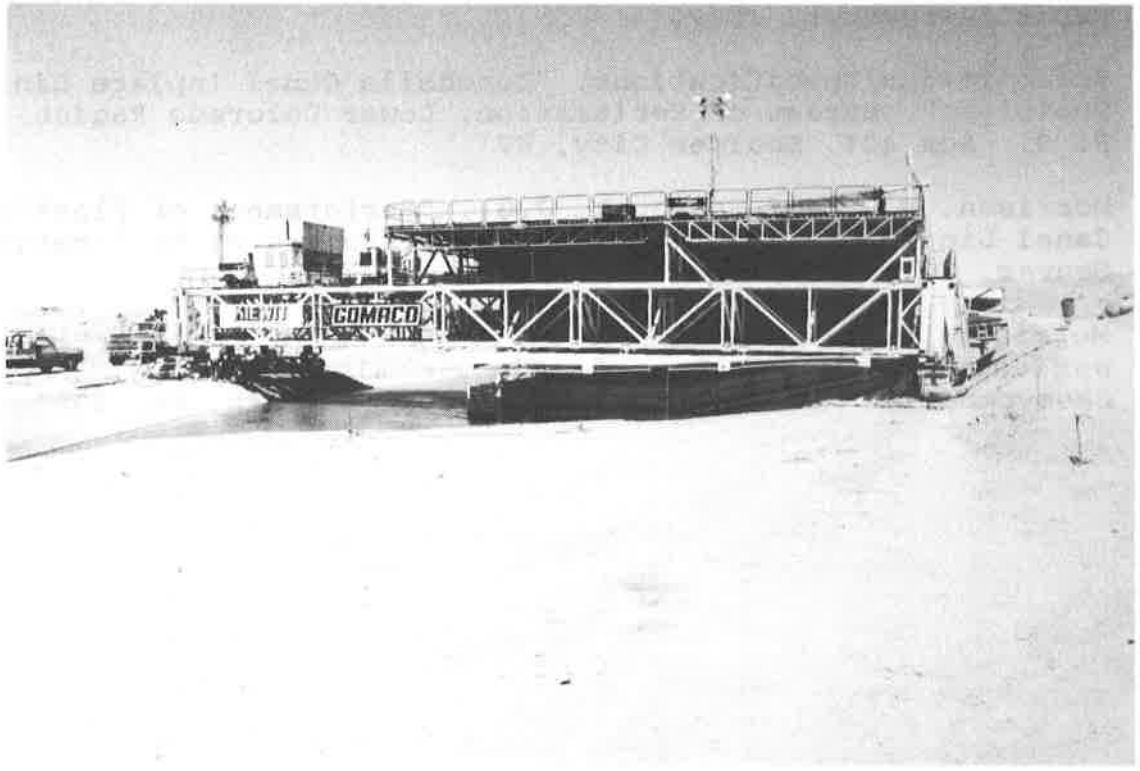

FIGURE 4. Rear view of Paving Machine

SUMMARY

The selection of PVC liner for this project has proven to be an excellent choice. The custom fabrication of the PVC liner for handling during placement by this equipment was accomplished with only 15% additional cost for the geomembrane liner. In addition,

method of remediation for existing canals that have been in service for many years. The development of equipment and process to place a PVC geomembrane underwater, without disturbing or restricting the water supply will be a boon to the eventual long term maintenance of this water supply system. This project is being viewed by engineers and water professionals from around the world. Its eventual involvement into a significant industry is becoming a more substantial possibility each day.

REFERENCES

1. Workshop on Inplace Lining Prototype - Coachella Canal, American Water Foundation - May 8, 1989, Palm Springs, California.

2. Rebant, Daniel B., "Underwater Lining of Canal Promises Huge Savings in both Water and Money", Geotechnical Fabrics Report, November, 1989.

3. Solicitation/Specifications, "Coachella Canal Inplace Lining Prototype", Bureau of Reclamation, Lower Colorado Region, P. O. Box 427, Boulder City, NV

4. Morrison, W.R. and Starbuck, J.G., "Performance of Plastic Canal Linings" Report #REC-ERC-84-1, Bureau of Reclamation, Denver, Colorado, 1984.

5. Morrison, W.R. and Swihart, J.J., "Bureau of Reclamation Experiences with PVC Seams", The Seaming of Geosynthetics, Geosynthetics Research Institute, Philadelphia, PA, 1989.

Use of Geosynthetics in Lautaro Dam

Luis Arrau
Ministry of Public Works, Chile
Donaldo Astorga
Ministry of Public Works, Chile

ABSTRACT

The Lautaro reservoir is a 30 m high and 42 million m^3 capacity earth dam. In an observation boring, pressures higher than 3 m water column above the ground level were measured at the downstream toe of the dam. The solution was a system of filter, drain and overburden protection. Taking into account the ground conditions, costs and other technical requirements, the best solution for the filter was a geotextile. The works were carried out and the filtrations now flow without any risk for the dam.

INTRODUCTION

The valley of Copiapó River is the first of the transverse valleys of the Chilean Norte Chico ("small north") with intensive agricultural exploitation. Located about 800 km to the north of Santiago, it shows outstanding climate conditions to cultivate grapes for export and other exquisite things. At present, the land of the valley has no price, since their owners are seldom ready to sell. The above, however, is only applicable when water for irrigation is available.

In this respect, there are two supply sources: the Copiapó River and the aquifer of the valley, from which water is pumped. Water from both sources is applied to the grape yards through dip irrigation.

The water of the river is at present controlled by the Lautaro storage dam located at 27°30' south latitude, about 90 km to the east south of the city of Copiapó. This is an homogeneous earth dam with a maximum height of 30 m, 3H:1V upstream slope and 2H:1V downstream slope, and a length of 815 m long. The dam is directly founded on fluvium in a highly seismic zone. The storage dam has a 42.3 million m^3 capacity and it acts, at the same time, as recharging source of the water table and flood control.

During the filling of the storage dam in 1983, it was observed that high water levels at the lake led to excessive pressures on the aquifer, thus allowing water to leak abundantly in a wide sector downstream of the dam. This condition jepardized the safety of the dam. Because of this the Irrigation Directorate of the Ministry of Public Works investigated ways allowing the use of the storage dam at full capacity with a proper safety.

BACKGROUND INFORMATION ON THE DAM

The Lautaro dam was constructed between the years 1928 and 1939, Arrau (1986). The left abutment rests on the debris cone of Amolanas Creek. The right abutment rests on a fractured shale outcropping, where the hydraulics facilities are located. The foundation soil beneath the dam is sandy gravel of Copiapó River mixed with the material from floods and Amolanas Creek. In the middle of the valley, under the dam, the bed rock is about 140 m below the natural ground surface. The waterproofing works in the wall axis did not reach a depth more than 15 m below the natural ground surface. For this reason, there is a large section under the dam through which the ground water may flow. The results of borings performed show that the valley filling has an alluvial nature rather than fluvial.

A diversion tunnel with a cross-sectional area of 17.3 m^2 and a length of 105 m long is located in the rock of the right abutment. The intake work is a cylindrical tower followed by a valve chamber with 3 valves inside. The delivery of irrigation water is carried out through a smaller section tunnel joining the diversion tunel. Water is directly delivered to the Copiapó River and then convey by the irrigation channels. A spillway with a rapid of variable width is located in the right abutment. The maximum capacity of the spillway is 600 m^3/s, which corresponds to the 1,000 year return period flood.

In 1969, some waterproofing works were carried out through groutings in the right abutment, since some leaks had been detected in the joint between the concrete works and the rock. In a first stage, 1,578 m of drillings were grouted. Later, this work was supplemented by 1,752 m of additional drillings.

In the left abutment of the dam, there is a small delivery work designed to deliver water to a turbine which at present is not used.

THE PROBLEM OF LEAKS

Due to the rise of water level in the lake by the cycle of rainy years beginning in 1981, it was observed that an old drilling (D-2) located just at the foot of the wall used to measure the pressures of the aquifer, was working as artesian well with a volume of flow of about 2 l/s. The lake was 3.6 m below the maximum normal level and the well already showed 3 m pressures of water column over the ground surface. This situation, plus the leakage downstream at the foot of the dam, was considered hazardous. The use of the dam was limited to 70% of its capacity as maximum and the safety for greater water levels was not guaranteed.

As part of the diagnostic studies, borings were performed in the top of the dam, as well as in the slopes, at the foot of the wall, and in the flooded zone downstream. The main purpose of the borings was to analize the water table behavior, permeability of soils, artesian volumes of flow and characteristics of the materials making up the body of the dam and its foundation. Figure 1 shows a dam layout with the location of borings and test pits carried out. Figure 2 shows the cross section of the dam in the highest sector.

In general terms, at medium levels of depth in the lake, the hydraulic gradients measured downstream the dam were not excessive. Estimates, however, indicated that for maximum levels of waters in the storage dam, the expected leakage was about 500 l/s and the outlet gradients may locally approach the critical value.

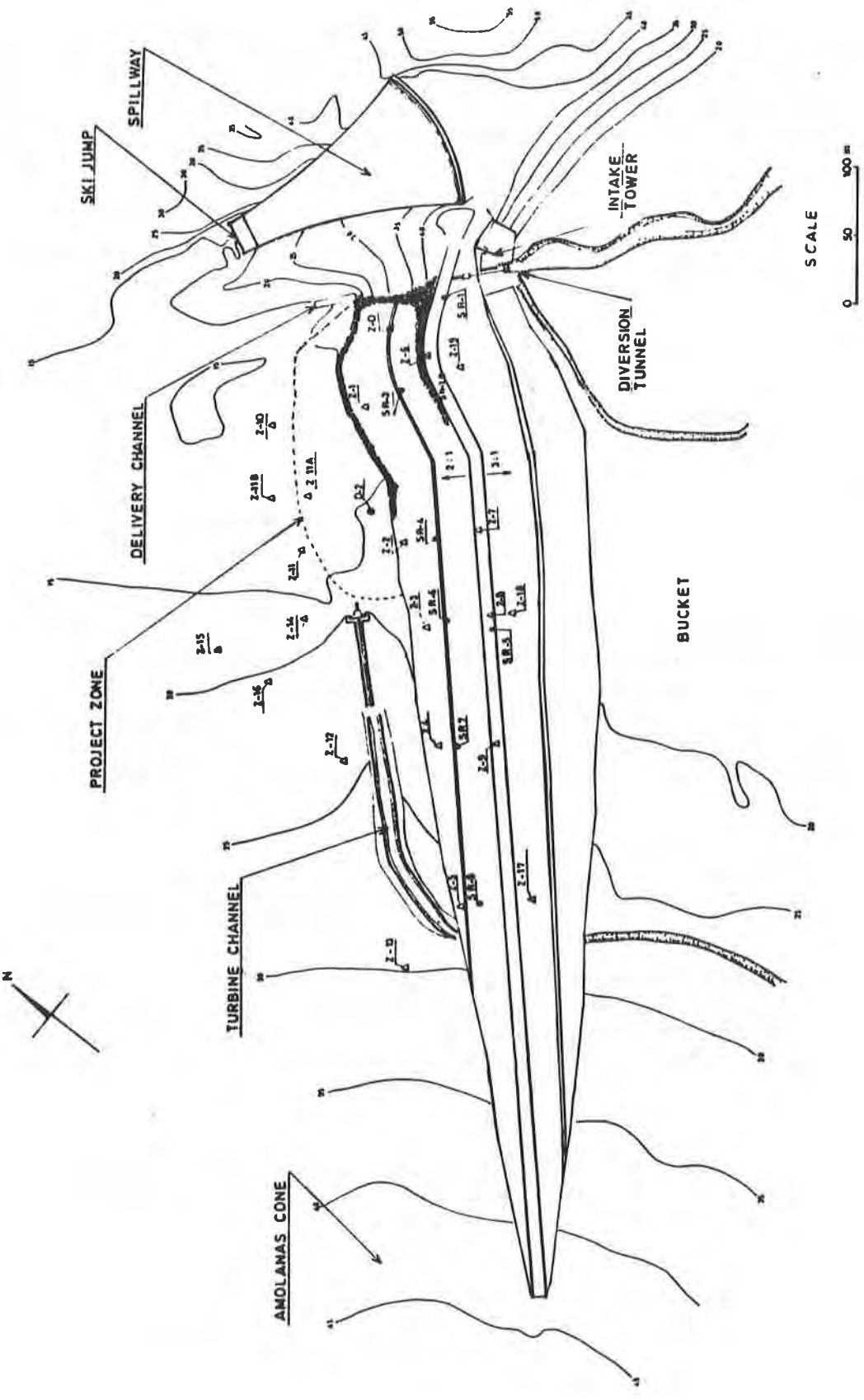

Figure 1. Dam plant and location of pits and exploration borings.

This situation might lead to the washout of fine particles of the soil, with the risk of generating piping. On the other hand, the stability analyses for the slopes of the dam showed that most of the times the critical surfaces of failures reached the foot or a sector very near to it. Safety factors very close to 1.0 under a static situation were reached with semi-saturated wall and a normal level of water in the storage dam.

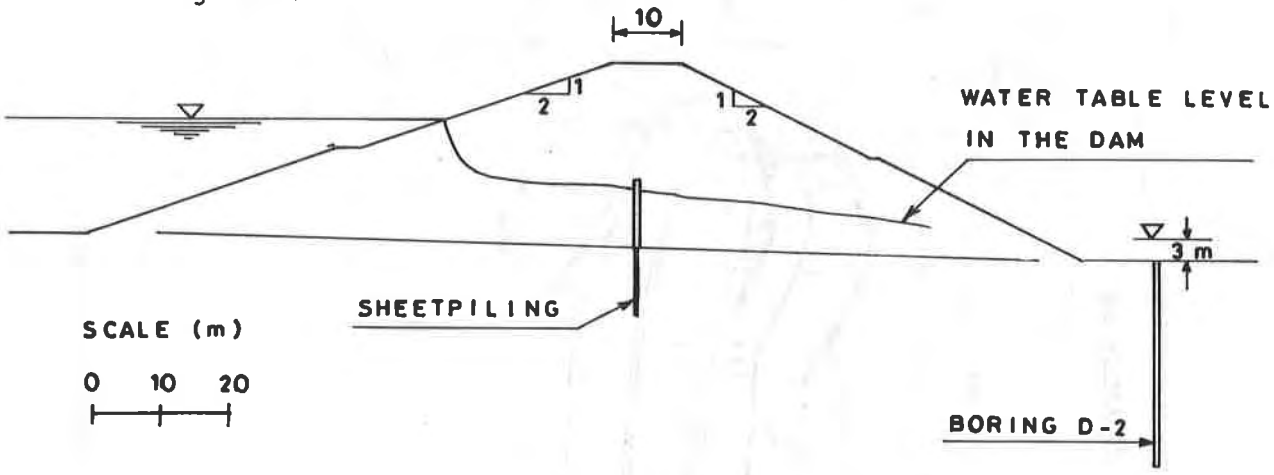

Figure 2. Cross section of Lautaro storage dam. Boring D-2 is shown where pressures up to 3 m water column were measured.

It was considered that the above was a hazardous situation, which was unacceptable due to the fact that the collapse of the dam may cause serious damages downstream and may even result in the loss of human lives. In the valley there are indeed many villages; the city of Copiapó has a population of 69,000 people.

THE SOLUTION

The problem of leaks in the reservoirs may be tackled under two different criteria: (i) to eliminate or reduce leaks; or (ii) to accept them in a controlled way.

In the case of Lautaro storage dam, the first solution is almost impossible due to the large aquifer existing under the dam. In order to eliminate the leaks, a large grout curtain, or the waterproofing of the reservoir area of the storage dam would be needed. Figure 3 shows a longitudinal section of the dam indicating the position of the bed rock of the valley.

The alternative of accepting the leaks assuring that no damages will be produced is attractive, since this is an irrigation storage dam in a zone having water requirements not below 500 l/s during the year. Therefore, leaks are not losses of the resource for the system. Considering the above, the feasibility was verified and it was thought that it was suitable to construct a drain-filter to avoid the washout of particles and to allow the drainage, as well as a stabilizing berm over the bottom part of the slope and a gravel fill over the drain-filter system. This system should cover the critical zone of leaks. The works so designed have the double purpose of safely draining the leaks, and increasing to reasonable levels the safely factor for the slope sliding downstream.

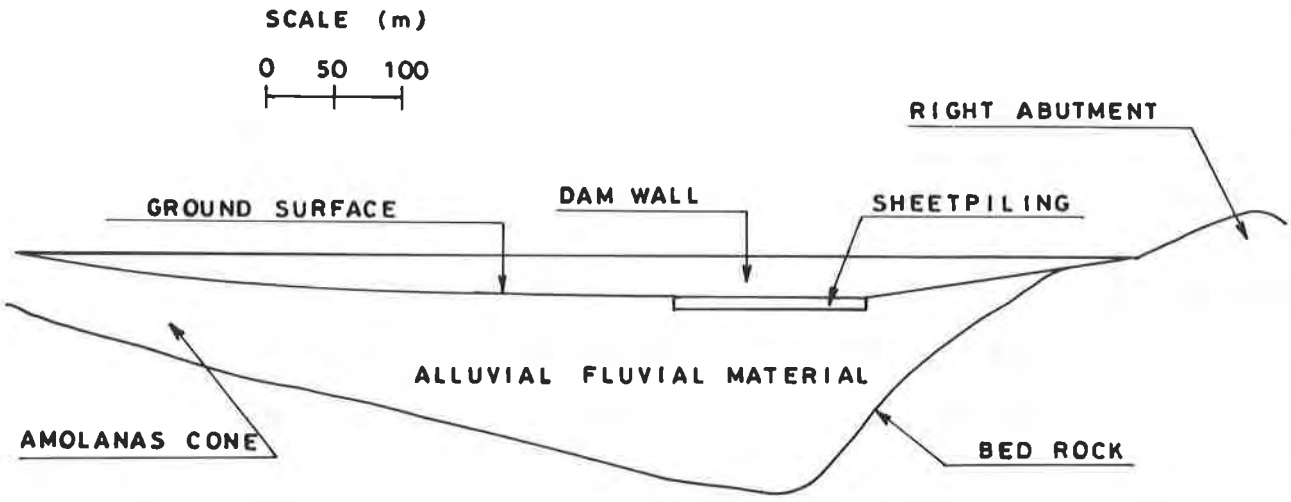

Figure 3. Longitudinal section through the axis of Lautaro storage dam

The alternatives to implement the chosen solution are the use of a graduated soil filter or the use of a geotextile.

The use of the surface fluvial of the valley to construct the system of drain-filter requires a strict selection to obtain a suitable graduation. This means the installation of a selecting plant and of a field soil laboratory to carry out quality control during the placement. The solution with a graduated filter involved the placement of a select layer of at least 0.3 m thick, Bureau of Reclamation (1980). This solution, however, had the advantage of collaborating as weight; therefore, part of the thickness of the gravel fill to be placed over the drain may be reduced.

For the alternative solution with a geotextile as filter, constructive advantages were obtained. These advantages include less severe quality control for the filter and time savings. The geotextile, however, does not contribute the total weight over the soil; therefore, the thickness of the gravel fill had to be increased.

A comparison of costs for both solutions was made, the use of geotextile being more economical. The values used for comparisons are indicated below:

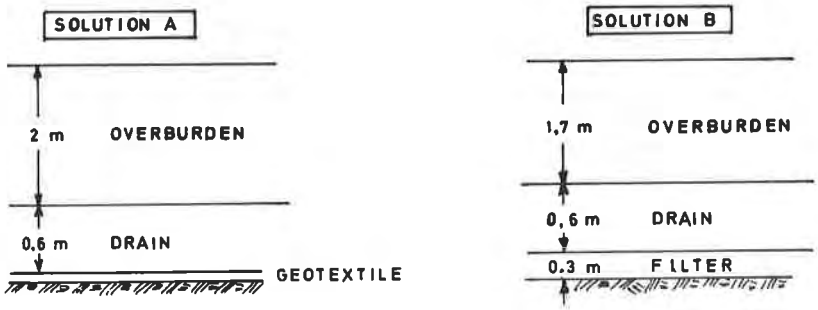

Costs

Gravel fill	US$ 71,175.-	Gravel fill	US$ 60,499.-
Drain	US$ 47,132.-	Drain	US$ 47,132.-
Geotextile	US$ 14,719.-	Filter	US$ 37,642.-
Total Sol. A	US$133,026.-	Total Sol. B	US$145,273.-

Cubical contents

Gravel fill	17,574 m^3	Gravel fill	14,938 m^3
Drain	5,272 m^3	Drain	5,272 m^3
Geotextile	10,984 m^2	Filter	2,636 m^3

Unit prices

(june 1989, 1 US$ = Ch$ 280)

Gravel fill	US$ 4.05 /m^3
Drain	US$ 8.94 /m^3
Geotextile	US$ 1.34 /m^2
Filter	US$14.28 /$m^3$

By consideration of a bigger safety of the solution, the constructive advantages, saving of controls and time, and the advantage of costs, the decision was to construct the alternative with geotextile. A well chosen geotextile guarantees that once it is placed, there will be no migration of fines. The adopted solution consisted of a geotextile acting as filter, a gravel layer over it to act as drain and, later, a compacted gravel fill. Figure 4 shows a cross section with solution adopted.

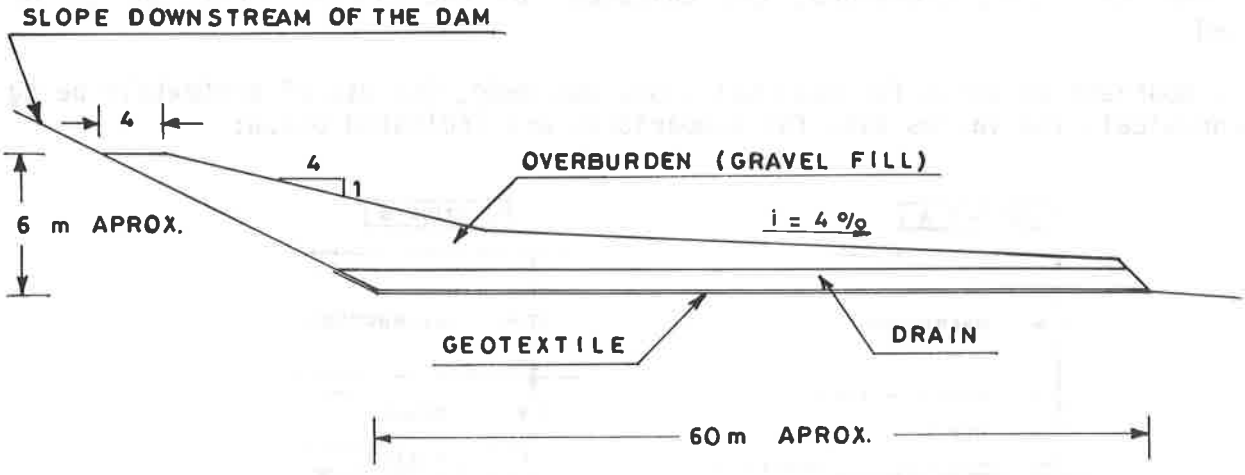

Figure 4. Cross section with drain-filter system and overburden

DESIGN OF THE FILTER-DRAIN SYSTEM

In order to select the geotextile, the following conditions were the most important ones: nonwoven geotextile; a geotextile with pore openings that minimize the washout of fines; a geotextile permeability allowing the right drainage of the maximum leaks expected; a geotextile with adecuate tensile strength, puncture resistance and elongations so that it will not become damaged during construction.

According to the recommendations of geotextile manufacturer, the following design ratios were proven:

$$0.85 \text{ mm} \leq D_{85} \text{ soil} \quad (1)$$

$$P_{95} \text{ geotextile} \leq 2 \bullet D_{85} \text{ soil} \quad (2)$$

$$K \text{ geotextile} \approx 10 \text{ to } 100 \text{ times } K \text{ soil} \quad (3)$$

where D_{85} soil = mesh diameter allowing the pass of 85% of the soil in weight; P_{95} = pore diameter 95% of geotextile (See figure 5); K = permeability coefficient.

Figure 5 shows the range of particle size distribution of the soil to be protected downstream the dam, along with the size distribution of pores of the geotextile used as filter.

According to Figure 5, the average D_{85} diameter of the soil is 20 mm. The dimension of P_{95} pores of the geotextile is 0.19 mm according to Figure 5. With these values, ratios (1) and (2) are more than enough fulfilled. On the other hand, the estimated permeability of the soil over the base of average D_{10} diameter (0.05 mm) resulted $2.5 \bullet 10^{-5}$ m/s, Lambe and Whitman (1972). Considering that the chosen geotextile has a $3 \bullet 10^{-4}$ m/s permeability according to the manufacturer, it was concluded that it reasonably fulfilled ratio (3) for most of the soil to be protected.

Based on the previous results, the availability in the market and the unit price, a nonwoven geotextile was chosen, which has been used for 10 years in our country with good results, and having the characteristics indicated in Table 1.

Table 1. Physical properties of the geotextile

Physical Properties	
Grab Tensile (lbs) ASTM D 1682-64 (1975)	150
Elongation (%) ASTM D 1682-64 (1975)	70
Modulus (lbs) ASTM D 1682-64 (1975)	1200
EOS (sieve) ASTM D422-63 (1972)	70 - 100
Flux (gal/ft^2/min) ASTM D 4491	62
k (cm/sec) ASTM D 4491	$3 \bullet 10^{-2}$
Trap. Tear (lbs) ASTM D 4491-80	74
Puncture (lbs) ASTM D 751-79	42
Abrasion Resistance (lbs) ASTM D 3881-80	44

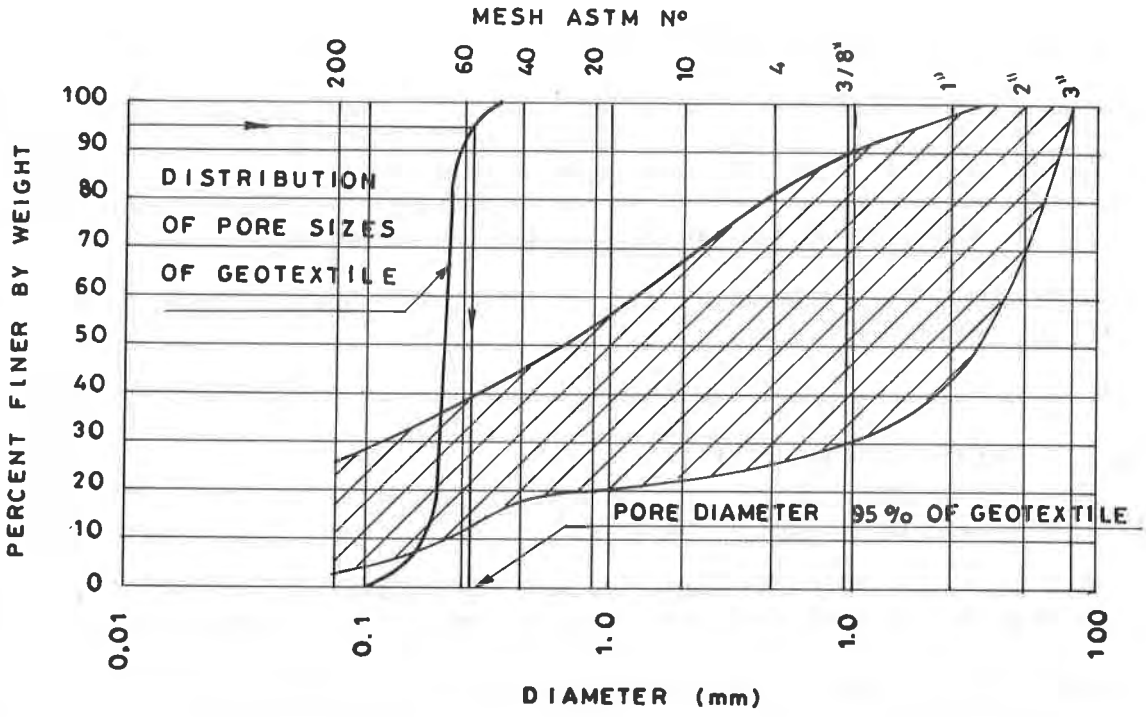

Figure 5. Range of particle size distribution of the soil and distribution of pores of the geotextile to be used in the drain-filter system.

The drain characteristics were defined by the sieve analyses of gravel borrowed fill. In the specifications for this material, a maximum particle size of 6" and a minimum size of $\frac{1}{4}$" was requested. For the drain, a permeability coefficient of 0.28 m/s was estimated. With a hydraulic gradient of 0.007, a maximum estimated volume of flow of 0.8 l/s/m and, a safety coefficient of 1.5, the required thickness of the drain is 0.6 m. Figure 6 shows some details of the drain-filter and gravel fill.

For the gravel fill to be placed on the drain, clayish or sandy gravel with a maximum size of particle not higher than 6" was specified, considering the availability of borrowed fill close to the work.

CONSTRUCTION OF THE DRAIN-FILTER

On July 19, 1989, the reparation works of Lautaro storage dam began. In addition to the construction of the drain-filter, the contract included the construction of a drainage channel for leakage, a structure for metering the discharge at the beginning of the channel, repair and expansion of the delivery channel of water towards the Copiapó River, replacement of the rockfill in the slope downstream the dam, repairs of some slabs of the spillway, and repair of the foundation of the ski jump existing at the end of the spillway. The contract life was 180 days for the total works indicated above, Contex (1989). Picture 1 shows the condition existing before the beginning of the reparation works.

The flooded zone downstream of the dam, where the drain-filter was to be placed, initially looked like a swamp with much vegetation, as is typical of this condition, and a great number of trees. First a clearing and general escarpment of

all the zone to be covered by the geotextile was carried out. The area was graded with bulldozers, and all sticks, tree roots and gravels with sharp edges that may damage the geotextile were removed. In some sectors, a compacted layer of 5 cm thick sand was placed. Later, for a greater safety, a 5 ton dead weight vibrating roller was passed over the whole area.

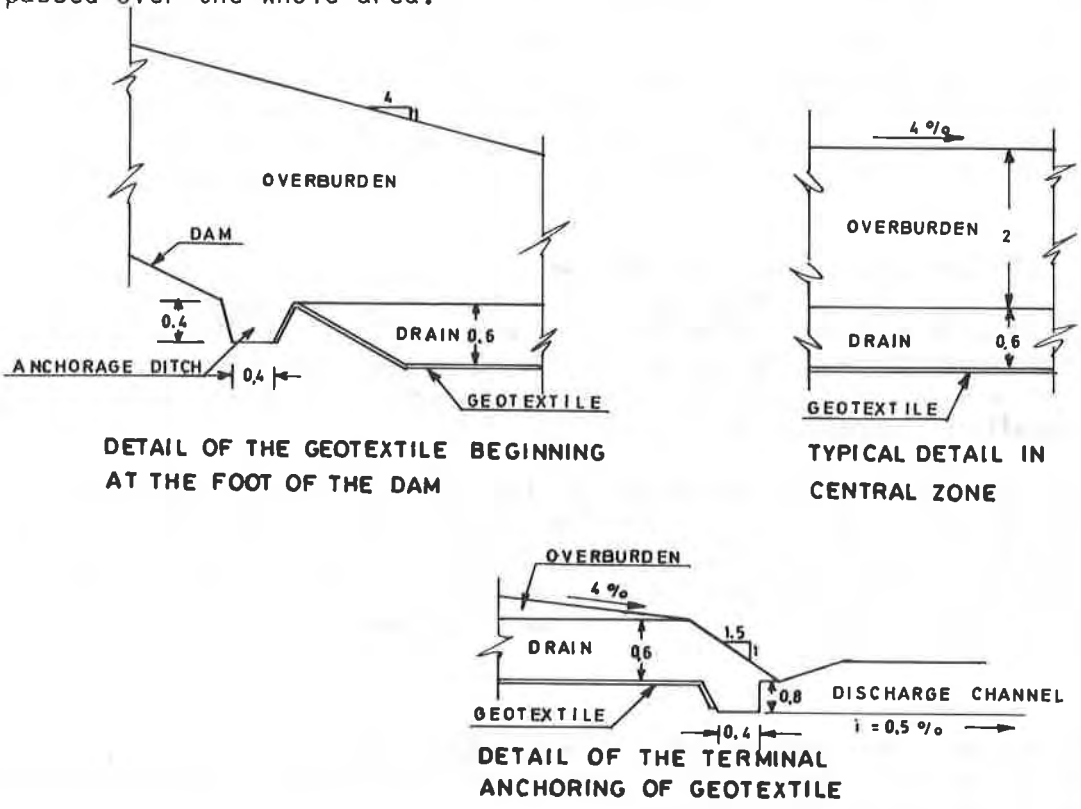

Figure 6. Typical details of the drain-filter system

The placement of the geotextile began in the right side of the dam, gradually advancing to the left side. The overlappings of geotextile were of 30-50 cm. Then, the specified drain was placed over the geotextile, taking care of not impairing the latter. The unloading of trucks with drain material was never done directly over the geotextile, but over a layer of the same material previously placed. The spreading of the accrued material was performed with a bulldozer. Then, the compacting of the drain was carried out with a 5 ton dead weight vibrating roller.

Later, the gravel fill material obtained from a borrowed fill of Amolanas Creek was placed over the drain. The spreading of the bill was carried out with a bulldozer and a motor grader. Compacting was carried out by passing the above mentioned roller 4 times through each point. Picture 2 shows the placement of the gravel fill drain over the geotextile. Once the process was ended in a sector, the material placed was removed to examine the condition of this geotextile. No significant alterations to the geotextile were observed.

As a whole, as part of the contract, 10,980 m^2 of geotextile were placed, as well as 6,340 m^3 of drain, and 28,630 m^3 of gravel fill, including the stabilizing berm over the slope downstream the dam. The Picture 3 shows the aspect of the zone downstream the dam at the end of the gravel fill placement.

REMARKS AFTER THE CONSTRUCTION

From December 1989, on which date the reparation work of Lautaro storage dam ended, some remarks have been made on the behavior of the drain-filter in an indirect way. The current flow of leakage is similar to that measured before the reparation for a very similar level of the lake. This suggests that the drain-filter system is operating as foreseen. Leak waters are clean and clear. No washout of fine particles has been detected. In addition, the location of the drain-filter system and the drainage channel to lower elevations of the natural level of the ground, allowed to dry the whole area at the foot of the dam and downstream the same.

Lautaro storage dam has many piezometers to control water tables and pressures inside the wall and the foundation soil. Measurements carried out in such piezometers indicate a normal behavior of water table and pressures, but now there is an additional safety granted by the drain-filter and the overload on the drain filter:. There are no hazardous exit hydraulic gradients and the safety factor of the slope downstream increased to a value over 1.5.

In order to confirm the behavior of the drain-filter system under a more stressing situation, we shall wait until the next thawing season of 1990. At this season the water level of the storage dam generally rises. In any case, there is a control program at present implemented by the Irrigation Directorate, which enables the gathering of very complete information month by month.

CONCLUSIONS

The design and construction of the reparation works of Lautaro storage dam allow to get interesting general conclusions about the use of geotextiles, among which the following may be pointed out:

- The use of geotextile as filter was more economical, simpler and safer than the traditional filter of granular material. The need of having a material selecting plant was avoided, as well as an intensive field quality control to guarantee a properly graduated granular filter.

- In those cases in which a granular drain is required over the filter, such as in the case of Lautaro storage dam, geotextile allows a much wider range of particle size for this drain than that required by the graduated filter of granular material.

- The geotextile used outstandingly simplified the constructive work. This advantage makes it especially attractive to be used in emergency works and in isolated and hard-to-reach places.

- The geotextile allowed the mechanization of the works, which was expressed in a significant saving of time of construction. This advantage is especially important when repairing works that are needed to be used as soon as possible.

- Controls carried out after the construction, that is during the brief period of time elapsed from the end of the work, show that the drain-filter system operates properly and as expected. The volume of leakage has not changed related to those measured before the construction of the work for similar

levels of the storage dam, this meaning that the drain is effective. In addition, no washout of fines has been observed in the leak waters, this proving that the geotextile is effectively fulfilling its capacity of filter and preventing the piping and erosion.

REFERENCES

Arrau, L., (1986) "The importance of Alluvion Control. The Lautaro Storage Dam Case", ICID Bulletin, Vol. 35, N°1, January 1986.

Bureau of Reclamation, (1980) "Diseño de Presas Pequeñas", Cía. Edit. Continental S.A., novena impresión.

Lambe, T.W. y Whitman, R.V. (1972), "Mecánica de Suelos", Edit. Limusa-Wiley S.A.

CONTEX, (1989) "Informe Final Obras Complementarias Embalse Lautaro", Internal report to Irrigation Directorate.

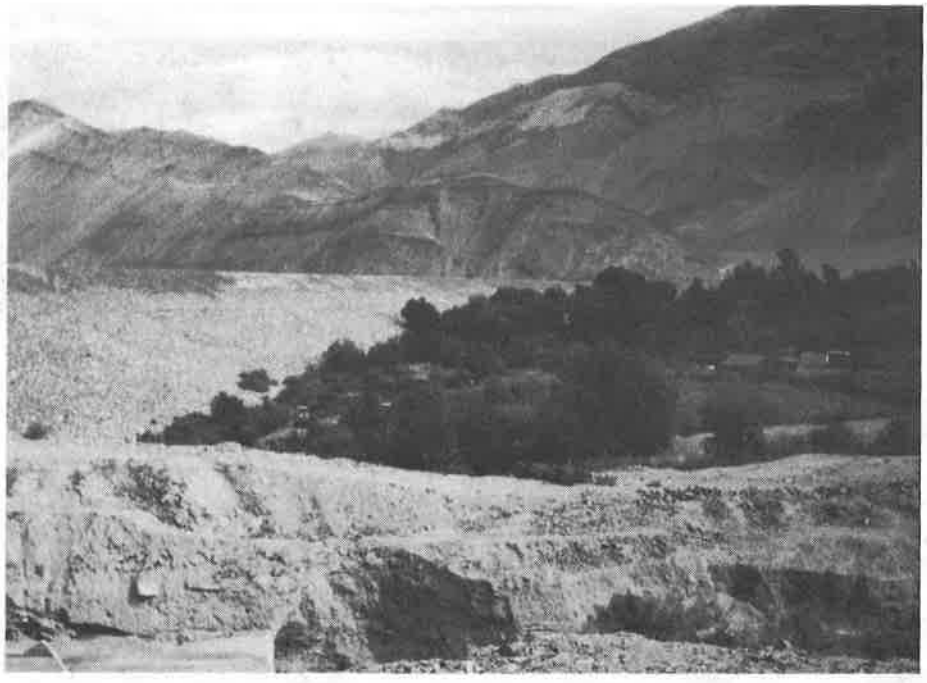

Picture 1. Aspect of the zone downstream of the dam before the construction of the works.

Picture 2. Placement of the drain over the geotextile during the constructive stage.

Picture 3. Placement of the overburden at the end of the construction period.

Witbank's 60Ml Floating Cover Reservoir: A Review of the First Five Years

Richard B. Turner
Hawkins, Hawkins & Osborn, South Africa
Peter L. Davies
Aquatan, South Africa

INTRODUCTION.

Background. Early in 1984 the town of Witbank called for tenders for the construction of a 30Ml reinforced concrete reservoir at their Ryno Ridge water storage site. This site already contained one 5Ml circular reinforced concrete reservoir and a water tower and provision was made for the construction of a second 30Ml reservoir after about ten years as well as for two future water towers.

At the request of J W Davey Construction (Pty) Ltd and Aquatan cc, Hawkins, Hawkins and Osborn prepared designs for one 30Ml and one 60Ml geomembrane lined and covered reservoir. In adjudicating the tenders (Table 1), the Town Engineer evaluated the 50 year projected costs for both the concrete reservoirs and the 60Ml geomembrane lined and covered reservoir allowing for the replacement of the cover after 25 years. As a result of the projected saving of 14% on the cost of the equivalent concrete reservoirs (Table 2) the Contract for the construction of a 60Ml geomembrane lined and covered reservoir was awarded to J W Davey Construction (Pty) Ltd on 30 May 1984. Detail design was done during June and July of that year, and construction of the reservoir was completed in time for an official opening on 6 December 1984.

Site Conditions. Witbank is an industrial and mining town with a population of about 150 000. It is situated on the Transvaal highveld 150km east of Johannesburg at about 29° 15'E and 25° 50'S with an elevation of 1600m above sea level. There are about 22 coal mines in the vicinity of the town including several feeding coal fired power stations.

Largely as a result of favorable prevailing winds and improved emission levels from the local steel mill and the power stations, the air pollution in the town and in the vicinity of the reservoir is relatively low as indicated in Table 3.

The climate in the town is moderate with temperatures varying from about 7°C to about 22°C and with an average annual rainfall of 722,5 mm.

The level of ultraviolet radiation at Witbank is 26 MJ/m2.

TABLE 1: PRICES OF KEY TENDERS[3]

TENDERER	CAPACITY OFFERED (Ml)	TENDER PRICES		UNIT PRICE (R/m³)
		SPECIFIED (R)	ALTERNATIVE (R)	
J W DAVEY CONSTRUCTION (PTY) LTD	30		948 000	31.60
PETER FABER CONSTRUCTION (PTY) LTD	30		1 174 000	39.13
GILLIS MASON	30	1 208 000		40.27
		1 219 000		40.63
5 OTHER TENDERS	30	TO		TO
		1 267 000		42.23
J W DAVEY CONSTRUCTION	60		1 269 000	21.15
OTHER TENDERS	30	1 290 000		43.00
		TO		TO
		1 563 000		53.30
H WELKE	58		2 797 000	48.22

TABLE 2: ESTIMATED TOTAL COST OF WITBANK RESERVOIR OVER 50YR LIFESPAN[4]

YEAR	EVENT	COST (RAND) AS AT DEC. 1984	
		30 Ml REINFORCED CONCRETE RESERVOIR	60 Ml MEMBRANE RESERVOIR
1985	COMPLETION OF CONSTRUCTION	1 378 128	1 821 682
2000	CONSTRUCT SECOND 30 Ml CONCRETE RESERVOIR	1 378 128	
2010	REPLACE COVER MEMBRANE		537 068
TOTAL COST AT END OF LIFESPAN (2035)		2 756 256	2 358 750

TABLE 3: MONTHLY MAXIMUM AIR POLLUTION READINGS (SO_2 µg/m³)

SITE	MONTHLY MAXIMUM READING (SO_2 µg/m³)											
	OCT 88	NOV 88	DEC 88	JAN 89	FEB 89	MAR 89	APR 89	MAY 89	JUNE 89	JULY 89	AUG 89	SEPT 89
CIVIC CENTRE	12	27	3	28	20	8	47	16	30	24	19	18
FERROBANK *	71	87	43	63	48	86	97	125	50	118	112	123
EXTENSION 10	15	32	8	12	8	9	37	15	48	37	30	29
TASBET PARK**	37	23	8	30	13	15	28	12	17	31	34	32

* AT STEEL MILL
** NEAR RESERVOIR SITE

Reservoir. The design parameters at tender stage called for the new reservoir to have a top water level 2,0m below that of the existing reservoir which allowed for a nearly balanced cut to fill earthworks design for the alternative tender. However due to the greater flexibility of an earthworks structure to accommodate variable founding conditions it was possible to raise the reservoir top water level to match that of the existing concrete reservoir. Although this resulted in unbalanced fill and cut quantities and was largely the cause of the increase in cost from the tender amount of R1 269 000 (Table 1) to the contract amount of R1 821 682 (Table 2).

The incorporation of a 1,2m high concrete anchor wall, which also acted as a retaining wall, at the top of the bulk earthworks (Fig. 1) allowed for a substantial reduction in the total volume of fill required while accommodating a walkway round the reservoir as well as providing a natural barrier to access onto the cover membrane. The embankments were constructed with an inner slope of 1:2 and an outer slope of 1:1.5.

Liner and Pipework. The liner consisted of a 1 mm thick Hidriline (HDPE) geomembrane laid over a 270 gm/m2 nonwoven needle punched geotextile which acted both as a protective layer for the liner geomembrane and as a drainage path to the four under drains laid in the reservoir floor. Each under drain discharges through a different outlet to facilitate the location of any leak that could develop in the liner membrane. Under drains consisted of 100mm slotted uPVC drains in a 300 x 300mm surround of 10mm crushed stone wrapped in a single layer of 270g/m2 nonwoven needle punched geotextile. Inlet, outlet and scour pipes, which were laid below the floor level, each ended in an open topped concrete chamber covered with a galvanized mild steel grid to prevent the cover membrane being drawn into any of these large (900mm diameter) pipes. The overflow structure was built into the top perimeter anchor wall with a flap valve to prevent inflow of air under the cover.

Cover Design. The cover was constructed of 1,14mm 5 ply Hypalon with two layers of 16 x 8 leno weave 140 x 250 denier yarn scrim reinforcement supplied by Burke Industries Inc., of San Jose, California and designed under licence from Globe lining Inc., of Long Beach, California. The floats were laid in a rectangular herringbone pattern over the projected floor area with no floats over the sloping sides of the reservoirs. One access hatch was placed over each of the inlet, outlet and scour chambers which were just outside the float rectangle. No air vents were installed in the cover as it was considered that these should only be installed where found absolutely necessary. A single submersible pump in a floating sump was installed on the cover to remove the accumulated surface water.

Completion. Construction of the reservoir was completed at the end of November 1984, and it was officially opened on 6 December 1984.

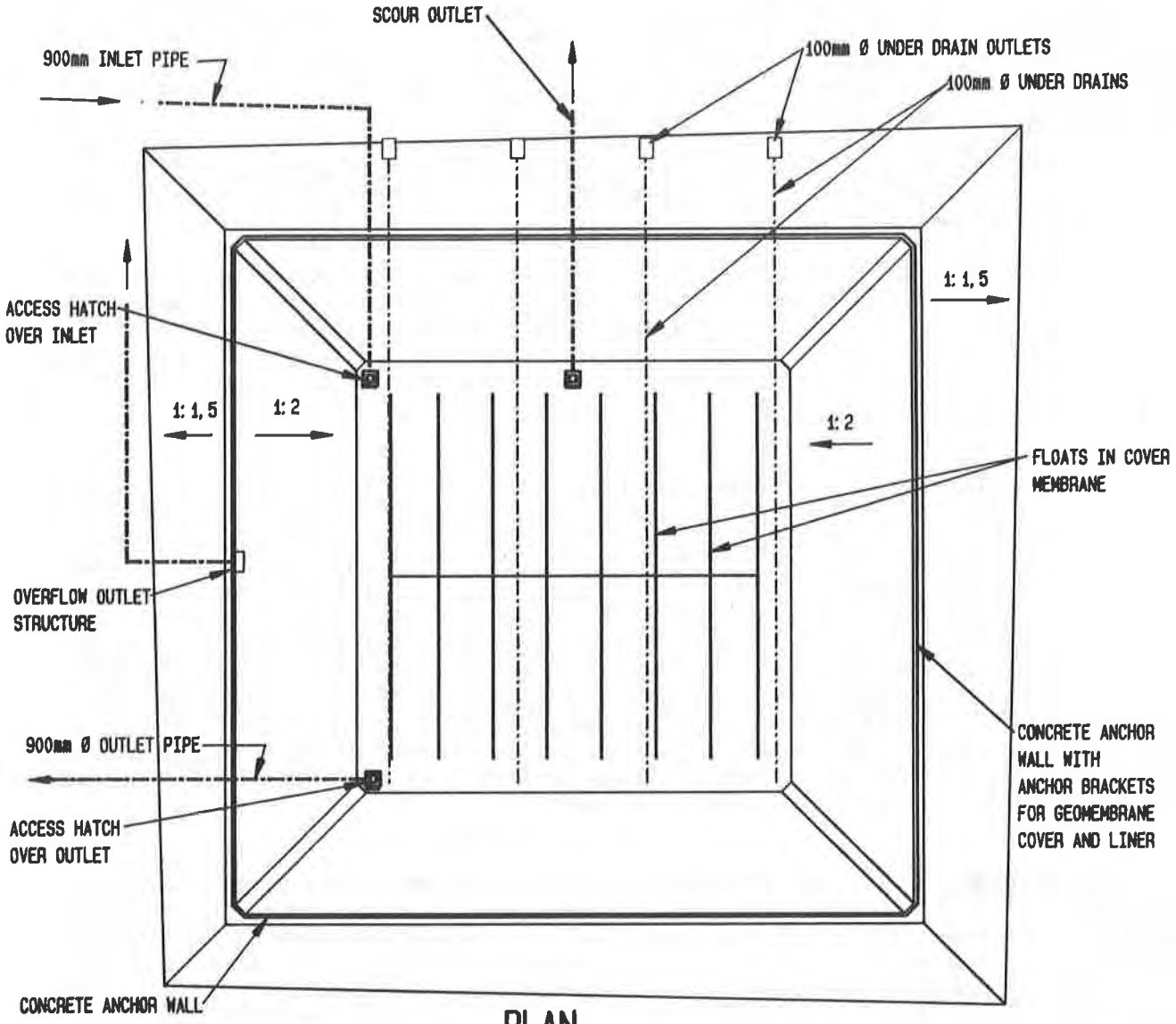

PLAN

1: 1000 APPROX.

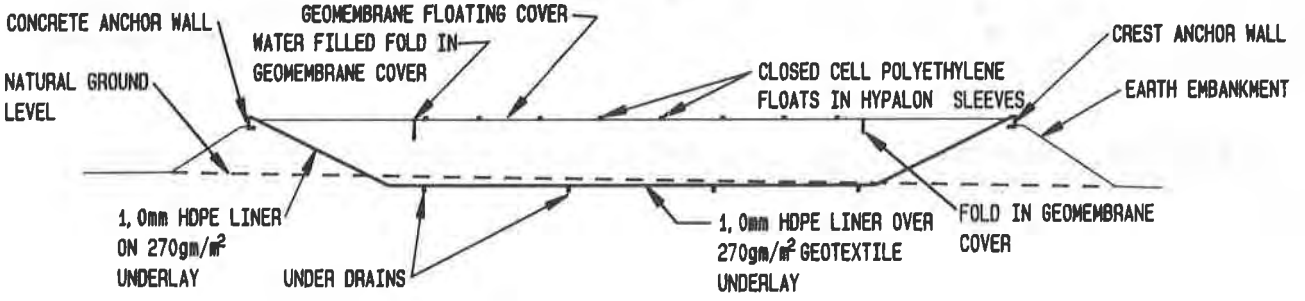

TYPICAL SECTION THROUGH RESERVOIR

1: 1000 APPROX.

FIG. 1: WITBANK RESERVOIR: GENERAL DETAILS

PERFORMANCE TESTING.

Proposed Program. As this was the first major geomembrane lined and covered reservoir to be constructed in South Africa a performance testing program was initiated to monitor the performance of the reservoir and the cover membrane in particular. The main aims of this testing were:-

(a) to allow early prediction of the length of useful life of the cover membrane.

(b) to determine locally the performance criteria of this type of reservoir to facilitate future evaluation and comparison with other types of reservoir construction.

Cover Membrane Aging Performance. The series of tests that were proposed to monitor the aging performance of the cover membrane were:-

(a) Tensile properties of membrane
(b) Tearing resistance - initiation and propagation
(c) Weld strength - in shear and peel
(d) Puncture resistance
(e) The effect of water in reservoir on the roof membrane

Twenty test sections of geomembrane were installed at the top of the southern embankment since this was the area receiving the greatest exposure to sunlight and ultraviolet radiation. It was originally proposed that samples be taken annually for performance testing to determine the effects of aging. To date samples have been tested after 6 months, 1 year, 2 years, 3 years and 4,5 years exposure.

Reservoir Performance. A series of tests was proposed to monitor the performance of this type of reservoir as compared to a conventional concrete reservoir. Control tests were to be done on the adjacent 5 Ml concrete reservoir which is fed by the same supply pipeline from the water purification works.

The following parameters were to be monitored over the first year of operation and thereafter as necessary:-

(a) Water analysis
(b) Temperature gradient and mean temperature
(c) Silt accumulation rate
(d) Maintenance and general observations

Test Procedures. The methods used for each of the tests referred to above were as follows:-

(a) Tensile properties of cover membrane: The tensile properties monitored are the membrane and reinforcement strengths at break and the membrane elongation at break. Test values were determined, in accordance with ASTM D412, using an Instron Universal Testing machine at a crosshead speed of 50mm/min. Twelve specimens were tested. Each was cut and tested in machine direction with a width of 4mm and having one unbroken strand of reinforcement across the width.

(b) Tearing resistance: The tear propagation resistance was determined in accordance with the requirement of ASTM D1938 using a rip separation speed of 200mm/min. Twelve specimens were cut and tested in the machine direction.

The initial tear resistance was determined in accordance with the requirements of ASTM 1004-66 with a separation speed of 200mm/min. Twelve specimens were cut at an angle of 45^{o} to the machine direction.

(c) Weld strength: The peel strength of the weld was determined on 12,7mm wide specimens on an Instron machine with a crosshead speed of 50mm/min. Twelve samples were tested on each occasion.

The sheer strength of the weld was also tested on twelve 12,7mm wide specimens on an Instron machine with a crosshead speed of 50mm/min.

(d) Puncture resistance: The puncture resistance of the membrane was determined using an instrumented Drop Impact Testing Machine on specimens at 23^{o}C and at 0^{o}C. A 16mm diameter hemispherical impact head was used. The speed of the impact head at the moment of impact was 4,4 m/s. Specimens were clamped in circular clamps with a 105mm internal diameter opening. The specimen was supported on a flat steel surface with a 40mm diameter circular opening at the impact point. The energy needed for complete penetration of the system was calculated from time/force curves.

(e) The effect of water in the reservoir on the roof membrane: Three samples of the roof membrane are immersed in the reservoir. The first of these is due for testing in January 1995 (i.e. after 10 years immersion). The same tests as in (a) to (d) inclusive above will be done on the immersed samples.

(f) Water analyses: Water analyses were undertaken by the Town Council's laboratory staff using standard methods of analysis on samples taken from both the concrete and geomembrane reservoirs at nominal monthly intervals. On the geomembrane reservoir a sample was taken from below each access hatch and through the cover by means of an hypodermic syringe. Samples were tested for free chlorine , E-Coli and for total viable organisms.

(g) Vertical temperature gradient: The vertical temperature gradient of the water in the reservoir was monitored using a Honeywell continuous chart recorder and negative temperature coefficient thermistors suspended vertically below the cover approximately 3m South-West of the manhole over the inlet pipe at intervals of 50, 100, 200, 300, 500, 1000, 2000, 3000, 5000 and 7000mm respectively below the cover. The temperatures were recorded during August 1985 which was estimated to correspond to the Winter minimums. The recorder was set to run continuously on the basis of 10 minutes on and 50 minutes off.

(h) Rate of silt accumulation: The rate of silt accumulation in the reservoirs was measured by placing a 600 x 500mm polyethylene box on the floor in each reservoir. In the concrete reservoir the box was placed below the access manhole and in the geomembrane reservoir below the manhole over the scour outlet. The physical quantities and appearance of deposits in these boxes were examined and the sediment was chemically analyzed.

(i) Maintenance and general observations: The Town Engineer's Department was to have kept maintenance records for the reservoir but due to the infrequency of maintenance requirements this has fallen behind. Other factors would be subject to visual examination.

TEST RESULTS.

Tensile Properties. The variation in the tensile properties of the cover membrane with age is shown in Figs. 2 and 3. Fig. 2 shows an initial sharp rise in tensile strength which is expected since the surface of the geomembrane will initially cure relatively quickly until the uncured material is effectively sealed off from the weathering effects of the atmosphere by a skin of cured material on the surface of the.geomembrane. As this cured surface forms the rate of change in the strength of the membrane slows considerably. The test results show that the increase in tensile strength of the membrane appears to have flattened off at about 24% above the initial value for the strength of the membrane at break. The results of the strength at break tests for the membrane over the next three to five years will be important in being able to define the trend of the values with a view to being able to predict at an early stage what the useful life of the membrane cover is likely to be and when a replacement cover may be required. Testing should be carried out at approximately 12 month intervals up till December 1994 and thereafter at three to five year intervals.

The strength at break values for the reinforcement vary between 12,9kg/cm and 15,1kg/cm with no trend apparent at this stage. However, as the scrim reinforcement is totally encapsulated by the Hypalon layers it is subject only to the effects of temperature variation. With the mild climate at Witbank the strength of the scrim would not be expected to vary with time. The variation in strength could probably be attributed to minor variations in the scrim yarn itself. Although no significant changes with item in the strength at break of the scrim reinforcement are expected the test should continue to be included in the monitoring program.

Fig. 3 shows the elongation at break test results. For the same reasons as described under the paragraph on tensile properties above a sharp initial drop in the value for elongation at break followed by a flattening off is expected. The test results show such a sharp initial drop in the value from the original 266% to about 140% over the first two years and thereafter a flattening out to a steady value of about 100%. The testing over the next three to five years will be essential to confirm this trend. Thereafter testing at three to five year intervals should be adequate.

Tearing resistance: The effect of aging on the resistance to propagation of a tear is shown on Fig. 4. Again the initial drop in resistance appears to have steadied at a level of about 2 kg force. The tests over the next three to five years will be important in confirming this trend.

The resistance to initial tearing does not yet appear to be approaching a steady state as shown in Fig. 5 and the results of the tests over the next five years will be important in determining whether or not the membranes resistance to the initiation of a tear has stabilized and at what value it has stabilized. In practical terms however it is considered that the resistance of the material to the starting of a tear from a plain edge of the membrane is not of critical importance to a floating cover installation since the edges of individual strips of the membrane are all welded to adjacent sheets and the only actual sheet edges are clamped under the peripheral anchor bracket. A more appropriate property for testing would be the initiation of a tear within the body of the membrane. Conversely the tear propagation test is important since it simulates the membrane's resistance to the propagation of a tear that could have been started as a cut caused by some other object.

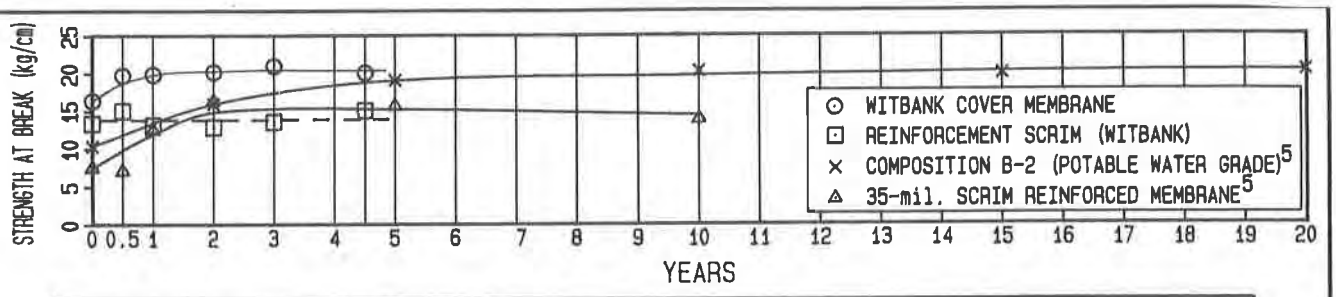

MEMBRANE	STRENGTH AT BREAK (kg/cm)									
YEARS	0	0.5	1	2	3	4.5	5	10	15	20
WITBANK COVER MEMBRANE	16.4	19.8	19.9	20.2	21.0	20.1				
REINFORCEMENT SCRIM (WITBANK)	13.4	15.1	13.2	12.9	13.6	15.1				
COMPOSITION B-2 (POTABLE WATER GRADE)5	10.4			16.0			19.1	20.3	19.9	20.3
35-mil. SCRIM REINFORCED MEMBRANE5	7.5	7.1	12.5	16.4			15.7	13.9		

FIG. 2: MEMBRANE STRENGTH AT BREAK[1,2]

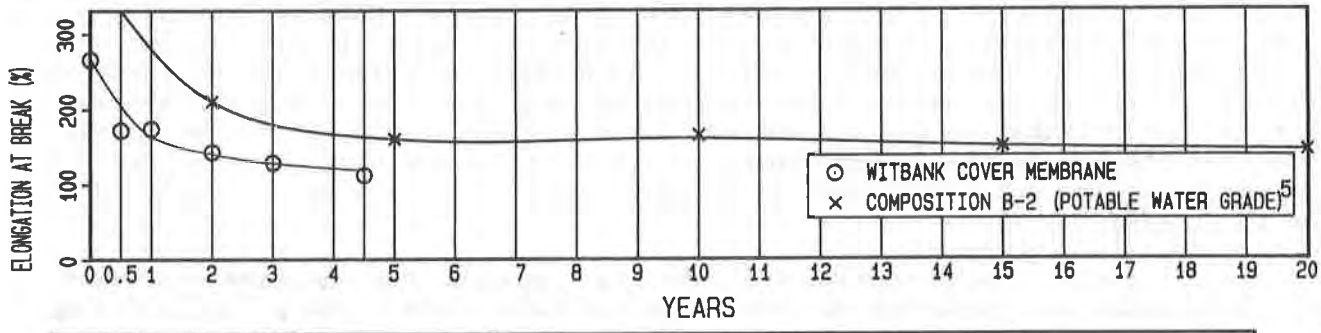

MEMBRANE	ELONGATION AT BREAK (%)									
YEARS	0	0.5	1	2	3	4.5	5	10	15	20
WITBANK COVER MEMBRANE	266	172	178	143	129	112				
COMPOSITION B-2 (POTABLE WATER GRADE)5	380			210			160	165	150	145

FIG. 3: MEMBRANE ELONGATION AT BREAK[1,2]

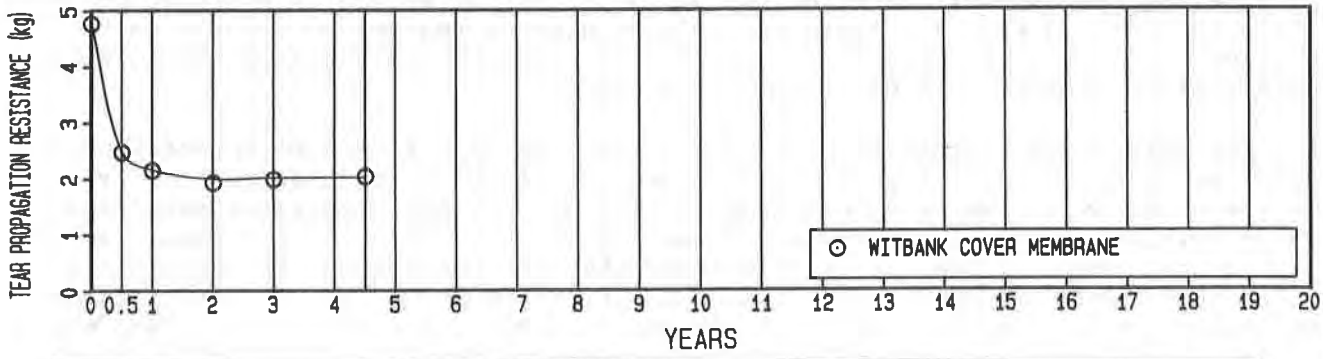

MEMBRANE	RESISTANCE TO TEAR PROPAGATION (kg)									
YEARS	0	0.5	1	2	3	4.5	5	10	15	20
WITBANK COVER MEMBRANE	4.77	2.47	2.15	1.93	1.99	2.04				

FIG. 4: RESISTANCE TO TEAR PROPAGATION[1,2]

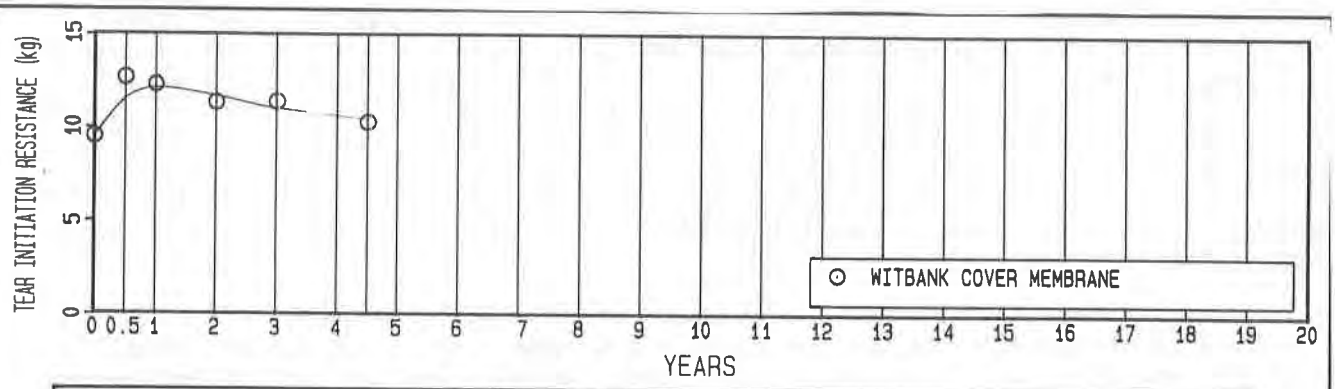

MEMBRANE	YEARS	RESISTANCE TO TEAR INIIATION (kg)									
		0	0.5	1	2	3	4.5	5	10	15	20
WITBANK COVER MEMBRANE		9.53	12.69	12.31	11.35	11.39	10.29				

FIG. 5: MEMBRANE RESISTANCE TO TEAR INIIATION[1, 2]

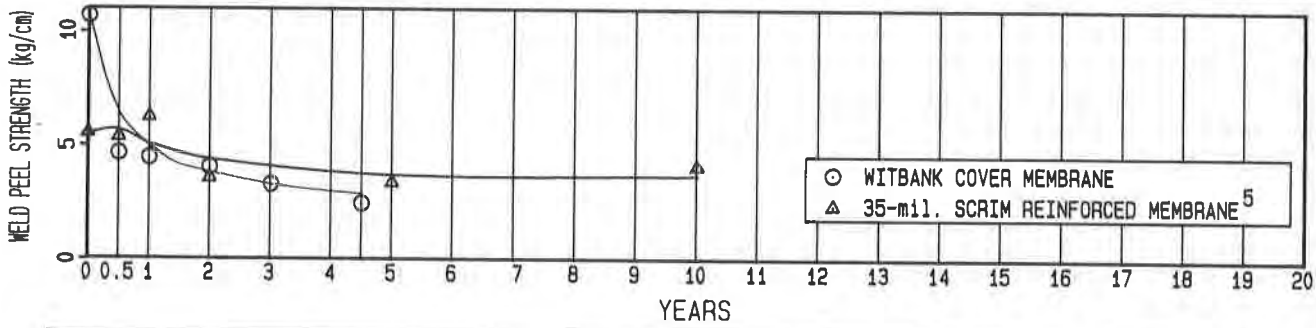

MEMBRANE	YEARS	WELD PEEL STRENGTH (kg/cm)									
		0	0.5	1	2	3	4.5	5	10	15	20
WITBANK COVER MEMBRANE		10.70	4.66	4.47	4.06	3.29	2.46				
35-mil. SCRIM REINFORCED MEMBRANE[5]		5.53	5.36	6.25	3.57			3.39	4.11		

FIG. 6: WELD PEEL STRENGTH[1, 2]

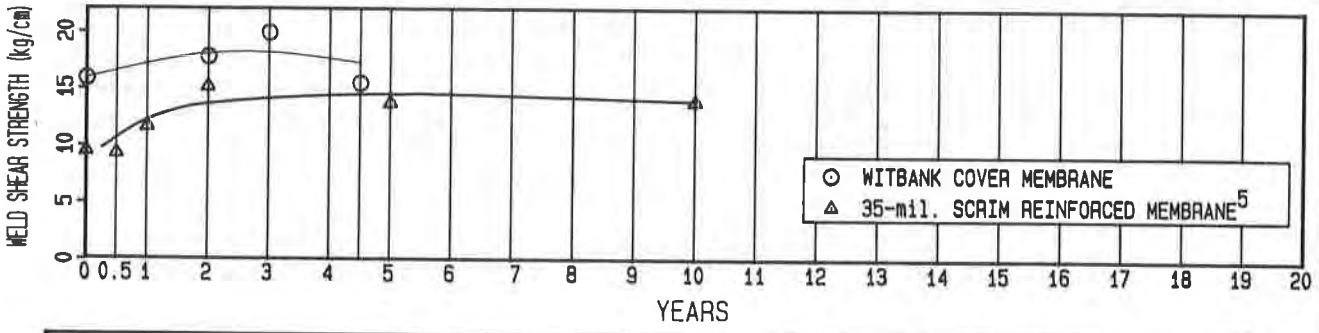

MEMBRANE	YEARS	WELD SHEAR STRENGTH (kg/cm)									
		0	0.5	1	2	3	4.5	5	10	15	20
WITBANK COVER MEMBRANE		15.89			17.79	19.89	15.47				
35-mil. SCRIM REINFORCED MEMBRANE[5]		9.47	9.29	11.61	15.18			13.75	13.97		

FIG. 7: WELD SHEAR STRENGTH[1, 2]

Weld Strength: Fig. 6 shows the results of the weld peel strength test. In this case the peel strength values are lower than expected and are continuing to decrease. The results of the next three to five years tests will determine whether or not the peel strength will reach a steady state. However, unlike the shear test which simulates actual loading conditions on the seams, this test does not directly simulate actual loading conditions on the cover membrane seams. It is consequently considered that in the case of floating cover membranes the shear test is of far greater value and importance than the peel test.

Fig. 7 shows the results for the seam shear test. In each case the break occurred in the parent material and not in the seam and in addition comparison with the strength at break of the original unweathered parent material the strength in the vicinity of the seam has been greater in all cases.

Thus although there is some concern regarding the present trend and the low values for the seam peel strength in the tests done to date, the seam shear strength tests are considered to be of far greater importance because of their direct simulation of possible loading conditions in practice. Since these seam shear strength values are well above the required levels it is concluded that the seams are still in good condition and do not yet pose potential problems. However results of the seam strength tests should be closely monitored particularly over the next three to five years. It is also recommended that a section of the actual cover membrane should be cut out and tested together with the next test panel on the south wall.

Puncture Resistance. Although the trend indicated by the test results for the variation of puncture resistance with age as shown in Fig. 8 continues downward it appears to have started flattening out but only testing over the next three to five years can confirm this.

Effect of Water in the Reservoirs on the Roof Membrane. To date tests have only been done on test samples laid on top of the cover membrane on the south embankment. A further three test samples have been suspended in the reservoir water and the first of these is due for testing in January 1995 - after 10 years immersion. However neither of these sets of specimens reproduces the actual operational condition of the cover where the underside is in contact with the water and the top face is exposed to the weathering effects of sunlight and air pollution etc. Unlike the test samples the actual cover membrane is subject to the cooling effect of the water contact as well as the daily variation in the temperature gradient across it. It is therefore recommended that a test sample should at this stage and again at the end of the ten, fifteen and twenty year periods be cut from the floating portion of the roof for testing together with one of the test samples. This would allow for determining the correlation of the test sample properties with those of the floating portion of the cover membrane so that conclusions drawn from test results on the test samples can be extrapolated to the floating membrane with confidence.

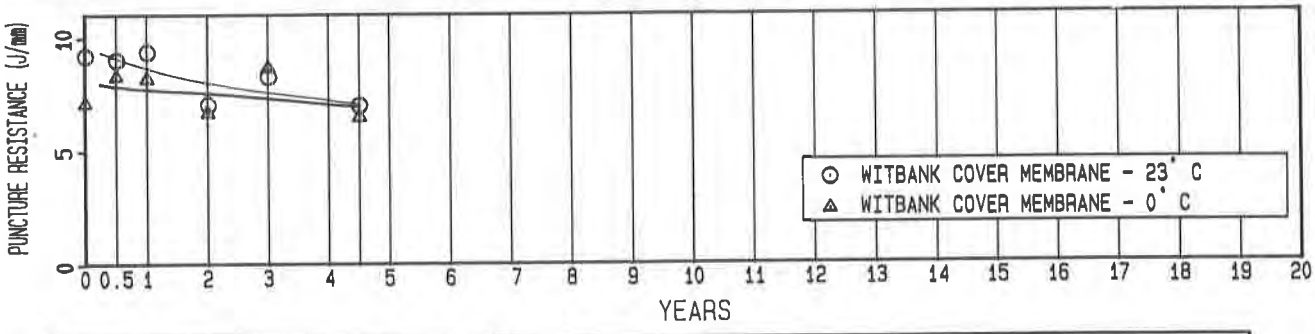

MEMBRANE	PUNCTURE RESISTANCE (J/mm)									
YEARS	0	0.5	1	2	3	4.5	5	10	15	20
WITBANK COVER MEMBRANE - 23°C	9.22	9.04	9.39	7.05	8.29	7.00				
WITBANK COVER MEMBRANE - 0°C	7.12	8.33	8.21	6.69	8.70	6.50				

FIG. 8: PUNCTURE RESISTANCE[1,2]

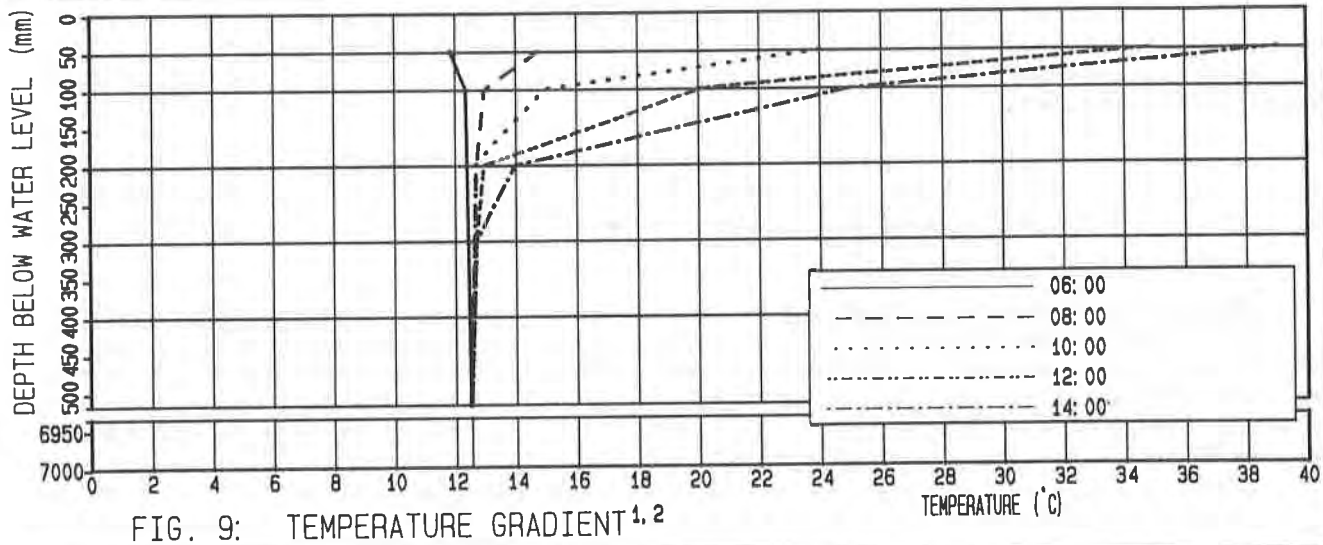

FIG. 9: TEMPERATURE GRADIENT[1,2]

Water Analysis. All the water samples analyzed in the first eighteen months of operation showed a free-chlorine presence of less than 0,1mg/l and a zero E. Coli count at 44°C. The results of the tests for total viable organisms measured as the plate count at 37°C are shown in Table 4.

Generally the geomembrane covered reservoir showed higher levels for total viable organisms and in the first year these levels were above the allowable limit of 100 total viable organisms per ml on three occasions. During this period there were four likely causes for the high total viable organisms counts. The first was that the access hatches were not air tight and surface blown dust could have entered the reservoir. This, together with the fact that the covers were not totally light tight, is likely to have allowed some algae growths in the vicinity of the access hatches where high organism counts were recorded. Also, the flap valve over the overflow outlet was not available for installation until the middle of 1986. As this outlet was on the windward side of the reservoir it is possible that a considerable amount of dust and other airborne pollutants were blown into the reservoir. A further reason is that with the water temperature reaching 35°C or higher just below the cover membrane a suitable environment is created for the growth of viable organisms and algae.

At the time of the first test report when the above results were noted it was recommended that additional chlorine be introduced to the reservoir to kill off the viable organisms. This was apparently done and the overflow outlet flap valve was installed.

Although no further testing of samples from the reservoir has since been done, no cases of high levels of total viable organisms have been reported from any of the reticulation sampling points where regular testing is undertaken.

Vertical Temperature Gradient. The temperature was found to vary only in the top 300mm below the cover. Below this level the temperature was found to remain virtually constant between 11°C and 13°C. At 200mm below the cover the maximum temperature reached about 14°C while at 100mm below the cover the maximum temperature reached was about 25°C. The maximum recorded temperature was 38°C at 50mm below the cover which was about 10°C higher than the ambient temperature. As expected the temperature gradient was found to be cyclic varying from a maximum at 14:00 to a minimum between 04:00 and 06:00 each day. Fig. 9 shows a typical warming cycle during which there would be no recirculation due to the thermosyphoning. During the cooling cycle however thermosyphoning may occur to a small degree although it does not appear to have any effect on the temperature of general body of water in the reservoir.

Silt Accumulation. A higher rate of silt accumulation is experienced in the geomembrane reservoir then in the adjacent concrete reservoir. The observed rate of accumulation in the geomembrane reservoir appears to be of the order of 4 to 5mm per year. Table 5 lists the deposits collected in the bins during the first year of operation and during 36 to 54 months after commissioning of the reservoir. Table 6 gives the analysis of the deposits found at the end of the first year of operation. The sediment comprised mainly of iron salts which could originate from the water purification process and for corrosion of steel pipelines supplying the reservoirs. There is no obvious reason why a higher deposition rate should occur in the membrane reservoir other than the length of the retention time.

TABLE 4: TOTAL VIABLE ORGANISMS AT 37°C (PLATE COUNT) IN WATER [1,2]

DATE OF ANNALYSIS	POLYMER MEMBRANE RESERVOIR									CONCRETE RESERVOIR	
	AT ACCESS MANHOLE OVER						UNDER COVER			AT ACCESS MH	
	INLET		OUTLET		SCOUR		NORTH	SOUTH	EAST	SURFACE	AT DEPTH
	SURFACE	AT DEPTH	SURFACE	AT DEPTH	SURFACE	AT DEPTH					
85-05-14	2	2 @ 1m	2	3 @ 1m	3	2 @ 1m	-	-	-	2	2 @ 1m
85-07-29	300	-	300	-	-	-	-	-	-	NIL	-
85-08-05	240	34 @ 3m	210	40 @ 3m	-	-	11	31	16	-	-
85-10-02	5	2 @ 3m	28	3 @ 3m	30	7 @ 3m	10	7	8	2	2 @ 3m
85-12-02	-	-	-	-	-	-	3	4	52	2	2 @ 3m
85-12-30	41	5 @ 3m	6	4 @ 3m	64	6 @ 3m	2	4	3	14	6 @ 3m
86-01-20	16	4 @ 3m	4	3 @ 3m	18	6 @ 3m	6	5	4	10	2 @ 3m
86-03-25	-	-	228	255 @ 2m	-	-	308	268	255	12	7 @ 2m

TABLE 5: SILT ACCUMULATION: DESCRIPTION OF DEPOSITS [1,2]

PERIOD	GEOMEMBRANE RESERVOIR	CONCRETE RESERVOIR
85-03-07 TO 85-10-21	3mm Colloidal matter	1mm Layer of grit and colloidal matter and small lumps and nodules
YEAR ENDING 90-02-21	(i) 8 to 12 small hard unidentified particles (ii) 5mm thick layer of sediment with some floc but mostly silt, which did not have the consistancy of clay.	(i) Three pieces of rust off the access ladder. (ii) About a dozen unidentified hard particles half the size of a pin head possible gravel. (iii) 25mm of floc in a soft layer on the bottom of the bin.

TABLE 6: ANALYSIS OF SEDIMENT IN RESERVOIR [1]

PRODUCT	CONCENTRATION (minerals in mg/kg)	
	GEOMEMBRANE RESERVOIR	CONCRETE RESERVOIR
VOLATILE RESIDUE (%)	20.50	12.18
FIXED RESIDUE (ASH) (%)	79.50	87.82
TOTAL (%)	100.00	100.00
ZINC	706.30	598.20
COPPER	69.50	435.80
MANGANESE	329.15	4992.00
LEAD	128.70	43.50
IRON	29053.00	121236.00
CADMIUM	< 0.01	< 0.01
NICKEL	125.20	261.00
CHROMIUM	17.30	229.80

Maintenance and General Observations. It was noted that with the prevailing wind being from the northwest the positioning of the surface water removal pump was not ideal as the wind tended to drive the water away from the pump with a resultant accumulation of surface water at the eastern end of the reservoir.

The location of the access hatches just outside the rectangle of the herringbone float layout tended to hamper the natural fold of the membrane in straight lines on the perimeter of that rectangle. It is thus recommended that where a rectangular herringbone float pattern or similar is used in a floating cover membrane the access hatches should be located within the natural perimeter of the float layout.

The presence of moles in the earthworks embankment was noted. It was recommended that the embankments be treated to eradicate the moles and any other rodents to avoid the possibility of their damaging the embankment.

During the first five years of operation vandalism had been limited to two or three occurrences of minor damage resulting in repair costs of less than R1 000,00 altogether. The maintenance costs attributable to the reservoir were so low that the Municipality did not keep separate records of the costs. Normal maintenance consisted of a visual inspection of the reservoir cover, the embankments and the under drain outlets whenever any member of the Town Engineer's staff made a routine visit to the reservoir site. The only cost normally attributed to the reservoir was the operating costs (electricity) for the surface water removal pump and since the pump was small and the pumping head low the cost was negligible. To date it has not been necessary to wash down the cover.

CONCLUSIONS.

Predicted Life of Reservoir. At this stage the results of the testing program are not clear enough for a prediction to be made on the actual length of the useful life of the reservoir, However, the results of the key tests - tensile strength of membrane; tear propagation; weld shear strength and puncture resistance - are such that one could conclude that the useful life should exceed twenty years.

Leakage. Other than one leak during the Maintenance Period caused by faulty backfilling around the outlet chamber which was immediately detected and repaired within one week, no leaks or loss of water has been experienced since the reservoir was commissioned. No seepage has been noted from the under drains. Should a leak ever be experienced, the Town Council is confident that it could be repaired rapidly with minimal loss of use of the reservoir while a similar problem with one of their concrete reservoirs would cause major disruption.

Test Program. It is considered that the test program as originally envisaged and carried out is serving a useful purpose to the Town Council, the linings contractor, and to the future of geomembrane lined and covered reservoirs in general.

Maintenance. The maintenance costs on this reservoir have been very low being limited mainly to the electricity consumption of the surface water removal pump and repair of minor vandalism. Regular inspection of the cover and under drain outlets etc., has been done during routine visits to the reservoir site and have therefore not been charged separately.

Performance and Operation. The Town Engineer and his staff are pleased with the performance and operation of the geomembrane lined and covered reservoir and would select this type of reservoir before a concrete reservoir in future.

RECOMMENDATIONS.

Testing Program. It is recommended that the testing program as originally proposed be continued for at least the twenty year period. The frequency of testing could be reduced as all the mechanical properties near steady conditions i.e. after ten years the period between tests could be increased to three to five years.

Testing of Cover Membrane. It is recommended that when the next test sample is taken for testing a specimen be cut from the floating cover membrane so that test results on the samples can be correlated to test results on the actual cover membrane.

Access Hatches. It is recommended that the access hatches be sealed to prevent the ingress of dust or algae spores and that the underside of the hatch cover be printed black to reduce the possibility of light entering through it.

Maintenance and Operation. It is recommended that the cover, the under drain outlets and the embankment be inspected at least once per month.

Water Quality Testing. It is recommended that a sampling point be established on the outlet from the geomembrane reservoir, possibly in the adjacent pumphouse, if possible, and that water quality testing be undertaken on a monthly basis.

Surface Water Removal System. Surface water removal systems should be designed to allow for flexibility in the location of the pump unit so that it can be moved to the point where the surface water collects naturally.

SUMMARY.

In general the geomembrane reservoir has performed well and met all the expectations of those who committed themselves to what was then an untried system in South Africa. The Witbank Town Engineer and his assistants have stated that on the strength of their experience with this reservoir they would at present select a geomembrane reservoir in preference to a concrete reservoir.

ACKNOWLEDGEMENTS.

Permission by the Town Engineer of Witbank for publishing tender, reservoir performance testing results and other information used in this paper is acknowledged with appreciation.

Permission by Aquatan cc to publish performance testing results and other information used in this paper is also acknowledged with appreciation.

In particular, the author wishes to thank Mr A Pretorius, the Town Engineer, Mr H Cronje and Mr L Uys of the Witbank Town Council, Mr P J Meyer of Aquatan cc, Mr S M Lloyd of the Department of Health and Population Development and personnel from the Council for Scientific and Industrial Research and the Weather Bureau for their help in preparing this paper.

BIBLIOGRAPHY.

1. BUILDING TECHNOLOGY, Division of, CSIR — 60Ml POLYMER-MEMBRANE RESERVOIR AT RYNO RIDGE: RESEARCH PROJECT Interim Report No 1 : 1989-05-06

2. BUILDING TECHNOLOGY, Division of, CSIR — 60Ml POLYMER-MEMBRANE RESERVOIR AT RYNO RIDGE : RESEARCH PROJECT Interim Report No 4 : 1989-09-08

3. HAWKINS, HAWKINS AND OSBORN — FLOATING COVER SYSTEM PROVES ITSELF ON LOCAL RESERVIOR

4. MALAN, G J and YOUNG, C G — POLYMER-MEMBRANE LINED AND COVERED POTABLE WATER RESERVOIRS

5. SCHOENBECK, Melvin — PERFORMANCE OF CHLOROSULFONATED POLYETHYLENE GEOMEMBRANES AFTER LONG TERM WEATHERING EXPOSURE

Evaluation of Field Seams Quality by the Impact Test Procedure

A. L. Rollin
Ecole Polytechnique, Canada
M. Lefebvre
Ecole Polytechnique, Canada
J. Lafleur
Ecole Polytechnique, Canada
M. Marcotte
Solmers International, Canada

ABSTRACT

Although recent research has contributed to enhance geomembrane seam quality, the authors believed that evaluation methods must still be improved in order to correctly assess the long term behavior of lined facilities. Structural molecular abnormalities, additive dispersion, unbonded areas, brittleness and micro-stress cracks within the bonded strip are usually not detected by the commonly used testing procedures.

An investigation on geomembrane brittle seam failures observed during field installation has been conducted and it has lead to the development of a new testing procedure applicable to both site and factory made seams.

This testing procedure, based on impact resistance, has been developed to determine the energy level required to fail specimens upon impact. The required energy level is evaluated using a drop-weight apparatus and depends upon the sheet's temperature and thickness as well as the quality of the seam itself.

The advantages of the impact test procedure are discussed and the results obtained during a recent testing program are presented. The energy required to fail specimens of different brittleness levels has been evaluated and these results are compared to shear and peel test results.

The use of this technique to evaluate the brittleness of geomembrane seams is mandatory to support the long term service life of HDPE geomembranes and should complement other methods.

INTRODUCTION

The growing use of High Density Polyethylene (HDPE) geomembranes as liners in hazardous and solid waste disposal facilities as well as in water retaining reservoirs requires the proper evaluation of their stress-strain characteristics as well as the risks associated with their long term performance.

The long term service life of an HDPE geomembrane depends upon the material's durability as well as the quality of the sheet's installation on the work-site. While material properties can be closely monitored during the manufacturing process, the behavior of the geomembrane seam is highly dependant on site conditions.

Polyethylene sheets can be assembled by different welding techniques such as extrusion, thermal fusion and ultrasonic welding. Basically, a quantity of energy is necessary to melt the polymer at the sheets' interface to produce a monolithic material. The transfer of energy from the source to the sheets is achieved by conduction, convection and/or radiation using a heating element, air, hot extrudate or even friction.

The quality of field seams depends on factors related to the geomembrane properties, the welding parameters, the expertise of the operators and on-site constraints such as design, climatic and site conditions. All of these factors may affect the bond strength and brittleness of the polymeric material.

Commercial welding equipment has been designed to adequately seam available geomembranes under normal field conditions. The reliability of the seams depends largely on the expertise of the trained operators, since proper equipment performance requires appropriate calibrations. Quality control testing programs must then be implemented in order to assess high quality seams. These programs should include simple test procedures that must easily be performed on-site as well as in the laboratory as to rapidly assess watertightness, bond strength (shear and peel resistance) and the brittleness of the seams.

Sheets are welded together to resist structural stress and to prevent leaks. The bonding is assessed by one of several non-destructive methods used to detect any discontinuity in a seam without measuring the relative strength of the bond. (Rollin et al.(9))

As a complement to these tests, two destructive tests are usually performed on site and in laboratory to perform welding machine calibration and to quantify the bond strength of the seam itself. These tests are namely the shear and the peel tests. The results of these tests are usually used as acceptance criteria.

The shear test simulates the stress induced by mechanical and thermal deformations on a seam. The shear strength at yield of the seam is thus obtained and careful examination of the failed seam reveals whether the seam failed before or after the liner itself. The seam specimen submitted to this shearing action is usually more rigid than the sheet itself such that the elongation of the specimen takes place within the base material. The coefficient of acceptance (Fs = seam shear strength/sheet yield tensile strength) is normally greater than 100%. This coefficient of acceptance is usually used as a minimum requirement criteria.

The peel test is used to evaluate the adhesion strength between two welded sheets. It is accomplished by applying an increasing load such that the interface is subjected to a peeling force that attempts to separate the welded sheets. The acceptance criteria commonly used is refered to as the Film Tear Bond (FTB). The specimen must fail before the interface separates. A quantitative peel strength acceptance coefficient (Fp = peel strength at break / sheet tensile yield strength) is an improvement over the FTB criteria. Recent publications by Peggs (3) and Rollin (2) have indicated that evaluation of seam quality is better achieved by using the peel test than by using the shear test.

However, it is important to note that the brittleness of a geomembrane seam is not evaluated nor detected by either of these two tests.

GEOMEMBRANE BRITTLENESS

Although adequate quality control programs were implemented during the installation of the geomembranes, some cases on long term failures of seams have recently been reported by differents authors (Rollin et al.(2), Peggs (10), Halse et al.(11).

The long term performance of a polymeric material can be reduced by weathering, chemical and bacteriological attacks and more likely by excessive welding conditions such as applying very high pressure, generating great thermal shock and overheating of the sheets (Rollin et al (4)).

Brittle failures of the seams or of the sheet itself originate from crazes or micro-stress cracks existing within the base material. Using microscopic analysis, observation of these stress cracks indicates that their presence can be related to inadequate welding conditions, production problems of the sheet itself, carbon black dispersion, too tight rolling of the sheet on a mandrel and other phenomena.

Micro-stress cracks originating from inadequate welding conditions have been presented in a preceeding paper (Rollin et al.(2)). To stress the importance of proper carbon black dispersion within a geomembrane sheet and to relate this parameter to the long term performance of a geomembrane, a micro-photograph of a cross-section of a four year old geomembrane is presented in Figure-1. Transversal micro-cracks originating at the interface between the polymer and a lump of carbon black can be observed at each undispersed carbon black element.

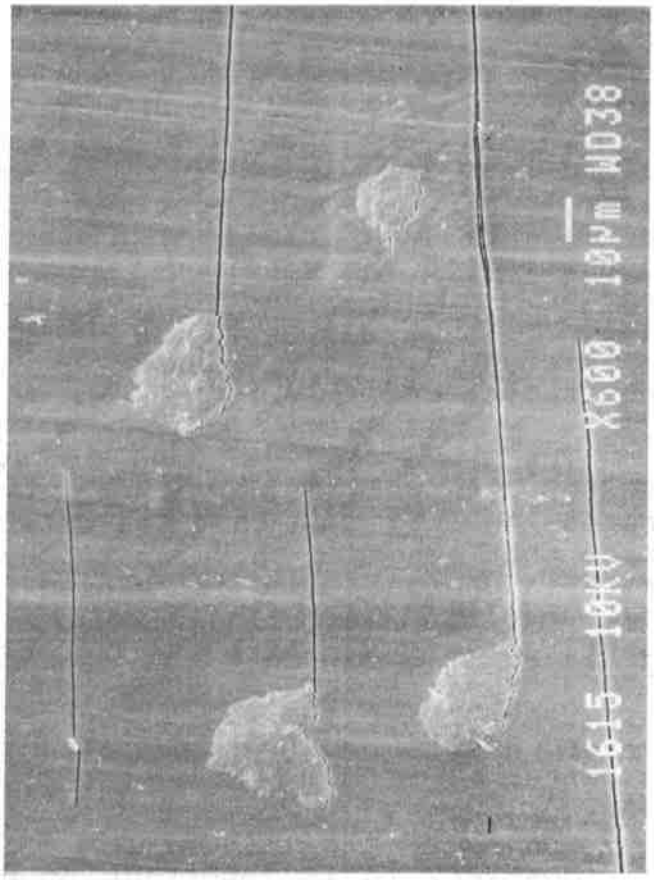

Figure-1: Section of a 4 years old HDPE geomembrane

HDPE geomembranes are materials sensitive to field and welding conditions and must be handled with care. As stated previously, excessive conditions are responsible for molecular rearrangement resulting in an increased brittleness of the geomembranes. Their long term performance will be altered and the geomembranes will degrade accordingly. A brittle product will not resist adequatly to impact stress or to heavy vehicle circulation.

Any quality assurance program must incorporate a test to measure the fragility of the geomembrane and refer to a brittleness criteria. Microscopic analysis is certainly a complementary test that can be used to assess the fragility of a seam. Unfortunately, the technique is costly and apparatus' are not easily available. A more simple and rapid test to detect seam brittleness has thus been developed: the impact test.

THE IMPACT TEST

The apparatus

The apparatus developed to assess the brittleness of HDPE geomembrane seams consists of a vertical cylinder used as a guide to a falling mass on a specimen as shown in Figure-2. This test shows the relationship which exist between an average failure energy and a specific level of brittleness as indicated in a recent paper (Rollin (8)).

This apparatus is an improved version of that used to test drainage pipes (AMI, 1987(1)). A metallic mass with a semi spherical tip weighing approximately 4000g is located at the upper end of a vertical cylinder (1130 mm high). The mass may be increased by increments of 230g (0.5 pound) as needed.

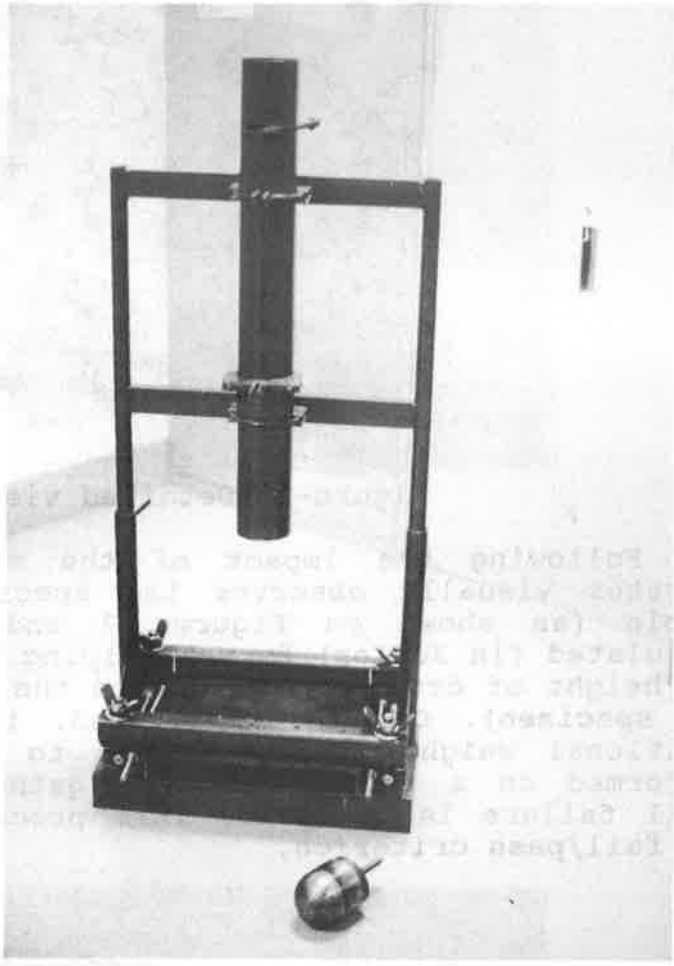

Figure-2: Overall view of the apparatus

A seam specimen of 400mm in length and width ranging from 200mm to 400mm is installed in a support clamp (Figure-3). The support is positionned such that the point of impact is located at the edge of the seam, half-way across the specimen's length.

The specimens to be tested are stored in a freezer where the temperature is maintained at approximately -3°C. Whenever the test is to be performed, a specimen is gathered, installed rapidly in the support and tested at approximately 0°C. This temperature has been selected for this testing program as a compromise in developing an accelerated test. The higher the temperature of the specimen, the greater the amount of energy needed to fail the specimen. The quantitative effect of higher testing temperature is currently under study.

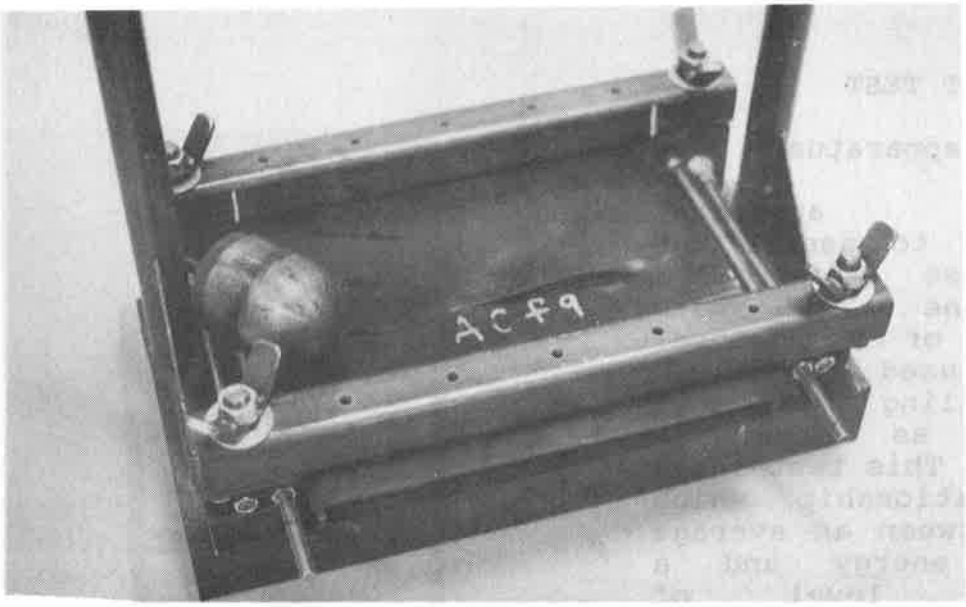

Figure-3: Detailed view of the support

Following the impact of the mass on the specimen, the operator visually observes the specimen. Upon failure of the sample (as shown on Figures 3 and 4), the energy is then calculated (in Joules) by multiplying the weight of the mass with the height of drop (distance from the tip of the falling mass to the specimen). On the other hand, if no failure is observed, additional weight is then added to the mass and the test is performed on a second specimen gathered from the same sample until failure is observed. This procedure is used to establish the fail/pass criterion.

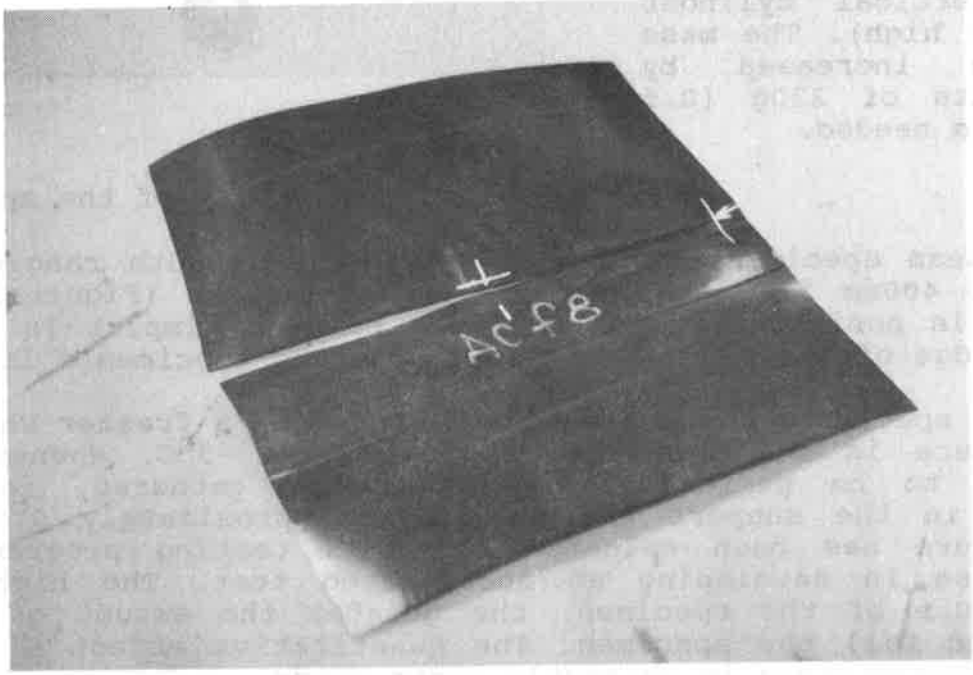

Figure-4: Example of a failed specimen

The testing program

This program was designed to evaluate the accuracy of the impact test method by testing specimens of seams of different brittleness level. Specimen of seams were produced from 1.5mm thick HDPE geomembranes using a hot air welding machine. Series of seams were performed programming different welding parameters: the speed, air temperature and the applied pressure. The values were selected in order to obtain normal welding conditions for two series and conditions known to induce brittleness at the seams edges (Rollin et al.(2)) for the others. Values of the different welding parameters and the samples identification are presented in Table-1

Series	Sheet temperature (°C)	Welding speed (m/min)	Air temperature (°C)	Welding pressure
AC a	23	0.50	400	normal
AC b	23	0.55 - 0.58	400	normal
AC d	23	0.50	430	normal
AC f	23	0.50	430	high

Table 1 . Welding parameters for each series

Seams identified as ACa were produced under acceptable welding conditions while seams ACb were performed with higher welding speeds. These samples must be identified as seams produced under normal conditions as compared to samples from seams ACd and ACf that were produced under respectively higher air temperature and higher applied pressure.

For each seam, five specimens were tested as suggested by Peggs (3) to evaluate their bond strength and their bond adhesion using both the shear and peel tests. Also cross-sections of these specimens were analysed with a scanning electron microscope (SEM) to evaluate the density of microcracks within their structure. This microscopic analysis was performed to confirm the presence of crazes and micro-cracks that can be related to the brittleness of the specimens (Rollin (4)).

IMPACT TEST PROCEDURE

The resistance of an HDPE sheet to an impact force can be expressed by the average energy, E_{50}, defined as the energy necessary to fail 50% of the tested specimens. Two different experimental approaches can be used:

a) the Probit method
b) the Bruceton Straircase method.

The Probit method consists in grouping an equal number of specimens (20 to 40 according to Pergelhof et al. (5)) selected at random from a seam into many sets and to test the specimens belonging to a set at a selected energy level, the energy used for each group being different.

The Bruceton Straircase method has been analyzed by Weaver (6) and presented in the ASTM-D-3029 standard (7). It consists of determining the average rupture energy (E_{50}) of a single batch of specimens by incremental increase of the falling mass. Following trial tests, an approximate value of the average energy is determined and a specimen is tested at this energy level. If failure is observed, an additional test is performed with a lighter mass equal to M - dM (where M is the weight of the falling mass and dM is the incremental weigth). Otherwise, if no failure is observed, the next test is performed with an increased mass, equal to the average value plus the incremental weigth (M + dM). This procedure is applied for all specimens to be tested until minimum and maximum energy are evaluated.

As recommended by Weaver (6), this technique is used to determine the average value but should not be used to evaluate the minimum and maximum energy values since only few specimens are tested at these limits. The main advantage of this method lies in the low number of specimens to be tested as compared to other methods (Progelhof (5)).

The energy increment was obtained by increasing or decreasing the falling mass' weight by 230g (0.5 pound) while the height of drop was kept constant at a value of 1130 mm. This procedure was retained to minimize the effect of impact velocity that could otherwise affect results. (ASTM-D-3029 (7)).

RESULTS

Impact test

The results obtained for each set of seam specimens are presented in Table-2 and in Figures 5 to 8. The average failure energy, E_{50}, and the related standard deviation and standard error for each seam are presented in Table-2 while the Bruceton Staircase graphical representation, showing the percent of rupture specimens as a function of the energy level, is used in the following figures: 5a and 5b, 6a and 6b, 7a and 7b and 8a and 8b.

Series	E_{50} (Joule)	Standard deviation σ	Standard error σ_E	Standard error σ_σ
AC a	50.67	0.943	0.375	0.273
AC b	49.04	3.479	1.007	1.584
AC d	40.62	2.443	0.773	1.051
AC f	42.09	5.220	0.673	1.274

Table 2 . Testing results for each series.

The energy level at which 50% of the specimens failed for both ACa and ACb seams is approximately 50 Joules while the energy levels observed for the seams identified as ACd and ACf are respectively 41 and 42 Joules with standard errors ranging from 1 to 2 percent. The standard deviation values related to a lowering of the average failure energy of 8 to 10 Joules for the brittle specimens support the precision of the method in measuring the brittleness of seams.

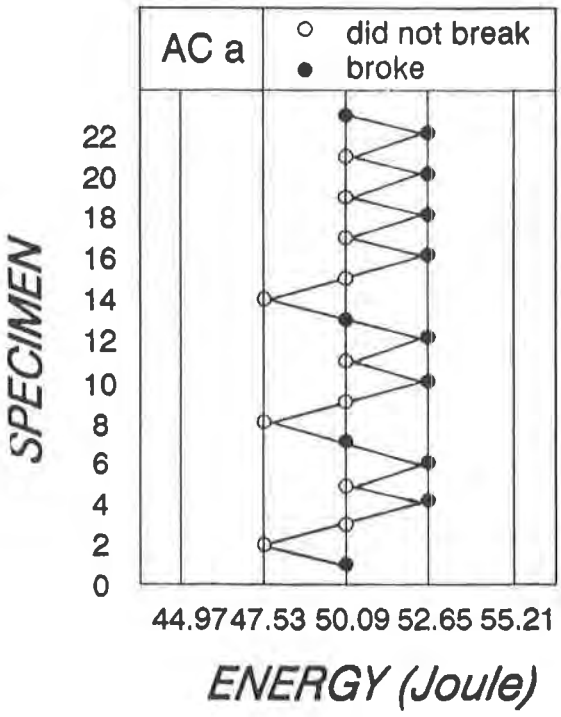

Figure 5a)

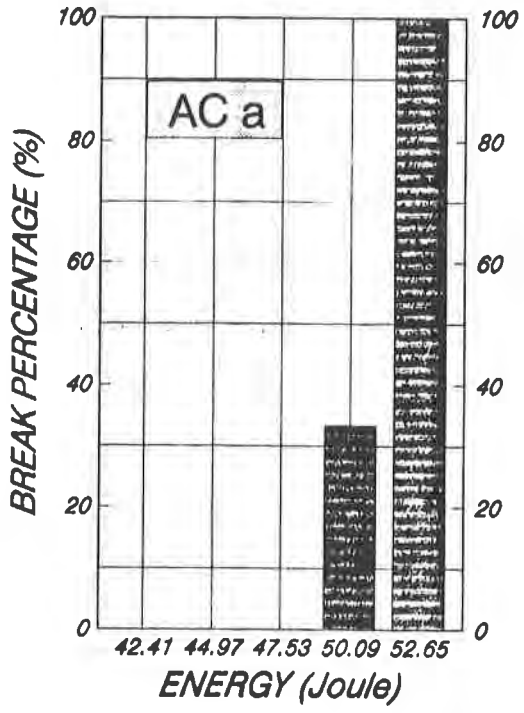

Figure 5b)

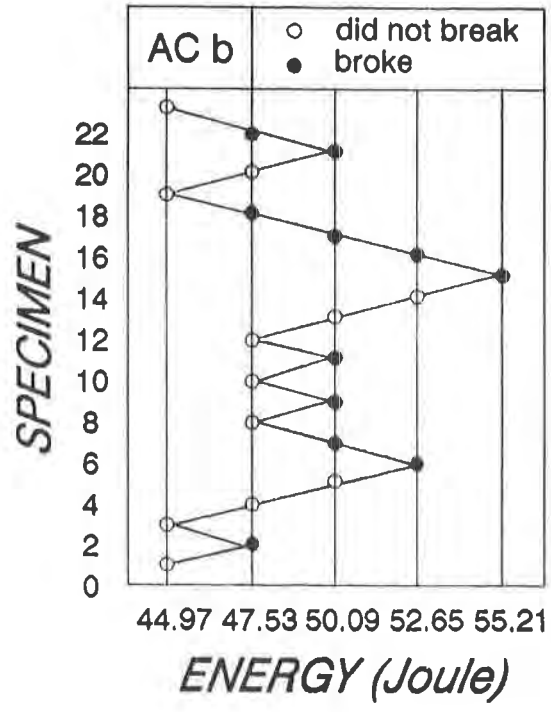

Figure 6a)

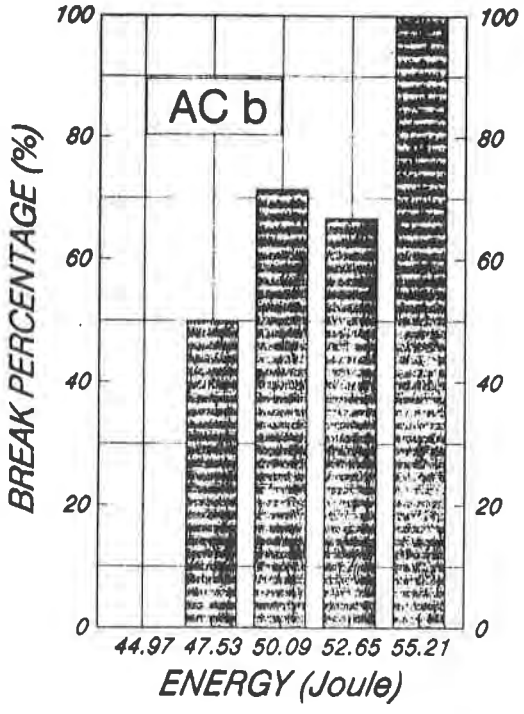

Figure 6b)

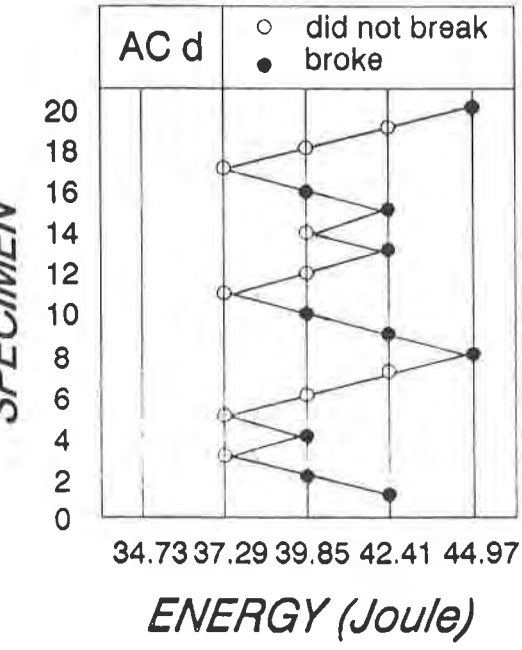

Figure 7a)

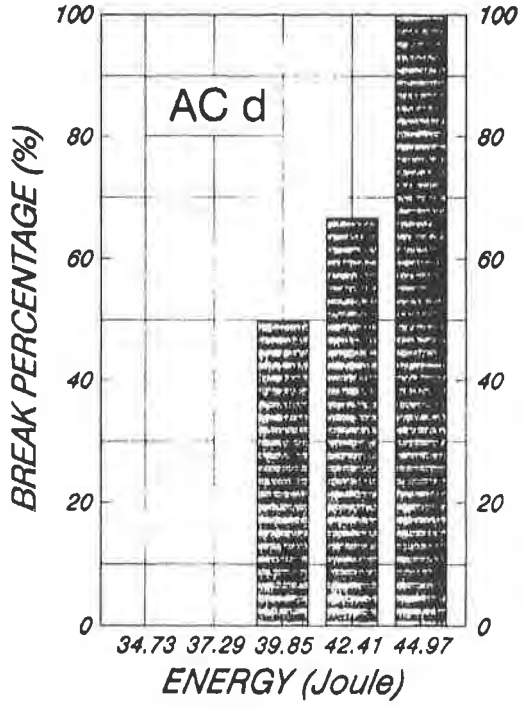

Figure 7b)

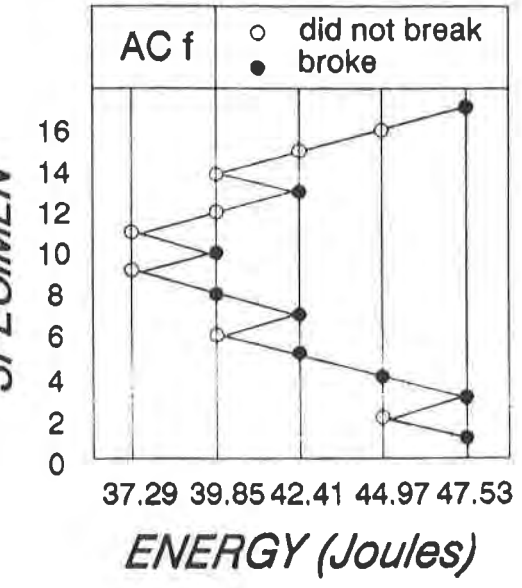

Figure 8a)

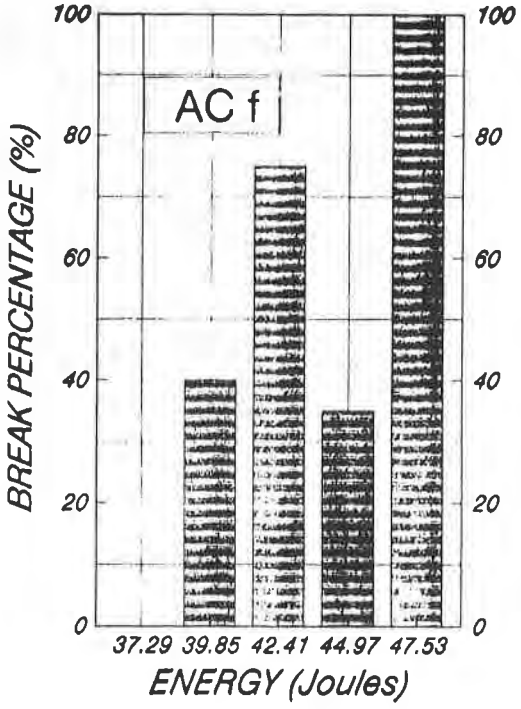

Figure 8b)

MICROSCOPIC ANALYSIS

The impact test results have been compared with microscopic detection results of micro-cracks within the brittle specimens. Micro-cracks were observed in all analysed specimens of ACd and ACf seams while the density of micro-cracks in specimens ACa and ACb was negligeable.

As an example, Figure-9 displays typical distribution of micro-cracks within a brittle specimen. Even though it is very difficult to quantify the density of microcracks within a sheet of geomembrane, the results observed support without a doubt the presence of micro-stress cracks within the seams that failed at lower value of impact energy. A program has been initiated to develop a procedure to measure the density of micro-cracks within geomembrane sheets and seams.

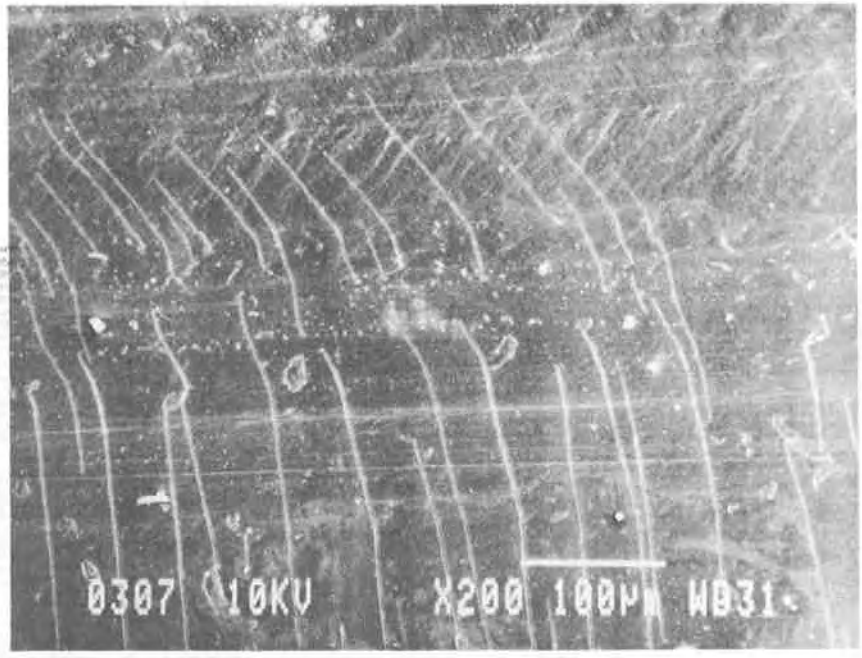

Figure 9: Typical cross-section of a brittle seam

SHEAR AND PEEL TESTS

The average results obtained from the shear and peel tests performed on five specimens of each seam are presented in Table3. Acceptance shear and peel coefficients (Fs and Fp), the elongation of the specimen under shear (E%) as well as the separation of the bond under peel (S%) expressed as a percentage are also presented in Table-3.

Finally, the standard deviations of these parameters are also presented to support the precision of the test results. The calculated values of the acceptance shear coefficient are greater than 100% without any significant variations of the elongation (strain).

The results of the peel test indicate that specimens of ACa, ACd and ACf seams resisted adequately while 10% of the specimens of seam ACb failed the FTB criteria. The average separation length of the bonds is equal to 45% of the bond width (80mm). These results support the fact that the quality of the adhesion was weaker for the seam ACb because of the higher welding speed.

SERIES	SHEAR TEST				PEEL TEST				
	STRENGTH		STRAIN		FTB (%)(1)	STRENGTH		SEPARATION LENGTH	
	$\bar{F}s(\%)$	σ_{ES}	$\bar{\varepsilon}(\%)$	σ_{E}		$\bar{F}p(\%)$	σ_{FP}	$\bar{S}(\%)$	σ_{S}
ACa	108	1.02	164	31.82	100%	64	4.34	17	6.99
ACb	108	1.26	135	27.70	90%	62	12.25	45	26.39
ACd	102	1.43	144	66.12	100%	66	4.28	19	18.42
ACf	101	1.25	131	27.44	100%	65	8.20	15	16.63

(1) FTB: These results display the percentage of tests respecting criteria.

Table 3: Shear and peel tests results

CONCLUSION

The seam's resistance to peeling indicates that the adhesion of the seam ACb is weaker than that of the other seams while the impact test indicates that seams ACd and ACf were more brittle than the other seams.

The weaker adhesion of the seam ACb can easily be explained by the relatively high welding velocity. Since not enough heat has been transferred to the sheets' interface under these conditions, one can consider that this action could not modify the base material. This is supported by the impact test results that did not indicate any significant differences in the rupture energy between specimens of seams ACa and ACb.

On the other hand, seams ACd and ACf were performed under purposely inadequate welding conditions in order to create enough micro-stress crack to induced brittle behavior. The impact test detected the increased brittleness of seams ACd and ACf while conventional testing procedures (shear and peel tests) were unable to do so. These results are supported by a Scanner Electron Microscopic (SEM) analysis that shows the increase in the density of micro-stress cracks found within those seams.

These results clearly indicate that the impact test should be a complementary test to any quality assurance program using the shear and peel tests, however may not serve as a substitute to these tests.

The impact test

The proposed impact test can evaluate the level of brittleness of HDPE geomembrane seams by determining an average failure energy. From the results obtained from 83 specimens selected at random out of 4 different seams, that the impact test is sensitive enough to detect differences in the quality of those seams. In the future, the impact test should be implemented in a quality assurance program to detect any brittle seam that may affect the long term performance of the HDPE liners. This test can easily and rapidly be performed on site as well as in the laboratory. The size of the apparatus and the cost of the necessary equipment are minimal.

The results presented in this paper have been obtained on welds performed using a hot air welding technique and a 1.5mm thick geomembrane. More results are presently been gathered to correlate the brittleness level of seams produced using other welding techniques, different testing temperature and different sheet thickness'. The impact test has been sensitive enough to detect brittle specimens.

BIBLIOGRAPHY

1- Ami, S. R. (1987), "Drainage Pipe Testing Manual" , Canadian International Development Agency technical report, Hull, Canada.

2- Rollin, A.L., Vidovic,A., Denis, R. and Marcotte, M.,(1989), "Evaluation of HDPE Geomembrane Field Welding Techniques ; Need to Improve Reliability of Quality Seams", Proceedings of the Geosynthetics'89 Conference, San Diago, USA pp 443-455.

3- Peggs, I.D. (1987), "Evaluating Polyethylene Geomembrane Seams", Proceedings of the Geosynthetics'87 Conference, New Orleans, USA, pp 505-518

4- Rollin, A.L., Vidovic, A., Denis, R. and Marcotte, M.,(1989), "Microscopic Evaluation of HDPE Geomembrane Field Welding Techniques", Proceedings Symposium on Microstructure and Performance of Geosynthetics, Orlando, USA, (under press)

5- Progelhof, R.C., Throne, J.L. and Patel, U. (1985), "Drop Weight Testing: What it Tells Designers", Modern Plastics Encyclopedia, pp 1985-6

6- Weaver, O.R. (1986), "Using Attributes to Measure a Continuous Variable in Impact Testing Plastic Bottles", Material Research and Standards, vol. 6, no. 6, June pp 285-292

7- ASTM-D-3029 (1984), "Standard Test Methods for Impact Resistance of Rigid Plastic Sheeting or Parts by Means of Tip (falling weight) ".

8- Rollin, A.L., Vidovic, A. and Ciubotariu, V. (1989), "Assesment of HDPE Geomembrane Seams", Proceedings of the Second International Landfill Symposium, Sardaigna, pp XIX. 1-11.

9- Rollin, A. L., Fayoux, D., Benneton, I . P . et Emond, G. (1990), "Non-Destructive and Destructive seam Testing" , Rilem Technical Publication "Geomembranes: Identification and Performance testing" Editor: Chapman and al., Chap. 4, (under press)

10- Peggs, I.D., (1988), "Failure and Repair of Geomembrane Lining Systems", Geotechnical Fabrics Report, 13-16, november 1988

11- Halse, Y., Koerner, R. and Lord, A. E., (1989) "Laboratory Evaluation of Stress Cracking in HDPE Geomembrane seams", Proceeding GRI-2, Durability and Aging of Geosynthetics, Journal Geotextiles and Geomembranes, Elsevier, May 1989

Analysis of Pinhole Seam Leaks Located in Geomembrane Liners Using the Electrical Leak Location Method: Case Histories

Daren L. Laine
Southwest Research Institute, USA

ABSTRACT

Twelve samples of small seam leaks were examined in the laboratory to determine the exact size of pinhole leaks detected using the electrical leak location method and the probable cause of the geomembrane liner failure. Each sample was viewed using a scanning electron microscope and thin sections were made of several samples. In addition, water leak rates were determined for several seam leaks.

Two facilities were examined for this paper. Facility A is a twelve-acre waste water containment pond double-lined with 60 mil high density polyethylene (HDPE), and facility B is a two-acre 80 mil HDPE lined double composite hazardous waste landfill. Twenty-one leaks were located in the geomembrane liner of facility A, and ten leaks were located in the geomembrane liner of facility B. Prior to inspection of each liner using the electrical leak location method, the liner seams were inspected using the air pressure method and the conventional vacuum box method.

The electrical leak location method, developed at Southwest Research Institute, was used to inspect the geomembrane liners of two waste containment facilities. The electrical leak location method provided for inspection of 100 percent of the geomembrane liner material that was covered with water. Some of the leaks were pinhole-sized and smaller. Samples of material containing these leaks were removed for laboratory analysis to determine the reasons for the leaks, and the leak rate.

The laboratory analysis and the leak rate tests indicates that small leaks can have a significant contribution to overall liner performance. Leak rates of two 0.04 inch diameter leaks were 1.85 gallons per day and 3.5 gallons per day with one foot of water pressure.

INTRODUCTION

The electrical leak location method provides for inspection of 100 percent of the geomembrane liner material that is covered with water. The method is very sensitive for locating small leaks and is capable of detecting 0.03 inch-diameter holes from a distance of two feet or more. The method is used to complement standard quality assurance measures for new geomembrane lined installations and to locate leaks in existing facilities.

Two waste containment facilities were inspected with the electrical leak location method developed at Southwest Research Institute. Twenty-one leaks were located in facility A and ten leaks were located in facility B. Even though the electrical leak location method is very sensitive, for locating leaks in geomembranes, the method cannot determine the size of the located leak. Therefore, twelve small seam leaks were removed and examined in the laboratory to determine the size of the leaks detected using the electrical leak location method and the probable cause of the leak. [And viewed using a scanning electron microscope] Thin sections were made of several samples. In addition, water leak rates for several seam samples were measured in the laboratory. The resulting leak rates revealed the importance of locating and repairing all small leaks.

Survey Method. Figure 1 shows a diagram of the operating principals of the electrical leak location method. When no leaks are present in the geomembrane liner, the high electrical resistivity of the geomembrane liner material prevents electrical current flow from the water to the earth ground. When a voltage is impressed across a geomembrane liner with no leaks, a relatively uniform voltage distribution is found in the liquid or soil cover above the liner. If a leak exists in the liner, conductive fluid will flow through the leak, establishing a path for electrical current and an anomaly in the measured electrical potential. Leaks can be accurately located within less than one inch by searching for the point of highest electrical potential using electrical leak location instrumentation.

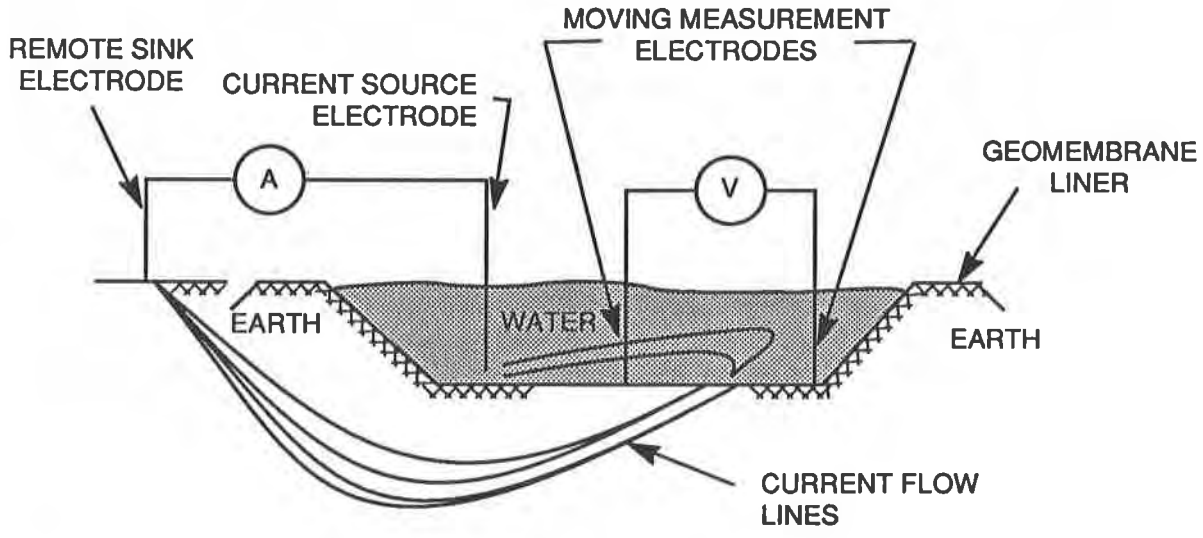

FIGURE 1. DIAGRAM OF THE ELECTRICAL LEAK LOCATION METHOD

Facilities Surveyed. The electrical leak location method was used as a pre-service quality control inspection technique for two geomembrane lined facilities. Facility A is a twelve-acre waste water containment facility double-lined with 60-mil HDPE primary and secondary geomembrane liners and facility B is a two-acre hazardous waste landfill lined with a double composite system with each composite liner consisting of an 80-mil geomembrane and an underlying clay layer.

The two facilities had rigorous quality control requirements for all phases of the liner installation. This included field tests of peel and shear strength of seam samples, laboratory analysis of seam samples, and quality control inspection of all non-destructive liner testing. An independent quality control engineering company was responsible for inspection and verification of the liner installation. All seams were tested prior to the electrical leak location method inspection with air pressure for double wedge welded seams or vacuum box for extruded seams or both conventional test methods.

Twenty-two leaks were located in facility A, and ten leaks were located in facility B using the electrical leak location method. The leaks were verified in the field by visual inspection or the use of a vacuum box test. However, several leaks could not be easily identified using the vacuum box test. Therefore, several sections that failed the electrical leak location testing were cut from the geomembrane liner for laboratory analysis.

LABORATORY ANALYSIS OF LEAK SAMPLES

Analysis Technique. Twelve seam leak samples were examined to determine the size, location, probable cause, and liquid flow rate through each leak hole/path. The samples were examined with an optical microscope to determine the exact location of the leak. If the leak position could not be determined with microscope examination then an electrical continuity test was used to pin point the leak position.

After the leak position was determined the sample was placed in a pressure test vessel to determine the water leak rate. Figure 2 shows a diagram of the leak rate test vessel. However, the leak rate test could not be conducted on all samples because not all the samples could be mounted onto the vessel with a water-tight fit due to the configuration of the samples.

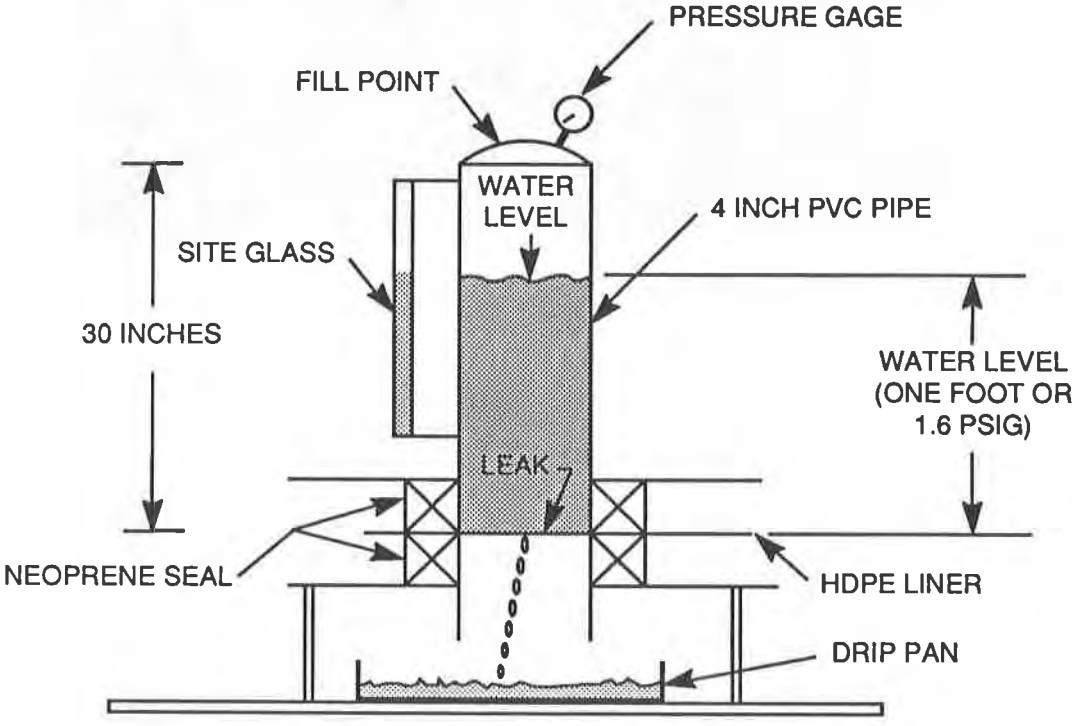

FIGURE 2 - DIAGRAM OF THE LEAK RATE PRESSURE TEST VESSEL

A scanning electron microscope (SEM) was used to examine the samples in detail for determination of the leak size and probable cause. Thin sections of the leaks were made for the detail examination.

Results of Laboratory Examination

Facility A, Sample One

Figure 3 is a top view of a fillet weld repair patch showing noticeable grind marks of the parent material on each end of the repair. The location of the detected leak is at the far left end of the fillet weld. A close view of the left side of the fillet weld is shown in Figure 4. However, the leak path or cause of the leak are not immediately obvious.

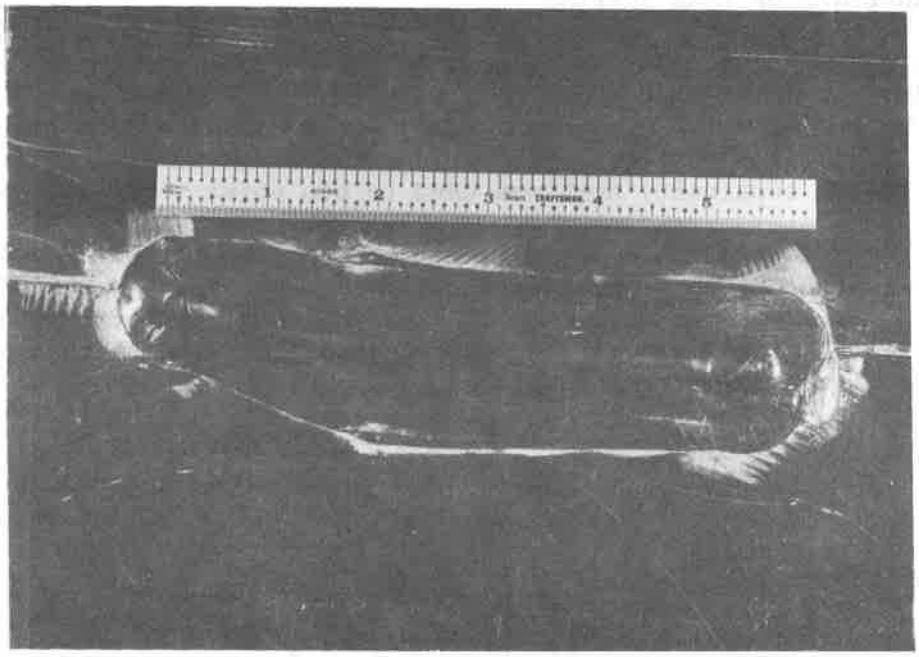

FIGURE 3. TOP VIEW OF EXTRUSION FILLET WELD ON 60 MIL HDPE LINER

A thin-section cut was made through the parent material at the end of the fillet weld. Figure 5 shows a SEM backscatter image of the area at 35 degrees from horizontal. A crack that represents the interface between the two non-bonded liner sheets is located in the center of the figure. Figure 6 shows an end view of the area in greater detail. The interface between the two liner sheets is fully recognizable, indicating that the initial welding process did not achieve molecular interpenetration of the material. In addition, over-grinding of the upper 60-mil HDPE liner is shown.

The leak was initially caused by the incomplete bonding of two geomembrane sheets during the welding process. A repair of the area resulted in over grinding of the parent material with subsequent liner failure. If the fillet weld were continued for an additional 0.25 inches, the leak path would have been repaired. Figure 5 shows excellent bonding of the fillet weld to the liner sheet.

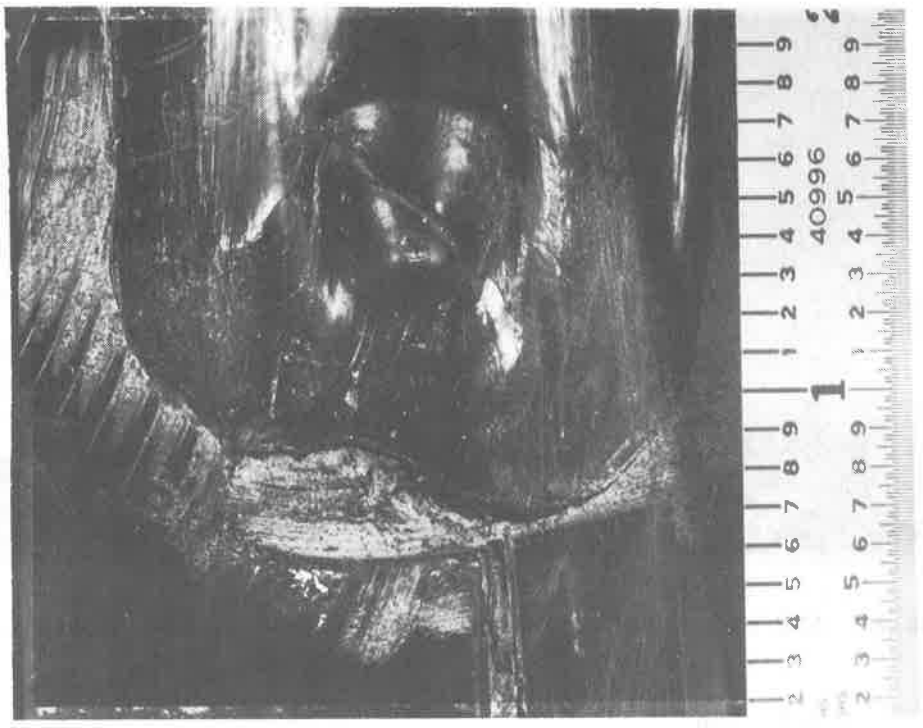

FIGURE 4. VIEW OF LEFT SIDE OF EXTRUSION FILLET WELD SHOWN IN FIGURE 3

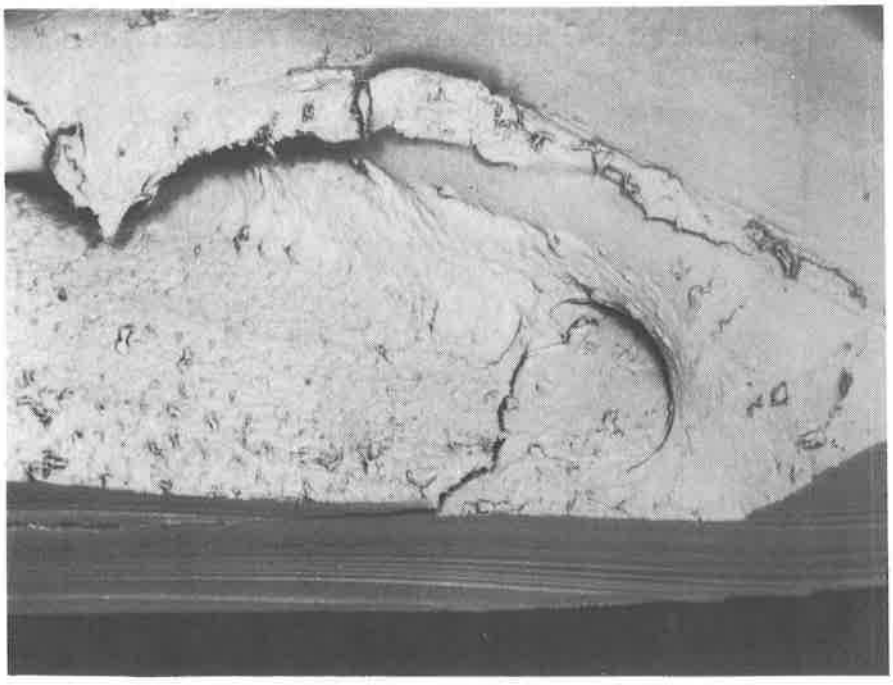

FIGURE 5. SEM VIEW OF EXTRUSION FILLET WELD SHOWING INTERFACE OF TWO 60-MIL HDPE LINERS

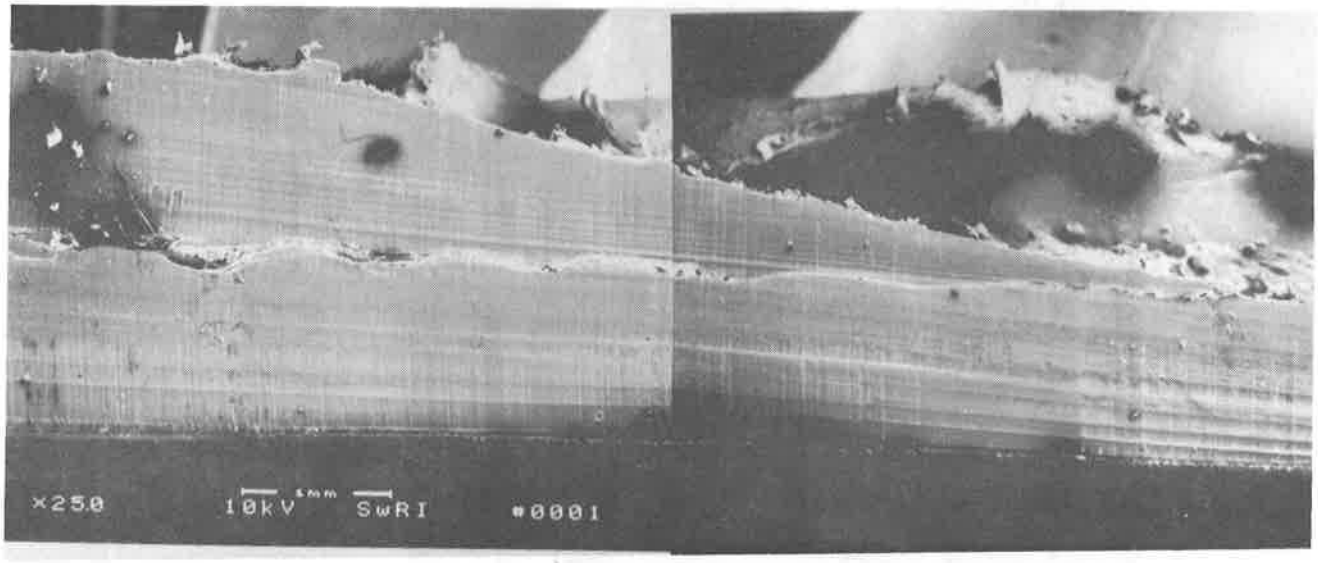

FIGURE 6. SEM OF THIN-SECTION CUT THROUGH 60-MIL HDPE LINER NEAR END OF EXTRUSION FILLET WELD

Facility A, Sample Two

Sample Two is another fillet weld repair patch of a double wedge welded seam. Figure 7 shows a top view of sample two and the three sheets that are welded together at this location. Sheet 1 (top sheet) and Sheet 2 (middle sheet) were double wedge welded together and then both sheets were doubled wedge welded to Sheet 3 (bottom sheet). The leak is located at the right end of the fillet weld repair.

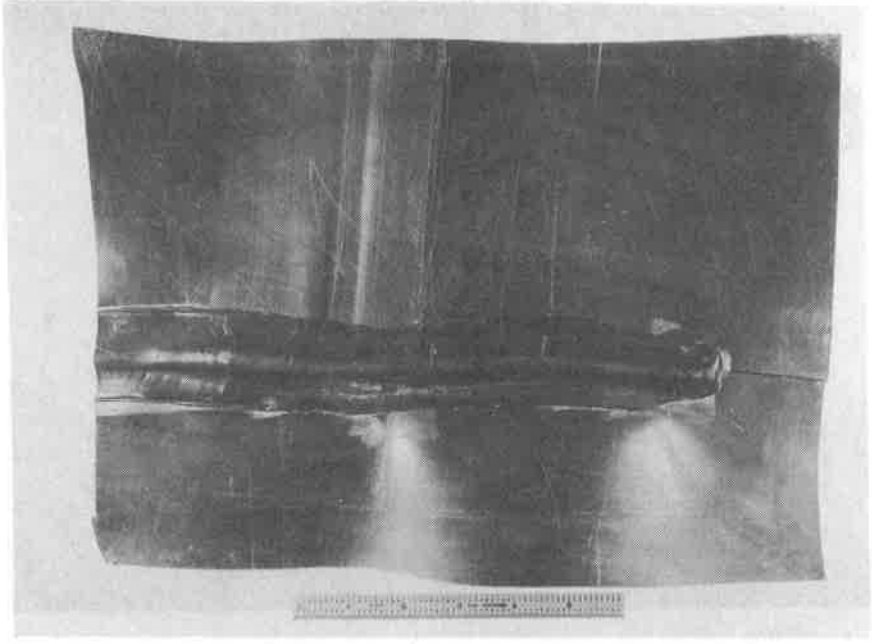

FIGURE 7. TOP VIEW OF AN EXTRUSION FILLET WELD AT THE INTERSECTION OF THREE 60-MIL HDPE LINER SHEETS

Figure 8 shows a leak path in a sample cut perpendicular to the weld axis. The leak path is along the edge boundary of Sheets 1 and 2 where an incomplete fillet weld was formed to Sheet 3. Figure 9 shows a side view of a cut parallel to the long axis of the weld. The open area indicated at Position "A" is the air channel between Sheet 1 and Sheet 2 that is made during the double wedge weld process. There is excellent overlap and fusion observed between Sheets 1 and 2. The open area indicated at Position "B" is an incomplete wedge weld between Sheet 1 and Sheet 3. Figure 10 shows an enlargement of this area. Sheet 3 is located at the bottom, Sheet 2 the center sheet, and Sheet 1 at the top sheet. The left side of the picture shows good interpenetration of the original liner material indicating proper seaming of the three sheets.

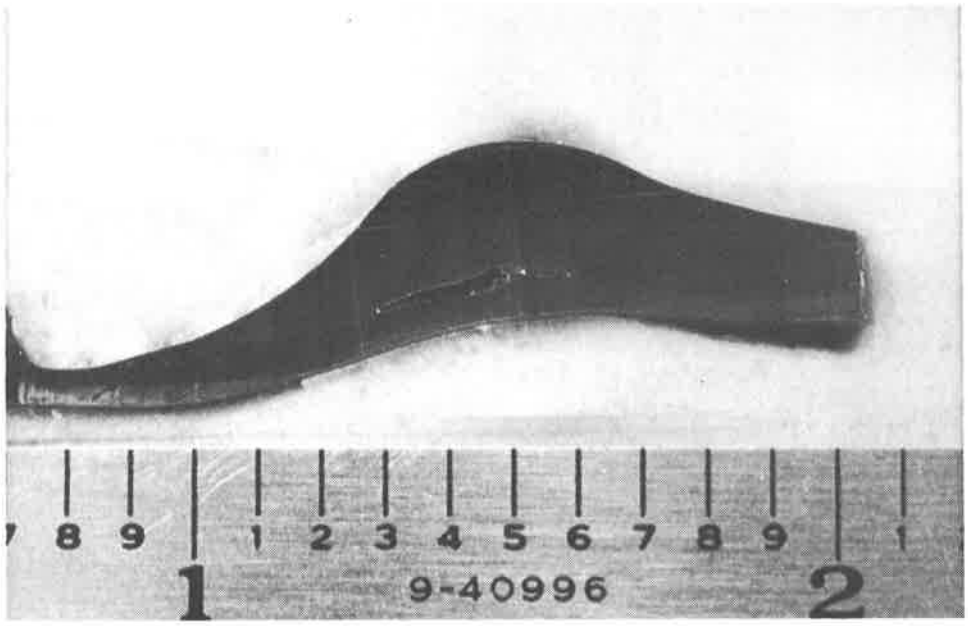

FIGURE 8. END VIEW OF CUT THROUGH THE EXTRUSION FILLET WELD PERPENDICULAR TO THE WELD AXIS

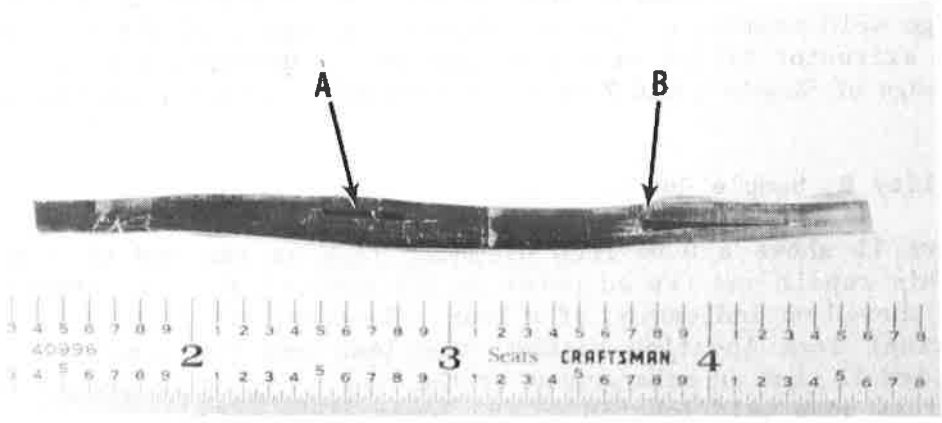

FIGURE 9. SIDE VIEW OF CUT ALONG LONG AXIS OF EXTRUSION FILLET WELD SHOWING AIR CHANNEL AT LOCATION "A" AND LEAK PATH AT LOCATION "B"

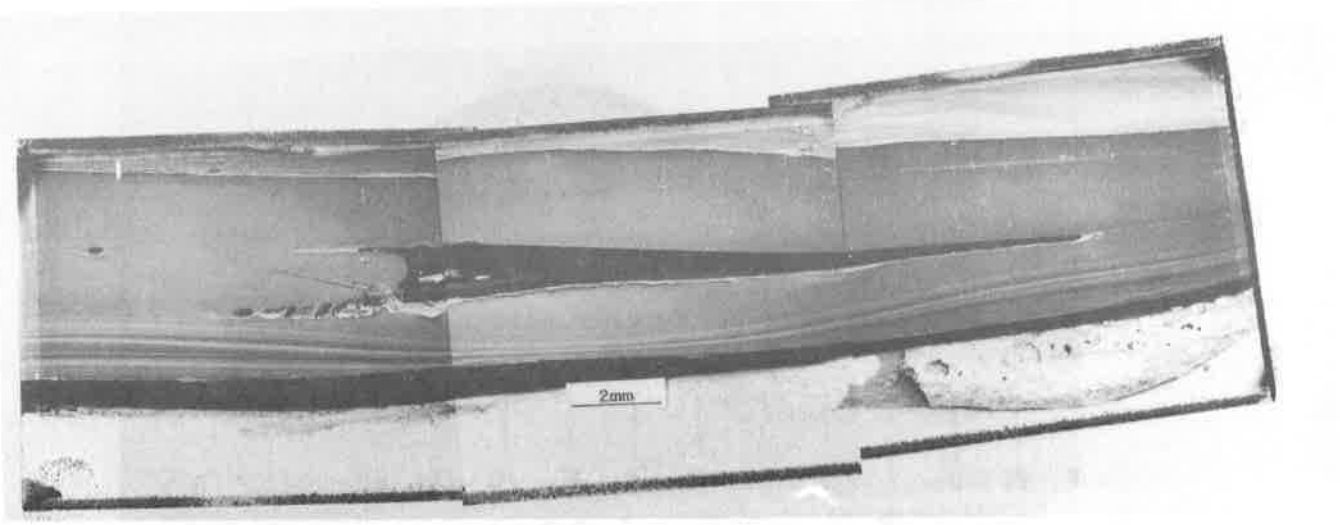

FIGURE 10. VIEW OF LEAK PATH SHOWING PROPER WELD OF THREE 60-MIL HDPE LINERS ON THE LEFT SIDE OF FIGURE

The leak shown in Figures 7 through 9 is a combination of two leak paths. The original leak path is located between Sheets 1 and 3 and was formed by the incomplete double wedge weld seaming of the two sheets. A repair of the area was attempted by placing an extrusion fillet weld over the area. However, a second leak was formed along the edge of Sheets 1 and 2 were the extrudate did not properly bond to the sheet material.

Facility B, Sample One

Figure 11 shows a 0.04-inch diameter leak at the end of a hand fillet weld repair. This repair was tested prior to the electrical leak location survey with a vacuum box showed no indication of a leak. However, after the leak was located with the electrical leak location method, the leak was confirmed with a vacuum box. Figures 12 and 13 show an enlargement of the leak. Figure 13 shows a noticeable break of the factory seam weld located on the lower right side.

Figure 14 shows a thin-section cut taken perpendicular to the leak showing the leak path and break in the factory weld. Figure 15 shows that the break does not continue through the entire length of the factory weld but continues approximately 0.02 inches into the weld and then terminates. Figure 16 shows a close up view of the factory weld break where the break ends.

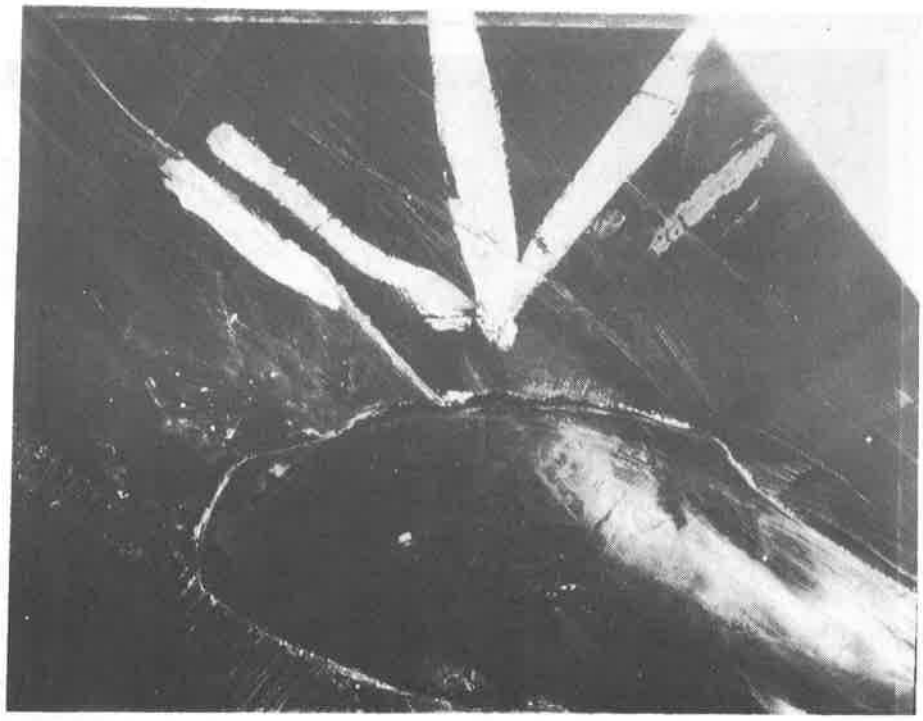

FIGURE 11. VIEW OF 0.04-INCH DIAMETER LEAK AT END OF EXTRUSION WELD ON 80-MIL HDPE LINER

FIGURE 12. SEM IMAGE VIEW OF 0.04 INCH DIAMETER LEAK

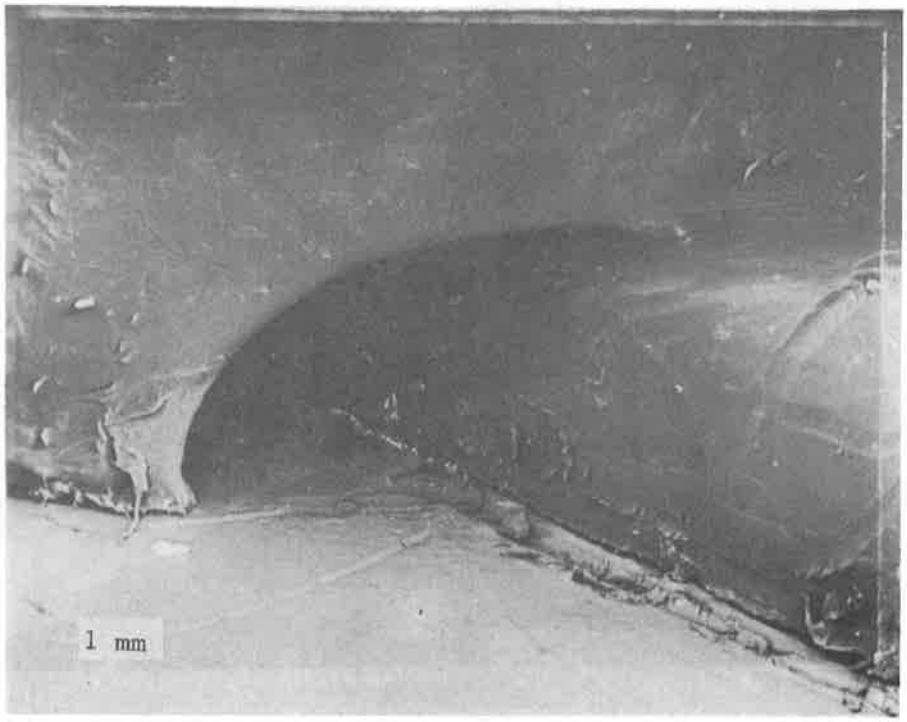

FIGURE 13. SEM IMAGE OF 0.04 INCH DIAMETER LEAK SHOWING BREAK IN FACTORY SEAM WELD

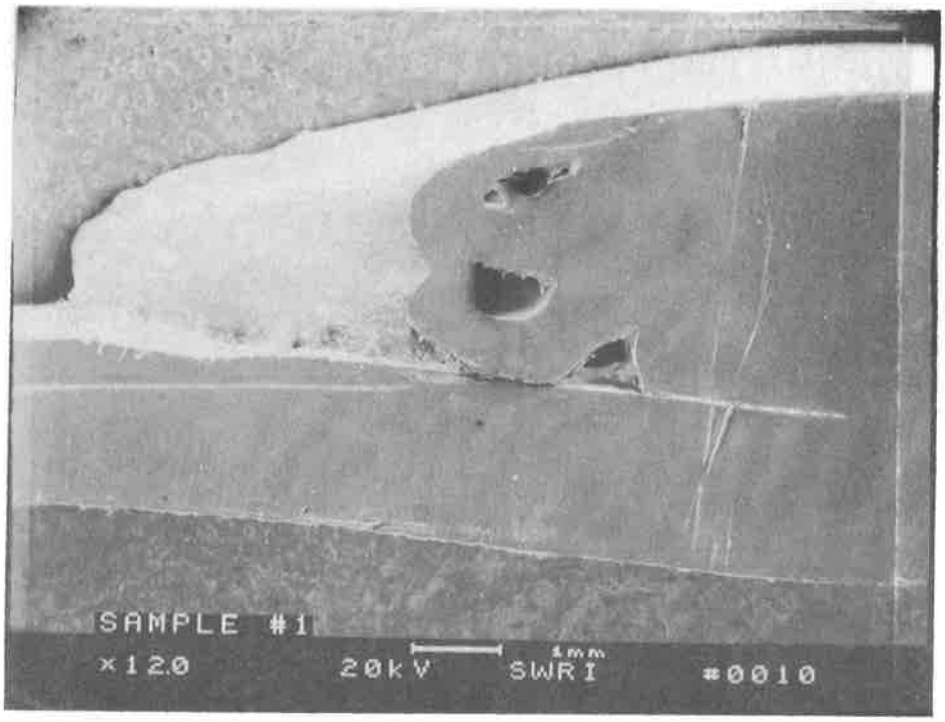

FIGURE 14. SEM IMAGE OF THIN SECTION CUT PERPENDICULAR TO 0.04-INCH DIAMETER LEAK

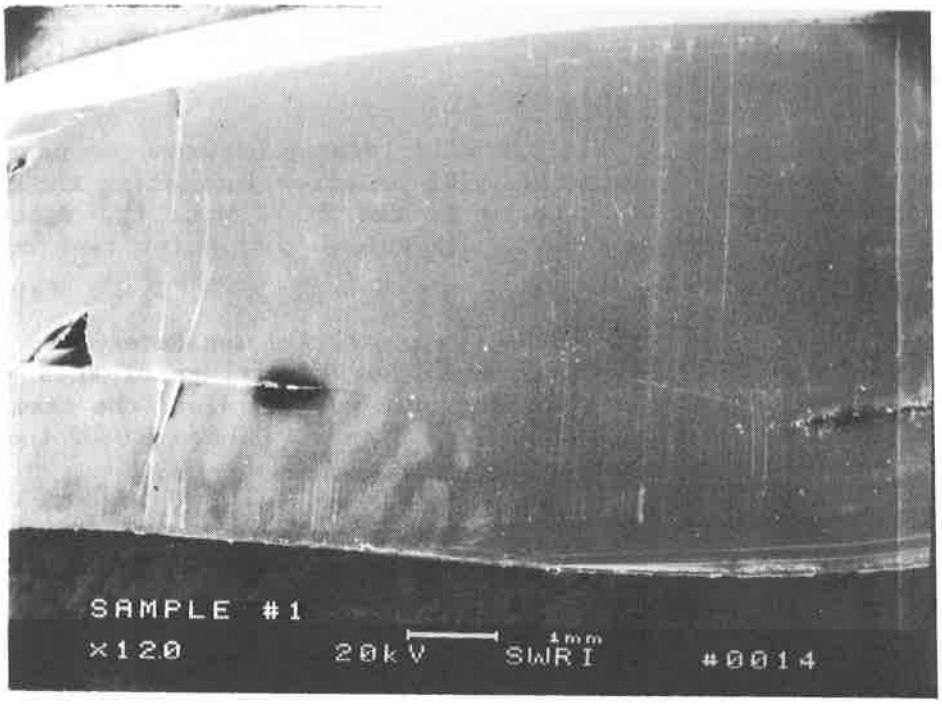

FIGURE 15. SEM IMAGE OF BREAK IN FACTORY WELD

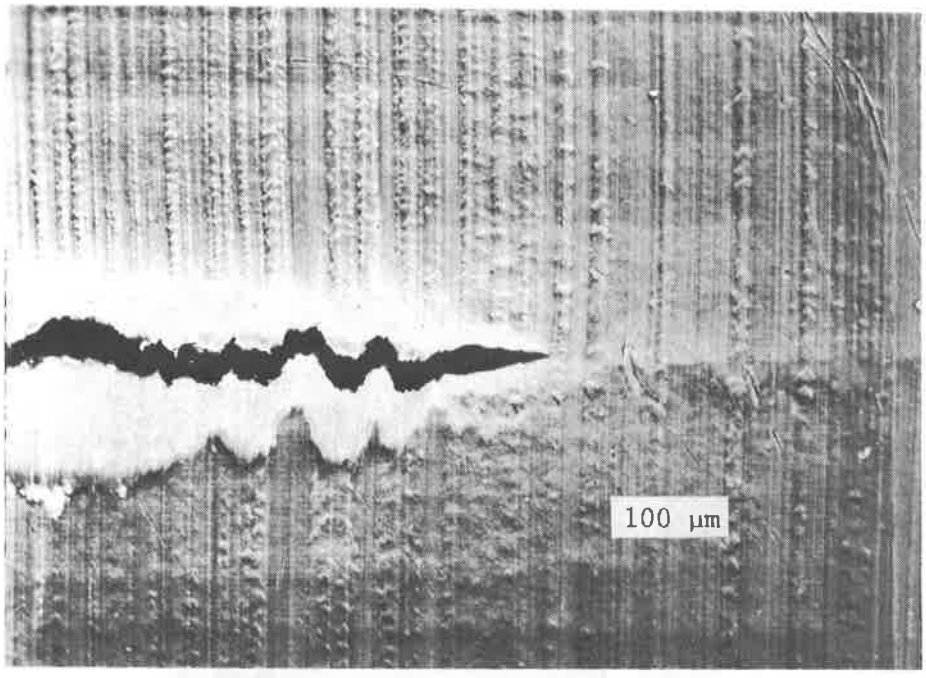

FIGURE 16. SEM IMAGE SHOWING END VIEW OF BREAK IN FACTORY WELD

As shown from the previous figures, the leak path for this sample is very complicated. The leak path was determined to be along the edge of two HDPE panels where the hand fillet weld was not properly bonded to the sheet and then exiting to the sub-grade through the break in the factory seam weld. The water leak rate for this sample was 1.85 gallons per day with one foot of water pressure.

Facility B, Sample Two

Sample two is a leak in a field weld located between two panels. Figure 17 shows a cut-out of the liner material with an arrow indicating the location of the leak. The leak could not be located in the field with the vacuum box method. However, the leak was confirmed by an electrical continuity test conducted in the laboratory.

A 0.04-inch diameter hole in the liner material was determined to be the cause of the leak in the liner. Figure 18 shows an SEM picture of this small hole. To determine the exact path of the leak, the seam was cut along the seam axis to expose any potential flaws in the welded material. Figure 19 shows a 0.02 inch by 0.006 inch flaw at the interface of the two welded panels.

Facility B, Sample Three

The leak shown in Figure 20 is at a hand extruded repair patch placed over a defective seam. The leak is seen as the small white dot opposite the large white arrow. The white dot is from light shining through the leak hole in the liner. After locating the leak with the electrical leak location method, a vacuum box was used to verify the location. However, the leak could not be detected in the field using the vacuum box. We assume that the vacuum box pulled sub-grade material or water through the leak during the vacuum test giving false test results.

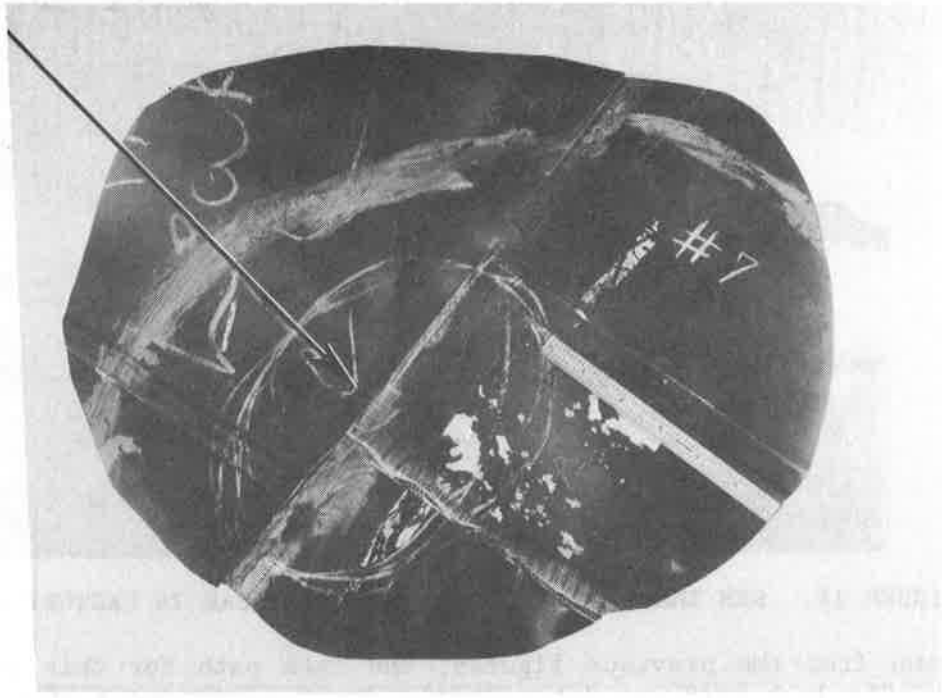

FIGURE 17. VIEW OF LINER MATERIAL SHOWING THE TWO WELDED LINER PANELS AN ARROW INDICATES THE POSITION OF THE LEAK

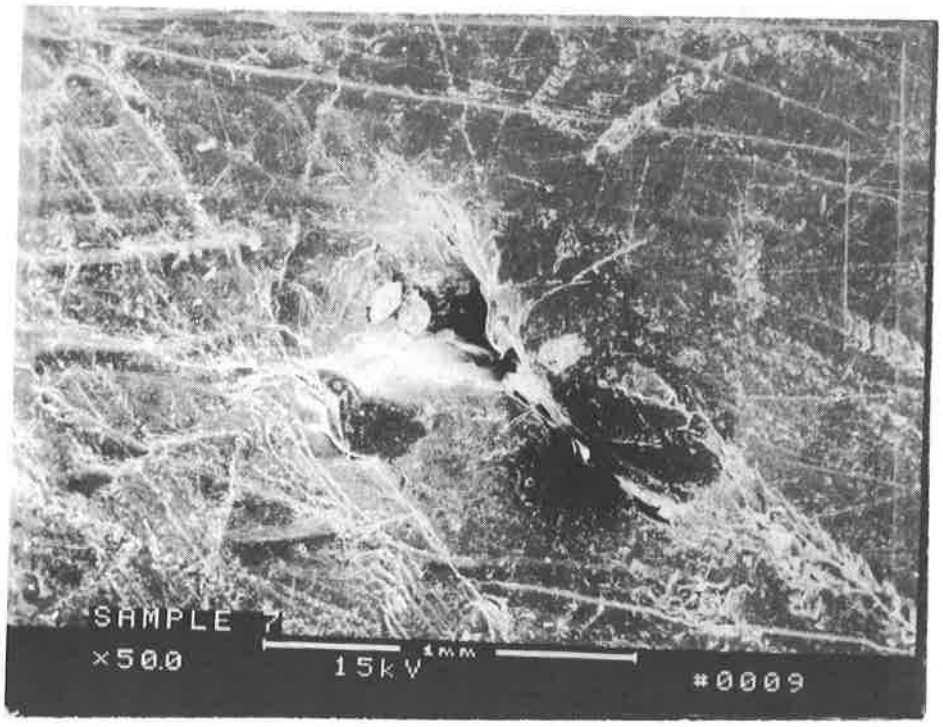

FIGURE 18. SEM IMAGE OF 0.04 INCH CUT IN 80 MIL LINER MATERIAL

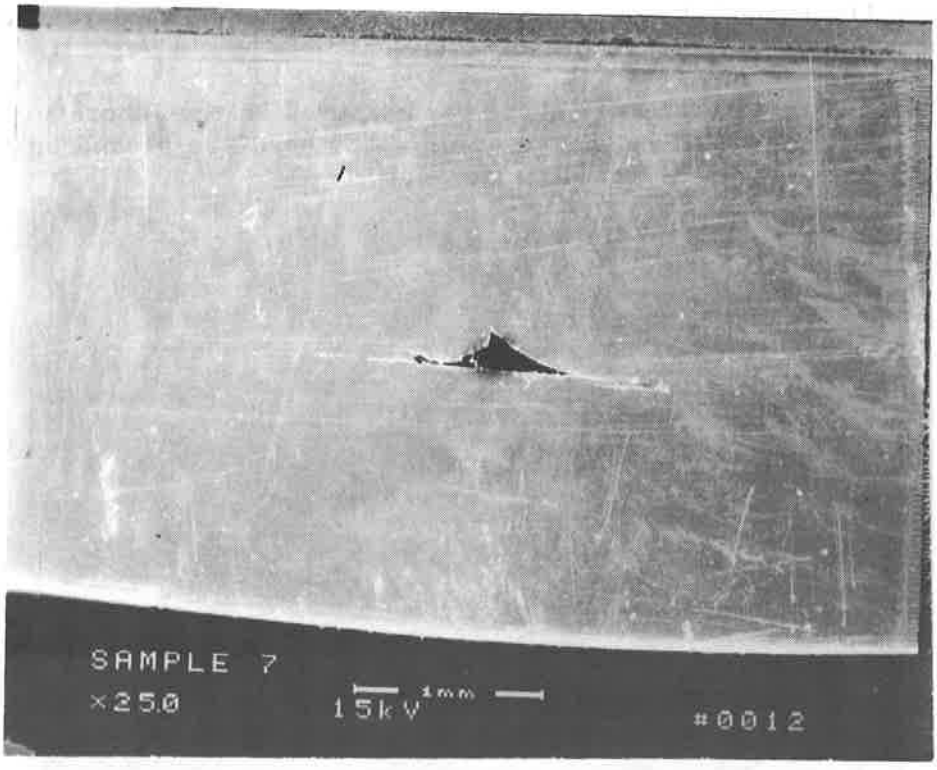

FIGURE 19. SEM IMAGE OF SEAM WELD SHOWING 0.02 BY 0.006 INCH FLAW

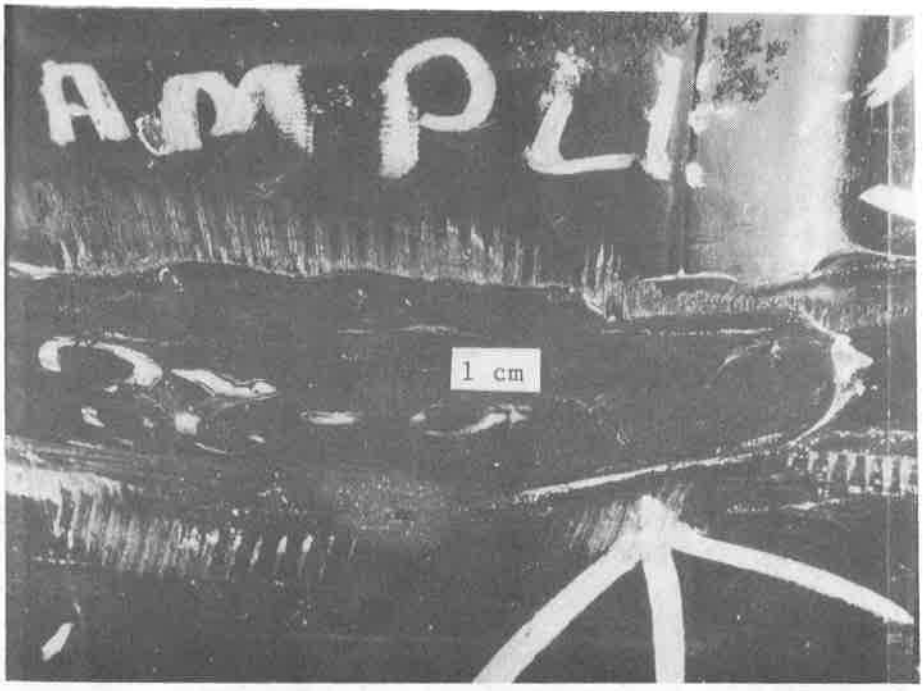

FIGURE 20. EXTRUSION REPAIR PATCH ON 80 MIL HDPE LINER SEAM

Figure 21 shows a SEM thin-section of the leak. This figure shows the HDPE material has thinned to less than 0.15 inches. The thinning may have been caused by overheating of the liner material during the repair process and then subsequent thinning as the liner cooled and contracted. Also note the apparent over-grinding of the material during the repair preparation.

The water leak rate for sample three was measured in the laboratory. The sample was placed in the test vessel and one-foot of water head was placed on the material. The resultant leak rate was 3.5 gallons per day.

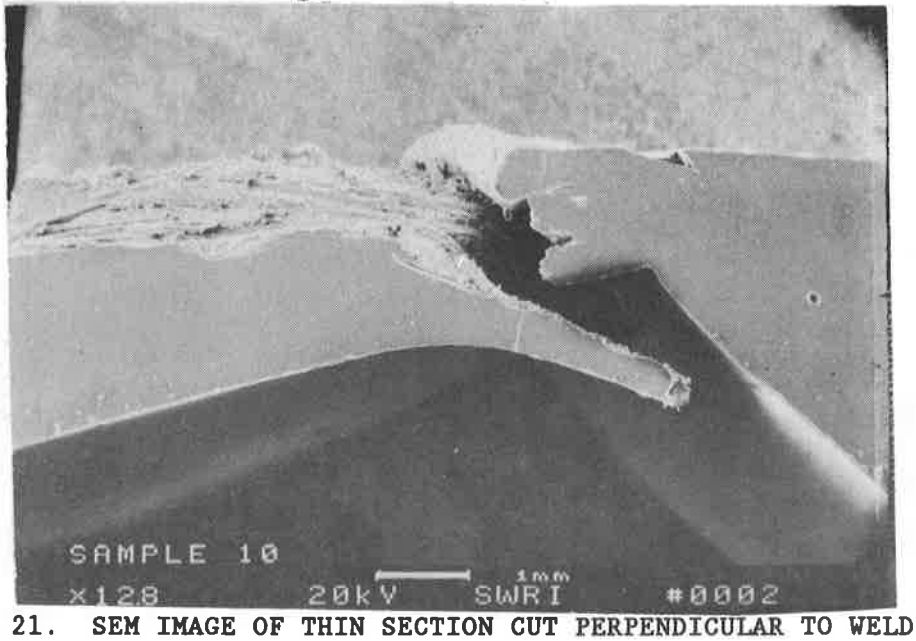

FIGURE 21. SEM IMAGE OF THIN SECTION CUT PERPENDICULAR TO WELD AXIS

CONCLUSION

The electrical leak location method was successfully used to locate leaks in two geomembrane lined waste containment facilities. Several of the smaller leaks were analyzed in the laboratory to determine the size and probable cause of the leaks.

The water leak rate of two small leaks was measured to determine the maximum water leakage through the liner. The data indicated that small leaks are an important contributing factor in overall liner performance. This data indicated that up to 3.5 gallons per day could leak from one small leak with one foot of head pressure. We have previously reported (6) that the electrical leak location method locates an average of twelve leaks per acre of liner material tested. Therefore, approximately 42 gallons/acre-day may leak from a facility that has an average of 12 holes per acre. This leak rate assumes that all the leaks in the liner are small and have a combined area of approximately 0.015 square inches with a head of one foot (1.6 psig). This leak rate also assumes free flow through a geomembrane hole.

The electrical leak location method has demonstrated that geomembrane installations can benefit from an electrical method leak location survey as a part of the construction quality assurance program. The leak location surveys should be conducted with as high a leak detection sensitivity as practical and all leaks found should be repaired, regardless of size. Therefore, pre-service testing of new installations using the electrical leak location method will enhance the overall performance of the containment facility by locating small leaks that may go undetected using conventional leak location equipment.

REFERENCES

1. Brown, K.W., J.C. Thomas, R.L. Lytton, P. Jayawickrama, and S.C. Bahrt, Quantification of Leak Rates Through Holes in Landfill Liners, *EPA Project Summary*, EPA/600/S2-87/062 Nov. 1987.

2. Struve, Fred, Extrusion Fillet Welding of Geomembranes, *Proceedings of the 3rd GRI Seminar*, December 14-15, 1989.

3. Giroud, J.P., R. Bonaparte, Leakage through liners constructed with Geomembranes - Part I. Geomembrane Liners, *Geotextiles and Geomembranes 8*, 1989.

4. Ojeshina, Anthony O., Extrusion Flatwelding, *Geotextiles and Geomembranes 9*, 1990.

5. Kolbasuk, Gary M., Hot Wedge Fusion Welding of HDPE Geomembranes, *Geotextiles and Geomembranes 9*, 1990.

6. Laine, D.L., Michael P. Miklas, Jr., Detection and Location of Leaks in Geomembrane Liners Using an Electrical Method: Case Histories, *Presented at the 10th National Conference Superfund '89*, November 27-29, 1989, Washington, DC.

7. Darilek, G.T., D. L. Laine, Understanding Electrical leak Location Surveys of Geomembrane Liners and Avoiding Specification Pitfalls, *Presented at the 10th National Conference Superfund '89*, November 27-29, 1989, Washington, DC.

8. Laine, D.L., M.P. Miklas, Jr., and C.H. Parr, Loading Point Puncturability Analysis of Geosynthetic Liner Materials, *EPA Project Summary EPA/600/S2-880/40 August 1988*.

Performance of Mount Elbert Forebay Reservoir Flexible Membrane Lining After 10 Years of Service

W. R. Morrison
U. S. Department of the Interior, Bureau of Reclamation, USA
E.W. Gray, Jr.
U. S. Department of the Interior, Bureau of Reclamation, USA

INTRODUCTION

The Bureau of Reclamation completed the first phase of initial filling for the Mt. Elbert Forebay Reservoir in March 1978. By September of that year, it was apparent that water levels in observation wells along the south ring of the reservoir were rising in response to the initial filling. In 1979 concerned that leakage through the 1.5-m thick compacted earth lining in the reservoir was threatening stability of an ancient landslide in the hillside between the reservoir and the Mt. Elbert Pumped-Storage Powerplant, Reclamation decided to install a geomembrane for seepage control in the reservoir. The geomembrane installed in the summer of 1980, consisted of a 1.14-mm reinforced chlorinated polyethylene (CPER) material, figure 1.

At that time, the installation at Mt. Elbert constituted the world's largest single-cell flexible membrane lining application to date (117 ha), and represented a milestone in the use of geosynthetic materials in the United States, if not in the world. Also, to meet Reclamation's time schedule for power on-line, the installation had to be accomplished in one construction season to allow sufficient time to fill the reservoir and conduct acceptance tests on the generating units and other accessory equipment.

The reservoir, located approximately 24 km southwest of Leadville, Colorado, impounds 14.2 X 10^6 m^3 of water of which 8.8 x 10^6 m^3 is used to develop 200 MW of electrical power during peak demand. Two 103-MW hydroelectric turbine-generators are used to generate the power. The generators have also been designed to operate as 127-MW motors to drive the turbines in reverse to pump the water from Twin Lakes, which form the afterbay for the powerplant, back to the forebay reservoir during nonpeak hours. The maximum depth of the reservoir is 21 m with a weekly fluctuation of about 9 m.

BACKGROUND

The original reservoir, built under contract between 1975 and 1977, was formed by constructing a small dike in the open southwest corner and a 27-m high-zoned earth embankment across the open north side of a topographic depression. A portion of the hillside between the forebay reservoir and the lower Twin Lakes, had been geologically mapped as an ancient landslide.

Figure 1. Aerial view taken June 1980, looking south across the Mt. Elbert Forebay Reservoir. The first portion of placed geomembrane is visible in the near right side of the reservoir and the processing plant is located in the center of the reservoir area. Also, the inlet-outlet structure (upper left-hand corner), forebay dam (foreground), slopes protection material around the perimeter of the reservoir, and subgrade areas being prepared by the contractor are visible.

Considerable concern had been expressed that seepage from the reservoir might reactivate the slide, and a 1.5-m thick compacted earth lining was placed under the entire reservoir. Water was introduced into the Forebay to a depth of 7.5 m during the period of November 1977 through March 1978. Water levels in several of the piezometers and observation wells located in the valley hillside between the forebay reservoir and the powerplant, began to rise shortly after completion of this first introduction of water into the forebay. By the summer of 1979, the water level had risen nearly 2.4 m in one well and up to 2.0 m in several others. Since other wells had either not responded or experienced water level decreases, the continuous rise experienced in some wells was considered to be attributable to water in the Forebay, rather than cyclical changes in the groundwater level.

Because the original 1.5-m thick compacted lining failed to provide adequate seepage control, a decision was made to dewater the reservoir and install a flexible membrane lining over the entire Forebay bottom and side slopes.

Once the decision was made to install a geomembrane in the reservoir, an extensive "state-of-the-art" survey was conducted, within the limited time frame available, to select a material for long term service under the unique and severe climatic and operating conditions to be encountered at the site (Reclamation 1981). At the time the membrane lining was selected, technical information on physical properties of membrane materials, installation of membrane linings, and material performance was available almost exclusively from membrane producers and their technical staffs. Even though geomembrane materials had been tested in various environments, longevity data for many products were nonexistent due to frequent changes in the chemical makeup of the materials as industry strived to improve its products. The designers of the membrane lining at Mt. Elbert consulted with scientists, engineers, manufacturers, fabricators, and installers of membrane materials in order to learn the essentials of designing and installing the lining. It was decided that the key to a successful installation and performance of the membrane lining was a quality assurance program involving inspection and testing throughout the entire manufacturing, fabricating, and installation process. State-of-the-art specifications for geomembrane material selection and installation were then written and were backed by a substantial quality assurance program.

CONSTRUCTION

Specifications for the membrane lining were issued in January, 1980 (Reclamation 1980 a); the contract for installation was awarded April 16, 1980, and final installation was completed September 20, 1980. The principal features covered by the specifications for the lining work included: removing of all existing reservoir slope protection; excavating and processing the top 0.6 m of the compacted earth lining; preparing the subgrade; manufacturing, fabrication, testing, and installing the geomembrane; placing earth cover; and replacing the slope protection materials.

Geomembrane. - The specifications provided alternate bidding schedules for installation of one of the following three lining materials: 1.14-mm reinforced chlorosulfonate polyethylene (RSPE), 1.14 mm reinforced chlorinated polyethylene (CPER), and 2.0-mm high density polyethylene (HDPE). The contractor selected CPER because of its availability to meet the construction schedule.

This geomembrane was of three-layer construction consisting of two equal thicknesses of chlorinated polyethylene (CPE) laminated to one layer of 10 by 10 1,000-denier polyester scrim. The specified physical properties requirements for this geomembrane are given in table 1.

The membrane lining was factory fabricated into "blankets," each 1300 m^2 in size and weighing approximately 2268 kg. Two shapes of blankets were furnished: 61 by 21 m containing 14 factory seams made with a Leister ™ hot-air gun and 30 by 43 m containing 28 factory seams made dielectrically. The latter blankets were installed on the side slopes in order to avoid making field seams at or near the toe of the slope. To install the membrane lining, labor crews unfolded

Table 1

Test Method and Physical Properties Requirements for CPER Lining

Property	Test Method	Minimum Requirement
Thickness	ASTM: D751-79	1.04 mm
Breaking strength each direction	ASTM: D 751-79 Grab Method	890 N
Tear strength each direction	ASTM: D 751-79 Tongue Tear Method B	334 N
Bonded seam strength in shear	ASTM: D 751-59 Grab Method A	890 N
Bonded seam strength in peel	ASTM: D 1876-78	No spec requirements
Dimensional stability (percent change, maximum)	ASTM: D 1204-78 1 hour at 100 °C	2 percent
Low temperature bend	ASTM: D 2136-78 3 mm mandrel; 4 hours at -40 °C	Pass
Mullen burst	ASTM: D 751-79 Method A	2.07 MPa
Ply adhesion	ASTM: D 413-76 Machine Method	1400 N/m

and positioned the blankets as shown on figure 2. Adjacent blankets were overlapped a minimum of 150 mm. A three-man crew thoroughly cleaned the contact surfaces with cleaning solvent and then applied the manufacturer's bodied solvent CPE adhesive to a minimum width of 100 mm. After the field seams were tested and approved, a cap strip was applied over the field seam. A 0.45-m protective earth cover material was then placed over the geomembrane, figure 3.

Details of the construction work and the quality assurance program conducted during the installation of the flexible membrane lining are summarized in the literature listed in the references at the end of this paper (Morrison, et. al., 1981, Reclamation 1980 b, Frobel and Gray 1984).

PERFORMANCE

Reservoir. - After completion of the membrane lining installation in 1980, the reservoir was refilled beginning in January 1981. By June 1981, the reservoir had been filled to elevation 2940 m. Since that time, the reservoir has remained above elevation 2935 m except for short periods of pool drawdown.

Piezometers and observation wells installed in the hillside south of the reservoir continue to be monitored. Several of the observation wells which began to rise during initial filling began a gradual decline as soon as the reservoir was drained in 1979. Others continued to rise primarily due to time lag and did not show signs of leveling off and declining until well after the lining was installed and the reservoir refilled. At the time of this writing, the water levels in the observation wells in the hillside south of the reservoir continue to decline. The foundation beneath the Mr. Elbert Forebay Dam on the north side of the reservoir is still not saturated. Inclinometers installed along the south side have not indicated any movement of the old landslide mass. Also, the riprap on the side slopes has remained stable with no evidence of slippage.

Test Section. - Included in the specification for the work was a 5-year maintenance warranty period on the membrane lining. To monitor the performance of the lining during the warranty period and for long-term research purposes, a special test section was installed in the forebay reservoir. The 6- by 30-m test section was installed at a location within the reservoir that would allow periodic access for retrieval of the membrane lining test coupons.

Eleven test panels (or coupons) comprised the total test section. Each test panel was made up of all three types of seams used in the project which included hot air, dielectric, and bodied solvent adhesive field seams. The test panels were placed on a 50-mm layer of fine sand directly above the Mt. Elbert Forebay membrane lining and then covered with the same 0.45 m of earth cover. Thus, the panels can be extracted and tested without disturbing the original CPER membrane lining. Test panels were retrieved on a yearly basis for the first 5 years, in 1987 after 7 years of burial, and in 1990 after 10 years of burial.

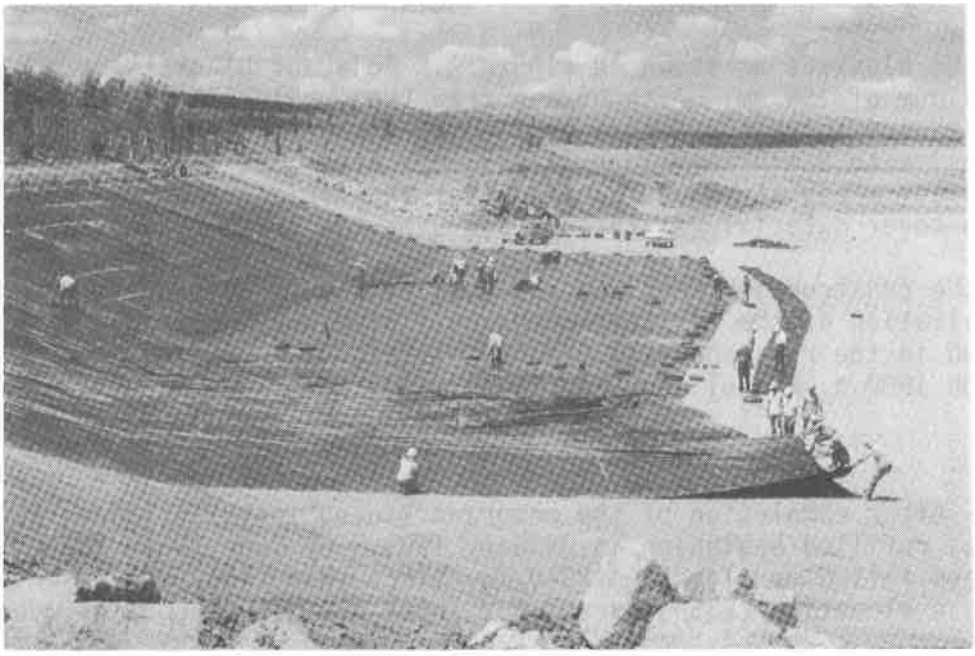

Figure 2. Installation of geomembrane on reservoir side slopes.

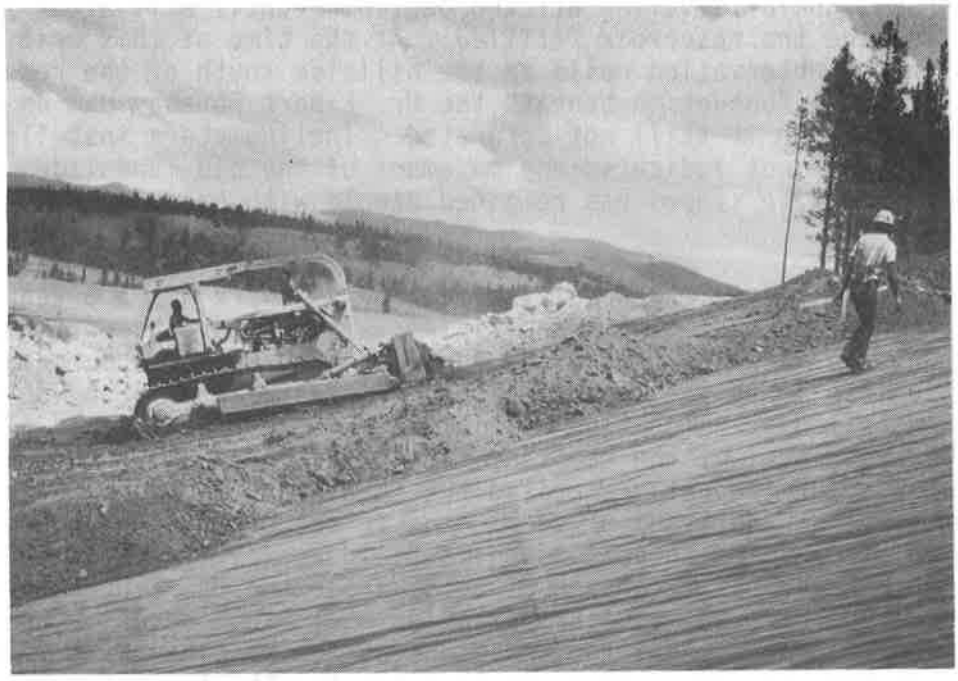

Figure 3. Placement of protective soil material on geomembrane.

The following physical and mechanical property tests are conducted on the coupons to determine changes in the CPER sheet material and seams:

1. Weight
2. Mullen burst hydrostatic resistance (ASTM D 751-79, method A)
3. Breaking strength (ASTM D 751-79, Grab Method A)
4. Ply adhesion (ASTM D 413-76, Machine Method Type A)
5. Tear strength (ASTM D 751, Tongue Tear Method B)
6. Seam peel strength (ASTM D 1876-78)
7. Seam shear strength (ASTM D 751)
8. Large-scale hydrostatic pressure resistance. This test was developed by Reclamation (Hickey 1969, Frobel, 1981). The procedure is now being adopted by ASTM under committee D-35, on Geotextiles, Geomembranes and Related Products. For the Mt Elbert evaluation, the coupon samples were tested over a 10- to 12-mm aggregate subgrade at a hydrostatic head of 43 m which was the same pressure that was used on samples of the unaged membrane lining material.

Original test specimens were taken from the same blanket samples as those used to fabricate the test section. Thus, results from extracted coupons can be compared directly with the test results obtained for the original blanket material.

Laboratory Water Immersion Tests. - To obtain additional information on the aging characteristics of the Mt. Elbert membrane lining, laboratory water immersion tests were conducted on random samples of the 1.14-mm CPER lining and the 0.5-mm CPE sheet material used in the manufacturing of the membrane lining. The reinforced material specimens with both sealed and unsealed edges were immersed to determine if there were any major differences due to possible water wicking through the exposed scrim. The samples were immersed in Denver laboratory tapwater for 5 years. The temperature of the running tapwater varied between 10 and 15 °C during this immersion period. Samples were removed yearly for testing. The same tests listed above except breaking strength and large-scale hydrostatic testing were conducted on the CPER samples. For the CPE sheet material, the following tests were conducted:

1. Weight changes
2. Breaking strength (ASTM D 882)
3. Elongation at break (ASTM D 882)
4. Tear resistance (ASTM D 1004, Die C)

Test results. - Test results for the field samples are summarized in table 2 to 5. Generally, any significant changes in the CPER lining and seams occurred within the first 3 years of service. Since then there has been very little change through 10 years of exposure. The following summary observations after 10 years of service can be made:

1. Condition. - Visual inspection of the coupon samples indicated that they are in good condition with no signs of deterioration.

2. Weight gain. - The CPER moisture absorption through 5 years of burial leveled off around 18 percent which was slightly below that noted for the laboratory immersion samples (see figure 4) for the same period of time.

3. Mullen burst resistance. - This property primarily reflects the strength of the reinforcing scrim and, on a limited basis, the contribution of the composite structure. This mechanical property has dropped approximately 19 percent in value, reflecting some decrease in scrim strength. However, the retained burst resistance is still above the original minimum requirement.

4. Large-scale hydrostatic test. - There were no significant changes in puncture resistance after 5 years of exposure. Testing on the 10-year coupon samples has been delayed until modifications to the pressure cell have been completed.

5. Ply adhesion. - This property reflects the strength of the lamination between the two CPE plies. It is dependent upon how much material passes or "strikes-through" the opening of the reinforcing scrim during manufacturing. For example, the tighter the weave of scrim, the lower the ply adhesion value. The test also reflects to some degree the scrim/CPE bond. This property exhibited a decrease in value with the change being quite variable. The reduction, however, is an indication of some loss in the scrim to CPE bond and/or the CPE to CPE polymer strength at the "strike through."

6. Tear resistance. - Determination of this property utilizing the tongue tear method was inconclusive due to "roping" or accumulation of scrim during testing, and thus did not reflect true strength characteristics. This "roping" was primarily due to the water absorption causing a weakening of the CPE/scrim bond allowing easier pullout of the reinforcing material. In future testing, tongue tear specimens will be wider in an effort to obtain a true tearing of the reinforced geomembrane without pullout of the scrim yarns.

7. Breaking strength - This property primarily reflects the strength of the reinforcing scrim. The determination of the breaking strength by the grab method has some limitation since there is a tendency to "collect" or concentrate the scrim fiber in tension between the grips, thus, producing fairly high tensile breaking loads. The test values dropped an average of 25 percent, but the retained strength was still above the original minimum requirements. It should be noted that ASTM Committee D-35 is now in the process of developing a wide-width tensile test method for all geomembranes and this should result in better assessing the performance strength of these materials.

8. Seam peel strength. - The factory seams made by the hot-air method showed a loss in peel strength of about 18 percent after 10 years of exposure, although higher losses were obtained at earlier sampling periods. A ply separation failure mode, typical for this type of reinforced geomembrane, was also observed during testing. The factory seams made dielectrically showed a loss in peel strength of about 54 percent. However, the retained peel strength of 3.6 kn/m is still twice the value of the current minimum requirement of National Sanitation Foundation Standard 54, "Flexible Membrane Lining" (NSF 1985). During testing of the 10-year coupon samples, ply separation was not observed for the dielectric factory seams. The adhesive field seams performed better than the factory seams. The adhesive field seam without a capstrip showed a loss in peel strength of about 10 percent, while the seams with the capstrip exhibited a much lower change indicating that the capping material was performing its intended function.

9. Seam shear strength. - The shear strength of the factory-made seams has shown the greatest change in mechanical properties. After 10 years of exposure, the factory seams made by the hot air method showed a loss in shear strength of about 40 percent while those made dielectrically showed a loss of about 54 percent. The failure mode was generally the same for both types of factory seams. This involved failure at the seam edge of the top sheet and scrim pullout. The adhesive field seam showed a much lower loss in shear strength.

In observing the mode of failure, the loss in shear strength does not reflect actual seam failure (i.e., CPE to CPE bond using adhesive or thermal welding) but rather a pullout of the reinforcement (polyester scrim) at the seam overlap. It is apparent that the scrim/CPE bond within the CPER laminate has deteriorated, and this weakening of the bond is being reflected in loss in mechanical properties such as the Mullen burst, ply adhesion, and most notably the overlap seam shear strength. Because the specified overlaps for the factory seams resulted in only 24 mm of a "scrim to scrim" bond, this overlap was the only contributing contact area for the seam shear values. On the other hand, the adhesive field required a 100-mm-wide bonded area and thus, had more "scrim to scrim", contact area which resulted in a less dramatic loss in tensile shear strength. In all cases of seam shear testing, the scrim pulled out of the overlaps relatively easily as compared to the tests conducted on the original unaged materials.

Test results conducted on random samples of the 1.14-mm CPER during the 5-year laboratory water immersion period are summarized in table 6. The testing of sealed versus unsealed edges showed no major differences in mechanical properties due to possible water wicking through the exposed scrim. Consequently, only the test results for the specimen with unsealed edges are presented in table 6. The results generally paralleled those observed for the field samples. The moisture absorption for the laboratory immersion samples leveled off around 21 percent as shown in figure 4.

Test results for 0.5-mm CPE material are summarized in table 7. The moisture absorption was similar to that noted for the reinforced material. It appeared that the moisture absorption caused some softening of the material as reflected in a reduction in its tensile and tear strength properties.

Table 2. Mt Elbert Test Section Results After One Year of Exposure

Property	Specification Requirement	Hot Air seam panel			Dielectric seam panel		
		Original data	One year data (range)	Percent change	Original data	One year data (range)	Percent change
Weight gain (percent)				8.62			8.62
Mullen burst (kPa)	2070	2958.0	2868.3 2724-2930	-3.0	2764.9	2571.8 2482-2655	-7.0
Tear strength (kN)	0.33	0.33	0.33 0.30-0.38	1.0	0.30	0.35 0.29-0.40	17.1
Ply adhesion (kN/m)	1.40	1.59	1.28 1.21-1.33	-20.5	1.87	1.41 1.38-1.44	-24.8
Breaking strength (kN)	0.89	1.26	1.33 1.21-1.40	4.9	1.26	1.25 1.18-1.30	-1.4
Bonded seam shear (kN)	0.89	1.33	0.90 0.82-0.97	-32.2	1.23	0.56 0.50-0.61	-54.1
Bonded seam peel (kN/m)	NR***	6.13	5.06 4.92-5.85	-17.4	6.92	6.06 5.83-6.20	-12.4
Adhesive field seam shear (kN)	NR***	1.34	1.21 ** 1.15-1.26	-9.9	1.34	1.22 * 1.16-1.30	-8.9
Adhesive field seam peel (kN/m)	NR***	6.04	6.30 ** 5.32-7.63	4.3	6.04	5.88 * 5.60-6.60	-2.6

* - Field seam with cap strip
** - Field seam without cap strip
*** - Not required

Table 3. Mt Elbert Test Section Results After Three Years of Exposure

Property	Specification Requirement	Hot Air seam panel			Dielectric seam panel		
		Original data	Three year data (range)	Percent change	Original data	Three year data (range)	Percent change
Weight gain (percent)				15.60			15.60
Mullen burst (kPa)	2070	2999.3	2716.6 2551-2758	-9.4	2813.2	2392.6 2241-2482	-14.9
Tear strength (kN)	0.33	0.35	0.30 0.28-0.32	-15.4	0.28	0.30 0.28-0.32	5.3
Ply adhesion (kN/m)	1.40	1.51	1.21 1.14-1.23	-19.7	1.84	1.30 1.23-1.37	-29.5
Breaking strength (kN)	0.89	1.26	0.99 0.94-1.04	-21.7	1.26	0.66 0.58-0.75	-47.5
Bonded seam shear (kN)	0.89	1.34	0.61 0.59-0.63	-54.6	1.22	0.56 0.48-0.59	-54.5
Bonded seam peel (kN/m)	NR***	5.69	4.13 3.99-4.27	-27.4	7.37	5.73 5.46-5.95	-22.3
Adhesive field seam shear (kN)	NR***	1.34	0.95 ** 0.89-0.10	-29.2	1.34	1.01 * 0.89-1.14	-24.6
Adhesive field seam peel (kN/m)	NR***	6.04	5.39 ** 5.17-5.92	-10.7	6.04	5.85 * 3.66-8.09	-3.2

* - Field seam with cap strip

** - Field seam without cap strip

*** - Not required

Table 4. Mt Elbert Test Section Results After Seven Years of Exposure

		Hot Air seam panel			Dielectric seam panel		
Property	Specification Requirement	Original data	Seven year data (range)	Percent change	Original data	Seven year data (range)	Percent change
Weight gain (percent)				16.90			16.90
Mullen burst (kPa)	2070	2923.5	2840.7 2758-2965	-2.8	2985.5	2558.0 2448-2655	-14.3
Tear strength (kN)	0.33	0.32	0.32 0.27-0.35	-1.6	0.31	0.27 0.26-0.28	-13.4
Ply adhesion (kN/m)	1.40	1.61	1.24 1.21-1.28	-22.8	1.79	1.37 1.26-1.42	-23.5
Breaking strength (kN)	0.89	1.26	0.91 0.77-1.17	-27.7	1.26	0.77 0.75-0.80	-38.7
Bonded seam shear (kN)	0.89	1.34	0.59 0.52-0.65	-55.9	1.21	0.49 0.48-0.50	-59.5
Bonded seam peel (kN/m)	NR***	6.06	3.38 3.22-3.59	-44.2	6.46	3.75 3.61-3.82	-42.0
Adhesive field seam shear (kN)	NR***	1.34	1.17 ** 1.07-1.22	-12.6	1.34	1.09 * 0.98-1.18	-18.3
Adhesive field seam peel (kN/m)	NR***	6.04	6.51 ** 5.71-7.20	7.8	6.04	7.74 * 6.81-8.98	28.1

* - Field seam with cap strip

** - Field seam without cap strip

*** - Not required

Table 5. Mt Elbert Test Section Results After Ten Years of Exposure

Property	Specification Requirement	Hot Air seam panel			Dielectric seam panel		
		Original data	Ten year data (range)	Percent change	Original data	Ten year data (range)	Percent change
Weight gain (percent)				ND			ND
Mullen burst (kPa)	2070	2923.5	2392.6 2344-2448	-18.2	2895.9	2302.9 2275-2379	-20.5
Tear strength (kN)	0.33	0.29	0.30 0.27-0.33	1.1	0.33	0.29 0.27-0.31	-12.8
Ply adhesion (kN/m)	1.40	1.54	1.47 1.44-1.52	-4.2	1.77	1.65 1.58-1.75	-6.9
Breaking strength (kN)	0.89	1.26	1.01 0.89-1.10	-20.3	1.26	0.89 0.69-1.06	-29.3
Bonded seam shear (kN)	0.89	1.28	0.78 0.74-0.81	-39.3	1.16	0.55 0.51-0.58	-52.8
Bonded seam peel (kN/m)	NR***	5.38	4.41 3.87-5.03	-17.9	7.84	3.61 3.40-3.73	-54.0
Adhesive field seam shear (kN)	NR***	1.34	1.18 ** 1.09-1.27	-12.0	1.34	1.09 * 1.00-1.13	-18.6
Adhesive field seam peel (kN/m)	NR***	6.04	5.46 ** 4.66-6.69	-9.6	6.04	6.09 * 4.52-8.12	0.9

* - Field seam with cap strip
** - Field seam without cap strip
*** - Not required

Table 6. Water Immersion Test Results - 1.14 mm CPER

Property	Original data (range)	One year data (range)	Percent change	Three year data (range)	Percent change	Five year data (range)	Percent change
Weight gain (percent)	-	-	15.58	-	19.25	-	21.07
Mullen burst (kPa)	2909.7 (2448-3075)	2330.5 (2275-2413)	-19.9	2706.3 (2551-2861)	-7.0	2526.3 (2344-2655)	-13.2
Tear strength (kN)	0.35 (0.24-0.44)	0.43 (0.41-0.44)	20.2	0.43 (0.42-0.43)	20.3	0.37 (0.35-0.40)	5.1
Ply adhesion (kN/m)	1.54 (1.31-1.73)	1.24 (1.19-1.30)	-19.3	1.51 (1.47-1.54)	-2.3	1.38 (1.33-1.42)	-10.2
Hot Air seam shear (kN)	1.19 (0.89-1.37)	0.61 (0.60-0.63)	-48.7	0.93 (0.89-0.97)	-22.1	0.60 (0.60-0.60)	-49.3
Hot Air seam peel (kN/m)	5.50 (4.64-6.81)	4.82 (4.52-5.06)	-12.4	6.01 (5.78-6.22)	9.2	3.64 (3.57-3.69)	-33.8
Dielectric seam shear (kN)	1.30 (1.00-1.41)	0.64 (0.62-0.66)	-51.0	0.89 (0.89-0.89)	-31.7	0.77 (0.77-0.77)	-40.6
Dielectric seam peel (kN/m)	6.74 (6.01-7.49)	5.80 (5.69-5.92)	-14.0	4.11 (3.94-4.20)	-39.0	4.10 (3.96-4.25)	-39.2
Adhesive seam shear (kN)	1.23 (1.21-1.25)	1.15 (1.12-1.18)	-6.5	1.32 (1.29-1.36)	7.4	1.20 (1.14-1.25)	-2.7
Adhesive seam peel (kN/m)	5.38 (4.01-7.41)	5.22 (4.76-6.13)	-2.9	6.02 (5.60-6.30)	12.1	5.24 (4.69-5.69)	-2.6

Table 7. Water Immersion Test Results - 0.50 mm CPE

Longitudinal test direction

Property	Original data	One year Test value	One year Percent change	Three year Test value	Three year Percent change	Five year Test value	Five year Percent change
Weight gain (percent)	-	-	16.9	-	20.4	-	20.9
Tensile strength (kN/m)	6.39	5.76	-9.9	5.59	-12.6	5.39	-15.6
Elongation (percent)	490.0	492.0	0.4	498.0	1.6	493.0	0.6
Modulus (kN/m)	1.91	0.93	-51.4	1.24	-34.9	1.63	-14.7
Tear strength (N)	18.68	12.01	-35.7	12.01	-35.7	15.57	-16.7

Transverse test direction

Property	Original data	One year Test value	One year Percent change	Three year Test value	Three year Percent change	Five year Test value	Five year Percent change
Weight gain (percent)	-	-	16.9	-	20.4	-	20.9
Tensile strength (kN/m)	5.53	4.78	-13.6	4.59	-17.1	4.47	-19.3
Elongation (percent)	587.0	587.0	0.0	581.0	-1.0	568.0	-3.2
Modulus (kN/m)	1.49	0.93	-37.6	0.91	-38.8	1.17	-21.2
Tear strength (N)	18.24	13.79	-24.4	14.23	-22.0	17.35	-4.9

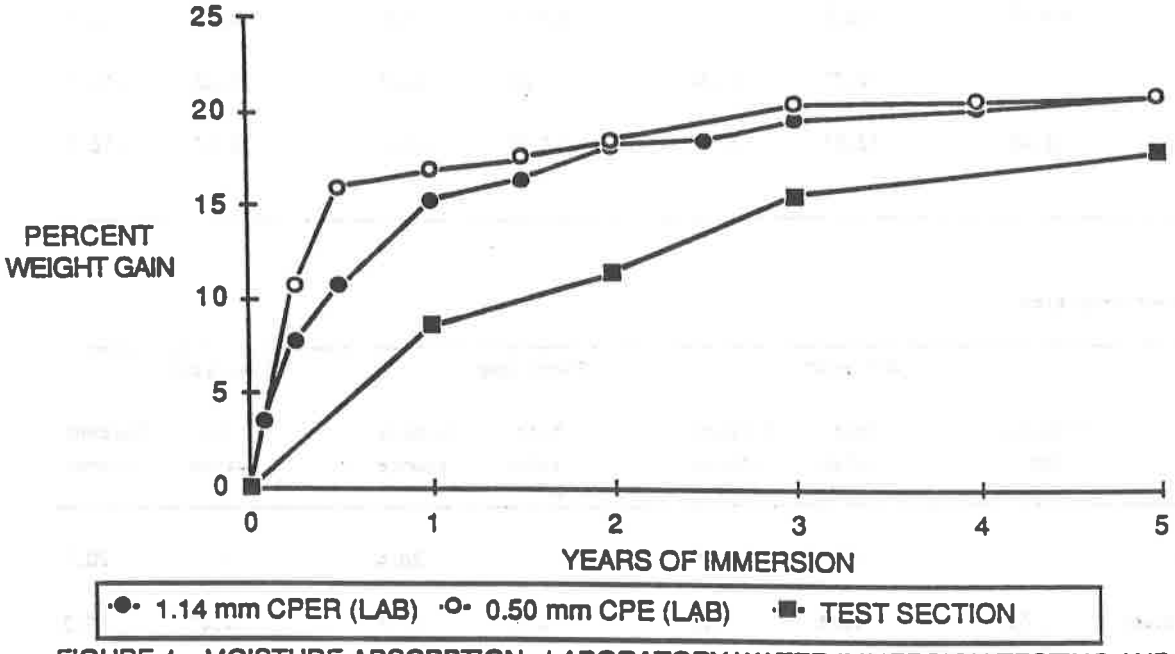

FIGURE 4. MOISTURE ABSORBTION - LABORATORY WATER IMMERSION TESTING AND MT. ELBERT TEST SECTION RESULTS

SUMMARY

Results of studies conducted on the geomembrane installed in 1980 in the Mt. Elbert Forebay Reservoir, indicate that the material is performing satisfactorily after 10 years of service. The studies involved continuous monitoring of the instrumentation on the hillside between the forebay reservoir and powerplant, and periodic retrieval of coupon samples from the field test section for laboratory testing and evaluation.

Continuous monitoring of the instrumentation on the hillside has indicated no movement of an old landslide mass. Water levels in observation wells and piezometers in the hillside continue to decline from levels reached during or shortly after first filling of the reservoir after the geomembrane lining was installed. Results of laboratory tests conducted on the coupon samples indicate that the lining has experienced some water absorption resulting in a decrease in its strength properties. The water absorption has caused some weakening of the polyester reinforcing scrim, the bond between the CPE and scrim, and CPE to CPE bond. Most of the changes in the strength properties occurred within the first 3 years of service and are not considered detrimental to the overall integrity of the lining. In fact, the retained strengths of all the geomembrane's mechanical properties are above the minimum specification requirements for the original unaged material except for the seam shear strength. The lower shear strength of the seams, however, should not affect the integrity of the lining with regard to seepage control.

As part of the construction work in 1980, an extensive quality assurance (QA) program was developed and conducted in an attempt to obtain a top quality installation. Prior to this time, QA programs for flexible membrane lining work were generally very minimal, and in some cases nonexistent. The installation at Mt. Elbert was a major milestone with respect to advancing the state-of-the-art on the use of geomembranes for seepage control, both in the United States and worldwide.

FUTURE WORK

Field instrumentation monitoring will continue at the Mt. Elbert Reservoir. Test coupon No. 8 will be removed in 1995 after 15 years of exposure. This will leave three coupons for future testing.

Because the test results indicated that moisture absorption can influence the strength and bonding characteristics of the reinforcing scrim, and consequently the geomembrane composite, studies are needed to develop better test methods which include the effects of moisture absorption for evaluating the tear and tensile strength properties of fabric reinforced membrane. Unfortunately test methods have essentially remained unchanged since 1980. This is primarily due to the fact that reinforced geomembranes have been used much less the past 10 years for seepage and pollution control in comparison to unreinforced materials, such as HDPE, polyvinyl chloride (PVC), and more recently very low density polyethylene (VLDPE). These unreinforced geomembrane materials have less potential for moisture absorption than fabric reinforced geomembranes.

ACKNOWLEDGEMENTS

The prime contractor for the installation work was the Green Construction Company, Des Moines, Iowa. The B. F. Goodrich Company, Akron, Ohio, manufactured, fabricated and installed the geomembrane lining. Reclamation personnel involved in the work were William Fraser, Project Construction Engineer, William McCormick, Field Engineer, Edward Gray Jr., Principle Designer; and William Morrison and Ronald Frobel who provided technical assistance on the geomembrane material.

The authors express special thanks to Mrs. Linda Parkhill who assisted in compiling and evaluating the test data.

REFERENCES

Bureau of Reclamation 1980a. Specifications DC-7418, Mt. Elbert Forebay Reservoir Membrane Lining, Fryingpan-Arkansas Project, Colorado

Bureau of Reclamation 1980b. Construction Considerations, Mt. Elbert Forebay Reservoir Membrane Lining, Fryingpan-Arkansas Project, Colorado

Bureau of Reclamation 1981, Design Summary for Mt. Elbert Forebay Reservoir Membrane Lining, Fryingpan-Arkansas Project, Colorado

Frobel, R. K. and E. W. Gray, 1984. Performance of the Fabric-Reinforced Geomembrane at Mt. Elbert Forebay Reservoir. Proc. Conf. on Geomembranes, Denver, Colorado, Vol. 2, pp 421-426.

Morrison, W. R., E. W. Gray, D. B. Paul and R. K. Frobel 1981. Installation of Flexible Membrane Lining in Mt. Elbert Forebay Reservoir, Bureau of Reclamation Report NO. REC-ERC-82-2.

National Sanitation Foundation 1985. Standard Number 54, Flexible Membrane Liners.

GEOSYNTHETIC DURABILITY

Puncture Resistance of Geomembranes Using a Truncated Cone Test

Donald Hullings
EMCON Associates, USA
Robert Koerner
Drexel University, USA

ABSTRACT

An experimental study to evaluate the puncture behavior of geomembranes alone and with geotextile protection is discussed. Truncated cones were used as the puncturing points, which allowed a critical cone height (CCH) to be determined. CCH values for flexible geomembranes, such as polyvinyl chloride (PVC) and very low density polyethylene (VLDPE), were so high that geotextile protection is generally not considered to be necessary. Conversely, the significantly lower CCH values for high density polyethylene (HDPE) and chlorosulfonated polyethylene (CSPE-R) strongly suggest that geotextile protection is generally required.

The geotextile portion of the study indicates that increasing mass per unit area is the major factor for increased puncture protection. Clearly, thickness (as cushioning) outweighs strength (as reinforcement) in preventing puncture. Other aspects of the study, such as post-treatment of the geotextile, fiber type (i.e., continuous vs. staple) and polymer type (PET vs. PP) reveal only nominal changes in the puncture performance of the geomembranes.

INTRODUCTION

Although geomembrane punctures are of great concern, little guidance is available for a rational design procedure or even a database upon which to base such a procedure. Current index puncture test methods are lacking because they fail to model the actual behavior of geomembranes. Design is therefore often based on past experience or intuition.

The test method used in developing this paper attempts to solve this problem by simulating the puncture mechanism in a performance oriented test. Hydrostatic pressure was used to compress the geomembrane over a representative subgrade. This type of test was originally developed by the U.S. Bureau of Reclamation, Frobel (1981). The subgrade can consist of natural stone or standardized shapes to simulate different conditions as done by Rigo (1977). Tests using standard shapes utilize some form of pyramid, Frobel (1987), or truncated cone, Laine (1988) and Pape (1990).

In order to alleviate the problem of geomembrane punctures, geotextiles are often placed between the geomembrane and the subgrade to improve puncture resistance. Little is currently known, however, about the mechanisms involved. This type of hydrostatic puncture test can be easily adapted to include a geotextile to investigate the protective mechansims.

GEOSYNTHETICS INVOLVED IN TEST PROGRAM

Four different types of geomembranes were tested to include a range of the materials that are currently being used. These included 1.5 mm high density polyethylene (HDPE), 0.91 mm chlorosulfonated polyethylene (CSPE-R), 0.50 mm polyvinyl chloride (PVC), and 1.0 mm very low density polyethylene (VLDPE). The thicknesses were chosen to represent those most often specified. Different thicknesses of the same type of geomembrane, although a factor in puncture resistance as shown by Frobel (1987), were not evaluated. Some of the properties of the geomembranes studied are shown in Table 1. The strength values shown are for yield in HDPE, for break in CSPE-R, and at ultimate for VLDPE and PVC.

Table 1 - Geomembrane Properties

Property	Method		HDPE	CSPE-R	VLDPE	PVC
Thickness	-	mm	1.5	.91	1.0	.51
Strength	D4595	MPa	19	30	10	16
Elongation	D4595	%	16	25	400	310
CBR puncture	GRI GS1	N	4300	3300	1500	1100
ASTM puncture	D4833	N	610	640	190	200

Geotextiles were also incorporated into the test program to investigate the improvement in puncture resistance they provide for geomembranes. Geotextiles were tested only in combination with, and placed below, a geomembrane. A continuous polyester fiber needle-punched nonwoven geotextile of mass-per-unit area from 140 to 1100 grams per square meter (g/sq.m), designated as NP1, was used as protection to determine the effect of varying mass-per-unit area. Different varieties of nominal 270 g/sq.m needle-punched geotextiles (NP2 to NP5) were included to examine the influence of polymer and fiber type. Two other geotextiles, a heat-set nonwoven (HS1) and a slit-film woven (W1), were also used to judge their suitability for this application. Table 2 summarizes the characterisitics of each geotextile.

Table 2 - Geotextiles

Textile	Polymer	Fiber	Mass/area (g/sq.m)	Tensile Strength (kN/m)	(%)	Puncture ASTM(kN)
NP-a	PET	cont.	140	8.8	62	27
NP1-b	PET	cont.	250	24.0	70	51
NP1-c	PET	cont.	550	44.5	72	95
NP2	PP	cont.	270	16.1	78	46
NP3	PP	staple	270	15.8	68	54
NP4	PET	staple	390	13.2	97	53
NP5	PP	staple	280	24.6	61	78
HS1	PP	staple	200	13.2	50	37
W1	PP	slit film	150	25.2	25	41

PET = polyester
PP = polypropylene

TESTING DEVICE

The test apparatus used for this series of experiments is shown schematically in Figure 1 and is similar to other researchers' equipment used in previous investigations. It consists of a 56 cm inside diameter pressure vessel that contains a strong metal frame. A thick wooden plate, which fits inside the vessel, is supported by the frame. This base supports the subgrade (either natural stone or standard shapes, as used in this study). The base has holes drilled into it so that after the geomembrane fails, water will flow through and into the bottom of the vessel. A water outlet at the bottom acts as a leak detection system.

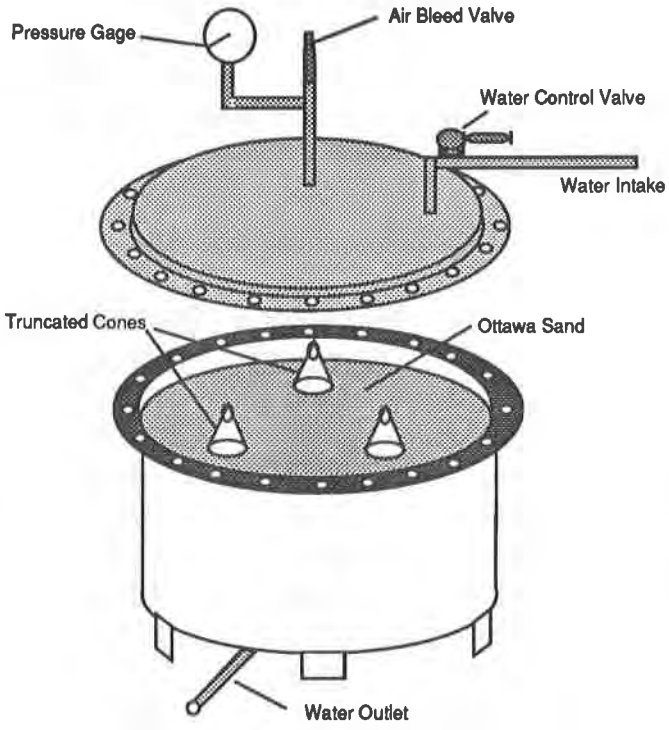

Figure 1 - Test Device

The geosynthetic test specimen is placed on a 5 cm flange, which encircles the top of the lower half of the vessel, so that it just touches the subgrade. The top part of the vessel is then placed on the sample and secured to the lower half by bolts that lock the geomembrane (or geomembrane and geotextile composite) in place. The top portion of the apparatus has a water intake valve, an air bleed valve, and a pressure gauge. Water is introduced into the top of the vessel, displacing the air

until the top half fills with water. The water pressure is then increased until the geomembrane fails or the limit of the system (550 kPa) is reached. Failure is indicated by a sudden drop in pressure and the simultaneous flow of water from the bottom of the vessel.

While many materials could have been used as a subgrade, three equally spaced plexiglass truncated cones were chosen. Using such an artificial but standard protrusion, allows the subgrade's condition to be varied with control. The reproducibility of the test results was also improved. The cones (shown schematically in Figure 2) were secured to the wooden base and Ottawa sand was placed around the cones. The amount of sand added controlled the effective height of the cones so that the subgrade condition could be easily varied.

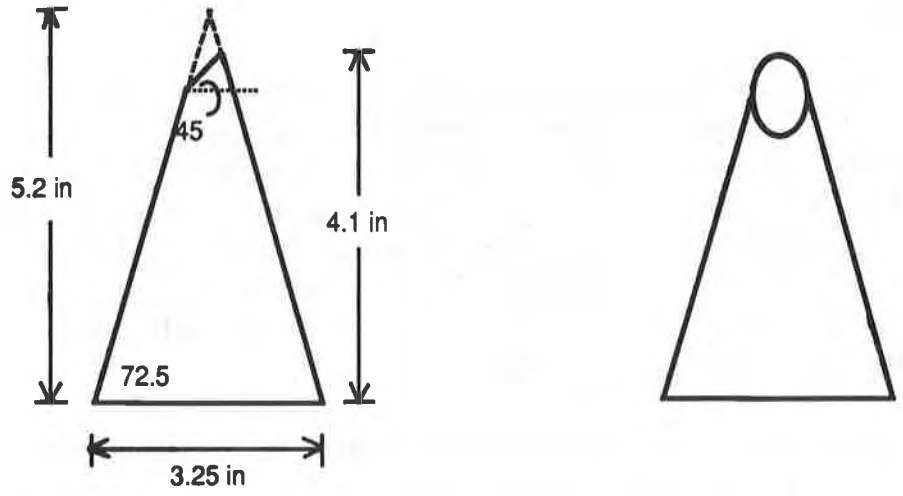

Figure 2 - Truncated Cones

PRELIMINARY TESTING

Before studying the effect of cone height, other subgrade conditions had to be established. For each geomembrane, an effective cone height first had to be found that would cause failures and reveal the effect of cone spacing. The spacing between cones was varied from 10 cm (cone bases touching) to 35 cm (cones were close to the vessel's perimeter). For

all four geomembranes, the lowest failure pressures were recorded at intermediate spacings. At moderate spacings the cones acted as three individual protrusions; this was believed to be the worst case. For all further testing the cones were placed with the truncated edges facing the same direction and spaced 25 cm apart (measured from center to center of each cone) to form the corners of an equilateral triangle.

The load rate was also determined. Load rates were varied from 410 kPa/hour to 3.5 kPa/hour for HDPE and CSPE-R. Slightly lower failure pressures for HDPE were noted as the load rate decreased but no dependence on load rate was seen for CSPE-R. Since the load rate did not appear to be a significant factor, a relatively fast rate of 410 kPa/hour was used for most tests so that a large database could be created. Where different load rates were used, reference is made to their significance.

CONE HEIGHT

This investigation focuses primarily on the effect of the height of protrusions in the subgrade. Since standard truncated cones were used, the subgrade height condition was varied by using different amounts of sand to change the effective cone height. The heights required to cause failure in various geomembranes ranged from about 1 cm for 1.5 mm HPDE to almost 9 cm for 1.0 mm VLDPE. These results suggest that puncture resistance cannot be measured only in terms of strength since VLDPE has lower strength than HDPE (see Table 1).

The behavior shown in Figure 3 prompted the establishment of a new term, the critical cone height (CCH). This is the cone height below which the geomembrane does not fail and is used to characterize puncture resistance. The CCHs for various types of geomembranes alone (i.e. without geotextile protection) are shown in Table 3. Note that these values are valid only under the test conditions described.

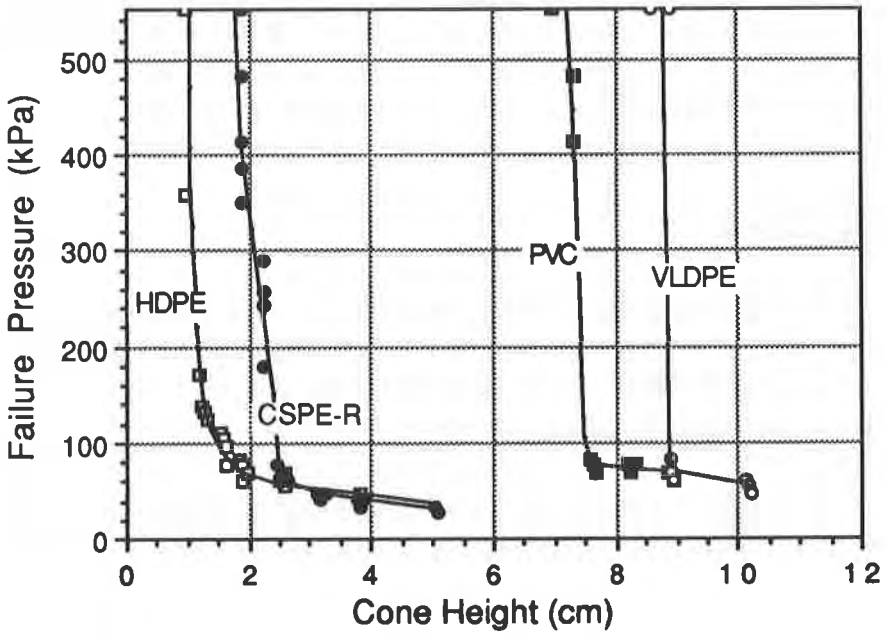

Figure 3 - Failure Pressure vs. Cone Height for Geomembranes

Table 3 - Critical Cone Heights

Geomembrane	CCH (cm)
1.5 mm HDPE	1.0
0.91 mm CSPE-R	1.8
0.50 mm PVC	7.0
1.0 mm VLDPE	8.9

Further consideration of Figure 3 indicates that there is an apparent grouping of high modulus and low modulus geomembranes. The high modulus geomembranes, HDPE and CSPE-R, have low CCHs. HDPE had localized yielding around the apex of the cone and eventually over extended in this region. CSPE-R had the scrim reinforcement break at the cone tip followed by failure in the plies. Testing performed at lower rates did not show that the CCH for either geomembrane depended significantly on the rate.

The low modulus geomembranes are the relatively flexible PVC and VLDPE. The flexibility results in greater elongations and larger CCHs and thus greater puncture resistance. When failures did occur they seemed to be due to extension beyond the maximum elongation of the geomembrane. Because such large heights (i.e. greater than 7 cm) are required to produce failures, further testing involving load rate and geotextile protection was not performed.

GEOTEXTILE PROTECTION

Because puncture resistance is so important for geomembranes, geotextiles are often used below geomembranes to improve resistance. Tests on HDPE and CSPE-R with geotextiles show that the resistance is increased over a wide range of cone heights. The amount of protection afforded probably depends on the mass-per-unit area. To quantify this amount the first series on geomembrane protection tests focused on using different weights of one geotextile type, designated NP1 (a), (b), and (c).

Figure 4 is a plot of cone height versus failure pressure for HDPE alone and with protection. The effect of the geotextile is demonstrated in two ways: increased CCH and increased puncture strength over intermediate heights. For small heights (less than 1 cm) the geotextile is not necessary since the geomembrane alone does not fail. For large cone heights (greater than 6 cm) the geotextile fails and therefore does not provide significant protection. Higher mass per unit area geotextiles result in higher puncture resistance for HDPE geomembranes.

For CSPE-R, less improvement is noted when a geotextile is used than with HDPE. As Figure 5 shows, no change in CCH is apparent but strength is increased for intermediate heights. Note that CSPE-R is already fabric reinforced and is more flexible than HDPE, which may explain the smaller improvement (i.e., some improvement over HDPE is already designed in). As with HDPE, increases in puncture resistance are directly related to mass-per-unit area of the geotextile.

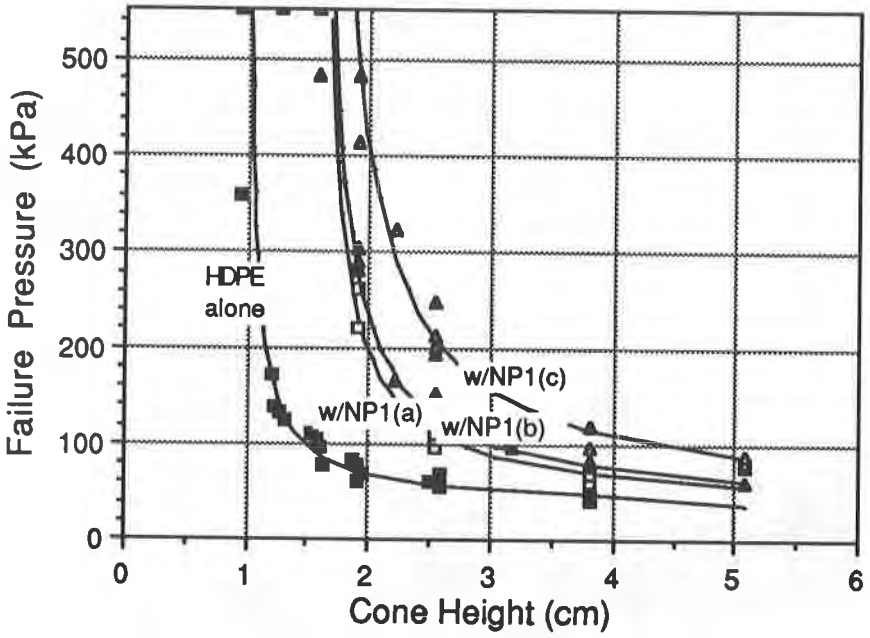

Figure 4 - HDPE with Geotextile Protection

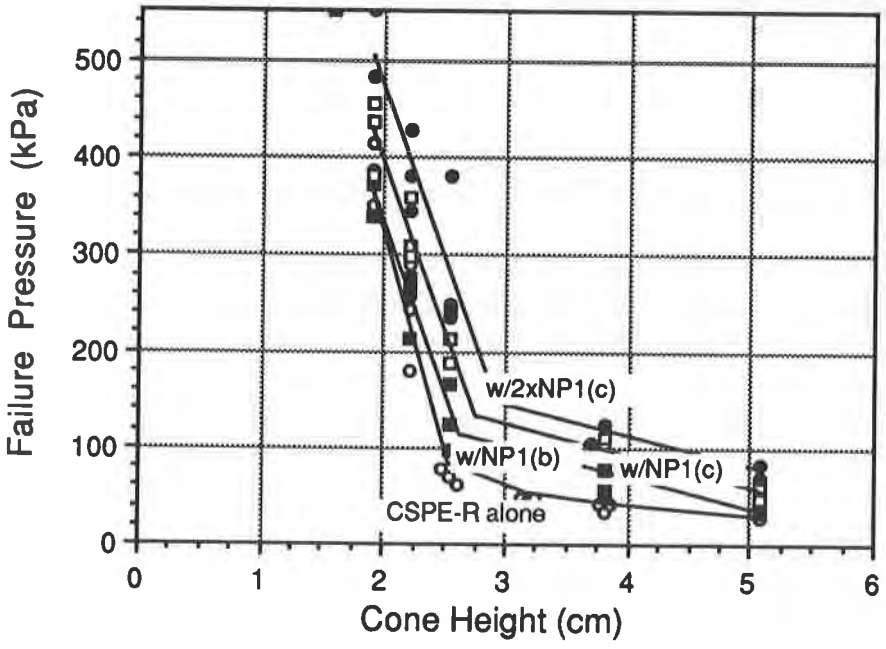

Figure 5 - CSPE-R with Geotextile Protection

The two preceding graphs were based on a specific type of geotextile, but other varieties may also be used. Figure 6 demonstates that the amount of protection provided varies with geotextile construction, filament type, and polymer type. Since only one cone height (2.5 cm) was used for the set of tests, cone height was not considered as a variable. All of the needle-punched geotextiles were of the same nominal weight so that the mass-per-unit area was also not considered. All values shown are the average of at least three tests.

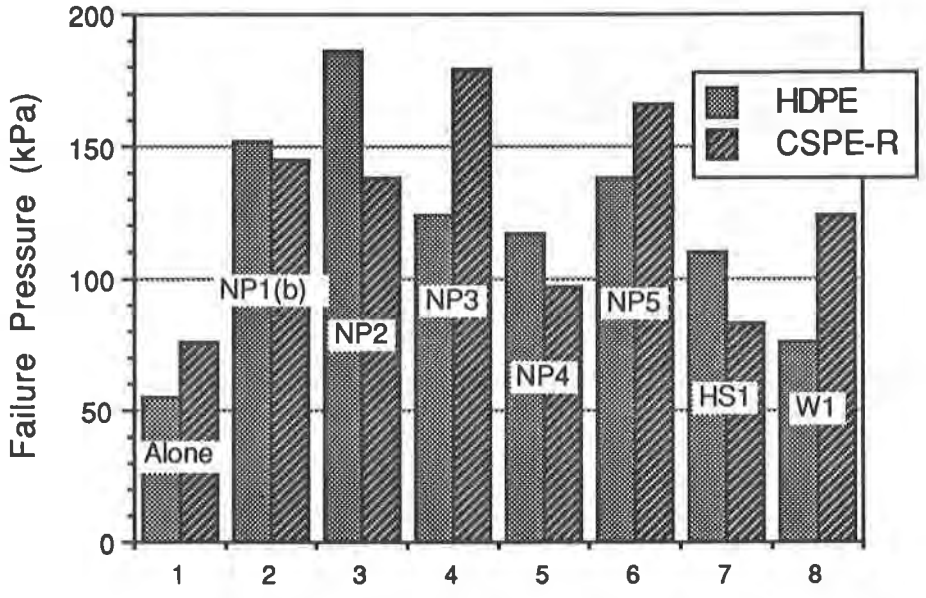

Figure 6 - Puncture Improvement from Different Geotextiles

Regarding Figure 6, the following results are noted:

- Continuous filament fibers (NP1b and NP2) may perform better for HDPE, but staple fibers (NP3, NP4, and NP5) provide more improvement for CSPE-R.
- Polymer type did not appear to make a difference, although the higher density of polyester means less material is used than in polypropylene fabrics.
- Since only polypropylene geotextiles were burnished, the effect of post-treatment could not be determined.
- Heat-set nonwovens or slit-film wovens show the lowest improved puncture performance: however, their mass-per-unit area was lower than that of the needle punched nonwovens.

Other experiments were performed to better understand the factors influencing geotextile protection of geomembranes. The first set of tests used 18 cm by 18 cm geotextile pads placed over the cones instead of a full-sized geotextile that was secured to the vessel flange. No tensile force is believed to have been mobilized in the pads since they were not secured. For HDPE, full-size geotextiles afforded better protection indicating that tensile strength plays a role. Tensile strength represents an 80 percent improvement over the cushioning effect of the geotextile alone. For CSPE-R, however, the cut pads resulted in higher puncture resistance indicating that 100 percent of the protection comes from a cushioning effect and that securing the geotextile was actually detrimental.

In another series of tests, a woven geotextile was placed between the nonwoven geotextile and the geomembrane. This experiment was also designed to distinquish between the different phenomena of protection. The woven geotextile was inserted to add tensile strength to the geotextile protection. For HDPE, the woven geotextile did not change the puncture resistance of the geomembrane/continuous-fiber geotextile composites, but did increase the resistance for the staple geotextiles by 40 to 200 percent. For CSPE-R, the woven geotextile insert increased the puncture resistance for all composites. In all cases the failure pressures were more than twice the pressure for the nonwoven/CSPE-R composites at a cone height of 2.5 cm.

These results indicate that the geotextile functions in at least two different ways. It can act as a separator between the geomembrane and the subgrade, providing a cushion that effectively "smooths" the subgrade. Cushioning increases with mass-per-unit area, since more material is available, but does not necessary involve tensile strength. It can also act as reinforcement, which is a quite different function dependent on tensile strength and the modulus of elasticity. The geotextile spans the distance between protrusions and reduces elongations in the geomembrane.

CONCLUSIONS

Geomembrane puncture resistance depends greatly on the subgrade condition and must not be overlooked. The results of many standardized index puncture tests commonly reported as puncture strength do not completely describe the phenomena and may be misleading. To focus attention on the subgrade, the use of a critical cone height is therefore

suggested to characterize the condition that will cause failure. The CCH, which can be determined for each type of geomembrane, considers the flexibility of the geomembrane. As shown below in Table 4, using the CCH results in a ranking of the geomembrane puncture resistance almost the exact opposite of the ranking based on strength properties.

Table 4 - Ranking of Geomembranes by Strength Properties
(where 1 is highest or best value)

Geomembrane Type	ASTM Puncture	CBR Puncture	Tensile Strength	CCH
60 mil HDPE	2	1	2	4
36 mil CSPE-R	1	2	1	3
20 mil PVC	4	3	4	2
40 mil VLDPE	3	4	3	1

Conversely, ranking with the stiffness, modulus or elongation as shown in Table 5 agrees very well with CCH values. In the table, a rank of 1 indicates the least stiff and lowest modulus geomembrane. CCH is believed to be more important than strength properties in Tables 4 for determining the suitability of a geomembrane against puncture failure.

Table 5 - Ranking of Geomembranes by Flexibility Methods
(where 1 is the most flexible or best value)

Geomembrane Type	Stiffness	Modulus	Elongation (at Failure)	CCH
60 mil HDPE	4	3	3	4
36 mil CSPE-R	3	4	4	3
20 mil PVC	1	1	2	2
40 mil VLDPE	2	2	1	1

A geotextile may be added below the geomembrane to improve the puncture strength, and in some cases to improve the CCH. The most important factor for increasing the puncture resistance is the mass-per-unit area of the geotextile. Note that the higher weight varieties have more material and incrementally more strength. The added bulk material

increases the effectiveness of the cushion while the strength helps to reduce the elongation of the geomembrane between protrusions. Other characterisitcs such as geotextile post-treatment, fiber type, and polymer type also affect both the cushioning and reinforcement functions but to a significantly lesser extent than the mass-per-unit area. The relative importance of each mechanism depends on the type of geomembrane and the subgrade condition. In general, cushioning is more important for increased puncture resistance; reinforcement plays a minor but increasing role as protrusion height increases.

ACKNOWLEDGEMENTS

The authors would like to thank the United States Environmental Protection Agency for their financial support and all members of the Geosynthetic Research Institute for their continued guidance.

REFERENCES

Frobel, R.K., Design and Development of an Automated Hydrostatic Flexible Membrane Test Facility, REC-ERC-80-9, Water and Power Resources Service, Denver, CO, Jan. 1981.

Frobel, R., Youngblood, W. and Vandervoort, J., "The Composite Advantage in the Mechanical Protection of Polyethylene Geomembranes: A Laboratory Study," Geosynthetics '87, New Orleans, USA, 1987, pp. 565-576.

Laine, D.L., Miklas, M.P. and Parr, C.H., Loading Point Puncturability Analysis of Geosynthetic Liner Materials, EPA/600/2-88/040, U.S. Environmental Protection Agency, Cincinnati, Ohio, March, 1988.

Pape, J.T. and Huang, L., "Large-scale Testing of Waste Containment Sealing Under Point Loading in High Pressure Testing Device," Geotextile, Geomembranes, and Related Products, Rotterdam, 1990.

Rigo, J.M., Correlation of Puncture Resistance over Ballast and the Mechanical Properties of Impermeable Membranes, University of Liege, Belgium, 1977.

Effects of Outdoor Exposure on a High Density Polyethylene Geomembrane

Y. G. Hsuan
Geosynthetic Research Institute, Drexel University, USA
A. E. Lord Jr.
Geosynthetic Research Institute, Drexel University, USA
R. M. Koerner
Geosynthetic Research Institute, Drexel University, USA

ABSTRACT

The engineering properties and the physical properties of a seven year old high density polyethylene geomembrane were evaluated. The test samples were taken from three seamed panels which had been exposed to four different levels of sunlight, heat, and air over the seven year period.

The engineering properties, such as the sheet's yield strength, and the peel and shear strength of the seams, were not affected significantly by the different levels of exposure. On the other hand, the physical properties, such as stress crack resistance on sheets and seams, and oxidative induction time (OIT), have shown some degree of alteration. The OIT of the exposed samples was much lower than OIT of the covered and partially covered samples. The stress cracking resistances of the exposed seamed samples were somewhat lower than those unexposed samples, suggesting that surface embrittlement due to oxidation might accelerate crack initiation. For the sheet samples, stress cracking performance of all four locations were fairly similar indicating that the internal of the liner was not affected after seven years exposure. There was no discernible differences at the different locations in crystallinity, and the carbonyl keytone group was not detectable in these samples. This indicates that the changes in the geomembranes in this time period were only in the "microscopic" structure.

INTRODUCTION

The design of geomembrane lined facilities is based on property values of the as-manufactured materials. However, the properties of polymeric materials change with time particularly when exposed to outdoor environments. Such exposure is unavoidable for at least such time until covering. However, in some cases the geomembrane might be uncovered indefinitely, e.g. in surface impoundments above the liquid level. This particular study focuses on a high density polyethylene (HDPE) geomembrane lined surface impoundment.

In general, the outdoor degradation of HDPE can be initiated by thermal and ultra-violet radiation which leads to the formation of free radicals, R•. These free radicals will react rapidly with any oxygen present, starting a series of autoxidation chain reactions, as shown in Equations (1) to (3).

$$RH + Energy \rightarrow R\bullet \quad (1)$$

$$R\bullet + O_2 \rightarrow ROO\bullet \quad (2)$$

$$ROO\bullet + RH \rightarrow ROOH + R\bullet \quad (3)$$

For polyethylene, degradation can result in both chain scission or cross linking depending on the amount of oxygen present. These processes are expressed in following equations[1]:

$$—CH_2CH_2CH_2— \ (RH) + Energy \rightarrow —CH_2\dot{C}HCH_2— \ (R\bullet) + O_2 \quad (4)$$

This will yield one of the following products:

1) Chain scission under oxygen excess :

$$—CH_2\underset{\displaystyle OOH}{\underset{|}{C}}HCH_2— \ (ROOH) \rightarrow —CH_2CHO + \bullet CH_2— \quad (5)$$

2) Cross-linking under oxygen deficiency:

$$—CH_2\underset{\displaystyle —CH_2CHCH_2—}{\underset{|}{\overset{\displaystyle O}{\overset{|}{C}}}}HCH_2— \ (ROR) \quad or \quad —CH_2\underset{\displaystyle —CH_2CHCH_2—}{\underset{|}{C}}HCH_2— \ (R\text{-}R) \quad (6)$$

Protection for HDPE geomembranes from degradation in the above described manner is accomplished by adding antioxidants and carbon black. The antioxidants act as sacrificial substances. They react readily with oxygen in the polymer to prevent the onset of the autoxidation chain mechanism. On the other hand, carbon black functions as a UV screening agent and/or absorber. These two additives assist each other in prolonging the onset of rapid oxidation in the polymer. However, the antioxidants do have a finite lifetime. After they have been consumed, the polymer will start to oxidize, becoming more brittle and eventually become susceptible to stress cracking.

In this study, an HDPE geomembrane from a seven year old surface impoundment was investigated. Four different locations were evaluated with three samples taken at each exposure location. Each of the locations had different exposure conditions. Mechanical tests and thermal analyses were performed on the samples so that the changes in engineering and physical structural properties could be determined. The short term engineering properties, which are called the "macroscopic" properties, include sheet tensile strength and seam shear and peel strength. The physical structural properties which are called the "microscopic" properties, include stress cracking resistance, oxidative induction time, melting points, crystallinity, melt flow index, and the ketone carbonyl content.

EXPOSURE CONDITIONS OF THE GEOMEMBRANE

The surface impoundment under investigation in this study was seven years old. It was a domestic solid waste leachate storage facility which has subsequently been decommissioned and reconstructed. It should be noted that the liner had not "failed" in any manner whatsoever. The reason for the reconstruction was to replace the surface impoundment with an underground storage tank system. The liner material was a 1.5 mm (60 mil) HDPE geomembrane. The seams were made by a hot air welding process.

Test samples were taken from the west side of the surface impoundment. A total of twelve samples were taken from three different panels at four various locations: three samples were taken from the portion of the liner continuously exposed to the atmosphere (AIR), three were taken from the backfilled anchor trench (AT), three were from the action zone (ACT), and three were taken from the bottom (BOT). These locations are illustrated in Figure 1. The three different panels were designed as S1, S2, and S3. As can be noted, the BOT samples were always covered by liquid so their exposure to sunlight and high temperature was the least. They will be used as the control reference during the comparison. The AIR samples were subjected to the most severe conditions: air, heat, and sunlight combined. For the ACT samples, the amount of exposure was dependent on the level of liquid, but it was probably at the intermediate level between BOT and AIR. Although the AT samples were not directly exposed to sunlight, they were still subjected to air and some degree of heat.

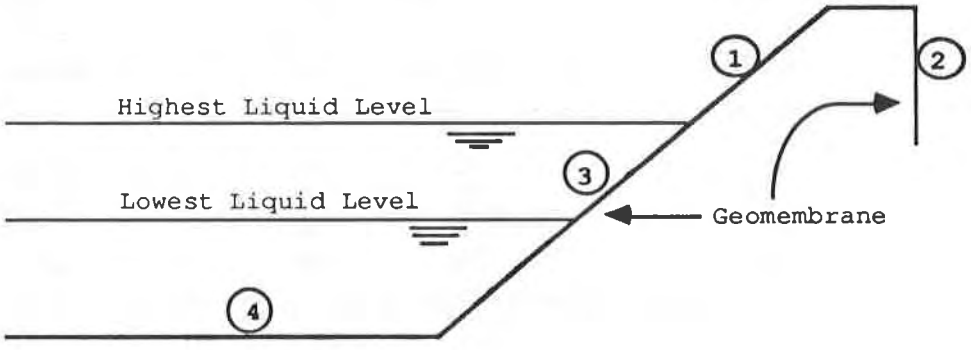

(1) "AIR" Locations - Specimens taken from the liner continuously exposed to the atmosphere

(2) "AT" Locations - Specimens taken from the backfilled anchor trench

(3) "ACT" Locations - Specimens taken from the action zone of the fluctuating liquid level

(4) "BOT" Locations - Specimens taken from the bottom of the impoundment covered by liquid

Fig. 1 - The Four Locations Where The Test Samples Were Taken

TEST PROCEDURES AND RESULTS

Mechanical Tests. Short term tensile tests and long term constant load tensile tests were conducted on all twelve samples.

(1) Short Term Tensile Properties. The macroscopic property changes of the twelve samples was measured by their short term index tensile properties. The tensile tests for the sheet materials were performed according to ASTM D 638 [2]. The peel and shear tests were performed on 25 mm (1 inch) wide seam specimens. All tests proceeded at a strain rate of 0.85 mm/sec (2 inch/min). Five specimens were tested for each sample and their average values are given in Table 1.

The tensile strength of the sheet material within each panel is very similar. Also, there is not much difference in the peel and shear strength of the seams connecting the panels, except for the S1 (BOT) in shear and S3 (ACT) in peel. Both of these have relatively low strength compared to the others within their own group and are considered to be outliers. The data suggests that there is no substantial macroscopic change in the geomembrane sheets and seams after seven years exposure at the site.

Table 1. Results of Short Term Tensile Tests on Sheet and Seam Materials

Location	Sheet Tensile	Seam Shear		Seam Peel	
	(KN/m)	(KN/m)	(%)	(KN/m)	(%)
S1					
AIR	34	32	94	20	59
AT	36	31	88	23	66
ACT	35	32	90	18	50
BOT	40	30	75	19	47
S2					
AIR	40	30	75	21	52
AT	40	30	74	20	49
ACT	39	30	77	20	53
BOT	40	29	73	21	52
S3					
AIR	44	34	77	22	50
AT	46	32	69	26	57
ACT	46	32	70	19	41
BOT	44	31	71	23	52

(2) Constant Load Tensile Test. It is known that HDPE geomembranes will increase in brittleness after being oxidized[3]. This, in turn, leads to a reduction in stress crack resistance. The tests to monitor such behavior are the notched constant load test (NCLT) for sheet materials and the seam constant load test (SCLT) for seamed materials.

a) Sheet materials. The stress cracking resistance of the twelve geomembrane sheet samples was evaluated using NCLT. The test procedure has been described in detail in previous papers[4,5]. Due to the limitation of available material, only one specimen was examined for each of the samples. The applied stress was 30% of the yield stress at 50°C which was used in order to obtain brittle failures. The test was terminated when each of the specimens failed. Figure 2 reveals the morphology of a typical fracture surface which illustrates that brittle failure did indeed occur. The failure times are shown in Table 2.

The failure times of all sheet specimens are listed in Table 2. The variation of the failure times between different locations within a single panel is very small. It seems that the constant out-door exposure has not caused substantial changes in the internal structure of the material.

b) Seamed materials. The seam constant load test (SCLT) procedure[5] was used to evaluate the stress cracking performance of twelve of the geomembrane seams. The seam section of sample S3 (ACT) had been damaged, hence no test was performed. One specimen was tested for each seam sample. The applied stress was 45% of the yield stress of the sheet material at 50°C. The purpose for using a higher applied stress in seam tests was to achieve shorter testing times. This is because no notch is introduced in the seam test specimens. The initiation is only dependent on the stress concentration resulting from the seam geometry. Hence the length of time for crack initiation to take place is generally quite long. The failure mode at this stress level is close to at the transition between ductile and brittle failure modes. A typical fracture surface is revealed in Figure 3. The test was terminated when each of the specimens failed. The failure times were recorded and are presented in Table 2.

In all three panels, the AIR specimens failed in the shortest time period, followed by the ACT specimens (except S3). The longest failure times occurred either in AT or BOT specimens. For S1 and S2 panels, the longest failure times appeared in AT specimens, whereas in S3, it appeared in BOT specimen. These results are in general agreement with the amount of geomembrane exposure to oxygen, high temperature and UV exposure. The differences in stress cracking performance resulted from the SCLT and the NCLT will be discussed later in the paper.

Table 2. Results of Constant Load Test for Sheets and Seamed Materials

Location	Failure Time for Sheets (hours)			Failure Time for Seams (hours)		
	S1	S2	S3	S1	S2	S3
AIR	502	502	502	378	602	899
AT	504	672	625	1484	1896	1540
ACT	639	519	556	957	1030	1426
BOT	503	658	718	982	1421	1835

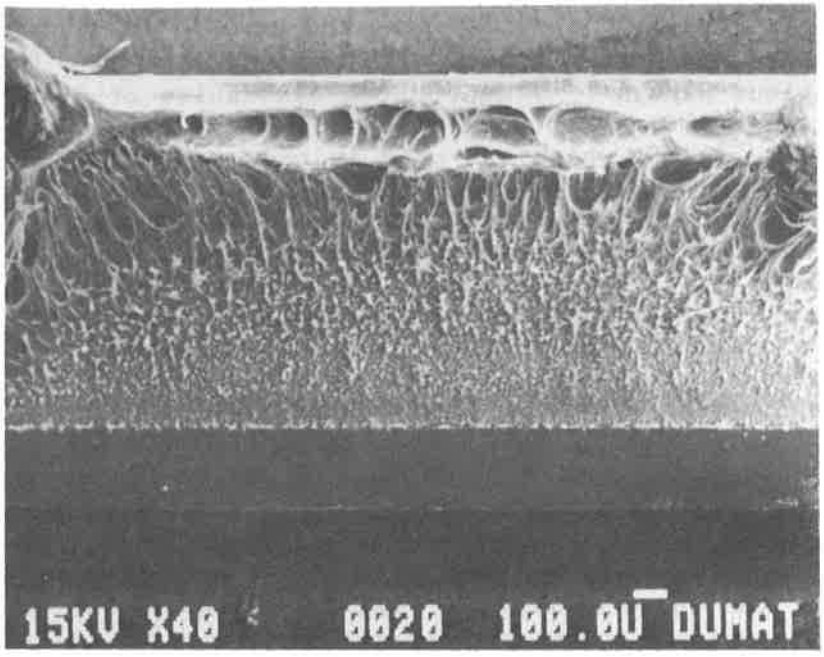

Fig. 2 - Fracture surface of a sheet specimen

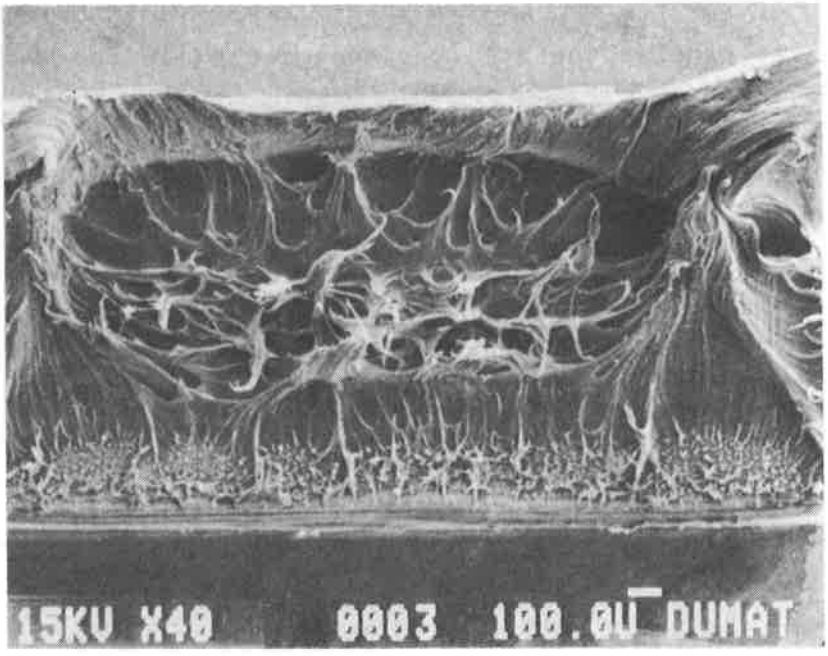

Fig. 3 - Fracture surface of a seam specimen

Melt flow and analytical tests. The microscopic properties of the twelve samples were monitored using melt flow and thermal analyses methods. The results will be viewed with respect to the exposure location and then correlated to the mechanical properties just described.

(1) Melt Flow Index (MI). The molecular weight of polyethylene is qualitatively related to the melt flow of the polymer. Typically, a high molecular weight polymer will have a low melt flow index under the same test conditions, and vice-versa. Since oxidation can induce chain scission in the polymer lowering the molecular weight, it can increase the melt flow value[6]. The melt flow index of twelve exposed samples were examined. The test procedure followed ASTM D 1238[7], using condition E. The results in the conventional units of grams per 10 minutes are tabulated in Table 3.

Table 3. Results of Melt Flow Index Tests

Location	MI (g/10 min)		
	S1	S2	S3
AIR	0.17	0.17	0.16
AT	0.20	0.20	0.20
ACT	0.17	0.17	0.16
BOT	0.19	0.19	0.20

The results from the AIR and ACT samples show consistently low MI values. Conversely the AT and BOT have the highest MI values. This seems to suggest that the AIR and ACT samples consisted of more of the high molecular weight chains than the others. If this hypothesis is correct, the NCLT failure times of AIR and ACT specimens should be longer than the others. However, this was not the case, as was seen in Table 2. One other possible explanations for the low MI values may be due to cross linking of the polymer. The materials might be thermally degraded during the preheat and extrusion period of the test. Since there was not much air (i.e. oxygen) available inside the test furnace, the degradation might lead to cross linking, as described by Equation (4)[1].

Clearly there are some uncertainties involved during this particular test. Melt index may not be a suitable technique to evaluate the change of molecular weight caused by this level of degradation.

(2) Crystallinity. Chain scission during oxidation produces smaller chains which can crystallize more easily, resulting in increases in crystallinity[6]. If this has occurred, the results should be correlated to the constant load tensile tests since these properties are associated with one another[8].

Differential scanning calorimetry (DSC) was used to monitor the melting behavior of the materials. The response curves were obtained by heating a specimen of known mass to 200°C at the rate of 20°C/min. The entire test was performed under

nitrogen atmosphere at a flow rate of 50 ml/min. The amount of crystallinity was calculated from the heat of fusion (proportional to the area under the melting peak) which is the energy required to melt the crystalline phase. The test specimens were heated twice. After the first heating cycle, the specimens were immediately quenched in liquid nitrogen and then heated again. This thermal process is necessary for yielding a consistent thermal history for the test specimens. The information provided by the second heating cycle was used for comparing differences between samples. A typical thermal curve is showed in Figure 4. The heat of fusion of each sample was calculated and is listed in Table 4. In addition, the crystallinity was calculated using 276 J/g as the heat of fusion of 100% crystalline HDPE material[9]. The results are also given in Table 4 along with the onset and maximum melting points.

Table 4. Results of Differential Scanning Calorimetry (DSC) Tests

Locations	Melting Point "onset" (°C)	Melting Point "max." (°C)	ΔH (J/g)		Crystallinity (%)	
			1st*	2nd+	1st*	2nd+
S1						
AIR	117	124	154	133	56.8	48.2
AT	117	124	152	133	55.1	48.2
ACT	117	124	158	139	57.2	50.4
BOT	117	124	143	134	51.8	48.6
S2						
AIR	117	124	145	123	52.5	44.6
AT	117	124	134	120	48.6	43.5
ACT	117	124	144	128	52.1	46.4
BOT	117	125	136	116	49.3	42.0
S3						
AIR	117	124	136	119	49.3	43.1
AT	117	125	153	136	55.4	49.3
ACT	117	124	158	137	57.2	49.6
BOT	117	125	148	134	53.6	48.6

* 1st - first heating cycle
+ 2nd - second heating cycle

As noted in Table 4, all specimens have very similar melting temperatures. Although there is some variation in crystallinity (based on 2nd heating cycle) between the different panels, within a particular panel the values are very similar. The only exception is the S3 (AIR) specimen which has a substantially lower value compared to the others within its panel. There is also no substantial variation in the crystallinities at the 1st heating cycle.

Two suggestions can be proposed based on the above data. One is that no chain scission has occurred in the polymer since the crystallinity remained almost constant. The second one is that this technique is not sensitive enough for monitoring small changes in the crystallinity. It seems that the second possibility is more likely since other measurements have indicated that some changes have

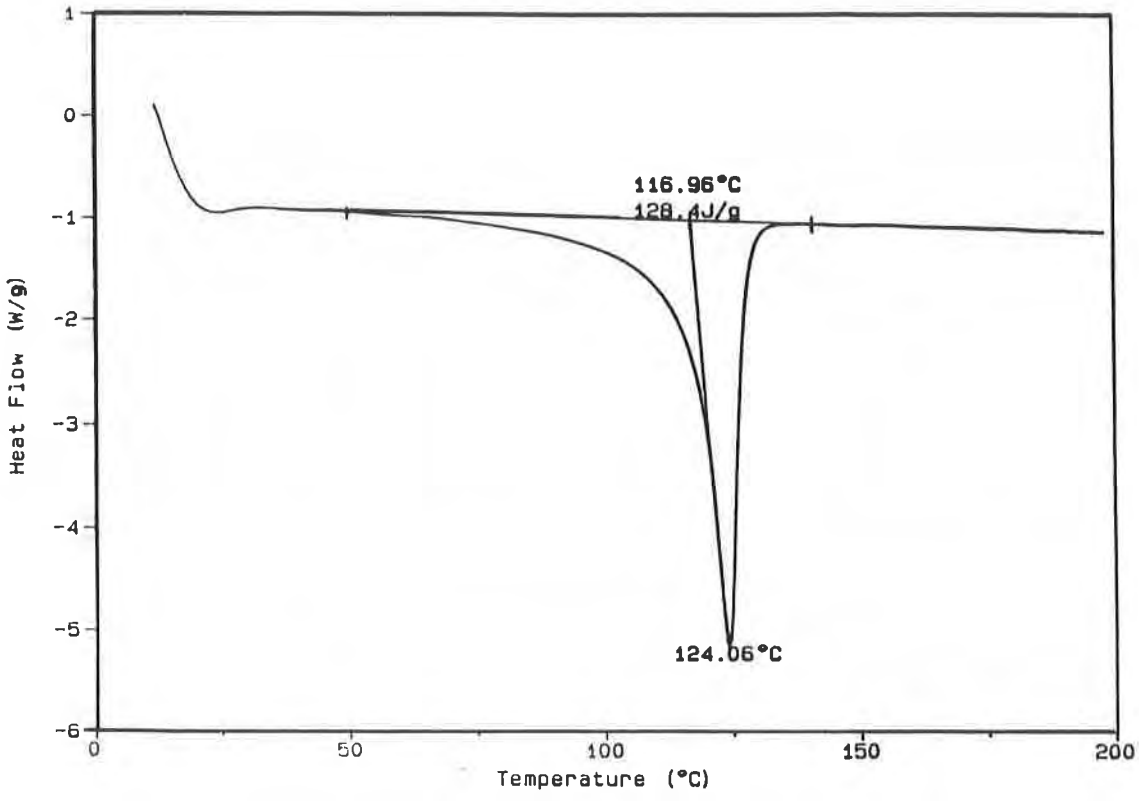

Fig. 4 - A Typical DSC Thermal Curve for HDPE Geomembrane

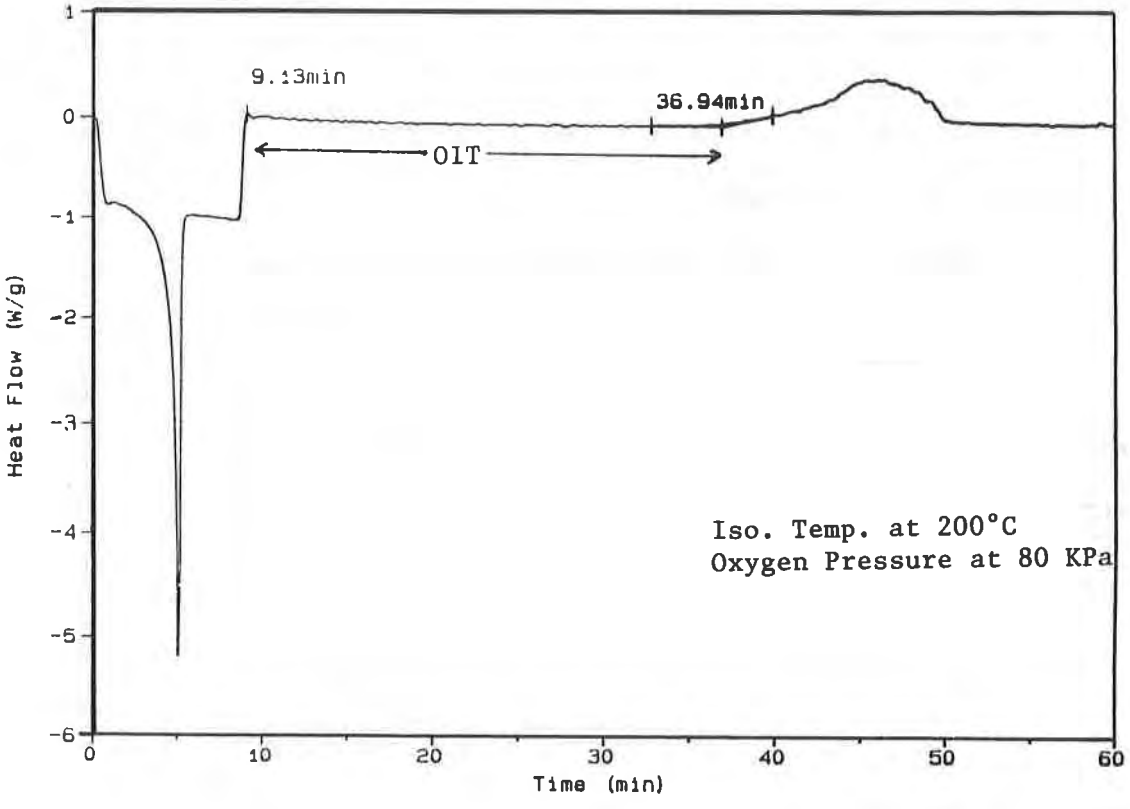

Fig. 5 - An Isothermal Oxidation Curve of HDPE Geomembrane

occurred.

(3) Oxidative Induction Time. The total amount of antioxidants in the geomembrane compound can be evaluated using isothermal DSC to measure the oxidative induction time (OIT). OIT is the length of time between the onset of the isotherm and the onset of the exotherm resulting from oxidation[10]. The longer the OIT, the higher the total antioxidants content available within the material.

Isothermal DSC tests were performed in both sheets and seams samples. The weight of test specimen was 3.0 mg, and each specimen was taken across the thickness of the sheet, from top to bottom. The specimen was placed in a closed aluminum specimen holder and heated from 20°C to 200°C at the rate of 20°C/min. It was then held at 200°C until the onset of oxidation. The entire test was performed under an oxygen atmosphere at the pressure of 80 KPa and a flow rate of 20 ml/min. A typical thermal curve is illustrated in Figure 5. Table 5 shows the OIT results of the twelve sheet and seam samples.

For the sheet materials, the AIR specimens produced the shortest OIT and the BOT specimens produced the longest within the same panel. In panels S2 and S3, the AT specimens yielded the second highest OIT followed by ACT. However, such order was reversed in panel S1, ACT being longer than AT. This contradiction may also be reflected in the inconsistent stress cracking behavior in S1 panel, as shown in Table 2.

For the seamed materials, the OITs of AIR specimens were again the lowest values. However, the remaining tests on the seamed material did not show the same trend as with the sheet materials. In both the S1 and S3 panels, the OIT values of BOT and ACT specimens were very similar, and they were longer than those of the AT values. In the S2 panel, BOT has the longest OIT followed by AT and then ACT. The data scatter may be partially associated with the welding method. The heat distribution of hot air seaming is very difficult to control. It is rather sensitive to the surrounding environment. This could cause non-uniform consumption of antioxidants along the seam.

Table 5 - Results of Oxidative Induction Times (OIT)

Locations	OIT for Sheets (min.)			OIT for Seams (min.)		
	S1	S2	S3	S1	S2	S3
AIR	5	16	14	9	6	8
AT	23	29	30	26	27	13
ACT	31	24	22	30	20	25
BOT	37	35	35	31	32	25

(4) Fourier Transform Infrared Spectrometer (FTIR). The oxidation of polyethylene produces a substance containing carbonyl ketones (-C=O-), as shown in Equation 5. The existence of this molecular group can be detected by FTIR. The carbonyl ketone group shows a strong absorption peak in the range of 1710-1720 cm^{-1}[11]. This might be the strongest evidence for the oxidation of HDPE.

A qualitative study was conducted on one panel, S2, of samples. The test was performed in a Perkin Elmer 1760X, FTIR. Approximately one gram of material was taken from each of the four sheet samples, and was ground to powder at liquid nitrogen temperature. A small amount of the polymer powder was mixed with potassium bromide. The mixture was then placed in a specimen holder and examined using the diffuse reflectance mode.

Figures 6 and 7 show the absorption spectra of S2 (AIR) and S2 (BOT) specimens. There is no obvious peak appearing in the 1710-1720 cm^{-1} range corresponding the ketone group, hence the oxidation was not significant enough to be detected. However, a strong absorption peak can be observed at around 1733 cm^{-1} which corresponds to the ester group (-COO-). It also appears in the other two specimens. One of the commonly used antioxidants in HDPE geomembrane product is Irganox 1010[10] which contains an ester group. The strong ester peak may overlap a small ketone peak. In Figure 6, the ester peak does show a small shoulder which may be due to the ketone peak.

DISCUSSION

The results of the five test methods used to evaluate the HDPE geomembrane and its seams are summarized in Table 6. Here it is seen that the short term tensile strength remains almost the same within each panel. This suggests that the seven years of exposure to the local environment has not significant affected the macroscopic short term engineering behavior of the geomembrane sheets or its seams.

On the other hand, subtile microscopic changes have been observed in properties such as OIT and stress crack resistance (SCR). The consumption of antioxidants in the AIR samples was much higher than in other samples, as shown by the OIT values. Since these OIT values are the average across the thickness, the OIT on the top surface of the liner probably would be even lower. This is because photo-oxidation first takes place on the surface and gradually migrates into the lower material[12,13]. Inside the geomembrane, a small amount of oxidation could still occur. Oxygen in the air can diffuse into the geomembrane and react with the preexisting free radicals which have been formed during the extrusion process[1,6]. In addition, the heat from the sun acting on the AIR samples can accelerate the diffusion rate. However, the OIT gradient across the thickness was not determined here.

One of the very first physical indications of an oxidized polymer will be the embrittlement which leads to a reduction in stress cracking resistance. The data from the constant load tests indicate that the AIR specimens is slightly more brittle than the others. For the AIR seam specimens, the surface embrittlement due to photo-oxidation may have accelerated the crack initiation leading to the shorter failure times. A similar phenomenon was also observed by Choi and Broutman[12]. In this case, OIT can provide some indication of the seam stress cracking performance.

For the sheet materials, their brittle failure times in a single panel were very similar. This suggests that the global internal structure of exposed and unexposed materials are very close. However, the notch constant load test is unable to challenge the surface embrittlement. This is because the 20% (0.3 mm) notch depth may have already passed through the surface oxidized layer. Choi and

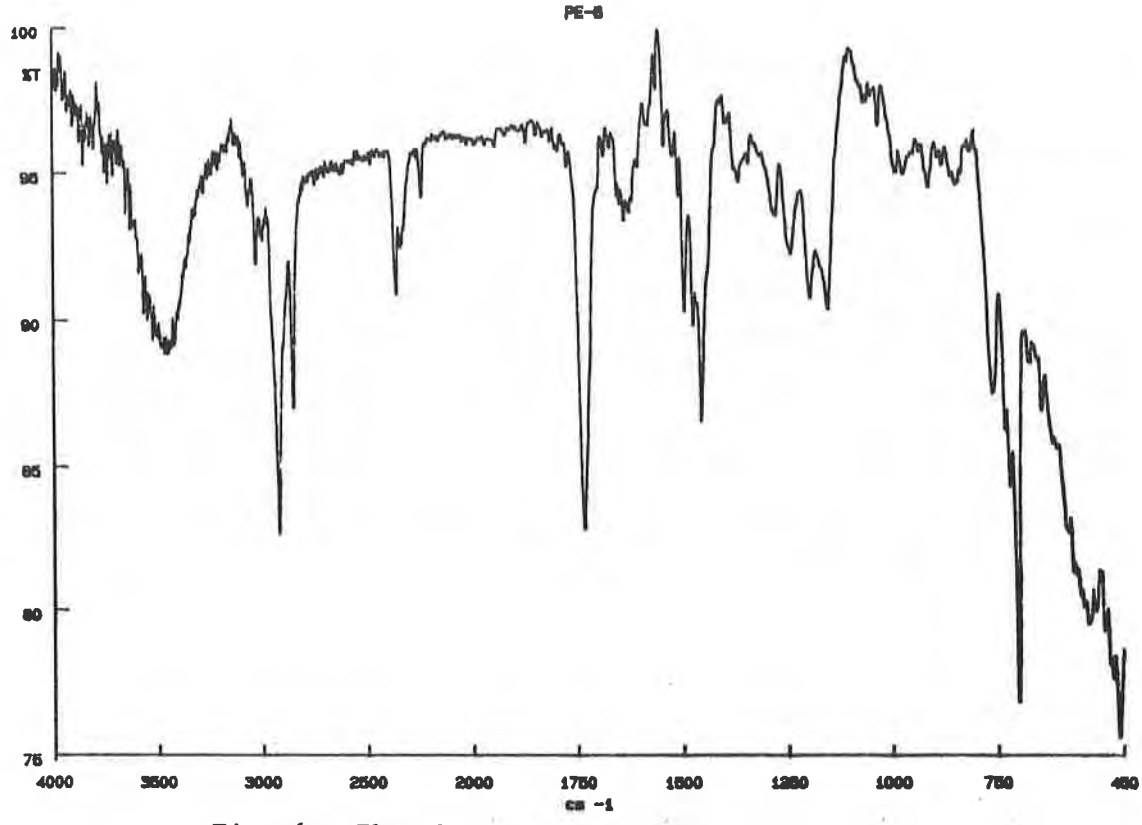

Fig. 6 - The absorption spectra of AIR specimen

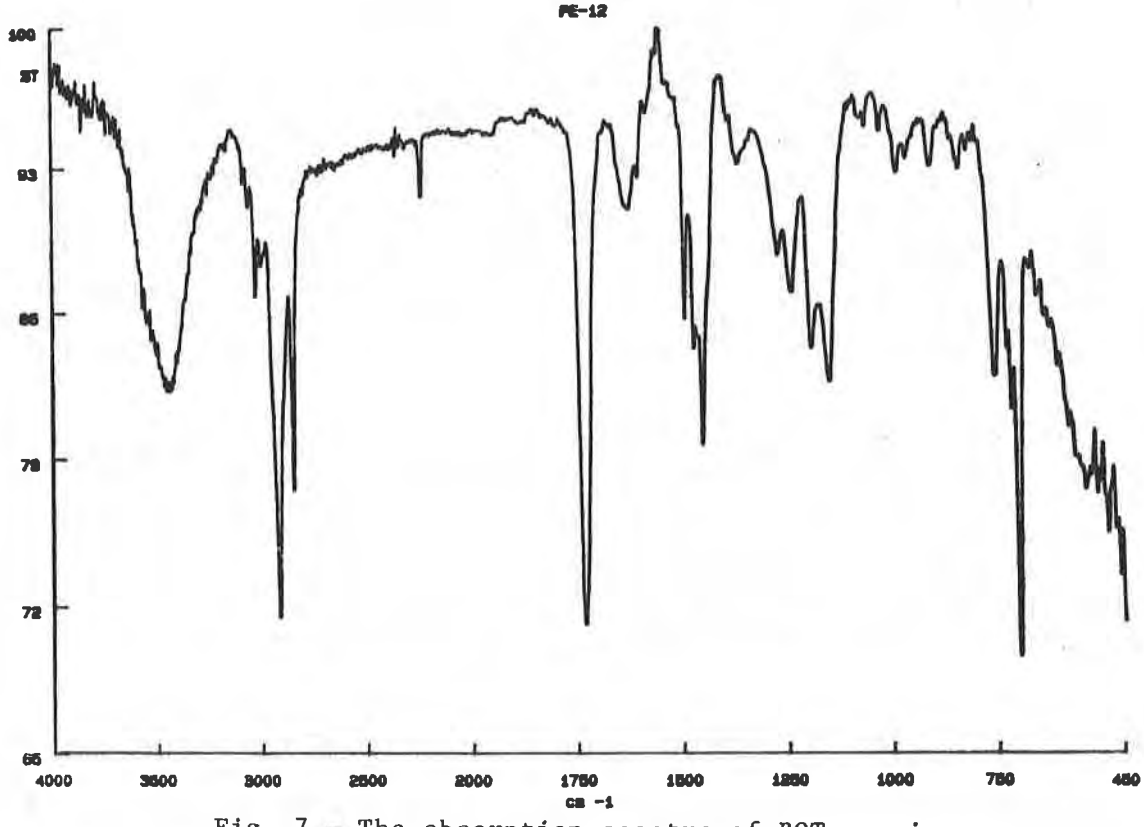

Fig. 7 - The absorption spectra of BOT specimen

Table 6 - The Summary of Five Quantitative Test Data

Samples	Tensile Tests			SCR		OIT		Crystallinity (2nd cycle)	MI (Cond.E)
	Sheet (KN/m)	Seam Shear (%)	Seam Peel (%)	Sheet (hr.)	Seam (hr.)	Sheet (min.)	Seam (min.)	(%)	(g/10 min.)
S1									
AIR	34	94	59	502	378	5.1	9.2	48.2	0.17
AT	36	88	66	504	1484	23.3	26.0	48.2	0.20
ACT	35	90	50	639	957	31.4	30.4	50.4	0.17
BOT	40	75	47	503	982	37.0	31.3	48.6	0.19
S2									
AIR	40	75	52	502	602	16.3	6.3	44.6	0.17
AT	40	69	57	672	1896	29.1	27.4	43.5	0.20
ACT	39	77	53	519	1030	23.5	20.4	46.4	0.17
BOT	40	73	52	658	1421	34.9	31.7	42.0	0.19
S3									
AIR	44	77	50	502	899	14.0	8.3	43.1	0.16
AT	46	69	57	625	1540	29.6	13.3	49.3	0.20
ACT	46	70	41	556	1426	22.3	24.6	49.6	0.16
BOT	44	71	52	718	1835	35.3	25.1	48.6	0.20

Broutman[12] found that the oxidized layer was 0.1 mm thick after 250 hours U.V. exposure.

The results of OIT and stress crack performance suggest that there may be some nominal amount of oxidation occurring in the exposed samples, specifically on the top surface. However, there is no increase in crystallinity, or only a small amount. During aging, secondary crystallization occurs. It reorganizes the crystal phase within the polymer by the growth of some crystallites, accompanied by the dissolution of others[14]. This transition does not substantially increase the total crystallinity of the material. It seems that the small change in the HDPE crystallinity may be unable to be detected by DSC. For such small variation, other crystallinity sensitive properties, such as specific volume, chain mobility from the NMR line width, and X-ray crystallinity, may possible be used to indicate changes[15].

The contradictory behavior between melt index and brittle failure time suggests that melt flow index probably is not a sensitive technique to monitor changes in the molecular weight due to oxidation. The samples with low OIT values could be thermally degraded and cross-linked during the melt index test, yielding a false indication.

Although FTIR is a very useful technique, the complex additive packages in HDPE geomembranes creates significant problems for interpreting the results. The quantitative analysis will be difficult to perform unless the additives in the HDPE are well defined and oxidation has proceeded to a large extent.

CONCLUSIONS

From six different mechanical and chemical tests on a seven year exposed HDPE geomembrane and its seams, the following results have been observed:

1) The short term tensile properties, such as yield strength for the sheets, and peel and shear strength for the seam, remained the same after seven years exposure to the atmosphere, (using the BOT samples as the control reference level).

2) The melt flow index test may not be sensitive enough to monitor changes in subtile molecular weight caused by oxidation.

3) FTIR is a useful technique to detect oxidation in HDPE geomembrane. However, in this case, it was not sufficiently sensitive to observe the small amount of oxidation that occurred. This may be due to the strong masking effect of the antioxidants additives.

4) The measurement of crystallinity by DSC may not be sensitive enough to detect the small amount of chain scission and aging in the polymer for this exposure period.

5) For the various analytical techniques used in this study, OIT appears to be more appropriate than the other test methods to detect small amount of oxidation in an exposed and aged HDPE geomembrane.

6) The surface embrittlement caused by the exposure has accelerated the crack initiation to the degree as indicated in the seam constant load tests.

7) It should be recognized that the changes in the geomembrane are only on the molecular level and they do not influence the engineering properties. In this regard, the OIT and constant load test seem to be the most sensitive techniques of those methods that were utilized.

8) It would be of significant interest to determine possible degradation/aging effects in other aged HDPE geomembranes and also to look at degradation/aging effects in other types of polymeric geomembranes (e.g. PCVC, CSPE, EIA, etc.,)

9) It should be clearly recognized that the HDPE geomembrane in this situation performed very well in its 7-year exposure period. The changes monitored at the different locations were very subtile. In fact, the precision and bias of these tes methods have not been estabilished and the tabulated data in the paper should take cognizance of this consideration.

REFERENCE

1. Grassie, N., and Scott, G., "Polymer Degradation and Stabilization" Cambridge University Press, 1985.

2. ASTM D 683, "Test Method for Tensile Properties of Plastics". Vol.08.01

3. Gray, R.L., "Accelerated Testing Methods for Evaluating Polyolefin Stability", Geosynthetic Testing for Waste Containment Applications: ASTM STP 1081, R.M. Koerner, Ed.,1990

4. Halse, H.Y., Lord, A.E., Jr., Koerner, R.M., "Ductile-to-Brittle Transition time in Polyethylene Geomembrane Sheet", Geosynthetic Testing for Waste Containment Applications:ASTM STP 1081, R.M. Koerner, Ed.,1990

5. Halse, H.Y., Lord, A.E., Jr., Koerner, R.M., "Methods to Evaluate the Stress Crack Resistance of High Density Polyethylene FML Sheets and Seams", 16th Annual Research Symposium of the U.S. EPA, Cincinnati, Ohio April, 1990

6. Bandyopadhyay, P.K., Shaw, M.T., and Weiss, R.A., "Detection and Analysis of Aging and Degradation of Polyolefins : A Review of Methodologies", Polym. Plast. Technol. Eng., 24 (2 & 3), pp.187, 1985

7. ASTM D 1238, "Test Method for Flow Rates of Thermoplastics by Extrusion Plastometer", Vol.08.01

8. Lustiger, A. and Markham, R.L., "Structure Variation Among Different Lots of Polyethylene Pipe", Ninth Plastic Fuel Gas Pipe Symposium, 1985

9. Wunderlich, B., and Cromier, J. Poly. Sci., A-2, 5, pp.987, 1967

10. ASTM D 3895, "Test Method for Oxidative Induction Time of Polyolefins by Thermal Analysis"

11. Conley R.T., "Infrared Spectroscopy", Allyn and Bacon, Inc., Boston, 1966

12. Choi, S.W., and Broutman, L.J., "Ductile-Brittle Transitions for Polyethylene Pipe Grade Resins", Eleventh Plastic Fuel Gas Pipe Symposium, pp.296, 1989

13. Whelton, W.S., and Wrigley, N.E., "Long-Term Durability of Geosynthetics Soil Reinforcement", Geosynthetic'87 Conference Proceedings, New Orleans, Vol. 2, pp.442, 1987

14. McCready M.J., and Schultz J.M., "Effect of Crystallization Time on the Properties of Melt-Crystallized Linear Polyethylene", Journal of Polymer Science: Polymer Physics Edition, Vol. 17, pp.725, 1979

15. Petermann, J., Miles, M., and Gleiter, H., "Growth of Polymer Crystals During Annealing", J. Macromol. Sci.- Phys., B12(3), pp. 393, 1976.

ACKNOWLEDGMENT

The authors would like to thank you Mr. Mark Swyka, Wehran EnviroTech Inc., for providing the test materials and performing the tensile tests. We also would like to thank Mr. Richard Thomas, TRI, for grinding the HDPE geomembranes. Equipment, supplies and materials for performing the study are part of the Geosynthetic Research Institute which is funded by a consortum of 37 member organizations. Our appreciation is extended to them for their participation.

The Resistance of Membranes in Cover Systems to Root Penetration by Grass and Trees

Robert E. Landreth
U. S. Environmental Protection Agency, USA

ABSTRACT

Increased emphasis in being placed on multi-layered cover systems for waste management facilities to minimize the need for further maintenance and to minimize the infiltration of moisture into the unit. These cover systems contain geosynthetic materials that perform specific design, drainage and barrier functions.

A major concern is long-term (greater than 30 years) performance of materials used, especially barrier materials. Grasses and woody plants planted or growing naturally on the cover may produce root systems capable of penetrating the barrier materials. The U.S. Environmental Protection Agency has undertaken a study to evaluate the resistance of commercially available membranes to the penetration force of grasses and trees.

This paper will describe the issues of concern, the experimental set-up, and the results from three lysimeters excavated after two growing seasons.

INTRODUCTION

The state of the art in landfill technology has improved significantly in the past few years through research, design experience, and regulatory requirements. The construction of cover systems, at closure, for waste management facilities at first seems simple, but high-confidence techniques remain to the developed. One of the primary goals of a cover system is to have minimum maintenance while still performing its intended function-minimizing moisture infiltration. While maintenance is maintained it is reasonable to expect mowing to occur at least annually if not more often. Mowing at this frequency should minimize the establishment of deep rooted vegetation. One issue that has not been clearly resolved for maintenance-free cover systems is whether roots from natural vegetation will develop to the point of penetrating the membrane barrier layer. This paper will discuss a small in-house study to investigate the potential for woody plant roots to penetrate commercially available membranes.

The literature contains relatively few reports on root penetration of membranes although it is well recognized that plant systems (grasses) easily grow upward through membranes unless the natural seed bearing soil is sterilized before membrane placement. Laboratory studies Dexter (1986), and Stolzy and Berkley (1968) have shown that roots do exert a pressure but probably insufficient to penetrate

membranes. These studies also indicate that the root after encountering strong untilled sub-soil will grow horizontally until the soil dries out, at which the plant may die, or until weak planes of resistance allow for the continued downward growth. The U.S. Department of Agricultural (USDA) Elkins and Van Sickle (1984) has investigated the use of roots from selected grasses to penetrate plow pans to increase the production of agriculture crops.

One of the early studies to investigate the ability of membranes to resist root penetration was by the Soil Conservation Service at Utah Station Lauritzen (1953). This study evaluated fiberglass reinforced asphaltic membrane, paper-backed membrane, asphaltic coated asbestos membrane, butyl-coated fiberglass and a sprayed membrane. Alfalfa was planted and the extent of root penetration noted. The results indicated the asphaltic coated asbestos liner to be more resistant than other asphaltic liners tested and that the butyl liner also showed no penetration of the roots. Additional tests using different plants was planned.

In a study by the Bureau of Reclamation U.S. Dept. of Interior, Bureau of Reclamation (1961) nutgrass roots penetrated 0.15 mm and 0.2 mm (6 and 8 mil) polyethylene and 0.2 mm (8 mil) vinyl plastic films. Roots and rhizomes of Johnson and nutgrass in another test series were able to penetrate 0.13 mm (5 mil); 0.15 mm (6 mil); 0.2 mm (8 mil) and 0.25 mm (10 mil) polyethylene and 6.2 mm (8 mil) vinyl and 0.63 mm (25 mil) butyl rubber.

These studies clearly suggest that grass root penetration through membrane should be considered. The membrane materials used in the studies were relatively thin in comparison to currently recommended membrane thickness U.S. Environmental Protection Agency (USEPA) (1989) for use in cover systems.

The experimental landfill test cells employed for this study are located at the USEPA Center Hill Research Facility in Cincinnati, Ohio. The test cells were originally installed to evaluate the impact of co-disposing industrial wastes with municipal solid wastes (U.S. Environmental Protection Agency (USEPA) (1985). At the completion of that project the wastes were removed and the test cells were cleaned.

EXPERIMENTAL FACILITIES AND TEST PLAN

The facility consists of fifteen outside cells buried in the ground. The cells are 1.8 m (6 ft) in diameter and 3.6 m (12 ft) deep although the total depth was not a consideration in the design of the experiment. They are constructed of 4.76 mm (3/16 in.) steel covered with a coal-tar epoxy. The test cells were back-filled with a washed pea gravel to a depth of 2.7 m (9 ft.), the membrane under consideration placed on the bottom and up and over the side, and then finished filling with a good quality top soil, Figure 1. In selected cells the membrane was slit with a knife to simulate tears or punctures in the membrane. Each test cell was planted with six tree seedlings obtained from the local Soil Conservation Service. The types used for this study were black walnut, Eastern Redbud, River Birch Tulip and Mountain Ash. Blue grass was then seeded and fertilized to complete the cover system.

Four commercially available membranes that might be used in waste management facilities for landfill cover systems were selected for the study. An additional material from a local hardware store was used for comparison to the higher quality membranes. The commercially available materials and their physical properties are shown in Tables 1 and 2.

The test plan was relatively simple. Once the vegetation and trees had established themselves, estimated to take 2 to 4 years, the system would be stressed to determine the fate of the root system. Stressing the vegetation would be accomplished by covering the test cells with shields to reject rainfall. Water would be introduced under the membranes to encourage the roots to grow through the membrane for moisture. Depending on growth performance the cells would be dissected (4 to 6 years) to determine the fate of the roots and the performance of the membrane barrier.

PRELIMINARY RESULTS

The initial development of the grasses and trees were hampered by a drought in the Cincinnati area. However, external watering helped to establish a good strand of grass and only a few trees were lost. It should be noted that natural growth of weeds, primarily Johnson grass, was also established and thrived in this environment.

As mentioned previously the test cells had been used in a co-disposal research study using industrial wastes. Selected wastes used in the co-disposal study were later defined as hazardous requiring sampling inside and outside of the cells for potential contamination. As part of the Center Hill permit, test cell contents suspected of containing hazardous wastes were removed. Trees from each test cell to be removed were transplanted to other cells that were to remain in the study. Fortunately, the removal of the test cell contents allowed for a preliminary review of growth of the roots and performance of the membranes.

As expected there was an abundance of root mass near the top of each cell. At the edge, immediately adjacent to the membrane, the root mass was at its maximum density. However, when the soil was removed and the membrane could be pealed back from the test cell wall there was no evidence of any root penetration. Figure 1 and 2 illustrates the root masses near the edge.

Figure 1. Root Mass within the Soil Matrix

Figure 2. Root Mass at Edge of Tank

The tree roots had not developed to the full depth of the soil. However, the Johnson grass roots had reached the bottom of the top soil. Figure 3 shows the root from Johnson grass reaching the membrane. The root split and was growing horizontally across the top of the membrane. This same phenomenon was observed in severally other locations of the test cells that were disassembled.

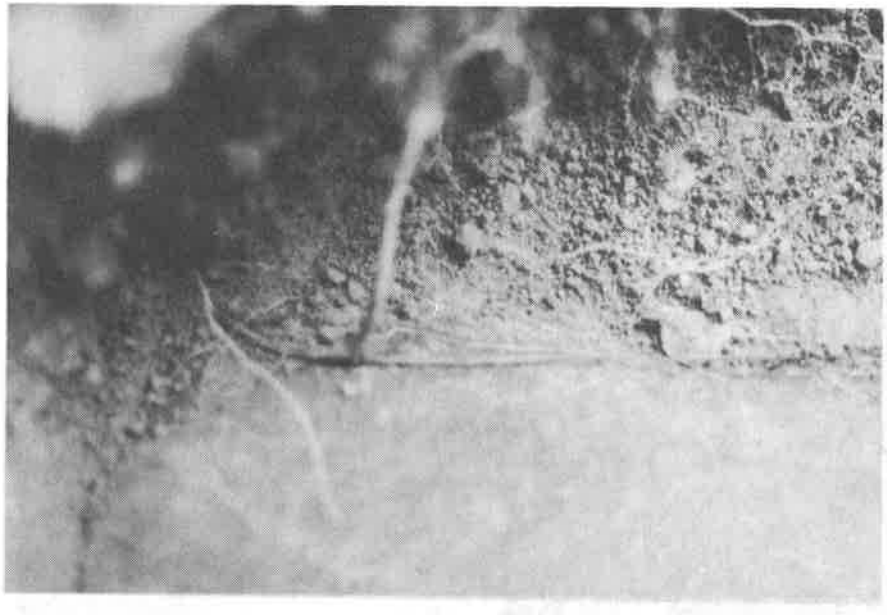

Figure 3. Johnson Grass Roots at Soil Membrane Enterface

Table 1. Analytical and Physical Properties of Unreinforced FMLs

Property	Direction of test	FMLs[a] PVC	LLDPE	CPE
Analytical properties				
Volatiles at 105±2°C, %		0.46	0.14	0.14
Extractables, %		35.23[b]	2.28[c]	14.30[d]
Ash, %		1.65	...	...
Carbon black content, %		...	2.27	...
Specific gravity of FML		1.243	0.945	1.349
Density of polyethylene, g/cm^3		...	0.936	...
Physical properties				
Thickness, ml		20.0	20.2	30.6
Tensile properties:				
Tensile at yield, psi	Machine	...	2340	...
	Transverse	...	2550	...
Elongation at yield, psi	Machine	...	20	...
	Transverse	...	15	...
Tensile at break, psi	Machine	2990	3985	1785
	Transverse	2815	3650	1550
Elongation at break, %	Machine	335	875	325
	Transverse	345	920	495
Stress at 100% elongation, psi	Machine	1435	1925	1255
	Transverse	1895	1875	780
Tear strength, ppi	Machine	360	775	280
	Transverse	345	715	215
Hydrostatic resistance, psi		72	140	98
Puncture Resistance				
Thickness, mil		20.0	20.4	30.5
Stress, lb		31.1	32.7	41.3
Elongation, in.		0.69	1.00	0.99

[a]PVC = polyvinyl chloride; LLDPE = linear low-density polyethylene; CPE = chlorinated polyethylene
[b]Extraction solvent: 2:1 blend of carbon tetrachloride and methyl alcohol
[c]Extraction solvent: methyl ethyl ketone
[d]n-Heptane

Table 2. Analytical and Physical Properties of Fabric-Reinforced Chlorosulfonated Polyethylene FML

Property	Direction of tests	Values
Analytical properties		
Volatiles, %		0.24
Extractables, %		6.15
Specific gravity		1.518
Physical properties		
Thickness, mil		37.9
Tensile properties:		
Breaking strength of fabric[a], lb	Machine	265
	Transverse	310
Elongation of fabric, %	Machine	20
	Transverse	27
Breaking strength of rubber, lb	Machine	180
	Transverse	265
Elongation of rubber, %	Machine	60
	Transverse	80
Ply adhesion, ppi	Machine	9
	Transverse	10
Hydrostatic resistance, psi		418
Puncture resistance, lb		186

[a]Grab test

SUMMARY AND CONCLUSIONS

The potential detrimental action of vegetation roots penetrating membrane barriers used in waste management cover systems is being investigated in fifteen test cells. The vegetation consisted of both grasses and trees with some intrusion of Johnson grass. Although the study was initiated under drought conditions a good stand of grass was developed and the trees are growing well.

Early dissection of 3 test cells established that a good root mass was developing from grass and weed root masses had reached the membrane surface but there was no evidence of any damage to the membranes.

These results represent only a short period of generation in the life of a landfill cover. The RREL plans to operate the test cells for several more years.

ACKNOWLEDGEMENTS

The author wishes to acknowledge the Water Saver Company of Denver, CO and the Gundle Lining Systems of Houston, TX for providing the membranes used in the study. We also appreciate the assistance of Dr. Henry Haxo of Matrecon, Inc., Alameda, CA for providing the analytical data for the membranes.

REFERENCES

Dexter, A.R., (1986) "Model Experiments on the Behavior of Roots at the Interface Between a Tilled Seed-Bed and a Compacted Sub-soil", Plant and Soil, 95, 149-161.

Elkins, Charles B., and Van Sickle, K., (1984) "Punching Holes in Plowpans", Solutions, July/August, pp. 38-41.

Lauritzen, C.W., (1953) "A Test of Durability of Canal Lining Materials is Their Ability to Resist Root Penetration", Farm and Home Science, September, pp. 58-59.

Stolzy, L.H. and K.P. Berkley, (1968) "Mechanical Resistance Encountered by Roots Entering Compact Soils", Soil Science Vol. 105, No. 5, pp. 297-301.

U.S. Dept. of Interior, Bureau of Reclamation, (1961) "Resistance of Canal Lining Materials to Penetration by Plant Growth Progress Report No. 1", Chemical Engineering Laboratory Report No. W-2, November 15, Denver, Colorado.

U.S. Environmental Protection Agency (USEPA), (1985) "Evaluation and Disposal of Waste Materials within 19 Test Lysimeters at Center Hill," Report No. EPA/600/2-86-035, Office of Research and Development, Hazardous Waste Engineering Research Laboratory, Cincinnati, OH. NTIS PB-86-176336.

U.S. Environmental Protection Agency (USEPA), (1989) Technical Guidance Document: Final Covers an Hazardous Waste Landfills and Surface Impoundments Report No. EPA/530-SW-89-047 Office of Solid Waste and Emergency Response, Washington, D.C.

The Chemical Resistance of Geotextiles to be Used in Secondary Containment Systems for Underground Storage Tanks

Randy C. Pucetas
Hoechst Celanese Corp., USA
Karen L. Verschoor
Texas Research Institute Environmental Inc., USA
Sam R. Allen
Texas Research Institute Environmental Inc., USA
C. Joel Sprague
Nicolon Corporation, USA

ABSTRACT

U.S. Environmental Protection Agency (EPA) regulations require underground storage tank systems (UST's) which prevent releases due to structural failure and which are equipped with leak detection devices. This paper addresses the chemical compatibility of various nonwoven needlepunched geotextiles to be used in leak detection systems for UST's. EPA Method 9090 chemical compatibility testing was performed with liquids commonly found in UST's and the results reported.

INTRODUCTION

Geotextiles are currently used in waste containment facilities as liner cushions, filters, drainage layers and gas vents. New regulations concerning the construction and operation of UST facilities have posed the possibility of using geotextiles in UST applications as well.

This paper describes the work performed at Texas Research Environmental, Inc. (TRI) to determine the chemical compatibility of various geotextile materials with petroleum products. The major objectives of this testing program were to produce data that demonstrate the chemical resistance of the geotextiles to petroleum products typically stored in underground storage tanks. The testing examined changes in various mechanical and hydraulic properties of the materials after exposure to various exposure media at 22°C and 50°C for 30, 60, 90, 120 and 150 days with guidance from EPA Method 9090.

PROCEDURE

The following geotextiles were studied:
. 4.3 oz/yd^2 continuous filament, resinated, polyester
. 7.5 oz/yd^2 continuous filament polyester
. 8 oz/yd^2 staple polypropylene (lightly burnished)
. 8 oz/yd^2 staple polypropylene (heavily burnished)
. 8 oz/yd^2 continuous filament polypropylene
. 8 oz/yd^2 staple recycled polyester

The following organic fuels and chemicals were used for exposure media:
. Automotive unleaded gasoline
. Diesel Fuel
. Jet Fuel (JP-5)
. Toluene
. Ethanol

The 7.5 oz/yd^2 continuous filament polyester geotextile was exposed to all exposure media, while the other geotextiles were exposed to unleaded gasoline only.

Samples of all geotextiles were exposed to the fuel and/or chemical media in glass jars capped with teflon lined lids and filled with the appropriate exposure media. These jars were maintained at 22°C ± 2°C and 50°C ± 2°C. The 50°C jars were placed in a heated water tank. The use of jars allowed for control of folitization and added a measure of safety when dealing with the flammable materials.

The exposure environments were monitored to maintain consistency in exposure conditions. The jar headspace above the geotextile samples was kept to a minimum to minimize evaporation. Constant levels of exposure media were maintained by the periodic addition of fresh media after removal of samples for testing at prescribed intervals. Care was taken to assure that all geotextile samples were fully exposed.

Exposed and unexposed geotextile samples were tested for the following properties:

Test	Method
Puncture resistance	ASTM D4833
Mullen burst strength	ASTM D3786
Grab strength and elongation	ASTM D4632
Permittivity	ASTM D4491
Trapezoidal tear strength	ASTM D4533

Geotextile test coupons were cut from stock and randomly selected for testing. Mass per unit area (osy) and thickness (mil) were recorded for all unexposed test coupons before subsequent exposure and testing for correlation to extraneous mechanical property test results. All samples were tested damp. After removal from the exposure jars, exposed samples were rinsed three times in deionized water, pat dried with absorbent material and stored in polyethylene bags until tested.

Ten replicates were tested for each test method. Trapezoidal tear and grab strength tests were performed in the machine direction only. Puncture resistance tests were performed using a 5/16 inch diameter flat beveled probe.

Initial permittivity test results showed a large reduction in geotextile flow properties. This observed change was found to result from sample retention of exposure media residue. To eliminate this bias, TRI pressure flushed each permittivity test coupon with test water held in the apparatus reservoir (as in a falling head test) before subsequent testing. This additional rinsing served to effectively remove retained residue in each test coupon.

Upon review of the 120 day interim report, TRI/Environmental was requested to perform 150 day testing using specimens that had been allowed to "dry" before subsequent analysis for various index properties. The rationale for this testing was based on an understanding that observed losses in mechanical strength properties of the geotextiles may be attributed (or partially attributed) to retention of exposure media residue by test specimens. Softening and swelling of the geotextile component polymers may take place as they absorb organics present in the exposure media, resulting in a reduction of fiber tensile strengths and friction between the fibers. The objective of the 150 day testing was to characterize this phenomenon as it affected the results generated during this chemical compatibility study.

All samples tested during the 150 day testing period were first rinsed using the procedure outlined above. Samples were then dried at ambient temperature to allow volatile organics to evaporate. Finally, samples were dried in an air oven at 30°C for twelve hours, soaked in deionized water for twenty four hours, pat dried with absorbent towels and tested damp.

TEST RESULTS

To take into account and also minimize the effects of dimensional variability, a normalization procedure was implemented which incorporated each test coupon's individual physical properties into each mechanical test result.

Normalization of test results was accomplished by using correction factors generated by defining the fractional relationship between each test coupon's physical properties and the average roll values measured for the entire product roll. Physical property data from all geotextiles included in the test pool were used to generate the average roll values for each product roll. The resulting correction factors were then multiplied by the original mechanical property test results to generate "corrected" values.

Determination of the appropriate physical characteristics to use in the normalization procedure was based upon the specific test being analyzed. The following physical properties were used to normalize each mechanical property test result.

Test	Normalizing Property
Puncture resistance	thickness
Mullen burst strength	thickness and mass/unit area
Grab strength/elongation	mass/unit area
Trapezoidal tear strength	thickness

The following correction factor formula was used for normalization of Mullen burst strength data to achieve an equal weighting of each normalizing property:

$$\text{Correction Factor (Mullen burst)} = \frac{(\text{avg roll osy}/\text{coupon osy}) + (\text{avg roll mil}/\text{coupon mil})}{2} \quad [1]$$

The normalized test results are presented graphically in Fig. 1, showing percent strength retained versus exposure time.

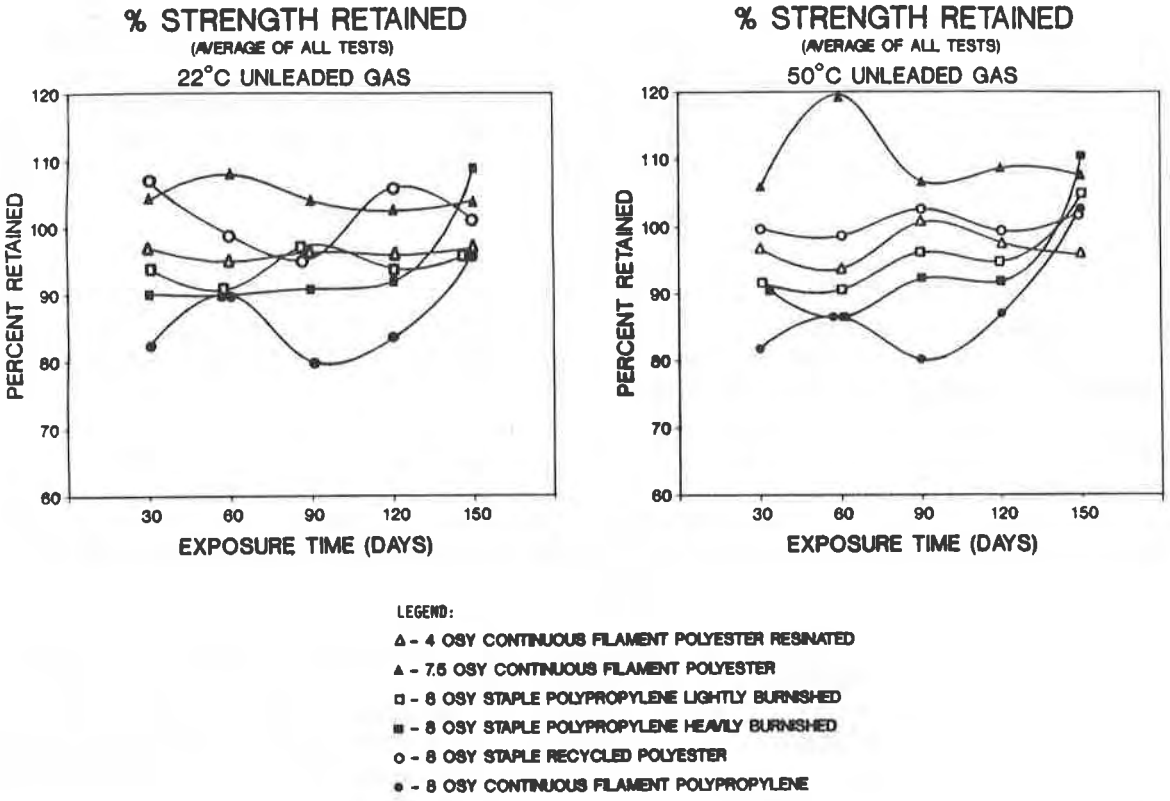

Figure 1: Normalized Test Results

The permittivity test results indicated no significant decreases for any of the geotextiles.

The 7.5 oz/yd^2 continuous filament polyester geotextile exhibited insignificant strength reductions in the other exposure media.

DISCUSSION

Changes in normalized mechanical properties measured for the polyester geotextiles were within the range of expected experimental variability associated with the applicable methods throughout the test periods at both temperatures. (In general, variability of as much as ± 10 to 15% may be expected for index testing of geotextile product and can be attributed to experimental factors.) Any loss of performance attributed to chemical interaction should be consistent across measurements of several index properties and would be expected to show changes outside the range of expected variability. Consistent and significant property changes were not observed for the polyester products.

All of the polypropylene geotextiles demonstrated a slight loss in certain mechanical properties, apparently as a result of exposure to unleaded gasoline. This is thought to be attributed to absorption of the exposure media into the polymer as well as surface retention of the exposure media by the test specimens. Upon drying of the polypropylene geotextiles, after the 150 day exposure, lost strengths were partially recovered, indicating degradation was a result of plasticization rather than chain scission.

Since the test results did not show a significant reduction in strengths, it appears that geotextiles of the type tested are suitable for use in leak detection systems for UST's.

Molecular and Rheological Changes in Polyethylene Occurring From Heat Seaming HDPE Liners

Mark W. Cadwallader
Gundle Lining Systems Inc., USA
Jeffrey R. Burkinshaw
Phillips 66 Co., USA

INTRODUCTION

The question is often asked: "How are polymeric molecular properties affected during seaming of HDPE liners?" What about molecular properties such as crystallinity and molecular weight, for instance? This paper explores that question with the help of differential scanning calorimetry (DSC), gel permeation chromatography (GPC), and melt rheology.

These characterizations of polymeric structure and behavior supplement those previous studies which have already focused on 1) gross morphology effects of seaming visible by cutting a microtome section and using a microscope, 2) testing of seams for Environmental Stress Crack Resistance, and 3) destructive testing of seams in peel and shear.

The present study confines itself to studying the behavior of polyethylene molecules at seams in terms of 1) their arrangement (crystallinity through thermal analysis), 2) size (molecular weight and distribution), and 3) flow behavior (rheology). It does not deal with oxidative stability of the seams, which depends at present state-of-practice primarily on heat stabilizers, not on the polyethylene itself.

SEAMING EFFECTS ON THERMAL BEHAVIOR OF THE POLYMER

Heats of Fusion. When a material undergoes a phase change as it does when it is converted from a solid to a liquid, heat energy is absorbed. When a material melts, this heat that is absorbed is called the "heat of fusion".

Secondary bonding of various types occurs between the molecules when a substance is in its solid phase. If this bonding results from an ordered arrangement of molecules, the material is said to possess crystallinity. Such is the case with polyethylene. Since increased crystallinity results in more and better secondary bonding (better "fusion" so to speak) the heat of fusion is a function of the crystallinity. Thus, percent polymer crystallinity can be calculated by measuring the heat energy required to melt a polymer and then dividing this value by that obtained for a maximum crystalline sample. The heat

of fusion for polyethylene of maximum crystallinity is 276.3 J/g (1).

Figures 1 and 2 display melting point curves for HDPE, with integration to find the heat of fusion. Since polymers melt over a range of temperatures, two melting points are listed. As the figure indicates, melting point "onset" temperature is found by extrapolating back to the baseline the tangent to the steepest part of the heat flow curve. The other melting point listed is the point of maximum heat flow. This latter point is the traditionally reported melting point of HDPE.

Table 1 lists a number of separate calculations of heats of fusion and crystallinities for a small piece of HDPE. Error analysis gives us a picture of the sensitivity of the procedure. Error is greater for the heat of fusion than for the melting points. This is because unlike melting temperature, heat of fusion is dependent on sample size; thus error in weight determination becomes important. Results in Table 1 are for a heating range of 10 degrees C per minute.

TABLE 1

PERCENT CRYSTALLINITY DETERMINED FROM
SEPARATE SPECIMENS ADJACENT TO EACH OTHER
IN A SAMPLE OF HDPE

Specimen	"Onset" (^{o}C)	Maximum (^{o}C)	AH (J/g)	% Crystallinity
1	115.59	127.36	156.24	56.6
2	116.80	127.03	147.57	53.5
3	116.34	125.97	158.17	57.3
4	115.51	127.89	150.43	54.4
5	116.34	127.27	158.02	57.2
6	116.79	127.72	149.51	54.2
7	115.56	126.76	158.01	57.3
Average	116.13	127.23	153.99	55.8
Standard Deviation	1.05	.14	1.9	1.6

Percent Crystallinity During Welding. To determine the effect welding has on the crystallinity of HDPE, two different samples of welding rod for a fillet extrusion weld were tested for percent crystallinity. Since the same resin and percent carbon black as go into sheet production are added to the welding rod, percent crystallinity of the rod is typical of the HDPE. Table 2 lists results for the welding rod samples.

FIGURE 1

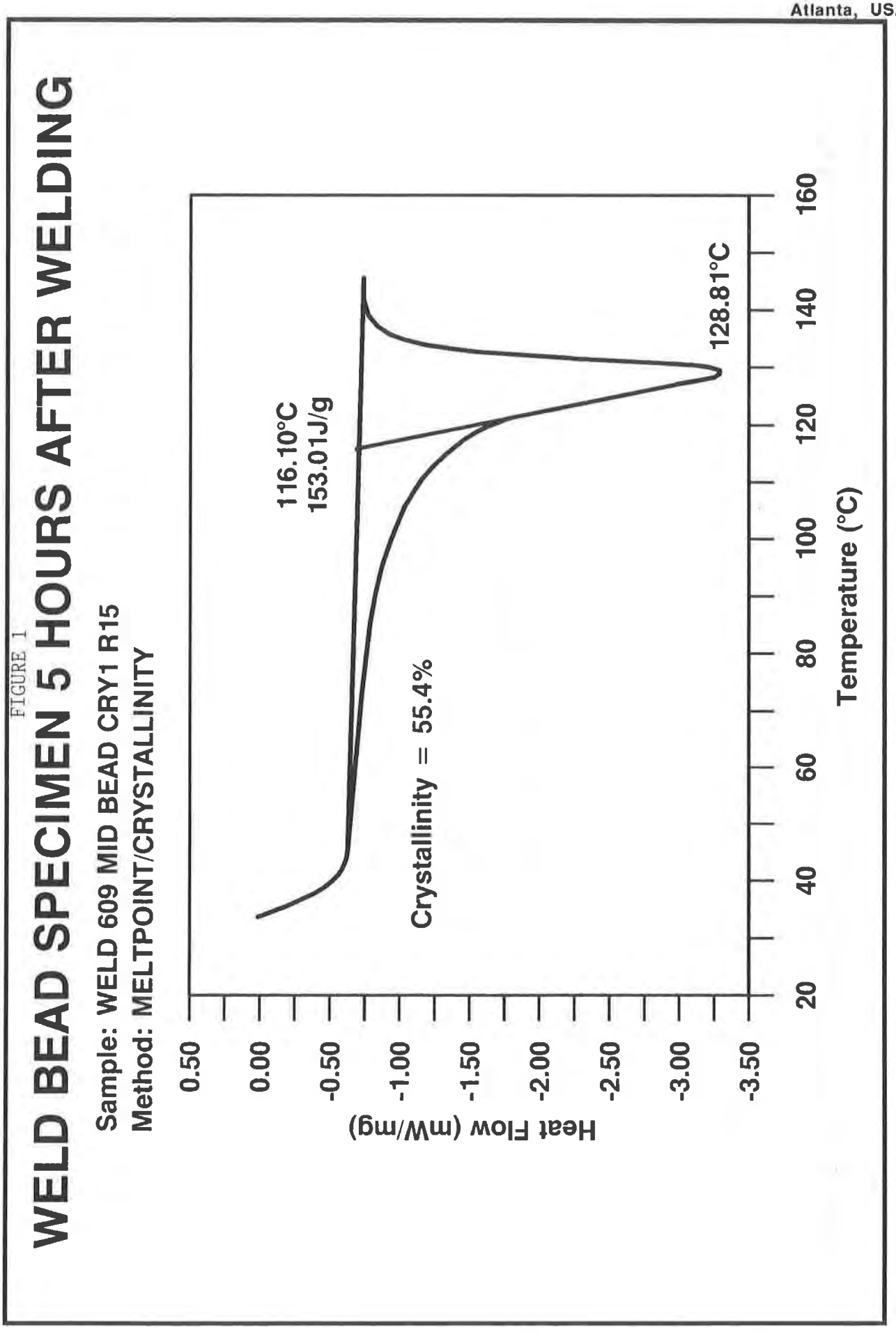
WELD BEAD SPECIMEN 5 HOURS AFTER WELDING
Sample: WELD 609 MID BEAD CRY1 R15
Method: MELTPOINT/CRYSTALLINITY
116.10°C
153.01J/g
128.81°C
Crystallinity = 55.4%
Heat Flow (mW/mg)
0.50
0.00
-0.50
-1.00
-1.50
-2.00
-2.50
-3.00
-3.50
20
40
60
80
100
120
140
160
Temperature (°C)

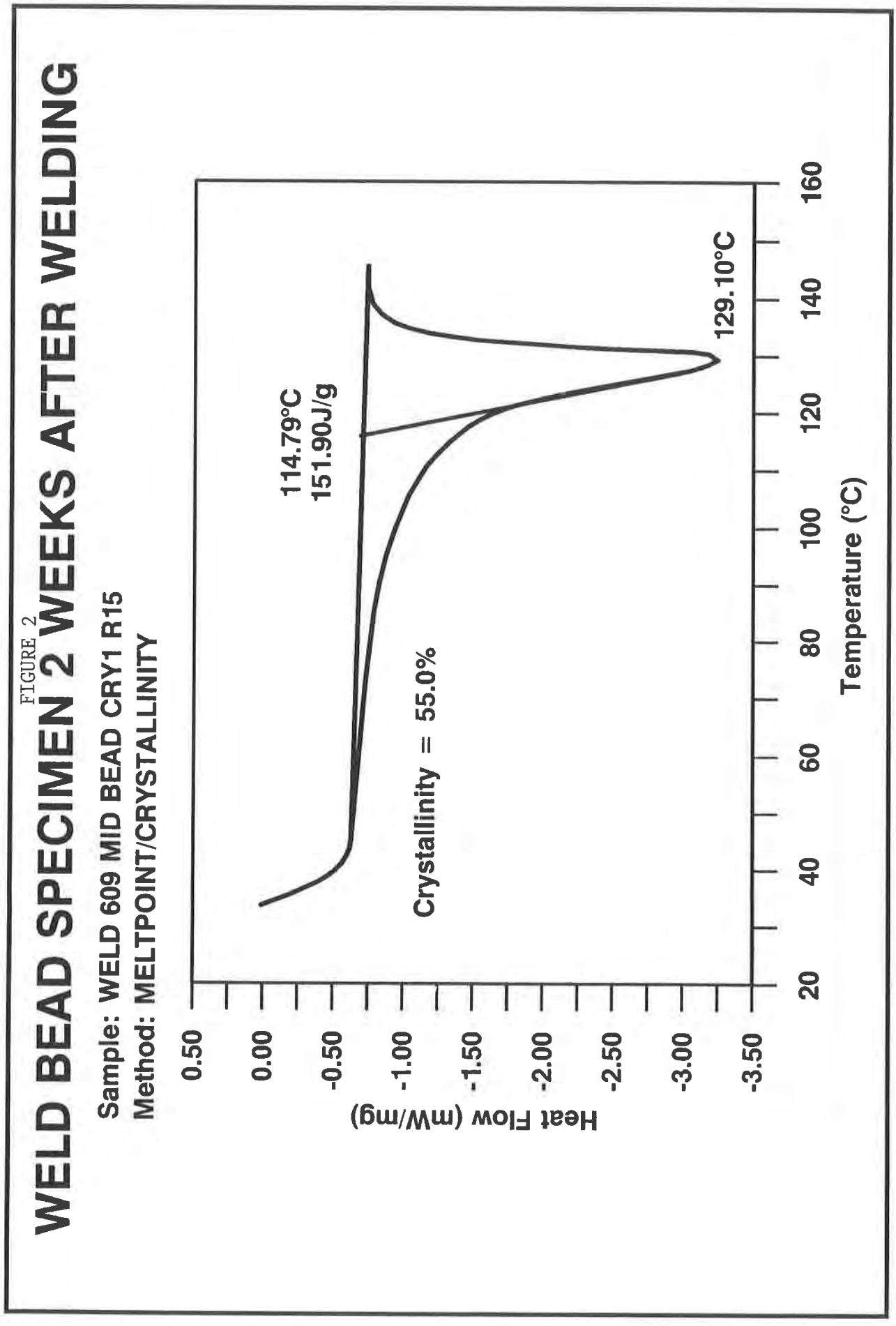
WELD BEAD SPECIMEN 2 WEEKS AFTER WELDING
Sample: WELD 609 MID BEAD CRY1 R15
Method: MELTPOINT/CRYSTALLINITY
114.79°C
151.90J/g
129.10°C
Crystallinity = 55.0%
Heat Flow (mW/mg)
0.50
0.00
-0.50
-1.00
-1.50
-2.00
-2.50
-3.00
-3.50
20
40
60
80
100
120
140
160
Temperature (°C)

FIGURE 2

TABLE 2

PERCENT CRYSTALLINITY OF WELDING ROD SAMPLES

Welding Rod Batch #607

Specimen Position	1st Melt Cycle	2nd Melt Cycle	Average	Deviation
Front of Weld Rod	53.6	53.9	53.8	0.2
Front of Weld Rod	54.9	55.4	55.2	0.3
Middle of Weld Rod	57.1	59.3	58.2	1.1
End of Weld Rod	58.1	57.4	57.8	0.4
Average	55.9	56.5		
Standard Deviation	1.8	2.0		

Density = .942 g/cm3

% Carbon Black = 2.1%

Welding Rod Batch #609

Specimen Position	1st Melt Cycle	2nd Melt Cycle	Average	Deviation
Front of Weld Rod	54.0	56.2	55.1	1.1
Middle of Weld Rod	49.2	50.2	49.7	0.5
End of Weld Rod	50.8	52.5	51.7	0.9
End of Weld Rod	47.4	48.9	48.2	0.8
Average	50.4	52.0		
Standard Deviation	2.4	2.8		

Density = .941 g/cm3

% Carbon Black = 2.2%

Seam samples between separate sheets of HDPE were made with each of the welding rod samples. Percent crystallinity was determined at five separate locations through each weld, as pictured in Figure 3. Tables 3 and 4 present the results of this testing for each of the seam samples. Percent crystallinity in the weld bead was then monitored through two weeks time. These results for each sample are also included in Tables 3 and 4.

FIGURE 3

SAMPLE LOCATIONS IN FILLET EXTRUSION WELD

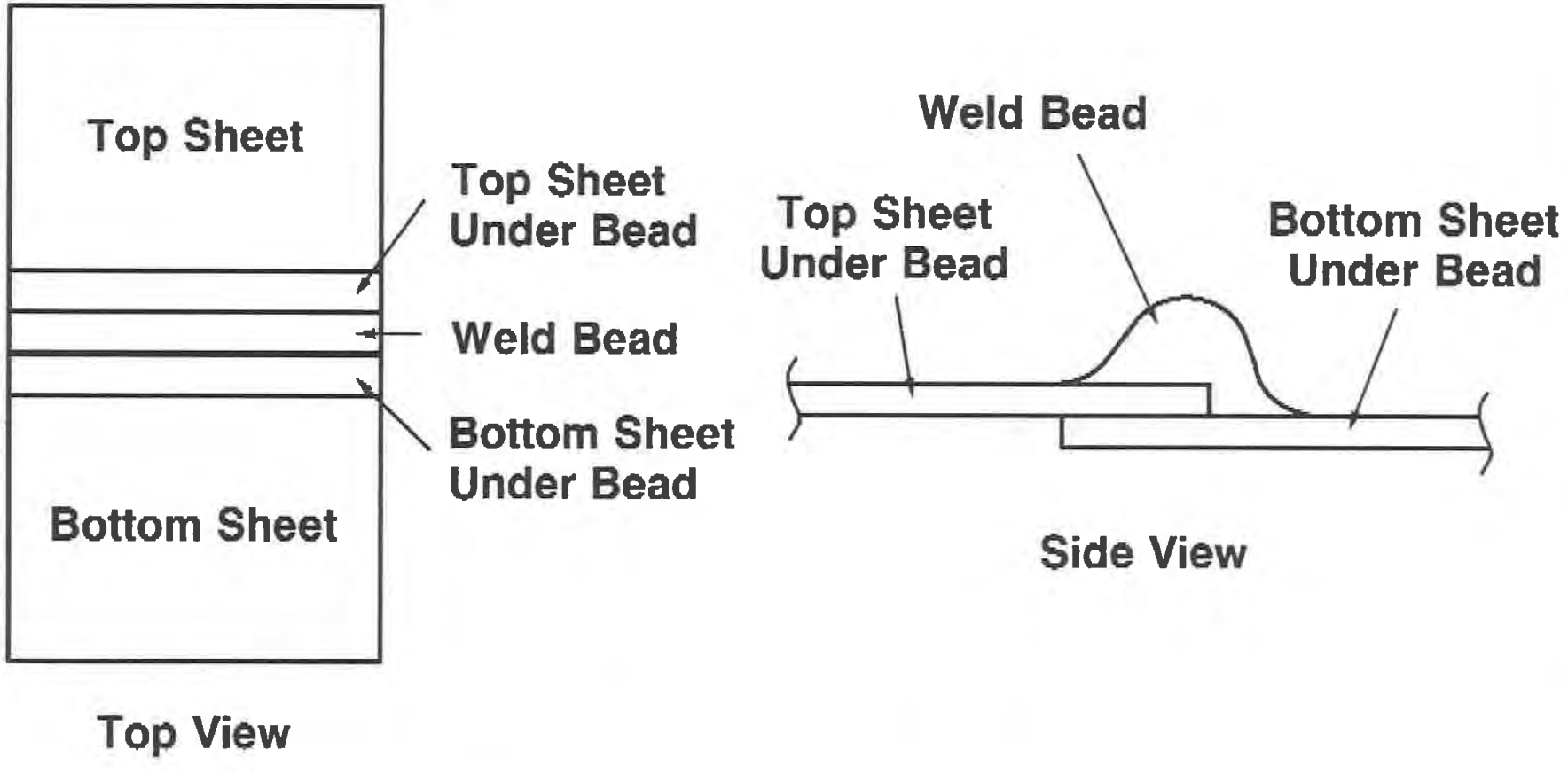

TABLE 3

PERCENT CRYSTALLINITY ACROSS SEAMS
WELDED WITH WELDING ROD BATCH #607 SAMPLE

Specimen Position	1st Melt Cycle	2nd Melt Cycle	Average	Deviation
Top Sheet	49.2	49.8	49.5	0.3
Top Sheet Under Bead	55.1	55.2	55.2	0.1
Bottom Sheet Under Bead	53.2	57.5	55.4	2.2
Bottom Sheet	50.1	48.5	49.3	0.8
Weld Bead (ca. 4 hrs. after welding)	53.7	53.9	53.8	0.1
Weld Bead (8 days after welding)	54.0	53.7	53.9	0.2
Weld Bead (11 days after welding)	51.3	55.4	53.4	2.1
Weld Bead (15 days after welding)	51.9	54.4	53.2	1.3
Average of Weld Bead	52.7	54.3		
Standard Deviation of Weld Bead	1.1	0.8		

TABLE 4

PERCENT CRYSTALLINITY ACROSS SEAMS
WELDED WITH WELDING ROD BATCH #609 SAMPLE

Specimen Position	1st Melt Cycle	2nd Melt Cycle	Average	Deviation
Top Sheet	59.7	57.5	58.6	1.1
Top Sheet Under Bead	51.6	55.7	53.7	2.1
Bottom Sheet Under Bead	54.2	56.8	55.5	1.3
Bottom Sheet	53.1	54.9	54.0	0.9
Weld Bead (ca. 5 hrs. after welding)	55.4	56.2	55.8	0.4

TABLE 4 (continued)

PERCENT CRYSTALLINITY ACROSS SEAMS
WELDED WITH WELDING ROD BATCH #609 SAMPLE

Specimen Position	1st Melt Cycle	2nd Melt Cycle	Average	Deviation
Weld Bead (8 days after welding)	54.4	52.3	53.4	1.1
Weld Bead (11 days after welding)	53.4	51.6	52.5	0.9
Weld Bead (15 days after welding)	55.0	54.7	54.9	0.2
Average of Weld Bead	54.6	53.7		
Standard Deviation of Weld Bead	0.8	1.8		

A hot wedge weld study of thermal effects in the polymer was also conducted at three different sample locations in a dual hot wedge weld capped with a fillet extrusion weld (see Figure 4). One sample (Sample A) was taken out of the bottom sheet near the hot wedge seam. A second sample (Sample B) was taken out of the bottom sheet underneath the inside track of the hot wedge seam. And a third sample (Sample C) was taken out of the bottom sheet underneath the outside track of the hot wedge seam which had been capped with a fillet extrusion weld. Samples were confined to the bottom sheet so that a consistent polymer base could be assumed in order to compare effects of seaming. Sample A had no welding history. Sample B had one hot wedge weld track history. And Sample C had one hot wedge weld track history and one fillet extrusion weld history.

Table 5 presents the results for Samples A, B, and C, with measurement of peak melting point, heat of fusion, and percent crystallinity.

TABLE 5

POLYMER BEHAVIOR FOR DIFFERENT HEAT HISTORIES ACROSS COMBINATION
DUAL HOT WEDGE/FILLET EXTRUSION SEAMS OF FIGURE 5

	Sample A Sheet	Sample B Hot Wedge Seam	Sample C Hot Wedge Fillet Weld
THERMAL ANALYSIS (DSC)			
Tm,C	129.4	128.2	130.4
del Hf, J/g	178.2	178.4	179.2
Tm (rescan), C	129.1	128.5	130.3
del Hf (rescan), J/g	176.0	176.3	174.2
Initial Crystallinity, %	62.3	62.4	62.6

FIGURE 4

SAMPLE LOCATIONS IN WEDGE WELD WITH ADDITIONAL EXTRUSION WELD

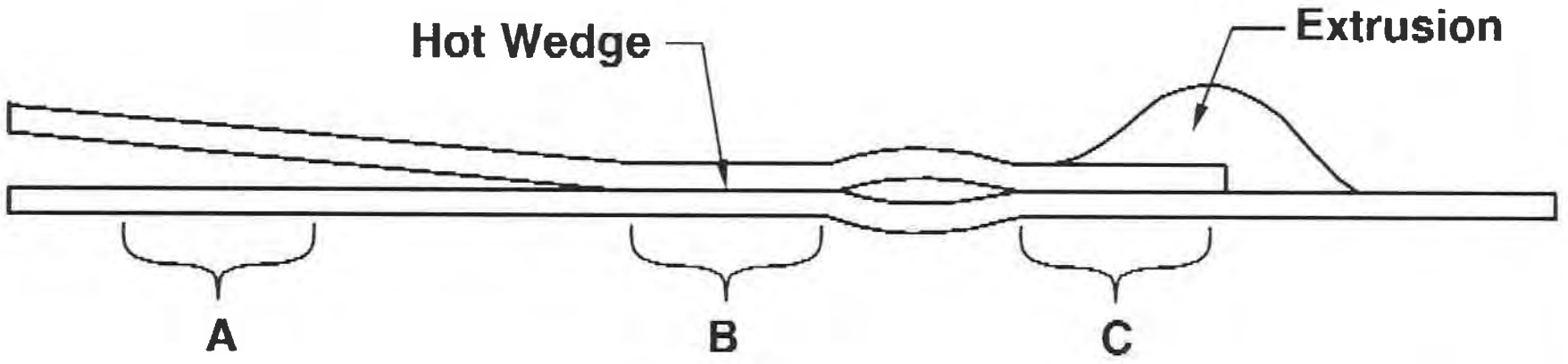

Sample A - 80 mil HDPE Sheet

Sample B - 80 mil HDPE Sheet Hot Wedge Weld

Sample C - 80 mil HDPE Sheet Hot Wedge Weld & Extrusion Weld

TABLE 5 (continued)

POLYMER BEHAVIOR FOR DIFFERENT HEAT HISTORIES ACROSS COMBINATION DUAL HOT WEDGE/FILLET EXTRUSION SEAMS OF FIGURE 5

	Sample A Sheet	Sample B Hot Wedge Seam	Sample C Hot Wedge Fillet Weld
MOLECULAR WEIGHT (GPC)			
Mw/1000	191	210	211
Mn/1000	10.1	10.2	10.0
[1]HI	18.8	20.6	21.1
MELT RHEOLOGY (RMS)			
[2]Gx*10-5, dyn/cm2	3.75	3.64	3.83
Vis*10-5 @0.1 s-1	4.73	4.83	5.08
Vis*10-4 @100 s-1	1.73	1.73	1.82
[3]tan d @0.1 s-1	1.50	1.46	1.45
[3]tan d @100 s-1	0.79	0.79	0.79

[1] HI = Heterogeneity Index = $\frac{Mw}{Mn}$

[2] Gx = crossover modulus; where G' = G", i.e., storage modulus = loss modulus

[3] tan d = $\frac{G''}{G'}$ = $\frac{\text{loss modulus}}{\text{storage modulus}}$

Experimental. The DSC measures the temperature difference between an aluminum pan containing sample materials and an identical empty reference pan. Because the sample material absorbs heat during melting, the sample and reference pans will change temperatures at different rates as they are heated in the calorimeter. The differential temperature gradient between sample and reference pans is characteristic of the sample being tested. Heat flows are calculated from the differential temperatures and integration of the heat flows gives the heat of fusion for the sample.

Percent crystallinities for the fillet extrusion weld studies were calculated from heats of fusion measured by a Dupont Model 910 DSC. Sample specimens were weighed to the nearest 0.1 mg. In addition, specimens were cut to constant dimensions and the weights were confined to a 5.0 mg + 0.5 mg range. This helped reduce error in the heat of fusion due to variation in sample size. The DSC was programmed for a temperature range from 30 degrees C to 150 degrees C. A Perkin-Elmer Model DSC-7 was used for the hot wedge measurements of Figure 4 and Table 5.

Table 6 displays the results of testing to determine the significance of heating and cooling rates during DSC calculation of percent crystallinity. Rates of heating and cooling have been thought to affect crystallinity, but the results in Table 6 indicate that changing the temperature gradient has a minimal effect

TABLE 6

VARIATION IN PERCENT CRYSTALLINITY DUE TO
HEATING AND COOLING RATES DURING DSC OPERATION

Sample	Condition	1st Melt Cycle	2nd Melt Cycle	3rd Melt Cycle	Average	Standard Deviation
60 mil HDPE	5°C/min heating 6°C/min cooling	51.9	53.5	51.6	52.3	0.8
60 mil HDPE	10°C/min heating 6°C/min cooling	54.1	50.5	51.1	51.9	1.6
60 mil HDPE	15°C/min heating 6°C/min cooling	52.6	53.4	53.2	53.1	0.3
60 mil HDPE	20°C/min heating 6°C/min cooling	50.8	52.8	52.6	52.1	0.9
60 mil HDPE	5°C/min heating 1.7°C/min cooling	57.3	60.1	58.5	58.6	1.1
60 mil HDPE	10°C/min heating 1.7°C/min cooling	51.8	54.8	53.8	53.5	1.2
	Average	53.1	54.2	53.5		
	Standard Deviation	2.1	2.9	2.4		

on the final values. Comparing standard deviations for the data in Table 6 with the data in Table 1, error in the percent crystallinity determination is not much more for the data with varied heating rates (standard deviation of 2.1 vs. 1.6).

Because stresses set up during processing have been thought to alter the internal crystallinity of the product, sample specimens were taken through more than one melting cycle. The first cycle would eliminate any built-in stresses from product manufacture which might have altered the crystallinity. By this line of thinking, permanent changes in crystallinity, unbiased by production/installation stresses, would show up after the first melt cycle released those stresses. However, in the case of the Table 6 samples average crystallinities remained constant through three melt cycles. The more than one melt cycle concept was kept through the study of crystallinity in the seaming process, using a 15 degrees C/min. heating gradient and a 6 degrees C/min. cooling gradient.

EFFECTS OF SEAMING ON MOLECULAR WEIGHT

Samples A, B and C across the dual hot wedge seam in Figure 4 were also compared for changes in molecular weight and distribution. The different samples were compared by gel permeation chromatography (GPC) and results are displayed in Figure 5 and Table 5. A Waters Model 150-CV was used for the GPC data.

EFFECTS OF SEAMING ON RHEOLOGICAL BEHAVIOR

Engineers have traditionally been concerned with two distinct types of materials: the viscous fluid and elastic solid. Although synthetic liners are solids as used in geotechnical engineering, they exhibit viscous flow behavior because they are actually hybrid materials; viscoelastic materials.

Figure 6 displays some of the mechanical models which have been used to represent elastic, viscous, and viscoelastic behavior. These models are spring, dashpot, and combinations of spring and dashpot respectively.

To characterize a viscoelastic material in dynamic mechanical testing, polymer scientists define a 1) storage modulus, G′ and 2) a loss modulus, G″ (2). The storage modulus is the ratio of stress to strain which is in-phase with the oscillations of an oscillating plate rheometer. In this case the shear energy is stored during the deformation as with a spring, indicating elastic behavior. The loss modulus is the ratio of stress to strain which is out-of-phase with the oscillations of an oscillating plate rheometer. In this case the shear energy is dissipated during the deformation as with a dashpot, indicating viscous behavior. The phase angle between stress and strain is given by the loss tangent, tan d = G″/G′. And the crossover modulus (Gx) is defined as the frequency of oscillation where G′ = G″, in the dynamic test of varying frequencies.

Table 5 reports crossover modulus Gx, loss tangent tan d, and viscosity. It also reports the rheological information at low shear, 0.1 s-1, and high shear, 100 s-1, allowing us to draw conclusions from the shear sensitivity before and after welding. A Rheometrics Mechanical Spectrometer (RMS) Model RMS-800 was

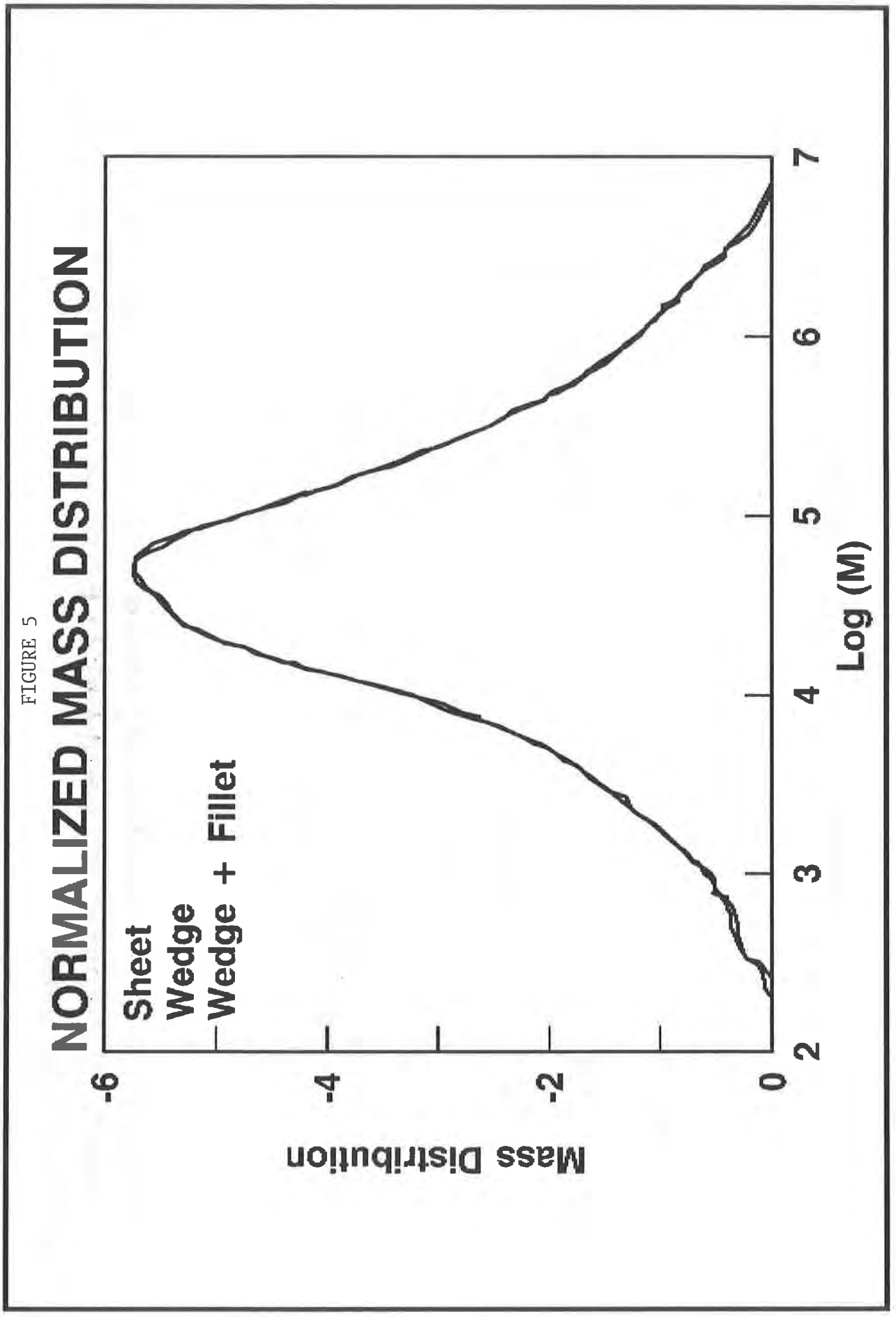
NORMALIZED MASS DISTRIBUTION
Sheet
Wedge
Wedge + Fillet
Mass Distribution
-6
-4
-2
0
2
3
4
5
6
7
Log (M)

FIGURE 5

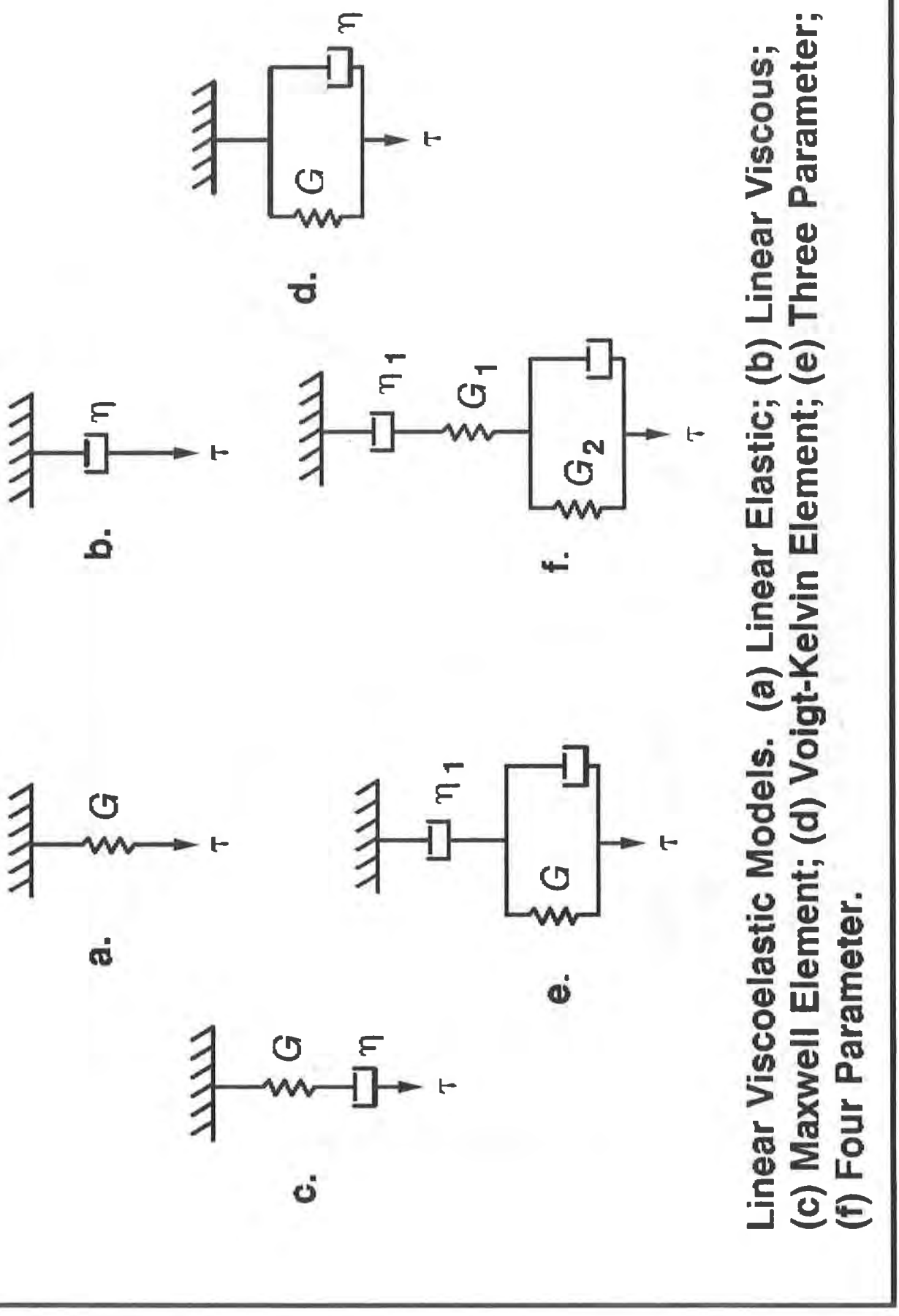

FIGURE 6

Linear Viscoelastic Models. (a) Linear Elastic; (b) Linear Viscous; (c) Maxwell Element; (d) Voigt-Kelvin Element; (e) Three Parameter; (f) Four Parameter.

used to collect this data.

Properties of viscoelasticity are important in the application of HDPE geomembranes because they are responsible for important design considerations such as elastic recovery below yield point, stress relaxation, and creep.

Stress relaxation, for example, means that the stresses in constant strains in the liner (such as bends and folds) will be relieved in time as viscous dissipation sets in. This is why with constant-strain stress crack testing (e.g., ASTM D1693, the bent strip test) the procedure is usually completed before 1000 hours. Beyond that time, the material has conformed to the bent condition and the stresses have dissipated. Here is one reason why extra slack, leading to more bends and folds, is better policy for synthetic liner installation than installing a liner which is too tight. In the one case the stresses are relieved in time through viscous dissipation. In the other case they may not be.

CONCLUSIONS

Crystallinities in the weld bead stabilized within four hours of welding. The standard deviation of four separate measurements over a two week period was less than the standard deviation of the separate measurements in Table 1. Figures 1 and 2 display melting point curves from the weld bead five hours and two weeks, respectively, after welding with the welding rod #609 sample.

No stresses which alter percent crystallinity were set up by either the sheet manufacturing or welding process. Standard deviations between melt cycles were no different than standard deviations between separate specimens.

The variation in crystallinity through the weld did not show a consistent trend. For the welding rod #607 sample, the crystallinity of the sheet appeared to increase because of contact with the welding action. Top and bottom sheet crystallinities underneath the weld bead were higher than sheet crystallinities away from the weld. Yet for the #609 sample, the top sheet underneath the weld bead was considerably less than the top sheet itself away from the weld.

In the hot wedge seam study thermal behavior of the polyethylene showed no significant differences in percent crystallinity due to welding heat history (see Table 5). Therefore, welding effects, if any, on the crystalline content of the sheet appear minimal, and not as significant as normal variation in percent crystallinity through the sheet.

Analyzing the molecular weight and rheological properties through the different heat histories of Samples A, B, and C we observe very little change, but there is a consistent trend. The heterogeneity index (Mw/Mn) increases with increasing heat history and so does viscosity at low shear. In addition, the loss tangent decreases with increasing heat history. The loss tangent decreases because the elastic storage modulus component increases with additional crosslinking faster than the viscous loss modulus does. These observations support what we would suspect, i.e., some branching, crosslinking, or rearrangement of polymer chains, occurring from the extra heat history.

Once again, however the effects of seaming in this study were quite minimal.

REFERENCES

1. Phillips 66 Co., Research Laboratories, Bartlesville, OK.
2. Rosen, Stephen L., Fundamental Principles of Polymeric Materials, pg. 272, John Wiley & Sons, New York, NY, 1982

Residual Stress Measurements in Geomembrane Sheets and Seams

A. E. Lord Jr.
Geosynthetic Research Institute, Drexel University, USA
R. M. Koerner
Geosynthetic Research Institute, Drexel University, USA
M. H. Wayne
Geosynthetic Research Institute, Drexel University, USA

ABSTRACT

By virtue of their manufacturing method and subsequent processing, it is very likely that geomembranes have some amount of residual stress at the time of their final field placement. The more crystalline is the polymer, the higher is the likelihood for such stresses, thus this paper is directed toward polyethylene geomembranes. While the long-term implications are unknown, a method to quantify residual stresses is necessary and is the focus of this paper.

An existing ASTM method for determining residual stresses in metals based on surface hole drilling and strain gage measurements has been adopted for geomembranes. A number of test sequences are reported in this paper on both sheet and seams. In general, it was found that the surface residual stresses in the sheets are about 1.4 MPa (200 lb/in^2), i.e. about 10% of yield stress, and are compressive at the surface of the sheets. When the sheets are annealed, this value decreased approximately 25% to 75%. Four types of fusion seams (extrusion flat, extrusion fillet, hot wedge, and hot air) were also investigated and these processes tend to reduce the stresses and in a few cases tension was measured. It was also significant to learn that the stresses vary for a long time after the hole is drilled which seems to illustrate the dynamic and complex behavior of residual stresses in polymers.

INTRODUCTION AND BACKGROUND

Residual stress (also called locked-in, inherent or self-stress) has been defined[1] as "the self-equilibrating internal stress existing in a free body when no external stresses are applied". Residual stresses arise during manufacturing and fabrication processes and also during installation procedures. Simply put, residual stresses arise when regions which have undergone different deformations (mechanically or thermally-induced) must match together.

At static equilibrium, the total force operating on any plane section cut through the system or body must be zero. That is,

$$\int \sigma_r \, dA = 0 \qquad (1)$$

where "σ_r" is the residual stress and "dA is" the element of area. The total moment of the forces on any section through the system must also be zero, i.e.,

$$\int dM = \int \sigma_r \, r \, dA = 0 \qquad (2)$$

where "dM"' is the element of moment and "r" is the position vector from the axis of rotation to the point of application of the stress. The application of Equations (1) and (2) leads to some of the most powerful methods for determining residual stresses of which many references, and even books, have been written (2-5).

In general, it has been observed that brittle materials are more susceptible to residual stress problems than ductile materials[3]. However, this may arise because the measurements are easier to obtain. Since this paper deals with geomembranes, which are extremely flexible in comparison to ceramics, glass, metals, etc., the phenomenon is likely to be quite complicated and difficult to measure. Even the unstressed reference state used for comparison of a measured value is quite elusive and probably unknown. Thus the problem is a formidable one.

Other than the work of Peggs[6], which is of a qualitative nature, there is no other study known to the authors on residual stress determination in geomembranes. The closest work seems to be that performed in the natural gas pipeline transmission area. The material is HDPE of a very similar nature to the geomembranes commonly used in geosynthetic engineering (with the exception of the lack of carbon black). Of course gas transmission pipelines are much stiffer than geomembranes due to their shape and thickness. Chaoui, et al [7] show that there can be quite large variations in the results for residual stresses determined by different techniques. The most reasonable results appear to be in the range 0.2-5.0 MPa (30-700 lb/in^2); the longitudinal residual stresses being somewhat higher than the circumferential stresses. These authors also monitored the released strain, due to cutting the sample, and found that a final value of the apparent residual stress was not reached until three months after the cutting. They state "this finding warrants a special effort to reconsider our vision of residual stresses in polyethylene pipe as a time dependent phenomenon". This is probably even more pertinent to the residual stress in a relatively flexible material like geomembranes. It is not known to what extent results from the HDPE natural gas pipe area will carry over (if at all) to the geomembrane area. The work is mentioned mainly because the authors feel they represent residual stress determination which is closest to the geomembrane area.

RESIDUAL STRESSES IN GEOMEMBRANES

The extrusion processing method of making semi-crystalline geomembranes can certainly give rise to the existence of residual stresses. The resin, along with its additives, is melted and forced through an extrusion die into a thin sheet. There are three variations commonly practiced in the manufacture of high density polyethylene (HDPE) sheet:

- Horizontal cast index extrusion produces a long strip which is approximately 450 mm wide and after placement is indexed through counter-rotating calenders into a continuous sheet while the next strip is being extruded. This system produces very wide sheet, up to 11 meters, of relatively thick gauge.

- Horizontal continuous flat extrusion produces full width sheet fed through counter-rotating calenders in a continuous manner. This system produces sheet

up to 5 meters in width at very controlled thicknesses.

- Vertical continuous circular extrusion produces a blown film that is stabilized, sized and lifted by air both inside the cylinder and on its outside. At the top of the cylinder it is folded over a horizontal bar, slit on its underside, opened and rolled onto the core. Systems of this type produce sheet from 5 to 11 meters in width in the entire range of geomembrane thicknesses.

The molten extrudate in all of the above processes leaves the die in a relatively stress free state until initial solidification occurs. Here the different extrusion processes described above can easily lead to the existence of some residual stresses. The subsequent step of calendering or drawing to the proper thickness, however, is where the residual stresses are likely to be mobilized to their maximum values. All three methods differ greatly in this respect. Cast index extrusion , continuous flat sheet extrusion and continuous blown film extrusion are so different in their extrudate ejection, extrudate placement, dwell time before sizing, method of sizing, cool-down procedure and final roll take-up that major differences might certainly be anticipated.

One way of possibly illustrating these differences in an indirect manner is to heat samples of the final sheets above their melting points and note their contraction during the process. Both the magnitude of the contraction and the degree of anisotropy appear to illustrate that residual stresses in geomembranes might be production dependent. It remains to be seen, however, what is the meaning and relevance of these differences.

Whatever the differences caused by the production of the geomembrane sheet, stress relaxation within the polymer structure can negate some, or all, of the potential long term effects. The entire area of stress relaxation has had very little focused research by the geosynthetics community. It is undoubtedly important insofar as field performance is concerned.

Irrespective of the in-situ residual stresses in the geomembrane sheets, the situation becomes further complicated when it comes to field seaming. Two very different seaming procedures (each with variations) are common in joining HDPE sheets. In one of the procedures, molten extrudate is placed on the roughened sheets to be joined. Heat flow, local melting and some material flow occur which produces the final bond upon cooling. There necessarily exists an enormous thermal gradient between the molten extrudate and the cold sheets. Figure 1(a) shows a thin film photomicrograph of such a weld produced by the flat extrusion process. The fillet extrusion process produces similar patterns. The residual stresses in the original sheet may be relieved, enhanced or be unaffected at various locations in the seamed region. Fusion seaming is the other type of process used to join HDPE sheet. Here a hot wedge, hot air or ultrasonic wave pass between the sheets to be joined and actually melts the opposing surfaces. A set of nip rollers follows closely behind which forces the sheets together until the area is adequately cool to support itself. The nip rollers actually squeeze some of the molten sheet material out from the pressurized area forming very complex flow lines. Figure 1(b) shows a thin film micrograph of a hot wedge seam.

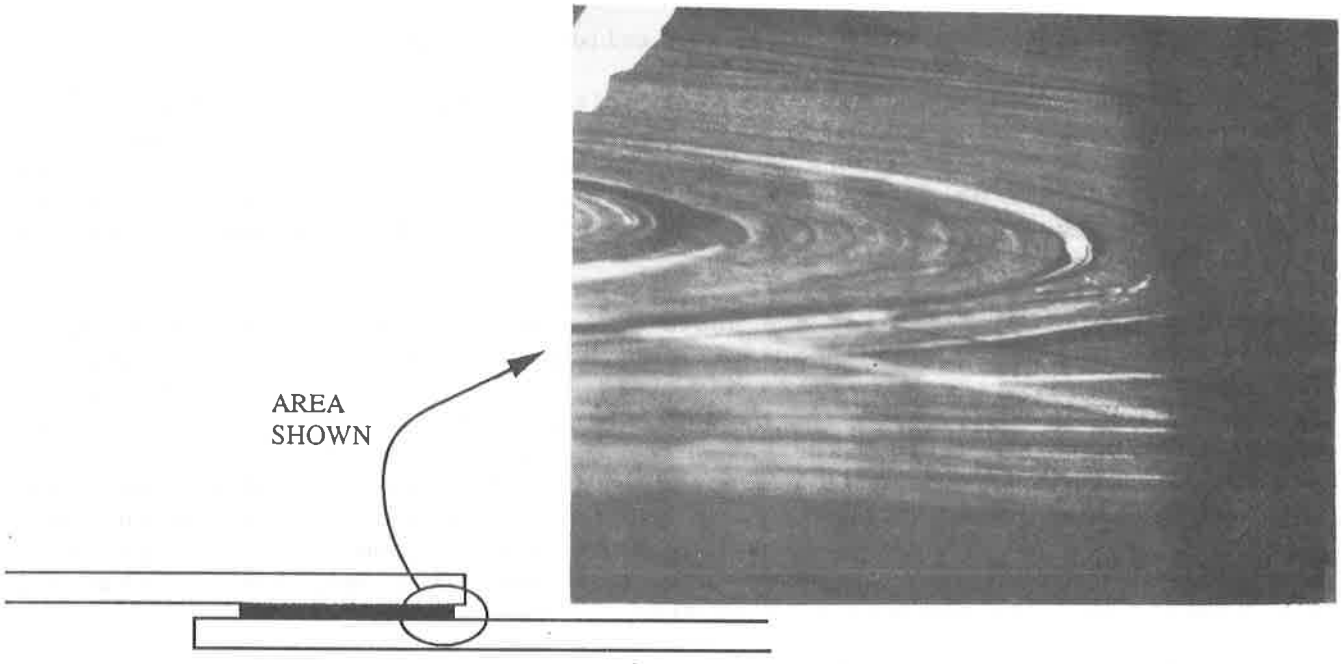

(a) Thin Film Cross Section of Extrusion Flat Seam (50 X)

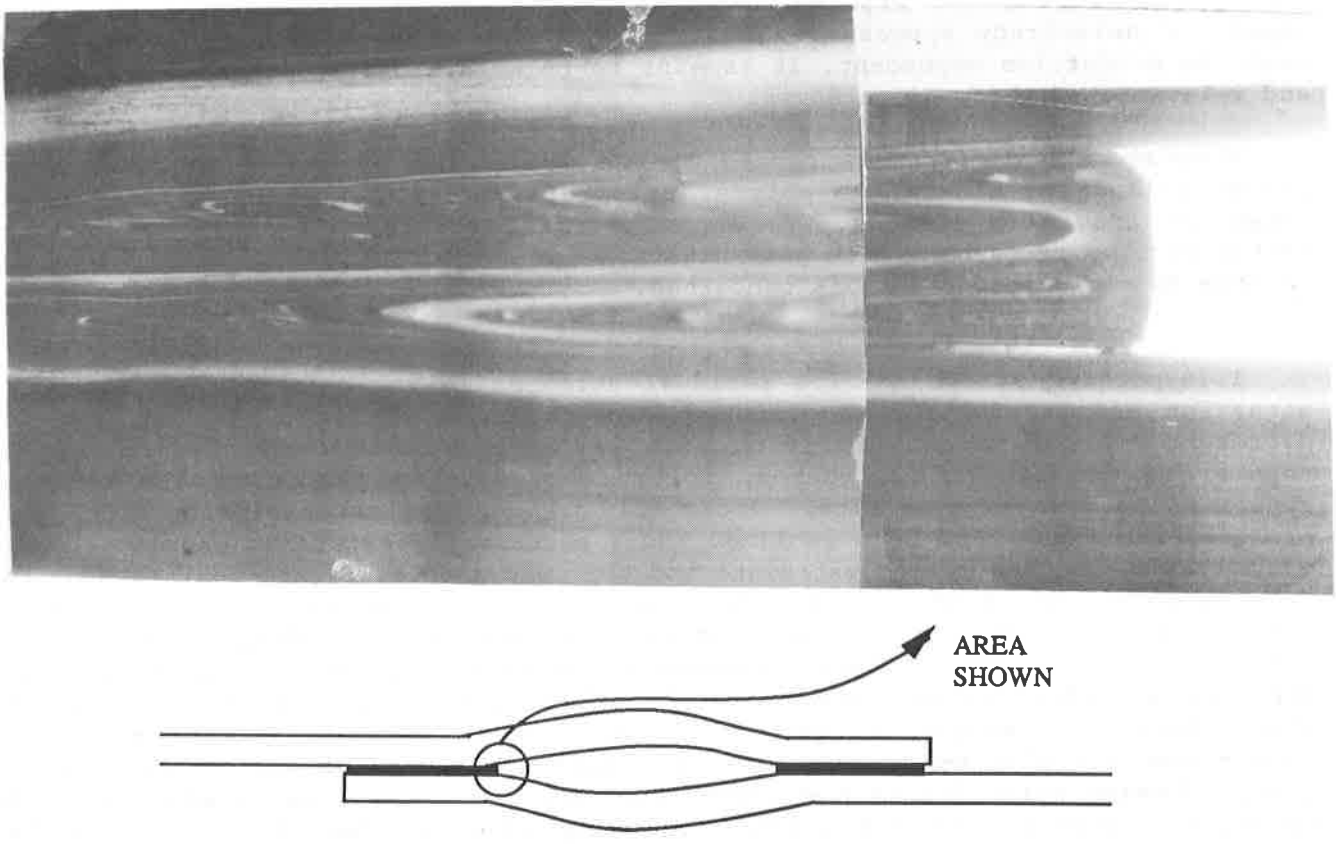

(b) Thin Film Cross Section of Hot Wedge Seam (50 X)

Fig. 1 TYPICAL FLOW PATTERNS THAT EXIST IN HDPE GEOMEMBRANE SEAMS

Quite clearly the photographs of Figure 1 illustrate that an already complex situation of residual stresses in geomembrane sheets can be radically modified in the seamed region. Whatever are these implications, it is necessary to determine the magnitude and type of residual stresses in a quantifiable manner. Only then can one begin to evaluate the potential impact of their existence.

METHODS OF MEASURING RESIDUAL STRESSES

While there are several nondestructive evaluation methods to determine residual stresses (e.g., X-Ray diffraction, ultrasonic velocity and magnetic effects), their application to geomembranes seems quite remote. Destructive methods whereby the residual stresses are relieved and a distortion occurs seem to be considerably more promising. To illustrate how this might occur consider the horizontal plate illustrated in Figure 2. The imaginary springs within the plate are meant to illustrate the residual stresses which are shown on the top and bottom springs as compression and as tension in the center spring. If some of the material on the top side of the plate were carefully removed, the compression stresses on the bottom spring would be relaxed and transmit some to the center spring which would tend to go into a more compressed state. The result would be an upward curling, or bending, of the plate as shown in the lower sketch. Both remaining springs would have to come to equilibrium with one another as suggested in equations 1 and 2. This concept allows for a number of destructive test methods which have been used to determine residual stresses, both their quantity and their sign. (Note that throughout this paper conventional mechanics --- of tension being positive and compression being negative will be used, i.e. geotechnical engineering sign convention will not be used).

The destructive testing methods used to determine residual stresses use strain gages mounted on the specimen and then proceed to either cut strips or slits, or drill holes to relieve the stresses. The resulting strains are then used with linear elasticity to determine the original residual stress. We will use the hole drilling method since neither strips nor slits are possible with flexible and thin materials like geomembranes.

THE HOLE DRILLING/STRAIN GAGE TECHNIQUE

The technique of hole drilling to relieve residual stresses with simultaneous sensing of relieved strains was originated by Mather [8] in the 1930's. While he used mechanical extensometers, the technique currently uses strain gages. In this technique a very small hole is drilled into the surface of the material in the vicinity of the strain gage(s). The surface residual stress in the plane of the sample can be determined from the measured relief strains and a calibration under a known single load or by comparison to Kirsch's appropriate elastic theory solution when the geometry is applicable [9]. There is an ASTM Standard Test Method for its use in measuring residual stresses in metals [10].

Figure 3 presents the usual configuration where the various parameters are defined as follows:

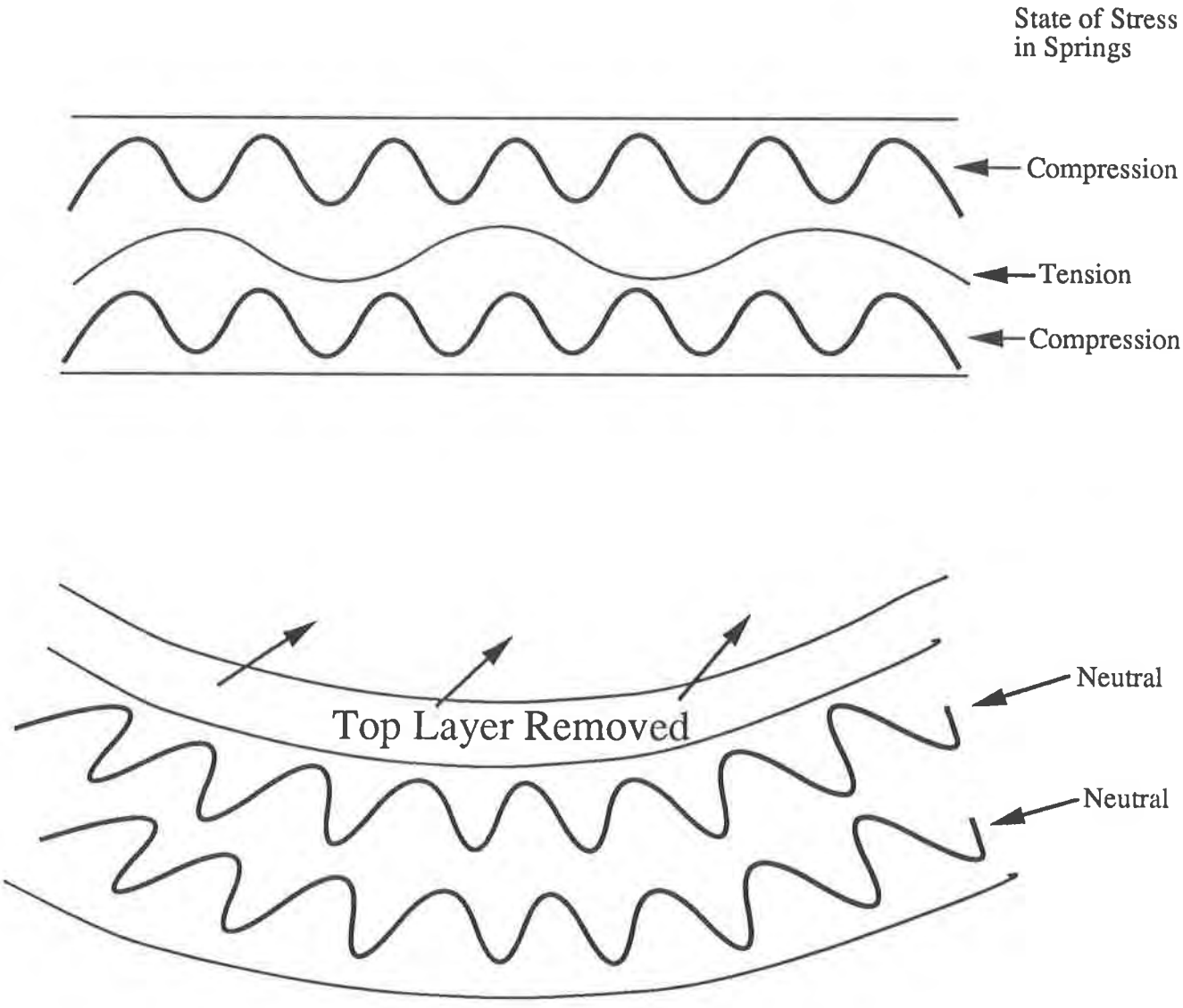

Fig. 2 - Spring Analogy Applied to Residual Stress Determination in a Plate, Modified from Baldwin. (4)

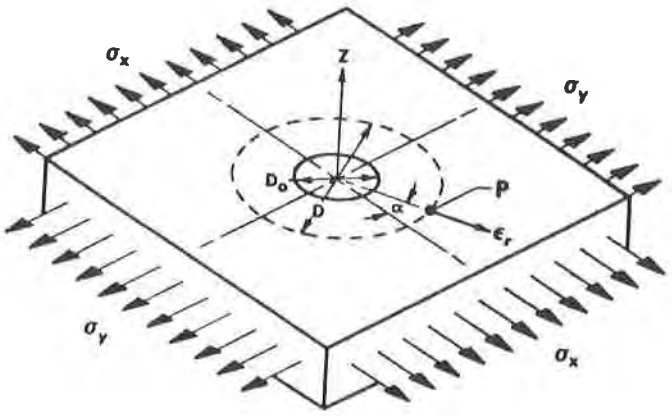

Fig. 3 - Generalized Residual Stresses Acting on a Membrane and Definition of Symbols

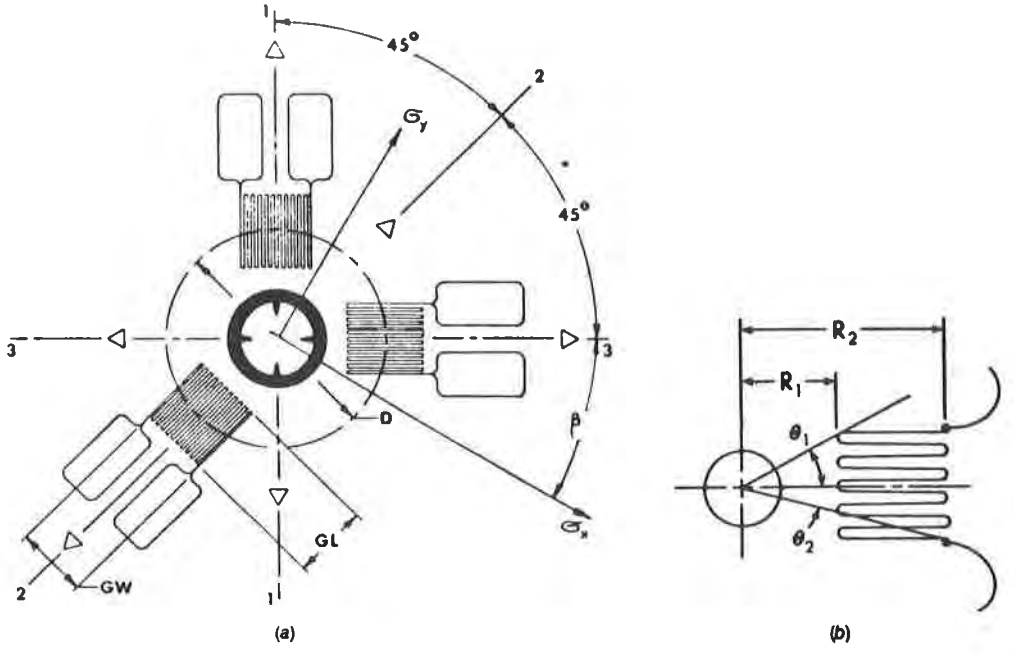

Fig. 4 - General Strain Gage Rosette Layout for Hole Drilling Method Showing (a) Typical Configuration and (b) Detail of a Single Gage

ε_r = radial strain relieved at point P,

$$A = -\frac{1+\mu}{2E} \times \frac{1}{r^2}, \quad (3)$$

$$B = -\frac{1+\mu}{2E}\left(\frac{4}{1+\mu} \times \frac{1}{r^2} - \frac{3}{r^4}\right), \quad (4)$$

σ_x, σ_y = principal stresses present in the structure before drilling,

α = angle between the directions of ε_r and σ_x,

E = Young's modulus,

μ = Poisson's ratio,

$$r = \frac{D}{D_0} \text{ (see Fig. 3)}, \quad (5)$$

D = diameter of gage circle, and

D_0 = diameter of drilled hole.

The relieved surface strain is related to the principal stresses which are relieved by the following equation:

$$\varepsilon_r = (A + B \cos 2\alpha)\, \sigma_x + (A - B \cos 2\alpha)\, \sigma_y \quad (6)$$

Measuring the relieved strains ε_1, ε_2 and ε_3 at three points P_1, P_2 and P_3, respectively, provides sufficient information to calculate the principal stresses σ_x and σ_y and their orientation a with respect to an arbitrarily selected reference. It is assumed that the stress variations in the x and y directions are small and that the variation within the depth of the hole is negligible.

If the strain gages are placed as shown in Figure 4, the analysis for σ_x, σ_y and α becomes quite straight forward. The resulting equations follow:

$$\sigma_x = \frac{(\varepsilon_1 + \varepsilon_3)}{4A} + \frac{\sqrt{2}}{4B}\sqrt{(\varepsilon_1 - \varepsilon_2)^2 + (\varepsilon_2 - \varepsilon_3)^2} \quad (7)$$

$$\sigma_y = \frac{(\varepsilon_1 + \varepsilon_3)}{4A} + \frac{\sqrt{2}}{4B}\sqrt{(\varepsilon_1 - \varepsilon_2)^2 + (\varepsilon_2 - \varepsilon_3)^2} \quad (8)$$

$$\tan 2\alpha = \frac{\varepsilon_1 + \varepsilon_3 - 2\varepsilon_2}{\varepsilon_3 - \varepsilon_1} \quad (9)$$

It should be noted that strain gage rosettes especially designed for this technique are available from several commercial suppliers.

This type of arrangement will be used in the work to follow for an evaluation of

residual stresses in HDPE geomembrane sheet and seams.

STRAIN GAGE BONDING, CALIBRATION AND HOLE DRILLING

The strain gage rosettes were bonded to the surface of the HDPE geomembrane sheet and seams at the desired location where the residual stresses were to be determined. The procedure used was as follows:

- The surfaces were rubbed with #100 sandpaper to remove the surface oxides and waxes.
- The areas were then cleaned with trichlorethylene which was allowed to evaporate.
- The gages were bonded with Eastman 910 bonding agent.
- The bonded gages were allowed to cure for at least 30 minutes, see Figure 5(a).

In order to verify the adequacy of the bonding, several geomembranes were tested in wide width tension and the gages gave reasonable values of strain and modulus up to the yield of the material, see Figures 5(b).

As noted previously, the constants A and B require determination either experimentally or theoretically. When both can be done (as in our situation) a check can be performed as a calibration procedure. To determine A and B experimentally one begins with a strain gaged geomembrane which is in a relatively residual stress free state and applies a known uniaxial stress, σ_c, see Figure 5(b). The strains ε'_1 and ε'_3 are determined under a known load. Then a hole is drilled at the center of the strain gage rosette (see Figure 6) and the new values ε''_1 and ε''_3 are determined under the same load. The constants A and B are determined as follows (from reference 10):

$$A = \frac{(\varepsilon_1)_{cal} + (\varepsilon_3)_{cal}}{2\,\sigma_c} \tag{10}$$

$$B = \frac{(\varepsilon_1)_{cal} - (\varepsilon_3)_{cal}}{2\,\sigma_c} \tag{11}$$

where

$$(\varepsilon_1)_{cal} = \varepsilon''_1 - \varepsilon'_1 \tag{12}$$

$$(\varepsilon_3)_{cal} = \varepsilon''_3 - \varepsilon'_3 \tag{13}$$

The best results achieved from a number of tests (using E = 689 MPa and m = 0.4) were:

$$A_{expt} = -0.12 \times 10^{-6}\,(kPa)^{-1}$$

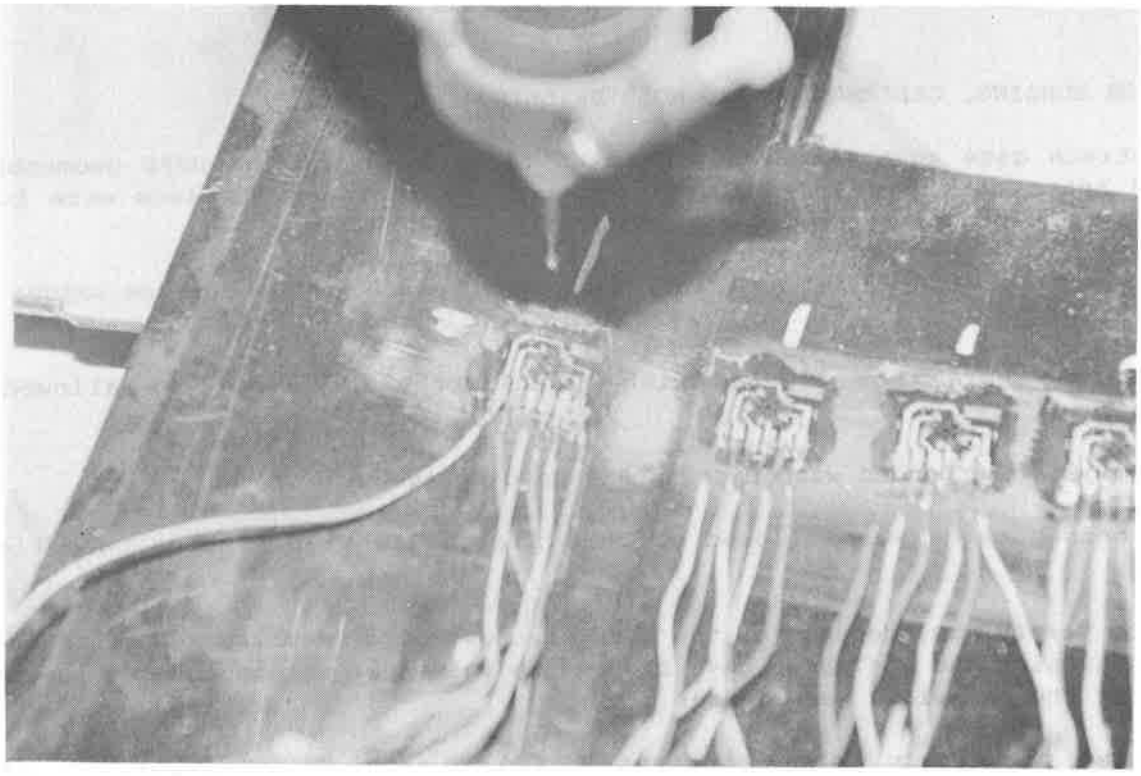

Fig. 5(a) - Detail of Strain Gage Rosettes Bonded to HDPE Geomembrane

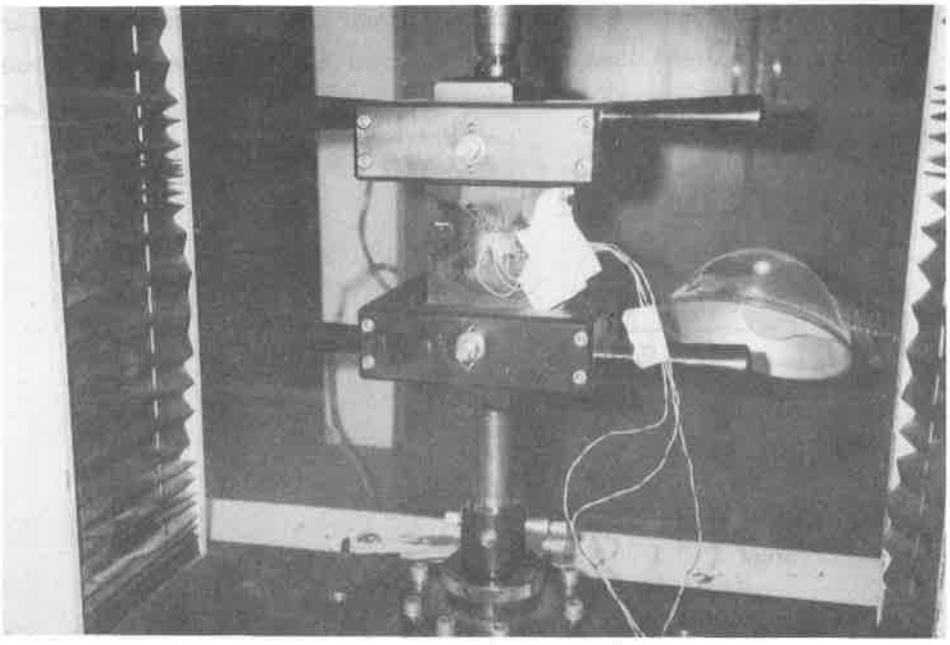

Fig. 5(b) - Calibration Testing of HDPE Sheet with Strain Gages Attached

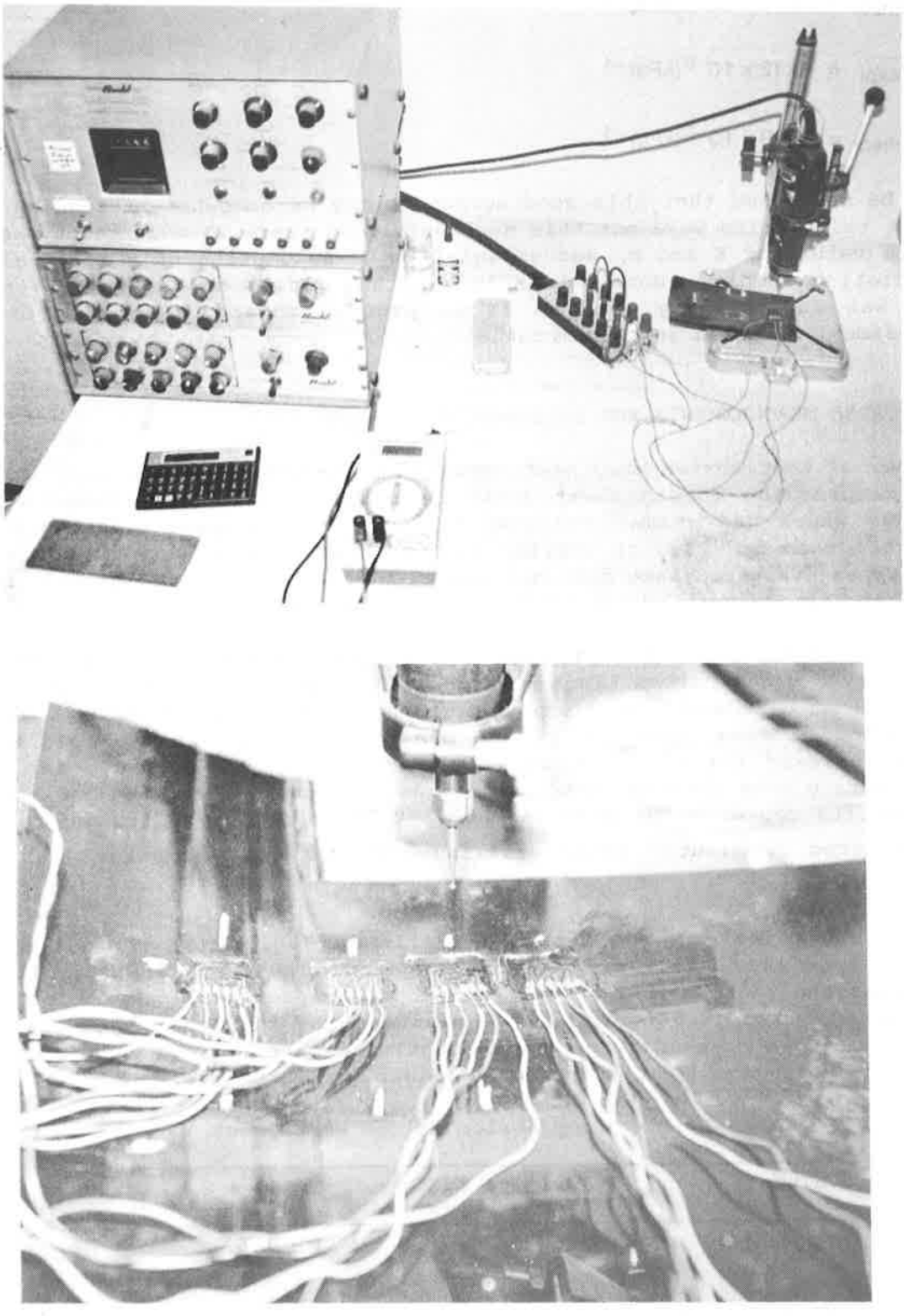

Fig. 6 - Method of Hole Drilling and Strain Gage Readout System

$$A_{theor} = -0.10 \times 10^{-6} (kPa)^{-1}$$

$$B_{expt} = -0.12 \times 10^{-6} (kPa)^{-1}$$

$$B_{theor} = -0.29 \times 10^{-6} (kPa)^{-1}$$

It should be mentioned that this good agreement may be somewhat misleading for all attempts at calibration were not this successful and there is uncertainty as to the appropriate values of E and m, and especially the assumption of a residual stress free calibration sample. Nonetheless it was the opinion of the authors that the agreement was sufficiently good so as to proceed towards measuring of actual surface residual stresses in geomembranes.

RESIDUAL STRESS MEASUREMENTS AND TEST RESULTS

A number of test series were performed in the course of this study. The first was in a compression molded sheet (with no seam). This was followed by actual geomembranes which had seamed regions. Thus the strain gage rosettes could be placed on the seam and then at varying distances away from it on the sheet. The four seam types evaluated were dual hot wedge, flat extrusion, fillet extrusion and hot air. Each forms a test series making a total of five.

Test Series 1 - Compression Molded Sheet - This test series utilized HDPE pellets (density = 0.948 g/cc; carbon black = 2.3%; melt index = 0.15 g/10 min) to form a 150 mm by 150 mm size and 5 mm thick sheet. The material was melted at 200 deg C for 30 minutes under a pressure of 4.0 MPa. The heat was turned off and slow cooling was allowed for 12 hours under a pressure of 0.4 MPa. As with all the tests, the strain gage rosettes were mounted as previously described and a hole was drilled into its center. The hole was about 0.75 mm deep. The strains ε_1, ε_2 and e_3 were measured 30 minutes after drilling and the residual stress values were calculated accordingly.

The results are given for two separate trails in Table 1(a) where compressive stresses of approximate 10% of yield were measured. (Comparison of #1 and #2 probably gives the reproducibility of the method.) A separate sample prepared the same way was annealed at 80 deg C for 7 days and the results are given in Table 1(b). Here it can be seen that the residual stresses are reduced considerably, but are not relaxed to zero, i.e., they remain slightly compressive.

Table 1(a) - Compression Molded HDPE Sheet

Value	Trial # 1	Trial # 2
σ_{max} (MPa)	- 1.50	- 1.82
σ_{min} (MPa)	- 1.42	- 1.59
α (degrees)	22	12

Table 1(b) - Compression Molded Sheet Annealed at 80 deg C for 7 days

Value	Trial # 3
σ_{max} (MPa)	- 1.18
σ_{min} (MPa)	- 0.24
α (degrees)	12

Test Series 2 - Dual Hot Wedge Seam and Sheet - This test series consisted of residual stress measurements on the air channel of a dual hot wedge seam, on one of the tracks and then several measurements on the sheet material at gradually increasing distances from the edge of the outer track. Table 2(a) gives the first set of data at time zero (i.e., after the hole was drilled) and at a 30 minutes delay after the hole was drilled. The results are again seen to be compressive and of a similar magnitude as the compression molded sheet previously discussed. Surprisingly, the seamed region (both on the air track and directly on the seam) did not have significantly lower stresses than the sheet material. After 30 minutes there was a reduction of stresses but only slightly. The tensile value at 30 minutes cannot be explained.

This sequence of tests was repeated with the new data given in Table 2(b). For the most part the stresses are slightly lower, however still compressive. Once again, a tensile stress is observed in the air channel between seams and some very low values away from the seam. The reasons for the differences are not known particularly considering that the lines were taken only 75 mm apart.

Table 2(a) - Dual Hot Wedge Seam

Value @ 0 min	Air Channel	Over Track	12 mm Away	37 mm Away	62 mm Away
σ_{max} (MPa)	- 1.31	- 1.27	- 1.67	- 1.55	- 1.47
σ_{min} (MPa)	- 0.63	- 0.90	- 0.81	- 0.63	- 0.51
α (degrees)	16	- 40	22	14	32
Value @ 30 min	**Air Channel**	**Over Track**	**12 mm Away**	**37 mm Away**	**62 mm Away**
σ_{max} (MPa)	+ 1.37	- 0.79	- 1.15	- 1.20	-1.40
σ_{min} (MPa)	- 1.00	- 0.67	- 0.50	- 0.25	-0.36
α (degrees)	8	23	20	- 17	44

Table 2(b) - Dual Hot Wedge Seam (75 mm From Table 2(a) Values)

Value @ 0 min	Air Channel	Over track	12 mm Away	37 mm Away	62 mm Away
σ_{max} (MPa)	- 0.64	-	- 0.74	- 1.03	-1.68
σ_{min} (MPa)	- 0.42	-	- 0.44	- 0.52	-0.77
α (degrees)	- 33	-	25	45	23
Value @ 30 min	**Air Channel**	**Over track**	**12 mm Away**	**37 mm Away**	**62 mm Away**
σ_{max} (MPa)	+ 0.09	-	- 0.59	- 0.77	-2.48
σ_{min} (MPa)	- 0.52	-	- 0.13	- 0.04	-1.69
α (degrees)	- 23	-	0	42	34

Test Series 3 - Extrusion Flat Seam - This third test series examined the residual stress on the sheet directly above an extrusion flat seam and at a distance of 100 mm away from the seam. Data was taken directly after hole drilling and then 30 minutes later. Table 3 gives the results of these tests where all stresses are again compressive but unlike the previous hot wedge data, the stresses are now higher at the seam than they are a distance away. The data suggests that the stresses relaxed somewhat in the 30 minute tests after hole drilling.

Table 3 - Extrusion Flat Seam

Value @ 0 min	Above Seam	100 mm Away
σ_{max} (MPa)	- 1.80	- 0.90
σ_{min} (MPa)	- 1.17	- 0.39
α (degrees)	0	45
Value @ 30 min	**Above Seam**	**100 mm Away**
σ_{max} (MPa)	- 1.07	- 0.63
σ_{min} (MPa)	- 0.38	- 0.45
α (degrees)	- 30	19

Test Series 4 - Extrusion Fillet Seam - Duplicating the previous test series but now with an extrusion fillet seam data was taken immediately adjacent to the seam and at 100 mm away from the seam on the geomembrane sheet. Table 4 presents the data where residual stresses are all compressive. The 30 minute dwell time had the effect of relaxing the stresses a slight amount.

Table 4 - Extrusion Fillet Seam

Value @ 0 min	Adjacent to Seam	100 mm Away
σ_{max} (MPa)	- 0.72	- 0.08
σ_{min} (MPa)	- 0.81	- 1.11
α (degrees)	6	- 38
Value @ 30 min	**Adjacent to Seam**	**100 mm Away**
σ_{max} (MPa)	- 0.32	- 0.11
σ_{min} (MPa)	- 0.63	- 0.94
α (degrees)	17	- 27

Test Series 5 - Hot Air Seam - Unlike the other seamed samples which had been made weeks or months before testing, this test series was on a hot air seam made only hours after it was fabricated. Data was taken immediately after the hole was drilled and then again after 30 minutes. Strain gage rosettes were placed directly above the seam and at 100 mm away from it. The data of Table 5 shows that the sheet was again in compression but that the seamed region was in tension. The effect remained for the 30 minutes after the hole was drilled.

Table 5 - Hot Air Seam (Recent Fabrication)

Value @ 0 min	Above Seam	100 mm Away
σ_{max} (MPa)	+ 0.83	- 0.73
σ_{min} (MPa)	- 0.57	- 1.21
α (degrees)	23	5
Value @ 30 min	**Above Seam**	**100 mm Away**
σ_{max} (MPa)	+ 0.87	- 0.27
σ_{min} (MPa)	- 0.34	- 1.08
α (degrees)	28	5

DISCUSSIONS AND CONCLUSIONS

It appears that by using the hole drilling/strain gage technique we are obtaining reasonable values for the surface residual stresses in bulk geomembranes and various geomembrane seam types. These apparently are the first indication of the magnitude of these residual stresses and hence are of some interest to designers of facilities utilizing geomembranes. Certainly these are preliminary

values and subject to many sources of error, but at least a start has been made.

The values only apply to the average residual stresses in a depth of about 0.75 mm below the surface. It will be much more difficult if not impossible, to obtain the very important depth variation of the residual stresses in the geomembrane and geomembrane seams.

Compressive residual surface stresses of the order of 5 to 10% of yield are consistently observed in all types of HDPE geomembranes investigated in this study. The surface residual stresses in the seamed area are much more complicated. Although they are of the same general magnitude as the bulk compressive stresses, the stresses in the seams are quite often tensile. If measurements are made long enough, after drilling, the sign of the seam stresses is almost always tensile.

As mentioned earlier, no care was taken in determining either the age of the bulk material or the age of the weld. The very brief study of the hot air seaming indicates in a preliminary fashion that the stress relief must be quite rapid after welding. [It is important to note that in welding of steel plate, for example, very often residual stresses in the weld area approach the yield stress of the steel (1-5).]

In the authors' opinion it is probably not prudent to pursue further the measurement of residual stresses in geomembranes, due to all of the difficulties and uncertainties involved in such measurements.

REFERENCES

1. Residual Stresses and Stress Relaxation, ed. by E. Kula and V. Weiss, Proc. of 28th Sagamore Army Materials Research Conf., Lake Placid, NY, July 13-17, 1981, Publ. by Plenum Press, New York, 1982, pp. 1-2.

2. Residual Stress Measurements, R. G. Trueting, J. J. Lynch, H. B. Wishart and D. G. Richards, from ASM 33rd National Metal Congress and Exposition, Detroit, October 15-19, 1951, published by Amer. Soc. for Metals, Cleveland, Ohio, pp. 4-5.

3. Evaluation of Residual Stresses, K. Heindlhofer, 1948, McGraw Hill, New York.

4. W. M. Baldwin, Jr., "Residual Stresses in Metals," Proc. ASTM 49, (1949), pp. 539-586.

5. Residual Stress, I. C. Noyan and J. B. Cohen, Springer-Verlag (Materials Research and Engineering Series), 1987.

6. I. D. Peggs and D. S. Carlson, "Examination of the Microstructure of Geomembranes and Geomembrane Seams by Light Transmission Microscopy," Proc. 4th Int'l. Conf. on Geotextiles, Geomembranes and Related Products, The Hague, 28 May - 1 June 1990, A. A. Balkema Publishers, Rotterdam (1990), p. 500.

7. K. Chaoui, A. Moet and A. Chudnovsky, "Residual Stress Analysis in Fuel Gas Pipes," Proc. 10th Plastic Fuel Gas Pipe Symp., New Orleans, LA, Oct. 27-29, 1987, pp. 316-323.

8. J. Mathar, "Determination of Metal Stresses by Measuring the Deformation Around Drilled Holes," Trans. ASME 86, (1934), pp. 344-358.

9. G. Kirsch, V.D.I., Vol. 42 (1898).

10. "Standard Test Method for Determining Residual Stresses by the Hole-Drilling Strain Gage Method," ASTM Designation: E 837-85, Annual Book of Standards, Vols. 03.01.

Determination of Long-Term Tensile Strength of Geosynthetics: A State-of-the-Art Review

Tony M. Allen
Washington State Department of Transportation, USA

ABSTRACT

Designers of geosynthetic reinforced structures must be assured that long-term stresses in the reinforcement do not exceed the strength of the reinforcement at any time during the design life of the structure. Currently available methods for determining long-term geosynthetic strength are reviewed and discussed. Mechanisms of degradation and aging of geosynthetics in-service are reviewed in detail. Other factors which affect the selection of the long-term strength to be used for design, such as the geosynthetic macrostructure, type and location of connections, type of design procedure used, and type and criticality of the structure are also discussed. Finally, recommendations are made regarding design procedures appropriate for the determination of long-term strength and areas of research needed.

INTRODUCTION

Geosynthetics function as soil reinforcement in applications such as reinforced embankments and slopes, and geosynthetic walls. Geosynthetics have been used in such applications, though infrequently at first, for over 15 years. Early use was limited to either temporary or relatively short design life permanent applications which were noncritical in nature. Due to the cost effectiveness of geosynthetic structures, their use by designers and owners has grown significantly in recent years, not only in numbers of structures, but also in criticality and structure design life. Hence, recent efforts regarding such structures have been focused on the development of more thorough approaches to quantifying long-term tensile strength, as this issue has been a weak link in geosynthetic reinforcement design.

The current state-of-practice regarding the issue of long-term strength varies widely among designers from no consideration at all to total exclusion of cost effective geosynthetic structures as an option. Design methods and standards regarding long-term strength recently documented in the literature generally incorporate a partial factor of safety approach, with each partial factor of safety accounting for a different strength degradation mechanism (8, 30, 32, 55). The most notable of these standards are those developed by AASHTO-AGC-ARTBA Task Force No. 27 and standard GG4 developed by the Geosynthetic Research Institute at Drexel University. However, the scope of these documents is limited, which can lead to confusion on how to apply them to the many situations encountered by designers.

The degradation mechanisms which affect long-term geosynthetic strength are reviewed and discussed in terms of what is known from recent research and in terms of the framework established by these recently documented design methods and standards. Based on this review and discussion, a rational approach to determining long-term design strength of geosynthetics for all reinforcement applications is presented. Variables addressed by this approach include ultraviolet light degradation, installation damage, creep, chemical aging, and biological degradation, type, design life, and criticality of the structure, geosynthetic macrostructure, type and location of connections, and type of design procedure used. Areas where research is needed to adequately assess the effect a given variable has on long-term geosynthetic strength are also presented and discussed.

GEOSYNTHETIC STRUCTURE VARIABLES

Geosynthetic structure variables include criticality and type of structure, and type of design procedures used. Tensile strength computation procedures become more rigorous as criticality of a structure increases. The difference between a critical and noncritical structure should be assessed by the engineer or may be set by regulatory authority. Guidelines for assessing criticality of a structure are presented in Table 1. Note that the categories are subjective and sound engineering judgement is required.

The guidelines set in Table 1 can be adjusted somewhat if a well defined performance monitoring program which will produce an early warning of failure is implemented for the structure. Also note that geosynthetic reinforced embankment applications are almost always temporary in nature, as the geosynthetic is only needed until the soil has consolidated and gained strength. Therefore, limitations for embankments in permanent applications are not shown.

Table 1. Definition of Criticality of Geosynthetic Reinforced Structures (Adapted from Allen and Holtz, 1991).

APPLICATION	Noncritical and Temporary*	Noncritical and Permanent*
Structure Design Life	< or = 5 years	< or = 50 years
Maximum Structure Height Embankment Reinforced Slope Retaining Wall	 7 m 15 m 15 m	 n/a 5 m 5 m
Soil Chemistry	3 < pH < 10	chemically neutral: 6 < pH < 8 and low concentrations of deleterious chemicals
Average Soil Temperature	< or = 20°C	< or = 20° C
Risk of Loss of Life if Failure Occurs	----	low
Loss of Services and/or Economic Loss if Failure Occurs	----	minimal
Reinforced Soil Structure Supports Other Structures	no, unless other structures are temporary and noncritical	no

* Geosynthetic structure applications not meeting these requirements should be considered critical.

The tolerance of each type of geosynthetic structure to deformation and/or failure of the reinforcement may influence the design strength selected. For example, relatively rigid concrete faced walls can tolerate less deformation than relatively flexible reinforced embankments, with reinforced slopes somewhere in between. Intuitively, long-term deformations resulting from creep and loss of strength in the geosynthetic reinforcements must be considered when designing these structures. The amount of deformation which can be tolerated may directly affect the long-term strength level selected.

However, limit equilibrium methods, which cannot predict deformations, are used for the design of most geosynthetic reinforced structures. The most common method of dealing with the deformation issue is to limit the applied reinforcement load to insure that the 5 percent reinforcement strain level is not exceeded (55). Yet, strain measured in geosynthetic walls designed with limit equilibrium techniques has generally been less than 1 percent (5, 15, 53), indicating that these designs are conservative. This conservatism appears to be attributable to the stability analysis technique, soil strength parameters, and the geosynthetic tensile properties used for design. It is common practice to use in-isolation (i.e., in-air) geosynthetic modulus values to calculate the load at 5 percent strain rather than in-soil modulus values. Doing this could result in design modulii which are too low, resulting in a prediction of reinforcement strain which is too high. Furthermore, it is common practice to select design soil strength parameters conservatively and to use factors of safety applied to the calculated reinforcement load of 1.2 for temporary structures to 1.5 for permanent structures (3, 43). Provided such measures are taken, it appears unwarranted at this time to limit the reinforcement design load to the load at the 5 percent strain level based on the previous experience just cited, at least for walls and slopes. Measured strains in geosynthetic reinforced embankments have been on the order of 5 percent or more (49). Therefore, limiting the strain in the reinforcement to the 5 percent level is warranted to insure serviceability of reinforced embankments. Much research is needed in this area.

GEOSYNTHETIC MATERIAL VARIABLES

Geosynthetic material variables include ultraviolet light degradation, installation damage, creep, chemical aging, biological degradation, geosynthetic macrostructure, and geosynthetic connections. The effect of these variables on long-term geosynthetic strength is represented in equation form as follows (32):

$$S_a = \frac{S_{ult.}}{FS_{UV} \times FS_{ID} \times FS_{CR} \times FS_{CA} \times FS_{BD} \times FS_{SM} \times FS_{JCT}} > T_{applied} \qquad \text{(EQ.1)}$$

where,

S_a = allowable long-term geosynthetic strength;
$S_{ult.}$ = ultimate wide-width strength of geosynthetic;
$T_{applied}$ = tension applied to geosynthetic;
FS_{UV} = partial factor of safety for ultraviolet light degradation;
FS_{ID} = partial factor of safety for installation damage;
FS_{CR} = partial factor of safety for creep;
FS_{CA} = partial factor of safety for chemical aging;
FS_{BD} = partial factor of safety for biological degradation;
FS_{SM} = partial factor of safety for strength reductions due to seams and connections;

FS_{JCT} = partial factor of safety to account for effect of junction strength of grid structures.

Since geosynthetics will typically be buried in soil or covered, strength loss due to UV degradation occurs only at the beginning of the structure design life. Strength loss due to installation damage also occurs only at the beginning of the structure design life. The partial factor of safety for seams and connections account for stress concentrations in the geosynthetic which reduces its ultimate strength. The partial factor of safety for junction strength accounts for long-term soil/geosynthetic interaction. Strength loss due to creep, biological degradation, and chemical aging are losses which can occur throughout the life of the structure. These potential strength losses are discussed for the three most common geosynthetic polymers in use today, namely polypropylene (PP), polyethylene (PE), and Polyester (PETP).

Factor of safety ranges are presented for each degradation mechanism based on the strength loss data and recommendations presented by various researchers. The ranges of safety factors presented are designed for use in noncritical applications in soils which are chemically neutral at average in-soil temperatures of 20° C or less. Product specific scientific data appropriate for the expected soil environment should be obtained for critical applications. The type of scientific data needed is discussed for each degradation mechanism.

Ultraviolet Light Degradation. If a geosynthetic is left exposed to sunlight during the structure's design life, ultraviolet light (UV) degradation must be considered. Though soil burial does stop UV exposure, there is some evidence to suggest that extended exposure to UV light before soil burial may accelerate geosynthetic degradation processes in soil (28). Therefore, exposure to UV light before soil burial should be minimized.

UV degradation is a photo-oxidative process which attacks only the surface of the polymer fibers (63). Chain scissions within the polymer occur, resulting in material embrittlement and eventual failure (50). Degradation is a function of fiber thickness, polymer type, and presence of stabilizers such as carbon black. The type, amount, and distribution of stabilizer controls resistance. Rate of degradation is a function of radiation intensity, which is affected by both geographic location and elevation, and temperature (50). Van Zanten (57) provides an excellent summary of the types of UV stabilizers used and how they function.

Polyolefins are especially susceptible to UV degradation and must be protected either chemically or physically. Carbon black, which effectively shades the oxidation-prone molecules, is the most common method of protecting polyolefins. Polyesters are not as prone to photo-oxidation but may suffer moderate strength loss, depending on the choice of pigments used in the polymer (26).

Specific test results for a number of geotextiles exposed to UV light degradation has been reported by Raumann (46). The geotextiles tested varied in thickness, polymer type, and degree of UV stabilization. The results demonstrate the variability among products and the need to assess resistance on a product by product basis. Strength losses due to UV degradation for extruded high density polyethylene (HDPE) geogrids have been found to be much less than for geotextiles due to their great filament thickness (63). Wrigley (63) presents long-term

weathering data for HDPE and PP grids which show that some geogrids will provide acceptable strength retention when exposed for 50 years or more.

The most common method of evaluating susceptibility to UV degradation is an accelerated weathering test. ASTM D-4355 is the most widely used test method and covers both UV light exposure and exposure to water. A total exposure time of 500 hours in a weatherometer, per ASTM D-4355, with a strength retention of 90 percent is typically the highest level of resistance manufacturers will certify to today. This level of resistance is, in general, recommended for geosynthetic structures where the geosynthetic will be exposed to sunlight for more than five years. Less strength retention after 500 hours could be acceptable for shorter design life applications, but generally not less than 70 percent. There is not a direct correlation between weatherometer exposure time and outdoor exposure time for all geosynthetics. This correlation must be made for accurate long-term weathering resistance prediction.

It is recommended that UV degradation be considered in determination of design tensile strength. A partial factor of Safety of 1.0 can typically be utilized if manufacturers' recommendations for storage and handling are followed and the geosynthetic is not left exposed over its design life. Quality control samples can be obtained from a project site and quickly tested to ensure extended exposure has not occurred.

Installation Damage. Significant loss of strength can occur during installation. The amount of loss is a function of gradation, angularity and maximum size of the backfill particles, weight and type of construction and compaction equipment, initial lift thickness over the geosynthetic, and the weight and type of geosynthetic.

The majority of the available data regarding installation damage strength losses has been obtained under uncontrolled conditions and are of limited usefulness. Strength losses reported in those studies vary from 10 to 70 percent (20). Seven studies do provide data under more controlled conditions (1, 20, 34, 38, 55, 59, 63), though in two of these studies (34, 55) the installation conditions and definition of survivability level relate more to reinforced fills over soft soils rather than a reinforced slope or mechanically stabilized earth wall.

The concept of survivability level of a given installation condition has been defined by Christopher and Holtz (14) for separation and fill reinforcement over soft ground applications. The concept of survivability level has not been specifically established for reinforced slope or wall applications, though this definition can be modified to accommodate walls and slopes based on the trends observed to date. Survivability as defined by Christopher and Holtz (14) is summarized in Table 2. A modified survivability definition for walls and slopes is shown in Table 3.

Measured strength retention versus the installation condition survivability level reported in the seven studies previously mentioned are presented in Figures 1 through 5. The appropriate survivability definitions in Tables 2 and 3 were used to develop the figures. There is considerable scatter in the data, and therefore only general trends regarding strength losses during installation can be determined. Some judgement is required to determine the survivability level, damage sustained by a geosynthetic tends to be nonuniform, and variations in geosynthetic weight within the groupings contribute to the data scatter. This

Table 2. Survivability Levels for Separation and Embankment Applications (Adapted from Christopher and Holtz, 1984).

SUBGRADE PREPARATION CONDITIONS:	Low ground-pressure equipment (< 27 kPa),15-30 cm initial lift	Medium ground-pressure equipment (> 27 kPa, < 55 kPa),15-30 cm initial lift	High ground pressure equipment (> 55 kPa), 15-30 cm initial lift
Subgrade is smooth and level	LOW	MODERATE	HIGH
Subgrade has been cleared of large obstacles	MODERATE	HIGH	VERY HIGH
Minimal site preparation is provided	HIGH	VERY HIGH	NOT RECOMMENDED
TYPE OF COVER MATERIAL		Medium ground pressure equipment (> 27 kPa, < 55 kPa),30 cm initial lift	High ground-pressure equipment (> 55 kPa), 30 cm initial lift
Fine sand to 2-inch minus gravel, rounded to subangular	----	LOW	MODERATE
Coarse angular aggregate with diameter up to one-half lift thickness, may be angular	----	MODERATE	HIGH
Some to most aggregate with diameter greater than one-half lift thickness, angular and sharp-edged, few fines	----	HIGH	VERY HIGH

Table 3. Survivability Levels for Slope and Wall Applications.

TYPE OF COMPACTION EQUIPMENT	BACKFILL CHARACTERISTICS	INITIAL LIFT THICKNESS (cm)		
		< 15	15 to 30	>30
Tracked equipment	fine to coarse, subrounded silty sand	LOW	LOW	LOW
	well-graded subrounded to subangular sandy gravel (75 mm minus)	MODERATE	LOW	LOW
	poorly graded angular gravel (75 mm minus)	VERY HIGH	HIGH	MODERATE
Full size steel roller or rubber tired equipment	fine to coarse, subrounded silty sand	MODERATE	LOW	LOW
	well-graded subrounded to subangular sandy gravel (75 mm minus)	HIGH	MODERATE	LOW
	Poorly graded angular gravel (75 mm minus)	NOT RECOMMENDED	VERY HIGH	HIGH

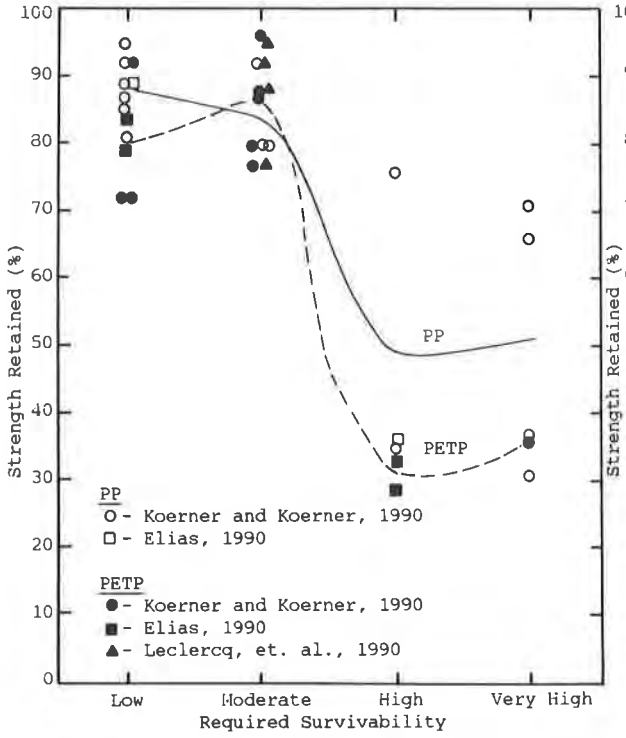

Figure 1. Installation Damage for Lightweight Nonwovens (<270 gm/m²).

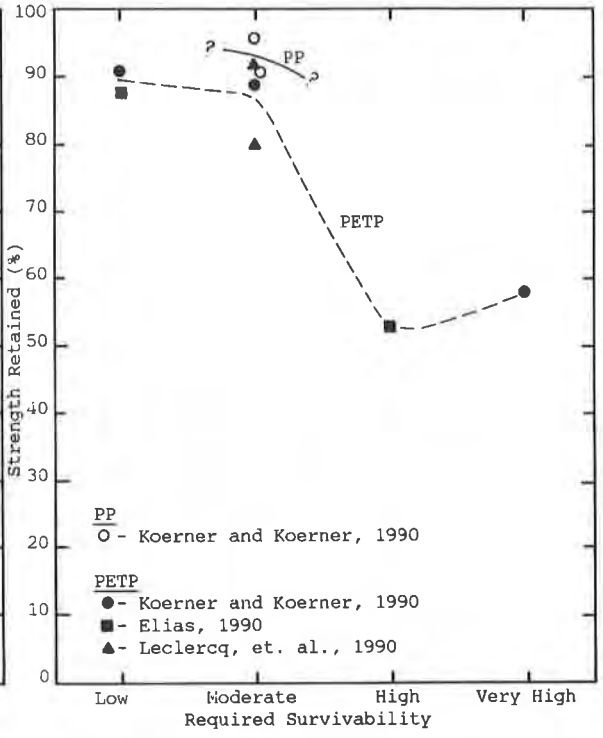

Figure 2. Installation Damage for Moderate to Heavy Nonwovens (≥270 gm/m²).

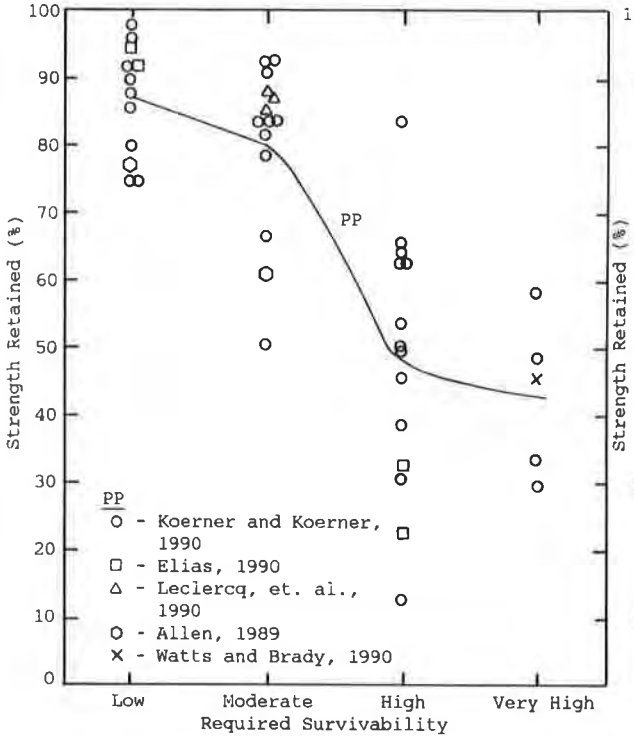

Figure 3. Installation Damage for Lightweight Wovens (<270gm/m²).

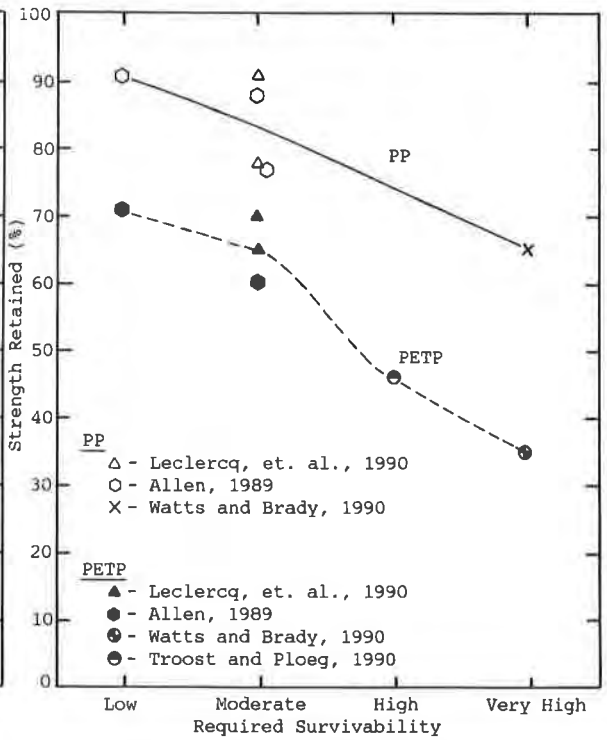

Figure 4. Installation Damage for Moderate to Heavy Wovens (≥270 gm/m²).

data shows the following trends:

1. Lightweight or thin geosynthetics suffer larger strength losses than moderate to heavyweight or thick geosynthetics;

2. Woven geotextiles suffer slightly larger strength losses than nonwovens, most likely due to the greater stiffness woven geotextiles possess. Grids suffer the least strength loss, most likely due to the great thickness of grid filaments;

3. PETP geosynthetics generally suffer greater strength losses than PP or PE geosynthetics. This is reasonble considering that PETP, at normal in-soil temperatures, is well below its glass transition temperature whereas the other two polymers are above their glass transition temperatures. This causes PETP to behave in a more brittle manner and to be more sensitive to the notching caused by abrasion than PP and PE.

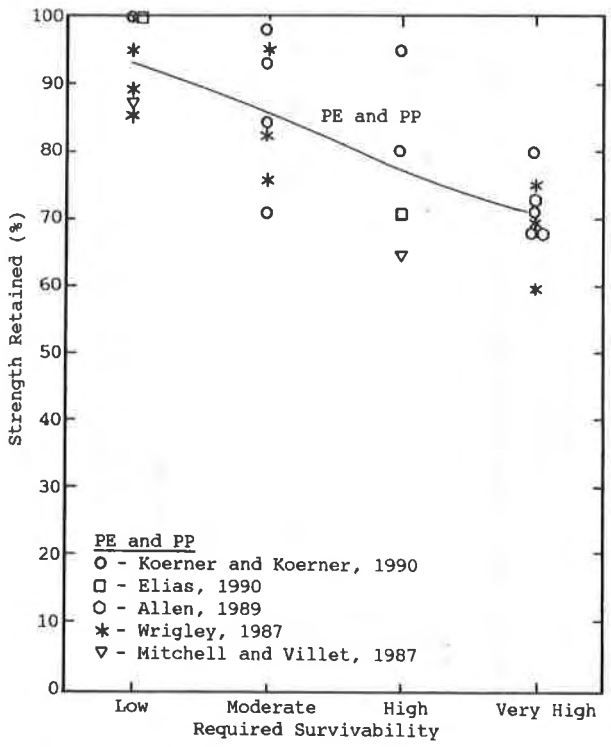

Figure 5. Installation Damage for Geogrids (all weights).

The available data also shows that installation damage mainly affects strain at failure and has minimal effect on modulus (1, 55, 59.). Viezee, et. al., (58) found this trend to be very strong for individual PETP yarns subjected to installation damage. The work performed by Elias (20), however, appears to be an exception to this trend in that he found the geosynthetic modulus to be reduced almost as much as strength. The failure strain and modulus retention after damage obtained in these studies are tabulated in Table 4. Troost and Ploeg (55) noted that the geotextiles they tested did show some nominal loss in modulus when installation damage was high, due to fibers which had been cut. This indicates that the modulus of the fibers themselves is not affected, but that only the modulus of the geosynthetic structure is affected by installation damage. Installation damage, in effect, creates local defects in the fibers causing premature rupture. The importance of this will become evident when considering the effect of installation damage on creep.

Ranges of the partial factor of safety for installation damage for various geosynthetics are presented in Table 5. The factor of safety is simply the inverse of the average percent strength retained for each survivability level shown in Figures 1 through 5. Higher factors of safety than shown in the table may be needed if the soil is very angular and/or gap graded, if the initial lift over the geosynthetic is relatively thin (say, less than 15 cm), or if the geosynthetic weight is near the bottom of the weight ranges shown in the table.

Table 4. Effect of Installation Damage on Strength, Strain, and Modulus.

STUDY	GEOSYNTHETIC TYPE	UNDAMAGED STRENGTH (KN/M)	AFTER INSTALLATION		
			Strength Retained	Failure Strain Retained	5 % Secant Modulus Retained
Allen (1989)	PE geogrid	76.4	73%	70%	95%
	PE geogrid	94.2	68%	63%	102%
	PP slit film woven	31.0	60%	64%	97%
	PP stitch/bond woven	62.0	77%	83%	101%
	PP stitch/bond woven	92.3	88%	75%	122%
	PETP multifil. woven	186.3	60%	61%	115%
Watts and Brady (1990)	PP woven	190.0	64%	67%	"no change"
	PP woven	46.1	46%	55%	"
	PETP woven	187.9	35%	50%	"
	PE geogrid	53.9	87%	75%	"
Troost and Ploeg (1990)	PETP multifil. woven	150.0	46%	not reported	85%
	PETP multifil. woven	400.0	65%	"	90%
	PETP multifil. woven	600.0	75%	"	94%
	coated PETP geogrid	55.0	82%	"	103%
Viezee, et. al. (1990)	PETP multifil. yarn	77.8 N	81%	77%	100%
Elias (1990)	PETP nonwoven needle	48.0	54%	not reported	67%
	PETP nonwoven needle	17.7	21%	"	33%
	PETP nonwoven needle	9.8	25%	"	33%
	PP silt film woven	33.6	20%	"	37%
	PP woven monofil.	48.5	34%	"	61%
Leclerq et al. (1990)	PETP nonwoven needle	13.1	77%	71%	not reported
	PETP nonwoven needle	41.9	92%	75%	"
	PETP nonwoven needle w/PETP grid	28.4	80%	72%	"
	PETP nonwoven bonded	5.3	95%	84%	"
	PETP nonwoven bonded	12.4	92%	85%	"
	PETP nonwoven bonded	17.7	88%	87%	"
	PETP mutifil. woven	115.2	70%	82%	"
	PETP mutifil. woven	158.7	65%	83%	"
	PP slit film woven	21.4	87%	101%	"
	PP slit film Woven	37.8	88%	81%	
	PP slit film woven	40.8	85%	90%	"
	PP slit film woven	96.3	91%	99%	"
	PP monofil. woven	55.0	78%	78%	"

Table 5. Partial Factor of Safety to Account for Installation Damage.

GEOSYNTHETIC POLYMER	GEOSYNTHETIC TYPE	GEOSYNTHETIC WEIGHT (g/m^2)	RANGE OF SAFETY FACTOR	
			HIGH SURVIVA-BILITY	LOW SURVIVA-BILITY
PP and HDPE	Nonwoven	< 270	2.0	1.15
		> 270	1.8	1.05
	Woven	< 270	2.5	1.2
		> 270	1.4	1.1
	Grid	all weights	1.4	1.0
PETP	Nonwoven	< 270	3.2	1.25
		> 270	1.8	1.1
	Woven	< 270	?	?
		> 270	2.2	1.4
	Grid	all weights	?	?

Even larger factors of safety may be needed if the construction equipment is allowed to make sharp turns on the first lift of soil above the geosynthetic. The factors of safety for high survivability should be used if the expected installation conditions are not known during design. Lightweight geosynthetics, especially woven geotextiles, can potentially suffer large strength losses and therefore should be used cautiously for geosynthetic reinforced structures. Since there are many variables which affect the amount of installation damage, the factors of safety shown in the table should only be used for preliminary design or for geosynthetic structures in noncritical applications. On-site installation damage tests performed on the geosynthetics to be used should be conducted for structures in critical applications or if severe installation conditions are expected. An appropriate methodology for conducting installation damage tests is provided by Elias (20).

Creep. Creep is simply the viscoelastic response of the reinforcement to sustained load. Creep results in time dependent deformation which may continue to occur as long as the reinforcement is loaded. It is of primary importance in the design of polymeric reinforced structures.

a. Creep Variables. Up to three phases of creep have been observed for geosynthetics: primary, secondary, and tertiary. Primary creep is characteristically linear when plotted on a logarithmic time scale. Secondary, or steady state creep, is characteristically linear when plotted on an arithmetic time scale. Tertiary creep is the rupture phase of creep and is characterized by a rapidly increasing creep rate with time. Geosynthetic structure tends to dominate primary creep, whereas the polymer material tends to dominate secondary and tertiary creep (2).

The creep response for the polymer material is related to the polymer type and grade, and manufacturing techniques. These will control the degree of molecular orientation and entanglement between molecules, the percent crystallinity, the molecular length, and hence the long-term strain response (18). The polymer creep response is also affected by load level and temperature (2). Since the polymer material dominates secondary and tertiary creep, these polymer characteristics will generally control when and at what load level a given geosynthetic will rupture.

The geosynthetic macrostructure also affects the overall creep response of the geosynthetic, as time dependent straightening of the fibers within the geosynthetic structure can occur, resulting in increased total creep strains. This macrostructure creep can control the total creep strain observed, at least when tests are conducted in-isolation. Strains due to macrostructure creep, when tested in-isolation, increase with increasing complexity of the geosynthetic structure, and can vary from 0 percent for grids to approximately 50 percent strain for needlepunched nonwoven geotextiles (18). Load level has a significant effect on creep of the geosynthetic macrostructure, while temperature has little effect, though there is some data to indicate that some resins used in bonded nonwovens may be temperature sensitive (2).

Soil confinement tends to restrict movement of individual filaments, preventing their realignment in the direction of load, thereby substantially reducing the magnitude of geosynthetic macrostructure creep. McGown, et. al., (40) found the reduction in primary creep to be especially large (on the order of 40 to 60 percent) for nonwoven geotextiles confined in sand. They also found

that the secondary creep rate is substantially reduced due to soil confinement in sand. They subsequently concluded that in-isolation creep testing grossly overestimates the long-term creep strains which would occur confined in-soil. This may explain the excellent long-term performance to date of test walls constructed of needlepunched nonwoven geotextiles in Colorado (4).

Koerner, et. al., (37) has postulated that creep behavior of the soil influences the creep behavior of the geosynthetic. Therefore, one must consider the possibility that the effect of soil confinement on geosynthetic creep may not be as great in more creep susceptible soils such as silts and clays.

Geosynthetic creep in-soil is obviously a very complex phenomena, and is not well understood. In-soil creep may not become fully understood until a working stress analysis for geosynthetic reinforced structures is developed which would allow the stress-strain regime within the structure to be analyzed and predicted. It is recommended that design creep limits be conservatively determined using in-isolation creep tests until more is known. Research regarding this issue is highly recommended.

b. Long-Term Creep Strength and Creep Prediction. The creep behavior of a geosynthetic can become unacceptable for two reasons: (1) the occurrence of tertiary creep and creep rupture, and (2) long-term creep deformation which exceeds the deformation tolerances for the structure. The partial factor of safety for creep, FS_{CR}, is generally associated with the first failure mode. Serviceability criteria, such as limiting the long-term strain to 5 percent or less, is associated with the second failure mode.

Table 6. Partial Factors of Safety to Account for Creep.

APPLICATION	POLYMER TYPE	RANGE OF FS's
Noncritical, Temporary	PP PE PETP	2.5 to 3.0 2.3 to 3.0 1.7 to 2.0
Noncritical, Permanent	PP PE PETP	3.3 to 5.0 2.7 to 5.0 2.0 to 2.5

Table 6 presents ranges of partial factors of safety to prevent creep rupture for various polymer types in noncritical structures, which are based on the observations and test results obtained by a number of researchers (2, 18, 21, 41, 43). These ranges were established at a temperature of 20° C. Higher temperatures will generally require higher partial safety factors for creep. The high end of the safety factor range should be used if little is known about the specific product to be used and the proposed structure is at the limits of the guidelines set in Table 1 for noncritical structures. Long-term product specific creep data, which can be extrapolated with confidence to the structure design life, should be obtained for any product proposed for use in critical structures. Long-term creep data is defined as data from creep tests with a minimum duration 10,000 hours. This duration is consistent with Task Force #27 and GRI:GG4 guidelines.

No standardized method exists for extrapolating creep data to design lives typical for permanent geosynthetic structures, though some methods have been proposed. Geosynthetic creep data can be extrapolated up to one log cycle of time without the use of some form of accelerated creep testing (30, 32). This one log cycle extrapolation can be aided through the use of tools such as isochronous load-strain curves, creep isochronous stiffness curves, and Sherby-Dorn plots. McGown, et. al., (42) illustrates the use of these tools for this purpose, as shown in Figures 6 and 7.

The temperature dependence of creep can be used to advantage to accelerate creep and extrapolate data more than one log cycle of time. This temperature dependence is related to the mobility of the molecular chains within the polymer, as movement in various portions of the molecule (i.e., side groups, branches, molecular backbone segments, and even crystallite features) must be activated by certain threshold temperatures (22). The most important threshold temperature regarding creep is the glass transition, as molecular mobility and potential for creep is generally low below and high above this temperature. Because PP and HDPE are well above their glass transitions, and PETP well below its glass transition at normal in-soil temperatures, creep of PP and HDPE has a strong (actually exponential) temperature dependence, whereas PETP creep has little temperature dependence (2, 63). Because of this, care must be used in selecting the design temperature, as relatively short exposure to high temperature can have a greater overall effect than constant exposure to the average temperature (51).

The temperature dependence of HDPE grids has been used in conjunction with a time-temperature superposition principle to extrapolate creep data (63). Due to the complex molecular structure of oriented semi-crystalline polymers, this principle could only be applied over limited stress and strain ranges where linear viscoelastic behavior could be expected (63). Beyond these ranges, the time-temperature super-

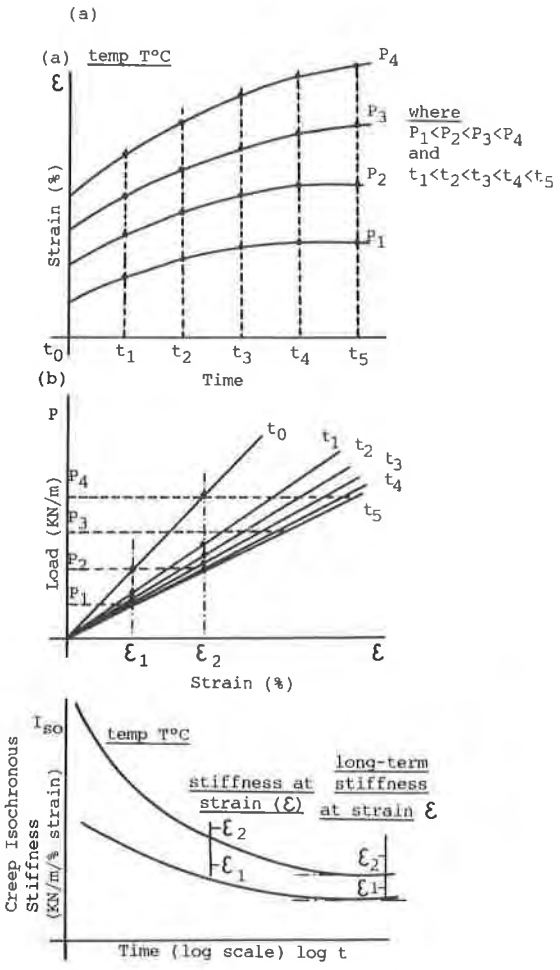

Figure 6. The Development of Geogrid Creep Isochronous Stiffness Curves from Creep Test Data: a) Creep Test Data; b) Isochronous Load-Strain Curves, and c) Creep Isochronous Stiffness Curves (After McGown, et. al., 1984; Reprinted by Permission of the Author and Thomas Telford Publications, Copyright 1984).

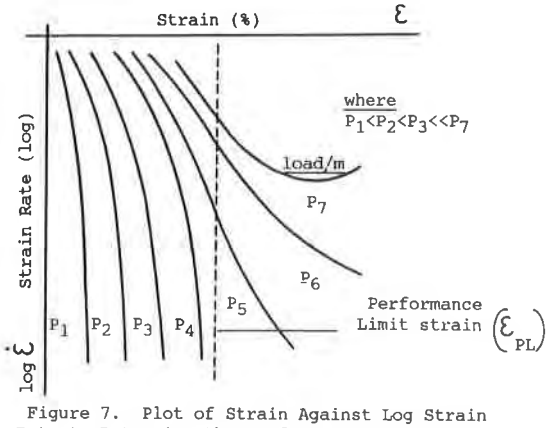

Figure 7. Plot of Strain Against Log Strain Rate to Determine the Performance Limit Strain (after McGown, et. al., 1984; Reprinted by Permission of the Author and Thomas Telford Publications, Copyright 1984).

position relationship becomes more approximate. Bush (9) illustrates how to apply this principle, as shown in Figure 8.

Since the temperature dependence of PETP creep is very small, it follows that larger ranges of temperature would be required to apply the time-temperature superposition principle to PETP. The data available for extrapolating creep of PETP using time-temperature superposition is very limited (30). Though this method does appear to be promising, more research is needed to evaluate its applicability to geosynthetics other than HDPE grids.

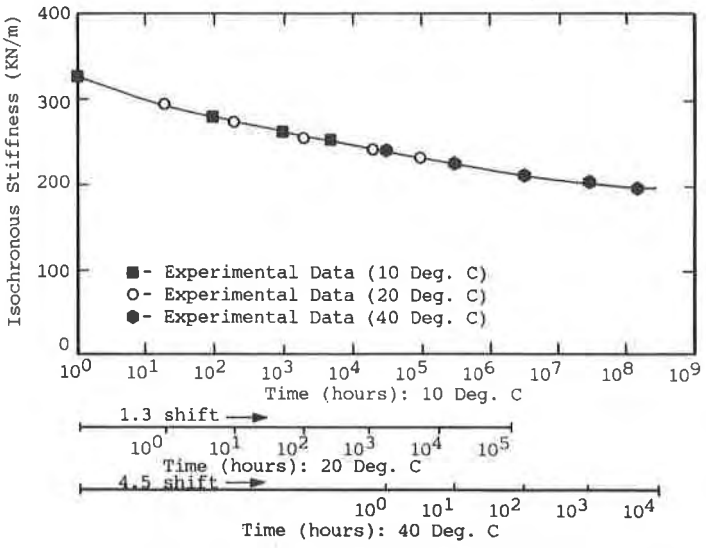

Figure 8. Time-Temperature Superposition for HDPE grid (After Bush, 1990; Reprinted by Permission of A. A. Balkema Publishers, Copyright 1990).

Other methods proposed for use in extrapolating short term creep data to long design lives include the use of rheological models coupled with empirical or theoretical approaches, such as the two-process model described by Wilding and Ward (60). The two-process rheological model consists of two springs and two dashpots placed in parallel, as shown in the bottom model in Figure 9. Figure 10 illustrates the two-process model and its manifested creep behavior. This type of model allows the secondary creep rate at lower loads to be extrapolated from the creep rates measured at higher loads. The rheological model can then be used to model the overall creep behavior of the geosynthetic in question. Research which confirms the validity of this method for creep extrapolation of all geosynthetics is needed.

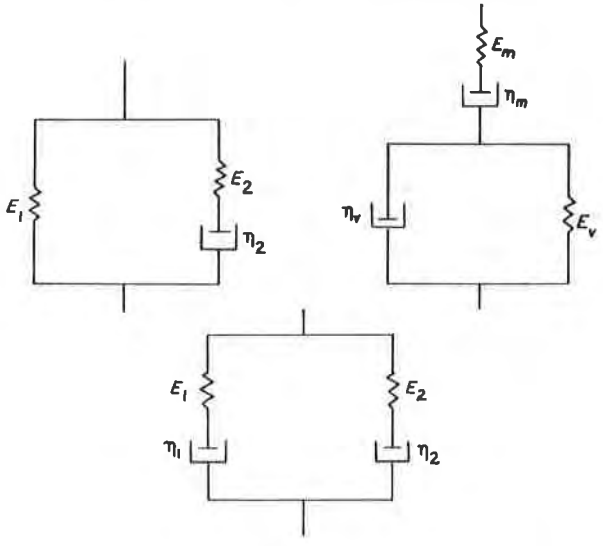

Figure 9. Mechanical Models of Creep and Recovery (after Wilding and Ward, 1981; Reprinted by Permission of Butterworth-Heinemann Ltd., Copyright 1981).

Regardless of the method used to extrapolate creep behavior, some estimate of the maximum allowable strain must be made. If this maximum allowable strain is based on the first failure mode, creep rupture, the ratio of the creep strain at the beginning of tertiary creep to the failure strain in a conventional load-strain test must be estimated. This ratio is often considerably greater than 1.0 for PP and PE and approximately equal to 1.0 for PETP (18). Data obtained by Allen, et. al., (2) shows that this ratio is a function of the secondary creep rate, at least for the PP geotextiles tested. Such a relationship, as shown in

Figure 11, could be used in conjunction with the creep extrapolation tools previously mentioned to estimate when creep rupture would occur. A lower bound approach or a factor of safety should be applied to such data if this method is used to account for material property variations. Until more is known, a minimum factor of safety of 1.5 applied to the creep rupture strain is recommended. This relationship has so far only been defined for secondary creep rates which would result in creep rupture in 10,000 hours or less. It has been postulated that a ductile to brittle transition could occur at longer times and very low secondary creep rates, resulting in reduced creep rupture strains. If this is possible for highly oriented semicrystalline polymers, then any attempts to extrapolate data such as shown in Figure 11 must be done with extreme care. Creep data at very low creep rates and long times is desperately needed. If this strain at failure data is not available, then an alternative is to select the load level at which the strain rate continues to decrease with log-time within the required design lifetime and which would preclude brittle or ductile failure (55).

If this maximum allowable strain is based on the second failure mode, excessive deformation, the amount of strain required for this purpose based on in-isolation tests is very difficult to estimate for slopes and walls in-situ, as discussed previously. Good engineering judgement is required.

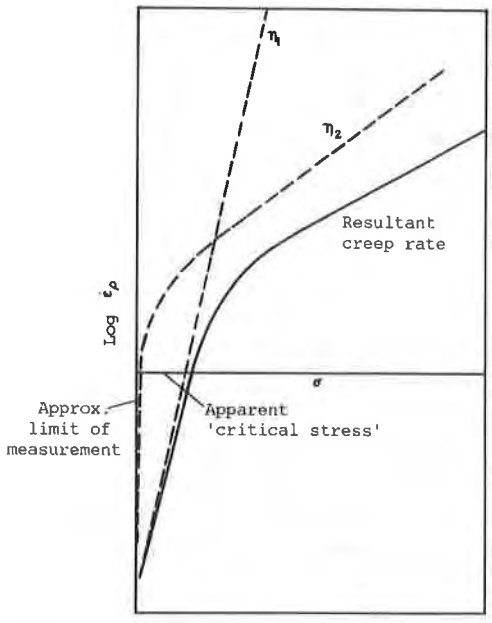

Figure 10. Schmetic Representation of Plastic Flow for the Two-Process Model; Creep Strain Rate $\dot{\epsilon}_p$ vs. Applied Stress (After Wilding and Ward, 1981; Reprinted by Permission of Butterworth-Heinemann Ltd., Copyright 1981).

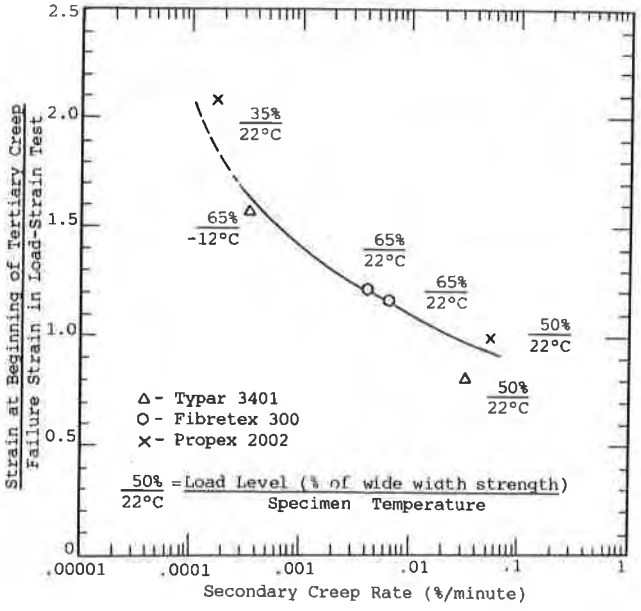

Figure 11. Ratio of Creep to Load-Strain Failure Strains Versus Secondary Creep Rate (After Allen, et. al., 1983).

Whatever method is used to determine the partial safety factor for creep in critical structures, enough creep data must be obtained for each given product to establish the creep behavior patterns observed. This requires creep data at

several load levels. Some creep data must also be carried into secondary and tertiary creep so that failure patterns can be recognized. It is preferable to use more than one method to extrapolate the creep data, if possible. Doing this provides confirmation of the accuracy of the extrapolation.

Chemical Aging. Chemical aging of geosynthetics is the result of both soil environmental factors and polymer chemical structure and composition factors. One can expect the greatest amount of chemical degradation to occur, in general, with polymers which have low molecular weights, low percent crystallinity, low density, and which have low draw ratios, considering a given polymer type (20). The use of improper polymer additives or leachable antioxidants may also allow degradation to occur more easily (13, 20). Regarding environmental factors, one can expect the greatest amount of degradation to occur, in general, at relatively high temperatures, in moderate to high moisture conditions, in soils which are active chemically, especially regarding soil pH and quantities of certain types of ions present, and with the geosynthetic under stress (20). The thickness of the polymer fibers may also have a strong effect on chemical aging, as degradation mechanisms are dependent on diffusion processes or exposure and removal of surface material (62, 63).

Chemical degradation mechanisms include oxidation, environmental stress cracking, hydrolysis, and attack by specific chemicals and solvents (i.e., such as hydrocarbons, strong acids and bases, or sulfates). Chain scission, chain slippage, crosslinking reactions, changes in crystallinity, and/or changes in end group composition can occur, resulting in embrittlement and polymer degradation (20, 36, 57).

a. Oxidation. Degradation due to oxidation occurs due to heat (thermo-oxidation) and exposure to ultraviolet light (photo-oxidation). Photo-oxidation has been discussed previously and is therefore not discussed further here.

Oxidation is, in general, a problem for PP and PE, but is minimal for PETP (57). PE is, in general, less susceptible to oxidation than is PP (57). The intrinsic resistance to oxidation of PE relative to PP is related to the methyl (CH_3) side group for PP which creates reactive sites on the polymer backbone (12).

Van Zanten (57) describes how oxidation of polyolefins takes place and how antioxidants help to prevent this reaction. Oxidation occurs through a series of consecutive free radical reactions, starting with the dissociation of a hydrogen atom from the main chain. The propogation phase (chain reaction) then begins, forming hydroperoxides, continuing with a branching phase and ending with a series of terminating reactions (57). The end result is the breakdown and/or crosslinking of the molecular chains and embrittlement of the polymer (31). Horrocks and D'Souza (25) reported that reduction in strain at failure due to oxidation was more marked than reduction in strength. Other evidence of oxidation include the absorption of oxygen in the polymer and the formation of carbonyl groups (56).

Antioxidants are added to the polymer to prevent oxidation during processing and use. Primary antioxidants prevent oxidation by breaking down radical reactions in the propogation and branching phases whereas secondary antioxidants provide additional help by eliminating hydroperoxides (57). A mixture of primary and secondary antioxidants in certain proportions is often added to a polymer to provide the most effective stabilization package. An excellent summary of the

types of antioxidant packages often used for various polymers are provided by Van Zanten (57).

As antioxidants are used up, the resistance of the polymer to oxidation will decrease. The rate of oxidation of the polymer is dependent on how much antioxidant is present initially, at what rate it is used up, how well it is distributed within the polymer to provide uniform protection, and how fast it can be leached out by flow of fluids, such as water, around and into the polymer (57). Leaching has been found to be a significant problem for certain antioxidants, such as Irganox 1010 and Topanol CA, based on research in the Netherlands (61). The potential for leaching of antioxidant is dependant on the size of the antioxidant molecule (larger molecules leach less), the type and structure of the polymer, and temperature (56).

The rate of oxidation and corresponding degradation is also influenced by the presence of certain ions in the surrounding environment, which act as catalysts for the oxidation reaction. Certain transition metal ions, such as iron, manganese, and copper, have been shown to significantly affect the oxidation rate of polyolefins (19, 56, 57, 61). Aluminum ions may also increase the rate of oxidation based on the experience of the author. Initial research indicates that these ions increase the rate of polymer degradation by a factor of 2 to 5 (19, 57). Recent research by Van Langenhove (56) indicates that for some metal ions, especially copper, the oxidation rate is accelerated by a factor of up to 10. Copper had the greatest effect, followed by iron and then manganese.

Little has been done regarding the concentrations of the metal ions necessary to cause a significant acceleration in the rate of oxidation. Some initial work has been performed by Wisse, et. al., (61) and Van Langenhove (56), in which PP geotextile oxidation was evaluated through immersion tests in solutions of various concentrations of metal ion. They both found that geotextile oxidation increased up to a limit once a certain concentration was reached, though one of the studies also found that oxidation became less severe at even higher concentrations of metal ion. The reason for this is not clear.

Van Langenhove (56) also presents data regarding the effect of environmental oxygen availability on the oxidation rate. The oxygen content in water is approximately 1/3 to 1/7 that in air. It has been concluded that in water the rate of oxidation and degradation is reduced by a factor of 3 to 4, when only the influence of the presence of oxygen is considered (56, 61). However, the presence of water, especially water vapor, has been shown to reduce potential lifetime of the polymer by a factor of 3 to 7 (56). Horrocks and D'Souza (25) state that moisture may promote antioxidant hydrolysis or even enter into the polymer oxidation chemistry. These factors tend to counteract one another regarding polymer lifetime. It is not clear at this point what the ultimate result on rate of oxidation would be when all of these factors are combined.

The effect of temperature on the rates of reaction of the various chemical processes, including oxidation of polyolefins, is well known. The formula of Arrhenius, in which a linear relationship between the reciprocal of temperature and the logarithm of time is assumed, has been applied to chemical degradation of geosynthetics by a number of researchers (36, 51, 56, 57, 61). In general, the Arrhenius relationship indicates that increasing temperature increases the rate of oxidation exponentially, showing the importance of temperature when considering potential polymer degradation. Current studies indicate that, in general, the

Arrhenius relationship holds true for polyolefin oxidation, though some deviations are possible, as shown in Figure 12 (56, 61). Factors which could cause this deviation include activation energy which is dependent on temperature and interaction between diffusion and solubility of stabilizers (56).

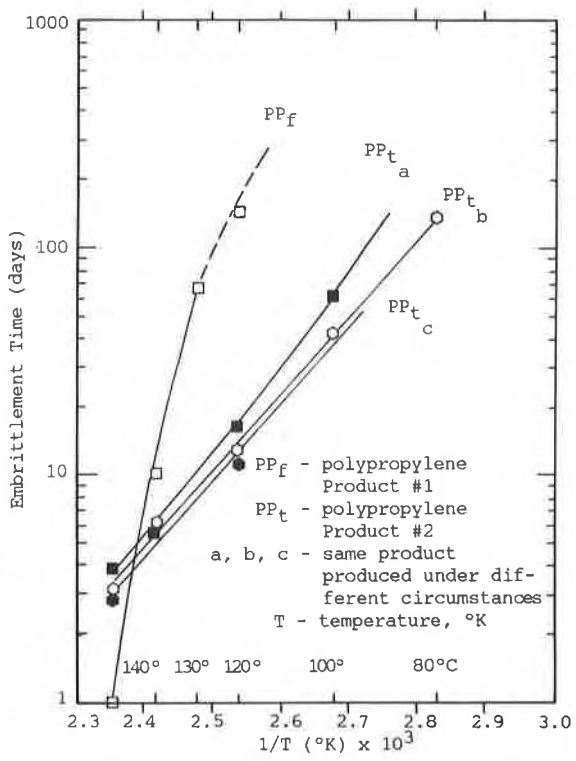

Figure 12: Embrittlement Time as a Function of Temperature During Oven Aging (After Van Langenhove, 1990; Reprinted by Permission of A. A. Balkema Publishers, Copyright 1990).

Strength losses due to oxidation in polyolefin geosynthetics measured in-service for 10 years or less has, in general, been found to be relatively small, ranging between no strength loss (39) to 20 percent strength loss (19, 24). Severe oxidation of a PP geosynthetic has been observed after 8 to 15 years of service in soil with high iron content in the Netherlands (19).

b. Environmental Stress Cracking. Environmental stress cracking (ESC) occurs when a polymer is subjected concurrently to a particular chemical environment and stress, resulting in the formation of cracks and premature brittle failure. It appears that ESC results in molecular chain disentanglement rather than chain breakage or chemical change (63). ESC is mainly a problem for PE, but can also occur for PP in extreme environments (31, 63). Chemicals which promote ESC in PE include weak acids and bases, alcohols, metallic soaps, solvents, and petroleum-based products (20).

The potential for ESC to occur in PE has been known since 1946 (63). A number of studies have made it possible to engineer the molecular structure of PE to prevent ESC. HDPE resistance to ESC can be improved by increasing its average molecular weight, decreasing its molecular weight distribution, increasing its crystalline content if the polymer is loaded in tension, reducing the crystallite and/or spherulite size, increasing the degree of orientation, and using copolymerization (63). Strength losses due to ESC for HDPE with the incorrect molecular structure can result in the polymer life being shortened by one to two orders of magnitude of time, at least for PE bars (64). Potential strength loss due to ESC has not been well defined for all the various types of HDPE used in geosynthetic reinforcement. Wrigley (63) reports that no significant strength loss due to ESC was observed for Tensar PE grid subjected to a constant load for up to 2000 hours in air and in a surfactant solution known to promote ESC. Jones and Ingold (31), however, reported substantial losses in strength and elongation (i.e., on the order of 40 percent) for PE geogrids subjected to rather severe laboratory test conditions. They also reported that some solutions can cause elongation to increase during ESC.

c. Hydrolysis. Hydrolysis occurs when water molecules react with the polymer molecules, resulting in chain scission, reduced molecular weight, and strength loss. Of the three polymers discussed, only PETP is susceptible to

hydrolysis. The water molecules react with the ester linkage in the PETP molecules (62). Hydrolysis is simply the very slow inverse reaction of the synthesis of PETP when water is present.

Risseeuw and Schmidt (47) report that in neutral water this reaction is catalyzed by the carboxyl end groups (-COOH) of the macromolecule itself. In an acid environment this catalysis still occurs, but additionally the H^+ ions catalyze the reaction. In an alkaline environment the hydrolysis reaction mechanism is slightly different in that the ester bond is split by an OH^- ion, producing a new carboxyl end group and an $-O-CH_2CH_2-$ ion that immediately reacts with the carboxyl group, giving a COO^- ion.

Most researchers agree that the susceptibility of PETP to hydrolysis is dependent on the polymer molecular weight and its distribution, with high molecular weight PETP having better resistance than low molecular weight PETP (17, 20, 23, 47, 62). Since the carboxyl end groups apparently play a significant role in the hydrolysis reaction, the number of these end groups may also be significant to the resistance of PETP to hydrolysis (47).

Risseeuw and Schmidt (47) have concluded that PETP fibers with molecular weights of 15,000 to 20,000 g/mole and carboxyl end group contents of 50 meq/kg or less will not be seriously affected by hydrolysis during their service life in general geosynthetic applications. Higher molecular weights (i.e., on the order of 30,000 g/mole) may be needed for more extreme environments, with pH of 10 or less. Ingredients beside the basic resin such as stabilizers and antidegradant fillers may also affect the resistance of PETP to hydrolysis (23).

There is some confusion regarding the role of diffusion of water into the polymer structure during hydrolysis. Apparently, hydrolysis occurs mainly within the amorphous regions of the polymer, as diffusion can occur more easily there than in the crystalline regions (17, 37, 62). Molecular orientation also appears to reduce hydrolysis for the same reason (17). Furthermore, tests conducted by Halse, et. al., (23) indicate that surface attack of PETP fibers due to hydrolysis cannot fully describe the strength losses observed, as specimens which lost little strength still showed extensive surface attack. This would indicate that some diffusion into the polymer must be taking place. However, Risseeuw and Schmidt (47) conclude that hydrolysis mainly takes place on the surface of the fiber, as dialectric properties of the material work as a barrier which prevents hydroxyl ions from penetrating the fiber core. Jaillioux and Verdu (29) further state that hydrolysis must be an erosion phenomena by superficial degradation, based on their observation that elongation at break remains almost unchanged while the rupture strength decreases.

Hydrolysis can be catalyzed by certain ions. As mentioned previously, acids (H+) can catalyze hydrolysis to a limited extent, but the effect of alkali catalysis (OH-) is much more pronounced for PETP (29). Alkali catalysis can be particularly severe if calcium ions are present when the pH is 9 or more, as would be the case near concrete or in dolomitic areas (20, 23).

Temperature also has a strong influence on the rate of hydrolysis, and hydrolysis can be particularly significant at temperatures above 50° C (62). If diffusion into the polymer is involved, changes in temperature will affect the rate of diffusion and thereby the rate of hydrolysis (62). Temperature also affects the hydrolysis reaction rate itself. Risseeuw and Schmidt (47) show that

the rate of hydrolysis for the PETP's which they tested appears to generally follow an Arrhenius relationship.

It must also be noted that the environment surrounding the geosynthetic need not be saturated, as hydrolysis can occur at humidities below 100 percent (47, 51). The relationship between relative humidity and hydrolysis rate appears to be approximately linear (47).

Segrestin and Jailloux (51) and Risseeuw and Schmidt (47) highlight the potential for strength loss due to hydrolysis to accelerate with time once a certain threshold strength loss is reached, at least at higher temperatures or high pH. This behavior should be considered when extrapolating short-term losses to expected long-term losses.

Actual strength losses due to hydrolysis measured for PETP geosynthetics in-service for 7 to 10 years in relatively neutral soil conditions have varied from no strength loss (16, 38) to 35 percent loss (27). A recent review by ICI (26) indicates that hydrolysis is PETP in-service in neutral pH conditions may result in a 50 percent strength loss in 50 to 150 years. Risseeuw and Schmidt, (17), however, have estimated that only a 20 percent loss would occur during this same time period. Woven PETP straps lost 45 percent of their strength in 17 years in a highly alkaline environment near a concrete wall face, most likely due to hydrolysis (39). Strength losses of 30 to 50 percent occurred in 4 months for one PETP geosynthetic subjected to immersion in high pH solutions, whereas another PETP geosynthetic showed no strength loss in that same environment (23).

Some geosynthetics use coatings of PE or PVC on the PETP fibers in an attempt to protect them from potential hydrolytic degradation. Based on the available research, these coatings appear not to prevent moisture from reaching the PETP core, making the value of these coatings as a barrier to hydrolysis rather limited (20, 51). Their ability to resist construction damage such that they remain intact as a barrier may also be questionable, depending on the thickness of the outer sheath (20). More research regarding the use of coated geosynthetics for long-term applications is needed to evaluate these concerns.

d. Predicting Long-Term Strength Loss Due to Chemical Aging. Chemical aging is a very complex process with many variables. It is not possible to predict long-term chemical aging based on analytical techniques, considering what is currently known. Therefore, tests which simulate one or more aspects of chemical aging must be conducted for each geosynthetic. Test programs performed to date to assess potential long-term degradation of geosynthetics have centered in tow main areas: accelerated laboratory aging tests, and evaluation of geosynthetics in-service in soil burial conditions. Both types of test programs have utilized physical and analytical test techniques to evaluate long-term changes in the geosynthetics due to chemical aging. Both types of test programs have advantages as well as some significant drawbacks.

Evaluation of long-term chemical aging of geosynthetics in-service requires that the initial physical and molecular properties of the geosynthetics to be evaluated, both before and after installation, as well as the soil chemical environment, be known with some degree of certainty. This is often not the case for existing geosynthetic structures. Very long observation periods are required, on the order of 10 years or more, to obtain degradation data adequate for long-term extrapolation. Furthermore, the in-service test environment is often highly

variable, resulting in many uncontrolled variables such as temperature, moisture, availability of oxygen, and types and homogeneity of ions present. Such conditions are very difficult to analyze and obtain understanding of the mechanisms of degradation occurring. However, evaluation of geosynthetics in-service provides the very important advantage that real conditions, especially regarding stress and the availability of water, oxygen, and various types of ions to the geosynthetic, are modelled.

These variables can be controlled in accelerated laboratory aging tests, which is a significant advantage. However, the types of tests performed to date to simulate chemical aging do not adequately model real conditions. Laboratory tests typically used include oven tests and immersion tests. Oven tests, which are typically used to evaluate oxidation resistance for geosynthetics, consist of circulating constant temperature air with or without humidity through the geosynthetic. Obviously, the availability of oxygen to the geosynthetic is much greater in this test than would occur in soil and is therefore a rather severe test. Immersion tests are typically used to evaluate hydrolysis, environmental stress cracking, exposure to specific chemicals, and to evaluate the effect of transition metals on oxidation rates. Immersion tests are also rather severe when compared to in-soil conditions, as water, ions, etc. in this test have easier access to the polymer than when in soil. If oxidation is to be evaluated by an immersion test, the ions will have easy access to the polymer whereas oxygen will not. For all of these types of laboratory tests, the relationship between laboratory conditions and real in-soil conditions needs to be established.

Laboratory tests are often accelerated by temperature or by use of more severe chemical types or concentrations than found in-soil. This is done to insure that useful test results are obtained within a reasonable period of time. The Arrhenius time-temperature relationship, as mentioned previously, has been used for this type of testing with at least some success at relatively high temperatures. However, there is practically no data available regarding the applicability of this relationship at more normal in-soil temperatures. Reaction mechanisms and activation energies may not be temperature independent, as shown in Figure 12. This must be considered when extrapolating to lower temperature and longer times. The accuracy of using higher than normal chemical concentrations or severe chemical types to allow extrapolation to more normal conditions has also not been verified.

Whether laboratory tests are conducted or evaluation of geosynthetics in-service is performed, both polymer fingerprinting tests as well as physical property tests should be conducted to provide understanding regarding the effects of aging. The wide width tensile test is the most important physical property measurement to make, though other types of tensile tests have been used. Some of the chemical fingerprinting techniques available include thermogravimetric analysis (TGA), differential scanning colorimetry (DSC), infrared spectroscopy (IR), melt index (MI), flow rate ratio (FRR), gel permeation chromatography (GPC), and microscopic analysis. Cassidy, et.al., (11) and Rollin and Rigo (48) explain some of the details of these methods and are highly recommended as references.

Obviously, degradation due to chemical aging is a very complex phenomenon which is difficult to model. Whatever the type of laboratory test program utilized, such as an oven test, immersion test, or some type of controlled laboratory soil burial test, the laboratory test results must be

correlated to the degradation observed for geosynthetics in-service to be of the most benefit. Conversely, an evaluation program of geosynthetics in-service should have a companion lab testing program so that degradation factors can be isolated and understood.

In the interim, a summary of the range of potential long-term strength losses recommended by various researchers (20, 26, 32, 47, 55, 57) can be made for use in designing geosynthetic structures in noncritical applications and chemically neutral soils, as defined previously. This summary is presented in Table 7 in terms of a partial factor of safety for use in Equation 1. The high end of the range should be selected for design, except as noted, unless specific long-term chemical aging data is available for the geosynthetics proposed for use. Geosynthetic structures in critical applications should not be attempted without adequate long-term data on the performance of the geosynthetic in the anticipated environment.

Table 7. Partial Factors of Safety to Account for Chemical Aging.

APPLICATION	POLYMER TYPE	RANGE OF FS's
Noncritical, Temporary	PP PE PETP	1.0 to 1.25[a] 1.0 to 1.25[a] 1.0 to 1.25[a]
Noncritical, Permanent	PP PE PETP	1.25 to 2.0[b] 1.1 to 1.5 ? 1.25 to 2.0[c]

a. Range depends on severity of soil chemistry.
b. High end of range reflects potential for antioxidants to leach out. If antioxidants in proposed geosynthetic are known to be highly leach resistant, use low end of range.
c. Does not apply to determination of strength loss of PETP where in contact with a concrete facing. Higher safety factors may be needed.

Biological Degradation. Biological degradation can occur as the result of three forms of microbiological attack: direct enzymatic degradation, chemical production by microorganisms which may result in deterioration of the polymer, and polymer additive degradation (20). A recent study in which biological degradation of PE, PP, and PETP geosynthetics was investigated showed no strength loss after one year of exposure to various leachates (35). The study showed that the biofilm was not even physically attached to the fibers, thus biodegradation could not occur (35). Several other biodegradability studies have obtained similar results (20). Koerner (33) has concluded that biological degradation is a nonproblem for the high molecular weight polymers commonly used for geosynthetics, as the microorganisms cannot find the molecular chain endings. A partial factor of safety for biological degradation of 1.0 is therefore recomended for temporary and noncritical permanent applications.

There is some evidence that very low molecular weight polymers and polymer additives can be consumed and degraded by microorganisms (57, 63). Therefore, caution is advised regarding the use of low molecular weight forms of the polymers. Caution is also advised regarding the use of coatings to protect the polymer fiber from degradation in this regard, as the biological stability of these coatings is unknown. Some PVC's are known to be susceptible to biological degradation (57).

For critical applications, one should be assured that the geosynthetic is composed of a high molecular weight polymer. Some relatively short-term biological degradation tests, such as ASTM G-21, G-22, and G-29 could be performed to insure the adequacy of the polymers (20).

Synergism of Degradation Mechanisms. Currently, synergism of the various degradation mechanisms is taken into account through the use of partial factors of safety multiplied together and applied to the ultimate tensile strength of the material, as shown in Equation 1. Multiplying the partial factors of safety together assumes the worst case regarding this synergism. This assumption is appropriate at this time until the synergism of these mechanisms is more fully understood.

Some recent research has been aimed at investigating how degradation mechanisms such as creep, installation damage, and chemical aging work together to produce an overall strength loss. Studies performed by Viezee, et. al., (58) and Billing, et. al., (7) show that the long-term creep rate of geosynthetics is not affected by previous installation damage. Instead, only the strain at break is affected. This correlates well with the concept that only the modulus of the geosynthetic macrostructure, rather than the filaments themselves, is affected by installation damage. Therefore, when considering the synergy of creep and installation damage, it may be more appropriate to estimate the safe stress by using the reduction in strain expected rather than multiplying estimated strength losses for each mechanism together as is currently done. Extrapolated isochronous load strain curves could be used to relate the safe strain to the safe stress. More research is recommended to verify this conclusion.

The synergy of chemical aging and biological degradation with creep (or stress) and installation damage appears to be much more complex. Based on their research, Viezee et. al., (58) have concluded that aging processes probably only affect deformation processes during the rupture phase. Horrocks and D'Souza (25) conclude that breaking strain is a more sensitive measure of chemical degradation than breaking stress. However, Jailloux and Verdu (29) reported that hydrolysis causes rupture strength to decrease while elongation at break remains unchanged. It appears that the effect of chemical aging on elongation and creep may vary depending on the polymer and the chemical aging mechanism. Accounting for the synergy between installation damage and creep with chemical aging using a relatively simple reduction in failure strain may not be possible, at least in some cases. Furthermore, stress may have an effect on the rate of chemical degradation. Popov et. al., (45) and Peeva and Evtimova (44) found that below a safe stress, which was found to be approximately 20 percent of ultimate, PP and PE oxidation was inhibited during stressing. Above this stress level, stress ceased to have an inhibiting effect as polymer structure defect zones opened up. Horrocks and D'Souza (25) found that once a critical stress of 10 percent of ultimate is exceeded, oxidative degradation increases, possibly due to increased concentrations of oxidatively sensitive species. They also found that temperature influences the safe stress and its effect on synergy between chemical aging and stress.

The complexities of the synergy between chemical aging and other degradation mechanisms are poorly understood at this point, and additional research in this area is much needed. The synergy between biological degradation, chemical aging, and stress is virtually unknown, though it has been speculated that the end products of microbial decay could provide the chemical environment needed to initiate environmental stress cracking or other forms of chemical degradation (31).

Seams and Connections. Currently, partial factors of safety for the various degradation mechanisms are applied to the ultimate strength of the geosynthetic

reinforcement. The wide width tensile strength of the geosynthetic is appropriate for this use if the long-term strength at the zone of maximum stress in the reinforced soil structure is desired. If geosynthetic seams which are perpendicular to the direction of stressing are allowed, the wide width seam strength should be used as the ultimate strength. The seam will become the weak link in the reinforcing layer. If the long-term strength of the geosynthetic connections to a wall face is to be analyzed, then the short-term connection strength should be used as an ultimate strength; or better yet, long-term creep tests on the connections should be conducted. Long-term facing connection strength should always be checked, as the environment at the face is usually more severe in terms of temperature, moisture, and ions present than deep within the reinforced soil mass. The Poitiers wall is an excellent example of this (39).

Geogrid Junctions. Another issue which must be addressed is the role of junction strength in long-term strength determination if a geogrid is used. GRI Standard Practice GG4 for stiff geogrids (32) conservatively recommends that the ultimate junction strength be used directly in the long-term strength equation if through-the-junction creep testing was not performed. Current Task Force 27 guidelines for geosynthetic walls require that the summation of the junction strengths within 300 mm length of grid be equal to or greater than the ultimate strength of the grid element to which they are attached (55). The ultimate wide width strength of the grid is then used in the long-term strength equation. Whether or not junction strength has any effect on reinforcement design strength is currently a subject of some controversy (10, 52). Junctions can lose tensile strength in the long-term due to creep and chemical degradation and can lose strength initially due to installation damage and U.V. exposure, resulting in premature failure. However, little research has been done on this subject.

The consequences of premature junction failure are not clear at this time. Recent research performed by Berg and Swan (6) indicate that removal of the cross ribs can significantly reduce the ultimate pullout coefficient. When considering long-term pullout capacity, this reduction in the interaction coefficient may not be all that important, as for typical design geometrics and granular backfills, even doubling the calculated pullout length required will not exceed the minimum pullout length of 3 feet typically used for geosynthetic wall design. It is possible, however, that a reduced interaction coefficient could result in increased long-term deformation over the length of the stressed reinforcement layer, as the grid would be less restrained by the soil. The amount of long-term deformation which could result from this is unknown, but should be researched.

The determination of amount of the load actually applied to each junction is very difficult, adding additional complexity to an already complex issue. The spacing of the junctions transverse and parallel to the direction of stressing as well as the nonuniform distribution of stress along the length of the geogrid reinforcement influences the magnitude of the load applied to each junction. The current Task Force 27 recommendations regarding junction strength are recommended until more is known about this subject.

Research Needs. Determination of long-term geosynthetic strength is extremely complex due to the large number of varieties of PP's, PE's and PETP's, each with different resistances to certain environments, and due to the many types of soil environments possible. Future research in this area is a formidable task indeed! Two research approaches are possible:

1. Establish some method of classifying polymers regarding their ability to resist chemical degradation using chemical fingerprinting techniques (13), as well as other forms of degradation, and determine maximum strength losses which can be expected for polymers of the various classifications for a given soil environment. Maximum expected strength losses would need to be determined through laboratory tests and evaluation of strength losses in-service.

2. Establish an analytical approach to determine the expected geosynthetic strength and/or strain loss utilizing certain key polymer and soil properties. Included in this approach could be the use of accelerated laboratory tests which have been correlated to real in-service performance of geosynthetics.

Either research approach is valid. It may be necessary to proceed with both approaches at first to establish the final direction for the research. Specific research needs are discussed in the individual sections in this paper. Currently, research in this area is rather fragmented. A unified effort among the various researchers is recommended.

CONCLUSION

There are many variables which affect long-term geosynthetic strength, making its determination difficult. A rational approach has been provided to assess the effect each of these variables has on long-term strength. Geosynthetic structures have proven to provide cost effective solutions to geotechnical problems, yet this issue of long-term geosynthetic strength has been the main stumbling block preventing their wide-spread use in soil reinforcement applications. Situations where geosynthetic structures can be used and their long-term strength determined, based on what is currently known, have been defined. Obviously, much is yet to be learned regarding long-term geosynthetic strength. The economic benefits warrant the further development of geosynthetic reinforced structures.

ACKNOWLEDGEMENTS

The author wishes to thank Mr. Ryan Berg for his efforts in reviewing the manuscript and for his technical assistance.

REFERENCES

1. Allen, T. M. (1989), "Strength Losses Occurring Due to Installation Damage for Several Geosynthetics", WSDOT Unpublished Report.

2. Allen, T. M., J. R. Bell, and T. S. Vinson (1983), "Properties of Geotextiles in Cold Regions Applications ", Transportation Research Report No. 83-6, Oregon State University.

3. Allen, T. M. and R. D. Holtz (1991), "Design of Retaining Walls Reinforced with Geosynthetics", ASCE/GED Specialty Conference, Session 3C, Boulder, Colorado (submitted for publication).

4. Bell, J. R., R. K. Barrett, and A. C. Ruckman (1983), "Geotextile Earth-Reinforced Retaining Wall Tests: Glenwood Canyon, Colorado", Transportation Research Record 916, pp. 59-69.

5. Berg, R. R., R. Bonaparte, R. P. Anderson, and V. E. Chouery (1986), "Design, Construction, and Performance of Two Geogrid Reinforced Soil Retaining Walls", Proceedings of the Third International Conference on Geotextiles, Vienna, Vol. II, pp. 401-408.

6. Berg, R. R. and D. B. Swan (1990), "Evaluation of Pullout Mechanisms", Proceedings of the International Reinforced Soil Conference, Glasgow (submitted for publication).

7. Billing, J. W., J. H. Greenwood, and G. D. Small (1990), "Chemical and Mechanical Durability of Geotextiles", Proceedings of the Fourth International Conference on Geotextiles, Geomembranes, and Related Products, The Hague, pp. 621-626.

8. Bonaparte, R. and R. Berg (1987), "Long-Term Allowable Tension for Geosynthetic Reinforcement", Proceedings Geosynthetics '87 Conference, New Orleans, LA, pp. 181-192.

9. Bush, D. I. (1990), "Variation of Long-Term Design Strength of Geosynthetics in Temperatures up to 40°C", Proceedings of the Fourth International Conference on Geotextiles, Geomembranes, and Related Products, The Hague, pp. 673-676; please order from: A. A. Balkema, Old Post Road, Brookfield, Vermont 05036.

10. Carroll, R. Jr. (1988), "Specifying Geogrids", Geotechnical Fabrics Report, Vol. 6, No. 2, pp. 40-43.

11. Cassidy, P. E., M. Mores, D. J. Kerwick, and D. C. Koeck (1990), "Recent Advances in Chemical Compatibility Evaluation of Geosynthetic Materials", Proceedings of the Fourth International Conference on Geotextiles, Geomembranes, and Related Products, The Hague, pp. 658-689.

12. Charron, R. M. (1989), "Polymers for Synthetic Lining Systems: Some Molecular Structure-Property-Application Relationships", Proceedings Geosynthetics '89 Conference, San Diego, pp. 408-420.

13. Christopher, B. R., Personal Communication, April 3, 1990.

14. Christopher, B. R. and R. D. Holtz (1984), Geotextile Engineering Manual, FHWA DTFH 61-80-C-0094, Washington, D.C.

15. Christopher, B. R., R. D. Holtz, and T. M. Allen (1990), "Instrumentation for a 12.6 m High Geotextile Reinforced Wall", Proceedings of the International Reinforced Soil Conference, Glasgow (submitted for publication).

16. Colin, G., M. T. Mitton, D. J. Carlson, and D. M. Wiles (1986), "The Effect of Soil Burial Exposure on Some Geotechnical Fabrics", Geotextiles and Geomembranes, No. 4, pp. 1-8.

17. Davis, G. W., (1988), "Aging and Durability of Polyester Geotextiles", Proceedings Durability and Aging of Geosynthetics, G.R.I., Philadelphia.

18. den Hoedt, G. (1986), "Creep and Relaxation of Geotextile Fabrics", Geotextiles and Geomembranes, No. 4, pp. 83-92.

19. den Hoedt, G. (1988), "Durability Experience in the Netherlands", Proceedings Durability and Aging of Geosynthetics, G.R.I., Philadelphia.

20. Elias, V. (1990), "Durability/Corrosion of Soil Reinforced Structures", FHWA/RD-89/186.

21. Finnigan, J. A. (1977), "The Creep Behavior of High Tenacity Yarns and Fabrics Used in Civil Engineering Applications", Proceedings, International Conference on the use of Fabrics in Geotechnics, Paris, Vol 2, pp. 305-310.

22. Hall, C. (1981), Polymer Materials, John Wiley and Sons, Inc., New York, NY.

23. Halse, Y., R. M. Koerner, and A. E. Lord, Jr. (1987), "Effect of High Alkilinity Levels on Geotextiles. Part 2: NaOH Solution", Geotextiles and Geomembranes, No. 6, pp. 295-305.

24. Hoffman, G. L. and R. Turgeon (1983), "Long-Term in Situ Properties of Geotextiles", Transportation Research Record 916, pp. 89-94.

25. Horrocks, A. R. and J. A. D'Souza (1990), "Physiochemical Changes in Laboratory-Aged Oriented Polypropylene Tapes - The Effects of Stress and Humidity", Proceedings of the Fourth International Conference on Geotextiles, Geomembranes, and Related Products, The Hague, pp. 709-714.

26. ICI (1986), "The Durability of Polyester, Polyaramid and Polyethylene Materials in Soil Reinforcement Applications", Report to British Standard Technical Committee CBS/56.

27. Ingold, T. S. and K. S. Miller (1986), "Short, Intermediate, and Long Term Stability of Geotextile Reinforced Embankments Over Soft Clays", Proceedings of the Third International Conference of Geotextiles, Vienna, pp. 337-342.

28. Jailloux, J. M. and P. Segrestin (1988), "Present State of Knowledge of Long-Term Behavior of Materials Used as Soil Reinforcements", International Geotechnical Symposium on Theory and Practice of Earth Reinforcement, Japan, pp. 105-110.

29. Jailloux, J. M. and J. Verdu (1990), "Kinetic Models for the Life Prediction in PET Hygrothermal Aging: A Critical Survey", Proceedings of the Fourth International Conference on Geotextiles, Geomembranes, and Related Products, The Hague, pp. 727.

30. Jewell, R. A. and J. H. Greenwood (1988), "Long-Term Strength and Safety in Steep Soil Slopes Reinforced by Polymer Materials", Geotextiles and Geomembranes, Vol. 7, Nos. 1 and 2, pp. 81-118.

31. Jones, M. and T. S. Ingold (1985), "Durability of Polyolefinic Soil Reinforcements", 8'th European Congress on Corrosion, Vol. 1, pp. 9-1 to 9-7.

32. Koerner, R. M. (1990), "Determination of the Long-Term Design Strength of Stiff Geogrids", GRI Standard Practice GG4.

33. Koerner, R. M., Personal Communication, April 2, 1990.

34. Koerner, R. M. and G. R. Koerner (1990), "A Quantification and Assessment of Installation Damage to Geotextiles", Proceedings of the Fourth International Conference on Geotextiles, Geomembranes, and Related Products, The Hague, pp. 597-602.

35. Koerner, G. R. and R. M. Koerner (1989), "Biological Clogging in Leachate Collection Systems", Durability and Aging of Geosynthetics, Elseiver Publishing Company (London), pp. 260-277.

36. Koerner, R. M., A. E. Lord, Jr., and Y. H. Halse (1988), "Long-Term Durability and Aging of Geotextiles", Geotextiles and Geomembranes, No. 7, pp. 147-158.

37. Koerner, R. M. et. al., (1980), "Stress-Strain-Time Behavior of Geotextiles in Uniaxial Tension", Proceedings Symposium on Geotextiles, ASCE, Portland, OR, pp. 31-52.

38. Leclercq, B., M. Schaeffner, P. H. Delmas, J. C. Blivet, and Y. Matichard (1990), "Durability of Geotextiles: Pragmatic Approach Used in France", Proceedings of the Fourth International Conference on Geotextiles, Geomembranes, and Related Products, The Hague, pp. 679-684.

39. Leflaive, E. (1988), "Durability of Geotextiles: The French Experience", Geotextiles and Geomembranes, No. 7, pp. 23-31.

40. McGown, A., K. Z. Andrawes, and M. H. Kabir (1982), "Load-Extension Testing of Geotextiles Confined In-Soil", Proceedings Second International Conference on Geotextiles, Las Vegas, NV, Vol. III, pp. 793-798.

41. McGown, A., K. Z. Andrawes, K. C. Yeo, and D. D. DuBois (1984), "The Load-Strain-Time Behavior of Tensar Geogrids", Proceedings Symposium on Polymer Grid Reinforcement in Civil Engineering, Paper No. 1.2, pp. 1-7.

42. McGown, A., N. Paine, and D. D. DuBois (1984), "Use of Geogrid Properties in Limit Equilibrium Analysis", Proceedings Symposium on Polymer Grid Reinforcement in Civil Engineering, Paper No. 1.4, pp. 1-5.

43. Mitchell, J. K. and W. C. B. Villet (1987), "Reinforcement of Earth Slopes and Embankments", Transportation Research Board, NCHRP Report 290.

44. Peeva, L. and S. Evtimova (1984), "Effect of Mechanical Stress on Oxidation of Polymers", European Polymer Journal, No. 11, pp. 1049-1051.

45. Popov, A. A., N. N. Blinov, B. E. Krisyuk, and G. E. Zaikov (1982), "Oxidative Destruction of Polymers Under Mechanical Load", European Polymer Journal, Vol. 18, pp. 413-420.

46. Raumann, G. (1982), "Outdoor Exposure Tests of Geotextiles", Proceedings Second International Conference on Geotextiles, Las Vegas, NV, Vol. II, p. 541-546.

47. Risseeuw, P. and H. M. Schmidt (1990), "Hydrolysis of HT Polyester Yarns in Water at Moderate Temperatures", Proceedings of the Fourth International Conference on Geotextiles, Geomembranes, and Related Products, The Hague, pp. 691-696.

48. Rollin, A. L. and J. M. Rigo, ed. (1990), Geomembranes Identification and Performance Testing, Rilem PC103, Elsevier, London.

49. Rowe, R. H., M. D. MacLean, and A. K. Barsvary (1984), "The Observed Behavior of a Geotextile-Reinforced Embankment Constructed on Peat", Canadian Geotechnical Journal, No. 21, pp. 289-304.

50. Schneider, H. and M. Groh (1987), "An Analysis of Durability Problems of Geotextiles", Proceedings Geosynthetics '87 Conference, New Orleans, pp. 434-441.

51. Segrestin, P. and J. M. Jailloux (1988), "Plastic Materials in Soil Reinforcement: The Question of Durability", Rotterdam, pp. 1-8.

52. Simac, M. R. (1988), Letter: "Geogrid Article Prompts Response", Geotechnical Fabrics Report, Vol. 6, No. 4.

53. Simac, M. R., B. R. Christopher, and C. Bonczkiewicz (1990), "Instrumented Field Performance of a 6 m Geogrid Soil Wall", Proceedings of the Fourth International Conference on Geotextiles, Geomembranes,and Related Products, The Hague, Vol. I, pp. 53-59.

54. Task Force No. 27 (1989), "Design Guidelines for Use of Extensible Reinforcements (Geosynthetic) for Mechanically Stabilized Earth Walls in Permanent Applications", Joint Committee of AASHTO-AGC-ARBTA on Materials.

55. Troost, G. H. and N. A. Ploeg (1990), "Influence of Weaving Structure and Coating on the Degree of Mechanical Damage of Reinforcing Mats and

Woven Geogrids, Caused by Different Fills, During Installation ", Proceedings of the Fourth International Conference on Geotextiles, Geomembranes, and Related Products, The Hague, pp. 609-614.

56. Van Langenhove, L. (1990), "Conclusions of an Extensive BRITE-Research Program on Ageing", Proceedings of the Fourth International Conference on Geotextiles, Geomembranes, and Related Products, The Hague, pp. 703-707; please order from: A. A. Balkema, Old Post Road, Brookfield, Vermont, 05036.

57. Van Zanten, V., Ed., (1986) Geotextiles and Geomembranes in Civil Engineering, Wiley-Halsted.

58. Viezee, D. J., W. Voskamp, G. den Hoedt, G. H. Troost, and H. M. Schmidt (1990), "Designing Soil Reinforcement with Woven Geotextiles - The Effect of Mechanical Damage and Chemical Aging on the Long-Term Performance of Polyester Fibres and Fabrics", Proceedings of the Fourth International Conference on Geotextiles, Geomembranes, and Related Products, The Hague, pp. 651-656.

59. Watts, G. R. A. and K. C. Brady (1990), "Site Damage Trials on Geotextiles", Proceedings of the Fourth International Conference on Geotextiles, Geomembranes, and Related Products, The Hague, pp. 603-607.

60. Wilding, M. A. and I. M. Ward (1981), "Creep and Recovery of Ultra High Modulus Polyethylene", Polymer, Vol. 22, pp. 870-876.

61. Wisse, J. D. M., C. J. M. Broos, and W. H. Boels (1990), "Evaluation of the Life Expectancy of Polypropylene Geotextiles Used in Bottom Protection Structures Around the Ooster Schelde Storm Surge Barrier - A Case Study", Proceedings of the Fourth International Conference on Geotextiles, Geomembranes, and Related Products, The Hague, 1990, pp. 697-702.

62. Wong, T. and A. R. Slaters, Jr. (1988), "Plasticization and Hydrolysis: The Effects of Water on Polyethylene Terephthalate in Geotechnical Applications", Proceedings Durability and Aging of Geosynthetics, G.R.I., Philadelphia, PA.

63. Wrigley, N. E. (1987), "Durability and Long-Term Performance of Tensar Polymer Grids for Soil Reinforcement," Materials and Science Technology, Vol. 3, pp. 161-170.

64. Zapas, L. J. and J. M. Crissman (1979), "Static Fatigue of Polyethylene in Uniaxial Creep in the Presence of Stress Cracking Agents and Solvents", Journal of Engineering and Science, pp. 469-475.

TECHNICAL ADVANCES / INNOVATIONS

Eccentric Plate Loading Tests on Geogrid-Reinforced Subgrades

Vito A. Guido
The Cooper Union, USA
Christopher H. Bakkala
Thornton-Tomasetti, P. C., USA
John J. Nocera
Malcolm Pirnie, Inc., USA

SYNOPSIS

Many foundations must resist in addition to vertical loads bending moments about one or both axes. Typical foundations which must resist moment are those for retaining walls, abutments and bridge piers. The allowable bearing capacity of an eccentrically loaded footing is greatly reduced from that of a concentrically loaded footing, depending on the magnitude of the eccentricity. The insertion of reinforcement in the subgrade below the footing should increase the load bearing capacity and reduce the displacement and/or rotation of an eccentrically loaded footing. Presented herein are the results of model eccentric plate loading tests on geogrid-reinforced subgrades. The parameters investigated were: degree of eccentricity, number of layers of reinforcement, size of the reinforcement, position and orientation of the reinforcement in the subgrade material and relative density of the subgrade material. In general, the load bearing capacity of the geogrid-reinforced subgrade increased above its unreinforced counterpart for a given eccentricity of applied load and for most cases increased above the load bearing capacity of a concentrically loaded plate on an unreinforced subgrade. The rotation of the plate and not the average settlement was used, and for the range of parameters investigated, the rotation of an eccentrically loaded plate on a geogrid-reinforced subgrade never achieved the theoretical zero rotation of a concentrically loaded plate, however, the rotations were greatly reduced.

INTRODUCTION

Presented herein are the results of 58 model eccentric plate loading tests on geogrid-reinforced subgrades. It was the intent of the testing program to investigate the capacity of eccentrically loaded plates on geogrid-reinforced subgrades to sustain increased loading and reduce rotation from the unreinforced subgrade case. This was done by varying several parameters and observing their effects on the load-bearing capacity and rotation.

LABORATORY MODEL

All 58 model eccentrically loaded plate tests were performed in a square stiffened wooden box, 48 in.(1.22 m) wide and 36 in.(0.92 m) deep. These 58 model tests are the latest in a series of approximately 300 model plate loading tests on geosynthetically-reinforced sand subgrades. Based on the results of this large number of tests it has been observed that the size of the test model used minimizes edge effects. The soil used as a subgrade material was a poorly graded sand (SP), see Table 1 for properties of the sand. For all relative densities investigated, the sand was placed in 2 in.(50.8 mm) lifts. In all but eight of the tests, the relative density of the subgrade material was kept at 55% to demonstrate the large benefits to be had from the placement of reinforcement in a potentially unsuitable subgrade material.

The reinforcement used in the subgrade below the eccentrically loaded plate was an SS1(BX1100) geogrid manufactured by Tensar. According to the manufacturer's literature the BX1100 is a high tensile strength biaxially oriented polymer grid formed from polyolefine resine. In addition, the grid geometry supplies an interlocking and supporting mechanism for both granular and cohesive soils. According to ASTM D 4595-86, Standard Test Method for Tensile Properties of Geotextiles by the Wide-Width Strip Method, the ultimate tensile strength of an SS1(BX1100) Tensar geogrid in the cross machine and machine directions is 1430 lbs/ft (20.5 kN/m) and 860 lbs/ft (12.5 kN/m), respectively. For typical dimensions of the BX1100 grid see Figure 1.

TABLE 1. PROPERTIES OF THE SUBGRADE SOIL

Uniformity Coefficient, C_u	1.90
Coefficient of Gradation, C_c	1.23
Effective Size, D_{10}, mm	0.086
Specific Gravity, G_s	2.66
Minimum Dry Unit Weight, γ_{dmin}, pcf(kN/m^3)	83.40 (13.10)
Maximum Dry Unit Weight, γ_{dmax}, pcf(kN/m^3)	99.60 (15.65)
Angle of Internal Friction, ϕ (deg)	
at Relative Density, D_r = 55%	37
D_r = 65%	38
D_r = 75%	40
D_r = 85%	42

The subgrade soil was loaded at its surface through a square aluminum plate with a 12 in.(305 mm) width and 1 in.(25.4 mm) thickness. The plate had three - 0.5 in.(12.7 mm) diameter and 0.375 in.(9.5 mm) deep holes drilled into it, whose purpose it was to receive a pin that projected from the lower socket of a machined steel ball-and-socket joint. See Figure 2 for the location of these holes. Hole 1 was at the center of the plate and holes 1, 2 and 3 had a 1 in.(25.4 mm) center-to-center spacing along the x-axis. The ball-and-socket assembly is able to rotate freely through an angle of approximately sixty degrees, well beyond the ranges to be expected and certainly much greater than what

would be tolerated by the rest of the apparatus. A static load was applied to the plate by a 25 ton(223 kN) capacity hydraulic cylinder and hand pump. The load applied in small increments, was recorded on a 10 ton(89 kN) capacity load ring which was attached to the upper socket of the ball-and-socket joint. The load was then transmitted through the ball to the lower socket and finally to the plate. The resulting displacements were recorded by four dial gages placed at the four corners of the plate, such that each gage piston rested on the plate at a point 0.25 in.(6.35 mm) in from each edge, see points U1, U2, D1 and D2 in Figure 2. To ensure that undamaged reinforcement was used, each test was performed with new BX1100 grid cut into square sheets. The geometry of the test model is shown in Figure 3.

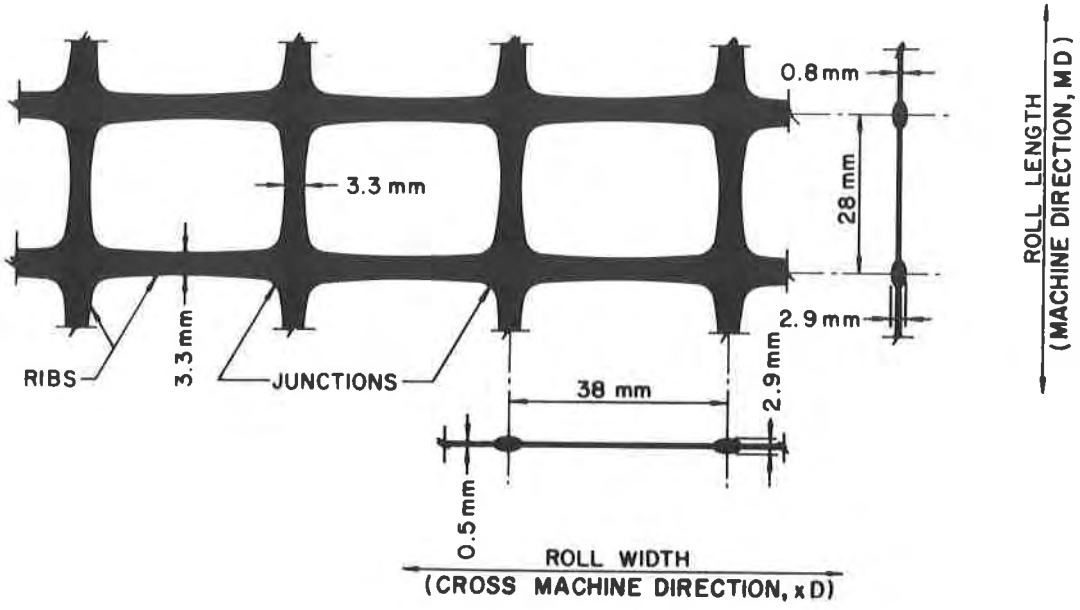

Figure 1 Typical Dimensions of Tensar SS1(BX1100) Grid

TEST RESULTS

For all the tests performed the depth below the plate to the first layer of reinforcement, u, was kept constant at 2 in.(50.8 mm) or in dimensionless form u/B of 1/6, where B is the width of the plate or 12 in.(305 mm). In addition, the vertical distance between layers of reinforcement, Δz, was kept constant at 2 in.(50.8 mm) or in dimensionless form $\Delta z/B$ of 1/6. The effect of six parameters on the load bearing capacity and rotational characteristics of eccentrically loaded plates on geogrid-reinforced subgrades were investigated. They were:

1) Degree of eccentricity, e, or in dimensionless form e/B.
2) Number of layers of geogrid-reinforcement, N.
3) Width size, b, of the square sheet of geogrid-reinforcement, or in dimensionless form b/B.
4) Position of the sheet of geogrid-reinforcement, either the centroid of the sheet vertically under the centroid of the plate or

vertically under the applied eccentric load.

5) Orientation of the sheet of geogrid-reinforcement, either the grid is oriented with the longitudinal (machine direction) parallel to the x-axis (see Figure 2) or the grid is rotated 90° with the transverse (cross machine direction) parallel to the x-axis.

6) Relative density of the sand, D_r.

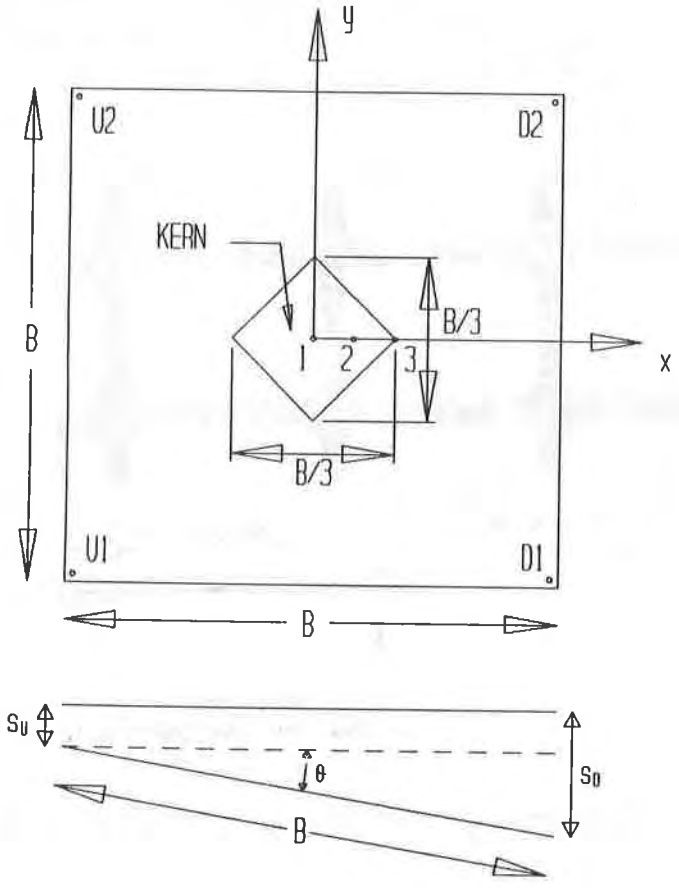

Figure 2 Loading Plate

The following definitions were devised to facilitate in expressing and comparing the test data.

1) Average uphill settlement, s_U, is the average of the displacements recorded on the dial gages positioned at points U1 and U2 (see Figure 2).

2) Average downhill settlement, s_D, is the average of the displacements recorded on the dial gages positioned at points D1 and D2 (see Figure 2).

3) Average settlement, s, is the average of the average uphill settlement and the average downhill settlement. This can be expressed in dimensionless form as the settlement ratio, s/B.

4) Rotation, θ, in radians (rads) can be expressed as

$$\theta = (s_D - s_U)/(B - 0.5) \qquad (1)$$

where s_u, s_p and B are in inches (see Figure 2).

5) The bearing pressure, q, will be taken as the average applied bearing pressure, or

$$q=P/A \qquad (2)$$

where P is the applied load and A is the area of the plate (B^2).

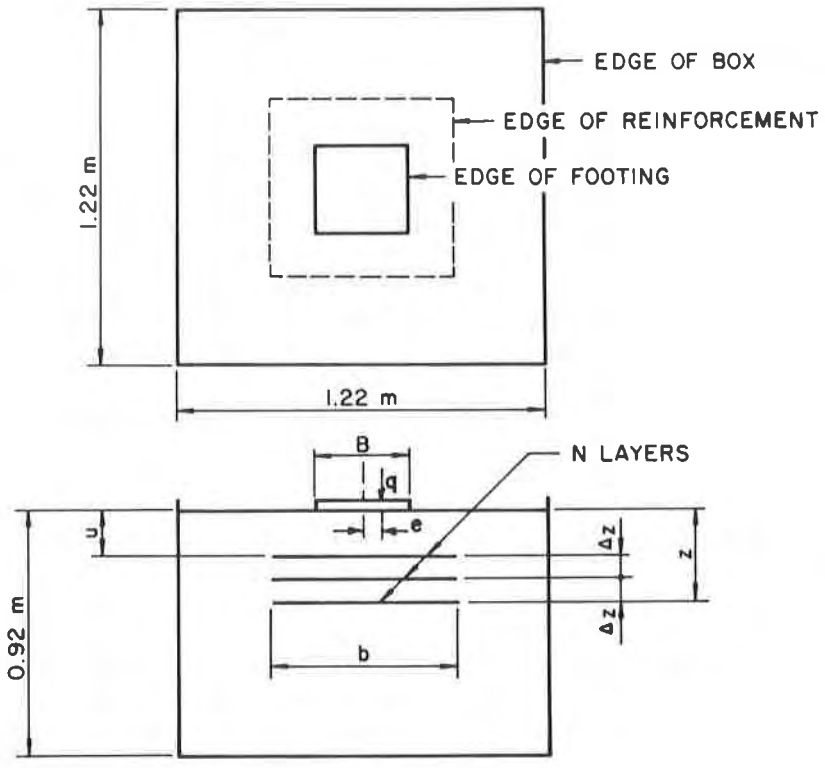

Figure 3 Geometry of the Test Model

6) The ultimate bearing capacity, q_u, for a given test for both the average settlement and rotation should be the same according to Meyerhof (1990), when defined as the bearing pressure at which the curves pass into inclined straight lines. At an eccentricity of 1 in.(25.4 mm) or e/B=1/12, this was the case for the unreinforced sand subgrade. Upon the introduction of reinforcement into the subgrade and at e=2 in.(50.8 mm) or e/B=1/6 (at the edge of the kern) for both the unreinforced and reinforced subgrade, the average settlement curve and the rotation curve deviate and yield very different values of ultimate bearing capacity. Since the bearing pressure-settlement ratio curves for e/B=1/12 and 1/6, for the case of the unreinforced sand subgrade were very similar and those for rotation very different; it was decided to use the settlement ratio curves to determine the ultimate bearing capacity. Guido et al (1987) used a settlement ratio of 0.07 to evaluate the ultimate bearing capacity of concentrically loaded plates on geogrid-reinforced sand subgrades. To be consistent with their research the same settlement

ratio was used for the eccentrically loaded plates. The bearing capacities for the unreinforced sand subgrade resulting from Meyerhof (1953) do not agree with the values obtained experimentally and presented herein. This is possibly due to the value of the settlement ratio used to evaluate the ultimate bearing capacity.

7) The bearing capacity ratio will be defined as

$$BCR = q_u/q'_{uo} \quad (3)$$

or

$$BCR' = q''_u/q'_{u1} \quad (4)$$

where q'_{uo} is the ultimate bearing capacity for a concentrically loaded plate on an unreinforced sand subgrade, q_u is the ultimate bearing capacity for either a concentrically or eccentrically loaded plate on either an unreinforced or reinforced sand subgrade and q'_{u1}, and q''_u are the ultimate bearing capacities for an eccentrically loaded plate with e/B=1/12 on an unreinforced and reinforced sand subgrade respectively. Equation (4) was used only when the relative density parameter was investigated because a value of q'_{uo} was obtained only at a relative density of 55% and not at the remaining values investigated. In addition, in Figures 5 and 7 the value of rotation, θ, plotted for a particular case corresponds to the ultimate bearing capacity, q'_{uo} and in Figure 8 to q'_{u1}.

Degree of Eccentricity. In order for the applied pressure across the loading plate to be solely in compression, the applied load must be inside the kern (see Figure 2). For a square plate the boundary of the kern is located a distance B/6 from the centroid of the plate. If the applied load is outside the kern a portion of the plate will have an applied pressure which is tensile. As the load is applied further outside the kern, the zone of tensile stress gets larger. Since soil can take very little if any tensile stress, albeit the reinforcement can, it was decided for this initial investigation to keep all the eccentricities inside or on the boundary of the kern, ensuring only compressive stresses were being applied to the soil. The eccentricities investigated were e/B=0, 1/12 and 1/6, no double eccentricities were attempted for this investigation.

In Figures 4 and 5, N=0 represents the unreinforced sand subgrade. It can be seen that when N=0 there is a 16% and 19% reduction in the bearing capacity from the e=0 condition for e/B=1/12 and 1/6, respectively, and the rotation increases from 0 to 0.088 rads and 0.170 rads, respectively. From Figures 4 and 6 it can be seen that the placement of the geogrid-reinforcement in the sand subgrade increased the load bearing capacity and from Figures 5 and 7 that the rotation of the plate decreased from the unreinforced condition, regardless of the degree of eccentricity. Further discussion of the degree of eccentricity will be included in conjunction with the effect of the other parameters investigated.

Number of Layers of Geogrid-Reinforcement. The effect of the number of layers of geogrid-reinforcement can be found in Figures 4 and

5. In general, the benefits of an increased bearing capacity and a reduction in rotation diminish with an increase in the number of layers of reinforcement. The optimum number of layers of reinforcement is approximately 3 (except for e/B=0), additional layers tend to yield no additional benefits. Similar results have been observed for concentrically loaded plates by Binquet and Lee (1975) and Guido et al (1985), (1987) and (1989).

A comparison of curves (a), (b) and (c) in Figure 4 indicates that except for N=1 and e/B=1/6 the bearing capacity increased above the concentrically loaded unreinforced subgrade case (for e/B=1/6, 46%, and 80% above its unreinforced case). However, a comparison of the same curves in Figure 5 indicate that although the rotations are reduced considerably (for e/B=1/12, over 300%), zero rotation is never reached regardless of the number of layers of reinforcement.

At N=1, the curve for e/B=1/12 is approximately equal to the curve for e/B=0. As N increases the BCR tends to level off quickly with increasing N for e/B=1/12, whereas for e/B=0 at N=3 the BCR is still increasing. After N=1, curve (b) remains below curve (a). Curve (c), e/B=1/6, remains below curves (a) and (b) for all values of N up to 2, after which its bearing capacity exceeds that of e/B=1/12 but is less than that of e/B=0. An e/B=1/6 places the load on the boundary of the kern; due to experimental inaccuracies it may actually be slightly outside the kern, inducing tensile stresses to develop. These tensile stresses would be picked up by the reinforcement and may actually yield a higher bearing capacity than if they did not exist. This can account for the higher bearing capacity at N=3, of e/B=1/6 than that of e/B=1/12. However, in reference to rotation there is a steady decrease in rotation for both e/B=1/12 and 1/6 with the rotations for e/B=1/12 always less than those for e/B=1/6 for all values of N, and neither reaches the zero rotation of e/B=0.

Width Size of a Square Sheet of Geogrid-Reinforcement. For a square sheet of geogrid-reinforcement, the width of the sheet is designated by b or the sheet has a width ratio of b/B. A comparison of curves (a), (b) and (c) in Figure 6 show a steady increase in the bearing capacity ratio with increasing b/B. Similar results have been observed for concentrically loaded plates by Fragaszy and Lawton (1984) and Guido et al (1985), (1987) and (1989). Within the sand subgrade there exists a zone of soil extension and only that portion of the geogrid-reinforcement within this zone will have its tensile strength effectively mobilized. Geogrid-reinforcement area beyond this zone will serve only as anchorage. For eccentrically loaded plates where the reinforcement was placed concentrically below the plate, a large portion of the reinforcement was neither in the zone of soil extension or anchorage, and the grid had no function.

Curve (c) in Figure 6 falls between curves (a) and (b) indicating a greater bearing capacity ratio at all values of b/B for the larger eccentricity, e/B=1/6, than for e/B=1/12. An e/B=1/6 places the applied load at the boundary of the kern, and as was discussed previously some tensile stresses may have been induced in the reinforcement enabling the reinforced sand subgrade, at this larger eccentricity, to withstand a

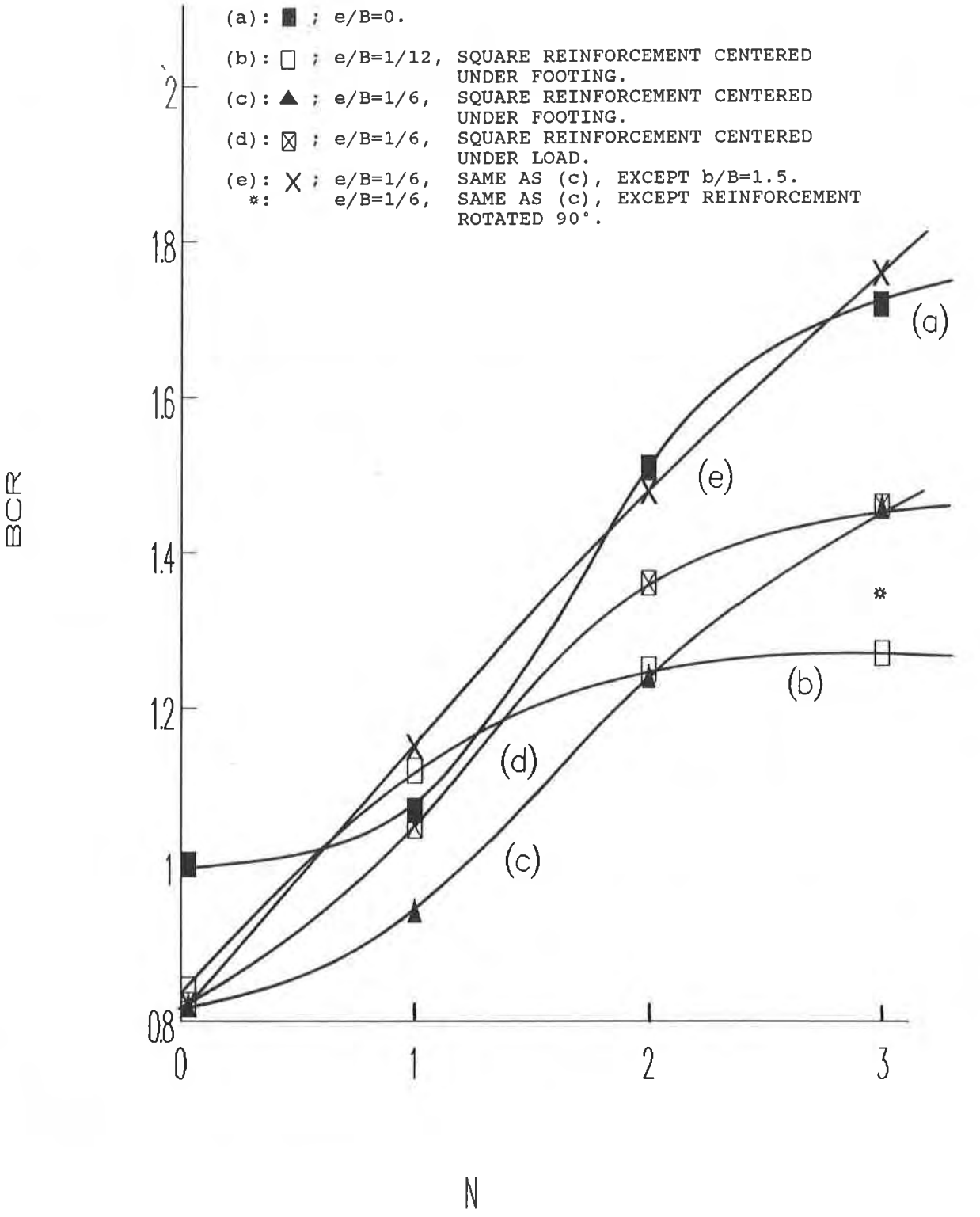

Figure 4 Variation of BCR with the Number of Layers, u/B=1/6, Δz/B=1/6, b/B=1.0 AND D_r=55%

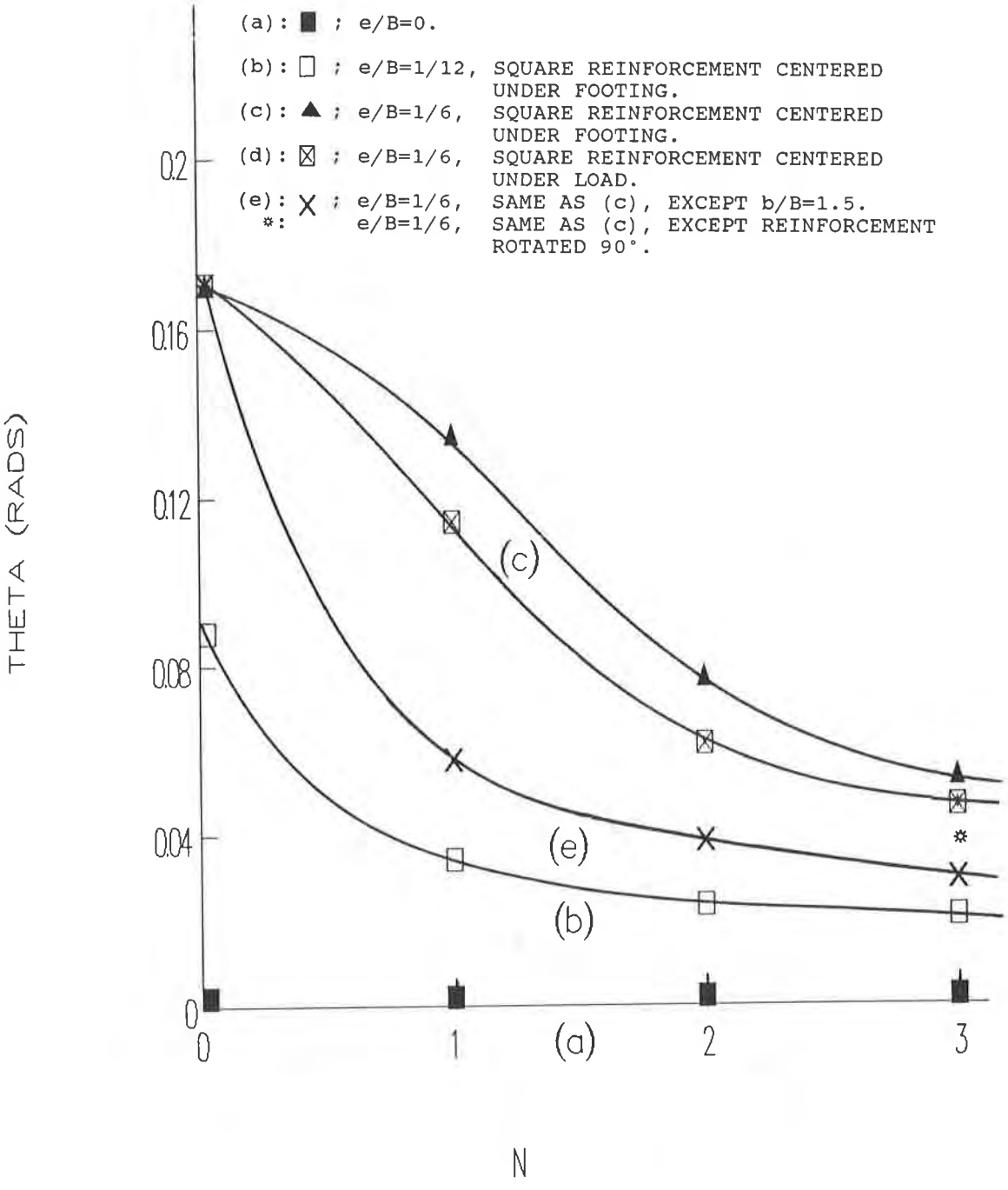

Figure 5 Variation of $\bar{\theta}$ with the Number of Layers, u/B=1/6, Δz/B=1/6, b/B=1.0 and D_r=55%

higher load than at the lower eccentricity. In addition, if the same curves are compared in Figure 7 it can be seen that the largest rotations occur for e/B=1/6 and all curves approach a limiting value at approximately b/B=2.0. The zero rotation associated with a concentrically applied load is never achieved for any of the

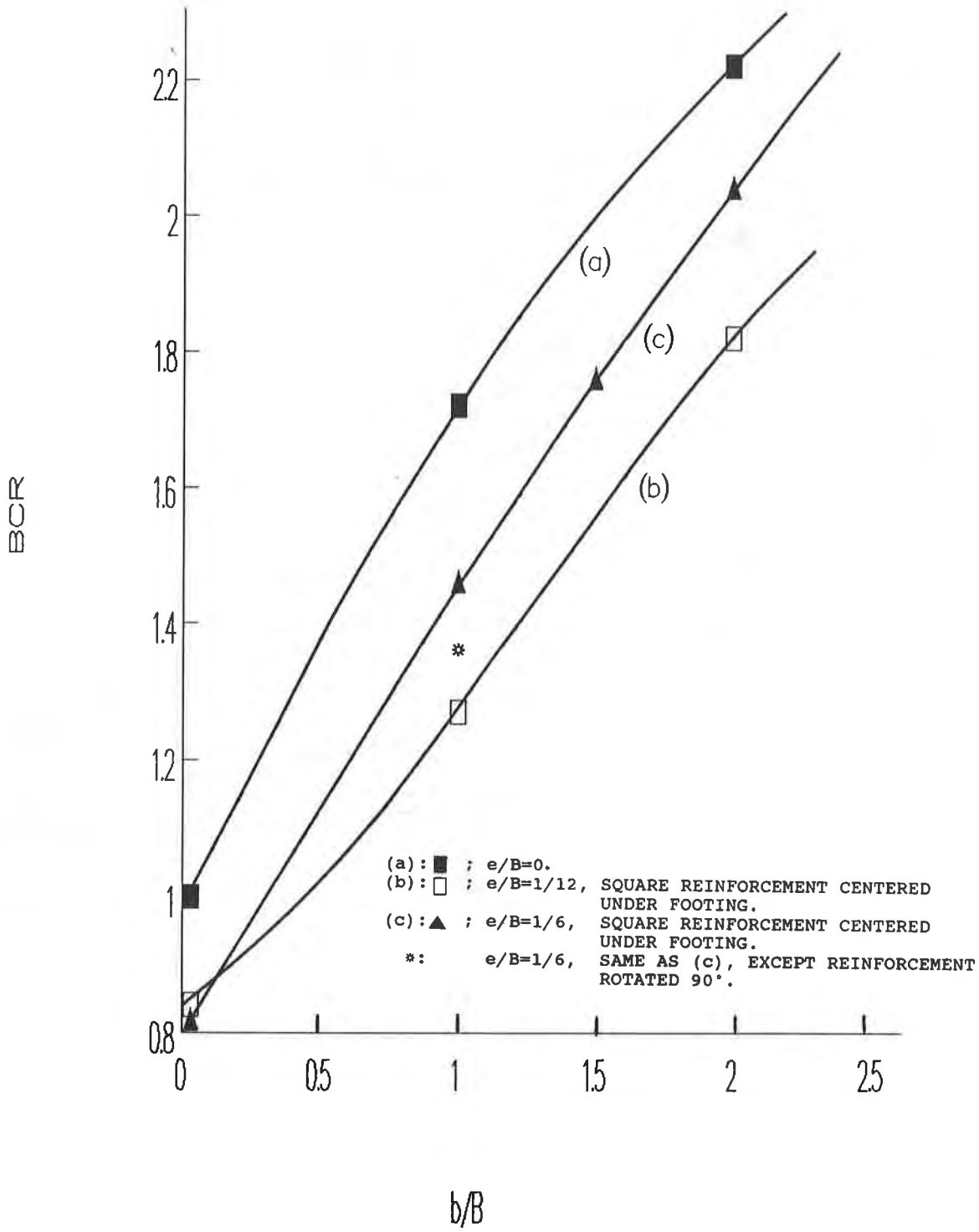

Figure 6 Variation of BCR with the Width Ratio, u/B=1/6, Δz/B=1/6, N=3 and D_r=55%

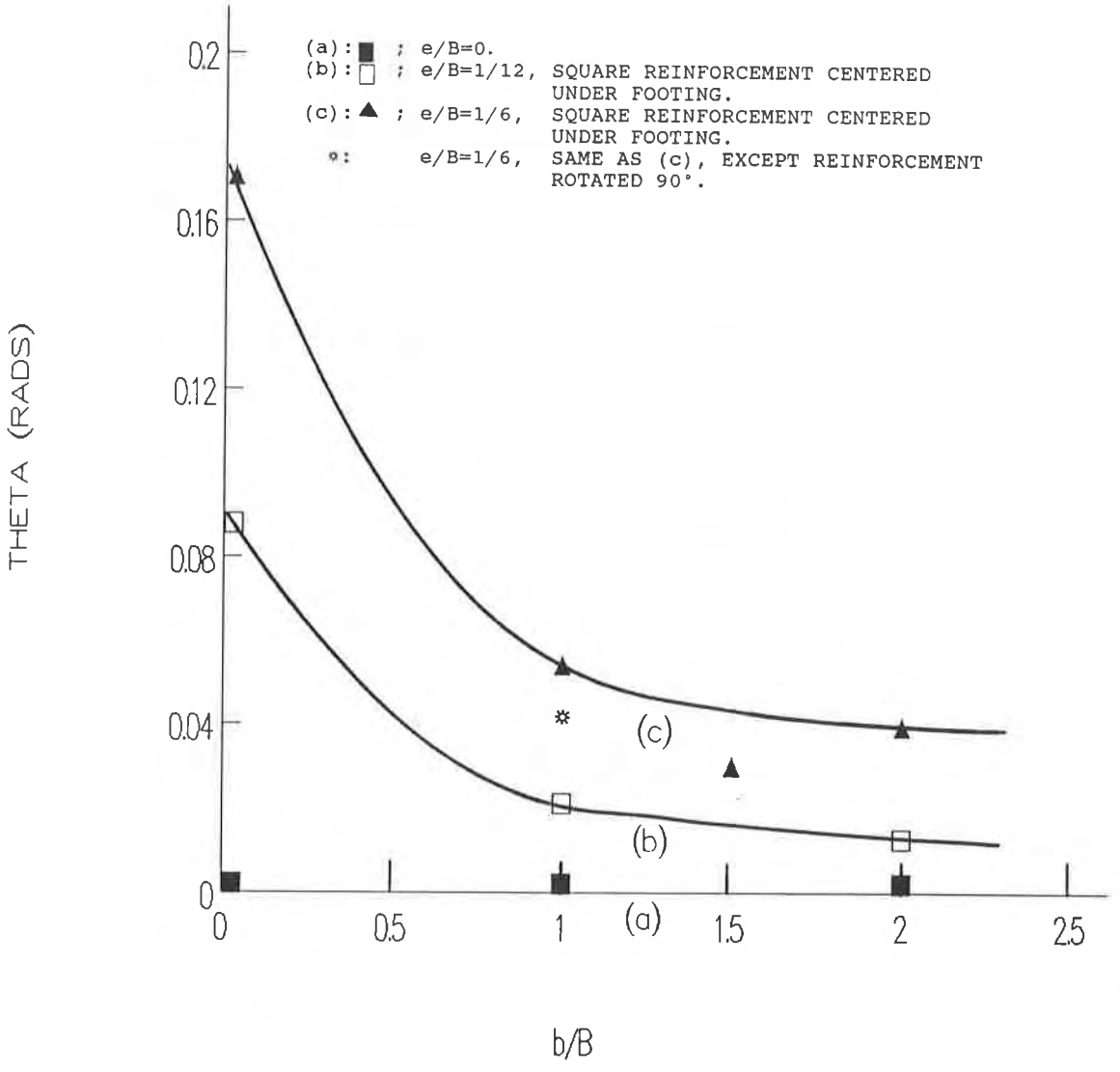

Figure 7 Variation of Θ with the Width Ratio, u/B=1/6, Δz/B=1/6, N=3 and D_r=55%

eccentricities. If a comparison of curves (a) and (e) in Figure 4 is made it can be seen that for b/B=1.5 the bearing capacity of the plate with an eccentricity of e/B=1/6 is almost identical with that of the concentrically loaded plate. However, the rotation of the plate for b/B=1.5 and e/B=1/6 does not achieve zero rotation.

Position of the Sheet of Geogrid-Reinforcement. Two positions of the sheet of geogrid-reinforcement were investigated: the centroid of the sheet was place directly under the centroid of the plate or the centroid of the sheet was placed directly under the applied load. A comparison of curves (c) and (d) in Figures 4 and 5, indicates that

those tests performed with a square sheet of geogrid-reinforcement placed with its centroid directly beneath the applied load yielded higher bearing capacities and lower rotations than those tests performed with a square sheet of geogrid-reinforcement placed with its centroid directly beneath the centroid of the plate. By placing the reinforcement directly beneath the applied load, more of the reinforcement is being placed in the zone of soil extension and is being utilized more effectively.

Orientation of the Sheet of Geogrid-Reinforcement. Of the 58 tests performed, all but two had the grid oriented with the machine direction parallel to the x-axis (see Figure 2). The remaining two had the grid oriented with the cross-machine direction parallel to the x-axis. These two tests (N=3, b/B=1.0, square sheet of reinforcement under centroid of footing and e/B=1/6) yielded identical results. Their results plotted as isolated points in Figures 4, 5, 6 and 7 should be compared to curve (c). It can be seen that when the grid is placed with the machine direction parallel to the x-axis the bearing capacity is larger than when it is rotated 90° from this orientation, and the rotations are comparable. By placing the machine direction parallel to the x-axis, actually more ribs are being placed parallel to the axis about which bending is occurring, than if the cross-machine direction had been placed parallel to the x-axis, and a better interlocking of the soil and grid occurs to resist bending. This in turn will increase the bearing capacity and have less of an effect on rotation.

Relative Density of the Sand. Figure 8 shows the variation of BCR' and θ with the relative density of the sand. Curve (a) indicates that there is a steady increase in the bearing capacity of the reinforced sand subgrade over its unreinforced case, for e/B=1/12, up to approximately a relative density of 80%. An increase in relative density above this value yields no further benefits. In addition, curve (b) indicates a steady decrease in the rotation up to approximately the same relative density of 80%. This indicates that under the aggravated condition of eccentric loading the inclusion of reinforcement in a poor quality subgrade will not be as beneficial as an inclusion in a better quality subgrade.

CONCLUSIONS

Presented herein are the results of a series of laboratory model eccentrically loaded plate tests on a geogrid-reinforced sand subgrade. The results have shown that the insertion of the geogrid into the subgrade has substantially increased its load bearing capacity and reduced its rotation. Based upon the test results, the reinforcement should be placed within an effective depth (z/B) of from 0.5 to 0.7 below the base of the plate. This is less than the z/B=1.0 presented by Guido et al (4) for a concentrically loaded plate on a geogrid-reinforced sand subgrade. When a plate is eccentrically loaded the effective area of the plate is reduced and therefore, the depth of soil below the plate which influences the bearing capacity is reduced. This is illustrated by the reduction in z/B from 1.0 for e/B=0 to 0.5 to 0.7 for e/B greater than 0.

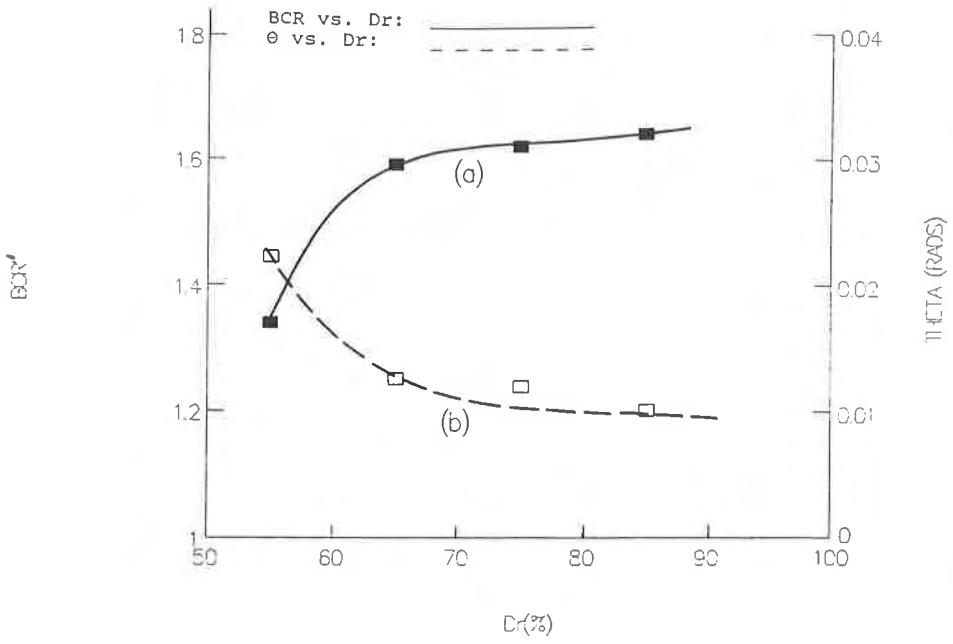

Figure 8 Variation of BCR and Θ with Relative Density, u/B=1/6, Δz/B=1/6, N=3, b/B=1.0 and e/B=1/12

The square sheet of geogrid-reinforcement should be placed with its centroid directly below the point of application of the load. In this way the reinforcement is utilized to its fullest by having the majority of its area placed in the zone of soil extension. In addition, the geogrid should be oriented in the sand subgrade with the machine direction transverse to the axis about which bending of the plate is taking place. This will insure that a maximum number of ribs will be placed parallel to the axis of bending, increasing the interlocking between the soil and the grid and therefore, increasing its load bearing capacity and decreasing rotation.

At low relative densities (Dr=55%) there is a 35% increase in the load bearing capacity over the unreinforced case, whereas at high relative densities (Dr=80%) there is a 65% increase in the load bearing capacity over the unreinforced case. Therefore, although a low compaction effort coupled with reinforcement yields substantial load bearing capacity, there is a relatively greater benefit to placing the reinforcement in a well compacted subgrade. Depending on the required load bearing capacity of the subgrade, it may prove cheaper to compact the subgrade to a high relative density without reinforcement. However, if the desired load bearing capacity is unattainable by these means, placement of multiple layers of reinforcement in the subgrade coupled with a greater compaction effort may be able to produce the desired results.

The use of geosynthetics as soil reinforcement has gained wide spread use. Their application in situations involving concentrically applied loadings is becoming more of a design and construction

alternative. The case of an eccentrically applied load is not so rare as not to warrant the use of geosynthetics in subgrade materials. Two very common applications would be in subgrades below retaining structures and transmission towers.

Further research is needed prior to the use of geosynthetics in the design and construction of reinforced subgrades underlying eccentrically loaded footings. Only one geosynthetic was tested in this investigation, the Tensar BX1100 geogrid; other grids, geotextiles and geocells should also be tested. In addition to granular subgrades, cohesive soils should be investigated. Further testing should be done on the orientation of the geogrid within the subgrade, on application of the load outside the kern and on double eccentricity. There is a definite place for the use of geosynthetics in subgrades underlying foundations subjected to bending moment.

REFERENCES

Binquet, J. and Lee, K.L., (1975) "Bearing Capacity Tests on Reinforced Earth Slabs", ASCE Journal of Geotechnical Engineering, 101(GT12), p.p. 1241-1255.

Fragaszy, R.J. and Lawton, E., (1984) "Bearing Capacity of Reinforced Sand Subgrades", ASCE Journal of Geotechnical Engineering, 110(GT 10), p.p. 1500-1507.

Guido, V.A., Biesiadecki, G.L. and Sullivan, M.J., (1985) "Bearing Capacity of a Geotextile-Reinforced Foundation", Proceedings of the Eleventh International Conference on Soil Mechanics and Foundation Engineering, San Francisco, Vol. 3, p.p. 1777-1780.

Guido, V.A., Knueppel, J.D. and Sweeney, M.A., (1987) "Plate Loading Tests on Geogrid-Reinforced Earth Slabs",Proceeding of the Geosynthetics '87 Conference, New Orleans, Vol. 1, p.p. 216-225.

Guido, V.A., Christou, S.N. and Sobiech, J.P., (1989) "A Comparison of Texturized and Non-Texturized GEOWEB-Reinforced Earth Slabs", Proceeding of the Geosynthetics '89 Conference, San Diego, Vol. 1, p.p. 215-230.

Meyerhof, G.G., (1953) "Bearing Compacity of Foundations Under Eccentric and Inclined Loads", Proceedings of the Third International Conference on Soil Mechanics and Foundation Engineering, Zurich, Vol. 1, p.p. 440-445.

Meyerhof, G.G., (1990) private communication to V.A. Guido.

On the Design of Reinforced Embankments on Soft Brittle Clays

B. L. J. Mylleville
The University of Western Ontario, Canada
R. K. Rowe
The University of Western Ontario, Canada

ABSTRACT

Finite element analyses are used to examine the effect of geosynthetic modulus on the behaviour of reinforced embankments constructed on very soft brittle clay deposits with and without a higher strength surface crust. Results are presented which illustrate how the calculated shear strains in the very soft underlying foundation are influenced by the geosynthetic modulus and selection of a limiting strain in design. It is demonstrated how an examination of shear strain in the foundation soil may be used to assess the potential for problems if the soil is susceptible to strain softening. Implications for practical design are discussed.

INTRODUCTION

It is now well recognized that the modulus of geosynthetic reinforcement greatly influences the performance of embankments constructed on soft cohesive deposits. The purpose of this paper is to discuss the effects of reinforcement modulus on the development of strain in both the geosynthetic and the underlying foundation soil, with emphasis on very soft brittle cohesive soils. The type of foundation soils being considered are typical of soft elastic-perfectly plastic soils with and without a higher strength surface crust.

Results obtained from carefully performed finite element analyses are used to illustrate that potential problems may arise due to strain softening in some brittle soils as a result of adopting allowable reinforcement strains recommended in the literature in a design situation. Some recommendations are made relating to the design approach which should be adopted for these situations.

NUMERICAL MODEL

Results from small strain elasto-plastic finite element analyses are presented in this paper. The program used was a modified version of program AFENA, developed by Carter (1985). Specific details regarding the formulation are discussed by Rowe and Soderman (1987) and Rowe and Mylleville (1988).

The results presented here were obtained using a finite element mesh with 12171 degrees of freedom. The high degree of refinement of the finite element mesh required the use of an ETA10-P supercomputer to perform the analyses.

Reinforced embankments were "constructed" by turning on gravity within rows of elements. This involved up to 12 lifts and a total of up to 250 load steps in the analysis.

PROBLEM DESCRIPTION

The type of problem being considered is that of a geosynthetic reinforced embankment constructed on a soft clay foundation as shown in Figure 1. Embankments of crest width B=18 m, were "constructed" on a soft clay deposit to a height h above original ground level, using 2 to 1 side slopes.

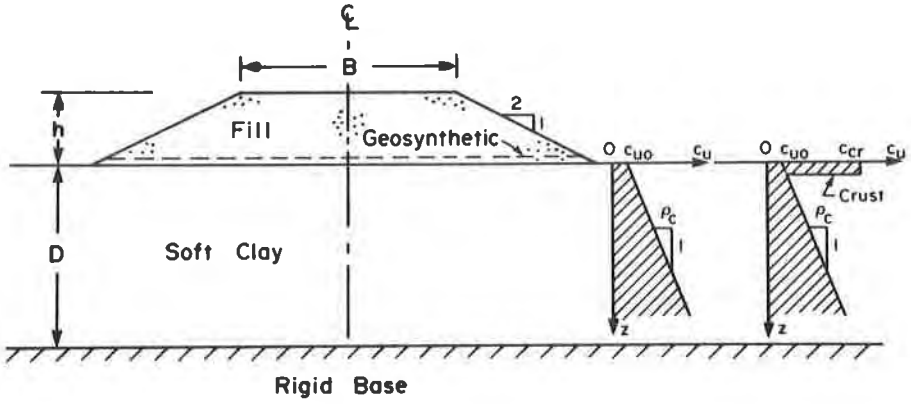

Figure 1. Typical embankment on a soft clay foundation

The granular embankment fill was modelled as having a stress-dependent Young's modulus based on Janbu's equation (see Rowe and Soderman (1987)). The parameters used in the numerical model for the granular fill were ϕ=32°, γ=20 kN/m^3, Poisson's ratio, ν=0.35 and dilatancy, ψ=0°.

The depth of clay deposit D, being considered is 15 m which is in turn underlain by a rigid base as shown in Figure 1. When constructing embankments on soft clay deposits, the most critical stage in terms of stability usually corresponds to that at the end of construction. The finite element results presented herein are predictions of embankment behaviour based on short term undrained (ϕ=0) analyses (taking Poisson's ratio to be 0.48).

The soft foundation soil was modelled as having an undrained shear strength and undrained modulus which increase linearly with depth from some surface value as shown in Figure 1. Some results are presented for undrained strength profiles with and without a higher strength surface crust. Strength profiles such as those shown in Figure 1 are commonly encountered in soft, normally or slightly overconsolidated clays. The ratio of undrained modulus to undrained strength (E_u/c_u) considered was E_u/c_u=500. The clay foundation was assumed to have a unit weight, γ of 16.5 kN/m^3 and coefficient of earth pressure at rest, K_o' of 0.60.

This paper examines results obtained using a construction sequence in which a 375 mm thick granular working mat is first placed directly on the surface of the clay deposit and the geosynthetic reinforcement is then placed on top of this granular working mat. The embankment is subsequently "constructed" to failure and ultimate collapse by placing horizontal lifts of granular fill on top of the geosynthetic. The fill-geosynthetic interface friction angle was taken to be 32°. The finite element model allows for slip at the clay-fill interface below the reinforced embankments as well as slip at the fill-geosynthetic interface.

To determine the embankment fill thickness and geosynthetic strain at failure, factored strength parameters were used in the finite element analyses. For a given foundation with nominal strength parameters c_{uo} and ρ_c, adopting a factor of safety FS=1.3, the factored strength parameters used in the analyses are $c_{uo}^*=c_{uo}/1.3$ and $\rho_c^*=\rho_c/1.3$. Thus, the fill thickness at failure computed using factored parameters corresponds to the allowable fill thickness under working conditions for the nominal strength parameters and a "factor of safety" equal to 1.3.

SOFT BRITTLE CLAY DEPOSITS

Inevitably, two important factors governing the behaviour of embankments constructed on soft brittle clay deposits are the strength characteristics of the underlying foundation and the modulus (stiffness) of the geosynthetic reinforcement. Figure 2 shows the relationship between applied pressure, γH (due to the embankment load, where H is the maximum thickness of fill at a given point in time), and the maximum strain developed in the geosynthetic reinforcement obtained from several finite element analyses.

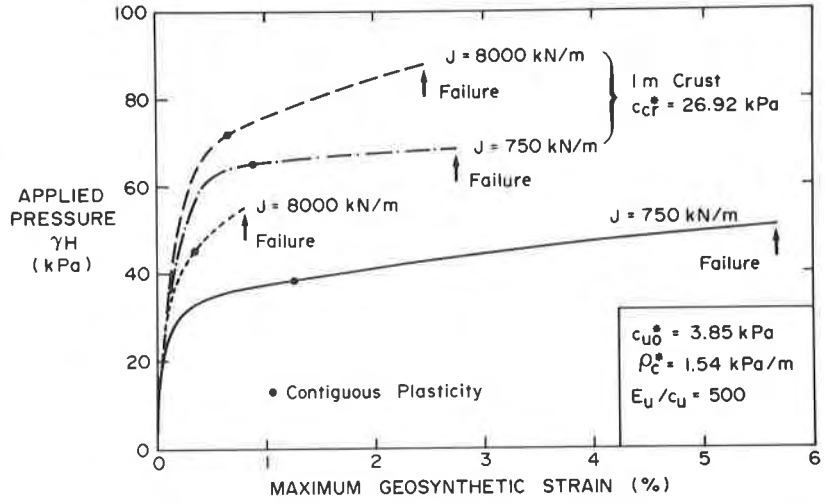

Figure 2. Effect of geosynthetic modulus on the maximum strain in the reinforcement

Analyses were performed for foundations assuming an undrained strength profile which increases with depth at a rate, ρ_c, from some surface strength, c_{uo}. Analyses were performed with and without a higher strength surface crust of strength c_{cr} and thickness 1 m (see also Figure 1 for a definition of the various strength terms). The nominal strength parameters considered were c_{uo}=5 kPa, ρ_c=2 kPa/m and for the profiles with a crust, c_{cr}=35 kPa. Factored parameters c_{uo}*, ρ_c* and c_{cr}* were used in the analyses.

The curves shown in Figure 2 both start at an applied pressure equal to 7.5 kPa because of the assumed construction technique (i.e. placement of 375 mm working mat prior to placement of the geosynthetic reinforcement) and terminate at a maximum geosynthetic strain corresponding to that at failure of the embankment. From a practical standpoint, a reinforced embankment is assumed to have failed at a fill thickness where the increment in vertical displacement is equal to or exceeds the increment in fill thickness just added. The addition of more fill will not result in a net increase in embankment height (for a detailed discussion regarding the failure and collapse of geosynthetic reinforced embankments, refer to Rowe and Soderman (1987)).

The shape of the curves shown in Figure 2 can be explained in terms of the behaviour of reinforced embankments on soft foundations. Initially, the maximum strain in the geosynthetic reinforcement increases slowly with increasing applied pressure and the foundation carries most of the load due to the embankment. However, once contiguous plastic failure occurs in the underlying foundation soil, the reinforcement must carry any additional load which must be resisted along the potential failure surface and hence the geosynthetic strains increase rapidly. The exception to this is the curve shown in Figure 2 for a very stiff reinforcement, J=8000 kN/m, on a very soft foundation with no surface crust (to be discussed in subsequent paragraphs).

To examine the effect of reinforcement modulus on the behaviour of embankments constructed on very soft brittle clay deposits without a surface crust, consider the lower two curves shown in Figure 2. The underlying clay foundation is assumed to have nominal strength properties c_{uo}=5 kPa and ρ_c=2 kPa/m, however factored parameters are used in the analysis (i.e. c_{uo}*=5/1.3 = 3.85 kPa and ρ_c*=2/1.3 = 1.54 kPa/m, where 1.3 is the assumed design factor of safety). The fill thickness (applied pressure) at failure obtained using factored parameters is therefore the allowable design height under working conditions (provided that the permissible strain for the geosynthetic is not exceeded). At failure, the maximum strain is approximately 5.7% for the embankment reinforced with a geosynthetic of modulus, J=750 kN/m and the fill thickness at failure is 2.5 m. This represents a 47% improvement in failure thickness when compared to the unreinforced failure height of 1.70 m. Increasing the modulus to a very high value of say, J=8000 kN/m has resulted in a marginal increase in fill thickness to 2.80 m (i.e. 0.3 m increase) and resulted in a substantially lower strain of 0.8%. The very high modulus reinforcement has significantly altered the behaviour of the embankment system. This is best illustrated by examining Figures 3 to 8 which compare the response of the two reinforced embankments under discussion.

Shown in Figure 3 is the velocity field at failure for the embankment reinforced with a geosynthetic of modulus, J=750 kN/m. The arrows indicate the direction and relative magnitude of soil movement at failure. The shape of the failure mechanism resembles that of a classical slip circle.

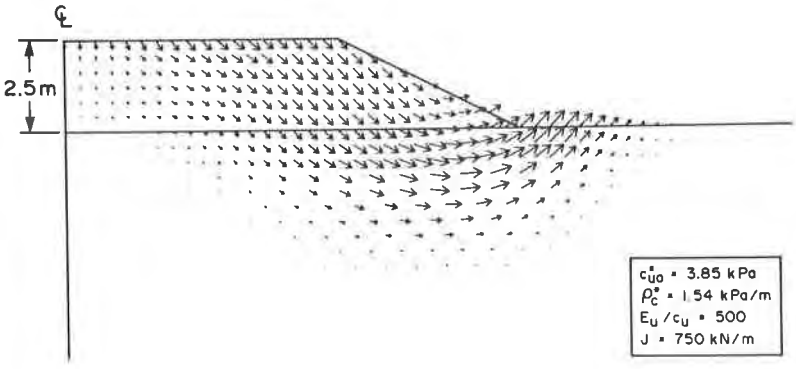

Figure 3. Velocity field at failure; J=750 kN/m

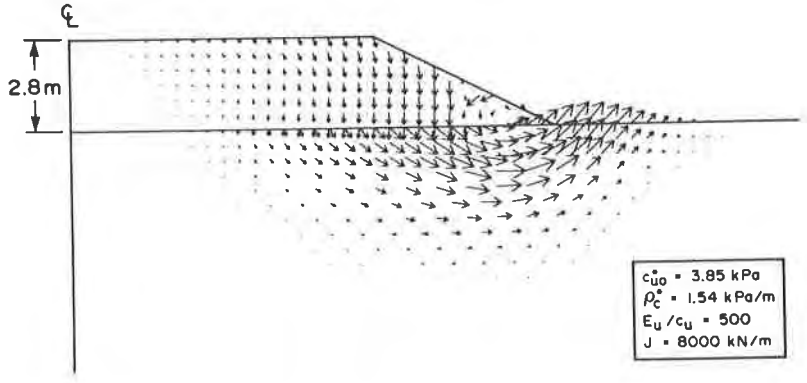

Figure 4. Velocity field at failure; J=8000 kN/m

Increasing the modulus of the geosynthetic to a very high value, J=8000 kN/m results in a velocity field as shown in Figure 4. What is interesting to note is that the inclusion of a very stiff reinforcement has substantially reduced the lateral component of displacement in the embankment fill, which is tending to move downward as a semi-rigid block and there is considerable slip at the fill-clay interface as indicated by the dual arrows shown in Figure 4. The movement of the fill is constrained by the reinforcement and the clay is squeezed out underneath. This type of behaviour is similar to that observed for steel strip reinforced embankments discussed by Rowe and Mylleville (1988) and Mylleville and Rowe (1988). In this case, failure is a bearing capacity type failure (rather than failure based on consideration of deformations). The fill thickness to cause collapse can be estimated reasonably well using a technique proposed by Rowe and Soderman (1987) where the heavily

reinforced embankment is idealized as an equivalent rigid footing. Interestingly enough, (based on an examination of the velocity field, Fig.4) it would appear that there is an effective crest width, B^* (which is less than B), corresponding to the failure mechanism. Using this reduced crest width B^*=9 m, the theoretical bearing capacity fill thickness was estimated to be 2.7 m. This compares reasonably well with the fill thickness of 2.8 m at failure for this heavily reinforced embankment which is tending to behave as a semi-rigid footing. It is noted that in this case the more than ten fold increase in reinforcement modulus (from 750 kN/m to 8000 kN/m) has not resulted in a significant increase in failure height because the embankment with a 750 kN/m reinforcement was already relatively close to the maximum capacity imposed by bearing capacity even though with a J=750 kN/m geosynthetic, failure is still a rotational type failure.

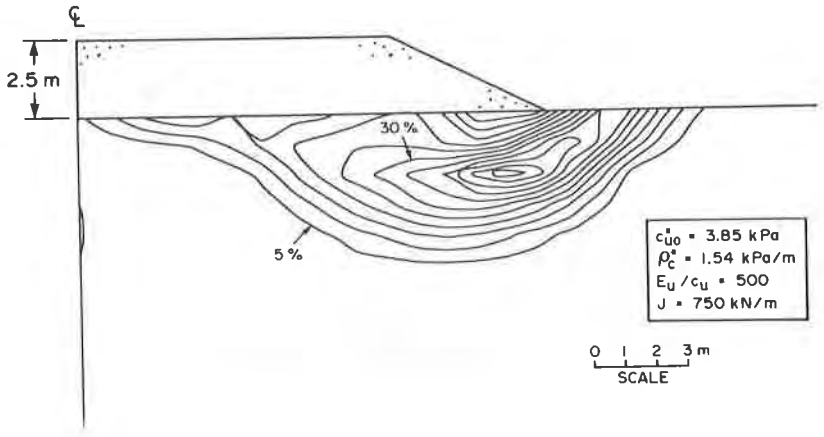

Figure 5. Contours of maximum shear strain at failure: 2.5 m fill thickness - 5% contour interval (from Rowe and Mylleville (1990))

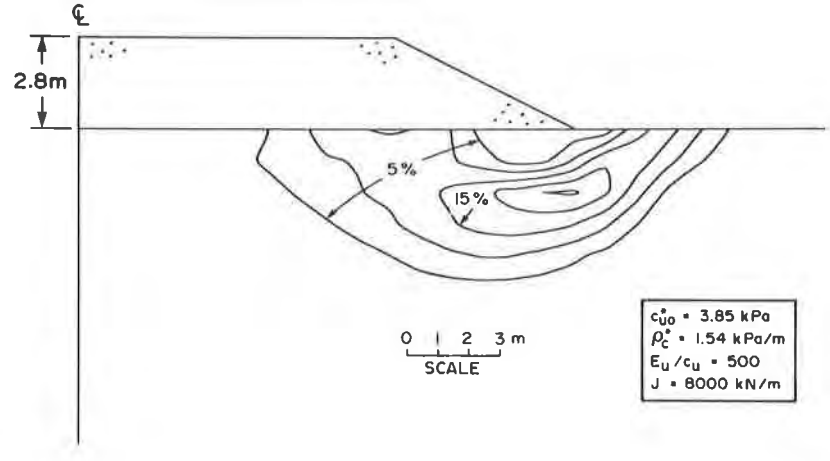

Figure 6. Contours of maximum shear strain at failure: 2.8 m fill thickness - 5% contour interval

Figure 5 shows contours of maximum shear strain at failure in a portion of the underlying clay foundation beneath the embankment reinforced with a geosynthetic having a modulus, J=750 kN/m. The contours for J=8000 kN/m are shown in Figure 6. For purposes of further discussion, maximum shear strain, ϵ_{sh}, is defined as the maximum engineering shear strain in the soil or in other words, the diameter of the Mohr's circle of strain (i.e. $\epsilon_{sh}=\epsilon_1-\epsilon_3$) expressed in percent. The first thing to note is that in both cases, at failure a band of intense shearing develops which is coincident with the failure mechanism in the underlying foundation soil (see also Rowe and Mylleville (1989)). At failure, for the embankment reinforced with a geosynthetic having a modulus, J=750 kN/m, there is a band of foundation soil which experiences maximum shear strains in excess of 30%. At that point, the maximum strain in the geosynthetic was found to be 5.7%. On the other hand, for the case of a very stiff reinforcement, say J=8000 kN/m, a significant band of foundation experiences maximum shear strains in excess of 15% as shown in Figure 6. The maximum strain in the geosynthetic was found to be 0.8%. Thus the stiffer reinforcement has slightly increased the fill thickness to cause failure but at the same time it has significantly reduced the shear strains experienced by the foundation soil.

Various investigators (La Rochelle et al. (1988); Lo and Morin (1972)) have found that sensitive clays may reach peak strengths at axial strains of 1% or less. Under undrained (constant volume) conditions this would correspond to a maximum shear strain, ϵ_{sh} approximately equal to 1.5%. Development of significant zones of shear strain in excess of 1.5% may pose potential problems with respect to strain softening and the results from conventional finite element or limit equilibrium analyses may be unconservative. It becomes evident from Figures 5 and 6 that the failure heights obtained assuming a plastic soil would overestimate the true failure height for a brittle soil since extensive softening would be expected to have occurred. Problems with softening may also arise under working conditions.

Shown in Figures 7 and 8 are the contours of maximum shear strain under working conditions (i.e. analyses were performed using nominal (unfactored) parameters) for the two cases under consideration. As can be seen from Figure 7, for an allowable fill thickness based on a limiting strain in the order of 5% and a geosynthetic of modulus, J=750 kN/m, there is an extensive zone of foundation soil which experiences maximum shear strains in excess of 1.5%. This zone is large enough to create problems if the soil is susceptible to softening at 1.5% strain. The calculated maximum strain in the geosynthetic for the "allowable fill thickness" under working conditions is only 1.3%. It should be noted that these "working conditions" are based on a stability calculation that considers peak strength, neglect strain softening and permits a strain in the geosynthetic at failure of 5 to 6%. As previously discussed by Rowe and Mylleville (1990), adopting a lower limiting strain of say 2% to obtain an allowable fill thickness from a conventional plastic analysis may help to reduce the maximum shear strain developed in the foundation soil to a more acceptable level.

Plotted in Figure 8 are contours of maximum shear strain under working conditions for the very high modulus reinforcement, J=8000 kN/m. The inclusion of a very stiff geosynthetic has dramatically reduced the extent of the zone of foundation soil which experiences shear strains in excess of 1.5%. The maximum strain in the geosynthetic under working conditions is only 0.3%. If the embankment height had been limited to 2.5 m (which corresponds to 0.5% maximum strain in the geosynthetic using factored strength parameters; see Fig.2) then under working conditions (i.e. using nominal strengths) the maximum calculated shear strains are only about 1%.

A general observation which can be made is that for the soft brittle clay deposit just discussed, a very high modulus geosynthetic (e.g. J=8000 kN/m) may not be required to realize a substantial improvement in failure height compared to the unreinforced case. However, keeping in mind that the very high modulus reinforcement may change the failure mechanism and may warrant special consideration from a design standpoint, it does however significantly reduce the magnitude of maximum shear strains experienced by the foundation soil.

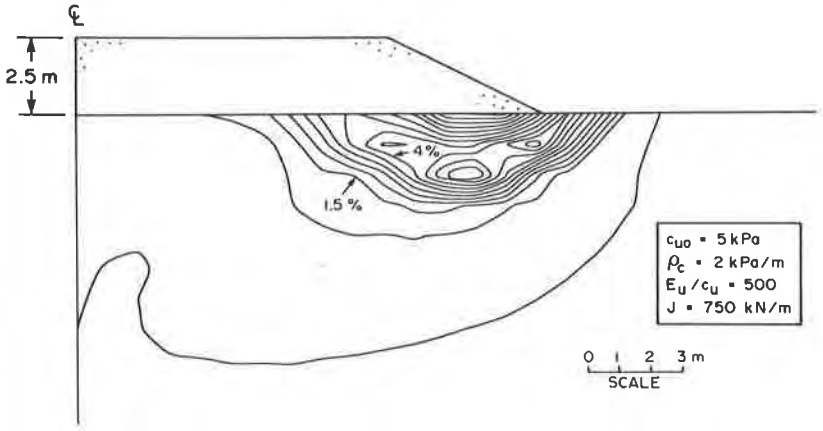

Figure 7. Contours of maximum shear strain under working conditions: 2.5 m fill thickness - 0.5% contour interval (from Rowe and Mylleville (1990))

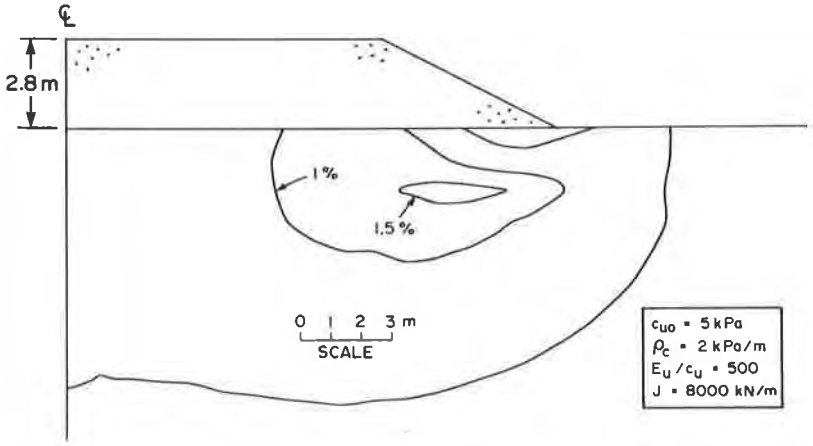

Figure 8. Contours of maximum shear strain under working conditions: 2.8 m fill thickness - 0.5% contour interval

SOFT BRITTLE CLAY DEPOSITS WITH A SURFACE CRUST

Many of the soft brittle clay deposits encountered, for example in eastern Canada and Scandinavia have a higher strength surface crust. Humphrey and Holtz (1989) and Rowe and Mylleville (1990) have demonstrated that a surface crust can substantially improve the stability of embankments. The presence of a higher strength surface crust may have a number of beneficial effects when compared to the case without a crust. The higher strength surface crust may help to increase the allowable embankment fill thickness, reduce the strain in the reinforcement and reduce the magnitude of maximum shear strains experienced by the foundation soil.

In this section, results of finite element analyses are presented which examine the effect of geosynthetic modulus on embankment performance. Two geosynthetic modulus values are examined: J=750 kN/m and J=8000 kN/m. The clay foundation is assumed to have a 1 m thick surface crust with a nominal undrained shear strength, c_{cr}=35 kPa. Beneath the crust the strength profile increases with depth at a rate of 2 kPa/m from an initial value of 7 kPa directly under the 1 m crust. The analyses were performed using factored parameters therefore the fill thickness at failure corresponds to the allowable fill thickness under working conditions.

One should keep in mind that for analyses with a high stiffness/strength surface crust, tensile stresses are attracted to the crust. Close examination of the results did show some tensile stresses to exist outside of the embankment, however only in the extreme upper portion of the surface crust. If the tensile stresses had propagated through the crust into the underlying soil, then this would constitute failure. Nevertheless, the results presented here should be regarded as upper bound solutions. If the crust was naturally fractured to any significant extent, then the improvement discussed below may not be fully realized.

The upper two curves in Figure 2, show the relationship between applied pressure and maximum geosynthetic strain for the analyses which will be discussed. The embankment reinforced with a geosynthetic of modulus J=750 kN/m, failed at a fill thickness of 3.4 m. The fill thickness at failure for the unreinforced case was found to be 3.2 m , hence it would seem the influence of the crust dominates with only a minimal improvement in failure load due to the inclusion of the geosynthetic.

The use of a higher modulus reinforcement, say J=8000 kN/m resulted in a fill thickness of 4.4 m at failure which represents a 38% improvement in failure load compared to the unreinforced case. However, one observation which can be made looking at Figure 2, is that the high modulus reinforcement (i.e. J=8000 kN/m) results in a somewhat more ductile response (i.e. beyond contiguous plasticity, the geosynthetic strain increases at a slower rate with increasing load to failure).

Figure 9 shows contours of maximum shear strain at failure for the case of a geosynthetic with modulus J=750 kN/m. Within the zone of intense shearing, the soil experiences maximum shear strains in excess of 10%. The contours of maximum shear strain at failure for the case of the very stiff geosynthetic are shown in Figure 10. The maximum shear strains experienced by the foundation soil are in excess of 14%, however the failure load is greater compared to that of the previous case (i.e. 4.4 m viz. 3.4 m). It should be noted that the maximum shear strains within the zone of intense shearing are comparable in magnitude to those shown in Figure 6 for the analysis without a crust and a considerably lower failure load. This once again illustrates the beneficial effect of a surface crust.

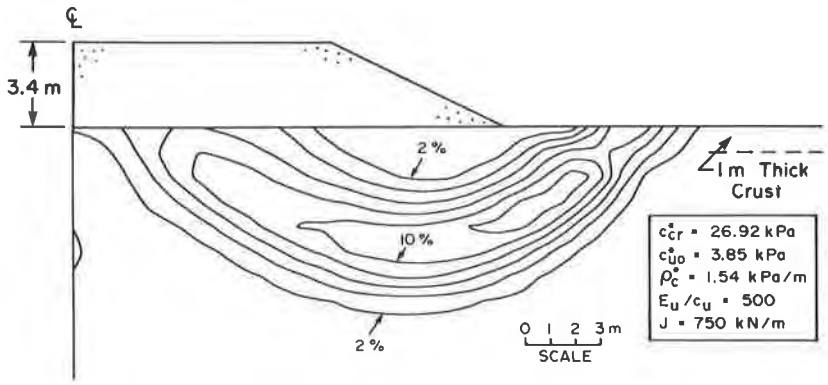

Figure 9. Contours of maximum shear strain at failure: 3.4 m fill thickness - 2% contour interval (from Rowe and Mylleville (1990))

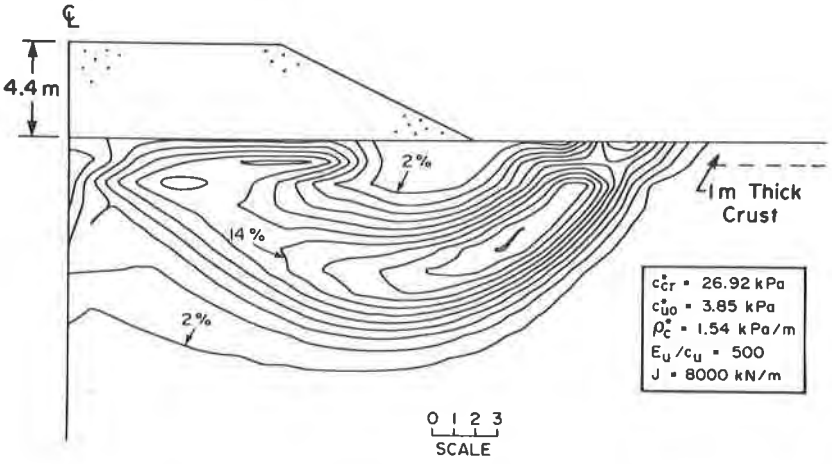

Figure 10. Contours of maximum shear strain at failure: 4.4 m fill thickness - 2% contour interval

Contours of maximum shear strain under working conditions for J=750 kN/m and J=8000 kN/m are plotted in Figures 11 and 12 respectively. For the case of J=750 kN/m, the maximum value is just in excess of 1%, whereas for the case of J=8000 kN/m the value is in excess of 1.6% (keeping in mind that in the latter case, the foundation soil is subjected to 38% more load). Looking at Figure 12, there is a significant zone of soil where the calculated shear strains are in excess of 1.5%, hence the potential for problems exists if the foundation soil is susceptible to strain softening. Adopting a lower limiting strain of say 0.5% in design (see Fig. 2), the calculated shear strains which correspond to a fill thickness of 3.5 m are plotted in Figure 13. The maximum value is just in excess of 1%. This suggests that adopting a 2% limiting strain in design for the very stiff geosynthetic may be unconservative, since the foundation soil may be subjected to shearing strains large enough to cause problems with softening.

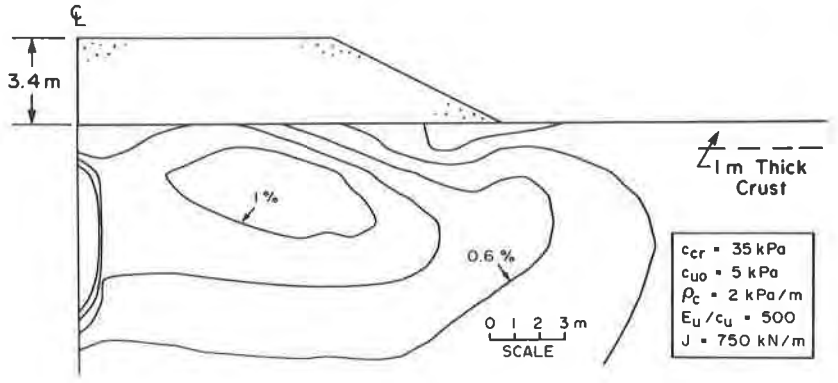

Figure 11. Contours of maximum shear strain under working conditions: 3.4 m fill thickness - 0.2% contour interval (from Rowe and Mylleville (1990))

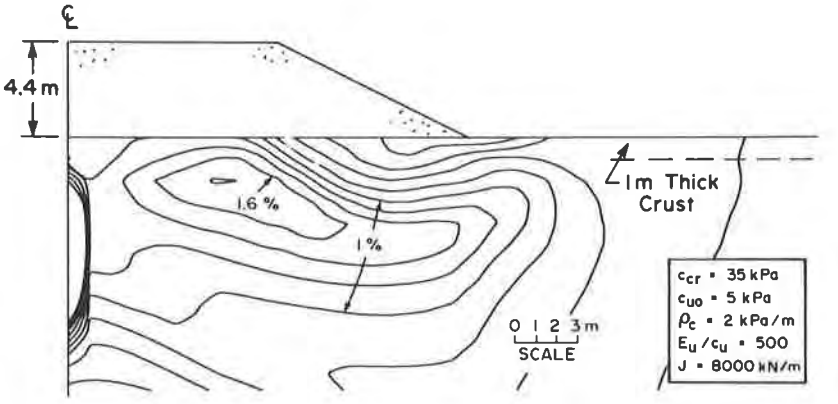

Figure 12. Contours of maximum shear strain under working conditions: 4.4 m fill thickness - 0.2% contour interval

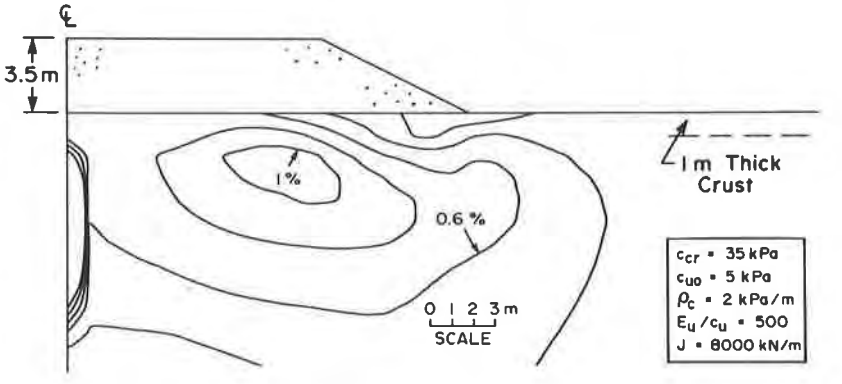

Figure 13. Contours of maximum shear strain under working conditions: 3.5 m fill thickness - 0.2% contour interval

IMPLICATIONS FOR PRACTICAL DESIGN

A number of results of finite element analyses have been presented which illustrate some important points one should keep in mind when designing reinforced embankments on soft brittle clay deposits. Calculated values of maximum shear strain in the foundation soil have been examined to assess the potential for strain softening.

Based on the results discussed, it would seem that for very soft brittle soils without a crust that the use of a very high modulus (i.e. J=8000 kN/m compared to J=750 kN/m) results in a greater fill thickness and reduction in shear strains in the foundation soil under working conditions. This may not be particularly significant for plastic soils but may be important if the soil is susceptible to softening. The use of a very high modulus reinforcement tends to change the failure mechanism to a bearing capacity type problem with significant slip of the foundation soil beneath the heavily reinforced embankment. As a result, the strain mobilized in the reinforcement tends to be quite low. Adopting a limiting strain in the order of 2% as recommended in the literature for sensitive brittle soils (Bonaparte and Christopher (1987)) may lead to unconservative designs in some cases. A limiting strain of say 0.5% may be more realistic for high modulus geosynthetics on soft soils susceptible to strain softening if one is going to design based on peak strength.

For soft brittle soils with a surface crust, it would seem that very little improvement in fill thickness is realized by the inclusion of a geosynthetic with a modulus, J=750 kN/m. The presence of the higher strength crust seems to dominate. On the other hand, the use of a very stiff geosynthetic, J=8000 kN/m results in a significant improvement in allowable fill thickness. However, under working conditions, the improvement in fill thickness results in calculated shear strains which may be large enough to cause problems if the foundation soil is susceptible to softening. Again, for the very high modulus geosynthetic, a limiting strain as low as 0.5% may be necessary to reduce the calculated shear strains to an "acceptable" level. This low value of limiting strain results in an allowable fill thickness which is for all practical purposes the same as that for the lower modulus geosynthetic.

It should be emphasized that the foregoing analyses and discussion assumed that the design was based on peak strength. An alternative would be to use post-peak strengths corresponding to the expected strains or in this case the limit on allowable strain would be higher and the strength would be lower. The designer could assess the economic implications of either design to "prevent softening" or design to accept softening and use post-peak strength.

CONCLUSIONS

The results of finite element analyses have been used to examine the effect of geosynthetic modulus on the behaviour of reinforced embankments constructed on very soft brittle clay deposits. A rigorous examination of strains in the geosynthetic and underlying foundation soil has resulted in a number of interesting observations.

It was found that increasing the geosynthetic modulus from J=750 kN/m to J=8000 kN/m resulted in an improvement in failure load and a significant reduction in shear strains in the underlying foundation soil. However, for the high modulus geosynthetic (i.e. J=8000 kN/m), the reinforcement strains at failure are very low for a very soft deposit without a surface crust. The failure mechanism for the heavily reinforced embankment resembled that of a semi-rigid footing bearing capacity failure.

If the foundation soil is susceptible to strain softening then care must be taken in a design situation. Limiting reinforcement strains recommended in the literature may lead to designs which subject the soil to excessive shear strains, even under working conditions. Results are presented which suggest the use of a limiting strain as low as 0.5% in a conventional plastic analysis may be warranted if a very stiff reinforcement is used.

It has been demonstrated that for soft brittle soils with a higher strength surface crust, the effect of the crust dominates, even if a very high modulus geosynthetic is used. For the cases considered, it was found that under working conditions, the modulus of the geosynthetic had very little effect on the magnitude of calculated shear strains in the foundation soil. In other words, keeping the shear strains low to avoid problems with strain softening, resulted in a failure load (fill thickness) which was for all practical purposes the same whether a geosynthetic with a modulus of J=750 kN/m or J=8000 kN/m was used.

ACKNOWLEDGEMENT

The research reported in this paper was funded by NSERC Grant A1007 awarded to R.K. Rowe.

REFERENCES

Bonaparte, R. and Christopher, B.R. (1987) Design and construction of reinforced embankments over weak foundations. Transportation Research Record, No.1153, p.p. 26-39.

Carter, J.P. (1985) AFENA - A general finite element algorithm - User's manual - School of Civil and Mining Engineering, University of Sydney, N.S.W. 2006, Australia.

Humphrey, D.N. and Holtz, R.D. (1989) Effect of surface crust on reinforced embankment. Proceedings of Geosynthetics'89 Conference, San Diego, U.S.A., p.p. 136-147.

La Rochelle, P., Tavenas, R. and Leroueil, S. (1988) Les argiles de l'est du Canada et leur contribution à la compréhension du comportment de l'argile. (The clays of eastern Canada and their contribution to the understanding of clay behaviour). Canadian Geotechnical Journal, Vol. 25, No.3, p.p. 413-427.

Lo, K.Y. and Morin, J.P. (1972) Strength anisotropy and time effects of two sensitive clays. Canadian Geotechnical Journal, Vol. 9, No.3, p.p. 261-277.

Mylleville, B.L.J. and Rowe, R.K. (1988) Steel reinforced embankments on soft clay foundations. Proceedings of the International Geotechnical Symposium on Theory and Practise of Earth Reinforcement, Fukuoka, Japan, p.p. 437-442.

Rowe, R.K. and Mylleville, B.L.J. (1988) The analysis of steel reinforced embankments on soft clay foundations. Proceedings of the 6th International Conference in Geomechanics, Innsbruck, Austria, p.p. 1273-1278.

Rowe, R.K. and Mylleville, B.L.J. (1989) Consideration of strain in the design of reinforced embankments. Proceedings of Geosynthetics'89 Conference, San Diego, U.S.A., p.p. 124-135.

Rowe, R.K. and Mylleville, B.L.J. (1990) Implications of adopting an allowable geosynthetic strain in estimating stability. Proceedings of the 4th International Conference on Geotextiles, Geomembranes and Related Products, The Hague, Netherlands, p.p. 131-136.

Rowe, R.K. and Soderman, K.L. (1987) Stabilization of very soft soils using high strength geosynthetics: the role of finite element analyses. International Journal for Geotextiles and Geomembranes, Vol.6, No.1, p.p. 53-80.

Using Geosynthetics to Reduce Earth Loads on Rigid Retaining Structures

John S. Horvath
Manhattan College, USA

ABSTRACT

To date, geosynthetics usage with relatively rigid earth retaining structures (gravity and cantilever retaining walls/bridge abutments, below-ground structures, navigation locks) has been limited primarily to drainage. A relatively new geosynthetics application, reducing lateral earth pressures on such structures, is discussed in this paper. The key element of this application is a new type of geosynthetic, called a geoinclusion, which is a relatively compressible geocomposite that is placed between the structure and retained soil. The primary function of the geoinclusion is to allow controlled horizontal deformation of the retained soil and concomitant soil yielding, although the geoinclusion can easily be made multi-functional. Used alone, the geoinclusion results in reduction of lateral earth pressures to or below active levels. This is called the Reduced Earth Pressure (REP) Wall case. If closely spaced horizontal layers of tensile reinforcement are placed within the retained soil, lateral earth pressures can be reduced to close to zero. This is called the Zero Earth Pressure (ZEP) Wall case. This paper explores the sensitivity of the results in both cases to geoinclusion thickness and reinforcement stiffness for a hypothetical case of a 10-foot (3 m) high wall. Recommendations for practical applications and future research of these concepts are also given.

INTRODUCTION

Background. A soil mass containing horizontal layers of tensile reinforcement will support itself, assuming the presence of a facing to prevent localized loss of material. However, horizontal deformation of the soil mass is required for the reinforcement to be activated. The magnitude of deformation required depends on the stiffness of the reinforcement, among other factors. However, regardless of reinforcement stiffness, relatively rigid earth retaining structures (gravity and cantilever retaining walls/bridge abutments, below-ground structures, navigation locks) usually will not move sufficiently for any reinforcement within the retained soil to be activated and contribute to the stability of the soil mass. Rather, the structure will retain the soil in a conventional manner. As a result, earlier trials of using soil reinforcement behind such structures did not meet with success, and the use of geosynthetics with such structures has, to date, been generally limited to prefabricated drainage panel geocomposites that function as chimney drains.

There are indications that the application of geosynthetics to relatively rigid earth retaining structures is undergoing significant change. Within the past five

years, the reduction of lateral earth pressures on such structures using geosynthetics has been attracting the interest of both practitioners and researchers. To overcome the rigidity of this type of structure, this recent work uses a new type of geosynthetic that will be called a geoinclusion. The geoinclusion is constructed primarily of relatively compressible material, and is placed between the structure and retained soil. The primary function of the geoinclusion is to allow controlled horizontal deformation of the retained soil and concomitant soil yielding. Partos and Kazaniwsky (1987) presented a case history in which a geoinclusion was used primarily to reduce the lateral earth pressure on a 20-ft (6.5 m) high portion of a basement wall. Field measurements indicated that they were successful in reducing the pressures to below the active level. This case also demonstrated that a geoinclusion can be multi-functional, as they used a commercially available geocomposite consisting of a 10-inch (250 mm) thick panel of expanded polystyrene (EPS) beads with a nonwoven geotextile facing that is marketed currently as a drainage panel. Application of a geoinclusion alone will be referred to as the Reduced Earth Pressure (REP) Wall concept.

McGown et al (1988) discussed using a geoinclusion with horizontal layers of tensile reinforcement within the retained soil. Their model tests demonstrated that even greater lateral-earth-pressure reductions could be achieved compared to using a geoinclusion alone. A significant finding of their work is that the reinforcement layers need to be closely spaced in the vertical direction for the lateral-earth-pressure reductions to be relatively uniformly distributed with depth. Edgar et al (1989) presented a case history where layers of geotextile reinforcement were placed behind existing highway bridge abutments undergoing reconstruction. They recognized the need to provide space for the soil mass to deform to activate the reinforcement, and placed a thin (fraction of one-inch-thick) layer of cardboard along the back of each abutment prior to backfilling. The success of the method depended on saturation of the cardboard with water after installation and its subsequent decomposition with time to create a void.

Purpose and Scope of Study. This work suggested to the writer that by proper matching of the geoinclusion compressibility and reinforcement stiffness, it should be possible to reduce the lateral earth pressure to close to zero. This amounts to allowing an otherwise conventional mechanically stabilized earth mass to develop behind, and essentially independent of, a relatively rigid earth retaining structure. The combined use of a geoinclusion and tensile reinforcement will be referred to as the Zero Earth Pressure (ZEP) Wall concept. To provide some guidance as to the relative stiffness of the geoinclusion and reinforcement necessary to achieve the ZEP-Wall condition, a research program was conducted by the writer between early 1989 and mid-1990. A study of the REP-Wall concept was included also. This research program, described in detail in Horvath (1990b), was devised to systematically vary what appeared to be key variables in the problem so that their relative influence on REP/ZEP-wall behavior could be assessed. The variables studied were:

1. soil stiffness. The soil type was limited to a sand, as coarse-grained soils are normally used with tensile reinforcement. Loose/normally consolidated, dense/normally consolidated, and dense/overconsolidated states were considered;

2. soil-wall friction. Both smooth and frictional interfaces between the retained soil and the back of the wall or geoinclusion were studied to evaluate the sensitivity of the results to this parameter;

3. geoinclusion. The modulus in compression was selected to approximate the behavior of the geocomposite drainage panel used by Partos and Kazaniwsky (1987). Three

thicknesses were studied: 2 inches (50 mm), 6 inches (150 mm), and 24 inches (600 mm). The 2-inch (50 mm) and 24-inch (600 mm) thicknesses represent the standard minimum and maximum thickness, respectively, for this product that were available at the time this study was begun. A baseline "free-field" case of no geoinclusion or reinforcement was studied also; and,

4. reinforcement. Material parameter values were chosen to approximate the stiffness of three commonly used types of tensile reinforcement: woven geotextile, polymer grid (geogrid), and steel (mesh or strips). To limit the number of variables, it was assumed that a layer of reinforcement was placed with each simulated layer of backfill, i.e., one-foot (300 mm) spacing vertically. As noted previously, the work by McGown et al (1988) suggested the need for closely spaced reinforcing. Also, the length of each reinforcement layer was made constant and relatively long (equal to the wall height) so that the potential for a pullout failure of the reinforcement was minimized. No attempt was made to investigate minimum or optimum lengths of reinforcement for a ZEP-Wall application, or sensitivity of the results to reinforcement length. Recent research summarized in Mitchell and Christopher (1990) suggests that relative reinforcement length significantly influences the horizontal deformations of a mechanically stabilized earth mass, so this factor should be included in future ZEP-Wall research.

Only a perfectly rigid wall was studied to eliminate wall stiffness as a variable at this stage of research. Nevertheless, a total of 87 separate combinations of variables were investigated.

Method of Analysis. The research performed for this study consisted of finite-element modeling of a simple, hypothetical problem. The computer code used was SSTIPNH, a microcomputer (PC) conversion by the writer of the well-known mainframe program SSTIPN. The general capabilities of SSTIPN are discussed in the user manual (1979), and the specific capabilities of SSTIPNH are discussed in Horvath (1990a).

PROBLEM STUDIED

Overall Geometry. Figure No. 1 shows the overall geometry of the problem investigated and the finite-element discretization used. Both the soil and geoinclusion were modeled using rectangular solid elements. Because a perfectly rigid wall was assumed, it was unnecessary to model the wall explicitly. Rather, the nodes on the left side of the mesh were fixed against movement. Not shown because of space limitations are the one-dimensional interface elements that were used above and below each layer of reinforcement.

SSTIPNH allows for the simulation of incremental construction. In this study, the geoinclusion (if present) was placed full-height on the wall, followed by the placement of soil in one-foot (300 mm) layers.

Soil Properties. SSTIPNH allows for non-linear stress-strain behavior of solid elements using the familiar hyperbolic model for both Young's Modulus and the Bulk Modulus, with Poisson's Ratio calculated from these two parameters. Elasto-plastic one-dimensional elements are also available to model the contact between dissimilar materials. The various model parameter values used in this study were based on Clough and Duncan (1971), Duncan et al (1980), and other data in the writer's files. Values are given in Table 1 for the soil (dense/overconsolidated state) and frictional soil-concrete interface. The latter parameters were used for the free-field analysis with no geosynthetics. One comment should be made concerning the soil. To approximate the

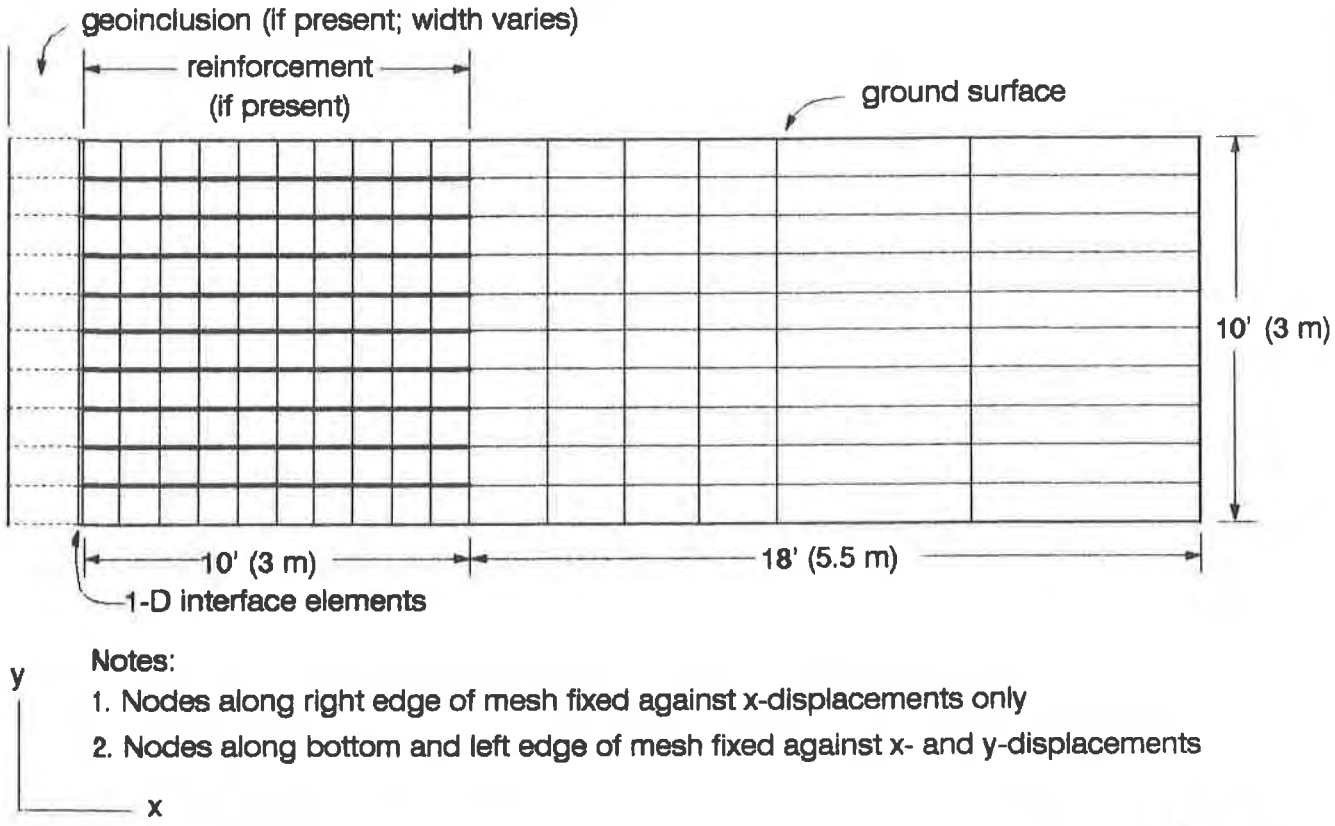

Figure No. 1. Problem Geometry and Finite-Element Mesh

effects of compaction, each layer was assumed to be overconsolidated with a K_0=1 immediately after placement. The writer recognizes that this is not a rigorous simulation of the compaction process (see Duncan and Seed (1986), and Seed and Duncan (1986) for a thorough discussion of this issue), but was all that could be achieved with the modeling capabilities in SSTIPNH.

Table 1. Soil/Soil-Concrete Interface Properties

solid elements:

Material	γ_t(pcf)	c(psf)	ϕ(deg)	$\Delta\phi$(deg)	K_0	K	n	R_f	K_b	m
sand	115	0	40	0	1	1000	.5	.8	300	.25

interface elements:

Material	c_a(psf)	δ(deg)	$\Delta\delta$(deg)	K_n	K_s	K_{sur}	n	R_f
concrete	0	32	0	1×10^9	4×10^4	6×10^4	1	.9

Geosynthetics Properties. The geoinclusion was modeled as a linear-elastic solid. Its Young's Modulus was based primarily on the test data reported in Partos and Kazaniwsky (1987). The values of the hyperbolic-model parameters used to approximate this behavior are given in Table 2. It was assumed that the geoinclusion was covered with a nonwoven geotextile on the soil side. The soil-geotextile interface was modeled using one-dimensional interface elements with the values given in Table 2. These values were based primarily on ones given in Koerner (1986).

The three types of reinforcement evaluated were each modeled as a linear-elastic spring element of zero thickness using what are called "nodal link" elements in SSTIPNH. The spring stiffness was allowed to have a transverse component as well as a normal (axial) component. The transverse component was used to simulate the component of tensile resistance of the reinforcement that develops as a consequence of differential vertical movement (Human et al 1986). The values used for the spring stiffness are given in Table 3. They were derived from typical moduli reported in manufacturer's literature, and rounded off for simplicity. The goal here was to approximate the stiffness of generic types of reinforcement rather than duplicate specific products. It is recognized that the relative stiffness difference between polymer grids and woven geotextiles available at the present time is less than the 10-to-1 ratio assumed.

The frictional interface between reinforcement and soil was modeled using one-dimensional interface elements, with separate interfaces above and below each layer of reinforcement. For the polymer grid and steel, a technique suggested by Human et al (1986) was used to account for the fact that there is at least partial continuity of soil through the reinforcement. This was accomplished by forcing the nodes of the solid soil elements immediately above and below the reinforcement to have the same horizontal displacement. The writer elected not to do this with the woven geotextile, as it was assumed to behave as an effective separator between soil above and below it. Thus, there could be relative horizontal displacement between the soil above and below the geotextile. Values for the interface parameters are given in Table 2, and were adapted from Koerner (1986) for the woven geotextile; Human et al (1986) for the polymer grid; and based on assumptions made by the writer for the steel.

Table 2. Geoinclusion/Soil-Geosynthetic Interface Properties

solid elements:

Material	γ_t(pcf)	c(psf)	ϕ(deg)	$\Delta\phi$(deg)	K_0	K	n	R_f	K_b	m
geoincl.	1	1	0	0	0	2.17	0	0	.72	0

interface elements:

Material	c_a(psf)	δ(deg)	$\Delta\delta$(deg)	K_n	K_s	K_{sur}	n	R_f
nonwoven geotextile	0	36	0	$1x10^6$	$1x10^3$	$1.5x10^3$	1	.9
woven geotextile	0	32	0	$1x10^6$	$1x10^3$	$1.5x10^3$	1	.9
polymer grid	0	25	3	$1x10^6$	$1x10^3$	$1.5x10^3$	1	.9
steel	0	40	0	$1x10^9$	$4x10^4$	$6x10^4$	1	.9

Table 3. Reinforcement Stiffness Parameters

	Spring Stiffness (lb/ft)	
Reinforcement	Normal	Transverse
woven geotextile	2,000	1
polymer grid	20,000	10
steel	2,000,000	1,000

DISCUSSION OF RESULTS

Introduction. Only the results involving soil in a dense/overconsolidated state with friction along interfaces are presented, as these represent the conditions likely to be encountered in practice. Complete results are presented in Horvath (1990b).

Geoinclusion Only. Initially, the REP-Wall case of a geoinclusion only was investigated. Figure No. 2 shows the lateral earth pressures calculated for the three geoinclusion thicknesses, plus the free-field results for no geoinclusion. The latter are essentially at-rest pressures with some increase in pressure near the top of the wall because of the simulated compaction effects. The horizontal component of the Coulomb active earth pressure is also shown for comparison. Note that the earth-pressure reductions from the geoinclusion alone are significant which is consistent with the work cited previously. For example, the measured earth pressures discussed by Partos and Kazaniwsky (1987) for a 10-inch (250 mm) geoinclusion were also somewhat less than the theoretical active stresses. They also reported a maximum compression of the geoinclusion of 0.6 inch (15 mm) which is consistent with values calculated for this study that are shown in Figure No. 3.

Combined Geosynthetics. The results for the analyses in which both a geoinclusion and reinforcement were used are summarized in Figure Nos. 4, 5, and 6. Each figure shows, for a different type of reinforcement, the lateral earth pressures without and with reinforcement. The calculated free-field (at rest) and theoretical active values are shown also. The principal observations from these results are as follows:

1. the use of geotextile reinforcement of the stiffness assumed in this study does not offer any improvement over the compressible inclusion alone. In fact, lateral earth pressures are actually slightly greater with the reinforcement. The reason for this unexpected result is not known at this time;

2. the polymer grid reinforcement produces a modest additional earth-pressure reduction compared to the geoinclusion alone; and,

3. the steel reinforcement produces significant additional earth-pressure reductions compared to the geoinclusion alone, and approaches the zero-earth-pressure condition.

The horizontal compression of the 24-inch (600 mm) geoinclusion for the various cases studied is shown in Figure No. 7.

CONCLUSIONS

The results of this study suggest that it is possible to significantly reduce lateral earth pressures on relatively rigid earth retaining structures by using a geoinclusion alone. The calculated results for both lateral earth pressures and geoinclusion compression are consistent with the limited field data available at the present time. The relationship between geoinclusion thickness and stress reduction is non-linear. A two-inch (50 mm) geoinclusion results in a reduction of peak lateral earth pressures of approximately 75% from the free-field (at-rest) case. Increasing the geoinclusion thickness six-fold to 24 inches (600 mm) causes an additional reduction of maximum pressures of approximately 15% of the original (free-field) stress. Therefore, the total stress reduction using a 24-inch (600 mm) geoinclusion is a maximum of 90%. It is uncertain at this time whether such significant stress reductions could be sustained for an extended period of time (tens of years) in practice because

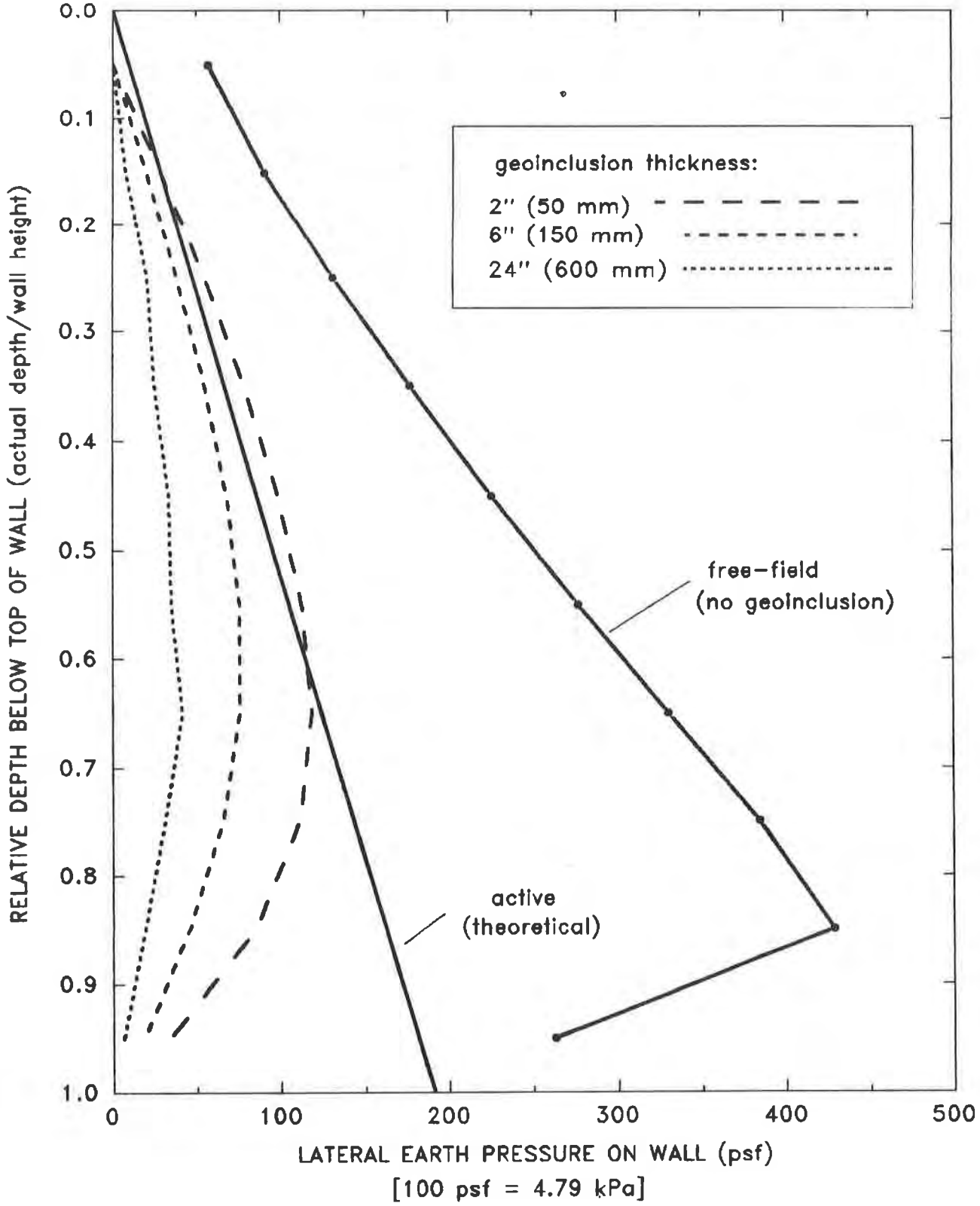

Figure No. 2. Lateral Earth Pressures for REP-Wall Case

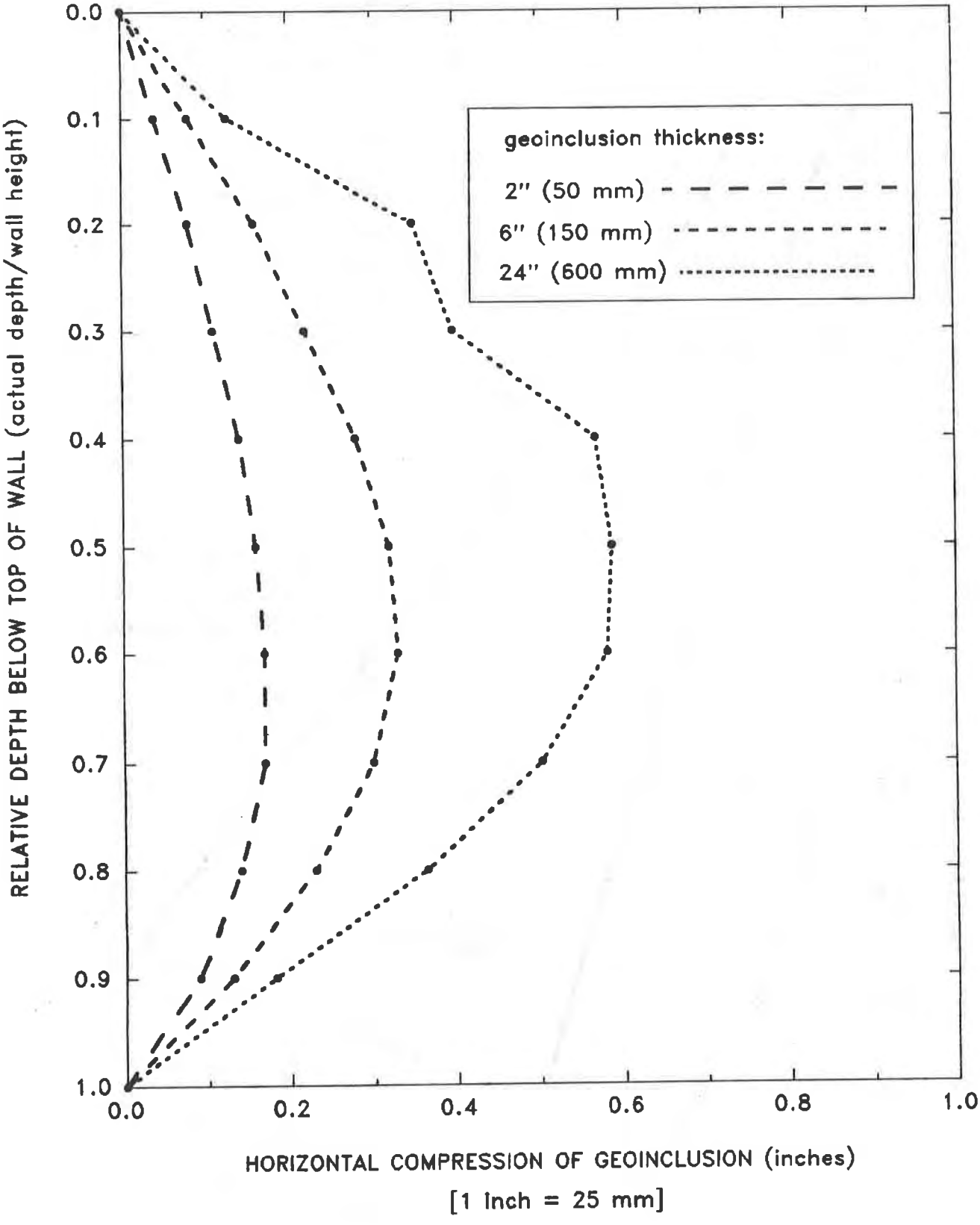

Figure No. 3. Compression of Geoinclusion – REP–Wall Case

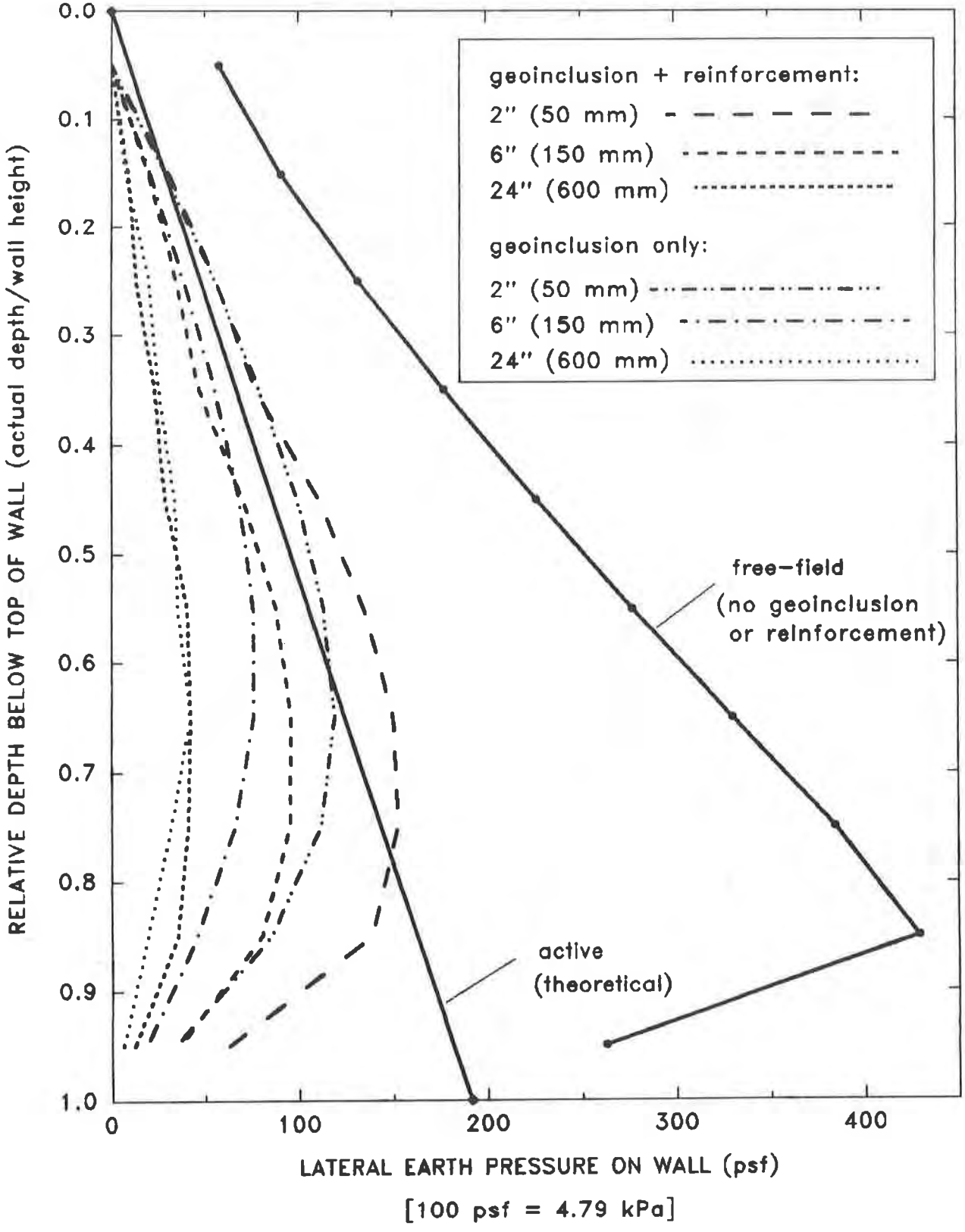

Figure No. 4. Lateral Earth Pressures for ZEP-Wall Case with Woven Geotextile Reinforcement

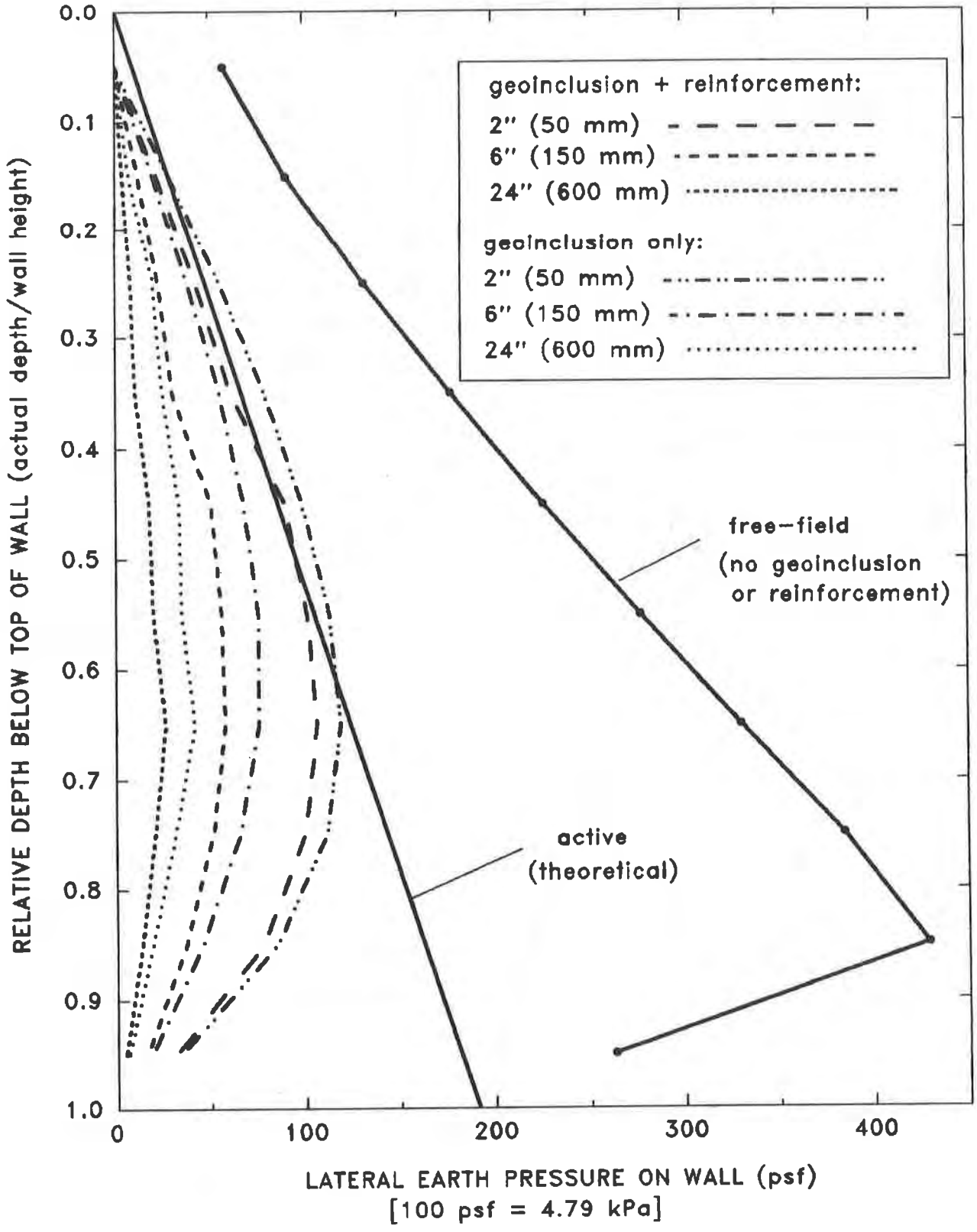

Figure No. 5. Lateral Earth Pressures for ZEP-Wall Case with Polymer Grid Reinforcement

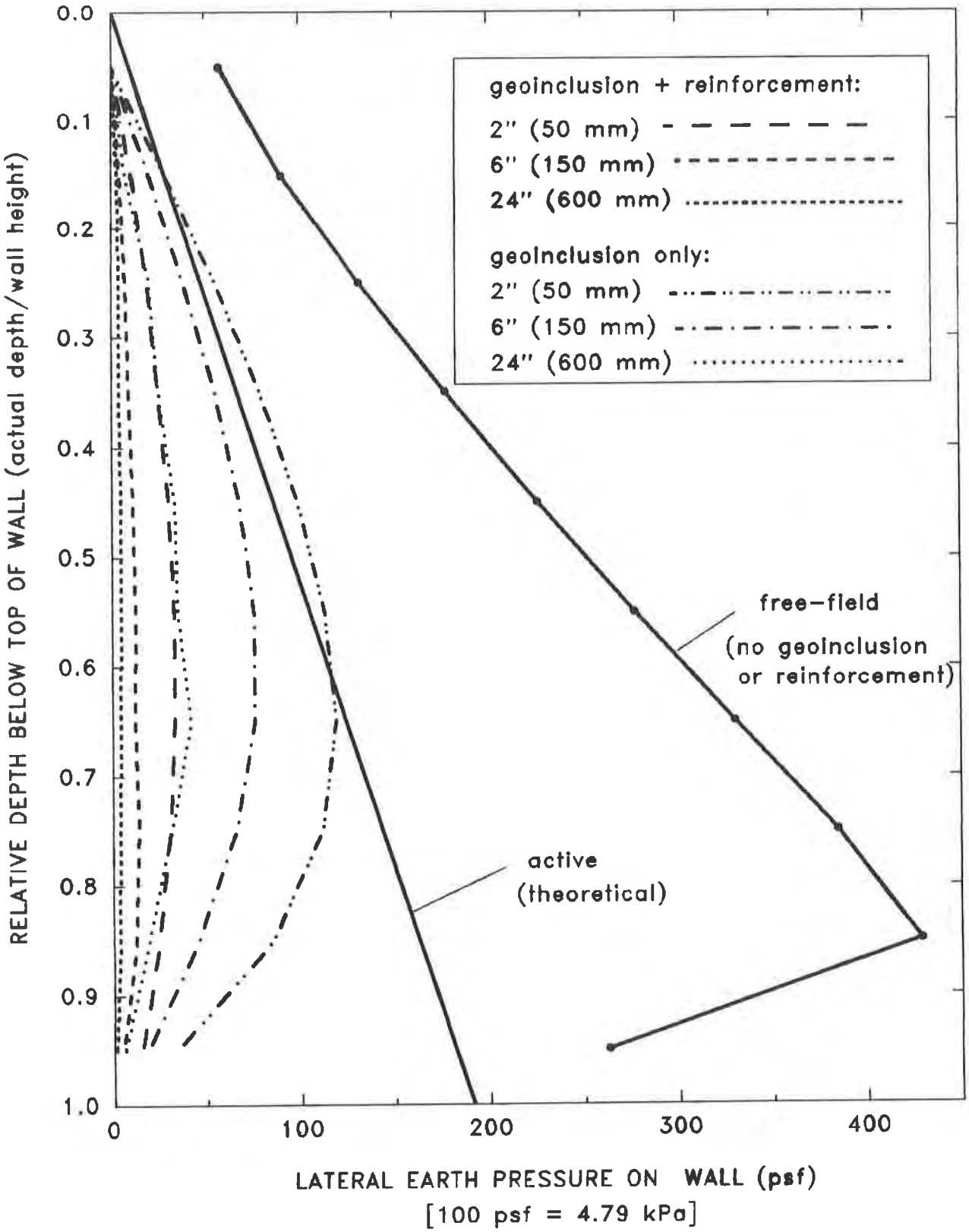

Figure No. 6. Lateral Earth Pressures for ZEP-Wall Case with Steel Reinforcement

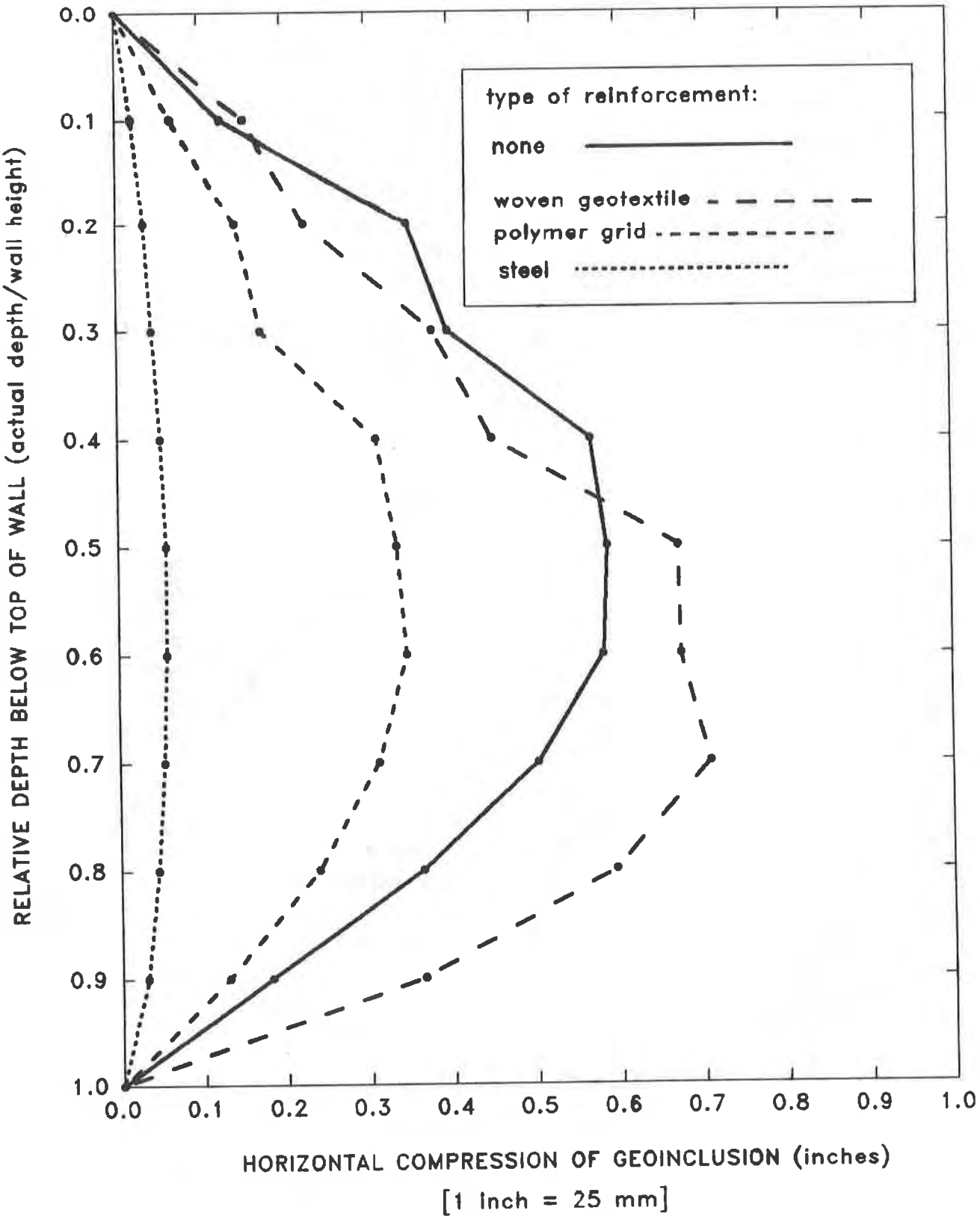

Figure No. 7. Compression of 24-Inch (600 mm) Geoinclusion

of creep of the polymeric materials that comprise the geoinclusion plus other effects. Until the long-term behavior of specific geoinclusion materials are studied, it would appears prudent to include relatively stiff reinforcement within the retained soil to aid in sustaining the stress reductions. This is because the long-term behavior of synthetic reinforcement materials is relatively much better understood at the present time. Use of sufficiently stiff reinforcement should also provide additional reduction in lateral earth pressures, so that a goal of achieving essentially zero lateral earth pressure should be achievable in practice. If very stiff reinforcement such as steel is used, the lateral earth pressures are relatively insensitive to the thickness of the compressible inclusion. If moderately stiff reinforcement such as a polymer grid or a woven geotextile (assuming the latter is significantly stiffer than that assumed in this study) is used, a relatively thick geoinclusion is required to achieve near-zero earth pressures.

RECOMMENDATIONS

Applications. Potential applications of the REP/ZEP-Wall concepts include both new construction and existing structures. In new construction, there may be cases where it is not desirable or economical to design the wall for normal earth pressures, as in the case history discussed by Partos and Kazaniwsky (1987). Future applications may include situations involve reducing pressures from swelling-susceptible fine-grained soils, or attenuating lateral-earth-pressure increases caused by a seismic event.

With regard to existing structures, there are many situations where a wall is subjected to lateral earth pressures that exceed the capacity of the wall and are causing distress of the wall. It may be more economical to reduce these pressures permanently using the REP/ZEP-Wall concepts rather than strengthen the wall structurally or replace it. This may also prove to be an economical way to retrofit existing earth retaining structures to safely accommodate lateral-earth-pressure increases caused by a seismic event.

The application of the REP/ZEP-wall concepts to reducing surface surcharge loads behind earth retaining structures is discussed elsewhere (Horvath 1990b, Horvath 1991).

Another important feature of the REP/ZEP-Wall concepts is that geoinclusions can be multi-functional. For example, the product used by Partos and Kazaniwsky (1987) is also a drainage material and possesses thermal insulation properties. With regard to the latter function, it has been recognized only recently (Horvath 1989, Murray and Farrar 1988, Segrestin and Jailloux 1988) that solar heat on the exposed exterior face of a retaining wall can propagate through the wall and into the ground, and increase significantly the creep rates in polymer-based reinforcement. Therefore, proper choice of the geoinclusion can regulate the heat flux between the open atmosphere and retained soil. Other possible functions for a geoinclusion include attenuation of noise and small-amplitude vibration caused by vehicular or rail traffic.

Future Study. There are three broad areas where future investigation is suggested:

1. large-scale model and/or full-scale field studies are required to verify the theoretical results presented in this paper. Particular areas of investigation include evaluating the effect on the reduced earth pressures of long-term creep of both the geoinclusion and reinforcement. The attenuation of vibrations, especially from earthquakes, is also a potentially fruitful area of research;

2. the entire REP/ZEP-Wall concept as applied to situations involving fine-grained soils should be studied both theoretically and experimentally. It is possible that a significant benefit of using geosynthetics behind relatively rigid earth retaining structures may be in this area, e.g., reduction of pressures from swelling-susceptible soils; and,

3. the application of the REP/ZEP-Wall concepts to flexible earth retaining structures such as sheetpile walls.

SUMMARY

Numerical modeling, supported to date by limited model and field testing, suggests that it is possible to achieve significant, even total, reduction in lateral earth pressures behind relatively rigid earth retaining structures. This is achieved by using a new type of geosynthetic called a geoinclusion, either alone or together with horizontal layers of synthetic reinforcement placed within the retained soil. These are referred to as the Reduced Earth Pressure (REP) Wall and Zero Earth Pressure (ZEP) Wall concepts, respectively. Another benefit is that additional functions can be incorporated within the geoinclusion, e.g., drainage, thermal insulation, and, possibly, attenuation of noise and vibrations.

ACKNOWLEDGEMENTS

A portion of the writer's time spent on the research summarized in this paper was supported by Manhattan College under its 1990 Summer Grant Program for Faculty Research. Computer hardware and software used in this study was provided by the Manhattan College Civil Engineering Department, Dr. Nicholas F. Morris/Chairperson, and Horvath Engineering, P.C. The writer is grateful for this support.

REFERENCES

Clough,G.W. and Duncan,J.M.(1971). "Finite Element Analysis of Retaining Wall Behavior." Journal of the Soil Mechanics and Foundations Division, ASCE, 97(12), 1657-1673.

Duncan,J.M., Byrne,P., Wong,K.S. and Mabry,P.(1980). "Strength, Stress-Strain and Bulk Modulus Parameters for Finite Element Analyses of Stresses and Movements in Soil Masses." Report No.UCB/GT/80-01, University of California, Berkeley, Calif.

Duncan,J.M. and Seed,R.B.(1986). "Compaction-Induced Earth Pressures under K_0-Conditions." Journal of Geotechnical Engineering, ASCE, 112(1), 1-22.

Edgar,T.V., Puckett,J.A., and D'Spain,R.B.(1989). "Effects of Geotextiles on Lateral Pressure and Deformation in Highway Embankments." Geotextiles and Geomembranes, 8(4), 275-292.

Horvath,J.S.(1989). Combined discussion of "Temperature Distributions in Reinforced Soil Retaining Walls" by R.T. Murray and D.M.Farrar, and "Temperature in Soils and its Effect on the Ageing of Synthetic Materials" by P.Segrestin and J-M.Jailloux, Geotextiles and Geomembranes, 8(2), 159-160.

Horvath,J.S.(1990a). "A Study of Some Miscellaneous Wall Problems." Research Report No.CE/GE-90-1, Manhattan College, Bronx, N.Y.

Horvath,J.S.(1990b). "The Use of Geosynthetics to Reduce Lateral Earth Pressures on Rigid Walls; Phase I: Concept Evaluation." Research Report No.CE/GE-90-2, Manhattan College, Bronx, N.Y.

Horvath,J.S.(1991). "Using Geosynthetics to Reduce Surcharge-Induced Stresses on Rigid Retaining Structures." To be presented at the Transportation Research Board 1991 Annual Meeting, Washington, D.C., January 1991.

Human,C.A., Seed,R.B., Mitchell,J.K., and Borja,R.I.(1986). "Predicted Behavior of the Stanstead Abbotts Trial Embankment," Proceedings of 'The Prediction Symposium on a Reinforced Embankment on Soft Ground', R.H.Bassett and K.C.Yeo(eds.), King's College, London.

Koerner,R.M.(1986). Designing with Geosynthetics. Prentice-Hall, Englewood Cliffs,N.J.

McGown,A., Andrawes,K.Z., and Murray,R.T.(1988). "Controlled Yielding of the Lateral Boundaries of Soil Retaining Structures." Geosynthetics for Soil Improvement - Geotechnical Special Publication No.18, R.D.Holtz(ed.), ASCE, 193-210.

Mitchell,J.K. and Christopher,B.R.(1990). "North American Practice in Reinforced Soil Systems." Design and Performance of Earth Retaining Structures - Geotechnical Special Publication No. 25, P. C. Lambe and L. A. Hansen(eds.), ASCE, 322-346.

Murray,R.T. and Farrar,D.M.(1988). "Temperature Distributions in Reinforced Soil Retaining Walls." Geotextiles and Geomembranes, 7(1&2), 33-50.

Partos,A.M. and Kazaniwsky,P.M.(1987). "Geoboard Reduces Lateral Earth Pressures." Proceedings of Geosynthetics '87, IFAI, 628-639.

Seed,R.B. and Duncan,J.M.(1986). "FE Analyses: Compaction-Induced Stresses and Deformations." Journal of Geotechnical Engineering, ASCE, 112(1), 23-43.

Segrestin,P. and Jailloux,J-M.(1988). "Temperature in Soils and its Effect on the Ageing of Synthetic Materials." Geotextiles and Geomembranes, 7(1&2), 51-69.

"User's Guide for SSTIPN" (1979).

Electrical Methods of Seaming of Geomembrane Sheet

E. O. Butts
Butts Consultants, Ltd., Canada
A. E. Lord, Jr.
Geosynthetic Research Institue, Drexel University, USA

ABSTRACT

This paper will describe electrical methods for joining geomembrane sheet. In both methods stainless steel resistance wire is wound (braided) around a core of the membrane material (of about 5 mm diameter). The core is then placed between the geomembranes to be seamed. (Only work with HDPE sheet will be discussed here.) No surface grinding preparation of the geomembrane is needed other than an alcohol wipe.

In the direct contact method, electrical connection is made at the ends of the stainless steel wires and current is then run through the wires. The wires heat up (via ohmic heating) and melt the core and adjacent geomembrane material. After the current is stopped, the material freezes and makes a bond between the sheets. A normal stress of 7-14 KPa (1-2 psi)) is maintained on the weld area during the seaming process. A maximum current of 6-15 amperes is used for about 120 seconds. The values of mechanical shear and peel strength for these welds are equivalent to those obtained with the more conventional welding techniques, and film tear bonds are usually observed. At present lengths of up to 10 meters (30 feet) can be processed.

In the non-contact method an electromagnetic induction coil, carrying high frequency electrical current (~250 KHz), passes directly over the braided core which has been placed between the geomembranes. The coil is only a few millimeters above the upper sheet. The wire heats inductively and melts the core and the adjacent geomembrane material. After the induction coil passes by, that portion of the wire ceases to be heated and the material freezes and makes a bond between the sheets. Here the mechanical stress of 7-14 KPa (1-2 psi) is applied immediately after the coil has passed. At present continuous seaming rates of 0.7-1.7 meter/minute (2-5 ft/min) are being used. Mechanical shear and peel strengths for these welds are also equivalent to those obtained by the more conventional welding techniques. Film tear bonds are usually observed.

Acceptable peel and shear values and film tear bonds have been achieved with the direct contact method in the underwater environment. Hence a unique aspect of the electrical seaming techniques is that they can in principle be applied to the repair of leaks in the "in-situ" situation.

INTRODUCTION

The fabrication of geomembrane seams is a most critical area. While "conventional" bonding techniques have been developed for specific geomembrane materials [1], there is always room for improvement in the methods and possibly for the introduction of new methods. Therefore it is of interest and importance to explore new bonding approaches. Two emerging techniques, electrical conduction bonding and electromagnetic induction bonding will be described here.

ELECTRICAL CONDUCTION SEAMING

In the electrical conduction seaming technique for plastics, electric current is passed through wires embedded in (or placed between) the vicinity of the parts to be joined. The temperature of the wires rises via ohmic heating and the heat is transferred to the plastic which melts and flows in the vicinity of the wires. Upon solidifying the parts are joined. Pressure is usually applied, either physically, or indirectly by differences in thermal expansion of the parts. Both ac and dc currents have been used. Welding times are typically the same as those common in geomembrane thermal techniques, for it is essentially a thermal technique. This particular seaming method is widely used in natural gas plastic pipelines and is usually called the "electro-fusion" technique [2,3]. Figure 1 gives a schematic diagram of the electro-fusion process which indicates that certain properties are measured in real-welding-time, and fed back to the control panel to readjust and optimize welding conditions.

The initial adaptation of this technique to geomembrane was by E. O. Butts Ltd. of Nepean Ontario, Canada [4]. HDPE sheet of density 0.945 g/cm^3 and thickness of 1.5 mm (0.060-inch) was used. Stainless steel (400 series) wires with diameters ranging 0.01 cm to 0.05 cm (0.004-inch to 0.020-inch) were coiled or braided around HDPE cylindrical cores (of the same density as the sheet) of either 3 mm or 5 mm diameter. The wires were braided onto the cores with a specially-adapted braiding machine which is shown in Figure 2a. The wires were embedded into the surface of the plastic cores via a heat treating process at the end of the braiding process (see Figure 2b). If the wires were not embedded in the core, the subsequent electrical welding did not proceed satisfactorily. Also it was imperative that there were no air bubbles in the original core material. Figure 3 shows braided core before and after embeddment. The final wire-wound cores had an electrical resistance of about 3-6 ohms/meter (1-2 ohms/foot).

The sheet surfaces were cleaned with isopropyl alcohol before the joining process. It was found that any grinding before assembly greatly deteriorated the final weld strength. The coiled core was then placed between the sheets. Figure 4 is a schematic diagram of the fabrication process. A force was applied normal to the sheets with the braided wire between. The pressure was 7-14 KPa (1-2 psi). Electrical current (ac) of 6-15 amperes was passed through the wires. The wires heat due to ohmic effects and melt the core and adjacent sheet material. Some material flow takes place. Typical core and sheet surface temperatures are shown in Figure 5. Core temperature was measured with an embedded thermocouple. Surface temperature was measured with an infrared pyrometer. Surface temperature gradients are shown on Figure 6. The current was stopped, after a prescribed time, and the material subsequently solidified, thereby bonding the sheets together. Under the present experimental circumstances, maximum weld lengths of about 2 meters (6 feet)

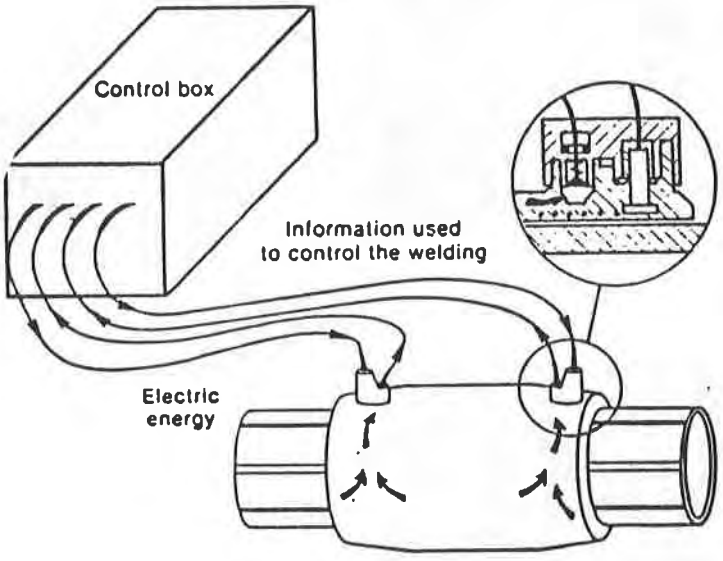

Figure 1 - Schematic Diagram of an Electrofusion Pipe Coupling Process (From Reference 4)

(a)

(b)

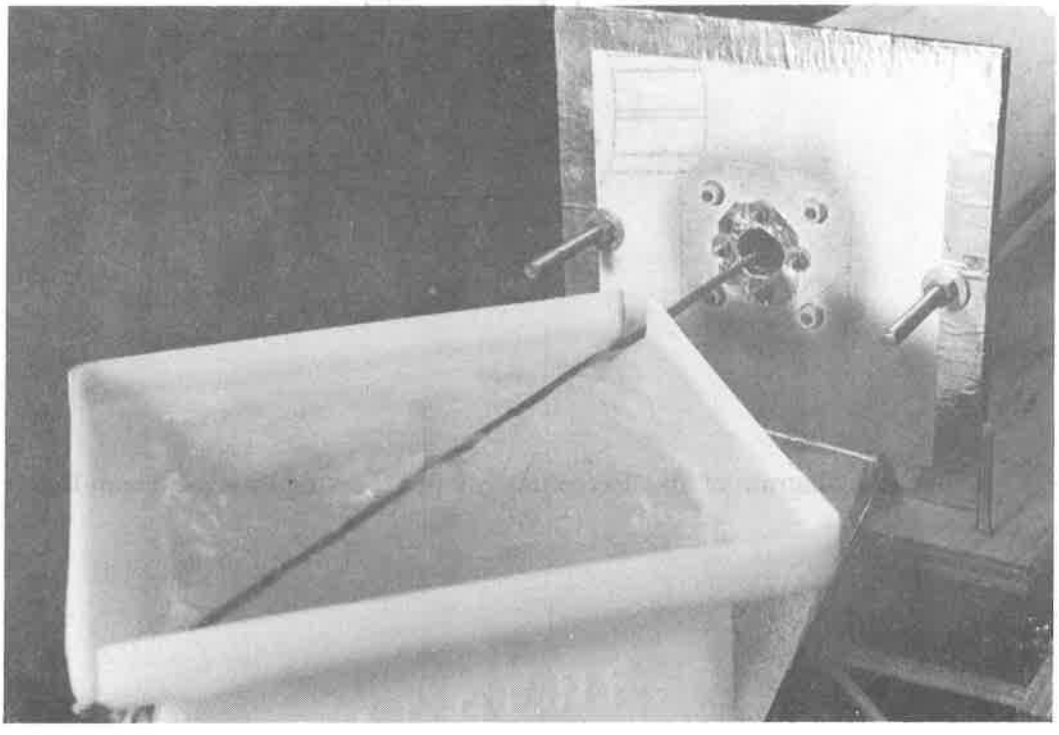

Figure 2 - (a) Braiding machine to produce braided core (b) Embedding oven and cooling tank

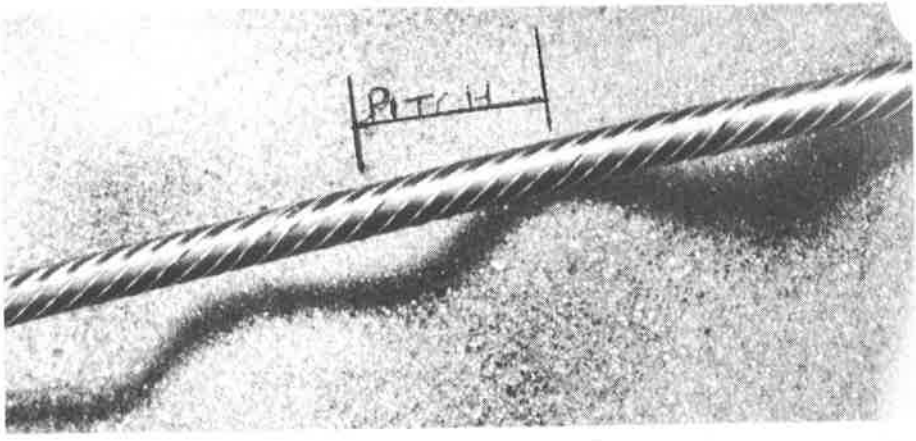

(a)

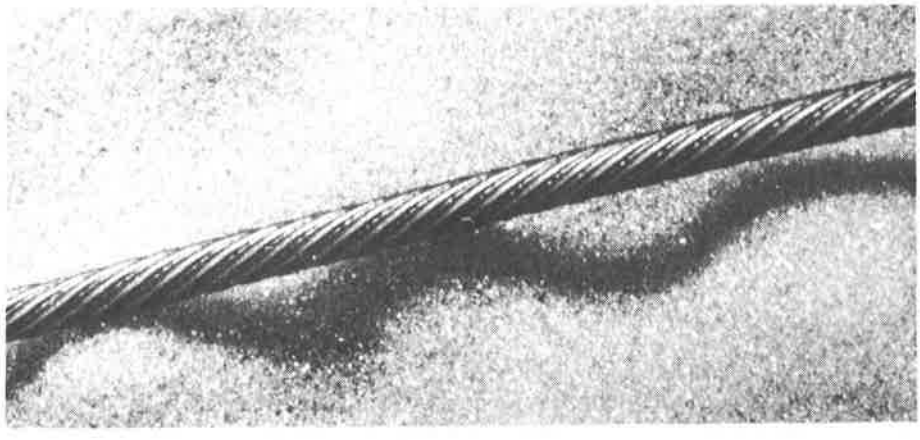

(b)

Figure 3 - Braided core (a) Before embedding (b) After embedding

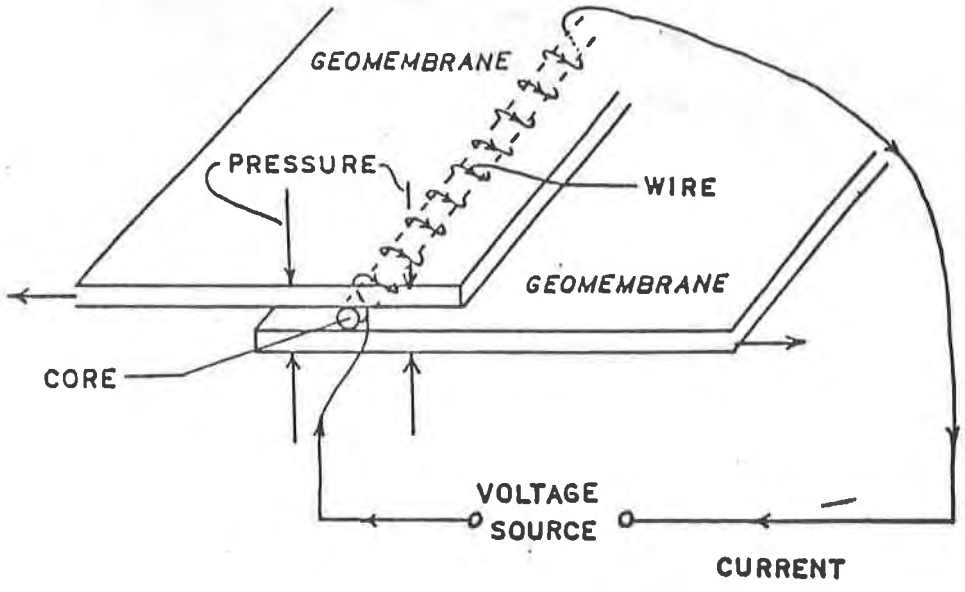

Figure 4 - Schematic Diagram of the Electrical Conduction Method of Joining Geomembrane Sheet (This method is called "Fustich" by the developers)

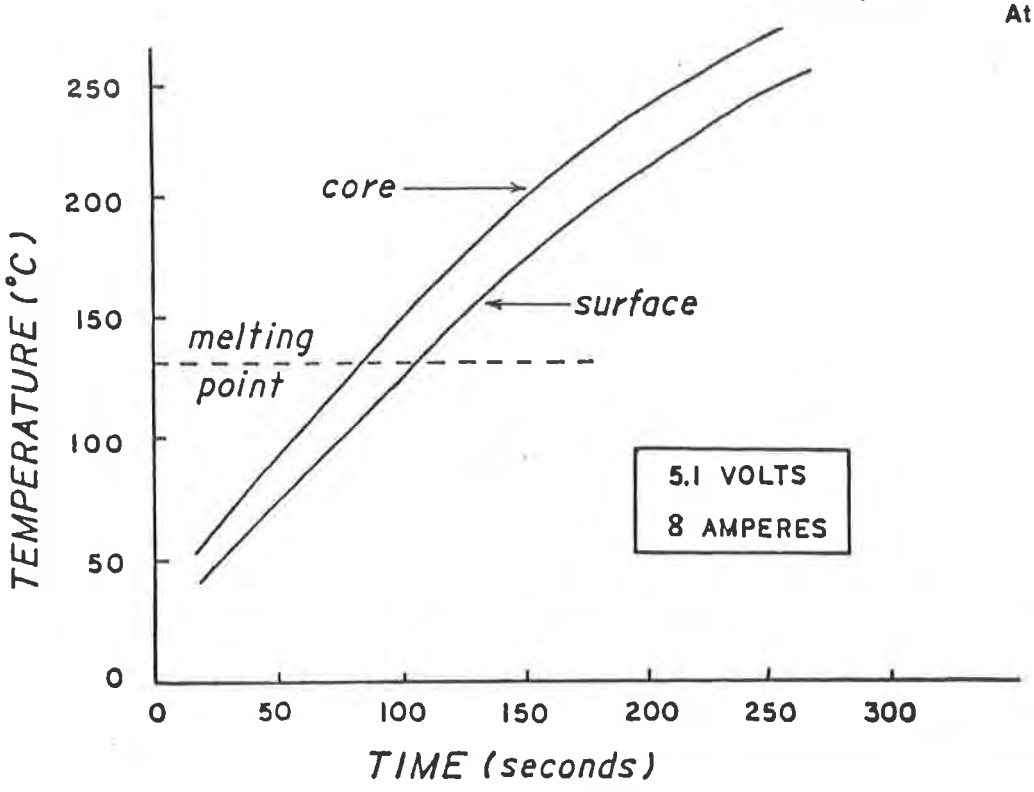

Figure 5 - Typical Core and Sheet Surface Temperatures During the Electrical Conduction Welding Process (From Reference 4)

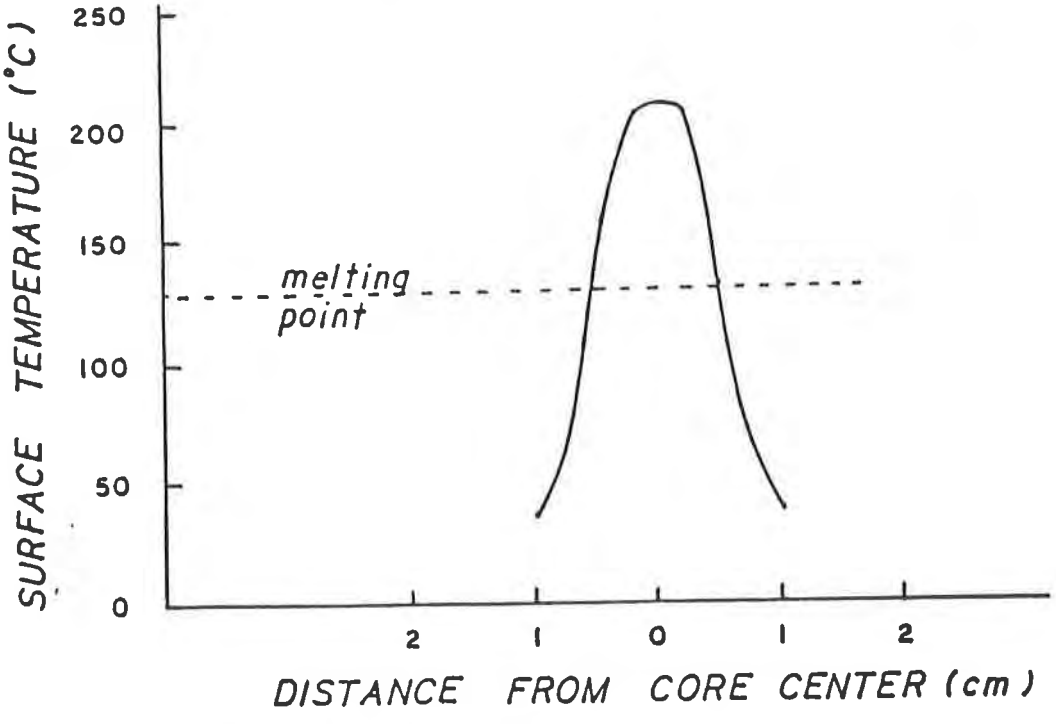

Figure 6 - Typical Lateral Sheet Surface Temperature Gradients in the Electrical Conduction Welding Process (From Reference 4)

can be made with a single application of the current electrodes. However in special experiments lengths up to 10 meters (30 ft) have been made (see Figure 7).

Mounted and polished cross-sections of electrical conduction welds give no indication of large voids in the immediate vicinity of the interface between wire and polymer (see reference 5).

Standard shear and peel tests were performed under ambient conditions on 25 mm (1.0 in.) wide samples at an extension rate of 5 cm/minute (2-inches per minute). In the electrical conduction welds, shear strengths of 90% (of sheet) and peel strengths of 80% (of sheet) are consistently realized. These values are comparable to other seaming techniques currently available. Film tears bonds are consistently realized. Seams which gave somewhat lower values than those given above usually showed exposed wires after failure. Good mechanical strengths were obtained with input electrical energy (voltage × current × time) between 7,000 and 10,000 Joules. The average power was between 40 and 70 watts. These values apply for a 1/3 meter (one foot) length of seam.

Two types of long term mechanical tests are being evaluated. In the first type [4], 12 mm wide, hand-cut seamed samples were put under an initial stress of 7000 kPa (1000 psi) and cycled between -20°C and +50°C once daily. The stress did relax somewhat during certain of these tests. In other tests, the stress was kept reasonably constant. After six months of testing, no seam failures have occurred in the four samples of electrical conduction welds. In the second type of long term testing, a fixed stress of 7000 kPa is applied to 12 mm\wide, die-cut samples of seamed material under ambient conditions. After one year of ambient temperature testing, no failures have occurred in the electrical conduction weld (or in any of the other three commonly-used types of welds also being tested). More extensive long term tests on electro-fusion bonds indicates that the presence of these foreign bodies (i.e., metal wires) does not shorten the lifetime of the joints [2,3].

ELECTROMAGNETIC INDUCTION SEAMING

In electromagnetic induction seaming, an electrical conductor and/or hysteretic material (in the form of wires, particles, strips, etc.) is placed at the interface to be joined. A non-contacting, induction coil containing high frequency electric current passes over the area to be seamed. The time-varying magnetic field caused by the current in the coil induces eddy currents and/or hysteresis loss in the embedded materials. Hence the area is heated, melts, flows, solidifies and bonding takes place. Pressure is usually applied to the interface. Frequencies mentioned range from 3-7 MHz [6] and 80-320 KHz [4], depending on the application. A wide variety of plastic assembly and sealing applications have been performed [6]. The electromagnetic induction method has been mentioned briefly in the natural gas pipeline literature [3], but with no details as to its use.

The initial adaptation of this technique to geomembranes was also by E. O. Butts Ltd. [4]. Figure 8 is a schematic diagram of the fabrication process of electromagnetic induction seaming. As with the electrical conduction method described previously, HDPE sheet of 0.945 g/cm^3 density and 1.5 mm thickness was used in the tests. The braided core, made by the same process as described for the electrical conduction method is placed between the two (cleaned) sheets. An

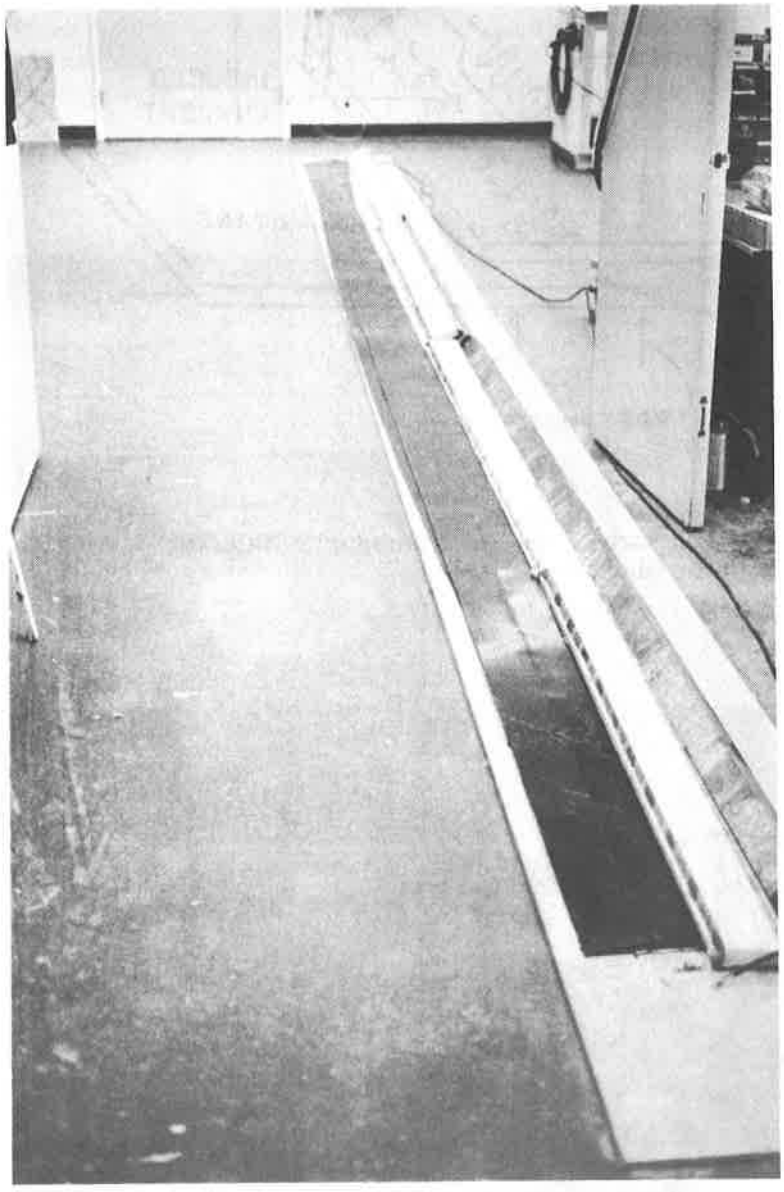

Figure 7 - Production of Electrical Conduction Weld in geomembranes of 10 meter length

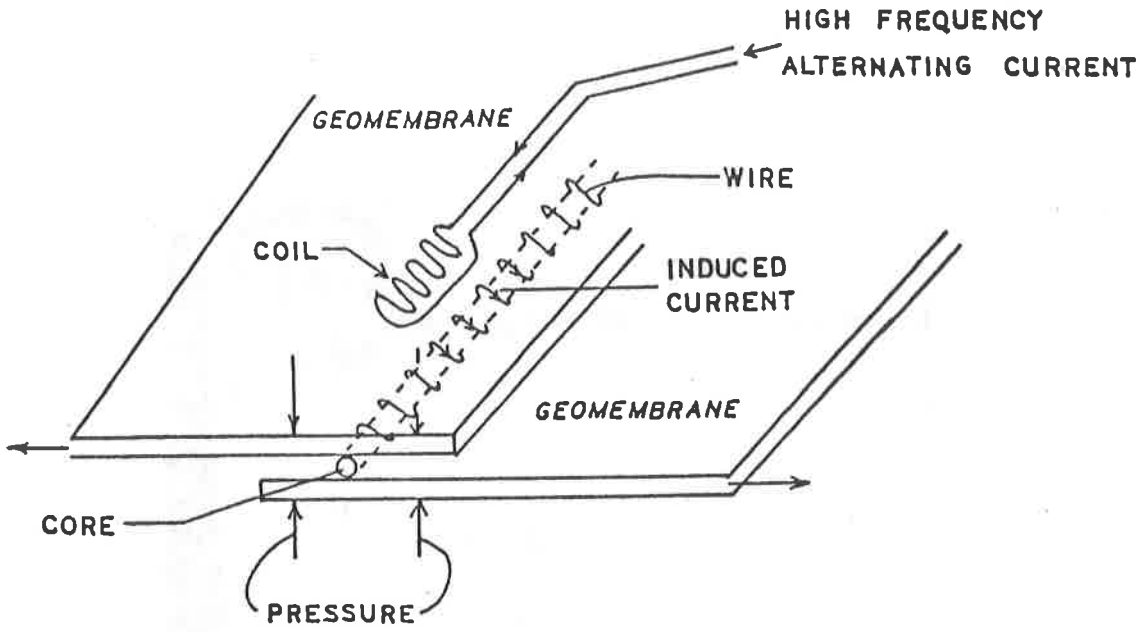

Figure 8 - Schematic Diagram of the Electromagnetic Induction Method of Joining Geomembrane Sheet

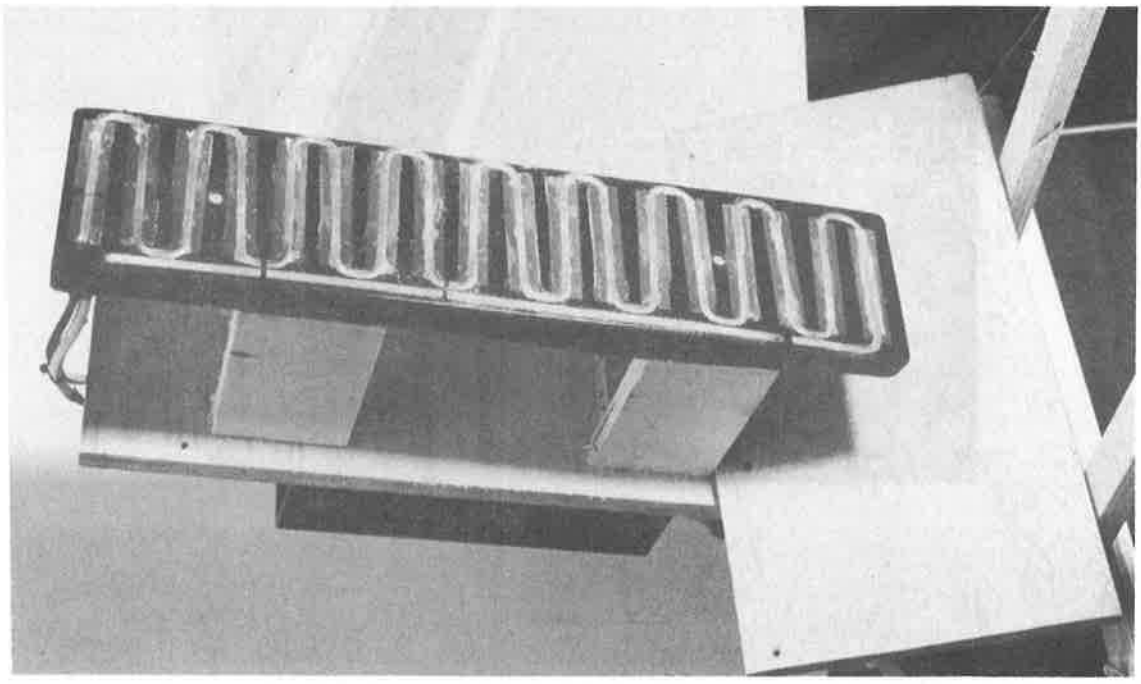

Figure 9 - Specially-Fabricated Electromagnetic Induction Coil

electromagnetic coil (see Figure 9) carrying high frequency alternating current of about 250 KHz is passed directly over the braided core. No contact whatsoever is made between the electromagnetic coil and the sheet. The coil is a few millimeters above the top geomembrane sheet. Figure 10 shows the experimental setup for producing the electromagnetic induction welds. Eddy currents are induced in the embedded braided wire by the time-varying magnetic field. This results in ohmic heating which melts the core and a certain amount of the adjacent sheet material. After the coil has passed, the eddy currents cease and the material solidifies and bonds the sheets together. A normal mechanical stress of 7-14 KPa (1-2 psi) was applied immediately after the coil has passed.

Rates of about 0.7-1.7 meters/minute (2-5 ft/minute) have been achieved at this time. Results of mechanical testing of the seams give about 90% of the sheet value for and at least 80% (of sheet) for peel. These values are comparable to other seaming methods being used. Film tear bonds are usually observed.

OTHER USES OF ELECTRICAL METHODS FOR SEAMING GEOMEMBRANE SHEET

An interesting application of the electrical welding techniques just described is their use for underwater welding. Figure 11 shows a geomembrane seam being produced underwater by electrical conduction welding. The peel and shear results for these welds are completely acceptable, and film tear bonds result even in this very hostile environment. It is somewhat surprising that good welds are produced underwater, as the temperature of welding is considerably above the boiling point of water. The vigorous action of the boiling water in the near vicinity of the weld does not preclude the good bonding of the plastic itself. We do not claim to understand the entire mechanism of weld production. The attempts at producing welds underwater with induction seaming have not proved successful to date, but it is felt that with optimization of the welding parameters (as was the case in induction welding in air) that inductive welds can be made underwater.

Some other uses of the electrical welding techniques are:

- the sealing of lids on HDPE drums used for hazardous waste storage
- the sealing of long HDPE panels in slurry walls
- the sealing of jackets around steel pipes and tanks

CONCLUSIONS

The electrical conduction method, although widely used in the natural gas pipeline industry, is in its formative stages as a seaming method for geomembranes. Although good mechanical properties of geomembrane seams can be achieved, only short lengths of geomembranes can be seamed [4]. Furthermore no field trials have as yet been performed. Good seams have also been produced underwater.

The electromagnetic induction method has been used to join relatively small parts [6], but has not been used to any extent in the natural gas pipeline and not at all in the geomembrane joining areas as far as the authors are aware. Preliminary work done in this regard on geomembrane sheet [4] indicates some potential for the method. There are certain advantages in the electromagnetic induction method. These include:

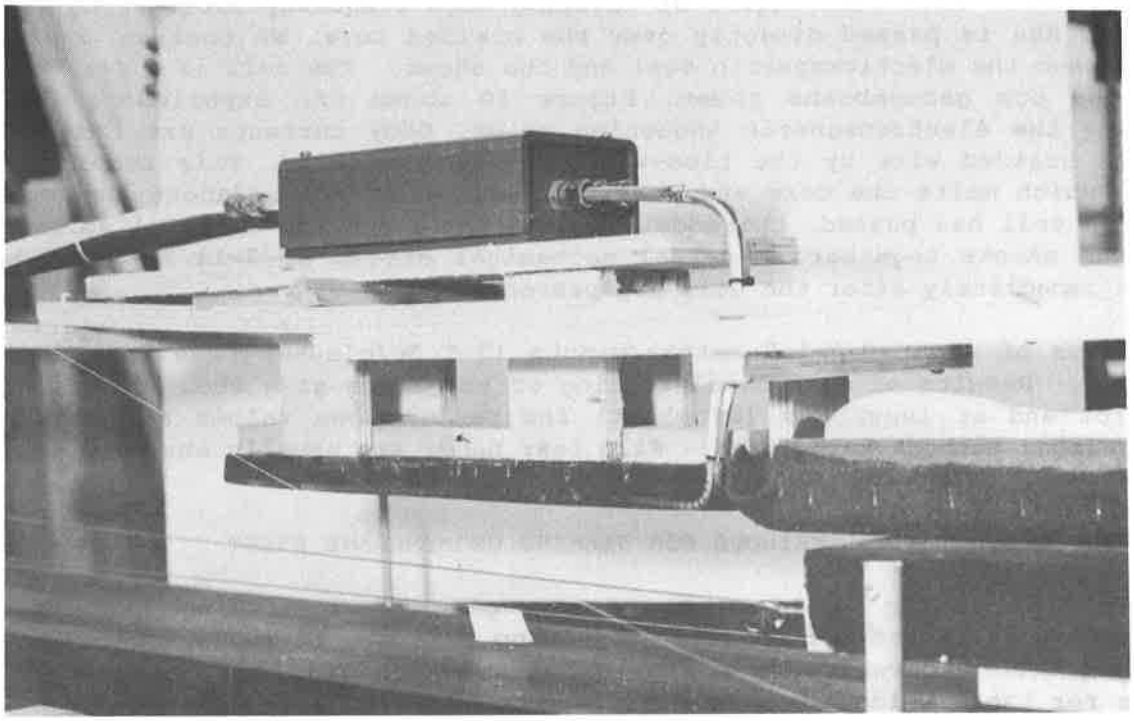

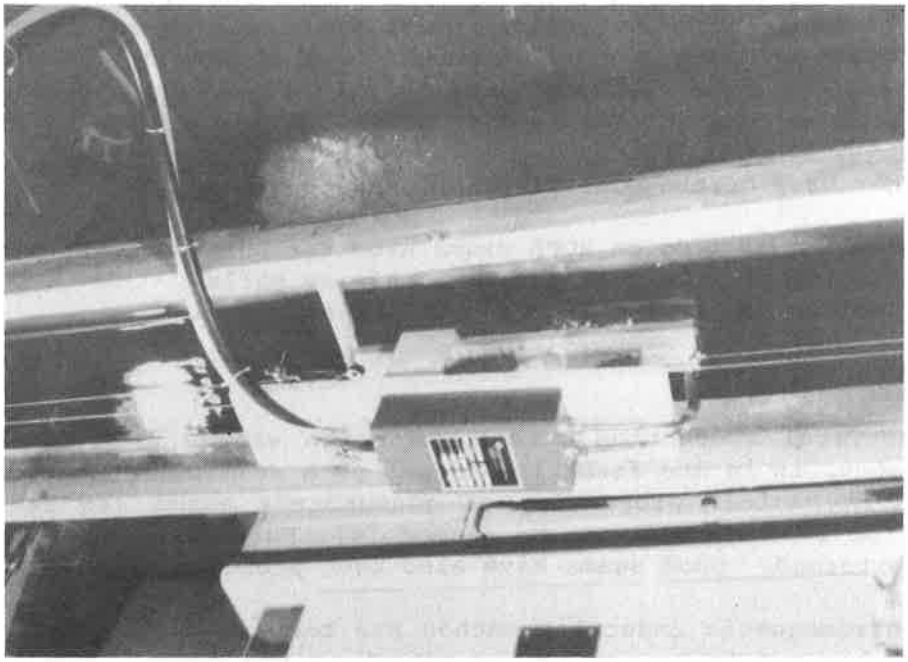

Figure 10 - Two Views of the Electromagnetic Induction Seaming Apparatus

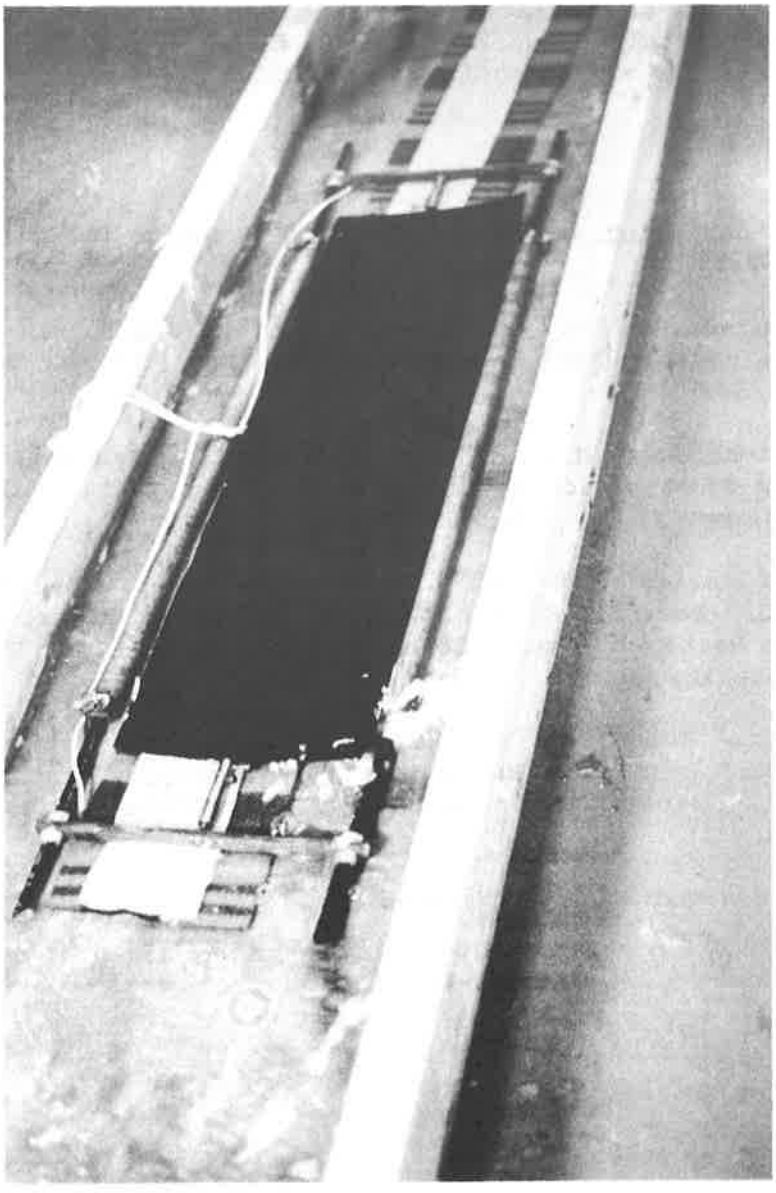

Figure 11 - Underwater Electrical Conduction Welding of Geomembrane Sheet

- The ability to go back over the the weld and re-heat if bonding was incomplete on the first pass.
- Real time readout of the welding parameters so that power adjustments can be made.
- Multicore, i.e., multiseam welds are essentially the same as one seam.

It is hoped that this discussion of electrical seaming techniques for geomembranes will be of help to workers in the field in gaining more perspectives as to what seaming methods are potentially available.

REFERENCES

1. Koerner, R. M., Designing with Geosynthetics, Prentice Hall, Englewood Cliffs, NJ, 1986, pp. 292-296.

2. Ewing, L. and Maine, L., "The Electrofusion of PE Gas Pipe Systems in British Gas," Proc. 8th Plastic Fuel Gas Pipe Symp., Nov. 29-30, Dec. 1, 1983, New Orleans, LA, pp. 102-109.

3. Ewing, L. and Richardson, W., "Polyethylene Gas Pipe Systems: An Appraisal of Joint Design and Construction Methods," Proc. 7th Plastic Fuel Gas Pipe Symp., Nov. 12-14, 1980, pp. 25-31, New Orleans, LA.

4. Welding Thermo Plastics, I.R.A.P. Collaborative Grant, CA-103-8-1277, Interim Technical Report, (Dec. 30, 1988) and Final Technical Report (Feb. 15, 1990), submitted to the National Researc Council of Canada by E. O. Butts Consultants, Ltd., Nepean, Ontario, Canada.

5. Lord, A. E., Jr., Halse, Y. H. and Koerner, R. M., "Emerging Methods for Geomembrane Seams," Proc. 3rd GRI Seminar The Seaming of Geosynthetics (Dec. 14 and 15, 1989), Geosynthetic Research Institute, Drexel University, Philadelphia, PA.

6. Literature from Emabond Systems, Norwood, NJ.

Membrane Action in a Two-Layer Soil System Reinforced By Geotextile

Philippe L. Bourdeau
Purdue University, USA

ABSTRACT

A numerical model is formulated to assess tensile membrane action in a two-layer soil system reinforced by a geotextile. The analysis is based on a two-dimensional plane strain model of the static equilibrium of an elastic membrane placed at the interface between a granular base and a compressible subgrade. The theory of stochastic stress diffusion in particulate media is used to describe the transmission of load through the gravel base, and a Winkler model is assumed for the subgrade. The model incorporates a Mohr-Coulomb criterion for the frictional interaction at the gravel-fabric interface, and it allows for incomplete anchorage. The numerical solution is provided by an iterative finite difference scheme. The influence of the anchorage conditions on the load-deflection response of the system is illustrated, and it is shown that the performance of high tensile modulus fabrics may be affected to a higher degree by an incomplete anchorage than lower modulus fabrics.

INTRODUCTION

Independently of their drainage and filter effects, geosynthetic inclusions placed at the interface between granular base and compressible subgrade can act in three ways to reinforce unpaved roads [1]: provide (a) granular base restraint, (b) subgrade soil restraint, and provide (c) membrane support.

If friction, or interlocking, is effective at the interface between the base course and the tensile resistant fabric, lateral spreading of the granular material under vertical surface loading is restrained, resulting in improvement of both strength and stiffness of the base course. A similar mechanism increases the bearing capacity of the subgrade by influencing its failure mode. Lateral restraint has been shown to occur with moderate surface deflection when geogrids are used as reinforcing elements [2, 3]. A design method based on this concept has been proposed recently [27].

At larger strain, interface deflection associated with rutting can lead to significant membrane tensile forces, which partly support the wheel loads and reduce the pressure on the subgrade. A number of analytical models [e.g., 4, 5, 6, 7] consider this latter effect as the dominant mechanism in reinforced unpaved roads, when high modulus geotextiles with soil-fabric friction properties sufficient to provide a full anchorage are used. In this type of analysis, the assumption of either a fixed edge condition or an arbitrary geometric shape for the deflected membrane is generally made. Thus, the influence of anchorage conditions and tensile modulus of the fabric inclusion on the development of its membrane action cannot be clearly demonstrated using these models. A recent study [8] has shown that the load-diffusion approach proposed by Bourdeau et al. [9] for reinforced particulate media may be appropriate to investigate this aspect of soil-fabric interaction including partial slippage at the soil-inclusion interface. This paper summarizes the formulation of this concept. Its application to a two-layer soil system is illustrated.

MEMBRANE ACTION MODEL

The analytical method is a two-dimensional plane strain model of the static equilibrium of an elastic membrane, placed at the interface between a granular base course and a compressible subgrade (Fig. 1).

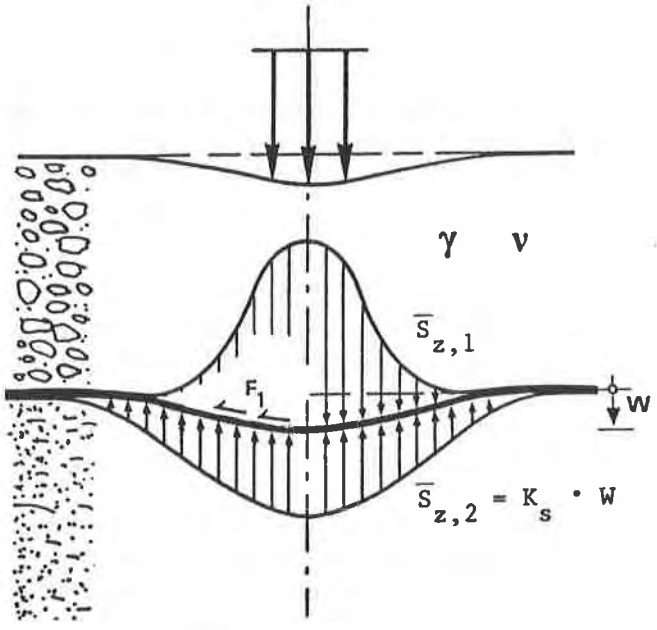

Figure 1. Two-dimensional plane strain model of the static equilibrium of an elastic membrane. $\bar{S}_{z,1}$, $\bar{S}_{z,2}$: Load induced vertical stresses at the interface.

The conventional approach to assess the transmission of traffic load through a road base course is to compute stresses using the linear theory of elasticity. This method was applied by Nieuwenhuis [4] to

reinforced unpaved road modeling. Such solutions require the assumption of an equivalent continuum. Furthermore, unless anisotropy is explicitly introduced, the elastic solutions are unable to account for the state of compaction of the material and its effect on the distribution of stresses in the base course. Another approach [e.g., 6, 10, 7] consists in assuming that the aggregate spreads the surface load at an arbitrarily chosen angle, and in replacing the bell-shaped distribution of vertical stress at the gravel-geotextile interface by a uniform distribution confined to the interior of this angle.

In the present model, the transmission of applied load through the gravel base is described using the theory of stochastic stress diffusion in particulate media developed by Sergeev [11] and Harr [12]. A detailed formulation of the theory can be found elsewhere [13, 14]. Instead of assuming continuity and homogeneity of the granular material, its particulate and inherently random nature is recognized, and boundary value problems are solved using probabilistic arguments. The transmission of applied loads results from the propagation of contact forces between particles. This can be modeled as the progression with depth of a vertical force undergoing random lateral fluctuations when proceeding from a particle to its neighbor. For two-dimensional plane strain conditions, this discrete process is a one-dimensional random walk where vertical steps are substituted for time steps, and the random fluctuations occur in the horizontal direction. As very small steps are considered, this leads in the limit to a diffusion-type equation:

$$\frac{\partial \bar{S}_z}{\partial z} = D \frac{\partial^2 \bar{S}_z}{\partial x^2} \qquad (1)$$

where $\bar{S}_z(x,z)$ is the expected vertical stress induced by the surface applied load at a point (defined by the coordinates x and z) in the granular material, and D is the coefficient of diffusion which governs the rate at which the granular base course spreads the applied surface load. Term D can be expressed as [11, 12]:

$$D = \nu \cdot z \qquad (2)$$

where the coefficient of diffusivity, ν, is a state parameter of the material. From a structural viewpoint, ν is influenced by such factors as stress induced anisotropy of the granular assembly, intergranular friction properties, and porosity of the medium. Conceptually, ν is related to the coefficient of lateral earth pressure and can account for the state of compaction of the gravel base [15]. Consequently, the coefficient of diffusivity is a stress-dependent parameter. It is noted that the present simplified formulation, Eq. (1), assumes a constant value for ν for the range of applied load being considered.

For a line load of intensity P acting normal to the surface (at the origin of coordinates) the solution of Eq. (1) is a bell-shaped Gaussian density function:

$$\frac{\bar{S}_z(x,z)}{P} = \frac{1}{z\sqrt{2\pi\nu}} \exp\left[\frac{-x^2}{2\nu z^2}\right] \qquad (3)$$

In the case of an applied load, P, uniformly distributed over a strip of width 2a, Harr [12] obtained:

$$\frac{\bar{S}_z(x,z)}{P} = \psi\left(\frac{x+a}{z\sqrt{\nu}}\right) - \psi\left(\frac{x-a}{z\sqrt{\nu}}\right) \qquad (4)$$

where ψ is the cumulative Gaussian distribution function:

$$\psi(x) = \int_o^x \exp\left[-\frac{t^2}{2}\right] dt \qquad (5)$$

In an unreinforced system where the lateral deformation of the granular base course is not confined by interface friction, it was shown [13] that the initial value upon loading of the coefficient of diffusivity, ν_o, can be approximated by the coefficient of earth pressure at rest, K_o. Thus, ν_o can be assessed as a function of the angle of internal friction of the granular base using Jaky's formula [22]. When the applied load is increased and the granular material approaches a yielding state, the coefficient of diffusivity can vary within the range of values bounded by the active and passive coefficients of earth pressure, K_a and K_p, respectively.

In contrast, as noted in the previous section, the lateral deformation of the gravel base of a reinforced system is restrained. Therefore, in a first approximation it is assumed that the coefficient of diffusivity remains under applied loading, equal to its initial value ν_o. Computations based on Eq. (3) show that large values of the coefficient of diffusivity ν contribute to smoother distributions of vertical stresses $\bar{S}_z$ and lesser rutting of the structure.

Following [16] and [4], the compressible subgrade is assumed to offer a reaction to loading proportional to its deflection (Winkler model), i.e.:

$$\bar{S}_{z,2}(x) = k_s \cdot w(x) \qquad (6)$$

where $\bar{S}_{z,2}$ is the vertical stress at the fabric-subgrade interface, w(x) is the membrane deflection, and k_s is the coefficient of subgrade reaction. The coefficient of subgrade reaction can be derived from plate load tests, taking in account the actual size of the loaded area [23].

Model wall tests [17] and pull-out tests performed with woven polyester fabrics [18] have shown that full frictional resistance of the geotextile is achieved with only small interface displacements. The post-peak drop in soil-fabric friction observed during these tests or reported from other experimental studies appears to be negligible (e.g. Ref. 25, 26). Accordingly, a rigid-perfectly plastic friction law is adopted to represent the behavior of the soil-fabric interface in shear. A Mohr-Coulomb yield criterion is invoked for the frictional stress at the gravel-fabric interface. If tensile strain is developed in the fabric, the frictional stress, τ, mobilized at the interface between the base course and the reinforcement is proportional to the resultant normal (vertical) stress at the point considered:

$$\tau(x) = F_1 \cdot (\bar{S}_{z,1}(x) + \gamma H_1) \qquad (7)$$

where $\bar{S}_{z,1}$ is the vertical stress at the gravel-fabric interface, γ is the unit weight of the gravel base, H_1 is the thickness of the base course and F_1 is the interface friction coefficient. Friction developed at the fabric-subgrade interface is neglected. It should be noted that Eq. (7) disregards the slope of the deflected membrane, and thus provides an upper-bound on the actual frictional stress developed at the gravel-fabric interface.

The determination of friction between soil and geotextile is generally made using a modified direct shear box. A description of the current testing techniques can be found elsewhere (e.g. Ref. 24).

Solution for Full Anchorage Condition

Consider the equilibrium conditions of the membrane as shown in Fig. 2. The tangential stress $\tau(x)$ opposes the direction of displacement of the membrane, and equilibrium in the horizontal direction implies:

$$T_H(x) + \int_o^x \tau_H(x)\,dx = T_o \qquad (8)$$

where τ_H is the horizontal component of the frictional stress at the interface, $T_H(x)$ is the horizontal component of the tensile force in the membrane, and T_o is the horizontal tensile force, at the origin of coordinates.

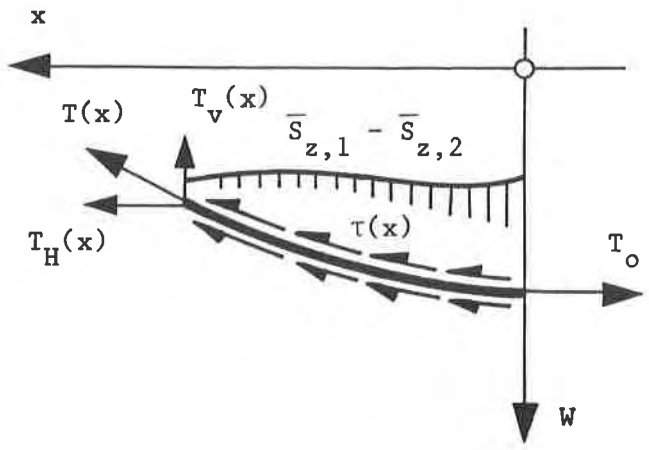

Figure 2. Forces acting on the deflected membrane

Equilibrium in the vertical direction is written as:

$$T_v(x) - \int_o^x (\bar{S}_{z,1} - \bar{S}_{z,2})\,dx + \int_o^x \tau_v(x)\,dx = 0 \qquad (9)$$

where τ_v is the vertical component of the frictional stress.

Taking the derivative of Eq. (9) with respect to x, and replacing $\bar{S}_{z,2}$ by its expression (Eq. 6) result in:

$$\frac{dT_v}{dx} + \tau_v(x) + k_s \cdot w(x) = \bar{S}_{z,1}(x) \qquad (10)$$

and from simple geometric considerations:

$$\frac{dT_H}{dx} \cdot \frac{dw}{dx} + T_H \frac{d^2w}{dx^2} + \tau_H \frac{dw}{dx} + k_s \cdot w = \bar{S}_{z,1} \qquad (11)$$

Finally, substituting the derivative of Eq. (8) into Eq. (11) gives:

$$T_H(x) \frac{d^2w(x)}{dx^2} + k_s \cdot w(x) = \bar{S}_{z,1}(x) \qquad (12)$$

The deformation condition of the reinforcement is:

$$\int_0^L \left[1 + \left(\frac{dw}{dx}\right)^2\right]^{1/2} dx - L = \frac{1}{E_m} \int_0^L T_H(x) \left[1 + \left(\frac{dw}{dx}\right)^2\right]^{1/2} dx \qquad (13)$$

where E_m is the elongation modulus [N/m] of the fabric of total length 2L.

The boundary conditions are:

$$\frac{dw}{dx} = 0 \quad for \; x = 0 \qquad (14a)$$

$$T_H = 0 \quad for \; x = L \qquad (14b)$$

The second condition (Eq. 14b) expresses that frictional anchorage is sufficient to prevent unbalanced tensile forces from occurring at the free edges of the geotextile.

Assuming that F, L, P, K_s, γ and H_1 are given, the system of differential equations (1), (7), (8), (12) and (13) subjected to boundary conditions Eqs. (14a, 14b) was solved numerically using the finite difference method. A derivation of this solution and its computer implementation can be found elsewhere [19,28].

Outputs of the numerical model consist of the membrane tensile forces T(x), the active length L_a and the deflection w(x). The active length of the reinforcement, L_a, is defined as the distance from the origin to the point where the effective tensile force and mobilized friction are equal to zero: L_a is the half-length of geotextile required to ensure full frictional anchorage. The computed deflection, w(x), is the deflection of the membrane placed at the interface between the base course and the subgrade. It differs from that of the road surface because the gravel base is compressible. However, the compressibility of the gravel material can generally be disregarded, compared to that of the soft subgrade.

Parametric studies performed with the model (Ref. 9) indicated that both required tensile resistance and active length of the inclusion are reduced when the coefficient of subgrade reaction or the coefficient of diffusivity of the granular base is increased. Simultaneously, the benefit provided by the reinforcement, expressed in terms of relative reduction of contact pressure on the compressible subgrade, is also reduced.

Solution for Incomplete Anchorage

According to the friction model adopted for gravel base-geotextile interface response, the anchoring process develops with a progressive mobilization of soil-geotextile friction, starting beneath the loaded area and extending to the outside zones. In the zone directly affected by the diffusion of the applied vertical load through the gravel layers, the friction forces available at the interface increase with this load. In the outside zones, the amount of anchoring resistance available increases with the length of the geotextile. This mechanism leads to a limiting value of the maximal tensile force, T_{max}, which can be balanced by the available anchoring resistance:

$$T_{max} = (P/2 + \gamma H_1 L) F_1 \qquad (15)$$

where P is the applied vertical load per unit of width.

Suppose the applied load is increased to the value at which the frictional anchoring resistance is fully mobilized. Beyond this limiting value, the maximal tensile force in the reinforcement would be bounded by Eq. (15). A further increase of applied load δP would produce a subsequent increase of available anchorage resistance of only:

$$\delta T_{max} = \frac{\delta P}{2} \cdot F_1 \qquad (16)$$

thus leading to a lower rate of reinforcing effect, as compared to the load-settlement response of a fully anchored system. However, one can reasonably assume that the reinforcing effect gained by the system at the previous loading increments, with a developed tensile force smaller than T_{max} in Eq. (15), would not be lost. This aspect of the soil-geotextile interaction can be handled in the model described above by incorporating the tension cutoff rule in Eqs. (15) and (16) to the numerical solution algorithm.

EXAMPLE

Large scale strip loading tests performed on a two-layer (uncompacted gravel over peat) system with various fabric tensile moduli and anchorage conditions have been reported by Douglas et al. [20] and Douglas and Kelly [21]. Theoretical predictions from the model described herein were compared to these test results and were found in qualitative agreement with the observations. A detailed discussion on this comparative study can be found in Ref. 8. The present example is derived from this previous study. Table 1 summarizes the geometry of the case considered, as well as the set of mechanical parameters adopted. The coefficient of diffusivity

TABLE 1. Parameters Used in the Computations

geometry	width of load area	0.25 m
	half length of fabric	1.20 m
	gravel base thickness	0.15 m
applied load	average pressure	up to 60 kN/m^2
reinforcement	tensile modulus	up to 120 kN/m
	tensile strength	unbounded
	gravel-geotextile friction coefficient	0.40
gravel base	dry unit weight	15.9 kN/m^3
	diffusivity coefficient	0.40
peat subgrade	stiffness coefficient	170 kN/m^3

for stresses in the gravel base is assumed to be of the order of the at-rest coefficient of earth pressure, K_o, for uncompacted material with a friction angle of 37°. The computations were performed with free and fixed edge conditions for the reinforcement, with the same length of tensile inclusion in both cases. The fixed edge case simulates a situation where the displacement of the edge of the fabric is artificially prevented, and thus represents an upper bound on anchorage resistance.

The load-settlement response at the interface of the system is presented, Fig. 3a, for a tensile modulus of the order of magnitude of a woven fabric modulus. The free and fixed edge results are compared to an unreinforced situation. Surface deflections observed by Douglas and Kelly [21] are also indicated. Figure 3b gives the results for a tensile modulus of the inclusion representative of nonwoven fabrics. The computed maximum tensile force and maximum interface deflection are plotted as a function of the inclusion tensile modulus in Figs. 4a and 4b, respectively, for an applied pressure of 60 kN/m^2. Experimental data reported by Douglas and Kelly [21] are also indicated in Fig. 4b, including the deflection observed with a very low modulus polyethylene film instead of a geotextile. Recall that the computed curves in Figs. 3a to 4b represent the membrane deflection and not the surface settlements, which are also shown (from Douglas & Kelly's measurement). The theoretical model seems to be at least qualitatively in agreement with the observed behavior: the trend in the prediction is increasingly nonlinear when the tensile modulus is increased. It is noted that in these experiments, the

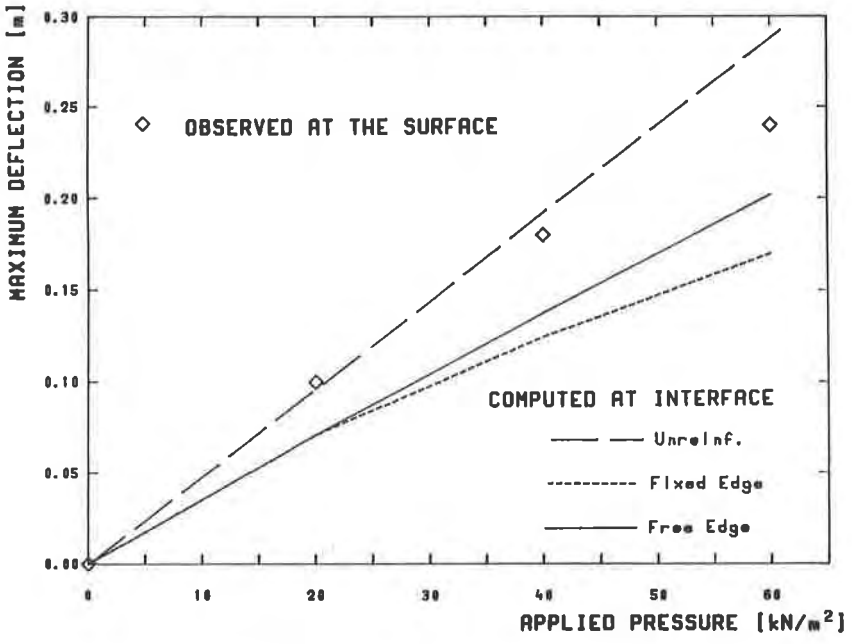

a) Woven geotextile (average tensile modulus = 121 kN/m)

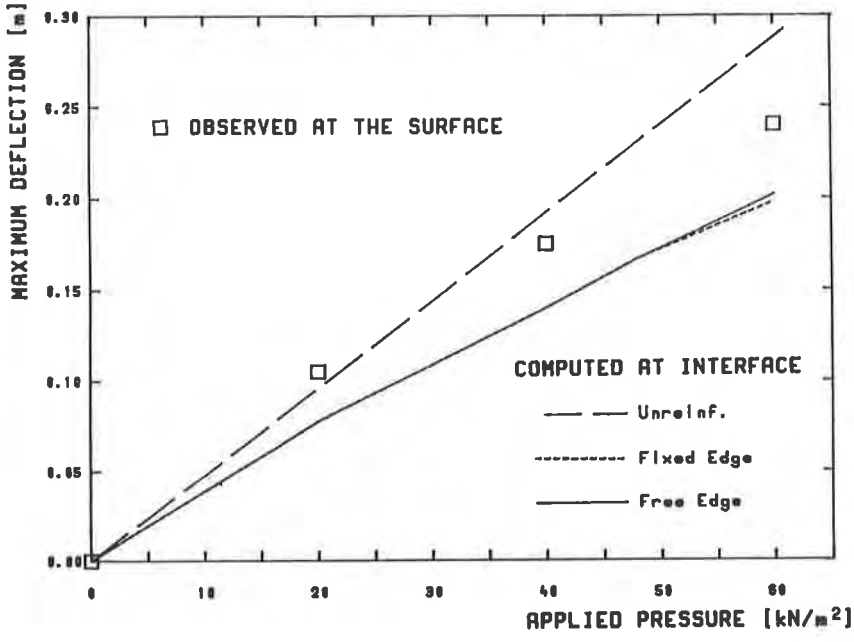

b) Nonwoven geotextile (average tensile modulus = 26 kN/m)

Figure 3. Results of the numerical modeling (see input data in Table 1). Maximum deflection at **interface** as a function of applied pressure, compared to **surface** settlement measured by Douglas and Kelly (Ref. 21).

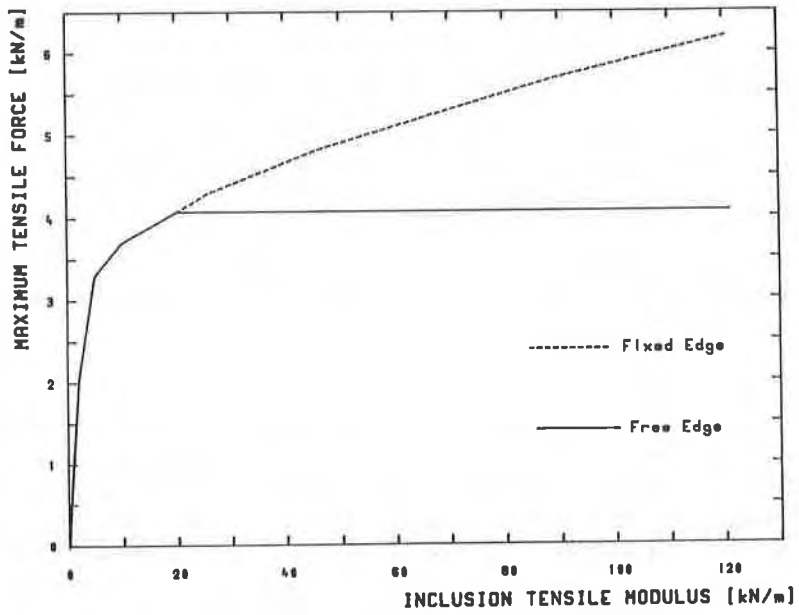

a) Influence of geotextile tensile modulus on maximum tensile force

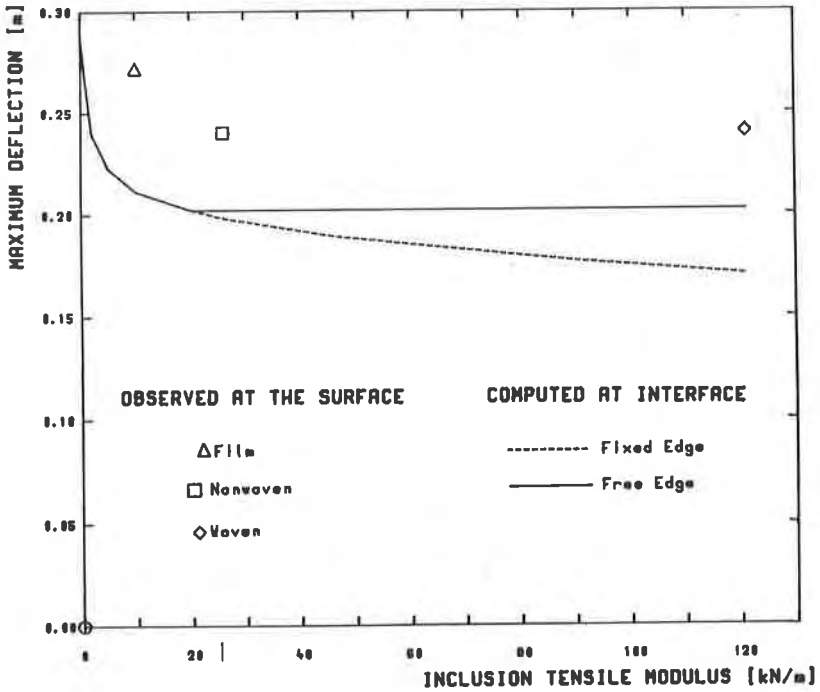

b) Influence of geotextile tensile modulus on maximum deflection

Figure 4. Results of numerical modeling (see input data in Table 1), compared to surface settlement measured by Douglas and Kelly (Ref. 21); applied pressure is 60 kN/m^2.

gravel base was not compacted prior to loading. Therefore, surface settlements should be larger than interface settlements, due to compression in the gravel layer. This is the case in Figs. 3a and 3b when the settlements observed at the surface by Douglas & Kelly are compared to the settlements computed at the interface with membrane inclusion, for both hypotheses of end fixity. If the presence of a tensile inclusion is not assumed ('unreinforced' hypothesis), the computed settlements at the interface are larger or equal to the settlements observed at the surface. Therefore, it is reasonable to conclude that noticeable reinforcing effects were developed in the tests reported by Douglas & Kelly.

The influence of the anchorage conditions is clearly apparent for the woven fabric (Fig. 3a). In the free edge case, full mobilization of the available anchorage resistance is reached at an applied pressure of about 20 kN/m^2, and with further increase in load the reinforcement effect is not fully efficient, as compared to the fixed edge case. With the nonwoven fabric, full mobilization of the free anchorage is reached at a higher applied pressure of about 50 kN/m^2, and at a pressure of 60 kN/m^2 the difference in deflection in the axis of the load is still very small, between the two edge conditions. This contrast in the behavior of the two reinforced system is a consequence of the difference in the tensile modulus of the inclusions considered and of the non-linearity induced by the soil-geotextile interaction (Figs. 5 and 6). Such a result could explain why woven and nonwoven fabrics lead to very close reinforcing effects in some situations. However, it should be pointed out that, according to the model proposed herein, full frictional anchorage is not a necessary condition for the reinforcement mechanism, although incomplete anchorage does not allow the full benefit of high modulus fabric to be gained.

CONCLUSION AND SUMMARY

A numerical model of the soil-geotextile interaction in two-layer systems reinforced by tensile inclusions has been formulated. The analytical method is a two-dimensional plane strain model of the static equilibrium of an elastic membrane placed at the interface between a granular base course and a compressible subgrade. The transmission of load through the gravel base is described using the theory of stochastic stress diffusion in particulate media. Within this framework, account is made for the lateral restraint interaction between the reinforcement and the granular base in a simplified way by assuming the coefficient of diffusivity being equal to the coefficient of lateral earth pressure at rest. A constant coefficient Winkler subgrade model is assumed for the pressure-displacement response of the compressible soil. At the gravel-geotextile interface, friction is evaluated using the Mohr-Coulomb criterion.

Incomplete frictional anchorage is allowed in the model, and the influence of this particular feature was demonstrated. High modulus fabrics may not provide more reinforcing effects than low modulus

fabrics in case of incomplete anchorage, as a consequence of the non-linearity of the soil-geotextile interaction mechanism.

ACKNOWLEDGEMENTS

This study was partly performed at the Soil Mechanics Laboratory of the Swiss Federal Institute of Technology, Lausanne, under contract No. 25/84 with the Swiss Federal Department of Transportation,

Communication and Energy, Division of Highways. Support during the preparation of this paper was provided by Purdue University.

The author wishes to acknowledge the contributions of the late Dr. Jacques Chapuis and the suggestions of Professor Robert D. Holtz. The manuscript was typed by Cathy Ralston.

REFERENCES

(1) HAUSMANN, M. R., Geotextiles for unpaved roads - a review of design procedures. Geotextiles and Geomembranes, Vol. 5 (1987), pp. 201-233.

(2) MILLIGAN, G. W. E., FANNIN, R. J., and FARRAR, D. M., Model and full-scale tests of granular layers reinforced with a geogrid. Proc. 3rd International Conference on Geotextiles, Vienna (1986), Vol. 1, pp. 61-66.

(3) LOVE, J. P., BURD, H. J., MILLIGAN, G. W. E., and HOULSBY, G. T., Analytical and model studies of reinforcement of a layer of granular fill on a soft clay subgrade. Canadian Geotech. J., Vol. 24 (1987), pp. 611-622.

(4) NIEUVENHUIS, J. D., Membranes and the bearing capacity of road bases. Proc. International Conference on the Use of Fabrics in Geotechnics, Paris (1977), Vol. 1, pp. 3-8.

(5) BENDER, D. A. and BARENBERG, E. J., Design and behavior of soil-fabric-aggregate system. Transportation Research Record 671 (1978), pp. 64-75.

(6) GIROUD, J. P. and NOIRAY, L., Geotextile-reinforced unpaved road design. J. of the Geotechnical Engineering Division, ASCE, Vol. 107 (1981), No. GT9, pp. 1233-1254.

(7) SELLMEIJER, J. B., KENTER, C. J. and VAN DEN BERG, C., Calculation method for fabric reinforced road. Proc. 2nd International Conference on Geotextiles, Las Vegas (1982), Vol. 2, pp. 393-398.

(8) BOURDEAU, P. L., HOLTZ, R. D. and CHAPUIS, J., Effect of anchorage and modulus in geotextile-reinforced unpaved roads. Geotextiles and Geomembranes (1988), Vol. 7, pp. 221-230.

(9) BOURDEAU, P. L., HARR, M. E. and HOLTZ, R. D., Soil-fabric interaction. An analytical model. Proc. 2nd International Conference on Geotextiles, Las Vegas (1982), Vol. 2, pp. 387-391.

(10) RAUMANN, G., Geotextiles in unpaved roads: design considerations, Proc. 2nd International Conference on Geotextiles, Las Vegas (1982), Vol. 2, pp. 417-422.

(11) SERGEEV, I. J., The application of probability - process equations to the theory of stress distribution in non-cohesive soil foundation beds. Soil Mech. and Fdn. Engng., No. 2 (1969), pp. 84-88.

(12) HARR, M. E., Mechanics of Particulate Media. A Probabilistic Approach, McGraw-Hill, New York (1977).

(13) BOURDEAU, P. L., Analyse probabiliste des tassements d'un massif de sol granulaire, These de Doctorat es Sciences Techniques, No. 628, Swiss Federal Institute of Technology, Lausanne (1986).

(14) BOURDEAU, P. L., Probabilistic analysis of settlements in loose particulate media. Proc. 5th Int. Conf. on Applic. of Statistics and Probability in soil and Structural Engng. Vancouver (1987), Vol. 2, pp. 977-984.

(15) BOURDEAU, P. L. and RECORDON, E., Dimensionnement des chaussees souples. Point de vue probabiliste. Annales de l'Institut Technique du Batiment et des Travaux Publics, No. 420 (1983), pp. 1-15.

(16) ROSNER, J. C. and HARR, M. E., Identification of subgrade characteristics from prototype testing of landing mats. HRB Record, No. 337 (1979).

(17) HOLTZ, R. D. and BROMS, B. B., Walls reinforced by fabrics: results of model tests. Proc. Int. Conf. on the Use of Fabrics in Geotechnics, Paris (1977), Vol. 1, pp. 113-118.

(18) HOLTZ, R. D., Laboratory studies of reinforced earth using a woven polyester fabric. Proc. Int. Conf. on the Use of Fabrics in Geotechnics, Paris (1977), Vol. 3, pp. 149-154.

(19) BOURDEAU, P. L., FABRIC4: A computer program for fabric-reinforced two-layers systems. Users guide. Internal report, Swiss Federal Institute of Technology, Lausanne (1988).

(20) DOUGLAS, R. A., BESSEY, R. B. and SMALL, R. P., The use of geotextiles in forest road construction. Proc. Second Canadian Symposium on Geotextiles and Geomembranes, Edmonton (1985), pp. 88-96.

(21) DOUGLAS, R. A, and KELLY, M. A., Geotextile 'reinforced' unpaved logging roads: the effect of anchorage. Geotextiles and Geomembranes, Vol. 4 (1986), pp. 93-106.

(22) JAKY, J., The coefficient of earth pressure at rest (in Hungarian), J. Society of Hungarian Architects and Engineers, Budapest (1944), pp. 355-358.

(23) TERZAGHI, K., Evaluation of coefficient of subgrade reaction. Geotechnique, Vol. 5 (1955), No. 4, pp. 297-326.

(24) VAN DEN BERG, C. and MYLES, B., Geotextile Testing. An Inventory of Current Geotextile Test Methods and Standards. International Geotextile Society, Brussells (1986).

(25) DEGOUTTE, G. and MATHIEU, G., Experimental research of friction between soil and geomembranes or geotextiles using a 30 x 30 cm^2 shear box. Proc. 3rd Int. Conf. on Geotextiles, Vienna (1986), Vol. 4, pp. 1251-1256.

(26) GOURC, J. P., RATEL, A. and DELMAS, P., Design of fabric retaining walls: the "Displacement Method". Proc. 3rd Int. Conf. on Geotextiles, Vienna (1986), Vol. 4, pp. 1067-1072.

(27) MILLIGAN, G.W.E., JEWELL, R. A., HOULSBY, G. T. and BURD, H. J., "A New Approach to the Design of Unpaved Roads. Ground Engineering, Vol. 22 (1989), No. 3, pp. 25-29 (Part 1), Vol. 22, No. 11, pp. 37-42 (Part 2).

(28) BOURDEAU, P. L., Modeling of Membrane Action in a Two-Layer Reinforced Soil System, Computers and Geotechnics, Vol. 7 (1989), pp. 19-36.

A Probabilistic Review of Geotextile Reinforced Slope Design

Shi-Chieh Cheng
Drexel University, USA
Barry Christopher
Polyfelt, Inc., USA

ABSTRACT

Slope stability analyses were performed on two geotextile reinforced slopes which were constructed as part of the FHWA study on the "Behavior of Reinforced Soil Structures". Both reinforced with geotextiles and non-reinforced conditions were evaluated. The uncertainties around the input parameters, including the geotechnical and geosynthetic properties, introduce a measurable uncertainty on the prediction of the slope stability and the required strength from reinforcement. Probabilistic methods were used to evaluate these uncertainties and the results can assist the geotechnical engineer in accounting for them through quantification of the risk involved in design.

INTRODUCTION

Reinforcement strength requirements for reinforced slopes are currently analyzed using modified versions of the classical limit equilibrium slope stability methods. A circular or wedge-type potential failure surface is assumed, and the relationship between the driving and resisting forces or moments determines the slope's factor of safety. Reinforcement layers intersecting the potential failure surface are assumed to increase the resisting force or moment based on their tensile capacity and orientation. Usually, the shear and bending strength of stiff reinforcements are not taken into acount. The tensile capacity of a reinforcement layer is taken as the minimum of its allowable pullout resistance behind the potential failure surface and its allowable design strength. A wide variety of potential failure surfaces must be considered, including deep-seated surfaces through or behind the reinforced zone. The slope stability factor of safety is taken from the the critical surface requiring the maximum reinforcement. Detailed design of reinforced slopes is performed by determining the factor of safety with successively modified reinforcement layouts until the target factor of safety is achieved.

This practice assumes that the target factor of safety for the reinforced case is equally "safe" to a flatter unreinforced slope with the same factor of safety. However, acceptable factors of safety for unreinforced slopes have been established through experience and the risks of designing at low factors of safety (i.e. typical factor of safety = 1.3) are somewhat known. The inclusion of reinforcement in the design introduces another level of uncertainty over that already contained in slope design due to the variability of soil properties and site conditions. As such, it would appear prudent for the designer to question the "equally safe" assumption of the current practice. Also, as a consequence of uncertainties associated with the input parameters,

uncertainties will arise on the value of the required reinforcement. Probabilistic analysis can be used to quantify uncertainty and assertain the relationships between design and risk.

The use of probability and statistics principles to account for uncertainty in geotechnical engineering analysis and design has become popular in recent years (Harr, 1987). It is possible to employ the probabilistic analysis techniques in predicting the slope stability while considering the uncertainties of the input parameters. One approach that can be undertaken is to treat the input variables as random variates represented by a mean value, a standard deviation (or coefficient of variation), and a probability density function (PDF). All or any desired number of variables contained in the deterministic slope stability equations (models) can be treated as random variables. Factor of safety and/or required reinforcement tensile strength, being a function of these random variables, also become random variables with a mean, standard deviation, and probability density function, and can be further analyzed probabilistically. It must be noted that these probabilistic techniques only serve as supplements or complements to the existing deterministic procedures rather than replacing them. Further, the purpose of this paper was to analyze the uncertainty in a specific deterministic approach. No attempt was made in this paper to evaluate the general slope stability analysis methods, as the reinforcement procedure relies upon a specific failure surface that requiring the maximum reinforcement.

The following section of this paper presents a brief review of the U.S. Federal Highway Administration deterministic design procedures for evaluating the reinforcement requirements in a reinforced slope (Christopher, et. al., 1989). The anchorage capacity of reinforcement, although an important part of the analysis, is a separate issue and, due to length restriction, will not be addressed in this paper. Next, fundamentals of a probabilistic method called Point Estimate Method (PEM) (Rosenbleuth, 1975) are presented as applicable to the study, and the essential features of the probabilistic models developed for the analysis are described. A case study involved two different slopes from a FHWA study are presented and discussed to demonstrate the applications and usefulness of these models. The summary and conclusions of the study appear in the final section of the paper.

DETERMINISTIC REINFORCED SLOPE DESIGN

Several simplified approaches are available for the design of slope reinforcement, many of which are contained in the FHWA Geotextile Engineering Manual (1985). The method used in this paper is the conventional rotational slip surface method as illustrated in Figure 1.

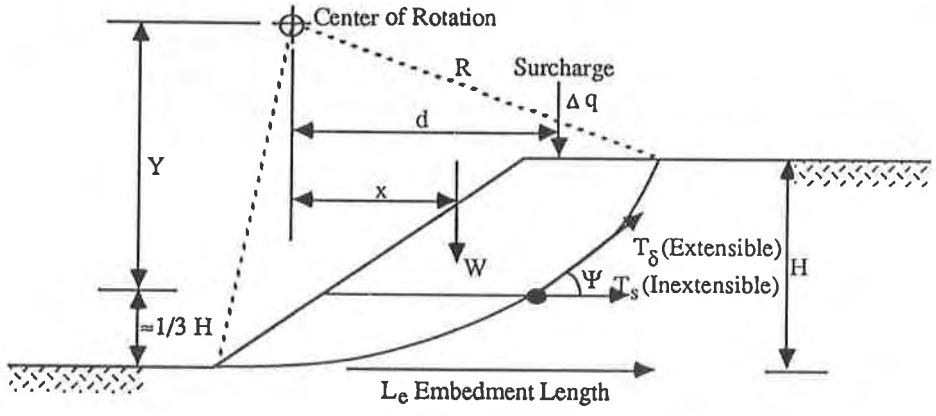

Figure 1 - Rotational Shear Approach to Required Strength of Reinforcement

The complete analysis should include both external and internal stability. In this paper, only the strength of the reinforcement to provide internal stability was considered. The steps involved are described as follows:

(1). Check unreinforced stability: To determine the size of the critical zone to be reinforced, examine the full range of potential failure surfaces found to have safety factor less than or equal to the target safety factor for the slope ($F.S._R$).

Factor of safety of unreinforced slope:

$$F.S._u = \frac{\text{Resisting Moment } (M_R)}{\text{Driving Moment } (M_D)} = \frac{\int_0^{L_{sp}} \tau_f \, R \, dL}{(Wx + \Delta q \; d)} \qquad (1)$$

where: $F.S._u$ = unreinforced slope safety factor
W = weight of sliding earth mass
L_{sp} = length of slip plane
Δq = surcharge
τ_f = shear strength of soil

(2). Calculate the total reinforcement tension (T_s) required to obtain $F.S._R$: This step should be performed for each potential failure circle inside the critical zone in step (1).

Factor of safety of reinforced slope:

$$F.S._R = F.S._u + \frac{T_s \; D}{M_D} \qquad (2)$$

or

$$T_s = (F.S._R - F.S._u) \; \frac{M_D}{D} \qquad (3)$$

where: T_s = sum of available tensile force per width of reinforcement for all reinforcement layers
D = moment arm of T_s about the center of rotation
= R for extensible reinforcement
= Y for inextensible reinforcement
$F.S._R$ = target minimum slope safety factor

PROBABILISTIC FUNDMENTALS

A fundamental principle in the probabilistic analysis is that a random variable (independent or dependent) can be decribed by a collection of statistical parameters, rather than a single value. These parameters include the mean, standard deviation, coefficient of variation, coefficient of skewness and coefficient of kurtosis. When two or more random variables are involved in the analysis, correlation coefficients can also be included. Associated with each random variable is also a probability density function (PDF) indicating the probability

distribution (e.g. normal, lognormal, Beta, etc.). The definitions and standard formulas for these parameters are covered in standard probability/statistics texts (see for example, Benjamin and Cornel, 1970).

When one or more of the independent variables in a model, (or equation), are random variates that are represented by a mean, a standard deviation and a PDF, the values for the same statistical parameters can be established for the dependent variables by methods like Taylor series expansion, Monte Carlo simulation or, the Point Estimate Method (PEM) which is recently developed by Rosenbleuth (1975), can be employed. To find the PDF, one can use the the Pearson's system, as described by Elderton and Johnson (1969). Armed with these parameters, one can easily establish a "reliability index" for the factor of safety ($\beta_{F.S.}$) (Baecher, 1986) or "reliability index" for the safety margin (β_{SM}) (Harr, 1987) defined as the difference between resisting and driving moment, where:

$$\beta_{F.S.} = \frac{\overline{F.S.} - 1.0}{s_{F.S.}} \tag{4}$$

and

$$\beta_{SM} = \frac{\overline{SM}}{s_{SM}} \tag{5}$$

where: $SM = (M_R + T_s\, D) - M_D$

CASE STUDY

Two slopes constructed for a study by FHWA (Figure 2 and Figure 3) were used in this paper, one with 0.5H : 1.0V slope and the other with 1.0H : 1.0V slope. Both slopes were constructed with silt type soils to a height of 7.62 m. The geotechnical parameters; moist unit weight(γ) and internal friction angle (ϕ') resulted from consolidated undrained test with pore pressure measurement are shown in Table 1. A rotational failure surface analysis (Equation 1) was performed on each slope to determine the most critical unreinforced failure surface which required the maximum reinforcement tensile strength. Table 1 list the results of this deterministic analysis.

Table 1. Deterministic Reinforced Slope Analysis

	H : V	γ (kN/m^3)	ϕ' (°)	M_D (kN-m)	M_R (kN-m)	$F.S._u$	$F.S._R$	T_s (kN/m)
Slope 1	1 : 1	20.1	35	508.1	485.8	0.956	1.3	60.8
Slope 2	0.5 : 1	20.1	35	1334.5	875.4	0.656	1.3 (1.5)	117.1 (153.5)

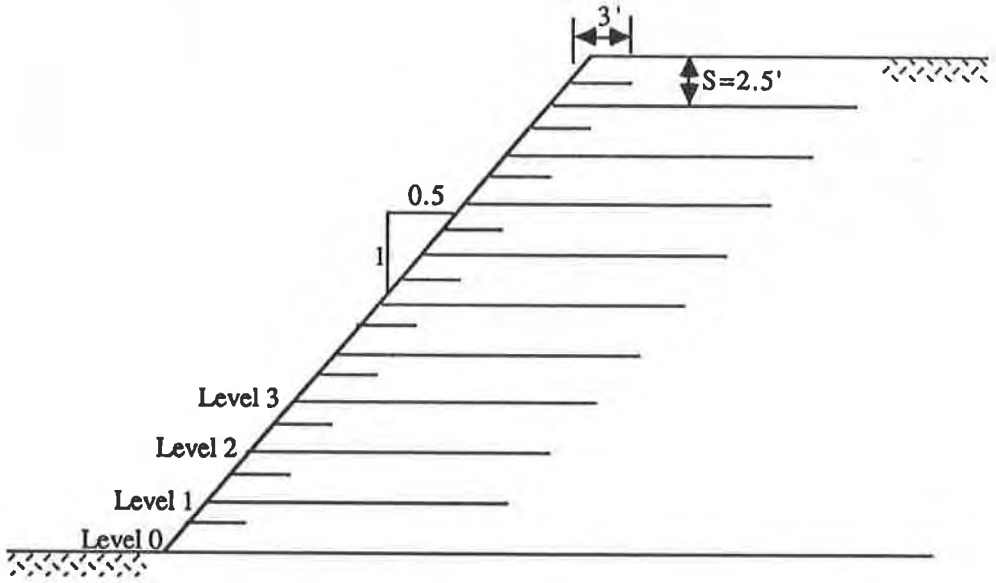

Figure 2 - 0.5H to 1.0V slope

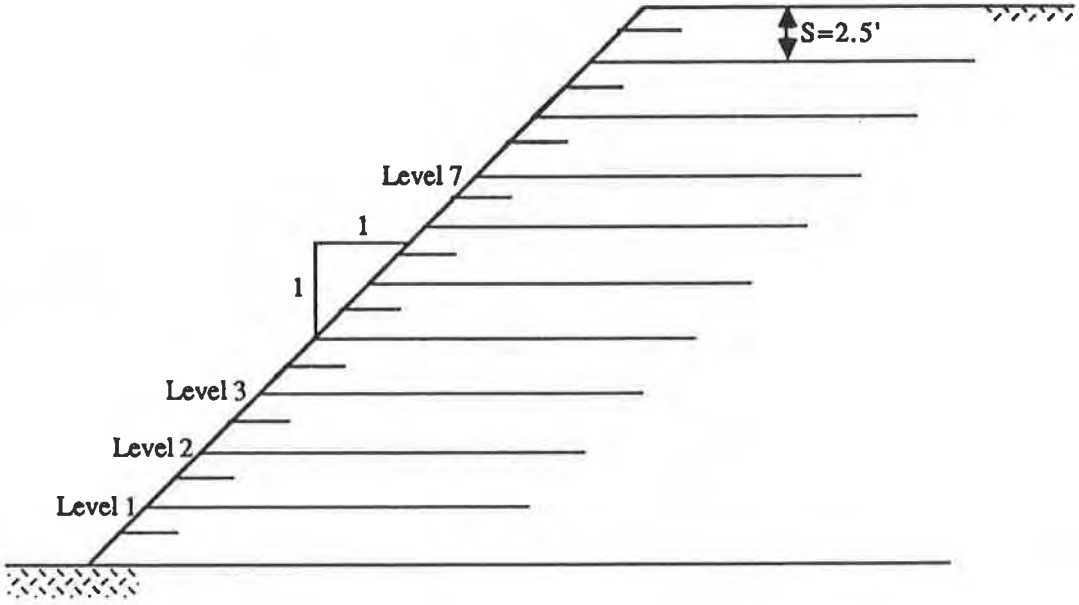

Figure 3 - 1.0H to 1.0V slope

Variabilities of Material Properties. Variability of the factor of safety for the slope can be analyzed by applying the Point Estimate Method and including the uncertainty of the random variables in Equation 1. If the geometry of the sliding mass and surcharge loads are treated as deterministic, then the random variables in the equation include shear strength (τ_f) and weight of the sliding mass (W). Weight of the sliding mass, or driving moment (M_D), is a function of the moist unit weight (γ). As for shear strength (τ_f), based on Mohr-Coulomb failure criterion, is dependent variable of cohesion (c), unit weight (γ) and internal friction angle (ϕ). The uncertainty of each variate can be expressed in terms of its coefficient of variation. The coefficient of variation for soil properties when correctly evaluated have been reported by several researchers. Table 2 list some of the reported values by Harr (1987) and by Lee et. al., (1983). It should be noted that the variability will increase significantly over those listed when these properties are assumed rather than determined through appropriate test methods. In this paper, the variability values used for unit weight and friction angle are 5% and 12% respectively.

Table 2 - Coefficient of Variation for Soil Properties

Reference	Unit Weight	Undrained Cohesion	Friction Angle
Harr (1987)	4%	40%	7 - 12%
Lee et. al. (1983)	1 - 10%	25 - 30%[1] 20 - 50%[2]	5 - 15%[1] 12 - 56%[2]

Note: 1: for sands. 2: for clays.

The variability of the strength of the reinforcement will, of course, vary with the type of reinforcement. For geosynthetics, which are of principle consideration in this paper, a coefficient of variation of approximately 10% for the wide width tensile strength of the material can be expected based on the writers' experience in performing a substantial number of such tests on numerous geosynthetics as well as results of recent ASTM round robin program to establish coefficient of variation of wide width tensile test method.

A fair assumption is that each soil layer acts independently and that no correlation exists between soil layers. As matter of fact, only one layer of soil was considered in this study as the multi-layer analysis are not considered in the deterministic analysis. However, there may be correlations within any soil layer (between soil parameters) or a soil layer and the reinforcement. For example, the friction angle of the embankment soil will increase linearly with an increase in the unit weight of the embankment (US Navy, 1982, DM - 7.1/2). Therefore, γ and ϕ should be positively correlated. Nevertheless, a study by Cheng (1990) on the probabilistic analysis of coal refuse disposal facility indicated the correlation between γ and ϕ have little influence on the result of the analysis. Rather, the correlation between the cohesion (c) and ϕ, which is negatively correlated, have a much higher impact on the results of the analysis in the same study. Since in this study, the cohesion value is not considered, no correlation will be considered in performing probabilistic analysis of the unreinforced slope. As for the reinforcement, it would appear to be

independent of the embankment soil if the friction angle is greater than that required to achieve the full strength of the reinforcement. This is usually the case for granular soils. However, an argument can be made that as the resisting moment (M_R) of the slope increases the strength of the reinforcement (T_s) required to achieve a particular factor of safety ($F.S._R$) will decrease and, thus, they are negatively correlated. By the same token, a positive correlation can be established between driving moment (M_D) and T_s.

Probabilistic Analysis of Unreinforced Slope. Based on Equation 1, the unreinforced factor of safety is the ratio between the resisting moment (M_R) and driving moment (M_D). The resisting moment is a function of the unit weight and friction angle of the soil, and the driving moment is only a function of the unit weight. The results of the probabilistic analysis using the PEM method are listed in Table 3. As anticipated, there is little difference between the deterministic and probabilistic $F.S._u$. The degree of variability of the driving moment basically has a linear relationship with respect to the variability of the unit weight (both are 5%). The variability of the resisting moment is a little higher than the variability of the friction angle (15.5% vs 12%). This is due to $\tan\phi$ which is used in the computation rather than just ϕ combined with the 5% variation from unit weight. The variability of the $F.S._u$ is generally controlled by the resisting moment which has a higher degree of variation than the driving moment, which in turn is controlled by the variation of the friction angle. This observation confirmed the previous study by Cheng, 1990.

Table 3 - Summary of the Probabilistic Analysis on Unreinforced Slope

	0.5H : 1.0V			1.0H : 1.0V		
	Mean	STD*	CV**	Mean	STD	CV
M_D (kN-m)	1334.5	66.7	5%	508.1	25.4	5%
M_R (kN-m)	882.5	137.2	15.5%	489.7	76.1	15.5%
$F.S._u$	0.663	0.1081	16.3%	0.966	0.160	16.6%
$F.S._u$ Determin.	0.656			0.956		

Note: *: standard deviation. **: coefficient of variation

Probabilistic Analysis of Reinforced Slope. To analyze the reinforced slope probabilistically, Equation 2 can be utilized with modification as follows:

$$F.S._R = \frac{M_R + T_s D}{M_D} \qquad (2a)$$

The reason for the modification will be discussed in the next section as Equation 3 requires the same kind of modification for probabilistic analysis. The independent variables in Equation 2a include the resisting moment, the driving moment, and the required reinforcement. The variability for the first two variables can be found in Table 3 (15.5% and 5%). The variability of the required reinforcement is based on the material test property which was 10% as mentioned before and the deterministic results for required reinforcement listed in Table 1 will be used as the mean values for each case. Table 4 lists the results of the probabilistic analysis of reinforced slopes. In addition, an unreinforced slope that having minimum safety factor of 1.3 (1.84H : 1.0V) was also analyzed probabilistically and listed in the same table to examine the "equally safe" assumption.

Table 4 - Summary of the Probabilistic Analysis on Reinforced Slope

	0.5H : 1.0V Reinforced	1.0H : 1.0V Reinforced	1.84H : 1.0V Unreinforced
$F.S._{Deterministic}$	1.300	1.300	1.300
T_s (kN/m)	117.1	60.8	0
$\overline{F.S._R}$	1.309	1.311	1.303
$s_{F.S._R}$	0.138	0.168	0.213
$CV_{F.S._R}$	10.6%	12.8%	16.3%
$\beta_{F.S.}$	2.24	1.85	1.42
β_{SM}	2.33	1.90	1.45
$\overline{SM}$ (kN-m)	407.4	156.3	43.9
s_{SM} (kN-m)	175.1	82.1	30.4
CV_{SM}	43.0%	52.5%	69.2%

The results in Table 4 provide some very important information with respect to the "equally safe" assumption. The estimated mean value for each case are almost the same, which is expected. However, differences are observed in the standard deviation and corresponding coefficient of variation, with the unreinforced slope having the highest variability (16.3% vs. 12.8% and 10.6%). The significance of this information is more apparent in the results of the reliability index (β) which provides a measurement of the risk involed (see Appendix). Both reinforced slopes have a much higher reliability than the unreinforced slope as the numbers indicate. In other words, designed using the same factor of safety, the reinforced slope would actually be safer than the unreinforced but flattened slope. Probabilistically speaking, the 0.5H : 1.0V reinforced slope is the only completely "safe" slope, since common geotechnical design is typically based on β values varying between 2 and 3. Comparing the two reinforced slopes, one can draw the conclusion that the higher the T_s required, the higher the reliability of the slope.

Probabilistic Analysis of Required Reinforcement. Another way to analyze the reinforced slope probabilistically is to treat the required reinforcement as the dependent variable. It should be repeated here that it is not the purpose in this paper to evaluate the uncertainty of the failure suface as part of the whole system reliability. Equation 3 can be used for the determination of the reinforcement tension (T_s) required. On the surface it seems that the independent variables include the driving moment (M_D), the unreinforced factor of safety ($F.S._u$), and the reinforced factor of safety ($F.S._R$). One can argue whether $F.S._R$ is deterministic or probabilistic. Based on Equation 2, $F.S._R$ should be a random variable since the independent variables on the right side of the equation are random variates. On the other hand, $F.S._R$ is usually a pre-determined value (e.g. required $F.S._R = 1.3$), and in this case, is not influenced by the material properties nor the geometry of the slope. For the sake of discussion, the authors calculated both cases, the results of which are listed in Table 5. The results indicate that $F.S._R$ should be treated deterministicly due to the exceedingly high variability when $F.S._R$ is treated probabilistically. Based on the summary of the results, it can be seen that the coefficient of variation is 80.6% and 38.3% in respective cases when $F.S._R$ is taken as a random variable.

Furthermore, the Equation 3 should also be modified to the following form:

$$T_s = \frac{F.S._R * M_D - M_R}{D} \qquad (3a)$$

There is no difference when comparing Equation 3 with 3a deterministically. But, caution must be taken when using these equations probabilistically. The difference is in its independent variables. The independent random variates are M_D and M_R in Equation 3a. As for Equation 3, the independent variates are $F.S._u$ and M_D. The $F.S._u$ can be further expressed as M_R/M_D, which means that if Equation 3 was used the variability from unit weight ($M_D = f[\gamma]$) seems to be double counted. For practical purpose, the effect can be considered to be insignificant as long as the degree of variability of M_D is low compared to other variates. A comparison of the results based on these two equations are list in Table 6. The results indicated that the variability of T_s could be under-estimated if Equation 3 is used. The following demonstrate the calculations of the statistical moments of required tensile reinforcement using the PEM method.

The statistical moments of required tensile reinforcement are calculated based on Equation 3a are as follows:

$$E[T_s^n] = P_{++}(T_{s++})^n + P_{+-}(T_{s+-})^n + P_{-+}(T_{s-+}) + P_{--}(T_{s--})^n \qquad (6)$$

In order to establish the PDF of T_s by the use of the Pearson's system, the coefficients of skewness and kurtosis are needed in addition to the mean and standard deviation and can be obtained from the central moments of the T_s, which has the general form as follows:

$$E[(T_s - \overline{T_s})^n] = P_{++}(T_{s++} - \overline{T_s})^n + P_{+-}(T_{s+-} - \overline{T_s})^n + P_{-+}(T_{s-+} - \overline{T_s})^n + P_{--}(T_{s--} - \overline{T_s})^n \quad (7)$$

By the use of the above two equations, the first four statistical moments of T_s; namely mean, standard deviation or coefficient of variation, coefficient of skewness, and coefficient of kurtosis, can be shown as follows:

The estimated mean value of required reinforcement: $\overline{T_s} = E[T_s]$ (8)

The estimated variance: $s_{T_s}^2 = E[(T_s - \overline{T_s})^2] = E[T_s^2] - E[T_s]^2$ (9)

The estimated coefficient of variation: $CV_{T_s} = \frac{s_{T_s}}{\overline{T_s}} \times 100\%$

$$= \frac{\sqrt{E[(T_s - \overline{T_s})^2}}{E[T_s]} \times 100\% \quad (10)$$

The estimated coefficient of skewness: $\beta_{1_{T_s}} = \frac{E[(T_s - \overline{T_s})^3]}{s_{T_s}^3}$ (11)

The estimated coefficient of kurtosis: $\beta_{2_{T_s}} = \frac{E[(T_s - \overline{T_s})^4]}{s_{T_s}^4}$ (12)

All the results in Table 5 show a PDF of the type II, which is a symmetrical distribution. The purpose of finding the PDF of output results is to further quantify the probability of the output result (required reinforcement) fall short of a certain specified value. This is because the specified $F.S._R$ may not be sufficient to ensure the safety of the slope. Nevetheless, this is outside of the scope of this paper and no further disscussion will be included.

Based on an overall observation of Tables 3, 4, and 5, the validity of the probabilistic analysis is obvious since they both show consistant results compared to the deterministic analysis. It can be further concluded that with variability in the input parameters, the output results also show significant variability. The question now is why the different levels of variability, namely 19.0% vs 48.6%, based on the same input values. The answer is the geometry of the structure. A 1H : 1V slope must have a higher critical factor of safety than a 0.5H : 1V slope (0.966 vs. 0.663). Consequently, a smaller difference between the resisting moments and the driving moments. When this is the case, the use of PEM may result in a certain condition that M_R is higher than M_D, which in turn will cause higher variation in the T_s values. This is exactly what happened in the case of the 1H : 1V slope. But in reality, this is not the concern of the design engineer since the factor of safety are close to one or even higher to begin with. On

the other hand, when the initial unreinforced slope has a low factor of safety, then M_R will always be lower then M_D. Thus, a much higher value of T_s is required which will also result in a lower variation of T_s.

Table 5 - Summary of the Probabilistic Analysis on Required Reinforcement

	$F.S._R = 1.3$							
	0.5H : 1.0V				1.0H : 1.0V			
	$\rho = 0$	$\rho \neq 0$	$\rho = 0$	$\rho \neq 0$	$\rho = 0$	$\rho \neq 0$	$\rho = 0$	$\rho \neq 0$
$\overline{T}_s$ (kN/m)	116.1 152.5*	115.2 151.4*	116.1	116.1	59.5	58.5	59.5	59.5
STD_{T_s}	44.5 50.2*	28.3 32.8*	22.1	26.6	47.9	29.1	28.9	33.7
CV_{T_s}	38.3% 32.9%*	24.6% 21.7%*	19.0%	22.9%	80.6%	49.7%	48.6%	56.7%
β_1	0.060 0.064*		-.00004	.00008	0.046		-.00003	-.00001
β_2	1.780 1.717*		1.816	1.291	2.000		1.533	1.224
Criterion	-0.001 -0.001*		0.0	0.0	-0.0008		0.0	0.0
Type	II I*		II	II	II		II	II
	$F.S._R$ Probabilistic		$F.S._R$ Deterministic		$F.S._R$ Probabilistic		$F.S._R$ Deterministic	

Note: *: for $F.S._R = 1.5$

Another factor which influences the output variability that has not been considered probabilistically is the radius of the failure circle (D) in Equation 3a. It is feasible that two similar failure circles have two completely different radii. The difference in radii will greatly influence the T_s in standard deviation although the $F.S._u$ may not be significantly different. Nevertheless, the trend is the lower the $F.S._u$, the lower the variation of the T_s. This can be a very good parameter for the design engineer to use in terms of the choice between reinforcing the slope or flattening the slope. Because the reinforced slope will have a higher reliability than its counterpart when the $F.S._u$ is lower or the $F.S._R$ is higher.

Table 6 - Comparison Between Equation 3 & 3a

	0.5H : 1.0V				1.0H : 1.0V			
	Equation 3		Equation 3a		Equation 3		Equation 3a	
	$\rho = 0$	$\rho \neq 0$	$\rho = 0$	$\rho \neq 0$	$\rho = 0$	$\rho \neq 0$	$\rho = 0$	$\rho \neq 0$
$\overline{T_s}$ (kN/m)	115.8	116.3	116.1	116.1	59.1	59.8	59.5	59.5
s_{T_s} (kN/m)	20.5	23.1	22.1	26.6	28.5	29.9	28.9	33.7
CV_{T_s}	17.7%	19.9%	19.0%	22.9%	48.2%	50.0%	48.6%	56.7%
β_1	0.078		-.00004	.00008	0.031		-.00003	-.00001
β_2	1.302		1.816	1.291	1.052		1.533	1.224
Criterion	-0.002		0.0	0.0	-0.0002		0.0	0.0

CONCLUSIONS AND RECOMMENDATIONS

A probabilistic analysis was performed on two research slopes. The results illustrated the usefulness of the probabilistic technique. It was not the intention of the authors to replace the traditional deterministic analysis; rather, the main purpose is to compliment and/or supplement the traditional method. In other word, to sharpen the engineer's ability in the decision making process. The following are conclusions of this study:

(1). The practice of assuming a reinforced slope is equally "safe" as a flatter unreinforced slope with the same factor of safety is a correct and somewhat conservative assumption.

(2). Variability in the input soil parameters will result in significant variability in the required reinforcement.

(3). Equations 2a and 3a should be used when analyzing the reinforced slope probabilistically, and $F.S._R$ should be treated deterministically in Equation 3a.

(4). The correlation coefficient between M_D and M_R will cause higher variation in T_s although it won't change the mean value.

(5). The radius of the critical failure slope should be treated probabilistically and is recommended for future study.

(6). The lower the safety factor of the unreinforced slope the lower the variability of the required reinforcement.

(7). The quality of the output results is controlled by the quality of the input parameters.

(8) The probabilistic analysis can be further employed in the design of the distribution of the reinforcement materials. Since, it is natural that the reinforcement material also exhibit variability in terms of its wide width tensile strength.

ACKNOWLEDGEMENTS

The authors would like to thank Dr. Milton Harr for his inspiration in the application of probabilistic methods to geotechnical practice.

REFERENCES

Harr, M.E. 1987. Reliability Based Design in Civil Engineering, McGraw-Hill, New York, 290pp

Christopher, B.R., Gill, S.A., Giroud, J.P., Juran, I., Mitchell, J.K., Schlosser, F., and Dunnicliff, J. 1989. FHWA Manual "Reinforced Soil Structures Volume 1: Design and Construction", FHWA Report No. FHWA - R0 - 89 - 043, Washington, D.C.

Rosenblueth, E. 1975. Point Estimates for Probability Moments. Proceedings, National Academy of Science, 72(10): 3812 - 3814

Elderton, W.P. and Johnson, N.L. 1969. Systems for Frequency Curves, Cambridge University Press

Baecher, G.B. 1986. Geotechnical Error Analysis. Paper presented at the 65th annual meeting of the Transportation Research Board, Washington, D.C.

Christopher, B.R. and Holtz, R.D. 1985. FHWA Geotextile Engineering Manual, FHWA, Washington, D.C.

Benjamin, J.R. and Cornell, C.A. 1970. Probability, Statistics, and Decision for Civil Engineers. McGraw - Hill, New York

Lee, I.K., White, W., and Ingles, O.G. 1983. Geotechnical Engineering. Pitman

U.S. Department of the Navy. 1982. Soil Mechanics, Design Manual 7.1, Alexandria, Virginia

Cheng, S.C. 1990. Probabilistic Analysis and Risk Assessment of Coal Refuse Disposal Facilities. Ph.D. Dissertation, Department of Civil Engineering, West Virginia University

Effect of Geotextiles on Water Migration in Freezing Soils and the Influence of Freezing on Performance

Karen S. Henry
U. S. Army
Cold Regions Research and Engineering Laboratory, USA

ABSTRACT

It is believed that certain geotextiles can be used in place of granular capillary breaks to reduce frost heave because they have relatively large pore sizes and their fibers tend to repel water. An experimental program was conducted to verify that geotextiles reduce frost heave by inhibiting water flow to the freezing front and to examine the performance of soil-geotextile samples when subjected to more than one freeze-thaw cycle.

The addition of a needle-punched fabric reduced frost heave rate in the test soil by an average of 65%, while a heat-bonded fabric reduced frost heave by 37%. The presence of needle-punched fabric resulted in very high soil moisture tensions and soil pressure gradients above the fabric during freezing. Both of these conditions would decrease water flow rates to the portion of the soil which is freezing. Results of tests in which a soil/fabric system was subjected to three freeze/thaw cycles indicate little, if any, influence on the fabric's ability to reduce frost heave.

Estimates of unsaturated hydraulic conductivities were made by using Darcy's law in conjunction with measured soil pressure gradients in the soil and assumed water flow rates based on the rate of frost heave. The results of this procedure suggest that there is a relationship between soil moisture tension and hydraulic conductivity in the frozen fringe and conditions in the unsaturated soil below the freezing front.

INTRODUCTION

Frost heave. Frost heave refers to the expansion of soil upon freezing due to the formation of ice lenses in soil which can grow up to several centimeters in thickness. Frost heave and subsequent thaw weakening in soils have long been a concern because of the damage they cause to various structures, including pavement systems. One of the principal non-traffic-associated distress modes in pavements constructed in seasonal frost areas is distortion caused by heave and reconsolidation during the thaw period (Berg and Johnson 1983).

The three conditions necessary for frost heave are freezing temperatures, the presence of frost-susceptible soil and availability of water to the freezing front. If water is available, it will migrate towards the freezing front and form ice lenses. This can happen even in soils where the water table is a meter or more below the depth of frost penetration. The U.S. Army Corps of Engineers design guidance addresses the problem of frost heave either by limiting the amount of frost-susceptible soil subjected to freezing temperatures or by designing the pavement system to adequately carry traffic during the thaw melting period when it is in an extremely weakened state. Both methods call for the use of clean, non-frost-susceptible base course material. The availability of such material is decreasing and it is becoming more expensive to obtain and transport.

Geotextiles as capillary barriers. We have examined the use of geotextiles in soil to reduce frost heave when placed between the water table and the freezing front (Henry 1988, Henry 1990). If this proves to be a viable means of limiting frost heave, it offers the possibility of relaxing current pavement base course criteria. The base course thickness might be smaller and/or it could contain fines, while the pavement system would maintain good performance over its lifetime.

Sweden and Finland have utilized a layer of granular soil as a capillary barrier, placed above the water table and backfilled with frost-susceptible soil, to minimize frost heave and related damage in pavements (Fig. 1) (Rengmark 1963; Taivenen 1963). This technique is thought to reduce water availability to the freezing front and is less expensive than replacing the entire section with non-frost-susceptible material. The sand or gravel has low capillarity and unsaturated hydraulic conductivity due to its large pores and therefore reduces the water availability to the freezing front.

One of the first uses of geotextiles was to replace graded granular filters for erosion control. In an analogous application, geotextiles may replace granular capillary barriers. The pore sizes of many geotextiles are about the same as those in a medium sand. Furthermore, some fabrics are hydrophobic and thus tend to repel water, an attribute that will further restrict water flow to the freezing front when the fabric is placed above the water table. However, if the water table rises above the capillary barrier, saturating the geotextile, it can no longer restrict water flow to the freezing front.

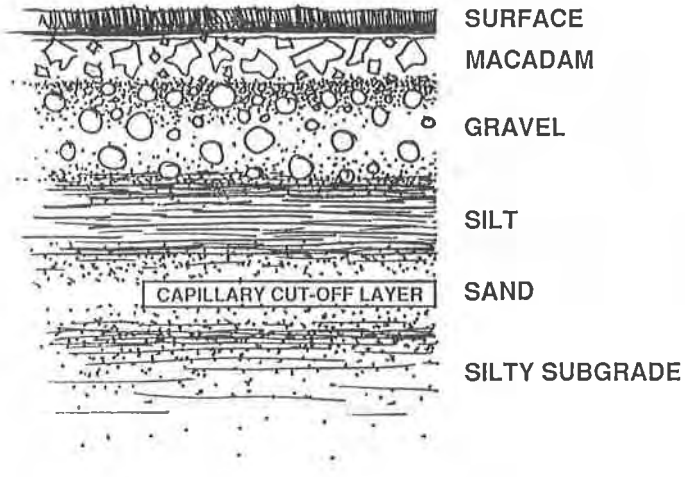

Figure 1. Cross section of granular capillary barrier in pavement section.

Using a delivered cost of $1.38/m^2 ($1.15/yd^2), for geotextile and $11.46/metric ton ($10.40/ton) for delivered clean, non-frost-susceptible base course material (typical costs in Hanover, N.H.) the geotextile costs about the same as a 5-cm (2.5 inch) thick-

ness of base course material. This means that if construction costs are the same for placing the different materials, the geotextile would be cost effective if it could replace more than 5 cm of base course material. The cost savings would be further enhanced if the geotextile could serve more than one function. For example, it could serve as a separator, or replace a granular filter between the base course and the subgrade as well as a functioning as a capillary barrier to a base course containing fines.

Purpose and scope. We conducted an experimental freezing program utilizing soil-geotextile samples and reference samples of soil alone. The principal objective of the program was to verify that geotextiles reduce frost heave by reducing water migration to the freezing front. We also investigated the consequences of subjecting the soil-fabric samples to more than one freeze-thaw cycle and the effect of the distance between the water table and the freezing front. The purpose of this paper is to present and discuss results of the investigation, except those regarding the effect of distance to the water table, which are reported in another publication (Henry 1990).

PREVIOUS WORK

Initial studies. Two early laboratory investigations provide evidence that geotextiles reduce frost heave in soils (Hoover et al. 1981 and Allen et al. 1983). In addition, one field study conducted to investigate the reinforcement aspects of a geotextile fabric, indicated improved road performance with respect to frost related damage (Hoover et al. 1981).

The investigation by Allen et al. (1983) found that hydrophobic geotextiles placed in soil above the water table in open system freezing tests reduced frost heave, while a hydrophilic geotextile increased heave. Chamberlain (pers. comm.) also found that polypropylene geotextiles reduced frost heave when placed above the water table in open system soil freezing tests.

Recent work. Two recent studies at CRREL have used a needle-punched and then a heat bonded polypropylene geotextile in the laboratory to reduce frost heave in soils (Henry 1988, Henry et al. 1990). The first study found that fabric thickness affects performance in reducing frost heave, and that an optimum thickness is likely to be a function of soil type. Data suggested that pore size distribution and hydrophobicity of the geotextile were also important factors in determining a fabric's performance in a specific soil type.

In the second study, results showed that the geotextile's ability to mitigate frost heave decreased after having been exposed to long-term saturated vertical water flow prior to freezing, but not after being exposed to pumping in saturated soil (Henry et al. 1990). It was speculated that the vertical water flow introduced soil fines into the fabric.

In the same study, scanning electron microscopy revealed that no significant damage occurred to the fabric as a result of freezing in water or soil. However, soil particles adhered to the fabric fibers and were lodged in pores of the fabric removed from soil samples after they were frozen. It is likely that this type of contamination with soil particles would hinder a fabric's performance as a capillary barrier. Since clogging of the fabric pores was associated

with soil freezing, it is logical to investigate the effects of repeated freezing on the fabric's ability to reduce frost heave.

In all previous work, no means of verifying the cut-off of soil water flow across the fabric was employed. Thus, one of the objectives of this study was to verify that the fabric reduces water supply to the freezing front.

EXPERIMENTAL METHOD

Equipment. Soil was frozen in a 15-cm-diameter, 106-cm-long soil column that was instrumented with thermocouples and tensiometers to monitor temperature and soil moisture tension, respectively (Fig. 2). The top 15 cm of the column consisted of six 2.5-cm-wide acrylic rings, lined with a rubber membrane. This configuration allows for maximum frost heave (Chamberlain 1986). An aluminum heat transfer plate, through which glycol was circulated from a temperature bath, was used to freeze the soil column from the top down. A weight of 4.5 kg was placed on top of the soil column to simulate overburden pressure on a pavement subgrade. The entire soil column was insulated with 5 cm of fiberglass insulation to ensure unidirectional freezing. Water was supplied to the base of the soil column through a porous stone with a Mariotte tube water supply. The Mariotte tube was raised or lowered to adjust the water table height.

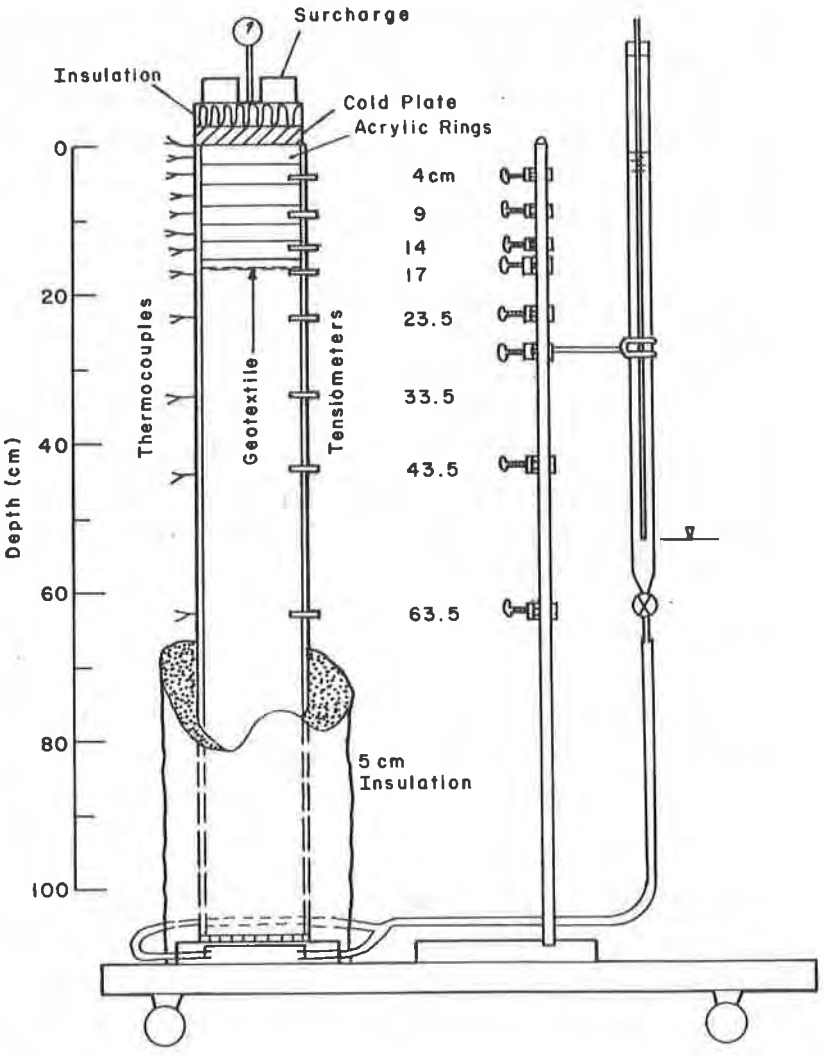

Figure 2. Test equipment for freezing soil-geotextile samples.

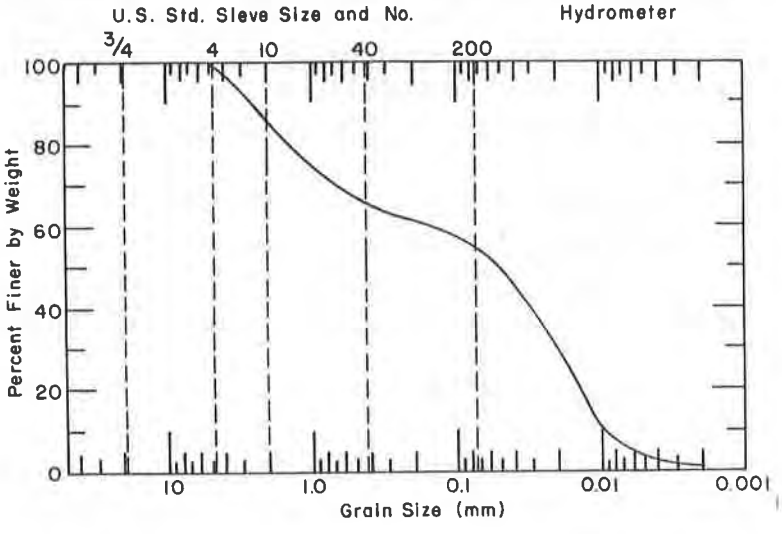

Figure 3. Grain size distribution curve for test soil.

For the tests containing fabric, a single layer of geotextile was placed at a depth of 17 cm, on top of the fixed portion of the soil column. The fabric was sealed around the edges with silicone cement to fix it in place as well as to prevent water from migrating around the sides during freezing.

Test soil and characterization. Two soils, a fine sand and a silt, were mixed in 50/50 proportions by weight to produce the test soil. The soil and fabric were matched in an effort to minimize fabric clogging and blinding. Figure 3 shows the grain size distribution curve of the test soil. It is classified as a low plasticity silt, ML, according to the Unified Soil Classification System.

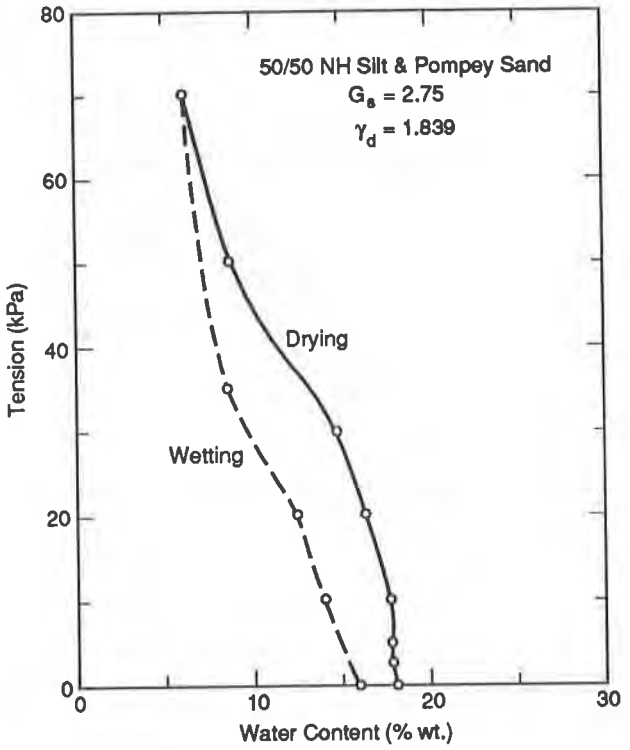

Figure 4. Soil moisture characteristic for test soil.

The test soil was further characterized by determining a soil moisture characteristic and an unsaturated hydraulic conductivity curve (Fig. 4 and 5, respectively). The experimental procedures for the soil moisture characteristic and unsaturated hydraulic conductivity determinations are described in Ingersoll (1981). This information is important for freezing soils because, as soil freezes, water is drawn to the freezing front. The soil between the freezing front and the water table may dry under these conditions. Having the information from the soil moisture characteristic and unsaturated hydraulic conductivity curves allows estimation of water content and hydraulic conductivity by measuring soil moisture tension.

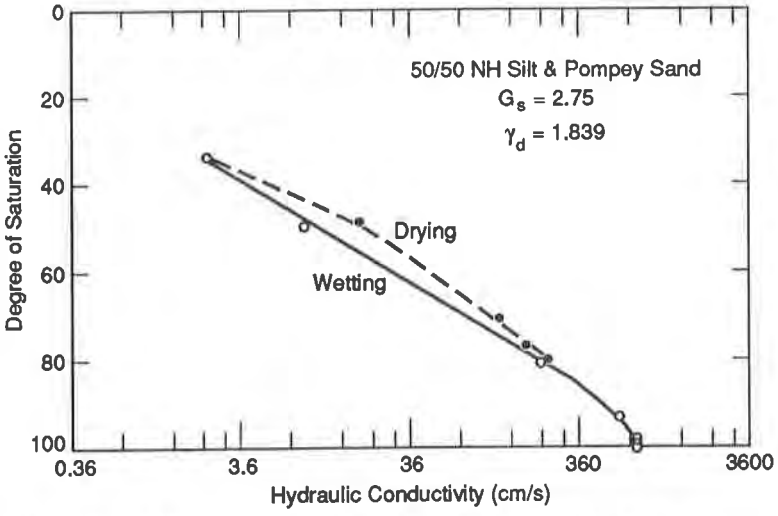

Figure 5. Unsaturated hydraulic conductivity as a function of water content for test soil.

Test geotextiles. Two fabrics were used in this program; the majority of the experiments employed a needle-punched polypropylene. A heat bonded polypropylene was also used in three tests. Table 1 contains properties of the two fabrics as supplied by the manufacturers:

Table 1. Properties of geotextiles tested.

Construction and material	Thickness (cm)	Weight (g/sq m)	Hydraulic conductivity (cm/sec)	Equivalent opening size (mm)
Needle-punched polypropylene	0.38	0.407	0.30	0.15
Heat-bonded polypropylene	0.038	0.136	0.03	0.23–0.15

Table 2: Experimental conditions and results for soil-geotextile freezing tests.

Test no.	Depth of water table (cm)	Fabric description	Comments	Average Heave rate Days 4–9 (mm/day)
1	25	new		2.05
2	85	frozen 1×	Molded new top	1.17
3	55	new		0.78
4	55	none		1.84
5	85	new		0.72
6	85	used l×		0.85
7	85	used 2×, frozen 1×		0.65
8	25	used 3×, frozen 1×		0.64
9	25	new		1.17
10	25	used 1×		1.08
11	25	used 2×		1.44
12	25	used 3×, frozen 1×		1.72
13	25	none	Same top for tests 13–15	4.84
14	55	none		3.88
15	85	none		2.99
*16	25	new		2.33
*17	25	used 1×		2.66
*18	85	new		2.47
19	25	none	Same top for tests 19–20	3.26
20	85	none		3.34
21	85	new		1.45
22	85	none	Same top for tests 22–24	2.74
23	85	none		2.98
24	85	none		3.13

* Tests with heat-bonded geotextile.

Test procedure. Prior to freezing, the soil column was saturated by raising the water table to the top, and then it was left to equilibrate overnight in a 0°C coldroom. The water table was dropped to the test level just prior to the start of freezing. The sample was then frozen from the top down at a rate of approximately 11.5 mm/day. In all cases, the water table was maintained at a constant level below the fabric during freezing. Measurements of temperature, soil moisture tension, frost heave and water uptake into the sample were taken at least daily. Freezing took place over 12 to 14 days.

Experimental plan. Table 2 lists all of the freezing experiments conducted in this program, including comments about the various test conditions and results in terms of average heave rate for days four through nine. A total of 24 freezing tests were conducted.

RESULTS AND ANALYSIS

Overview of experimental results. The experimental results clearly show that the addition of a geotextile to the sample resulted in lower frost heave than would have otherwise occurred. Figure 6 shows heave as a function of time for all of the tests. Every test with fabric heaved less than every test without fabric, regardless of test conditions. The shapes of the frost heave curves are different for the samples containing needle-punched fabric than for the reference samples or those with heat-bonded fabric. The reference soil samples heaved at an approximately constant rate, while frost heave curves for the samples containing needle-punched geotextiles start to level out after the first few days of freezing. The frost heave curves for the heat-bonded fabric have an intermediate shape.

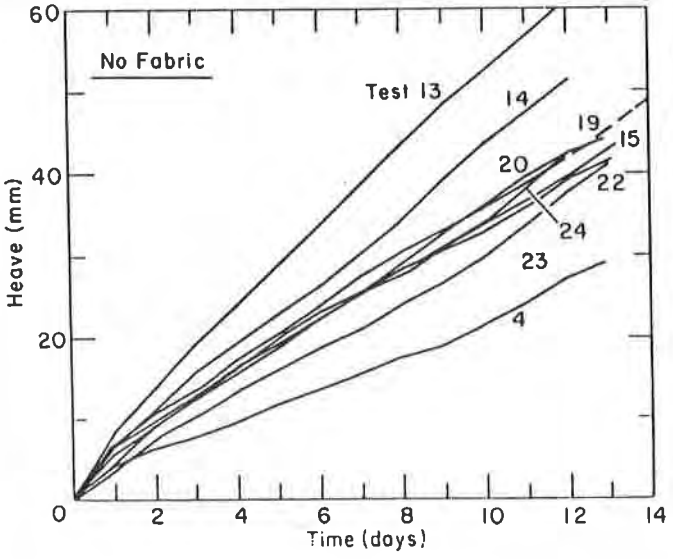

Figure 6a. Frost heave vs. time for reference samples of soil only.

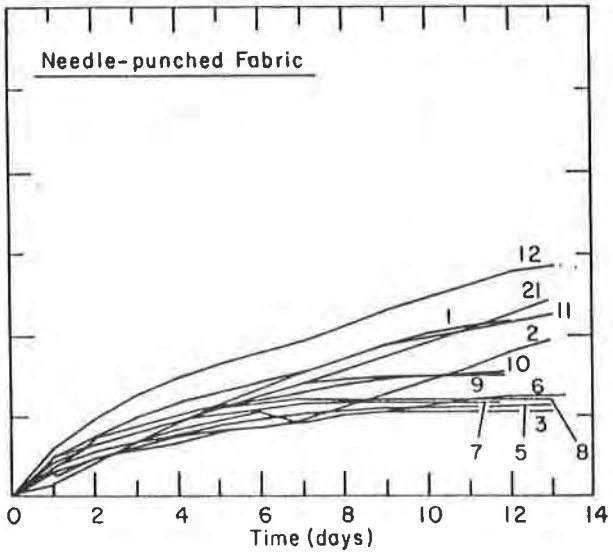

Figure 6b. Frost heave vs. time for soil-geotextile samples containing needle-punched fabric.

Rate of frost heave from day 4 through day 9 of each test was chosen to be the dependent variable. Two other quantities were considered—total frost heave at day 12 of the test or frost heave for a given level of frost penetration. These were eliminated as dependent variables since the differences in the shapes of the frost heave curves make them dependent on the length of the test and possibly exaggerate the effect of a geotextile. In addition, frost heave rate in laboratory freezing tests under very similar conditions is used by the Corps of Engineers to classify the frost susceptibility of soils (e.g. Chamberlain 1986).

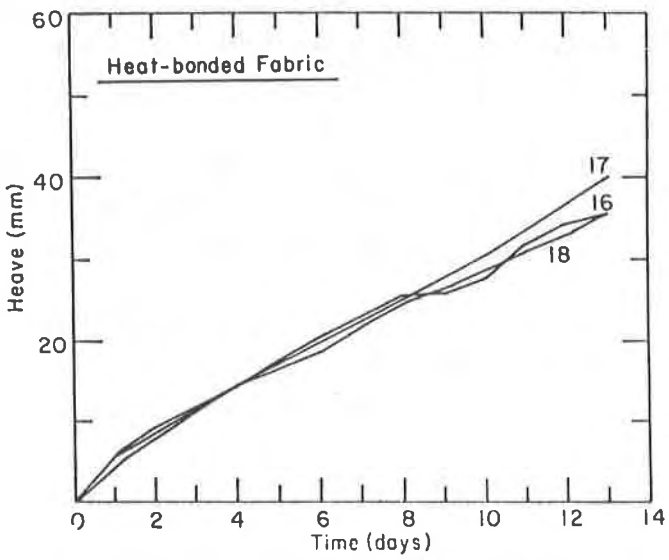

Figure 6c. Frost heave vs. time for soil-geotextile samples containing heat-bonded fabric.

To quantify the influence of the geotextiles on rate of frost heave, the difference in average heave rate (days 4 through 9) for identical test conditions was calculated for fabric-soil samples and reference soil samples, and then converted to a percentage reduction of the soil-only sample heave rate. Whenever there was a replicate test condition, the average of the tests was used. For example, test 22 was compared with the average of tests 5 and 21. The presence of needle-punched fabric reduced heave rate an average of 65%, with the range of reduction being 58 to 79%. The presence of the heat-bonded fabric reduced frost heave an average of 37%. These computations assumed that there is no significant interaction among the three independent experimental variables—water table location, number of freeze thaw cycles and presence of fabric. There is no obvious reason to believe that these experimental variables interact.

Although the heat-bonded fabric performed poorly in comparison to the needle-punched fabric in these tests, this has not been true in other tests with different soil types (e.g. Allen 1983, Henry 1988 and Henry et al. 1990), so that it is important not to dismiss this type of fabric as a potential capillary barrier. How effectively a capillary barrier performs is likely to be a function of both the soil and fabric properties; one important consideration is probably their relative pore size distributions (e.g. Henry 1988).

Frost penetration variability. It is important to establish that the experimental results were not affected by significantly different rates of frost penetration. The average frost penetration rate for soil samples containing fabric was 11.76 mm/day with a standard deviation of 1.1 mm/day. Samples without fabric froze at an average rate of 11.06 mm/day with a standard deviation of 0.68 mm/day. Thus, there is a statistical difference between the frost penetration rates for the two conditions. This difference is not large enough, however, to make a significant difference in frost heave rate (Penner, 1972; Chamberlain, 1981). If

anything, under these experimental conditions, one would expect the faster penetration rate to result in more frost heave (Penner, 1972).

Experimental variability. Remolding the top 15 cm of the sample, which is subjected to frost heave, caused considerable variability in the experimental results. The percent relative standard deviation of results for identical test conditions but different tops was 30.3%. This fact considerably hindered quantitative data analyses. Therefore, meaningful comparisons could only be made among results obtained from a given molded top, or alternatively, for replicate tests when each result came from a test with a different molded top. For example, if tests 8 and 12, with three freeze-thaw cycles, are averaged and compared with the results of tests 1 and 9, with one freeze-thaw cycle, the apparent effect is that frost heave is reduced by 27% for the higher number of cycles. This result is counterintuitive, and examination of the data from tests nine through twelve, all of which were performed using the same column top, show a trend for increased frost heave with increased freeze cycles.

Effect of fabric on moisture transmission to the freezing front. Soil moisture tension profiles below the freezing front from tests 8, 16 and 19 on the 7th day of freezing are shown in Figure 7. They typify the soil moisture tension profiles seen in samples containing the two different fabrics and the reference samples. The soil moisture tension profile from test 8 (Fig. 7a) shows that the needle-punched fabric acts to prevent or slow down moisture transmission to the region above it, whereas the other two tests do not show the pronounced break in soil

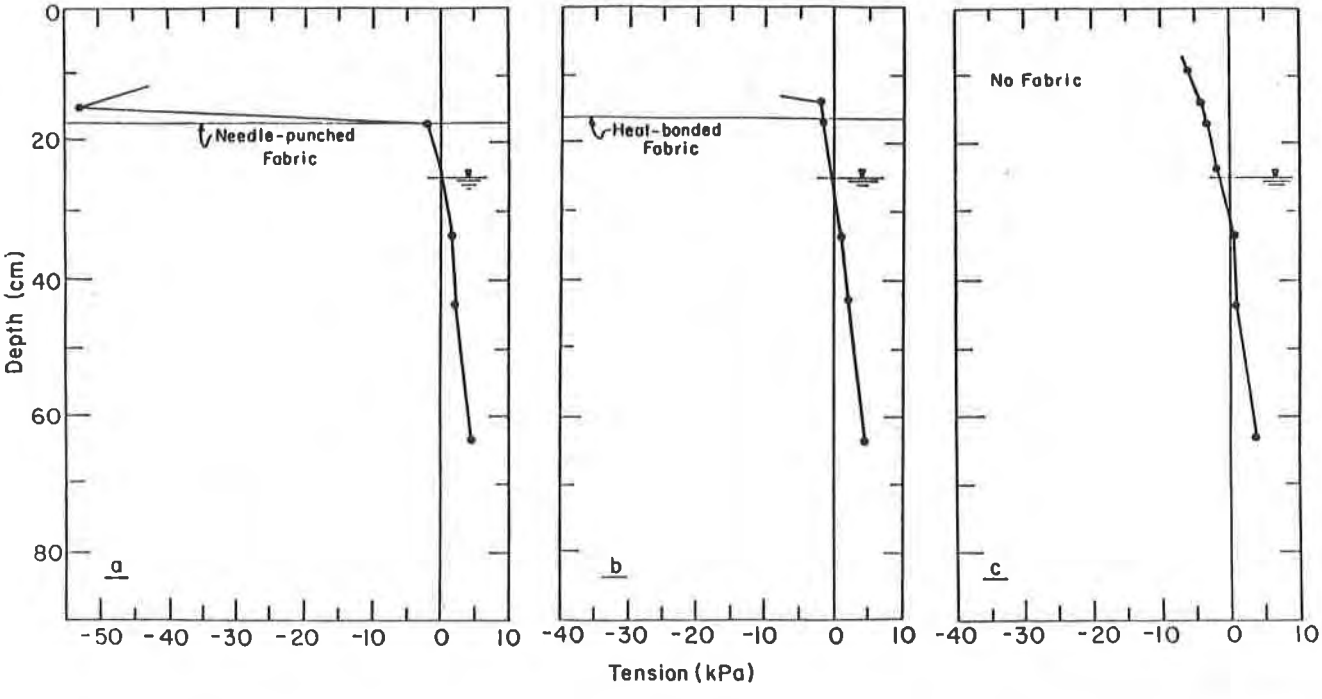

Figure 7a. Soil moisture tension profile on day 7 of freezing for test 10.

Figure 7b. Soil moisture tension profile on day 7 of freezing for test 16.

Figure 7c. Soil moisture tension profile on day 7 of freezing for test 19.

moisture tension across the fabric. The high soil moisture tension between the fabric and the freezing front in Figure 7a results from drying of the soil in this region: as water is drawn from this region to the freezing front, it can't be replaced at the same rate. The observation that this region dries above the needle-punched fabric indicates that it is impeding the upward moisture flow to the freezing front.

Estimates of the lower bounds of hydraulic conductivity in the unfrozen soil below the freezing front were made to determine whether the geotextiles were limiting frost heave by controlling the unsaturated hydraulic conductivity of the soil below the freezing front. Since the effects of fabric on freezing rate were most pronounced during the latter days of freezing, data from days 10 to 12 of the freezing tests were studied. Darcy's law was used to calculate the hydraulic conductivity that would be necessary to sustain the average frost heave rate. The assumption was made that frost heave was due entirely to upward water migration in the soil, and the possibility that additional soil water was provided to the freezing front by frost penetration or desiccation of the soil was ignored.

The unsaturated hydraulic conductivity required to sustain heave rate was calculated using:

$$K_{\text{unsat}} = \frac{Q}{\frac{\Delta H}{\Delta Z}}$$

where Q was obtained by converting the frost heave rate to an equivalent water flow rate and $\Delta H/\Delta Z$ was obtained from soil moisture tension measurements in the soil below the freezing front and converting them to equivalent hydraulic head and correcting for elevation head. Table 3 shows frost heave rate, highest soil moisture tension measured below the freezing front, the hydraulic head gradient and the K value calculated from these data.

Figure 8 shows the calculated K values as a function of the highest measured tension in the soil below the freezing front for all of the tests. The line and regression equation shown in Figure 8 were computed by a least squares fitting of a log vs. log scale plot of the hydraulic conductivity data obtained from the unfrozen test soil (i.e., the data shown in Fig. 4 and 5). This is a common way to express the unsaturated hydraulic conductivity vs. soil moisture tension relationship (Hillel 1982). Note that there is a small difference in the dry densities of the soil samples in the freezing tests, which averaged 1.77 g/cm^3 and the dry density of the unfrozen soil used to the determine the unsaturated hydraulic conductivity curve (1.84 g/cm^3). This difference in density should not result in large differences in soil moisture tension or, by implication, in the unsaturated hydraulic conductivity vs. tension data (Taylor and Box 1961).

In general, the estimated unsaturated hydraulic conductivity for tests containing no fabric is higher than that for tests with fabric. This is a result of two factors—higher frost heave rates and lower hydraulic gradients. The tensions predicted using the estimated K values (Table 3) and the unsaturated hydraulic conductivity curve in Figure 8 are signifi-

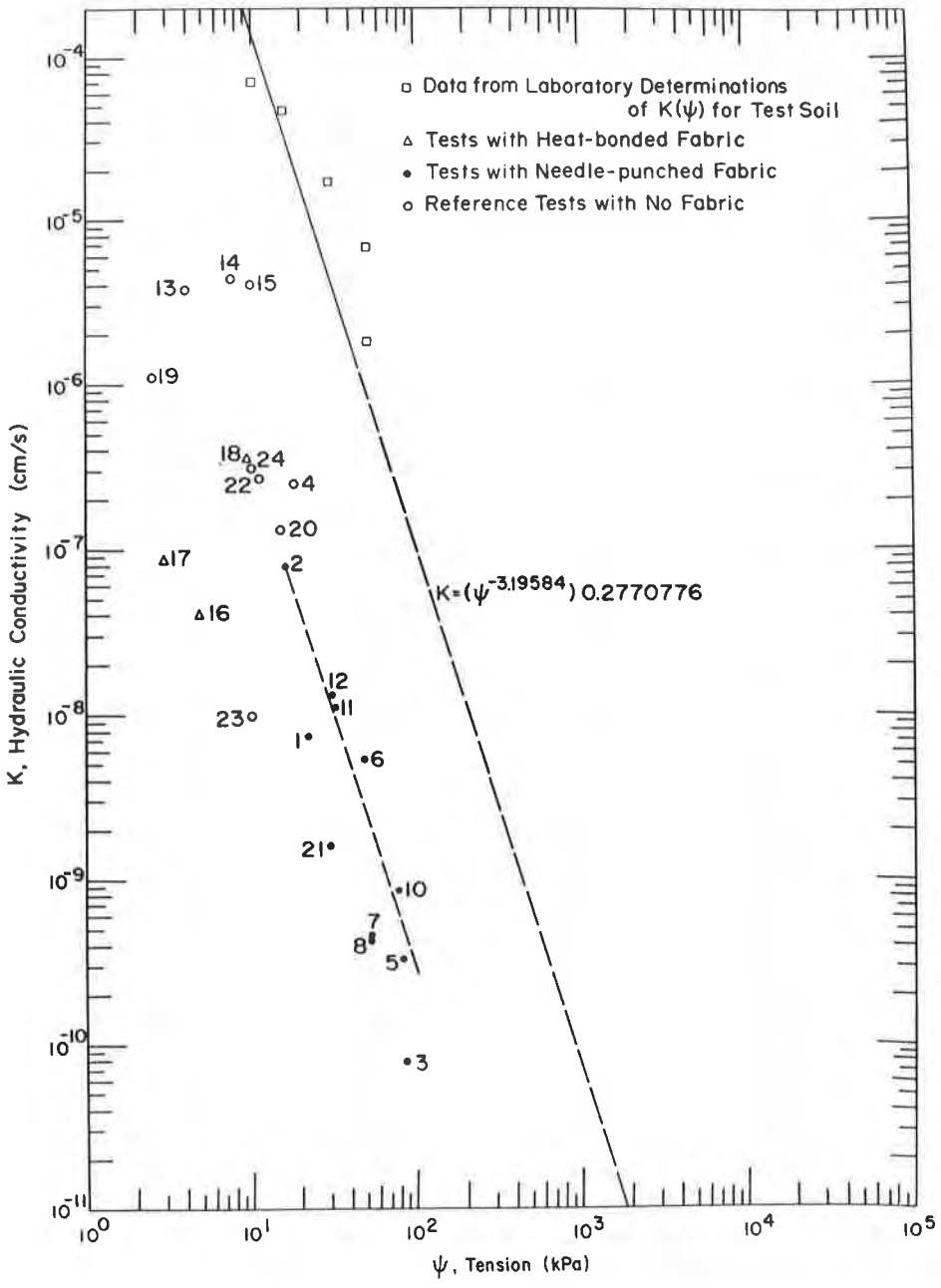

Figure 8. (Estimated) hydraulic conductivity vs. soil moisture tension data for soil-geotextile freezing tests.

cantly greater than the observed tensions. Furthermore, the relationship between the estimated values of K and the observed tensions parallels the unsaturated hydraulic conductivity curve. There is no evidence for an experimental condition that would result in lower soil moisture tensions existing in the outer portion of the soil column where the tensiometers are located, such as poor seals around the tensiometers or non-horizontal ice lenses that would indicate radial heat loss (vs. unidirectional freezing). It is also important to note that the upper limit of the tensiometers used in the freezing tests is 100 kPa.

Table 3. Experimental data used to estimate unsaturated hydraulic conductivity in freezing soil-geotextile samples. Data are averaged for days 10–12 of freezing.

Test no.	Frost heave rate	Highest tension below freezing front	Hydraulic head gradient ($\Delta H/\Delta Z$)	$K(\Psi)$ (cm/sec)
1 (N)	1.01	18	145.2	7.4×10^{-9}
2 (N)	1.71	16	22.9	7.9×10^{-8}
3 (N)	0.02	86	274.3	7.7×10^{-11}
4	2.70	12	11.4	2.5×10^{-7}
5 (N)	0.08	82	247.1	3.4×10^{-10}
6 (N)	0.63	48	124.1	5.4×10^{-9}
7 (N)	0.65	53	151.9	4.5×10^{-9}
8 (N)	0.64	53	162.1	4.2×10^{-9}
9 (N)	1.17	— — — — Insufficient test data — — — — —		
10 (N)	0.18	68	222.3	8.6×10^{-10}
11 (N)	1.07	34	105.0	1.1×10^{-8}
12 (N)	1.48	30	123.1	1.3×10^{-8}
13	4.14	4	1.2	3.7×10^{-6}
14	4.12	6.5	1.0	4.4×10^{-6}
15	2.80	9.5	0.74	4.0×10^{-6}
16 (H)	2.78	5	73.8	4.0×10^{-8}
17 (H)	3.11	3	37.8	8.7×10^{-8}
18 (H)	1.91	9.5	5.8	3.5×10^{-7}
19	3.26	2.5	3.1	1.1×10^{-6}
20	3.34	11.5	27.9	1.3×10^{-7}
21 (N)	1.79	7.3	116.8	1.6×10^{-8}
22	3.61	11	14.0	2.7×10^{-7}
23	2.75	10	29.9	9.8×10^{-8}
24	3.50	10	11.2	3.3×10^{-7}

(N)—Test with needle-punched fabric
(H)—Test with heat-bonded-fabric

It is logical to consider that higher tensions do exist in the soil, but they were not be measured in this experiment. If such tensions existed above the freezing front, they could not be reliably measured by tensiometers, which do not operate below freezing. There is acceptance for the concept of a "frozen fringe" that exists in a freezing soil between the zone of ice lens formation and the freezing front (Loch and Miller 1975). This is a region where ice is forming in the soil pores but no ice lenses are yet forming. Furthermore, laboratory experiments show that the hydraulic conductivity of this layer is quite low (Black and Miller 1990). Thus, it is likely that the hydraulic conductivity and pressure gradients existing in the frozen fringe limit frost heave. The observation that the data shown in Figure 8, which reflects conditions in the unfrozen soil below the freezing front, parallel the unsaturated hydraulic

Table 4. Average heave rates (days 4 through 9) for freezing tests on soil and soil-geotextile samples.

Test no.		Fabric	W.T.	No.of times previously frozen	Heave rate 4–9 mm/day	% change in F.H. from 1st test
	5	needle-	85	0	.715	
1	6	punched	85	1	.85	+19%
	7		85	2	.65	−10%
	22	none	85	0	2.74	
2	23		85	1	2.974	+ 8%
	24		85	2	3.125	+12%
	9	needle-	25	0	1.17	
	10	punched	25	1	1.08	-8%
3	11		25	2	1.435	+ 8%
	12		25	3	1.72	+ 32%
	16	heat	25	0	2.33	
4	17	bonded	25	1	2.66	+12%

onductivity curve suggests that there is a relationship between the hydraulic conductivity nd soil moisture tension in the frozen fringe and conditions in the adjacent unfrozen soil.

The effect of freezing on fabric performance. Four series of tests were performed to con-ider the effect of repeated freezing on frost heave. They are listed in Table 4 along with verage rates of frost heave and the percent change in heave rate from the first freeze cycle. reezing temperatures actually penetrated the fabric in tests six and eleven. In all other tests, he frost line remained above the fabric.

Only the reference soil sample (tests 22, 23 and 24) shows consistent increase in heave rate vith repeated freeze cycles for three consecutive freeze cycles. It is not unusual for a soil to how increased frost susceptibility in a second and third freezing test in the laboratory (e.g. hamberlain, 1986). The samples containing needle-punched fabric do not show such a trend, vith the possible exception of the fourth freeze cycle (test 12) of the third test series, which as an increased heave rate of 32% over the first freeze cycle. Thus, the data indicate no change n fabric performance with two freeze-thaw cycles, regardless of whether the fabric was frozen. owever, the observations that the soil-fabric sample showed a marked increase in frost eave on the fourth freeze cycle indicate a need to subject fabrics to numerous freeze-thaw ycles to investigate the long-term fabric performance in reducing frost heave.

Even though all fabrics removed from the soil samples contained soil particles, the fabric emoved from the soil column after test 12 contained more soil particles than usual on the top urface. Soil particle presence in fabric would probably hinder its ability to reduce unsatur-ted water flow by altering the pore size distribution and wetting properties of that layer.

Unfortunately, the fabrics weren't weighed before and after being tested, a procedure which would have given more quantitative information on the amount of soil gained by the fabric during testing.

Freezing tests for an 85-cm water table on a soil sample and a soil-geotextile sample are shown in Figure 9. This figure shows that the fabric continues to reduce frost heave in successive freeze cycles, as long as the freezing front remains above it. On day 39, when the frost penetrated the fabric, the soil-geotextile sample started to heave at a rate similar to the reference sample, as expected.

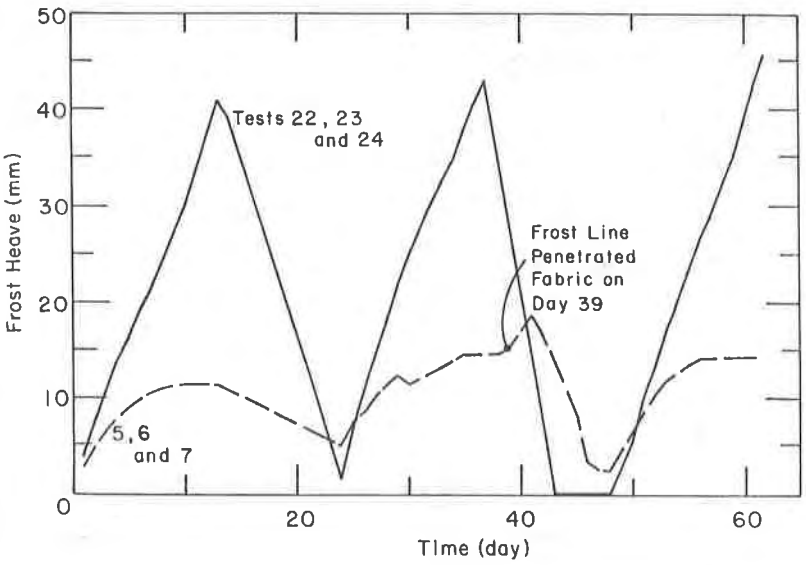

Figure 9. Frost heave vs. time for three freeze cycles on a soil-geotextile sample (tests 5, 6 and 7) and a reference sample (tests 22, 23 and 24).

CONCLUSIONS

Based on the results of this soil-geotextile laboratory freezing program, the following conclusions are made:

1. Geotextiles limit frost heave in soils when placed above the water table and below the depth of freezing by reducing unsaturated water flow to the freezing front. A needle-punched polypropylene fabric placed between the water table and the freezing front resulted in high moisture tensions above the fabric as well as high pressure gradients in the unfrozen soil.

2. Study of the literature indicates that the physical conditions that actually limit the rate of frost heave probably occur in the frozen fringe. Data from this study suggest that the limiting conditions of the frozen fringe are related to those in the unfrozen soil below the frozen fringe.

3. The effect of subjecting a soil-geotextile sample to up to three freeze cycles does not noticeably degrade its frost heave performance compared to reference soil samples. Furthermore, freezing the fabric itself does not appear to influence its subsequent performance, although it is ineffective while frozen.

RECOMMENDATIONS

1. Future testing of geotextiles for reducing frost heave in soils should subject samples to many freeze-thaw cycles and should include a procedure to measure the amount of soil gained by a geotextile when it is frozen in a soil sample.

2. Past work and work reported in this paper work have repeatedly shown that properly selected geotextiles can reduce frost heave in laboratory freezing tests. It is timely that field testing of geotextiles ensue before more extensive laboratory work is undertaken. If field trials of geotextile capillary barriers are successful, then design criteria should be developed to insure their proper use.

ACKNOWLEDGMENT

Mr. Jonathan Ingersoll, Civil Engineering Technician, conducted all of the freeze tests for the test program discussed in this paper.

REFERENCES

Allen, T., J.R. Bell and T.S. Vinson (1983) Properties of geotextiles in cold regions application. Transportation Research Report 83-6, 275 p. Transportation Research Institute. Oregon State University, Corvallis.

Berg, R.M. and T. Johnson (1983) Revised procedure for pavement design under seasonal frost conditions. CRREL Special Report 83-27, U.S. Army Cold Regions Research and Engineering Laboratory, Hanover, N.H.

Black, P.B. and R.D. Miller (1990) Hydraulic conductivity and unfrozen water content of air-free frozen silt. Water Resources Research, Vol 26, No. 2, pp. 323–329, February.

Chamberlain, E.J. (pers. comm.) Research Civil Engineer, USACRREL, 72 Lyme Road, Hanover, N.H.

Chamberlain, E.J. (1981) Frost susceptibility of soil: Review of index tests. CRREL Monograph 81-2, U.S. Army Cold Regions Research and Engineering Laboratory, Hanover, N.H.

Chamberlain, E.J. (1986) Evaluation of selected frost-susceptibility test methods. CRREL Report 86-14, U.S. Army Cold Regions Research and Engineering Laboratory, Hanover, N.H.

Henry, K.S. (1988) Use of geotextiles to mitigate frost heave in soils. In Proceedings, Fifth International Conference on Permafrost, Trondheim, Norway, pp.1096–1101.

Henry, K.S., S. Taylor and J. Ingersoll (1990) Effects of freezing on the microstructure of a geotextile. In Geosynthetics: Microstructure and Performance, ASTM STP 1076, pp. 147–164, Philadelphia.

Henry, K.S. (1990) Geotextiles as capillary barriers. Geotechnical Fabrics Report, March/April, pp 30–36.

Hillel, D. (1982) Introduction to soil physics. New York, Academic Press, 364 p.

Hoover, J.M., J.M. Pitt, L.D. Handfelt and R.L. Stanley (1981) Performance of soil-aggregate-fabric systems in frost-susceptible roads. Linn County, Iowa. Transportation Research Record No. 827, pp. 6–14.

Ingersoll, J.E. (1981) Method for coincidentally determining soil hydraulic conductivity and moisture retention characteristics. USACRREL Special Report 81-2, USACRREL, 72 Lyme Rd., Hanover, N.H.

Loch, J.P.G and R.D. Miller (1975) Tests of the concept of secondary frost heaving. Soil Sci. Soc. Amer. Proceedings, Vol. 39, pp.1036–1041.

Rengmark, F. (1963) Highway pavement design in frost areas in Sweden. Highway Research Record No. 33, pp.137–150.

Taivenen, O.A. (1963) Preventive measures to reduce frost heave in Finland. Highway Research Record No. 33, pp. 202–216.

Taylor, S.A. and J.E. Box (1961) Influence of confining pressure and bulk density on soil water matric potential. Soil Science, Vol. 91, No. 1, pp. 6–10.

GEOSYNTHETICS '91

February 26-28, 1991 Radisson Hotel, Atlanta, GA

CONFERENCE PROCEEDINGS

Radisson Hotel
Atlanta, Georgia, U.S.A.
February 26-28, 1991

Volume 2

Sponsored by the North American Geosynthetics Society (NAGS)
and the Industrial Fabrics Association International (IFAI)
under the auspices of the International Geotextile Society (IGS)

DISCLAIMER:
The opinions expressed and the technical data provided herein are those of the author(s) and does not necessarily represent the opinion of the geosynthetics industry, the Industrial Fabrics Association International, or the North American Geosynthetics Society.

SPONSORED BY

February 26-28, 1991 **Radisson Hotel, Atlanta, GA**

CONFERENCE PROCEEDINGS

Radisson Hotel
Atlanta, Georgia, U.S.A.
February 26-28, 1991

Volume 2

Sponsored by the North American Geosynthetics Society (NAGS)
and the Industrial Fabrics Association International (IFAI)
under the auspices of the International Geotextile Society (IGS)

Printed in U.S.A.

Table of Contents

Volume I

Waste Containment Case Histories

Landfill Stabilization Through the Use of Geosynthetics ____ 1
Russell H. Fetrow
Russ Fetrow Engineering, Inc., USA
Maxwell M. Mick
ET AL
Russ Fetrow Engineering, Inc., USA

Geogrid Liner Support at Empire Sanitary Landfill ____ 15
Alan Stephens
Empire Sanitary Landfill, Inc., USA
Richard Bodner, P. E.
Martin & Martin, Inc., USA

Private Industry Maximum Security Landfill Case History ____ 23
Michel Marcotte
Solmers Internationale Consulting Engineers, Canada
Sophie Lagace
Solmers Internationale Consulting Engineers, Canada
Robert Denis
Solmers Internationale Consulting Engineers, Canada
Denis Faucher
PPG Canada Inc., Canada

The Evolution of Geosynthetics in a Landfill Lining System ____ 31
Jan Hutwelker
American Resource Consultants, USA
Thomas Pullar
American Resource Consultants, USA
Francis Taylor
Palco Linings Inc., USA

Application of Geosynthetics in the Design of Fully-Drained Mineral Waste Storage Facilities ____ 61
W. A. Cincilla
Knight Piesold and Co., Consulting Engineers, USA
G. A. Zagorski
Fluid Systems, Inc., USA

Geomembrane Applications in Australia ____ 77
Roger J. Parker
Golder Associates PTY LTD, Australia
Mike A. Sadlier
Polyfelt Geosynthetics PTY LTD, Australia

Waste Containment Interface Stability

Soil-Geosynthetics Interface Strength Characteristics: A Review of State-of-the-Art Testing Procedures ____ 87
Deanne L. Takasumi
CH2M Hill, Inc., USA
Kenneth R. Green
CH2M Hill, Inc., USA
Robert D. Holtz
University of Washington, USA

PVC Geocomposite for Improved Friction and Performance Properties ____ 101
David C. Lauwers
Occidental Chemical Corporation, USA

Landfill Liner Side Slope Design to Minimize Geomembrane Tensile Stress ____ 113
Michael Quinn
Barton & Loguidice, P. C., USA
Martin Chandler
Barton & Loguidice, P. C., USA

Structural Geogrids Used to Stabilize Soil Veneer Covers ____ 125
Vicky E. Chouery-Curtis
Tensar Environmental Systems Inc., USA
Stephen T. Butchko
Tensar Environmental Systems Inc., USA

Stability of High Refuse Slopes on Synthetic Lining Systems at the Bee Canyon Landfill ____ 145
Suji Somasundaram
The Earth Technology Corporation, USA
Kris Khilnani
The Earth Technology Corporation, USA

Shear Strength of Sand-Geomembrane Interfaces for Cover System and Lining Design ____ 159
S. J. Druschel
ABB Environmental Services Inc., USA
T. D. O'Rourke
Cornell University, USA

Geosynthetic Material Response to Landfill Cap Settlement and Subsidence ____ 175
Ronald K. Frobel, P. E.
R. K. Frobel & Associates, USA

Environmental Applications

Underwater Geomembrane Placement ____ 187
Fred P. Rohe
Environmental Protection, Inc., USA

Use of Geosynthetics in Lautaro Dam ____ 195
Luis Arrau
Ministry of Public Works, Chile
Donaldo Astorga
Ministry of Public Works, Chile

Witbank's 60Ml Floating Cover Reservoir: A Review of the First Five Years ____ 207
Richard B. Turner
Hawkins, Hawkins & Osborn, South Africa
Peter L. Davies
Aquatan, South Africa

Evaluation of Field Seams Quality by the Impact Test Procedure ____ 223
A. L. Rollin
Ecole Polytechnique, Canada
M. Lefebvre
Ecole Polytechnique, Canada
J. Lafleur
Ecole Polytechnique, Canada
M. Marcotte
Solmers Internationale, Canada

Analysis of Pinhole Seam Leaks Located in Geomembrane Liners Using the Electrical Leak Location Method: Case Histories ____ 239
Daren L. Laine
Southwest Research Institute, USA

Performance of Mount Elbert Forebay Reservoir Flexible Membrane Lining After 10 Years of Service ____ 255
W. R. Morrison
U. S. Department of the Interior, Bureau of Reclamation, USA
E.W. Gray, Jr.
U. S. Department of the Interior, Bureau of Reclamation, USA

Geosynthetic Durability

Puncture Resistance of Geomembranes Using a Truncated Cone Test ____ 273
Donald Hullings
EMCON Associates, USA
Robert Koerner
Drexel University, USA

Effects of Outdoor Exposure on a High Density Polyethylene Geomembrane ____ 287
Y. G. Hsuan
Geosynthetic Research Institute, Drexel University, USA
A. E. Lord Jr.
Geosynthetic Research Institute, Drexel University, USA
R. M. Koerner
Geosynthetic Research Institute, Drexel University, USA

The Resistance of Membranes in Cover Systems to Root Penetration by Grass and Trees ____ 303
Robert E. Landreth
U. S. Environmental Protection Agency, USA

The Chemical Resistance of Geotextiles to be Used in Secondary Containment Systems for Underground Storage Tanks ____ 311
Randy C. Pucetas
Hoechst Celanese Corp., USA
Karen L. Verschoor
Texas Research Institute Environmental Inc., USA
Sam R. Allen
Texas Research Institute Environmental Inc., USA
C. Joel Sprague
Nicolon Corporation, USA

Molecular and Rheological Changes in Polyethylene Occurring From Heat Seaming HDPE Liners ____ 317
Mark W. Cadwallader
Gundle Lining Systems Inc., USA
Jeffrey R. Burkinshaw
Phillips 66 Co., USA

Residual Stress Measurements in Geomembrane Sheets and Seams ____ 333
A. E. Lord Jr.
Geosynthetic Research Institute, Drexel University, USA
R. M. Koerner
Geosynthetic Research Institute, Drexel University, USA
M. H. Wayne
Geosynthetic Research Institute, Drexel University, USA

Determination of Long-Term Tensile Strength of Geosynthetics: A State-of-the-Art Review ____ 351
Tony M. Allen
Washington State Department of Transportation, USA

Technical Advances/Innovations

Eccentric Plate Loading Tests on Geogrid-Reinforced Subgrades ____ 381
Vito A. Guido
The Cooper Union, USA
Christopher H. Bakkala
Thornton-Tomasetti, P. C., USA
John J. Nocera
Malcolm Pirnie, Inc., USA

On the Design of Reinforced Embankments on Soft Brittle Clays ____ 395
B. L. J. Mylleville
The University of Western Ontario, Canada
R. K. Rowe
The University of Western Ontario, Canada

Using Geosynthetics to Reduce Earth Loads on Rigid Retaining Structures ____ 409
John S. Horvath
Manhattan College, USA

Electrical Methods of Seaming of Geomembrane Sheet ____ 425
E. O. Butts
Butts Consultants, Ltd., Canada
A. E. Lord, Jr.
Geosynthetic Research Institue, Drexel University, USA

Membrane Action in a Two-Layer Soil System Reinforced By Geotextile ____ 439
Philippe L. Bourdeau
Purdue University, USA

A Probabilistic Review of Geotextile Reinforced Slope Design ____ 455
Shi-Chieh Cheng
Drexel University, USA
Barry Christopher
Polyfelt, Inc., USA

Effect of Geotextiles on Water Migration in Freezing Soils and the Influence of Freezing on Performance ____ 469
Karen S. Henry
U. S. Army
Cold Regions Research and Engineering Laboratory, USA

Volume II

Failures and Solutions

Case History of a 9 m High Geogrid Reinforced Retaining Wall Backfilled with Cohesive Soil ____ 485
W. J. Burwash
Golder Associates Ltd., Canada
J. D. Frost
Purdue University, USA

A Shattered Geomembrane Liner Case History: Investigation And Remediation ____ 495
Ian D. Peggs
GeoSyntec Consultants, USA
Jules P. Winfree
GeoSyntec Consultants, USA

Geosynthetic Considerations in a Landfill on Compressible Clays ____ 507
Gregory Richardson
ENSCI, Corp., USA
Dick Reynolds
R. G. Gerber, USA

Technical Advancements/Testing & Research

Results of Laboratory Tests on a Geotextile/Bentonite Liner Material ____ 517
Hsin-Yu Shan
University of Texas - Austin, USA
David E. Daniel
University of Texas - Austin, USA

Load Test of a Large-Scale Geotextile-Reinforced Retaining Wall ____ 537
John W. Billiard
Canonie Environmental Services Corp., USA
J. T. H. Wu
University of Colorado at Denver, USA

Case History Comparison of Geosynthetic-Reinforced Soil Walls ____ 549
Alan F. Claybourn
Woodward-Clyde Federal Services, USA
Jonathan T. H. Wu
University of Colorado at Denver, USA

Creep Measurements on Polymeric Reinforcement ____ 561
R. J. Fannin
University of British Columbia, Canada
S. Hermann
Norwegian Geotechnical Institute, Norway

Comparative Behaviour of Metal and Tensar Geogrid Strips Under Static and Repeated Loading ____ 575
Thomas Hamilton Hanna
University of Sheffield, UK
Mabrouk Touahmia
University of Sheffield, UK

Short and Long Term Performance of Polymeric Geogrids ____ 587
I. Juran
Polytech University, USA
K. H. Farrag
Louisiana State University, USA
L. Richmond
Conwed Plastics, USA

Effectiveness of In-Membrane Test in Simulating Strength and Deformation Characteristics of a Nonwoven Geotextile Under Operational Conditions ____ 601
Hoe Ing Ling
University of Tokyo, Japan
Jonathan T. H. Wu
University of Colorado at Denver, USA
Fumio Tatsuoka
University of Tokyo, Japan

Large-Scale Pullout Tests: Assessment of Procedure and Results 615
G. E. Bauer
Carleton University, Canada
A. O. A. Halim
Carleton University, Canada
Q. Shang
University of Western Ontario, Canada

Effect of Pores Structure of Nonwoven Geotextiles on Their Clogging Behavior 629
Shobha K. Bhatia
Syracuse University, USA
Jacek Mlynarek
Ecole Polytechnique, Canada
Andre L. Rollin
Ecole Polytechnique, Canada
Jean Lafleur
Ecole Polytechnique, Canada

Load Distribution in Geogrids With Low Junction Efficiency 643
C. Bonczkiewicz
STS Consultants Ltd., USA
B. Christopher
Polyfelt Inc., USA
M. Simac
Intersol Engineering, USA

Comparative Hydraulic Performance of Resinated Geotextile Overwraps 653
R. Anne Gallup
GeoSyntec Consultants, USA
Robert C. Bachus
GeoSyntec Consultants, USA
Scott M. Luettich
GeoSyntec Consultants, USA

The Effect of Repeated Traffic Loading on Geosynthetic Reinforcement Anchorage Resistance 665
M. Nimmesgern
FMPA (Otto-Graf-Institut), Germany
David Bush
Netlon Limited, UK

Transportation Applications

Geogrid Reinforcement and Stabilization of a Highway Subgrade 673
Terry L. Yarger
Montana Department of Highways, USA
Francis E. Harrison, Jr.
Tensar Earth Technologies, USA
Earle William Mayberry
Tensar Earth Technologies, USA

Response of a Geogrid Earth Reinforced Retaining Wall With Full Height Precast Concrete Facing ____ 691
K. L. Fishman
State University of New York at Buffalo, USA
C. S. Desai
University of Arizona, USA

Geotextiles For Subgrade Stabilization in Permanent Roads and Highways ____ 701
Barry R. Christopher
Polyfelt, Inc., USA
Robert D. Holtz
University of Washington, USA

North Las Vegas: Reconstruction of Cheyenne Avenue Incorporating A High Geosynthetic Moisture Barrier ____ 715
Dave Guram
Phillips Fibers Corporation, USA
Mark Marienfeld
Phillips Fibers Corporation, USA
Dave Smiley
Phillips Fibers Corporation, USA
Dan Nesbitt
G. C. Wallace, Inc., USA

Raleigh Street Embankment-Orlando, Florida ____ 727
Robert L. Goehring, P. E.
Professional Services Industries, Inc., USA

Heavy Construction Applications

Utilization of Geotextile - Reinforced Retaining Wall for Stabilizing Weathered Mudstone Slope ____ 739
Dave Ta-Teh Chang
Chung-Yuan University, Taiwan, ROC
Tien - Chien Chen
Chung-Yuan University, Taiwan, ROC
Kuan-Hsien Su
Chung-Yuan University, Taiwan, ROC

Design and Construction of a Geotextile Wall ____ 775
Douglas Chandler
Shannon & Wilson, Inc., USA
Thomas Kirkland
Shannon & Wilson, Inc., USA

Geogrid Reinforced Soil Wall Bridge Replacement at Picnic Point, Snohomish County, Washington ____ 765
Roland D. Maynard, P. E.
Snohomish County Department of Public Works, USA
Steve E. Thomsen, P. E.
Snohomish County Department of Public Works, USA
Paul W. Grant, P. E.
Shannon & Wilson, Inc., USA

Design and Analysis of Three Reinforced Soil Retaining Walls ____ 781
Michael R. Simac
Intersol Engineering Inc., USA
Dr. Richard J. Bathurst
Royal Military College of Canada, Canada
Richard A. Goodrum
Mirafi, Inc., USA

High Clay Embankment Over Cannon Creek Constructed With Geogrid Reinforcement ____ 799
R. F. Hayden
Hayward Baker, Inc., USA
G. R. Schmertmann
University of California - Berkeley, USA
B. Q. Qedan
Arkansas Highway and Transportation Dept., USA
M. S. McGuire
Opterra, Inc., USA

A Case History of the Design and Construction of a Reinforced Soil Wall Using D. S. F. Fabric Geotextiles for the Purpose of Stabilizing a Major Landslip ____ 823
Peter Rankilor
Manstock Geotechnical Consultancy Services Ltd., United Kingdom

Reinforcement of a Failed Embankment Over Slough Mud ____ 839
Richard Barrows, P. E.
Oregon State Highway Division, USA
George Machan, P. E.
Oregon State Highway Division, USA

Commercial/Industrial Applications

Surcharge Embankments at Walt Disney World ____ 849
Ian Kinnear
Jammal & Associates, Inc., USA
Frank Wood
Disney Development Company, USA

Geogrid Reinforced Containment Dykes for Mountainside Oil Tank Farm in Seismic Zone ____ 861
Thomas T. Heike
SNC Inc., Canada
Michael A. Patterson
SNC Inc., Canada
John R. Kerr
Tensar Earth Technologies, Canada

A Simplified Design Method For Silt Fences ____ 879
Gregory N. Richardson
ENSCI, Corp., USA
Percy Middlebrooks
Georgia Department of Transportation, USA

Modular Block Faced Polymer Geogrid Reinforced Soil Walls U.S. Postal Service Combined Carrier Facility ____ 889
Robert B. Anderson
Tensar Earth Technologies, Inc., USA
Fred N. Boyd
U. S. Postal Service, USA
Larry Shaw
Gifford Hill, USA

Design and Construction of an 18 Foot High Geogrid Stayed Concrete Block Wall "A Case History" ____ 903
Douglas J. Yovaish
Michael D. Sims & Associates, USA
Stephen W. Berry
Michael D. Sims & Associates, USA

Geogrid Reinforced Soil-Cement Arch Over Accelerator Ring ____ 917
John P. Gnaedinger
STS Consultants Ltd., USA
Safdar A. Gill
STS Consultants Ltd., USA

Application of Geosynthetics to the W.H. Zimmer Generating Station Project ____ 935
Rudolph Bonaparte
GeoSyntec Consultants, USA
Joseph E. Fluet
GeoSyntec Consultants, USA
Ronald D. Johnson
Tensar Earth Technologies, Inc., USA
Vicky Chouery-Curtis
Tensar Earth Technologies, Inc., USA

Modular Concrete Retaining Wall and Geogrid Reinforcemnet Performance and Laboratory Modeling ____ 951
John C. Kliethermes
Service Engineering, USA
Kenneth Buttry
University of Wisconsin-Platteville, USA
Earl McCullough
University of Wisconsin-Platteville, USA
Richard Wetzel
University of Wisconsin-Platteville, USA

FAILURES

Case History of a 9 m High Geogrid Reinforced Retaining Wall Backfilled with Cohesive Soil

W. J. Burwash
Golder Associates Ltd., Canada
J. D. Frost
Purdue University, USA

ABSTRACT

A 9 m high retaining wall reinforced with geogrids and backfilled with cohesive soil was constructed in Calgary, Alberta, Canada in 1984. The wall performed satisfactorily for 16 months when signs of settlement were first observed in the fill behind the wall. Conditions gradually deteriorated and over the next 22 months settlement of the backfill approached 0.9 m in one area. The top of the retaining wall rotated outwards about the toe and a deflection of 310 mm was recorded with a slope indicator over a 17 month period. In June, 1987 approximately 3 years after completion of construction, the upper 6 m of wall was replaced with a free standing 2h:1v slope.

This paper describes the only known documented case history of a major geogrid reinforced retaining wall backfilled with cohesive soil. Details are given for design of the wall, its construction and performance, and causes for its failure are postulated.

INTRODUCTION

In the fall of 1983 tenders were called for construction of the geotechnical components of a commercial development in Calgary, Alberta. Design called for construction of a retaining wall to support an asphalt surfaced parking lot. The wall was up to 9 m in height and was to consist of vertical steel H-piles, timber lagging and deadman anchors. An alternative design using high strength geogrids (Tensar SR2) to replace the deadman anchors but still using the H-pile and timber lagging facade was accepted by the owner on the basis of lowest price.

As a part of the alternative design, it was decided to use low plastic clay till as backfill to the retaining wall. Drainage was to be provided by a 600 mm wide zone of granular fill adjacent to the timber lagging. A 75 mm void was to be constructed between the geogrid facing and the H-pile and timber lagging to allow for possible post-construction movement. Foundation soils consisted of a deep deposit of very stiff low plastic clay till with the groundwater table well below the ground surface.

The wall was constructed in the spring of 1984 and performed satisfactorily until September 1985 when signs of settlement were first observed. Conditions gradually deteriorated and in January 1986 a slope indicator was placed on the face of the wall to monitor outward movement. Subsequent measurements showed that the wall facing was rotating about its base and after 17 months the deflection at the top of the wall was 310 mm. Settlement of the parking lot behind the retaining wall was observed to continue over the same period and was estimated to be up to 0.9 m by June, 1987. At that time the upper 6 m of the wall was replaced with a free standing 2h:1v slope.

DESIGN DETAILS

The geogrid reinforced wall consisted of two segments called the north and northwest walls oriented at an angle of 142° as shown on Figure 1 with a total length of 59.4 m and a maximum height of 9.0 m. Design details are given on Figures 2 and 3 and are discussed briefly in the following paragraphs.

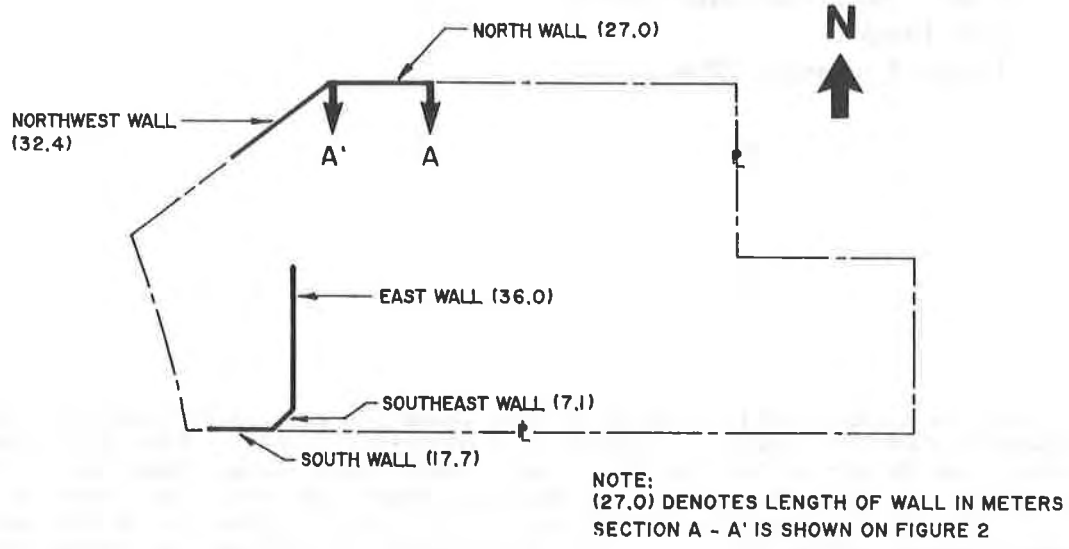

Figure 1 Key Plan

The H-piles consisted of W250 x 49 steel sections placed in 600 mm diameter augered holes which were about 3 m deep; the holes were then backfilled with 20 MPa concrete. The H-piles were positioned at 2.2 m centres. The pressure treated timber lagging was 75 mm thick and 150 mm wide and positioned on the inside of pile flanges and held in place by wooden blocks wedged into the opposite flange.

The wall reinforcement consisted of Tensar SR2 which is a high strength oriented polymer grid which was first marketed commercially in the early 1980's. The wall was reinforced by up to 10 layers of geogrid with lengths up to 6.8 m. The geogrids were incorporated into the wall design using the "wrap around" method shown in Section B-B' of Figure 3; a temporary spacer was placed between the H-piles and the geogrids to produce a 75 mm wide void which, if necessary, could accommodate creep of the geogrids. Geogrid sheets were joined together with a Bodkin joint consisting of a 6 mm diameter rebar woven through the ribs of the geogrid. The "double layering" technique reduced the quantity of required geogrid over the single layering method. The lower layer extended 2 m beyond the active pressure zone and was separated from the upper layer by a minimum of 300 mm of soil; the upper layer was extended back to give a length of geogrid (L) to height of wall (H) ratio (L/H) of at least 0.7.

The outer 600 mm of soil contained by the geogrids was granular fill which provided drainage. The top layer of geogrid was fastened to the top of the H-pile so that the soil was flush with the back of the wall.

The backfill consisting of low plastic clay till (typical liquid limit of 30 and plastic limit of 15 and 25% sand, 50% silt and 25% clay sizes) was similar to the foundation soils and was compacted to a minimum of 95% standard Proctor dry density. The earthworks was compacted under the scrutiny of a full-time inspector who conducted 105 in situ density tests; where tests did not meet the standard, the soil was given further compaction and retested until the density requirement was met.

A second wall termed the "south, southeast and east wall" (collectively called the south wall) was constructed at the same time as the north-northwest wall using similar methods but with some significant differences; the maximum height was 5.4 m

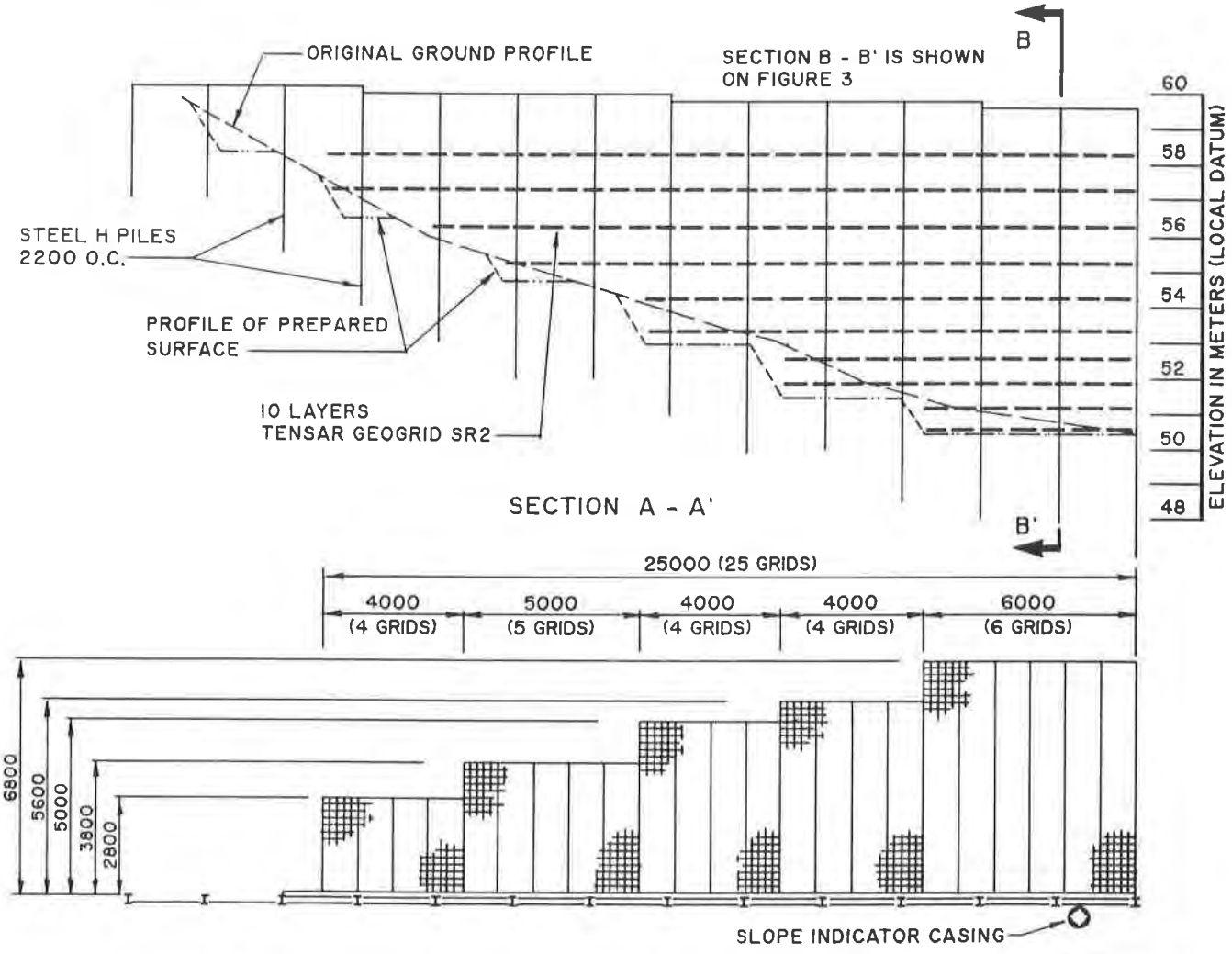

Figure 2 Plan and elevation of North wall

(compared to 9.0 m) and the embedded depth of H-piles was 8 m (compared to 3 m) at maximum wall heights with spacings varying from 1.5 to 2.2 m (compared to 2.2 m). It is significant that the south, southeast and east walls suffered no distress.

DETAILS OF ANALYSIS

External Stability

Geogrid walls must satisfy the same external stability criteria as conventional gravity retaining walls (Tensar, 1986): (i) sliding (ii) overturning (iii) bearing capacity and (iv) global stability.

The length of reinforcement was selected so that a factor of safety of at least 1.5 wa0s provided to prevent the possibility of the entire reinforced mass being mobilized outwards by the force of the lateral pressure. The lateral earth pressure was calculated using the Rankine theory with an angle of internal friction (ϕ) of 30°.

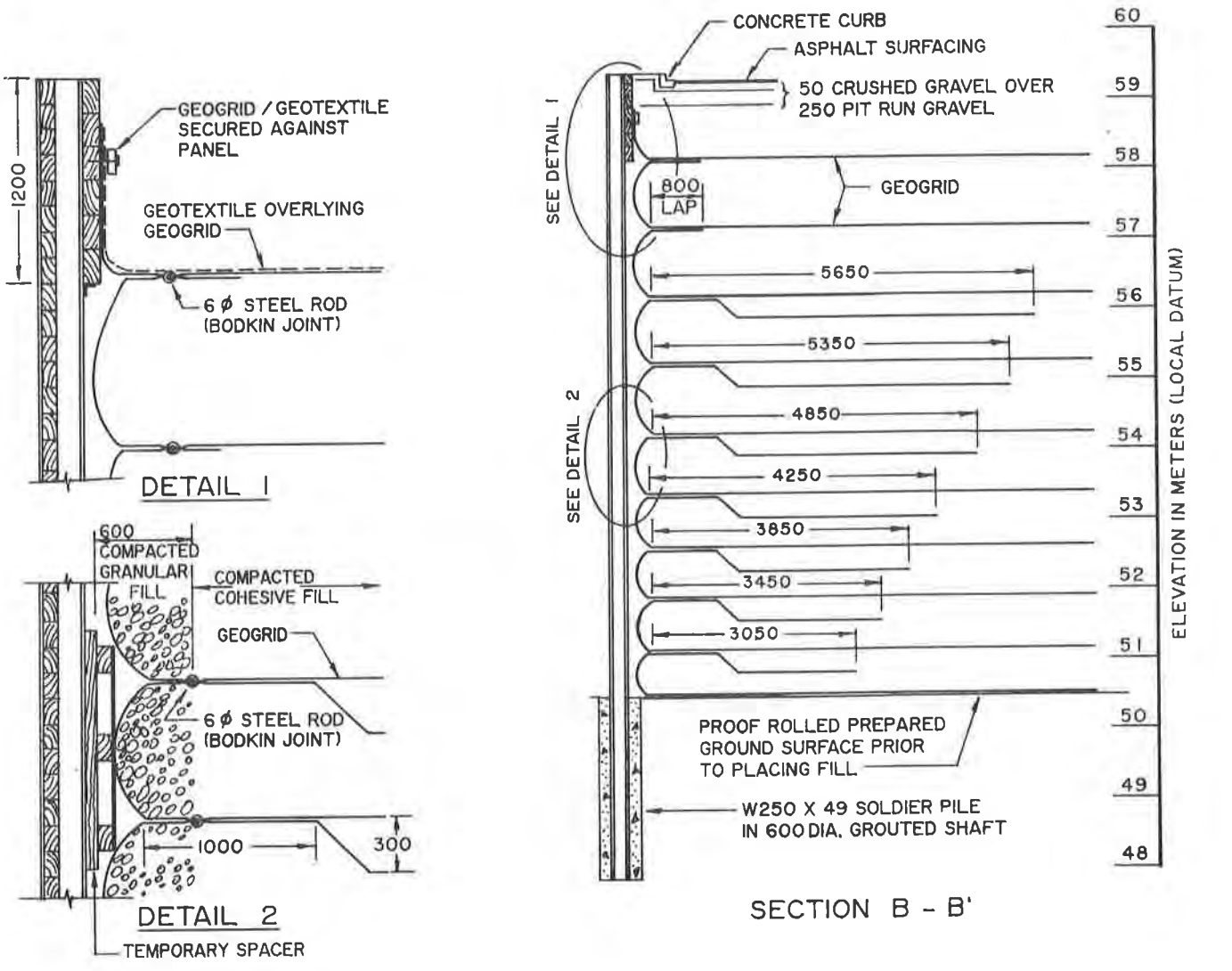

Figure 3 Typical section and design details

The critical sliding surface was found to be between the geogrid and the compacted clay; an interaction coefficient of 0.6 was used based in part upon the findings of the Bolton Institute of Technology (1982) and partly by experience with glacial tills in the Calgary area. Using these input parameters it was determined that a ratio of 0.7 for length of reinforcement to height of wall (L/H) was required.

A minimum factor of safety of 2.0 is normally used to prevent the possibility of overturning about the toe of the wall. For L/H of 0.7 the overturning requirement was exceeded. In addition, for L/H of 0.7 the resultant earth pressure force lies within the middle one-third of the base width to preclude theoretical tension at the base of the reinforced zone. The maximum bearing pressure at the toe of the wall was calculated to be about 315 kPa. Assuming an undrained shear strength of 200 kPa for the very stiff foundation soils, the ultimate bearing capacity exceeds the imposed toe pressure by a factor greater than 3 which is consistent with normal practice.

Conventional stability analyses showed that the factor of safety with respect to global or deep seated shear failure exceeded the conventional minimum factor of safety of 1.5.

Internal Stability

Internal stability ensures that the geogrid reinforcement is positioned so that tension failure of the geogrids and pullout from the soil mass beyond the assumed failure plane is prevented.

Tensar geogrid SR2 has a peak tensile strength of 79 kN/m but a long term design load of 29.2 kN/m is used in permanent engineered structures to ensure that deformation of the structure remains within acceptable limits over its service life. A factor of safety of 1.5 was then applied to the long term design load to give the allowable design strength. The geogrids were then spaced so that the tension induced in the geogrids was less than the allowable strength. The top geogrid was placed 1.2 m below finished grade and the bottom layer at the level of the ground surface outside the toe of the wall. The lower geogrid layers were spaced as close as 300 mm apart.

Adequate anchorage length was required so that the geogrids would not pull out of the soil behind the assumed failure plane based on the Rankine method of analysis. The L/H ratio of 0.7 required to ensure adequate resistance against sliding provided more than sufficient pullout resistance.

HISTORY OF EVENTS

A history of events from completion of the wall until its reconstruction three years later is discussed below and is given in abbreviated form on Table 1.

TABLE 1 - SUMMARY OF EVENTS

DATE	TIME FROM COMPLETION OF CONSTRUCTION	EVENT
May 1984	0	Wall completed
Sept. 1985	16 months	Cracks first observed in asphalt and obvious signs of settlement noticed.
Feb. 1986	21 months	Slope indicator installed. Settlement noticeably greater.
Aug. 1986	27 months	Parking lot cordoned off for safety reasons
Nov. 1986	30 months	Additional site investigation performed
June 1987	37 months	Wall reconstructed

The wall was completed in May 1984. Signs of distress were first observed 16 months later in September 1985; settlement of the ground surface and cracking of the asphalt pavement was readily apparent near the juncture of the north and northwest walls. Conditions gradually deteriorated and wall movement was suspected. In February, 1986 a slope indicator was placed on the outside face of the wall (see Figure 2) where ground surface settlement was greatest. Readings were taken over the next 17 months and the results are plotted on Figures 4 and 5. The results showed that the facade was rotating about the toe and that the rate of displacement was in general constant. After 17 months the facade had moved 310 mm which was 3.4% of the

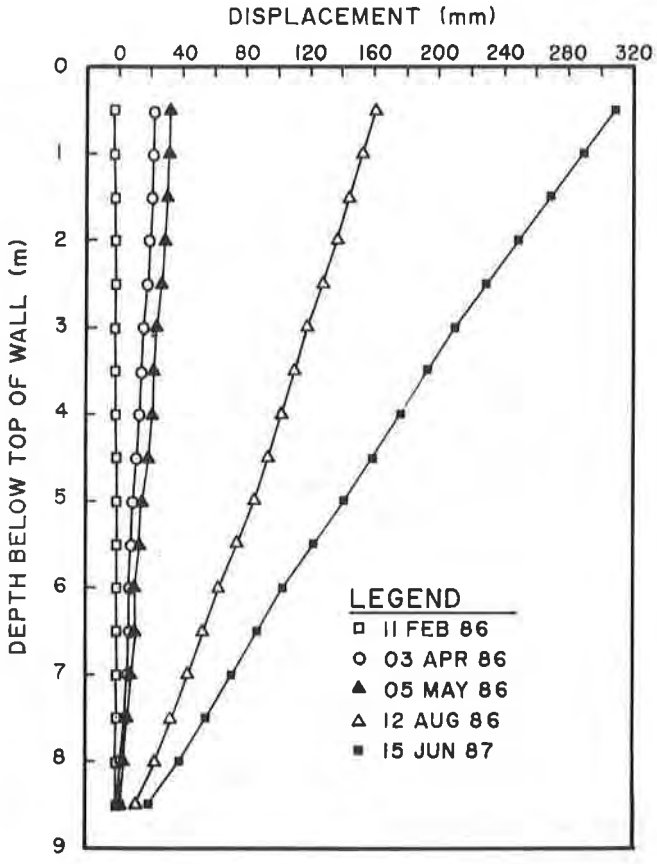

Figure 4 Displacement of wall vs. depth

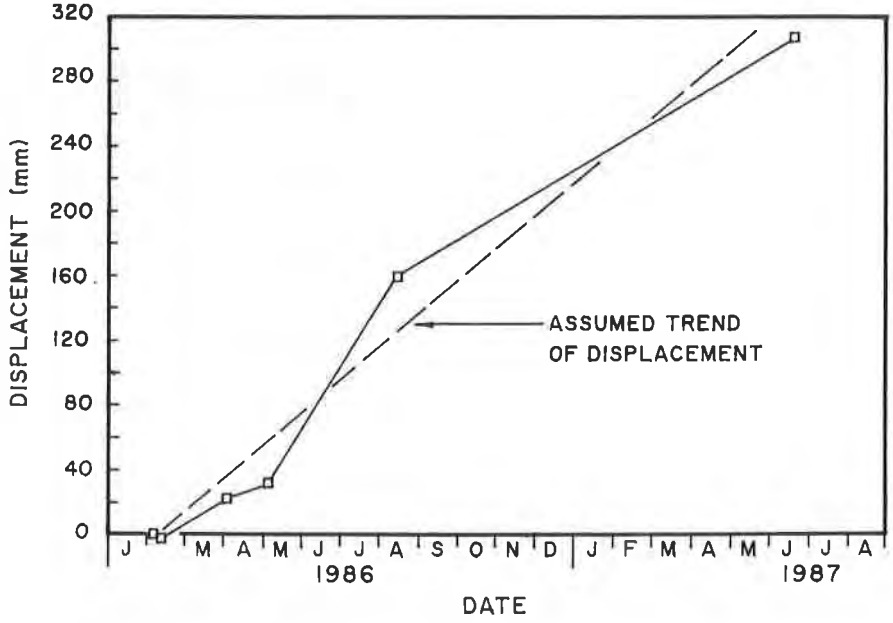

Figure 5 Displacement of top wall vs. time

height of the wall or 2.0° rotation about the toe. It is noted that these measurements were initiated some 21 months after end of construction and 5 months after the first evidence of distress; thus, actual displacements were most likely larger. By August of 1986 it was apparent that the distress showed no sign of abating and the wall was designated as unsafe and the parking lot near the wall was cordoned off.

In November, 1986 three boreholes were put down behind the juncture of the north and northwest walls. The results showed that the clay backfill had softened to a depth of about 3 m. Construction records showed that the average moisture content of the clay backfill at placement was 10.5% which was 4.0% dry of the optimum value of 14.5%. However, in comparison, the moisture content determined on samples from the boreholes which were put down 30 months after completion of construction showed a noticeable increase particularly in the upper 3 m where values were typically 1.5 to 3.0% above optimum or 5.5 to 7.0% above the placement moisture content. The increase was less apparent at depth and less noticeable at increasing distances from the wall.

In June 1987 the upper 6 m of the wall was removed and replaced with a free standing 2h:1v slope. The lower 3 m of the wall was left in place. A site survey conducted just before reconstruction showed maximum settlement in the order of 0.9 m (approximately 10% of the height of the fill). Maximum settlement at the back of the reinforced zone was about 0.5 m or about 5.5% of the height of the fill.

DISCUSSION

When this wall was constructed (1984) it was the highest known Tensar reinforced wall in existence. Previously a 7 m high wall had been constructed in England using Tensar geogrids (Netlon, 1983). A 12 m high geogrid reinforced slope had been constructed in 1982-1983 near Waterdown, Ontario (Busbridge, 1984) and was the first known use of geogrid for slope stabilization in Canada. Both projects were successfully completed without noticeable deformation. Berg et al (1986) described two retaining wall systems (with heights up to 6.0 m) used in Tucson, Arizona and Lithonia, Georgia using precast concrete panels. These walls were constructed in 1984 and 1985, approximately the same time as the wall described in this paper. Maximum deformation at the top of the walls was about 1.0° to 1.4° depending upon pretension in the geogrid and construction techniques; both walls were judged to be performing well. Comparatively, the rotation of the Calgary wall was estimated conservatively at about 2.0° before reconstruction.

A number of possible causes that could have been responsible for the distress of the wall were considered and are discussed below:

1. Settlement of Foundation Soils and Backfill

The glacial till underlying the wall is heavily overconsolidated and relatively incompressible under the weight of 9 m of fill and would account for less than 4% of the observed settlement. A study conducted by Rivard and Goodwin (1978) concluded that for clay till similar to that at the Calgary wall site and compacted to 95% standard Proctor dry density that the settlement would not exceed 1% of the embankment height. Further, it would be expected that 75% of the settlement would occur during construction. Thus, for a 9 m high fill, post-construction settlement would be expected to be about 22 mm which is about 2.4% of the observed settlement. The combination of foundation and fill settlement represents little more than 6% of the observed settlement. Clearly, the observed settlement pattern greatly exceeds the predicted performance.

As discussed previously compaction was inspected by a full-time inspector. However, of the 105 tests conducted only 8 were within 4 m of the wall face. The reasons for this are unknown but it is speculated that congestion near the face of the wall resulting from the materials and methods used was a contributing cause (the geogrids, the slipform, the Bodkin joint and the two soil types). This congestion could have hampered compaction efforts near the face of the wall and resulted in sub-standard compaction. This possibility is not inconsistent

with the fact that the settlement 6 m from the wall was about one-half that at the face of the wall although this may partly be associated with loss of lateral support resulting from the rotational movement of the wall facing. Regardless of the source of settlements, there is still a large magnitude of settlement not accounted for in the prediction analysis. Further, the fill behind the south wall which was placed using the same materials and methods showed no obvious signs of settlement.

2. Internal Erosion

The possibility of soil fines being washed from the backfill, through the geogrids, and into the void between the geogrids and the timber lagging and possibly even being transported through the lagging was considered. However, during reconstruction there was no evidence of fines in the void nor were there any fines deposited at the toe of the wall. Hence, internal erosion was not considered to be a contributing cause.

3. Saturation of Backfill

The post construction site investigation showed that the moisture content of the clay backfill had increased significantly from that measured during construction of the wall. The upper 3 m of the fill appeared to be saturated and was much softer than when placed.

The parking lot was graded to a catch basin located 21 m from the wall. The area surrounding the catch basin was designed to act as a holding pond and extended up to the wall; water would pond in this area after heavy rainfalls and would in time flow through the storm sewer system. The difference in elevation between the paved surface at the wall and at the catch basin was designed to be 200 mm. This difference in elevation was eventually reversed by the subsidence. It is suspected that the subsidence caused failure of the storm sewer leading from the catch basin; runoff water would then seep through the cracks in the asphalt and into the clay backfill. This series of events is consistent with the saturated condition of the clay backfill.

It is noted that heavy rainfall (40 mm in 24 hrs) preceded observation of the first signs of distress in September, 1985. The rainfall could have caused ponding which would allow a source of free water into the clay backfill.

A series of laboratory tests were conducted on samples of clay backfill recovered during the reconstruction. Samples were compacted to 95% standard Proctor dry density at the placement moisture content (10.5%) and consolidated in an oedometer under a pressure of 100 kPa to simulate loading at mid-height of the wall. At completion of consolidation, the samples were inundated and settlement of 0.7 to 0.8% of the height of the sample occurred immediately. The dry state of the backfill (about 4% less than optimum) contributed to the observed collapse type settlement. However, this settlement even when combined with foundation and backfill settlement still does not explain the magnitude of the observed settlement. The behaviour of the clay at low confining pressures, e.g. within 3 m of finished grade is expected to be different from that observed in the oedometer tests; the clay may swell in this zone. The loss of lateral support of the soil resulting from swelling and strength loss could lead to rotation of the wall which was not modeled in the oedometer tests and may explain some of the discrepancy between the predicted and observed settlement.

An unconsolidated undrained triaxial test conducted on a sample of the clay compacted to 93% Proctor density at a moisture content of 10.5% gave a compressive strength of 375 kPa. A similar sample when saturated gave a compressive strength of only 49 kPa and the moisture content had increased to 18.7%. These test results are consistent with that observed in the field, e.g., the clay gained moisture and lost considerable strength.

CONCLUSIONS

The distress to the retaining wall is believed to be related to saturation of the clay backfill which was placed 4% dry of optimum. The saturation occurred by ponding of surface runoff near the face of the wall. Laboratory tests have shown that saturation of the clay backfill placed dry of optimum water content resulted in significant loss in strength and collapse type settlement. It is postulated that the clay fill behaved as cohesionless backfill until saturated when its strength was significantly reduced. The geogrids were then subjected to strain to compensate for the resulting loss in strength. The lateral restraint offered by the embedded H-piles may have masked the lateral deformations which went unnoticed for 1.3 years.

It is believed that the south wall performed successfully because it was never subjected to the same increase in moisture content. This is likely due to the imposed surface drainage in that area and the fact that the H-piles at this location were more deeply embedded than at the north-northwest wall. Considering the lower height of wall they offered much more lateral restraint.

REFERENCES

Berg, R.R., Bonaparte, R., Anderson, R.P., and Chouery, V.E. "Design, Construction and Performance of Two Tensar Geogrid Reinforced Soil Retaining Walls", Proceedings of the III International Conference on Geotextiles, Vienna, Austria, April, 1986.

Bolton Institute of Technology, "Shear Box Tests on Tensar SR2 Embedded in London Clay", report to Netlon Ltd., March, 1982.

Busbridge, J.R. "Stabilization of CP Rail Slip at Waterdown, Ontario, Using Tensar Grid", Institute of Civil Engineers Proceedings, Symposium on Polymar Grid Reinforcement in Civil Engineering, London, England, 1984.

Netlon Ltd., "Construction of a 7 m High Vertical Faced Soil Wall", Case Study Report, 1983.

Rivard, P.J. and Goodwin, T.E., "Geotechnical Characteristics of Compacted Clays for Earth Embankments in the Prairie Provinces", CJG, Vol. 15, 1978, pp. 391-401.

Tensar Technical Note, "Guidelines for the Design of Tensar Geogrid Reinforced Soil Retaining Walls", The Tensar Corporation, Georgia, USA, 1986.

A Shattered Geomembrane Liner Case History: Investigation And Remediation

Ian D. Peggs
GeoSyntec Consultants, USA
Jules P. Winfree
GeoSyntec Consultants, USA
J.P. Giroud
GeoSyntec Consultants, USA

ABSTRACT

Prior to very cold weather in early 1989, the exposed high density polyethylene geomembrane liners of 5 of 13 evaporation, ash, and other ponds at a major power station in the western United States were observed to contain small cracks in and adjacent to the seams. During and after the cold weather, several seams cracked from the top of the side slopes to the bottom, and many of them extended as branching cracks into the geomembrane panels.

This paper describes the analyses performed to determine the nature of the cracking, the experimentation required to determine the material's performance characteristics so that proper repairs could be made, and the nature of the repairs.

INTRODUCTION

A number of brittle cracking failures of high density polyethylene (HDPE) geomembranes have been reported (Peggs and Carlson, 1989). The majority of these failures have occurred in the side slopes of liquid impoundments where the liner has been left uncovered and subject to large temperature variations and, therefore, significant thermally induced tensile stresses (Peggs et al., 1990).

In the winter of 1988/89 and, to a lesser extent, the winter of 1989/90, record low temperatures appeared to be responsible for extensive, spectacular shattering failures of a number of HDPE liners in the western and northwestern United States and western Canada. Moreover, similar fracture phenomena have been noted, but to a much lesser extent in other (warmer) parts of North America such as Tennessee. Cracking has occurred in many different HDPE liners and many different types of seams.

At one site 5 of 13 liners approximately 4 years old exhibited branching brittle cracks in the geomembrane panels extending from cracks along the edge of the seams. Three or four other liners at this site contained relatively short cracks with brittle fracture faces along the edges of the seams. The seams were extruded lap seams.

It was essential to the owners of this site that damage be repaired and that, most importantly, preventive measures be incorporated in repaired liners and in existing liners that had not suffered the extensive visible damage but which had, undoubtedly, suffered some less obvious damage. A detailed investigation of the cause of cracking and development of a permanently effective repair procedure was supported by the owners of the facility. This paper outlines the materials properties aspect of the investigation and how this contributed to defining the repair procedure.

BRITTLE (LOW DUCTILITY) CRACKING

Two types of brittle stress cracking have been observed in HDPE geomembranes and pipes: slow crack growth (SCG) and rapid crack propagation (RCP). SCG is stress cracking that occurs during application of constant tensile stress well below the yield stress of the HDPE. Stress cracks in HDPE geomembranes are typically 20 to 100 mm long. The longer, often branching RCP cracks that propagate beyond stress crack initiation sites grow very rapidly, at speeds as high as 500 m/s. The factors that produce both SCG and RCP are not well established for polymer materials (Mruk, 1989).

SITE INVESTIGATION

The site is located in the mid-western United States where temperatures vary from -30°C to 40°C. This temperature range, particularly the lower temperature, is typical of sites where shattering failures have occurred (GeoSyntec, Inc.).

During the on-site investigations, the following features of the geomembrane were noted and the following information generated:

- Short (20 mm) stress cracks were the first damage features observed.
- There were more stress cracks in ponds where the level of impounded water was low.
- At temperatures close to freezing (during the site visit), the geomembrane was considerably taut from bridging across corners of the rectangular ponds, and the liners on the side slopes were taut.
- Seam cracks extended from the anchor trench to the toe of the slopes (22 m); the crack opening displacement at mid-slope was approximately 200 mm).
- Branching cracks propagated into the geomembrane at an angle to the seam (upward in the top half of the slope, downward in the bottom half of the slope).
- The branching cracks traversed patches and seams without change of direction or evidence of blunting.
- On one slope, the shattering occurred at one seam one night and then occurred at an adjacent seam the following night; apparently, stress relief due to the first crack was insufficient to prevent another failure only twenty meters away.

- Damage did not predominantly occur on one slope facing one direction.
- The liners in "identical" ponds did not all fail.
- The liner in the pond containing the fewest visible stress cracks had been installed with compensation panels to allow for liner contraction at low temperatures; designed compensation panels had not been installed in the other liners.
- There was some indication that the seriously damaged liners had been installed at high ambient temperatures and would, therefore, require the largest amount of compensation in order to be stress-free at the lowest operating temperature.
- Other features of the liners such as manufacturing data, surface shading, subgrade settlement or slumping, and elapsed time for installation did not appear to bear any relationship to the amount of damage.

SAMPLING

Samples were removed from the field for systematic laboratory testing and examination to determine:

- the extent of incipient stress cracking;
- geometries and fractography of small stress cracks;
- identification and location of crack initiation areas;
- fracture characteristics of one small, but complete, seam and geomembrane crack system;
- geomembrane behavior in a biaxial stress mode at low temperatures; and
- detectability of incipient or partially penetrating stress cracks.

The manufacturer/installer of the original geomembrane provided samples of geomembrane (with which repairs were to be made) for testing and provided seams containing artificial stress cracks "repaired" by novel proprietary methods for evaluation.

LABORATORY INVESTIGATIONS

The laboratory investigations were quite extensive and, therefore, can only be summarized here.

Fractography. Many fracture faces were examined at moderate to high magnification with different light conditions. The following features were revealed.

- The branching cracks in the geomembrane had the very smooth features of RCP.

- The cracks along seams showed a combination of RCP and SCG; the RCP initiated at SCG cracks.
- In general, the stress cracks found on the top surface of the bottom geomembrane at the edge of the seam propagated by SCG downward through the thickness of the geomembrane.
- After penetrating through the geomembrane and growing sideways about the initiation point by SCG, RCP was initiated and the crack traveled rapidly in the plane of the geomembrane.
- Many stress cracks had initiated where the original seam had been repaired with an extruded fillet bead.
- Other stress cracks were initiated where there was evidence of overheating during seaming.
- A few stress cracks initiated where there was no visible cause for initiation.
- The sample representing the small complete crack system presented a microcosm of all the key features above; propagation was from a single initiation site in a repaired section of the seam.

Microtome Sections. Thin slice (~ 15 μm) cross sections (microsections) of seams were prepared with a microtome from samples removed from undamaged seams in each pond. The microsections were examined by transmitted light microscopy using polarizing filters at magnifications up to 400. Of 50 microsections examined, 20 showed evidence of actual stress cracking. The seam cracking problem was, therefore, far more extensive than visibly apparent. There was no relationship between the frequency of damage in the microsections and the visible damage in each pond; the visibly undamaged liners contained as many stress cracks as the visibly damaged liners. This observation simply demonstrates the inability to define all the effects which synergistically combine to initiate stress cracking.

Seam Tests. Some of the same seam samples used to prepare microsections were subjected to conventional peel and shear tests. Of 25 specimens tested, only two specimens had relatively low (<50%) shear elongation values. The remainder showed acceptable behavior. In construction quality assurance seam testing programs, elongations less than 100% may be considered to be unacceptable. (Elongation is calculated using the distance between the grip and the nearer edge the seam as the gage length. The seam must be centered between the grips.) Of 20 specimens tested, a few showed varying degrees of peel separation up to 30%; other parameters were acceptable. By some present standards (Peggs, 1989), peel separations in excess of 10% can be considered excessive; however, at the time of liner installation, 30% peel separation followed by failure of the geomembrane would not typically have been cause for concern. These criteria incorporating shear elongation and peel separation were not in place during the installation of the liner but are criteria that have recently been found to indicate the potential for stress cracking problems (Peggs, 1989).

Uniaxial and Multiaxial Tensile Tests. Uniaxial tensile tests using American Society for Testing and Materials (ASTM) D638 Type IV specimens were performed at room temperature and at -30°C. In addition, and to more closely simulate the biaxial stresses that occur in the field, tests were performed with specimens of various sizes, from 25 mm wide and essentially zero gage length to 300 mm wide and 50 mm gage length.

The strength values increased and strain decreased with decreasing temperature as shown in Table 1. It was very difficult to perform a satisfactory biaxial (wide strip) test as evidenced by the fact that generated strength values are lower than those from the uniaxial test. Biaxial strength values should always be higher, and strain values lower, than uniaxial test values.

Table 1. Tensile Properties of Installed Geomembrane as a Function of Temperature

Test Method	Temperature (°C)	Yield Stress(MPa)	Yield Strain(%)	Break Stress(MPa)	Break Strain(%)
Uniaxial	25	20.7	12	29.0	850
	-30	35.0	6	35.6	422
Biaxial (wide strip)	25	---	---	15.7	230
	-30	---	---	26.5	160
Pneumatic Burst	23	24.0	5.6	24.0	5.6
	-26	27.0	2.5	25.9	4.6
	-38	32.0	1.8	29.7	2.9

To determine the relative ductility of the geomembrane material under biaxial overstress at seams, some specimens 300 mm wide and with a gage length of 50 mm were tested at room temperature with seams centered across the gage length. On some specimens, artificial, nonpenetrating stress cracks were simulated by razor cuts along the edge of the seam. In all cases, whether failure initiated at the artificial stress cracks or elsewhere at the seam edge, fractures showed material thinning and elongation characteristic of ductile failures (Peggs, 1989).

This type of behavior was further confirmed by testing large specimens (0.6 m diameter) in a multiaxial burst testing chamber. The specimens were strained pneumatically from one side. Both geomembrane and seamed specimens were tested. The geomembrane specimens were tested at temperatures between room temperature and -38°C (Peggs and Carlson, 1990); at -38°C, they displayed strains at yield of less than 2%. Such strain values are lower than those on which design figures are often based. Despite these low strain values and the fact that the biaxial and multiaxial stress-strain curves do not show the distinct visible yield peaks of the uniaxial curves the majority of failures occurred in a ductile manner, albeit in a very local region.

The one exception that showed brittle fracture characteristics was a seamed specimen that was tested at -38°C. It failed with an RCP crack along the seam and with several branching RCP cracks into the geomembranes on either side of the seam. It was a small version of the complete crack system removed from the field. Microscopic examination of the fracture faces revealed, as with all other samples showing RCP cracks, that the final RCP cracking had been initiated at a pre-existing SCG stress crack. It is, therefore, confidently postulated that the RCP shattering fractures are initiated at stress cracks and that, if the stress cracks are not present, the shattering will not occur.

It is concluded from this phase of the work that the brittle stress cracking failures seen in the field are not the result of simple overstressing under biaxial or multiaxial stress conditions and are, in fact, the result of a completely different phenomenon.

Dimensional Changes. Changes in dimensions of an HDPE geomembrane derive from two sources: reversible thermal contraction and expansion, and irreversible contraction due to the annealing of residual stresses remaining from the manufacturing process. These two processes, the latter resulting primarily from exposure to elevated temperatures are, primarily responsible for the induced tensile stresses that initiate cracking at low temperatures.

The coefficient of linear thermal expansion (CTE) of HDPE is high and increases significantly when temperature increases over the practical range of interest, -40°C to 90°C. The latter temperature, and even higher temperatures, have been measured on black HDPE exposed to summer sun.

Measurements of CTE on small 1 mm cube specimens by thermomechanical analysis (TMA) showed a distinct increase in expansion rate at temperatures between 20 and 50°C, probably related to a change in the unit cell of HDPE from monoclinic to orthorhombic. On large specimens, 250 mm square, this change is more gradual but the CTE increases when temperature increases over the range of interest (Peggs et al., 1990). Typical values of CTE of HDPE geomembrane are:

Temperature Range	Mean CTE
-40 to 10°C	1.4×10^{-4}/°C
-40 to 20°C	1.6×10^{-4}/°C
-40 to 30°C	1.9×10^{-4}/°C
-40 to 40°C	2.3×10^{-4}/°C

The temperature indicated is the temperature of the geomembrane, not the environmental temperature which could be different to the geomembrane temperature.

The conventional National Sanitation Foundation (NSF) 54/ASTM D1204 dimensional stability test, in which dimensional change is measured while a specimen is heated at 100°C for 15 minutes, was performed but was continued for 3200 hr. The specimens shrank by as much as 1.5% and still had not reached an equilibrium dimension (GeoSyntec, 1989-1990).

Dimensional change data (i.e., dimensional instability and thermal contraction) must be used to determine the amount of slackness to be built into any lining system when the lining is installed or when compensation panels are installed at a later date (Giroud and Peggs, 1990). The temperature at which the slackness is measured must be the actual geomembrane temperature and not the atmospheric temperature.

Mechanical and Physical Properties. The following conventional properties of the geomembrane removed from the field were measured: low temperature brittleness, puncture strength, density, carbon black content, carbon black dispersion, and tear resistance. All were found to meet NSF 54, manufacturer, and project specifications.

Stress Cracking Resistance. Constant tensile load tests on ASTM D638 Type IV specimens that were notched on one side through 20% of the thickness of the geomembrane were performed. Tests were performed on geomembrane samples removed from the field, seam samples removed from the field (notched in the bottom geomembrane along the edge of the seam), and on the geomembrane proposed for the repairs to the liner. Specimens were tested until they failed or they were removed prior to failure and the notch extension measured.

The stress cracking resistance of the geomembrane at the edge of the seam was found to be less than that of the basic installed geomembrane. Apparently, the seaming process compromised the durability of the geomembrane. This happens in most but not all HDPE geomembranes when they are seamed (Peggs and Carlson, 1990). Tests were also performed on geomembrane at the edge of seams that had been repaired (for unknown reasons) by laying an extruded fillet bead along the edge of the seam. The stress cracking resistance of the geomembrane had been reduced to approximately 17% of its original value which explains why many of the stress cracks in the field were associated with reseamed seams.

The stress cracking resistance of the proposed repair material was found to be superior to that of the installed material.

The reasons for the increased susceptibility to stress cracking of the geomembrane at the edge of the seam were next examined by microstructural means.

Geomembrane Microstructure at Edge of Seam. The microstructure of the geomembrane just outside and just underneath the edge of the seam (where stress cracking was observed) was examined for density variations as well as crystallinity and oxidative induction temperature (OIT) variations. These results have been given in more detail elsewhere (Peggs and Carlson, 1990) and generally showed that the density and crystallinity were higher adjacent to the location of the stress cracks. This subject needs much further investigation, but it is not surprising that the heat-affected zone of the geomembrane adjacent to the seam can be adversely affected by the seaming process.

The laboratory observations supported the field observations that many stress cracks had been initiated at repaired seams where two applications of thermal energy reduced stress cracking resistance of the geomembrane.

Clearly, it is inadvisable to repair seams by laying down an additional extruded bead. Neither should existing, partially penetrating stress cracks be repaired this way.

Seam Repair Protocols. It was proposed to repair seams containing stress cracks by a wide bead extrusion technique. A wide (100 mm) bead was proposed so that the heat affected zone in the parent geomembrane would be well removed from the heat affected zone of the original seam, thereby preventing an excessive reduction in the stress cracking resistance of the geomembrane. It was, therefore, necessary to test the repair for effectiveness and to ensure that the repair technique would not reduce the stress cracking resistance of the geomembrane to a level lower than that produced by the original seaming technique.

Penetrating "stress cracks" were cut in seams removed from the original pond liner and submitted to the installer for repairing. The seaming parameters (temperature and speed) were varied until a satisfactory seam was thought to have been produced. Microsections of the repaired seams were examined under the microscope, and long gage length specimens were subjected to constant tensile load stress cracking tests. The gage length included the repaired stress crack with the notch cut at the edge of the repair bead. The objective of the test was to find a repair procedure that would promote failure at the edge of the repaired seam in a time equal to, or greater than, that at a seam of the originally installed geomembrane.

The specimens from the first attempted repair protocol failed in the repaired stress crack. The second attempt produced many voids along the extruded bead/geomembrane interface, and the seam was not subjected to the stress cracking test. The next repair protocol produced a failure at the edge of the seam, as desired, but at a very short time. After several attempts, a seaming protocol was found that produced a stress cracking failure at the edge of the repair in the same time as at a seam of the originally installed geomembrane. This last protocol (proprietary) was used in the field to make repairs.

Identification of Seams Containing Nonpenetrating Stress Cracks. It became necessary, finally, to find a nondestructive method of locating penetrating and nonpenetrating stress cracks in the field. Several methods, listed below, were investigated in the laboratory:

1. Visual observation.

   This method would require a well-trained eye.

2. Ultrasonic shadow technique.

   In this method an ultrasonic signal is injected in the geomembrane on one side of the seam, traverses the seam, and is monitored on the other side of the seam. Defects within the seam affect the transmitted signal and are, thereby, identified.

It was found that the technique would clearly identify an artificial notch penetrating through 10% of the thickness of the geomembrane where there had previously been no notch, but the change in signal was swamped by the variations in signal along the length of a typical seam. The method was, therefore, impractical to use.

3. Dye penetrant.

   The dye penetrant method was also found to be impractical since it was impossible to distinguish between dye in stress cracks and dye in scratches and grinding gouges.

4. Powder penetrant with video monitoring.

   This method offered the most potential for practical use. White talc (baby powder) was dusted along the edge of a seam then wiped off with a rag. The powder was trapped inside a stress crack and, therefore, highlighted the stress crack. The seam was then traversed along its length by a video camera mounted in a carrier, and the view was observed on a small portable TV monitor. The seam characteristics could be reviewed at any time by replaying the video tape.

   During field trials the technique was found capable of identifying stress cracks that had not initially been seen by the naked eye but it also missed a few cracks that had been previously identified. The main drawback of the method was that it did not provide a "go, no-go" acceptance criterion and would require an experienced operator to make subjective acceptance/rejection decisions.

The final field survey for stress cracks was made using visual observations.

Repair Procedure. All of the data generated in the test programs were taken into consideration in the design of the repairs.

All damaged seams and panels were replaced with new material containing an adequate amount of slackness calculated using the temperature of the liner at the time of the repair. The new panels were installed during the coolest time of the day so the minimum amount of slackness would be required.

In addition to repairing visually damaged seams and panels every third seam was cut from the trench to the toe of the slope and the geomembrane allowed to relax. Compensation panels, typically 1 m wide, were installed at each cut seam. The compensation panels were tapered at the anchor trench and at the toe of the slope. The uncut seams were visually examined for stress cracks and repairs were made using the wide bead extrusion technique.

REPAIR PERFORMANCE

Repairs, initiated in the late summer of 1989, have been completed. The repairs that were made have successfully withstood one and one-half winters, without the appearance of any additional cracks. The liners are clearly

expanding and contracting but they are never taut. The built-in compensation is remaining uniformly distributed and is not migrating away from, or across, the slopes.

CONCLUSIONS

Design, construction, and maintenance of effective, durable HDPE lining systems require an understanding of the mechanical performance of the geomembrane under biaxial stress conditions at the lowest operating temperature, coupled with a knowledge of thermal contraction and dimensional shrinkage performance in order that geomembranes may be installed to be essentially stress-free at their lowest expected operating temperatures.

Seaming methods in each type of geomembrane need to be investigated to determine those methods that least affect the stress cracking resistance of the adjacent geomembrane. Until such time as this information is known, seams should not be repaired by reseaming. It is most advisable that all HDPE liner installations receive adequate professional construction quality assurance to ensure that seams are produced so that stress cracking resistance of the seam and the adjacent geomembrane is maximized.

ACKNOWLEDGMENTS

The authors acknowledge the technical support of D.S. Carlson, S.G. Peggs, L.G. Tisinger, and R.M. Charron; the administrative support of G.E. Saunders and S.A. Meeker; and the reviews performed by J.R. Mollenauer, R.C. Bachus, and J.P. Giroud.

REFERENCES

GeoSyntec, Inc., proprietary reports, 1989-90.

Giroud, J.P., and Peggs, I.D., "Construction and Quality Control of Geomembrane Liners", Proceedings of ASCE 1990 Annual Civil Engineering Convention and Exposition, San Francisco, CA, Nov 1990, pp. 190-225.

Mruk, S.A., "Plastic Piping Terms and Definitions", Proceedings of Eleventh Plastic Fuel Gas Pipe Symposium, American Gas Association et al., San Francisco, CA, Oct 1989, pp. 16-29.

Peggs, I.D., and Carlson, D.S., "Stress Cracking of Polyethylene Geomembranes: Field Experience", Durability and Aging of Geosynthetics (Ed., R.M. Koerner), Elsevier Applied Science, London, 1989, pp. 195-211.

Peggs, I.D., "Destructive Testing of Geomembrane Seams", Seaming of Geosynthetics, (Ed., R.M. Koerner), Elsevier Applied Science, London, 1990, pp. 125-134.

Peggs, I.D., and Carlson, D.S., "The Effects of Seaming on the Durability of Adjacent Polyethylene Geomembrane", Proceedings of the Symposium on Geosynthetic Testing for Waste Containment Applications, Las Vegas, NV, Jan 1990, pp. 132-142.

Peggs, I.D., Carlson, D.S., and Peggs, S.J., "Understanding and Preventing 'Shattering' Failures of Polyethylene Geomembranes", Proceedings of the 4th International Conference on Geotextiles and Geomembranes, The Hague, The Netherlands, May 1990, Vol 2, pp. 549-553.

Geosynthetic Considerations in a Landfill on Compressible Clays

Gregory Richardson
ENSCI, Corp., USA
Dick Reynolds
R. G. Gerber, USA

INTRODUCTION

In mid-August, 1989, a 500,000m^3 landslide occurred at a commercially operated landfill in central Maine. The landfill material consisted of municipal solid waste (MSW) that rested on a thick deposit of marine clay-silt which provided a natural barrier to leachate seepage.

The movement lasted about 15 seconds. During the slide, huge vertical crevices formed in the landfill. Trash dropped 6 to 9 meters into scarps formed in the underlying clay as the soil slid out from underneath. During the period over 125 mm of rain fell. During the slide, 6 large crevices opened up in the trash pile. Some of the crevices were 15 meters wide and up to 9 meters deep. Soil was disturbed by the landslide up to 100 meters beyond the original toe of the landfill. Due to remolding, some of the clay lost 90% of its original undrained shear strength. At some locations, the remolded clay and silt flowed over undisturbed soil at a shallow depth. Analysis of the slide indicated that a rotational failure first occurred under the original landfill slope. The rotation left steep unsupported slopes within the trash pile and the underlying clay and silt. Blocks of trash and clay then followed the direction of the initial movement.

This paper discusses why the slide occurred and its implications on the design of future landfill cells at this site. Specific attention is focused on the dissipation of excess pore water pressures that result from the consolidation of the underlying clays and on the impact of differential settlements on the leachate collection systems.

SITE HISTORY AND GEOLOGY

In the 1970's a local landowner began the operation of a small municipal solid waste disposal facility on a 120 hectare site in central Maine. In contrast to many town dumps located in abandoned gravel pits, this site offered a good natural clay barrier to protect the area's ground water resources. The landfill is underlain with 15 to 20 meters of marine clay-silt deposits.

The marine clay-silt is regionally referred to as a clay. It is apparent from radiographs of undisturbed samples in Shelby tubes, that the soil is composed of clay and silt lenses laid down in an environment of varying energy levels. Bloom (1960) indicated that the clay and silt are part of the Presumpscot Formation deposited during the last glacial period, or about 10,000 years ago. Extensive deposits of this Formation occur over much of coastal Maine. The top 2 to 4 meters of the marine clay and silt are often weathered and fissured. Below the weathered zone, the soil has vertical permeabilities obtained from undisturbed samples in the range of 10^{-7} to 10^{-8} cm/sec. Occasional sand seams in the formation cause the horizontal permeability to be about one order of magnitude higher.

THE NATURE OF THE LANDSLIDE

During the slide, 6 large crevasses opened up in the trash pile. Figure 1 shows the landfill just after the landslide. Some of the crevasses were 50 feet wide and up to 30 feet deep. Soil was disturbed up to 300 feet beyond the original toe of the landfill by the landslide. Due to remolding, some of the clay lost 90% of its original undrained shear strength. At some locations, the remolded clay and silt flowed over undisturbed soil at a shallow depth.

Post-failure analysis of the slide indicates that a rotational failure first occurred under the original landfill slope. The rotation left steep unsupported slopes within the trash pile and the underlying clay and silt. Blocks of trash and clay then followed the direction of the initial movement.

STABILITY EVALUATION

While the marine clay and silt offers an ideal natural barrier to the seepage of leachate, the strength of the soil limits the weight of fill which may be placed on top of it. As the landfill expanded, monitoring wells were installed and laboratory tests on soils were run. Some of the monitoring wells included field vane shear tests (ASTM D2573-72) and 76mm Shelby tube sampling. Laboratory testing included classification, strength, and consolidation testing. Figure 2 shows typical laboratory Atterberg and consolidation (σ_{vm}) test data, as well as vane shear data, for the marine clays and silts. Typical consolidation load-strain response of the marine clays and silts are shown on Figure 3. The upper 10 meters of the profile is over consolidated while the deeper marine clays are normally consolidated.

Using the vane shear data and what was thought to be a reasonable value for the density of the landfill, a height limitation of 17 meters was placed on the existing MSW landfill in mid 1986. With fill above that level, it was calculated that the factor of safety against a slope failure would be below 1.25 for short term conditions and that was not acceptable. Laboratory testing subsequent to the landslide and back-calculations from the slide itself has shown that the field vane test values were in fact considerably lower than the actual shear strengths developed in the clay-silt.

However, another factor that strongly influenced the stability of the landfill slopes was the density of the landfill material. In the early stages of the operation, the owner had little historical on-site data to indicate the landfill density. Consequently, a density that seemed appropriate, based on the appearance of the fill was used. A value of 590 kg/m^3 (1000 lb/cy) was estimated and this value seemed to be corroborated by historical information discussed by Weiss (1974). By mid-1987, weight and volume data was available to indicate that the density of the trash and cover was on the order of 1250 kg/m^3 (2125 lb/cy). At that time, the height of the landfill was nearing 12 meters. Considering clay strength increase due to consolidation the minimum calculated factor of safety of the landfill slopes was approximately 1.25 with the height at 12 meters and the density at 1250 kg/m^3.

From late 1987 to early 1989, the height of the MSW landfill was gradually increased to about 18 meters. Biweekly readings from inclinometers indicated a maximum lateral movement of 19mm per year. This rate was judged to be high, but acceptable.

Construction began on a westerly cell expansion in the late Spring of 1989. Trees were cleared, the topsoil was stripped from the clay and silt, and all weathered soil was removed below the topsoil. Some of the weathered soil was mined for cover material for other landfills. Since digging into the clay and silt would also increase the capacity of the landfill, the plans called for the removal of 2 to 2.5 meters of soil in the expansion area at the toe of the landfill. Because the new area was to include a compacted clay liner and a geomembrane and the original area had not, a leachate collection trench was dug adjacent to the toe of the old landfill. In hind sight, it was obvious that removing strong soil at the toe, which was supporting the existing landfill slope, and then cutting a leachate collection trench deeper into the ground at the toe, were not prudent steps to take. Following a 10 day period when over 125 mm of rain fell, the landslide occurred.

After the failure, the owner performed a dozen large-scale density tests and 6 direct shear tests in the trash. Each density test involved digging about 8 m^3 of trash out of the fill, cross sectioning the excavation to measure its volume, and then weighing the excavated material. The results of the density tests indicated an average total density of 1534 kg/m^3 (2,600 lb./cy). To measure

the shear strength of the trash, the owner constructed a 1.5m² square shear box. The box was loaded with large concrete blocks to vary the normal force in the test. Figure 4 provides a summary of the results.

Back calculations at the time of failure showed that the shear strength of the marine clay can be expressed by the equation (Koutsoftas and Ladd, 1985)

$$USR = S(OCR)^m$$

where

USR = Ratio of the soil's undrained shear strength to the effective vertical consolidation stress
S = Undrained strength for normally consolidated clay
OCR = overconsolidation ratio, $6_{vm}/6_{vo}$
m = 0.8

For this site, S of the marine clay was found to be approximately 0.23 kg/sq.cm. Thus, with time and as waste is added to the landfill mass, the OCR will reduce and the shear strength of the clay will increase at a rate less than the vertical consolidation stress.

To properly function on top of consolidating marine clay profiles, landfill systems must be designed to allow for drainage of pore water from the consolidating clay and to survive the differential settlements resulting from such drainage. The previous review of the landfill failure clearly shows that successful commercial operation of such facilities is dependent upon excess pore water pressures dissipating in a timely manner so that the strength of the marine clay will increase and thus allow more waste to be placed. This cycle of loading, soil strengthening through consolidation, and increased loading is central to the safe and economic operation of such facilities.

CONSOLIDATION DRAINAGE

As waste is placed atop the marine clays, excess pore water pressures are generated within the clays and begin to move towards a drainage face. If the marine clays have a horizontal stratigraphy, then the drainage flow direction near the center of the landfill will be primarily vertical. Contemporary landfills incorporating a composite liner (geomembrane and soil liner) may pose a significant restriction on the rate at which pore waters can dissipate.

The compacted soil component of the composite liner is placed wet of optimum but at a water content that still leaves the soil partially saturated. The fine grained nature of this soil, however, results in a capillary draw of moisture from the underlying saturated marine clays. Note that this in itself may result in an initial minor settlement of the landfill. As the

water suction of the compacted clay layer is satisfied, the pore volume available to absorb the consolidation generated drainage is significantly diminished. The capillary draw of moisture is, however, essential to preventing the potential desiccation of the clay liner. **Thus, provisions must be made to prevent the buildup of consolidation generated pore water pressures beneath the synthetic liner without destroying the capillary link between the marine clay subgrade and the overlying compacted clay liner.**

A proposed solution to this problem is shown on Figure 5 and consists of a parallel row of drains placed at the clay liner-subgrade interface. The spacing of the drains can be determined by adapting the general equation for mounding of infiltration liquids between the rows of horizontal drains as follows:

$$H_{max} = L \left[\sqrt{\frac{e}{K} + \text{Tan}^2\alpha} - \text{Tan}\,\alpha\right]$$

where L is the spacing between the horizontal drains, e is the infiltration velocity, and α is the slope of the interface. For this application α can be assumed to be zero such that

$$H_{max} = L \sqrt{\frac{e}{K}}.$$

The infiltration velocity of the consolidation waters were calculated for this site using the initial 25% of consolidation (e - .006 inch/day). Assuming the soil liner satisfies the criteria that $K<1 \times 10^{-7}$ cm/sec, then the spacing between the drains must be approximately twice the thickness of the soil component of the composite liner. For typical liners, this results in a drain spacing of 3 to 4 feet. The volume of water entering each drain daily is limited by the low permeability of the soils surrounding each drain and in this case has a maximum value of 0.3 $inch^3$/day/ft. Geosynthetic drainage products will commonly have capacities many orders of magnitude greater than required for this application.

The proposed drainage elements must withstand the normal pressure generated by the weight of the waste mass placed above it and the differential settlements discussed in the following section. This combination of drainage capacity, strength, and flexibility can be obtained using a geotextile wrapped perforated-pipe fitted with mechanical slip joints. The mechanical slip joints eliminate the expense of rigid fusion joints and allow the pipe to elongate as differential settlements develop. Additional drainage system options include geosynthetic highway edge drain and wick drain systems. Laboratory transmissivity tests must be performed on these alternatives to confirm their ability to remain operational under the anticipated long-term normal stresses.

A hydraulic outlet must be designed to allow the consolidation water collected by the drain pipes to be removed. For the specific facility in questions, sufficient topographic relief exists to allow a simple gravity drain to serve this function. Sites having limited relief would require lift stations to remove the collected

water.

DIFFERENTIAL SETTLEMENT CONSIDERATIONS

The consolidation of the marine clays will produce differential settlements of the clay liner due to the variations in waste depth. Such variations are largest at the perimeter of the landfill where the largest gradients of waste thickness occurs. The normal stresses acting on the marine clays due to the waste embankment can be calculated using the chart given on Figure 6. Using the normal stress from this chart, the anticipated long-term differential settlements can be calculated and are also plotted on Figure 6. Such differential settlements of the subgrade can place the composite liner in tension and reduce the effectiveness of the leachate collection systems. Strains in the liner elements due to differential settlements can be calculated using the following equation:

$$\epsilon = (L^2 + (S_1 - S_2)^2)^{\frac{1}{2}}/L$$

where L is the distance between two points and S_1 and S_2 are the consolidation settlements of those two points. This strain level must typically be less than 10% to prevent tension cracking of the clay liner (Gilbert and Murphy, 1987).

Leachate collection systems are typically designed for slope angles of 2%. Additionally, it is common for such systems to drain to the perimeter of the landfill to allow easier removal of the collected leachate from the landfill. Thus, the interior of the landfill will typically have a higher floor elevation than the perimeter. Long-term consolidation settlements, however, will be larger at the center of the landfill and, thus, tend to reduce the slope of the leachate collection system. Referring to Figure 6, it can be seen that nearly 3/4 of the original 2% slope will be lost due to long-term consolidation of the underlying marine clays.

SUMMARY

The 60-feet of marine clays that make this site environmentally attractive for a landfill also result in significant potential long-term operational problems for the landfill. Such long-term considerations include the following:

- Staged placement of the waste must be done in a manner that allows the underlying clays to consolidate and increase in shear strength.
- Drainage of consolidation waters from the underlying clays must be provided for in the final design.
- Slopes of leachate collection systems must be sufficient that long-term differential settlements do not reduce or reverse the flow gradients.

The role of geosynthetic components during these long-term settlements must be clearly understood and evaluated by the design engineer.

The authors wish to thank Steve Cole, of Cole & Associates, and Bob Gerber, of G. R. Gerber, Inc., for their comments and sharing of experiences from sites in Maine.

REFERENCES

Bloom, A.L., "Late Pleistocene Changes of the Sea Level in Southwestern Maine," Maine Geological Survey, Augusta, Maine, 1960.

Koutsoftas, D.C. and Ladd, C.C., "Design Strength for an Offshore Clay," Journal of the Geotechnical Engineering Division, ASCE, March, 1985.

Perloff, W.H., et al, "Stress Distributions Within and Under Long Elastic Embankments", Highway Research Record No. 181.

Weiss, S., Sanitary Landfill Technology, Noyes Data Corporation, Park Ridge, NJ, 1974.

Gilbert, P. A. and Murphy, W. L., Guidance Manual for Prediction and Mitigation of Settlement Damage to Covers of Hazardous Waste Landfills (Draft), prepared for EPA-RRRL, Cincinnati, Ohio, 1987.

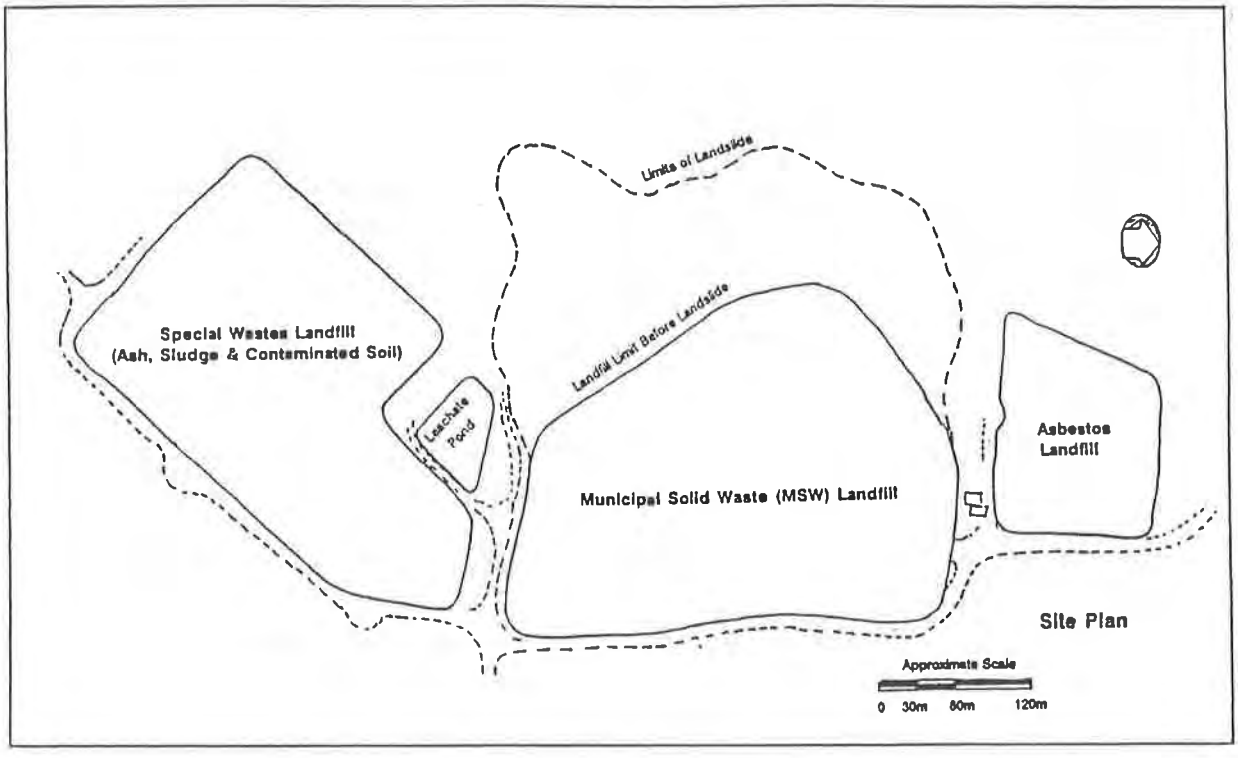

FIGURE 1: LANDFILL BOUNDARIES AFTER FAILURE

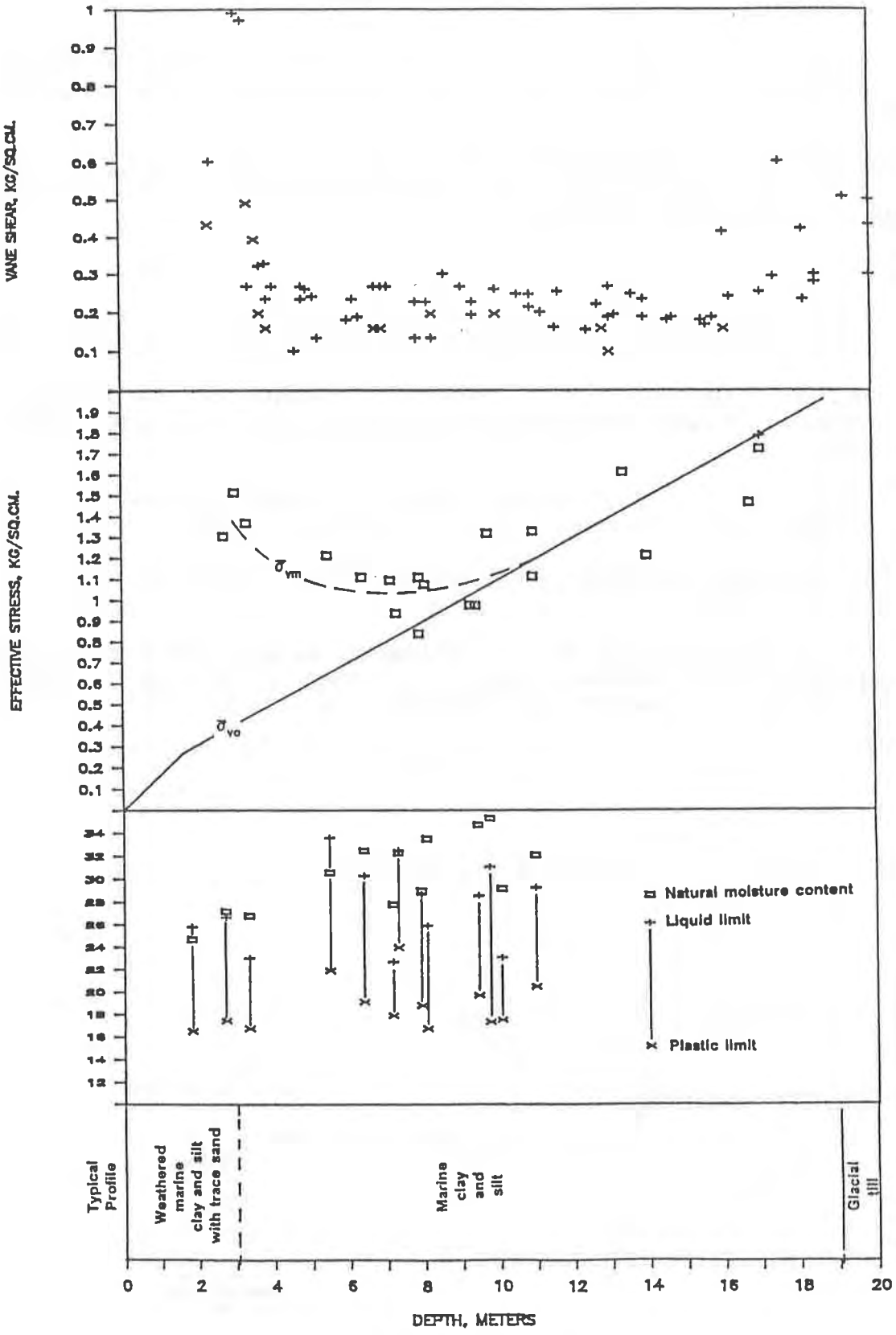

FIGURE 2: SOIL CONDITIONS AT NORRIDGEWOCK , MAINE

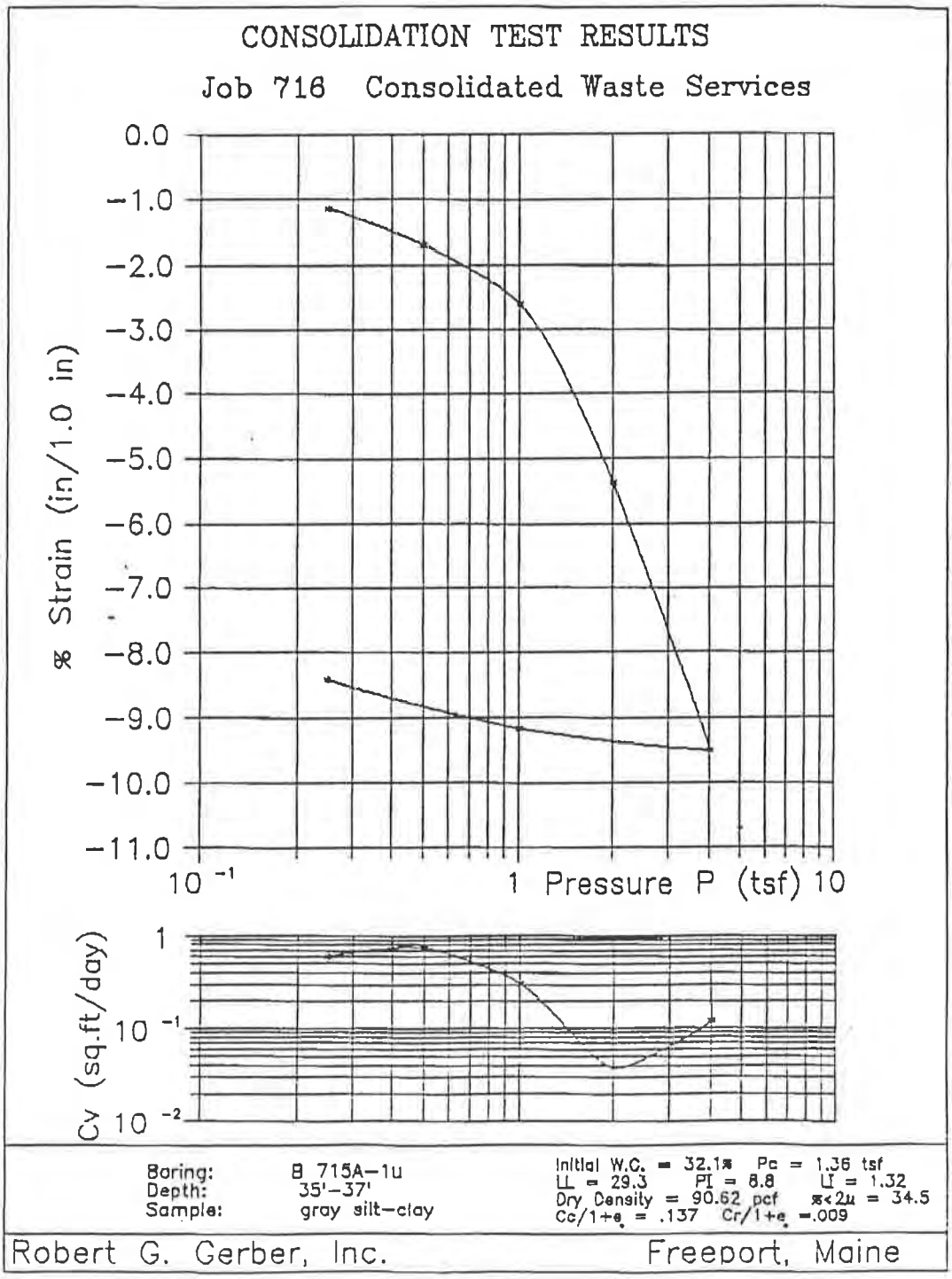

FIGURE 3: CONSOLIDATION DATA: SUBGRADE SOILS

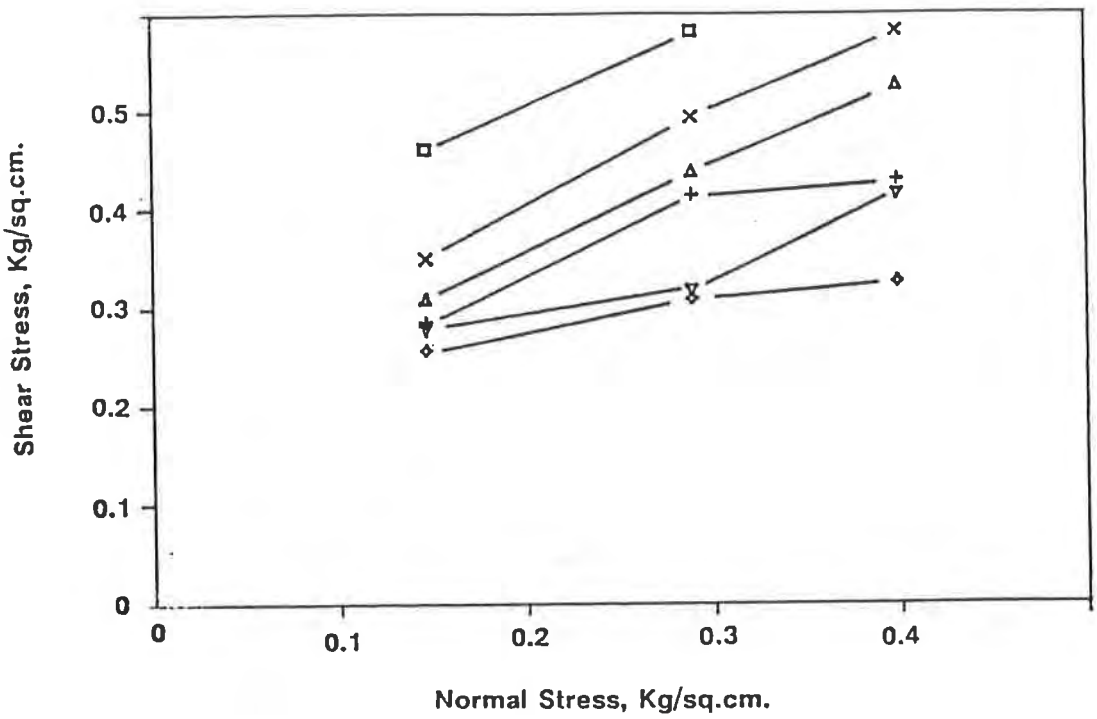

FIGURE 4: MSW DIRECT SHEAR TEST RESULTS

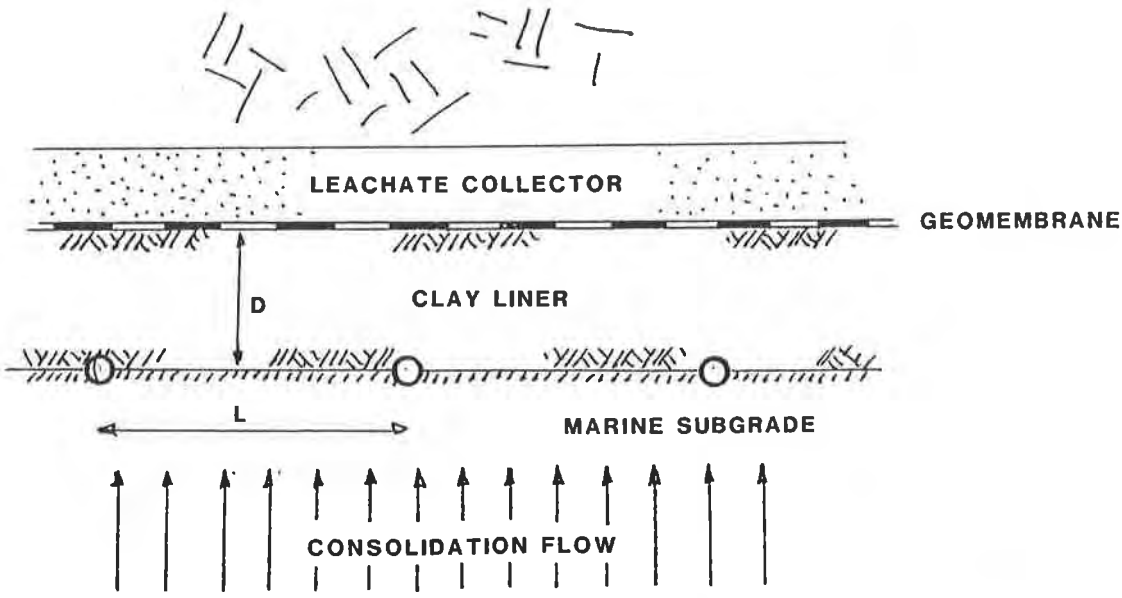

FIGURE 5: SUB-LINER CONSOLIDATION DRAINS

TECHNICAL ADVANCES / TESTING & RESEARCH

Results of Laboratory Tests on a Geotextile/Bentonite Liner Material

Hsin-Yu Shan
University of Texas - Austin, USA
David E. Daniel
University of Texas - Austin, USA

ABSTRACT

Laboratory tests were performed to evaluate the hydraulic properties and shearing characteristics of a bentonitic blanket. The material investigated contains sodium bentonite sandwiched between two geotextiles. The material was found to have an angle of internal friction of about 10° when the bentonite was fully hydrated and sheared under drained conditions. The hydraulic conductivity to water was sensitive to the effective confining stress applied to the bentonite but was equal to approximately 2×10^{-11} m/s (2×10^{-9} cm/s) at a low confining stress and 2×10^{-12} m/s (2×10^{-10} cm/s) at a higher confining stress. The material was found to be somewhat self healing if punctured, desiccated, or frozen under controlled laboratory conditions. The material was attacked by some chemicals, but hydration with water prior to permeation by organic chemicals led to much lower hydraulic conductivity than permeation of unhydrated material directly by organic compounds. Tests show that the material must be hydrated with water, and not concentrated organic chemicals, in order to achieve low hydraulic conductivity.

INTRODUCTION

Compacted soil is widely used as a low-permeability component of liner and cover systems for waste-disposal units. Recently, thin bentonitic blankets have been suggested, and in some cases used, as an alternative material to compacted soil. To date, the main use of bentonitic blankets has been to back up a geomembrane so that the geomembrane and bentonitic blanket will function together as a composite liner (Schubert, 1987). The advantages of composite materials in minimizing leakage rates through liners are discussed by Giroud and Bonaparte (1989).

The research described in this paper was conducted to develop a base of scientific and engineering data on one bentonitic blanket material. Tests were

performed to evaluate: (1) shear strength; (2) hydraulic conductivity to water; (3) hydraulic conductivity to chemicals; and (4) effect of wet/dry and freeze/thaw cycles upon hydraulic conductivity.

BENTONITIC BLANKET INVESTIGATED

The Material. The bentonitic blanket that was selected for testing was Claymax®, which is manufactured by the James Clem Corporation, Chicago, Illinois. This material was selected because more information and experience existed for it than other bentonitic blanket materials. Claymax® consists of approximately 1 lb/ft^2 (4.9 kg/m^2) of sodium bentonite sandwiched between a slit-film, woven, polypropylene geotextile containing nylon fibers needlepunched into the geotextile and a very light, open-weave, spun-lace polyester backing that helps to hold the bentonite in place. The primary polypropylene geotextile typically weighs 3 to 6 oz/yd^2 (102 to 204 g/m^2) while the backing weighs approximately 3/4 oz/yd^2 (25 g/m^2). Other geotextiles can be substituted for special designs. A non-toxic, water-soluble, sodium-enriched, organic adhesive is used to bond the bentonite to the geotextiles. Claymax® is manufactured in sheets that measure approximately 4 m in width and 30 m in length. The sheets are placed on rolls and stored at the factory prior to delivery.

To install this material in the field, the manufacturer recommends placing the bentonitic blanket on a smooth subgrade and overlapping adjacent sheets by at least 6 in. (152 mm). The material is said to be self sealing at the overlaps: the bentonite oozes out of the openings in the geotextiles when the bentonite is hydrated, and a seal forms.

Advantages and Disadvantages of Bentonitic Blankets. Bentonitic blankets have several potential advantages over compacted soil liners: installation is simpler; less space is occupied by the liner (leaving more space for waste); repair is simpler; installation can be accomplished with light-weight equipment (soil liners are compacted with heavy rollers, which can damage underlying geosynthetics); once a material is thoroughly characterized, there should be no need to re-characterize it (each compacted soil liner material is different and must be individually studied and characterized); bentonitic blankets are not as vulnerable to desiccation as wet, compacted clays during and immediately after installation; and the cost of a bentonite blanket is more predictable than the cost of a compacted soil liner.

The main disadvantages of bentonitic blankets are that the material must be properly covered before it hydrates (rainstorms during installation can prematurely hydrate the material before it is covered), experience with the material is limited, independent test data and analysis are limited, the shear strength of hydrated

bentonite is low, the thinness of the blankets makes them vulnerable to damage by puncture, the bentonite may be attacked by chemicals, and the thin blankets may be vulnerable to damage if exposed to wet/dry or freeze/thaw cycles. Despite these concerns, the advantages of bentonite blankets are compelling, and the materials deserve careful testing and analysis by the scientific and engineering communities.

MATERIALS AND METHODS

Materials. Ordinary Claymax® supplied by the manufacturer was used in this research. The polypropylene geotextile weighed approximately 4 oz/yd^2 (136 g/m^2). Test specimens were cut from larger sheets at randomly-selected locations.

Methods. The shear strength of the bentonitic blanket was evaluated with the direct shear apparatus. Circular specimens with a diameter of 60 mm were sheared through the bentonite under different normal (vertical) loads. Dry test specimens were sheared at a strain rate of 16 mm/hr. Hydrated materials were soaked at the desired normal load until vertical deformation ceased (about 2 to 3 weeks) and were then sheared at a rate of 0.02 mm/hr, which produced failure in 3 to 5 days.

Hydraulic conductivity tests were performed using flexible-wall permeameters and the general procedures outlined by Daniel et al. (1984). The test specimens were cut out from larger pieces of the material with a sharp knife. Except for two tests, the specimens were all 152 mm (4 in.) in diameter. Two tests were performed on specimens that measured 305 mm (12 in.) in diameter. Rigid porous discs were placed above and below each test specimen, with a sheet of filter paper separating the test specimen from the porous disc. The specimens were confined with a latex membrane. In addition, the specimens that were permeated with chemicals other than water were wrapped in Teflon® tape prior to placement of the latex membrane over the Teflon®. The test specimens were permeated with either distilled water, tap water, or various chemicals. All tests with chemicals other than water were performed on test specimens that had first been fully hydrated at the applied compressive stress with tap water (the hydraulic conductivity to tap water was determined prior to introducing a chemical so that the hydraulic conductivity with the chemical could be compared directly with the hydraulic conductivity for water). Most test specimens were not back-pressure saturated (because the primary interest on this research project was use of bentonitic materials as a low-hydraulic-conductivity barrier material in covers, which are not likely to ever become 100 percent saturated with water). However, some comparative tests were performed with backpressure saturation. When backpressure was used, the backpressure was 275 kPa (40 psi). In all tests, with or without backpressure, permeation continued until rates of inflow and outflow were equal (within ± 5%) and the hydraulic conductivity ceased to change with time.

Tests were falling-head tests, although the drop in head was less than 10% of the original head. The tests were performed keeping the hydraulic gradient as small as possible, keeping in mind the need to utilize a hydraulic gradient that was large enough to produce sufficient flow so that the tests could be completed in a few months time. A hydraulic gradient of approximately 20 was used for tests with water, and a gradient of 80 to 100 was used for permeant liquids other than water. Hydraulic conductivity was calculated utilizing the final thickness of the specimen, which was determined by constantly monitoring the thickness of the bentonitic blanket with a cathetometer and by checking the thickness when the test was complete and the apparatus dismantled. Test specimens were permeated at different levels of effective stress. Unless otherwise noted, the effective stress was 14 kPa for tests with water and 35 kPa for tests with chemicals other than water.

Some test specimens were artificially "punctured" and then hydrated and permeated to evaluate the effect of the puncture. The circular punctures were made by cutting three holes in the pattern shown in Fig. 1 through the test specimen. Some test specimens were fully hydrated and then desiccated. Desiccation was accomplished by air drying the material with a vertical stress of about 1 kPa acting to keep the material from shrinking as a block. (Without the small vertical stress, the wet specimens shrank during drying as a block to a smaller, uncracked, circular specimen; with the small vertical stress, the diameter decreased only slightly during desiccation, and large cracks developed in the bentonite during drying).

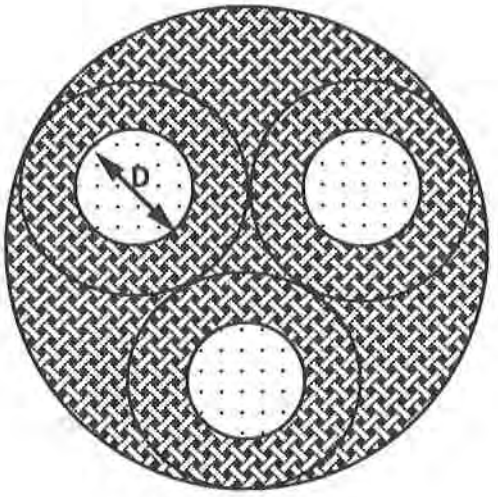

Figure 1. Pattern of the Holes Cut for Tests to Study the Effect of Punctures.

Some fully hydrated test specimens were permeated, then removed from the permeameter and frozen, and later thawed and repermeated. The specimens were frozen three-dimensionally by placing a disc-shaped test specimen in a freezer (-10° C) for approximately 24 hours. Thawing was accomplished by removing the specimen from the freezer and allowing it to thaw at room temperature (approximately 22° C).

Swelling tests were performed using a Wykam-Farrance back-loading oedometer. Each test specimen was cut to a diameter of 50 mm and the original thickness was measured. A constant vertical stress was applied to each test specimen. When the height of the specimen ceased to decrease after the vertical stress was applied (usually after just a few minutes), water was introduced into the cell and the specimen was allowed to compress or swell freely at the constant vertical stress. Changes in height were monitored continuously until the height ceased to change. The final swell or compression for a given vertical stress was recorded.

RESULTS OF SWELL TESTS

The results of swell tests are shown in Fig. 2. Under low overburden pressure, the thickness increased substantially when the bentonitic blanket was hydrated. No change in the thickness of the specimen occurred when the overburden pressure was approximately 140 kPa (3000 psf). At vertical stresses > 140 kPa, the material compressed when it was soaked. Normally, one would expect to measure a much higher swelling pressure for compacted or consolidated bentonite. However, this material is constructed from loosely placed bentonite granules. Hydration at a stress > 140 kPa evidently causes the granules to compact, which offsets swelling of the granules themselves.

RESULTS OF DIRECT SHEAR TESTS

The Mohr-Coulomb diagrams for dry and hydrated bentonitic blanket specimens are shown in Figs. 3 and 4, respectively. The failure envelopes were determined by linear regression. For dry specimens, the apparent cohesion was 26 kPa and the angle of friction was 28°. For hydrated specimens, the apparent cohesion was 4 kPa and the angle of friction was 9°. The failure envelope for hydrated specimens may be curved at low normal stress and the actual effective cohesion may be essentially zero. The manufacturer reports that unpublished test results typically indicate an angle of internal friction of about 10 to 15° for the hydrated material sheared under drained conditions.

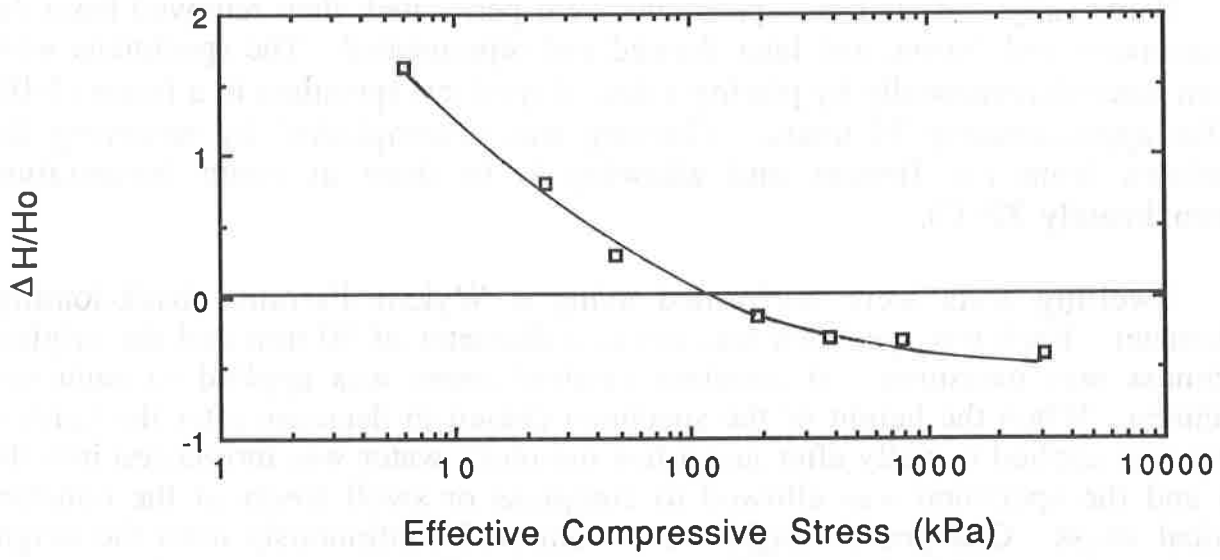

Figure 2. Height Change (ΔH) Vs. Effective Overburden Pressure from Swelling Tests (H_o = Height of Specimen before Testing)

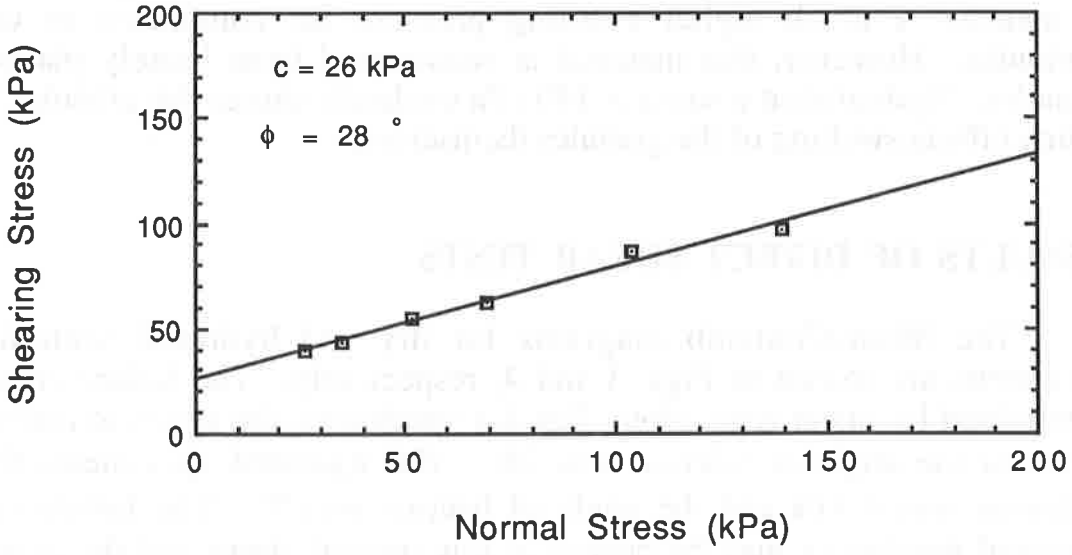

Figure 3. Mohr-Coulomb Diagram for Dry Test Specimens

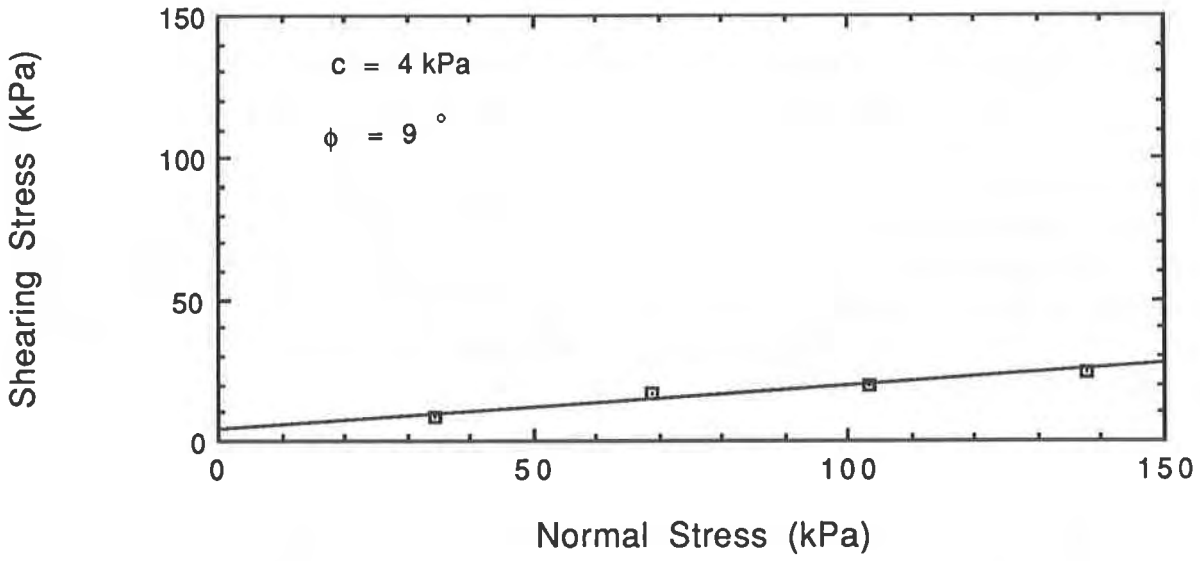

Figure 4. Mohr-Coulomb Diagram for Hydrated Test Specimens

The friction angle measured in this study is similar to the range of values reported by the manufacturer but near the low end of the range reported. An angle of internal friction of 9° is quite low, and the designer is cautioned to anchor properly this type of material when it is placed on slopes approaching or exceeding 9°.

RESULTS OF HYDRAULIC CONDUCTIVITY TESTS

Hydraulic Conductivity to Water. The relationship between hydraulic conductivity of the bentonitic blanket permeated with water and effective stress is shown in Fig. 5. At low effective stress, for example, 14 kPa (2 psi), the hydraulic conductivity was about 2×10^{-11} m/s (2×10^{-9} cm/s). When effective stress was increased to 138 kPa (20 psi), the hydraulic conductivity became as low as 3×10^{-12} m/s (3×10^{-10} cm/s). Given the order-of-magnitude variation in hydraulic conductivity shown in Fig. 5, it is very important that effective stress be reported along with the hydraulic conductivity value. This is especially true when one bentonitic blanket is compared with another; hydraulic conductivities measured at the same effective stress should be compared.

Effect of Punctures. The effects of punctures on the hydraulic conductivity of the bentonitic blanket are listed in Table 1. The test specimens were examined after dismantling the permeameters, and it was found that the bentonite had swelled

and fully filled the holes that were initially 12 and 25 mm in diameter. The bentonite paste that occupied the holes was not as thick as elsewhere, and thus the overall hydraulic conductivity of the test specimens increased slightly as a result. Two out of three of the 75 mm-diameter holes did not seal themselves and were left with openings of about 12 mm diameter. The measured hydraulic conductivity fluctuated but was as high as 2×10^{-6} m/s. The actual hydraulic conductivity was probably much higher; the hydraulic-conductivity apparatus was not designed to measure high hydraulic conductivity accurately, and the flow rates were limited by head losses in tubings, porous discs, and the protective filter paper that separated the test specimens from the porous discs.

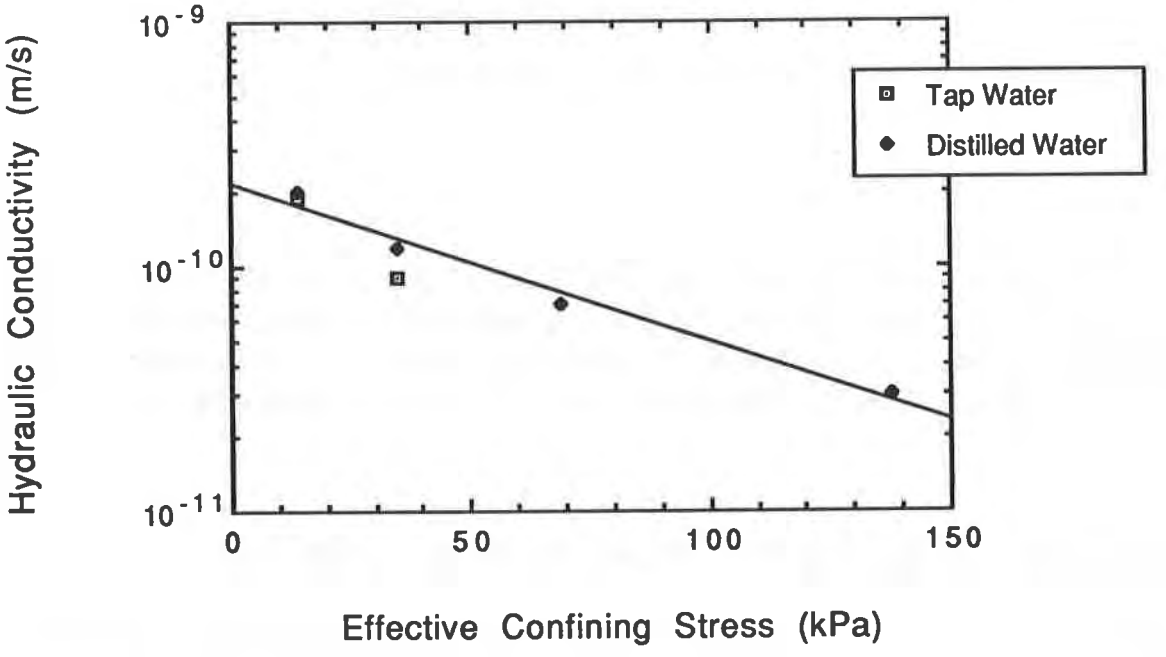

Figure 5. Relationship between Hydraulic Conductivity and Effective Confining Stress.

These tests demonstrate that under controlled laboratory test conditions, bentonitic blankets have some self-healing capability. Small holes or imperfections in the materials are probably of little consequence so long as the bentonite is not impeded from swelling to fill the holes once the material is hydrated.

Table 1 Effect of Punctures

Diameter of Punctures	Hydraulic Conductivity (m/s)
No punctures	2×10^{-11}
12 mm	3×10^{-11}
25 mm	5×10^{-11}
75 mm	$> 2 \times 10^{-6}$

Effect of Wet/Dry Cycles. The results of tests aimed at studying the effect of desiccation on hydraulic conductivity are summarized in Table 2. It was found that the hydraulic conductivity of the bentonitic blanket did not change after 3 wet/dry cycles. When the specimens had been desiccated, cracks as wide as about 2 mm were observed. A typical crack pattern is sketched in Fig. 6. The hydraulic conductivity was on the order of 1×10^{-6} m/s at the beginning of repermeation after drying. The cracks closed within a few hours and outflow stopped as bentonite hydrated. It was not until bentonite was fully hydrated that outflow started again.

Table 2 Effect of Wet/Dry Cycles

	Hydraulic Conductivity (m/s)			
Specimen	Original	After First Cycle	After Second Cycle	After Third Cycle
DS-1	1.7×10^{-11}	1.9×10^{-11}	1.7×10^{-11}	1.8×10^{-11}
DS-2	1.9×10^{-11}	1.7×10^{-11}	2.0×10^{-11}	-
DS-3	1.8×10^{-11}	1.7×10^{-11}	-	-

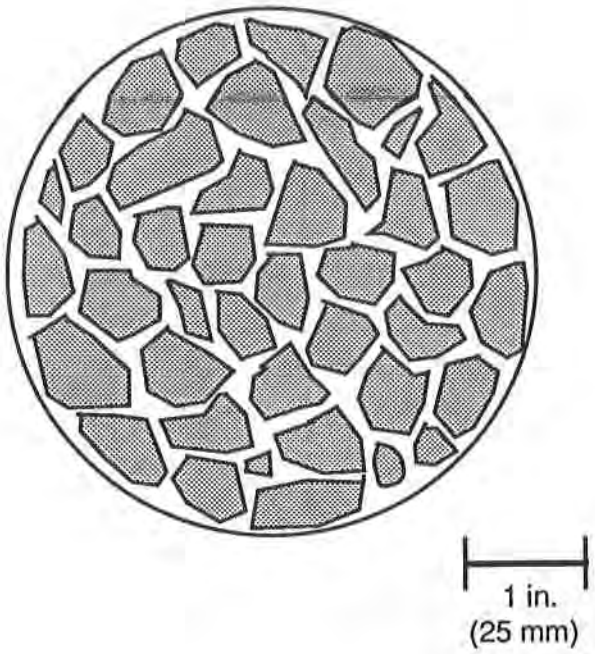

Figure 6. Typical Crack Pattern in Desiccated Specimens.

These tests, like the puncture tests described earlier, point to the self-healing capability of the bentonitic material. So long as small punctures or cracks did not fill with a permeable material, the bentonite self-healed when hydrated with water.

Effect of Freeze/Thaw Cycles. The hydraulic conductivity of the test specimen before freezing was 2×10^{-11} m/s. After five freeze/thaw cycles, the hydraulic conductivity of the specimen was found to still be 2×10^{-11} m/s. Under these conditions, freeze/thaw had no effect.

Hydraulic Conductivity to Chemicals. The results of hydraulic conductivity tests with various chemicals are summarized in Table 3. All of the test specimens were first permeated with tap water for about 1.5 months and were then permeated with the chemicals for about 6 months. The results of the control test with tap water as the permeant liquid are shown in Fig. 7. The hydraulic conductivity increased with time initially but stabilized at 7×10^{-11} m/s (7×10^{-9} cm/s) after 1 pore volume of flow. (A pore volume of flow is defined as the cumulative quantity of flow divided by the volume of water contained in the pores of the bentonitic material.)

Table 3 Results of Hydraulic Conductivity Tests with Different Chemicals

Liquids	Total Pore Volumes of Flow of Chemical	Hydraulic conductivity (m/s) To tap water	Final
Methanol	0.6	7×10^{-12}	3×10^{-12}
50% methanol	2.2	7×10^{-12}	9×10^{-12}
Heptane	0.2	7×10^{-12}	1×10^{-12}
Sulfuric acid	3.1	8×10^{-12}	6×10^{-13}
0.01 N $CaSO_4$	2.2	9×10^{-12}	1×10^{-11}
0.5 N $CaCl_2$	24.2	9×10^{-12}	8×10^{-11}
Tap water	2.7	-	7×10^{-12}

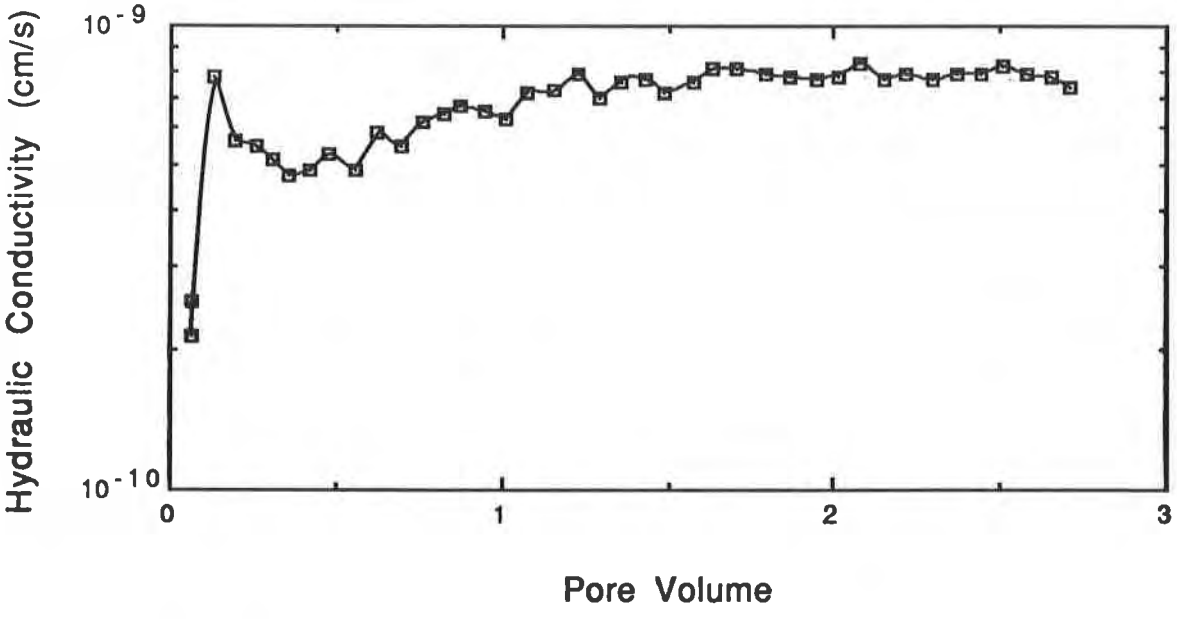

Figure 7. Hydraulic Conductivity to Tap Water

Pure methanol was chosen to represent a neutral, polar organic chemical. The hydraulic conductivity of the bentonitic blanket decreased to 3 x 10^{-12} m/s (3 x 10^{-10} cm/s) after 0.6 pore volumes of effluent fluid was collected (Fig. 8). The thickness of the specimen increased about 20% after the permeant liquid had been switched to pure methanol. The result was contradictory to the findings of most other investigators (Brown and Anderson, 1983; Foreman and Daniel, 1987; Uppot and Stephenson, 1989) who found that methanol increased the hydraulic conductivity of clayey soils. However, Fernandez and Quigley (1988) found that the hydraulic conductivity of their compacted clay sample decreased when permeated with pure methanol in flexible-wall permeameters. Uppot and Stephenson (1989) found that the hydraulic conductivity of kaolinite and Mg-montmorillonite decreased during the first pore volume of flow when permeated with pure methanol. Since less than 1 pore volume of methanol passed through the test specimen, it is possible that hydraulic conductivity of the bentonitic blanket would have increased had there been more flow.

The hydraulic conductivity of the bentonitic blanket to 50% methanol solution was found to be almost the same as that to water (Fig. 9). Bowders and Daniel (1987) observed the same results from kaolinite and illite-chlorite permeated with 50% methanol.

Heptane was selected as a representative neutral, nonpolar organic. As recommended by Foreman and Daniel (1986) the test specimen was permeated with pure methanol before introducing heptane into the specimen to avoid surface-tension exclusion of the heptane from soil. As shown in Fig. 10, heptane was introduced into the specimen after it had been permeated with 0.44 pore volumes of pure methanol. The hydraulic conductivity was as low as 1 x 10^{-12} m/s (1 x 10^{-10} cm/s) and only 0.22 pore volumes of effluent fluid was collected after 3 months of permeation with heptane.

The hydraulic conductivity of the bentonitic blanket to sulfuric acid went through changes that are typical for soils permeated with inorganic acids. After sulfuric acid was introduced into the specimen, the outflow rate, Q_{out}, became larger than the inflow rate, Q_{in} (Fig. 11). Water was being driven out of the material, and thickness of the specimen decreased. The hydraulic conductivity increased slightly to 2 x 10^{-11} m/s (2 x 10^{-9} cm/s) in the initial stages of acid permeation (Fig. 12). The effluent liquid was brownish yellow, and a small amount of solids was present, which provided evidence of dissolutioning. Later, probably because precipitates clogged the pores, the hydraulic conductivity decreased to as low as 6 x 10^{-13} m/s (6 x 10^{-11} cm/s). Also, the pH of the effluent liquid decreased continuously during the test (Fig. 13). Had the test continued to very high pore volumes of flow to exhaust the buffering capacity of the soil, the hydraulic conductivity probably would have eventually increased.

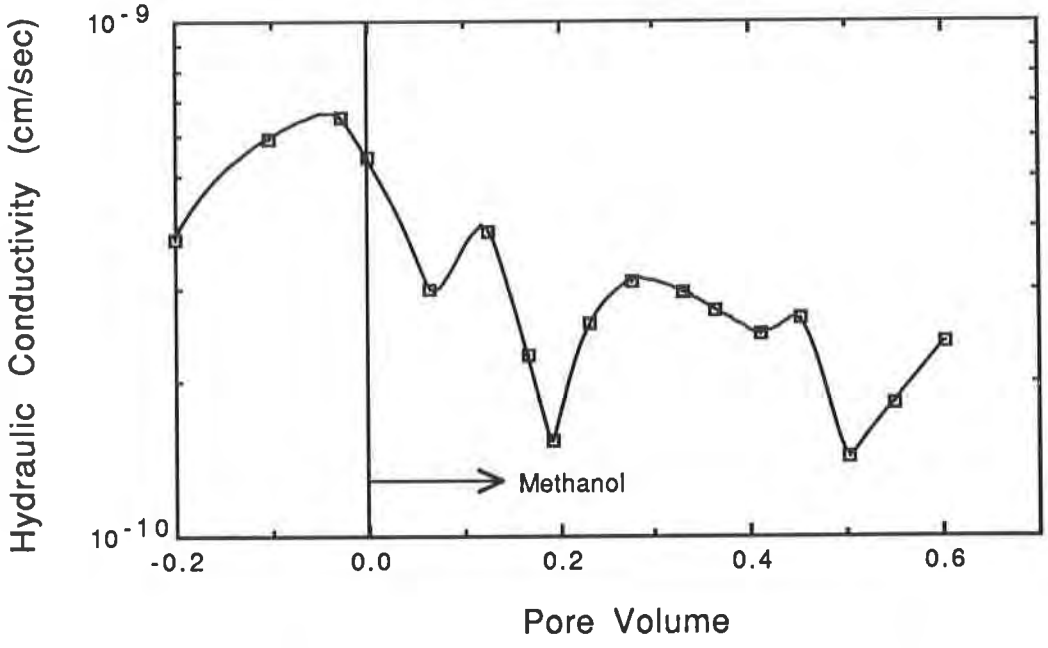

Figure 8. Hydraulic Conductivity to Pure Methanol

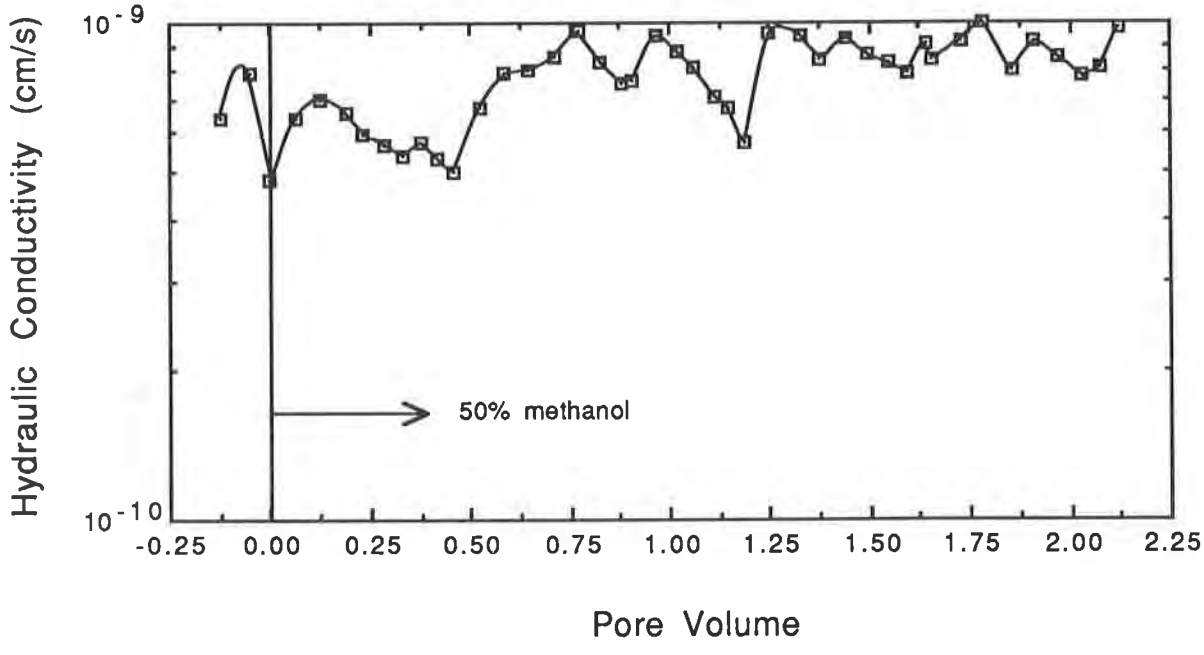

Figure 9. Hydraulic Conductivity to 50% Methanol/Water Solution

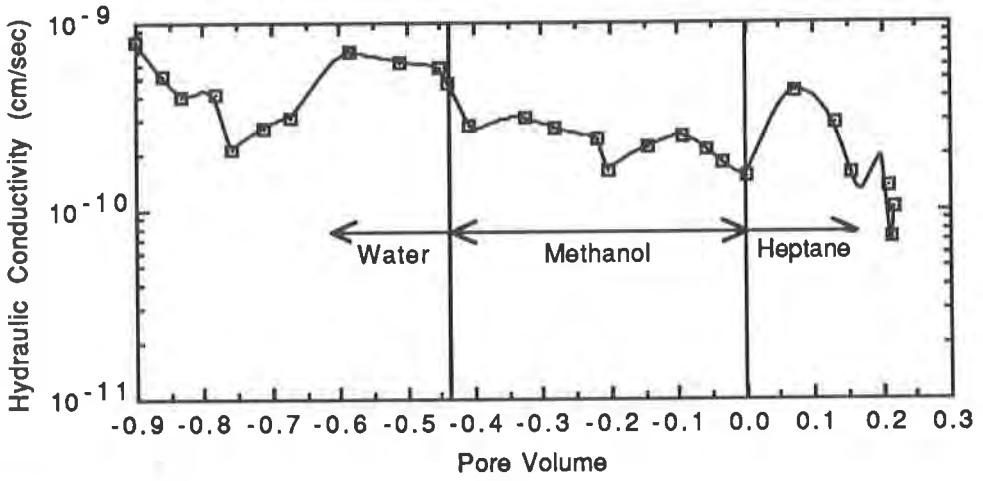

Figure 10. Hydraulic Conductivity to Heptane

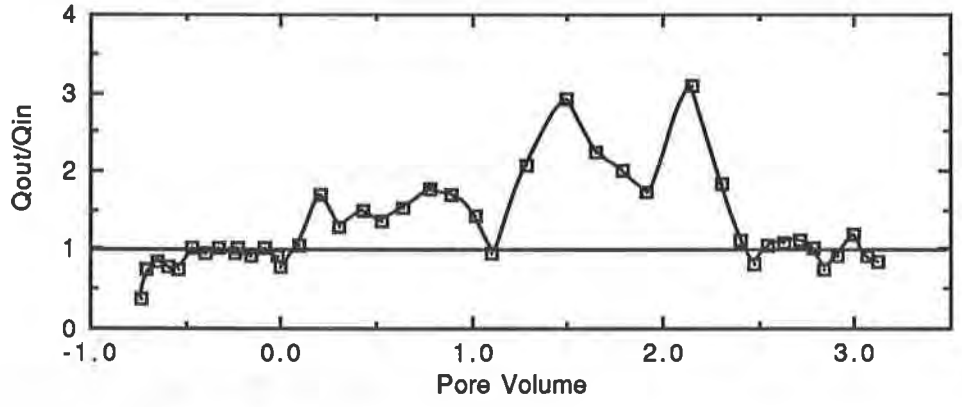

Figure 11. Variation of Outflow/Inflow Ratio from Test with Sulfuric Acid (pH=1.5)

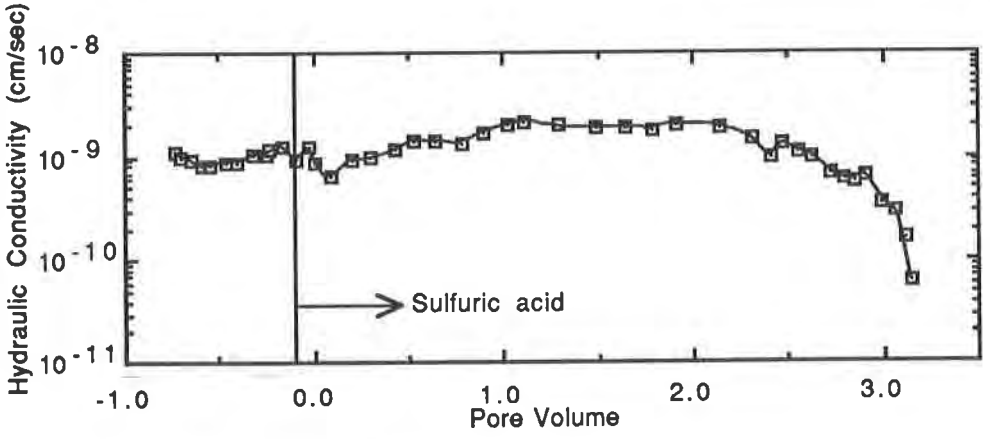

Figure 12. Hydraulic Conductivity to Sulfuric Acid (pH=1.5)

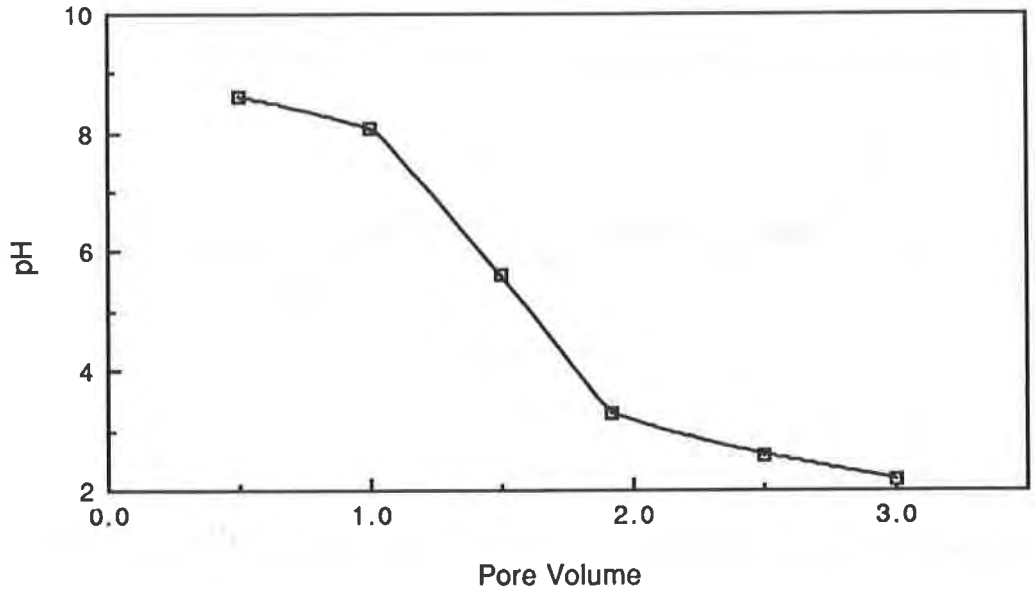

Figure 13. pH Value of Effluent Liquid from Test with Sulfuric Acid

The 0.01 N calcium sulfate solution had little influence on the hydraulic conductivity of the bentonitic blanket. The final value of hydraulic conductivity was found to be 1 x 10^{-11} m/s (Fig. 14) and there was little change over time. During the test period, a large amount of gas was produced, probably by anaerobic bacteria. Gas occupied the pore spaces of the porous disk at the effluent end and impeded the flow. The tubings were repeatedly flushed to drive to gas out. The permeant was switched to 0.01 N calcium chloride solution in an attempt to minimize the problem of the gas formation from the production of H_2S. However, the problem remained. The periodic generation and removal of gas was probably the cause of the fluctuations shown in Fig. 14.

The hydraulic conductivity of the test specimen permeated with 0.5 N calcium chloride solution increased about an order of magnitude to 8 x 10^{-11} m/s (Fig. 15). The outflow rate was larger than inflow rate throughout the test and especially between 0 and 2 pore volumes of flow (Fig. 16). The thickness of the specimen decreased 46%. It appears that calcium replaced sodium, which reduced the thickness of adsorbed water layer and caused the bentonite to shrink.

It should to be mentioned that during the period in which the specimens were permeated with water, although no backpressure was applied, the specimens took in water from both the influent and effluent ends. There was no outflow for approximately four weeks. The same phenomenon was also observed by Edil and Erickson (1985) when they permeated specimens of bentonite-sand mixture. They

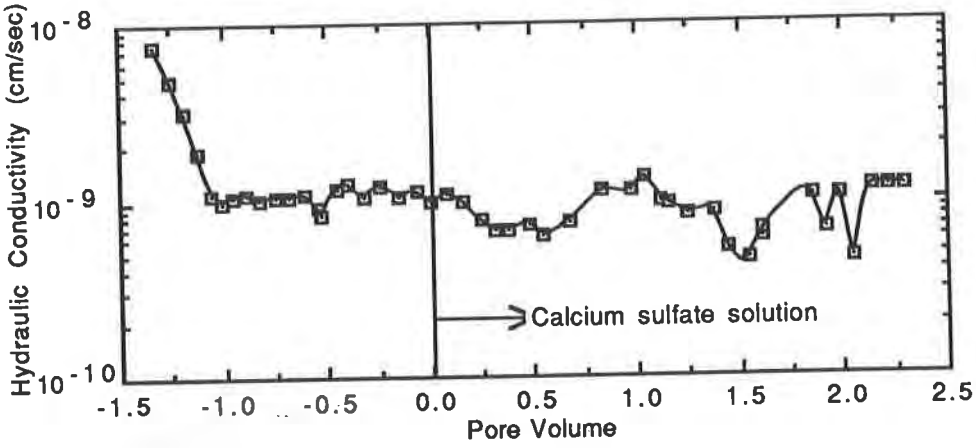

Figure 14. Hydraulic Conductivity to 0.01 N Calcium Sulfate Solution

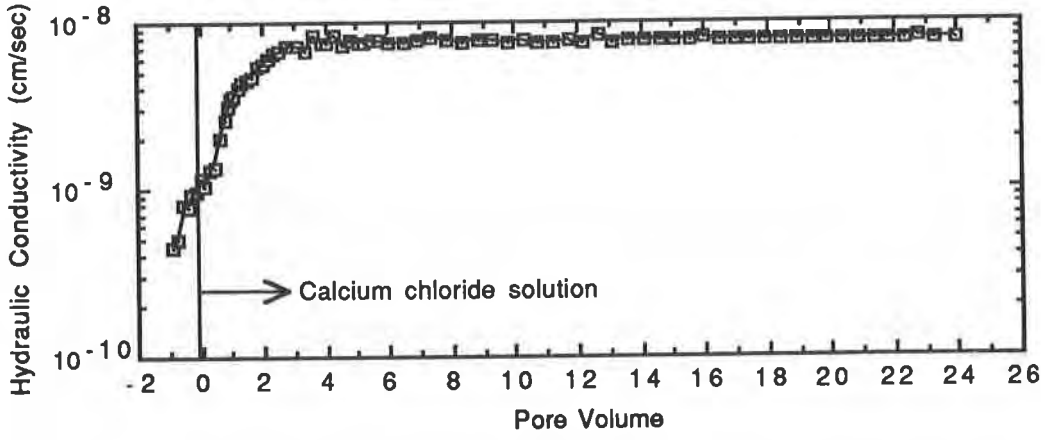

Figure 15. Hydraulic Conductivity to 0.5 N Calcium Chloride Solution

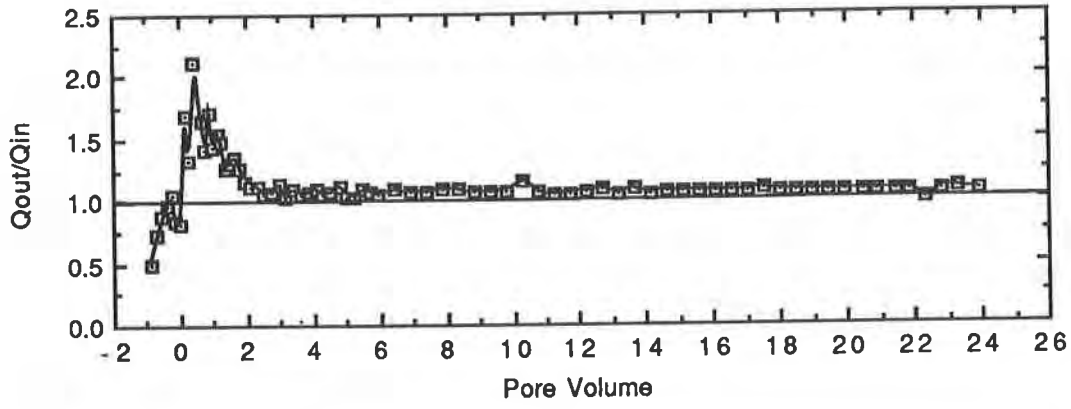

Figure 16. Variation of Outflow/Inflow Ratio from Test with 0.5 N Calcium Sulfate Solution

point out that highly active bentonite may have a threshold water content below which all water entering the specimen is absorbed.

It should also be mentioned that much different results were obtained when dry test specimens were permeated directly with concentrated organic chemicals, like methnaol and heptane, rather than prehydrated with water prior to permeation. When the bentonitic blanket was exposed directly to a concentrated organic chemical, the material did not attain a hydraulic conductivity below 1 x 10^{-7} m/s (1 x 10^{-5} cm/s) even after 10 pore volumes of flow. The bentonite must be hydrated with water prior to exposure to concentrated organic liquids in order to achieve low hydraulic conductivity. For bentonitic blankets used in liner systems, the ability of the material to hydrate and achieve low hydraulic conductivity when exposed to leachate should be evaluated.

CONCLUSIONS

In this study, several characteristics of a bentonitic blanket (Claymax®) were investigated. The hydraulic conductivity to water was found to be 2 x 10^{-11} m/s at low confining stress (14 kPa) and 3 x 10^{-12} m/s at a confining stress at 138 kPa.

The material swells at pressures ≤ 140 kPa. When fully hydrated and sheared under drained conditions, the angle of internal friction was found to be approximately 9°.

The material was found to be capable of sealing punctures of diameters up to 25 mm with only a slight increase in hydraulic conductivity. Desiccation cracks formed when saturated material was dried, but when the material was rewetted, the cracks closed and the hydraulic conductivity returned to the original, low value. Hydraulic conductivity of the material appeared to be not affected by freeze/thaw action.

Results from hydraulic conductivity tests with chemicals showed that a diluted organic chemical did not affect the hydraulic conductivity of the material. Pure organic chemicals and an inorganic acid caused decreases in hydraulic conductivities, but the period of testing was probably too short to allow observation of the potential long-term damaging effects of these chemicals. When the material was permeated with 0.5 N calcium chloride solution, an order of magnitude increase in hydraulic conductivity occurred and the material underwent shrinkage. The increase in hydraulic conductivity and bulk shrinkage were evidently caused by the replacement of sodium ions in the bentonite with calcium ions. All tests with chemicals were performed on test specimens that had been pre-soaked with tap water.

The tests described in this paper show that thin bentonitic blankets have low hydraulic conductivity to water, resist chemical attack when prehydrated with water, and have outstanding self-healing characteristics. Low shear strength of the hydrated material was observed. Clearly these types of materials have some desirable characteristics and warrant further testing and evaluation.

ACKNOWLEDGEMENTS

The project has been funded in part with federal funds as part of the program of the Gulf Coast Hazardous Substance Research Center (GCHSRC) which is supported under cooperative agreement R815197 with the U.S. EPA and in part from the Texas Hazardous Waste Research Center. The authors thank the director of the GCHSRC, Mr. William Cawley, for his support. The contents do not necessarily reflect the views and policies of the GCHSRC, the U.S. EPA, or the State of Texas, nor does the mention of trade names or commercial products constitute endorsement or recommendation for use. The authors also thank William and Martin Simpson of the James Clem Corporation for providing the test material and information on Claymax®.

REFERENCES

Bowders, J. J., and Daniel, D. E. (1987), *Journal of Geotechnical Engineering,* ASCE, Vol. 113, No. 12, pp. 1432-1448.

Brown, K. W. and Anderson, D. (1983), "Effects of Organic Solvents on the Permeability of Clay Soils," U.S. EPA, EPA-600/9-83-016, Environmental Protection Agency, Cincinnati, Ohio.

Daniel, D. E., Trautwein, S. J., Boynton, S. S., and Foreman, D. E. (1984), "Permeability Testing with Flexible-Wall Permeameters," *Geotechnical Testing Journal*, Vol. 7, No. 3, pp. 113-122.

Edil, T. B., and Erickson, A. E. (1985), "Procedure and Equipment Factors Affecting Permeability Testing of a Bentonite-Sand Liner Material," in *Hydraulic Barriers in Soil and Rock, ASTM STP 874,* American Society for Testing and Materials, Philadelphia, pp. 155-170.

Fernandez, F., and Quigley, R. M. (1988), *Canadian Geotechnical Journal*, No. 25, pp. 582-589.

Foreman, E. F., and Daniel, D. E. (1986), *Journal of Geotechnical Engineering,* ASCE, Vol. 112, No. 7, pp. 669-681.

Giroud, J. P., and Bonaparte, R. (1989), "Leakage through Liners Constructed with Geomembranes - Part II. Composite Liners," *Geotextiles and Geomembranes,* **8**, pp. 71-111.

Schubert, W. R. (1987), "Bentonite Matting in Composite Lining System," in *Geotechnical Practice for Waste Disposal '87*, R. D. Woods (ed), American Society of Civil Engineers, New York, pp. 784-796

Uppot, J. O., and Stepheson, R. W. (1989), *Journal of Geotechnical Engineering,* ASCE, Vol. 115, No. 1, pp. 115-131.

Load Test of a Large-Scale Geotextile-Reinforced Retaining Wall

John W. Billiard
Canonie Environmental Services Corp., USA
J. T. H. Wu
University of Colorado at Denver, USA

ABSTRACT

A controlled load test was performed to investigate the performance of a geotextile-reinforced retaining wall until a failure state was reached. A five-layer geotextile-reinforced retaining wall 5 feet 1 inch high was designed using the Forest Service method and erected in the laboratory using a typical sequential construction technique. The test wall was loaded by applying incremental vertical surcharge loads on the top surface until excessive deformation of the facing had occurred.

To provide insight into the behavior of the retaining wall under load, the wall was instrumented to measure the strain of the geotextile, deflection of the top surface and vertical wall face, and movement of the soil mass within the interior of the wall. Strain was measured by 20 strain gages attached along the embedded length of the geotextile layers. External displacements of the wall were measured with dial indicators, and internal movement was monitored by tracing the displacement of the soil mass. A complete description of the measurement techniques is provided in this paper.

Results of the controlled test provided valuable data for validation of numerical analysis of geotextile-reinforced retaining wall behavior under load. In addition, the test also provided insight to the validity of design assumptions and the ultimate factor of safety associated with the Forest Service design method.

INTRODUCTION

This paper describes the design, construction, and load test performed on a 5-foot 1-inch-tall geotextile-reinforced retaining wall. The Forest Service design method was used to obtain the test wall geometry. The five-layer test wall was constructed inside a test apparatus designed for the study of earth structures under plane strain conditions. An incremental surcharge load was exerted over the top surface to an equivalent of more than 25 feet of fill. Deformations as a result of the load were measured using strain gages and deflection instrumentation. Results of the load test are presented herein to

provide insight on the behavior of a geotextile-reinforced earth test wall under load.

DESIGN OF THE TEST WALL

The Forest Service design method, Steward, et al. (1983), was incorporated for this study of a geotextile reinforced earth retaining wall. The design method, chosen for its popularity in practice, uses an assumed active Rankine failure plane in the determination of the reinforcement lengths. The method provides the layer thicknesses, given a factor of safety in rupture, or conversely, provides a factor of safety against rupture, given a layer thickness.

The design of a geotextile-reinforced earth wall involves the calculation of three internal safety factors. These include: 1) rupture; 2) embedment pullout; and 3) overlap pullout. External safety factors include bearing capacity, sliding, overturning, and overall performance. As this test wall was constructed in a confined apparatus resting on a rigid floor, only internal safety factors were considered for the design.

The test wall geometry is illustrated in Figure 1. This test wall was designed to have a rupture factor of safety of 1.0 at 850 pounds per square foot (psf) of uniform surcharge. In other words, this test wall was designed to fail by rupture at a surcharge greater than 850 psf. With the given safety factor of 1.0 for rupture, the layer spacings were calculated so that every layer had an equal opportunity for rupture failure at 850 psf. The layer thicknesses used in the test wall varied from 0.85 foot thick at the bottom (layer number 5) to 1.24 feet thick at the top (layer number 1). No factor of safety was used to reduce the allowable fabric strength.

To restrain an undesirable fabric pullout failure mode, the factor of safety in embedment and overlap pullout was greater than 1.0 at 850 psf surcharge for all layers. With 3-foot-long embedment lengths beyond the assumed Rankine failure plane, and 1.5-foot-long overlap lengths, the factor of safety for pullout at a uniform pressure of 850 psf for layers 1, 2, 3, 4, and 5 were calculated to be 2.5, 5.3, 8.2, 11.1, and 14.2, respectively.

DESCRIPTION OF TEST APPARATUS

Steel Box - As shown in Figure 1, the 5-foot 1-inch-high test wall was constructed inside a steel-supported test apparatus. The overall interior dimensions of the box were 5 feet 6 inches tall by 2 feet 6 inches wide by 8 feet long. Each side of the box was constructed with standard 3-inch steel channels laterally supported against bending by standard 2-inch steel angles. Lateral movement of the side walls was restrained by using standard 2-inch angles bolted across the top and ends of the box. Four 3/8-inch thread rods were bolted to the bottom of the vertical channels to restrain lateral movement at the bottom of the box.

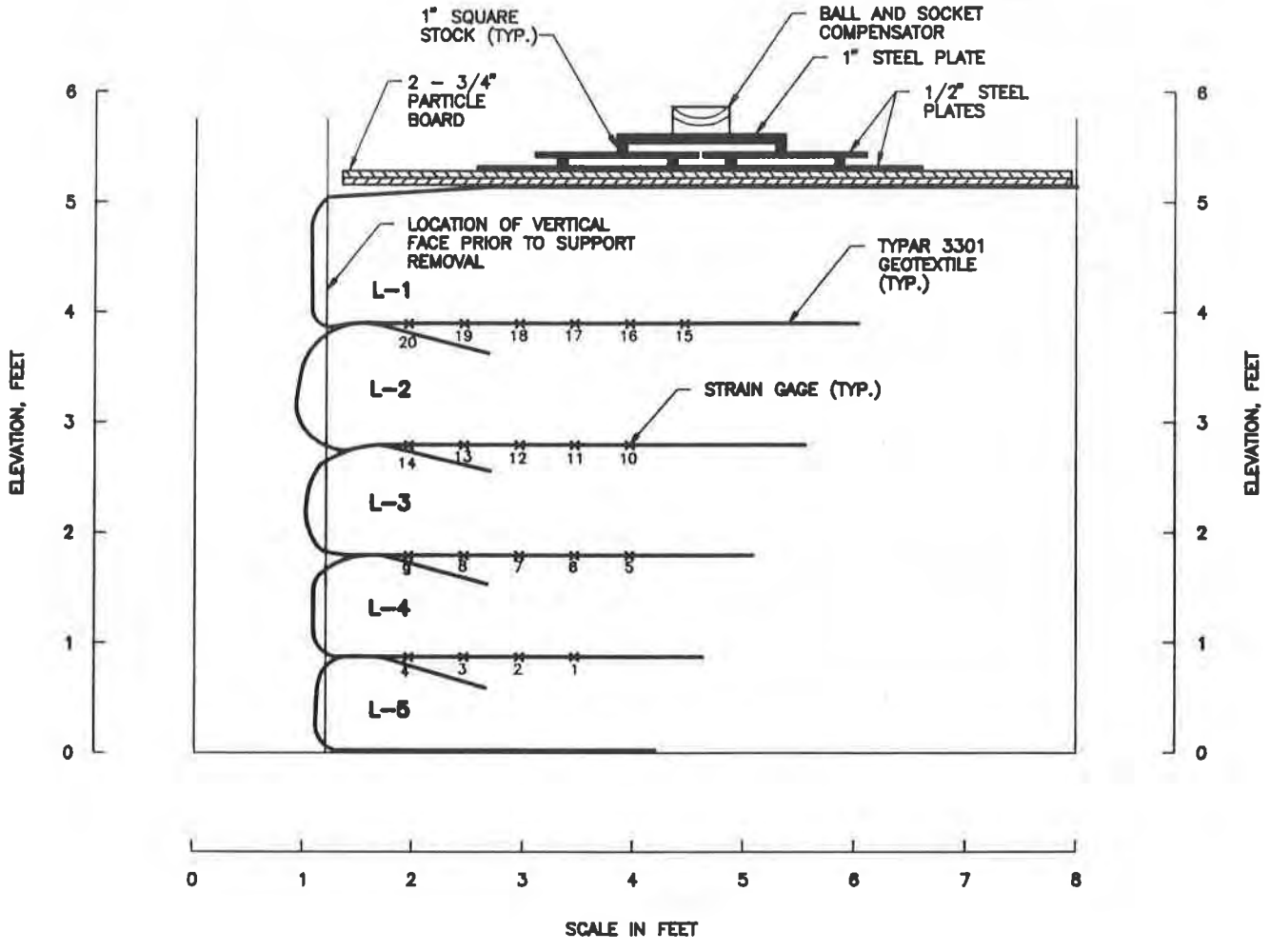

FIGURE 1: TEST WALL GEOMETRY AS CONSTRUCTED

Acrylic Plastic Walls - Acrylic plastic sheets 1/2 inch thick were fastened to the interior sides of the steel walls. A limited number of bolt connections were used in an effort to prevent the cracking of the plastic from stress concentrations during the loading and to ensure a smooth wall surface.

Teflon Sheeting - Two layers of teflon sheets, 3 mills (0.003-inch) thick by 12 inches wide were placed along the full interior of the acrylic sides. This was accomplished to eliminate, as much as possible, any side friction between the soil and acrylic. The interface side wall friction, associated with the soil/teflon/acrylic interface at the side walls, had a friction angle of about 5 degrees (measured in a direct shear apparatus). Elimination of side friction was required to maintain the idealized plane-strain condition crucial for simulation of a very wide test wall.

Loading Frame - The test wall loading frame consisted of two 4-inch-diameter steel posts placed to straddle the midpoint of the test wall and bolted to dead man connections in the laboratory floor. Each dead man mounted in the laboratory floor was capable of providing adequate vertical resistance for this test. A steel beam was bolted across the top of each post to provide a jacking point for the hydraulically induced load.

DESCRIPTION OF INSTRUMENTATION

Strain Measurement - Strain measurements at select points on the geotextile for the top four layers (layers 1, 2, 3, and 4) were obtained for each increment of load during the test. The measurements were made by attaching high elongation strain gages (+/- 20% strain) to the fabric by means of a unique non-standard method of attachment, Billiard (1989). A total of 20 strain gages were used in the test wall with a layout as shown in Figure 1.

The strain gages and method of attachment were calibrated prior to the load test in a planar tensile fabric pull test. Results of the pull test indicated that the strain gages read fabric strains accurately up to 10% tensile strain. Once mounted on the fabric, the gages were protected against degradation by soil particles. The exact methods used for the attachment and protection of the strain gages will be found in a subsequent paper to be published in the near future.

Exterior Lateral and Vertical Deflection Measurement - Seven dial indicators graduated to 0.001 inch were used to obtain deflection data at each load increment during the test. Two dial indicators were located at the top of the test wall to measure the vertical deflection at the front and back of the wall. Five dial indicators were used to measure the lateral deflection at the center of each of the five layers. Figures 2, 3, and 4 illustrate the deflections measured at surcharge pressures near the beginning, middle, and end of the test.

Side Wall Movement Grid - A grid network made up of yarn was placed against the interior side of one acrylic-faced wall prior to placement of fill. The yarn was placed an average of three inches center to center in the vertical and

horizontal planes. The grid was constructed to allow unrestricted movement of the soil mass throughout the test.

The grid could be easily seen through the acrylic plastic sheet after the construction of the test wall. The locations of key grid points were marked on the exterior of the acrylic wall by means of a marker pen. During the test, the movement of these intersections was traced using another pen. At the end of the test, the final locations of the specific points were marked, and the internal movement of the soil mass was traced.

MATERIAL PROPERTIES

The geotextile-reinforced earth wall was constructed using a low weight (2.9 ounce/square yard) spunbonded nonwoven polypropylene geotextile with a wide width tensile strength of 420 lbs/ft at 60% elongation. The soil was a gravelly sand cohesionless soil (USCS-SP) with a phi angle of 39 degrees (measured by a drained triaxial test). Minimum and maximum relative densities were measured to be 91.7 and 108.1 lbs/ft^3, respectively. Placement of the soil into the test wall was accomplished by raining the sand down out of a large bag suspended from a crane at a constant fall height. Placement unit weight (dry) was estimated to be approximately 95 pounds per cubic foot.

TEST WALL CONSTRUCTION AND LOADING

The five-layer geotextile-reinforced retaining wall was constructed within the test apparatus using typical sequential construction practices. The test wall was loaded within hours of completion to prevent fabric and soil creep. Figure 1 illustrates a view of the test wall geometry as constructed.

The bottom portion of each fabric layer (embedment) was placed on leveled fill, and a small amount of fill material was placed on the fabric to hold it in place. The tail of the geotextile was then pulled tight to remove any wrinkles in the fabric. In this manner, the geotextile would immediately mobilize tensile resistance allowing the strain gages to record deformation upon loading.

After the test wall was constructed, load plates were placed on top of layer 1. A ball and socket compensator device was used between the load plates and the hydraulic jack to keep the jack ram plumb during the test. Load increments of 2,000 pounds were applied to a total of 20,000 pounds, at which time the load was increased in increments of 3,000 pounds until termination of the test at 44,000 pounds (average surcharge pressure of 2,855 psf).

RESULTS

Figures 2, 3, and 4 graphically illustrate the strain and deflection data obtained at load increments near the beginning, middle, and end of the test. Evaluation of the data and figures produced the following observations:

i) The largest lateral deflection of the wall occurred in Layer 2 throughout the test;

ii) The maximum strain developed in Layer 1;

iii) The strains in Layer 2 were smaller than those in Layer 3, indicating that the large deflection of Layer 2 was due in part to geotextile interface slippage in Layer 2; and

iv) At the average surcharge pressure of 2,660 psf, the tensile strain at gage 16 in Layer 1 jumped from 8% to 18%. At the same time, the sound of sand "flowing" inside the test wall was detected. It was suspected that a failure condition might have been reached at that surcharge.

The test was terminated at a surcharge load of 2,855 psf as a result of excessive lateral face deformation. Even though the wall was designed to fail by rupture at a surcharge of 850 psf, the ultimate load of 2,855 psf (more than three times the calculated value) did not produce a "classic" Rankine failure plane.

Figure 5 illustrates a potential failure plane developing near the end of the test as obtained from the locus of peak strain in each reinforcement layer. The potential failure plane illustrated resembles more of a log-spiral failure plane than the assumed Rankine failure plane used to design the test wall.

Figure 6 illustrates the locations and full-scale movement traces of three selected points of the soil mass throughout the load test. The paths within the soil mass were traced using the grid system discussed previously.

Evaluation of the data illustrated in Figure 6 indicates the soil near the wall face (point A) moved downward and outward (in the same direction of the wall face) at about the same rate. For the points away from the face in Layers 2 and 1 (points B and C), the downward movement was initially larger than the outward movement. As the surcharge pressure increased, the outward movement increased faster than the downward movement and eventually became greater than the downward movement. These internal movement data are especially valuable for validation of analytical models such as the finite element model.

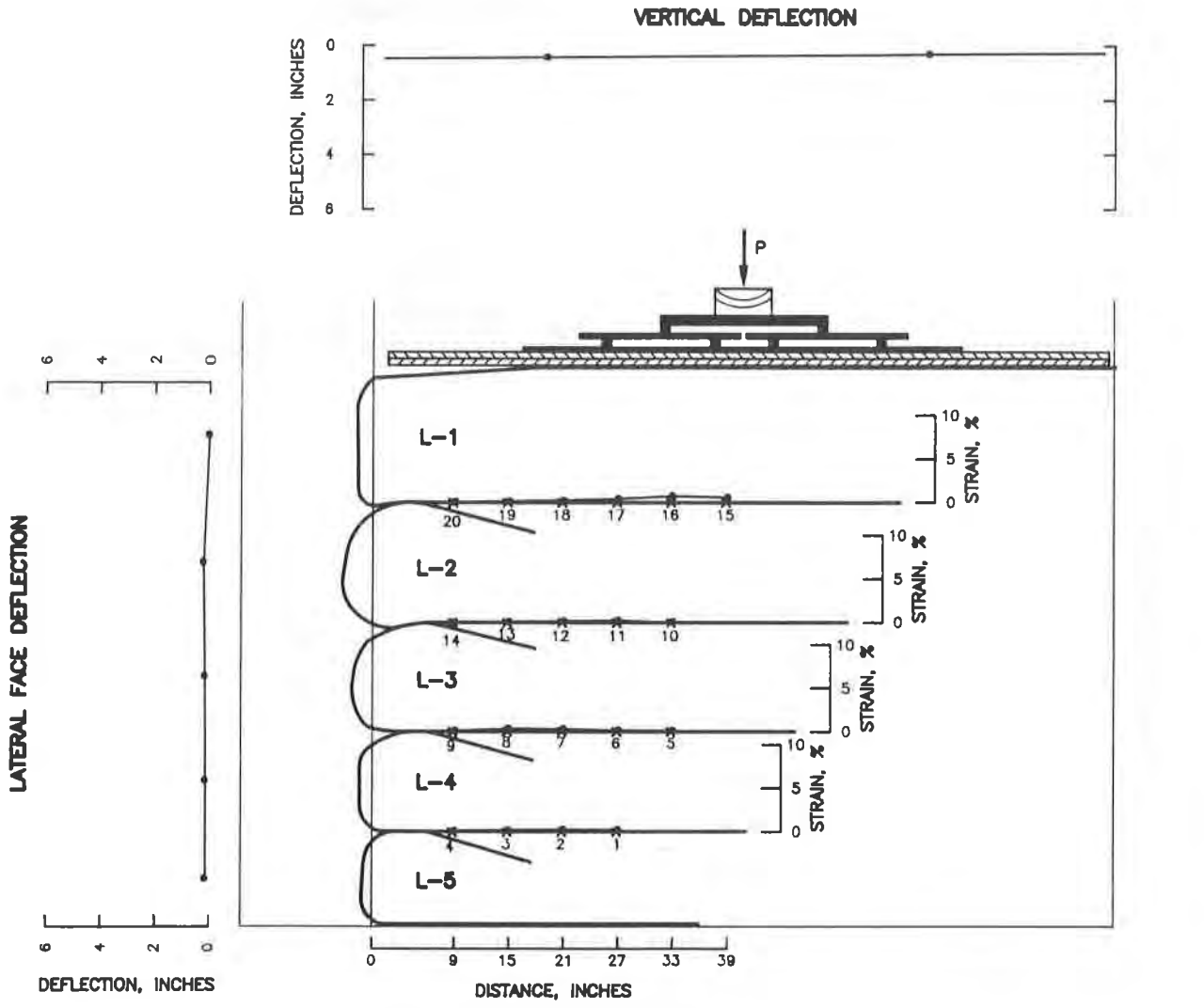

FIGURE 2: MEASURED RESPONSE AT A SURCHARGE PRESSURE OF 295 PSF

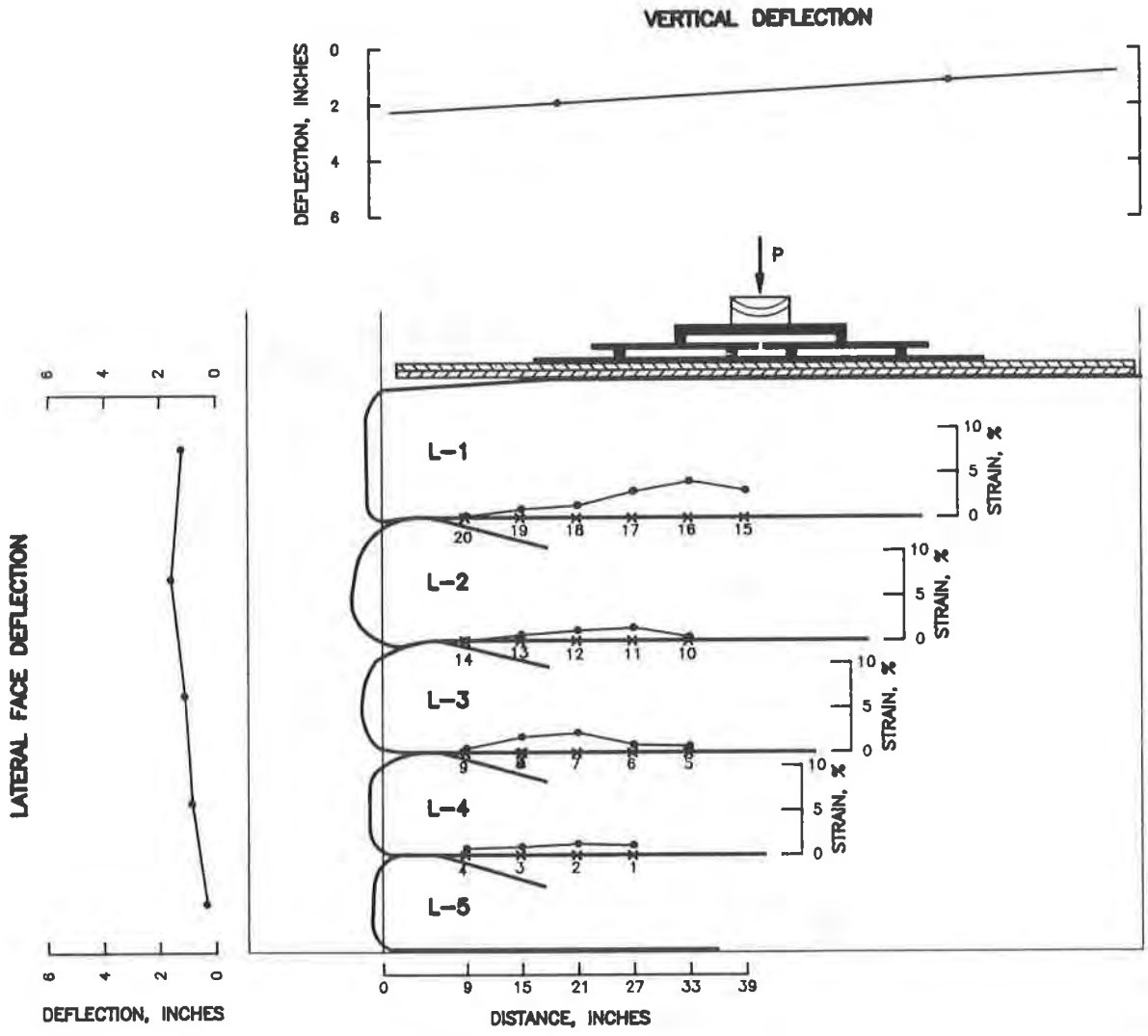

FIGURE 3: MEASURED RESPONSE AT A SURCHARGE PRESSURE OF 1380 PSF

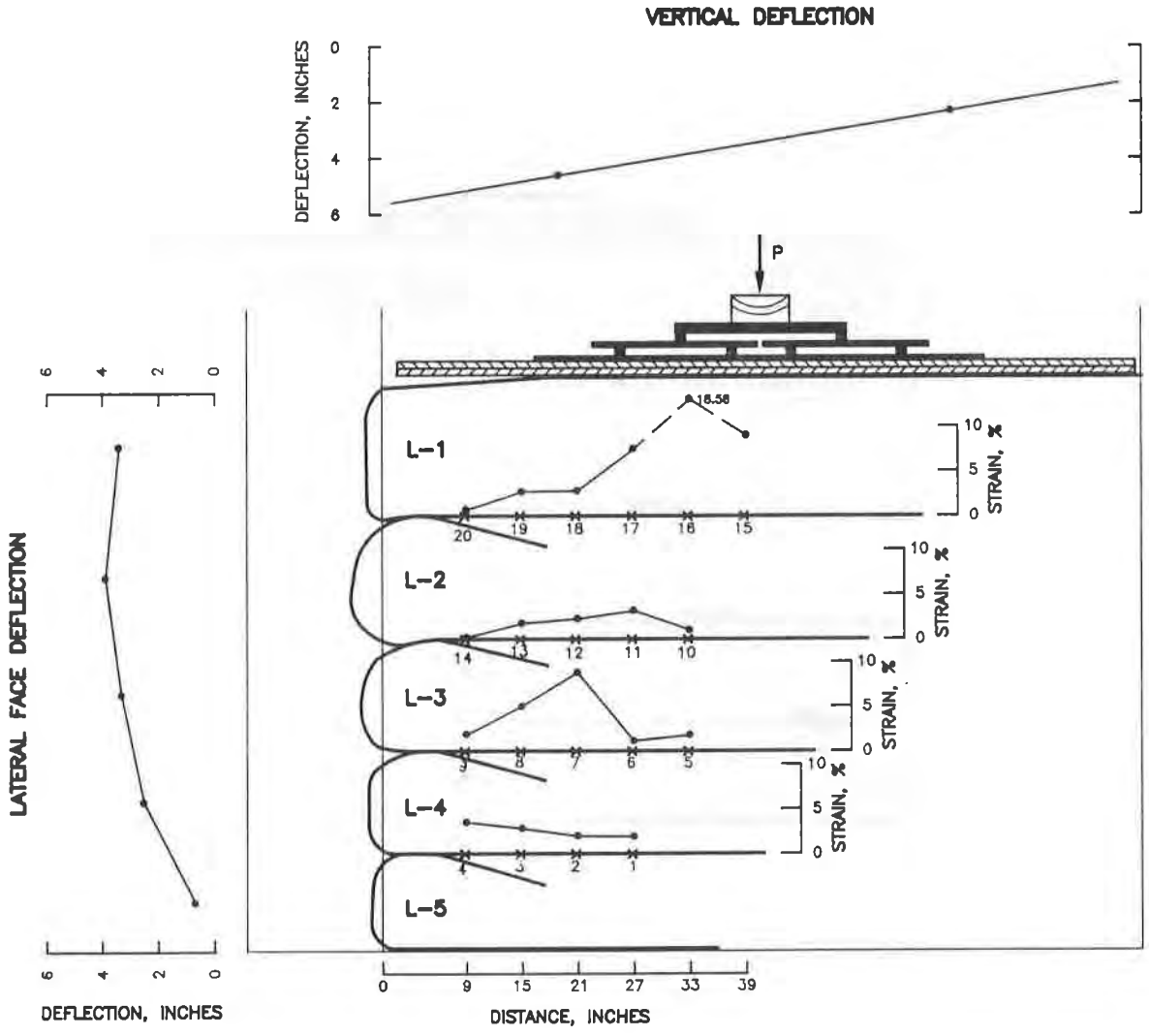

FIGURE 4: MEASURED RESPONSE AT A SURCHARGE PRESSURE OF 2660 PSF

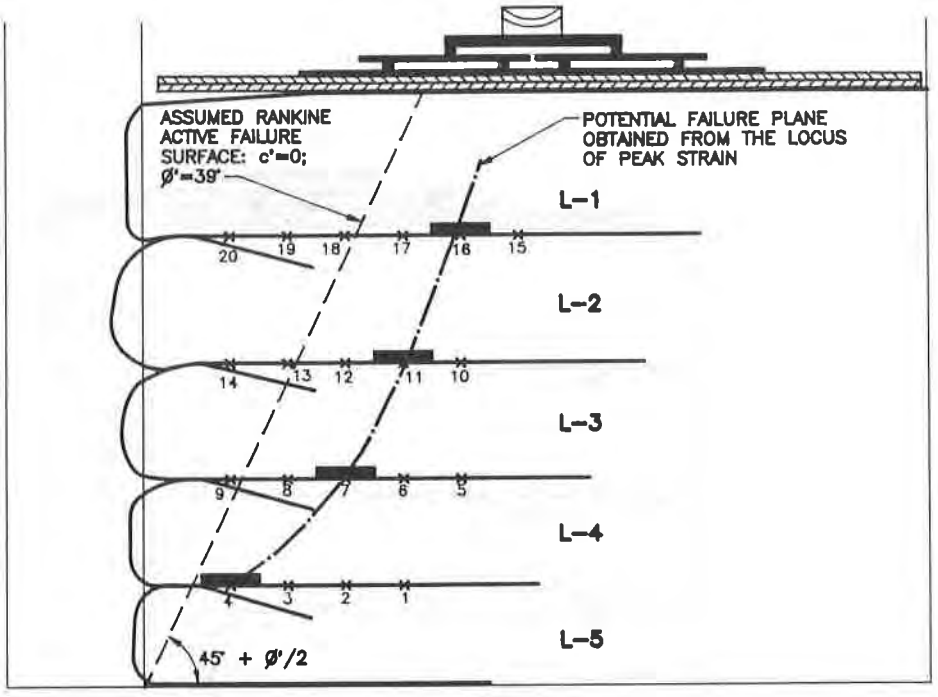

FIGURE 5: LOCUS OF MAXIMUM STRAIN AT SURCHARGE PRESSURES GREATER THAN 2000 PSF

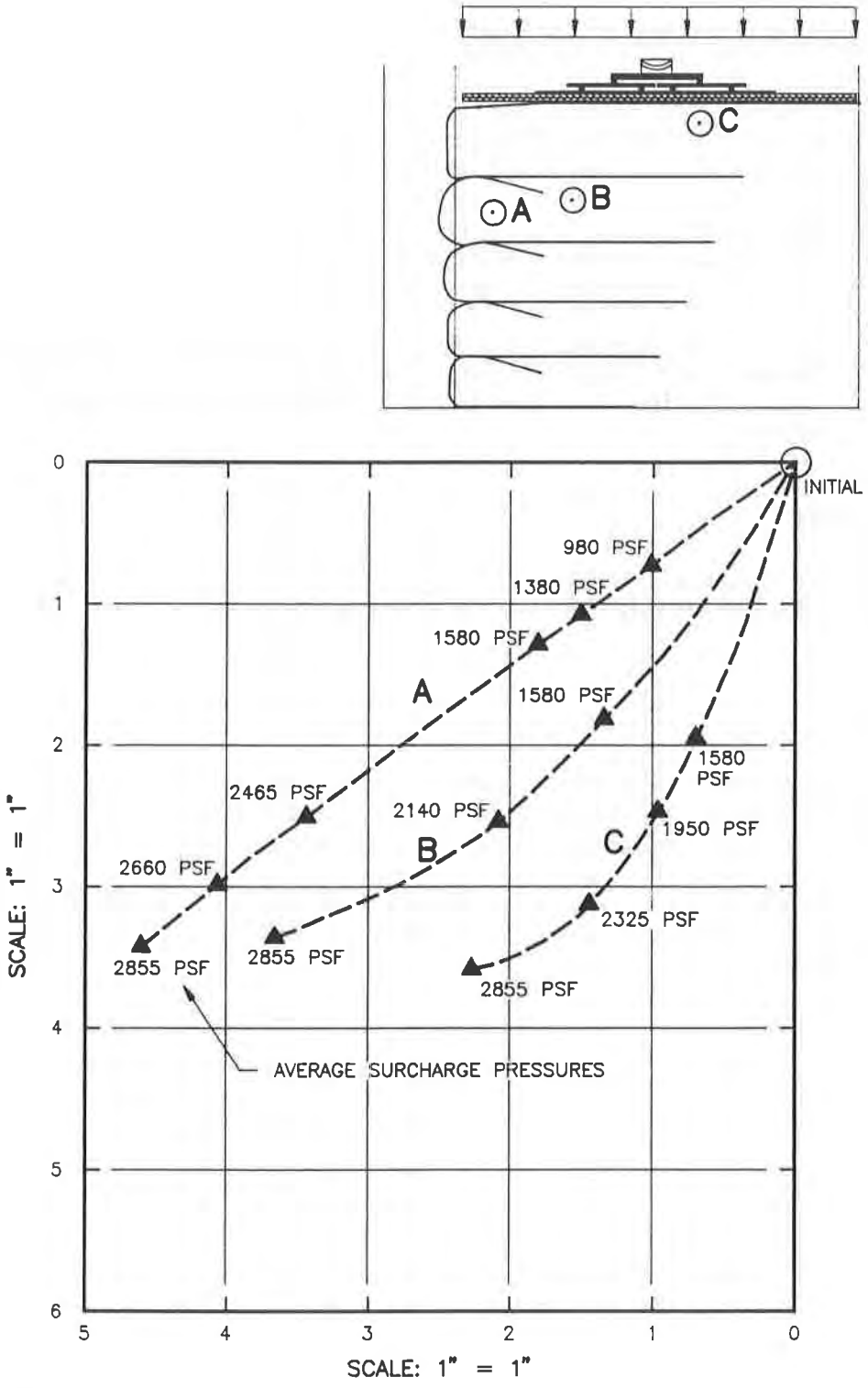

FIGURE 6: FULL SCALE MOVEMENT OF SOIL MASS AT POINTS A, B, AND C

CONCLUSIONS

The results of this load test suggest:

1. The Forest Service method yields a very conservative design. A classic failure condition was not developed at a surcharge load three times that of the calculated load.

2. The assumption of a Rankine planar failure surface used by the Forest Service method does not appear to be valid. The locus of peak strain in the reinforcement layers (Figure 5) resembles a log-spiral curve.

3. The strains and displacements measured in the test provide valuable "controlled" test data for verification of analytical models for investigating the performance of geotextile-reinforced retaining walls.

ACKNOWLEDGMENTS

The author would like to express his gratitude and appreciation to REEMAY for providing financial assistance for this research work.

REFERENCES

John E. Steward, Ron Williamson, and John Mohney, (1983),"Guidelines for Use of Fabrics in Construction and Maintenance of Low-Volume Roads," Federal Highway Administration, Report Number FHWA-TS-78-205

John W. Billiard, (1989), "Performance of a Large Scale Fabric Wall during Load Test," Master's Thesis, University of Colorado at Denver, Denver, Colorado.

Case History Comparison of Geosynthetic-Reinforced Soil Walls

Alan F. Claybourn
Woodward-Clyde Federal Services, USA
Jonathan T. H. Wu
University of Colorado at Denver, USA

ABSTRACT

The design of geosynthetic-reinforced soil walls in engineering practice is currently conducted using a number of diverse design methods. These are typically based on relatively simple analytical models that may not represent the complex stress and strain distributions that actually occur. Since relatively little investigation of the behavior of these structures has been conducted to date, most of the analytical models used are based more on assumptions than on supporting empiricism. The result is diverse results among the various methods.

A study was conducted to review and compare six published design methods representing North American practice. They are: the Forest Service method (Steward, Williamson and Mohney, 1977, revised 1983); the Broms method (Broms, 1978); the Collin method (Collin, 1986); the Bonaparte et al. method (Bonaparte, et al., 1987); the Leshchinsky and Perry method (Leshchinsky and Perry, 1987); and the Schmertmann et al. method (Schmertmann et al., 1987).

The study was conducted in two parts. The first part compared the results of designs for various wall heights and geometries. The results of that portion of the study will be presented in another paper. The second part, presented in this paper, involved comparing the results of tests conducted on two geosynthetic-reinforced test walls that were loaded to failure (by others) with the results predicted by each of the design methods without using any of the prescribed safety factors.

The comparisons of the design predictions with the test wall results indicated there are differences among the methods. More importantly, the study results indicate there is a tendency for the methods to underestimate the amount of reinforcement required for a high wall. This has probably not been a problem due to the safety factors typically used in design and since relatively few high walls have been constructed. However, the results demonstrate the general lack of knowledge of high geosynthetic-reinforced soil walls.

INTRODUCTION

The concepts of reinforced soil and gravity retaining structures are both centuries old. The use of modern geosynthetic reinforcement to construct a reinforced soil mass, essentially a gravity retaining structure, is relatively new. Henry Vidal of France introduced a new era of relatively flexible retaining walls with the concept of reinforced earth (Vidal, 1966). Metal strips were used to anchor facing panels at the wall's face and to reinforce the backfill soil mass.

Geosynthetics have found some use in reinforced soil walls in the past 10 to 20 years and are becoming increasingly popular as their behavior becomes better understood. Similar in concept to the patented "Reinforced Earth" structures using metal strips, layers of geotextile or geogrid are embedded in a backfill soil to

construct a free standing wall. These walls tend to be quite flexible when compared with conventional structural retaining walls. Flexibility can be an advantage for some applications. Reinforced soil walls also frequently tend to be less costly than more conventional retaining structures. They are versatile in that the exposed face of the wall may consist of a variety of building materials, such as cast-in-place concrete, masonry, timber, precast concrete panels, or the reinforcement may be wrapped at the face and left exposed or provided with protection such as sprayed-on asphalt or gunite. Figure 1 shows several types of geosynthetic-reinforced soil walls. Regardless of the wall facing, the same basic design methodologies are used.

The design of geosynthetic-reinforced soil walls, like other retaining structures, must consider both internal and external stability. Evaluation of external stability typically considers the reinforced zone of the wall to be a semi-rigid structure, see Figure 2(a), and analyzes its potential for sliding, overturning or bearing capacity failure. Slope instability beneath or behind the wall are also evaluated. Internal stability addresses the structural integrity of the reinforced zone of the wall. Evaluation of internal stability requires consideration of tensile rupture/creep and pullout failure modes, as depicted in Figures 2(b) and 2(c). The internal stability is the subject of this study. A number of diverse methods for designing the required reinforcement strengths, lengths and spacings have been published.

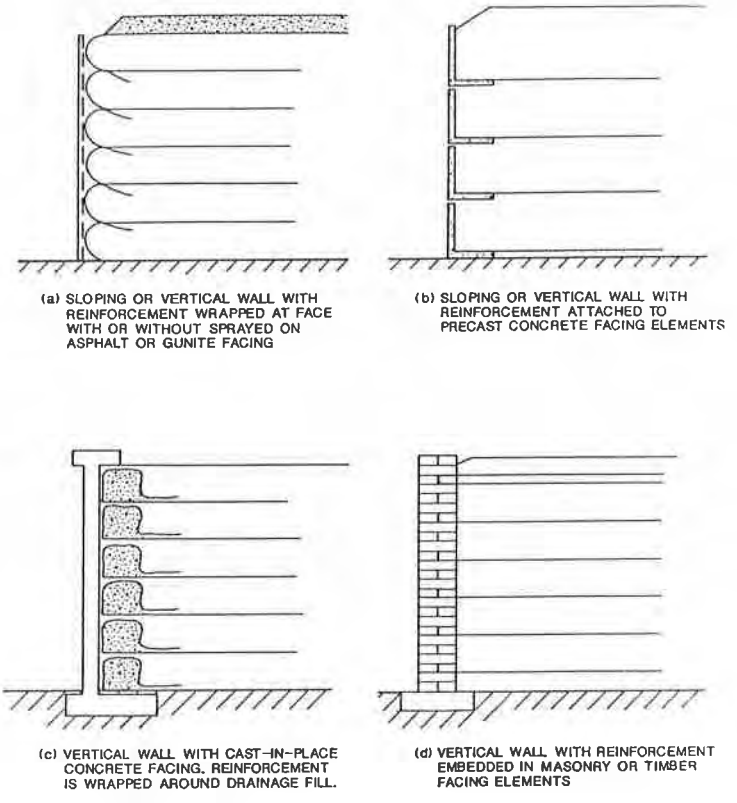

Figure 1 - Examples of Various Types of Geosynthetic-Reinforced Soil Walls

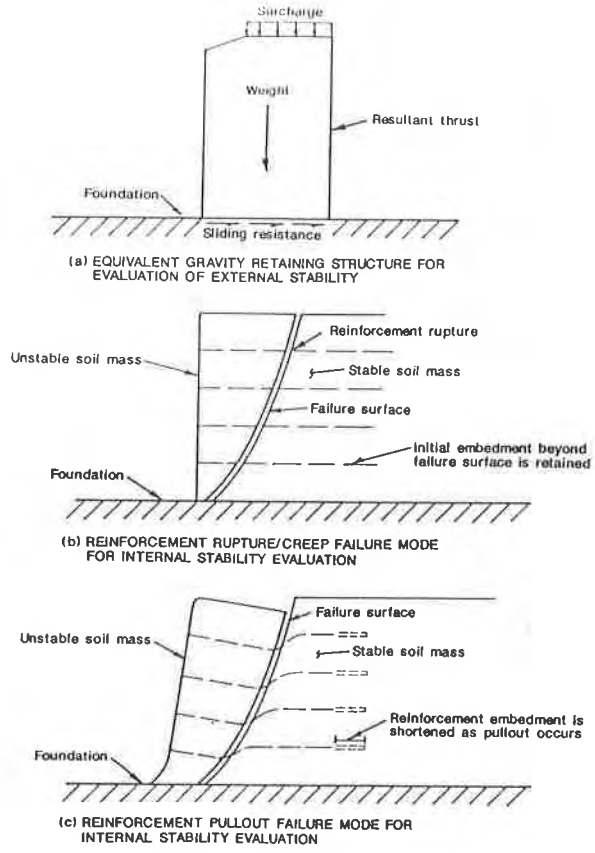

Figure 2 - Failure Modes Considered For Stability Analysis

DESCRIPTION OF STUDY

A study was conducted to compare design methodologies and the results obtained using various published design methods for geosynthetic-reinforced soil walls, and to compare two case histories of test walls that were loaded to failure with the results predicted by each of the methods. The results of the design method comparisons are included in a paper that has been submitted for possible publication in the ASCE Journal of Geotechnical Engineering. The case history comparisons are presented in this paper.

Six design methods for evaluating the internal stability of geosynthetic-reinforced soil walls were used for the comparisons. The selection of design methods was based on the authors' perception that they represent the range of methods most frequently used in North American practice. The following methods were used:

(1) Forest Service Method (Steward, Williamson and Mohney, 1977, revised 1983);
(2) Broms Method (Broms, 1978);
(3) Collin Method (Collin, 1986);
(4) Bonaparte et al. Method (Bonaparte, Holtz and Giroud, 1987);
(5) Leshchinsky and Perry Method (Leshchinsky and Perry, 1987); and,
(6) Schmertmann et al. Method (Schmertmann, Chourey-Curtis, Johnson and Bonaparte, 1987).

Computer spread sheet programs were written and used for applying the design methods to different situations. Hand calculations were used for the Schmertmann et al. method due to its ease of application.

DESCRIPTION OF METHODS

A number of approaches have been developed for the design of geosynthetic-reinforced soil walls. All of the methods normally considered applicable to routine design use limiting equilibrium analysis to determine factors of safety against failure. Most of them use conceptually simple analyses of destabilizing horizontal forces resulting from earth pressures and stabilizing horizontal forces provided by the reinforcement. Others use methods of evaluating force and/or moment equilibrium along an assumed failure surface similar to conventional slope stability analysis. These limiting equilibrium methods typically do not include stress-deformation analyses to evaluate performance nor do they realistically model the presumably complex soil/geosynthetic interaction mechanisms that actually occur.

Methods 1 through 4 listed above are based on lateral earth pressure considerations. Nearly all geotextile-reinforced soil walls that have been constructed in North America were designed by these methods (Yako and Christopher, 1987). Limiting equilibrium analysis is used to equate the horizontal forces due to lateral earth pressures tending to cause instability to the stabilizing tensile forces in the horizontal reinforcement. The only stresses considered are vertical and lateral earth pressures, the horizontal tensile stresses in the reinforcement, and the horizontal resistance to pullout of the reinforcement from behind a failure surface. Therefore, two independent safety factors are determined for each layer of reinforcement. The factor of safety for reinforcement rupture is the ratio of reinforcement strength to the lateral earth pressure thrust for the layer. The factor of safety for pullout is the ratio of pullout resistance to the lateral earth pressure thrust for the layer. Pullout resistance is provided by horizontal shear stresses resulting from the soil/reinforcement interface friction under the vertical confining stress on the portion of the layer behind the failure surface.

The tied-back wedge methods typically presume a planar failure surface through the reinforced mass described by a Rankine active failure condition. The stresses on a failure surface are not directly analyzed. The reinforcements extend beyond the assumed failure surface and are considered to be tension-resistant tiebacks for the assumed failure wedge. As a result, they are frequently collectively referred to as tied-back wedge analysis methods. Although the tied-back wedge methods have many similarities, they use different lateral earth pressure distributions to describe the horizontal forces that need to be resisted.

The remaining two methods used for the study (methods 5 and 6 listed above) employ the approach commonly used in conventional slope stability analysis, which involves analyzing the stresses on a failure surface. Leshchinsky and Perry used limiting equilibrium analyses of rotational (log-spiral) and translational (planar) failure surfaces. The method was based on earlier work by Leshchinsky which used techniques similar to those presented in "Variational Approach to Slope Stability" (Baker and Garber, 1977). The Schmertmann et al. method is based on limiting equilibrium analysis using wedge failure models. Straight line and bi-linear wedges are used for different aspects of the analysis. Extended versions of Bishop's modified and Spencer's methods of slope stability analysis were used to modify the results of the wedge analyses. Due to their complicated computations, the Leshchinsky and Perry and Schmertmann et al. methods both use design charts.

There are significant variations among the methods in the definition of safety factors. Some of the methods explicitly prescribe allowable strengths and safety factors while others provide only general guidelines. However, in general, the design methods use allowable strengths significantly lower than ultimate strengths and apply further safety factors to account for uncertainties in the behavior of the reinforcement and soil/reinforcement interaction mechanisms.

CASE HISTORY EVALUATIONS

Each of the six design methods was used to evaluate two actual cases of reinforced soil walls that were tested to failure under controlled conditions. The

purpose was to compare the analytical models used in the design methods without the influence of any of the assumed or empirical, and perhaps somewhat subjective, criteria for defining factor of safety and selecting allowable reinforcement strength. Ultimate wide width reinforcement tensile strengths were used and all safety factors were set equal to 1.0.

The first case involved a full-scale, geotextile-reinforced test wall constructed as part of a Federal Highway Administration (FHWA) study entitled, "Behavior of Reinforced Soil." At the time of this paper, the results have not been published. The information given in this paper was obtained through personal communication with the principal investigator of the study, Mr. Barry Christopher, formerly of STS Consultants, Ltd. This wall is subsequently referred to as the STS/FHWA Test Wall. Effectively, the wall was constructed up to a height at which failure occurred, 20 feet. It was constructed of granular soil with a reported internal friction angle of 39 degrees and reinforced with a relatively extensible non-woven polyester geotextile with a reported wide width tensile strength of 1320 pounds per foot (lb/ft). The reinforcements were 14 feet long and at equal spacings of 2.5 feet. The test wall was not designed to evaluate pullout and the reinforcement lengths were designed longer than were believed necessary. Based on his previous experience and on reinforcement strain data, Mr. Christopher estimated the wall's performance would have been the same with a reinforcement length as short as 10 feet. This length was selected as the "effective" reinforcement length for this study. The wall was quite flexible, with lateral deflection of the face on the order of one foot occurring during construction. Much of this deflection was reportedly due to initial slack in the reinforcements. The geometry of the STS/FHWA Test Wall is depicted in Figure 3 (a).

The other case was one of the large-scale model geogrid-reinforced walls constructed as part of a long-term research project at the Royal Military College of Canada (RMC). The walls have been the subject of investigation in a prediction exercise workshop sponsored by NATO (1987). The test wall used for this study is Test 3 presented in a paper by Bathurst, Benjamin and Jarrett (1988). That case is subsequently referred to as the RMC Model Wall. The geometry of this wall is shown in Figure 3 (b).

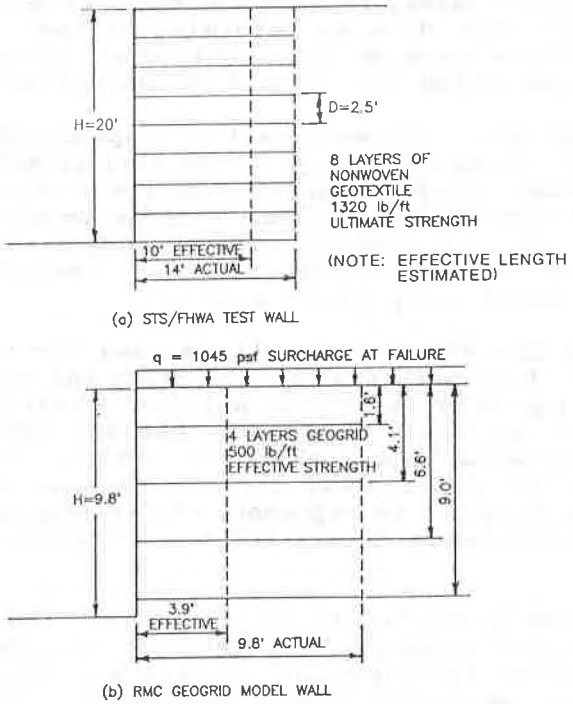

Figure 3 - Test Wall Configurations
(1 ft. = 0.3048 m.)

The major component of the RMC model test facility consisted of a reinforced concrete structure in which a geosynthetic-reinforced wall could be constructed up to approximately 12 feet high, approximately 8 feet wide and nearly 20 feet deep. A vertical surcharge was applied at the top of the wall by pressurizing pneumatic bags. An equivalent surcharge of up to approximately 20 feet of fill could be provided. The test used for this study involved a model wall approximately 9.8 feet high with four layers of geogrid reinforcement, each approximately 9.8 feet long, at depths 1.6, 4.1, 6.6 and 9.0 feet. The wall was constructed by slightly pre-tensioning the reinforcements and then carefully compacting granular backfill with a reported internal friction angle of 53° inside the concrete forms. The resulting wall was stiff for a geosynthetic-reinforced soil wall. Timber facing elements backed with foam rubber to reduce stress concentrations at the facing elements were provided. Reinforcement strain measurements were obtained at six points on each layer. An effective reinforcement length of 3.9 feet was reported for the test based on strain data. The reinforcement used consisted of a high-density polyethylene (HDPE) geogrid. This material possessed an ultimate wide width tensile strength of 840 lb/ft at 14% strain in the direction it was oriented. The model was surcharged in increments to approximately 250, 625, 1,045, 1,250, 1,465 and 2,090 pounds per square foot (psf). The 1,045-psf surcharge was sustained for 162 hours, during which time failure occurred. Lateral movement of the face of the wall of approximately one inch occurred at failure.

For each case, an effective reinforcement length is reported. This is the length beyond which the performance of the wall is presumed to be unaffected by further lengthening of the reinforcement for the loading conditions at failure. Therefore, no stresses are mobilized along the portion of reinforcement beyond the effective length. For an extensible reinforcement, the length of reinforcement over which the soil/reinforcement interface shearing resistance is only partially mobilized within the effective length is probably relatively short, resulting in a pullout safety factor of not much greater than 1.0 for the effective reinforcement length. For a stiff reinforcement, the shearing resistance may be partially mobilized over a significant length within the effective length resulting in a pullout safety factor significantly greater than 1.0 for the effective length. Since soil/reinforcement shear stresses were not measured and pullout did not occur for either test wall, pullout safety factors could not be determined. However, even though there is not sufficient data to determine pullout safety factors and the significance of the effective lengths is not well understood, they are presented to provide some context within which the calculated lengths may be judged.

Neither of the test walls failed in either rupture or pullout. The mode of failure reported for both cases was creep. This failure mode was used to describe a condition where there was a marked increase in the rate of lateral displacement of the wall face at the same time a failure surface developed, as evidenced by a scarp in the reinforced backfill surface. The authors assume this may effectively be considered a rupture failure considering the presumably high stress ratio required for relatively rapid creep to occur.

The comparisons of the six design methods used for this study with the two case histories described above were made by modifying the calculations to eliminate all considerations for margins or factors of safety. A reinforcement strength equal to the ultimate strength was used to evaluate the STS/FHWA wall. This was used since stress data was unavailable and since the authors believe the stress ratio must have been high for the rapid creep failure to have occurred. An effective strength of 500 lb/ft was selected to represent the average of the maximum mobilized stresses in the four reinforcement layers for the RMC model wall based on measured strains.

The comparisons were approached two ways. First, the reinforcement tensions predicted by each method were calculated for the test wall geometries. Second, each method was used to determine reinforcement lengths and spacings for the test wall heights and reinforcement strengths summarized above using a safety factor of approximately 1.0. Results of the analyses are presented in detail in Claybourn (1990). Figures 4 and 5 show the reinforcement tension calculated by each design method for each layer along with the ultimate (STS/FHWA Test Wall) or measured (RMC

Model Wall) reinforcement stress. The results show distributions of required reinforcement strength consistent with the lateral earth pressure distributions used by the tied-back wedge methods. Both the Leshchinsky and Perry and Schmertmann et al. methods and two of the four tied-back wedge methods indicate a requirement for increasing reinforcement strength with depth. However, the results of the RMC Model Wall indicate that, except for the bottom layer, the reinforcement stresses are probably better approximated by uniform rather than increasing distributions. The RMC Model Wall report indicated the low bottom layer stress was probably influenced by the model set-up.

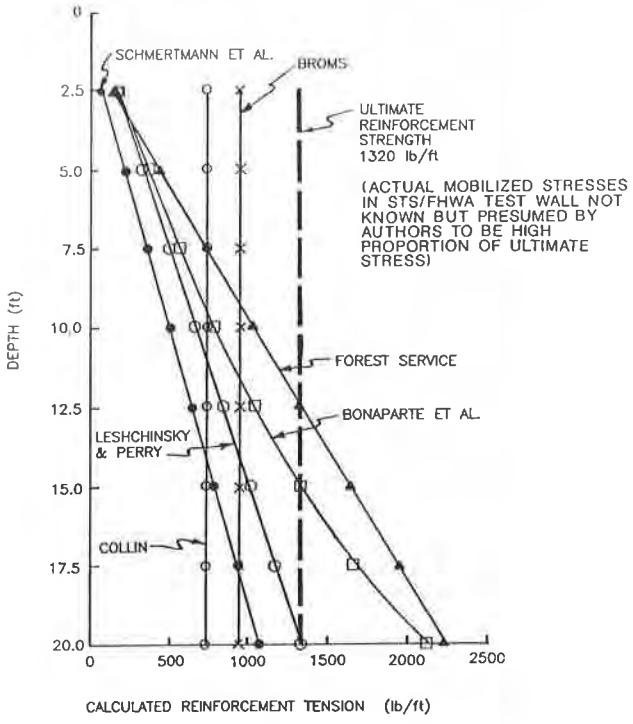

Figure 4 - Reinforcement Tension Calculated for STS/FHWA Test Wall Geometry (1 ft. = 0.3048 m.; 1 lb./ft. = 14.59 N./m.)

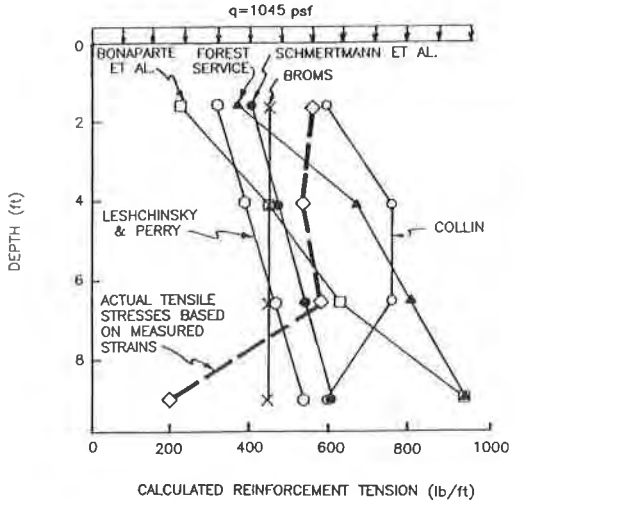

Figure 5 - Reinforcement Tension Calculated for RMC Model Wall Geometry (1 ft. = 0.3048 m.; 1 lb./ft. = 14.59 N./m.)

Figures 6 and 7 show the results in terms of reinforcement lengths and spacings calculated using each design method with all safety factors set equal to 1.0 using the test wall heights and reinforcement and soil strengths.

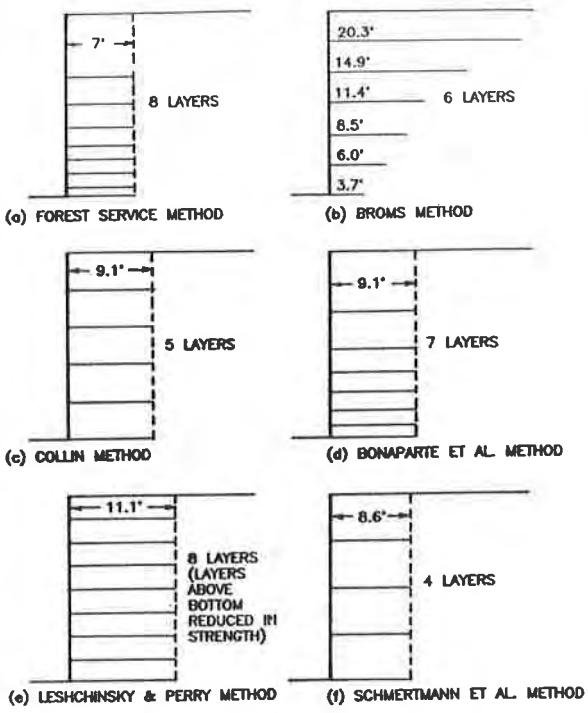

Figure 6 - Comparison of Methods for FS=1.0, 20-Foot High Wall with 1320-lb/ft Reinforcement strength (1 ft. = 0.3048 m.)

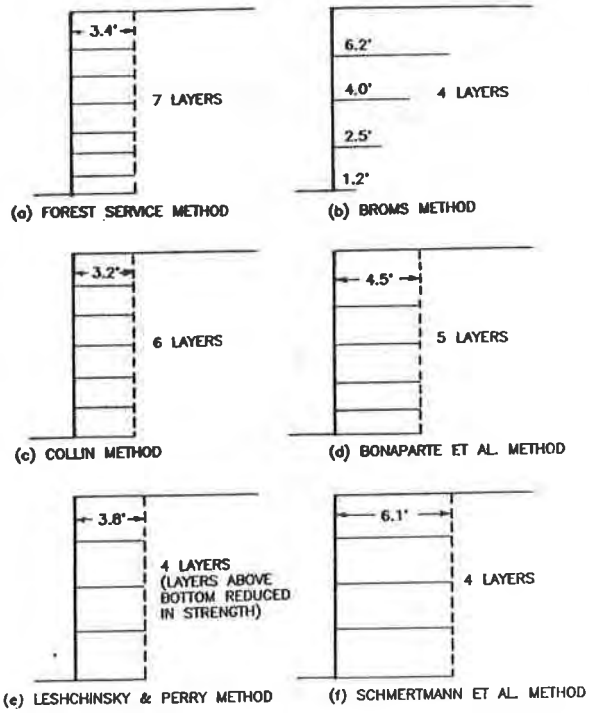

Figure 7 - Comparison of Methods for FS=1.0, 9.8-Foot High Wall with 500-lb/ft Reinforcement strength (1 ft. = 0.3048 m.)

The following comparisons may be made if it is assumed that the ultimate reinforcement strength was mobilized for the STS/FHWA Test Wall and that a reinforcement stress of 500 lb/ft was mobilized for the RMC Model Wall. Comparison of Figure 6 with Figure 3 (a) shows that all of the methods predict either the same number or fewer layers of reinforcement than used for the STS/FHWA Test Wall. The Broms Method is the only method of the six evaluated that does not use a uniform reinforcement length. It does, however, allow a reduction in the apparently excessive lengths of the upper layers. The lateral earth pressure distributions associated with the Forest Service and Bonaparte et al. methods result in wider reinforcement spacings at shallower depths. Similarly, the Leshchinsky and Perry Method, although specifying uniform spacings, allows a linearly decreasing distribution of required reinforcement strength above the bottom.

Comparison of Figure 7 with Figure 3 (b) shows that the distributions of reinforcements are similar to those described above for the STS/FHWA Test Wall. However, unlike the STS/FHWA Test Wall, the methods predict a requirement for the same number or more layers of reinforcement than used for the RMC Model Wall. A reason for this apparent inconsistency is not offered here. However, it should be noted that the STS/FHWA Test Wall was a relatively high flexible structure subjected to internal loading (self weight) while the RMC Model Wall was a much stiffer, smaller structure loaded externally.

CONCLUDING REMARKS

At present, there is not sufficient basis for determining which of the methods is best suited for design. For relatively high walls (i.e., 20 feet and higher), comparison with the STS/FHWA test wall indicates many of the methods may underestimate the number of layers of reinforcement required. However, The Schmertmann et al. Method has been used successfully for relatively high geogrid-reinforced slopes and walls. This demonstrates the general lack of knowledge concerning the behavior of high geosynthetic-reinforced walls. At present, the authors recommend the design of high walls be conducted with caution based primarily on the demonstrated success of existing walls. Analysis by several different methods can be beneficial in evaluating where relative unconservatism among the methods may lie.

Most of the current design methods are based more on assumptions and relatively simple analytical models than on supporting empiricism. There are significant differences in the analytical methods used. Further study by means of test structures and monitoring of production structures should lead to more consistent design methodologies, and ultimately in more economy and confidence in geosynthetic-reinforced structures.

REFERENCES

Baker, R. and Garber, M. (1977), "Variational Approach to Slope Stability," Proceedings 9th International Conference on Soil Mechanics and Foundation Engineering, Tokyo, Vol. 2, pp. 9-12.

Bathurst, R.J., Benjamin, D.J. and Jarrett, P.M. (1988), "Laboratory Study of Geogrid Reinforced Walls," Royal Military College of Canada, Kingston, Ontario, Proceedings, Symposium on Geosynthetics for Soil Improvement, American Society of Civil Engineers (ASCE) National Convention, Nashville, Tennessee, ASCE Geotechnical Special Publication No. 18, R.D. Holtz, Ed., pp. 178-192.

Bonaparte, R., Holtz, R.D. and Giroud, J.P. (1987), "Soil Reinforcement Design Using Geotextiles and Geogrids," Geotextile Testing and the Design Engineer, ASTM STP 952, J.E. Fluet, Jr., Ed., American Society for Testing and Materials, Philadelphia, pp. 69-116.

Broms, B.B. (1978) "Design of Fabric Reinforced Retaining Structures," Proceedings of the Symposium on Earth Reinforcement, ASCE, Pittsburgh, p. 282, as summarized in Reference Nos. 6 and 12 for this paper.

Claybourn, A.F. (1990), "A Comparison of Design Methods for Geosynthetic-Reinforced Earth Walls," M.S. thesis, Department of Civil Engineering, University of Colorado, Denver.

Collin, J.G. (1986), "Earth Wall Design," Doctoral Thesis, Department of Civil Engineering, University of California, Berkeley, 376 pages.

Eigenbrod, K.D. and Locker, J.G., (1987), "Determination of Friction Values for the Design of Side Slopes Lined or Protected with Geosynthetics," Canadian Geotechnical Journal, Vol. 24, No. 4, pp. 509-519.

Holtz, R.D. and Broms, B.B. (1977), "Walls Reinforced by Fabrics - Results of Model Tests," Proceedings of the International Conference on the Use of Fabrics in Geotechnics, Paris, Vol. I, p. 113.

Juran, I. and Christopher, B.R. (1989), "Laboratory Model Study on Geosynthetic Reinforced Soil Retaining Walls," Journal of Geotechnical Engineering, ASCE, Vol. 115, No. 7, pp. 905-926.

Juran, I., Knochenmus, G., Acar, Y.B. and Arman, A. (1987), "Pull-out Response of Geotextiles and Geogrids," draft submitted to the Symposium on Geosynthetics for Soil Improvement.

Koerner, R.M., (1986),"Designing WithGeosynthetics," Prentice-Hall.

Leshchinsky, D. and Perry, E.B. (1987), "A Design Procedure for Geotextile-Reinforced Walls," Proceedings of the Geosynthetic '87 Conference, New Orleans, Vol. 1, pp. 95-107.

Leshchinsky, D. (1985), "Design Manual for Geotextile-Retained Earth Walls," Research Report No. CE 85-51, Dept. of Civil Engineering, University of Delaware, Newark. 137 pages plus appendices.

Martin, J.P., Koerner, R.M., and Whitty, J.E. (1984), "Experimental Friction Evaluation of Slippage Between Geomembranes, Geotextiles and Soils," Proceedings of the International Conference on Geomembranes, Denver, Vol. I, pp. 191-196.

McGown, A., Andrawes, K.Z., Murray, R.T. (1988), "Controlled Yielding of the Lateral Boundaries of Soil Retaining Structures,"Proceedings, Symposium on Geosynthetics for Soil Improvement, American Society of Civil Engineers (ASCE) National Convention, Nashville, Tennessee, ASCE Geotechnical Special Publication No. 18, R.D. Holtz, Ed., pp. 193-210.

McGown, A., Andrawes, K.Z., and Kabir, M.H. (1982), "Load-Extension Testing of Geotextiles Confined In-Soil," Proceedings, Second International Conference on Geotextiles, Las Vegas, pp. 793-798.

National Cooperative Highway Research Program (NCHRP) Report 290 (1987), "Reinforcement of Earth Slopes and Embankments." 323 pages.

Schmertmann, G.R., Chouery-Curtis, V.E., Johnson, R.D. and Bonaparte, R., (1987), "Design Charts for Geogrid-Reinforced Soil Slopes," Proceedings of the Geosynthetics '87 Conference, New Orleans, Vol. 1, pp. 108-120.

Schneider, H.R. and Holtz, R.D. (1986), "Design of Slopes Reinforced with Geotextiles and Geogrids," Geotextiles and Geomembranes, Vol. 4, No. 2, T.S. Ingold, Ed., pp. 29-51.

Siel, B.D., Wu, J.T.H., and Chou, N.N.S. (1987), "In-Soil Stress-Strain Behaviour of Geotextiles," Proceedings Geosynthetics '87, New Orleans, pp. 260-265.

Steward, J.E., Williamson, R. and Mohney, J. (1977, Revised 1983), "Guidelines For Use of Fabrics in Construction and Maintenance of Low-Volume Roads," Chapter 5: Earth Reinforcement, USDA, Forest Service, Portland, Oregon, pp. 87-95 and 102-105.

The Tensar Corporation, "Slope Reinforcement with Tensar Geogrids, Design and Construction Guideline," Tensar Technical Note.

Terzaghi K. and Peck R. (1967), "Soil Mechanics in Engineering Practice, John Wiley and Sons, N.Y., 729 pages.

Vidal, H. (1966). "La Terre Armee," Annales de l'Institut Technique du Batiment et des Travaux Publics, Paris, Nos. 223-229, Jul.-Aug., pp. 888-938.

Yako, M.A. and Christopher, B.R. (1987), Polymeric Reinforced Retaining Walls and Slopes in North America," Proceedings, NATO Advanced Research Workshop on the Application of Polymeric Reinforcement in Soil Retaining Structures," Ontario, Canada, pp. 239-284.

Creep Measurements on Polymeric Reinforcement

R. J. Fannin
University of British Columbia, Canada
S. Hermann
Norwegian Geotechnical Institute, Norway

ABSTRACT

A sloped, reinforced soil wall was built in July 1987 and instrumented to measure force and strain in the geogrid reinforcement. Long-term performance data describing surcharge loading of the structure between October 1987 and April 1990 are used to describe creep behaviour of the uniaxial polymer grid. A comparison of field measurements to laboratory tensile creep data for the same material is used to evaluate the role of isochronous load-strain curves for design. The field measurements are also related to allowable values of limit strain that govern design and construction of similar reinforced soil retaining walls in the United Kingdom.

INTRODUCTION

Creep of polymeric materials refers to the continued, irrecoverable strain that is observed at constant load and which may ultimately lead to rupture. The mechanism by which creep strains occur is one of plastic flow, in a process of permanent deformation. With increasing applications of reinforcement in slopes and walls, and as liners for waste containment facilities, a thorough understanding of creep behaviour in geosynthetics is fundamental to any long-term design.

Currently our understanding of creep is based on interpretation of the results of laboratory tests carried out on isolated specimens, and it is well-recognized that the magnitude of creep strain in polymeric materials is predominantly influenced by the following:

- polymer type and draw ratio
- tensile load
- tensile strain
- temperature

Selection of the polymer, in combination with alignment of the molecules during manufacture by drawing of the material, broadly determine the potential for creep in any specific material. Given any potential for creep, the extent to which creep strains actually occur is governed by the ratio of tensile load to tensile strength in the material, by the magnitude of strain, and by ambient temperature.

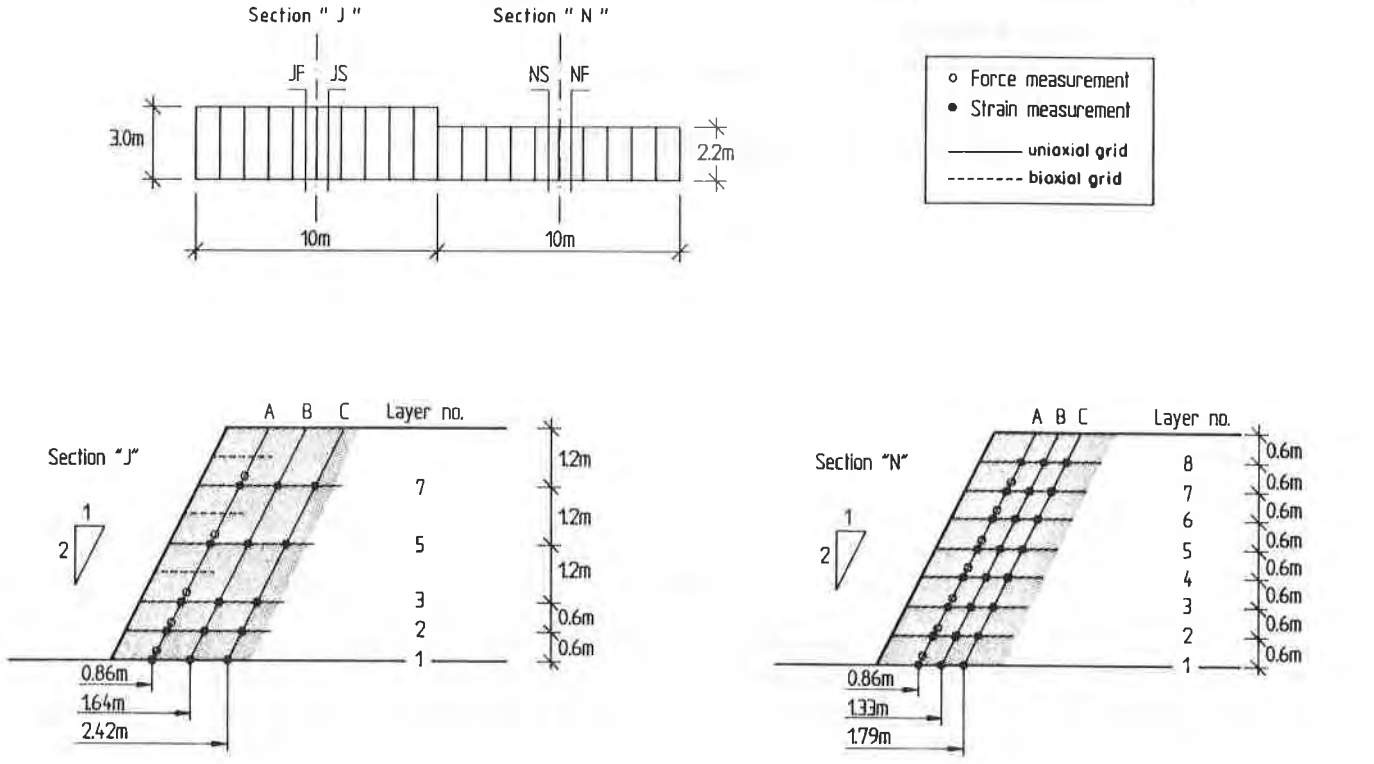

Figure 1. Arrangement of the reinforcement

A requirement for design of permanent structures reinforced with geosynthetics must be one of ensuring that creep strains which occur do not lead to a serviceability type of failure, that is a failure in which tensile forces required for stability are mobilized but at the expense of strain magnitudes that are unacceptable and may even lead to rupture. Long-term tensile tests at constant loads have been used to establish isochronous load-strain curves for some polymeric reinforcement materials. The curves identify clearly the significance of creep behaviour, McGown et al (1984). Such curves may also be used to establish appropriate allowable tensile strengths for a particular design life based on extrapolation of the laboratory testing data. As in many areas of geotechnical engineering there is a need for quality field data from instrumented structures to validate these approaches.

CONSTRUCTION AND LOADING OF THE STRUCTURE

A sloped (2V:1H) reinforced soil wall was constructed in July 1987 near Oslo, Norway. The 4.8m high structure comprises two sections, termed Section 'J' and Section 'N', each with a different arrangement and spacing of geogrid reinforcement as shown in Figure 1. The backfill soil is a uniformly graded medium coarse sand that was placed and compacted at optimum water content to a specification of greater than 92% of the maximum dry density in separate lifts 0.3m thick. Shearbox tests gave a value for the angle of friction in plane strain of 38° at large displacement.

A uniaxial geogrid was used for the layers of primary reinforcement and a biaxial geogrid was used for any layers of intermediate reinforcement. The geogrid is manufactured by drawing a continuous, punched sheet of high density polyethylene material to achieve the specified geometry and strength. Physical dimensions of the geogrid reinforcement are reported in Figure 2 (after Fannin and Hermann, 1990). Long-term tensile strength of the uniaxial geogrid is reported as 32 kN/m at a performance limit strain of 10%. Long-term tensile strength describes the strength of the material at $1x10^6$ hrs, from extrapolation of laboratory creep tests carried out to $1x10^4$ hrs. Facing panels for the structure were cut from a commercially available steel mesh, Ø 8mm c/c 150mm, and formed (2V:1H) to a panel height of 0.6m; they were supplied in lengths of 5m and covered with a fabric to prevent soil erosion at the face.

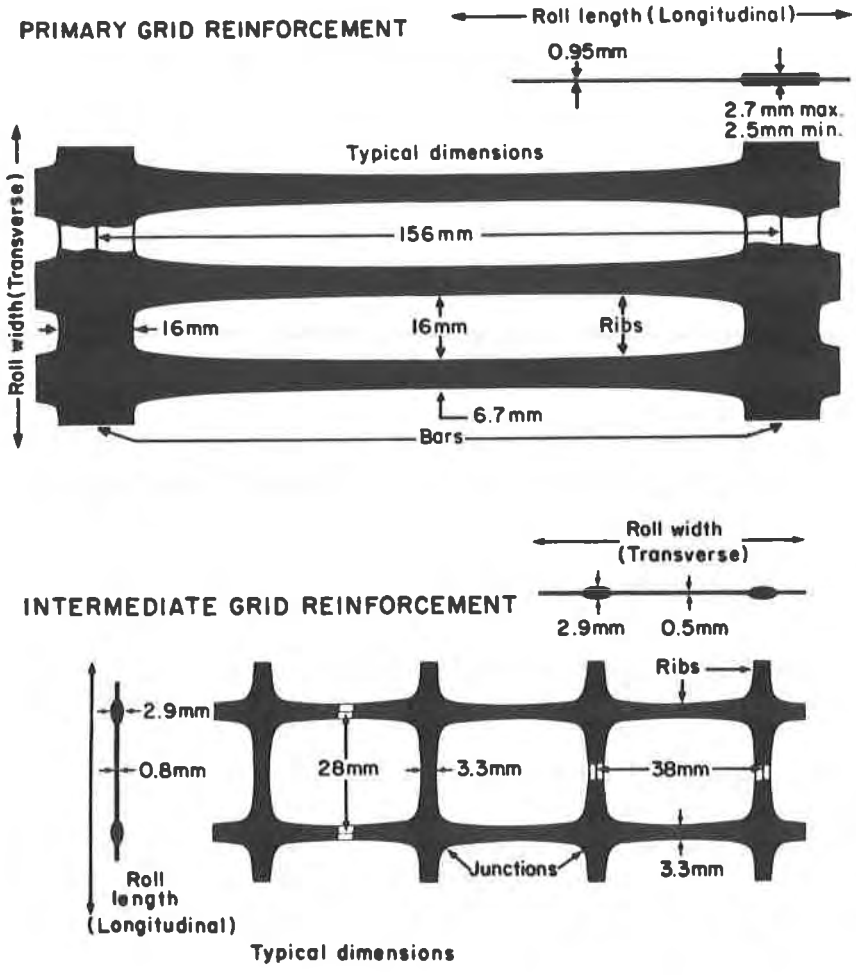

Figure 2. Geogrid reinforcement

Following completion of construction and a period of self-weight loading only, the structure was subjected to a cycle of surcharge load. Relatively small strains were recorded in the structure throughout this period, therefore in October 1987 a permanent surcharge load was applied by placement of a soil berm on the crest of the wall, see Figure 3. The condition of surcharge loading has remained unchanged since then. A summary of the loading sequence is given in Table 1.

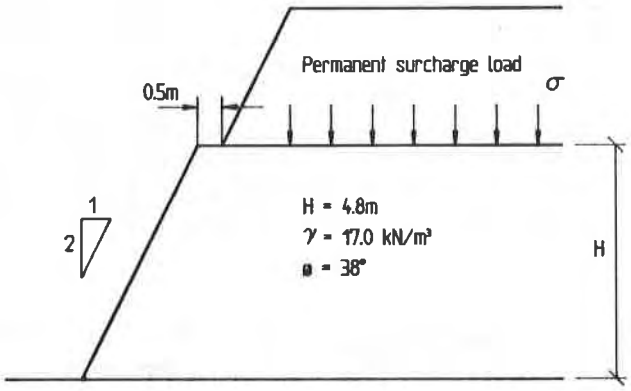

Figure 3. Permanent surcharge loading

Table 1. Loading sequence for the structure

Date	Loading	Description
July 1987	Self weight	
August to October 1987	Cycle of surcharge	Water tanks placed on crest σ_{max} = 28.7 kN/m^2
October 1987 to present	Permanent surcharge	Soil berm placed on crest $\sigma \simeq$ 50 kN/m^2

INSTRUMENTATION OF THE FIELD STRUCTURE

Instruments were placed in the structure to measure force in the reinforcement, strain in the reinforcement and in the soil, earth pressure and temperature, for which complete details are reported by Fannin (1988). Temperature is measured at eighteen locations in the reinforced soil zone, together with the air temperature, and the temperature in the instrument house where the readout units are located. These measurements of temperature are used to correct readings for differences in temperature between field measurement, installation (initial condition) and calibration. All instrumentation cables and hoses are taken to an on-site instrumentation house, which is supplied with mains electricity and is temperature controlled. Locations of strain and force measurement are illustrated in Figure 1. Following application of permanent surcharge loading to the structure, measurements of strain have been used to monitor creep behaviour.

Strain in the primary reinforcement is deduced from the output of inductance coils that are attached to the geogrid. Manufactured by Bison Instruments Inc., the coils comprise a metal winding which is embedded in an epoxy resin to form a flat disc. Discs are made to standard sizes, the dimensions of those used being a diameter of 54mm and a thickness of 7mm, with a central 6mm hole. The principle of operation is that of electromagnetic coupling, whereby the separation of a pair of coils may be related to the electromagnetic coupling between them. The coil pairs were fixed so that strain in the geogrid could be deduced at three locations on any layer of reinforcement. They were attached by a single nylon screw taken through the central hole in the coil and a similar hole drilled in the bar of the grid at the node, see Plate 1. A coplanar arrangement not only facilitates mounting, but was found to be least sensitive to a relative angular displacement of the coils. Application of an excitation current to one coil induces in the other a current that has both a phase and amplitude component: balancing of an inductance bridge allows a measurement to be made of the amplitude component which is directly related to the spacing of the coils.

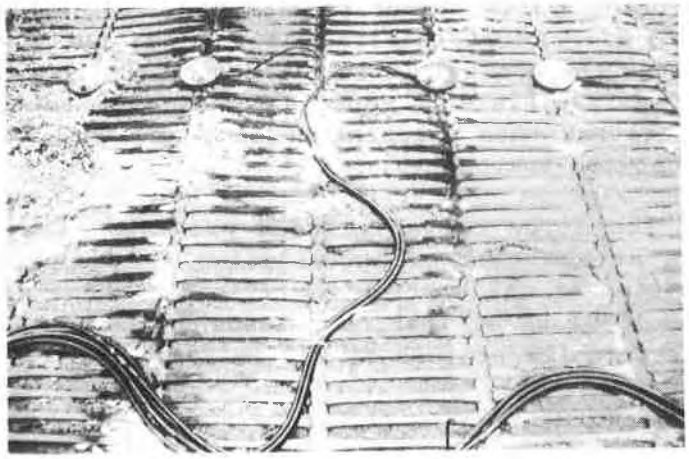

Plate 1. Inductance coils mounted on the geogrid

Examination of calibration certificates for coil pairs "in-air" shows predicted relative displacements to vary from actual relative displacements by ±0.05mm, for increasing relative displacements between zero and 7.5mm and an initial gauge length separation of 156mm, at a calibration temperature of 20° ±1°C. An initial gauge length separation of 156mm is the nominal spacing of the coils at the time of installation of the geogrid during construction.

Calibration of the coil pairs, which show a sensitivity to the presence of metal within four coil diameters, included corrections for ambient temperature of the system; relative temperature difference between the coils and meter box; embedment in the backfill soil; moisture content of the backfill soil. Complete account of these calibration factors is taken in reduction of the data. A reasonable indication of accuracy is given by the output from three pairs of dummy coils which are fixed at a constant separation on perspex blocks and embedded in the reinforced soil zone. They show a nearly constant, apparent strain of -0.1%, +0.1% and 0% respectively.

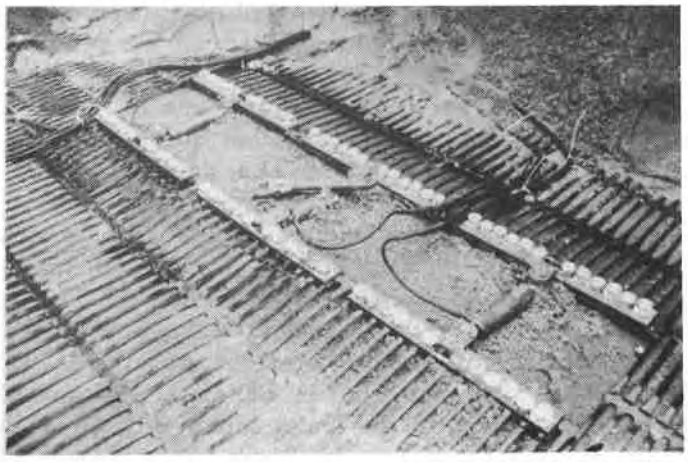

Plate 2. Load cells mounted on the geogrid

Force in the primary reinforcement is measured using vibrating-wire load cells designed and built by NGI. Installation was made by cutting away one series of longitudinal ribs across the nominal 1m roll width of the geogrid and mounting three cells to bridge the gap, see Plate 2. Special clamps connect the cells to the grid by a bearing action, rather than gripping action, and include provision against a transfer of bending between components.

Calibration of the force cells included provision for temperature effects, including temperature at the time of installation and temperature at the time of measurement. Examination of calibration certificates shows predicted loads differ from applied loads by ±0.01 kN or less, for loads between zero and a maximum value of 10 kN, at a calibration temperature of 20° ±1°C.

STRAIN IN THE GEOGRID REINFORCEMENT

Strain in the reinforcement is zero at the embedded end and is observed to increase to a maximum value close to the face of the wall. Generally the strain magnitudes are small, hence measurements at location 'A' on the instrumented grid are used to evaluate creep behaviour, see Figure 1. The variation of total strain with time at location 'A' is reported in Figures 4(a) and 5(a) for each layer of primary reinforcement, and for both sections of the slope. Time is reported as the elapsed time since completion of the surcharge loading in October 1987.

While the magnitude of strain is different in each layer, two characteristic responses are evident and are common to both sections of the structure. Strain in the base layers (layer No.1) is very small, and the characteristic response is one of little significant change with time. In contrast all other layers, with the exception of layer No.3 in Section 'JS', demonstrate a characteristic response of increasing strain with time. The magnitude of the increase is typically less than 0.5%. The rate of increase of strain with time is greater immediately after completion of surcharge loading, and the curves tend to a constant value of strain. This feature of the response is apparent from Figure 6, in which the mean value of strain in all layers except the base layer is plotted against time.

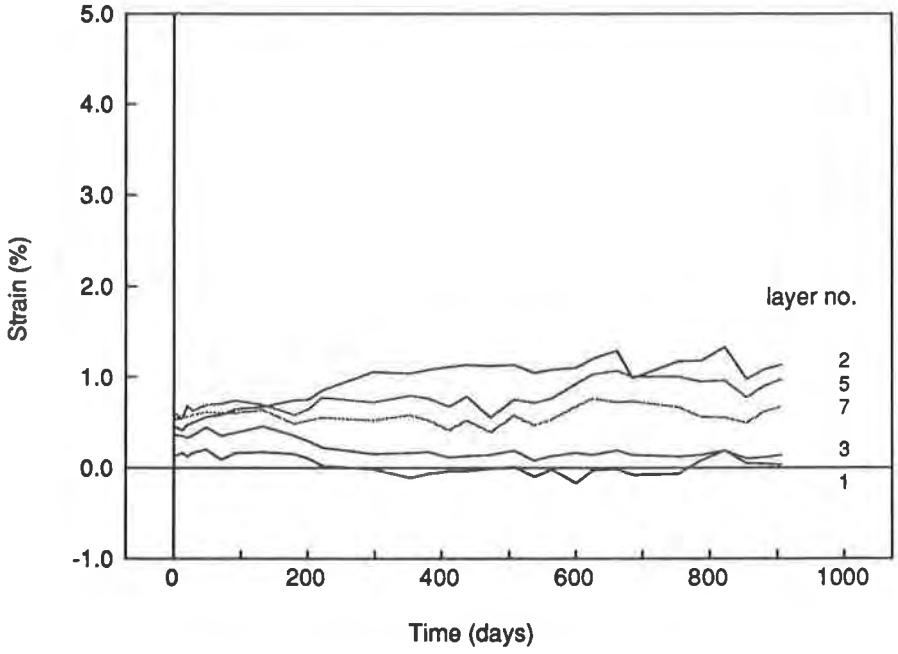

Figure 4(a). Section 'JS': strain measurements

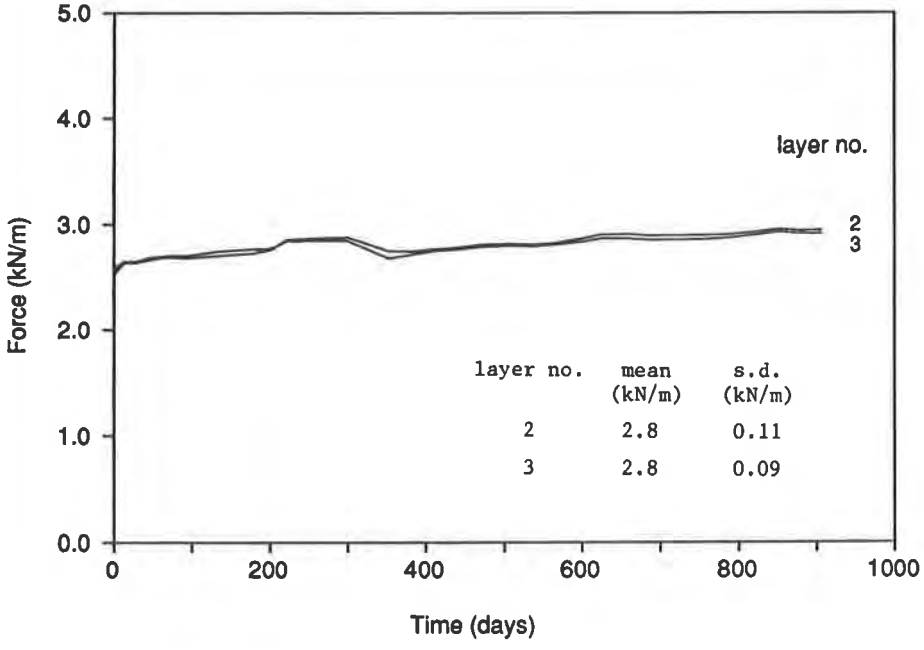

Figure 4(b). Section 'JF': force measurements

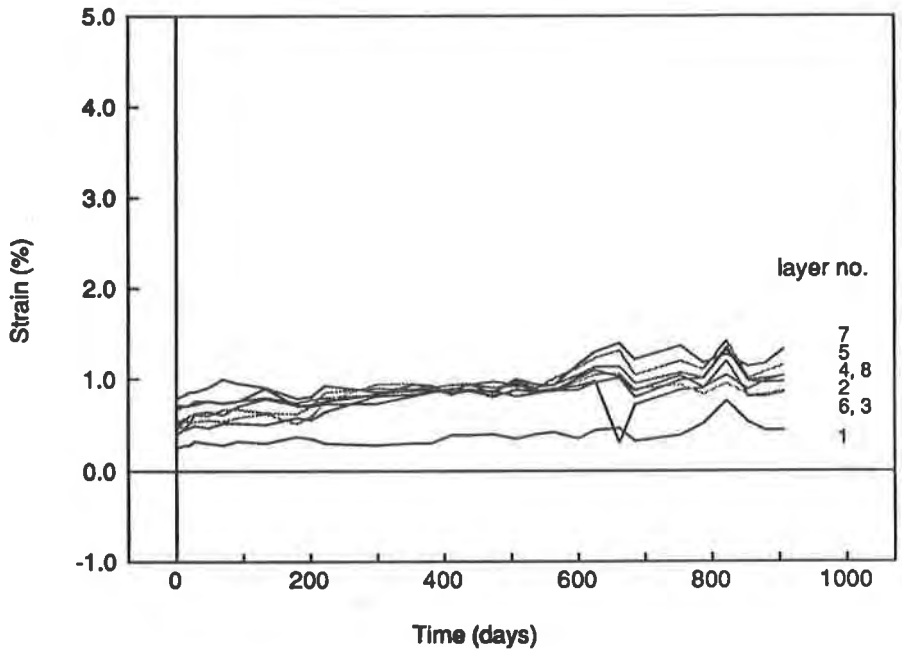

Figure 5(a). Section 'NS': strain measurements

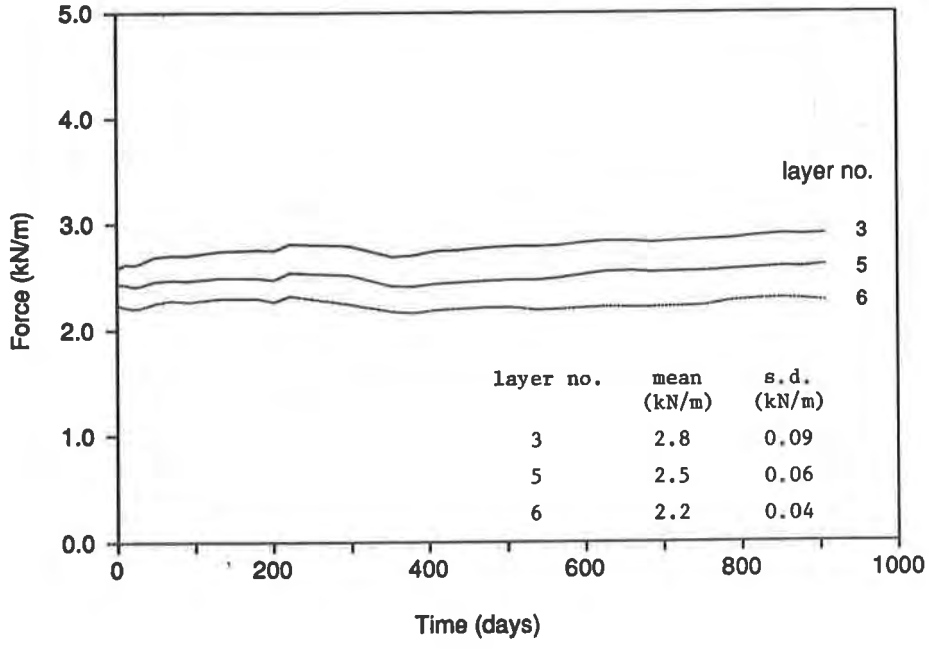

Figure 5(b). Section 'NF': force measurements

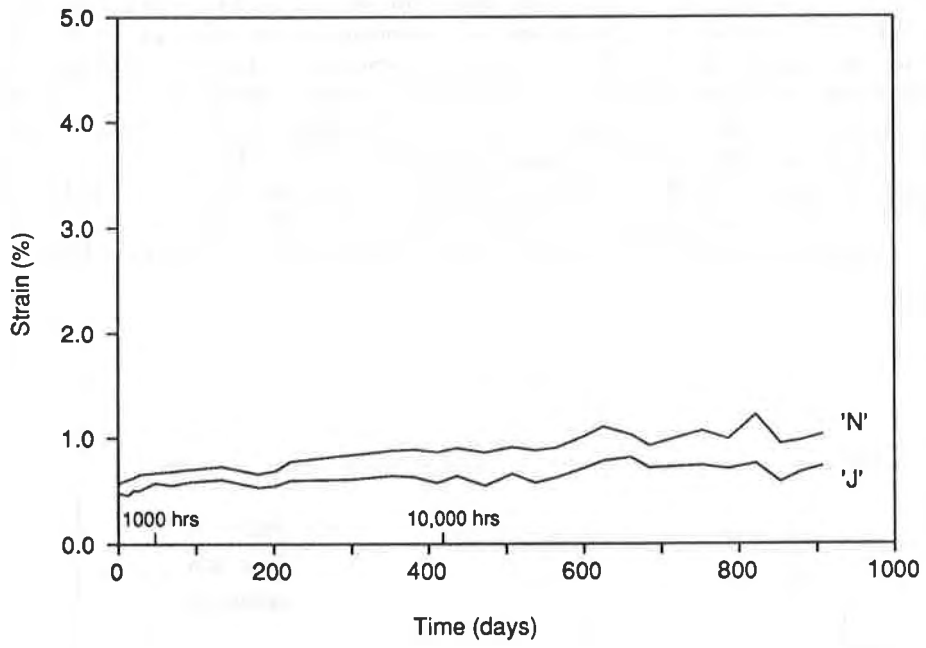

Figure 6. Variation of mean strain with time

FORCE IN THE GEOGRID REINFORCEMENT

Measurements of force in the reinforcement are also recorded at location 'A', though on an adjacent section of grid, see Figure 1. The measurements of force presented in Figures 4(b) and 5(b) are therefore directly comparable with the measurements of strain. A complete record of the variation of mobilized force with time throughout permanent surcharge loading is only available for five of the instrumented layers: some of the load cells sustained damage during an electric storm and are inoperable. As before the force at time zero is that in response to surcharge loading, and time is reported as the elapsed time since completion of surcharge loading. A mean and standard deviation for all measurements are reported with the curves.

The observations of force illustrate a characteristic response which again is common to both sections of the structure: although the reported values are not constant, there is no significant change in mobilized force with time. Rather there is evidence of a very moderate increase in force during the reported period of observation. It can be characterized as an increase of some 0.1kN/m on a magnitude of 2.5kN/m, which is less than 5%. This contrasts markedly with an increase of some 50% in the measured mean strains in the geogrid at location 'A' reported in Figure 6.

PREDICTION OF CREEP BEHAVIOUR

The field data which are reported describe a monitoring period of some 907 days, nearly 22000 hrs, following application of permanent surcharge loading. Throughout this period the measurements of force and strain describe a response to loading that is one of continued strain at nearly constant load. Observation shows the rate of increase of strain is not constant, rather it is decreasing with time and there is strong suggestion of a trend in the long-term to a rate of increase that is very small indeed. Measurements of soil temperature for this period show a variation between -0.5°C and 18°C. The variation is seasonal, as illustrated by the relationship between soil temperature and time reported for layer No. 5 in Section 'N' at location 'A', see Figure 7.

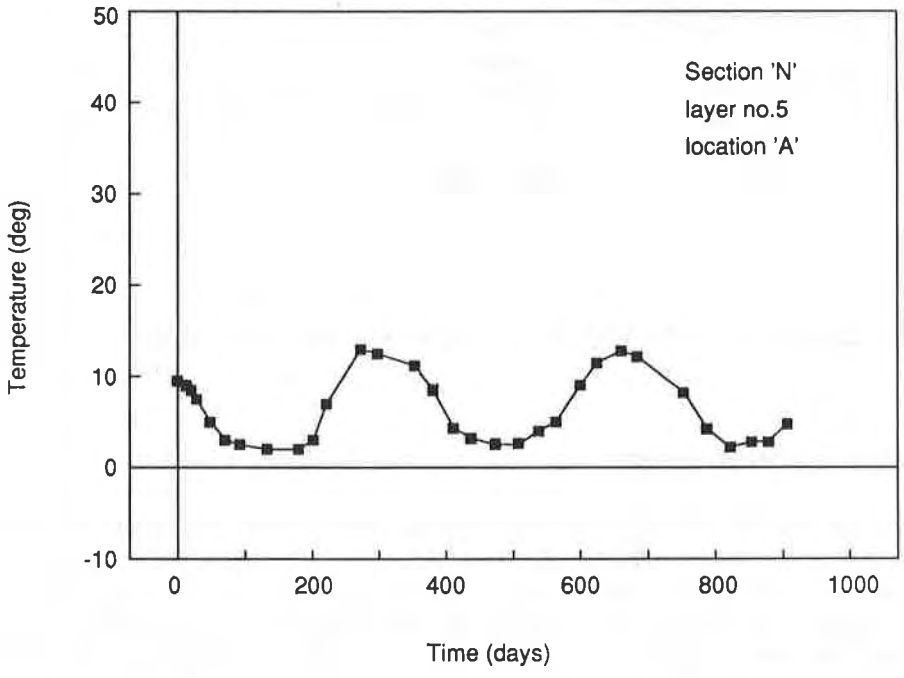

Figure 7. Variation of soil temperature with time

Laboratory data on the creep behaviour of the uniaxial geogrid are available as isochronous load-strain curves. Use of such curves for polymeric reinforcement has developed from work reported by McGown et al (1984) and by Yeo (1985), and it is proposed that the approach be adopted by the Canadian General Standards Board for tensile creep testing. Curves for 10°C and 20°C are reproduced in Figure 8 from data supplied by the manufacturer. While it is difficult to establish precisely values of force and strain from these curves at small strain magnitudes, a reasonable estimate of the range of strain for a tensile load of 2.5kN/m is from 0.5% at 1 hr to 0.75% at 1000 hrs, for 10° ±1°C.

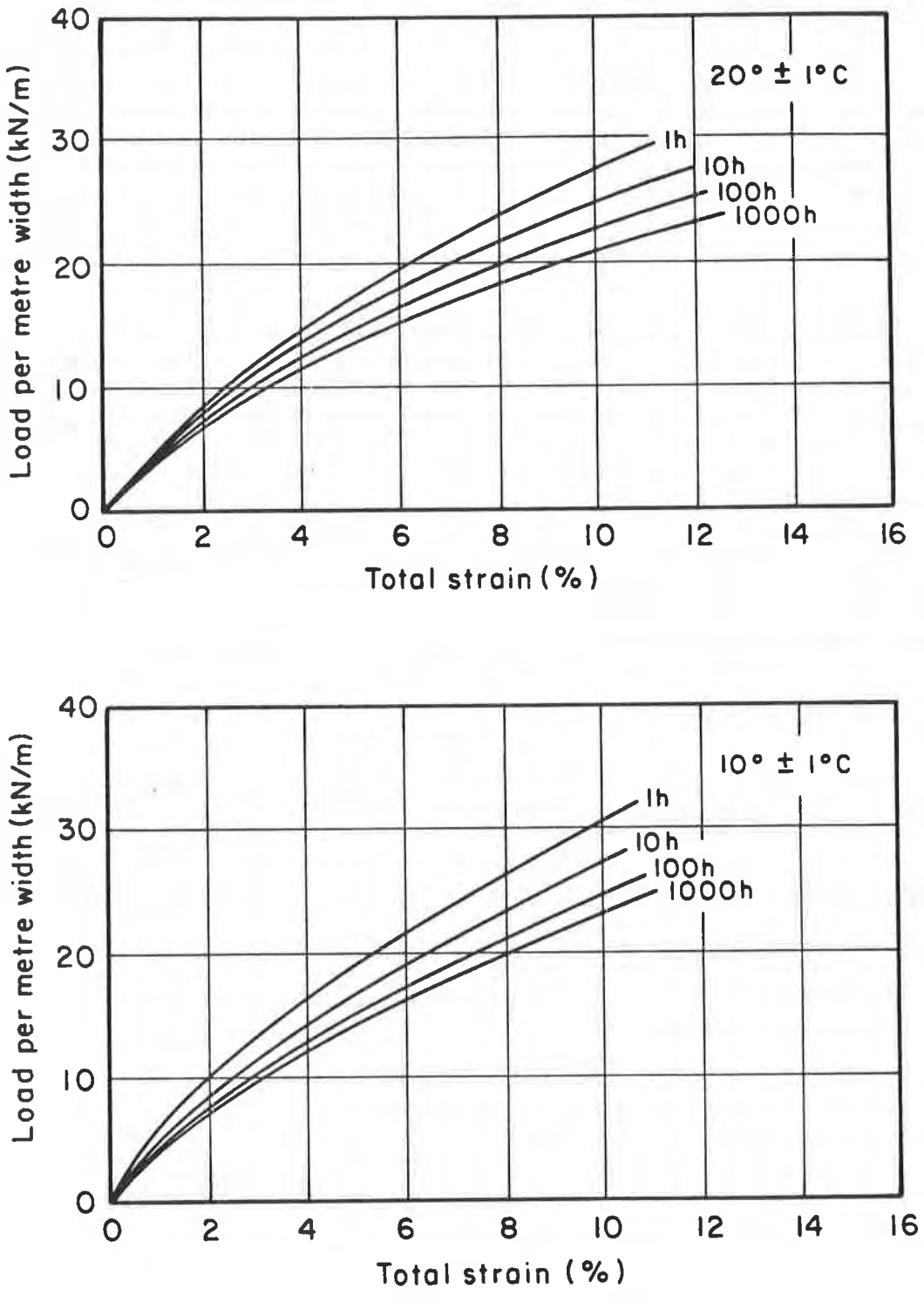

Figure 8. Isochronous load-strain curves for the uniaxial geogrid

In making a comparison of field data for the reinforced soil structure to such laboratory data it is important to recognize the pattern of loading imposed in each situation is not directly comparable. The field structure was incrementally loaded over a period of three days preceding completion of permanent surcharge loading, and the increment of mobilized force was in addition to that mobilized as a consequence of self-weight loading. In contrast, laboratory specimens for isochronous load-strain tests are loaded instantaneously. For this reason it is not possible to make a rigorous comparison of laboratory and field creep measurements. Yet the comparison shows good agreement between the observed response to loading of the reinforcement in the wall, and the predicted creep behaviour of the material from isochronous load-strain curves.

The predicted creep behaviour, at 10° ±1°C, is an increase in total strain from nearly 0.5% to 0.75% between 1 hr and 1000 hrs after loading, for a load of 2.5kN/m. The observed response in the reinforced soil structure, for layers of reinforcement mobilizing a nearby constant load in the range 2 to 3kN/m, is an increase in mean strain with time from some 0.5% to between 0.75% and 1.0% at 900 days (21,600 hrs) after surcharge loading, see Figure 6. The rate of increase of strain with time appears to be slowing, which again is a characteristic of behaviour evident in the isochronous load-strain curves, see Figure 8. The variation of mean strain with time reported for the field structure suggests creep data to 1000 hrs of loading does not completely describe load-extension behaviour of the polymeric reinforcement, and information for a longer period of time may be appropriate. Current creep test methods are usually taken to 10,000 hrs. This would appear to describe better the creep behaviour reported for the field structure.

DESIGN FOR LONG TERM CREEP

Requirements for design of geogrid reinforced soil structures in the United Kingdom are presented in Technical Memorandum (Bridges) BE 3/78 (Revised 1987) (DTP 1987) and the Roads and Bridges Agrement Certificate No.86/27 (BBA 1986). With regard to creep, criteria are presented in the Technical Memorandum as values of limit strain that are dependent on the method of wall construction. Consideration is given to a design life of 120 years, or 1.05×10^6 hrs. In the case of incremental construction using discrete facing panels, such that each layer of the structure may deform prior to placement of the next, the limit strain ignores any initial strain developed during the period of construction. For retaining walls the value of limit strain is 1 per cent, and for bridge abutments the value of limit strain is 0.5 per cent.

The arrangement and spacing of reinforcement in the instrumented reinforced soil structure, and the surcharge loading, were deliberately selected to mobilize large strains in the polymer grid. The data are for a period of some 22,000hrs following application of surcharge loading. Measurements of strain reported in Figures 4(a) and 5(a) show creep strains up to 0.5% for some layers of reinforcement, although mean values of creep strain for all layers except the base layer are somewhat less, see Figure 6.

In comparison to the requirements of limit strain described above, the observed creep strains are significant, although it is difficult to establish at this stage if they will exceed in the long-term the 1 per cent limit which applies to retaining walls. Since the arrangement of reinforcement in both sections of the wall was designed for self-weight loading only, the magnitudes of strain cannot be used in any

direct evaluation of the design approaches relating to creep. Rather the results imply a prediction of creep strains based on long-term creep tests is possible, and is appropriate to design of reinforced soil structures. The creep tests should be carried out for load magnitudes that are representative of field values.

CONCLUSIONS

1. The relationship between force and strain observed in the reinforced soil structure is described by isochronous load-strain curves established from creep tensile tests. Such curves are well suited to design criteria for long term creep based on values of limit strain.

2. Creep tensile tests to establish isochronous load-strain data for use in design should be carried out for loads that are representative of working conditions in field structures. Data to at least 10,000 hrs is required to facilitate long term predictions.

ACKNOWLEDGEMENTS

The reported study was carried out at the Norwegian Geotechnical Institute, in cooperation with the Norwegian Road Research Laboratory, and the assistance of Tor Helge Johansen is gratefully acknowledged. The work was funded by the Royal Norwegian Council for Scientific and Industrial Research. The geogrid reinforcement was supplied by Netlon Ltd.

REFERENCES

British Board of Agreement (1986). Roads and Bridges Agrement Certificate No.86/27. Tensar SR2 polymer grid for reinforced soil walls. BBA, Watford, Herts.

Department of Transport (1987). Technical Memorandum (Bridges) BE 3/78 (Revised 1987). Reinforced earth retaining walls and bridge abutments for embankments. London (Department of Transport).

Fannin, R.J. (1988) An instrumented field study of the analysis and design of geogrid reinforced slopes. Norwegian Geotechnical Report No.52757-10, Oslo.

Fannin, R.J. and Hermann, S. (1990). Performance data for a sloped reinforced soil wall. Can. Geotech. J. 27(5), pp. 676-686.

McGown, A., Andrawes, K.Z., A, K.C. and Dubois, D. (1984). The load-strain-time behaviour of Tensar geogrids. Symposium on Polymer Grid Reinforcement, ICE, London. Thomas Telford Ltd.

Yeo, K.C. (1985). The behaviour of polymer grids used for soil reinforcement. Ph.D. thesis, Dept. of Civil Engineering, University of Strathclyde.

Comparative Behaviour of Metal and Tensar Geogrid Strips Under Static and Repeated Loading

Thomas Hamilton Hanna
University of Sheffield, UK
Mabrouk Touahmia
University of Sheffield, UK

ABSTRACT

Static and slow repeated load tests were performed on 4m length of smooth steel, ribbed steel and Tensar geogrid reinforcing strips. Comparisons are made of the development of strip movement under load with number of alternating load applications. It has been clearly demonstrated that the synthetic geogrid strip reinforcement is more load efficient than either the smooth or the ribbed steel strips.

INTRODUCTION

It is now recognized that the designer of reinforced earth structures may have to consider (i) different types of reinforcing element and (ii) different types of loading e.g. static, repeated, dynamic. Extensive literature will be found on the behaviour of elements under static loading. However, little data are available in which different forms of reinforcement are compared by reference to tests under similar conditions. A reinforced earth element is a tensile resisting member embedded in a soil mass. Under applied external load the reinforcement will mobilize resistance along its length according to the laws of bond and bearing. Questions very often posed by engineers include: (a) does the surface roughness or shape of the reinforcement affect resistance to loading; (b) what is the significance of strip length; (c) what is the significance of applied normal stress; (d) what is the difference between a relatively flexible and a relatively rigid reinforcement; (e) how does a repeated load application affect the pull-out capacity and the "life" of a reinforcement? The ability of the engineer to give reliable answers to these questions is thwarted by a lack of reliable data. To provide a datum against which the performance of reinforced earth elements could be assessed a program of experimental work has been in progress for 15 years. This paper presents some of this work in an attempt to give an unbiased assessment of the performance of the synthetic geogrid strip relative to those of both the smooth and the ribbed steel strip. In this study efforts were made to work at large scale (about half scale) to avoid errors associated with "model" testing.

THE TEST SYSTEM

The test rig comprised a steel container, Figure 1, 0.3m by 0.3m by 4m in length. The internal walls of the rigid rig are smeared with a "frictionless grease", allowing a surcharge

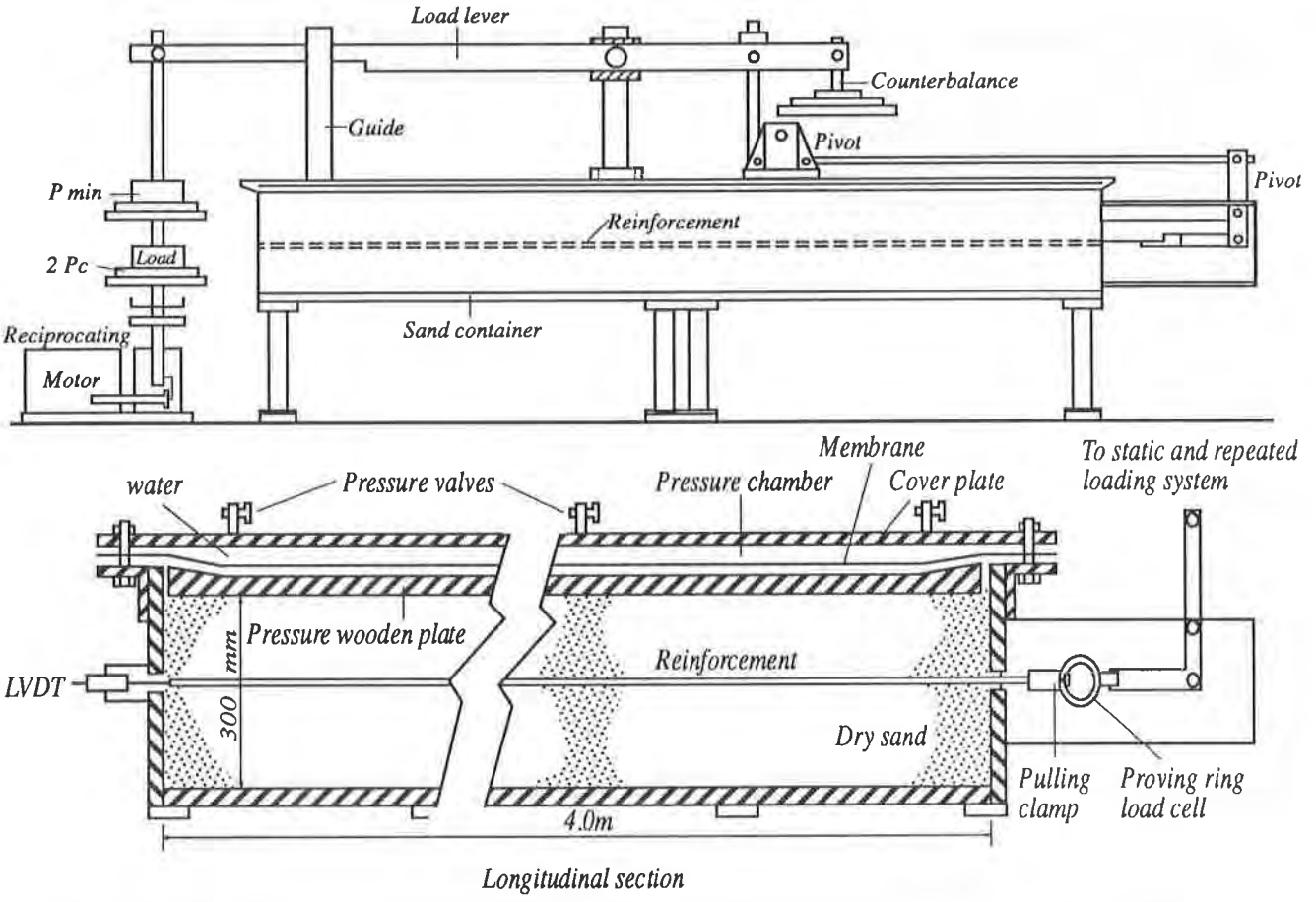

Fig. 1. The test apparatus

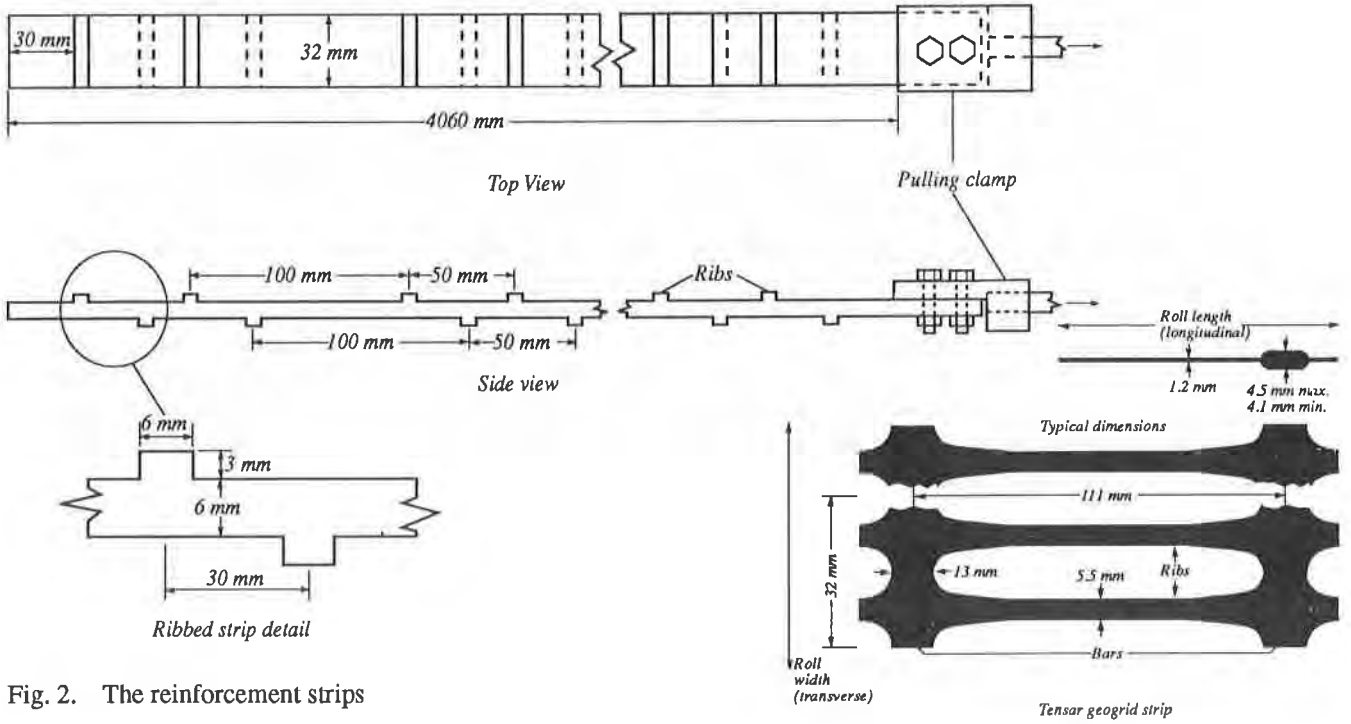

Fig. 2. The reinforcement strips

pressure, applied via a pressure plate loaded through a water bag, to be transmitted through the sand mass. The reinforcing element is located within the sand mass, emerging through the end of the sand box where it is connected to a special loading level system with the capacity to apply either static loads or slow repeated loadings. For the repeated loadings the load was changed every 20 seconds to give a square-shaped pattern between an upper and a lower load level. The load levels were related to the static pull-out capacity, P_u, of the steel strips and the index load (P.I.) of the synthetic geogrid strip. The Index Load is the ultimate rupture load. (Choek (1985)). Great care was taken to prevent impact loadings being caused. The surcharge pressure could be controlled from 0 to 200 kN/m^2 without causing any significant straining of the test rig.

The sand was used in a dry state being of medium size and uniformly graded ($U = D_{60}/D_{10} = 1.9$). The specific gravity was 2.67; maximum and minimum densities were 1.78 and 1.42 Mg/m^3 respectively with corresponding void ratios of 0.87 and 0.49. A raining method of sand placement gave an average and repeatable density of 1.57 Mg/m^3 with a relative density of 0.53.

Three reinforcing elements were chosen for test corresponding to a smooth steel strip, a high adherence (ribbed) steel strip and a plastic strip formed from synthetic geogrid material. The width of the strip finally chosen was 32mm to ensure that there were no edge effects from the test rig walls. For the smooth steel strip the thickness was 6mm. The ribbed steel strip was of the same material (yield stress = 680 N/mm^2 and modulus of elasticity 200 kN/mm^2) but with a series of projections 3mm high by 6mm in width attached to the strip according to the recommendations of Schlosser (1978). Both steel reinforcements were provided with special load cells, temperature compensated, at 400mm centres, the wires from the cells being carried in grooves machined along the length of the strip to a terminal at the free end. Care was given to both the longevity of the load cell and drift in calibration. No problems were encountered.

The third reinforcement was formed by cutting a strip (32mm wide) of two ribs in width and 35 bars in length from a roll of SR2 geogrid. The yield stress of the geogrid was 250 N/mm^2. The value of the modulus of elasticity was not determined because it is well known (Choek 1985) that the value is highly dependent on the rate of loading and temperature. Attempts were made to instrument the strip with load cells but none were successful.

Details of the steel and geogrid strips tested are given in Figure 2. For the geogrid strip special axial movement gauges were provided at five locations to measure the distribution of axial movement along the strip with applied load (Carr and Hanna (1970)).

STATIC LOAD TEST BEHAVIOUR

The results of constant stress load tests to failure for the three reinforcement types are shown in Figures 3(a) to (c) for three levels of normal stress, 50, 75 and 100 kN/m^2. In general the following conclusions are drawn:

(a) The largest pull-out load was generated by the steel ribbed strip, the smallest by the synthetic geogrid strip.

(b) The displacement to cause failure was smallest for the smooth steel strip and largest for the geogrid strip. Failure was defined as the load to cause either complete pull out of the strip or very large displacements of the strip for very small load increments.

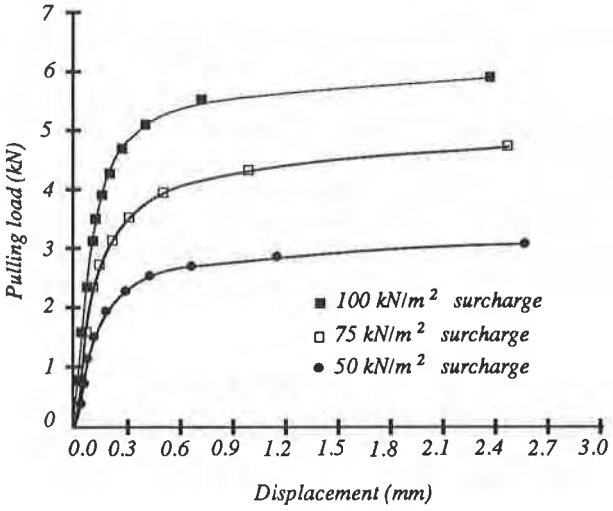

Fig. 3. (a) Load - displacement relationships, smooth strip

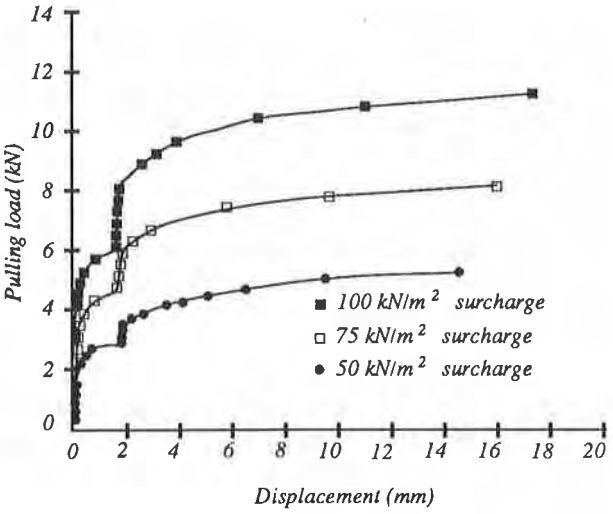

Fig. 3. (b) Load - displacement relationships, ribbed strip

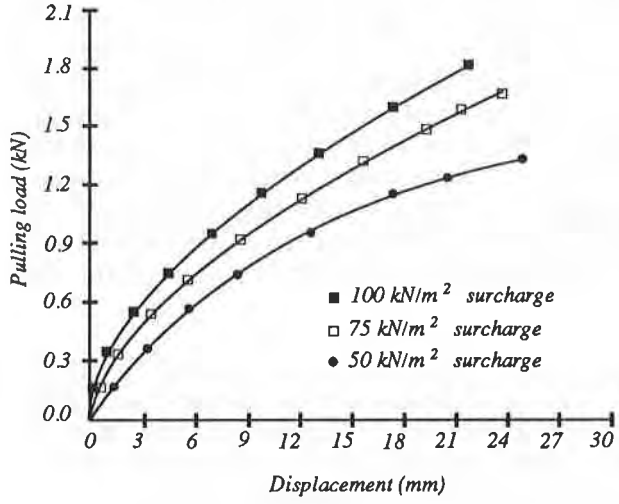

Fig. 3. (c) Load - displacement relationships, Tensar geogrid strips

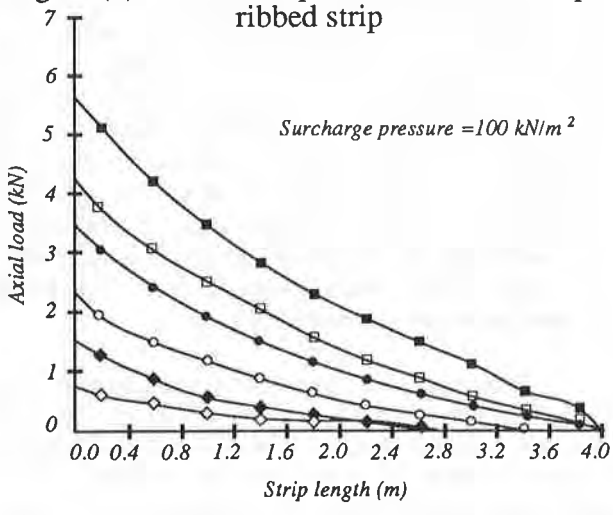

Fig. 4. (a) Load mobilization along smooth strip

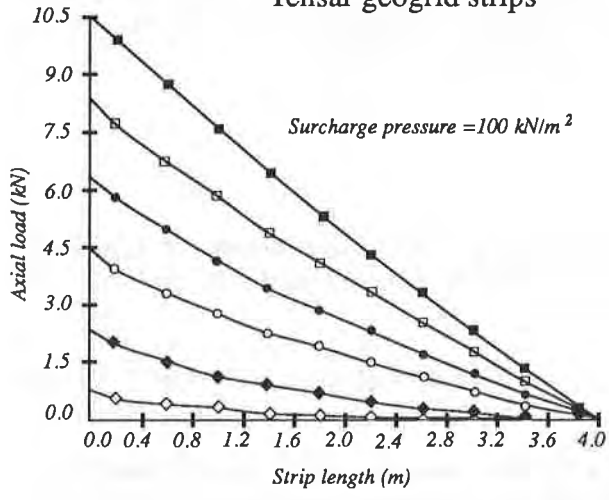

Fig. 4. (b) Load mobilization along ribbed strip

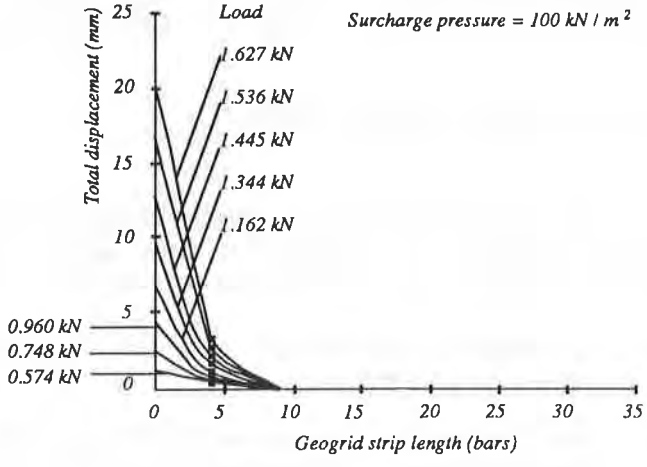

Fig. 5. Total displacement for various load increments

(c) Increase of confining pressure caused an increase in pull-out load, the relationship being approximately linear.

(d) The shapes of the pull-out load/displacement curves were very different: the smooth strip gave a near peak value at a displacement less than 1mm; the ribbed strip gave a peak load (approximately) at a displacement of about 4mm; the geogrid gave no peak load, the load increasing with displacement (Figure 3(c)).

(e) For the ribbed steel strip the effects of side friction and end bearing load development on the ribs are clearly evident at displacements between about 0.5 and 2mm.

It is clear that these trends are reflecting the complex interaction between the strains necessary to mobilize skin friction and bearing resistances and the effects of the axial flexibility of the geogrid strip. The ribbed and the geogrid strips are much more load efficient and have a much less 'brittle' load/displacement relationship than the smooth strip. Data for the smooth and ribbed strips are given in Figure 4 showing the distribution of load along the length of a 4m strip whilst the movements of the geogrid strip are given in Figure 5. A most interesting feature is observed. In contrast to the steel strips where the axial load was gradually mobilized over the full length of the strip; the load in the geogrid was mobilized along the front quarter of the strip only. It will be noted that the test was stopped at a displacement of 24mm of the end of the strip, the applied load being 50% of the Index load. Index testing was chosen to standardize the test conditions so that the geogrids may be compared under the same conditions and to establish a set of properties for the geogrids which may be referred to by end users to define strength and to relate to other testing conditions, Choek (1985). It is evident from Figure 5 that the geogrid strip still has a very large pull-out load reserve but the applied load was restricted to 1.63kN to prevent damage to the strip material. Unless a very low confining stress is used, it would be impossible to pull the strip out of the soil, failure of the strip material being easier.

Load testing was also performed on strips which had been subjected to cycles of repeated loading. Typical data are presented in Figure 6. Surprising results emerged: (i) the pull-out capacity of the smooth strip reduced significantly after 100,000 cycles of loading between 0 and 30% P_u; (ii) for the ribbed strip the reverse was found, the pull-out resistance being significantly increased after 6700 cycles of loading between 0 and 50% P_u ; (iii) for the geogrid strip there was very little change in behaviour even after 30,000 cycles of repeated loading, an expected result.

These findings clearly demonstrate that a smooth steel strip is not a reliable reinforcement if the applied loading is of a slow cyclic form. The ribbed strip is a much more reliable reinforcement. The geogrid, because of the very large reserve length unloaded, behaved in a similar manner to first time loading and, undoubtedly, is the most reliable of the three strips tested.

REPEATED LOAD TESTING

Because of the very different static load performances of the three strips it was expected that their behaviours under slow repeated loading would be very different. The application of a load to the strip causes resistance to be mobilized between the soil and strip, the mechanics being similar to those of loading a pile (Hanna, 1969). The removal of part of the applied load causes load to flow out of the strip with associated stress change. An enormous amount of

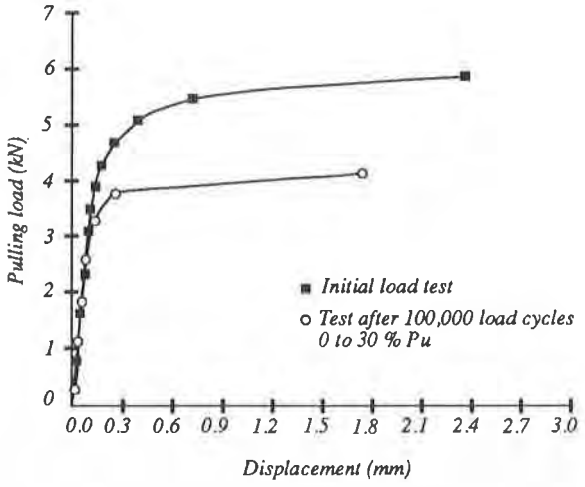

Fig. 6. (a) Load - displacement relationships before and after repeated loading, smooth strip

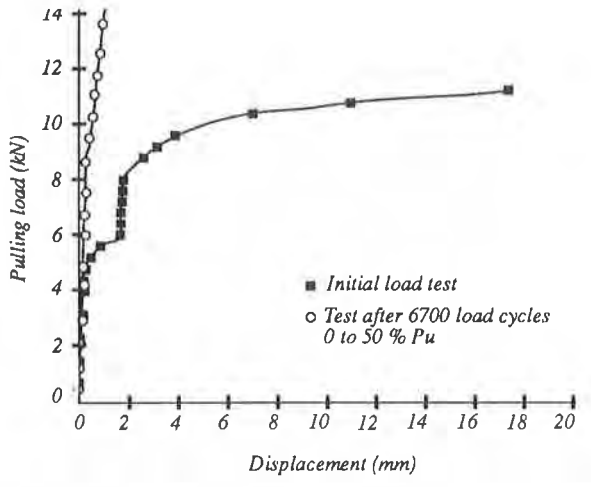

Fig. 6. (b) Load - displacement relationships before and after repeated loading, ribbed strip

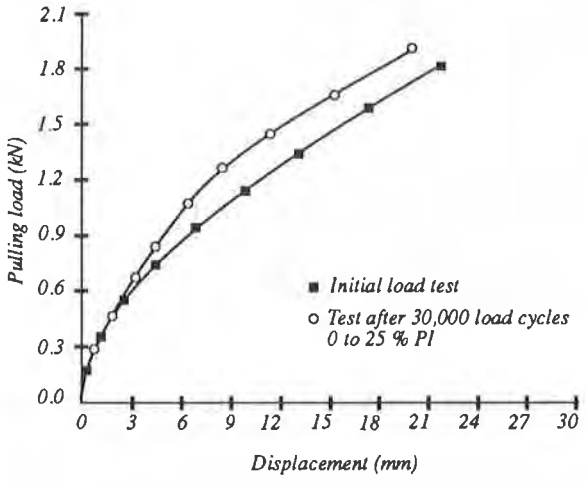

Fig. 6. (c) Load - displacement relationships before and after repeated loading, Tensar geogrid strip

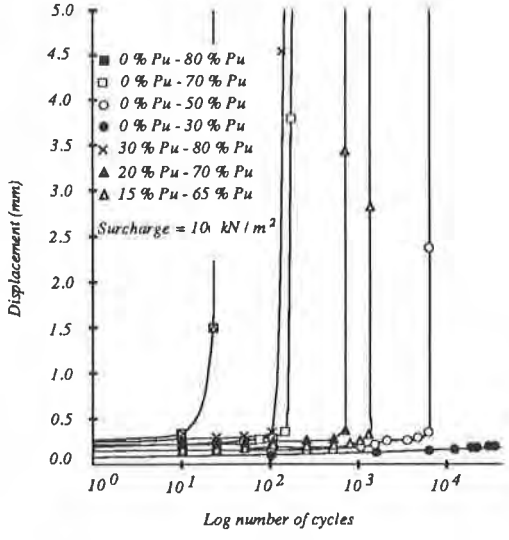

Fig. 7. (a) Displacement - log number of load cycles, smooth strip

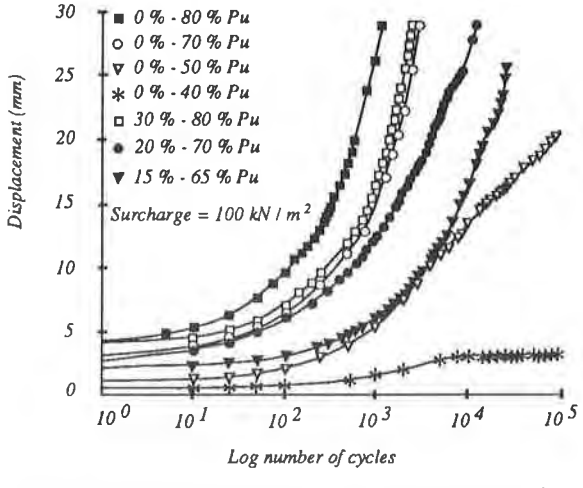

Fig. 7. (b) Displacement - log number of load cycles, ribbed strip

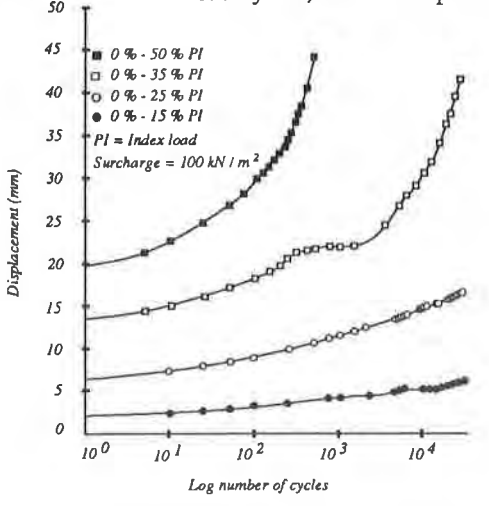

Fig. 7. (c) Displacement - log number of load cycles, Tensar geogrid strip

test data has been generated with some tests being taken to 100,000 cycles. Typical results only are presented for 4m strips. Data for other lengths of strip will be reported in another paper.

Displacement - log number of load cycles data are given in Figure 7 for the three strips tested. A range of load levels was used for one level of confining stress. For the seven load levels tested with the smooth steel strip failure by pull-out occurred in six cases, Figure 7(a), but for the load level 0 to 30% P_u the strip was still stable after 10^5 cycles the displacement at this stage being a fraction of a mm. It will be noted that in all cases the displacements were small and the strip appeared to be "stable". The reason for the relatively sudden change in behaviour may be related to the distribution of load along the length of the strip. Initially (on first loading) the distribution of loading was near linear along the strip length but, with increase in the number of load repetitions, the load distribution changed with more and more load being transferred towards the distal end of the strip. Typical data are given in Figure 8 for a repeated load level of 0 to 50% P_u.

The ribbed strip behaved in a very different manner as Figure 7(b) clearly shows. Firstly, for any number of load cycles the displacement of the strip was greater than for the smooth strip. Secondly, there was no "abrupt" change in behaviour, all of the strips gradually pulling through the ground with the exception of the test at 0 - 40% P_u which was still stable after 10^5 cycles. As mentioned earlier the mechanics of load mobilization for smooth and rough ribbed strips are quite different.

The geogrid strip gave performances somewhat similar to those of the ribbed strip, Figure 7(c), but there were differences. The movements were much larger; at all load levels no load was mobilized at or near the distal end of the strip; the test data do show that none of these strips failed by pulling through the sand mass.

The above data were presented in semi-log form making difficulty in comparing trends between the strips because of different levels of loading, different initial displacements on load and different modes of load mobilization. Lashine (1973) showed that an accelerated rate of displacement for repeated tests on a granular soil usually was irreversible and indicative of failure once such a stage was reached. The present data are replotted in this form of rate of displacement/cycle against the number of cycles, Figure 9. The smooth strip data clearly reflect the trends shown in Figure 7(a), namely that all strips failed by eventually pulling out although initially all rates of displacement kept decreasing with increases in the number of load cycles. An interesting feature is that the slopes of all plots are approximately the same. In general there was no indication that failure was imminent. None of the ribbed strip tests indicated failure, the rate of displacement in all cases decreasing with cycle number increase. The geogrid data, Figure 9(c) show a similar trend. These curves may be somewhat misleading because the scales of the vertical axis are different, reflecting the different amounts of movement of the strips. What is clear is the excellent performance of the geogrid strip compared with the two metal strips.

DISCUSSION OF THE FINDINGS

The test data clearly demonstrate the complex nature of repeated loading response of foundation elements. The cumulative effects of the repeated loads have been presented in the Figures. From a fundamental point of view the deterioration in the performance of a strip appears to be related to several partly understood factors including, (i) changes in load transfer along the strip length, (ii) changes in the normal confining stress along the strip with increase

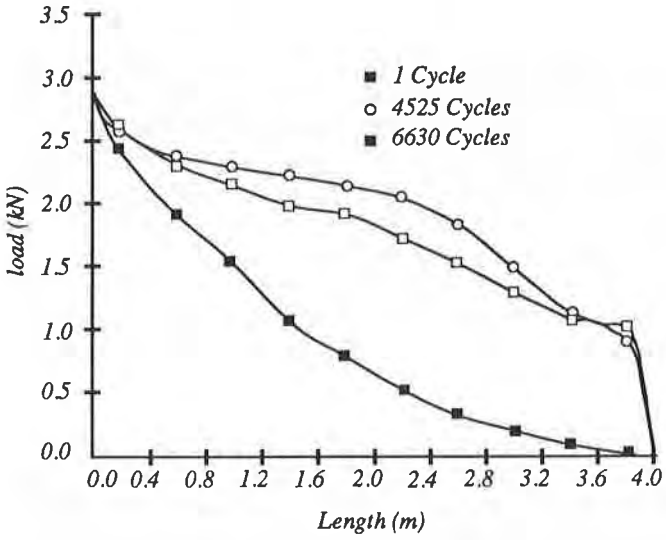

Fig. 8. Changes in axial load distribution with repeated loading , smooth strip

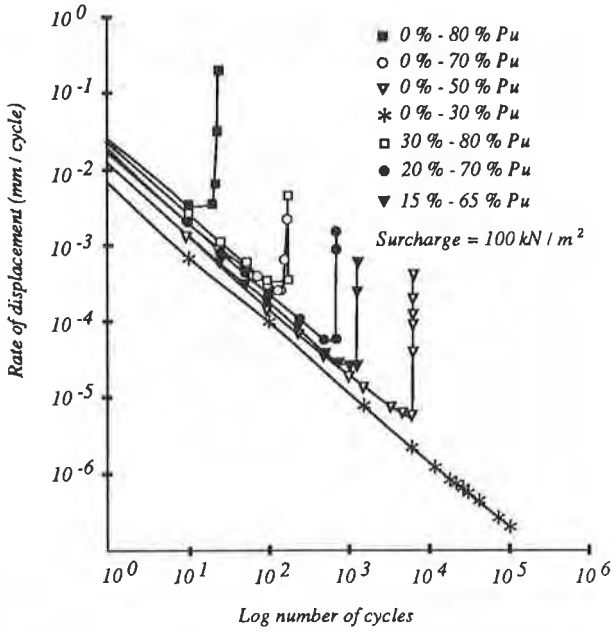

Fig. 9. (a) Rate of displacement / load cycle, smooth strip

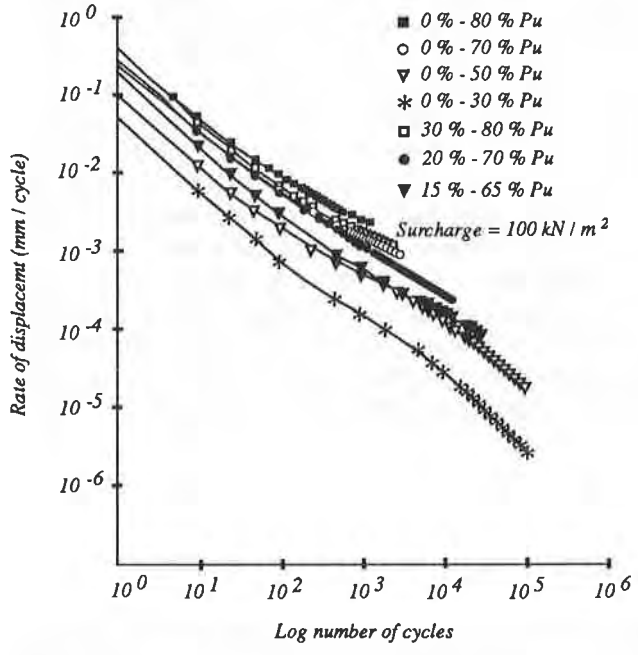

Fig. 9. (b) Rate of displacement / load cycle, ribbed strip

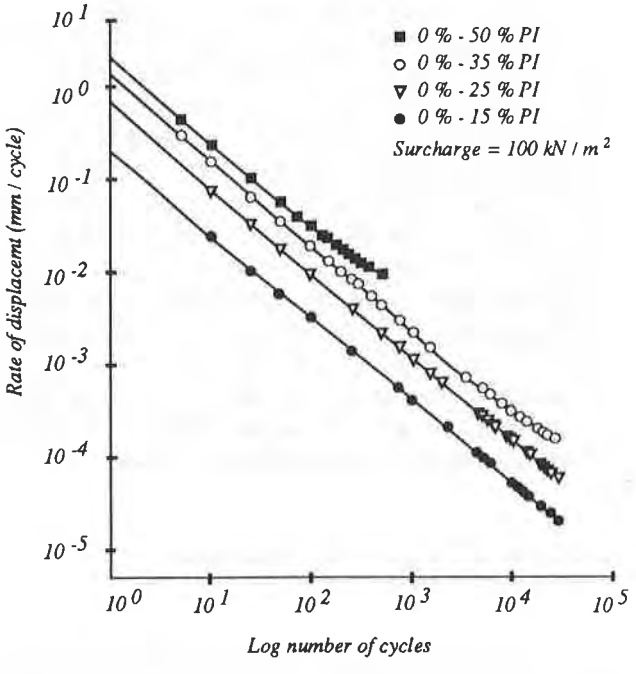

Fig. 9. (c) Rate of displacement / load cycle, Tensar geogrid strip

in the number of load repetitions, (iii) "compaction" of the sand due to local shear reversals causing breakdown of particles, (iv) locked-in stresses changing after each load cycle. In order to understand these complex and interrelated factors it will be necessary to carry out a wide range of further testing and calculations. The experimental work has established the changes in load transfer which occur. Changes in soil grading in the vicinity of the strips have shown a break-down of particles leading to a densification of the sand locally which, in turn, allows the strip to gradually pull out because the normal confining stress is reduced. This compaction of the sand mass may be the primary factor in controlling behaviour. Work by Morland and Sawicki (1983, 1985) has established reliable means of describing the compaction effects of shear hysteresis loading of sands. The theory has been applied with success to the modelling of pile behaviour under axial cyclic loading. It may be possible, at a later date, to extend these theories to the case of reinforced earth elements and thus develop a reliable method of predicting cyclic loading behaviour. The locked-in stress regime is a complex one. the experiments have shown that the locked-in stress increases with increase in the number of load cycles, a trend also observed with piles under repeated loading (Chan and Hanna (1979)). At the present time it has not been possible to analyse any of these causes but it has been possible to show the cumulative result. From an engineering consideration these test results, and much other data not reported here, establish the following:

(a) A ribbed or a grid strip is a much more efficient reinforcement element than a smooth strip both for static and repeated loading.

(b) With the relatively inextensible steel strips the applied load is mobilized over the full length of the strip. In contrast, the relatively extensible synthetic geogrid strip under load deformed much further than the steel but even at the highest test load, 50% P.I., the resistance to load was mobilized over the front quarter length of the strip, the remaining three-quarters of the strip being unstressed. The load was resisted primarily by the bars of the grid acting as a series of anchors or footings. On unload large residual loads were locked in the steel strips. It was not possible to measure load distributions in the synthetic geogrid strip but the evidence, as obtained from the longitudinal movement of this strip under load change, suggests that the locked-in loads on unload were small. It is clear that the mechanics of load mobilization for the steel strip (primarily in side friction) are different from those of the synthetic geogrid (primarily in bearing against the individual bars of the grid). Direct comparison of load carrying capacity between the steel strips and the synthetic geogrid is unwarranted because, in use, the grid reinforcement covers the plan area of the ground whereas the individual strips cover a small area only. From knowledge of strip spacing the relative load efficiencies of the grid versus the strip may be established. From a simple consideration it will be found that the synthetic geogrid has at least the same load capacity as the steel reinforcement. Also, at reasonable depths of embedment the synthetic geogrid will fail structurally rather than pull out.

(c) Under load the synthetic geogrid moves much further than the steel reinforcement but, for a given load, has a much greater reserve of pull-out capacity. In design allowance can be made for the larger movements. In contrast to the movements of the strips under static loading, the application of repeated loads generated quite complex trends. The smooth strips strained very little further under repeated loading for all load levels but suddenly started to pull out leading to catastrophic failure. The ribbed strips displaced much further under repeated loadings showing a gradual movement with the log the number of load applications. None of the strips failed by pulling out, the rate of displacement per load cycle decreasing. Clearly this strip is much more suitable to resist pull-out repeated loadings than the smooth strip. None of the synthetic geogrid strips failed during repeated loading. In no case did any of the applied load reach the distal end

of the strip. The behaviour of these grid strips was even better than the ribbed steel strips. From all of the test data generated to date it is impossible to predict when the onset of failure by pull-out starts. There is a need to develop further a degradation curve for repeated loading and apply it to the reinforced earth strip. All indications are that grid and ribbed reinforcements are suitable for cases of repeated loading. The grid is a more efficient element than a ribbed strip.

(d) Contemporary work on offshore piles subjected to a small number of repeated loads has led to the postulation of the use of cyclic stability diagrams, Poulos (1989). In such plots a normalized alternating load is graphed against a normalized mean load and stable and unstable zones defined for different numbers of repeated loadings. Attempts have been made to generate such stability plots for the strips tested. For the ribbed and the synthetic geogrid strips, as referred to earlier, failure of these strips did not occur despite up to 10^5 load repetitions. For the smooth strips failure occurred and these data have been assembled in a stability plot form, Figure 10(a) for 100 load cycles. A general master plot is given in Figure 10(b) for load repetitions up to 10^6.

(e) The testing of a reinforcing element after subjecting it to a series of repeated loads demonstrated the importance of the sand densification in the vicinity of the strip. The smooth strip gave a significantly reduced pull-out capacity, the other strips showing a significant increase (ribbed strip) and the geogrid behaving in a similar manner to its initial static loading. With the geogrid strip it was not possible to subject it to pull-out failure.

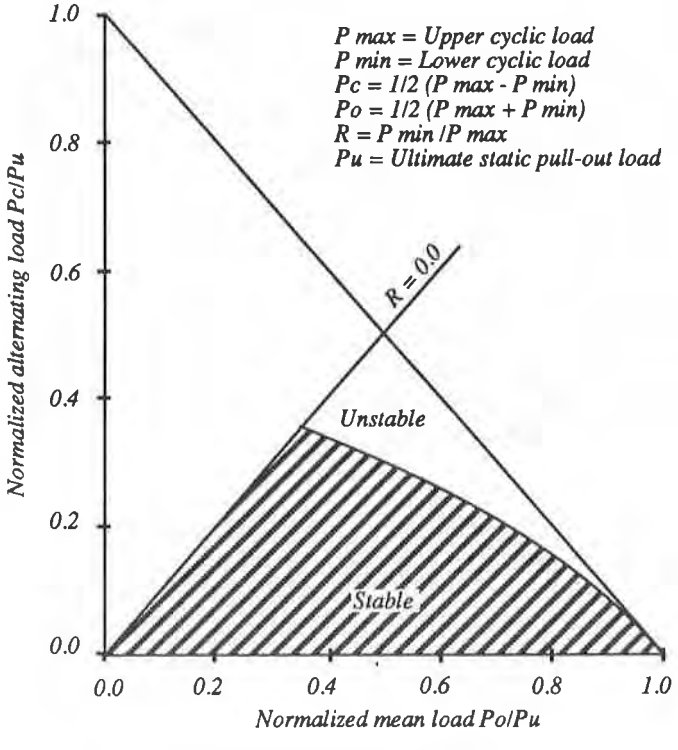

Fig. 10. (a) Cyclic stability plot for smooth strip, 100 cycles

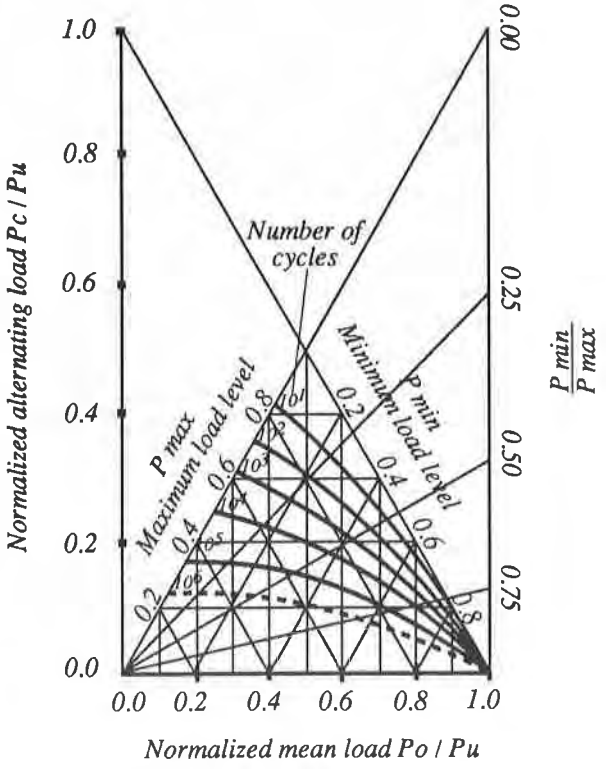

Fig. 10. (b) Cyclic stability plots for smooth strip, 10 to 10^6 cycles

CONCLUSION

The results of the large-scale tests indicate that the rate of accumulation of reinforcement movement increases with increase in the number of load repetitions, load amplitude and load level being controlling variables. Failure by pull-out resulted with the smooth strip only despite testing to 10^5 of load applications. The synthetic geogrid reinforcement is much more load efficient than either the smooth or ribbed strips under both static and repeated loadings. A particular feature was the inability of the geogrid to pull out of the sand, failure being by rupture of the reinforcement material. In many design cases deformation of the reinforcement will control. Comparative data are presented. Suggestions for future studies are made.

ACKNOWLEDGEMENT

The work described forms part of a general research project into the mechanics of foundation elements under slow repeated loadings. One author (M Touahmia) received financial support from the Algerian Ministry of Higher Education. The synthetic geogrid material was supplied by Netlon Ltd., Blackburn, U.K.

REFERENCES

1. Carr, R.W. and Hanna, T.H., (1971) "A note on sand movement measurement in the vicinity of circular shaped plate anchors", Proceedings American Society of Civil Engineers, Vol 97, No SM2.

2. Chan, S.F. and Hanna, T.H., (1980) "Repeated loading of single piles in sand", Proceedings American Society of Civil Engineers, Vol GT106, No 2, 171-188.

3. Choek, Y.K., (1985) "The behaviour of Polymeric Grids used for soil reinforcement", Thesis, University of Strathclyde.

4. Hanna, T.H., (1969) "The mechanics of load mobilization in friction piles", Journal of Materials, American Society for Testing and Materials, Vol 4, No 4, 924-937.

5. Lashine, A.K.F., (1973) "Deformation characteristics of a silty clay under repeated loading", Proceedings of the Eighth International Conference on Soil Mechanics and Foundation Engineering, Moscow, Vol 1, 237-244.

6. Morland, L.W. and Sawicki, A., (1983) "A mixture model for the compaction of saturated sand", Mech. Materials, Vol 2, 217-231.

7. Morland, L.W. and Sawicki, A., (1985) "A model for compaction and shear hysteresis in saturated granular materials", Journal Mechanics and Physics of Solids, Vol 33, 1-24.

8. Poulos, H.G., (1989) "Cyclic axial loading analysis of piles in sand", Proceedings American Society of Civil Engineers, Vol 115, No 6, 836-852.

9. Sivinianski, J., Tejchman, A and Sawicki, A., (1989) "A model of the pile-sand interaction for vertical cyclic loadings", Symposium, Universites Kaiserlautern-Danzig, October, 1-25.

10. Schlosser, F. and Elias, V., (1978) "Friction in reinforced earth", Proceedings Symposium on Earth Reinforcement, ASCE Annual Convention, Pittsburgh, USA, 735-763.

Short and Long Term Performance of Polymeric Geogrids

I. Juran
Polytech University, USA
K. H. Farrag
Louisiana State University, USA
L. Richmond
Conwed Plastics, USA

ABSTRACT

Design of reinforced soil walls with polymeric geogrids or geotextiles requires an appropriate testing procedure to evaluate the stress-strain properties of the reinforcement embedded in the soil and its long term pull-out performance. The current testing procedures are primarily based upon displacement-rate controlled pull-out tests which provide the peak and residual pull-out resistance parameters. However, these testing procedures do not yield any data regarding the long term pull-out performance of geogrid.

This paper presents typical results of both displacement-rate and load controlled pull-out tests. A data analysis procedure was developed to establish confined stress-strain properties and interface characteristics of the geogrid. A stepped load controlled pull-out testing procedure was used and Singh and Mitchell's creep model (1968) was adapted to analyze the time dependent geogrid displacement and to derive interface creep parameters.

INTRODUCTION

Determination of the stress-strain relationship of the geosynthetic reinforcement embedded in the soil is a difficult task. No standard testing procedure, yet, exists for this purpose. Several investigators (Siel et al., 1987; Rowe et al., 1985; El-Fermaoui and Nowatzki, 1982; and Juran and Chen, 1988) have used modified direct shear devices, in which the rear of the specimen was attached to the shear boxes, in order to establish the in-soil confined material properties of the geosynthetics. McGown et al. (1982) developed custom built apparatus, using air activated pressure diaphragms, to conduct extension tests on confined geotextile specimens. More recently, Knochenmus (1989) developed testing equipment for performing confined extension tests which permits conducting tests on both saturated and dry soil samples under controlled drainage and provides better simulation of the compaction process. However, there still exists a substantial need for the development of a standardized testing procedure to obtain the confined material properties which govern the behavior of the geosynthetic reinforced structures.

The extensibility of the reinforcement significantly affect the load transfer mechanism. Pull-out tests on geotextiles (Leshchinsky and Field, 1987) and geogrids (Juran and Farrag, 1990)

have demonstrated that the interaction between the soil and extensible inclusions results in a non-uniform shear displacement distribution along the inclusion. Therefore, displacement measurements along the extensible geosynthetic materials are required for a meaningful interpretation of the pull-out test results.

In this paper, the authors present the results of both displacement-rate controlled and load controlled pull-out tests performed on Conwed and Tensar geogrid materials. An Interpretation procedure for the displacement-rate controlled pull-out tests on instrumented geogrids was developed to permit the determination of both: (a) in-soil confined material properties, and (b) soil-geogrid interface characteristics. This procedure is evaluated through comparison of the interface properties derived from pull-out tests with those obtained directly from direct shear tests in a specially designed large direct shear box. The load controlled pull-out test results are used to assess the critical creep pull-out load and to predict the long term creep displacement under a specified pull-out load.

PULL-OUT FACILITY AND TESTING PROCEDURE

Several pull-out facilities have been designed and used to evaluate the pull-out performance of metallic and geosynthetic reinforcements. A detailed review of the available testing equipment (Juran et al., 1988) has shown a large variety in design schemes of testing facilities and in testing procedures which made it difficult to consistently compare the pull-out performance of different reinforcements. The review also indicated significant limitations pertaining to boundary effects of: (1) side wall friction reducing the normal pressure on the reinforcement, (2) soil confinement by top and bottom rigid plates, and (3) passive resistance of the rigid front wall to soil movement during pull-out. Moreover, the clamping of the reinforcement to the loading devices outside the box leads to an unconfined elongation of the front portion of the reinforcement.

The pull-out facility used in this study (Farrag, 1990; and Juran and Farrag, 1990) was designed to overcome most of these limitations. The modular design of the pull-out box (Figure 1-a) permits different box dimensions and soil thicknesses to be used for control and evaluation of the boundaries effect. The pull-out box also incorporates sleeves of appropriate lengths to eliminate the effect of the rigid front wall. The clamping plates pass through the sleeves into the soil to assure the confinement of the geogrid specimen during the test. Performance evaluation testing of the facility was conducted (Juran and Farrag, 1990) to assess the effect of the main testing variables (i.e. displacement-rate, soil thickness, and sleeve length) on the pull-out resistance. These tests led to establish a standard testing procedure using a displacement rate of 2 mm/min, a minimum sleeve length of 12 inch (30 cm) and a soil thickness of 2 ft (60 cm). The compaction process, and consequently soil relative density, has a major impact on soil dilatancy and soil resistance to pull-out. A sand compaction process which consists of coupling vibrations and hammering effects has been adapted to simulate field conditions. Calibration tests were performed to establish the compaction energy required to achieve the desired soil density.

The facility provides the capability of conducting two testing modes: (a) displacement-rate controlled, and (b) load controlled mode. In the displacement-rate controlled mode, the inclusion is subjected to a constant pull-out displacement-rate and the applied pull-out load is recorded. This testing procedure (which is most commonly used) provides the interface parameters related to the short term pull-out performance such as peak and residual pull-out resistance, interface stiffness modulus and front displacement. In the load controlled mode, pull-out loads are applied incrementally and maintained constant during a specified period. The displacement along the inclusion are recorded and data interpretation yields time-dependent response parameters related to the long term pull-out performance. In addition, a large direct shear box was constructed (Figure 1-b) to obtain the soil-geogrid interface parameters and, thereby, permit the evaluation of the data analysis procedure proposed to derive the interaction parameters from the test results.

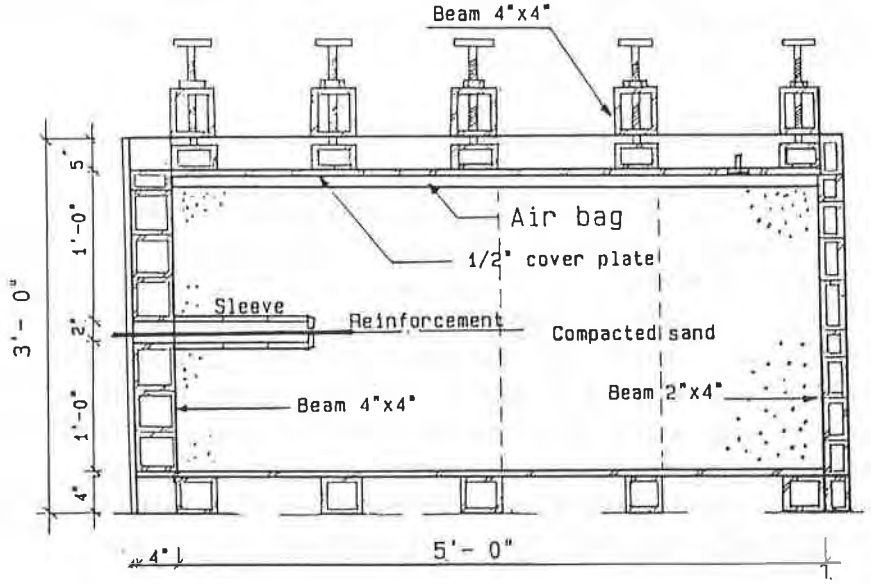

Figure 1-a. Cross Section of the Pull-out Box.

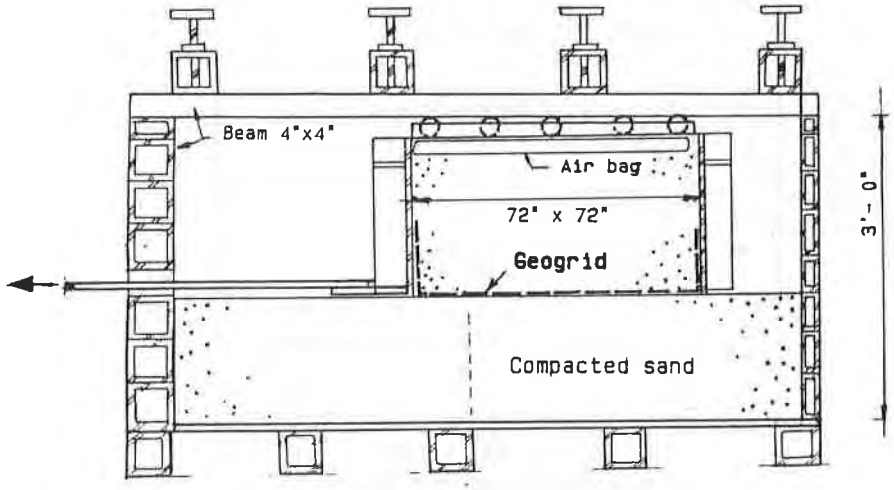

Figure 1-b. Cross Section of the Direct Shear Box.

TYPICAL PULL-OUT TEST RESULTS AND DATA ANALYSIS PROCEDURE

Interpretation of pull-out test results raises a major concern with regard to the specimen scale effect on the pull-out interaction parameters. For extensible reinforcement, the material elongation and the non-uniform shear stress distribution imply that the interface shear resistance is dependent on the sample dimensions. Therefore, an appropriate data analysis procedure has to permit the evaluation of the scale effect in extrapolating laboratory pull-out test results to full scale reinforcement lengths.

Application of the proposed data analysis procedure is illustrated through the interpretation of results of pull-out tests conducted on 'Conwed G-9027' and 'Tensar SR2' geogrids in a uniform blasting sand (average grain size diameter 0.2 mm and minimum and maximum dry density of 1.58 t/m^3 and 1.78 t/m^3, respectively).

Displacement-Rate Controlled Pull-out Tests:

Figures 2 and 3 show typical results of pull-out tests conducted on 'Conwed' geogrid (specimen dimensions 1 ft width and 3 ft length) under a displacement rate of 2 mm/min, confining pressure of 7 psi (48 KN/m^2), and an average soil density of 1.7 t/m^3. The load-displacement curves, shown in Figure 2, yield the interface stiffness modulus, peak pull-out resistance, and front displacement at the peak. The measurements of displacements at different nodes along the geogrid, shown in Figure 3, illustrate the progressive load transfer along the geogrid during pull-out. At early stages of pull-out response, the difference in slopes of nodal displacements indicates a progressive load transfer along the geogrid. As the pull-out resistance is attained, the slopes of the nodal displacements become practically equal, indicating that at slippage failure the geogrid moves as a rigid body without noticeable extension.

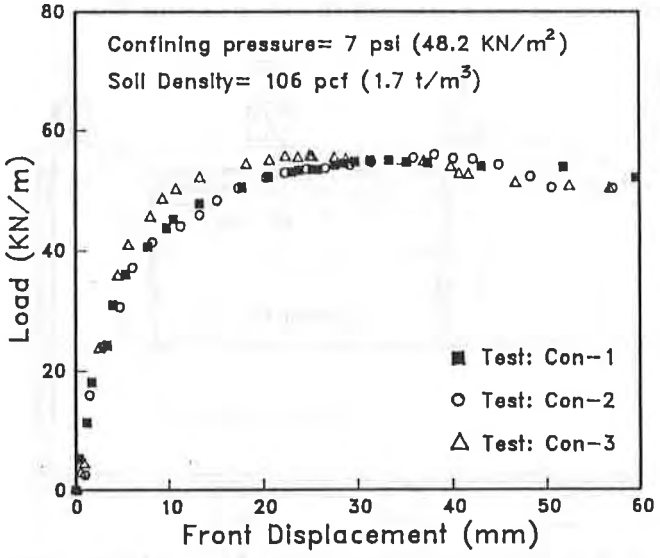

Figure 2. Typical Pull-out Test Results on Conwed G-9027.

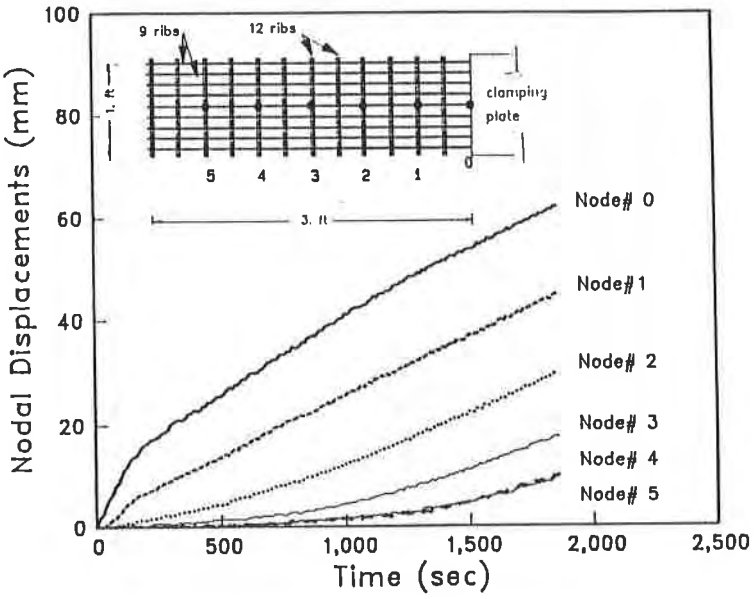

Figure 3. Displacement Measurements at different Nodes Along Conwed Geogrid.

The proposed data analysis procedure is illustrated through the interpretation of the results shown in Figures 2 and 3. This procedure consists of the following steps:

(1) From the time-Nodal displacements curves, the displacement distribution along the reinforcement can be plotted for different pull-out loading levels (Figure 4). The displacement of each node i results from the elongation of the element i (i.e. $\delta_{i-1} - \delta_i$) and its shear displacement δ_i.

(2) The strain ε_i of each element i can be calculated from the relation:

$$\varepsilon_i = [\, \delta_{i-1} - \delta_i \,] / \Delta x \qquad (1)$$

where, δ_{i-1} and δ_i are the displacements at nodes i-1 and i, respectively, and Δx is the length of element i.

(3) The in-soil confined tension force/unit width versus strain of the geogrid can now be plotted for the front element as shown in Figure 5. For the sake of comparison, the Figure shows also the unconfined material stress-strain relationship illustrating that the confinement effect results in a substantial apparent increase of the stiffness modulus E.t (Where t is the reinforcement thickness of the geogrid).

(4) The confined stress-strain properties (i.e. stiffness modulus E.t) obtained under a specified confining pressure are assumed to be unique (i.e. intrinsic material properties). These values can be determined from the slope of the stress-strain relationship obtained for each loading level.

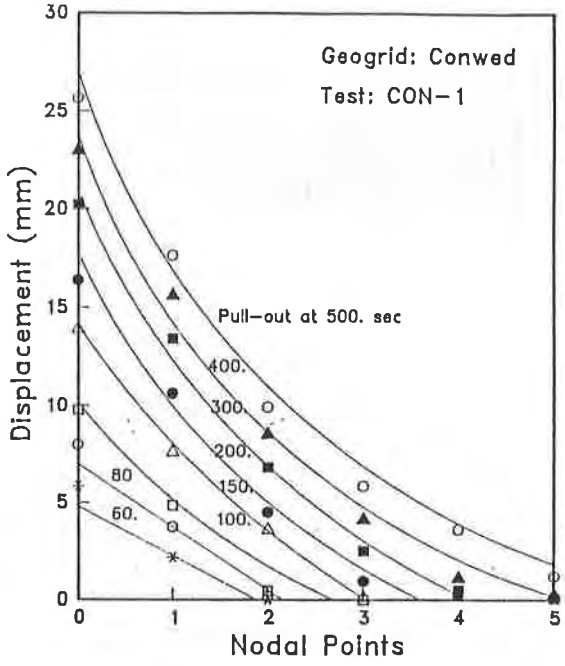

Figure 4. Displacement Distribution along the Conwed Geogrid in Pull-out Tests.

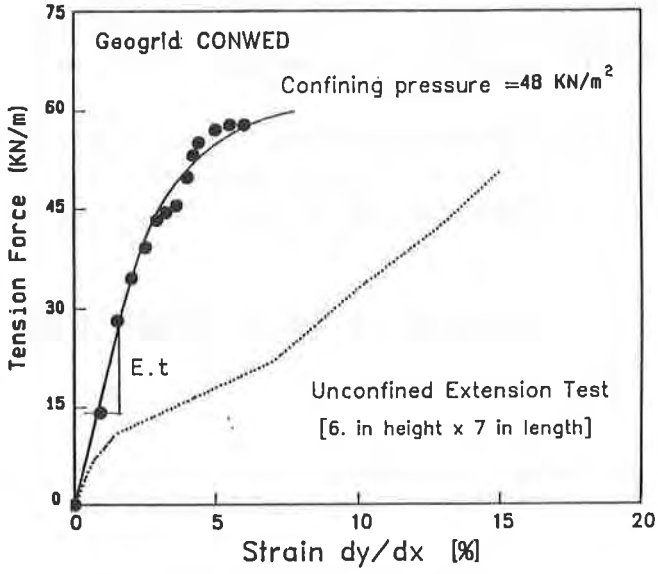

Figure 5. Confined and Unconfined Stress-Strain Relationships for 'Conwed G-9027' Geogrid.

(5) The tension force T_i at each loading level i can be calculated using the confined stress-strain relationship:

$$[T_{i-1} - T_i] /b = E.t. [\delta_{i-1} - \delta_i]/ \Delta x \qquad (2)$$

where b is the geogrid width.

(6) The shear stress distribution along the specimen can be calculated from the static equilibrium equation of each element:

$$[T_{i-1} - T_i] = \tau_i \cdot P \cdot \Delta x \qquad (3)$$

where P is the reinforcement perimeter (for the geogrid P=2b).

(7) The stress-strain relationship can be plotted for all the elements of the geogrid specimen as shown in Figure 6 for the Conwed geogrid.

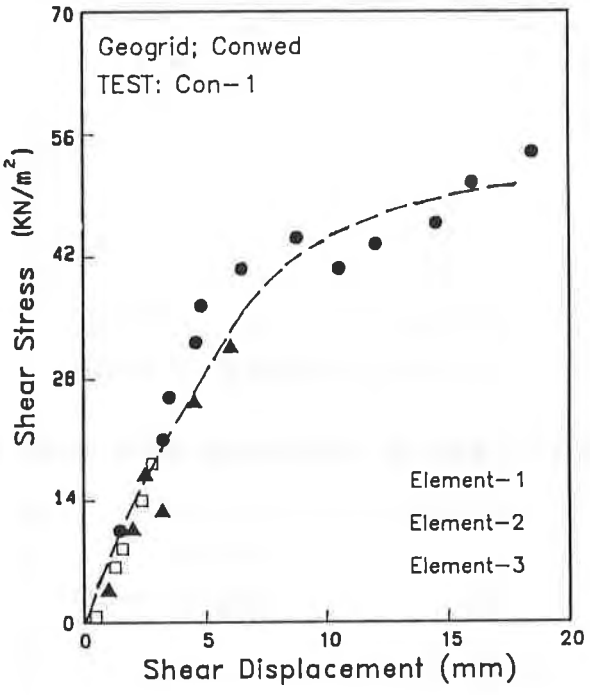

Figure 6. Shear Stress-Strain Relationship from Pull-out Tests on 'Conwed G-9027' Geogrid.

Displacement -rate controlled pull-out tests have also been conducted on instrumented 'Tensar SR-2' Geogrids. The pull-out load displacement curves, obtained for this geogrid under confining pressure of 7 psi (48 KN/m^2) and sand compacted to a dry density of 1.67 t/m^3, are shown in Figure 7. The displacements distributions along the specimen at different loading levels are shown in Figure 8. The proposed data analysis procedure was used to establish the in-soil confined material properties. The interface shear stress-displacement curves derived for the 'Tensar SR2' geogrid are shown in Figure 9. In order to validate the analysis procedure, the shear stress-displacement curves were compared with those obtained from direct shear tests, performed in the large direct shear box, on the sand geogrid interface. The results, shown in Figure 9, confirm the applicability of the proposed procedure. The established shear properties and the

confined material properties can then be used to back calculate the displacement distribution along any geogrid length and, thereby, to adequately extrapolate the laboratory pull-out test results to full-scale reinforcement length.

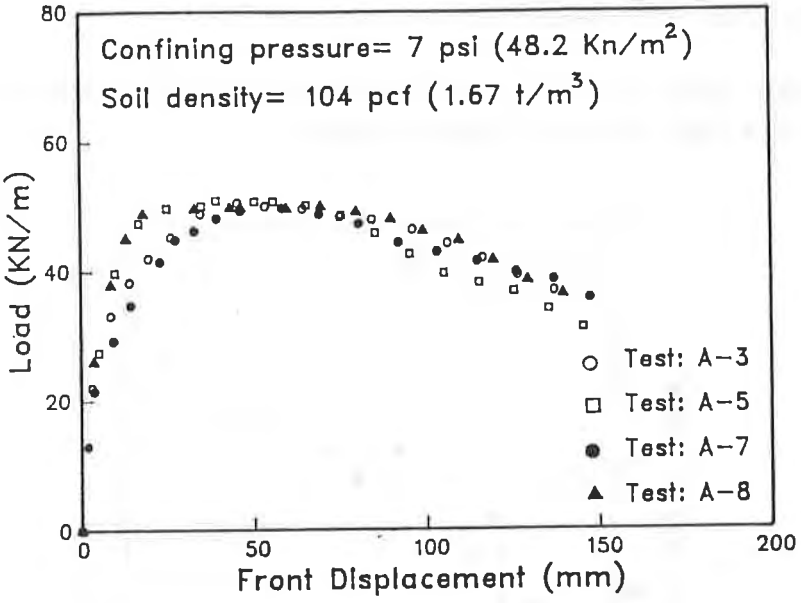

Figure 7. Typical Pull-out Test Results on Geogrid 'Tensar SR2'.

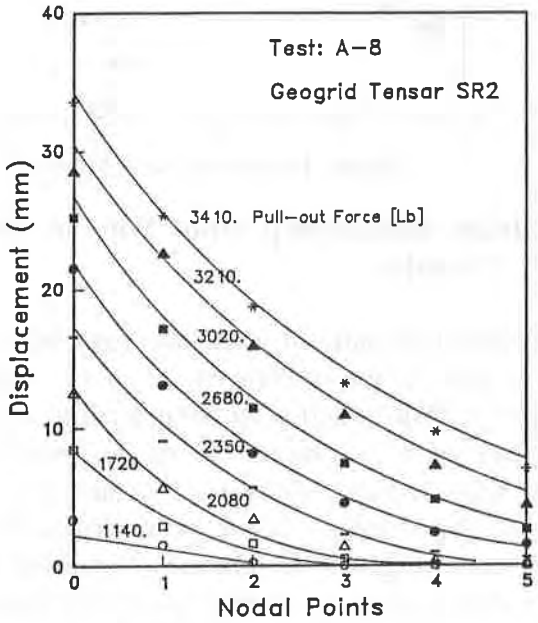

Figure 8. Displacement Distribution along Geogrid 'Tensar SR2'.

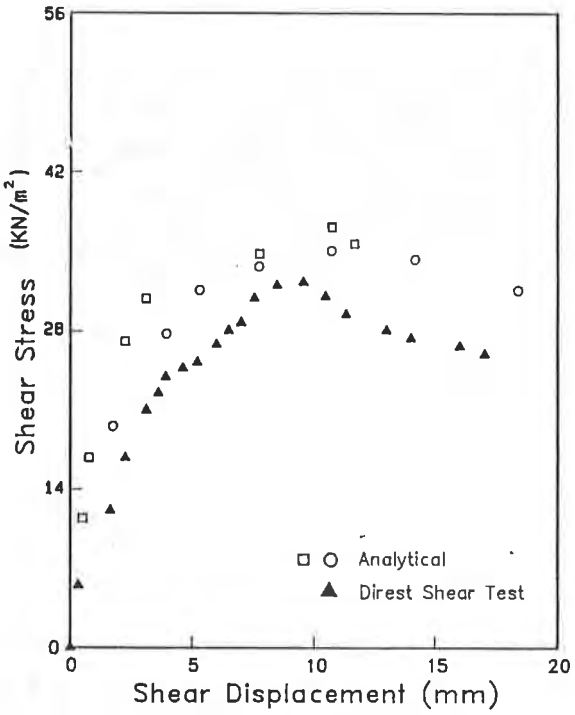

Figure 9. Shear Stress-Displacement from Pull-out Test and Direct Shear Tests.

Load Controlled Pull-out Tests:

Figures 10 and 11 show the results of stepped load controlled pull-out tests conducted on the 'Conwed' geogrid under a confining pressure of 7 psi (48 KN/m^2), at soil dry density of 1.7 t/m^3 for a loading period of 1800 min for each loading level. The figures show, respectively, the front displacement versus time and log displacement-rate versus log time relationships obtained under different loading levels (i.e. at loading levels defined as percentages of the maximum pull-out resistance Tmax obtained from displacement-rate controlled tests).

The figures show that the time dependent displacement rate ($\dot{\varepsilon}$) of the geogrid under a constant pull-out load (T) corresponds to the creep behavior that follows the relationship proposed by Singh and Mitchell (1968):

$$\dot{\varepsilon} = e^{\alpha T} \cdot \frac{1}{t^m} \qquad (4)$$

or,

$$\text{Log } \dot{\varepsilon} = [\ \alpha\ T + \text{Log } A\ ] - m\ \text{Log } t \qquad (5)$$

where m, α and A are interface creep displacement parameters defined as: m is the slope of the Log $\dot{\varepsilon}$ versus Log t curve, α is the slope of the Log $\dot{\varepsilon}$ versus T curve, and A is the intercept of the Log $\dot{\varepsilon}$ versus T curve plotted for a specified reference time, as shown in Figure 12. This model can be used to evaluate the long term pull-out displacement under loading levels smaller than the critical creep pull-out load.

The critical creep pull-out load (Tc) below which creep failure is unlikely to occur is determined following a data interpretation procedure which is similar to that used for ground anchors (Christopher et al., 1989). In this procedure, the measured front displacement, for each applied load, is plotted versus Log time (t). An upward concavity of the creep curve indicates an accelerated creep failure. The slope of the displacement versus Log time for the 'Conwed' plastics is plotted against the applied load to determine the critical creep load in Figure 13.

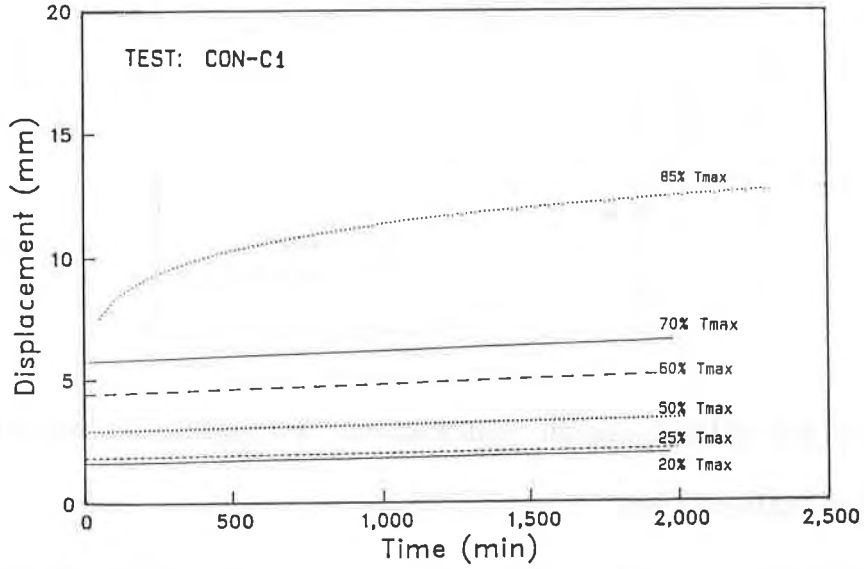

Figure 10. Displacement-Time Relationship for Load Controlled Pull-out Test.

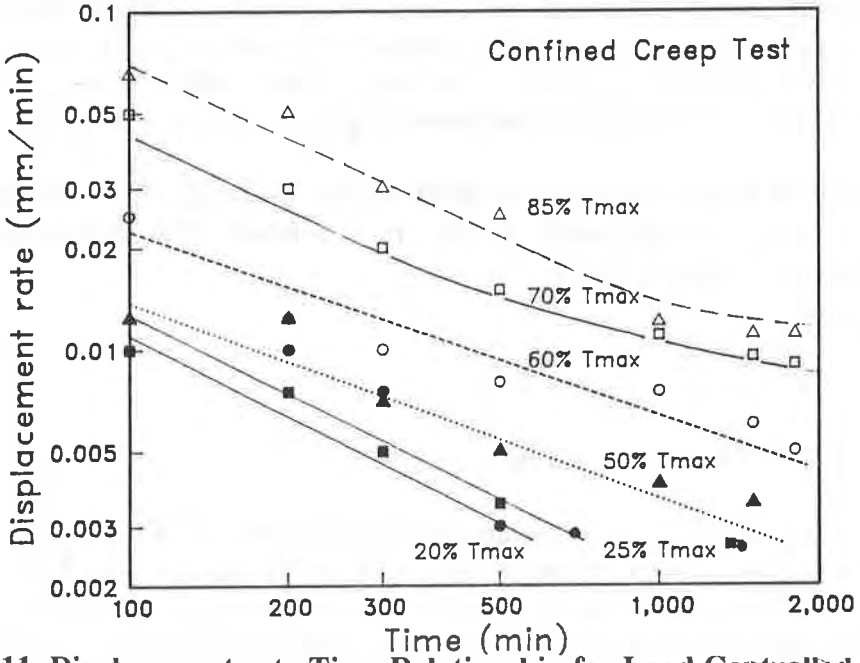

Figure 11. Displacement rate-Time Relationship for Load Controlled Pull-out Test.

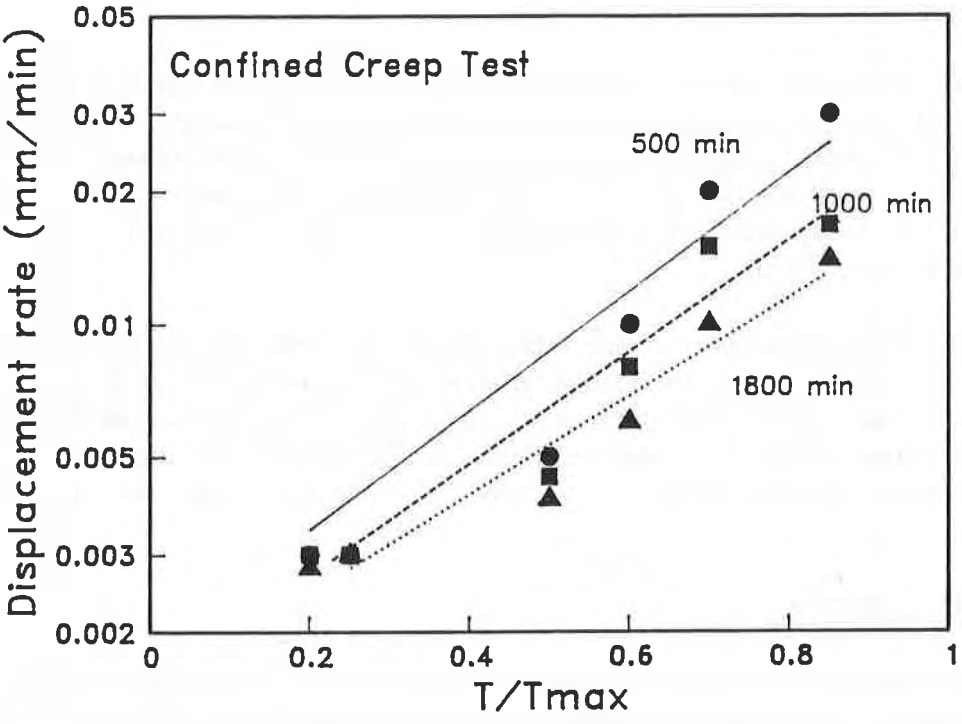

Figure 12. Displacement rate-Loading Level Relationship for Load Controlled Pull-out Test.

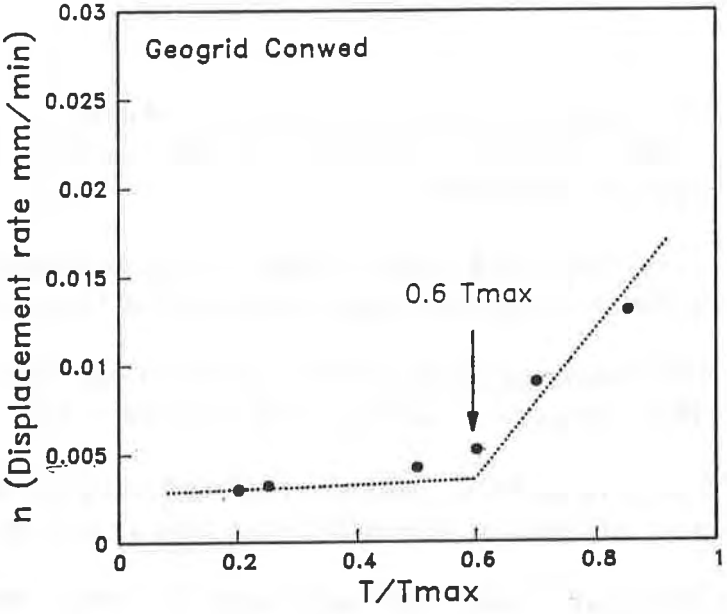

Figure 13. Determination of Critical Creep Pull-out Load from Load Controlled test.

CONCLUSIONS

Modeling load transfer in soils reinforced with geogrids is rather complex and involves several interaction mechanisms which are difficult to simulate. However, a simplified load transfer model for extensible geosynthetic reinforcement can be developed in order to rationally extrapolate laboratory pull-out test results to full-scale reinforcement lengths. Development of such a model requires an adequate pull-out testing procedure with the appropriate instrumentation along reinforcement in the soil.

The data analysis procedure outlined in this paper permits the determination of both soil-geogrid interaction parameters and in-soil stress-strain relationships of geosynthetic reinforcement from displacement-rate controlled pull-out tests. Creep interface characteristics can be determined from the interpretation of the load controlled pull-out test results. The data analysis yields relevant input design parameters for the evaluation of the short and long term pull-out performance.

ACKNOWLEDGEMENTS

This paper forms part of a continuing research carried out by the Geosynthetic Research Laboratory at Louisiana Transportation Research Center at Louisiana State University. The fund and assistance of 'Conwed Plastics' to conduct this part of research is gratefully acknowledged.

REFERENCES

(1) Christopher, B.R.; Safder, A.; Giroud, J.; Juran, I.; Mitchell, J.; Schlosser, F.; and Dunnicliff, J., (1989), "Reinforced Soil Structures, Design and Construction Guide," 2 Vol., FHWA Report No. RD-89043.

(2) El-Fermaoui, A.; and Nowatzki, E., (1982), "Effect of Confining Pressure on Performance of Geotextiles in Soils," 2nd. Int. Conf. on Geotextiles, Las Vegas, Vol. 3, pp. 799-804.

(3) Farrag, Kh., (1990),"Interaction Properties of Geogrids in Reinforced Soil Walls, Testing and Analysis," Ph.D. Dissertation, Louisiana State University, 267p.

(4) Juran, I., and Farrag, Kh.,(1990), "Design of Pull-out Facility for Geotextiles", Report submitted to Louisiana Transport. Research Center, State Project No. 736-12-24.

(5) Juran, I., Knochenmus, G., Acar, Y.B., and Arman, A. (1988), "Pull-out Response of Geotextiles and Geogrids (Synthesis of Available Experimental Data)," Proc. of Symp. on Geotextiles for Soil Improvement, ASCE, Geot. Publication 18, pp. 92-111.

(6) Juran, I.; and Chen, C.L., (1988) "Soil-Geotextile Pull-out Interaction Properties, Testing and Interpretation," Transp. Research Board, 67th Annual Meeting, Washington D.C.

(7) Knochenmus, G., (1989),"Stress-Strain Behavior of Non-woven Geotextiles under Confined Conditions," M.Sc. Thesis, Louisiana State University, 194 p.

(8) Leshchinsky, D., and Field, D.A., (1987), "In-Soil Load, Elongation, Tensile Strength and Interface Friction of Non-woven Geotextiles," Geosynthetics Conf., New Orleans, Vol. 1, pp. 238-249.

(9) McGown, A., Andraws, K.Z., and Kabir, M.H., (1982), "Load-Extension Testing of Geotextiles Confined in-Soil," 2nd. Int. Conf. on Geotextiles, Las Vegas, Vol. 3, pp. 793-798.

(10) Rowe, R.K., Ho, S.K., and Fisher, D.G., (1985), "Determination of Soil-Geotextile Interface Strength Properties,' 2nd. Canadian Symp. on Geotextiles, pp. 25-34.

(11) Siel, B.D., Tzong, W.H., and Chou, N.S., (1987), "In-Soil Stress-Strain Behavior of Geotextiles," Geosynthetics Conf., New Orleans, Vol. 1, pp. 260-265.

(12) Singh, A., and Mitchell, J.K., (1968), "general Stress-Strain-Time Functions for Soils," Journ. Soil Mech. and Found. Division, ASCE, SM1, Jan., pp.21-46.

Effectiveness of In-Membrane Test in Simulating Strength and Deformation Characteristics of a Nonwoven Geotextile Under Operational Conditions

Hoe Ing Ling
University of Tokyo, Japan
Jonathan T. H. Wu
University of Colorado at Denver, USA
Fumio Tatsuoka
University of Tokyo, Japan

ABSTRACT

It has been well recognized that most geotextiles have different load-elongation properties when they are tested in isolation and in the confinement of soil. Therefore, there are increasing doubts as to whether the in-air tests give adequate representation of geotextile's properties in its operative condition, particularly in reinforcement applications where load-elongation properties are very important to the design. In this study, a new test apparatus is proposed for obtaining the in-confinement strength and deformation properties of geotextiles. The test method is an element test and is capable of simulating the predominant operational condition of geotextile-reinforced soil structures. Using the test method, the strength and deformation properties of a spun-bonded nonwoven geotextile was investigated. Geotextile specimens with a width/length ratio of 8 were tested using three different confinement conditions: in-air, in the confinement of soil and in the confinement of rubber membrane while subjected to confining pressures. The results clearly demonstrate the importance of the confining effect. In the case of confinement tests, the effect of stress-confinement by a membrane is found to be similar to that by a soil under otherwise identical condition. It is believed that this test method is superior to the existing test methods for obtaining load-elongation relationship of geotextiles in the design of geotextile-reinforced soil structures.

1. INTRODUCTION

In the conventional methods of determining the strength and deformation properties of geosynthetics, for example, the grab method (ASTM D-4632) and wide-width strip method (ASTM D-4595), the operational conditions of the geosynthetics are not fully considered. The work of McGown et al. (1982) has lead many researchers to propose various test methods for geosynthetics under soil confinement conditions. However, the authors believe that these 'confined' tests failed to simulate the actual field condition. In McGown's test, the frictional resistance between the geosynthetic and the stationary confining soil has to be overcome before tensile strain in the geosynthetic can be developed. As a result, the applied load is a measure of the coupling resistance due to the friction and the confined stiffness of the geosynthetic. Besides, the test is a model test in which the stress distribution was nonuniform, therefore, the test results may be strongly subjected to the boundary effect. Similar drawbacks exist in the pullout test (e.g., Juran and Christopher, 1989), the direct shear test (e.g., El-Fermaoui and Nowatzki, 1982), and the zero-span test (Christopher et al., 1986) modified for measuring the load-elongation relationships of geosynthetics. It is very likely that these test methods tend to overestimate the strength and rigidity of geosynthetics.

In this study, an apparatus has been developed which measures the load-elongation relationship of geotextiles under in-air, in-membrane and in-soil conditions. Tests were conducted to investigate if the strain compatibility between the soil and the geotextile induces an interaction effect in addition to that of the stress confinement. The applicability of the in-membrane test for obtaining the load-elongation relationship of a geotextile under the operational condition was also investigated.

2.TESTING APPARATUS AND SPECIMEN PREPARATION

The apparatus shown in Figure 1(a) was designed for the in-soil test so that the strain would be compatible between the soil and the geotextile during deformation, which is believed to be the predominant operational

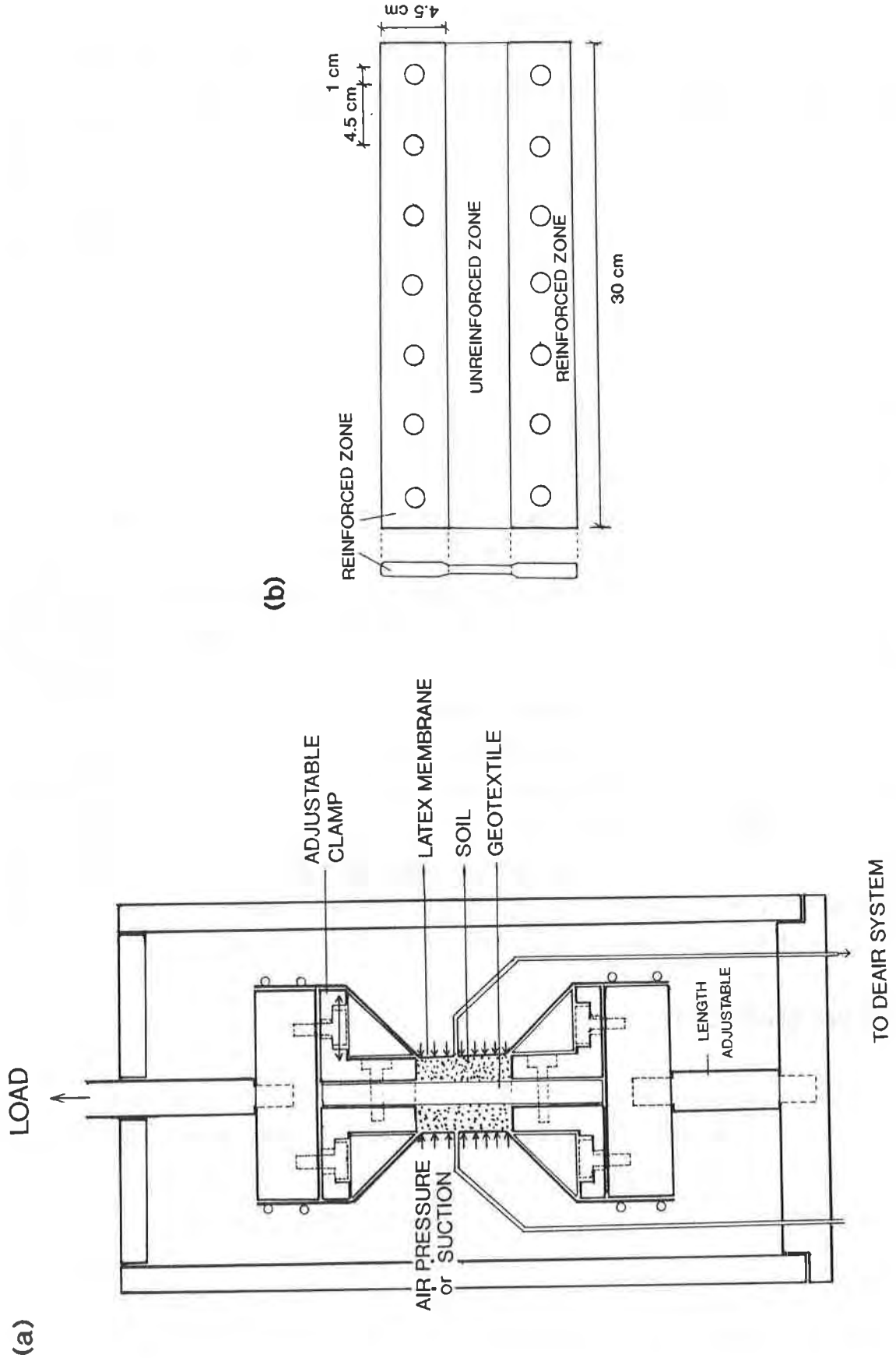

Figure 1. Configuration of (a) test apparatus (b) geotextile specimen

condition in the field before an ultimate state is approached. The apparatus allows for a geotextile a specimen of width (W) up to 30 cm while varying values of length (L) can be selected. For the case of the in-soil test, the geotextile specimen with the confining soil were enclosed in a rubber membrane and the confining stress was applied by a partial vacuum. Two frozen soil cakes, each with a thickness of 0.8 cm, were used to confine the geotextile specimen during sample preparation to avoid disturbances. The soil-geotextile system was then left overnight for the soil to thaw before the test was started. The specimen was loaded in a manner similar to the triaxial extension test.

In order to maintain as close as possible a plane strain condition, a large aspect ratio (W/L) was selected for the test. In addition, the geotextile specimens at the two clamping ends were reinforced using a slow-hardening epoxy. Ample time was allowed for the epoxy to penetrate into the geotextile matrix before getting set. A rapid-hardening epoxy may be used if the geotextile is of a small thickness. Circular holes were then drilled at a regular interval through the reinforced zone of the geotextile, as shown in Figure 1(b), through which screws were used to attach the geotextile to the loading apparatus using two sets of jaws. The jaws are adjustable sideways to accomodate geotextiles of different thicknesses. Due to the high rigidity (E=7000 kgf/cm^2) of the hardened epoxy relative to the unreinfored geotextile, the clamping system functioned very satisfactorily, as indicated by the drilled holes remaining intact even the unreinforced sections had been strained over 200 percent.

3. TESTING CONDITIONS

A spun-bonded nonwoven geotextile manufactured from polypropylene fibers was used in this study. It has a nominal thickness of 3 mm and a unit area weight of 300 gf/m^2. The in-air, in-membrane and in-soil tests were performed. The in-air tests were conducted to ensure that a sufficient W/L ratio be selected for the tests under the confinement of soil and membrane. The in-membrane and in-soil tests were performed at a confining pressure of 0.8 kgf/cm^2. The geotextile specimens were strained at a constant rate of 2

percent per minute in its machine direction until failure occurred. The room temperature was maintained around 20° C for the tests.

Figure 2 shows the load-elongation relationship of the geotextile for the in-air tests with different W/L ratios, wherein the strain is defined as the ratio of the elongation to the initial length of the geotextile. It is seen from these curves that the larger values of W/L ratio gave slightly larger initial rigidity. However, the results for the W/L=8 and 12 were rather close; therefore the ratio of 8 was selected for the in-membrane and the in-soil tests. Tests without using the geotextile, i.e., using only the confined soil enclosed by the membrane and with the membrane only, were performed so that the load-elongation relationships of the in-soil and the in-membrane tests could be corrected for the loads applied to the geotextile. Toyoura sand was used as the confining soil. The soil is a fine uniform sand mainly composed of quartz (D_{50} = 0.16 mm, U_c = 1.4).

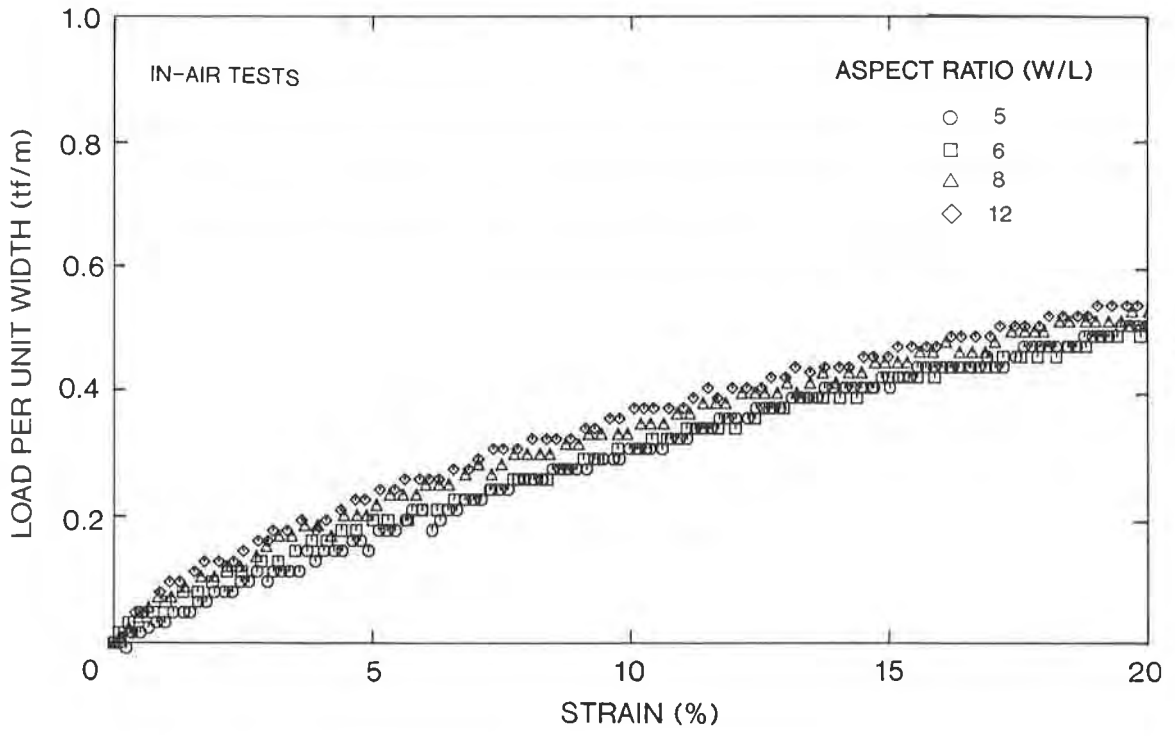

Figure 2. Load-elongation relationship of a geotextile with different aspect ratios

4. TEST RESULTS AND DISCUSSIONS

The results of the tests, after being corrected for the membrane and soil loads, are shown in Figures 3 and 4 for strain levels up to 20 percent and 250 percent, respectively. The corrected load for the in-soil tests was about 8 percent of the measured peak value and was negligible for the in-membrane tests. The two types of tests and the in-air test gave the same mode of tensile failure -- with the rupture line developed near the middle of the geotextile specimen. Confinement effect exists in this geotextile probably as a result of the constraint on the fiber reorientation. However, no significant difference can be seen from the in-membrane and the in-soil tests, except for some fluctuations in the measured load for the in-soil test. This may have been due to alternated positive and negative arching effect as a result of nonuniform normal pressure acting on the same portion of the geotextile when the soil was approaching continuous tensile failure and particle rearrangement, as illustrated in Figure 5. A portion of the geotextile tended to deform largely, with the load being relaxed to a level between those of the in-membrane and in-soil tests as a result of negative arching. The similar behavior was observed in preliminary tests for the geotextile with an aspect ratio of six. Apparently, such behavior as described above is not a material property but a model property which is a function of the dimension of the specimen. Therefore, it is rather difficult to evaluate accurately the load-elongation behavior from the in-soil test.

The use of soil as the confining material alleviated the coupling effect of the frictional resistance and the stress confinement. When a geotextile sheet is placed within a coarse-grained soil, the normal pressure acting on it would be nonuniform because of the relatively large ratio of the grain size to the geotextile thickness. The deformation and strength characteristics of the geotextile in such a case would be different from that under a uniform pressure. The extent of difference due to the nonuniform pressure will probably be similar to that of the in-soil and in-membrane tests observed in this study. Therefore, the in-soil test may only be needed when simulating the behavior of geotextile embedded in a coarse-grained soil or gravel.

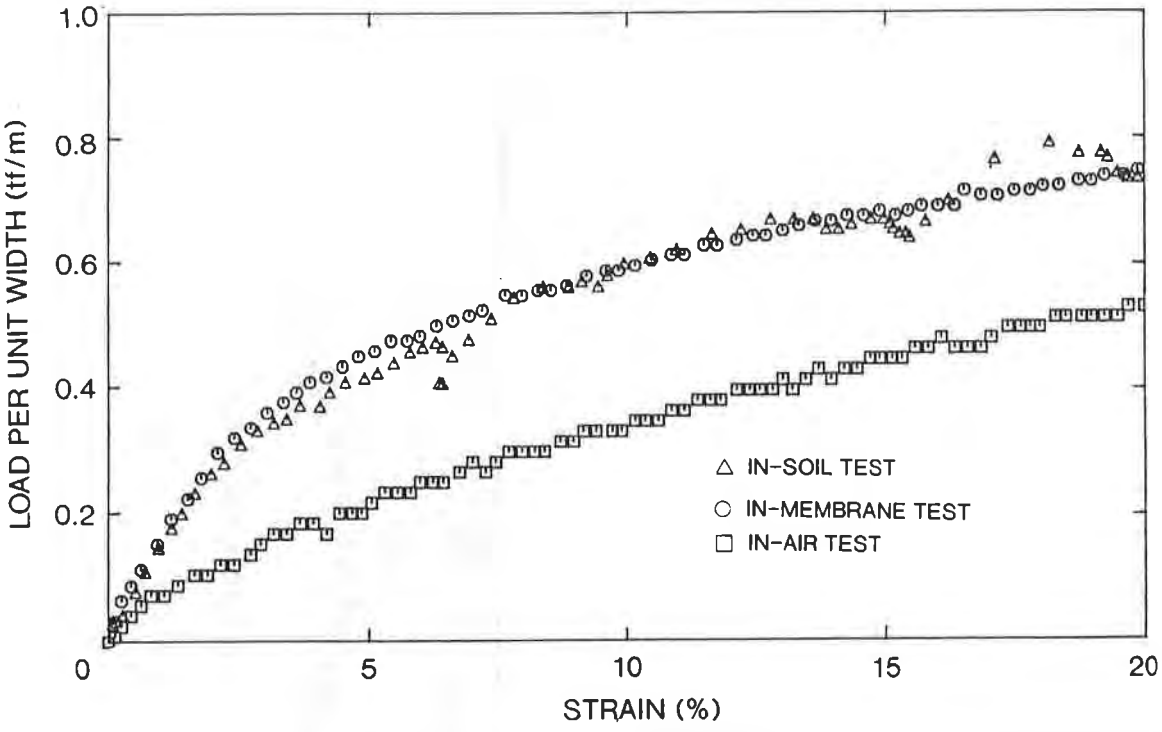

Figure 3. Test results for different methods of confinement at low strain level

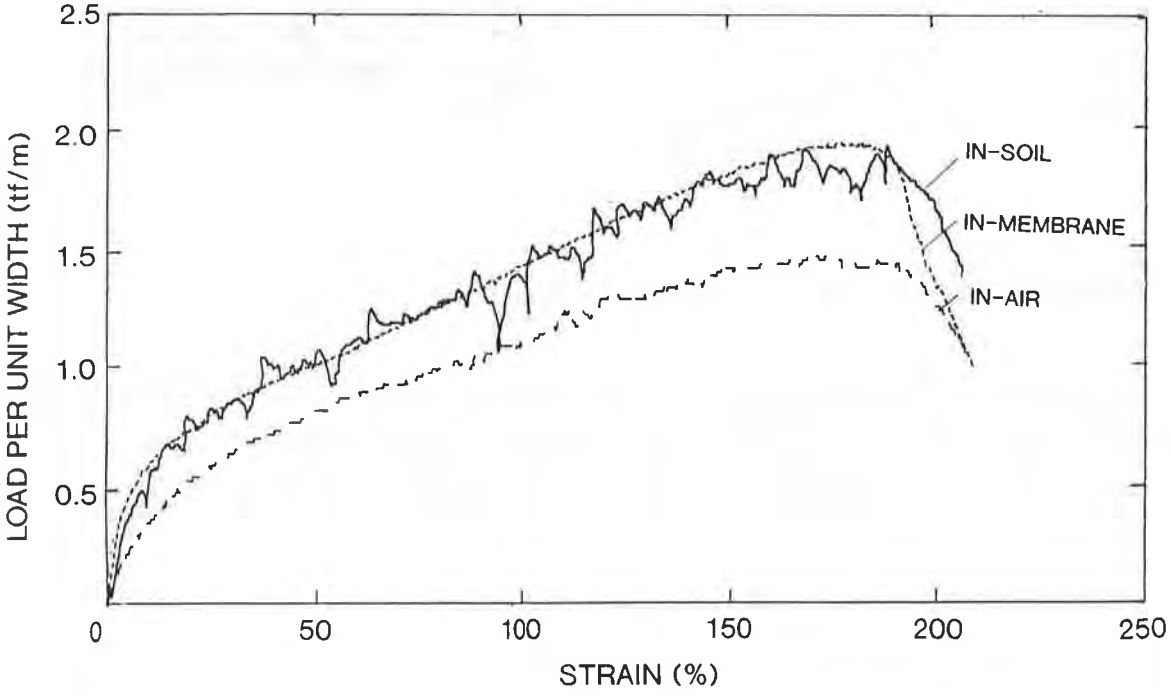

Figure 4. Test results for different methods of confinement (up to failure)

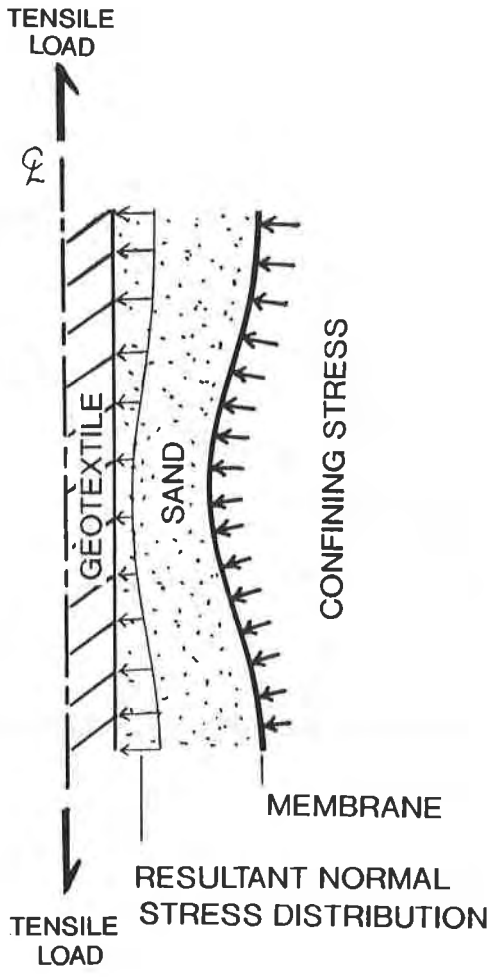

Figure 5. Arching effect in the in-soil test

4.1 Mathematical Model of Load-Elongation Relationship

Mathematical representation of the load-elongation relationships of the geotextile was also investigated. The relationship between the tensile load per unit width T, and axial strain ε, can be expressed by a hyperbolic equation as

$$T = \frac{\varepsilon}{a + b\ \varepsilon}$$

where 1/a and 1/b give, respectively, the initial tensile modulus and the ultimate load of the geotextile.

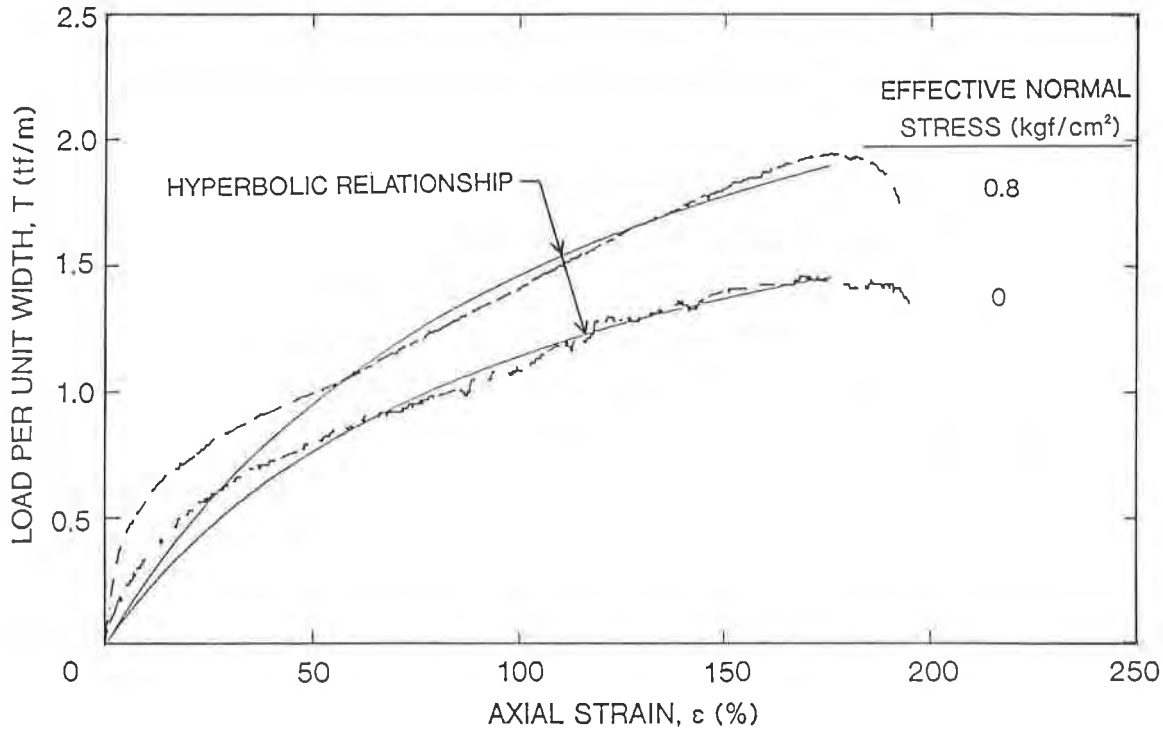

Figure 6. Hyperbolic relationship in expressing test results up to failure

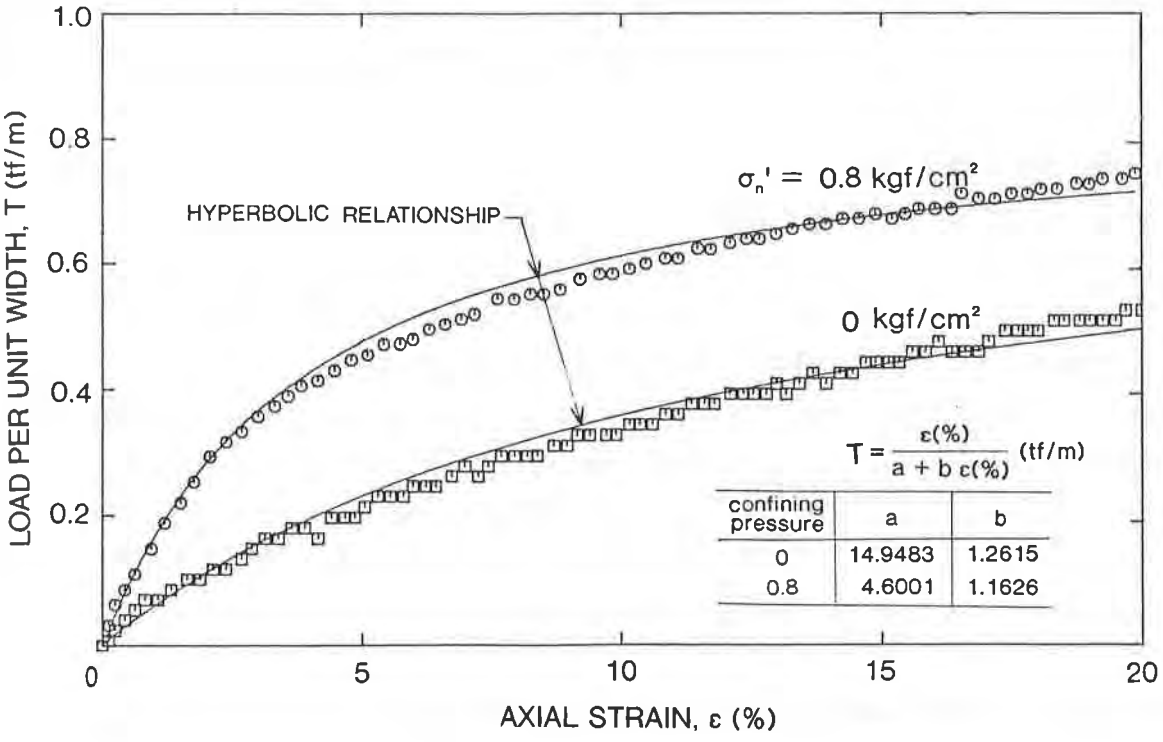

Figure 7. Hyperbolic relationship in expressing test results at low strain level

Figures 6 and 7 show the experimental curves and those fitted by the hyperbolic equation to 250 percent and 15 percent strain levels, respectively. The representation was found to be very good for strains up to 15 percent, but inadequate for the entire range of 0 to 250 percent strains. In field applications, the measured tensile strains in a geotextile are typically fairely small when used for reinforcing earth wall, usually less than 3 percent (see for example, Tatsuoka et al., 1990), therefore, the T versus ε relationship up to 15 percent strain, as shown in Figure 7, should be sufficient for representing the predominant operational conditions. For this particular geotextile, the values of a and b up to 15 percent strain level at different confining pressures are given in Figure 7.

4.2 Effect of Confinement on The Strength and Deformation Characteristics of Geotextile

Failure Strain. The spun-bonded geotextile was found to be a very ductile material. Failure occurred at an elongation of about 170 percent strain. The stress confinement did not give rise to a reduction in the failure strain when compared to the in-air test because a sufficient degree of 'plane strain condition' has been realized in the in-air test using a large aspect ratio and an effective clamping system.

Failure Strength. The failure strength of the geotextile was increased as a result of stress confinement (Figure 8). The increase was about 30 percent at a confining pressure of 0.8 kgf/cm^2 when compared to the in-air test. The linear relationship depicted in Figure 8 is merely an assumption and requires verification with additional tests at different pressures.

Tensile Moduli. The confinement gives a great increase in the secant tensile moduli of the geotextile at low strain levels (Figure 9). It can be seen that very significant differences in the modulus exist at strain levels up to about 10 percent. The difference in the initial modulus of the geotextile at 0 and 0.8 kgf/cm^2, as shown in Figure 8, was a factor of three times.

4.3 Comparison of In-Membrane and In-Soil Test Results

The in-membrane test yields nearly identical results with the in-soil test

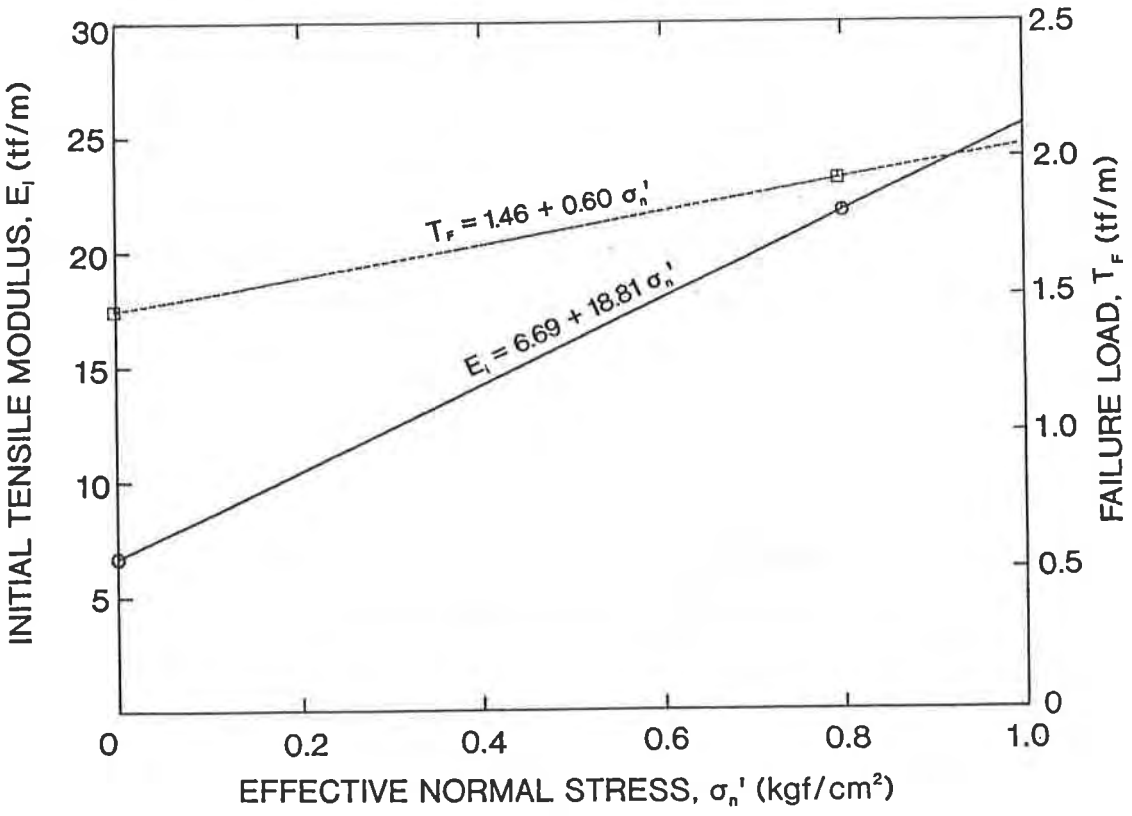

Figure 8. Effect of confinement on initial stiffness and strength of geotextile

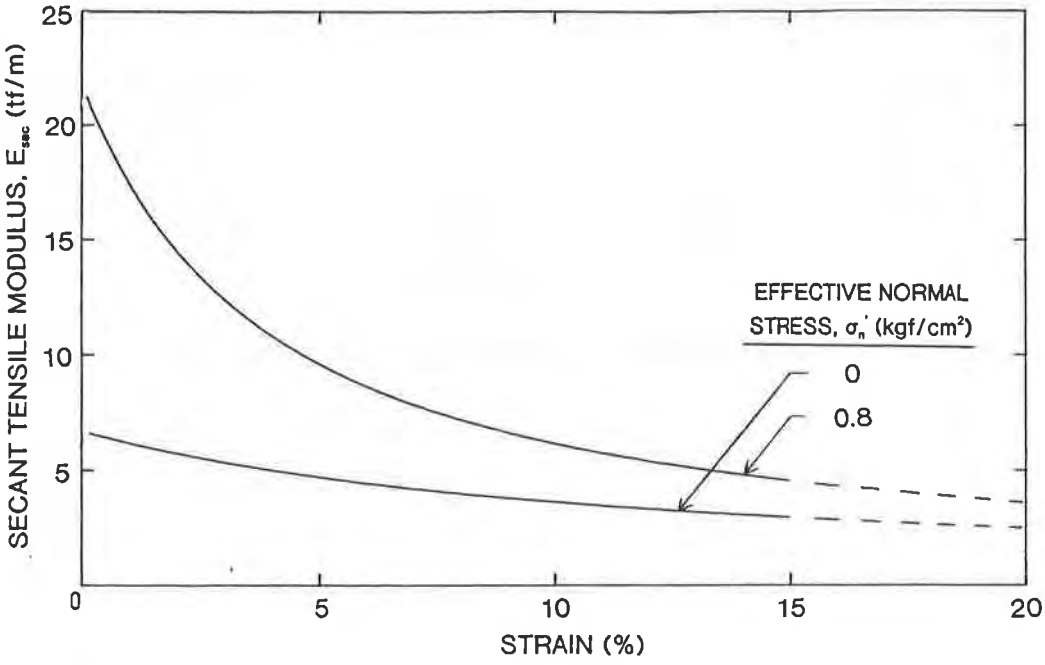

Figure 9. Effect of confinement on secant tensile modulus of geotextile

both at small and large strain levels (Figures 3 and 4). This implies that the in-membrane test is more than sufficient for simulating the in-soil load-elongation relationship of the geotextile. The results of the in-membrane test were also found to be very repeatable as can be seen from Figure 10. In-membrane test is a less time-consuming and less cumbersome test when compared to the in-soil test, and is recommended for the purposes of designs and construction specifications.

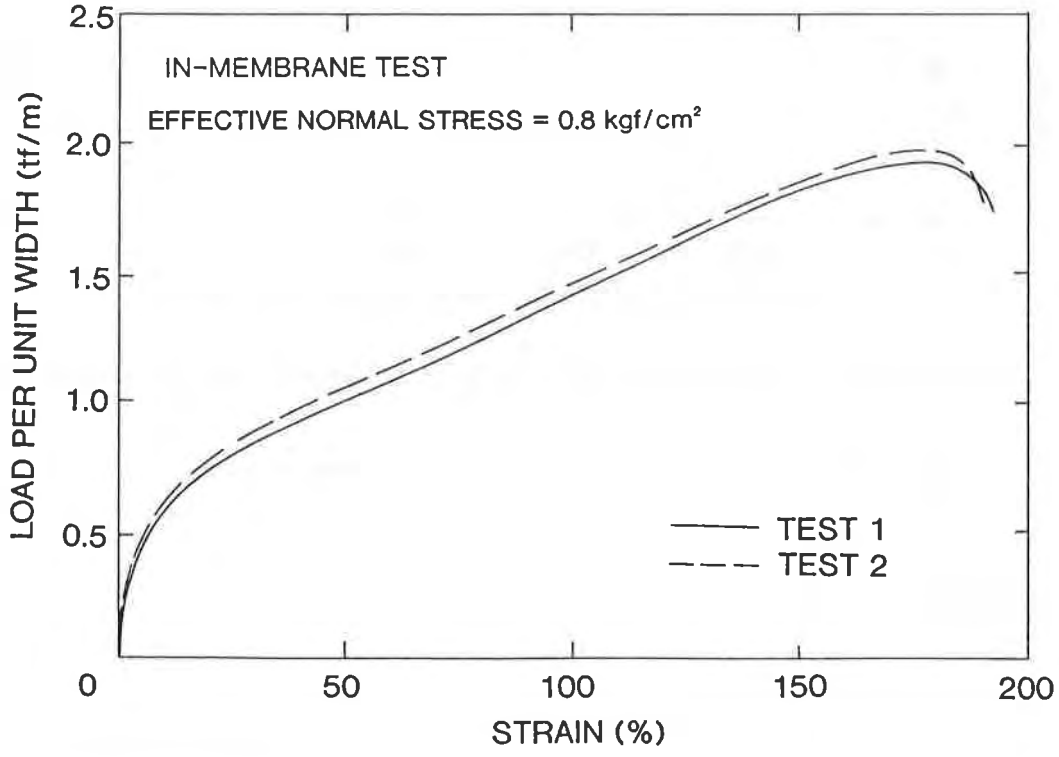

Figure 10. Repeatability of in-membrane tests

5. CONCLUSIONS

It is concluded that the stress confinement effect exists in the spun-bonded nonwoven geotextile. The effect is quite significant under a confining stress of 0.8 kgf/cm^2 in terms of both the failure load and the tensile rigidity. The in-membrane test yields the same effect of stress confinement as the in-soil test which suggests that the in-membrane test which is easier to perform and less time consuming is a superior alternative for simulating the field operational conditions of the geotextile.

Additional in-membrane and in-soil tests gave similar conclusions on a needle-punched nonwoven geotextile. However, the heat-bonded geotextile was not subject to any stress-confinement effect (Ling et al., 1990).

From these short-term test results, it is expected that the long-term behavior (creep behavior) of the spun-bonded and needle-punched geotextiles be very different under confined and unconfined conditions.

6. ACKNOWLEDGMENTS

The Authors would like to express their sincere thanks to Mr. T. Sato, the technician of the Geotechnical Engineering Laboratory, for his advices in the design of the test apparatus. This research was part of the work for the first author during his Master Program at the University of Tokyo with the study financially assisted by the Japanese Government. The research was partly supported by the Mitsui Petrochemical Industries Ltd. and the testing apparatus was manufactured at the machine shop of the Institute of Industrial Science, University of Tokyo.

7. REFERENCES

1. ASTM D-4632-86: Standard Test Method for Breaking Load and Elongation of Geotextiles (grab Method), Annual Book of ASTM Standards, 1987, Vol. 04.08, pp. 1122-1126.

2. ASTM D-4595-86: Standard Test Method for Tensile Properties of Geotextiles by the Wide-Width Strip Method, Annual Book of ASTM Standards, 1987, Vol. 04.08, pp. 1041-1055.

3. Christopher, B.R., Holtz, R.D., and Bell, D. (1986): New Tests for Determining the In-Soil Stress-Strain Properties of Geotextiles, Proceedings of Third International Conference on Geotextiles, Vienna, pp. 683-688.

4. El-Fermaoui, A. and Nowatzki, E. (1982): Effect of Confining Pressure on Performance of Geotextiles in Soil, Proceedings of the Second International Conference on Geotextiles, Las Vegas, pp. 799-804.

5. Juran, I. and christopher, B. (1989): Laboratory Model Study on Geosynthetic Reinforced Soil Retaining Walls, Journal of Geotechnical Engineering, ASCE, Vol. 115, No. 7, July, 1989, pp. 905-926.

6. Ling, H.I., Wu, J.T.H., and Tatsuoka, F. (1990): Short-Term Strength and Deformation Characteristics of Geotextiles under Typical Operational Conditions, submitted to Geotextiles and Geomembranes.

7. McGown, A., Andrawes, K. Z., and Kabir, M. H. (1982): Load-Extension Testing of Geotextiles Confined in Soil, Proceedings of the Second International Conference on Geotextiles, Las Vegas, pp. 793-798.

8. Tatsuoka, F., Murata, O., Tateyama, M., Nakamura, K., Tamura, Y., Ling, H.I., and Yamauchi, H. (1990): Reinforced Steep Clay Slopes with a Nonwoven Geotextile, Preprints of International Reinforced Soil Conference, Glasgow, U.K.

Large-Scale Pullout Tests: Assessment of Procedure and Results

G. E. Bauer
Carleton University, Canada
A. O. A. Halim
Carleton University, Canada
Q. Shang
University of Western Ontario, Canada

ABSTRACT

A total of twelve pullout tests were performed in a large test apparatus. Three soil types and one uniaxial geogrid were investigated. The soils, two granular backfills and a clay shale, were placed under site specific conditions. Strain distributions over the embedded portion of the geogrid were estimated from grid displacement measurements. The coefficients of sliding for all three soil/geogrids systems were determined.

INTRODUCTION

Reinforced soil structures, such as vertical walls and embankments, are a common phenomenon worldwide. Initially steel strips were used as reinforcing elements (Vidal, 1966) but during the last two decades geosynthetics are used to impart tensile strength to the soil. Polymer grids or meshes, so-called geogrids, have now been widely accepted as suitable reinforcement. They have the additional advantage over sheet reinforcement such as geotextiles and geomembranes, that they interlock with the soil particles by nature of their open structure or apertures. In order to determine how well a geogrid interlocks with a given soil it is common to carry out a pullout test. This pullout test serves two purposes: (1) it establishes a relationship between the soil and geogrid interaction behaviour, and (2) it provides a physical parameter, the pullout resistance or anchorage capacity of the geogrid with the soil. The latter is an important parameter in the design and stability analysis of reinforced soil structures. In order to obtain realistic parameters, the pullout test should be carried out in a large test tank using representative geogrid specimens and soils placed under similar conditions to those specified in the field. A large test facility would also overcome side and end effects of soil/geogrid interaction problems with which most small test aparatuses are plagued.

This paper discusses a fully automated large facility to test geogrids under pullout action. The box is 1.5 m (5 ft) long by 0.9 m (3 ft) wide and 1.2 m (4 ft) high. The apparatus was also used to obtain the stress-strain properties of geogrid specimens 1.5m(5 ft) in length and 0.8 m (2 ft 5 in.) in width.

This paper reports the results obtained with an uniaxial geogrid used for reinforced soil structures. The interaction behaviour of the geogrid was investigated in three soil types: a coarse sand, a well-graded crushed limestone aggregate and a silty clay. These soils were selected for the following reasons. The coarse sand is a common material and is generally specified as a suitable backfill for reinforced soil structures. The crushed limestone aggregate, in its well-graded form, has the best mechanical properties of a granular backfill according to the specifications of the Ministry of Transportation of Ontario. This aggregate is, of course, more expensive than sand backfills.

Clay soils have also been used as backfills due to their availability and economy, but little is known about their interaction behaviour with geogrids in particular under long-term conditions. In order to study some of the interaction responses, pullout tests in a compacted clay shale were performed. One series of pullout tests was carried out with the geogrid being sandwiched between a clay and sand interface. This was to simulate the condition of a granular embankment or wall being constructed on a clay foundation material with the reinforcement placed at the interface. All soil/geogrid systems were tested under three normal stresses. Auxiliary laboratory tests were also carried out for soil classification, and to determine the strength deformation properties of these soils.

TEST APPARATUS

The test apparatus consisted of a concrete tank 1.5 m long, 0.9 m wide and 1.2 m high. The inside of the tank was lined with polished stainless steel sheets in order to minimize side friction effects. Direct shear tests on sand and polished stainless steel interface yielded a wall friction angle in the order of 4^{o}. Calculations showed that the reduction in applied surcharge load at midheight of the tank was less than 1 percent due to wall friction. There was a horizontal slit about 200 mm (8 in.) wide at the front side of the tank to pull the geogrid through. The grid was placed horizontally on the compacted soil at the elevation of the slit. The free end of the grid was connected to a hydraulic actuator by a clamping device. Foam rubber pads were glued to the inside of the slit to prevent stress concentrations at the vicinity of the slit and loss of soil particles during a pullout test.

The pullout mechanism consisted of a set of clamping jaws for the grid. These jaws were stiff and assured a uniform pullout displacement across the width of the reinforcing grid. The hydraulic actuator was equipped with a load cell and an internal LVDT. The actuator in turn was bolted to a reaction frame which was anchored to

the concrete tank. A schematic diagram of the whole test assembly is shown in Fig. 1. Vertical surcharge loads were applied by a second actuator. In order to distribute the surcharge load uniformly, a rigid concrete slab was placed over the whole surface of the soil as shown in Fig. 1. The system could apply surcharge intensities equivalent to 30 feet of soil overburden.

TEST CONTROL AND DATA ACQUISITION SYSTEM

The data acquisition system consisted of a Hewlett Packard 9836 instrument controller with a 30 Mbyte hard disk subsystem, a Hewlett Packard 3497 data acquisition (control unit with 15 slots) providing up to 300 channels of mixed input. The pullout load versus the actuator stroke displacement was displayed on the monitor for visual observation. The control/data acquisition system was thus used to control load applications as well as to collect test data at pre-programmed time, load or displacement intervals. After a test the data were transferred to a floppy disk for further analysis.

INSTRUMENTATION

The pullout load was monitored continuously during a test by the load cell of the actuator which was connected to the data acquisition system. The stroke displacements of both vertical and horizontal actuators were also recorded by the build-in LVDT's. In addition the free end displacements of the geogrid were recorded by two independent LVDT's D_1 and D_2 as shown in Fig. 2. The movement of the geogrid embedded in the soil was monitored at three points, indicated as D_3, D_4 and D_5 in Fig. 2, through piano wires attached to LVDT's located at the back of the tank. The piano wired were fed through thin rigid nylon tubes to assure free movement of the wires. Table 1 gives a summary of the various quantities monitored in a test.

TEST PROCEDURE

The soil was compacted in lifts to 90 percent of modified Proctor density and optimum moisture content. The moisture content had little effect on the dry density for the granular soils. Soil density and water content were checked with a nuclear density probe and by taking frequent soil samples. The geogrid was placed on the soil surface as the elevation in the tank reached that of the horizontal pullout mechanism. The grid was connected to the clamping jaws and the piano wires. Filling of the tank was continued. The top cap (i.e., concrete slab) was placed on the soil surface and the vertical actuator was brought into contact. The vertical dial gauges were put in place and the specified surcharge load was applied and left on for a minimum of 12 hours in order to consolidate the soil. For granular backfills no settlement could be observed whereas for the clay shale uniform settlements between 0.25 and 0.5 in. were recorded after a 12 hour consolidation period depending on the surcharge intensity. All pullout tests were run at a rate of 10 mm/min (0.4 in/min). This rate is similar to that used by other researchers (Ingold, 1980; Mowafy, 1986 and Palmeira, 1990).

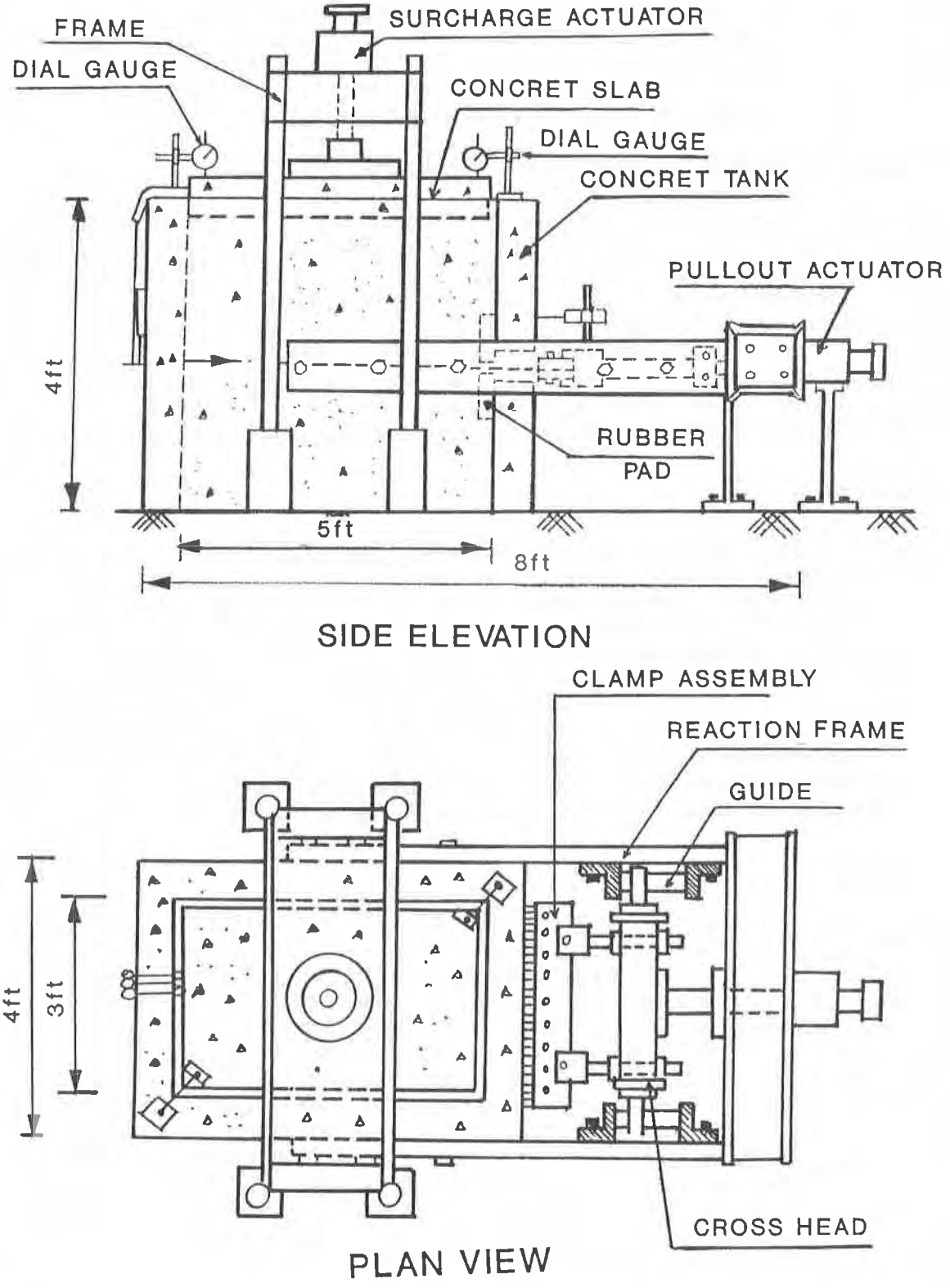

FIG.1 PULLOUT TEST APPARATUS

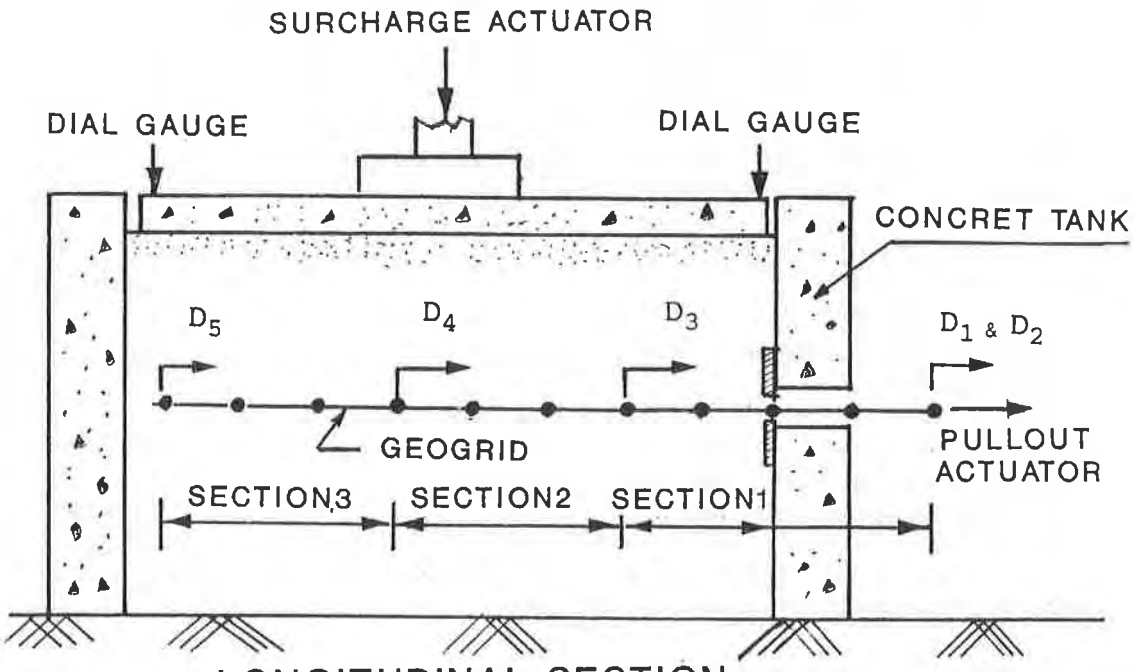

LONGITUDINAL SECTION

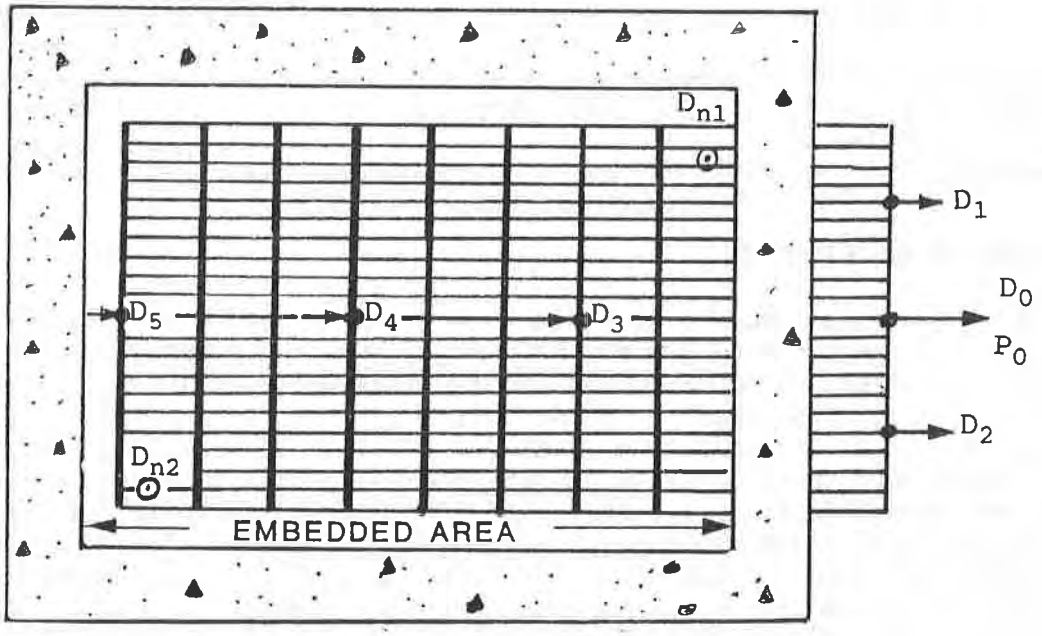

Legend: D = Points of Displacement Measurements with LVDT's

PLAN VIEW AT GRID ELEVATION

FIG.2 LOCATION AND ARRANGEMENT OF MONITORS

TABLE 1: MONITORED VARIABLES IN PULLOUT TESTS

SYMBOL	DESCRIPTION	TRANSDUCER
P_o	Pullout force, applied by 20t hydraulic actuator in horizontal direction	Actuator load cell
D_o	Pullout displacement, parallel to pullout force P_o	LVDT of pull-out actuator
D_1 D_2	Pullout displacement of free end of geogrid	LVDT #1 LVDT #2
D_3 D_4 D_5	Displacement measured at various points along centre line of geogrid to determine strain changes	LVDT #3 LVDT #4 LVDT #5
S	Surcharge load applied by 10t hydraulic actuator through concrete slab	Load cell of surcharge actuator
D_n	Vertical displacement of soil-reinforcement system	LVDT of surcharge actuator
D_{n1} D_{n2}	Vertical displacement and tilting of concrete slab	Dial Gauge #1 Dial Gauge #2

SOIL AND GEOGRID PROPERTIES

Soil Two granular soils and one cohesive backfill material were used in this study. The first material was a coarse sand with rounded particles having an average grain size diameter, D_{50}, of 0.7 mm (0.03 in). The modified Proctor density was 19.2 kN/m^3 (122.3 lb/ft^3) with an optimum moisture content of 11%. Compaction of the soil in the tank was done with a 10 kg (22 lb) hand tamper and using a free drop of about 300 mm (1 ft) until 90% of the modified Proctor dry density was achieved. The in-place dry density for all tests with this material was 18 kN/m^3 ± 2% (115 lb/ft^3). The density in the tank was measured with a nuclear density meter. Direct shear tests yielded a friction angle of 32° ± 1° and no cohesion was observed.

A well-graded crushed limestone aggregate was used in the second series of tests. This material should be considered as an upper limit material for strength and is generally not specified as backfill material for reinforced soil structures because of economic considerations. In the third series a silty clay was employed to investigate the anchorage capacity of geogrids in a clayey backfill material under short-time loading conditions. Direct shear tests

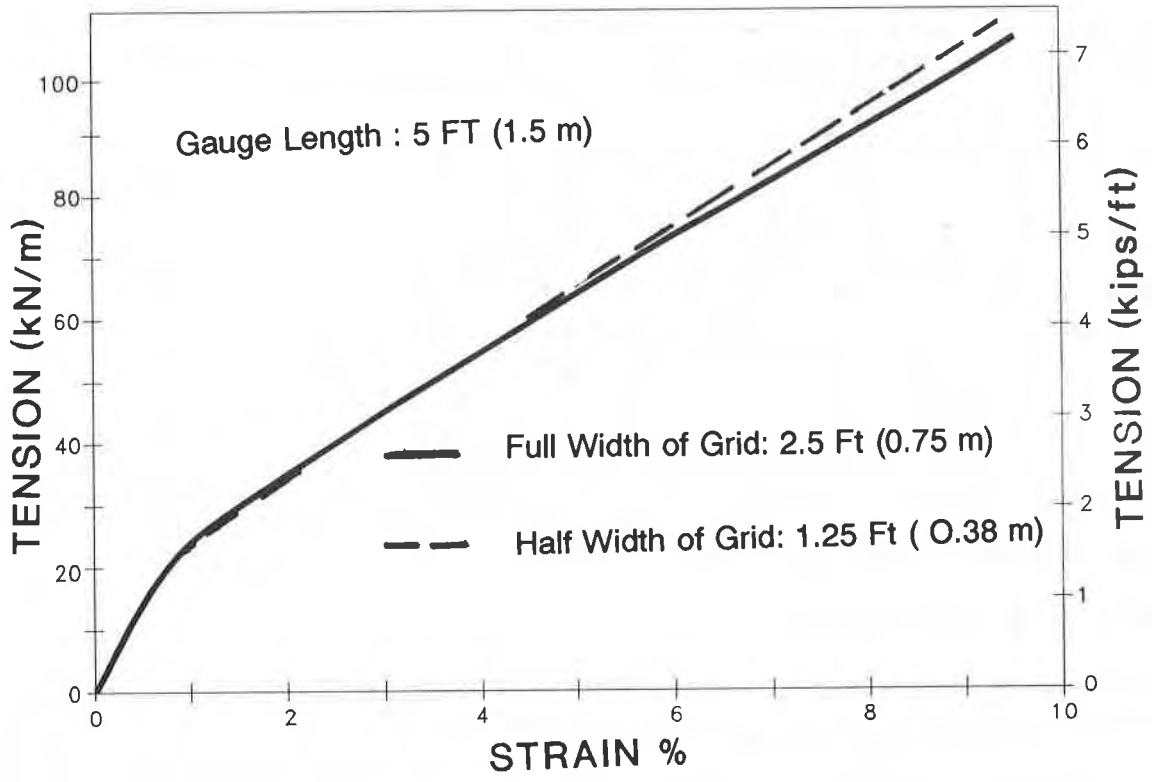

FIG.3 TENSION VS STRAIN (TENSAR UX 1600)

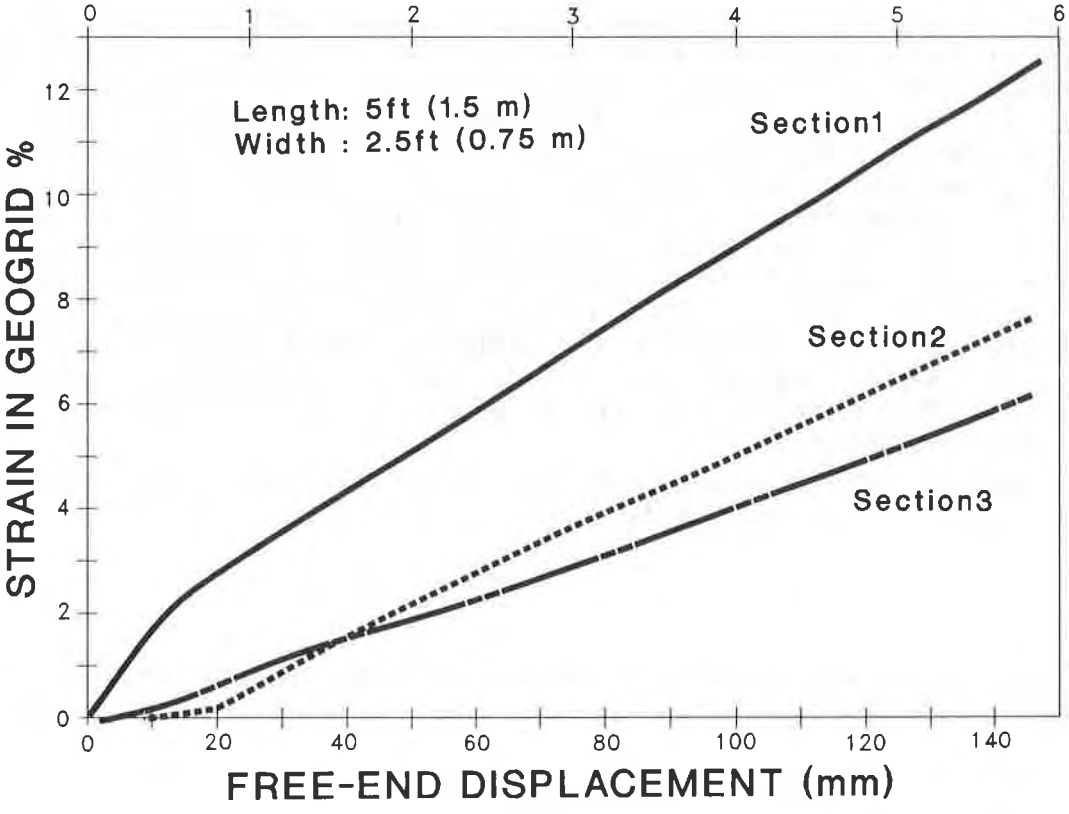

FIG.4 STRAIN DISTRIBUTION IN GEOGRID

were performed on specimens cut from the Proctor mold samples. These specimens were consolidated for 24 hours under similar normal stresses as were applied to the clay in the test tank.

From eighteen shear tests a cohesion parameter of 200 psf (7.5 kPa) and a friction angle of 16° was obtained for an optimum moisture content of 11% for the day. Clay samples from the test tank were also tested in direct shear and yielded parameters which agreed within 10% of those from the clay of the Proctor mold specimens.

The results from test tank specimens were used in the subsequent analysis. Additional direct shear tests were performed in which the bottom half of the shear box was filled with the coarse sand and the upper half with compacted clay. The strength parameters from the clay/sand interface tests were 2.92 kPa (62.5) psf for cohesion and 26° for a soil friction angle. It was anticipated that these results would be useful in predicting the pullout resistance of geogrids sandwiched between clay and sand layers.

Properties of Geogrid

Based on a series of comparative tests carried out by Mowafy (1986) using uniaxial and biaxial polymer grids, such as glassgrid, paragrid, and various types of Tensar biaxial geogrids, Tensar uniaxial geogrid UX1600 was selected in this study because of its good interlock strength with the two granular soils.

In order to obtain a stress-strain response of the UX1600 geogrid, several tensile tests were carried out with specimens 1.5 m (5 ft) in length and 0.75 m (2.5 ft) in width. The test set-up is shown in Fig. 2. In a second test the width of the geogrid specimen was reduced by one-half to 0.38 m (1 ft 3 in) in order to observe if the reduction in width would have any influence on the stress-strain relationship. A comparison of results for these two tests is given in Fig. 3 and are in excellent agreement with each other. The tensile moduli were computed from the bilinear curves. The initial tangent modulus (i.e., 0 to 1% strain) was found to be 2780 kN/m (190 kips/ft) and 900 kN/m (62 kips/ft) for strains greater than 2%. The values are in fair agreement with those obtained from a manufacturer's stress-strain plot which yielded corresponding values of 2650 kN/m and 895 kN/m.

The average tensile strain distributions over the three sections of the unconfined geogrid are given in Fig. 4.

TEST RESULTS

The pullout resistance of a reinforcing element sandwiched in a soil mass is commonly expressed as a dimensionless coefficient of sliding:

$$f = \frac{\tan\delta}{\tan\phi} = \frac{\tau}{\sigma_v \tan\phi} = \frac{p_m}{2A(\sigma_v \tan\phi + c)} \qquad (1)$$

in which P_m is the maximum pullout force; A is the nominal (plan) area of the geogrid in contact with the soil; τ is the shear or interlock stress developed between the soil/grid interface; σ_v is the vertical stress (overblurden pressure) at the reinforcement plane; δ is the friction angle between soil and reinforcement, ϕ is the angle of shearing resistance and c is the unit cohesion of the backfill material.

For geogrids and coarse granular soils Equation (1) is not strictly correct since grids develop interlock and bearing resistance of the cross-strands which could yield coefficients equal or even greater than unity. According to the guidelines of Task Force 27 (Federal Highway Administration, 1985) and in the absence of pullout test results with of geogrids in-site specific granular backfills, the coefficient of sliding can be estimated from:

f	% open area of geogrid
0.5	80% or more
0.7	51 to 79%
0.6	50% or less

A total of twelve pullout tests were carried out in the three soils and one series of tests was performed where the geogrid was sandwiched between a clay and a sand layer. In all cases the test set-up was as indicated in Figs. 1 and 2. The embedded end of the geogrid was unattached and the pullout force was applied at the portion of the grid protruding through the slit in the tank. For all tests the portion of the geogrid fully contained in the soil was 1.5 m long (5 ft) and 0.75 m wide (2.5 ft).

The pullout force versus the free-end displacement of the geogrid for three different surcharge loads and soil-reinforcement systems was obtained. A typical response is shown in Fig. 5 for the geogrid embedded in coarse sand. The maximum pullout resistance increased with an increase of normal stress on the geogrid as indicated by point "B" of the respective graphs.

The points "A" in Fig. 5 indicate when the embedded end of the polymer grid started to move under a particular normal stress. It should be noted that the pullout resistance still increased beyond point "A" due to progressive failure of the soil surrounding the mesh. At point "B" the maximum pullout force was reached and the free and the embedded ends of the grids moved at about the same strain rate. This may have implications on the performance of prototype structures which are usually designed based on the maximum pullout resistance, since the initial pullout resistance, occurring at point "A", is rarely known. Fig. 6 shows the pullout response of the polymer mesh sandwiched between coarse sand and clay. The maximum pullout forces are lower than the corresponding values in the coarse sand, but higher than the values obtained in purely cohesive clay. This observation also agrees with the results from the direct shear tests.

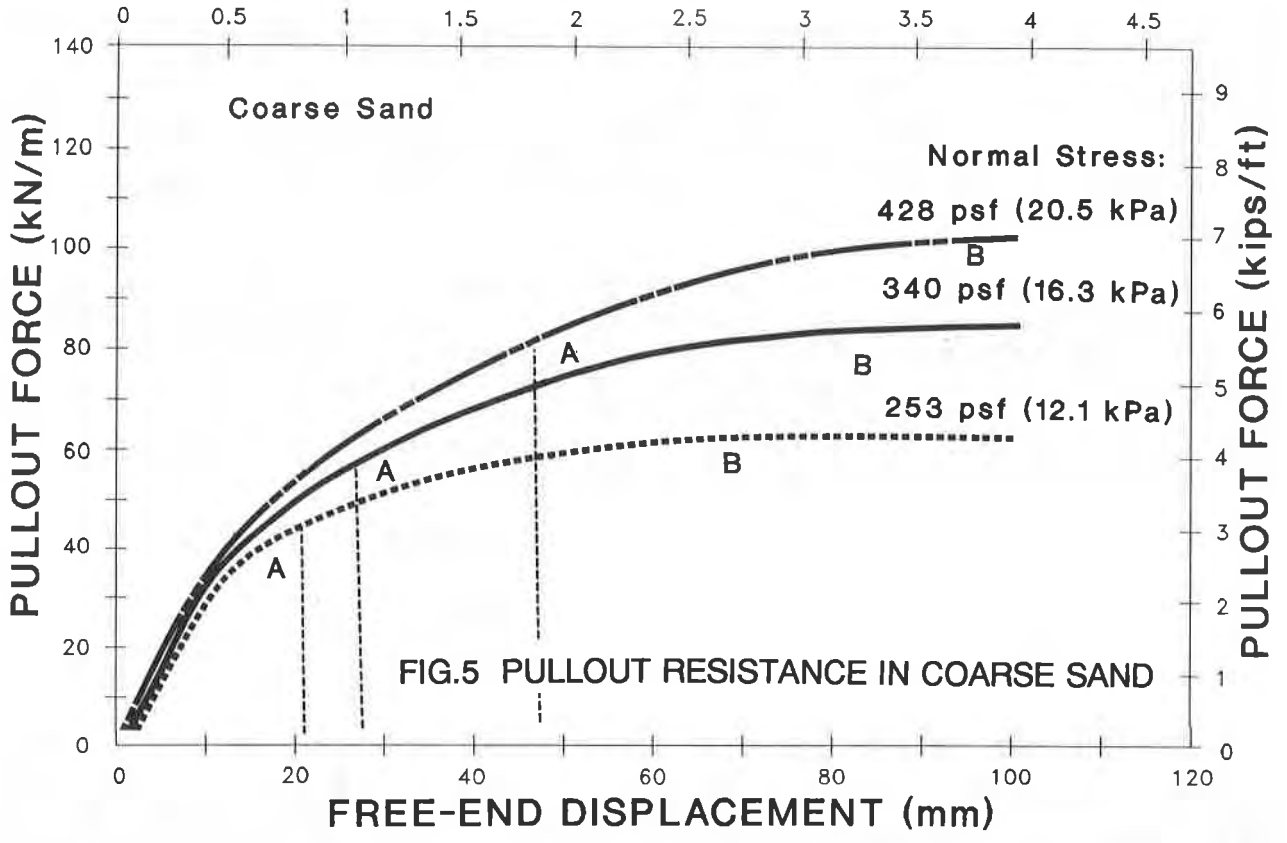

FIG.5 PULLOUT RESISTANCE IN COARSE SAND

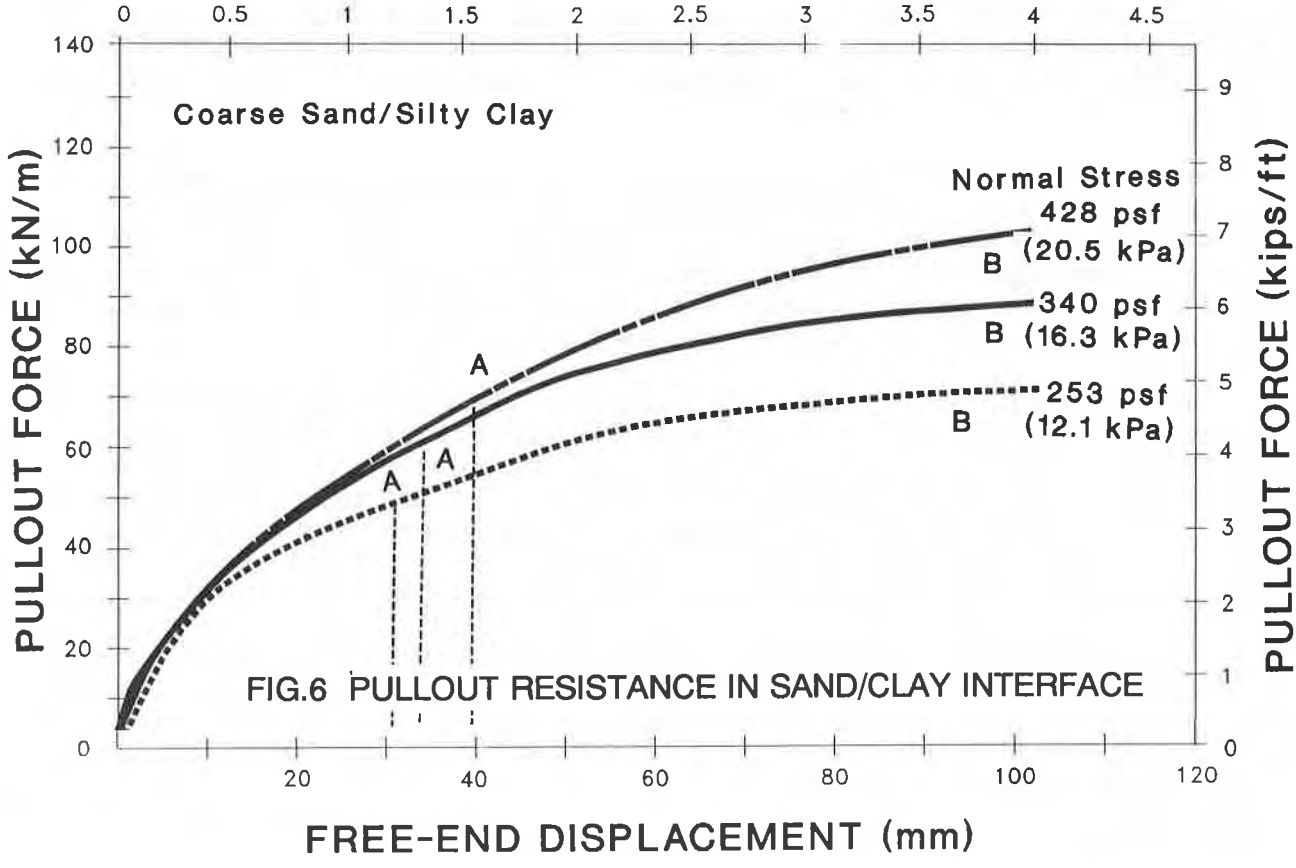

FIG.6 PULLOUT RESISTANCE IN SAND/CLAY INTERFACE

Fig. 7 presents the average strains mobilized along portions of the geogrid. As indicated in Fig. 2 the movement of the grid in contact with the soil were monitored at three points, D_3, D_4 and D_5, therefore the average strains can be calculated for Sections 1, 2 and 3 from the difference of respective LVDT displacement readings. It should be noted that Sections 2 and 3 are completely embedded in the soil whereas Section 1 is only partly embedded.

Figure 8 shows the strain mobilization with free end displacement of grid for the sand/clay interface. For both pullout tests (Figs. 8 and 9) the average strain mobilized was in the order of 2.5% when the embedded end started to move. The strains associated with the maximum pullout force (point "B" of curves in Figs. 7 and 8) were in the order of 6% for the coarse sand and 8% for clay/sand system. At higher surcharge loads these strains decreased slightly.

ANALYSIS AND DISCUSSION OF RESULTS

The results of the pullout tests are summarized in Table 2 together with the pertinent soil properties. The pullout resistance given in this table corresponds to the applied force when the embedded end of the geogrid started to move as indicated by point "A" of the load-displacement curves in Figs. 5, 6, 7 and 8. Additional resistance is mobilized due to stress restribution in the vicinity of the geogrid surface. This increase was in the order of 15 to 30% depending on the soil type and surcharge intensity. In the last column of Table 2 the coefficient of sliding is computed from Equation (1). The UX1600 geogrid has an open area of about 60% and the recommended coefficient of sliding is 0.7. The computed average values are 1.30 for sand, 0.73 for clay, 1.38 for crushed aggregate and 1.24 for the mixed soil interface. One must keep in mind that the values suggested by the Federal Highway Administration are "design" values and include some kind of safety factor. This coefficient of sliding for a grid is a function of particle size distribution and to a lesser extent of soil density. Angular well-graded particles seem to provide good interlock with the grid openings. Most of the pullout resistance in the clay soils is provided by surface adhesion and friction between the clay particles and the geogrid material. The coefficient of sliding is about 60% of the values obtained for the two granular materials.

CONCLUSIONS

A large test tank with associated equipment was employed to test representative specimens of a uniaxial geogrid under pullout action. It is suggested that the three soil types used in this investigation were placed under site specific conditions.

The test apparatus could also be used to test the unconfined geogrid in uniaxial tension. Reduction of grid width from 0.75 m (34 longitudinal ribs) to 0.38 m (17 longitudinal ribs) seem to have little effect on the strain-strain response and the associated tensile moduli.

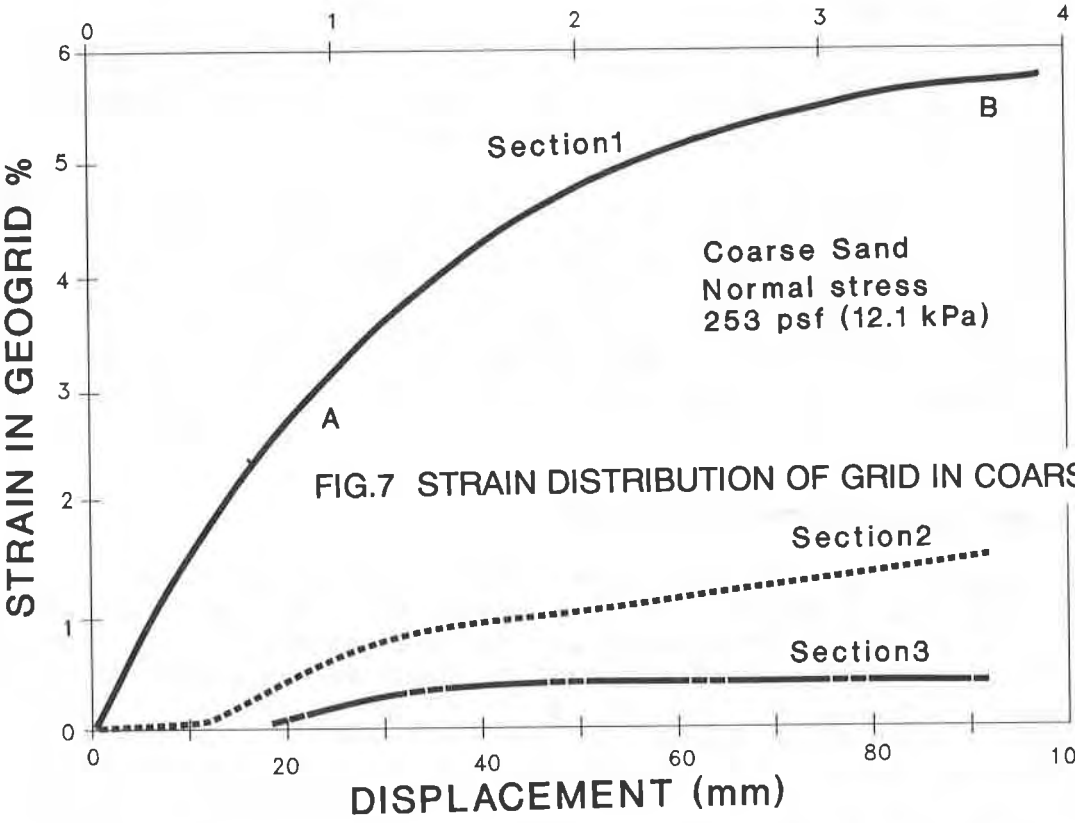

FIG.7 STRAIN DISTRIBUTION OF GRID IN COARSE SAND

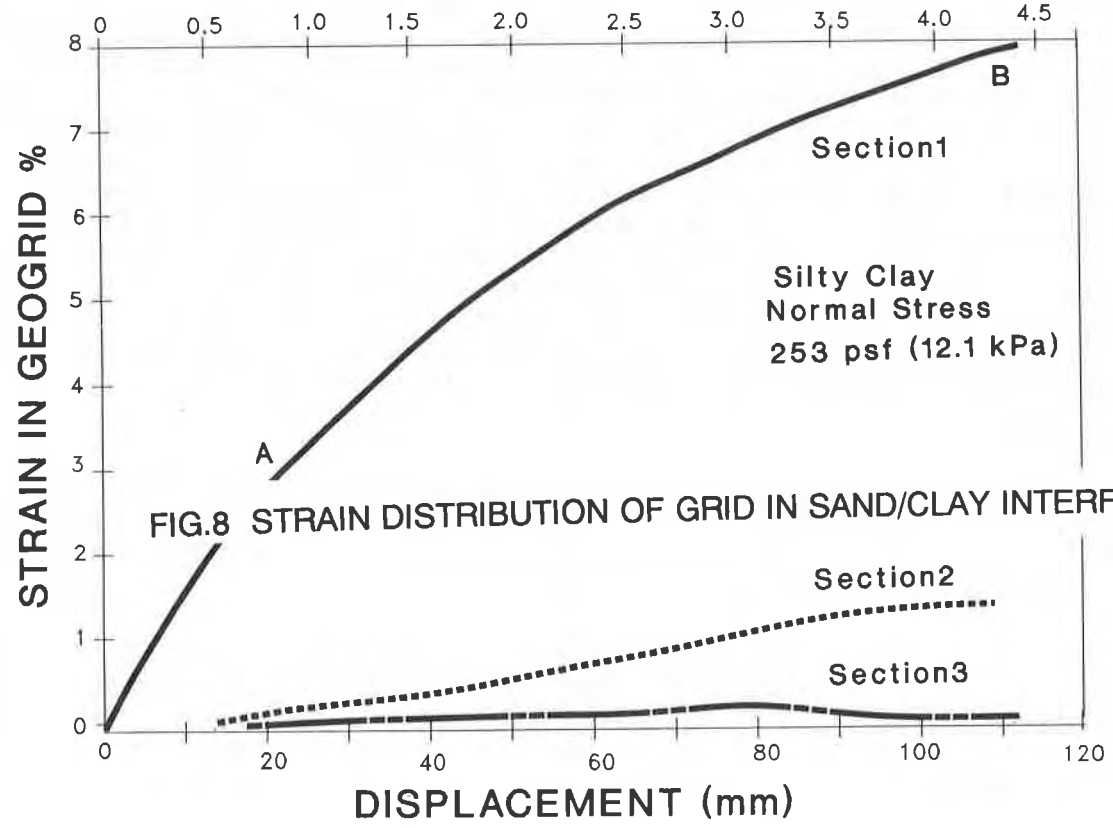

FIG.8 STRAIN DISTRIBUTION OF GRID IN SAND/CLAY INTERFACE

Two specific values of pullout resistances were obtained from a particular pullout force versus displacement relationship. The grid anchorage capacity was defined as the pullout force at which the unattached embedded end of the grid started to move. This is indicated as point "A" on the curves given in Figs. 5 to 8. The maximum pullout force was obtained after the geogrid underwent further displacement in the soil. This is indicated by point "B" in Figs. 5 to 8.

The coefficients of sliding obtained for the two granular materials were approximately twice the value suggested by FWA for design purposes. The clay shale yielded a coefficient of sliding of approximately 60% of the corresponding values for the granular materials.

TABLE 2. SUMMARY OF TEST RESULTS

SOIL	SOIL UNIT WEIGHT (kN/m^3)	COHESION (kPa)	FRICTION ANGLE (DEGREE)	NORMAL STRESS kPa	PULLOUT RESISTANCE RN/m	SLIDING COEFFIC. f
Sand	17.6	0	32	12.1	20.8	1.22
				16.3	29.9	1.28
				20.4	39.8	1.38
					Average	1.30
Clay	18.0	7.45	16	13.3	17.5	0.70
				17.4	20.0	0.71
				21.6	24.2	0.79
					Average	0.73
Crushed Aggregate	19.0	0	45	12.9	36.7	1.35
				16.3	50.6	1.38
				20.4	64.3	1.40
					Average	1.38
Sand/ Clay	17.6 18.0	2.92	26	12.1	25.0	1.26
				16.3	29.8	1.22
				20.4	35.9	1.24
					Average	1.24

REFERENCES

1. Ingold, T.S., 1983. Laboratory Pullout Testing of Geogrid Reinforcement in Sand, Geotechnical Testing Journal, Vol. 6, No. 3, pp. 101-111.

2. Mowafy, Y.M., 1986. Analysis of Grid Reinforced Earth Structures, Ph.D. Thesis, Civil Engineering, Carleton University, Ottawa.

3. Palmeira, E.M. and Milligan, G.W.E., 1989. Scale and other Factors Affecting the Results of Pullout Tests of Grids Buried in Sand. Geotechnique 39, No. 3, pp. 511-524.

Effect of Pores Structure of Nonwoven Geotextiles on Their Clogging Behavior

Shobha K. Bhatia
Syracuse University, USA
Jacek Mlynarek
Ecole Polytechnique, Canada
Andre L. Rollin
Ecole Polytechnique, Canada
Jean Lafleur
Ecole Polytechnique, Canada

ABSTRACT

Nonwoven geotextiles are used as filters in many drainage applications, such as roads, agriculture, consolidation, silt fences, tailing ponds, and landfills. For these applications, geotextiles must be chosen selectively to obviate any clogging problems. However, there is still much that is not known about the mechanisms governing particle migration in the soil layers in contact with a geotextile and within a geotextile structure. This knowledge is necessary to assess the long-term performance of a geotextile as a filter. The goal of this paper is to demonstrate the effects of the structure of various geotextiles on the filtration behavior of silty soil/geotextile systems. Long-term filtration laboratory test results on fourteen different nonwoven geotextiles and one silty soil are presented. The analysis of microphotographs shows that for different structures of geotextiles, different mechanisms affecting long-term filtration behaviors occur with the same silty soil. The results also indicate the significance of the Filtration Opening Size (FOS) as a parameter in filter criteria for silty soils.

INTRODUCTION

Four different conditions should be considered when analyzing the stability of soil/geotextile systems:

- soil properties: particle size gradation, relative density index, particle shape and permeability;
- geotextile properties: opening size, porosity, mass per unit area and permittivity;
- hydraulic conditions: gradients and flow directions;
- external conditions: type and function of the earth structure, type of loading (transient or steady) and nature of the adjacent soils.

Many filter criteria were developed to select geotextiles to perform as filter. In essence, a characteristic soil particle diameter, a soil uniformity coefficient and a geotextile characteristic pore size are used for the established filter criterion. In some cases, the hydraulic gradients (the French Committee on Geotextiles and Geomembranes - CFG criterion (1986)), the density index of the soil (the criterion

proposed by Giroud (1982)), the loading conditions (the Federal Highway Administration - FHA criterion, Christopher and Holtz (1988) and the Franzius Institute of Hannover - FIH criterion, Saathoff and Kohlhase (1986)), and the type of function (CFG criterion) are also considered.

The existing filter criteria, however, are not directly applicable to silty and broadly graded soils due to the lack of understanding of the geotextile's resistance to clogging with these soils. Lafleur et al. (1989) have shown that a certain migration of fines through the filter is necessary and unavoidable in the development of the self-filtration process when silty and broadly graded soils are involved. If nonrestricted, this migration can eventually result in the clogging of the filter. It was found that in some subsurface drainage systems which have used geotextile filters, the drains were filled with sediments in a very short period after installation. More than 70% of the sediments were in the silt size range (Rollin et al., 1987).

Because of probable failures, Koerner (1990) proposes that "if these conditions (i.e., 1. cohesionless silts, 2. gap-graded particle size distributions, and 3. high hydraulic gradients) are present, one should avoid the use of geotextiles altogether and should instead use a soil filter (although the chances are that it, too, will clog) or should open up the geotextile to the point where some soil loss will occur." It is therefore imperative to study the filtration behavior of nonwoven geotextiles in silty and broadly graded soils to understand the geotextile's resistance to clogging and its long-term performance, to develop a new generation of geotextiles to suit the nature and size of soil particles to be retained, and to develop new design criteria.

The purpose of this paper is to demonstrate the effects of the structure of various geotextiles on their long term filtration behavior of the silt/geotextile system. The phenomena involved with silt particle migration and retention within a soil/geotextile interface will be presented to understand the filtration mechanisms.

LABORATORY TESTING PROGRAM

Geotextiles. Five types of nonwoven geotextiles were selected for this study. Selected properties of these geotextiles were determined. These properties are a direct or indirect measure of the pore structure characteristics of the nonwoven geotextiles. The apparent Opening Size (AOS) and the Filtration Opening Size (FOS) parameters can be assumed as direct pore structure properties while mass per unit area, thickness and permittivity can be assumed as an indirect measure of pore structure characteristic. The AOS values of the geotextiles were determined by the dry sieving method as per ASTM standard test method D4751 - 87. The FOS values were determined by the hydrodynamic sieving method as per modified CAN/CGSB draft 148.1, No.10.2 -M. The indirect pore structure properties were determined as follows: mass per unit area according to CAN/CGSB 148.2 standard test method, thickness according to ASTM D35.03.80.06 draft standard method and water permeability by permittivity according to ASTM D4491- 85 standard test method. All these properties are presented in Table 1.

It can be seen that a significant difference exists between the direct pore structure parameters, the AOS values and the FOS values. The FOS values are always lower than the AOS values. (See Table 1.) As expected, the FOS values decrease with increasing mass per unit area of the geotextiles, as shown in Figure 1, (Rigo et al., 1989.

Table 1. Properties of Nonwoven Geotextiles

Type of geotextiles	Geotextile Identification	Mass per Unit Area (g/m^2)	Thichness (mm)	Opening Size		Permittivity (sec^{-1})	Fibres
				AOS (mm)	FOS (mm)		
I. Nonwoven needle-punched	A	119	1.19	0.149 to 0.210	0.193	2.3	Continuous
	B	140	1.64	0.195 to 0.210	0.180	2.3	filament
	C	241	2.78	0.125 to 0.210	0.103	1.4	polyester
	D	472	4.42	0.105 to 0.149	0.080	0.8	
	E	567	4.70	0.088 to 0.149	0.065	0.5	
II. Nonwoven needle-punched heat-treated	F	140	1.01	0.180	0.105	1.97	Polypro-pylene
	G	280	2.02	0.210	0.100	1.48	
	H	420	3.00	0.210	0.115	0.98	
III. Nonwoven heat-bonded	I	105	0.30	0.240	---	1.30	Continuous filament
	J	119	0.36	0.230	0.160	1.10	polypro-pylene
	K	140	0.38	0.170	0.110	0.80	
	L	210	0.46	0.080	0.047	0.30	
IV. Nonwoven needle-punched calandred	M	220	1.13	----	0.040	0.47	Polyester
V. Nonwoven needle-punched	N	345	2.82	----	0.105	1.33	Polypro-pylene

In Figure 2, microscopic view in plane and perpendicular cross sections of two geotextiles (type III, geotextile I, and type IV, geotextile M) are shown as examples to support the large difference in their structures. The geotextiles used in this research, even though they belong to the same family (nonwovens), are very distinct in structure. This difference could be attributed to the manufacturing process (age of machine, type of needles, length of fibers, etc.). It was shown by Rigo et al. (1989) that the process of manufacturing plays an important role when examining a pore structure of a geotextile. Although all the geotextiles used in the test program were needle-punched, they were supplied by five different manufacturers.

Soils. The filtration tests were performed using a silty Sil-Co-Sil 75 manufactured soil produced from high purity silica that is ground to nonplastic particles with average diameter of 0.003 mm. Its grain size distribution curve is plotted in Figure 3. The dimensions of characteristic particles of this silt are as follows: d_{85} = 0.04 mm, d_{60} = 0.0055 mm, d_{50} = 0.0045 mm, and d_{10} = 0.0024 mm.

Methodology. The most unfavorable situation which can occur along a drainage system was simulated in the laboratory testing program.

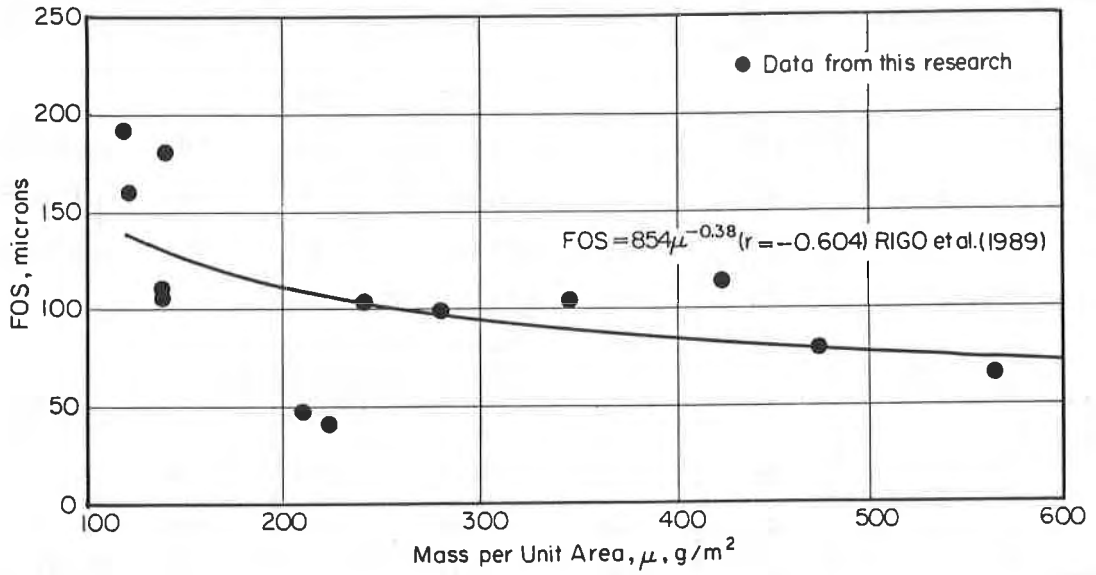

Figure 1. Variation of FOS with Mass per Unit Area for Nonwoven Geotextiles

First, since water must enter the pipes through perforations that represent only about 1% of the total area of the pipe, hydraulic gradients encountered close to these perforations are very high (Lagace, 1983). A gradient of 10 was used in this program to simulate this condition.

Second, installation of a drainage system in wet conditions occurs very often. It often considered an unfavorable situation since the disturbed soil around the drains can easily be eroded and carried by water (Bonell, 1984). To simulate these conditions, it was decided to mix the silt samples into a slurry (50% water and 50% silt in bulk volume) and place the slurry in the apparatus. Two other sample preparations were also attempted, but both proved inferior to the slurry method. The first of these was preparing sample by water pluviation; in this method, the heavier particles settled before the lighter particles, resulting in a nonhomogeneous mixture. The second technique involved placing the dry sample in the cylinder and then pouring water into the cylinder. The problem with this preparation was that a nonuniform level of soil sample was obtained. It was found that the slurry preparation technique produced the most uniform soil sample and that this technique has excellent reproducability.

To conduct the filtration tests, eight constant head permeameters were constructed following the long term filtration apparatus proposed and described by Rollin et al. (1987). The permeameter consists of two plexiglass tubes: a small inner cylinder (diameter 9.5 cm) and a larger outer cylinder (diameter 20.3 cm). The geotextiles were placed at the bottom of the inner cylinder. A total of 240 g of soil was mixed with the same volume of deaired water to form a slurry which was then poured over the geotextile. This resulted in a 3.5 cm high soil sample forming above the geotextile.

The deaired and chlorinated water was introduced into the permeameter by carefully pouring the water so as not to displace the soil particles. After filling the inner cylinder with water, the outer cylinder was filled. The first reading was

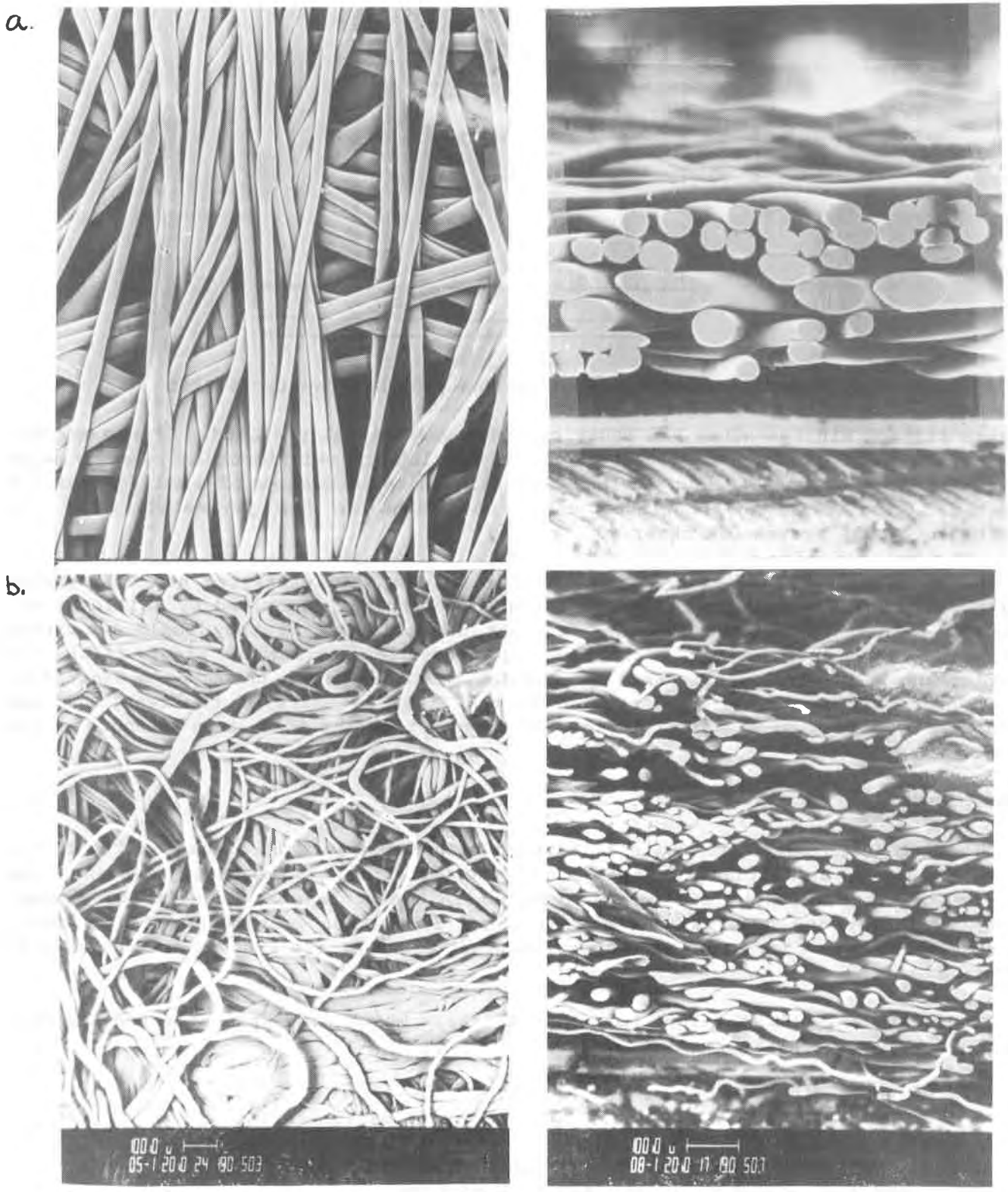

Figure 2. Micrographs of the In Plane and Perpendicular Cross Sections of the Geotextiles: a) Nonwoven, Heat Bonded Type, III Geotextile I and b) Nonwoven, Needle-Punched Type IV Geotextile M

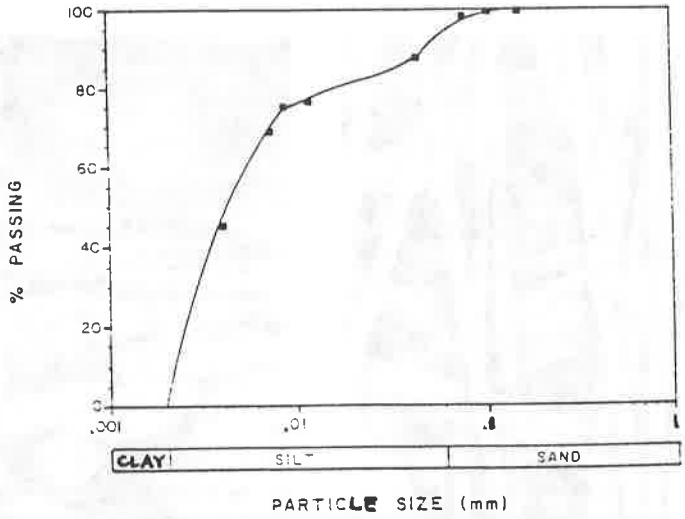

Figure 3. Gradation Curve of the 100% Sil-Co-Sil 75 Silt

taken fifteen minutes after the inner cylinder was initially filled. It was assumed that the initial period (first fifteen minutes), although very important, has no major significance when considering the long-term filtration mechanisms of a soil/geotextile system. The test was continued until no change in the permeability of the silt/geotextile system was observed.

After each test, the silt and geotextile samples were extracted and impregnated with ultra low viscosity epoxy by applying the technique described by Rollin et al. (1987). The encapsulated samples were cut and polished so they could be viewed through a reflected light microscope to study the structure after filtration performance. For all experiments, the filtration water was put through the centrifuge to measure the amount of soil passing in the first 24 hours of the test. It was observed that most of the particle loss occurred within the first 8 to 10 hours of the test.

TEST RESULTS

The long term soil/geotextile filtration mechanisms as well as geotextile filter performance can be evaluated by analysis of the following: permeability curves of the system, microphotographs of the soil/geotextile contact layer, quantity of washed-out particles, and observations of any other filtration phenomena noticed during system work. The results of all investigated silt/geotextile systems are compiled in Table 2.

There are only three filter retention criteria which are applicable for the silt used in this program:

- the EPM criterion, Rollin et al. (1990):
  FOS < 1.0 to 1.5 d_{85}, i.e., FOS < 40 to 60 micrometers

- the FHA criterion, Christopher and Holtz (1989):
  AOS = O_{95} < 1.8 d_{85}, i.e., AOS < 72 microns

- the Giroud criterion, Giroud (1982):
  O_{95} < C'_u to 2 C'_u. d_{50}

Table 2. Test Results

Geotextile Type	Type I					Type II			Type III				Type IV	Type V
Filtration behavior	A	B	C	D	E	F	G	H	I	J	K	L	M	N
1. Permeability curve 1) k_o/k_{150}	around 1 for all geotextiles													
2. Estimated Level of dogging (% of the pore volume)	≈ > 0 to 80%					≈ 25%			≈ 5%			0%	0%	25%
3. Quantity of wash-out particles (g/cm^2)	0.24	0.24	0.05	0.05	0.05	0.03 to 0.10			0.20 to 0.27			0	0.03	0.05
4. Particles piping 2)	yes	yes	no	no	no	no	no	no	yes	yes	yes	no	no	no

1) k_o - permeability at the start of the test
k_{150} - permeability after 150 hours.

2) Piping occured only within first 5 hours of the test.

if assuming that O_{95} = AOS and that C'_u = Cu, the following criterion can be calculated:

AOS < 10 to 21 micrometers

Based on the EPM criterion, only two of the geotextiles used would retain particles of the 100% Sil-Co-Sil 75 silt: type III geotextile L of FOS--47 micrometers and type IV geotextile M of the FOS--40 micrometers. None of the geotextiles of type I, II, and III for which the AOS was measured fits the FHA criterion as well as the Giroud criterion.

Surprisingly, however, the permeability curves presented as examples in Figure 4 show that all the geotextiles acted as proper filters. The initial permeability of all silt/geotextile systems was between 1.8×10^{-5} to 4×10^{-5} cm/sec and stabilized almost immediately after the beginning of the experiment. Once stabilized, the permeability of all silt/geotextile systems stayed in the same order of magnitude until the end of the experiment. It should be noted that the curves presented are typical permeability curves for silts which can be obtained in a constant head permeameter. If so, it can be concluded that geotextiles retained the silt particles and had no effect on the permeability of the silt/geotextile system. The same behavior was observed for all other systems, in support of the notion that the geotextiles act as the proper filters. On the other hand, through analysis of microphotographs, the quantity of washed-out particles as well the observed particle piping phenomenon there is a significant difference amongst the geotextiles.

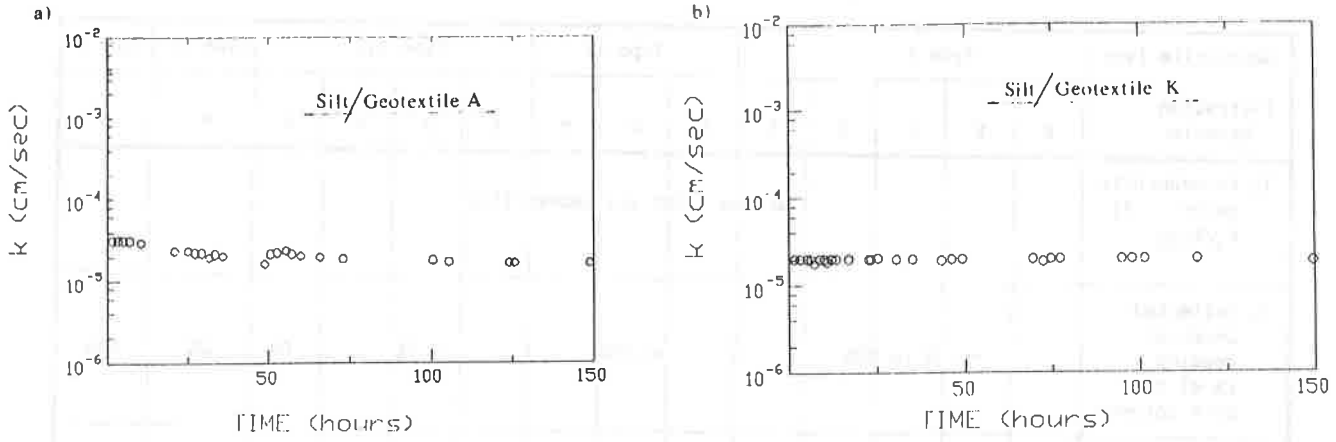

Figure 4. Typical Permeability Curves: a) Silt/Type I Geotextile A System and b) Silt/Type III Geotextile K System

Geotextiles - type I. In Figure 5a, a microphotograph of geotextile B with 100% Sil-Co-Sil 75 silt is shown. It can be seen that migration of fine silt particles resulted and that fines carried by the water were retained at the agglomerations of fibers within the geotextile structure. A vault network was formed between the fibers at the lower part of the geotextile. This network of vaults resulted in a decrease of the porosity; finer particles were stopped by this newly formed filter layer inside the geotextile. Because pore sizes of the geotextile are much larger than the diameters of fines, the particles could move within the pores, be retained at the vaults and finally be trapped (estimated fines filling 80% of the pore volume).

It is important to note that for this geotextile as well as for geotextile A, the piping phenomenon was observed within the first four hours of the tests. Surprisingly, a small amount of particles was washed out. Around 0.24 g/cm^2 (around 8% by weight) of particles passed through geotextiles A and B, whereas for geotextiles C, D and E a much smaller amount (around 0.05 g/cm^2 - 1.5% by weight) of soil loss was observed.

Geotextiles - type II. A microphotograph of geotextile F used to retain 100% Sil-Co-Sil 75 silt is shown in Figure 5b. It can be seen that a substantial amount of fines migrated in the geotextile (it is estimated that around 30% of the pore volume has been filled). The filtration mechanism is believed to be the same as for the geotextiles of type I.

The amount of soil passing through geotextiles F, G, and H was in the range of 0.03 g/cm^2 (1% by weight) to 0.10 g/cm^2 (3% by weight), which is, as shown by Lafleur et al. (1989), less than the amount of migration necessary for self-filtration to develop. Since the FOS of this geotextile is smaller (105 micrometers), the amount of particles trapped within the geotextile structure is lower than in the case of geotextile B (FOS = 180 microns). A particle network formation was observed at the soil/geotextile interface as it was presented recently by Mlynarek et al. (1989). The examination of microscopic cross sections showed two filter layers: layer one, which is composed of the fibers and particles trapped inside the geotextile, and layer two, which is formed upstream of the geotextiles.

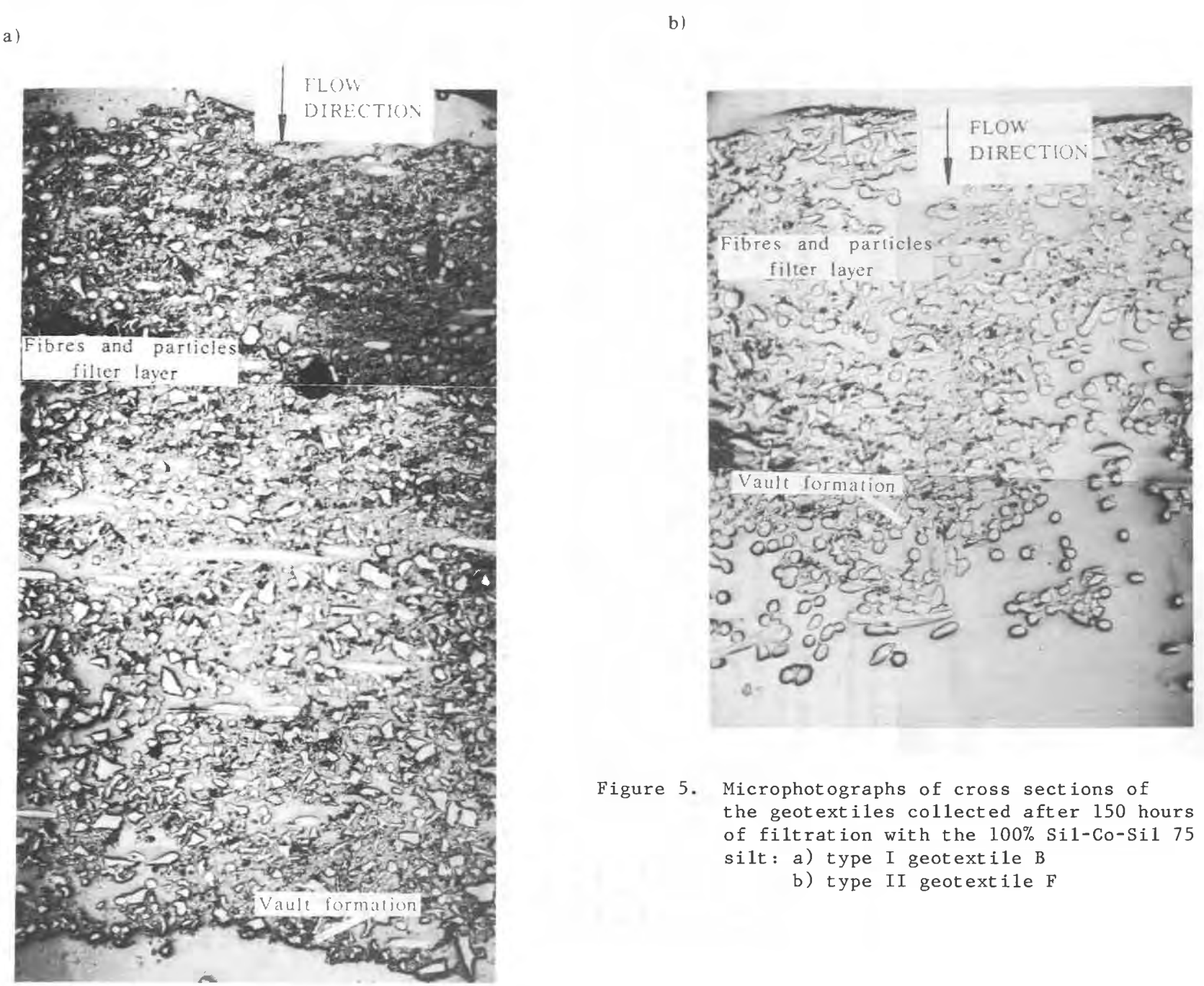

Figure 5. Microphotographs of cross sections of the geotextiles collected after 150 hours of filtration with the 100% Sil-Co-Sil 75 silt: a) type I geotextile B
b) type II geotextile F

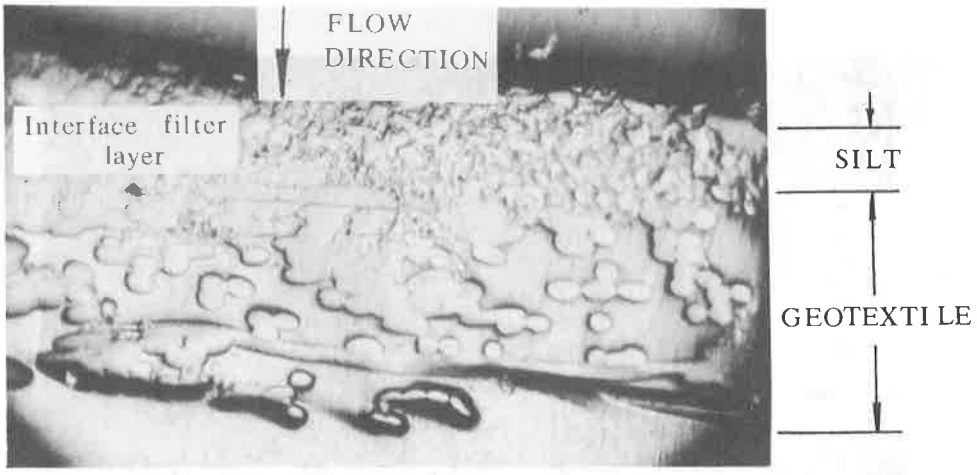

Figure 6. Microphotograph of Geotextile K after 150 Hours of Filtration Performance--Magnification 100x.

Geotextiles - type III. In Figure 6, a microphotograph of geotextile K is presented after 150 hours of performance. Very little clogging (around 5% of the pore volume) was observed in this geotextile in spite of its FOS of 110 micrometers which is almost the same as the FOS of the type II geotextile F (see micrograph in Figure 5b). For type III geotextiles, K, I, and J, the piping phenomenon was also observed. It was noted that it took place within the first five hours of testing and that during that time 0.20 g/cm^2 to 0.27 g/cm^2 soil passed through the geotextiles. After this time, no particle wash-out was observed. The wash-out value, 0.27 g/cm^2, is slightly higher than the threshold value of 0.25 g/cm^2 proposed by Lafleur et al. (1989) as necessary to develop self-filtration. It was only for geotextile L, which has the lowest FOS of the type III geotextiles (47 microns), that no particle piping and passage was noted.

From the microphotographs, it is clear that the filtration mechanism in the geotextiles of type III is completely different from those of types I and II. The only explanation for this is the individual structures of the geotextiles is different. First, the geotextiles I, J, K and L are much thinner than any other geotextiles. Their structures are different and in general there are not many fiber agglomerations inside to initiate the formation of vaults and natural filters. Because of this, as well as the opening size (excluding geotextile L), the particles which passed into the geotextiles were washed out from the system. However, during the first few hours of filtration the particle network was formed at the interface of soil and geotextile; this network began to act as a filter for other fines. This is why boiling was observed only at the beginning of the experiments, before this filter was formed.
The details of the mechanism of boiling are discussed in a forthcoming paper by Bhatia, et. al. (1991).

In contrast, geotextile L, which fits the EPM filter criterion for the 100% Sil-Co-Sil 75 soil (FOS < 60 microns), had no wash-out of fines. In this system, the interface filter was formed more rapidly due to the low value of FOS of the geotextile (47 microns).

Geotextiles - type IV. A microphotograph for geotextile M is presented in Figure 7. Geotextile M (FOS = 40 microns) was the second geotextile to fit the EPM filtration criterion for 100% Sil-Co-Sil 75 soil, i.e., FOS < 40 to 60 microns.

It was observed that the permeability curves of type IV geotextiles were very similar to those of type I (for example, see Figure 4) in spite of totally different structures. However, geotextile M apparently remained completely unclogged within the fibers, whereas all geotextiles of type I were significantly clogged. It is very important to notice that a very small amount of fines, 0.03 g/cm^2, were lost with geotextile M.

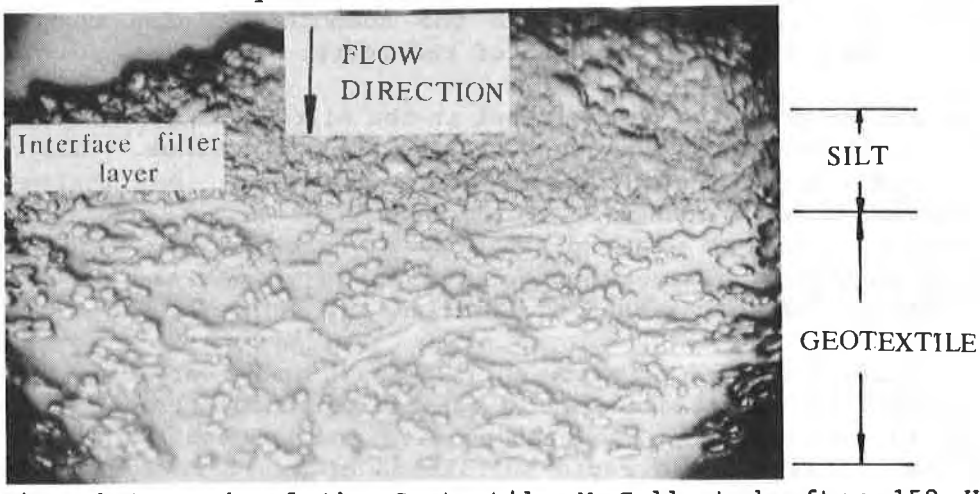

Figure 7. Microphotograph of the Geotextile M Collected after 150 Hours of Filtration--Magnification 100x

With this geotextile, only one filter layer was formed at the interface of silt/geotextile, because of the low FOS value. This layer is very efficient at retaining the fines and evacuating the water. It was found once more that differences in structure as well as filtration opening size played a crucial role in a natural filter formation within geotextiles and at the interface of both media.

Geotextile - type V. A microphotograph of type V geotextile N cross-section shows partial clogging (around 25% the pore volume) of the geotextile which is very similar to that of type II geotextiles (see Figure 5b). Also, no significant amount of fines passed through the fabric (around 0.05 g/cm^2).

DISCUSSION

Two important aspects of the long term filtration performance of soil-nonwoven geotextile filter systems are addressed: (1) is the structure of various nonwoven geotextiles important for the filtration behavior of silty soils? (2) do the filtration opening sizes influence the filtration behavior of geotextile/silty soil systems?

The analysis of the filtration curves of silt/geotextile systems indicates that the permeability criterion is not critically important for geotextile filters for 100% Sil-Co-Sil 75 silt. It was found that the permeability of a silt governs the long-term permeabilities of systems. The permeabilities of silt/geotextile systems were always in the range of a silt permeability, as presented in Figure 4.

The retention criterion seems to be most important when the geotextile filters are considered for silty soils. From the observations of microphotographs, it is clear that the structure of a geotextile has a great influence on the filtration mechanisms and on the level of clogging. It can be concluded that in some geotextiles (types II and V) appreciable levels of clogging (> 25% of the pore volume) occurred, while in the type I geotextiles higher levels of clogging were observed (80% of the pore

volume). However, there was always some (20% to 75%) unfilled pore space through which water could easily flow. The coefficient of permeability is still high enough to evacuate the water. Conversely, for geotextiles type III and IV it was found that a particle network was formed at the silt/geotextile interface. This network performs as a filter for other fines. It is the authors' opinion that in all systems stabilization was achieved at the end of the tests.

However, the authors also believe that in the silty soil/geotextiles type I, II and V, system's stabilization is very sensitive to any disturbance. This results from the structure as well as from the filtration opening sizes. Any increase in hydraulic gradient, combined with change in other hydraulic conditions, can influence this temporary equilibrium, as was explained by Mlynarek et al. (1987). The modified structure of partially clogged geotextiles is very weak and a minute increase in hydraulic gradient can break this equilibrium.

The filtration mechanism of silty soils appears to be very complex. It is obvious that the formation of vault networks is related to other filtration properties of the geotextile, in particular to the opening size and thickness. The selection of the proper geotextile favors the rapid initiation of vault network formation and of a filter layer at the soil/geotextile interface. In this research program, the crucial role of the opening size was observed in two geotextiles-type III geotextile L (FOS = 40 microns) and type IV geotextile M (FOS = 40 microns). For these geotextiles and silty soil, almost no fines went through the system. The geotextiles properly initiated a self-filtration layer at the interface immediately after the beginning of flow.

It can also be concluded that the thickness of the geotextile does not play an important role. The thickness of geotextiles ranged from 0.30 to 4.72 mm and had an insignificant effect on the long term silt/geotextile system permeability. This result confirms recently published findings of by Rollin et al. (1990) and Qureshi et al. (1990).

CONCLUSIONS

The purpose of this study was to demonstrate the effects of the structure of various geotextiles on the long-term filtration behavior of silt/geotextile systems. The most critical observed conditions which can occur along a drainage system (such as a high hydraulic gradient and an installation of a geotextile filter in wet conditions) were simulated in the laboratory.

The results obtained during the laboratory test program, using fourteen different nonwoven geotextiles and one manufactured silty soil, indicate the following:

1. Laboratory filtration tests to simulate the long-term field behavior of geotextile filters should be supported by microscopic analyses to understand the filtration mechanisms and visualize the clogging level of the geotextiles. This is particularly important for experiments using silty soils.

2. The structure of a geotextile plays a crucial role in the soil/geotextile structure modification mechanisms, while the retention ratio, FOS/d_{85}, affects the long-term permeability values.

3. Geotextile filters can be used as filters for silty soils if the proper filter retention criteria are met.

4. The Ecole Polytechnique filter retention criterion for silty soils, FOS < 1.5 d_{85}, should be applied if the hydraulic gradients are lower than 10 and steady state filtration conditions exist.

5. The general trend of soil geotextile system performance can not be evaluated from permeability curve analysis only.

6. All silt/geotextile systems were stable systems; the quantity of wash-out particles was in the range of 0 to 0.27 g/cm^2, which shows stable filtration conditions (Lafleur et al., 1989).

7. Thickness of the geotextile filter has an insignificant effect on the long-term filtration performance of the silty soil/geotextile performance.

It is proposed, for future research on geotextile filter criteria for silty and gap-graded soils, that analysis of the influence of hydraulic conditions on the silt/geotextile system performance is necessary. This research could lead to the proposal of more appropriate criteria depending on hydraulic conditions.

ACKNOWLEDGEMENTS

The support for this research was provided by the National Science Foundation (MSS 8910052) to the first author and it is gratefullly acknowledged. Appreciation is also extended to M.S. Qureshi, R.M. Kogler, and S. Umakanthan who performed laboratory tests as part of their Masters of Science degrees at Syracuse University.

REFERENCES

Bhatia, S.K., Umakanthan, S., and Mlynarek, J. (1991). "Performance of Thin Nonwoven Geotextiles as a Filter", paper in preparation to be submitted to journal of Geotextiles and Geomembranes.

Bonell, R.B. (1984) "Critical Hydraulic Gradient and Soil-Drain Envelopes," M.Sc. thesis, McGill University, Montreal, Canada.

CFG--The French Committee on Geotextiles & Geomembranes (1986) "Recommendations pour l'utilisation des geotextiles en filtration et drainage," Comite Francais des Geotextiles, Paris.

Christopher, B.R., and Holtz, R.D. (1988) "Geotextile Design and Construction Guidelines," U.S. Department of Transportation, Federal Highway Administration, Washington.

Giroud, J.P. (1982) "Filter Criteria for Geotextiles," Second International Conference on Geotextiles, Las Vegas, Vol. 1, pp. 103-108.

Koerner, B. (1990) Designing with Geosynthetics, 2nd ed., Englewood Cliffs, N.J., Prentice Hall, Inc.

Lafleur, J., Mlynarek, J., and Rollin, A.L. (1989) "Filtration of Broadly Graded Cohesionless Soils," Journal of Geotechnical Engineering, Vol. 115, No. 12, pp. 1747-1768.

Lagace, R. (1983) "Predicting Drain Silting Potential," Ph.D Dissertation, North Carolina State University, Raleigh, N.C.

Mlynarek, J., Lewandowski, J.B., Rollin, A.L., and Bolduc, G. (1988) "Soil-Geotextile System Interaction," International Seminar on Geotextiles, Gdansk.

Mlynarek, J., Rollin, A.L., Lafleur, J., and Bolduc, G. (1989) "Microstructural Analysis of Soil/Geotextile System," ASTM Symposium on Microstructure and the Performance of Geosynthetics, Orlando.

Qureshi, S., Kogler, R.M., and Bhatia, S.K. (1990) "Long-Term Filtration Behavior of Nonwoven Geotextiles", Proceeding of the 4th International Conference on Geotextiles and Related Products, The Hague, 28 May - 1 June, pp. 279-283.

Rigo, J.M., Lhote, F., Rollin, A.L., and Mlynarek, J. (1989) "Influence of the Geotextile Structure on the Pore Size Determination," ASTM Symposium on Microstructure and the Performance of Geosynthetics, Orlando.

Rollin, A.L., Broughton, R.S., and Bolduc, G.E. (1987) "Thin Synthetic Envelope Materials for Subsurface Drainage Tubes," Geotextiles and Geomembranes, Vol. 5, No. 2, pp. 99-122.

Rollin, A.L., Mlynarek, J., and Bolduc, G. (1990) "Study of Significance of Physical and Hydraulic Properties of Geotextiles Used as Envelopes in Subsurface Drainage Systems," 4th International Conference on Geotextiles, Geomembranes and Related Products, The Hague, pp. 363.

Saathoff, F., and Kohlhase, S. (1986) "Research at the Franzius Institute on Geotextile Filters in Hydraulic Engineering," Proceedings of the 5th Congress Asian and Pacific Regional Division, ADP/IAAR, Seoul.

Load Distribution in Geogrids With Low Junction Efficiency

C. Bonczkiewicz
STS Consultants Ltd., USA
B. Christopher
Polyfelt Inc., USA
M. Simac
Intersol Engineering, USA

ABSTRACT

Stress transfer in geogrids with low junction efficiency was investigated. Field pullout testing was performed, where resistance strain gauges were mounted on each side of the junction points along the length of the geogrid. Results were compared with the distribution of strain levels measured along the reinforcement during construction of a full-scale test wall.

INTRODUCTION

The stress transfer in geogrids with low junction efficiency is currently an area of much discussion. Questions regarding the influence of grid element junction strength on stress transfer, and specifically on the effectiveness of weak junctions to provide adequate pullout resistance, have been raised. Although several structures have been successfully constructed with such products, definitive research has not been performed to evaluate the pullout resistance of such materials. The capacity for using these products in reinforcement applications has, therefore, been limited due to the absence of data supporting their effectiveness.

A geogrid with low junction strength, (15% of its rib strength), was instrumented to obtain the data necessary to evaluate stress transfer. Its performance was evaluated by lab and field pullout testing and by monitoring construction of a full scale test wall. Stress transfer in the geogrid was evaluated under each loading condition by monitoring resistance strain gauges mounted along the length of the geogrid and specifically on each side of a junction point at several locations.

This paper describes the procedures used and results of the field and laboratory study. Data from resistance strain gauges is presented and the distribution of strain levels along the reinforcement is shown.

PROJECT DESCRIPTION

The geogrid evaluated in this study was Miragrid 5T manufactured by Mirafi, Incorporated. It is made of continuous filament polyester yarn formed into a biaxial grid by a knitting process. Strands are approximately 0.15 inches wide in the machine direction and 0.25 inches wide in the cross direction. The junction at each cross direction has about 15% of the strength of the machine direction element to which it is attached. This biaxial geogrid has approximately 1.2 inch strand spacing in both the machine direction and in the cross direction. The ultimate wide width strength in the machine direction is 223 pounds per inch at 15% maximum elongation and 134 pounds per inch at 19% maximum elongation in the cross-machine direction. Wide width strength test (ASTM D-4595) results with resistance strain gauge data are shown on Figure 1.

Initially, a trial pullout test was performed in the laboratory to evaluate the strain gauge reaction to loads anticipated in the field pullout tests. A normal stress equivalent to approximately 4 feet of overburden pressure was maintained vertically as the lateral load on the geogrid was increased until specimen pullout.

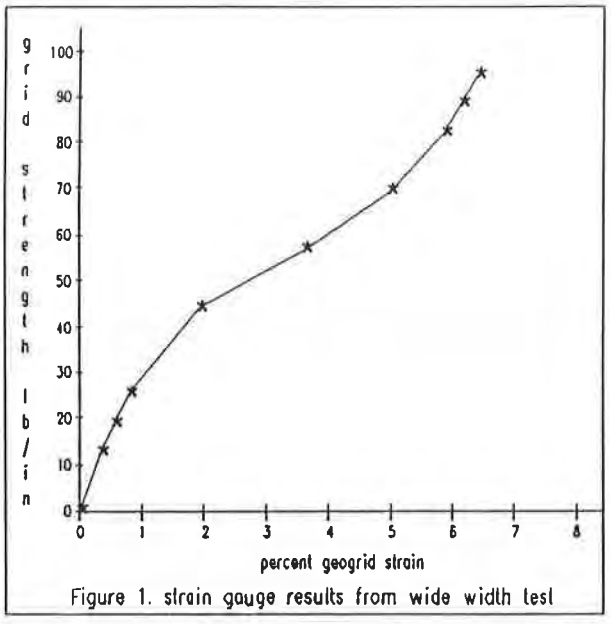

Figure 1. strain gauge results from wide width test

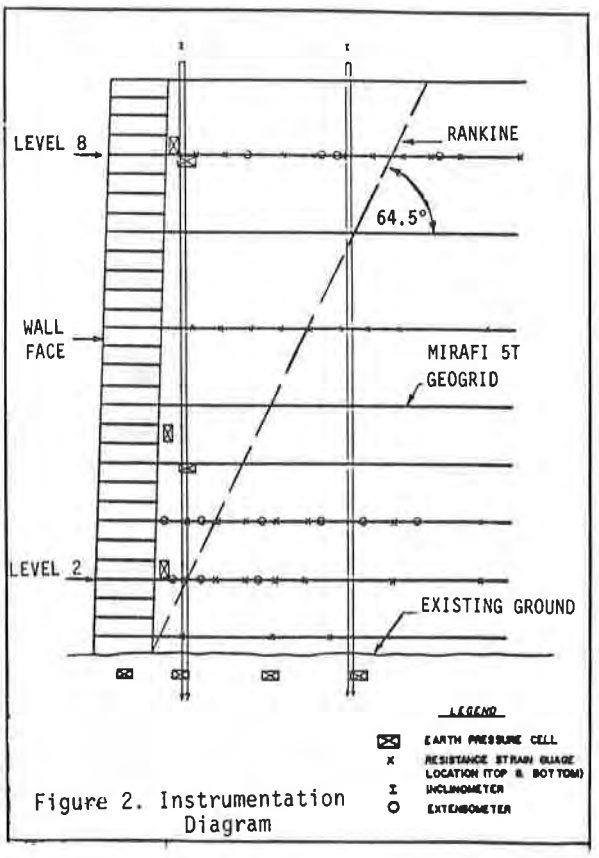

Figure 2. Instrumentation Diagram

The primary stress transfer evaluation was made by field pullout tests. Two instrumented field pullout specimens, four feet long by two feet wide, were laterally loaded from the face of a full scale, 20 foot high, reinforced wall at the same constant rate used in the laboratory pullout testing. The test specimens were subjected to four feet and seventeen feet of soil overburden pressure, respectively.

The transfer of stress along the geogrid was also evaluated from strain data obtained during construction of the field test wall. The lateral stresses in this part of the study built up internally as backfill was placed to construct the wall. To compare results, the lateral forces on the geogrid were estimated based upon a Rankine theoretical stress distribution for reinforced soil structures with extensible reinforcements and appropriate instrumentation measurements. The test wall was reinforced and instrumented as shown in Figure 2.

This full scale test wall was constructed by STS Consultants in Algonquin, Illinois at the FHWA reinforced soil research site in July, 1989. Precast concrete blocks were used for the wall face. The reinforced soil fill, retained fill, and subgrade all consisted of a well graded gravelly sand with less than 1% fines. The instrumented section was in the center of the 50-foot long wall. Details of construction and preliminary instrumentation results are reported in Simac et al. (1990).

EVALUATION PROCEDURES

As previously indicated, stress transfer evaluation was based on resistance strain gauge data from pullout tests and from test wall monitoring during construction. The resistance strain gauges were selected based on an extensive laboratory study using various gauges, bonding agents, and mounting procedures. The final gauging procedure was based on strain compatibility measurements between the gauge and LVDT measurements during wide width strength tests (ASTM D-4595). A Kwoya KFE-5-C1 strain gauge with high elongation capacity and correlating strain data was chosen.

Laboratory Pullout Testing - The primary purpose of the laboratory pullout testing was to evaluate the performance of the strain gauges under load. The results, although limited, provide additional information related to pullout performance and are therefore reported therein.

The laboratory pullout testing of Miragrid 5T was performed in a pullout box 53 inches long by 27 inches wide by 18 inches deep. The apparatus was described by Bonczkiewicz et al. (1990). For this study, a Miragrid 5T specimen, 24 inches wide with 48 inches inside the box, was used. Because of a load transfer sleeve in this apparatus, the effective embedment length was 42 inches. A resistance strain gauge was located 12 inches from the front of the box or 6 inches embedded into the soil.

A normal pressure of 4.0 psi, equivalent to approximately 4.5 feet of overburden, was maintained throughout the test. The geogrid specimen was embedded between two 6-inch layers of fine sand and pulled laterally at a constant rate of approximately 0.04 inches per minute as measured by a dial extensometer just outside the pullout box door. Load, front deformation and local strains at the strain gauges were monitored until pullout resistance provided by the geogrid decreased.

Field Pullout Testing - About 1 weeks after the reinforced wall was completed, the field pullout tests were performed, using procedures similar to those used in the laboratory pullout test. The field specimens were also 24 inches wide and were embedded 42 inches behind the wall facing units. Strain gauges were installed on the top and bottom of the geogrid and on the leading and trailing sides of an element junction at 0.8 feet and 3.5 feet from the front embedded edge of the specimen.

As previously indicated, the backfill used for the field wall was a gravelly sand. However, pea gravel was used inside the precast concrete face units and extended approximately one foot behind these blocks. The backfill was compacted by a vibratory compactor to 95% of the maximum standard proctor density (ASTM D-698) or 124 pounds per cubic foot. Two extra geogrid specimens were placed at 3.2 feet from the base of the wall for pullout testing. They were extended through the face using trimmed blocks and spacers to prevent vertical loading by the facing units. A solid metal plate placed over the spacers prevented loading from gravel inside the facing units.

One of the pullout specimens was installed in the center wall section constructed to a height of 20 feet. The other pullout specimen was placed in the access ramp area where final wall height was 7 feet. This allowed for 17 feet and 4 feet of overburden pressure, respectively, on the test specimens.

The hydraulic cylinder and load cell from the laboratory pullout apparatus were used to provide the pullout force in the field. A pullout rate of 0.04 inches per minute was also used. Gross external grid displacement was measured by a dial extensometer near the face of the wall, with eight strain gauges on the embedded geogrid to monitor internal local strains.

Field Monitoring During Construction - Resistance strain gauges were also applied to top and bottom of four reinforcement layers in the field test wall as shown in Figure 2. These geogrid layers were stressed by placement of overlying backfill soils. The readings of these strain gauges clearly indicate that an increase in stress occurred during construction of fill height above each instrumentation location. The average field test wall loading rate was approximately 1 ft/day.

PRESENTATION OF RESULTS

The results of the strain monitoring are presented in Figures 3 through 5. Figure 3 shows strains recorded in microstrain versus the lateral force applied in the three pullout tests performed. Strain across junction points is presented in Table 1 for the field pullout tests. The laboratory specimen had a pullout resistance of 37 lb/in. The field pullout tests with 4 feet and 17 feet of overburden pressure resulted in specimen failure in the unconfined area near the clamp at 130 and 97 lb/in resistance, respectively. Field wall performance data is shown in Figures 4 and 5 as microstrain versus fill height above the instrumented layer. The gauge location is referenced by distance from the face of the wall.

To illustrate the distribution of the strains and corresponding stress transfer during lateral loading, the strain data was re-plotted versus strain gauge location for several load conditions, as shown in Figures 6 through 9. These figures show a gradual difference in strains under load at low loads and a steeper strain distribution at higher loads. The field pullout test data in Figures 6 and 7 show strains at several pullout load (lateral stress) conditions. Almost no strain was measured at the far embedded end of the pullout test specimens. Since the strain level was not measured between 0.8 and 3.5 embedded feet, the actual strain distribution curve may be steeper than that shown. That is, the lateral force may have been transferred to the soil over a shorter distance than 2.7 feet.

The data included in Figures 8 and 9 are only that assumed to be on the embedded side of the failure zone, i.e., in the resisting area behind the active wedge zone. The strains measured in front of the areas shown were much lower. The lateral stress values included in Figures 8 and 9 along with the fill height are derived using a K_a value of 0.22 (=39). This value was chosen for comparison purposes only. However, it is in good agreement with that measured for this test wall (Simac et al. (1990)), and anticipated for this type of reinforcement in the FHWA design manual (1990).

DISCUSSION OF RESULTS

Data was presented from pullout tests and field wall performance monitoring at similar normal load and lateral load conditions. Although the actual loading methods differed, some comparisons can be made.

Table 1

Summary of Strain Gauge Data at
Junction Points from Field Pullout Tests

Overburden Stress	Pullout Force (lb/in)	Strain Across Node Embedded 1 Ft. (microstrain)	Strain Across Node Embedded 3.5 Ft. (microstrain)
4 psi	29	73	10
	45	90	8
	62	129	15
	96	2352	26
	112	3181	--
15 psi	29	2	--
	49	75	--
	70	100	--
	75	90	--

-- Denotes negative tension indicated across node.

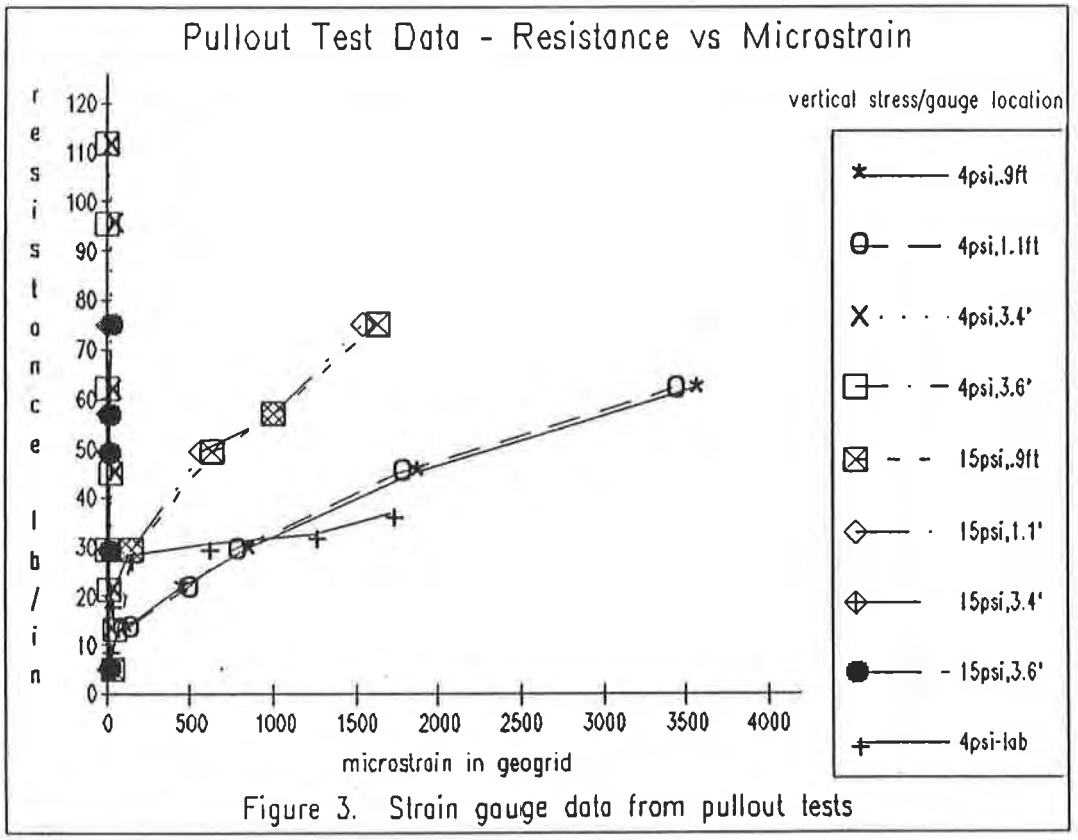

Figure 3. Strain gauge data from pullout tests

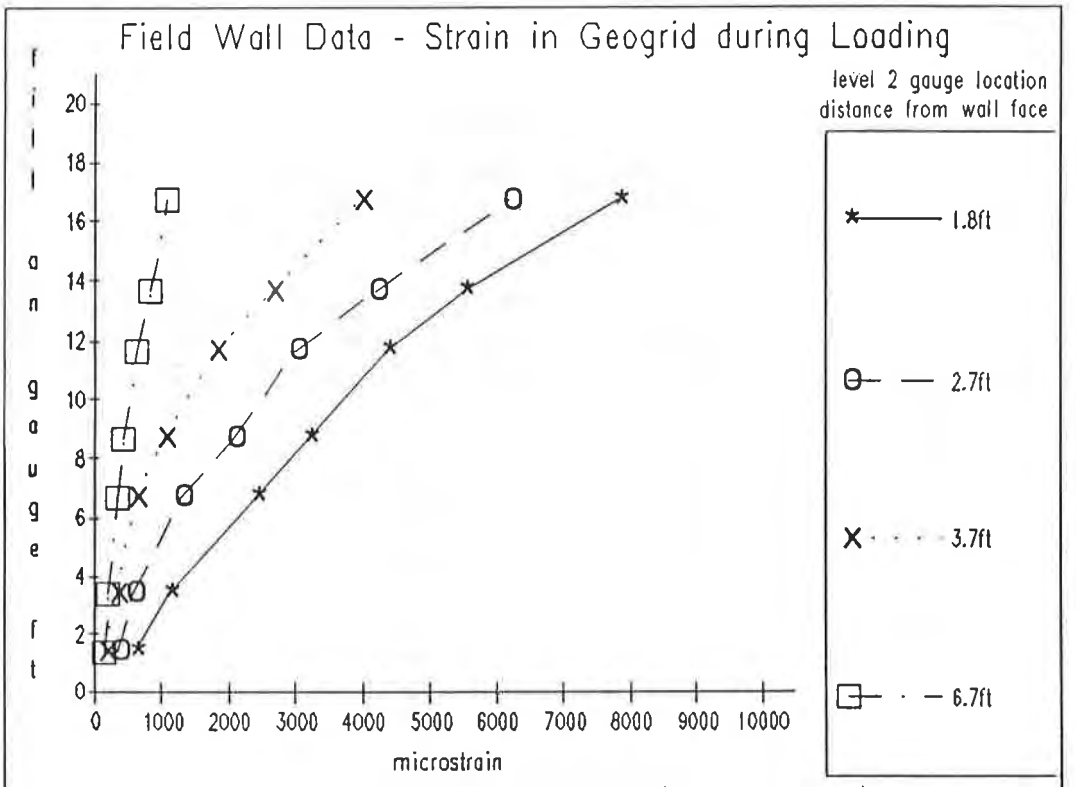

Figure 4. Strain in Level 2 Geogrid (2.7 ft Height)

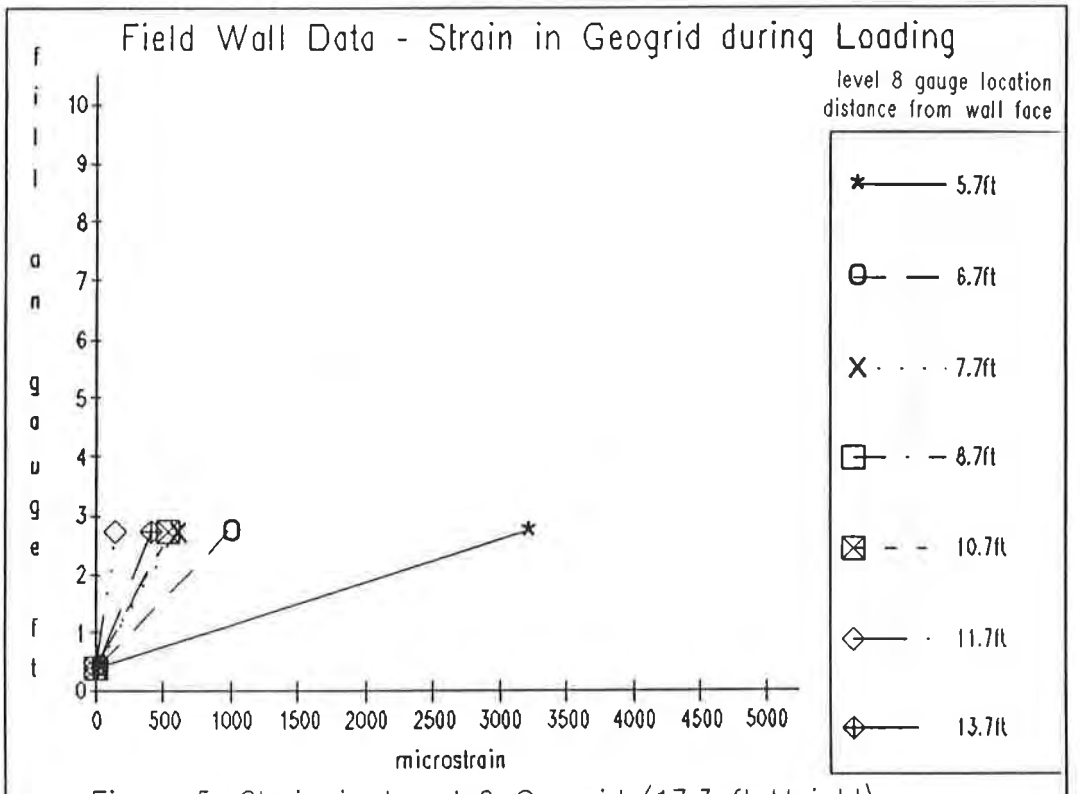

Figure 5. Strain in Level 8 Geogrid (17.3 ft Height)

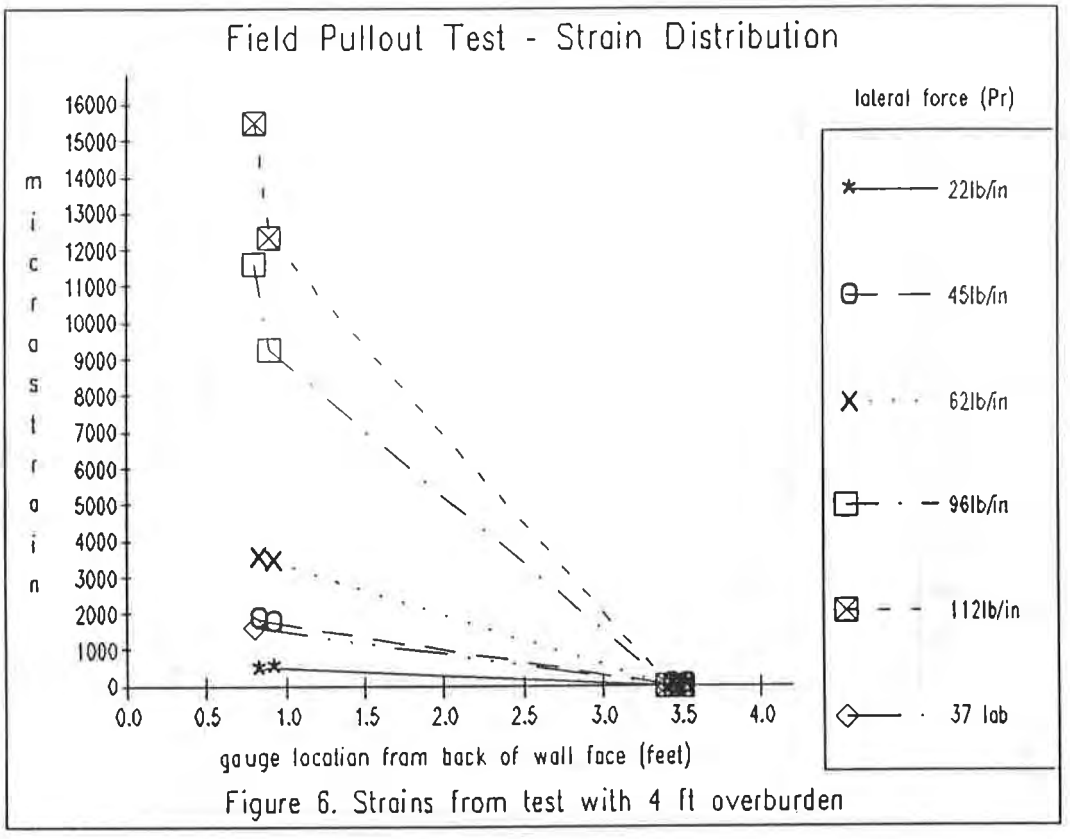

Figure 6. Strains from test with 4 ft overburden

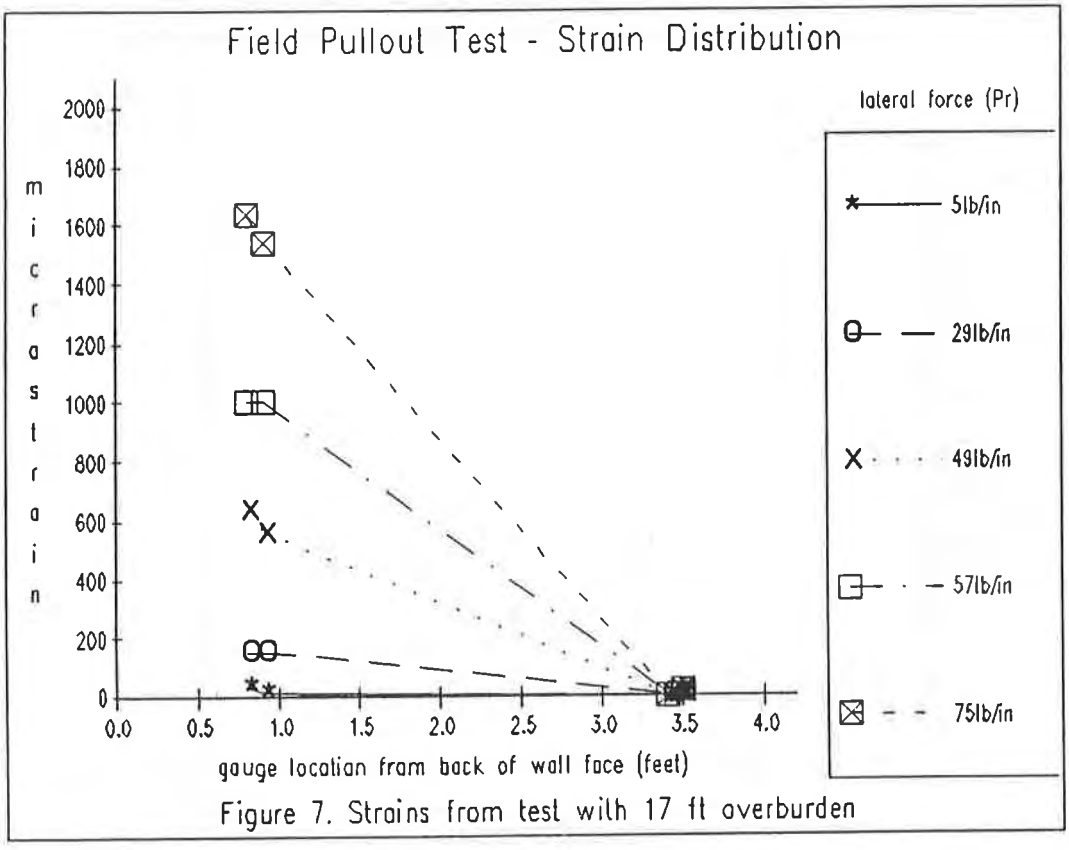

Figure 7. Strains from test with 17 ft overburden

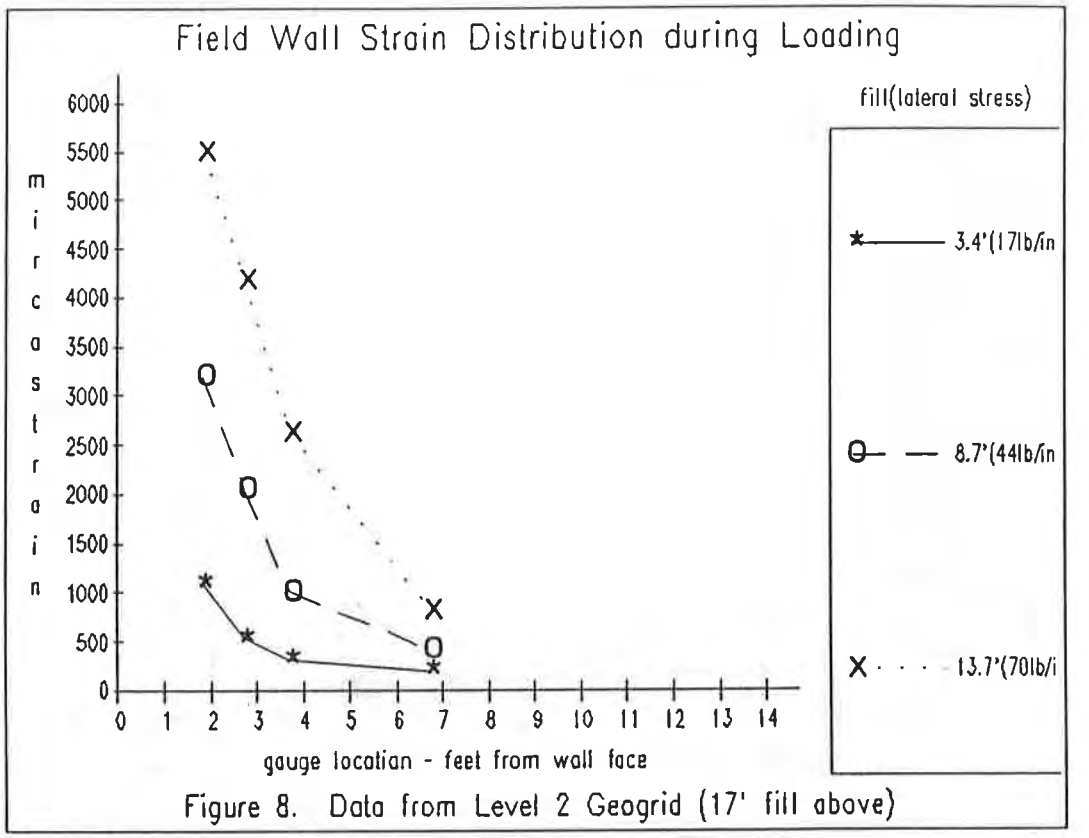

Figure 8. Data from Level 2 Geogrid (17' fill above)

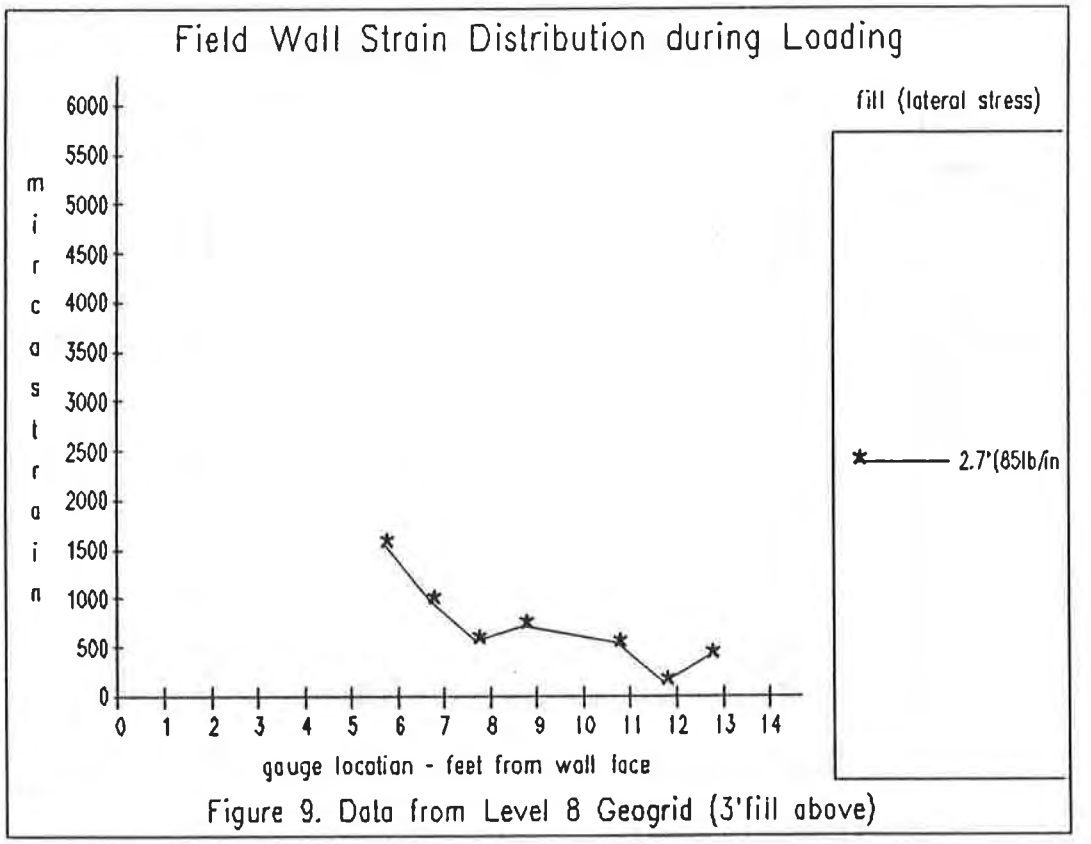

Figure 9. Data from Level 8 Geogrid (3'fill above)

Figure 3 shows that the field pullout samples developed about three times more resistance than the lab sample during testing. Differences in frictional shear values for the lab sand and the gravelly sand used in the field, as well as the influence of the pea gravel, most likely caused the different strain reaction under lateral loading. The initial portion of the lab data, however, was almost the same as the field data. Failure of the grid at loads lower than predicted by wide width testing may have been due to specimen exposure to weather before field pullout testing.

The field test wall performance data in Figures 4 and 5 show that most of the strain increase due to lateral loading occurs within 4 to 5 feet but decreases behind the point of maximum strain that was assumed to be the theoretical Rankine failure plane. The strains in the wall performance data probably included some creep due to the slow rate of loading. Nevertheless, the strains measured during field pullout testing at the lower normal stress condition were higher than the assumed comparable condition in the actual wall reinforcement layer.

When the strain data from the field pullout test with lower overburden is replotted in Figure 6, it is apparent that stress is transferred without loss across the node, up to pullout loads of 62 lb/in or 28% of ultimate grid strength at very low strains. At higher pullout loads, loss of strain across the node was shown to be greater. Therefore, less stress is transferred along the grid and more is taken by the soil. This figure also shows that the lab data agrees quite well with the field data despite the differences noted earlier. It should be noted that the highest strains recorded before grid failure at the face were only 10% of the maximum strain obtained from wide width testing of this geogrid.

The pullout test specimen with 17 feet of overburden above realized much lower strains. As shown in Figure 7, at these strains, there was less loss of strain across the node and therefore less transfer of stress to the soil. This data indicates that for the same geogrid, load transfer across junctions is more critical at large strains than small strains.

Comparing the strain distributions from Figure 8 with the pullout test strain distribution in Figure 7 at similar lateral stress levels shows that the pullout test strains were lower than those measured during wall construction. As previously discussed, the pea gravel at the wall face may have been a factor in this difference. The difference may also have been due in part to background strains in the field, perhaps from backfill compaction.

At the lower normal stress level, the pullout test strains were much greater than the strains measured during wall construction and plotted in Figure 9. This is due to the lack of confinement of the geogrid at the wall face during the pullout test.

The distribution of strains which were the focus of this study were found to be similar during both the field pullout and field construction monitoring. It was shown that strains were realized only 5 to 6 feet back from the lateral force source and that on the average, strains decreased by at least 50% in the first two to three embedded feet of geogrid. If field pullout tests and field strains are compared with the curve in Figure 1, the data indicates that tensile force at the embedded

gauge location was less than 16% of the reported grid wide width strength. Although there is an order of magnitude difference between the field strains measured during field pullout and field performance, the difference is minimal at comparable vertical stresses when expressed in terms of tensile force on the geogrid. These results exemplify the use of the pullout test to evaluate geogrid/soil stress transfer and provide design information for geogrids.

SUMMARY AND CONCLUSIONS

Strain data from a full scale test wall reinforced with Miragrid 5T was obtained from resistance strain gauges mounted on geogrid sections. When 3 foot long specimens were pulled horizontally, a strain distribution was found that was similar in shape to the stress distribution monitored behind the Rankine active wedge failure surface on geogrid reinforcement layers. The shape of the distribution curves indicates that substantial lateral stress can be transferred along a geogrid in the absence of high junction strength and that significant loads can be resisted by this geogrid without junction failure. At low strains (pullout loads) it appears that this geogrid develops a significant amount of pullout resistance in friction since there is little loss of strength across junctions. However, at large strains there is a significant strain differential indicating that the cross members are carrying load at high strains. On-going monitoring of the field structure should provide additional information related to creep at junctions as it relates to long-term performance.

ACKNOWLEDGMENTS

The authors would like to acknowledge R. Swager, D. Moe, C. Leucht and N. Trudeau for their work on this project and also Mirafi Inc. for the research project funding.

REFERENCES

1. Bonczkiewicz, C., Christopher, B., Atmatzidis, D., (1990), "Evaluation of Soil-Reinforcement Interaction by Large Scale Pull-out Tests", Transportation Research Record, No. 1188, January, 1990.

2. Christopher, B., Gill, S., Giroud, J., Junan, I., Mitchell, J., Schlosser, F., Dunnicliff, J., (1990), "Reinforced Soil Structures", Report No. FHWA-RD-89-043, Federal Highway Administration, Washington, D.C.

3. Simac, M., Christopher, B., Bonczkiewicz, C., (1990), Instrumented Field Performance of A 6M Geogrid Soil Wall", p. 53-59, 4th International Conference on Geotextiles, Geomembranes and Related Products, The Hague, Netherlands, May, 1990.

Comparative Hydraulic Performance of Resinated Geotextile Overwraps

R. Anne Gallup
GeoSyntec Consultants, USA
Robert C. Bachus
GeoSyntec Consultants, USA
Scott M. Luettich
GeoSyntec Consultants, USA

ABSTRACT

A comparative study is presented on the hydraulic performance of resinated needlepunched nonwoven geotextiles used as overwraps on a geocomposite drainage product. Index properties and hydraulic performance of the geotextile overwraps were evaluated through a laboratory test program consisting of a series of hydraulic transmissivity tests and hydraulic conductivity ratio (HCR) tests. The hydraulic transmissivity test results show that the increase of resin content in the geotextile overwraps increases the in-plane flow of the geocomposite drainage system. The HCR test results show that the increase of resin content in these geotextiles slightly increases the retention performance of the geotextile overwrap.

INTRODUCTION

Geocomposite drains typically consist of a geotextile filter overwrap which allows flow perpendicular to the plane of the geocomposite drain (normal flow) and a geosynthetic drainage core which conveys flow within the plane of the geocomposite drain (in-plane flow). Drainage performance of the system is dependent upon the reaction of the geosynthetic components to applied boundary conditions which include soil characteristics, normal stress, and hydraulic gradient. The focus of this paper is on the geotextile overwrap component reaction to these boundary conditions.

Failure of the geotextile overwrap to function properly may affect the hydraulic performance in both the normal flow and in-plane flow direction. In the normal flow direction, the geotextile overwrap functions as a filter allowing passage of drainage fluid and preventing excessive migration of adjacent soil particles. Improper functioning may cause geotextile clogging by excessive accumulation of soil particles within or adjacent to the geotextile structure. Alternatively, clogging of the drainage core may be caused by excessive passage of soil particles through the geotextile (i.e., poor retention performance) and deposition of the soil particles within the drainage core. Geotextile properties affecting the filtration performance are related to structural and hydraulic characteristics, including pore size distribution, porosity, and permittivity. While filtration performance is also

dependent on the adjacent soil type and hydraulic conditions, these effects are not within the scope of this paper.

With respect to in-plane flow of the geocomposite drain, the geotextile overwrap functions to minimize the decrease of the drainage core pore space caused by intrusion of the geotextile under pressure from the adjacent soil. A typical cross section of a geocomposite drainage core and its interaction with the surrounding soil is shown schematically in Figure 1. The cross sections of the geocomposite shows that the geotextile may bow (Figure 1b) or may bow and puncture (Figure 1c) due to the pressure exerted by the soil mass, thereby intruding into the in-plane flow drainage space. Geotextile overwrap properties affecting the in-plane flow performance are related to the strength and deformation characteristics including tensile strength, puncture resistance, and stiffness. In-plane flow performance is also dependent on the drainage core geometry, adjacent boundary soil type, and applied normal stress, but these effects are not within the scope of this paper.

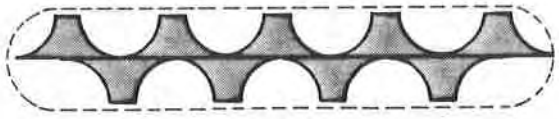

(a) geocomposite prior to its inclusion in the soil

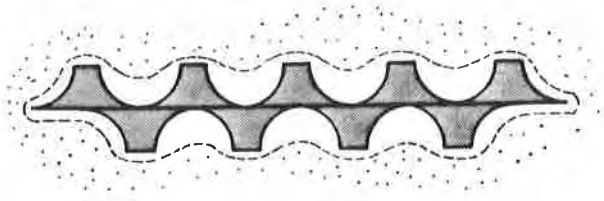

(b) bowing of geotextile between cusps

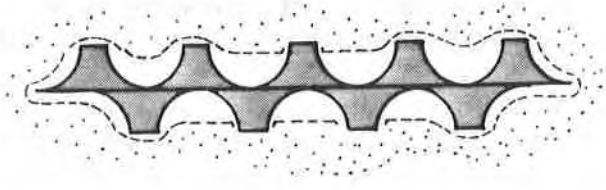

(c) combination of bowing and puncture of geotextile

Figure 1. Mechanisms of Geotextile Intrusion on a Double-Sided Cuspated Core

Quantifying the hydraulic performance of the geotextile and the drainage performance of a geocomposite drain may be achieved using laboratory tests. For normal flow across the geotextile-soil interface the Hydraulic Conductivity Ratio

(HCR) test can be used and for in-plane flow within the geocomposite drain the hydraulic transmissivity test can be used.

A product-development test program was conducted to quantify the hydraulic performance of three needlepunched nonwoven geotextiles with 1.5%, 3% and 5% resin added by weight. Resin was added primarily to increase the stiffness of the geotextile overwrap to improve the in-plane flow performance of the geocomposite drain; however, the effects of the resin on the normal flow performance of the geotextile was unknown. Therefore a laboratory test program was organized to evaluate performance in both flow directions. The following presentation includes a discussion of the selected materials and the geotextile properties. The test program is described, and results of the laboratory study are presented.

GEOTEXTILE INDEX PROPERTIES

The geotextile overwraps in this study are lightweight (approximately 135 g/m^2 (4 oz/yd^2)) needlepunched nonwoven polyester fabrics with 1.5%, 3% and 5% acrylic resin content by weight. Resin was added during manufacture of the geotextile. A micrograph of the fiber structure of the geotextile with 3% resin content is shown in Figure 2. In Figure 2a, some of the filaments seem to be bonded together along their longitudinal axes. This is particularly evident at the center and lower left portion of the micrograph. In Figure 2b, a close-up view shows that the resin appears to accumulate along the points of contact between the filaments but does not seem to significantly clog the pores of the geotextile.

Pore space reduction of the geotextile, caused by the resin, can be quantified by evaluating the pore size distribution using the mercury intrusion porosimetry technique (Prapharan et al., 1989). The pore size distribution results are summarized in Table 1 and Figure 3. As the resin content is increased, the following trends are observed:

- the total volume of intruded mercury decreases with increasing resin content; and
- an increase in resin content results in a slight decrease of the D_{10}, D_{50}, and D_{90} values, although the shape of the pore size distribution curve remains similar.

Physical strength-elongation data of the resinated geotextile are summarized in Table 2. Based on these data, the grab strength of the geotextiles increases with increasing resin content and the corresponding elongation values decrease. These effects are indicative of an increase in stiffness of the geotextile.

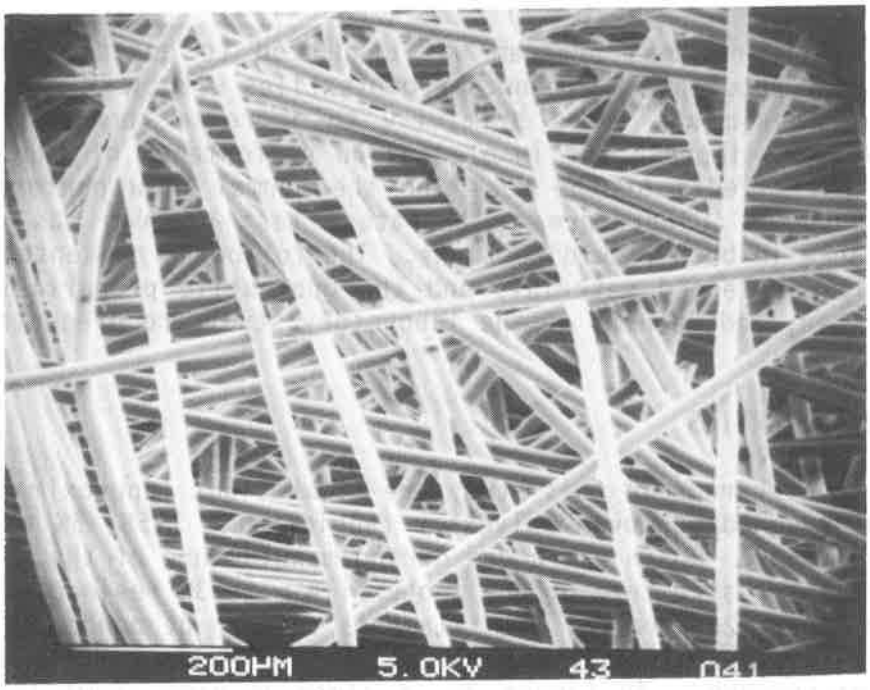

(a) enlarged view of geotextile structure

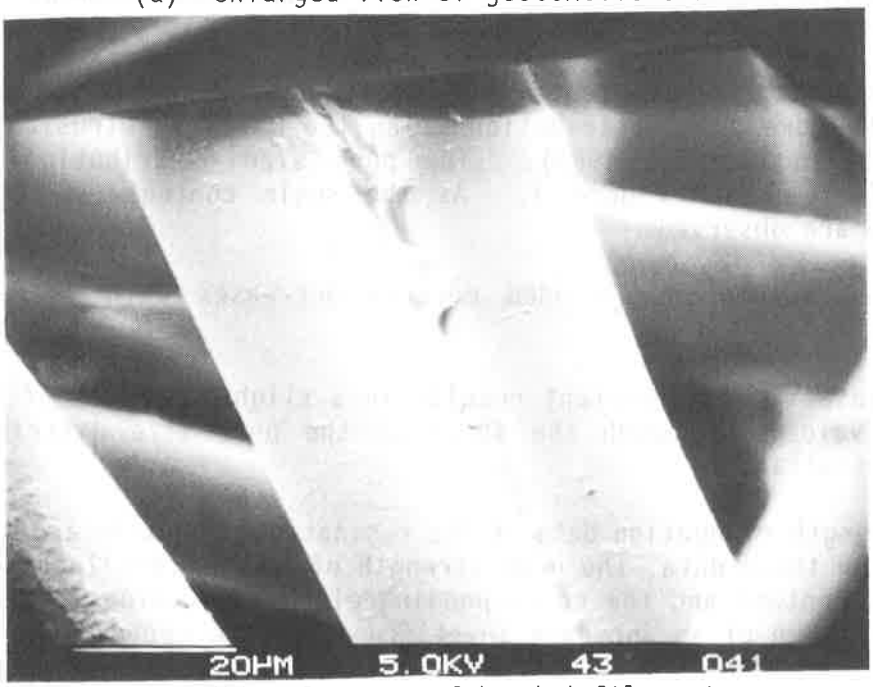

(b) close-up of bonded filaments

Figure 2. Micrographs of Resinated Nonwoven Geotextile Overwrap with 3% Resin Content (scale as shown on micrograph).

Table 1. Geotextile Density and Pore Size Distribution

Resin Content (%)	Mercury Intrusion Volume (ml/g)	Pore Diameter (μm)		
		D_{10}	D_{50}	D_{90}
1.5	6.95	90	118	180
3.0	6.67	85	125	180
5.0	5.81	80	110	165

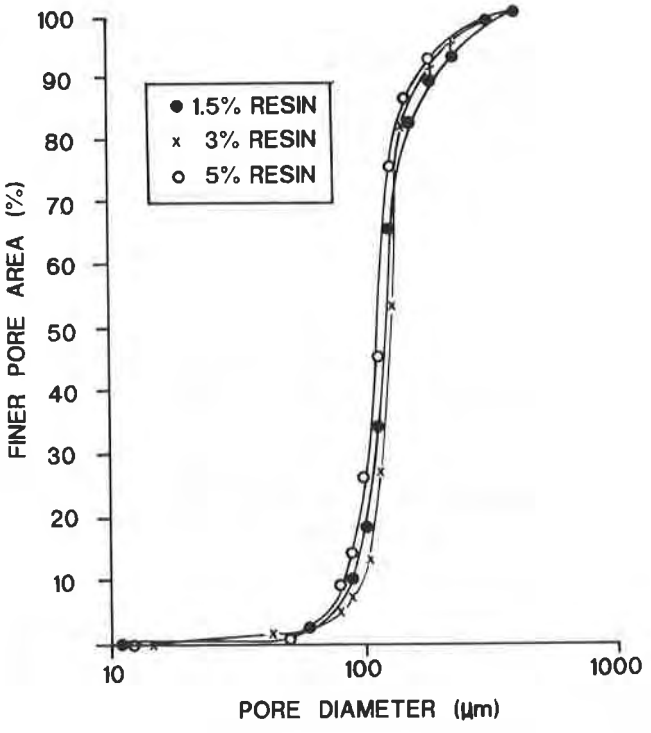

Figure 3. Geotextile Pore Size Distribution Curves

Table 2. Geotextile Strength Properties[a,b]

Resin Content (%)	Grab Tensile Strength[c,d] (Newtons)	Grab Tensile Elongation[c,d] (%)	Puncture Strength[e] (Newtons)
0	445	60	200
1.5	---	--	267
3	450	66	271
5	520	66	271

[a] strength values of the unresinated 135 g/m^2 (4 oz/yd^2) needlepunched nonwoven polyester geotextile are typical minimum average roll values as supplied by manufacturer literature
[b] 4.45 Newtons = 1 pound
[c] ASTM D4632
[d] minimum value of machine and cross direction
[e] ASTM D3787

It is noted that the principal focus of this project was to evaluate the hydraulic performance of resinated geotextiles. Therefore, limited strength test results were available as the resinated geotextiles were in the developmental stage. Strength tests on the unresinated geotextile were not conducted as part of the scope of work on this project, but the values reported in Table 1 are believed to be representative of the unresinated materials tested.

HYPOTHESES

From reviewing the geotextile properties which are affected by the resination process, the following two hypotheses are proposed:

- The tensile strength and stiffness increase as the resin content increases; therefore, the increased resin content of the geotextile overwrap will reduce geotextile intrusion into the drainage core as demonstrated by higher in-plane flow rates of the geocomposite.

- The resin accumulates along the points of contact between the geotextile filaments and the pore size decreases slightly with increasing resin content; therefore, as the resin content increases, the retention performance of the geotextile will be enhanced as demonstrated by lower HCR values.

TEST PROGRAM AND CONDITIONS

The laboratory test program was conducted to quantify and evaluate the hydraulic performance of the resinated geotextile overwraps. The program consists of a series of in-plane flow tests and a series of normal flow tests.

In-plane Flow Test Series. A total of three transmissivity test series were conducted with the only variable component of the test series being the resin content of the geotextile overwrap (0%, 3% and 5%). Falling head test procedures were utilized in accordance with the American Society for Testing and Materials (ASTM) test method D 4716. The boundary conditions used for the series are described below:

- a drainage core with a double-sided cuspated structure was used;
- a low-permeability compacted soil mixture of 10% bentonite and 90% Ottawa 20/30 sand (a uniform clean sand originating in Ottawa, Illinois which passes the 0.85 mm sieve (U.S. standard sieve No. 20) and is retained on the 0.60 mm sieve (U.S. standard sieve No. 30)) surrounded the geocomposite to ensure that water will flow within the drainage space of the geocomposite and to distribute pressure on the geotextile filter in a way that simulates field conditions;
- normal stresses of 10, 24, and 48 kPa (200, 500, and 1000 psf) were applied to observe the relationship between normal stress and in-plane flow reduction;
- tap water was used as the permeant; and
- hydraulic gradients ranging from 0.05 to 0.15 were used.

Normal Flow Test Series. The purpose of performing the HCR test series was to quantify the transient and stable flow rate across the soil/geotextile boundary at a prescribed hydraulic gradient and effective stress. Stable flow occurs when the measured hydraulic conductivity of the soil/geotextile boundary, $k_{s/g}$, reaches a constant value signalling the development of a filter network. This filter network may be a transitional filter zone (Lawson, 1982) adjacent the geotextile within the soil, or a vault network formation (Rollin and Lombard, 1988) at the soil/geotextile boundary. The constant $k_{s/g}$ value could also be indicative of clogging or blinding (Abouzakhm, 1986) of the geotextile. If a constant $k_{s/g}$ value is not reached, an unstable flow condition exists. This is characterized by either continuous soil loss occurring through the geotextile, or the progressive clogging of the geotextile. Trends of stable and unstable conditions are addressed by Gallup (1990).

A total of nine HCR tests were performed using the 1.5%, 3%, and 5% resinated geotextiles adjacent to three soil mixtures. HCR tests in this study were conducted using triaxial permeability equipment and falling head test procedures. Both the equipment and test procedures are described by Abouzakhm (1986) and Williams and

Abouzakhm (1989). The test configuration consists of a geotextile placed adjacent to a compacted soil mixture. Note that, in these tests, drainage core effects are not considered. Water is permeated through the soil/geotextile system until a stable condition occurs. Sample preparation and testing conditions are summarized as follows:

- the following three soil mixtures (by percent dry weight) of nonplastic silt and Ottawa sand were used:
  - 100% Ottawa sand (100% sand is used as a base test),
  - 95% Ottawa sand/5% silt, and
  - 90% Ottawa sand/10% silt;
- an effective confining stress of 69 kPa (1440 psf) was applied to the test configuration;
- de-aired, deionized water was used as the permeant; and
- hydraulic gradients in the range of 1 to 3 were used.

IN-PLANE FLOW TEST RESULTS

Results of the in-plane flow tests are shown in Figure 4 where the in-plane flow is plotted as a function of hydraulic gradient. The following observations and explanations are noted:

- At 0% resin content no effect of normal stress is apparent. The in-plane flow is low when compared to the quantity of flow through the geocomposites with 3% and 5% resin content. It is believed that the geotextile has intruded into the geocomposite core upon application of the lowest normal stress.
- At 3% resin content the effect of normal stress is characterized by a consistent decrease of in-plane flow with increase of normal stress. The quantity of in-plane flow through the composite with 3% resin content is greater than that of the composite with 0% resin content. The addition of resin apparently decreases geotextile intrusion thereby increasing flow through the composite and the amount of intrusion is dependent upon the magnitude of applied normal stress as measured by the reduction of in-plane flow.
- At 5% resin content, no consistent effect of normal stress is apparent. The quantity of in-plane flow is greater than that observed for the other two composites. It is believed that the 5% resin content minimized the geotextile intrusion so that the geotextile was stiff enough to resist deformation under the applied normal stresses.

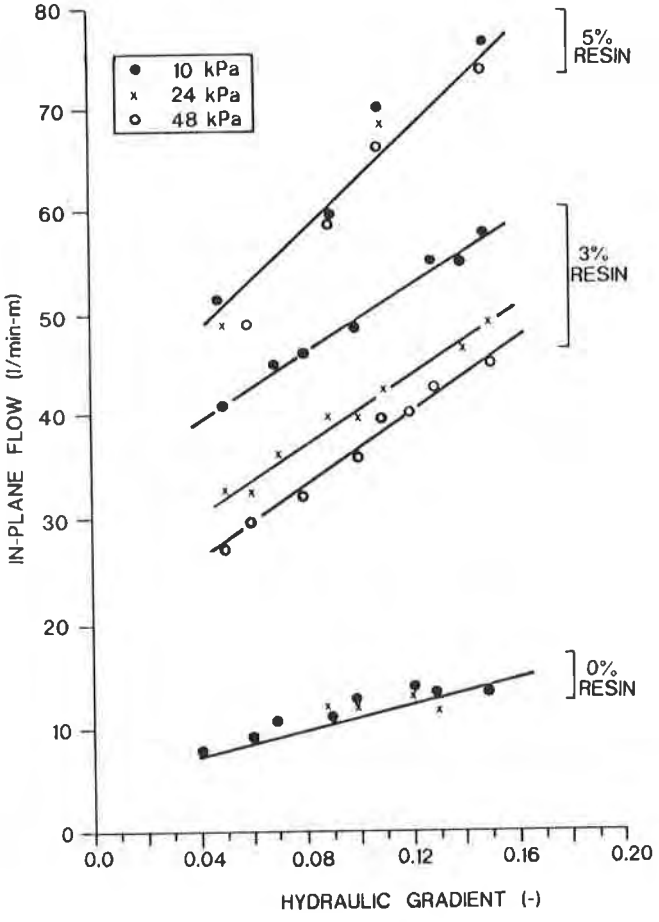

Figure 4. In-plane Flow Results

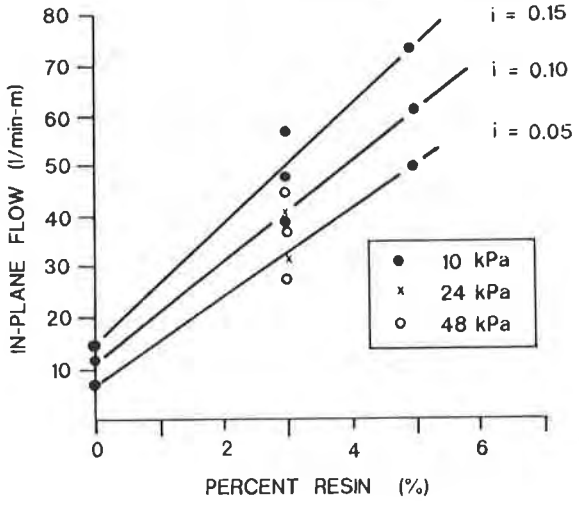

Figure 5. Relationship between Resin Content and In-plane Flow

The results show a consistent increase of geocomposite in-plane flow with increasing resin content of the geotextile overwrap. A summary graph of the relationship between in-plane flow and resin content is shown in Figure 5 for hydraulic gradients, i, of 0.05, 0.10, and 0.15.

NORMAL FLOW TEST RESULTS

The development of a stable flow condition during the HCR test for the three boundary soils is most effectively shown by the hydraulic conductivity versus pore volume curve illustrated in Figure 6. (One pore volume is defined as the volume of voids in the soil sample.) For the tests in this study, the average hydraulic conductivity measured during the passing of the first two pore volumes is assumed to be the "initial" hydraulic conductivity of the soil, k_s. Thereafter, the measured hydraulic conductivity is assumed to be that of the soil/geotextile filter network, $k_{s/g}$. Comments and observations pertinent to each of the three tests are included in the following paragraphs.

100% Sand Results. The following observations resulted from examination of Figure 6a:

- all three geotextiles show a stable $k_{s/g}$ value; and
- all three geotextiles showed a stable $k_{s/g}$ from the start of $k_{s/g}$ measurement.

The 100% Ottawa sand apparently does not contain particles which are likely to dislodge and move under these flow conditions. Therefore, each geotextile performed similarly.

5% Silt/95% Sand Results. The following observations result from examination of Figure 6b:

- all three geotextiles show a stable $k_{s/g}$;
- there was a slight difference in $k_{s/g}$ for the three geotextiles; and
- permeation of several pore volumes was required to reach a stable $k_{s/g}$.

This soil mixture contains small particles which apparently move at these hydraulic gradients. These particles continue to migrate until the $k_{s/g}$ decreases to a point where the particles are not transported at the resulting seepage velocity.

10% Silt/90% Sand Result. The following observations result from examination of Figure 6c:

- all three geotextiles show a stable $k_{s/g}$; and
- the $k_{s/g}$ for the 5% resinated geotextile was lower than the $k_{s/g}$ for the 1.5% and 3% resinated geotextiles.

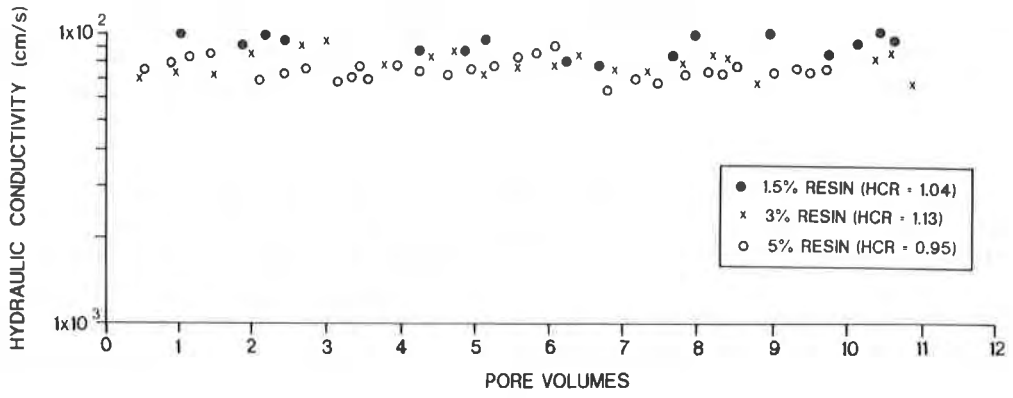

(a) 100% sand

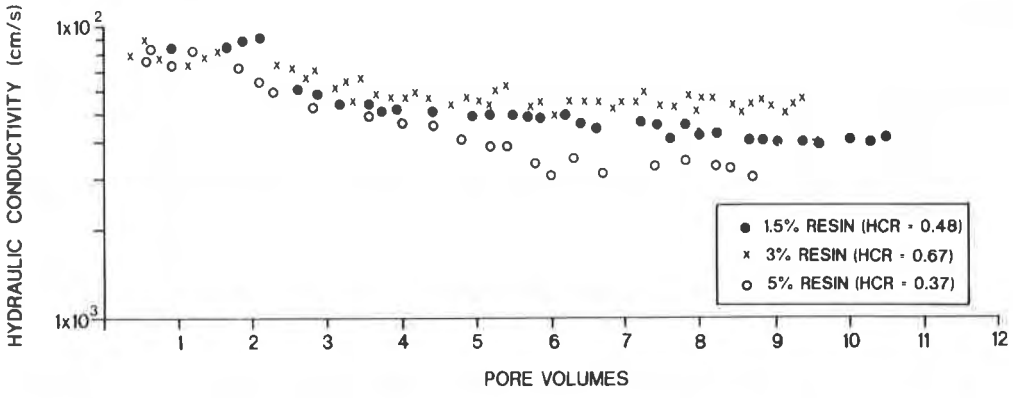

(b) 5% silt/95% sand

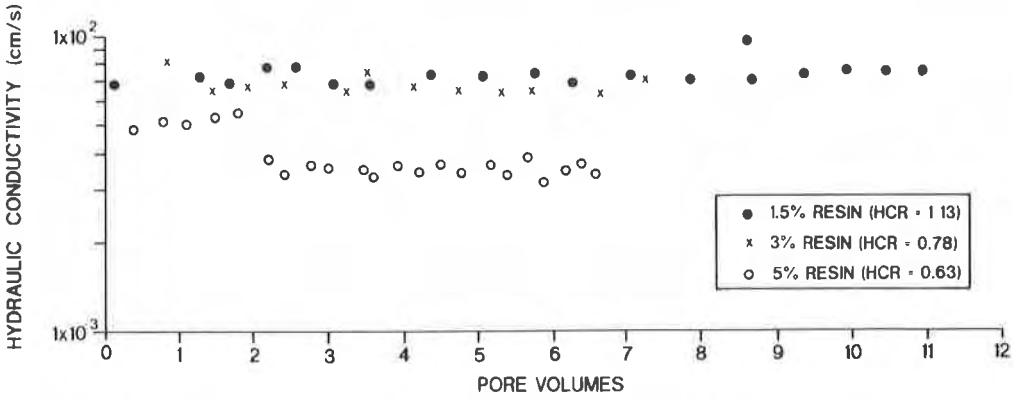

(c) 10% silt/90% sand

Figure 6. HCR Test Results

Like the previous soil mixture, this mixture contains small particles which move as a result of these hydraulic gradients. These particles continue to migrate until the $k_{s/g}$ decreases to a point where the particles are not transported at the resulting seepage velocity. The comparably smaller $k_{s/g}$ for the 5% resinated geotextile may be due to the smaller pore sizes caused by the increased resin content.

Discussion. It appears that the 5% resin in the geotextile affects silt migration. The HCR results for this geotextile were consistently lower than values from the geotextiles with 1.5% and 3% resin content. This relative comparison indicates that, with the increase of resin content, the internal pore structure of the geotextile is altered enough to increase retention performance of the geotextile. For all tests, however, a stable flow condition did develop.

CONCLUSIONS

Conclusions pertaining to the index properties of the resinated geotextiles include the following:

- geotextile grab strength and stiffness increased with an increase in resin content; and
- the pore size of the geotextile decreases slightly with an increase in resin content.

Conclusions pertaining to the hydraulic performance of resinated geotextiles include:

- an increase in resin content of the geotextile overwrap significantly increases in-plane flow through a geocomposite; and
- under similar soil conditions adjacent to the geotextile, the increase of resin content slightly increases the retention performance of the geotextile, resulting in a reduction of HCR values.

Overall, the hydraulic trends hypothesized on the basis of the geotextile property data were verified through laboratory testing. There may be an optimal resin content which provides enhanced hydraulic performance without significantly affecting the flow characteristics in the direction normal to the geotextile. Through laboratory testing of specific soil mixtures in this study, the addition of 3% resin to the needlepunched nonwoven polyester geotextile seemed an adequate amount for improving the tensile performance of the overwrap, while not greatly influencing the retention performance within the range of normal stresses used in the test program.

ACKNOWLEDGEMENTS

The testing program summarized in this paper was conducted at the Georgia Institute of Technology by R. Anne Gallup, E.I.T., under the direction of Neil D.

Williams, Ph.D., P.E. and Robert C. Bachus, Ph.D. All geosynthetic materials were provided by Mr. David E. Beck of Contech Construction Products. Financial Support of Contech Construction Products is acknowledged and appreciated. Special thanks goes to J.P. Giroud, Ph.D. of GeoSyntec Consultants for review of this paper.

REFERENCES

Abouzakhm, M.A., "*Permittivity of Geotextile/Soil Compositions*", A Special Research Problem Presented to the Faculty of the School of Civil Engineering at the Georgia Institute of Technology, Sep, 1986, 147 p.

Gallup, R.A. "*Factors Affecting the Performance of Geosynthetic Drainage Composites*", A Special Research Problem Presented to the Faculty of the School of Civil Engineering at the Georgia Institute of Technology, in partial fulfillment of the requirements for the Master of Science in Civil Engineering, Mar, 1990.

Lawson, C. R., "Filter Criteria for Geotextiles: Relevance and Use", *Journal of the Geotechnical Engineering Division*, American Society of Civil Engineers, Vol. 108, No. GT 10, Oct. 1982, pp. 1300-1317.

Luettich, S.M. and Williams, N.D., "Design of Vertical Wall Drains Using the Hydraulic Conductivity Ratio Test Method", *Proceedings Geosynthetics '89*, Vol. 1, San Diego, California, USA, 1989.

Prapharan, S., Holtz, R.D., and Luna, J.D., "Pore Size Distribution of Nonwoven Geotextiles", *Geotechnical Testing Journal*, ASTM, Vol. 12, No. 4, Dec, 1989, pp. 261-268.

Rollin, A. L., and Lombard, G. "Mechanisms Affecting Long-Term Filtration Behavior of Geotextiles", *Geotextiles and Geomembranes*, Vol. 7, Nos. 1 and 2, Elseiver Applied Science, 1988, pp. 119-145.

Williams, N.D. and Abouzakhm, M.A., "Evaluation of Geotextile/Soil Filtration Using the Hydraulic Conductivity Ratio Analysis", *Geotextiles and Geomembranes*, Vol. 8, 1989, pp. 1-26.

The Effect of Repeated Traffic Loading on Geosynthetic Reinforcement Anchorage Resistance.

M. Nimmesgern
FMPA (Otto-Graf-Institut), Germany
David Bush
Netlon Limited, UK

ABSTRACT

Reinforced soil structures supporting highways and railways carry permanent loads of self weight and transient surcharge loading due to traffic. These transient surcharges cause simultaneous increases of vertical stress on the reinforcement and horizontal stress to be resisted by the geosynthetic. Some concern was expressed that the continued application of transient surcharges from the traffic could cause progressive pullout of reinforcement from the anchorage zone.

A new dynamic pullout test has been devised to replicate these in-situ conditions. Results of the first testing is reported.

INTRODUCTION

In reinforced soil structures supporting roads and railways, the geosynthetic reinforcement will be subjected to the dead loads of the structure combined with repeated short duration live loads of the traffic. These transient loads cause a simultaneous increase of vertical stress on the reinforcement and horizontal stress to be resisted by the geosynthetic. Some concern was expressed by approval authorities that the continued application of transient loads due to traffic could cause progressive pullout of reinforcement from the anchorage zone, particularly in cases of lower overburden pressures.

A new dynamic pullout test has been developed to reproduce these in-situ conditions. A geosynthetic reinforcement (type Tensar SR80) was placed in a rounded granular fill in a pullout box with an area 1 m x 2 m. A vertical stress, equivalent to the overburden, was applied to the surface of the pullout box whilst at the same time the consequent horizontal anchorage tension was applied to the reinforcement. Horizontal and vertical dynamic loads equivalent to traffic induced loading, were applied simultaneously with a frequency of 5 Hz which is the normal frequency of loads applied through road pavements and mid-range frequency loading on railway track beds.

TEST CONDITIONS

The usual method for the calculation of reinforced soil design is based - for the internal stability - on the assumption of plane one- or two-part wedge mechanisms for limit equilibrium analysis. The assumed slip surfaces go through the reinforced soil and subdivide it into two parts: an active and a retaining part. This is shown on an example for a reinforced railway embankment in Figure 1. The geosynthetics, which are cut by the slip

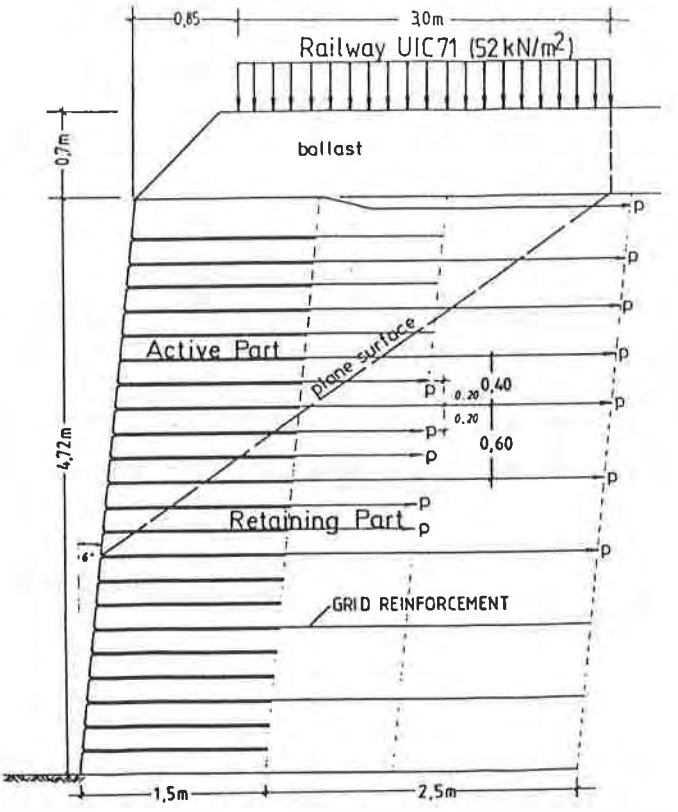

Fig.1 Example : Reinforced Railway Embankment

surface, try to hold the slipping parts in position using their tensile forces. These forces are firstly the tensile strength of the reinforcing material used and secondly the pullout-resistance in the backfill material. The pullout-resistance of each layer is obtained using the following equation.

$$P \leq 2 \cdot b \cdot l_i \cdot \gamma \cdot h_i \cdot \mu \qquad (1)$$

2	the factor 2 is needed because there are two faces
b	the width of the reinforcement in m/m
l_i	the length behind the slip surface in the layer i in m
γh_i	the weight of overburden in the layer i in kN/m
μ	a factor of friction ($\mu = \alpha \cdot \tan \varnothing_R$ where α is the coefficient of interaction)

This equation is only valid for static conditions. The example shown in Figure 1 has in addition to the static overburden a dynamic loading, which is - especially in the upper layers - relatively high. In order to investigate the nature and effect of this dynamic load, tests were carried out in the pullout box. The main detrimental effect expected is that due to the vibration a vertical motion of the grains will reduce the bond between soil and grid and a progressive pullout-failure will take place.

For the test a pullout box was used with the following dimensions:

length	2 m
width	1 m
height	1 m

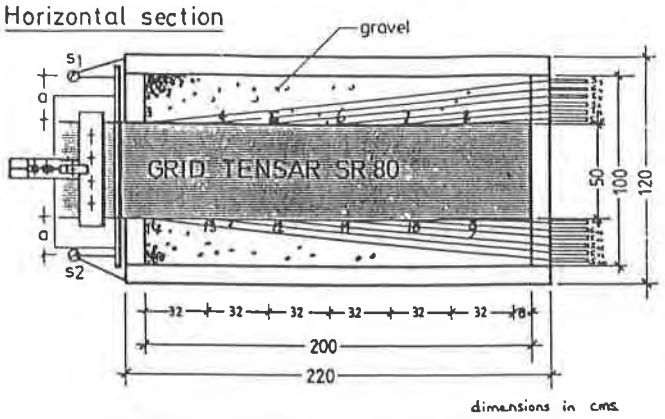

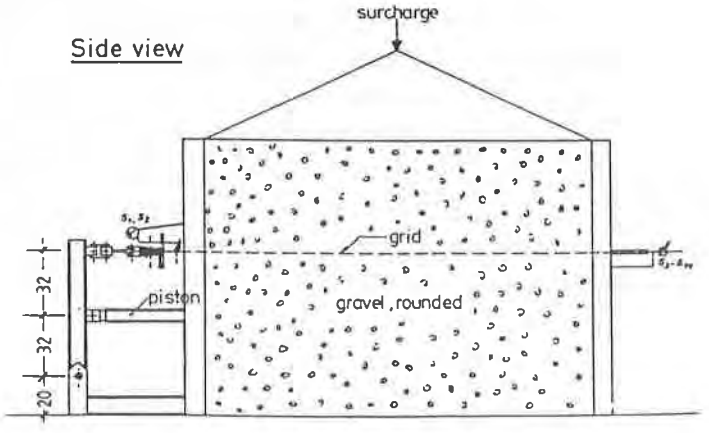

Fig.2 Pullout box

The box was split at mid-height. The lower half was filled, the reinforcement placed and the slack taken up. Extension measuring devices were fixed to the reinforcement before filling was completed. Figure 2 shows a section through the box. The soil material used for the test was a well graded sandy gravel typical of fills used in reinforced soil structures. The maximum grain size was 30 mm and particle size distribution is shown in Figure 3. Uniformity coefficient of the fill was 28.

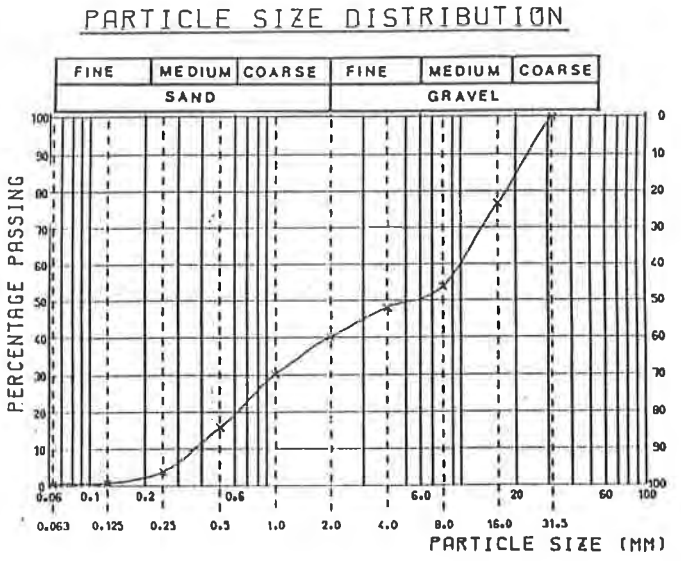

Fig.3 Particle size distribution

The deformation of the grid and the settlement of the overburden were measured using dial gauges. Two gauges were used to measure deformation in front of the box. To measure the deformation of the grid inside the box sheathed piano wires were connected to six positions on the grid inside the box and run to the rear of the box where deformation was measured by six pairs of dial gauges.

The pullout box had previously been used for static pullout tests and it was necessary to modify it and provide hydraulic loading for the dynamic pullout horizontal and vertical forces. The forces were applied using hydraulic cylinders. The required oil pressure was provided by a two-channel hydraulic pump, controlled by servo-valves. The reaction frames for the overburden force and the horizontal tensile force were very different and therefore the synchronising of the two hydraulic pistons was difficult. The sinusoidal-signal with 5 H_Z for the servo-valves was provided by wave generator with one channel for the vertical loading and one for the horizontal tensile force on the grid. The loads resulting from both cylinders were checked using load transducers and an oscilloscope as shown in Figure 4.

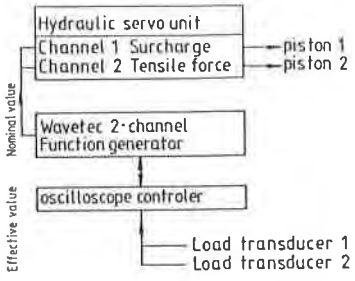

Fig.4 Steering components

LOAD CONFIGURATION

The static overburden was chosen as equivalent to the weight of 3 m of soil with γ = 19 kN/m^3, which is a surcharge of 57 kN/m^2. This static load was superposed by dynamic load of 10 kN/m^2 over the 2 square metre box. The tensile force per metre width of the reinforcement was determined from the equilibrium conditions and was calculated as a static load of 25 kN/m and a dynamic load of 4 kN/m. The loading regime represented typical conditions in the upper part of a structure in which the potential loss of anchorage is more likely to occur.

This loading pattern was applied until the deformations of the grid ceased to increase. The first loading pattern (Test 1) was applied for a total of 9.5 hours (171,000 cycles). In the second test the tensile horizontal force was increased to a static value of 36 kN/m and a superposed dynamic load of 4 kN/m was applied (Test 2) to try to initiate a pullout failure. This test pattern was run for 9 hours (162,000 cycles). The loading patterns for the two tests are shown in Figure 5.

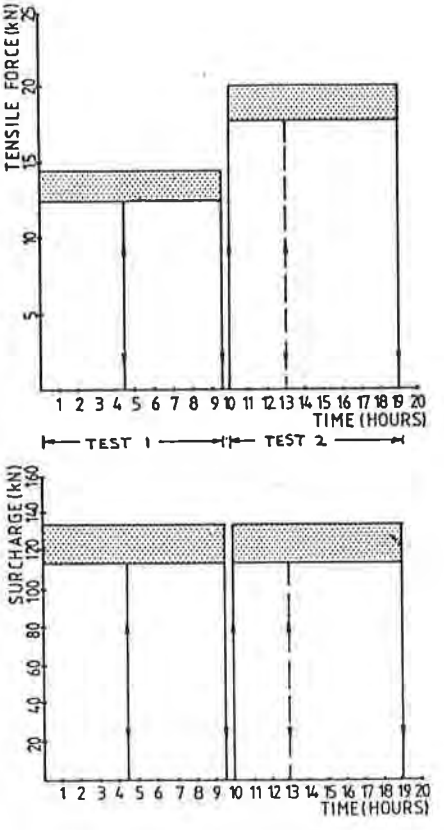

FIG.5 LOAD CONFIGURATION

TEST RESULTS

The results show that the potential pullout failure did not occur. During the first minutes of the test the deformations of the grid in front of box $(S_1 + S_2)/2$ increased relatively rapidly. Then the rate of deformation slowed down and reached a quasi constant value. After 4.5 hours (81,000 cycles) the test was stopped for the night and recontinued next morning. The same constant value of deformation was reached after about 3 hours (135,000 cycles total). Because the deformations remained sensibly constant for a further period of 2 hours the test was stopped after a total time of 9.5 hours (171,000 cycles). In Figure 6 the dependence of the deformation with time (cycles of load) is shown. It is necessary to take into consideration, that the distance between the measuring gauge and the soil in the front of the box was 130 mm. In this distance the grid was deformed elastically in free air without contact with soil to reach an elongation of almost 3%. The deformation of the embedded grid obtained from the wire extensometers are also shown in Figure 6. The distance between the individual extensometer measuring points was 320 mm.

FIG.6 Grid Deformation over Time (Test 1)

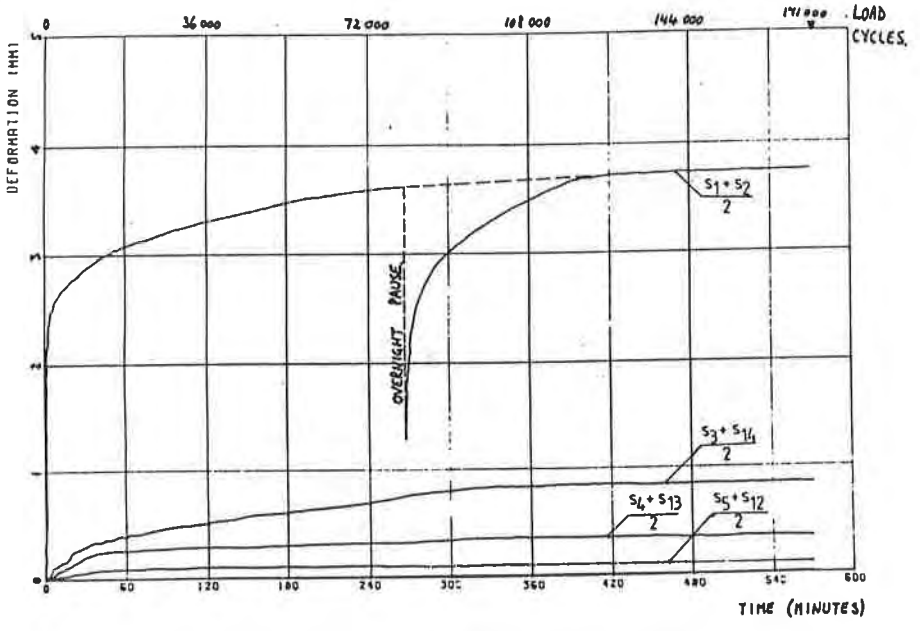

It is clear that deformation of the restrained grid within the soil is much less than the unrestrained grid in air. The deformation of the grid in soil diminishes rapidly and is not measurable on the final three pairs of instruments. Elongation between the first pair of measuring instruments (S3 and S14) and second from the front of the box (S4 and S13) is calculated at 0.15%. Between the second and third this has reduced to 0.08% and between the third and fourth is 0.03%.

The vertical settlement of the upper load plate during the first hours of the test is shown in Figure 7. After reaching an average settlement of 0.97 mm at the front and 1.07 mm at the rear of the plate within the first hour (18,000 cycles) of the test there was no additional measurable settlement during the remaining part of the test. Mean vertical compression was 0.1%.

Fig.7 Settlements

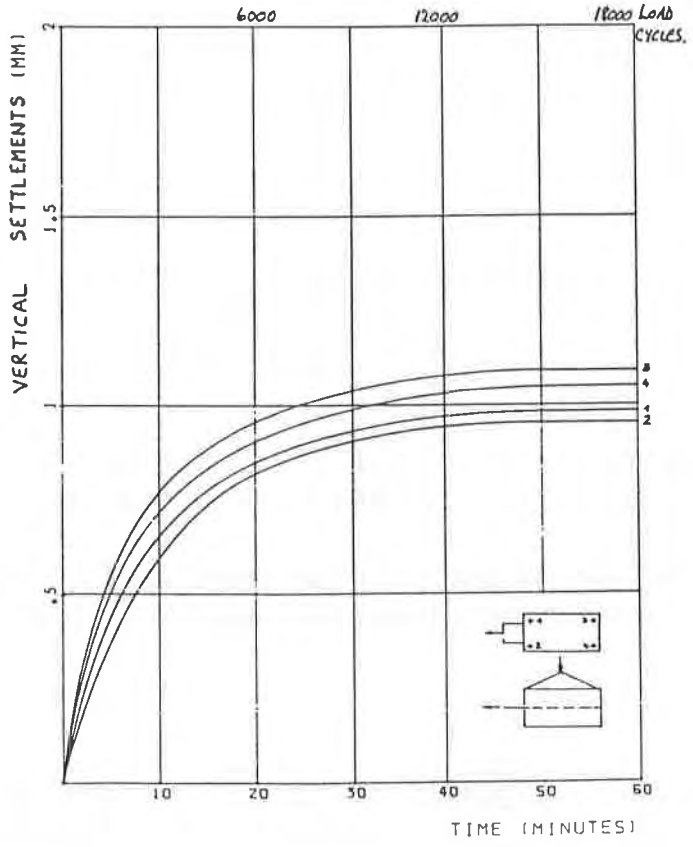

The same instrumented sample of grid was used in test 2 which was started with the same vertical loading as in test 1 but with an increased horizontal static tensile force of 36 kN/m and the same dynamic loading of 4 kN/m, superposed. The behaviour of the embedded grid (Figure 8) was similar to that of the first test. The deformations aspired asymptotically to sensibly constant value. In this test the in-air elongation reached 7.3 %. This was reduced to 1.26% elongation between the first and second embedded measuring points decaying to 0.10% between second and third and to 0.075% between third and fourth.

Once again there was no movement at the final three measuring points. Also with this higher static tensile force there was no pullout behaviour as was originally feared during the 9 hours (162,000 cycles) of the test.

It is evident in both test, that the deformation of the grid decreased rapidly within the first two ribs/transverse bars embedded in the soil. All pullout elongation was taken up

FIG.8 Grid Deformation over Time (Test 2)

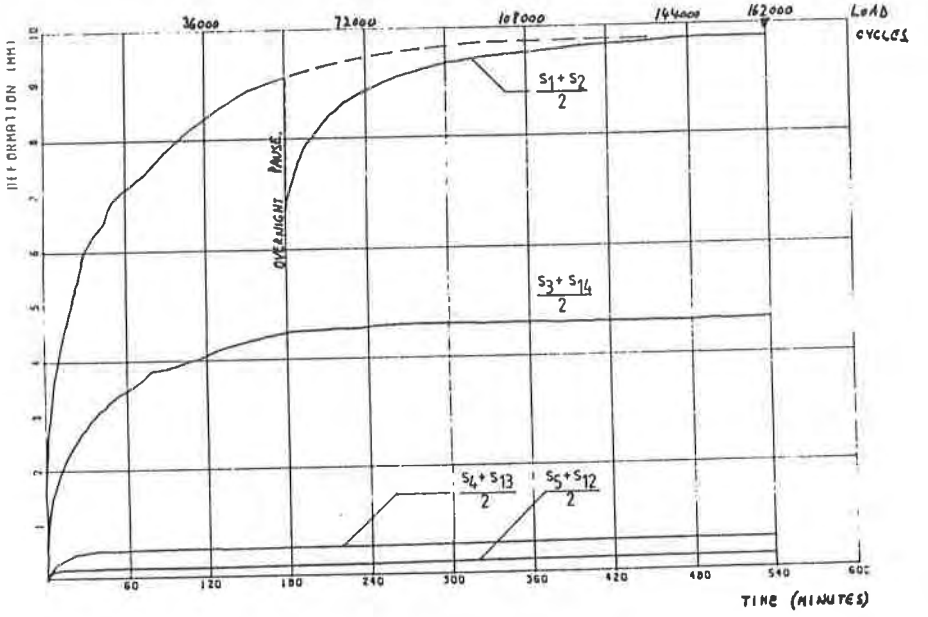

within the first metre of embedded length. This is a result of the high modulus grid with full strength integral junctions interlocking with the fill to prevent pullout.

At the end of the two tests the grid was inspected for damage. The grid was in good condition and all ribs and junctions were intact after 333,000 applications of cycled pullout and dynamic loading.

CONCLUSIONS

In order to study the pullout behaviour of a geogrid under dynamic loading conditions dynamic pullout tests were carried out in a large (1 m x 2 m in plan) pullout box. The overburden load was relatively small in order to simulate the upper layers of a reinforced soil structure. Two tests with different horizontal tensile forces were carried out. In addition to the static forces (pullout force and overburden load) a dynamic loading with a frequency of 5 Hz was superposed. The results of these two tests show that the dynamic load causes a small additional compaction of the backfill 0.1%. The feared behaviour that a vertical motion of the grains would reduce the anchorage capacity the grid did not occur. The grid reinforcement in-soil elongations were around 1% close to the box face and fell to one tenth of this value half a metre into the pullout box. The two tests were carried out for a total of about 333,000 load cycles. In each test the grid progressively anchored the dynamic loads full anchorage was provided over a one metre embedded length. In future, further tests should be carried out with higher loads, other reinforcement materials and backfill soils.

ACKNOWLEDGEMENTS

The research was carried out at FMPA (Otto-Graf-Institut) Stuttgart, Germany and funded by Netlon Limited, UK.

TRANSPORTATION APPLICATIONS

Geogrid Reinforcement and Stabilization of a Highway Subgrade

Terry L. Yarger
Montana Department of Highways, USA
Francis E. Harrison, Jr.
Tensar Earth Technologies, USA
Earle William Mayberry
Tensar Earth Technologies, USA

ABSTRACT

This paper presents a case history of a project where a biaxial geogrid was utilized to reinforce and stabilize a granular fill section, which served as a subgrade for a highway pavement. The site was located in a river flood plain, with existing soils consisting primarily of an organic silt, relatively low in shear strength, variable in moisture content, and subject to frost action.

The conventional solution to this situation is described, consisting basically of excavation of several feet of the objectionable material, and replacement with granular fill. The geogrid alternative is presented, where the reinforcing effect of the geogrid improves the load distribution characteristics of the granular fill, allowing a reduction in both the excavation quantity, as well as the quantity of granular fill. This alternative included the use of a non-woven, needle punched geotextile, which served as a filter. Design or analysis methods for both the conventional and geogrid alternatives are presented. Considerations relative to the performance of both are discussed, and comparative cost data are provided.

Additional background information or documentation provided and discussed includes: plans and cross sections, generic specifications and justification, description of construction procedures, photographs, and key participants.

INTRODUCTION AND SCOPE OF PROJECT

The project site is located on Spring Hill Road near Bozeman, Montana. This project was undertaken by the Montana Highway Department, and involved a reconstruction and partial realignment of Spring Hill Road. The reconstruction was undertaken due to poor existing pavement conditions on the road, which were judged to be a safety threat, as well as disruptive to the function of the highway. The poor performance of the existing pavement structure had been attributed to the soft, compressible soil conditions present on site (refer to following section describing site conditions). Measures taken to remedy the questionable foundation conditions present are described herein.

SITE DESCRIPTION

The subject site is located in the Gallatin River Flood Plain three miles west of the town of Bozeman, Montana. Although western Montana is generally thought of as a mountainous region, the vicinity of this site along the Gallatin River Flood Plain is relatively flat . Localized areas with shallow ground water are common.

Soil deposits generally present in the area consist predominately of silty and clayey soils with varying degrees or amounts of organics. Shear strengths of these alluvial deposits are generally low, particularly where relatively high moisture contents exist. Standard penetration Test N-valves varying from 1 to 25 were recorded, with the lower valves predominant. In addition, frost action is a significant concern, due to the silty nature of the soils, and the presence of moisture.

Precipitation in the immediate area is not unusually high, being on the order of 18 inches per year. However, very moist conditions are common in the spring, normally due to spring thaw, high water levels in lakes and rivers, and seasonal high precipitation levels. Ground water has been measured from 1.5 to 5 feet below the surface,

depending on the season of the year. Consequently, soft subgrade conditions are often seasonal as opposed to permanent.

Unfortunately, the tight schedule and fast response required by this project did not permit extensive collection and tabulation of data. Consequently, information was gathered from a variety of sources, and only limited data was actually collected for this project.

DESIGN ALTERNATIVES

For the Spring Hill Project, a geogrid reinforced subgrade improvement was undertaken, in lieu of a more conventional undercutting and replacement of the existing unstable subgrade or a grade raise. All alternatives are described in following sections.

Conventional Approach. The conventional approach to the problem previously described at Spring Hill Road consisted of over excavation below pavement subgrade level approximately 36 inches. The excavated material would then be replaced with 36 inches of an AASHTO designation A-1-b imported fill. This thickness of over excavation and replacement was determined largely from experience of the highway department on projects with similar conditions, as well as their observations of existing pavement conditions on Spring Hill Road. The thickness may also be verified using a Boussinesq analysis as shown below.

Assumptions:

Wheel Load - P = 12,000 lbs.
Tire Pressure - p = 120 p.s. i.
Subgrade Strength (assume undrained shear) - c_u = 1.5 p.s.i.

Note: c_u = 1.5 is quite low but probably reasonable with excessive spring moisture.

The allowable bearing capacity (q_u) of the existing subgrade is given by Terzaghi's bearing capacity relationship for cohesive soils:

$$q_u = N_c c_u \text{ (Equation 1)}$$

Where $N_c = 3.1$ for soft soils subject to local shear. Substituting,

$$q_u = (3.1)\ (1.5) = 4.65 \text{ p.s.i.}$$

The required thickness of fill necessary to prevent a bearing capacity failure is then given by Boussinesq's stress distribution relationship:

$$Z = R/[\{1/(1 - q/P)^{0.67}\}]^{0.5} \qquad \text{(Equation 2)}$$

Where R is the radius of tire contact pressure, and is given by:

$$R = (P/P\pi)^{0.5} \qquad \text{(Equation 3).}$$

Substituting:

$$R = \left(\frac{12.000}{120 \times 3.14}\right)^{0.5} = 5.6 \text{ inches}$$

$$Zu = 5.6/[\{1/(1 - \frac{4.65}{120})^{0.67}\} - 1]^{0.5}$$

$$Zu = 34.2 \text{ inches (use 36 inches)}$$

A grade raise was also considered in this alternative, rather than undercutting and replacement. However, the grade raise required to install this section would have resulted in excessive right-of-way requirements, due to the flat side slopes required.

Geogrid Reinforced Alternative. A geogrid reinforced alternative to the conventional approach described above was then proposed. With this alternative, the geogrid is utilized to reinforce the A-1-b material, improving its load distribution characteristics. Thus, less over excavation and less granular fill were required.

The calculations for determining the depth of over excavation and thickness of reinforced A-1-b material are shown below, and may be summarized as shown on figure 1. (Refer to previous section for assumption)

The allowable bearing capacity of a material in a reinforced condition is given by:

$$q_r = (6.2)\ (1.5) = 9.3 \text{ p.s.i.}$$

The required thickness of reinforced fill is then given by equation 2 using a reinforced bearing capacity of 9.3 psi:

$$Z = 5.6 /[\{1/(1 - \frac{9.3}{120}\ 0.67\} - 1]\ 0.5$$

$$Z_r = 23.8 \text{ inches}$$

As can be seen above approximately 24 inches of A-1-b material should have been adequate to reduce the applied stress to the existing subgrade material to an acceptable level. However, 30" was chosen as the design section, for the following reasons:

1. 30 inches of A-1-b reinforced with geogrid would have better load distribution characteristics and the original section; consequently, performance would likely be enhanced.

2. The reduction in excavation and import material of 6 inches was judged to be more than enough to offset the cost of the geogrid, thereby the geogrid alternative was less expensive than the conventional alternative, even if somewhat over designed.

3. The silty soils on site (predominately AASHTO classifications A-4, and A-2-4) are probably subject to frost action. In addition the borrow A-1-b material may also be subject to frost action. In light of this possibility, the better load distribution at the 30" alternative was desirable. Also, the ability of the reinforced fill material to better support loads over the localized soft spots that can develop due to thawing ice lenses in the spring was a significant added benefit.

Due to the frost concerns described above, a relatively light weight (4 oz .)

needle punch non-woven filter fabric was selected to be placed beneath the grid. The purpose of the geotextile was to serve as a filter to prevent contamination of the A-1-b material from fine material in the subgrade below, particularly during the spring thaw.

Other Alternatives. The possibility of using a single layer of relatively high strength geotextile as both reinforcement and a filter/separator was also considered. While high strength geotextiles have the capacity to act in a reinforcing mode similar to that described above, it was not considered for this application for the following reasons.

1. The relatively low initial secant modulus of most fabrics requires that fairly significant deflection take place prior to mobilizing reinforcement tension. This is generally not desirable with a paved surface road, and in this instance this was particularly undesirable because of the likelyhood of significantly reduced subgrade strength during the spring months of the year. A significant strength loss in the spring followed by severe deflections necessary to mobilize additional reinforcement tension could possibly lead to a pavement surface failure.

2. Due to the light weight and relatively high flexural rigidity of the geogrid, it was believed that installation would be simpler, particularly over very soft or unstable ground.

3. The relatively high flexural rigidity of the geogrid, as well as the better confining effect which it produces within the A-1-b material, was expected to enhance compaction, allow higher densitys to be achieved in the borrow material, with fewer passes of the compaction equipment and less likelihood of over stressing the subgrade.

COSTS

Unit costs for the project were estimated as follows:
$5.00 per ton ($9.00 dollars per cubic yard) for the borrow A-1-b material,
$5.00 per cubic yard for excavation of unstable or unsuitable subgrade material,
$1.50 per square yard for the geogrid in place.

Based on these unit costs, it was estimated that the 6 inch reduction of excavation and import material thickness, would result in a cost savings of $2.25 per square yard for the State. With an in place geogrid cost of $1.50 per square yard, the net savings realized by the highway dept. was approximately $0.75 per square yard, even though the geogrid reinforced alternative was anticipated to give superior performance. Based on a total project size of approximately 50,000 square yards, the total value of savings to the State was therefore approximately $40,000.00.

GEOSYNTHETIC SELECTION

Basis for Selection. In order to accomplish the intended effect, based on the design described above, it was recognized that a biaxial geogrid with a high tensile modulus,relatively high junction strength or efficiency, and high flexural rigidity should be specified.

High tensile modulus was judged to be important as it was desired to achieve the reinforcing effect with a minimal amount of vertical displacement. A reinforcing element with a low initial secant modulus would lead to much greater vertical deflection being necessary to mobilize the reinforcing effect of the reinforcing member. Also, it was believed that a higher initial secant modulus, and the minimal deflections associated with this property, would enhance compaction of the select material over the geogrid.

High junction strength was judged to be important to provide positive confinement of the material being reinforced, thus providing for enhanced load distribution characteristics. It was believed that a high junction efficiency geogrid, in excess of 90%, would assure good load transfer across the junctions of the geogrid, from the longitudinal to the transverse members. Without high junction efficiency, only a relatively small degree of confinement would be achieved due to friction along the longitudinal and transverse elements of the geogrid. In addition, relatively high junction strength and efficiency was believed to introduce less risk of construction damage, especially when high ground pressure compaction equipment is used. Ideally, a 100% junction efficiency would be desirable, but only about 90% can be pratically and routinely achieved.

A high flexural rigidity was specified for two reasons. The first is that the installation of a relatively stiff geogrid is easier. Laborers can walk on top of the geogrid during installation, even over very soft subgrades, without significant deflection. This

did not prove to be particularly important for this site, but at the time of specification preparation it was not known exactly how bad the subgrade would be. Also, the stiffness of the geogrid makes it much easier to install without wrinkles or slack. In addition to the ease of installation afforded by stiff geogrids, the relatively high flexural rigidity also aids in enhancing the load distribution characteristics of the reinforced material. This effect is sometimes described as the "snow shoe effect". This can be particularly important over soft to very soft subgrades.

Specifications. The specifications selected by the Montana Highway Department for the Spring Hill Project are summarized in the table below (from section 21.1 of the Special Provisions for the Project.

Specifications for the geogrid and construction methods will conform to the following:

a. The geogrid should be a polymer grid structure specifically fabricated for soils reinforcement.

b. The geogrid should be biaxial - having high tensile strength in two directions, perpendicular to one another.

Material Requirements:

The geogrid shall conform in all respects to the property (Interlock, Reinforcement, and Material) requirements listed below:

PROPERTY	TEST METHOD	UNITS	VALUE
Interlock			
-aperture size	I.D. Calipered (1)		
MD (2) (Logitudinal Rib)		in	1.00 - 2.00
CMD (3) (Transverse Rib)		in	1.00 - 2.00

PROPERTY	TEST METHOD	UNITS	VALUE
-open area	COE Method (4)	%	70 (min)
-thickness	ASTM D 1777-64		
ribs (50 mils)		in	0.03 - 0.04
junctions (160 mils)		in	0.11 (nom)

Reinforcement

-flexual rigidity	ASTM D 1388-64	mg-cm	
-MD (2)			250,000 (min)
-CMD (3)			325,000 (min)
-tensile modulus	ASTM D 638-82 (5)		
-MD (2)	(modified)	1 lb/ft	14,000(min)
-CMD (3)		1 lb/ft	19,500(min)
-junctions strength	ASTM D 638-82 (6)		
-MD (2)		%	90 (min)
-CMD (3)		%	90 (min)

Material

-polypropylene	ASTM D 4101 Group 1/Class 1/Grade 2	%	98.5(min)
-carbon black (content by weight)	ASTM 4218	%	1.0 - 1.5

NOTES:

* Nom = nominal values that shall not vary by more than +/- 15%

(1) Maximum inside dimension in each principal direction measured by calipers.

(2) MD - machine direction which is along roll length.

(3) CMD - Cross Machine direction which is across roll.

(4) Percent open area measured without magnification by Corps of Engineers method as specified in CW 02215 Civil Works Construction Guide, November 1977.

(5) Secant modulus at 2% elongation measured by tensile loading test ASTM D 638 modified to clamp single ribs of the grid structure at junctions and apply a constant rate of extension of the rib of 2 inches per minute at a temperature of

68 degrees F. No offset allowance is made in calculating secant modulus.

c. Geogrid shall be laid over the fabric.

d. Geogrid shall be oriented such that the roll length runs parallel to the road direction.

e. Geogrid sections shall be overlapped as indicated on the plans or as directed by the Engineer. Minimum overlap is 2 feet. Care shall be taken to ensure that geogrid sections do not separate at overlaps during construction. Placement of geogrid around curves will require cutting of geogrid product and diagonal overlapping to ensure that excessive buckling of grid material does not occur.

f. Granular fill material shall be placed in two lifts of 18, then 12 inches.

g. Rubber tired compaction equipment will be used over all geogrid sections. Vibratory compactors will not be allowed over geogrid/fabric sections.

h. Construction equipment shall not operate directly upon the geogrid. A minimum fill thickness of 18 inches is required prior to operation of equipment over the geogrid.

i. Granular fill material shall be back dumpled from trucks riding on tops of the reinforced fill and bladed onto geogrid in such a manner that the fill rolls onto the grid ahead. If ruts are created in the granular fill due to construction traffic, they shall be filled with dirt.

j. The contractor shall conduct his operations so as to minimize the possibility of rutting or pumping in the subexcavation section, i.e. haul thru ditch sections, use of lighter equipment and/or loads and staging operations to limit hauling through this area.

CONSTRUCTION SEQUENCE

Construction of the geogrid reinforced subgrade is indicated in figures 3 through 6 . The first step involves excavation of the necessary amount of unstable or unsuitable subgrade material. The next step involved unrolling the filter fabric and the

geogrid. These steps are indicated on figure 3. The A-1-b fill material was then placed over the geogrid and geotextile as shown in figures 4 and 5. The fill was spread in an initial lift of approximately 18 inches of thickness, followed by a second lift of approximately 12 inches. Initially, compaction was accomplished simply by earth work equipment traveling across the already placed fill lift as shown on figure 6. Note that in figure 6, deflection of the fill surface is minimal. Following installation of the stabilized subgrade, construction of the pavement structure proceeded in a conventional fashion.

CONCLUSIONS

The Spring Hill Road Project near Bozemen, Montana, as described herein is believed to be a good example of a cost effective use of biaxial geogrids in a subgrade reinforcement or stabilization application. Application of this technology to stabilization of soft or unstable subgrades should prove very economical for almost any instance, unless the granular fill used for stabilization is very inexpensive. In addition to the cost savings, other advantages are believed to be obtainable from this technology, due to the ability of the geogrid to aid and support in load distribution, even when significant strength loss in the fill can occur. The use of geogrids in this type of application is particularly applicable where it is desired that vertical surface deflections be kept to an absolute minimum.

Although this project involved reconstruction and stabilization of a low-strength subgrade, rather than reinforcement of a part of the pavement structure (such as aggregate base course or sub-base), the experience described above are believed to demonstrate to applicability and feasibility of geogrid reinforced base layers for pavement thickness designs, particularly over weak subgrades, and for projects with anticipated high aggregate costs.

ACKNOWLEDGMENTS

The authors wish to express their appreciation to the Montana Department of Highways, and to the following individuals: Bob Rask, formerly of the Montana Department of Highways, and to Dennis Dirks and Ron Daniels, of Contech Construction Products.

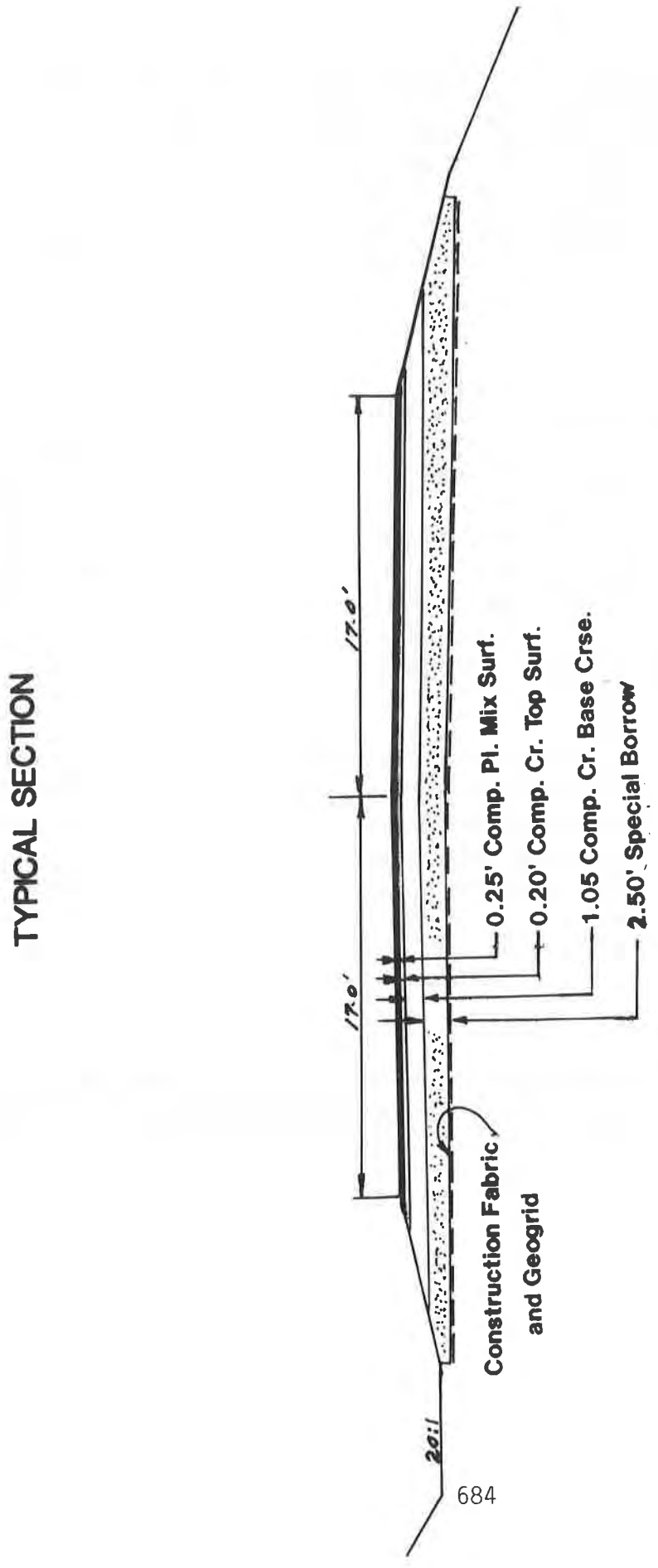

Figure 1 Geogrid Reinforced Alternative

Figure 2. Pavement conditions prior to reconstruction.

Figure 3. Excavation operations and installation of geotextile and geogrid.

Figure 4. End-dumping A-1-b borrow on geogrid.

Figure 5. Spreading A-l-b material over geogrid.

Figure 6. Initial compaction of surface A-1-b material.

Figure 7. Completed installation. Pavement surface has recently been chip-sealed.

Figures 8 & 9. Completed installation.
Note presence of water in side ditches.

REFERENCES

1. Terzaghi, K. and Peck, R. B., Soil Mechanics in Engineering Practice, John Wiley and Sons, New York, 1967.

2. Rodin, S. "Ability of a Clay Fill to Support Construction Plant," Journal of Terramechanics, 1965, Vol. 2, No.4.

3. Tensar, "Tensar Technical Note: BR5, Design Guideline for Subgrade Improvement under Dynamic Loading." The Tensar Corporation, Morrow, Georgia, 1986.

Response of a Geogrid Earth Reinforced Retaining Wall With Full Height Precast Concrete Facing

K. L. Fishman
State University of New York at Buffalo, USA
C. S. Desai
University of Arizona, USA

ABSTRACT

Results from field instrumentation of a geogrid reinforced earth retaining wall utilizing full height precast wall facing are presented and compared with back predictions from finite element analysis. In general, a reasonably good correlation of results is demonstrated but further refinements in the finite element analysis may lead to significant improvement with regard to quantitative comparison with measurements.

INTRODUCTION

A geogrid reinforced earth retaining wall utilizing full height precast concrete wall facing was instrumented in Tucson, Arizona. The purpose of the instrumentation was to study the response of the wall system and compare with design assumptions and calculations previously applied to wall systems utilizing strip reinforcements and articulated wall facing. Instruments were placed to measure geogrid strains, lateral earth pressure transferred to the wall face, strains in the reinforced wall fill, and vertical stress within the reinforced wall fill. Measurements were taken during and after wall construction.

In general, good agreement was obtained between maximum tensions in the geogrids computed with the design equations and those measured with gages attached to geogrids. However, neither the maximum tensions in the geogrids predicted with the design equation nor the maximum tensions obtained via the geogrid strain measurements were close to the safe working load for the geogrids. This seems to indicate a degree of conservatism in the design which may be attributed to uncertainty concerning the behavior of the wall system which utilized full height precast concrete wall facing. Although the data obtained from the instrumentation project provided some interesting results, further study is necessary before credibility may be assigned to conclusions drawn or increased understanding of the wall behavior leading to improved design is realized. In order to further verify observed behavior, a finite element analysis of the wall system was performed. Details of the finite element analysis and comparison between measured and computed response are presented in this paper. Recounts of the instrumentation project presented in this paper are derived from various previous publications [1,2,3,4].

DESCRIPTION OF WALL SYSTEM

The wall system serves as a grade separation for a highway project and was considered as an alternative to a conventional cantilevered retaining wall system or a reinforced earth retaining wall system utilizing steel strips as reinforcement. A schematic of the instrumented earth reinforced retaining wall is shown in Figure 1 (a) and (b). The two sections shown refer to separate wall panels which were instrumented. Instrument locations shown on these figures will be discussed later. In this paper "height" refers to the vertical elevation, and "depth" refers to the horizontal distances into the fill measured from the wall face. The instrumented wall panels had a height of 15.5 ft. (4.72 m). Wall facing consisted of 6 in. (15.24 cm) thick by 10 ft. (3.05 m) wide precast concrete panels. Geogrids were located at the elevations shown and extended to a depth of 12 ft. (3.66 m). On the top of the wall fill, a pavement structure was constructed consisting of a 4 in. (10.16 cm) base course covered by 9.5 in (24.13 cm) of Portland Cement concrete.

The specified soil reinforcement was Tensar's SR2 geogrid which is made of high density polyethylene, uniaxially oriented to obtain a high tensile strength equivalent to that of mild steel. It is reported to be resistant to chemical substances normally existing in soils. The geogrids have a maximum tensile strength of 5400 lb/ft (79 KN/,) and a secant modulus in tension at 2% elongation of 75000 lb/ft (1094 KN/m).

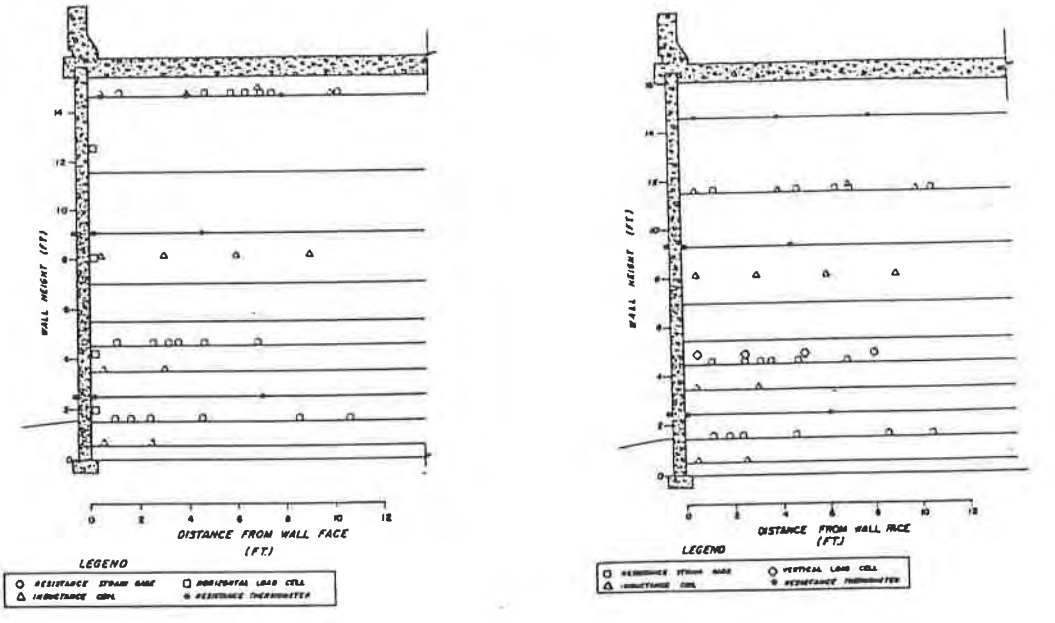

(a) Wall Panel 26-30 (b) Wall Panel 26-32

Figure 1. Schematic of Instrumented Reinforced Earth Retaining Wall

Construction Methods. Construction methods can have a major impact on the performance of the wall system. The construction procedures used on this project are discussed in detail in various reports [1,2,4]. Brief details are given below.

Full height precast concrete wall facing panels were hoisted and set vertically on a levelling pad. The panels were stabilized with struts such that initially the panels were battered inward.

As backfill proceeded, geogrids were secured to the wall face at proper elevations and then pretensioned. Fill was placed and spread onto the geogrid with a front end loader. The fill was added to the next goegrid layer and compacted. Compaction near the wall face was performed using a jumping jack, however, further from the wall face, a self propelled vibratory compacter was used. As the height of the wall increased, struts on the outside of the wall were loosened, allowing load to be transferred to the geogrids. This process was repeated for each geogrid level until the top of the all was reached.

Description of Instrumentation. The instrumentation program was designed as follows:

1) The fronts of the concrete facing panels were surveyed to record the movements of wall faces.

2) Resistance strain gages and inductance coils were fastened to geogrid reinforcement to measure the strains therein.

3) Inductance coils were placed in the reinforced wall fill to measure horizontal and vertical strains in the soil.

4) Pressure cells were installed in the reinforced wall fill to measure (a) the lateral earth pressure against the wall face, and (b) the distribution of vertical stresses along a geogrid.

5) Resistance thermometers were placed to measure the distribution of temperature within the reinforced soil mass.

Locations of instruments are shown in Figure 1 (a) and (b). All elevations refered to in this section are with respect to the base of the wall. Two adjacent wall panels were instrumented. They are denoted as wall panels 26-30 and 26-32. In general, instrument locations in the two walls were similar, so as to provide a cross check while some differences in instrument layout allowed for acquiring additional information, such as geogrid strains at different elevations or the measurement of vertical stress and lateral earth pressures against the wall facing.

Details of instrument calibration, performance and installation can be found in a Preliminary Report [1].

DESIGN EQUATIONS

The wall was designed in accordance with available reinforced soil methodology [5]. A value engineering study performed by Dames and Moore [6] provides a detailed description of the design for this particular project. Table 1 presents a summary of parameters used in the analysis. Wall fill refers to the reinforced soil material behind the wall face and back fill refers to material behind the wall fill, and to foundation material.

Table 1. Summary of Parameters Used in Analysis

Wallfill		
Internal Friction	ϕ_w	34°
Cohesion	C	0.0
Unit Weight	γ_w	125 lb/ft³ (19.6 KN/m³)
Backfill		
Internal Friction	ϕ_b	30°
Cohesion	C	0.0
Unit Weight	γ_b	115 lb/ft³ (18.0 KN/m³)
Geogrid		
Allowable Tension		1324 lb/ft (19.3 KN/m)

Considering the internal stability of a soil wall constructed with frictional fill, as was the case with the instrumented wall panels, the tensile force in the geogrid at level i, T_i, per unit width of wall is given by:

$$T_i = K_{aw}\, \sigma_{vi}\, V_i \qquad (1)$$

where V_i is the vertical spacing of the geogrids, σ_{vi}, is the maximum vertical stress at level i obtained by assuming a trapezoidal distribution of vertical stress along the length of a geogrid as described in ref. [5], and K_{aw} is the coefficient of active earth pressure for the wall fill.

Comparison between Measurements and Design Quantities. In general good agreement was obtained between maximum tensions in the geogrids computed with equation (1) and those obtained from measurements with gages attached to the grids.

Typical results from pressure cells placed to measure the distribution of vertical pressure at elevation 5.0 ft (1.53 m) are shown in Figure 2. Also shown in Figure 2 is the average vertical pressure at this elevation computed by multiplying the density with the fill height, and the assumed trapezoidal

distribution of vertical stress used in the design calculations. This figure indicates that the measured distribution of the vertical stress along the geogrid is nonlinear. The maximum vertical pressure occurs at a distance of about 60 in (152 cm) away from the wall face, with the lowest pressure measured near the wall face. Results from the instrumentation project did not yield a distribution of vertical stress consistent with design assumptions. Interaction between wall facing and wall fill may account for this, but further study is required before any conclusions may be drawn.

The design procedure assumes that no lateral earth pressure is transferred to the wall face, since all of it is transferred to geogrids as tension. Figure 3 presents results from pressure cells placed to measure lateral earth pressure against the wall face. The low pressure measured above 1/3 of the total wall height seems to approximately confirm this assumption. However, this assumption does not account for the increased lateral earth pressure near the base of the wall. When using full height panels as wall facing, restraint to displacement of the wall facing at the connection between the wall facing and the footing may inhibit load transfer between the soil and extensible reinforcement resulting in lateral earth pressure acting on the wall facing.

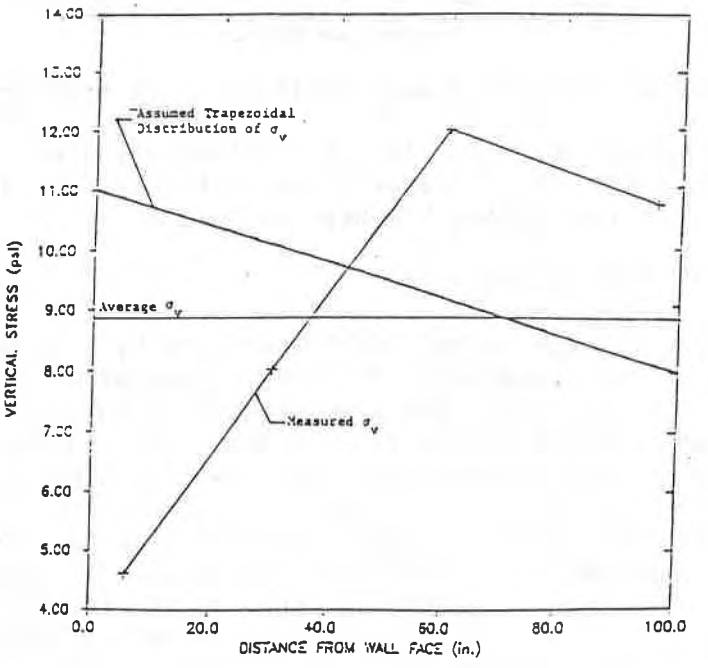

Figure 2. Measured Distribution of Vertical Stress at El = 5 ft.

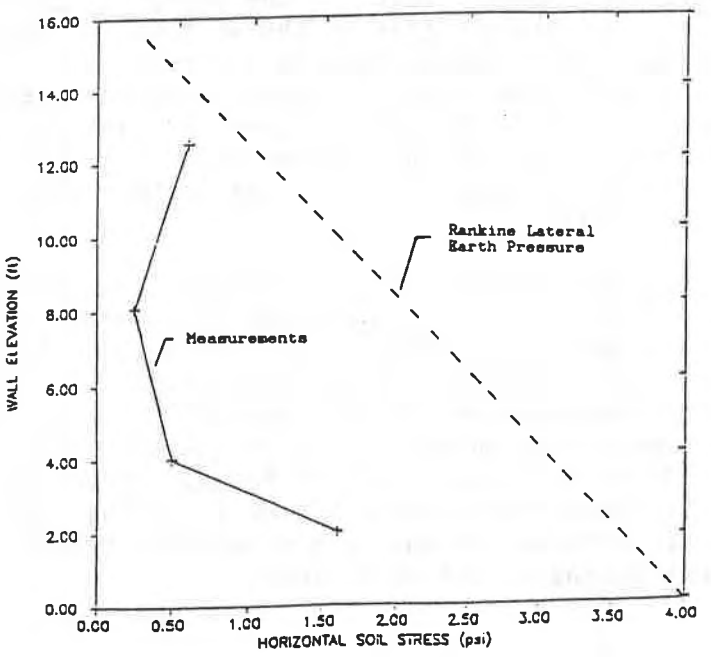

Figure 3. Measurement of Lateral Earth Pressure Near Wall Facing

Although the data obtained in the instrumentation project provided some interesting results further verification is desirable. As an alternative a finite element analysis of the wall system has been performed.

DESCRIPTION OF FINITE ELEMENT ANALYSIS

A finite element code called SSTIN developed by C.S. Desai and co-workers [7] is used in this study. Details of the finite element study presented in this paper are derived from ref. [8]. The element used is an eight node isoparametric element which is used to model the soil, geogrids, wall facing, and interfaces. All material behavior was assumed to be linearly elastic. The analysis was sensitive to including of the effect of confining pressure on Young's modulus for the soil. Young's modulus was assigned by estimating the confining pressure at each depth for the completed wall and the sequence of construction was not considered in this analysis. Material properties for the wall fill were determined from the results of triaxial tests performed on samples obtained from the site. Table 2(a) shows the variation of Young's Modulus with depth and Table 2(b) summarizes other parameters utilized in the analysis. Geogrid stiffness was determined from tension tests performed on samples obtained from the manufacturer. All testing was performed under the direction of C.S. Desai in the Constitutive Modelling Laboratory, University of Arizona.

Table 2(a). Variation of Soil Young's Modulus With Depth

Depth (ft.)	Modulus (psi)
0.0	492
5.0	2660
7.5	3716
10.0	4781
12.5	5837
15.5	7110

Table 2(b). Material Properties Utilized in Finite Element Analysis

Material	Young's Modulus (psi)	Poisson's Ratio	Unit Weight (pcf)
Soil	-----	0.3	120.
Geogrid	55555.	0.0	---
Wall Facing	3000000.	0.15	150.

Figure 4(a) depicts the mesh utilized for the analysis and Figure 4(b) is a schematic representation of salient details of the mesh. The mesh consists of 1871 nodes and 586 elements. Only the reinforced structure is represented in the mesh and the foundation material is not included. The mesh is loaded with gravity loads from the wall fill, a vertical surcharge of 152 psf (7.3 kPa) applied along the top boundary which represents the pavement structure, and by a Rankine lateral earth pressure due to the unreinforced back fill.

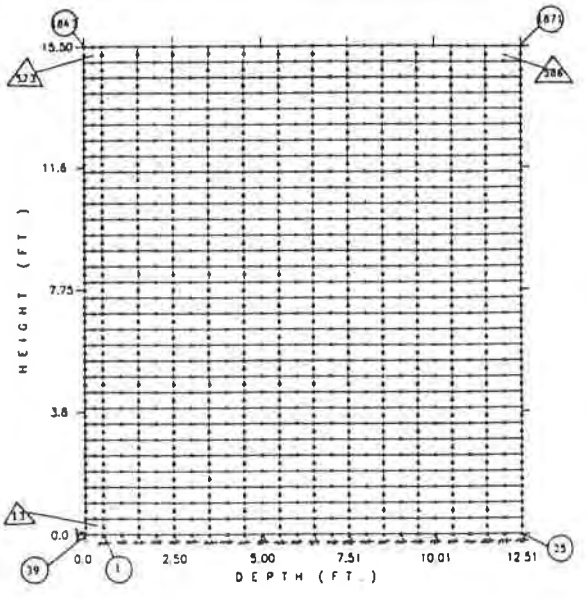

Figure 4(a). Mesh Used for Finite Element Analysis

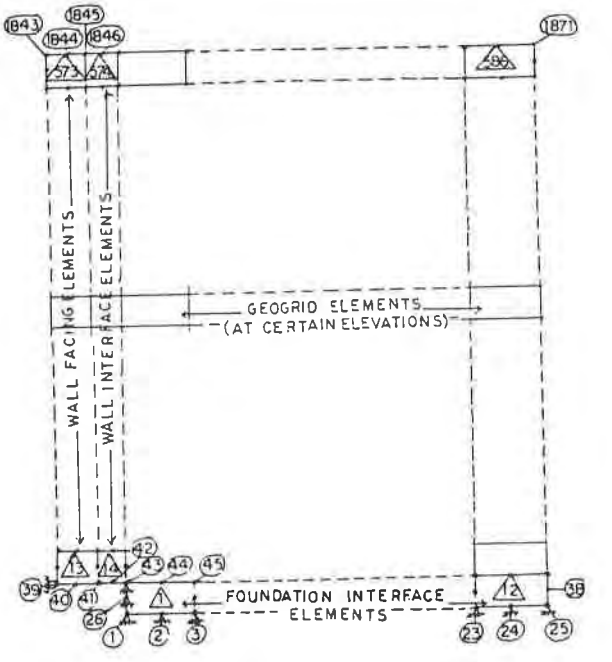

Figure 4(b). Details of Finite Element Mesh

Results from the finite element analysis are compared with observations, and are presented in Figures 5-7. Wall face movement is shown in figure 5. Both the finite element analysis and measurements demonstrate that the wall face rotates about the toe of the wall. The measured wall face movements are higher than those predicted with the finite element method by a factor of about two. This can be mainly due to the fact that the behavior of the soil is assumed to be linear.

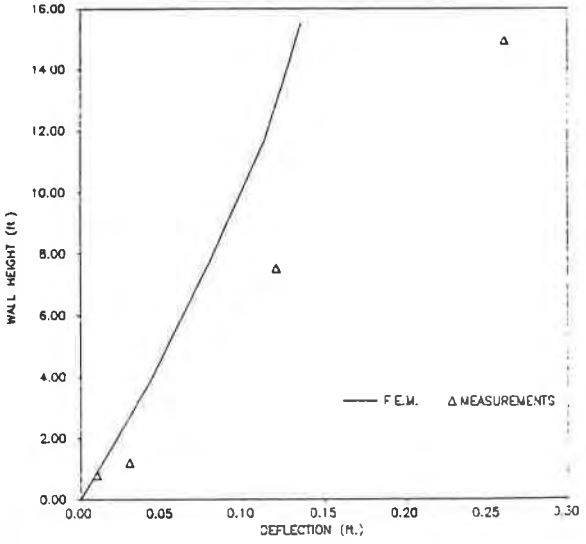

Figure 5. Comparison Between Measured and Predicted Wall Face Movements

Figure 6 (a) to (c) displays the distribution of tensile strains along geogrids at elevations of 1.5, 4.5, and 14.5 ft. (0.46, 1.37, and 4.42 m). Agreement between predicted and measured response is not always good. Excellent correlation prevails at elevation 1.5ft. (0.46 m) but, discrepancies exist at elevation 4.5 ft (1.37 m) and 14.5 ft. (4.42 m). The high inductance coil measurement recorded near the wall face at elevation 14.5 ft. (4.42 m) may be due to problems relative to response of these instruments close to the wall face.

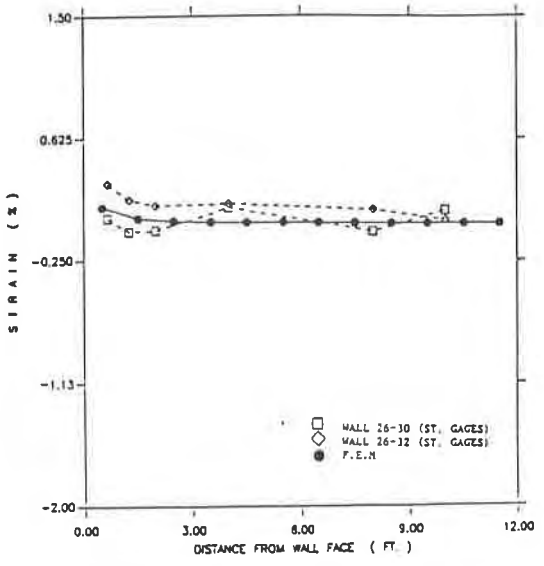

Figure 6(a). Geogrid Strain at Elev. 1.5 ft.

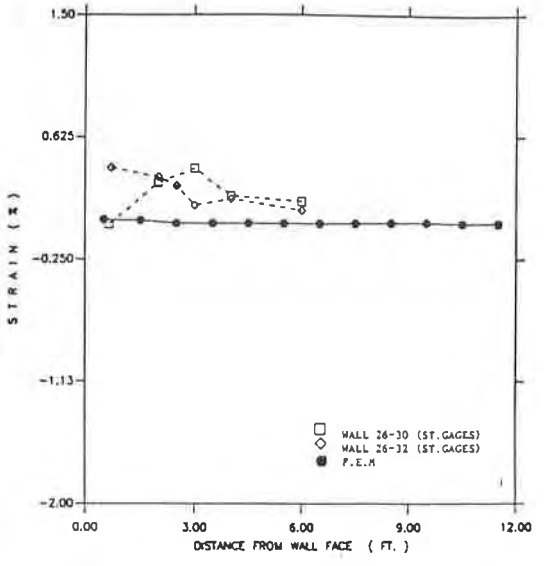

Figure 6(b). Geogrid Strain at Elev. 4.5 ft.

Figure 7 presents results in terms of horizontal stress carried by geogrids at different elevations. Horizontal stresses carried by geogrids are obtained by determination of the maximum geogrid tension and dividing by the geogrid spacing. Comparisons are made between measurements, results from finite element analysis, equation (1), and active earth pressure predicted by Rankine theory. The comparison shows that the results from finite element analysis are below measurements and predictions from equation (1) except near the base of the wall.

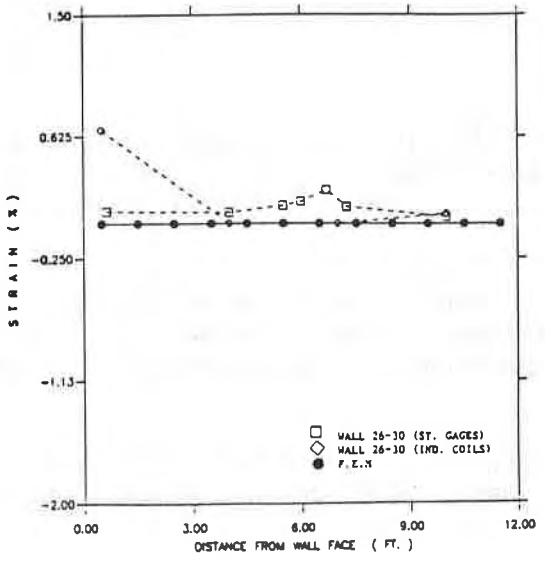

Figure 6(c). Geogrid Strain at Elev. 14.5

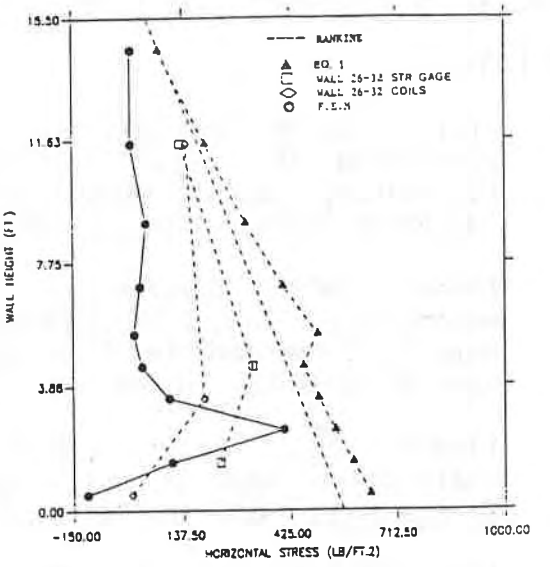

Figure 7. Lateral Stress Transferred to Geogrids

CONCLUSIONS

Good qualitative results were obtained from the finite element analysis when compared to most observations. Quantitatively, goegrid strains computed using the finite element analysis were smaller than measurements. In general, promising results were obtained from this preliminary study, but further refinements in the finite element analysis may lead to significant improvement with regard to quantitative comparisons with measurements. Refinements to the analysis should include consideration of the construction sequences, nonlinear soil behavior, and for interfaces between soil used for wall fill and geogrids.

ACKNOWLEDGEMENTS

The research study was conducted for Pima County Department of Transportation and Flood Control District (PCDT & FCD) on two reinforced retaining walls at the Tanque Verde/Wrightstown/Pantano Project in Tuscon, Arizona. The walls were built by M.M. Sundt Construction Company. Funding for the research study was provided by the Federal Highway Administration (FHWA) and the Tensar Corporation. The instrumentation project was originally conceived by Barry Berkovitz who was a staff engineer for PCDOT & FCD and is now with FHWA. Administration was conducted by the project manager Ali I. Fermawi of PCDOT & FCD. The research study was contracted with Desert Earth Engineering with active

participation of personnel from the Civil Engineering and Engineering Mechanics (CEEM) Department at the University of Arizona in Tucson, Arizona. Calibration and testing of the instruments were performed in the Constitutive Modeling Laboratory, CEEM Department. Those technical aspects including calibration of instruments, planning of instrumentation, interpretation and analysis of field data, laboratory testing for soil behavior and development of the finite element procedure and code were performed with active participation, guidance and direction of Professor C.S. Desai.

REFERENCES

1. Desert Earth Engineering, (1986) "Tensar earth-reinforcement wall monitoring at Tanque Verde-Wrightstown-Pantano Roads, Tuscon, AZ," Preliminary Report, submitted to Pima County Department of Transportation and Flood Control District, Tucson, AZ.

2. Desert Earth Engineering, (1987) "Tensar earth-reinforcement wall monitoring at Tanque Verde-Wrightstown-Pantano Roads, Tuscon, AZ," Final Report, submitted to Pima County Department of Transportation and Flood Control District, Tucson, AZ.

3. Fishman, K.L., Desai, C.S., and Sogge, R.L., "Field behavior of instrumented geogrid soil reinforced wall," ASCE Journal of Geotechnical Engineering, submitted March 1990.

4. FHWA, "Tensar geogrid reinforced soil wall," Experimental Project 1, Ground modification Techniques, U.S. Dept. of Transportation. Federal Highway Administration, FHWA-EP-90-001-005, January 1989.

5. Netlon Limited, (1984), "Guidelines for the Design and Construction of Reinforced Walls Using Tensar Geogrids," Netlon Limited, Kelly Street, Blackburn, BB2 4PS, England.

6. Dames and Moore, (1984) "Tensar SR2 reinforced retaining walls for Tanque Verde Road, Tuscon Arizona," Value Engineering Study. Job No. 13780-002-22, Submited to Pima County Department of Transportation and Flood Control District, Tucson, AZ.

7. Desai, C.S. and Lightner, J.G., (1979) "Improved numerical procedures for soil-structure interaction including simulation of construction," Report #VPI-E-7932, Virginia Polytech, Blacksberg, VA.

8. Harahap, A., "A study of earth reinforced retaining walls; Design, case histories and numerical analysis," Master's Project Report, submitted to the Dept. of Civil Engineering, State University of New York at Buffalo, Buffalo, NY, January 1990.

Geotextiles For Subgrade Stabilization in Permanent Roads and Highways

Barry R. Christopher
Polyfelt, Inc., USA
Robert D.Holtz
University of Washington, USA

ABSTRACT

A rational procedure for the design of permanent roads using geotextiles to reduce stabilization aggregate and overexcavation requirements is presented. The procedure is based on common geotechnical engineering principles and pavement design. Use of the methodology is demonstrated through a case history.

INTRODUCTION

One of the important uses of geotextiles is in the stabilization of soft subgrades for construction of both temporary and permanent roads. While design procedures are well established for geotextiles in temporary or unpaved roads (e.g. Barenberg, et al., 1975; Giroud and Noiray, 1981; Stewart, et al., 1977), design guidance for permanent roads is virtually nonexistent. Although geotextiles have been used successfully in numerous permanent roadway projects, very few papers on the subject have been published. Perhaps this is because geotextile design for permanent road appears to be based on intuitive judgement, or sometimes haul road design procedures are used, but without proper consideration of their impact on the entire pavement system. Both of these approaches have led to failures, and Christopher and Holtz (1985) describe two such cases. One failure occurred because the selected geotextile had insufficient strength; the other took place when construction equipment on a wet clayey silt subgrade caused the subgrade to pump. The geotextile was not sufficiently permeable to allow excess pore pressures to dissipate, and the subgrade never did stabilize properly. Hoffman and Shamon (1984) also report some premature failures of geotextiles in special test sections that were attributed to construction and traffic damage of the geotextile.

As a part of the preparation of some geotextile design guidelines for the Federal Highway Administration (Christopher and Holtz, 1989), procedures were developed for use of geotextiles in subgrade stabilization for permanent roadways. As the FHWA report is not readily available literature, this paper presents this procedure along with a review of principles upon which the design methodology is based. A case history in which the design methodology was successfully used will also be described.

PRINCIPLE OF USING GEOTEXTILES IN ROADWAYS

After the pioneering experiments by McGown and Ozelton (1973), it is well established that soft unstable roadway subgrades can be effectively stabilized by using a combination of geotextiles and aggregate. Sufficient aggregate thickness is required to reduce the stress from the anticipated traffic loading at the elevation of the subgrade such that the subgrade will support these loads. The geotextile in turn prevents penetration of the aggregate into the weak subgrade and conversely intrusion of the subgrade into the aggregate, thus maintaining the design aggregate thickness. This "separation" function alone allows for a reduction in aggregate, since without the geotextile additional "sacrificial" aggregate would have been require to maintain the same design thickness. In fact, a common practice in the design of permanent roads has been to empirically include additional aggregate in the design section to cover the assumed aggregate loss. Several roadway design methods include this additional subbase in the design requirements (Yoder and Witczak, 1975). Figure 1 shows the range of typical aggregate thickness loss as a function of subgrade strength assumed by many state highway engineers (FHWA, 1989). As shown in the figure, this loss can be substantial, sometimes in excess of 100%.

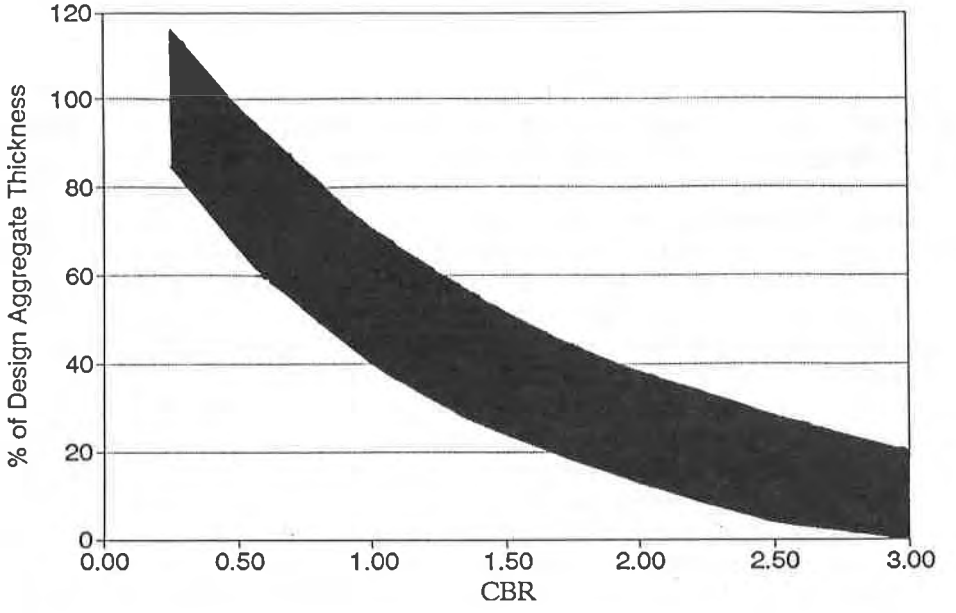

Figure 1. Aggregate loss to weak Subgrades (FHWA, 1989)

Subgrade stabilization problems most often occur at sites with fine-grained soils (silts and clays) with a high water content and some sensitivity to remolding. Usually the subgrade is weak and saturated due to a high ground water table. Therefore, equally as important as separation, a properly selected geotextile can improve drainage of the subgrade providing a means for dissipating excess pore water pressures which can buildup in the underlying soil during and after construction. Adequate drainage helps to maintain or may even increase the strength of the subgrade with time.

A secondary function of the geotextile in roadways is reinforcement. The geotextile provides a tensile component at the base of the aggregate which acts to restrain the aggregate. This "reinforcing" function provides two benefits. By resisting shear at the base of the aggregate, the geotextile decreases the shear stress that would have been transferred to the subgrade. By providing additional confinement due to lateral restraint at the base of the aggregate, the modulus of the aggregate is increased, which can also reduce the stresses transmitted to the subgrade. Haliburton, Lawmaster, and King (1980) and Gourc, Perrier and Riondy (1983) verified the lateral restraint concept and suggested that the reinforcement increases the resistance of the aggregate to "local failure" beneath the loaded area.

There is also a potential for the geotextile reinforcement to act as a membrane in tension and directly support the wheel load. However, membrane tension will only occur if the wheel loads rut the subgrade, a situation not ordinarily permissible in a permanent roadways. Giroud, Ah-Line and Bonaparte (1984) have shown that unless the rut depth is at least 0.1 to 0.15 m, the membrane effect is negligible (see also Holtz and Sivakugan, 1987).

BENEFITS OF GEOTEXTILES IN PERMANENT ROADS AND HIGHWAYS

At the present time, there is no method to quantitatively access the benefits of a geotextile to the structural support capacity of a pavement system. However, qualitatively the use of geotextiles to stabilize soft subgrades of permanent roads leads to several possible cost and performance benefits, including:

1. Reducing the intensity of stress on the subgrade and preventing the subbase aggregate from penetrating into the subgrade.

2. Preventing subgrade fines from pumping into the subbase.

3. Preventing contamination of the subbase (item 2) allows more open-graded aggregate to be considered in the design, further enhancing drainage of the pavement system.

4. Reducing the depth of excavation required for removal of unsuitable subgrade materials.

5. Reducing the aggregate thickness required to stabilize the subgrade.

6. Providing for less subgrade disturbance during construction, which results in a more competent subgrade.
7. Maintaining the integrity and uniformity of the pavement should settlement of the subgrade occur. (The geotextile does not prevent settlement of the subgrade, but their use can result in more uniform settlement (e.g. Boutrup and Holtz, 1983).)

8. Aid in reducing differential settlement in transition areas from cut to fill.

9. There is also a potential to use geotextiles as a "capillary break" to reduce frost heave (Henry, 1988) or to stop soil salts from being carried upwards where they could damage a concrete pavement.

The end result of using appropriately selected geotextiles can be a better designed roadway with reduced maintenance and potentially an extended life of the roadway system. In justifying the use of geotextiles, dollar values could be assigned to each of these potential savings, both in the initial construction cost and in the long term operation of the roadway system.

DESIGN APPROACH

Basically, the design of any roadway involves a study of the components of the system, including the pavement, aggregate base courses and subgrade. Consideration must be given to their behavior under load and their ability when placed in the roadway section to carry that load under various climatic and environmental conditions. All roadway systems, whether permanent or temporary, derive their support from the underlying subgrade. Thus, the geotextile functions are similar for either temporary or permanent roadway applications. However, due to different performance requirements, there is an essential philosophical difference in the design approach. The main difference in performance relates to rutting which is allowed to occur during the design life of a temporary road without impairing service and the obvious desire to have no rutting in permanent roads. Since all temporary roadway design methods which incorporate geotextiles allow some rutting (on the order of 50 to 300 mm) to occur, use of these approaches for permanent roadway design must be approached with caution. However, it is possible to incorporate temporary roadway design methods into the design of permanent roadways, with the following limiting assumptions:

1. No structural support is provided by the geotextile, and therefore no reduction is allowed in the aggregate thickness required for structural support.

2. Aggregate savings is achieved through a reduction in the required stabilization aggregate not used for structural support.

3. An evaluation of settlement and drainage requirements must also be made, the same as for a conventional design.

Discussion of Assumptions. The first two assumptions are required to limit deformation of the system. To provide improved support the geotextile must placed in tension which requires some elongation. For most geotextiles elongation sufficient to provide significant strength improvement would be excessive and result in

pavement rutting. Even with high modulus geotextiles, very little research has been presented on the dynamic response of these materials and their long term creep potential under such loads. Until such research is available it is prudent to make this conservative assumption. The third assumption simply emphasizes standard practice which cannot be ignored when a geotextile is used.

Design Method. Our design method considers the first aggregate lift to be a stabilization layer that allows normal construction equipment access to the remaining lifts. Essentially, the first lift is a haul road, which will be exposed to relatively few passes of construction equipment and which can tolerate 50 to 100 mm of rutting. A geotextile is used to reduce the lift thickness of the first lift using temporary roadway design methods. Once the first lift is complete, the remaining construction can proceed normally.

The design consists of the following steps:

1. Estimate the need for a geotextile based on the subgrade strength (e.g. CBR < 3) and by past performance in similar types of soils.

2. Design the roadway for structural support using your normal permanent roadway pavement design methods (i.e. AASHTO, CBR, R-value, etc.) with no allowance for the geotextile.

3. Determine if additional stabilization subbase over that required for structural support has is required due to susceptibility of the subgrade soils to pumping and aggregate intrusion. If so, reduce the stabilization aggregate by 50% and include a geotextile in the design at the subbase subgrade interface.

4. Determine the additional subbase required for stabilization of the subgrade during construction activities. Using any well established geotextile supported temporary haul road procedure such as Stewart, et al. (1977), Giroud and Noiray (1981), etc. Use a 75 mm rutting criteria for construction equipment. Compare the geotextile/aggregate thickness requirement with the reduced stabilization aggregate, if any, from step 3 and add the greater thickness to the structural aggregate requirement.

5. Determine the geotextile pore size (e.g. AOS) and hydraulic properties required on the basis of the gradation and permeability of the subgrade, water table conditions, and the retention, filtration and permeability requirements for the geotextile (Christopher and Holtz, 1985). These criteria will be reviewed in the next section.
6. Determine the geotextile strength requirements to survive the anticipated construction activities (also reviewed in the next section.)

DESIGN CONSIDERATIONS

For the geotextile to perform effectively in the roadway system, careful consideration must be given to the required properties.

Separation. As discussed earlier, the primary function of a geotextile in this application is separation of the aggregate and the subgrade. To prevent migration of subgrade fines, the geotextile must be capable of retaining the underlying soils. Therefore a retention criteria similar to that required for filtration and drainage applications must be specified or a well-graded base course must be used to control fines migration. Retention criteria for geotextiles are well established and usually take the form of:

$$\text{Apparent Opening Size} < B\ D_{85}$$

where, B is a coefficient generally ranging from 1 to 2 and is based on the grain size (sand versus silts and clays) and the grain size distribution (uniformity) of the subgrade. A summary of suggested B values and other existing geotextile filter criteria are reviewed by Fischer, Christopher and Holtz (1990). A B value of 1 provides a conservative first order estimate of the requirements.

As a minimum, the FHWA through Task Force 25 (a joint committee of AASHTO-AGC-ARTBA) recommends that the geotextile have an Apparent opening size (AOS) less than 0.3 mm for fine grain soils (>50% passing the No. 200 US sieve), the majority of soil types where geotextiles are used. This criteria may be relaxed to < 0.6 mm for coarser soils.

The strength required of the geotextile to provide separation is basically that required of survive construction as will be discussed later in this section.

Drainage and Filtration. The subgrade must be allowed to drain through the geotextile or in the case of poorly draining aggregate (not recommended) drainage must occur in the plane of the geotextile. Otherwise, pore pressures could build up in the subgrade either during or after construction which could further weaken the subgrade or induce pumping and weaving. Task Force 25 recommends that the geotextile be at least as permeable as the subgrade. However this assumes that little or no clogging of the geotextile will occur. Numerous studies have shown that when clogging occurs, the geotextile permeability is reduced an order of magnitude. Since the some clogging is likely under the dynamic hydraulic loading conditions that are anticipated at the geotextile soil interface, an additional factor of safety of 10 is recommended, especially for permanent structures, with a minimum value of 0.1 cm/sec recommended by many state DOTs for geotextile drainage requirements (Koerner and Wayne, 1989). For poorly draining aggregates, the in plane permeability should equal to the required through plane permeability value.

Filtration relates to the proper pore size requirements to reduce the potential for geotextile clogging. This requirement is often ignored in roadway specifications but is a very important consideration as it relates to long term performance of the roadway system. The appropriate design procedure is to relate the opening characteristics of the geotextile to the grain size of the subgrade such that the geotextile will retain the coarser fractions but will allow the finer fractions to pass instead of clogging the geotextile.

Survivability. If the geotextile does not survive construction, then it will of course not perform as intended. Therefore it must have sufficient strength to withstand the anticipated construction conditions. An analysis of geotextile strength requirements with respect to various loading conditions are presented by Giroud (1981) and related to road applications by Christopher and Holtz (1985).

The FHWA through Task Force 25 has developed guidelines for minimum geotextile requirements based on research by Koerner and Koerner (1990) as well as other geotextile experience. The requirements are outlined in Tables 1 and 2 and relate the degree of exposure based on equipment, aggregate and subgrade conditions to the strength requirements for the geotextile.

Table 1. Construction Survivability Ratings (Task Force 25, 1989)

SITE SOIL CBR AT INSTALLATION		<1		1-2		>3	
EQUIPMENT GROUND CONTACT PRESSURE	(kN/m^2) (PSI)	>350 (50)	<350 (50)	>350 (50)	<350 (50)	>350 (50)	<350 (50)
COVER THICKNESS[1] (COMPACTED) (mm)	(in.)						
100[2,3]	(4)	NR	NR	H	M	M	M
150	(6)	NR	NR	H	H	M	M
300	(12)	NR	H	M	M	M	M
450	(18)	H	M	M	M	M	M

H = HIGH
M = LOW
NR = NOT RECOMMENDED

[1] Maximum aggregate size not to exceed one half the compacted cover thickness.
[2] For low volume unpaved roads (ADT < 200 vehicles)
[3] The 100 mm minimum cover is limited to existing road bases and not intended for use in new construction.

Table 2. Physical Property Requirements[1]
(Task Force 25, 1989)

<50% GEOTEXTILE ELONGATION / >50% GEOTEXTILE ELONGATION[2,3]

SURVIVABILITY LEVEL	GRAB STRENGTH ASTM D-4632 kN (LBS)	PUNCTURE RESISTANCE ASTM D-4833 kN (LBS)	TRAPEZOID TEAR STRENGTH ASTM D-4533 kN (LBS)
HIGH	1200 / 800 (270/180)	445 / 335 (100/75)	445 / 335 (100/75)
MEDIUM	800 / 510 (180/115)	310 / 180 (70/40)	310 / 180 (70/40)

1 Values shown are minimum roll average values.
Strength values are in the weaker principle direction.
2 Elongation as determined by ASTM D-4632.
3 The values of geotextile elongation do not imply the allowable consolidation properties properties of the subgrade soil. These must be determined by a separate investigation.

We recommend that high survivability geotextiles be used where construction equipment and field conditions cannot be carefully controlled. Moderate strength geotextiles should only be considered when the engineer can monitor field activities or in less critical applications.

DESIGN EXAMPLE

A permanent roadway project that was designed and constructed in 1983 will be used to demonstrate the design methodology. A new public street and service drive was to be constructed leading in to a townhouse community located in an East coast state. The anticipated traffic conditions were estimated at 1,500 vehicles per day for each lane. An investigation indicated surficial soils consisting of predominantly micacious silts with an in situ CBR value of 2 and localized areas of very poor soils (CBR of 0.5). The area was low and poorly drained, and existing roads in the area had poor maintenance records.

The standard design for these conditions under the local highway code consisted of 350 mm (14 in.) of subbase aggregate, 200 mm (8 in.) of base aggregate and 64 mm (2.5 in.) of bituminous concrete as shown in Figure 2 as alternative 1. The relatively thick subbase was required for subgrade stabilization. Based on the poor performance of other roads in this area, it was felt that even with the significant amount of stabilization aggregate, longterm maintenance would still be a problem due to subgrade intrusion. Therefore, an alternative design using a geotextile was proposed.

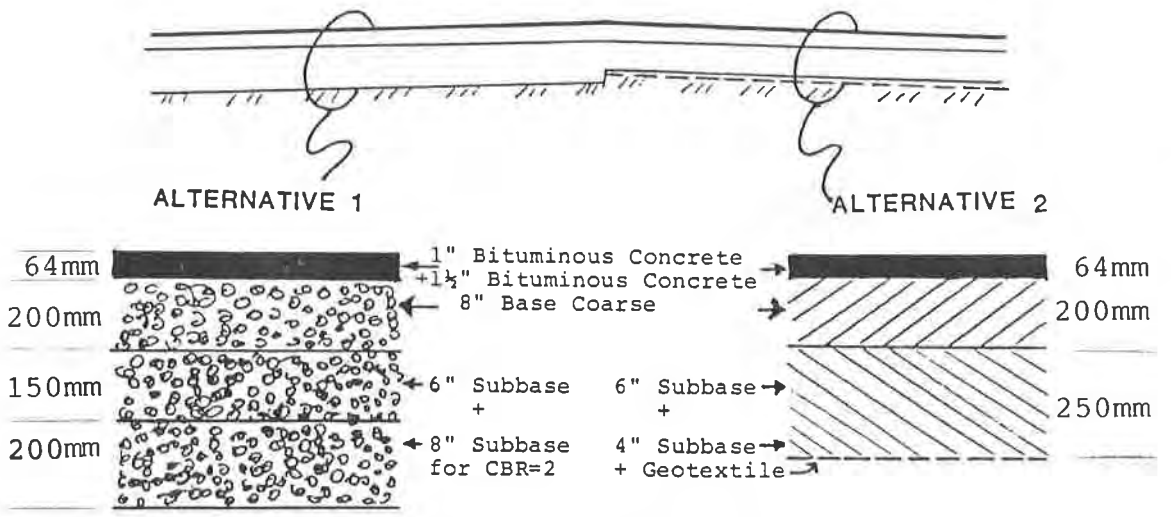

Figure 2. Design Example: Proposed Pavement Design for a Roadway near Washington, D.C. (Christopher and Holtz, 1985)

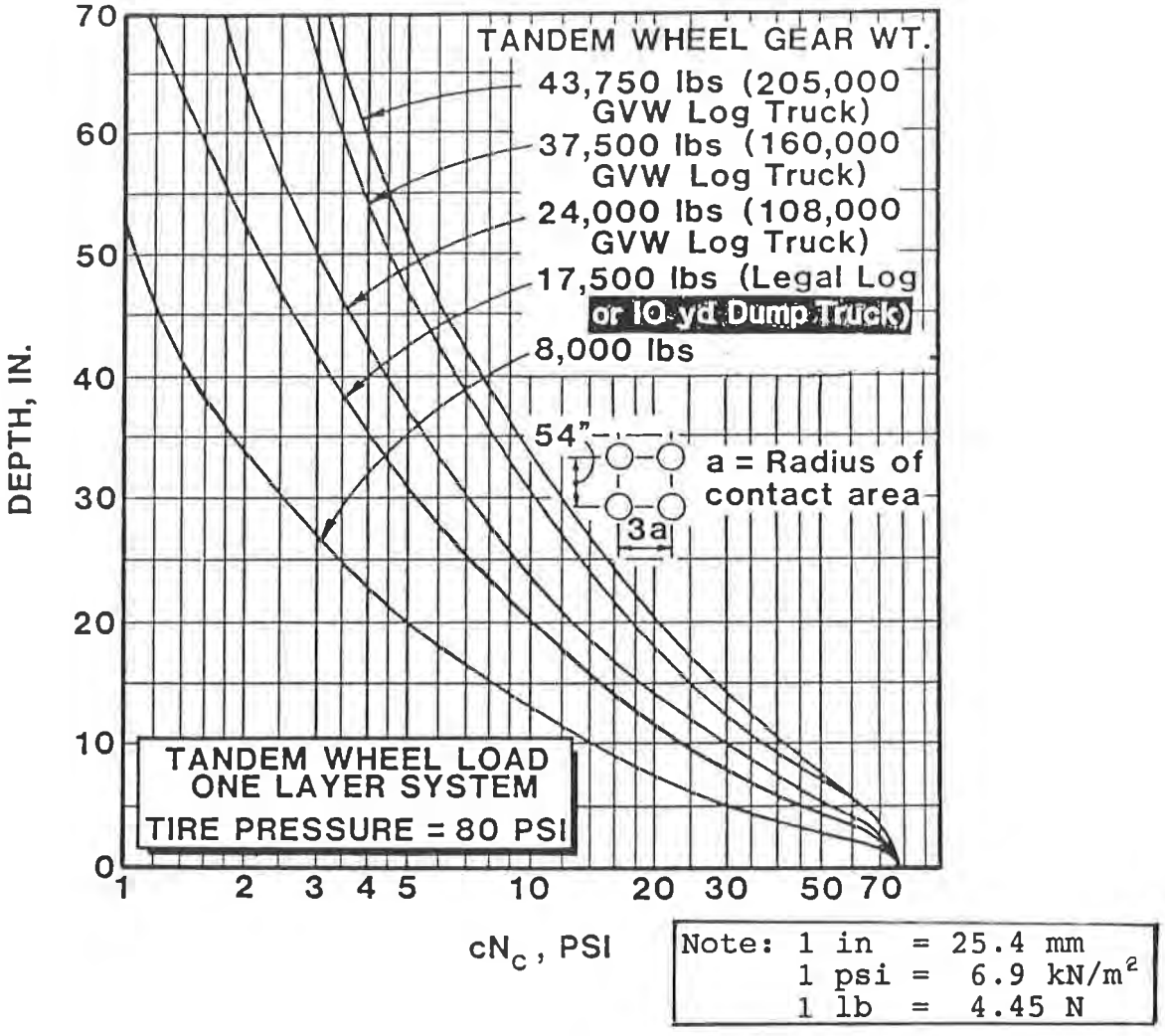

Figure 3. Typical Temporary Road Design Chart from U.S. Forest Service (Stewart, et. al., 1977)

The geotextile alternative was designed using the steps listed in the Design Approach section as follows:

Step 1. Ideal conditions for considering geotextile, e.g. low CBR, saturated subgrade, and poor performance history with conventional design.

Step 2. The structural design for the pavement section was based on AASHTO (1972) Interim Guide for Design of Pavement Structures using an equivalent design structural number for the anticipated loading and soil support conditions as follows (note AASHTO is based on English units):

Assumptions: Maximum Vehicles/Day = 3,000
95% Passenger,5% single unit,1 multiunit
Equivalent Daily 18k single-axle load (EAL) Applications = 10

Determine Structural Number $\overline{SN}$:
From AASHO (1977) Design Charts:
Given 20 years, CBR = 2, EAL = 10 and
Regional Factor = 2, therefore SN = 2.9

Thickness for Structural Support on Stable Subgrade:

Surface Base Subbase

$$\overline{SN} = a_1D_1 + a_2D_2 + a_3D_3$$
$$2.9 = 0.4(2.5") + 0.14(8") + 0.13D_3$$

D_3 = 6 in required for subbase, therefore

Structural design = 64 mm (2.5 in.) bituminous
+355 mm (14 in.) base & subbase

Step 3. Thickness of Additional Stabilization Aggregate in original design = 560mm -355mm = 205mm (8 in.), therefore, consider 200 mm (8 in.), or 100 mm (4 in.) + geotextile and compare with step 4.

Step 4. Design of Stabilization Aggregate with Geotextile

From Figure 3 (typical haul road design chart) and CBR = 2, Loaded Dump Trucks, <100 passes, and 3" ruts enter chart with 6.0 x c = 6.0 x 8 psi (for CBR = 2)

Aggregate required = 4.0 in. with geotextile

Since step 3 = step 4, use 100 mm (4 in.) additional aggregate.

Step 5. Geotextile Filtration Property Requirements

Given: Silty Soils with D85 = 0.075mm, and k_{soil} = 0.0005 cm/sec

AOS < BD_{85} and $k_{fabric} > 10\ k_{soil}$

From Christopher and Holtz (1985), B for silt type soil = 1.8

AOS < 1.8 x 0.075mm < 0.14mm

minimum k_{fabric} > 0.005 cm/sec

k_{fabric} > 0.05 cm/sec was specified due to wet conditions

Step 6. Geotextile Survivability Property Requirements

Given: CBR = 2, Loaded Dump Trucks with 550 kN/m^2 (80 psi) ground contact pressure, minimum of 200 mm (8 in.) cover,

Use: High Survivability Geotextile Property Requirements from Table 2.

The geotextile alternative shown as Alternative 2 in Figure 2, was selected and , as previously mentioned, installed in 1983. Recent inspection of the project indicated the roadway was performing as intended with no signs of distress or need of repair.

CONCLUDING REMARKS

A procedure has been developed for using geotextiles to reduce the thickness of stabilization aggregate often required for the construction of roadways on soft unstable subgrades. The procedure considers the first construction or stabilization aggregate lift to be a temporary haul road, and designs it accordingly using well established methods. It is assumed that no structural support is provided by the geotextile and thus no reduction in the thickness of the pavement section is permitted. Aggregate savings is achieved by a reduction in the thickness of the stabilization aggregate. A case history describing the successful application of the method is given in the paper.

REFERENCES

Barenberg, E.J., Dowland Jr., J.H. and Hales, J.H. (1975), "Evaluation of Soil-Aggregate Systems with Mirafi Fabric," UIL-ENG-75-2020, University of Illinois at Urbana-Champaign.

Boutrup, E. and Holtz, R.D. (1983), "Analysis of Embankments of Soft Ground Reinforced with Geotextiles," Proceedings of the Eighth European Conference on Soil Mechanics and Foundation Engineering, Helsinki, Vol. 2, pp. 469-472.

Christopher, B.R. and Holtz, R.D. (1985), "Geotextile Engineering Manual," Federal Highway Administration Report Number FHWA-TS-86/203, Washington, D.C., 1044pp.

Christopher, B.R. and Holtz, R.D. (1989), "Geotextile Design and Construction Guidelines," STS Consultants Ltd. and Geoservices, Inc. Report to Federal Highway Administration, Contract No. DTFH-86-R-00102, Washington, D.C. 300pp.

FHWA (1989), "Geotextile Design Examples," Geoservices, Inc. report to the Federal Highway Administration, Contract No. DTFH-86-R-00102 Washington, D.C.

Fischer, G.R., Christopher, B.R. and Holtz R.D. (1990), "Filter Criteria based on Pore Size Distribution" Proceedings of the Fourth International Conference on Geotextiles, Geomembranes and Related Products, The Hague, Vol. 1, pp. 289-294.

Giroud, J.P. (1981), "Designing with Geotextiles", Materiaux et Constructions, Vol. 14, No. 82, (July-August 1981), 257-272.

Giroud, J.P., Ah-Line, C. and Bonaparte, R. (1984), "Design of Unpaved Roads in Trafficked Areas with Geogrids," Proceedings of the Symposium on Polymer Grid Reinforcement, ICE, London.

Giroud, J.P. and Noiray (1981), "Design of Geotextile-Reinforced, Unpaved Roads," Journal of the Geotechnical Engineering Division, ASCE, Vol. 107, No. GT9, September, pp.1,233-1,254.

Gourc, J.P., Perrier, H, and Riondy, G. (1983) "Unsurfaced Roads on Soft Subgrades: Mechanism of Geotextile Reinforcement," Proceedings of the 8th European Conference on Soil Mechanics and Foundation Engineering, Helsinki, Vol. 2, pp.495-498.

Haliburton, T,A., Lawmaster, J.D. and King, J.K. (1980), Potential Use of Geotextile Fabric in Airfield Runway Design," Report to U.S. Air Force Office of Scientific Research, Oklahoma State University, Stillwater, 121 pp.

Henry, K (1988), "Use of Geotextiles to Mitigate Frost Heave in Soils," Proceedings of the V International Conference on Permafrost, Trondheim, pp 1096 - 1101.

Hoffman, G. and Shamon (1984), Report on Research Conducted for the Pennsylvania Department of Transportation at the Pennsylvania State University Pavement Durability Research Facility.

Holtz, R.D. and Sivakugan (1987), "Design Charts for Roads with Geotextiles," Geotextiles and Geomembranes, Vol. 5, No. 3, pp 191-199 Koerner and Koerner (1990)

Koerner, R.M. and Wayne, M.H. (1989), "Geotextile Specitications for Highway Applications," Federal Highway Administration Report Number FHWA-TS-89-026, Washington, D.C., 90 pp.

McGown, A. and Ozelton, M.W. (1973), "Fabric Membranes in Flexible Pavement Construction Over Soils of Low Bearing Strength," Civil Engineering and Public Works Review, Vol. 68, No. 798, January, pp. 25-29.

Stewart, J., Williamson, R. and Mohney, J. (1977), "Guidelines for Use of Fabrics in Construction and Maintenance of Low-Volume Roads," USDA, Forest Service, Portland, Oregon. Also published as Report No. FHWA-TS-78-205.

Yoder, E.J. and Witczak, M.W. (1975), Principles of Pavement Design, Second Ed., John Wiley & Sons, New York, 1980.

North Las Vegas: Reconstruction of Cheyenne Avenue Incorporating A High Geosynthetic Moisture Barrier

Dave Guram
Phillips Fibers Corporation, USA
Mark Marienfeld
Phillips Fibers Corporation, USA
Dave Smiley
Phillips Fibers Corporation, USA
Dan Nesbitt
G. C. Wallace, Inc., USA

Abstract

The case history describes the reconstruction of a 5-mile section of Cheyenne Avenue in North Las Vegas, Nevada by incorporating a specially designed moisture barrier.

Local engineers had previously unsuccessfully tried several stabilization procedures on sections of this roadway, which led them to recommend an innovative alternative to stabilize the moisture sensitive clays in the roadway subgrade soils.

The new design approach consists of maintaining the subgrade at a constant moisture content to eliminate shrinking and swelling of these problem soils. The subgrade is encapsulated on three sides by placing a geosynthetic moisture barrier fabric, both horizontally and vertically to a predetermined width and depth over and beside the expansive clay subgrade.

The geosynthetic moisture barrier used had nonwoven geotextile on both sides of an impermeable film allowing it to also remove water in its horizontal plane. This will help remove the water percolating downwards from the surface, keeping the roadbase drained.

As it was placed beneath the base stone, the moisture barrier also provides the frictional, separation and soil stabilization effects of a nonwoven geotextile. Details will be given on the project design and its implementation. Installation procedures followed on the project will be discussed. Seaming techniques used to join the moisture barrier fabric will be reviewed. Unanticipated construction problems encountered during construction and their resolution will be discussed.

Introduction

Cheyenne Avenue, a two-lane highway between Losee Road and Rancho Drive in North Las Vegas, Nevada was originally constructed in 1970. Within a few years, signs of pavement distress started to appear. In the late seventies,

the pavement had deteriorated so badly due to swelling and shrinking subgrade that the road became extremely wavy. This became a major safety hazard with truck trailers reportedly becoming uncoupled from the tow vehicles. Severe alligator cracking was also evident. In 1980, the worst section was reconstructed by over-excavating up to 6 ft., replacing with select fill material, type 2 and 3 road base, and 4" of A.C. surfacing. However, deterioration due to shrinking and swelling continued. Between 1982 and 1988 the old and new sections of pavement were rehabilitated by repeatedly milling off humps and patching the badly alligatored areas. In 1987, the city of North Las Vegas contracted the services of G. C. Wallace, Inc., to redesign Cheyenne Avenue into a four-lane, modern highway with two paved parking lanes. In the reconstruction design, G. C. Wallace, Inc., explored various subgrade stabilization alternates. One system was a paving fabric saturated with asphalt to be used as a moisture barrier within the pavement. Due to anticipated installation problems in the vertical trenches this system was discarded. Lime treatment was not considered due to negative experiences with lime in Las Vegas on Stewart Avenue and Owens Street. The design engineers opted for a geosynthetic moisture barrier to be designed into the project. The moisture barrier selected was Petromat* MB, manufactured by Phillips Fibers Corporation and consisting of an impermeable membrane sandwiched between two layers of nonwoven geotextile. The design was reviewed and approved by Nevada Department of Transportation, Nevada Regional Transportation Council, city of Las Vegas and the city of North Las Vegas.

Site Geology And Site Condition

Natural soils consist of soft to moderately hard clays, gravelly clays, and silty clays and gypsum. Tests performed on soils by Western Technologies, Inc., Las Vegas, Nevada, indicated that the on-site clay soils range from having a low to very high expansion potential, and the gypsum is slightly soluble in water. In addition, some of the clay soils can exhibit large expansion pressures. Based on chemical tests, the on-site soils also contain a sufficient concentration of sodium sulfate to be susceptible to chemical expansion. In addition, Cheyenne Avenue crosses some adverse geologic features which are: compaction faults, area subsidence and fissure zones. There is a potential for vertical and horizontal displacements across the compaction faults. The conclusion of the subsurface investigation report conducted by Western Technologies Inc. was, "It is not economically feasible to overexcavate enough clay soils to allow the placement of enough non-expansive soils to provide the required surcharge. Also, the potential for displacement due to compaction faults cannot be eliminated. Pavement recommendations are intended to provide the best pavement life and service within practical economic consideration."

*Trademark Phillips Petroleum Company

Concept Of A Moisture Barrier

Moisture barriers are specialty geomembranes which, when installed properly, can solve expansive soil problems. Conservative estimates of the damage caused by the expansive soils in the United States exceed 10 billion dollars a year. More than half of these damages occur to roads and streets. The expansive soil subgrades which shrink and swell with variations in moisture content are described as being in the "active zone." An active zone may range from 3 to 10 feet deep beneath the ground surface. This zone is subject to surface water recharge and evaporative water discharge. For example, if the active zone beneath a road is 5 feet thick and experiencing 10% swelling, the road surface will actually move up 6 inches. Likewise, a 10% shrinkage will cause the road surface to move down 6 inches. The movement usually occurs locally, nonuniformly, creating a rolling road surface and road deterioration resulting in a need for premature rehabilitation. Figures 1 and 2 illustrate these conditions. Cheyenne Avenue road conditions fall into this category.

By incorporating a moisture barrier, on new projects or on rehabilitation projects, the moisture content of the subgrade is held constant and the subgrade soil remains inactive with no shrinking or swelling. Geosynthetic moisture barriers are deigned to maintain a constant moisture content by stopping infiltration into and evaporation out of the active zone.

Depending upon the actual site conditions, the geosynthetic moisture barrier can be used as part or as all of the moisture barrier system to shield the active subgrade soil zone from infiltration and evaporation as shown in Figures 3 & 4. In the existing road rehabilitation shown in Figure 3, a paving fabric membrane interlayer system is used as the horizontal moisture barrier, and the geomembrane moisture barrier is used vertically. In Figure 4, the geomembrane moisture barrier was used both horizontally and vertically such as applied to this Cheyenne Avenue project.

To seek ways to minimize the destruction caused by expansive soil conditions, Texas Department of Transportation has been using geomembrane moisture barriers since 1976. According to the Texas Department of Transportation, moisture barriers used both vertically and horizontally are cost effective. The active zone in some areas of Texas is at least 8 feet deep and to maintain constant moisture content under the roadway, they utilize a 9 feet deep vertical moisture barrier. In addition to its moisture barrier function, properly designed geosynthetic moisture barriers placed beneath the aggregate base function also as strong geotextiles and provide the following benefits:

1. Provides a separation layer to keep base aggregate from pushing into the subgrade and subgrade from intruding into the aggregate. This allows a clean, free-draining base aggregate to be used.

2. Stabilizes a weak subgrade allowing approximately a 1/3 reduction in structural section thickness or an increase in the overall performance factor of safety if structural section reduction is not realized.

3. Reduces overall project cost due to savings in structural materials both initially and by preventing aggregate loss by keeping the aggregate separated from the subgrade soil.

Selection Of The Moisture Barrier For Cheyenne Avenue

The city of Las Vegas had previous successful experience with the Petromat MB geomembrane used as a horizontal moisture barrier on city streets. It was used in a test installation to evaluate the ability of Petromat MB to keep subgrade moisture content constant, thereby improving pavement performance. The design engineers and local officials on the Cheyenne Avenue project requested further evidence that this unique product could withstand anticipated construction stresses and survive the installation without any damage.

The city of North Las Vegas performed a field test of their own to evaluate the survivability and waterproofing capabilities of the Petromat MB moisture barrier. The test consisted of placing a 10 ft X 20 ft piece of material on the ground, dumping 6 inches of crushed, hard angular rock on top of the membrane as a base course, and compacting the stone to simulate the harsh realities of field installation. After compaction, they scraped off the rock from the geosynthetic moisture barrier and visually inspected it for rupture or any other damage. No damage was observed. In order to test for water migration through the membrane after the survivability test, the membrane was placed on a wooden frame having a wire mesh screen as a support. Then water was poured onto the moisture barrier which was observed for 8 hours to monitor any leakage. They did not observe any leakage. This convinced the specifiers that Petromat MB could be successfully used for this project. The Phillips Petromat MB selected for this project is a composite of two layers of nonwoven needlepunched polypropylene fabric with a polyethylene film bonded between the two nonwoven fabric layers. This unique product offered the membrane protection and the proper frictional surface necessary for use as a horizontal moisture barrier. The typical properties of the moisture barrier supplied for the project are listed in Table 1.

Cheyenne Avenue Pavement Design

The pavement design consisted of installing the horizontal moisture barrier across the full width of the roadway including the median section and the vertical moisture barrier along each edge of the road underneath the curb and gutter section and the 5 feet wide sidewalk section on the road edges. The horizontal moisture barrier was covered with 18 inches of type-2 base having a maximum size of 1½ inches aggregate. The base was overlain with

7 inches of asphalt binder mix which was placed in two lifts. The binder mix was overlain with a 3/4" thick open-graded mix to provide a high-skid resistance-riding surface. The actual typical section of the project is shown in Figure 5.

Moisture Barrier Installation

Before the start of construction, the representatives of Southern Nevada Paving Inc., the contractor; Phillips Fibers Corporation, the manufacturer; and G. C. Wallace Inc., project quality assurance engineers, had a preconstruction meeting to discuss the installation phase of the moisture barrier.

Since the project was a part reconstruction of an existing roadway and part widening with new construction, the construction of the roadway proceeded in two phases. Phase one was construction of the new half of the roadway so that the traffic could move without disruption on the existing roadway. Once that was completed, the old highway was excavated to subgrade level and reconstructed to the new design. The sequence allowed movement of traffic without disruption regardless of construction. The Petromat MB moisture barrier was supplied in two sizes, i.e., 12 feet wide by 300 feet long rolls and 6 feet wide by 300 feet long rolls due to construction logistics.

The installation of Petromat MB started from the outer, vertical trenches inwards. The first 12 feet wide roll was installed partially in the trench and partially on the roadway subgrade. Since the trench dimensions were 1 foot by 3 feet, the first roll of moisture barrier covered the bottom 1 foot of the trench, 3 feet upwards on the inside of trench, and 8 feet of the horizontal roadway subgrade. The outer edges of the trenches and top and bottom were lined with 4 NP Supac, a nonwoven needlepunched polypropylene geotextile specially engineered for drainage applications, to form an edgedrain. A 6-inch perforated pipe was installed in the roadway edgedrain to remove water quickly. The typical section of this installation is shown in Figure 5. The reason for the edgedrain is that although the North Las Vegas area is an arid environment, when it does rain, the run-off can cause localized flooding. The drain was provided to remove the seepage from the surface run-off quickly before it percolates into the subgrade. The edgedrain will also remove water from the road base aggregate layer over the moisture barrier.

In the first new construction phase of the project, four consecutive rows of Petromat MB were installed by shingling each successive row with an overlap of 6 inches. This procedure provided a 36.5-foot-wide membrane-lined roadway section. Each overlap was seamed by using Phillips Fibers Corporation's recommended sealing method which produced a watertight seam. The seaming

method used involved placing a hot rubberized asphalt mastic material along the seam and then immediately rolling the seam in place. This system, developed by Phillips, results in a strong, waterproof seam which is easily performed just ahead of the aggregate placement over the moisture barrier.

As soon as the moisture barrier was in place, 18 inches of aggregate base meeting the Nevada Department of Transportation's specification of type-2 base material was placed over it. The base was compacted in two lifts at optimum moisture content to attain maximum density, and no damage was incurred by the moisture barrier. The base was overlain with 7 inches of asphalt concrete in two 3½-inch thick lifts. The surface will be covered later on with a 3/4-inch thick layer of open-graded asphalt mix, generally known as pop-corn mix, to provide surface drainage and high skid resistance. As soon as the first phase of new construction was completed, the roadway was opened to traffic. Then, the existing roadway was excavated and regraded to the final subgrade level. The second phase of moisture barrier was installed by following exactly the same sequence as followed in the first phase installation of new section. A gap of 11 feet wide was left in the middle of the roadway which was covered with a 12-foot-wide moisture barrier tying both halves of the moisture barrier system together. The aggregate base course and asphalt binder layers were also placed by following exactly the same procedure as defined earlier. At the completion of the project, two New Jersey-type traffic barriers were constructed with an 8 feet wide decorative median in the center as shown in Figure 6. To remove surface water quickly, storm drains were constructed every so often. Underdrains were connected to storm drains. At each storm drain drop inlet, Petromat MB was flashed (cut and sealed with mastic) to the drain similar to how roofing obstructions are flashed to keep the entire system waterproof.

Construction Problems

The project went very smoothly. Traffic was kept to a minimum on moisture barrier installation. There were minor folding problems in the first roll, which was partially placed in the trench, when stone was dumped in the trench. The dropping of the aggregate into the trench pulled the roll somewhat, thus causing the horizontal portion of the moisture barrier to fold. Any folding at seams was treated with extra seaming mastic to assume a good seam. Wind was a problem off and on, however, due to past installation experience under similar conditions, the contractor was advised to place some ballast on the membrane during installation regardless of the conditions. Also, a minimum amount of moisture barrier was placed ahead of the base aggregate placement. Otherwise, the project went more smoothly than actually expected. The contractor, the city of Las Vegas, and the design engineers responsible for the quality control and quality assurance were all pleased with the ease in which the geosynthetic moisture barrier system was installed.

Conclusion

The project was just completed in 1990. It will be monitored for long term performance on this difficult to stabilize section.

Past projects constructed using this system are performing excellently.

Table 1

Moisture Barrier Fabric Specification

Moisture Barrier Fabric - Composite fabric shall consist of two layers of nonwoven needlepunched polypropylene fabric with a minimum layer of 4 mils thick polyethylene film bonded between the two nonwoven fabric layers. The moisture barrier shall meet the following minimum properties:

Property And Test Method	Value
Weight (oz/yd^2) ASTM D-3776	9.0
Thickness (mils) ASTM D-1777	50
Tensile Strength (lbs) ASTM D-4632	150
Elongation (%) ASTM D-4632	35
Mullen Burst (psi) ASTM D-4833	260
Puncture (lbs) ASTM D-4833	80
Trapezoidal Tear (lbs) ASTM D-4533	45
Permeability (cm/sec) ASTM D-4491	0
Resistance To Soil Burial ASTM D-3083	No Change
Abrasion Resistance (% strength retained) ASTM D-4886 (can be abraded on either side of fabric)	60

Note:

1. The nonwoven needlepunched fabric on both sides of the membrane is to provide a high degree of survivability, i.e., during installation and construction it provides a cushion against sharp objects that is not available in single-sided membranes. Also, without a film exposed, the product has very good friction against both underlying soil and against the cover material.

2. Seaming of the moisture barrier fabric shall be done in accordance with manufacturer's recommendation.

3. Petromat MB, as manufactured by Phillips Fibers Corporation of Greenville, South Carolina, meets the properties listed above.

FIGURE 1

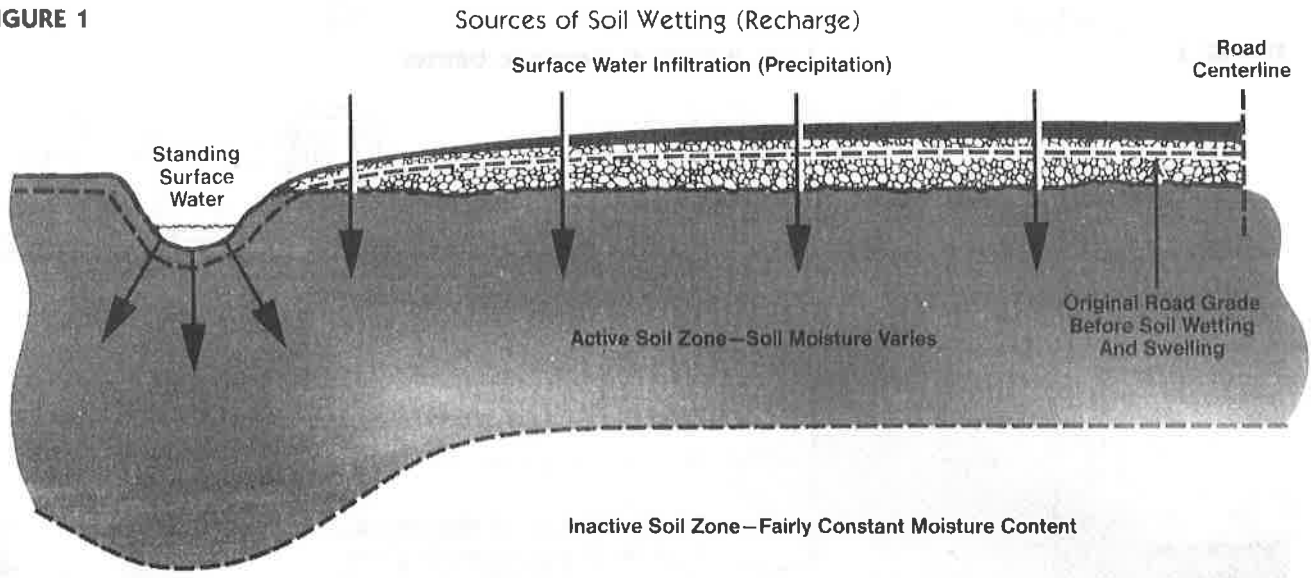

FIGURE 2

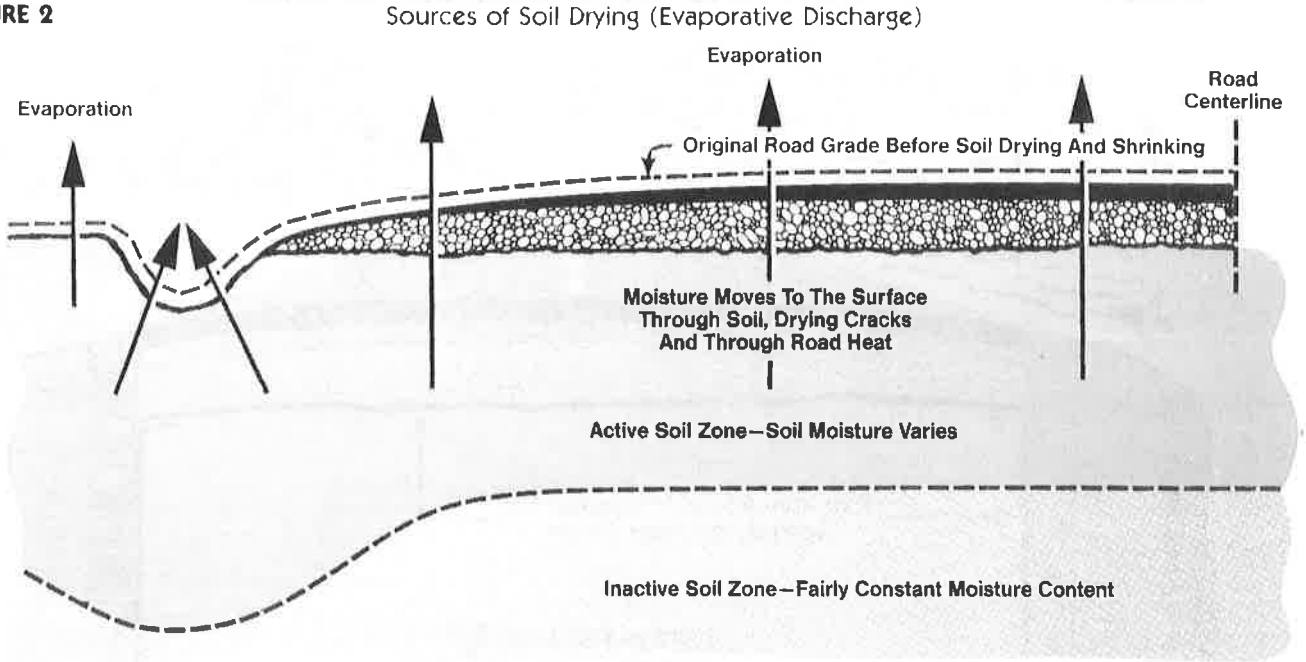

FIGURE 3

1) As a vertical moisture barrier

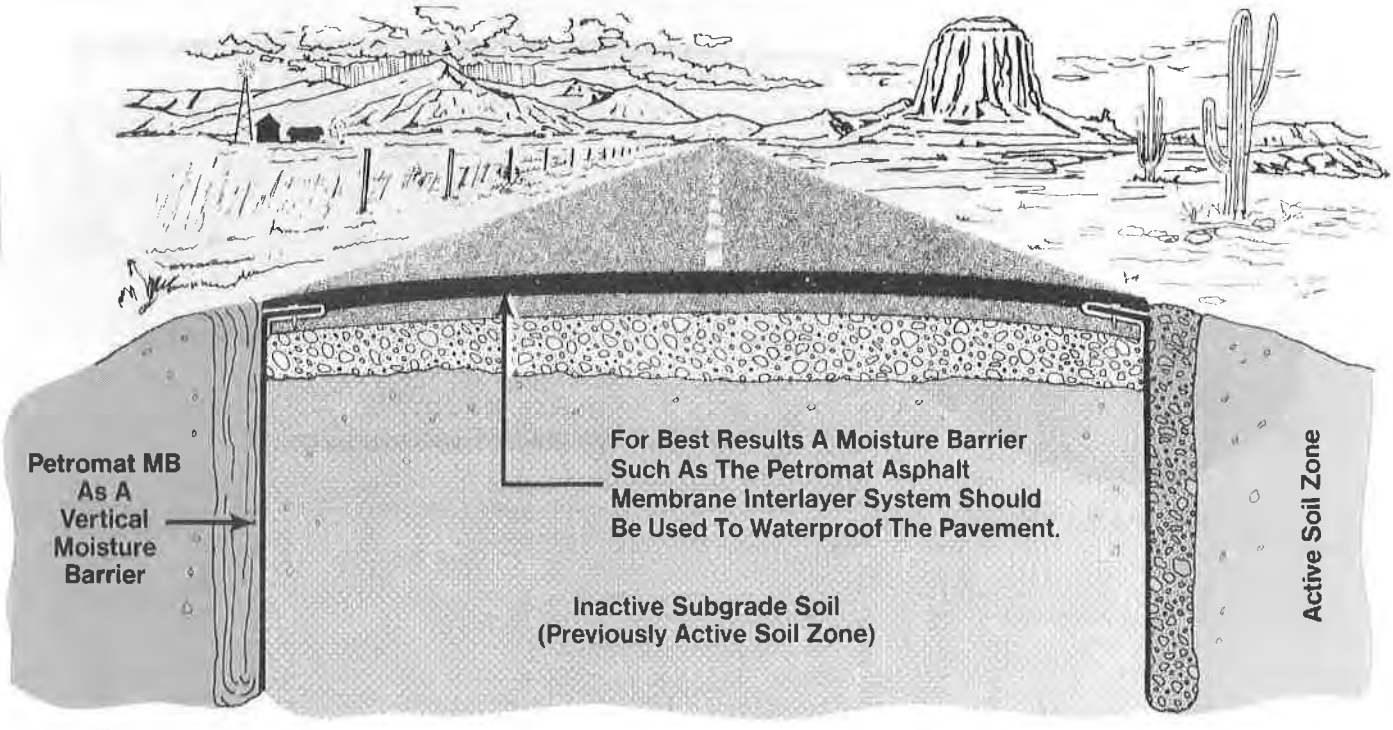

FIGURE 4

2) As a vertical and horizontal moisture barrier

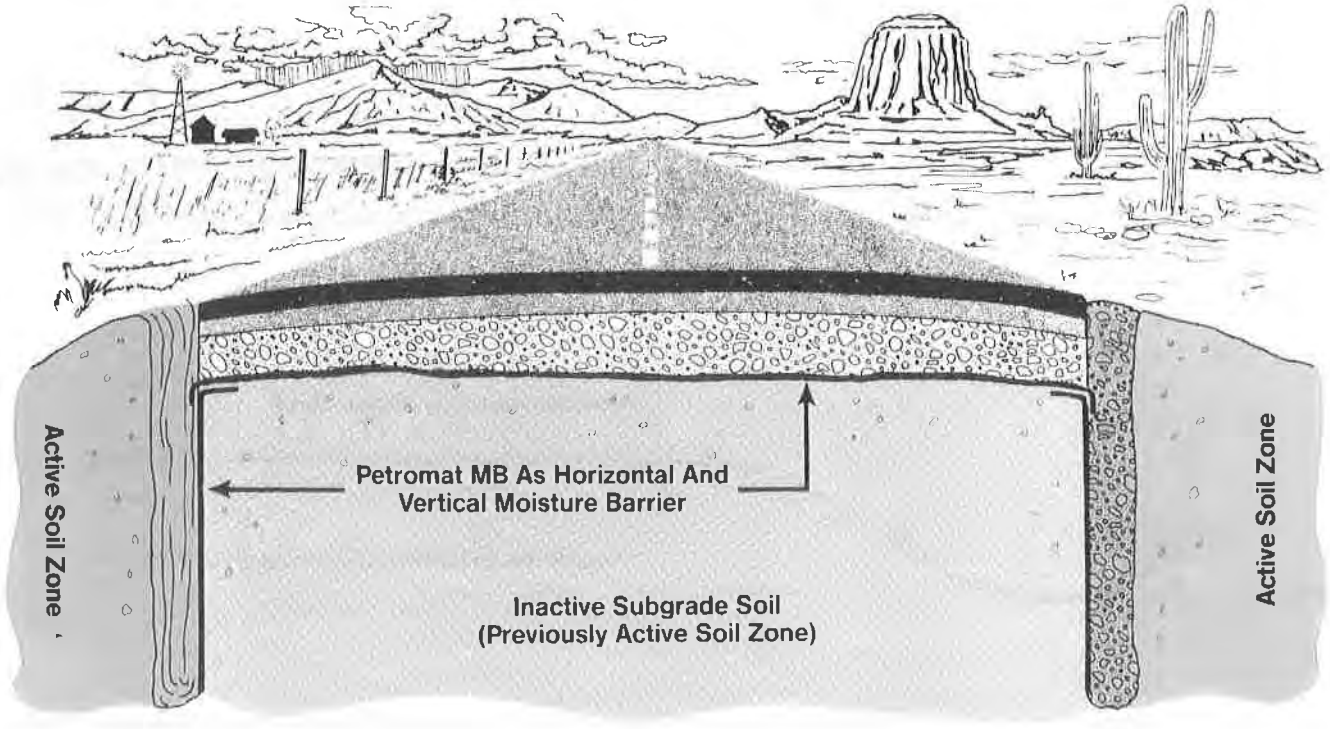

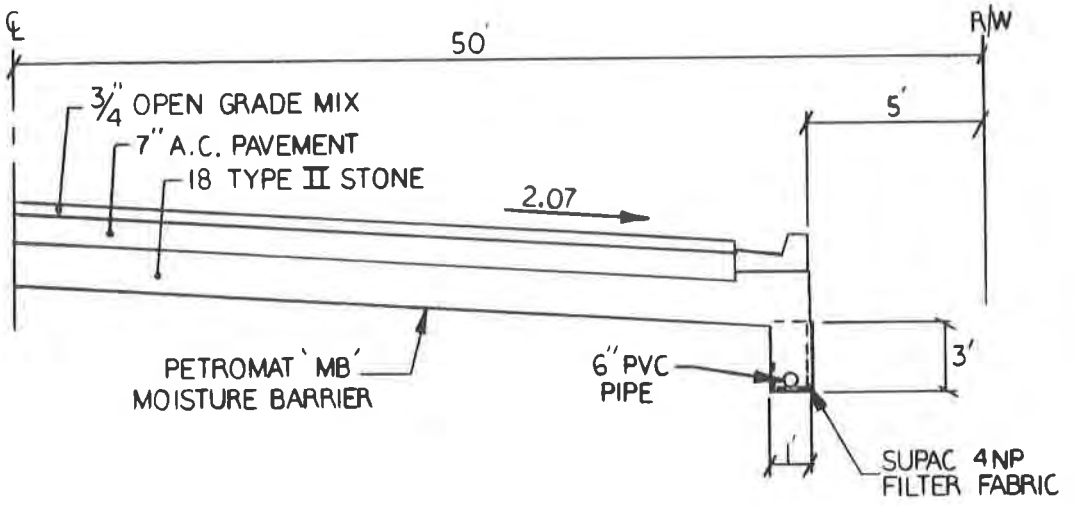

MEDIAN TYP. SECTION

FIGURE 5

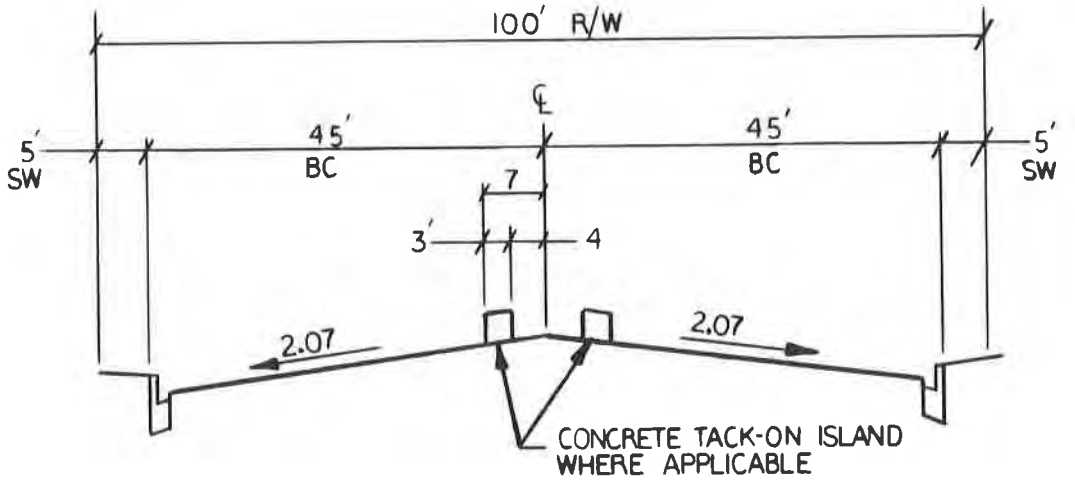

MEDIAN TYP. SECTION

FIGURE 6

References

1. Cedergreen, Harry R., "Poor Pavement Drainage Could Cost $15 Billion Yearly." Engineering News-Record, ViewPoint, June 8, 1978

2. Humphries, K., Guram, S., Chu, T., "Soil Moistures As A Factor In Subgrade Evaluation." ASCE Symposium On Pavement Design, 1975

3. Hunter, Dal, "Lime-Induced Heave In Sulfate-Bearing Clay Soils," Journal Of Geotextile Engineering Volume 114, No. 2, Feb. 1988

4. Jones, D. E., and Holtz, W. G., "Expansive Soils - The Hidden Diaster," - Journal Of Civil Engineering Proceedings ASCE Volume 43

5. Krohn, J. P., and Slossan, J. E., "Assessment Of Expansive Soils," Volume 1, Forth International Conference On Expansive Soils

6. Lytton, R. L., et al, "Study Of Expansive Clays In Roadway Structure Systems," Center For Highway Research, University Of Texas Austin Reports 118-1 through 9

7. Lytton, R. L., and Gay, D. A., "Moisture Barrier Effects On Pavement Roughness," Texas Transportation Institute, Texas A & M University 1988

8. Steinburg, M. L., "Deep Vertical Fabric Moisture Barrier In Swelling Soil," Transportation Research Record 790, TRB

9. Steinburg, M. L., "Horizontal Placement Of A Geotextile On A Subgrade To Control A Swelling Soil," Research Report 187-9, Texas Department Of Highways And Public Transportation

10. Steinburg, M. L., "Monitoring The Use Of Impervious Fabrics, Geomembranes In The Control Of Expansive Soils." Research Report 187-12, Texas Department Of Highways And Public Transportation

Raleigh Street Embankment-Orlando, Florida

Robert L. Goehring, P. E.
Professional Services Industries, Inc., USA

INTRODUCTION

Professional Service Industries, Inc. was retained in late 1985 to study alternatives for constructing Raleigh Street, a four-lane roadway in the MetroWest Development. MetroWest is a large multi-use development in southwest Orlando, Florida. Figure 1 presents a map of the site vicinity.

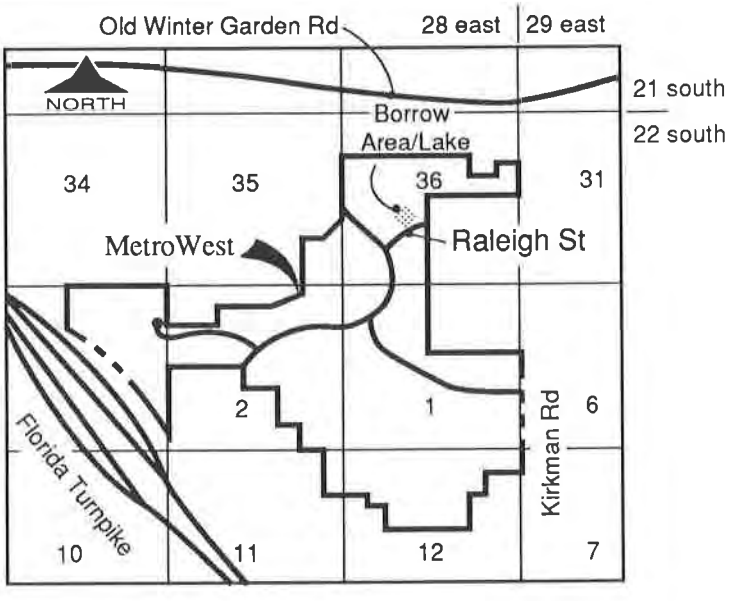

Figure:1 Site vicinity map

Geotechnical evaluations for the Raleigh Street Project were made more complicated by the presence of an old borrow pit that was present adjacent to the proposed roadway. For a distance of about 50 feet, the north shoulder of Raleigh Street was to pass within 20 feet of the deep water filled pit. The proposed roadway was to be constructed 35 to 40 feet above the surface of the lake/pit. In Central Florida, where topography is relatively flat, such a large natural grade separation is rare.

SCOPE OF PROJECT

Because of the large grade separation required, our scope of services was initially very general. We started this project with only one purpose: to find the most economical way to build Raleigh Street across the corner of the borrow pit. To accomplish that purpose, the engineers at Professional Service Industries, Inc. provided the following services:

1. Evaluated the existing soil conditions with Standard Penetration Test borings on land and wash borings in the lake/borrow pit.

2. Identified several feasible construction alternatives.

3. Ranked the alternatives and helped the project civil engineer estimate costs for each alternative.

4. Expanded upon the selected alternative and provided construction level drawings/concepts.

5. Provided technical support while the design was reviewed by the City of Orlando (the road was to be dedicated at a later date.)

6. Attended a pre-construction meeting to discuss the selected alternative and methods of construction with the project contractor.

7. Provided full-time monitoring of construction activities with technicians as supported by project engineers.

8. Provided follow-up consultations to the owner during and after the construction.

SUBSOIL CONDITIONS

For the purpose of investigating the type and condition of the subsoils beneath the proposed embankment, a total of three (3) Standard Penetration Test borings were performed at the approximate locations shown on Figure 2. The structural borings were extended to depths of 55 feet at each end of the embankment and to a depth of 90 feet in the center where the maximum amount of fill was needed. The general stratification found in those test borings is presented in profile form on Figure 3.

In order to provide drill rig access on the natural slopes, a bulldozer was needed to provide a level bench for the drill rig to operate on. This required providing 13 to 19 feet of sand fill at the boring locations. Below these recently placed fill soils, borings encountered alternating layers of dark reddish-brown slightly silty fine sand and grayish-brown fine sand to depths of 50 to 55 feet.

In the deepest test boring, soils below 55 feet consisted of alternating layers of clayey fine sand, sandy clay and silty fine sand, all with traces of phosphates. This material is locally known as the Hawthorn Forma-

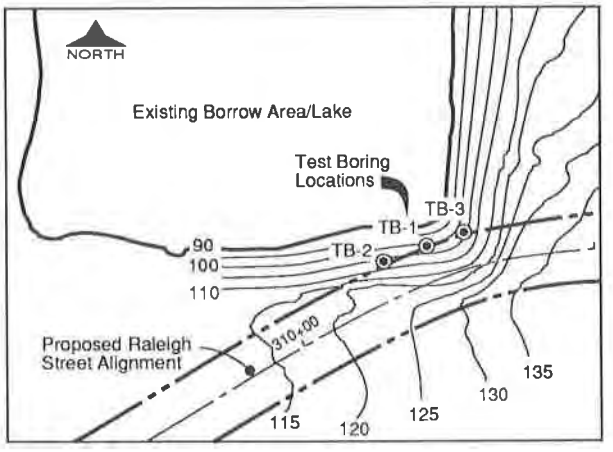

Figure:2 Plan view/boring locations

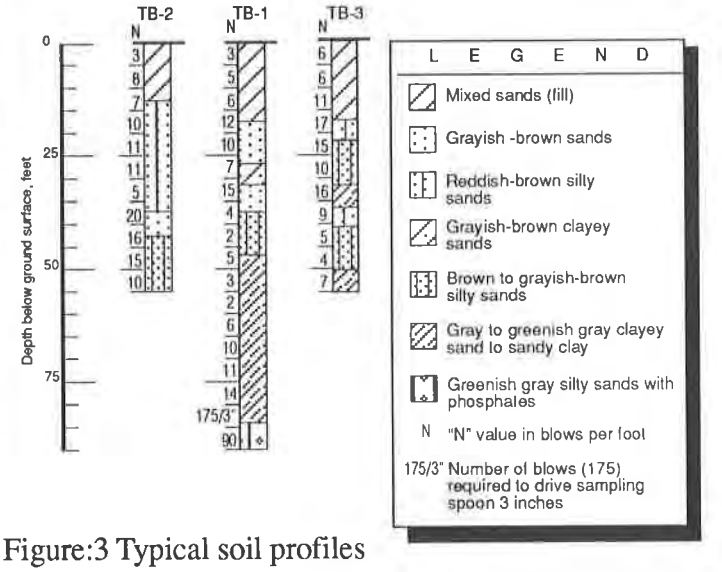

Figure:3 Typical soil profiles

tion and has a characteristic greenish-gray color. The deepest test boring was terminated at a depth of 90 feet in the Hawthorn Formation. From previous experience in this area, we estimate the underlying limestone may be at depths of 125 to 160 feet below grade at the project.

To determine the approximate contour of the borrow pit bottom, depth soundings were made by the project surveyor along transects. These soundings revealed an irregular lake bottom with several deep holes near the proposed embankment. Within 20 feet of the proposed embankment toe, the water was 20 to 30 feet deep.

At the time of our field investigation, the shallow groundwater table was not encountered in the top 10 feet of the borings. Because of the clean sand present in the upper 55 feet, we expected the groundwater levels at the proposed embankment to remain at or slightly above the adjacent lake level.

FEASIBLE ALTERNATIVES

After reviewing the test boring results, it was evident that foundation support conditions would not be the limiting factor at this site. Rather, it was clear that slope stability issues wn the fill would control the design.

From the available information, four conceptual alternatives were presented to the owner. Those options included:

1. Move the roadway alignment to the southeast away from the borrow pit. This would allow flattening of the side slope between the shoulder of the road and the edge of the existing lake.

2. Fill into the borrow pit at a slope of 3 horizontal to 1 vertical (3H:1V) starting at the edge of the right-of-way. This option would require placing more than half of the fill into the water in an uncontrolled manner.

3. Install a vertical sheet pile or step-down type retaining wall system between the waters edge and the edge of the right-of-way.

4. Steepen the slopes to as great as 0.5H:1V. This would require restricting filling to above the water line and reinforcing the embankment with geogrid to increase the stability. At the time of this project, no other project of this magnitude and steepness had been attempted in the Central Florida area.

EVALUATION OF ALTERNATIVES

After a lengthy discussion, the first alternative (moving the roadway) was rejected because of curve geometry/alignment and development considerations. Had the alignment been moved, the owner would have suffered significant loss of valuable real estate and been forced to reapply for project permits, possibly delaying construction.

During consideration of the second alternative, preliminary earthwork estimates showed a substantial amount of fill would be required in the borrow pit if 3H:1V slopes were attempted. The large quantities estimated were due in part to the concern that any fill placed below the water line would tend to "flow" and reach a slope as flat as 8H:1V. When discussing this option with the project contractor, he indicated he was very nervous about the possibility of loosing a significant amount of fill due to the uneven bottom of the old borrow pit. The combination of this tendency to flow and the presence of several deep holes in the borrow pit made the second option very costly.

The third option considered involved installation of a vertical sheet pile or poured in-place, step-down retaining wall system. Because of the 30 to 40 foot vertical drop necessitated in a horizontal distance of 20 to 50 feet, both types of retaining walls quickly become uneconomical. Additionally, preliminary slope stability analyses showed that a multiple wall pattern could have a very low factor of safety against a deep seated slope failure.

The last option evaluated considered construction of a very steep embankment (0.5H:1V) reinforced with high strength geogrid. While geogrid reinforcement had been used for embankment stabilization in other parts of the country, design and construction of a major embankment like Raleigh Street had not been attempted in Central Florida. Design of a geogrid option was also complicated by the fact that the embankment geometry and slope steepness was constantly changing throughout the curve. When considering this option, we recognized that none of the local contractors had ever attempted construction with geogrid material. This lack of local experience was expected to result in higher costs for placement and construction.

PREFERRED ALTERNATIVE

Based on conceptual designs, construction costs for the geogrid reinforced slope was estimated to be on

the order of $200,000. This cost was significantly less than other conventional alternatives such as filling the lake at a flatter slope ($300,000) or constructing a retaining wall (over $400,000.) This apparent cost savings and the aesthetic benefits of a "living" sodded face led the owner to select the geogrid option for further study.

Two variations of the geogrid reinforced steepened slope option were carried through final design. Those alternatives were referred to as Option 1: Heavy Reinforcement; and Option 2: Moderate Reinforcement with Toe Berm. Figure 4 shows the concept for the steepest section of the Heavy Reinforcement option and Figure 5 shows a similar section for the Moderate Reinforcement with Toe Berm.

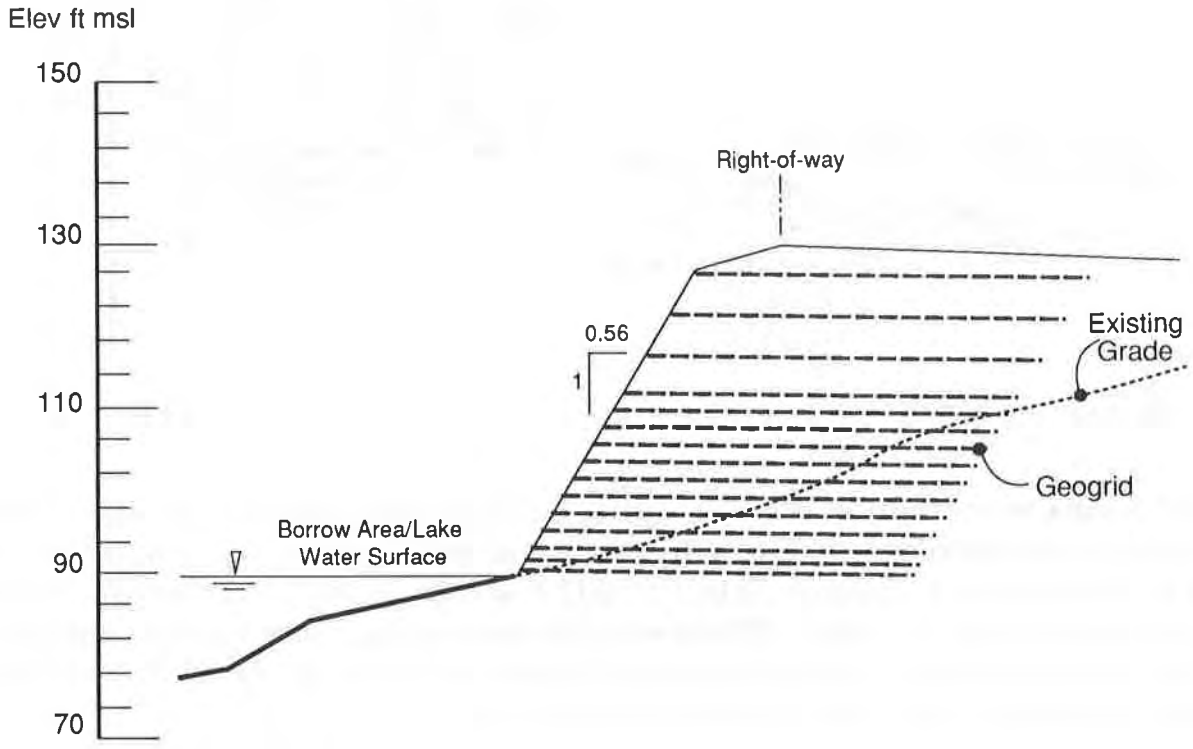

Figure:4 Heavy reinforcement option

After final design had been completed, the contractor priced both the Heavy Reinforcement option and the Moderate Reinforcement with Toe Berm option. Because of his concern over filling into the lake, the Heavy Reinforcement option was the lowest price option. The remainder of this paper addresses various aspects of design and construction of that Heavy Reinforcement option.

GEOGRID DESIGN PARAMETERS

One of the first elements considered when conducting the slope stability analysis was the design parameters of the geogrid reinforcement. A search of available manufacturers literature was made. It quickly be-

came evident that very few products were available at the time that would provide: proven field experience, laboratory test data supporting elongation properties/pull-out capacity, and technical support by the manufacturer. Not only did we, the design engineer, have to feel good about the design, but we also had to overcome doubts from the contractor and the City of Orlando that this innovative solution was sound and workable.

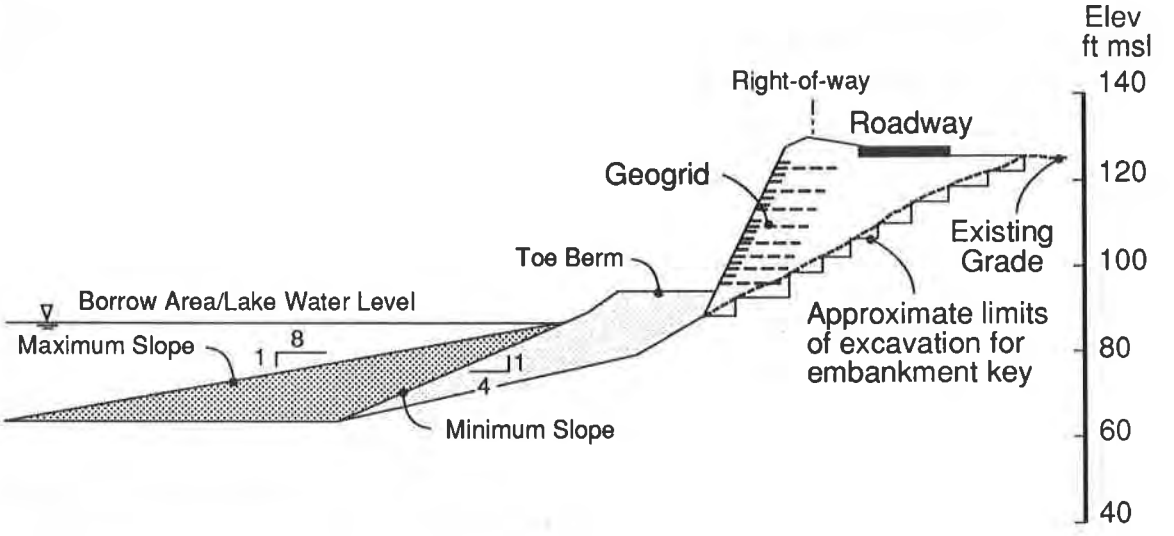

Figure:5 Moderate reinforcement with toe berm

After our initial search, two types of high strength uniaxial polyethylene based geogrid were selected for the primary embankment reinforcement. The two types of geogrid haddesign strengths of 2,000 to 2,200 pounds per foot of width at 5 percent elongation. To hold the sod facing in place, a low-strength biaxial geogrid with good ultra-violet resistance was selected. While the strength was not a major factor for this anchoring layer at the face, the selected geogrid had a design strength of 350 pounds per foot in the roll direction. All three types of geogrid were readily available from standard production stock.

DESIGN ISSUES

Embankment Settlement Because new fill up to 40 feet high was planned for the embankment, overall foundation settlement was considered. Based on site-specific standard penetration test-borings and extensive local experience, we estimated total embankment settlement would be 2 to 3 inches. Since the foundation soil is mostly cohesionless sand with some sandy clay, we anticipated most of the settlement would occur during initial fill placement. Longer-term settlement due to consolidation of the deeper clayey soil and densification of the sand fill was expected to be negligible(less than $^1/_2$ inch).

Geogrid Analysis Because of the complex geometry of the roadway in relation to the corner of the borrow pit (see Figure 2), seven (7) different cross-sections and geogrid layouts were needed to economically reinforce the embankment. To accurately model the embankment, a detailed site grading plan was first developed then seven typical cross-sections were drawn and analyzed.

Each cross-section was designed to have a factor of safety against major slope instability of 1.5 or greater. This factor of safety against overall slip circle type failure was selected considering the lack of local experience with this type of construction and the fact that the City of Orlando had to feel comfortable that the design would be conservative.

Because of the sloping toe below lake level, initial trial designs using published nomographs were found to be unconservative. All subsequent design used the STABGM computer program developed by Virginia Polytechnical Institute.

For our analysis, we assumed that the foundation and embankment soils would act as cohesionless materials. Based on past experience in the area, we used a phi angle of 30 degrees for the foundation soils below the lake level and a somewhat higher phi angle of 35 degrees for the clean well compacted fine sand to be placed in the embankment. In an attempt to maximize the efficiency of the geogrid used in the embankment, we selected the option in the computer program which applied the geogrid strength on the tangential surface of the failure arc. We felt this approach was justified considering the relatively high factor of safety (1.5) to which we were designing the embankment.

Geogrid Layout For the heavy reinforcement option, the STABGM program showed circular failure arcs extending 30 to 44 feet back from the face of the slope. To provide adequate length for the geogrid reinforcement to develop full pull-out, our design extended the primary geogrid reinforcement back from the face of the slope distances of 38 to 49 feet. Vertical spacing of the geogrid ranged from 1 to 6 feet in a manner similar to shown on Figure 4. Closer spacing of the geogrid was provided at the base of the embankment to maximize the moment arm available to resist the sliding forces. It is interesting to note that if a toe berm had been used, the geogrid length could have been reduced by as much as 20 to 25 feet per layer. Additionally, the Heavy Reinforcement option required a maximum of 15 layers of geogrid while the Moderate Reinforcement option with toe berm required only 8 layers of geogrid at the most critical section.

Because the heavy reinforcement option employed up to 15 layers of geogrid, a geogrid layout plan was developed for each elevation to be reinforced to help reduce confusion. Examples of these layouts for elevation 92 and 116 feet msl are shown on Figures 6 and 7. Notice that the length and shape of the plan view of the embankment changed significantly in the two views.

Because of the multiple layouts needed to convey the design, this method of presentation became known on the project as the "Drawer Concept". The geogrid layout for each elevation was presented on its own drawer/sheet.

Erosion Protection To provide erosion protection at the face of the embankment, sod wrapped in a low strength geogrid material was provided. Figure 8 shows the typical detail for this facing. Had the aesthetic function of this embankment not been a consideration, a geotextile could have been substituted for the sod. After reviewing the site grading plan, it was decided that the sod would have to be held in place on slopes steeper than 2H:1V. This included about 3/4 of the embankment area.

As a side issue, there was some discussion about the type of sod to use for this project. In an effort to provide a very low maintenance sod that would be self-seeding and require very little water, we selected a

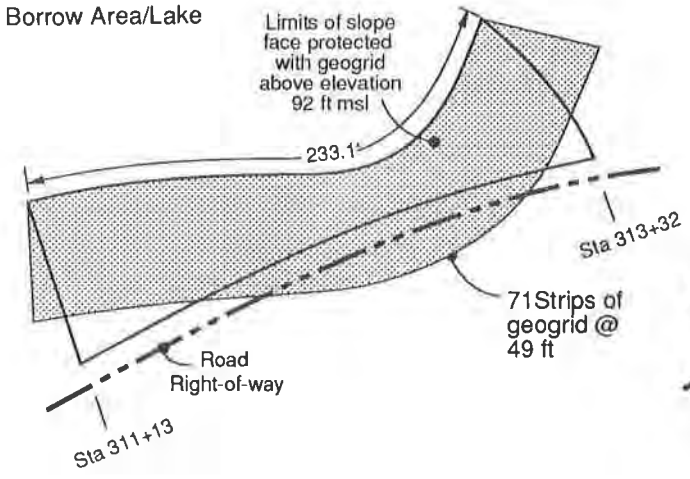

Figure:6 Typical geogrid layout plan for elevation +92.0 msl

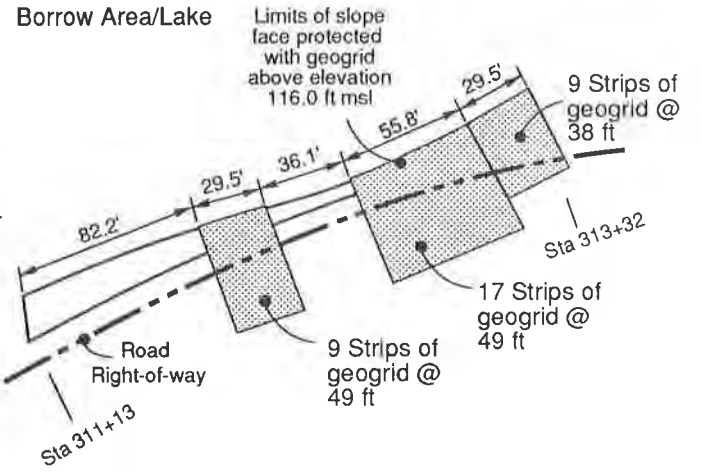

Figure:7 Typical geogrid layout plan for elevation +116.0 msl

variety of bahia grass. We also commented to the owner that after construction, he may wish to plug the face of the embankment with some type of creeping vine.

Tensile Splicing Where the primary uniaxial reinforcement was too short, a field tension splice was needed to maximize use of the roll. This splice consisted of folding one end of the grid and interweaving it between the openings of the piece of grid to be added. A section of 1/2 inch diameter PVC irrigation pipe slipped through the two pieces of grid then served to form a tension splice. Such a splice had been tried in previous projects and served well.

Corner Reinforcement As an off-shoot of the geogrid layout plans, it became evident that in the steepest section of the embankment at the corner, "fanning" of the grid radially would occur. This "fanning" action would result in the lake side face being fully reinforced with grid adjacent to each other and the roadway side

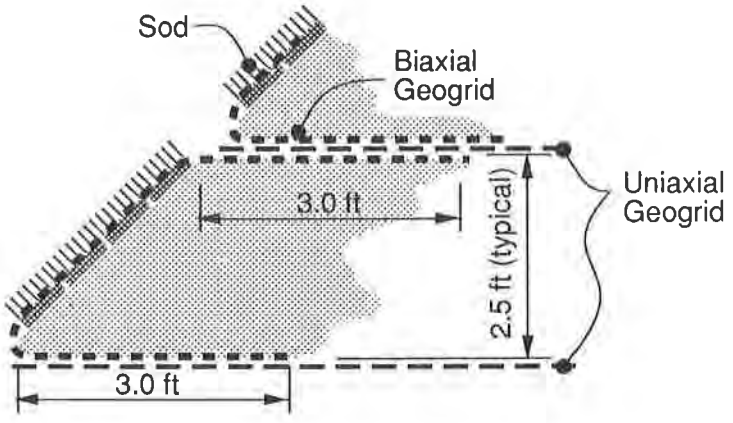

Figure:8 Typical embankment face detail

of the embankment having adjacent strips of uniaxial grid spread by several feet. Figure 9 illustrates this effect. The project peer reviewer initially questioned this practice contending it significantly reduced the effective reinforcement in the corner. The engineers at Professional Service Industries, Inc. countered this

Figure:9 Geogrid fanning

argument by showing the shear resistance of the adjacent soil wedges was greater than the loss of strength through spreading the material. This additional strength was available due to the three-dimensional arch formed by the embankment and the buttressing effect of theflattened slopes on either side of the steep section. In relatively straight sections of the embankment, the uniaxial geogrid was laid side-by-side with no overlap or gap.

CONSTRUCTION CONSIDERATIONS

Because the contractor had never seen geogrid, let alone placed it, site work specifications were kept to the very simplest terms and a significant amount of instruction was performed in the field by the manufacturer and the project engineers. The following are some of the highlights of the specifications provided:

1. Bench the existing slope with vertical steps to key the new embankment into the original slope.

2. Provide a drainage blanket of clean fine sand at the bottom 5 feet of the embankment. Material with less than 5 percent fines passing the No. 200 sieve will be acceptable.

3. The surface of the fill should be kept horizontal at all times. Geogrid will be laid directly on top of the horizontal surface.

4. Fill should be spread over the geogrid using rubber-tired equipment working on the newly placed fill. This will ensure that the geogrid is not damaged by compaction or site vehicles traveling directly on top of it.

5. Fill soils should be placed in 12 inch thick maximum lifts and be compacted to a minimum density of 95 percent of Modified Proctor Density.

6. When positioning the geogrids, be sure that the correct direction with respect to strength of the material is used. The primary reinforcement will be laid in the long roll dimension perpendicular to the roadway centerline.

7. Reinforcement is to be placed horizontally in continuous strips with no overlapping. Where partial rolls of material are to be used, a positive tension connection should consist of a 1/2 inch diameter PVC pipe interweaved through the material.

Forming the Face Initially, the geogrid manufacturer thought that a plywood form would be required to hold the sand in-place until the sod facing had been wrapped and fastened by the next layer of fill. After attempting this forming on the first lift, the method was abandoned as awkward and slow. Instead, the contractor compacted the clean sand in a 1 foot lift leaving a near vertical face ready to receive the sod. The low strength facing grid was then pulled up and over the sod and tensioned by the crews. While this did not form a perfectly straight face, it worked reasonably well. The overall effect created was a "pillow-like" face.

Cutting the Geogrid Because this was the first exposure of the contractor to geogrid material, he had little idea of how to cut the material. Initially, he tried using scissors and tin-snips but found this slow and awkward. After the first day, the contractor cut the geogrid easily using a machete.

Survey Control Because of the complex geometry of this curving three-dimensional embakment, survey control on this job was of vital importance. Throughout the project, there was a constant battle to establish where the face of the embankment needed to be for the correct slope. The first two or three layers of the embankment were placed at an angle flatter than the design stated. To make up this deviation, the next 4 or 5 feet of the embankment was actually placed at angles steeper than the design called for. In fact, at one place in the steepest section of the embankment, the face is nearly vertical.

POST-CONSTRUCTION

Following completion of the embankment, the project engineers visited the site on numerous occasions. Within the first 30 to 60 days, the bahia sod showed excellent growth and put down roots. While some minor leakage of sand through the face occurred in the first 30 days after construction, no major washouts or erosion areas were observed. Figure 10 shows the embankment at about 30 days after construction. Several months after construction, the facing grid was only visible at close range.

Now that the embankment has been in-place almost 4 years, the sodded face appears to be part of the natural landscape at the project. Most residents don't even know that the near vertical slope was constructed using geogrid. The owner of the property has had to perform little or no maintenance on the face and does not even mow it. To-date, the owner has not taken our suggestion that a creeping vine could be installed on the face. The bahia sod seems to be re-seeding itself and holding up to the lack of attention very well.

During a recent site inspection after a prolonged dry spell, we noticed that a thin tension crack has developed in the Raleigh Street pavement at approximately the point where the geogrid stops and the natural embankment starts. This tension crack is almost unnoticeable, but indicates the filled embankment may have consolidated slightly through the seasonal fluctuation of groundwater. While not implemented for this project, the use of a non-woven geotextile in the upper several feet of the embankment may have minimized or prevented this minor tension cracking. Figure 11 shows the Raleigh Street embankment after three years in service.

Figure:10 Embankment thirty days after construction

Figure:11 Embankment after three years

SUMMARY AND CONCLUSIONS

The Raleigh Street reinforced earth embankment was the first one of its kind constructed in Central Florida. Because of that its design and construction had to surmount unique challenges. Conventional solutions to the problem of providing a 40 foot grade separation over a 20 foot horizontal distance were not as economical as using a steep geogrid reinforced slope.

Complex geometry at the corner of the existing borrow pit required sophisticated analysis and a detailed geogrid layout plan. Close field monitoring and survey control were imperative to build this embankment.

Long-term maintenance of the sod face has been minimal and no erosion or displacement problems have been observed after 4 years. Local residents have an aesthetically pleasing slope to view and have no idea that geogrid holds it in place.

ACKNOWLEDGEMENTS

The author wishes to recognize both S.W. Berry, P.E. and D.J. Yovaish, P.E. for their part in designing the Raleigh Street embankment. The owner of the project is Debra, Inc. The contractor on the project was Hubbard Construction of Orlando, and the Civil Engineer and Surveyor on the job was Bowyer, Singleton & Associates of Orlando.

HEAVY CONSTRUCTION APPLICATIONS

Utilization of Geotextile - Reinforced Retaining Wall for Stabilizing Weathered Mudstone Slope

Dave Ta-Teh Chang
Chung-Yuan University, Taiwan, R.O.C.
Tien - Chien Chen
Chung-Yuan University, Taiwan, R.O.C.
Kuan-Hsien Su
Chung-Yuan University, Taiwan, R.O.C.

ABSTRACT

This paper is to deal with the concept of utilizing the geotextile reinforced earth as the retaining structure for stabilizing mudstone slope in southwestern Taiwan. A two tiered wall used in this study was designed, with the lower and upper tiers having heights of 3 m and 2 m from toe, respectively. Two woven geotextiles and two types of fill material (alluvial sand and fly ash-cement treated weathered mudstone) were used in four test sections. Basing on the tensile and frictional behaviors of geotextile and backfill-geotextile interface, respectively, the wall design was made by the conventional tieback wedge analysis method. For comparison purpose, an instrumentation program was also developed and installed to monitor the field behaviors of the wall. Having with stood the rainfall season, the performance of the wall was evaluated and confirmed that the proposed concept for materials selection (geotextiles and backfills) is suitable for stabilizing the mudstone slope. And the fly ash-cement treated material, may be more effective for its lower cost.

INTRODUCTION

In southwestern Taiwan, a great part of mountainous area is covered by mudstone. When bare slopes are softened by rainwater serious disasters often follow by mud slides. In order to improve the unstable mudstone

slope the National Science Council in Taiwan has formed a special ten-year project to conduct broad research and study. The researchers' systematic study aims at evaluating the feasibility and efficiency of using geotextile and fly ash to reinforce the site and stabilize the backfill material. Based on the findings of previous laboratory studies, the project has established an instrumented geotextile reinforced test wall to evaluate efficiency in application and has also formulated guidelines for design, material selection and layout analysis.

The test site is located at Highway No.3 from stations 358 km+120 to 358 km+160. The upper slopes of this section have had significantly slided which have resulted in toe failure from the concrete gravity type retaining wall. For the geotextile reinforced earth, fly ash-cement treated weathered mudstone and alluvial sand were selected to be the backfills. At the same time, relevant tests and analysis are conducted according to the guidelines for design and the selection of materials. The tests include the wide width tensile strength test (ASTM D4594), creep test and the test for frictional properties of the geotextile with soils. The slope stability analysis and layout and detailed design of the reinforced earth structure will be conducted simultaneously. The STABL5/PC computer program (carpenter, 1986) is used for external stability analysis. And the conventional tieback wedge method is applied for the internal stability analysis and design of test wall. In order to understand the field performance and behavior of the wall, a special designed monitoring instrumentation system were also installed to collect necessary data.

BACKGROUND REVIEW

A common problem in an area of exposed mudstone is that the erosion of the mudstone will result in slope instability. King (1985) and Yen and Tsai (1985) indicated that both ground water and runoff water break the weak bonds of mineral particles of mudstone and then soften the strength to cause erosion and subsequent slope failure. Class F fly ash (with low self-cementing potential), a waste material from the thermal power plants in Taiwan, was firstly studied and recommended by Chang and Yu (1986 and 1987) for hancing the stabilization of weathered mudstone. In their studies, lime [$(Ca(OH)_2$] was used as modifier for

improving self-cementing potential. Chang et al. (1988) discovered later, the fly ash-lime can not only improve the strength of the weathered mudstone but also reduce the clogging possibilities for the geotextiles. Chang and Chen (1989) also found later that the cement which is relatively cheaper than lime, the cement could be substituted lime as the modifier for fly ash on the weathered mudstone treatment.

Since the sandy soil is the regular material for this kind of backfill, alluvial sand is to be selected for the purpose of comparison with fly ash-cement treated weathered mudstone in this experiment.

DESIGN, PLANNING AND EVALUATION

Description of Site Condition. The test site, near the Tsen-Wern Dam, is the typical mudstone slope failure area. Since the existing retaining wall was damage at the toe, and the drainage trench and pavement surface were not shown any sign of extrusion, it indicated that could be a typical toe failure mode of slope. About 20 sites with different degrees of similar failure over the adjacent area have been observed. Typical examples can be referred from Fig.1.

Fig. 1 Typical examples of retaining wall failure

Material Selection and Evaluation of Related Characteristics. Two major materials which being concerned for this study were backfills and geotextiles. For backfills, alluvial sand and weathered mudstone treated with fly ash-cement are used. It was based on the consideration as described previously. For geotextiles, five samples were evaluated basing on the wide width tensile strength and clogging resistance combining with the backfills (Gradient Ratio Test, Haliburton, et al., 1982). Two woven geotextiles, sample symbols as G-1 and N-1, were selected in this study for their suitable tensile behavior and low clogging potential (gradient ratio less than 3) with backfills. Typical results for tensile characteristic are shown in Fig. 2.

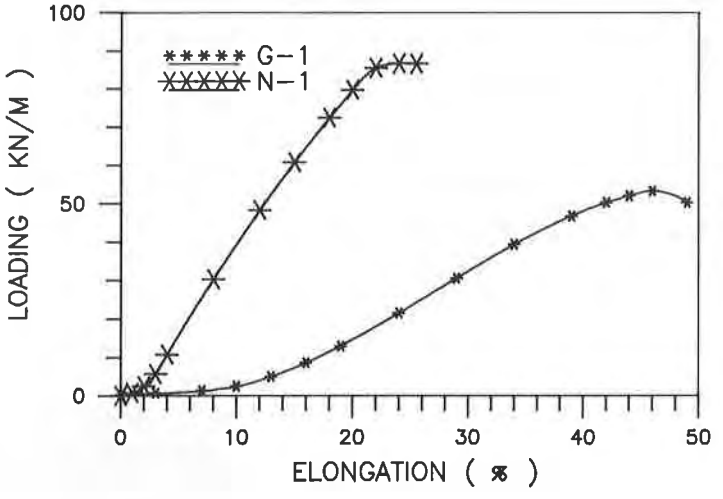

Fig. 2 Results of wide width tensile test of geotextiles

To obtain more understanding of the creep behavior of the test wall, the simple creep tests were conducted for the selected geotextiles. The test procedure was based on the Haliburton et al. (1982) suggested method with a specimen size of 7.5 cm×10 cm, the constant loads were controlled as 5%, 10%, 20%, and 30% of tensile strength for testing. The results were plotted in Fig.3 which shown that the creep strained for 48-hrs and 240-hrs periods exhibited no change with 20% load level. For 30% load level, only G-1 geotextile presented about 2% change of strain. Combining results from Fig. 2 and Fig. 3, strength level from 10% to 20% was selected

for wall design. The other property of soil- geotextile friction angle was determined by undrained direct shear test. In the test program, 12 cm-dia shear box was used, and unsoaked and soaked condition were controlled for series tests. By reviewing the result of friction angle (ϕ_{SF}), ranged from 28^{o} to 36^{o}, the conservative value of 20^{o} was decided to use for wall design which basing on the consideration of durability of soil-geotextile properties.

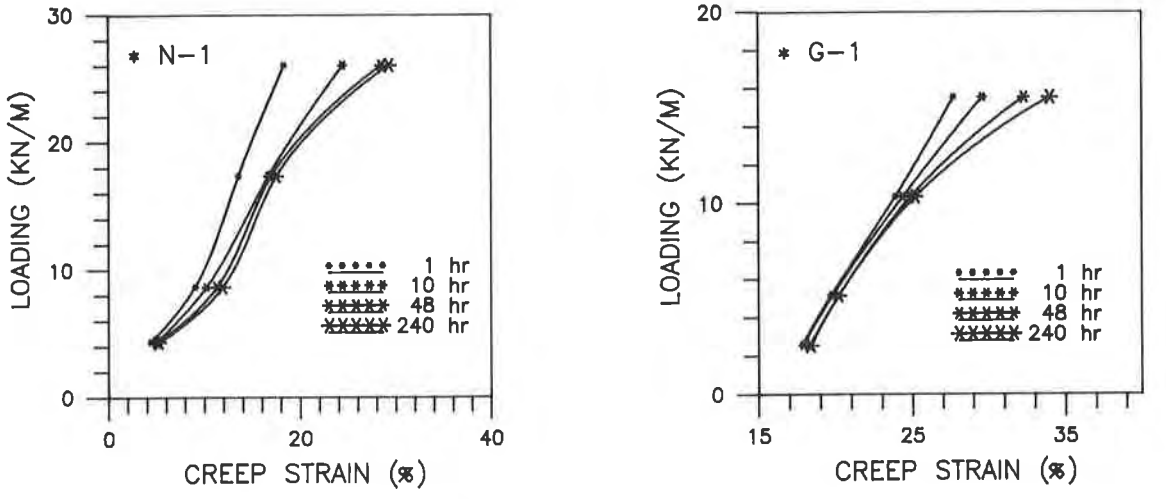

Fig. 3 Results of creep tests under various loading levels and periods

Design and Stability Analysis of Test Wall. A conventional tieback wedge analysis (Bell et al., 1975, Christopher and Hotlz, 1984) was performed to establish the reinforcing requirement for the wall. Wall was separated as the lower (3-m) and upper (2-m) tiers with 1.5 m horizontally from toe to toe, and reinforcement spacing was 50 cm vertically. Since this study is to evaluate stabilizing a sliding slope, the proper design should be rather conservative, The arrangement of geotextiles and backfills for the wall were subdivided into four sections. G-1 geotextile was used for the first and second sections, N-1 geotextile the was used for the third and forth sections. The fly ash-cement treated weathered mudstone was used for backfill in the second and third sections; sand material was used in the first and forth sections.

For slope stability analysis, the Spencer method through computer program " STABL5/PC " was applied. In the analysis, saturated condition and ø=0 state were considered and the results were obtained for original slope and slope with test wall. The typical results are shown in Fig. 4 and indicates that the proposed test wall can meet the safety requirement for stabilizing the unstable slope.

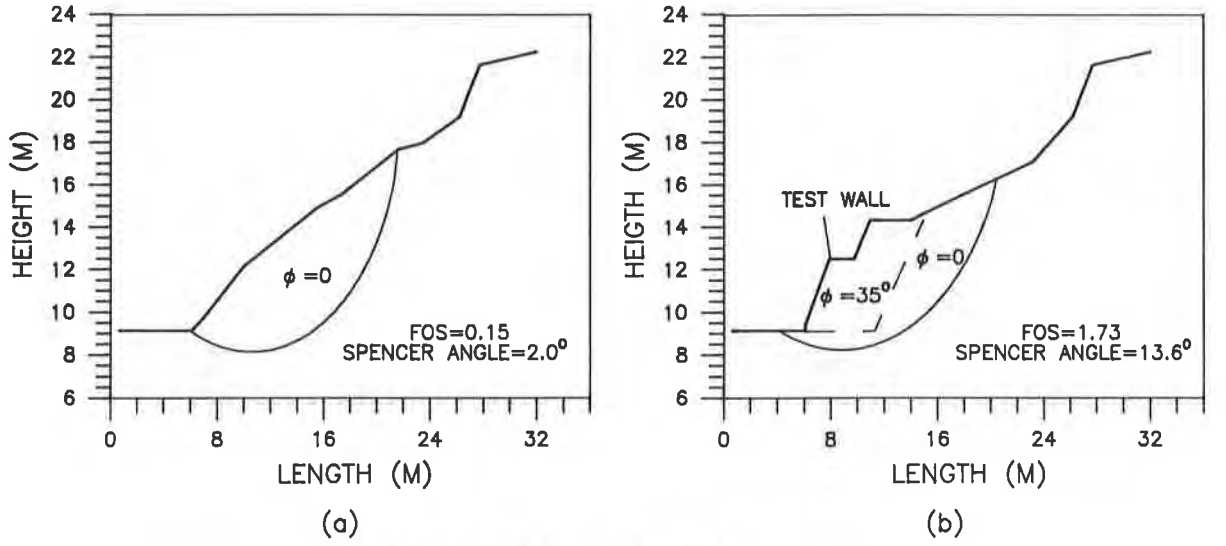

Fig. 4 Analysis of critical sliding circle for (a) original slope (b) slope with reinforced earth mass

Instrumentation Program and Construction of Test Wall. An extensive instrumentation program was developed for monitoring the performance of test wall. Six kinds of instrumentation system had been installed at the test site to (1) observe the settlement of foundation, (2) confirm the filtration efficiency of soil-geotextile system, (3) evaluate the elongation of geotextile, (4) study the stress development within the reinforced section, (5) observe the movement of wall and (6) evaluate the potential of slope movement. The typical units used and the systems arranged at the test site are presented in Fig. 5 and Fig. 6. For more details of special designed elongation measurement unit and tensiometer are shown in Fig. 7 and Fig. 8.

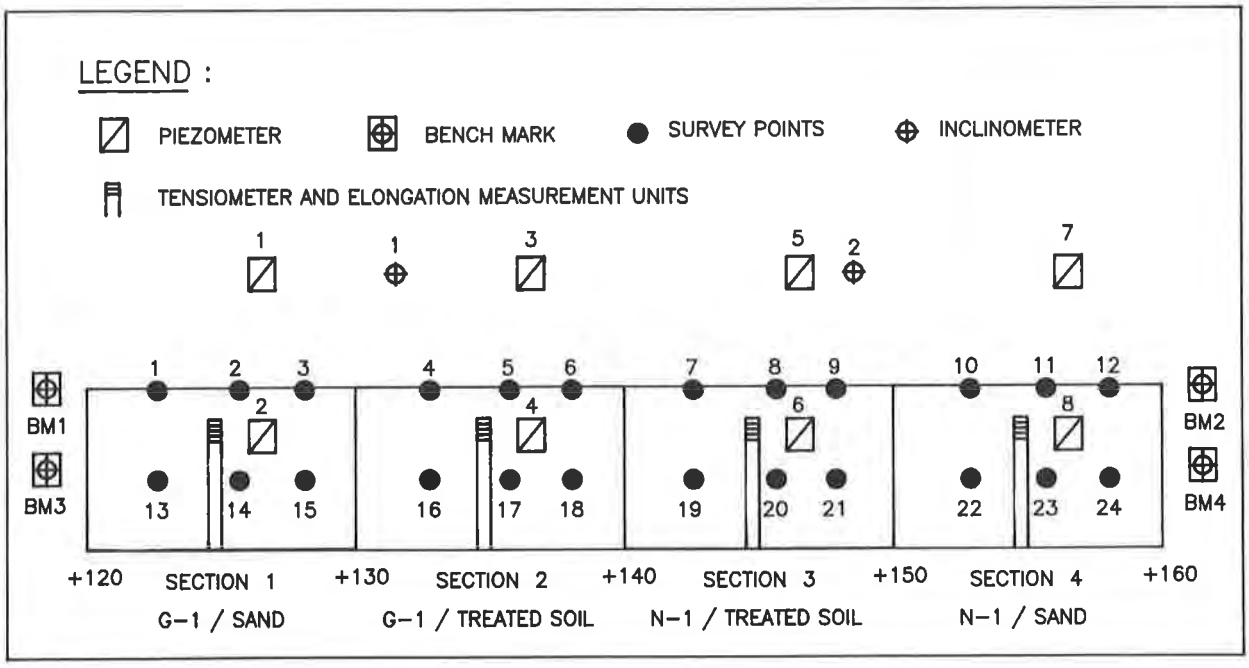

Fig. 5 Layout of instrumentation system

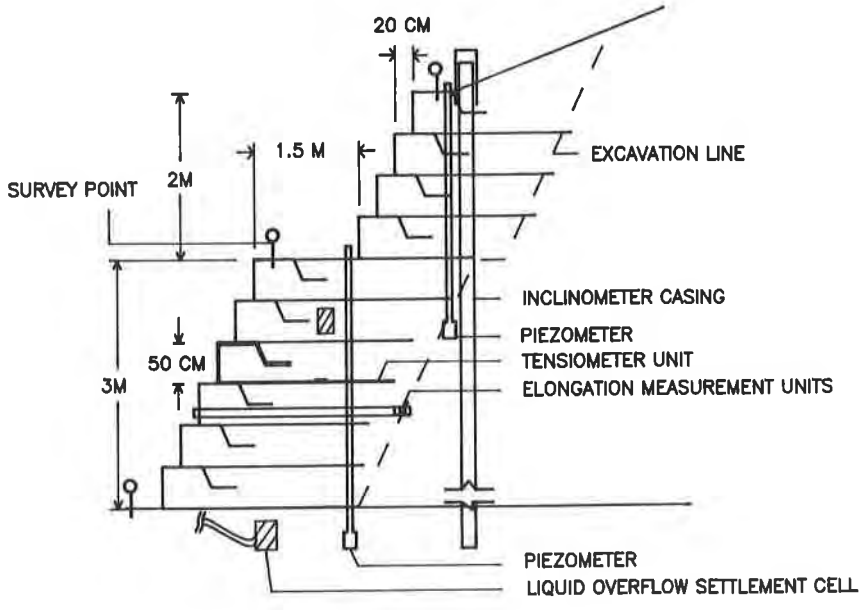

Fig. 6 Arrangement of instrumentation system from typical cross section

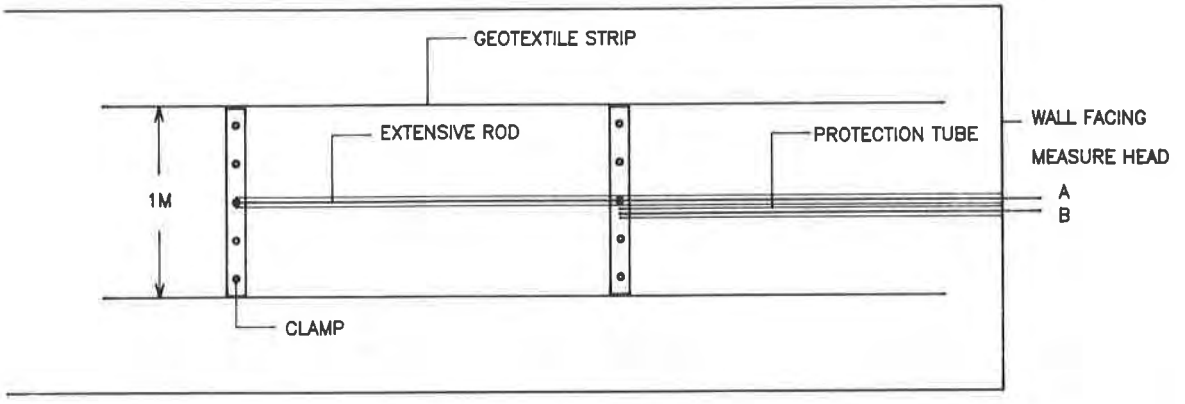

Fig. 7 Details of elongation measurement unit

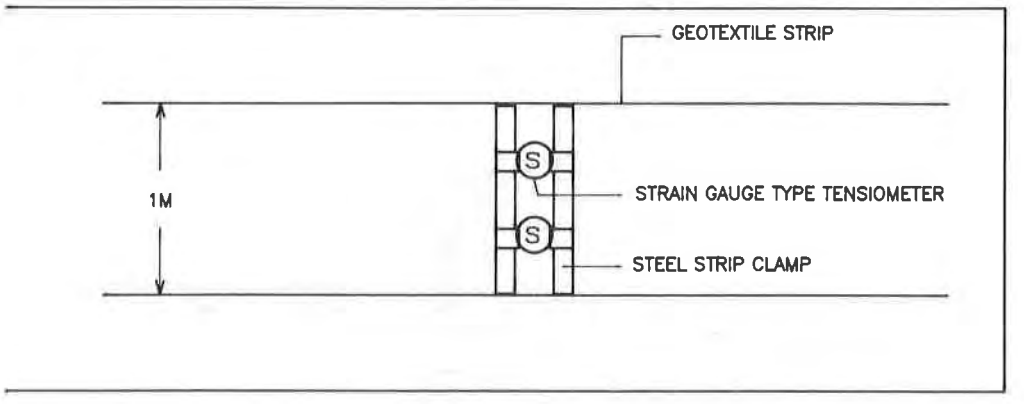

Fig. 8 Details of strain gauge type tensiometer

During construction, it was discovered that the foundation soil had been soaked and softened by the accumulated ground water. Fly ash and cement was then used to mix and compact with existing soil to stabilize the foundation. The laying of geotextile and construction of the wall followed the procedure recommended by Christopher and Holtz (1984). The photo of the finished test wall is provided in Fig. 9.

Fig. 9 Finished test wall

EVALUATION OF MONITORING PERFORMANCE OF WALL

Settlement of Foundation. Except No.1 unit was destroyed during construction, the summarized results for four sections (two units for each) are provided in Table 1. According to the periodical readings, the settlements of foundation were relatively uniform and the differential settlements were not significant. Based on the satisfactory performance of walls, it can be considered that the stabilized foundation bas been performed well.

Table 1 Summary of the settlement from wall foundation (cm)

Section	Unit	Observation Period, month								
	No.	0	1.1	2.2	3.1	4.3	5.7	6.3	10.3	11.2
Section 1	1	--	--	--	--	--	--	--	--	--
	2	0	3.2	4.5	5.5	6.7	8.0	8.1	9.2	10.1
Section 2	3	0	3.2	4.5	5.5	6.7	8.0	8.1	9.2	10.1
	4	0	2.1	3.6	5.7	6.0	7.2	7.8	10.6	11.0
Section 3	5	0	2.0	3.0	3.6	4.8	6.4	7.1	8.3	8.2
	6	0	4.4	6.4	8.3	9.5	10.7	11.1	11.7	11.9
Section 4	7	0	2.3	4.3	5.1	5.7	6.8	7.3	8.9	8.8
	8	0	2.9	5.9	6.4	8.2	9.2	10.3	11.7	12.0

Filtration and Drainage Performance. The piezometric heads obtained from the bottom and the mid-height units of wall are listed in Table 2. For these considerably low water pressure within the wall, it is confirmed that the selection of geotextiles based on the GR test is functioning successfully. The slight higher heads from fly ash-cement treated soil sections also presented the well performance. This indicates that the enlarged soil particles treated by fly ash-cement can be considered to be the filter material for mudstone.

Table 2 Summary of piezometric heads ,(m)

Piezometer No.	Observation Period, month								
	0	1.1	2.2	3.1	4.3	5.7	6.3	10.3	11.2
1 (B)	--	--	--	--	--	--	--	--	--
2 (M)	1.60	0.17	0.80	2.00	2.20	2.75	1.90	0.25	0.30
3 (B)	--	--	--	--	--	--	--	--	--
4 (M)	1.10	1.23	0.79	0.10	0.05	0.25	0.04	0.50	0.6
5 (B)	--	--	--	--	--	--	--	--	--
6 (M)	1.60	0.69	0.90	0.50	0.70	0.55	1.17	0.25	0.35
7 (B)	1.20	2.21	0.90	3.10	3.10	3.10	3.17	0.90	1.01
8 (M)	1.40	0.15	1.00	0.20	0.40	0.10	0.09	0.0	0.10
*(B) : located at bottom, (M) : located at middle height of wall									

Elongation and Stress Developments of Geotextiles. From Fig. 10, except section 1 being damaged during construction, the responded elongations of geotextiles were limited and insignificant. The values shown from Fig. 10 could be caused from the elongation due to responded stress, creep effects, settlement of foundation and outward movement by the sliding slope. Thus, the positive and the negative data were the reflected effects from the results combination.

According to the summarized data which plotted in Fig. 11, the stress development during service period of the wall has been evaluated as follow. Typhoon and heavy rainfall seasons started about two months after the wall had been completed, and the geotextiles were stressed about

4 months of bad weather period. After the typhoon season, the stress had gradually become stable in sections 1 and 3. In section 2, stress kept increasing and reached about 30% of tensile strength. For section 4 stress had not developed well. The phenomena described above matched the elongation behavior (in Fig. 10) quite well.

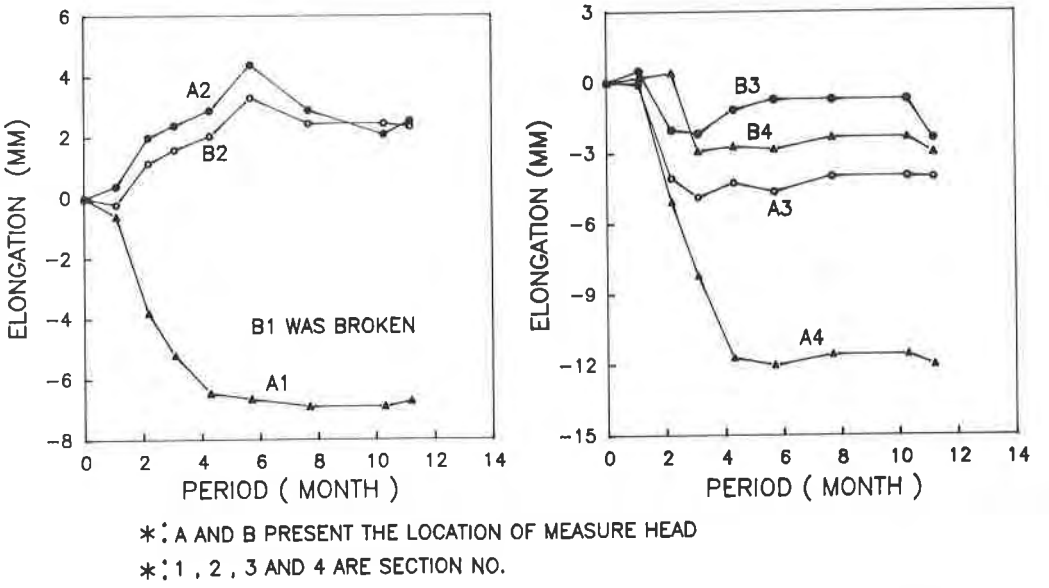

Fig. 10 Development of elongation of geotextiles

Potential of Slope Sliding. Since the inclinometer No. 2 was damaged during construction, only the results for No.1 are presented in Fig. 12. It shows that sliding of the slope occurred in the initial period, and became stable by the retaining reinforced mass. The results confirm that the geotextile reinforced earth wall, backfilled with sand or fly ash-cement treated weathered mudstone, can be effective in stabilizing the failed mudstone slope.

Lateral Movement of Test Wall. The lateral movement produced from the periodical readings are presented in Fig. 13. The results indicated that the potential of sliding of the slope was concentrated on sections 2 and 3. This shows that the middle area of the wall may produce the higher driven force and exhibited the greater movement. Except the effect of slope movement, the elongation of geotextile could be the other factor to cause the positive and negative movements of the test wall.

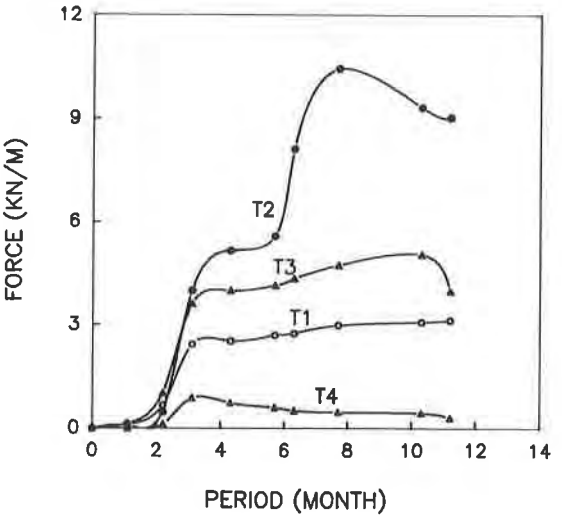

Fig. 11 Stress development from four sections

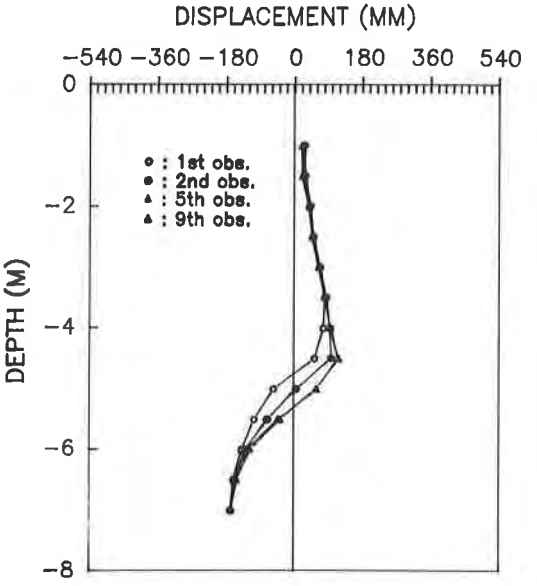

Fig. 12 Produced results from No.1 inclinometer

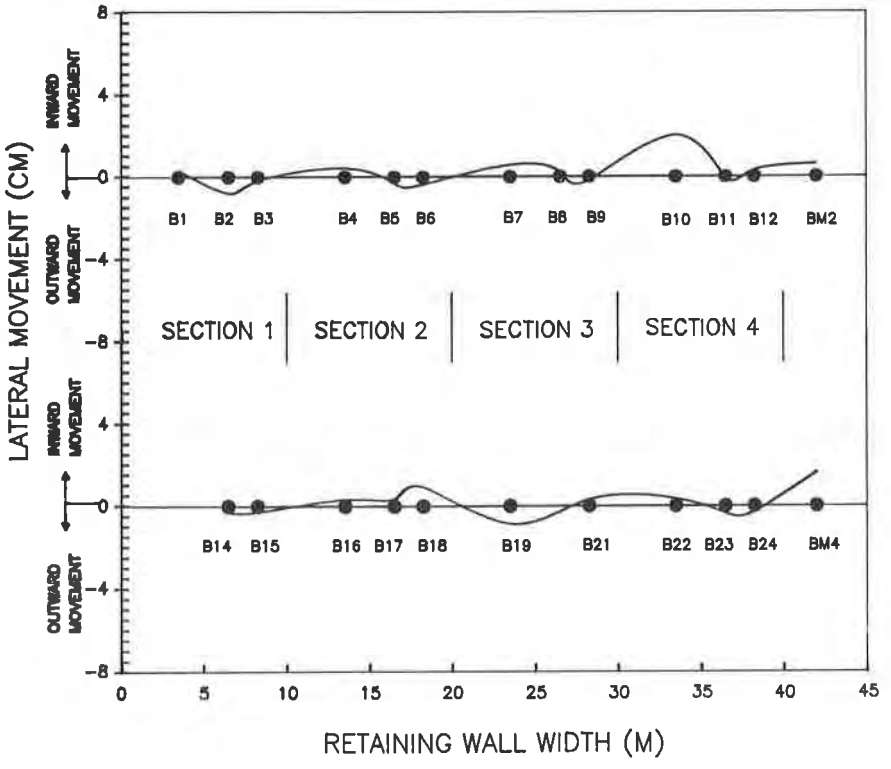

Fig. 13 Observations for lateral movement of reinforced earth wall from 24 survey points

Continuous observations had revealed that water had been seeping from wall facing, even in the dry season. It leads to believe that the softened area within the mudstone slope was still filled with the remaining ground water. At the same time, it is confirmed that the selected geotextiles and backfills have been functioned well as the suitable retaining and filter system to the mudstone slope. With comparing the overall behavior of test sections of two types of backfill, no significant difference had performed. For the cost-benefit reason, using the fly ash-cement treated material as backfill for geotextile reinforced earth wall may be considered more feasible.

CONCLUSION

A study of using the geotextile reinforced earth wall for stabilizing a weathered mudstone slope has yielded the following results:

(1) Having been subjected to the typhoon and heavy rainfall season, the test wall has performed well with the intended functions.

(2) The development of stress and elongation of geotextile within the wall can be considered as the results from the earth pressure of wall mass, settlement of foundation, creep effect and the driven force from the sliding slope.

(3) The proper selected geotextiles and backfills have formed the suitable filter system for draining remaining ground water in the mudstone slope. This may be a good answer to the problem that has been bothering local engineers for a long time.

(4) The more economic backfill----weathered mudstone treated by fly ash-cement performed as well as the commonly used sandy material.

ACKNOWLEDGEMENTS

Authors extend the deepest thanks to the National Science Council, Taiwan, Republic of China, for Grant Number, NSC-78-0414-p033-18,

which supported this study, also to the Taiwan Highway Bureau for extending their kind assistance in cooperation and support during the construction of the test site.

REFERENCE

Bell, J. R., Stilley, A.N., and Vandre, B. (1975) " Fabric Retained Earth Walls," Proc. 13 th Eng. Geol. Soils Eng. Symp., Moscow, Idaho.

Carpenter J. R. (1986) " STABL5/PC User Manual " Joint Highway Research Project, JHRP-86/14, School of Civil Engineering, Purdue University, IN. U.S.A.

Chang, T. T. and Yu, K. (1986) "Study on Lime and Fly Ash Stabilization for Lin Kou Lateritic Soil" (in chinese) Report No. NSC-74-0414-p033-01, National Science Council, Taipei, Taiwan, R.O.C.

Chang, T.T. and Yu, .k. (1987) "A study of Application of Fly Ash Stabilization for the Typical Taiwan Highway Subgrade Soils, " (in Chinese) Report No. 75-0010, College of Engnieering, Chung Yuan University, Chung Li, Taiwan, R.O.C.

Chang, T. T., Zhuang, F. S. and Chiag, C. E. (1988) "Clogging Study of Geotextile with Weathered Mudstone," Proceedings of Geosynthetics for Soil Improvement G. T. Div/ASCE, Nashville, TN, U.S.A.

Chang, T. T. and Chen, T. C. (1989) "Study of Geotextile with Fly Ash Treated Lateritic Soil and Weathered Mudstone for Slope Problem (II)," (in Chinese) Report No. NSC-78-0414-p033-18, National Science Council, Taipei, Taiwan, R.O.C.

Christopher, B. R., Holtz, R. D., (1984) "Geotextile Engineering Manual," U. S. DOT, FHWA Contract No. DTFH 61-80-C-00094. Washington, D.C. U.S.A.

Haliburton, T.A., Lawmater, J. D. and Mcguffey, V. E. (1982) "Use of Engineering Fabrics in Transportation Related Applications" Final Report Under Contract No. DTFH-80-C-0094. Washington, D. C.. U.S.A.

King, Y. P. (1985) "Slope stability of surface Treatment for Natural Mudstone Around Southwestern Taiwan, " (in Chinese) Report No. NSC-74-10, National Science Council, Taipei, Taiwan, R.O.C.

Yen, F. S. and Tsai, Y. H. (1985)"On the Physio-Chemical Properties of the Clay Minerals in the Main Mudstone Foothill of Southwestern Taiwan", (in Chinese) Report No. NSC-73-26, National Science Council, Taipei, Taiwan, R.O.C.

Design and Construction of a Geotextile Wall

Douglas Chandler
Shannon & Wilson, Inc., USA
Thomas Kirkland
Shannon & Wilson, Inc., USA

ABSTRACT

This project consisted of rehabilitating an existing access road to a private beachfront community near Everett, Washington. The road traversed a steep hillside prone to landslides. The downhill shoulder of the road consisted of a wedge of fill, the stability of which was questionable as evidenced by cracking and sloughing along the edge of the road.

Shannon & Wilson, Inc. was retained to study rehabilitation alternatives, to develop plans and specifications, and then to provide construction monitoring for the chosen alternative. The selected alternative consisted of excavating the downhill shoulder and replacing it with a geotextile-reinforced fill. The construction was completed in the autumn of 1989.

INTRODUCTION AND PROJECT DESCRIPTION

Sunny Shores is a private beachfront community located on the east shore of Puget Sound, north of Everett, Washington. Community access is via a private road that traverses a steep hillside prone to landslides. The access road, which is owned and maintained by the 38 members of the Sunny Shores Community Association, was originally cut into the steep hillside resulting in a 15- to 20-foot-high, near-vertical bank on the uphill side. The downhill shoulder was comprised of a wedge of fill with unretained slopes approaching 1 horizontal to 1 vertical (1H:1V). The stability of the downhill shoulder was questionable as evidenced by cracking and sloughing along the downhill edge of the road. The fill materials in one section of the road were reported to have been reinforced with timbers some time in the 1940s. Additional stability concerns were related to the probable rotting of this timber reinforcement.

The road was temporarily closed by a landslide in March of 1989. Shannon & Wilson, Inc. was retained to study rehabilitation alternatives, and then to develop plans and specifications for the chosen alternative. There were several basic objectives of the rehabilitation:

- replace the shoulder of the road where damaged by the landslide, and widen the remainder of the road if possible
- increase the stability of the downhill shoulder of the road

- maintain or improve the existing global stability of the road
- provide a guard rail
- provide a cost effective solution

A subsurface exploration program consisting of nine backhoe test pits was completed to determine the subsurface conditions along the road alignment. In general, the subsurface materials consisted of dense to very dense granular natural soil or fill materials or weathered rock for most of the road, with the downhill shoulder comprised of medium dense fill or slough with abundant roots and organics. The downhill shoulder was generally susceptible to sloughing and ravelling. In order to widen the road and provide guard rails, some means of providing a near-vertical face to the downhill shoulder was needed. Several general rehabilitation alternatives were considered including:

- retaining structure consisting of soldier piles with lagging
- conventional cast-in-place concrete retaining wall
- gravity retaining wall of gabions or concrete ecology blocks
- gravity retaining wall constructed by reinforcing the existing shoulder materials

The idea of reinforcing the existing granular fill that comprised the downhill shoulder was attractive because it would utilize the relatively high strength of most of the existing materials. Several combinations of reinforcement/wall facing alternatives were considered. In general, high strength reinforcement (such as geogrids) allow greater reinforcement spacing, but also require longer embedment lengths to develop the full tension in the reinforcement. Since a primary constraint in this case was to minimize the width of the excavation (so that the narrow road would remain passable to construction equipment throughout the construction), a relatively low-strength geotextile reinforcement placed at a relatively small spacing was advantageous for this project. It was also thought that the thinner reinforcement spacing would not be a disadvantage in this case since relatively small, hand-operated compaction equipment (requiring thin lifts to achieve compaction) would be required in the restricted available space for the construction anyway. Based on these factors, and the general simplicity of the system, the selected alternative was to use geotextile fabric for reinforcement, with a shotcrete covering for protection from vandalism and ultraviolet degradation.

The construction thus consisted of excavating the downhill shoulder embankment and replacing it with a geotextile-reinforced fill comprised of the non-organic excavated material. A typical test pit log showing the approximate relative location of the geotextile wall is shown in Figure 1. The resulting road was wide enough to allow the use of concrete Jersey barrier guard rails. The wall is founded in the underlying, very dense, glacially consolidated advance outwash and/or weathered sandstone.

DESIGN METHODS FOR INTERNAL STABILITY

Both the internal and external stability must be considered in the design of geotextile-reinforced fills. To provide for internal stability of the reinforced section, the general design methods described

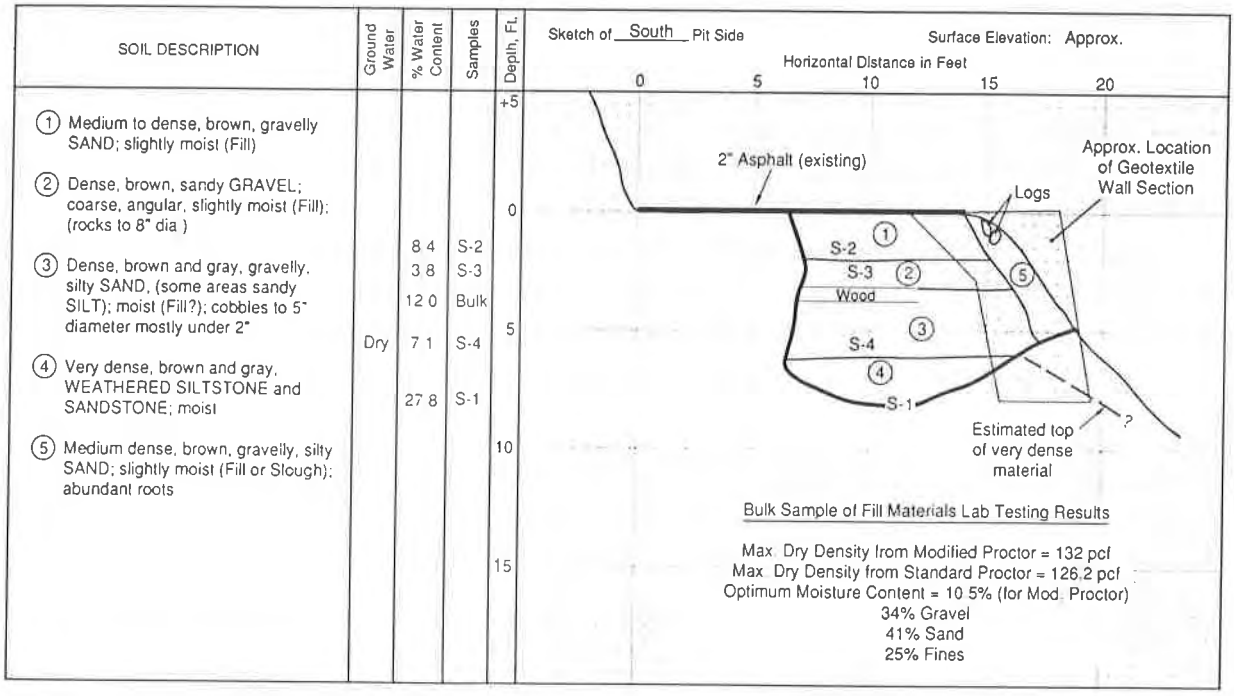

Figure 1. Typical test pit log showing relative location of geotextile wall.

by Koerner (1986) were used. Design factors that influence the internal stability of the wall include lift thickness (vertical spacing of the fabric), allowable stress in the fabric, fabric embedment length, the soil strength and unit weight, and the surface loading conditions.

The basic design criteria is to balance the fabric tensile strength and spacing with the horizontal stresses in the fill. The horizontal stresses in the fill are calculated assuming at rest conditions (which is conservative) where the coefficient of at rest earth pressure (K_o) is assumed to equal 1 - sin ϕ. Boussinesq elastic theory is used to account for the horizontal stresses induced by live loads on the road surface.

For this project, the design equations and factors were compiled into a spread sheet so that the sensitivity of the various design factors could be easily explored. The spread sheet allowed the designer to try different combinations of wall heights, design loadings, lift thicknesses, soil and fabric properties, and other pertinent design factors with ease. The final design assumed a 10-foot-high wall with 12-inch vertical fabric spacing down to the 6-foot depth, and 9-inch vertical fabric spacing for depths between 6 feet and 10 feet, and an allowable fabric stress of 800 pounds per linear foot.

The basic design elements of the wall are depicted in Figure 2. Based on the calculated required embedment length, the fabric embedment was specified to extend horizontally behind the toe of the wall a distance equal to the height of the fabric layer above the toe, or a minimum of 4 feet behind the face

of the wall. The design included a drainage chimney of imported sand and gravel filter/drainage material against the excavation face. A slotted drain pipe to collect seepage was specified at the base of the wall. The face of the wall was built at a batter of approximately 1H:6V and was covered with shotcrete to protect the geotextile fabric from ultra-violet rays and possible vandalism.

The geotextile specifications were generic in nature and specified minimum values of common test methods. The required allowable fabric tensile strength of 800 pounds per linear foot was specified by requiring a minimum Grab Tensile Strength of 200 pounds. Minimum elongation at maximum tensile stress, puncture strength, burst strength, and trapezoidal tear were specified to achieve minimum survivability for severe installation stresses as recommended by the AASHTO-AGC-ARTBA Task Force 25. Fabric opening characteristics of the fabric were specified to provide retention of the fill and to assure that the geotextile was more permeable than the surrounding materials (Christopher and Holtz, 1985).

A theoretical factor of safety of 1.4 for internal stability was used in the design of this embankment. Load testing of similarly reinforced embankments indicate that the actual factor of safety is higher than the calculated factor of safety (Koerner, 1986).

GLOBAL STABILITY

The external stability of the geotextile wall must also be considered. The external or global stability takes into account other possible modes of failure such as overturning, sliding, and foundation failures. These modes of failure are common to all wall systems and can be treated the same as other types of gravity retaining walls.

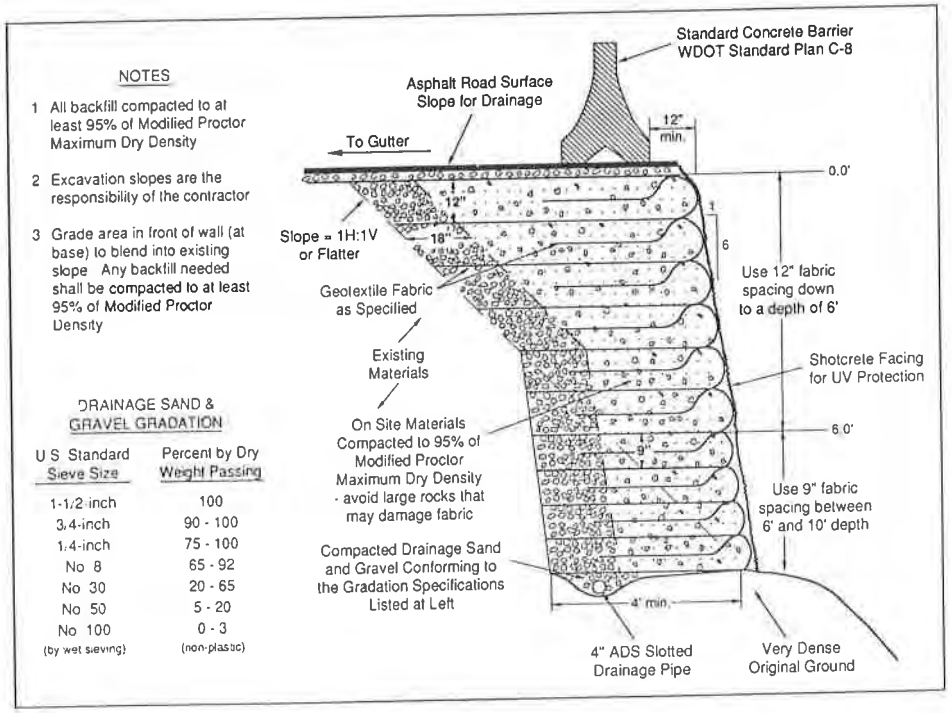

Figure 2. Typical wall section.

Rankine active earth pressures were assumed for the existing, in-place road materials in calculating the stability of the wall section against overturning and sliding at the base. Individual calculations were performed for several specific cross sections, and for the maximum section assuming average backfill conditions. The minimum factor of safety against overturning about the toe was 5.0, and the minimum factor of safety against sliding at the base was 2.5.

Global stability against foundation failures is not as straightforward. Foundation support at any particular location on the steep hillside is dependent upon both the local topography and the strength of the underlying slope materials. Since both the topography and slope materials vary along the length of the project, a detailed slope stability analysis at any one location would be of limited value.

A more general approach to the slope stability question was used in this case. The local geologic conditions indicated that the project area is relatively stable against deep-seated failures and fairly active with surficial failures. Observations which support this include:

- The subsurface materials were generally observed to be very dense, competent, granular materials that were weathered to a relatively shallow depth. This type of subsurface profile is generally not prone to deep-seated failures.
- Scarps from numerous surficial failures were noted in the project vicinity.
- The hillslope landform, which is a relatively uniform steep slope as opposed to hummocky terrain, is indicative of near-surface sloughing rather than deep-seated failures.
- The existing road has apparently had no problems resulting from deep-seated failures and, in fact, survived a substantial impact loading from the March 12, 1989 landslide with little damage other than to the downhill shoulder.

Since the previous existing configuration did not appear to be especially susceptible to deep-seated failures, and the proposed rehabilitation did not significantly increase the loading on the slope, it was reasoned that the proposed road rehabilitation would not significantly change the existing global stability of the Sunny Shores access road. It was recognized and communicated to the client that the risks from landslides originating from upslope of the road and from foundation failures would not be significantly changed by the rehabilitation and thus would still be present. Several recommendations separate from the road rehabilitation were provided to reduce these risks.

CONSTRUCTION

The construction sequence adapted from the U.S. Forest Service and presented in Koerner (1986) was followed. The general construction sequence is summarized as follows:

1) Excavate the loose shoulder materials down to the dense underlying materials.
2) Place the lowest geotextile layer directly on the foundation soil. In this case, suitable foundation soils were encountered at depths of between 5 and 10 feet below the previously existing road surface.

3) A wooden form of height slightly greater than the lift height was placed on the ground surface (or on the previously placed lift after the first layer was completed). This form was a series of metal "L" brackets with a continuous wooden brace board running along the face of the wall.

4) The fabric was then unrolled and positioned so that approximately 4 feet hung over the top of the form.

5) Backfill was then placed on the fabric up to approximately one-half of its lift height and compacted. Material was placed with an excavator and/or by hand methods. A freely draining sand was used as backfill for all areas within 1.5 feet of the excavation face, and the on-site materials were utilized for the remainder of the backfill. Compaction was to achieve at least 95 percent of the Modified Proctor maximum dry density and was accomplished using a "walk-behind" vibratory roller.

6) A windrow of soil was placed adjacent to the face of the wall up to the full lift thickness and the loose end of the fabric (i.e., its "tail") was folded back over the wooden form onto the windrow.

7) The remaining lift thickness behind the windrow was then completed atop the folded back geotextile tail to the planned geotextile spacing and suitably compacted.

8) The wooden form was removed from the front of, and the metal brackets from beneath the lift and reset on top of it in preparation of the next higher lift. A slight batter of 1H:6V was used for this wall.

Although the contractor had no previous experience building geotextile-reinforced walls, the construction went relatively smoothly. There were some initial difficulties in placing the fabric tightly (without wrinkles), and in achieving the specified compaction of the backfill due to the extremely dry conditions during construction. However, a small amount of practice in placing the fabric, and the addition of water to the backfill, solved these initial difficulties.

The rehabilitated road section was completed in the autumn of 1989 and is approximately 625 feet long, averaging about 7 feet high. The unit cost for the wall construction was $16.80 per square foot. The project was substantially completed within budget in 6 weeks at a total cost of $150,000, which included the wall construction, drain lines, collection basins, guard rails, and final paving of the entire road surface. A summary photo record of the project is shown in photos 1 through 6.

PERFORMANCE

The new wall has survived two upslope landslides which deposited soil and debris on the road during the winter of 1989-90, with no noticeable damage or deflections. There has been some localized settlement within the geotextile-reinforced fill in the area where the wall construction was first begun. The settlement caused localized cracking of the overlying pavement. The crack widths were monitored several months after they were first noticed. The widening of the cracks appeared to cease about 9 months after construction, at which time the cracks were repaired by the contractor.

The settlement is attributed to the initial placement of the geotextile too loosely, and/or possible poor compaction at the start of construction. The settlement apparently occurred gradually as the soil/fabric system gradually tightened up due to vibrations from traffic. No significant cracking of the shotcrete covering has been observed to date.

Another condition that is currently being monitored is due to the continued sloughing of slide debris which was deposited by the March, 1988 landslide immediately below the road. Most of the slide debris was removed prior to the construction, but in this area the equipment was not able to reach or access all the debris for removal. The sloughing has exposed the edge of a layer of very dense advance outwash gravel, which is underlying the road. The concern is for gradual undermining of the foundation support of the road. Several alternatives to protect the exposed gravel from erosion are currently being considered.

ACKNOWLEDGEMENTS

Project Owner:	Sunny Shores Community Association Mitch Cogdill, President
Engineer:	Shannon & Wilson, Inc. Seattle, Washington
Contractor:	Wilder Construction Company, Inc. Everett, Washington David Gent, Project Manager

REFERENCES

Christopher, B.T., and Holtz, R.D. (1985), "FHWA Geotextile Engineering Manual".

Koerner, R.M. (1986), "Designing with Geosynthetics", Prentice-Hall, Englewood Cliffs, New Jersey.

PHOTO RECORD

Photo 1. An aerial view of the Sunny Shores Road after a landslide closed the road (March 1989).

Photo 2. A view of the completed road traversing the old landslide path (November 1989).

Photos 3 through 6 show a view of the road before, during, and after construction.

Photo 3. Before construction (March 1989).

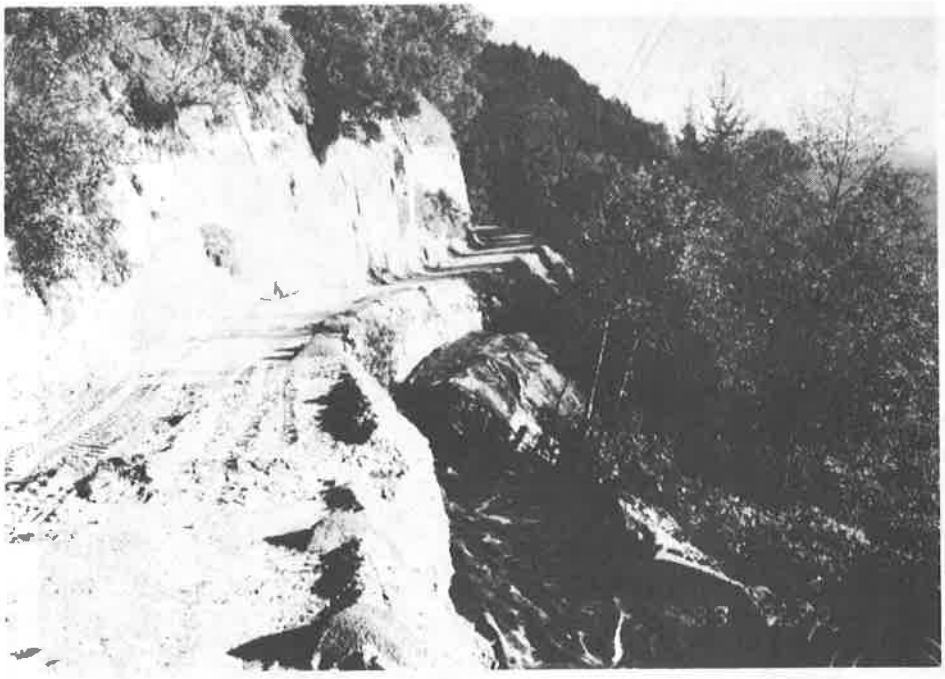

Photo 4. After excavating to the very dense underlying materials and preparing to place the first layer (September 1989).

Photo 5. Before paving and shotcreting (October 1989).

Photo 6. Substantially completed wall (November 1989).

Geogrid Reinforced Soil Wall Bridge Replacement at Picnic Point, Snohomish County, Washington

Roland D. Maynard, P. E.
Snohomish County Department of Public Works, USA
Steve E. Thomsen, P. E.
Snohomish County Department of Public Works, USA
Paul W. Grant, P. E.
Shannon and Wilson, Inc., USA

ABSTRACT

In 1957, a major landslide occurred along Puget Sound Boulevard at the project location requiring construction of a wood trestle bridge to span the slide. As a result of the deterioration of this bridge, Snohomish County hired a consulting firm in 1978 to develop a design package for the bridge replacement. Prior to finalization of the project, a major slide occurred in 1983 that caused closure of Puget Sound Boulevard for several months. In 1985, Snohomish County entered into an agreement with a local consultant to jointly perform a VE study on this project. The recommendation of the VE study was to replace the existing bridge with a reinforced soil wall. Final design of the reinforced soil wall was completed in May of 1987. The contract was awarded in June of 1987 and construction was completed in December of 1987. The bridge replacement project was a unique and economical solution to stabilize and span a slide zone utilizing a reinforced soil wall. By investing the time in conducting a thorough site investigation and by preparing a VE study, the County was able to save $2,000,000 and still effectively solve a reoccurring problem. The project was a FHWA Experimental Features project and was awarded the 1988 Award of Excellence by the Washington State DOT State Aid organization.

BACKGROUND

Puget Sound Boulevard is a narrow two lane road between the cities of Edmonds and Everett, Washington. Puget Sound Boulevard originally connected the communities of Norma Beach to the south and Picnic Point to the north (Figure 3). Several slides over the years have severed the southern section of Puget Sound Boulevard so that access is available only from the north. The topography is steep and affords limited access to the 30 residences in this area. The people who live here trade this inconvenience for a secluded park like setting that includes beautiful views to the west of Puget Sound and the Olympic Mountains.

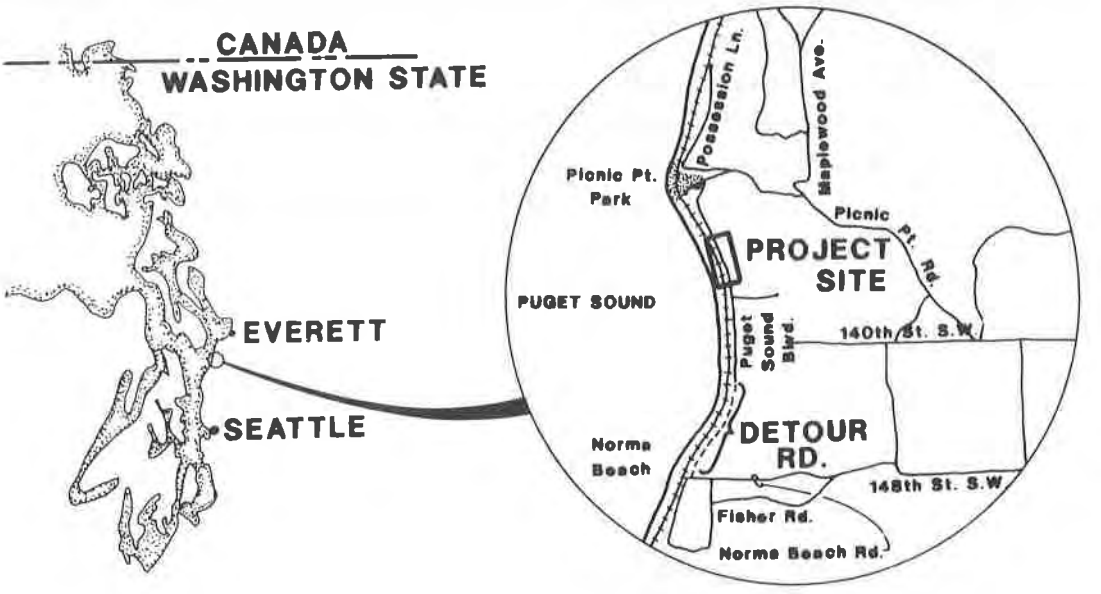

Figure 1. Vicinity Map

Site History. Puget Sound Boulevard area has been plagued by landslides in both ancient and recent history. Puget Sound Boulevard is located within a 2,000 foot (see Table 2 on page 14 for conversion from English to SI units) long ancient landslide which extends approximately from Puget Sound eastward to 700 feet east of the Boulevard (see Figure 2). It is believed that this original landslide occurred roughly 10,000 years ago. In 1957, a major landslide occurred at the project location requiring construction of a wood trestle bridge (Picnic Point Bridge) to span the slide. Later in 1961, a major landslide severed Puget Sound Boulevard 2100 feet south of the bridge. Subsequent landslides at both ends of the original section of the bridge in 1964 and 1969 resulted in the eventual lengthening of the structure on both ends. In total, approximately 20 landslides have occurred in the vicinity of the bridge since 1940 (8).

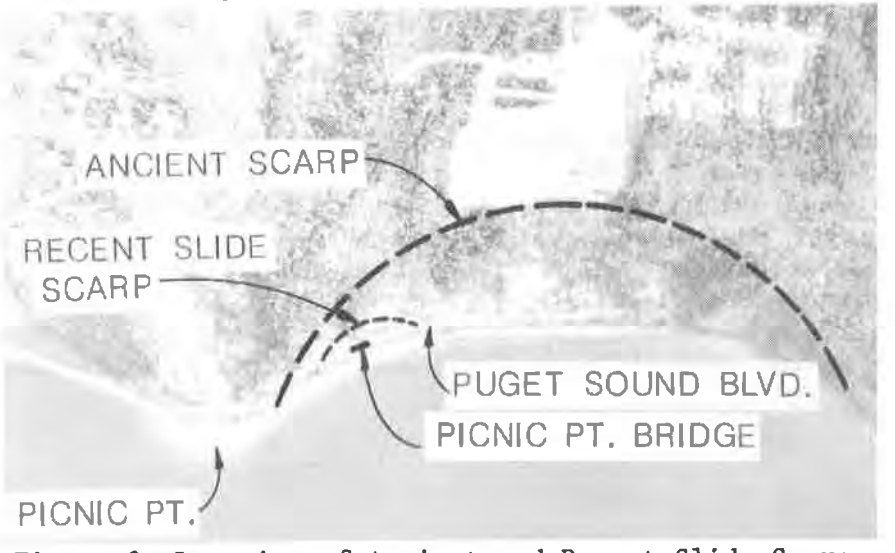

Figure 2. Location of Ancient and Recent Slide Scarps

Initial Design. Because the existing bridge was located in an area that had experienced numerous slides in the past and because of the structural condition of the bridge, Snohomish County entered into an agreement with an independent consultant in 1978 to develop plans and specifications for the replacement of the existing bridge (1,2,3 and 6). The consultant's suggestions for replacing the bridge consisted of removing unstable soil at the site and buttressing the hillside with two metal crib walls which would retain a structural granular fill and a temporary soldier pile and tieback wall. This design was developed for 800 feet of roadway alignment. The estimated cost for this design scheme was $3 million dollars (6).

Emergency Slide Repair. Prior to the finalization of the consultant's plans and specifications, a major slide occurred at the southerly end of the bridge that caused closure of Puget Sound Boulevard for several months. This slide occurred in the winter of 1983. When the slide progressed to the point of endangering an existing home, Snohomish County initiated an emergency slide repair project. This project consisted of construction of a permanent tieback wall on the uphill side of the existing road and a cantilever soldier pile wall located on the downhill side. Additionally, an ecology block wall was constructed along the western right-of-way of the County road to retain fill soils which were placed to help restore the roadway alignment. The cost of this repair for 150 lineal feet of roadway was approximately $500,000 (4,5).

Value Engineering Study. In 1985, Snohomish County entered into an agreement with the consulting firm of Sverdrup & Parcel and Associates to conduct a value engineering (VE) study of the original recommended design and to explore possible cost savings of other designs. The VE team consisted of personnel from Sverdrup & Parcell, Shannon & Wilson, Inc., Value Engineering Services Transworld and Snohomish County. The recommendation of the VE study was to replace the existing bridge with an reinforced soil wall which would be constructed over a subsurface drainage system beneath the upslope side of the roadway. The estimated cost for this design proposal was $1.2 million. This represented a cost savings of over 50% from the original design recommendations (12).

SUBSURFACE CONDITIONS

Thirty borings have been advanced in the area of the bridge replacement by various consultants (1,2,3,4,5,7). Subsurface conditions along the alignment typically consist of medium dense, sandy silts to silty sands overlying a very stiff to hard clayey silt at approximately elevation 40. This hard clayey silt layer acts as a barrier to the vertical movement of the groundwater. During extended periods of wet weather, groundwater seeps out of the slope at this contact point. This seepage causes the exposed soils to become saturated and loose their strength. This results in a slow, steady, downhill creep of the near-surface soils. A similar mechanism is generally assumed to be the cause of the slide which damaged the road in the winter of 1983 (4,5).

PROJECT DESIGN

In early summer of 1986, Snohomish County decided to proceed with the plans, specifications and estimate (PS&E) for construction of an earth reinforced wall. Construction was scheduled for the summer of 1987. Shannon and Wilson, Inc. was selected as the geotechnical consultant to work jointly with Snohomish County to develop the design and the PS&E package for this project.

Preliminary Considerations. Staging was an important consideration for this project. The existing bridge would have to be completely removed and the hillside excavated to make way for construction of the earth reinforced wall and subdrains while providing continuous access for the local residents. The project would also have to be constructed during the driest possible time of the year to reduce the possibility of increased slide activity caused by wet soil conditions.

Selection of Wall System. Three types of earth reinforced wall systems were chosen for this project and were listed as acceptable alternatives in the bid documents. The criteria for choosing the wall system was based on existing site conditions and the restraints listed above. The hillside on which the bridge was being replaced was unstable and likely to move and shift on a long term basis. The wall system needed to be somewhat flexible, able to move with the hillside and constructed of components that were easy to transport, lift and move around within the narrow available construction work area. The cost of the wall system was also a factor that affected the choice of the alternates. The following alternatives were considered:

1. Welded Wire Retaining Wall
2. Geogrid Wall
3. Geotextile Fabric Wall

Wall Design. The design of the wall required special considerations for both the temporary and permanent stability of the overall system. It was desired to maximize the amount of slide debris removal during construction to allow installation of the subdrains which would permanently lower the water table in the area. This in turn would provide a stable base for the earth reinforced wall.

The lowest possible ground water table was desired in order to improve the local factor of safety for the stability of the hillside. However, increasing the depth of the cut to install the drains decreased the stability of the hillside during the temporary construction. It was necessary to establish a critical balance between an allowable factor of safety during construction and a desirable factor of safety for the completed product. Stability analyses were conducted for the project to evaluate both the construction and long term factors of safety. The engineering properties used in the analysis, which are shown on Figure 3, were derived based upon prior experience with similar materials (fill and clay) or from back analysis of the stability of the existing slopes in the project area landslide materials. The results of the analysis indicated that a temporary cut to elevation 50 would allow a construction factor of safety slightly greater than 1 a permanent factor of safety of about 1.4.

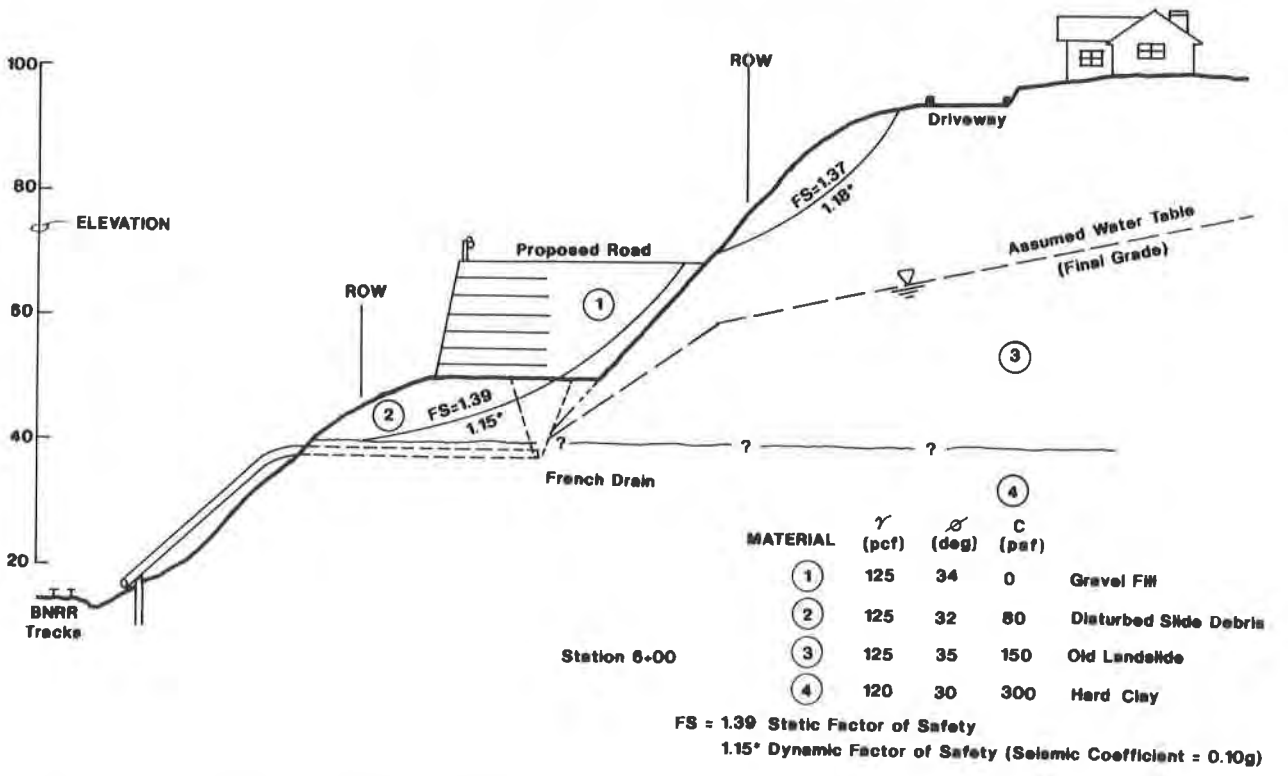

Figure 3. Stability of Final Design Conditions

The wall systems were designed utilizing industry recognized design methods and guidelines. These design guidelines provided information on the layer thickness, length of embedment of the grid and/or fabric, strength, and backfill material grain size parameters for the grids. A typical wall section is shown in Figure 4. The factors of safety (FS) for the wall shown in Figure 4 are compared with the FS established in the design criteria in Table 1 below.

Table 1. Computed FS vs Design Criteria FS

Condition	Computed FS	Design Criteria FS
Sliding	2.7	1.5
Overturning	4.1	2.0
Bearing Pressure	2.1	2.0
Pullout	1.9	1.5

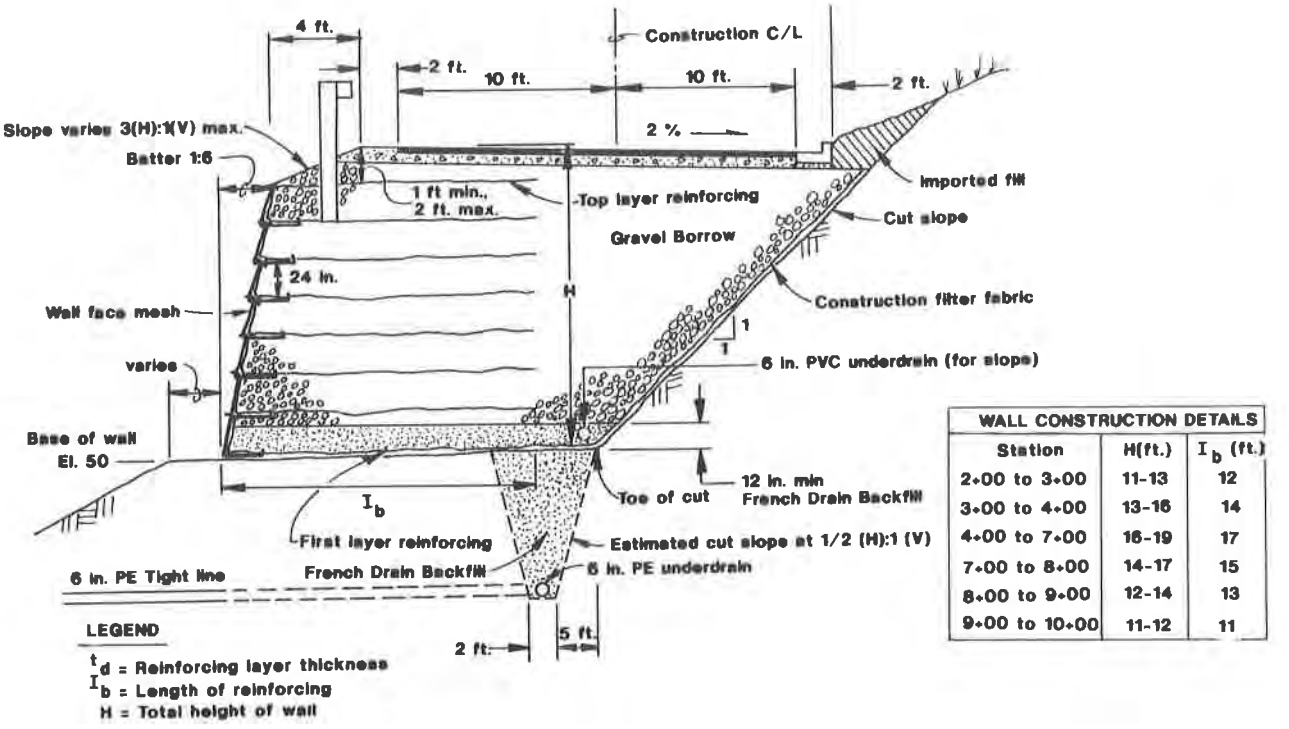

WALL CONSTRUCTION DETAILS

Station	H(ft.)	I_b (ft.)
2+00 to 3+00	11-13	12
3+00 to 4+00	13-16	14
4+00 to 7+00	16-19	17
7+00 to 8+00	14-17	15
8+00 to 9+00	12-14	13
9+00 to 10+00	11-12	11

Figure 4. Typical Wall Section

Following is a summary of the design parameters used for the three wall alternatives (8).

Welded Wire Wall. All wire and welded wire fabric had to conform to ASTM A-82 (wire) and ASTM A-185 (fabric), with a yield strength of 65 ksi. Required wire size numbers were W4.5, W7 and W9 depending upon the height of the wall. The required length of reinforcing is listed in Figure 4 above. The vertical spacing of the reinforcing layers was 18 inches. Wall face mesh and screens were to be installed at the face of the wall to retain the compacted gravel backfill within the structure. For long term protection, the wire mesh was to be hot dip galvanized with a 2.0 ounce per square foot zinc coated weight in accordance with ASTM A-123 after the mesh was bent and welded.

Geotextile & Geogrid Wall. The wall design required allowable long term design strengths of 1000 pounds per linear foot for walls 8 feet or less in height, and strengths of 2000 pounds per linear foot at locations overlain by 8 or more feet of wall height (long term strengths given are for a strain of 10%). The required length of reinforcing is listed in Figure 4 above. The vertical spacing of the reinforcing layers was 24 inches. For the geotextile wall, lapping perpendicular to the wall face was allowed provided that the minimum overlap was 3 feet. Splices parallel to the wall face were not allowed. For the geogrid wall, overlapping of 1-1/2 inches was required in the longitudinal direction and overlapping of 4 feet was required in the transverse direction. For both wall types, a shotcrete facing was required to protect the reinforcing material from ultraviolet strength degradation (8).

Subdrainage Design. The subdrain system design consisted of a trench drain extending from elevation 50 down to elevation 38. The purpose of the trench was to intercept the ground water at the impervious clayey silt layer. The trench drain system was designed as eight individual "L" shaped segments. This was done for ease of construction in anticipated caving soil conditions and to insure that the overall system remained operable, i.e., if one drain failed it would not interfere with operation of other drains in the system. Due to the need to get the subdrains constructed with a minimum of delay, no shoring or cribbing was used. This required excavating the trench, placing perforated drain pipe, and backfilling with drain sand in one operation without people in the trench. The trench was designed to be excavated with 1/2:1 side slopes to minimize the caving of soils. The pipe in the bottom of the trench was tightlined down the hillside to an existing Burlington Northern Railroad (BNRR) drainage ditch. This required obtaining drainage easements from BNRR as well as an agreement to use their drainage facilities for the County's project. The backfill for the trench drains was designed as a coarse drain sand or fine pea gravel to eliminate the need for filter cloth and compaction of lifts. Again, this was to speed construction time for the trench drains (8).

GENERAL CONSTRUCTION

Final design of the reinforced soil wall was completed in May 1987, and the contract was awarded in June 1987. The Engineer's estimate for the project was $750,500. A total of four contractors bid on the project. The low bid was $788,688 (this price included the additional construction of a detour road to the south to provide access for the contractor and residents during construction); the highest bid for the work was $872,732.

Shannon & Wilson, Inc. were again used on the construction phase of this project to inspect and advise on the construction of the trench drains and to help solve geotechnical related problems which were expected to arise during construction. Snohomish County was responsible for overall project management, contract administration, materials testing, and construction inspection.

Revised Wall Face Design. The contractor (Dell Johnson Construction, Inc.) proposed using the geogrid product to construct the wall using a revised wall face design (Figure 5a). An "L" shaped wire basket made of galvanized No. 5 wire, welded into a 4 inch square grid pattern was proposed at the wall face in place of wrapping the geogrid material around the wall face. The contractors motive for proposing the welded wire face was to eliminate the temporary wood form at the wall face and also to eliminate the permanent shotcrete facing, as the wire baskets with extra zinc galvanization and the UV protection of the geogrid material should provide adequate long term performance. The contractors proposal to use an alternate face design was reviewed, revised, and approved for use (9). Since the contractors revised face design was relatively new and had not been used on any previous highway projects, Snohomish County applied and received approval from FHWA to reclass the project as experimental. This would qualify the County for funds to repair any problems that might occur in the untested wall and face system.

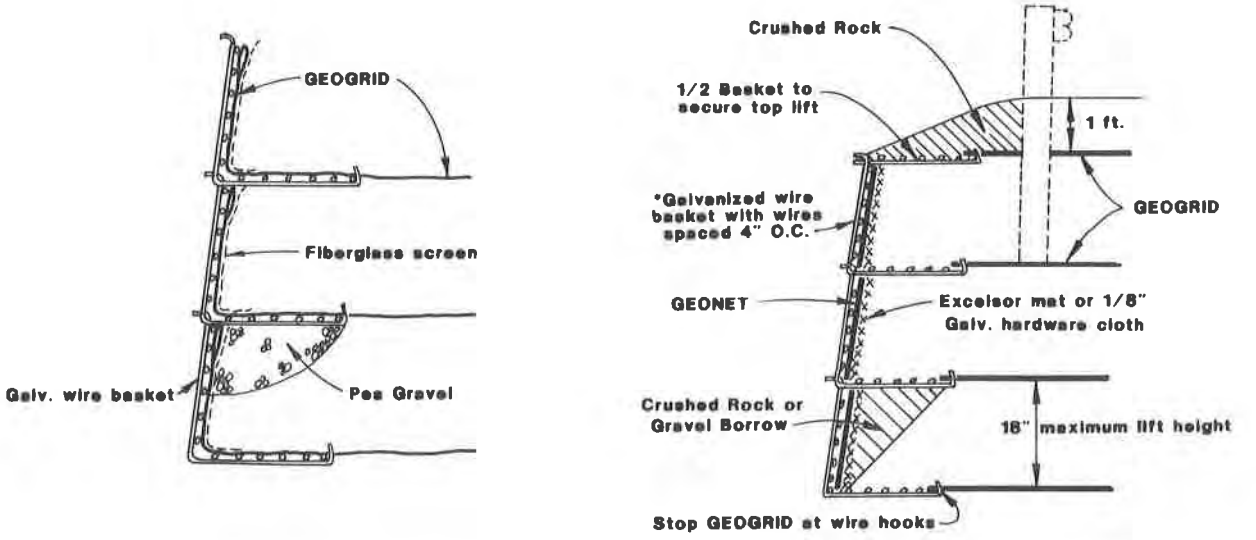

Figure 5. Revised Wall Face Detail,
(a) As-built, (b) Preferred Alternative

Demolition & Earthwork. The contractor was given a notice to proceed effective July 6, 1987. The first order of work was construction of the temporary detour road and the pedestrian trail around the site. The contractor then moved onto the bridge site and began bridge demolition and excavation to elevation 50 simultaneously. The contractor used a large track mounted hydraulic hoe to perform the combination demolition/excavation work by sitting on the existing wood trestle bridge and alternately loading dump trucks with bridge debris and then native soils to be wasted off site. This system worked well but the contractor could not reach the entire excavation area (Figure 6). As a result a portion of the material on the west side of the cut had to remain for excavation at a latter date. During excavation perched water conditions were encountered at elevation 50 in several locations (Figure 7). This soil was highly saturated with water and required some method of draining or bridging before the contractor could place equipment on the subgrade platform (elev. 50). This problem was solved by overexcavating 2 feet, constructing shallow temporary drains, and placing 2 feet of fill over a 4.0 oz/sy woven geotextile (11). This formed a work platform that was suitable for supporting construction traffic within a few days of installation of the platform. After the construction platform was completed, the contractor excavated and installed the trench drain system.

Figure 6. Bridge Demolition and Excavation

Figure 7. Saturated Soil Conditions at Elevation 50

Wall Construction. The reinforced soil wall was constructed in two foot lifts. Wire baskets were laid out in advance of the geogrid material along the staked alignment of the wall toe. The contractor then laid out the geogrid to the specified embedment length and held it down by hand shoveling fill material onto the loose ends (Figure 8). Drain sand (1st lift) was then belly dumped onto the geogrid. During the dumping operation the geogrid would push and wrinkle when the trucks drove across it. In addition, the trucks bogged down and would get stuck in the drain sand requiring a bulldozer to tow then through the job. The bulldozer tracks would sometimes pinch the wrinkles in the geogrid pulling the fabric up. This required hand digging several cubic yards of sand to repair the damages. The contractor soon modified his placement procedure by using wood stakes at the loose ends of the geogrid along with more hog rings along the joints and at the baskets to more firmly hold the geogrid in place. These changes greatly improved the contractors success at keeping the geogrid buried with a minimum of wrinkles. The placement of fill material for each lift was accomplished in 2-one foot lifts with vibratory compaction in each lift. Compaction within 2 to 3 feet of the wall face was by hand tamping and/or foot tamping near the bottom of each lift followed by compaction with a small walk behind mechanical compactor near the top of each lift. Each layer of baskets was placed with offsetting joints between lifts similar to laying bricks. This eliminated a continuous joint in the wire baskets. Each layer of geogrid was hooked to the wire face basket. Before staking each layer of geogrid, the contractor used pry bars and a wood jig with a carpenters level to adjust the wall face batter of the preceding lift. After proper adjustment for batter, the geogrid was staked in place and the first 1 foot of the next lift of fill material was placed over the geogrid and compacted. To maintain the batter of the baskets during fill placement, the contractor found it beneficial to use a tie wire. These tie wires were fastened at regular intervals between the horizontal and vertical legs of the baskets. The wires were installed after the geogrid and fiberglass screening were in place.

Figure 8. Beginning Wall Construction

Fill Material. The fill material specified was a pit run Gravel Borrow. At first the material was very clean and consequently difficult to compact to the required specification. In addition, haul trucks continued to get stuck in the fill material. The contractor then started hauling from a different location in the pit where the material contained more fines. This material still met the Gravel Borrow specification, but compacted to 95% of its maximum dry density utilizing less effort than the original material. The required density was obtained with 2-3 passes of a vibratory roller (Figure 9). Trucks stopped getting stuck and the contractors daily production rates increased. The task of placing wire baskets, geogrid, and screen material at the face was a labor intensive job. The contractor maintained a minimum of 4 people working in the grade to place these materials.

Figure 9. Compaction Was Performed Using a Vibratory Steel Drum Roller

Face Bulging. Bulging, amounting to 6-7 inches, was noted at the face of the wall in the lower lifts after 3 or 4 lifts had been completed. While it was initially believed that the bulging resulted from insufficient compaction of the pea gravel backfill used at the face of the wall (Figure 5a), it was later concluded that the bulging was more attributed to a combination of details and materials used at the wall face. Specifically, construction details at the wall face (Figure 5a) resulted in a condition in which significant vertical loading was transmitted through the wire cage at the wall face. This load occurred because the bottom layer of geogrid, which extended to the face of the wall, would not allow the soil to migrate between lifts. Hence, all the soil weight at the wall face was transferred to the wire baskets. Since the construction detail of the baskets did not permit relative vertical movement between the baskets, the vertical load resulted in a flexural failure of the wire in the baskets. The

amount of bulging and settlement was self-limiting as the load carried by the vertical elements in the wire baskets was transferred to the soil contained within the lift. Thus, the bulging turned out to be more of a nuisance aesthetically than a structural concern. A detail that would have reduced the wall bulging is shown in Figure 5b (10).

Roadway. The final lift of wire baskets were trimmed to match the roadway shoulder elevation and were tied back into the fill with another layer of geogrid attached to the tops of the trimmed wires and then backfilled. The rest of the roadway was constructed in a conventional manner. Storm drain facilities and curbing was installed on the finished roadway platform. The roadway was then graded and paved. Finally, the guard rail was placed to finish the project.

Performance. Movement during construction was monitored by taking inclinometer readings at various locations along the project. Inclinometer casings had been established from previous geotechnical investigations at the site. Locations were approximately 50 feet uphill (east) from the construction site and were situated between the roadway and the abutting houses. The monitoring showed no deep movement in the hillside during construction. However, localized surface sloughing was experienced along cut slopes during construction.

Snohomish County monitored the settlement and horizontal movement of the wall face for approximately 15 months following completion of the wall. This data indicated that settlements of the completed roadway were typically less than one-half inch and that the bulging which was noted at the face of the wall essentially stopped after construction of the final roadway lift.

Groundwater level measurements were made by Shannon & Wilson, Inc. during and subsequent to the call construction. These measurements indicated that the subsurface drains were effective in lowering the groundwater table 2 feet of more in borings located 30 feet uphill from the project. Clean flow occurs all year around from the subsurface drains, with total flow estimated to be about 10 gallons per minute or less over the entire project length (11).

SUMMARY

The Picnic Point Bridge replacement project was a unique and economical solution to stabilize and span an unstable area with a history of landslides. By investing the time in conducting a thorough site investigation and by performing a Value Engineering study, the County was able to save $2 million dollars and still effectively solve a reoccurring problem. In addition, the County was able to use state of the art design and construction techniques related to reinforced soil wall construction and obtain an aesthetically appealing project (Figures 10,11). These techniques should be valuable in solving future County road construction problems. The project was awarded the 1988 Award of Excellence by the WSDOT State Aid organization.

Figure 10. Completed Wall Section

Figure 11. View to the North After Completion of the Project

ACKNOWLEDGEMENTS

The Picnic Point bridge replacement project was designed jointly by Snohomish County and Shannon & Wilson, Inc. The authors wish to thank both the Washington State DOT and the FHWA for their financial and technical support on the project. Finally, the authors wish to thank Dell Johnson Construction, the general contractor for the project, for their efforts and craftsmanship in attaining a successful project.

Table 2. English to SI Unit Conversion Chart

1 inch = 25.4 millimeter
1 foot = 0.305 meter
1 ounce = 28.3 gram
1 square foot = 0.093 square meter
1 pound per foot = 14.59 newton per meter
1 pound per cubic foot = 0.157 newton per cubic meter
1 pound per square foot = 47.88 newton per square meter

REFERENCES

1. Hart-Crowser & Associates, In,., 1978, "Preliminary Geotechnical Evaluation, Picnic Point Bridge No. 589", report to HNTB, Sept. 22.

2. _____, 1980, "Phase II Preliminary Geotechnical Investigations, Picnic Point Bridge No. 589", report to HNTB, Nov. 19.

3. _____, 1983, "Geotechnical Engineering Study, Picnic Point Bridge Replacement", report to HNTB, April 28.

4. _____, 1984A, "Picnic Point Slide Repair South of Bridge No. 589", report to HNTB, August 7.

5. _____, 1984b, "Field Records, Picnic Point Slide Repair", field transmittal of soldier pile and tieback installation records to R. Andrews, Director, Snohomish County Dept. of Public Works, August 22.

6. HNTB, 1978, "Preliminary Engineering Study, Bridge No. 589, Picnic Point", report to Snohomish County Dept. of Public Works, Dec. 16.

7. Rittenhouse-Zeman & Associates, Inc., 1986, "Subsurface Explorations and Geotechnical Engineering Report, Roadway Stabilization for Puget Sound Boulevard, Picnic Point Bridge No. 589", report to Snohomish County Dept. of Public Works, May 12.

8. Shannon & Wilson, Inc., 1987, "Geotechnical Engineering Studies, Picnic Point Bridge Replacement, Snohomish County, Washington", report to Snohomish County Dept. of Public Works, March 24.

9. _____, 1987b, "Shop Drawing Review, Welded Wire Facing, Geogrid Wall, Picnic Point Bridge", letter to Snohomish County Dept. of Public Works, Aug. 3.

10. _____, 1987c, "Wall Bulge, Picnic Point Bridge Replacement", letter to Snohomish County Dept. of Public Works, Sept. 16.

11. _____, 1988, "Final Memo, Geotechnical Construction Observation, Picnic Point Bridge Replacement", letter to Snohomish County Dept. of Public Works, Jan. 18.

12. Sverdrup & Parcel and Associates, Inc., 1985, "Value Engineering Study on the Picnic Point Bridge Replacement", report to Snohomish County Dept. of Public Works, October.

Design and Analysis of Three Reinforced Soil Retaining Walls

Michael R. Simac
Intersol Engineering Inc., USA
Dr. Richard J. Bathurst
Royal Military College of Canada, Canada
Richard A. Goodrum
Mirafi, Inc., USA

ABSTRACT

Three case histories are presented using two commercially available computer software programs for analysis to incorporate geogrid reinforcement into retaining walls, with different interlocking modular concrete masonry block as the permanent facing element. Unique aspects of each project and how it effected the design and analysis of the reinforced soil wall is documented for each case history.

INTRODUCTION

In recent years, the use of geosynthetics particulary geogrids, for reinforced soil retaining wall construction has increased dramatically. The innovation and mass marketing of a number of proprietary interlocking masonry concrete-modular facing units has stimulated much of this growth. It is the experience of the writers that composite retaining wall systems with geosynthetic tensile reinforcement and precast modular facing units offer significant cost advantages over conventional retaining wall systems. Furthermore, these systems are easy to construct, aesthetically pleasing, use available on-site soils, tolerate settlement well, and are flexible in design layout.

The design and analysis methods to determine geosynthetic reinforcement requirements for these structures are well documented (e.g. Jones 1985, Mitchell 1987 and Koerner 1986, 1990). Additionally, the state-of-practice has been well stated and enhanced by the contributions of Christopher, et al (1990) and Task Force 27 (1990) which provide practical design guidelines and recommendations for selecting appropriate design parameters when using geosynthetic reinforcement. Finally, the performance of these composite systems has been well documented by instrumentation of full scale retaining walls as reported by Crowe et al (1989), Bathurst (1990) and Simac, et al, (1990).

While the state-of-practice in reinforced soil wall design is well established, calculations can be tedious. Hence, the implementation of these analytical procedures is particularly well suited to computer automation to achieve optimum solutions. Additionally these retaining walls, which are driven by keen competition, tend to be optimized for total installed cost in-place efficiency. Therefore, the designer must closely evaluate each wall section within stringent design criteria to optimize the economic impact of the wall system components. Computer automation has made this optimization of design possible.

The following three projects illustrate the use of computer software specifically written to facilitate the analysis and design process to determine geosynthetic tensile reinforcement requirements for retaining walls and slopes. Each project has unique site conditions or constraints which required modifications to the routine steps in the general reinforced soil retaining wall design methodology, that demonstrates the versatility of these computer programs.

COMPUTER PROGRAMS

Two commercially available computer programs were utilized in the design and analysis of these projects. Both programs are described briefly for completeness in this paper, but the reader can refer to the listed references for complete documentation.

MGRSW. The "MGRSW" program analyzes polymer reinforcement requirements for reinforced soil retaining walls, Bathurst (1989). A menu driven, user friendly interface prompts the engineer to enter the required design input parameters, such as; wall height, backslope angle, soil properties, surcharge conditions, geosynthetic reinforcement properties, and minimum factors of safety. The user friendly interface consists of a continuously updated graphic representation of wall geometry and reinforcement location, a designated screen area for wall and surcharge descriptions, and a dialogue area to respond to menu prompts. The program allows the designer to analyze two design strength types of reinforcement in the same wall, permits analyses to be stored and retrieved for reference and provides a graphic presentation of the final reinforcement and wall geometry on a dot matrix printer.

The "MGRSW" program first analyzes the requirements for external stability; i.e. sliding, overturning, and bearing capacity. Next, the program analyzes internal stability; i.e. tensile overstress and pullout, of the geosynthetic reinforcement configuration entered by the designer. The designer may alter the reinforcement design properties, number of layers, and/or vertical location to obtain allowable minimum factors of safety for internal stability. The program summarizes the results of analyses on a single output sheet, as shown in Figure 1.

The "MGRSW" program is based on a tied-back wedge model, using Rankine active earth pressure theory as documented in the users manual by Simac (1990). The program performs only total stress analysis on fully drained structures. The program follows closely the established design methodologies of Jones (1985), Mitchell (1987), Christopher, et al (1990) and Task Force 27 (1990). However, global stability analysis was specifically excluded from the program.

STABGM. "STABGM: A Computer Program for Slope Stability Analysis of Reinforced Embankments" was written by Duncan, et al (1985). The program provides a search routine to locate the most critical potential circular failure surface in a slope by implementing either the Bishops Modified Method of Slices or the Ordinary Method of Slices. The program allows the user to input; multiple soil layers, up to thirty layers of reinforcement, multiple groundwater surfaces, several pore pressure parameters, and seismic coefficients for pseudo-static analysis of dynamic loadings. A sample of the summary output is shown in Figure 2. The computer output also echoes all input data as shown in Figure 3.

JOB: CAROLINA PLACE
RUN: 1
DATE: 01-15-1991
ENGR: RAG

PROBLEM GEOMETRY:

Wall Height = 20.0 (ft)

SURCHARGE DETAILS:

Uniform surcharge starting at crest of wall
Magnitude = 250.0 (lbs/ft^2)

SOIL DATA:	COHESION (lbs/ft^2)	FRICTION ANGLE (degrees)	BULK UNIT WEIGHT (lbs/ft^3)
REINFORCED ZONE	0.0	30.0	130.0
BACKFILL	0.0	30.0	130.0
FOUNDATION	0.0	30.0	130.0

RESULTS OF EXTERNAL STABILITY CALCULATIONS:

Total Active Earth Force = 103.3E+02 (lbs/ft)
F.S. against sliding = 1.82
F.S. against overturning = 2.73
F.S. against bearing capacity failure = 2.83
BASE eccentricity = 2.09 (ft) > LT/6

REINFORCEMENT DETAILS:

Base Reinforcement length = 12.5 (ft)
Number of Reinforcement layers = 8

REINF. TYPE	LONG TERM ALLOWABLE LOAD	COEFF. OF SHEAR STRESS INTERACTION
MIRAGRID10T	2700.0 (lbs/ft)	0.75
MIRAGRID5T	1050.0 (lbs/ft)	0.75

SUMMARY OF INTERNAL STABILITY CALCULATIONS:

Assumed Earth Pressure distribution = Rankine, (i.e. Triangular)
Active Earth Force = 103.3E+02 (lbs/ft)
Minimum F.S. against grid tensile overstress = 1.49 in layer 1
Minimum F.S. against grid pullout = 1.56 in layer 8

RESULTS OF INTERNAL STABILITY CALCULATIONS:

LAYER NO.	TYPE NO.	ELEV. (ft)	L (ft)	FHORIZ (lbs/ft)	F.S. tensile Overstress	V.Stress (lbs/ft^2)	la (ft)	Anch.CAP (lbs/ft)	F.S. Pullout
1	1	1.3	12.5	1813	1.49	2431	11.7	24736	13.64
2	1	2.7	12.5	1405	1.92	2249	10.9	21310	15.17
3	1	4.7	12.5	1702	1.59	1989	9.8	16857	9.91
4	1	7.3	12.5	1676	1.61	1651	8.3	11846	7.07
5	1	10.0	12.5	1531	1.76	1300	6.7	7573	4.95
6	1	13.3	12.5	1028	2.63	871	4.8	3637	3.54
7	2	15.3	12.5	499	2.10	611	3.7	1940	3.89
8	2	16.7	12.5	680	1.54	429	2.9	1062	1.56

FIGURE 1: TYPICAL "MGRSW" OUTPUT (Program by MIRAFI Inc., 1990)

The "STABGM" program provides two options for incorporating the tensile reinforcement into the slope stability analysis. First, as a pure tangential force along the failure surface. Alternatively, the tensile reinforcement force can be considered to act solely horizontal, exerting a normal and tangential force on the failure surface. The program allows for variation of reinforcement tensile force along its length so pullout efficiencies of different geosynthetics can be modeled.

SUMMARY OF THIS STABGM RUN
Atomic Tire Retaining Wall+Slope,Deptford,NJ.,5Lyrs.MG 5T,REVISED

TANGENT	(X) CENTER	(Y) CENTER	FSMIN(BMM)
-15.00	111.00	-45.00	1.325
-10.00	121.00	-49.00	1.396
-5.00	135.00	-65.00	1.446
.00	113.00	-53.00	2.112

OVERALL MINIMUM FS = 1.325
(TANGENTIAL ORIENTATION)

FIGURE 2: TYPICAL "STABGM" OUTPUT (Program by Duncan, 1985)

CAROLINA PLACE MALL

Project. The Carolina Place Mall is being built in southern Mecklenburg County to service the rapidly growing suburban population of Charlotte, North Carolina. Due to the extremely large size of this retail project, over 1,000,000 square feet, it will be constructed in three stages. To separate these phases several temporary retaining walls, up to 18 feet high, were constructed for utility services and truck deliveries. All three locations required an "L" shaped wall in plan view to support and contain fill placement to meet planned finish grades at the site. Originally, cantilever cast-in-place concrete walls were proposed and bid for this project. However a reinforced soil retaining wall with concrete masonry modular facing was selected for construction, based on economics of the total structure.

Soil Conditions. The site is typical for the Piedmont region of North Carolina. A thin residual soil layer, 3 to 5 feet thick, consisting of sandy silt (SM), clayey silt (ML), or silty clay (CL) is underlain by 10 to 20 feet of partially weathered rock consisting of decomposed sandstone and siltstone. The partially weathered rock is easily broken down into a silty fine to medium sand (SP-SM), and was the fill source for retaining wall construction. A massive hard bedrock is encountered at a 15 to 20 foot depth below the surface. The existing groundwater table is in the massive bedrock and not expected to effect retaining wall design or construction.

The uniformity and abundance of the partially weathered rock or silty fine to medium sand, resulted in one set of consistent soil parameters being adopted for the analysis of all three walls: cohesion = 0 psf, $\emptyset$ angle = 30 degrees, and moist unit weight = 130 pcf.

```
        STABGM   Version  9.85 (MS-DOS)
 Slope Stability Analysis of Reinforced Slopes
          Bishop's Modified Method
       and/or Ordinary Method of Slices

Atomic Tire Retaining Wall+Slope,Deptford,NJ.,5Lyrs.MG 5T,REVISED

                C O N T R O L   D A T A
    NUMBER OF SPECIFIED CENTERS . . . . . .    0
    NUMBER OF DEPTH LIMITING TANGENTS . . . .   4
    NUMBER OF VERTICAL SECTIONS . . . . . .    14
    NUMBER OF SOIL LAYER BOUNDARIES . . . . .   8
    NUMBER OF PORE PRESSURE LINES . . . . . .   0
    NUMBER OF POINTS DEFINING COHESION PROFILE  0
    NUMBER OF REINFORCING LAYERS  . . . . . .   5
    SEISMIC COEFFICIENTS, S1, S2  . . . . . .  .00    .00
    UNIT WEIGHT OF WATER  . . . . . .  .62.40
SEARCH IS BASED ON BISHOP MODIFIED METHOD

SEARCH STARTS AT CENTER ( 103.0, -47.0) WITH FINAL GRID OF  2.0

ALL CIRCLES TANGENT TO DEPTH, -15.0, -10.0,  -5.0,    .0,

GEOMETRY
    SECTIONS    10.0  63.0  65.0  66.0  98.0  98.1  99.1  99.2 100.0 103.0 109.0 117.0 120.0 200.0
    T. CRACKS  -37.0 -37.0 -36.0 -36.0 -36.0 -25.0 -25.0 -25.0 -25.0 -23.0 -17.0  -8.0  -5.0  -5.0
    W IN CRACK -37.0 -37.0 -36.0 -36.0 -36.0 -25.0 -25.0 -25.0 -25.0 -23.0 -17.0  -8.0  -5.0  -5.0
    BOUNDARY 1 -37.0 -37.0 -36.0 -36.0 -36.0 -25.0 -25.0 -25.0 -25.0 -23.0 -17.0  -8.0  -5.0  -5.0
    BOUNDARY 2 -36.0 -36.0 -36.0 -36.0 -36.0 -25.0 -25.0 -25.0 -25.0 -23.0 -17.0  -8.0  -5.0  -5.0
    BOUNDARY 3 -36.0 -36.0 -25.0 -25.0 -25.0 -25.0 -25.0 -25.0 -25.0 -23.0 -17.0  -8.0  -5.0  -5.0
    BOUNDARY 4 -36.0 -36.0 -25.0 -19.0 -19.0 -25.0 -25.0 -25.0 -25.0 -23.0 -17.0  -8.0  -5.0  -5.0
    BOUNDARY 5 -36.0 -36.0 -25.0 -19.0 -19.0 -18.0 -18.0 -25.0 -25.0 -23.0 -17.0  -8.0  -5.0  -5.0
    BOUNDARY 6 -36.0 -36.0 -25.0 -19.0 -19.0 -18.0 -18.0 -19.0 -19.0 -19.0 -13.0  -5.0  -5.0  -5.0
    BOUNDARY 7 -13.0 -13.0 -13.0 -13.0 -13.0 -13.0 -13.0 -13.0 -13.0 -13.0 -13.0  -5.0  -5.0  -5.0
    BOUNDARY 8  30.0  30.0  30.0  30.0  30.0  30.0  30.0  30.0  30.0  30.0  30.0  30.0  30.0  30.0

SOIL PROPERTIES
     LAYER          COHESION   FRICTION ANGLE     DENSITY
       1              .0           .0             250.0
       2              .0         32.0             125.0
       3              .0         20.0             110.0
       4          25000.0        10.0             150.0
       5              .0         15.0             100.0
       6              .0         25.0             120.0
       7            800.0        25.0             125.0

REINFORCING FORCE DATA AT  5 LEVEL(S)   (TANGENTIAL ORIENTATION)
   Y =  -34.00    NO. OF FORCE POINTS =  4
          X       FORCE
        98.0        .0
        96.0     1050.0
        70.0     1050.0
        68.0        .0
   Y =  -32.00    NO. OF FORCE POINTS =  4
          X       FORCE
        98.0        .0
        96.0     1050.0
        70.0     1050.0
        68.0        .0
   Y =  -30.00    NO. OF FORCE POINTS =  4
          X       FORCE
        98.0        .0
        96.0     2700.0
        70.0     2700.0
        68.0        .0
   Y =  -28.00    NO. OF FORCE POINTS =  4
          X       FORCE
        98.0        .0
        96.0     2700.0
        70.0     2700.0
        68.0        .0
   Y =  -26.00    NO. OF FORCE POINTS =  4
          X       FORCE
        98.0        .0
        96.0     2700.0
        70.0     2700.0
        68.0        .0
```

FIGURE 3: TYPICAL "STABGM" INPUT (Program by Duncan, 1985)

Reinforcement. To optimize reinforcement performance and cost, two types of geogrids were used in the design. The geogrids were specified to meet a minimum long term, 75 year, design strength of 1050 and 2700 pounds per lineal foot (lbs/ft) respectively; and both have a minimum coefficient of shear stress interaction of 0.75; as defined by Task Force 27 (1990). Task Force 27 recommends specific reductions of the ultimate wide strip tensile strength ASTM D-4595, based on product specific creep site damage, and durability testing, to obtain a working design strength. High tenacity, continuous multi-filament polyester geogrids that met these design requirements were selected based upon cost effectiveness and availability.

Design and Analysis. The overall site geometry and competent foundation soils precluded any problems with global stability. The project design focused on the internal and external stability analysis of the reinforced soil section using the "MGRSW" program. To simplify construction across all wall sections, a constant elevation for each geogrid level was selected whenever possible.

The design was initiated at the tallest section, 18 feet exposed height and 20 feet total height. An optimized number of geogrid layers, length, and vertical spacing was determined to maintain a minimum factor of safety of 1.5 against all assumed failure mechanisms with the exception of overturning and bearing capacity which were evaluated using a 2.0 minimum factor of safety. A typical wall cross-section for this is shown in Figure 4.

To minimize changes in geogrid elevations across wall sections, all shorter wall heights were analyzed to ensure that minimum factors of safety were achieved using permutations of geogrid elevations based upon the highest section first. This was accomplished by analyzing walls with total heights equivalent to the maximum height less each geogrid placement elevation.

To maintain tight tolerances on modular facing alignment during construction, an efficient connection between the geogrid reinforcement and modular facing is required. For this facing system it was analyzed as a frictional connection between the block, drainage aggregate in block core openings and the geogrid (Simac, 1990). The connection provided adequate, 1.5, factors of safety on all design loadings, as well as for the pretensioning force applied to the geogrid during construction, which meets Task Force 27 requirements.

Two special geogrid reinforcement details were required to ensure proper placement. First, a corner detail was established, which required placement of geogrid perpendicular to the main wall face, over to face of the other leg of the "L" shaped wall. In only the reinforcement area common to both walls, reinforcement perpendicular to the 90 degree wall face would be installed one course above the original reinforcement (Simac, 1990). All other reinforcement was placed at same elevation.

Second, to accommodate some vertical electrical conduits, only the geogrid reinforcement cross members were severed from the tail up to the conduits. The "freed" longitudinal strands were worked around the vertically rising conduits while maintaining as closely as possible a geogrid pattern. This allowed the main, longitudinal, members to remain intact and maintain full tensile load capacity. The reduction of pullout capacity due to severing cross members was accounted for in the design.

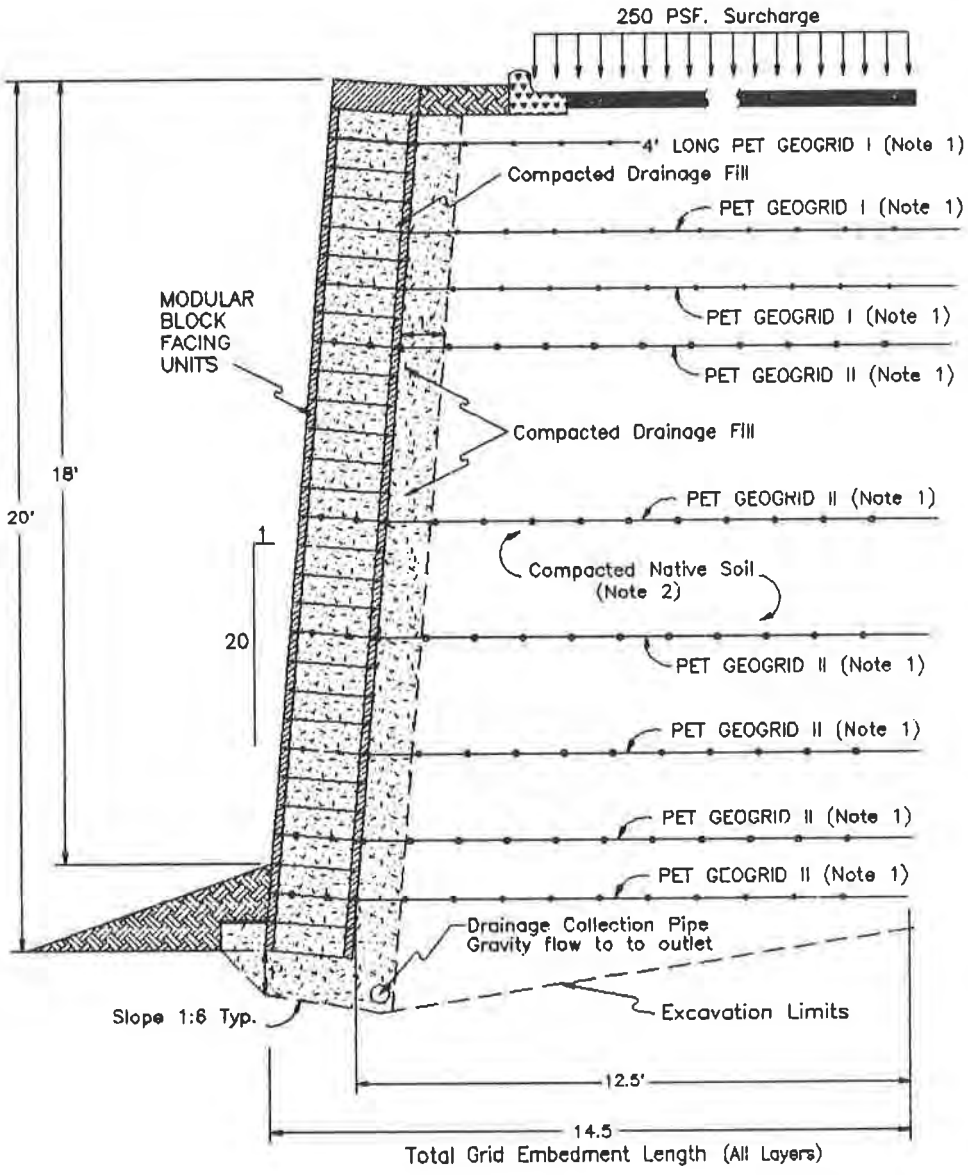

NOTES:
1) Geogrid is to be rolled out perpendicular to the wall face and pulled taut prior to fill placement.
2) Fill placed within the the reinforced soil zone is to be compacted to a minimum 90% modified proctor density (ASTM D-1557) or as determined by a soil engineer.

FIGURE 4: TYPICAL WALL CROSS-SECTION CAROLINA PLACE MALL

All three walls on this project were constructed in fall of 1990 and have performed well to date.

OAKLANDS FESTIVAL

Project. Oaklands Festival is a retail strip shopping complex in Exton, Pennsylvania. Almost 850 feet of retaining wall, averaging about 18 feet tall, was constructed to provide additional parking and delivery/fire truck access around the rear of the building. This large grade separation was required, since the eastern quarter of the site impinged on the flood plain of a large creek in the area. A hydrologic study of the area indicated that the 100 year flood elevation was approximately 285 feet above MSL. This design flood would partially submerge the lowest 650 lineal feet of retaining wall. A reinforced soil wall with modular concrete block facing was selected based on a 30% cost savings over cast-in-place concrete retaining wall.

Soil Conditions: The sloping site was characterized by residual soils consisting of 1 to 1.5 feet of organic topsoil (OL), 2 to 6 feet of clayey silt (ML), and 10 to 20 feet of sandy silt or silty sand (SP-SM). The groundwater elevation was normally around 280 feet above MSL, but could fluctuate seasonally up to 284 feet and during the design flood up to 285.5 feet above MSL.

To balance earthwork quantities at the site, it was anticipated that both the clayey silt and silty sand would be used as structural fill in the reinforced soil zone. The majority of the retained structural fill, that supports the building and parking areas, will be placed concurrently behind the reinforced soil wall construction. The height of walls, concurrent fill placement procedures, and the presence of underlying saturated foundation soils led to the prediction of as much as 2 inches of differential settlement along the wall length. The allowable soil bearing pressure was specified as 3000 pounds per square foot (psf). Existing site soil strength parameters were assigned by the project geotechnical engineer as shown in Table 1.

Table 1 Soil Strength Parameters, Oaklands Festival

Strength Property	Clayey Silt (ML)	Silty Sand (SP-SM)	Drainage Aggregate
Cohesion, psf	0	0	0
Total Stress Ø Angle, degrees	30	32	35
Effective Ø Angle, degrees	32	34	38
Moist Unit Weight, pcf	125	130	120

Reinforcement. To simplify construction and reduce installation costs, only one type of tensile reinforcement was desired. The site development requirement that both clayey silt and silty sand soils be used to balance earthwork quantities, necessitated that the reinforcement be a geogrid to maintain maximum pullout efficiencies on saturated/wet soil conditions. Additionally, to control precast modular block facing unit movement due to soil compaction during construction a minimum modulus of 25,000 lbs/ft at 2 percent strain was required for the reinforcement.

The geogrid specification required a minimum long term design load of 2700 lbs/ft and a minimum coefficient of shear stress interaction of 0.7; as defined by Task Force 27 (1990). A large aperture, high strength, continuous multi-filament polyester geogrid met these minimum performance criteria and was selected based upon cost-effectiveness.

Design and Analysis. To address the groundwater/hydrostatic loading conditions, an external stability analysis was performed on the retaining wall system using rapid drawdown conditions and effective stress soil parameters. Since the maximum groundwater elevation behind the reinforced zone is elevation 285.5 and the lowest wall elevation 281, a maximum 4.5 feet water head differential was anticipated. Additionally, 0.5 feet of water head was added should seepage forces develop. To model this maximum 5 foot head differential for external stability analysis, adjustment of the average moist unit weight in "MGRSW" was required because, only a single soil type can be entered into the program for the reinforced and backfill soil volumes respectively and the program also ignores the driving force of water.

To model the effective stress for resisting forces, the reinforced soil volume average unit weight was adjusted as follows:

$$UWavg = \frac{UWm\ (H-Hw) + (UWs - UWw)\ Hw}{H}$$

Where:
- UWavg = average moist unit weight, pcf
- UWm = moist unit weight, pcf, (measured)
- UWs = saturated unit weight, pcf,(calculated)
- UWw = unit weight of water, pcf, (62.4)
- H = height of wall, ft
- Hw = height of water, ft.

To model the effects of the driving forces of water pressure, an increase in the average unit weight of the retained backfill soil was determined as follows:

$$UWinc = UWw\ (Hw)^2 / H^2$$

Where:
- UWinc = increase in moist unit weight of backfill soil volume, pcf (Note: to be added to measured moist unit weight)
- UWw = unit weight of water, pcf, (62.4)
- Hw = height of water, ft
- H = height of wall, ft

The calculations were performed with both design soils and yielded similar results. These adjustments for use in "MGRSW" are accurate for total force computations (i.e. sliding) and conservative for moment computations (i.e. overturning and bearing capacity). Additionally, these adjustments slightly underestimate the total weight resisting overturning. Therefore, these calculations conservatively defined a total length of reinforcement, meeting all minimum safety factors of external stability analysis for the rapid drawdown condition. This represented a more critical condition than the total stress analysis for normal operating conditions and was ultimately adopted as the design length for geogrid reinforcement.

Internal stability of the reinforced soil volume was determined based on total stress soil parameters of the silty sand. This is appropriate since the total stress condition, i.e. normal operating condition, yielded greater forces in the reinforcement. The silty sand also represented the most conservative soil parameters. However, a blanket drain, consisting of free draining aggregate conforming to AASHTO No. 57 stone wrapped in a nonwoven geotextile, was specified for entire reinforced soil volume to an elevation of 287 feet, about 2 feet above the maximum flood elevation, see Figure 5. That blanket drain is anticipated to allow quick and free movement of water in and out of the reinforced soil volume, to preclude buildup of fluid pressure behind the wall facing units. The improved soil strength parameters of the drainage aggregate were conservatively ignored in both the internal and external stability analyses since the program can only accommodate one soil type.

To account for any temporary blockage in the drainage aggregate, those reinforcement layers within the blanket drain were analyzed to receive the full 5 feet of water pressure. This was accomplished by adding a force to those layers, equivalent to the applied fluid pressure acting over the contributary wall face area assigned to each reinforcement layer, see Simac, et al (1990). These calculations must be performed manually, then combined with the results of the "MGRSW" program.

Thus an optimized, but conservative design cross-section was established as shown in Figure 4. The cross-section requires a standard wall embedment of about 2.0 feet, plus a half foot for scour protection along the toe of wall. Additionally, rip-rap scour protection was specified for full wall embedment depth.

Other Considerations. A global stability analysis check of this design section indicated minimum factors of safety of 1.5 and 1.3 for the normal and flood water level conditions, respectively. Analysis of sliding on the geotextile filter interface yielded factors of safety significantly above the minimum 1.5 and therefore did not control the design. Also, the friction facing connection was analyzed and even under effective stress conditions yielded factors of safety greater than 1.5 which are above Task Force 27 requirements.

A storm drain culvert passes beneath the wall at one section. To accommodate locations where geogrid reinforcement intersects the storm drain culvert, the detail shown in Figure 6 was adopted. It allows the geogrid to be inclined up over the pipe by slitting the cross members parallel to and just outside the pipe.

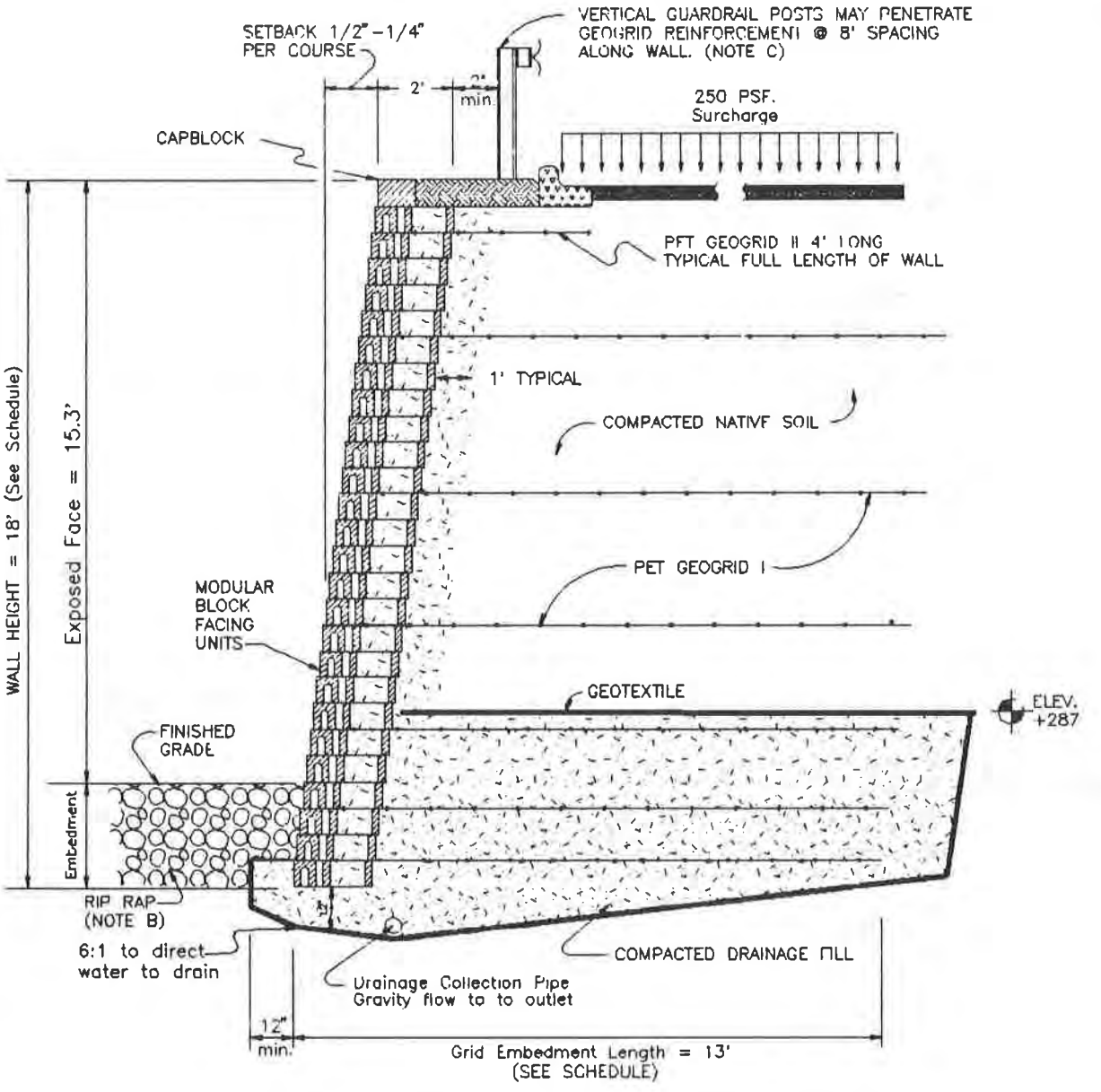

FIGURE 5: TYPICAL CROSS-SECTION -- OAKLANDS FESTIVAL

To simplify construction and reduce wall construction costs, the geogrid reinforcement elevations were held constant for as many wall panels, i.e. design heights, as practical. This is illustrated in the wall profile drawing shown in Figure 7. Therefore, the design of each wall section was greatly influenced by its neighboring sections with design proceeding away from the maximum height section, panel "N".

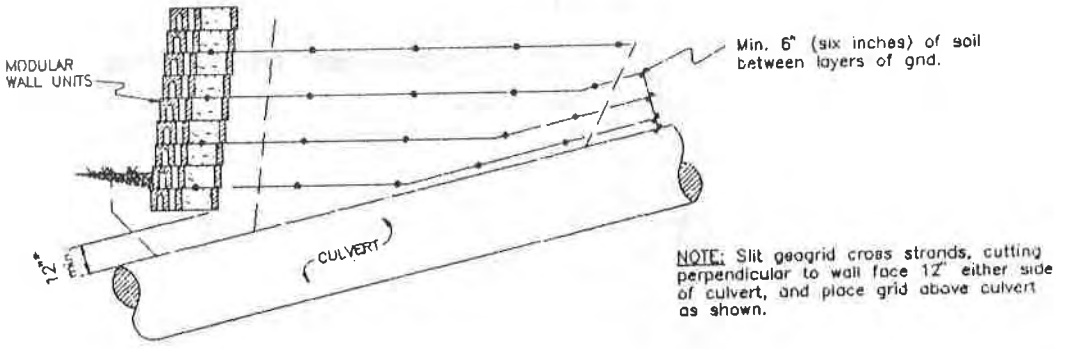

FIGURE 6: DETAIL FOR GRID PLACEMENT AT CULVERT OAKLANDS FESTIVAL

This wall was constructed in the summer of 1990 and has performed well to date. However, no significant flooding has occurred yet to truly test the design.

ATOMIC TIRE CENTER

Project. The Atomic Tire Center store in Deptford, New Jersey was nearing completion, when unexpected soil conditions were encountered during excavation for a 200 foot long by 8.5 foot high cast-in-place concrete retaining wall adjacent to the recently completed building. A subsequent geotechnical investigation confirmed a significant volume of loose uncompacted fill. Removal of the loose fill materials would have resulted in an increased wall height from 8.5 to 17 feet. Corrective measures were further complicated by the presence of a 20 foot high 1:1 (H:V) slope just below the toe of the wall.

Since the retaining wall was in a fill section and founded on loose soils in which up to 3 inches of settlement was expected, a flexible retaining system using a modular masonry concrete block facing was suggested to the engineer. A geogrid reinforced soil wall system could accommodate the expected vertical settlement and reduce or eliminate the need for excavation of the loose fill subsoils at the site and replacement with more competent materials. Although the site contractor proposed three other precast or masonry wall systems, the reinforced soil retaining wall approach with modular concrete facing offered a 25% cost savings over the least expensive alternative.

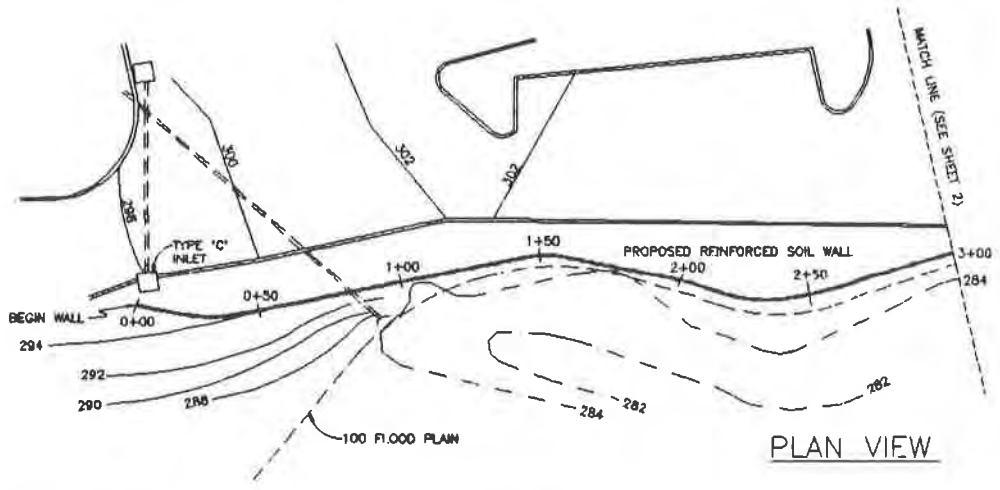

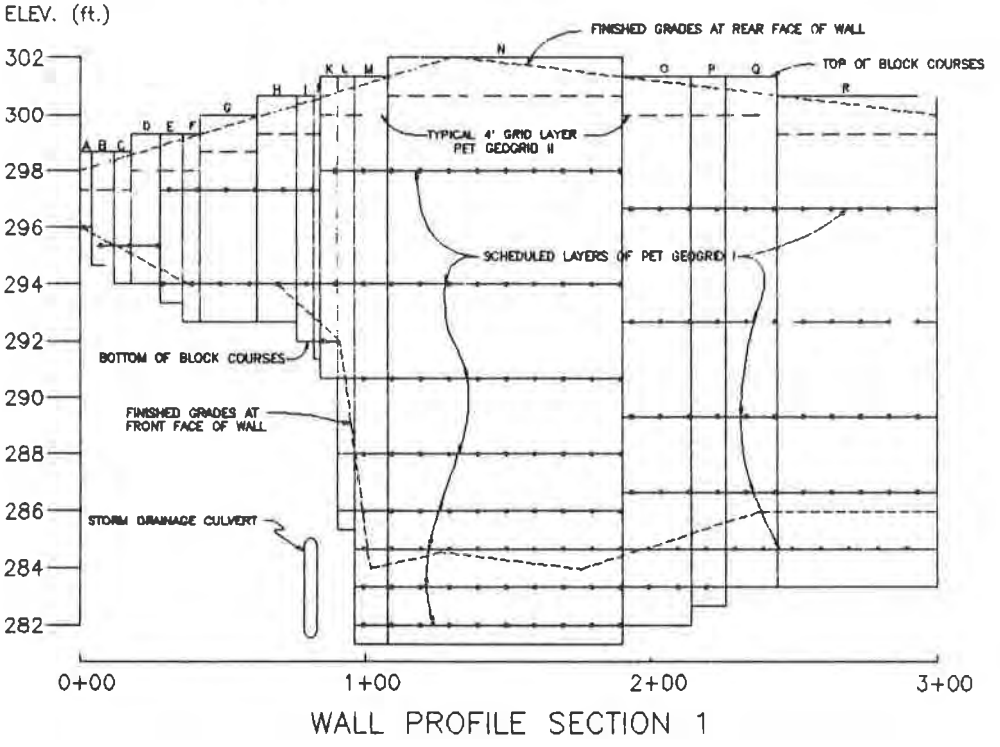

FIGURE 7: PLAN & PROFILE OF OAKLANDS FESTIVAL WALL

Soil Conditions. The reinforced soil retaining wall was built with imported sand fill. It was founded on 5 feet of loose miscellaneous fill that also formed a thin 2 to 3 feet cover down the 1:1 slope below the toe of wall. Beneath the loose fill, is a 6 to 8 feet thick loose, silty fine sand layer. Underlying the loose soils is a medium dense to stiff silty clay forming the main bearing stratum at the site. The groundwater table was not encountered during site exploration and hence was well below the toe of slope. The soil stratigraphy and strength parameters recommended by the project geotechnical engineer for these analyses are shown in Figure 8.

Reinforcement. Detailed global stability analysis indicated that high strength, geosynthetic reinforcement was required for this project to minimize the number of reinforcement layers. Additionally, a low profile reinforcement was required to develop the required friction facing connection to control horizontal deflection of the modular concrete block facing system during construction and to keep irregularities in block alignment to a minimum. The geogrid specification required a minimum long term design load of 2700 lbs/ft and a minimum coefficient of shear stress interaction of 0.7; as defined by Task Force 27 (1990). Based upon cost and geogrid performance, a large aperture high strength continuous multifilament polyester geogrid was selected.

Design and Analysis. Initially, a reinforced soil wall design was performed using "MGRSW" assuming an 11.3 feet high wall with a uniform surcharge of 250 psf and $\emptyset$ = 32 degrees soil in-fill. This analysis defined the basic minimum vertical configuration of reinforcement, comprising 5 layers of 1050 lbs/ft reinforcement each 8.5 feet long. A check of global stability using "STABGM" indicated the minimum factor of safety to be near 1.0 when the retaining wall was within a few feet of the crest of the 1:1 slope. Therefore, global stability would control the design and high strength, 2700 lbs/ft, reinforcement would be required.

Several alternatives were considered to improve the global stability:

a.) Lowering the bearing elevation of the wall. This solution would have increased the wall height significantly.

b.) Excavation and replacement of poor underlying soils. However, this alternative would have endangered the stability of the recently completed building foundations located behind the wall.

c.) Constructing a reinforced concrete cut-off trench to competent bearing soils, to act as a shear key. This strategy was deemed unconstructable in the loose soils.

d.) Increasing the geogrid reinforcement lengths to ensure global stability. However, the required geogrid lengths would have jeopardized the adjacent building foundations during construction.

e.) Moving the wall back from the crest of the slope twenty feet. This solution reduced parking spaces to below local zoning restrictions and was therefore deemed unacceptable.

Finally, it was decided by the owner to combine solutions "d" and "e" to obtain a workable situation. By moving the wall back 10 feet from the crest, angled parking could still be used to meet zoning restrictions. At the same time, destabilizing earth forces would be reduced to levels, at which a 20 feet high strength, 2700 lbs/ft geogrid length could maintain stability. This would allow earthwork to be completed without jeopardizing adjacent building foundations.

A global stability analysis of this configuration using "STABGM", indicated a minimum 1.3 factor of safety could be maintained using 5 layers of the specified high strength, 2700 lbs/ft, geogrid reinforcement. For this analysis, since the geogrid reinforcement was to intersect the failure plane on slices with fairly steep base inclinations and some vertical movement or rotation was expected due to the underlying loose soils. The tangential orientation was selected. A summary of this global stability analysis is shown in Figure 8. This reinforcement layout was rechecked using "MGRSW", which showed that all requirements for internal and external stability were also met.

The parking area above the wall was regraded to place the drainage swale in the middle of the area to keep water away from the wall face. Additionally, this allowed the storm sewer and catch basins to be just outside the reinforced zone.

This retaining wall has performed well in its first year of service. Differential settlement is less than the 2 inches predicted by one-dimensional consolidation analysis. The completed wall is shown in Figure 9.

SUMMARY AND CONCLUSIONS

The paper has reported details of the analysis, design and construction of three reinforced soil retaining walls constructed using continuous multifilament polyester geogrid reinforcement and modular concrete block facing.

The project designs and analyses were carried out using the current state-of-practice for these systems as outlined in the FHWA guidelines, Christopher, et.al. (1990) and the guidelines from AASHTO Joint Task Force 27 (1990). The implementation of analysis steps and the optimization of the wall design for cost and ease of construction was carried out using two commercially available PC-DOS programs, ("MGRSW" and "STABGM").

The experience of the authors in using these software packages is that the input parameters can be easily adjusted to accommodate non-routine site conditions. However, the use of commercial software must be restricted to experienced geotechnical engineers who are familiar with: the mechanical properties of the proposed wall components; the site soils and topography; and, the details of the analysis methods implemented in the computer packages employed.

ACKNOWLEDGEMENTS

The authors would like to express their appreciation to the design engineers on these projects Mr. Michael Arfman, Insite; Mr. Ed Ryan, E. P. Ryan Associates; and Mr. William Elton, Elton Engineers. Additionally, the authors thank Mr. Elliott Wolfe and Norman Amend for drafting these figures and Ms. Nancy Steffen for typing the manuscript.

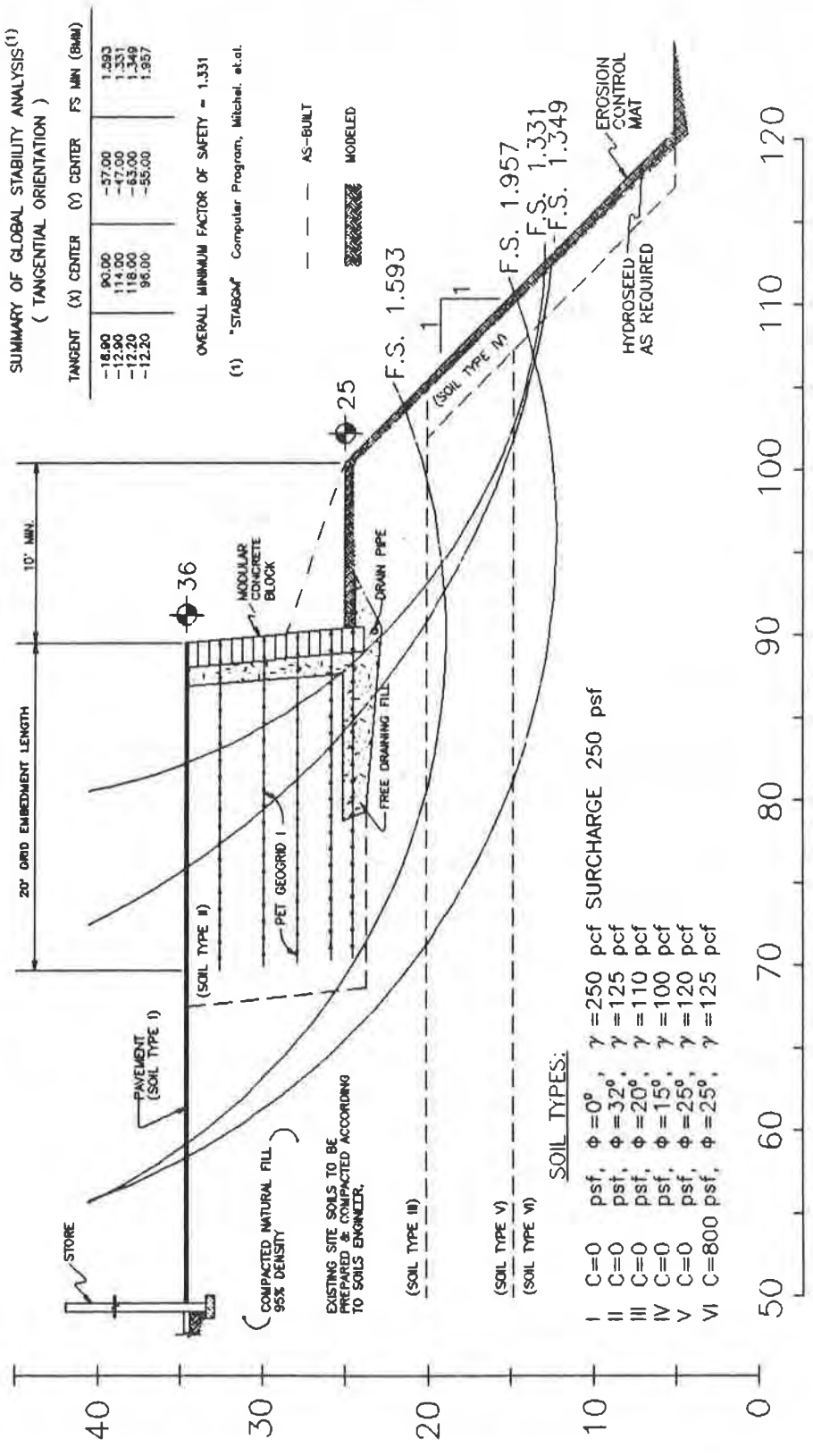

FIGURE 8: TYPICAL WALL & SLOPE SECTION ATOMIC TIRE CENTER

FIGURE 9: COMPLETED WALL, ATOMIC TIRE CENTER

REFERENCES

Bathurst, R.J., (1989), Technical Notes for MGRSW: An Interactive Design Program for Miragrid Reinforced Soil Walls, Bathurst, Jarrett and Associates, Inc.

Bathurst, R.J., (1990), "Field and Laboratory Instrumentation of Geosynthetic Reinforced Soil Retaining Walls", Symposium on In Situ Testing and Monitoring: Recent Advances and Applications, Toronto, Canada.

Christopher, B.R., Gill, S.A., Giroud, J.P., Juran, I., Mitchell, J.K., Schlosser, F. and Dunnicliff, J. (1990), "Design and Construction Guidelines for Reinforced Soil Structures - Volume I," and "Summary of Research - Volume II," Report No. FHWA-RD-89-043, Federal Highway Administration.

Crowe, R.E., Bathurst, R.J., and Alston, C., (1989), "Design and Construction of a Road Embankment using Geosynthetics", 42nd Canadian Geotechnical Conference, Winnepeg, Manitoba.

Duncan, J.M., Low, B.K., Schaefer, V.R. (1985), "STABGM: A Computer Program for Slope Stability Analysis of Reinforced Embankments", Virginia Polytechnic Institute, Blacksburg, Virginia.

Jones, Colin J.F.P. (1985), "Earth Reinforcement and Soil Structures", Butterworths, London, England.

Koerner, R.M. (1986, 1990), Designing With Geosynthetics, Prentice-Hall, Englewood Cliffs, New Jersey, (1986), 1st Edition (1990) 2nd Edition.

Mitchell, J.K., and Villet, W.C., (1987), "Reinforcement of Earth Slopes and Embankments", National Cooperative Highway Research Program Report 290, Transportation Research Board, Washington, D.C.

Simac, M.R., Christopher, B.R., Bonczkiewicz, C., "Instrumented Field Performance of a 6 m Geogrid Soil Wall" (1990), 4th International Conference on Geotextiles, Geomembranes and Related Products, The Hague, The Netherlands, A.A. Balkema.

Simac, M.R. (1990), "Design Methodology for Miragrid Reinforced Soil Retaining Walls", Mirafi Inc, Charlotte, North Carolina.

Task Force 27 (1990), In-Site Soil Improvement Techniques, "Design Guidelines for Use of Extensible Reinforcements for Mechanically Stabilized Earth Walls in Permanent Application", Joint Committee of AASHTO-AGC-ARTEA, AASHTO, Washington, D.C.

High Clay Embankment Over Cannon Creek Constructed With Geogrid Reinforcement

R. F. Hayden
Hayward Baker, Inc., USA
G. R. Schmertmann
University of California - Berkeley, USA
B. Q. Qedan
Arkansas Highway and Transportation Dept., USA
M. S. McGuire
Opterra, Inc., USA

ABSTRACT: Original plans for realignment of Arkansas State Highway 16 with a 76 ft (23.2 m) high embankment over Cannon Creek were cancelled when initial construction experience indicated that the available plastic and expansive clay fill was unstable in the design configuration. An embankment redesign option which incorporated geogrid reinforcement within the full-height of clay fill was successful upon project rebidding, with a savings of about $1.1 million (US) over conventional options. The geogrid reinforced embankment was constructed in 1988.

The design of the reinforced embankment considered short and long-term soil and geosynthetic properties and took into account both overall and surficial stability. Detailed reinforcement layout was determined from extended limit equilibrium slope stability analysis techniques and constructability factors.

An extensive instrumentation program including strain gages, extensometers, inclinometers, pore pressure sensors, settlement stakes and moisture-temperature indicators shows limited deformations during the first 24 months of embankment service and generally confirms the design assumptions. Virtually all measured horizontal strains have been less than 0.5 %. The measurements generally indicate relatively large near-surface deformations, thus suggesting the essential need for surficial reinforcement of expansive clay slopes. Continued monitoring of the instruments should provide more information on long-term embankment performance.

INTRODUCTION

Project Description

Arkansas State Highway 16 is a two lane secondary road which winds and twists over the Boston Mountains between Ozark and Fayetteville (Figure 1). Locally known as the Pig Trail, the road serves farm to market vehicles as well as provides a short cut link

between Central Arkansas and the growing Northwest corner of the State. A realignment project in 1986 involved the replacement of a hairpin curve and a one-lane bridge over Cannon Creek with a straightened roadway section, an embankment with a maximum side slope height of 76 feet (23.2m) and a four barrel concrete box culvert.

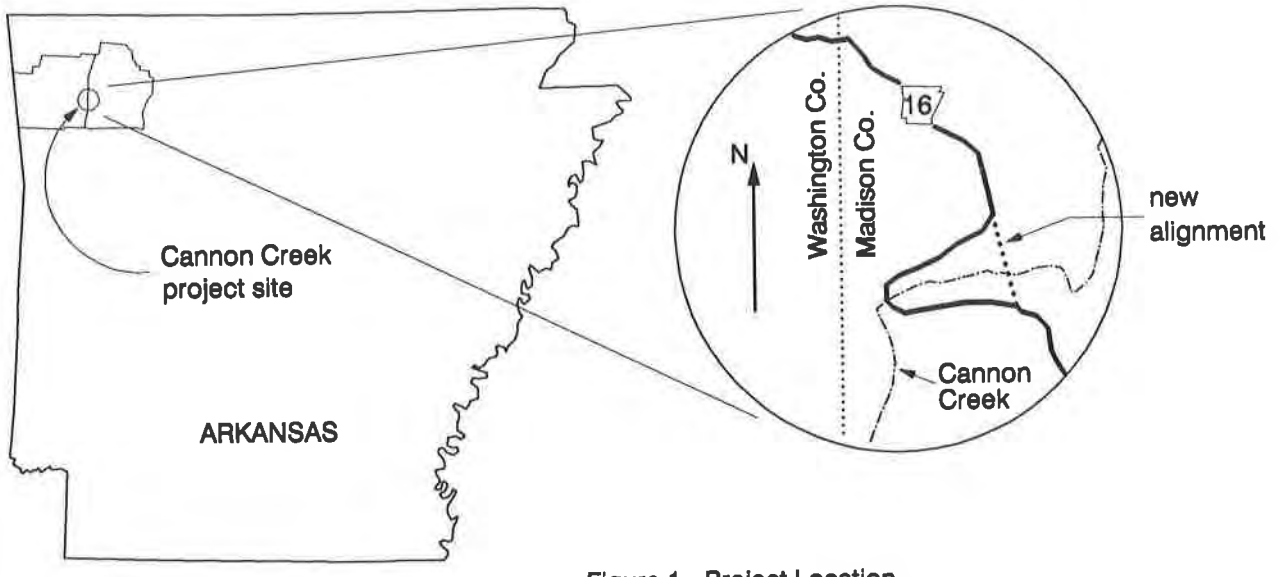

Figure 1 - Project Location

The design for the 800 foot (244.m) long realigned section of roadway embankment involved excavation of unclassified soil and weathered rock to depths of 45 and 15 feet (13.7 and 4.6m) from the southern and northern sides of Cannon Creek, respectively. The 132,400 cubic yards (101,300 cubic meters) of excavated material was to be placed in the ravine as fill to reach roadway level.

A 400 foot (122.m) width of right-of-way was purchased to accommodate the embankment with the 460 foot (140m) long skewed box culvert length at the base. Fill side slope heights ranged from 20 to 40 feet (6.1 to 12.2m) along much of the embankment to a maximum of 76 feet (23.2m) near the box culvert. Centerline fill heights also had a maximum of about 76-80 ft (23.2-24.4m) as shown in Figure 2. Side slopes for the embankment were to be graded to 2H:1V angles along the full length and two drainage swales were included as shown on Figure 3.

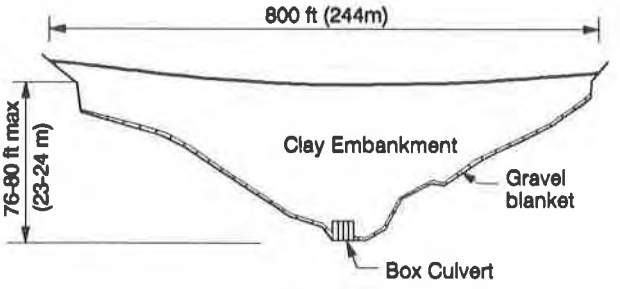

Figure 2 - Centerline Profile of Highway 16 Embankment

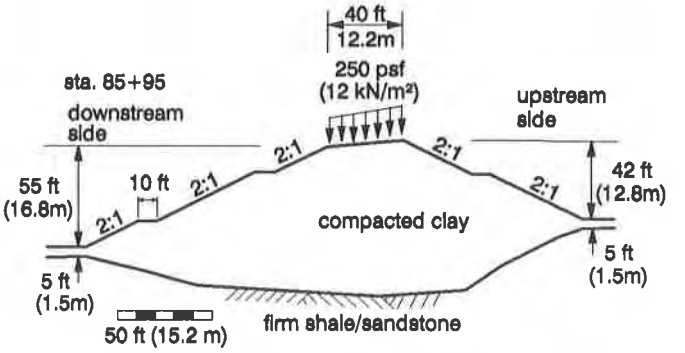

Figure 3 - Embankment Design Section at Sta. 85+95

Initial Construction

The reinforced concrete box culvert was built during the first phase of construction in 1988. Several slope failures developed in the clay fill placed next to the box culvert requiring the construction to be stopped. Investigations by Arkansas State Highway and Transportation Department (AHTD) geotechnical engineers found that the borrow soils being excavated on site were highly plastic clays with plasticity indexes of 20 to 40. Further, stability analyses revealed that the embankment could not be safely constructed with 2H:1V side slopes as planned.

Redesign Alternatives

The in-place box culvert and right-of-way restrictions were the primary factors controlling redesign alternatives. The two most economical options recommended for continuation of the project were either: 1) wasting the highly plastic clay soils from the excavations in favor of imported granular fill for the full embankment height or; 2) use of geogrid reinforcement to improve the stability of the on-site clay fill slopes. In each case, the magnitude of the changes required cancellation of the original construction contract and rebidding with the new design.

Both of the design alternatives included the original side slopes of 2H:1V since the box culvert was already in place and the right-of-way was limited. Both of the alternatives were included in the bidding documents but only one bid was submitted and that was from the original contractor. The bid amount of $3.3 million exceeded the allotted AHTD budget and another redesign process was begun.

Due to the high cost of imported granular fill, the third and final designs incorporated as a first option, the granular fill in only the lower half of the embankment and geogrid reinforced clay in the upper half. The full height, geogrid-reinforced embankment was also included as the second option, with the granular drainage blanket at the base changed from 10 feet (3.0m) in thickness to 2 to 4 feet (0.6 to 1.2m) to reduce cost.

On the second rebidding, the full-height geogrid reinforced clay embankment was the lower cost at approximately $2.1 million, a savings of $1.1 million over the earlier bid, and it was therefore selected for construction. The paper provides descriptions of soil property selection, geogrid specification, stability analyses, design layouts, construction seguences and results of instrumentation. The embankment is the highest fill for a roadway in the state of Arkansas and is believed to be the highest geogrid-reinforced plastic clay fill in North America. The project incorporated broad usage of geosynthetics including three grades of uniaxial geogrid, a biaxial geogrid for secondary reinforcement, a nonwoven geotextile as a drainage filter fabric, and a three-dimensional, polymer erosion protection mat on a steepened slope near the box culvert.

SOIL PROPERTIES FOR REINFORCED EMBANKMENT DESIGN

Soil Information

The designated material for the embankment fill was a highly plastic clay (AASHTO type A-7-6, USCS type CH). Atterberg limits tests performed on 9 samples recovered from borings in the borrow areas yielded the results shown in Table 1, with the high average plasticity index (PI=35) being consistent with local experience that the clay was expansive. Grain size analyses indicated that all samples had at least 70%, by weight, finer than the #200 sieve. The only other laboratory information available at the time of the design was the result of UU triaxial tests, performed by AHTD on compacted samples of the clay, which indicated an undrained shear strength of about 900 psf (43 kN/m^2). Observations of cut slopes in natural deposits of the fill clay near the project site provided additional information. It was observed that these 2H:1V slopes had experienced occasional, but not widespread, sloughing failures. (See Photo 1).

Soil shear strength and unit weight properties were selected based on available laboratory test data and field observations. As information was limited, reasonable yet conservative, estimates were required. Properties for both end-of-construction and long-term design cases were considered as described in the following paragraphs.

Strength Properties for End-of-Construction Design Case

The end-of-construction case was taken as an undrained loading condition which would be analyzed with total stress methods. The appropriate clay shear strength was therefore the undrained strength measured for the compacted clay in the UU triaxial tests, s_u=900 psf (43 kN/m^2). This strength should appropriately capture pore pressure effects for the total stress analysis as long as the laboratory and field conditions were reasonably similar.

Table 1 - Atterberg Limits Test Results for 9 Samples of the Embankment Soil

	low	high	average	std. dev.
LL	49	77	61	8
PL	20	30	26	3
PI	23	47	35	7

Table 2 - Statistical Summary of Geogrid Strain Gage Readings

Gage Set No.	align. wrt ribs	total # of gages	Date of zero read.	# of gages at end date	Date of end read.	Measured total strains (%) from zero to end date			
						ave	std dev	min	max
1	par.	34	7-8/88	22	1/90	0.11	0.09	-0.01	0.30
	perp.	4	7/88	1	1/90	-0.09	-	-	-
2	par.	28	8/88	22	1/90	0.08	0.07	-0.04	0.28

Table 3 - Material Quantities Used in the Embankment
(after Qedan, 1990)

Item Name	Unit	Quantity
Filter Fabric	Sq. Yd.	23,454
Drainage Gravel	Cu. Yd.	23,405
Geogrid (type 1)	Sq. Yd.	7297
Geogrid (type 2)	Sq. Yd.	14,363
Geogrid (type 3)	Sq. Yd.	51,918
Geogrid (intermediate)	Sq. Yd.	18,716
Fill Material	Cu. Yd.	206,233

There is reason to believe that the value of 900 psf may be conservative for this clay. For example, the NAVFAC manual (US Navy, 1982) gives s_u=2150 psf (103 kN/m^2) as a typical value for CH soil compacted to 100% standard Proctor.

Photo 1: Completed Embankment (Note sloughing cut slopes in background).

Strength Properties for Long-Term Design Case

The long-term case was taken as a drained loading condition which would be analyzed with effective stress methods. For such a massive structure, the length of time to reach the long-term condition in this CH soil would almost certainly be measured in years. The appropriate long-term clay shear strength would be specified with the effective strength parameters, Ø' and c'. As no drained strength testing data was available, conservative estimates for these parameters were made based on the information at hand.

The effective friction angle, Ø', for the clay would have a major influence on predicted embankment stability, and was estimated based on the following three considerations:

1) A correlation developed originally by Kenney (1959), and presented by Mitchell (1976), between $Ø'_{peak}$ and PI for clay soils indicated that for the reported range of PI the value of $Ø'_{peak}$ varies from 25-30°. Kenney specifically stated that this correlation was applicable to both natural and remolded clays.

2) Other correlations presented by Mitchell (1976) between $Ø'_{residual}$ and PI and LL indicated that for the reported ranges of PI and LL the value of $Ø'_{residual}$ varies from 9 to 22°.

3) Sloughing failures were occasionally observed in existing 2H:1V (slope angle, i , of 26.5°) cut slopes in the same soil. If these sloughs are analyzed with a simple long-term infinite slope approach, where FS= tan Ø'/tan i, then a lower bound estimate of Ø' for the natural soil deposit can be made if a value of FS which implies very widespread failures is used.

A value of FS= 0.85, which Sowers (1979) states means almost certain failure, gave Ø'=23°, and it could be reasonably expected that the as-compacted value for the clay would be greater. This estimate was very approximate because, among the uncertainties, it was not known that a long-term analysis was appropriate for the sloughs.

Based on these considerations, and the reasonable viewpoint that the displacement necessary to reduce strength to residual levels is relatively improbable in a structure internally reinforced with a high-modulus geosynthetic, the value of Ø' for the long-term analysis was conservatively estimated at 20°. This compares closely, for example, with the typical value of Ø'=19° for compacted CH soil given in the NAVFAC manual (US Navy, 1982).

The effective cohesion parameter, c', was set equal to 50 psf (2.4 kN/m²). This nominal value would have only minor influence on overall stability of the embankment, in that it would compromise about 5-10% of the soil shear strength for typical critical potential failure surfaces in the final design. For surficial stability this value would be more significant, but reasonable because the analysis procedure would not account for extensive light geogrid reinforcement to be placed at all slope surfaces.

Soil Unit Weight

The moist unit weight of the compacted clay fill, gm, was estimated to be 120 pcf (18.8 kN/m^3) for both end-of-construction and long-term design cases. It was judged that this value was almost certainly conservative because very high moist unit weights are not likely in plastic clay embankments. Concern over excessive positive pore pressure generation in plastic soils during compaction usually dictates that compaction specifications are written to minimize pore pressure development by requiring a relatively low degree of compaction and water content. Both these factors will reduce the moist unit weight. The project compaction specifications reported in Section 6.4 of this paper are in line with these assumptions.

REINFORCED EMBANKMENT DESIGN ASSUMPTIONS

Geometry

The design was based on four embankment cross sections that were cut perpendicularly to the roadway center line at stations that had the most critical combinations of slope height and existing ground geometry. At each section it was assumed that an equivalent uniform traffic surcharge of 250 psf (12 kN/m^2) was acting and that placement of a blanket drain under the embankment would result in a 5 ft (1.5m) thickness of compacted clay underlying the embankment toes.

One of the four critical design sections, at station 85+95, is given in Figure 3 and shows the embankment slope height (55 ft, 16.8m) and assumed ground geometry at this position. The embankment slope heights in this figure are not equal because the roadway center line does not cross the creek on a right angle with the ravine axis.

The project length was divided into about 8 zones such that each zone could be conservatively represented by one of the four critical design sections. The design process involved determining the necessary reinforcement layout for both embankment faces in each critical cross section, and then conservatively specifying the layout along the full length of the corresponding embankment zones. A slight horizontal curvature of the embankment center line, radius=1150 ft (350 m), was neglected. It was also assumed that transitional slopes at the ends of the embankments length that were flatter than 3H:1V would not require reinforcement.

Factor of Safety

The minimum factor of safety for all slope stability analyses of the critical sections was taken to be 1.3, as recommended by AHTD. This applied for both the end-of-construction and long-term conditions that are normally considered when designing cohesive soil embankments (Duncan et al., 1987).

Required Reinforcement Properties

The design was performed using three primary reinforcement grades, designated types 1, 2 and 3, assumed to have allowable 120-year design strengths of 1000, 2000 and 3000 lb/ft (14.6, 29.2 and 43.8 kN/m), respectively, in one material direction. Strength in the other direction was not needed for stability. No increase in design strength for shorter-term loading was considered, and it was assumed that the reinforcement would be placed in continuous horizontal layers. Design strengths were required to take into account the potential for site damage, material deterioration, and creep. Specifically, total in-isolation geogrid strain at the allowable design load was limited to 10% over 120 years, in order to limit long-term embankment deformations. The use of the in-insolation geogrid testing to develop design strengths for use in the limit equilibrium stability analysis is anticipated to result in geogrid strains significantly less than 10 percent and keep the soil from straining to residual strength.

An additional assumption was that the shear strength efficiency factor, f, between the CH embankment soil and the reinforcement material would have a minimum value of 0.7 for all the reinforcement types under the full likely range of confining pressures.

The efficiency factor is the ratio of soil-reinforcement to soil-soil interface shear strength under equal confining stress, and applies to both direct shear and pullout situations. This assumed value was later confirmed by sustained pull-out tests in the laboratory (Christopher and Berg, 1990) using clay samples shipped from the site.

Surficial Stability

The design would specify that continuous horizontal layers of intermediate reinforcement, consisting of lightweight geogrid extending 4.5 ft (1.4 m) into the slope, be placed on 1 ft (0.3 m) vertical intervals over the entire slope face (Figure 4). It was assumed that this reinforcement, along with any vegetation that was established, would ensure long-term stability of the slope face despite the expansive nature of the soil. The intermediate reinforcement was not directly modelled by the analysis procedure, but its effect was assumed to be conservatively accounted for by the use of a small effective cohesion value (c'=50 psf [2.4 kN/m2]) for the embankment soil. Intermediate reinforcement is believed to be a necessity when dealing with expansive clay soils.

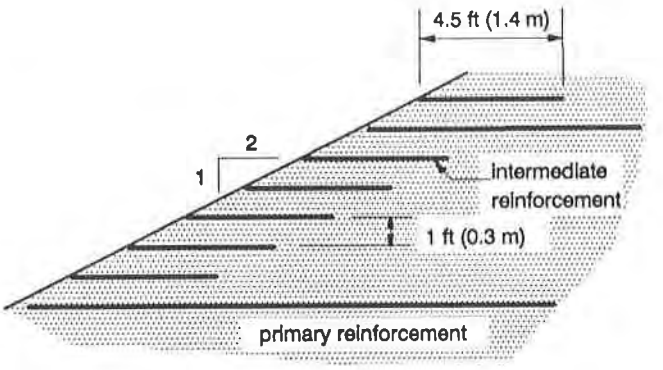

Figure 4 - Intermediate Reinforcement Scheme

Soil Pore Pressures

Embankment pore pressures were assumed to be zero for the long-term condition. This assumption was reasonable because the following control measures were to be incorporated in the project: a gravel blanket drain to intercept subsurface seepage; an effective embankment and roadway surface drainage system; and compaction specifications to minimize compaction-generated pore pressures. Any small compaction-generated pressures were assumed to dissipate before the long-term condition was achieved. End-of-construction pore pressures were assumed to be represented by the appropriate selection of undrained shear strength.

REINFORCED EMBANKMENT ANALYSIS METHODS

Stability of geosynthetic-reinforced soil embankments is generally evaluated in practice with extended versions of the classic limit equilibrium slope stability analysis methods (eg. Christie and El-Hadi, 1977; Jewell, 1982; Murray, 1982; Jewell et al., 1984; Leshchinsky and Reinschmidt, 1985; and Wright and Cuenca, 1986). These extended versions use different assumptions as to how the presence of tensile reinforcement influences computed slope stability safety factors.

Although these are equilibrium methods, strain compatibility between soil and reinforcement can be partially represented through consistent selection of soil and reinforcement strength properties.

Working stress analysis methods which directly account for strain compatibility, such as finite element methods or the model recently proposed by Juran et al. (1990), are not currently used in standard practice. Stability analyses for this project were performed with the extended limit equilibrium methods described in the following paragraphs.

Internal Stability

The term internal stability is herein associated with circular potential failure surfaces which intersect some or all of the reinforcement layers. Compound failure modes with potential circles intersecting some layers and passing behind others are therefore included in this category. Internal stability of the critical cross sections was evaluated using an extended version of Bishop's modified method of slices for circular potential failure surfaces (Bishop, 1955), as implemented in the TENSLOl computer code (Tensar, 1985). The extension involves adding an additional resisting moment into the overall moment equilibrium summation for each reinforcement layer intersected by the circle. The magnitude of each resisting moment increment depends on the tensile capacity of the layer and the orientation of the circle at the point of intersection (Figure 5), where the tensile capacity is the smaller of a) the reinforcement design strength or b) the safe pullout capacity of the layer due to its embedment behind the circle. The computer code made it practical to rapidly evaluate the most critical potential failure circle and corresponding safety factor for any specific cross section and reinforcement layout.

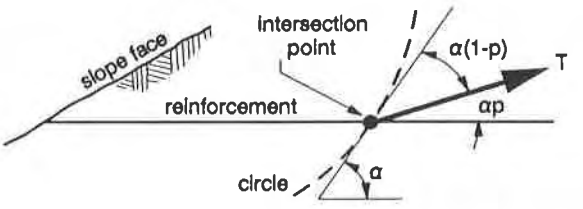

ΔM = resisting moment increment from reinf.
$= \min \{ RT [\cos(\alpha(1-p)) + \sin(\alpha(1-p)) \tan\phi] , RT \}$

where:
ϕ = soil friction angle
α = inclination of circle at intersection point
T = reinf. tensile capacity at intersection point
p = local reinf. rotation factor (assumed = 0.25)
R = radius of circle

Figure 5 - Details of Calculation of Reinforcement Resisting Moment Increment in Extended Modified Bishop Analysis

External Stability

A distinction between internal and external stability is somewhat arbitrary for this embankment. However, the term external stability will be herein associated with non-circular, compound failure surfaces which lie primarily behind the reinforcement mass and exit through the soil mass along a soil-reinforcement interface. The interfaces were preferential weak planes because of their assumed shear strength efficiency factor (f= 0.7). External stability of the critical cross sections was evaluated with both the simplified and complete Janbu

method of slices (Janbu, 1973). For both methods, the procedure for accounting for reinforcement layers which intersected the potential failure surface was not significant because their contribution to stability was small. In the complete Janbu method, however, the influence of reinforcement layers which crossed interslice boundaries was more significant, and was accounted for by a procedure similar to that recently described by Vanicek and Skopek (1989).

REINFORCED EMBANKMENT DESIGN PROCESS

End of Construction and Long-Term Cases

A first step in the design process was to determine whether end-of-construction or long-term conditions would control the design for each cross section. With this in mind, stability analyses without reinforcement were performed for both conditions. Observation of the minimum safety factors and locations of critical potential failure surfaces clearly indicated that, with the exception of the highest embankment section, long-term conditions were critical. For the highest section the decision was not obvious, but upon consideration of the selected end-of-construction soil and reinforcement strengths, it was judged that the long-term condition was critical. All reinforcement layout design was therefore performed for the long-term condition.

Reinforcement Placement Design

The main goal of the reinforcement design process for each critical section was a reinforcement layout that provided the required minimum safety factor for a wide range of potential failure surface shapes at all elevations in the embankment. As an additional constraint, the different reinforcement grades were used appropriately to minimize the reinforcement cost, and also hold the vertical spacing between primary layers to less than about 6 ft (1.8m). The maximum primary geogrid spacing of 6 ft (1.8m) was arbitrarily selected to control the size of localized unreinforced soil zones within the mass.

The process of developing an optimal reinforcement layout required many iterations in which the effect of layout changes on the minimum safety factor was evaluated with the internal stability computer code. Berg et al. (1989) have recently discussed how each different reinforcement layout can have a unique critical surface. External stability was also evaluated during this iteration process, and reinforcement lengths determined from the internal stability analyses often had to be increased to meet the external stability requirements.

The optimal layouts were subsequently adjusted where necessary to improve constructability. For example, layouts in adjacent slope zones were sometimes slightly modified to match up reinforcement layer elevations across the zone boundaries, or from the upstream to downstream face. In addition, it was attempted to hold layer lengths to convenient subdivisions of the expected product roll length of 98 ft (30 m). This was expected to minimize reinforcement wastage and reduce the construction time required for splicing and/or overlapping.

Final Reinforcement Layout

The final reinforcement layouts for two of the critical design cross sections are shown in Figure 6. These layouts represent continuous side-by-side placement of reinforcement pieces in each layer, though side splicing or overlapping was not required. Face views of the embankment, looking perpendicularly to the roadway center line, showing the complete reinforcement layout were also prepared for both the upstream and downstream embankment faces as an essential part of communicating the design to the contractor. The two face views were different because the roadway center line was not perpendicular to the creek ravine axis. Because the final reinforcement design for each of the four critical sections was applied along the entire length of their corresponding slope zones, the average minimum slope stability safety factor for the entire embankment was greater than 1.3.

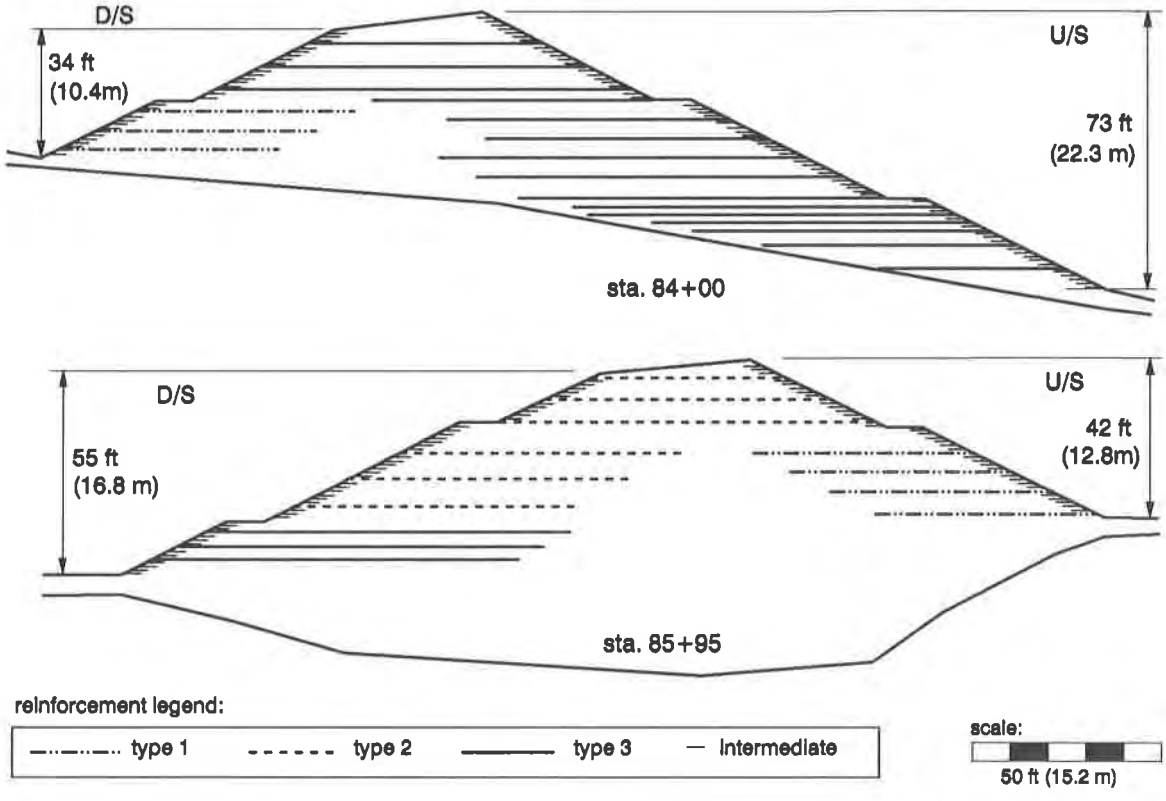

Figure 6 - Reinforcement Layouts for Two Design Sections

REINFORCED EMBANKMENT CONSTRUCTION

Site Preparation

Construction resumed in early 1988 with the contractor excavating the plastic clay fills which had been placed under the original contract. Fills were removed to bedrock and from around the box culvert. Prior to starting the geogrid-reinforced fill, a gravel drainage blanket 2 to 4 feet (0.6 to 1.2 m) in thickness was placed over the entire excavated surface. A nonwoven geotextile was placed at the interface of drainage gravel and the fill to prevent migration of soil particles into the gravel layer.

Geogrid Staging

Geogrid materials were shipped to the job in standard roll sizes and stored in the contractor's lay down area at the top of the ravine. A staging area was set up to sort the different types of geogrids and to cut them into the required lengths with small hand shears. After cutting the geogrids were rerolled, marked and then trucked to the fill location when needed.

Geogrid Placement

The selected geogrid materials for construction were Tensar UX1400, UX1500 AND UX1600 for primary reinforcement types 1, 2, and 3; and Tensar BX1100 for intermediate reinforcement. The first layer of primary geogrid reinforcement was placed in the fill approximately two feet above the top of the box culvert. Uniaxial geogrids were rolled out perpendicular to slope faces. Vertical spacings between the uniaxial geogrids ranges from 2 to 6 feet (0.6 to 1.8m).

Uniaxial geogrids were rolled out side-to-side without overlapping or tieing along the sides of the rolls. Geogrid rolls were overlapped end-to-end when required to splice lengths together. The minimum overlap length was 10 ft (3m) in the upper 10 ft (3m) of embankment and 4 ft (1.3m) for geogrid layers below 10 ft (3m) of the crest. Overlapped geogrids were separated by a minimum of 4 inches (10 cm) of soil fill material to prevent a weak plane which could be caused by a geogrid- to- geogrid interface.

The secondary, biaxial geogrids were rolled out parallel to the slope face at the outer edge of the embankment with 1 foot (0.3 m) vertical spacings between layers of uniaxial geogrids. All geogrids were placed by hand with unskilled labor. After rolling out, small hand shoveled piles of clay fill were placed on the end of geogrids rolls to hold them in place. No pins, ties or stakes were used. Total material quantities are listed in Table 3.

Fill Placement

Scrapers were used to haul the clay fill into place. Trafficking over the geogrids with the scrapers and other rubber-tired equipment was allowed at slow speeds less than 10 mph (16 kph) due to the high durability of the geogrid material. Dozers and blade-mounted, sheep-foot compactors were used to spread the fill into nominal 8 inch (20.cm) lifts. (See Photo 2). Sheep-foot rollers were used to compact the clay fill to the specified minimum 95 percent relative compaction according to AASHTO T-99 standards. Specified moisture contents ranged from optimum to 4 percent dry of optimum for the lower 30 feet (9.3 m) of embankment and from +2 percent to -2 percent of optimum in the upper embankment section.

Construction progressed according to schedule with the contractor noting little impact of the geogrid placement on the time required to place the fill. The selection of the geogrid reinforced, full height clay embankment solution over importation of granular fill in the lower half of the embankment and reinforced clay in the upper half resulted in a cost saving estimated to be over $200,000. A pending final report by AHTD will address the cost effectiveness of the geogrid reinforced embankment including the maintenance requirements.

REINFORCED EMBANKMENT INSTRUMENTATION AND PERFORMANCE

Instrumentation Scope

Due to the limited experience with geogrid reinforcement of high, plastic clay fills, an extensive instrumentation array was installed in the downstream face of the Cannon Creek structure during construction.

The instrumentation was designed to measure the performance of the geogrid-reinforced embankment with respect to horizontal and vertical movement of the soil, horizontal strain in the geogrid, and soil pore pressure and moisture content. Monitoring will continue for five years after completion of construction. The installed instruments are listed below under headings of the response to be measured:

Horizontal soil movement-
- 3 multipoint extensometers
- 3 inclinometers

Vertical soil movement-
- settlement stakes

Horizontal geogrid strain-
- 67 electrical resistance strain gages

Soil pore pressure-
- 2 tensiometers
- 3 pneumatic piezometers
- 5 soilmatrix potential sensors

Photo 2: Clay Fill Being Placed over Primary Geogrid Reinforcement

Soil moisture content-
8 moisture-temperature indicators
lab testing for initial moisture content

Details of the construction and instrumentation of the embankment are given in the AHTD post-construction report (Qedan, 1990). Presentation of instrumentation results in this paper will be limited to measurements of horizontal movement and strain from the extensometers, inclinometers, and strain gages.

Measurements of Horizontal Movements and Strains

a. Extensometers

Three horizontal multipoint rod extensometers were installed in the downstream face along a 160 ft (49m) running length of the embankment in the locations indicated in Figure 7. In each case the interval between anchors was 5 ft (1.5m) near the slope face and 10 ft (3m) for the remaining length. Relative movement between each anchor and the slope face was measured to 0.001 inch (0.025mm) at various times during construction with the first readings taken when the embankment crest was about 0 to 10 ft (0 to 3m) above each extensometer elevation. The total horizontal soil strains detected in each anchor interval during approximately the first 18 months after installation are presented in Figure 8.

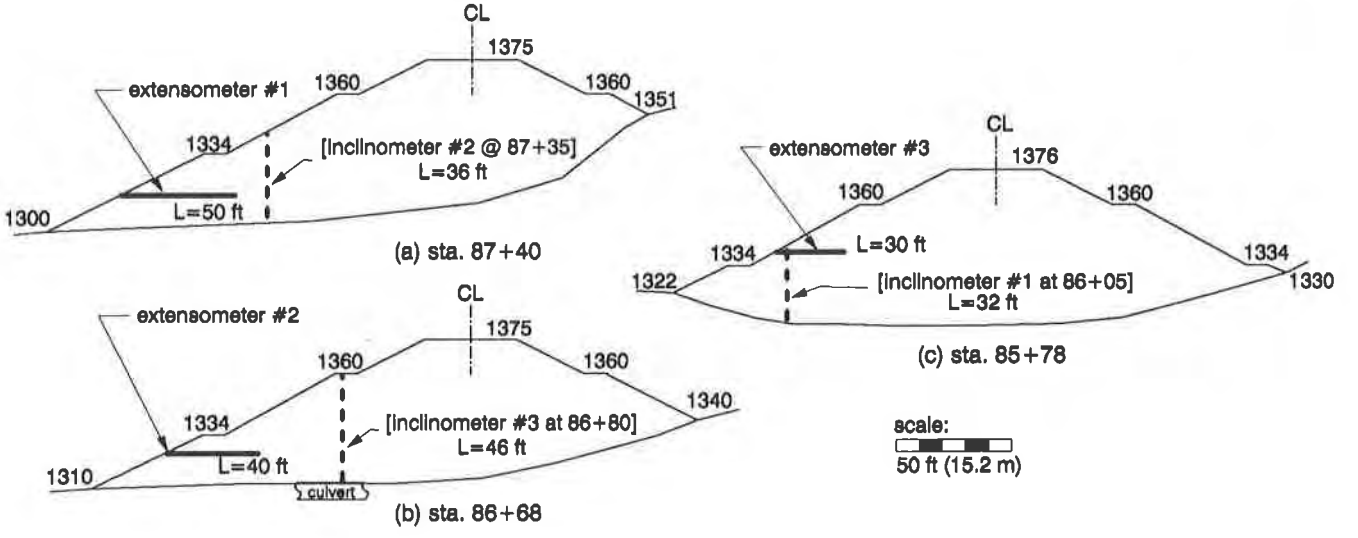

Figure 7 - Location of Extensometers and Inclinometers

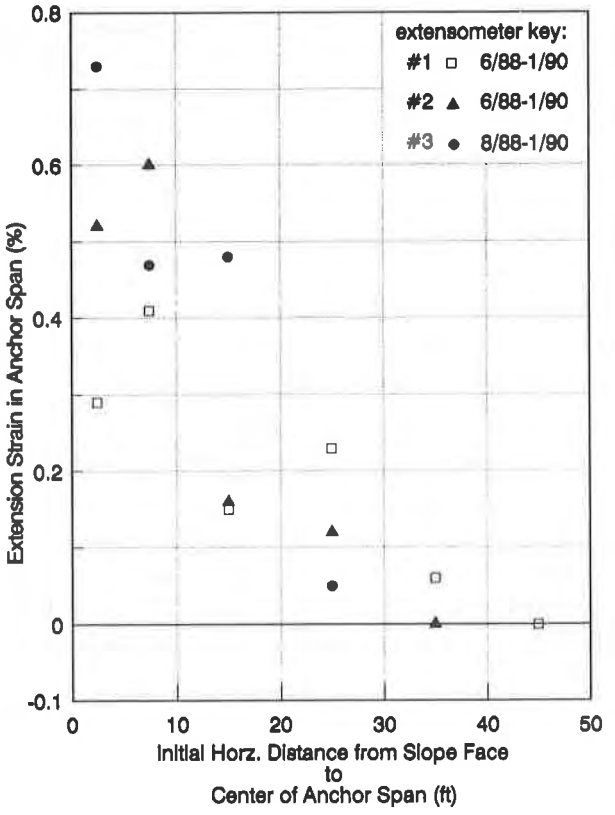

Figure 8 - Extensometer Results

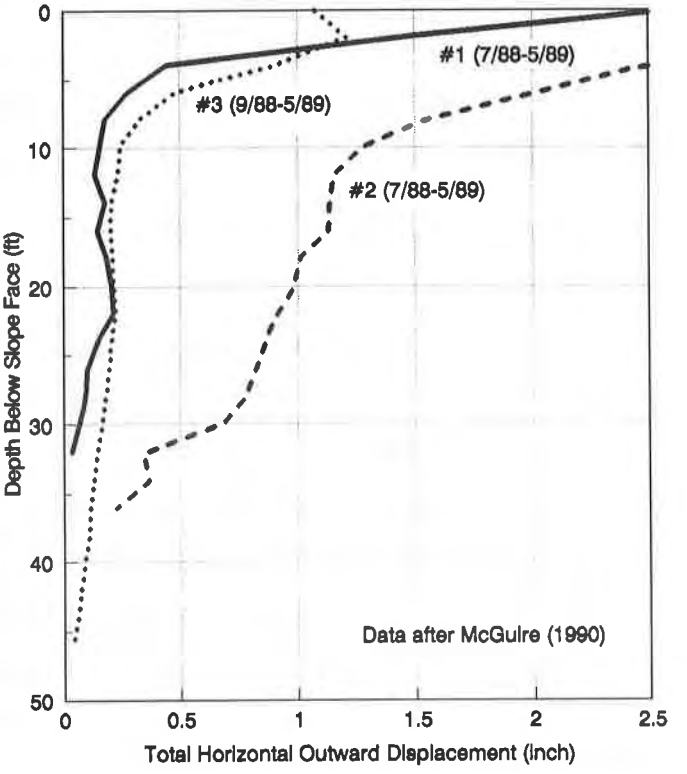

Figure 9 - Inclinometer Measurements

b. Inclinometers

Three slope inclinometers were installed in the downstream face along a 130 ft (40m) running length of the embankment in the locations shown approximately in Figure 7. Installation was performed when the embankment fill reached the planned inclimoneter elevations, and the first readings were taken within three days after installation.

The total outward horizontal movements detected by each inclinometer during approximately the first 12 months after installation are presented in Figure 9. Points of local maximum values on these plots, for example at depths of 14 and 22 ft for inclinometer #1, can be interpreted as locations of zones of relatively high horizontal displacement.

c. Strain Gages on Geogrids

Sixty-six strain gages were glued to geogrids reinforcing the downstream slope of the embankment. The first set consisted of 38 gages on type 3 geogrids at elevation 1326 ft placed along a 110 ft (34m) running length of the embankment, at 15-70 ft (5-21m) behind the slope face. The majority were placed on the geogrid tensile load carrying ribs, but four were placed on the geogrid cross bars perpendicular to the load carrying direction. A plan view of a representative geogrid structure showing typical strain gage positioning is given on Figure 10. Strain gage set #2 consisted of 28 gages on type 2 geogrids at elevation 1352 ft placed along an 83 ft (25m) running length of the embankment, at 30-50 ft (9-15m) behind the slope face. All of this set were placed on the geogrid load carrying ribs. The zero gage readings for sets #1 and #2 were made approximately 1-2 months and one week, respectively, after geogrid placement and therefore strains occurring during gage installation, geogrid placement and initial soil placement and compaction cannot be evaluated.

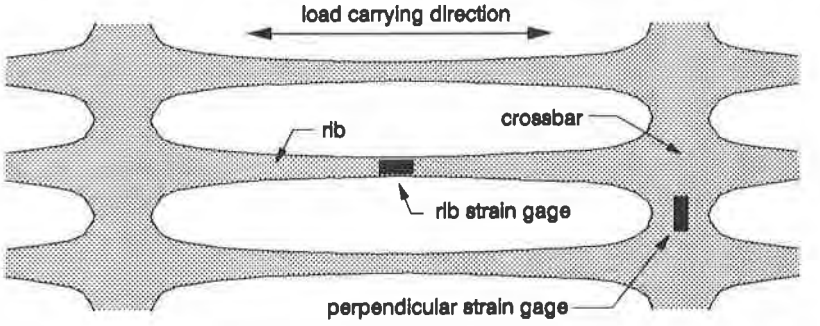

Figure 10 - Typical Strain Gage Installation Positions on Geogrid

A statistical summary of the total measured gage strains during the first 13-14 months after the zero gage readings is given in Table 2 for both gage sets. This summary includes only those gages which were working over the entire time span, and a single outlier reading from each set has been discarded. Because the gages in both sets were spread over many geogrid strips along significant running lengths of the embankment, it is judged inappropriate to present the gage readings in terms of a strain profile along a representative single geogrid strip. It is felt that the statistical summary is more appropriate as it reflects the spread in gage positions and the scatter in the readings to date.

Interpretation of To-Date Reported Measurements

a. Near-Face Soil Movement

The primary indication from the extensometer data (Figure 8) is that horizontal soil extension strain is greatest in the outer 10 ft (3m) of the embankment. Specifically, average measured strain in the outer 10 ft is approximately 0.5%, while the average strain in the zone 10-50 ft (3-15m) from the face is only 0.1%.

The significantly higher horizontal strain near the slope face is consistent with the inclinometer data (Figure 9) which shows dramatic increases in measured horizontal soil displacement within 5-10 ft (1.5-3m) depth from the slope face. Large movements in the near-face soils also seem consistent with the use of expansive clay fill given moisture access at the slope face.

Overall, the strong indication of significant near-face soil movement even in the presence of pervasive intermediate soil reinforcement shows the need for this reinforcement. It also suggests that the appropriate length for intermediate reinforcement in expansive clay slopes may be greater than the 4.5 ft (1.4m) length used for this project.

b. Internal Soil and Geogrid Strains

The extensometer data (Figure 8) indicates horizontal extension strain in the soil 10-50 ft (3-15m) behind the slope face in the range of 0.0-0.2% (ave. of about 0.1%). These values agree well with the geogrid strains of -0.04 to +0.30% (ave. of about 0.1%) measured in both strain gage sets from 15-70 ft (5-21m) behind the slope face (Table 2).

It also appears that horizontal soil movement is occurring well behind even the deepest extensometer anchor, as evidenced by the measured displacement of about 0.75 inch (19cm) for inclinometer #2 at a location close to 15 ft (5m) directly behind the deepest anchor of extensometer #1 (see Figure 7(a)).

A direct comparison of soil and geogrid strain can be made for extensometer #2 and a group of six working gages from set #1 which are both at elevation 1327, separated in station by only 10 ft (3m). During the 16 to 18 month period ending 1/90, extensometer #2 recorded a soil strain of 0.0% in the zone 30-40 ft (9-12m) behind the slope face and the six gages recorded a geogrid strain of 0.02-0.07% in the same zone.

The relatively good agreement between measured soil and geogrid strains summarized above must be considered with respect to two qualifying factors. First there was only one small area in the entire structure where gages and an extensometer were close enough for direct

comparison of strains. The second factor is that strains measured with small gages glued on the geogrid are not generally equal to the overall geogrid strains. This is because the glue itself is stiff relative to the polymer and may cause a local stiffening of the geogrid, possibly changing measured strains by 15% (Vishay Instruments, 1990) and because local strain measured at geogrid ribs may not equal the average strain in the geogrid structure (Bathurst et al, 1987).

c. Interpretation of the Inclinometer Data

This section presents an interesting use of the inclinometer data from this project that has been developed by McGuire (1990). The location of zones of relatively high lateral displacement that were indicated by the three inclinometers (Figure 9) were superimposed on a single embankment cross section at sta. 85+95. This superposition involved changes in station of 10-140 ft (3-43m), corresponding to changes of 0-20 ft (0-6m) in height of the downstream slope, and it was performed by holding constant the position of each inclinometer relative to the crest of the downstream slope. The superimposed high displacement locations were then compared to the position of the critical potential failure circle for sta. 85+95 from the internal stability design procedure already described. This comparison is given in Figure 11, and shows that the points of high lateral displacement fall fairly close to the critical circle.

The implications of this interesting comparison are not clear because of the following considerations. First, the limit equilibrium internal design procedure involves limiting stability conditions and its critical surfaces are not generally expected to be related to regions of high lateral working strains. Another factor is that the critical circle for comparison was for the long-term design case, and the inclinometer data is from only about 12 months after inclinometer installation. Finally, the superposition of inclinometer data from stations where slope heights vary significantly (from 55-75 ft [17-23m]) makes comparison to a single critical potential failure circle somewhat arbitrary.

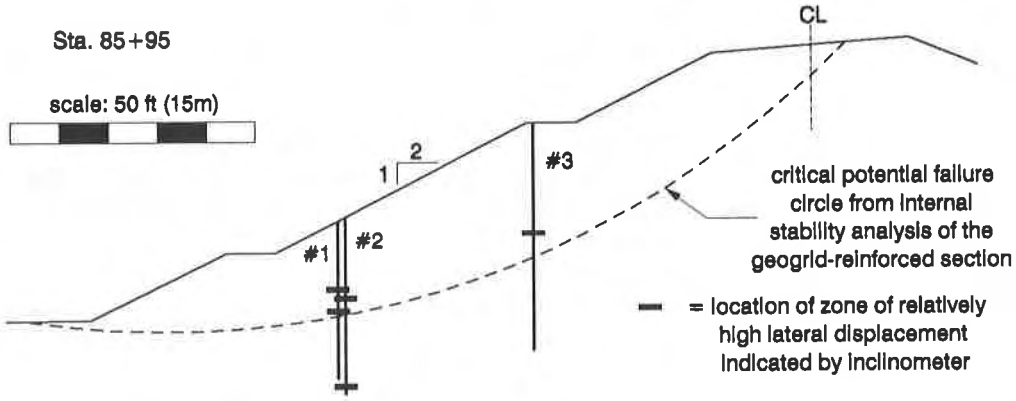

Figure 11 - Superposition of Inclinometer Data on Sta. 85+95

Despite these considerations, it appears that this type of comparison is potentially useful and may eventually reveal something about the relationship between working reality and limit equilibrium design procedures for reinforced soil structures.

CONCLUSIONS

The 76 ft (23.2 m) high geogrid-reinforced plastic clay embankment on Highway 16 is the largest roadway embankment in the state of Arkansas and is believed to be the highest reinforced cohesive soil embankment in North America. The selection of the geogrid reinforced solution over importation of granular fill in the lower half of the embankment and reinforced clay in the upper half of the embankment resulted in a cost saving estimated to be over $200,000.

Long-term loading conditions governed the reinforcement layout design, which was performed using detailed limit equilibrium stability methods that fully accounted for the interaction between the layout and the location of critical potential failure surfaces. Allowable geogrid design tensile strengths took into account site damage, material deterioration and creep.

An extensive instrumentation program was undertaken due to the limited experience of geogrid reinforcement of high clay fills. Measurements taken in the first 24 months of service indicates limited soil and geogrid deformation and generally confirms design assumptions. Maximum horizontal soil strains have occurred in the outer 5-10 ft (1.5-3.0m) of the embankment which is consistent with the expansive clay soils which have access to moisture at the slope face.

The indication of high strains near the slope face shows the essential need for the intermediate geogrid reinforcement at close vertical spacings in expansive soil slopes. It also suggests that the appropriate length of this reinforcement may be greater that the 4.5 ft (1.4 m) length used for this project. Strains near the ends of extensometers suggest that deeper instrumentation should have been installed.

Virtually all measured strains in the embankment to date are below 0.5%, and although these measurements do not include strains that occurred during the initial construction operations prior to device zeroing, it is judged that they indicate satisfactory overall performance of the embankment and relatively low levels of load in the geogrid reinforcement. The performance data indicates that deformation has not ceased and it is expected that this large plastic clay embankment will continue to deform as a fully drained soil loading condition gradually develops. Continued monitoring of the instrumentation until movements stop will provide useful information about the performance of reinforced cohesive structures.

Acknowledgements

The Highway 16 project was partially funded by the Federal Highway Administration(FHWA). Geotechnical engineers at the Washington, D.C. and Ft. Worth, Texas offices of FHWA were involved with evaluation and approval of the geogrid reinforced embankment.

The embankment design was developed by Raymond-Kaiser Engineers in Houston, Texas with the assistance of The Tensar Corporation located in Morrow, Georgia. Michael Cowell, Vicky Chouery-Curtis, and the first two authors were major participants in the design process while employed by the Tensar Corporation. The geogrid supplier was Contech Construction Products in Little Rock, Arkansas and the construction contractor was Machen Construction, Inc. of Little Rock.

Dr. Sam I. Thornton supervised the thesis of Mr. McGuire and provided constructive assistance in the early development of the paper.

References

Bathurst, R.J., Wawrychuk, W.F. and Jarrett, P.M. (1987), "Laboratory Investigation of Two Large-Scale Geogrid Reinforced Soil Walls", Proc. of NATO Workshop on Application of Polymeric Reinforcement in Soil Retaining Structures, June, p.71-125.

Berg, R,R., Chouery-Curtis, V.E. and Watson, C.H. (1989), "Critical Failure Planes in Analysis of Reinforced Slopes," Proc. of Geosynthetics '89 Conf., San Diego.

Bishop, A.W. (1955), "The Use of the Slip Circle in the Stability Analysis of Slopes," Geotechnique, v.5, p.7-17.

Christie, I.F. and El-Hadi, K.M. (1977), "Some Aspects of the Design of Earth Dams Reinforced with Fabric," Proc. Int. Conf. on the Use of Fabrics in Geotechnics, Paris, v.1, p.99-103.

Christopher, B.R. and Berg, R.R., (1990), "Pullout Evaluation of Geosynthetics in Cohesive Soils", 4th International Conference on Geotextiles, Geomembranes and Related Products, The Hague, Netherlands, May 28-June 1.

Duncan, J.M., Buchignani, A.L. and DeWet, M. (1987), "An Engineering Manual for Slope Stability Studies," Virginia Polytechnic Institute and State University, Dept. of Civil Engineering, March, p.3.

Janbu, N. (1973), ."Slope Stability Computations, " Embankment-Dam Engineering (Casagrande volume), John Wiley and Sons, New York, p.47-86.

Jewell, R.A. (1982), "A Limit Equilibrium Design Method for Reinforced Embankments on Soft Foundations," Proc. of 2nd Int. Conf. on Geotextiles, Las Vegas, August, v.3, p.671-676.

Jewell, R.A., Paine, N. and Woods, R.I. (1984), "Design Methods for Steep Reinforced Embankments," Proc. of Conf. on Polymer Grid Reinforcement, London, March, Thomas Telford Ltd., p. 70-81.

Juran, I., Ider, H.M. and Farrag, K. (1990), "Strain Compatibility Analysis for Geosynthetics Reinforced Soil Walls," ASCE Journal of Geotechnical Engineering, v.116, no.2, p.312-329.

Kenney, T.C. (1959), discussion of "Geotechnical Properties of Glacial Lake Clays," ASCE Journal of the Soil Mechanics and Foundations Division, v. 85, no. SM3, June, p. 67-79.

Leshchinsky, D. and Reinschmidt, A.J. (1985), "Stability of Membrane Reinforced Slopes," ASCE Journal of Geotechnical Engineering, v.111, n.11, p.1285-1300.

McGuire, M.S. (1990), "Reinforced Earth Embankment", MSCE Thesis, University of Arkansas, Fayetteville, Arkansas.

Mitchell, J.K. (1976), Fundamentals of Soil Behavior, John Wiley and Sons, New York, p. 284-285.

Murray, R. (1982), "Fabric Reinforcement of Embankments and Cuttings," Proc. of 2nd Int. Conf. on Geotextiles, Las Vegas, August, v.3, p.707-713.

Qedan, B. (1990), "Instrumentation of a 76 ft High Reinforced Earth Embankment, Cannon Creek Structures and Approaches (phase II): Post Construction Report", Arkansas State Highway and Transportation Dept., Materials and Research Division, Report No. FHWA/AR-90/001, January.

Sowers, G.F. (1979), Introductory Soil Mechanics and Foundations: Geotechnical Engineering, 4th edition, MacMillan, New York, p. 583.

The Tensar Corporation (1985), TENSLOl slope stability computer program, internal program.

U.S. Navy - Naval Facilities Engineering Command (1982), Foundations and Earth Structures, Design Manual 7.2 (NAVFAC DM-7.2), May, p. 7.2-39.

Vanicek, I. and Skopek, P. (1989), "Stability Calculation of Reinforced Soil Slope," Proc. of 12th ICSMFE, Rio De Janeiro, August, v.2, p.1321-1324.

Vishay Instruments, Inc., "Correction Equation for Strain Gages on Low Modulus Material", 63 Lincoln Highway, Malvern, PA, 19355.

Wright, S.G. and Cuenca, F. (1986), "Stability Computation Procedures for Earth Slopes Containing Internal Reinforcement," Center for Transportation Research, University of Texas at Austin, Research Report No. 435-1, November.

A Case History of the Design and Construction of a Reinforced Soil Wall Using D. S. F. Fabric Geotextiles for the Purpose of Stabilizing a Major Landslip

Peter Rankilor
Manstock Geotechnical Consultancy Services Ltd., United Kingdom

ABSTRACT

This case history represents an ideal example of the utilization of several different geotextiles and geogrids for a variety of purposes including soil reinforcement, separation, filtration and architectural landscaping.

In 1987, for the first time, high tenacity polyester D.S.F.[1] geotextile grids (Refs 1 & 2), were used to construct steep reinforced-soil retaining banks for the stabilization and reconstruction of a major landslip. Geotextile-wrapped ground drains and fin drains were used to intercept and remove groundwater. The final landscaping works included the use of polypropylene geogrids to construct reinforced-soil brick wall garden frontages on top of the main reinforced-soil banks. During the construction works, a polypropylene tape woven geotextile was used as a base for a steep (2.5H:1V) access road.

DESCRIPTION OF THE PROBLEM

The Landslip. The site of the landslip was a high, steep wooded hillside in the county of Cheshire in the United Kingdom. The hillside was subsequently assessed as standing with only a marginal factor of safety since a river at the base of the slope had cut a valley with over-steep slopes, exceeding 2H:1V in places. A domestic soil moving operation at the top of the slope had de-stabilized the crest and a major landslip took place, removing the crest of three domestic gardens and the upper two thirds of the hillside. Fig.1 is a plan of the landslip, showing its proximity to the houses; a cross-section of the slip is shown schematically in Fig.2.

Site investigation boreholes revealed that the hill contained no rock, but was entirely made of glacial sands with a thick band of clay part way up the slope. The slip had moved outward on the clay, thus making the slope very difficult to stabilize. Owing to this type of geometry, there was a tendency for the slip to keep moving in sporadic episodes, often corresponding to periods of heavy rainfall.

[1] D.S.F. stands for Directionally Structured Fibre fabrics made on Warp Knitting machines.

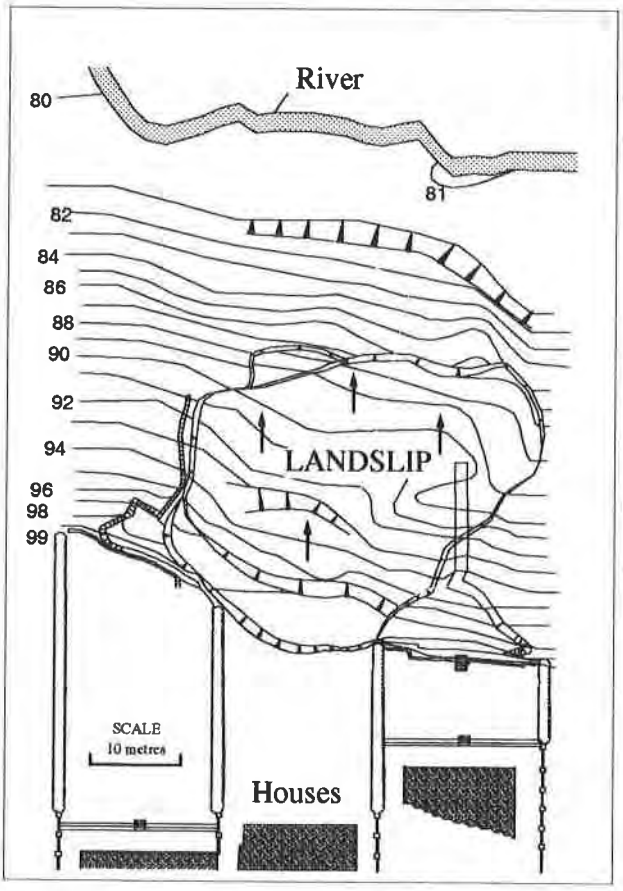

Fig.1 Plan of Landslip

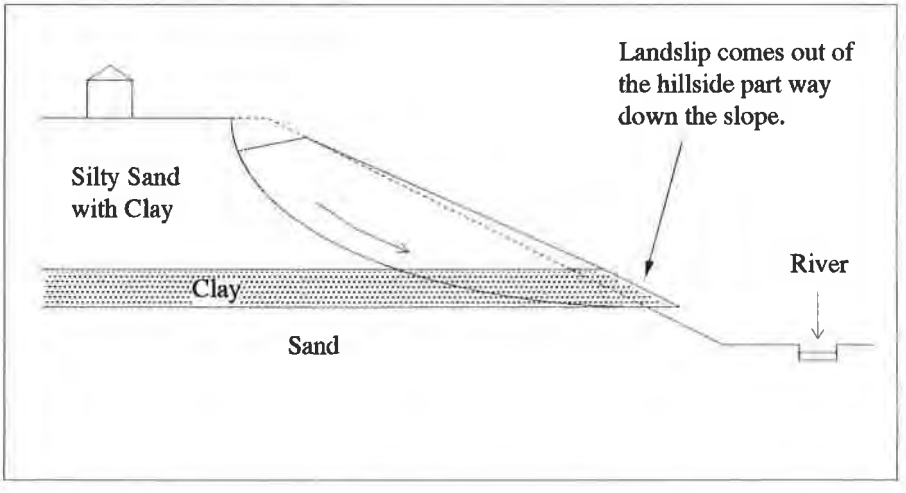

Fig.2. Schematic Cross Section of Landslip.

Stabilization options were limited by :- a) the need to stop the slip from moving further during operations, b) the need to restore the gardens to their original position; therefore the slope could not be cut back to a flatter angle, c) the fact that the slip came out two thirds of the way down the hillside, thus precluding the use of the traditional 'toe weight' solution.

Working conditions were aggravated by a) the fact that the slope was steep for the undertaking of civil engineering drainage works (up to 2.5H:1V) b) it being moderately wooded, with trees and roots hindering drain excavation b) the presence of excessive amounts of water egressing from the slope.

THE DESIGN SOLUTION

Extensive slip surface analyses were conducted and it was decided that the introduction of very effective downslope drainage could raise the safety factor of the slope to marginally above unity for long enough to permit remedial measures to be instigated.

Fig.3. shows a plan of the drainage system which was installed to deal with the ground water. These drains were up to 5 metres deep and were about eight metres apart. This was a particularly challenging part of the design in view of the wooded nature of the slope and its steepness. It was subsequently proved to be a practical proposal.

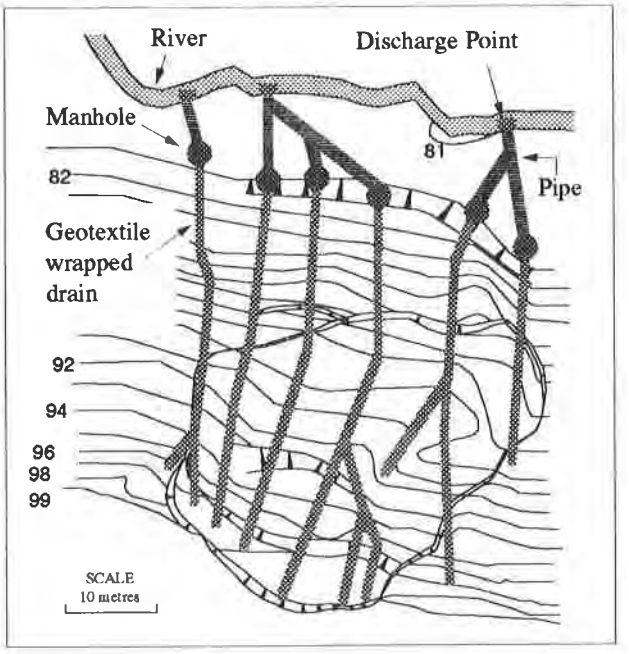

Fig.3 Plan of Drainage

With regard to lifting the safety factor to an acceptable final value of 1.35 (since a toe weight could not be used), the solution proposed was to introduce a highly permeable granular basal friction toe to the slip by removing the clay toe and replacing it with a reinforced soil bank (Fig.4). However, to cut away the entire toe would certainly de-stabilize the slope and cause further movement. Therefore, the design proposed that only a two metre wide slot would be cut out in the first instance. In this slot would be constructed a two metre wide reinforce soil block, using any suitable material from immediately adjacent, together with imported fill. Waste was to be carted off site. By this means, the reinforced bank would be constructed laterally across the base of the slip without destabilizing it since virtually as soon as a slot was constructed, it was to be filled with reinforced soil.

The design was for total stabilization to be achieved with the completion of the lower bank. Although the overall slope would then be stable, the reconstruction of the upper crest was problematic in view of its height and steepness. Therefore, a second reinforced soil bank was proposed to provide a strong bridge across the original failure surface and a stiff crest on which to reconstruct the landscaping and garden wall features. The two banks would also provide firm rooting for the replacement trees which were to be established on the reconstructed hillside.

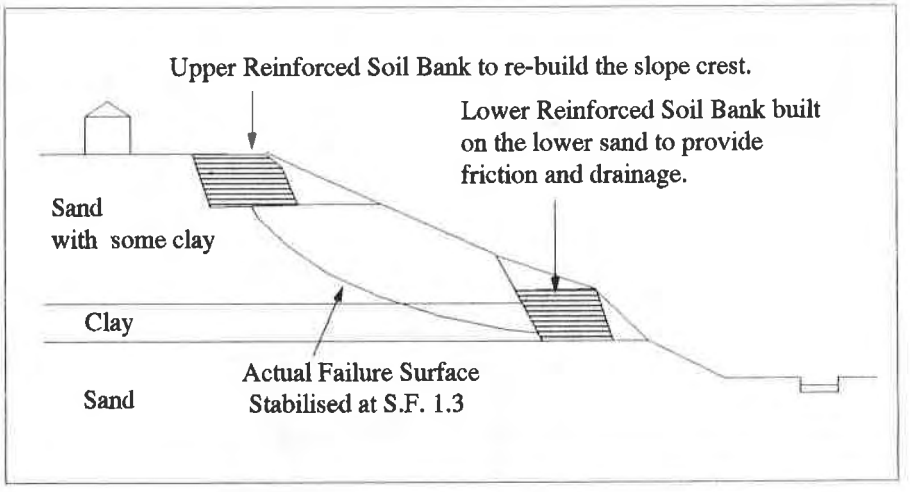

Fig.4. Schematic Design Solution Using Reinforced Soil Banks.

DESCRIPTION OF THE SITE WORKS EXECUTED

A number of longitudinal downslope drains were constructed to a depth of 5m. They were placed at 8m intervals apart and each drain was wrapped in a needlepunched nonwoven geotextile and backfilled with a carrier pipe and coarse granular drainage stone. These were excavated as the first phase of the work in order to remove excess groundwater and to raise the safety factor to the point where the slip just stopped moving. These drains were constructed successfully even though tree roots were present and the slope was steep. They worked well and the slip dried out.

Much thought was given as to whether to excavate the trenches from the top to the bottom of the slope or the opposite. It was clear that, from a drainage point of view, it would be easier to start the drain excavations at the bottom, thus allowing the ground to drain away by gravity as work progressed. However, this meant that the excavator would have to be winched up the slope if it was to avoid having to work over the open trenches, as shown in Fig.5. Eventually, option 4 (Fig.5) was adopted as the best alternative - excavating from the top down, since this meant that the excavator could stand below the trench and that its excavation stroke would be assisted by the weight of the digger. It would not need winching. The only disadvantage was that the trench had to be pumped continuously to dry it during excavation work. This was not easy to do, but was actually achievable.

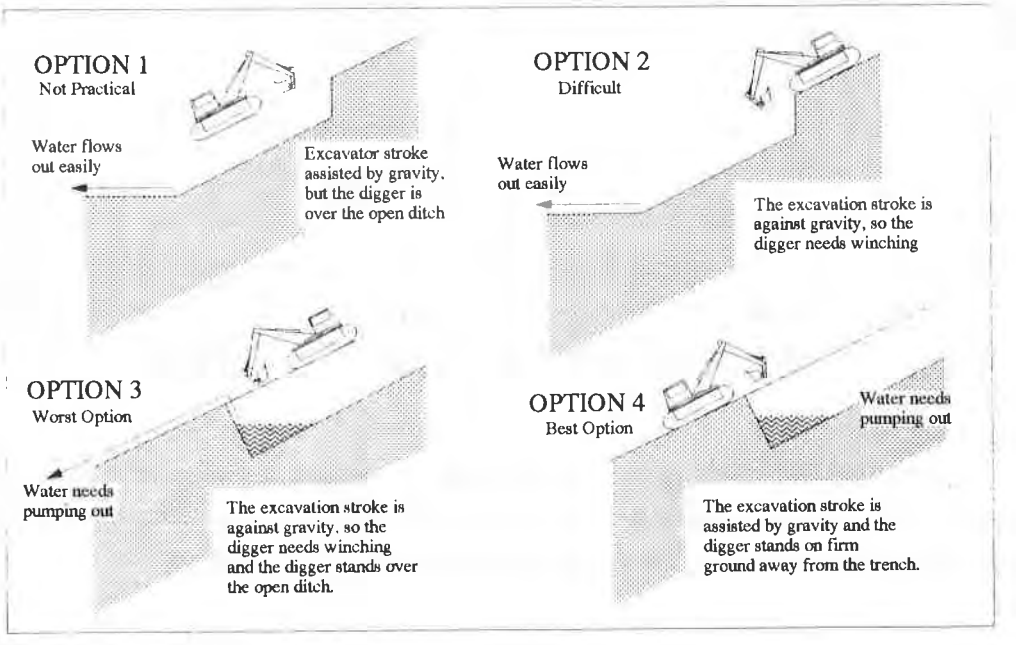

Fig.5. Options For Excavating Down-Slope Drains.

Then followed the placing of the lower bank. In order to maintain control of the overall slope, only narrow sections of the clay could be excavated at any time and replaced by reinforced soil blocks. This was done on a sequence basis as shown in Fig.6. The weight, granularity and permeability of the lower reinforced soil bank prevented further slippage of the slope outwards and stabilized the slip, raising the safety factor to 1.35.

As the lower reinforcing bank was constructed sideways in 2m wide modules, the pre-constructed ground drains were cut out as the bank reached each one. Each severed ground drain was re-connected beneath the bank and drains from the bank itself were connected into these lower ground drains as shown in Fig.7. The use of a geotextile wrap facilitated the cutting out of the drains and the re-connection of the drains, whilst keeping the stone clean.

Reinforcing Geotextile. Slip surface calculations were undertaken using the SARMA method, which enabled consideration to be given to non-circular surfaces. By insertion of different bank

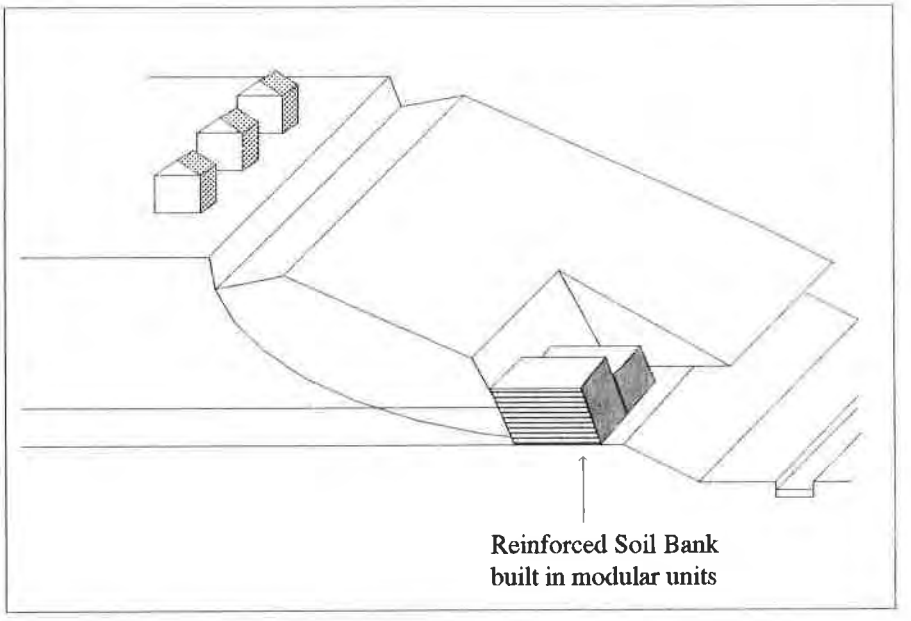

Fig.6. Modular Replacement of Slip Toe by Reinforced Soil Bank.

constructions, it was possible to calculate that banks measuring 5-6 metres high and about 4.5 metres deep, would stabilise the bank. As described below, considerations of strength, site damage factor and longevity led to a design requirement for a reinforcement with an ultimate tensile strength of 140 kN/m width.

Much reinforced soil work has been undertaken elsewhere using polyethylene grids, but these were only available with a maximum strength of around 110 kN/m. This led to consideration of either the newly developed D.S.F. geogrids or conventional woven geotextiles. For soil reinforcement

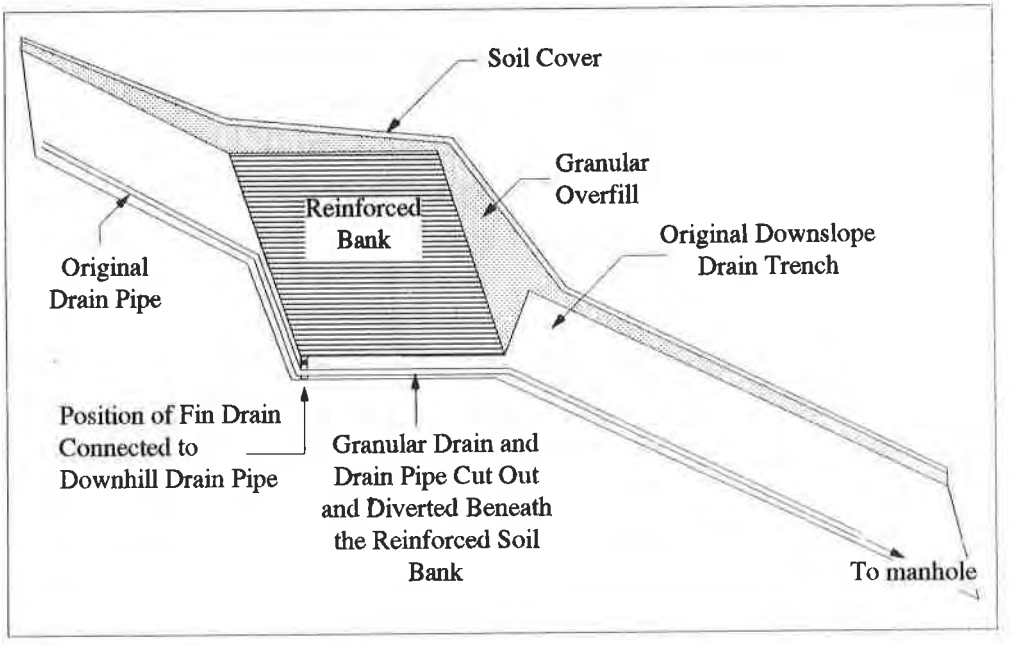

Fig.7. Cross Section of Downslope Drainage Ditch.

purposes, both of these products are made from high tenacity polyester multifilaments and were manufactured in strengths up to and exceeding the required value.

Grids have generally been preferred over recent years for soil reinforcement purposes and a D.S.F. geogrid was chosen in this case because of its strength, cost effectiveness, high grip and because its open grid structure would ensure the absence of any possible perched water on top of the reinforcing sheets. It was recognised that continuous sheet geotextiles have been successfully used in soil reinforcement work before, but it was a cause of potential concern that in the particular position that the banks would be built, with outflow of water from the cut slopes on which they were abutting, there was the possibility of a continuous textile becoming silted and actually trapping water. The design was based upon a free draining block of reinforced soil and the presence of an open grid would ensure that this was achieved and maintained in the long term.

The photograph in Fig.8 is a close-up view of the actual D.S.F. warp-knitted grid finally chosen and used for the works[2]. The product chosen was a mid-size reinforcing mesh, suitable for use with medium-to-coarse granular materials. It was a fabric with an ultimate strength of 140kN/m width and an effective mesh size of 15mm x 15mm. It can be observed that the predominant amount of polyester is laid in the warp direction, with only sufficient in the weft to provide stability and the necessary grip.

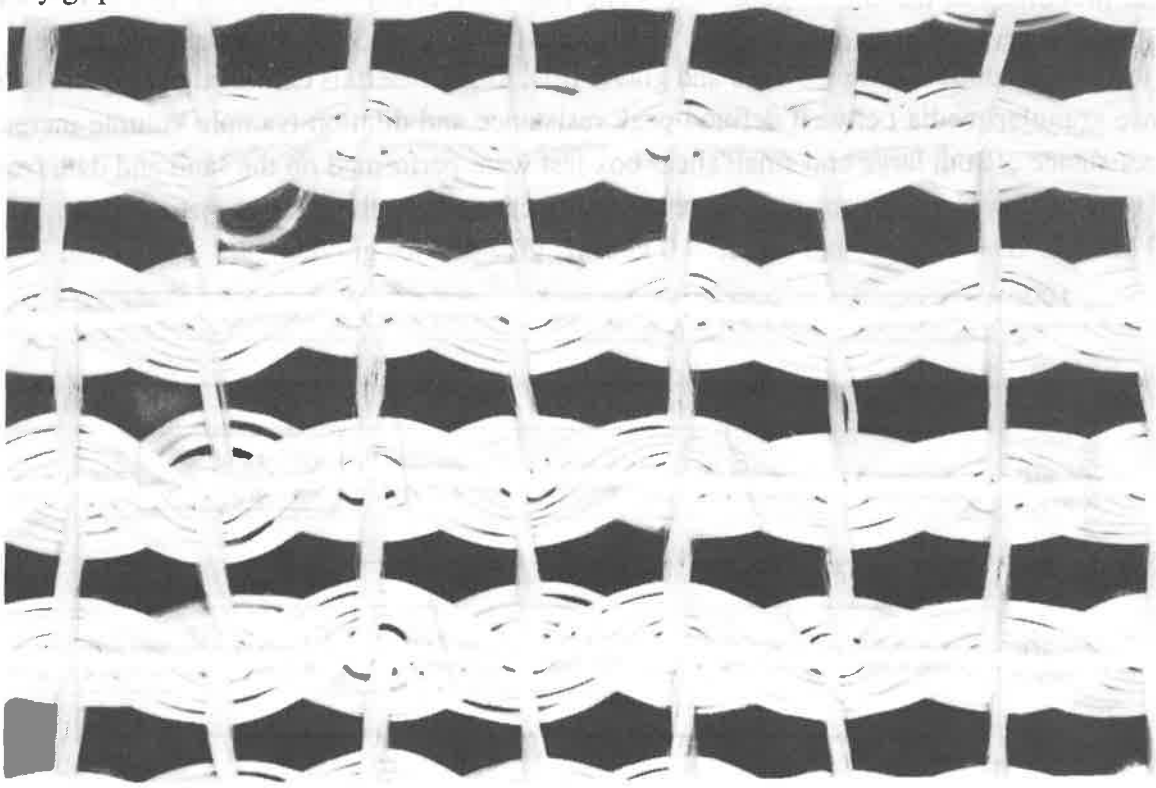

Fig.8. Photograph of the Warp Knitted, High Tenacity Polyester, D.S.F. Reinforcing Geotextile used in the Works.

2 A HITEN rectangular mesh grid manufactured by Fryma Fabrics Ltd., Nottingham, UK.

During the site investigation stage, samples of the sand throughout the site were taken and tested in the laboratory for particle size distribution and coefficient of friction for design input. As well as this, between design and implementation, larger samples were excavated and laboratory pull-out tests were undertaken to confirm the properties of the reinforcement geotextile in relation to standard and local material.

It was recognised that the soil/reinforcement interaction would be affected by the size of the soil particles used for the structural backfill between the banks. Accordingly, the geotextile grid was tested with different size fill, i.e. both sand and gravel. The inbuilt facility for the contractor to build the site from any free-draining granular material, otherwise irrespective of particle size and dependent only on internal angle of friction, was one of the factors leading to the substantial cost savings inherent in this method of construction. The contractor was able to use any from-site or local granular materials that came available during the course of the works, on an ad-hoc basis, subject only to simple laboratory confirmation testing. The banks, therefore, were constructed of variable size and quality of material, all meeting or exceeding the design specification. In some places it would be sands derived from the on-site works; in other places it would be imported gravels or sands, and in yet other places it might be a mixture.

The curves in Fig.9 show a typical sand and gravel fill material used for the assessment of the pull-out properties of the D.S.F. geotextile. The fills were always compacted to a dense state and typical maximum bulk densities obtained were around 1700 kg/m3 for both sand and gravel. Direct shear tests were conducted on the sand and gravel fills. Both materials exhibited the typical behaviour of dense granular media i.e. well defined peak resistance and dilation (sample volume increases) at peak resistance . Both large and small shear box test were performed on the sand and data from both boxes were in complete agreement. The resultant effective shear strength parameters were C' = 0 kN/m2, Ø' = 40° for sand and C' = 0 kN/m2, Ø' = 57° for gravel.

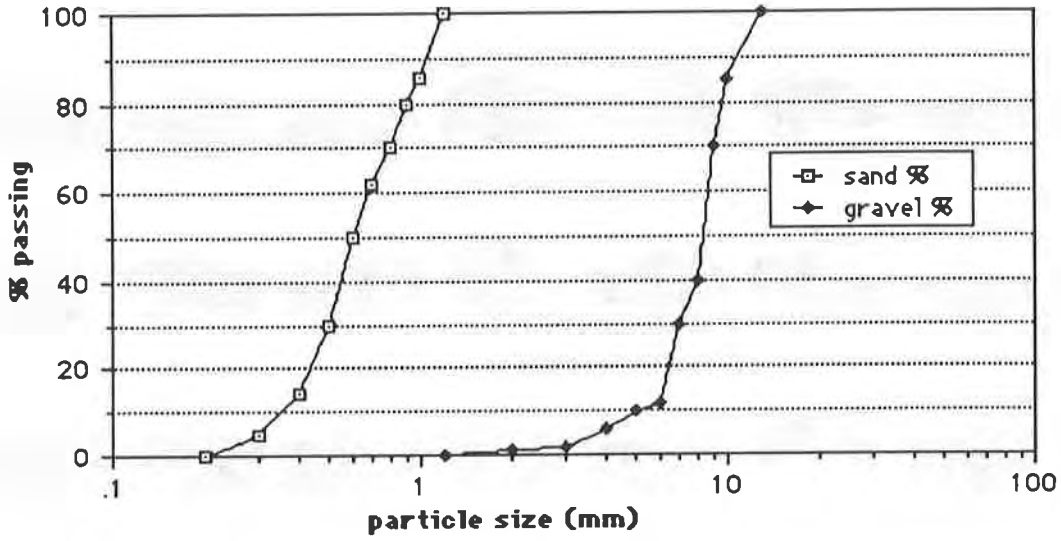

Fig.9 Sieve analyses of a sand and gravel used in the test program.

For small scale tests with the geotextile grid, a shear box with plan dimensions of 300mm x 300mm was used. The normal stress was exerted by a hydraulic ram and was measured on a load cell interposed between the machine loading head (which is connected to the hydraulic ram) and the top loading platen. It is essential to use such a load cell because of the dilation which occurs during shearing of the dense granular media used in this investigation. The sample height increase which occurs can cause the normal stress to rise (due to friction in the hydraulic ram) unless it is closely monitored and the hydraulic pressure adjusted accordingly.

The modified shear box as illustrated in Figure 10. The two halves of the box are connected together (with spacers) while the fabric is placed in the slot between them. Soil is compacted under and over the reinforcement fabric (1) and a load is placed on to the top (2). Both parts are then driven to the left by a ram (3), while the fabric, connected to the clamp (4) is pulled through the soil.

During the test, a change in soil volume is experienced as an indication of the interaction between fabric and soil. Pull-out failure is achieved when the pull-out load becomes constant, i.e. when the fabric tears or when the tail of the fabric reinforcement is pulled into the box. This keeps the area of the soil/geotextile interface constant during the shearing process.

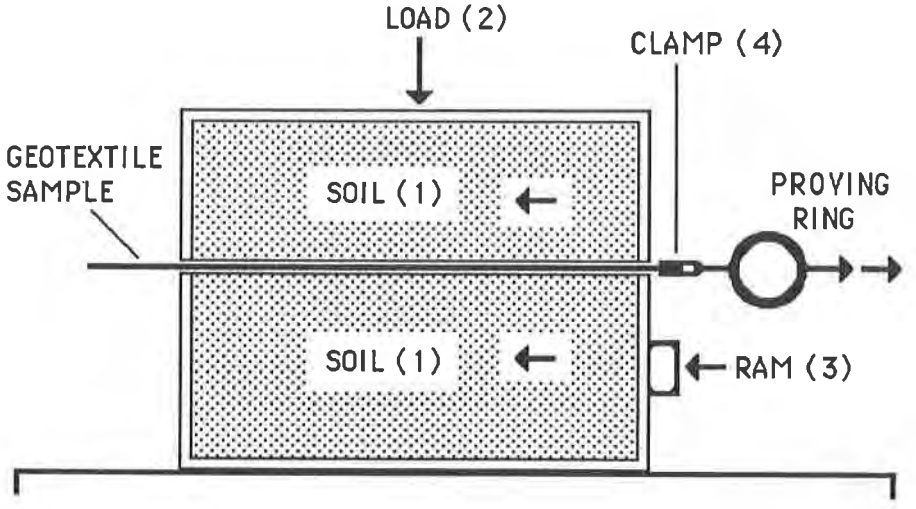

Fig.10. Diagram of Modified Shear Box used for Small Scale Pullout Tests.

Testing was also undertaken on a larger-scale pull-out box (as opposed to the modified shear box). The reinforcement was 2m long and a strip width of 0.3m was used. Essentially, pull-out tests are different in nature from soil/fabric shearing tests. In this case, since the fabric is pulled-out of the soil, the restraining force of the soil is applied to both sides at the same time. Depending on the type of textile being tested, soil dilation does not need to occur since fibres can "slide' between particles if it is of a sheet variety, but not so with grids. We were looking here, for a direct, pragmatic and practical indication of the actual pull-out behaviour of the textile under realistic loading conditions.

Depending upon the assumptions made, the lateral stress level within a surcharged reinforced bank, at a depth of six metres, can be calculated at around 30 kN/sq.m. In the design of a long-life stress-absorbing structure such as a slip-stabilising bank, special consideration had to be given to the multiple factors affecting the long term ability of the geogrid to perform its function. In simple terms, in view of the relatively new state of the art of reinforced soil, conservative partial safety factors must be applied to the design criteria. In view of the lack of knowledge at this time, these can only be arbitrary, but for example, the following would appear realistic in non-dimensional terms:-

As new ultimate tensile strength = 1

Factor to allow for site placement damage	gravel 0.65	sand 0.95
Factor to allow for 'no creep' condition		polyester 0.45
Factor to allow for chemical deterioration over 100 years		polyester 0.20
Factor to allow for short term UV degradation during construction		U.K nil

Since any type of fill was to be permitted, it was necessary to multiply the initial unit strength of the textile by 0.65 for fill placement damage. This then had to be factored by 0.45 to achieve a 'no–creep' condition leaving an effective strength of 0.29.

The 'damaged' 0.29 residual had also to be multiplied by 0.20 to allow for physico-chemical deterioration over a period of say 100 years. This would leave an effective strength of 0.06 times the original strength. This criterion is rigorous but it was applied as a simple multiplier to the others since it is not really known how it factors in relation to creep resistance. This approach was considered adequate to cover engineering requirements. Therefore, a working imposed stress on the geotextile of 140 x 0.06 = 8.0 kN/m width would be acceptable.

With a layer interval of 250 mm, there are four layers of geotextile to absorb the outward force, giving a working load in each layer of one quarter of 30 kN/sq.m. being 8 kN/m width. Owing to the high safety factors required for the reconstruction - in view of the proximity of domestic residences - a working stress of 8 kN/m width was considered sensible and cost-effective. Savings from any reduction in initial geotextile strength would be very small in relation to the overall cost of the project.

With regard to the frictional grip capability of the geotextile, Fig.11 is typical of the test curves produced and shows that the 6298G geotextile generated a slightly better grip within a gravel than a

sand. Information of this kind allowed the design to be developed around the lower bound parameters of the sand.

The maximum shearing resistance developed was, as might be expected from a grid, equal to sand-on-sand friction, although with grids, it is possible to obtain an apparent angle of friction greater than the internal angle of friction of the soil itself, dependent upon the relative strength of the weft elements. However, the graph demonstrates that with working tensile forces of around 8 kN/m width or less, each geotextile sheet would stabilise with only a very small displacement and at very low percentage strain.

It is interesting to note, for calculation purposes that when the 6298G geotextile was untensioned the percentage of the total plan area occupied by the fibres in the direction of sliding (the warps) was approximately 60%, decreasing to 40% as tension was placed on the fabric. It was also useful to have the opportunity of assessing the type and extent of damage imposed on a DSF geotextile under high confining stresses in different types of granular material.

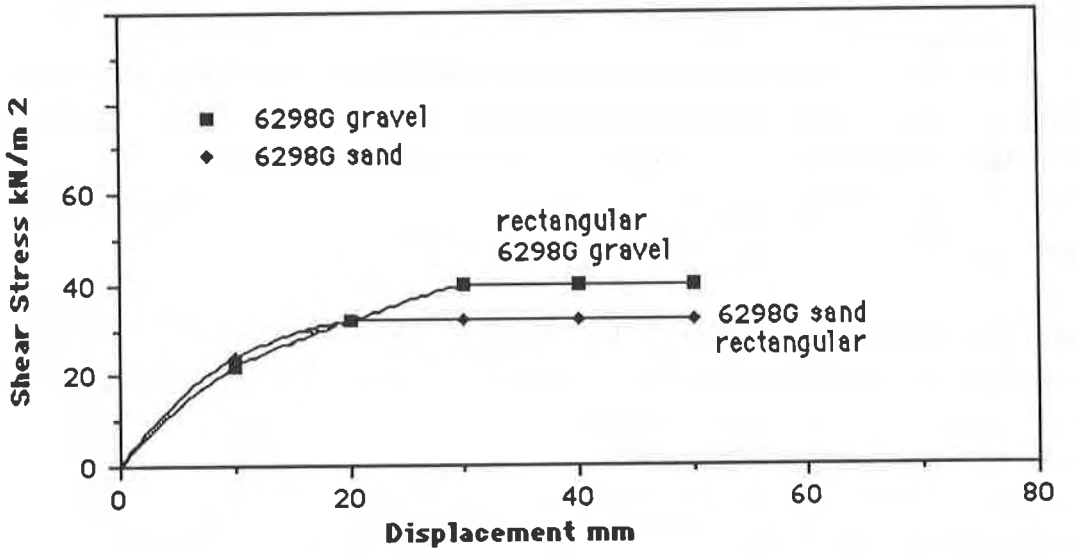

Fig.11. Typical Pullout Test Result from 300 x 300 mm Pullout Box.

Geotextile for Drainage Works. A 300 g.s.m. needlepunched nonwoven geotextile[3] was chosen. This was heavier than was strictly needed for filtration purposes, because strenuous laying conditions were expected to be encountered in the execution of the 5m deep drains being cut at a 2H:1V, or sometimes steeper, gradient. The excavation options for the trenches have been described previously.

Although not specified in the design, the contractor opted to install sheet piling to support the sides of the trenches, in order to give him a continuous excavation capability over longer lengths.

3 Bidim, manufactured by Du Pont, France.

Placing of the geotextile filter, the perforated pipe and the granular fill was done between the sheet piling, which was subsequently withdrawn by pulling. This technique worked because there were no pebbles or obstructions in the soil to bend the ends of the sheet piles. Had there been, it is almost inevitable that the textile would have been torn and replacement would have been necessary at great cost to the contractor.

The nonwoven needle punched geotextile behaved well and was placed with 5m of gravel cover without tearing. The subsequent re-excavation of the banks gave a useful opportunity to examine the geotextile and the way it had behaved during placing. It was found that it had not been damaged. The good extensibility of the nonwoven product allowed it to mould itself to the shape of the outer gravel layer as the gravel pressed against the trench sides. It did not puncture and good textile-to-ground contact was achieved.

Fin Drains. A fin drain measuring 300 x 25 mm in cross section (Ref.3) was placed in a vertical orientation behind each soil bank across the direction of maximum soil thrust. Ground water moving out of the rear cut slope would be drawn into this fin drain, which was linked laterally into the diverted drains passing below each bank (Fig.7). This ensured that ground water levels were kept down to below the rear base of the bank, notwithstanding the obvious permeability of the bank itself. It was clear that any lateral trench at the base of the bank would become subjected to the same high thrust forces being retained by the bank; therefore a crush-resistant fin drain[4] was required. The fin drain chosen had a 'pillar' type internal construction, being highly resistant to crushing, whilst retaining a good pipe-less in-plane flow capacity.

Erosion Control Geotextile. The placing of adequate topsoil cover on top of the reinforced soil banks was a problem in view of potential soil slip and rain erosion. The original slopes were up to 2.5H:1V, but the final soil slopes would be at almost 1H:1V in places. To secure the soil, a coarse granular overfill was place over the site to achieve the final approximate landscape profile (Fig.7). On top of this was placed about 25cm of good quality topsoil. Trees were planted through the soil and overfill into specially prepared pits. The soil had to be grassed and a 1000 g.s.m. woven jute[5] erosion control fabric was specified for the purpose. This type of fabric is comprised of a loosely woven open-mesh textile made from coarse jute fibres, was chosen particularly since it was felt that rain impact on the loose soil when freshly placed on the exposed slopes, would be the main danger. This was particularly so, since the work was being constructed and completed in the winter months. Geojute has been extensively tested for this purpose and is extremely effective. It's open mesh permits and encourages seed germination, whilst its fibre construction is sufficiently coarse to effectively deflect rain drop impact and stabilise the soil against rain splash. Jute will also absorb up to five times its own weight in water and thus each square metre will absorb the first 5000 cc of water falling on it. This reduces peak run-off figures from storm precipitation and the held water is available for use by vegetation after rainfall has ceased.

4 Hydraway, manufactured by Monsanto Corporation, USA.

5 Geojute erosion control mesh manufactured by Belton Industries, Atlanta, USA.

RECONSTRUCTION OF ORIGINAL CREST, SLOPE AND GARDENS

Construction of Crest. As shown in Fig.4, a second steep reinforced soil bank was constructed at the top of the slope to bridge the original slip circle plane and to re-establish the crest in its original position. The same reinforcing fabric was used as for the lower bank, and the same granular specification of $\phi > 30^0$ was adopted.

The upper bank was built right across the top of the slip surface on which movement had taken place. Naturally, at the top of the slope this was nearly vertical and a flat surface was excavated across it on which to place the bank. By this time, the drains and lower bank had stabilized the movement of the slip and considerably dried the site lower down. However, there were still minor water egresses which were tapped by the construction of ad-hoc drains - nonwoven filter fabric and gravel were used to catch the water and feed it into the main drains. This is an important facility, since it permits the location and interception of localized groundwater flows which could cause further instability if not treated.

The cross sectional geometry of the upper bank was virtually the same as the lower one except that the upper profile of the reinforced section was adjusted to provide a rounder curve at the top, to give a natural appearance when landscaped. Although this rounding of the upper crest was shown on the drawings, it was a particularly attractive feature of this construction technique, that the final profile could be specified on site 'by eye', with the engineer and client present, so that an aesthetically pleasing shape could be realized, based upon on-site observation at the time. Rigid supporting constructions would not be capable of such variable on-site adjustments at the time of construction, making this a powerful tool for the construction of slopes in aesthetically sensitive locations and for general landscape architectural design where realistic slopes and finishes must be achieved.

Reinstatement of Slope. Once the banks had re-stabilized the slope and re-established its structural framework, granular fill and topsoil were placed to achieve a satisfactory final profile and the erosion control fabric applied.

Geojute erosion control textile was selected by the contractor and placed on the crests and on other parts of the final landscaped steep surfaces, to prevent soil wash.

The placing was easy and the material was pinned down satisfactorily. However, the contractor ignored the specified overlap of 20cm and pinned the sheets edge-to-edge. Previous experience had shown jute to shrink after placing and this occurred on the site. The edges moved away from one another, leaving unprotected strips downslope which eroded. This demonstrated the effectiveness of the product and the contractor was required to re-fix all of the jute with the correct specified overlap. Subsequently there was no problem and the site was vegetated satisfactorily. Seeding and grassing were undertaken after construction by a sub-contractor and the jute kept the superficial slopes stable and erosion free, thus saving the cost of claims from the sub-contractor. He lifted, seeded and then replaced the jute which continued to protect the slope throughout the ensuing

growing season. He was able to plant trees through the jute and replace the jute around the stem to reduce erosion.

Reinstatement of Gardens and Walls. The upper granular reinforced bank, although buried under profiling fill and topsoil, provided an excellent base on which to construct the garden walls necessary for the landscaping. Fig.12 shows the cross-sectional concept of this part of the work. Concrete foundation strips were cast and stiff polypropylene geogrids[6] were set into the back of the walls to provide lateral restraint and soil reinforcement. The walls were constructed up to 1 metre high in single brick thickness with standard mortar. After the laying of the first few brick courses, a geogrid sheet measuring 60 cm. wide was pressed into the wet mortar on the last-laid bricks and further bricks were then added above it. Compacted sand and later garden soil was filled in behind the wall and into the grid. This was repeated as new courses of brick were laid until the top of the wall was reached. The gardens were then re-established overlooking the steep slopes and no movement was experienced in the walls or supported soil masses. The walls were constructed with vertical movement joints every 10 metres or so along the length, but no differential movement has been observed subsequently. The reason for choosing a different type of geogrid is primarily the fact that the grid is placed into the mortar cement between the bricks as the holding mechanism. Polyester is susceptible to degradation when exposed to highly basic environments and in particular to the by-products of setting concrete. It was decided, therefore not to use polyester for this purpose in case it should deteriorate at the anchor points within the brickwork. Further, the strength requirement of the polypropylene grid was more than adequate at 16 kN/m width for the reinforcement of a wall of approximately 1 metre height.

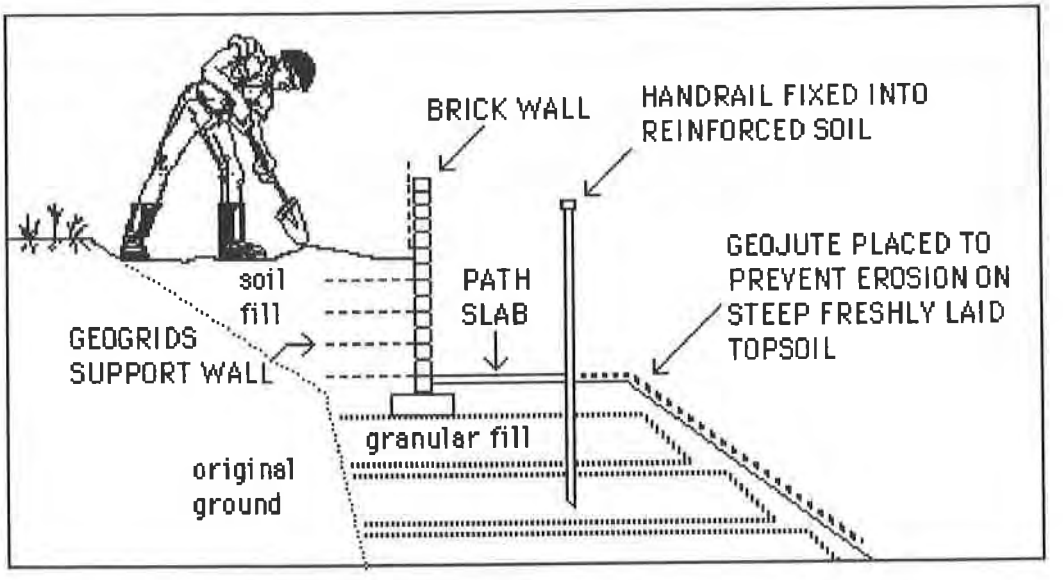

Fig.12. Cross-Sectional Diagram of Garden Wall Construction Using Geogrids.

Fig.'s 13 and 14 are photographs of the site showing the lower bank and upper bank, respectively, during construction works.

6 GM1 geogrid manufactured by the Tensar Corporation, Blackburn, UK.

Fig.13. View of Reinforced Soil Bank Being Built in Modular Units.

Fig.14. View of the Upper Bank Being Constructed to Re-Build the Original Crest.

CONCLUSION

This is the first known reinforced soil bank to use D.S.F. (Directionally Structured Fibre) geotextile grids.

The construction and placement of a major buried embankment by means of excavating the toe of a landslip is a design technique which uniquely utilizes the instant support power of reinforced soil banks.

The technique of cutting the longitudinal drains to lower the water table and then inserting the reinforced soil bank, connecting the drains beneath the bank, was successful and is a useful development of stabilization techniques for landslips.

The relatively undemanding design parameters chosen, allowed the use of mixed local sand from the site and imported granular materials. The granular materials within the reinforced bank were different from place-to-place, sometimes being entirely sand, sometimes being entirely granular coarse aggregate and in other places being a mixture of the two. This demonstrated the validity of the main design criterion being specified as an angle of friction.

This project demonstrates the ideal use of multiple different geotextiles and geogrids in the successful integrated solution of a complex and demanding earthworks project.

ACKNOWLEDGEMENTS

The author wishes to thank the warp knitting machine manufacturers Karl Mayer GMBH, Obertshausen, Germany, for their support in the development of the DSF geotextile fabrics used in this work. He also wishes to thank Manstock Geotechnical Consultancy Services Ltd., Manchester, U.K. for their permission to publish this paper.

REFERENCES

Rankilor, P.R., (1987) "The Classification and Fundamental Properties of Directionally Structured Fibre Geotextiles",Tech-Textil Conference Proceedings, Frankfurt. June 2nd - 4th.

Raz, S and Rankilor, P.R., (1990) "The Fundamental Definition and Classification of Warp Knitted DSF Geotextiles for Civil Engineering and Geotechnical End-Uses". I.G.S. Fourth International Conference, The Hague, The Netherlands, 28th.May - 1st.June .

Rankilor, P.R.(1985) "The Specification and Use of Geotextile Fin Drains". Geotextiles and Geomembranes. Elsevier Applied Science Publishers Ltd.

Reinforcement of a Failed Embankment Over Slough Mud

Richard Barrows, P. E.
Oregon State Highway Division, USA
George Machan, P. E.
Oregon State Highway Division, USA

ABSTRACT

Several days following surcharge placement, the approach embankment began to slide. A 5-foot high head scarp formed in the surcharge material and a mud wave developed into the slough. Piles under the adjacent existing south bound bridge were moving toward the slough. Field explorations and analyses of permanent stabilization options were conducted. It was determined that conventional stabilization methods were either impractical or too costly. Internal embankment reinforcement using geogrids was determined to be a cost-effective solution without delaying the construction schedule. This paper in addition to presenting the details to the case history investigates the appropriateness of the geogrid design used and presents a revised procedure and recommendations for additional research.

INTRODUCTION

First time use of geogrid for embankment reinforcement in the Oregon State Highway Division was the result of an embankment slide during construction. A limit equilibrium method was used in the geogrid design. The effect that allowable geogrid strain had on the overall level of stability (factor of safety) of the embankment was examined during design.

This paper presents a case history of geogrid use and investigates the validity of current approaches to geogrid design using limit equilibrium techniques.

BACKGROUND

The Shingle House Slough Bridge replacement project is located in Coos Bay, Oregon on U.S. Highway 101. The south bound approach embankment required placement of approximately 5 feet of fill with a 5-foot high surcharge (Figure 1). Foundation soils included a very soft 20-foot thick layer of clayey silt. Primary settlement of about 1.5 feet was expected and wick drains were installed to expedite the time required for primary settlement.

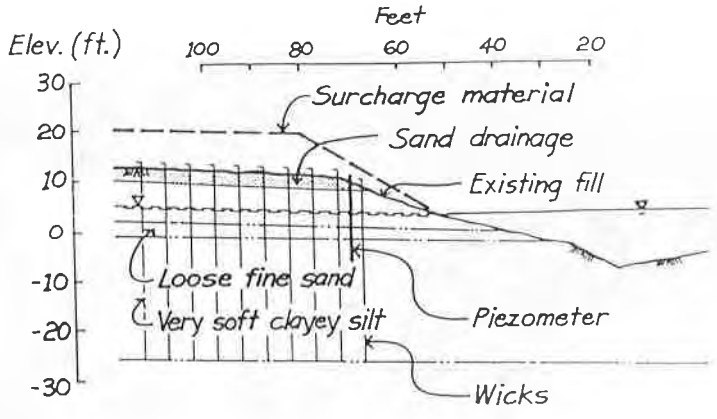

Figure 1. Southbound Approach Embankment Profile

Shortly after the surcharge material was brought to finish elevation, the embankment became unstable. Initially a 5-foot head scarp appeared in the embankment and the toe bulge appeared about 70 feet from the head scarp (Figure 2).

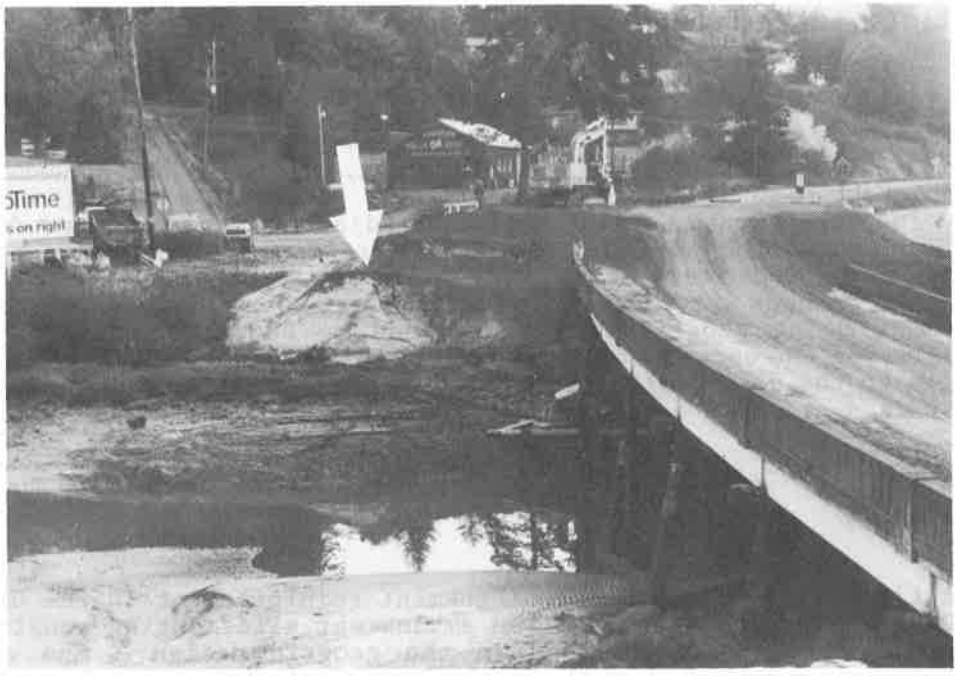

Figure 2. South Bound Approach Photo (Arrow Marks Dropped Portion of Embankment).

The circular failure mass began moving towards the slough and pushed piling out from under the adjacent existing bridge (Figure 3). A failure arc radius of 30 feet was interpreted.

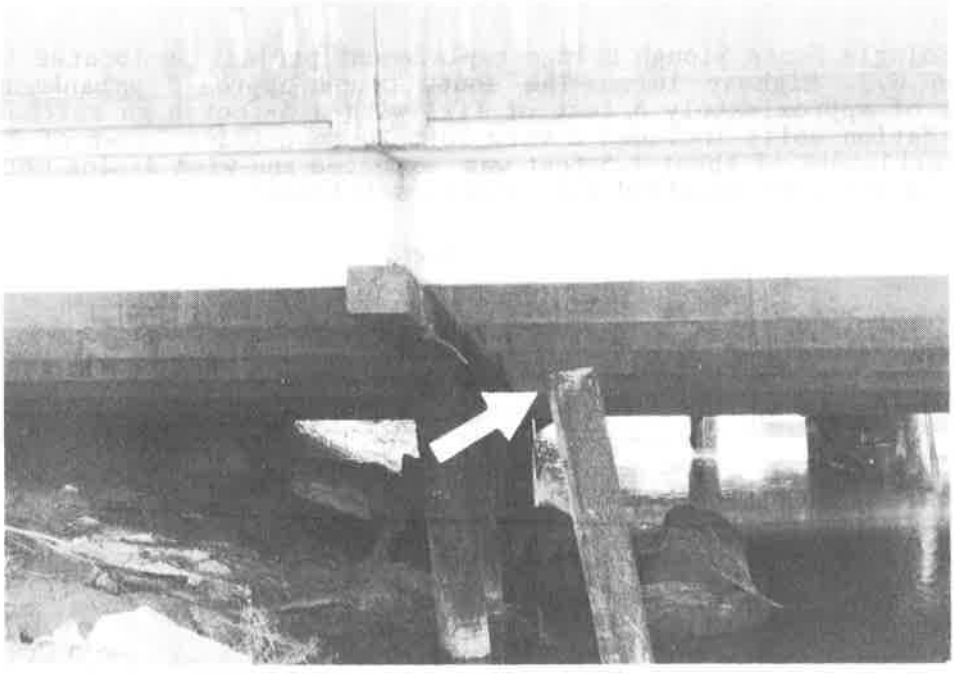

Figure 3. Bent #2 Displaced Pile Due To Embankment Instability.

TEMPORARY REMEDIAL ACTION

Initial remedial action measures were taken within 24 hours to protect the adjacent structure. The surcharge material near the abutment was unloaded to an elevation of 15 feet. Although this action slowed slide movement it did not stop it completely. The embankment was no longer receiving the benefits of the surcharge load for consolidation. The time allowed for embankment settlement had a major impact on the contractors critical path. Delaying the work by lengthening the settlement period would have resulted in a claim by the contractor and therefore was unacceptable.

A back analysis of the failure profile for a factor of safety equal to 1.0 indicated a shear strength of about 250 psf using Bishops modified method of circular stability analysis (Figure 4). A 5-foot high, 25-foot wide counterbalance was placed at the toe of the slide. A factor of safety of 1.1 with surcharge removed was calculated with this geometry. If the surcharge were to be restored, the factor of safety would drop to 0.8. This factor of safety was not adequate so additional stabilization measures were considered. Also, the counterbalance would eventually have to be removed because of its wetlands impact and therefore could not be part of a permanent solution.

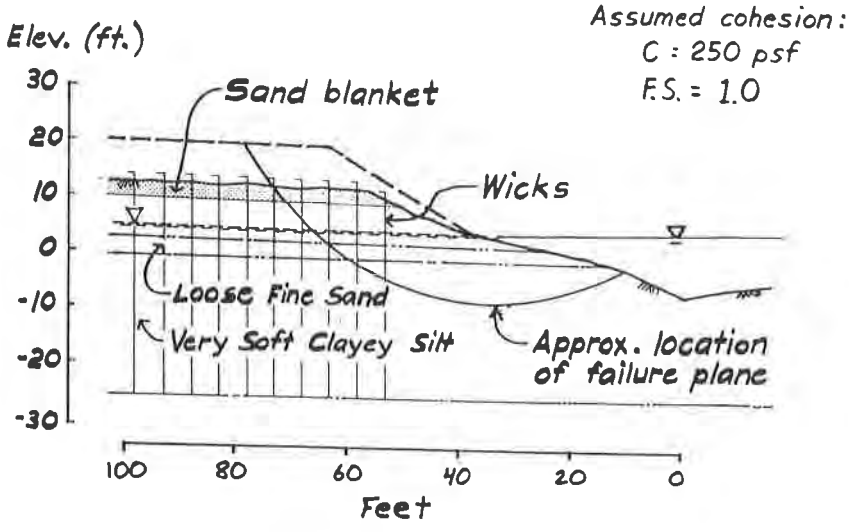

Figure 4. Stability Analysis Profile

ALTERNATIVES CONSIDERED

Lengthening the bridge to span over the poor foundation materials was considered, but redesign time and significant added cost made it an undesirable alternative.

Reinforcing the embankment with a geosynthetic was a viable alternative. The State of Oregon had about 10 rolls of geogrid material (Tensar SR-2) left over from a previous wall project making it an even more economical choice.

GEOGRID REINFORCEMENT OPTION

Geogrid reinforcement is considered most effective when placed near the base of the embankment. The lowest level the geogrids could be placed on this project was at the top of the sand drainage blanket in order to preserve the wick drains.

The design procedure included:

1. Circular stability analyses, with the slip circle passing through the geogrids. A range of slip circles was used to determine the length of geogrid needed to satisfy stability.
2. Geogrid embedment length to resist pullout, beyond the limits of the critical slip circle.
3. Spacing of geogrid layers.
4. Consideration of backfill between geogrid layers.

There were two important design cases to analyze. First was the short term case: a reinforced embankment with counterbalance and the surcharge restored. The long term case consisted of a reinforced embankment with both the surcharge and counterbalance removed and the pavement in place.

Three factors of safety were used, as follows:

* FS=1.0, Equilibrium condition
* FS=1.1, Stability required under short term loading
* FS=1.2, Long term stability required during design life. This value was considered to be appropriate because of the reliability of the analytical model from back-analysis.

The stability analysis steps consisted of:

1. Determining the required resisting force, T, at the geogrid level, following the stability analysis procedure by Broms (1977), Tensar (1982), and Jewell (1982).

$$T = \frac{[(F.S.) x \sum M_D] - \sum M_R}{Y}$$

Where:

F.S. = Design Factor of Safety

$\sum M_R$ = Sum of the Resisting Moments

$\sum M_D$ = Sum of the Driving Moments

Y = Moment Arm for Reinforcement Layers

2. Varying the number of geogrid layers and then calculating the required resisting force per geogrid layer. The results are shown on Figure 5.

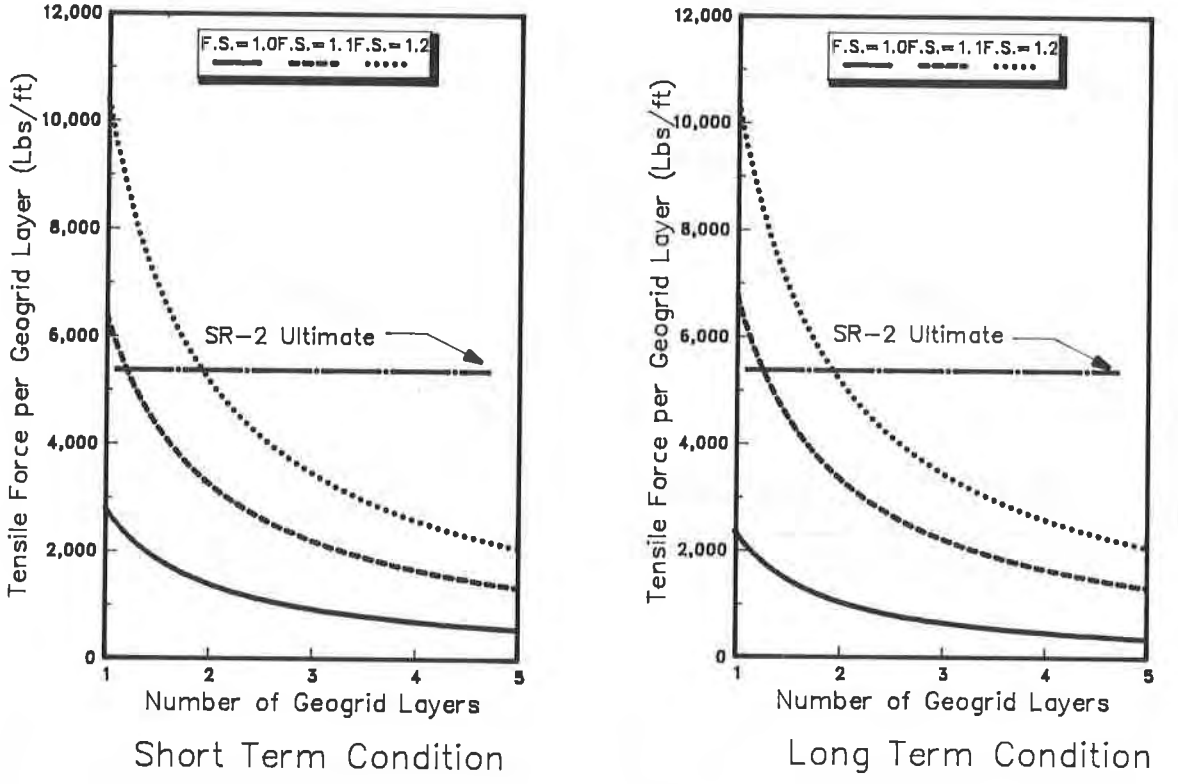

Figure 5. Required Resisting Force vs. Number of Geogrid Layers

3. Comparing the required resisting force per geogrid layer to the ultimate tensile strength to determine which combination of geogrid layers would provide an optimum working stress level.

4. Checking that the strain to mobilize the required geogrid resisting force was not excessive for embankment stability.

The analysis results, assuming 4 geogrid layers, are shown on Figure 6 for both the short and long term cases. The graph on the left shows the percent strains required to mobilize sufficient geogrid tensile strength to achieve various levels of stability (factor of safety). The strength-strain relationship was derived from isochronous curves for the geogrid. The graph on the right shows the same analysis results comparing the tensile strength required (as a percentage of ultimate tensile strength) to various levels of stability analyzed.

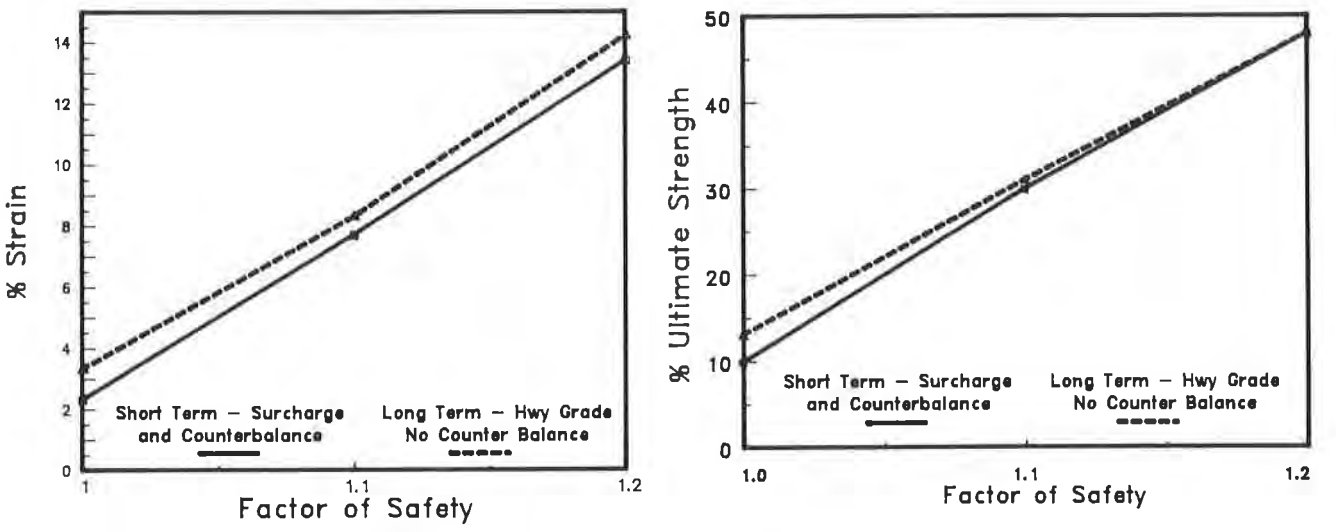

Figure 6. Geogrid % Strain and % Ultimate Tensile Strength vs Factor of Safety

The allowable working tensile load is usually selected in the range of 0.4 to 0.6 of the ultimate tensile strength to account for installation hazards and biological, chemical, and creep effects with time for embankment applications. The above figures demonstrate that at a FS of 1.2, the required geogrid tensile resistance would be less than 50 percent of ultimate, and would therefore appear to be acceptable. In the short term, under equilibrium conditions (FS=1.0), the design utilizes only 10 percent of the ultimate geogrid resistance which requires 2.3% strain to mobilize. This demonstrates how the design can be significantly impacted by the uncertainties of soil, groundwater, and geogrid conditions/properties with time.

Since the time to develop the embankment slide repair design was very short, we decided to recommend using 4 layers of Tensar SR-2 geogrid.

CONSTRUCTION AND PERFORMANCE

The embankment was excavated down to the foundation sand blanket level. Most of the wick drains were unharmed, while a few were either severed or pulled out. Each layer of geogrid was constructed by placing the reinforcement strips parallel to embankment center line. Each strip was placed against the edge of the adjacent strip; overlaps or hog rings were considered unnecessary. Where the geogrid strips were short of the design length, they were spliced together using a PVC pipe. The center of the geogrid strips were secured to the ground with wood stakes. Sand backfill was then placed in the middle and spread towards the ends of the strips in order to tension the geogrid. This process worked well and there was no damage or separation of the geogrid strips. The backfill was placed 6 inches thick and compacted prior to placing the next geogrid layer. Overall,

the procedure of placing the geogrid reinforcement and backfill was simple for the contractor and easy to inspect/control. A fifth geogrid layer was actually constructed to use up all the geogrid delivered to the site.

The embankment was subsequently monitored. No signs of movement or distress were noted. Four months later the pre-consolidation level was achieved and the surcharge was removed. The roadway was paved in one year. Two years of post-construction inspection have revealed no signs of pavement or embankment slope distress.

RECOMMENDED STABILITY ANALYSIS PROCEDURE

When faced with future slope stability applications and sufficient design time, it is recommended to apply more judgment to analysis assumptions. This would include the stability factor of safety, the geogrid working load, and the geogrid strain. In addition, there will usually be at least two design cases, including the short-term condition and the long-term condition. Each design case should be analyzed and the critical case should control the final design. If the less critical cases are significantly over-conservative, then the controlling design should be reassessed in the event any of the assump-tions could be made less conservative.

The following describes a procedure that is intended to be used on future projects that utilize geogrids/geotextiles for improving stability.

A. Short-Term Design Case

1. The first consideration should be the stability analysis without any reinforcement. The level of stability would need to be compared to the desired factor of safety F. S. The reinforcement force required to achieve equilibrium, FS = 1.0., should then be calculated.

   - For this project, the reinforcement load to achieve equilibrium would be 2,800 lbs./ft.

2. The desired FS should be selected considering: 1) the reliability of subsurface data and groundwater/pore-pressure conditions; 2) the type and duration of loading on the embankment; 3) the level of acceptable risk; and 4) any other impact that would occur during the short-term case.

   - For this project, an appropriate factor of safety would have been 1.1 because a) the subsurface data was well understood or back-calculated, b) the surcharge loading would only be for 4 months, and c) the level of acceptable risk was moderate.

3. Calculate the required tensile reinforcement from the stability analysis, using the desired F. S.

   - For this project, the required tensile reinforcement was 6,400 lbs./ft.

4. Select a geogrid (or geotextile) and determine the tensile strength vs. strain relationship consistent with the materials isochronous curves. This step would be repeated if different geogrids/geotextiles were being considered.

5. Initially select a geogrid working load, as a percentage of the ultimate tensile strength (or the strength corresponding to a limiting strain if the material has an excessive elongation). This is a very important selection which should be based on: 1) handling and installation hazards; 2) biological and chemical effects; 3) level of creep anticipated for the planned duration; 4) nature of the loading ; and 5) tolerance of the embankment to deformations.

- For this project, we would have selected 50 percent of the ultimate strength as a maximum value, which would be 2,700 lbs./ft., at a strain of 14%. The selection of 50 percent of ultimate strength is based on: a) no danger of damage to the geogrid during handling and installation, and b) no biological or chemical damage or creep concerns in the short 4 months duration for this design case.

6. Calculate the number of layers required by dividing the required tensile reinforcement (from step 3) by the geogrid working load (from step 5). Round up to the next whole number.

   - For this project, we calculated 2.4, which rounded up is 3 layers.

7. Determine the design working load by dividing the required tensile reinforcement (from step 3) by the number of layers (from step 6).

   - For this project, the design working load would be 2,133 lbs./ft. at a strain of 11.5%. The design working load is 40% of the ultimate tensile strength.

8. Calculate the working load and corresponding strain for the equilibrium condition, FS = 1.0. This would indicate the actual force and strain that would most likely be mobilized. The equilibrium working load is calculated by dividing the required tensile reinforcement for equilibrium (from step 1) by the number of geogrid layers (from step 6).

   - For this project, the equilibrium working load would be 933 lbs./ft. at a strain of 4.2%.

9. Plot the results of the working loads on the geogrid tensile strength vs. strain graph, as shown on Figure 7.

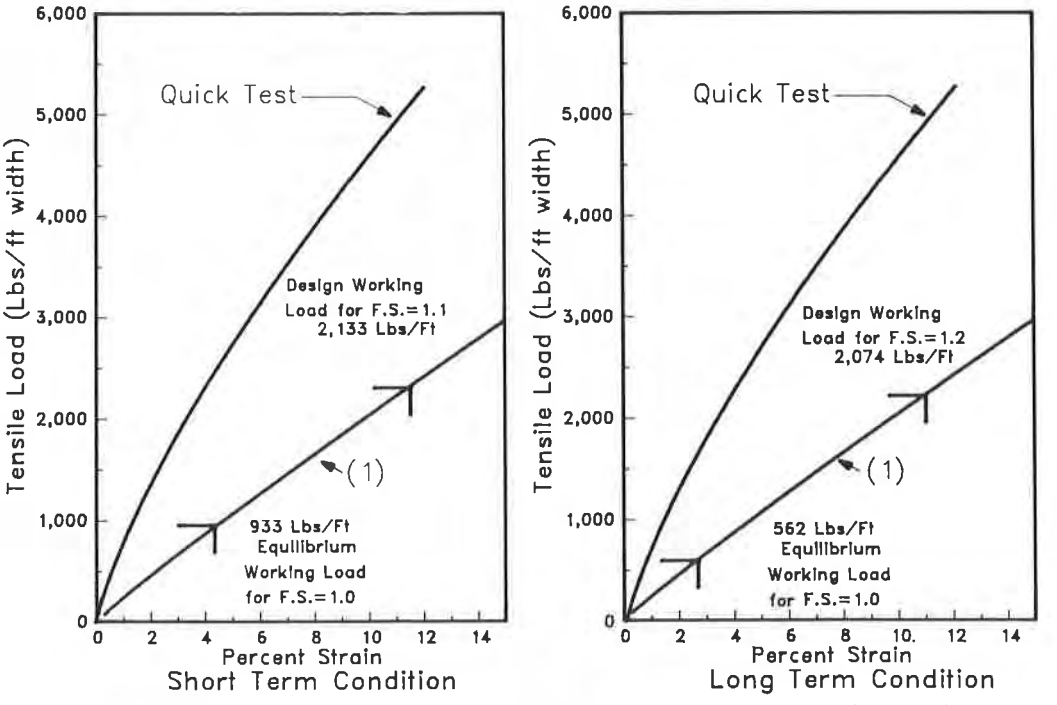

Figure 7. Working Tensile Load vs Strain Diagrams

10. Evaluate if the ranges of working loads and strains between the equilibrium and design FS levels are acceptable.

    - For this project, the ranges would have been acceptable.

11. If the working load/strains are not acceptable, either too low or too high, then repeat the analysis and reconsider the design FS, the working load level, and the reinforcement material.

B. Long-Term Design Case

The procedure for the long-term case would be similar to the short-term case. However, the assumptions used for the factor of safety and the working loads would probably be different.

- For this project, the long-term factor of safety was selected as 1.2 because of our confidence in the back-calculated subsurface data and the need for a low risk solution. The initial working load was selected at 40% of the ultimate tensile strength because of our concern for long-term creep, and biological and chemical effects. The combination of the increased FS and the decreased allowable design working load resulted in two more geogrid layers being required than for the short term case. The results of these long-term analyses are shown on Figure 7.

The results of the long-term case should be evaluated to determine if the working load and strain ranges are acceptable. If these values are excessive, then the geogrid material or number of layers should be changed until an acceptable solution is reached. Then the redesign should be evaluated for the short-term case conditions.

ADDITIONAL RESEARCH

The design method should be researched further to determine if the geogrid tensile strength should only be reduced to "working load" levels for equilibrium (FS = 1.0) analyses. For design factors of safety, it might be justifiable to use the ultimate strength or at least the strength at a higher level of strain (such as 10%). In the event that unfavorable long-term variations occur, additional geogrid and soil resistance would be mobilized, up to the ultimate strength level. The consequence would be increased strain and possibly small embankment deformations.

ACKNOWLEDGMENTS

The technical assistance provided by Steve Miller, of the Tensar Corporation, is gratefully acknowledged. The authors thank Ron Chassie, FHWA, for his technical guidance and review during the emergency repair effort, and Frank Morrison, Ken Eddy, and Jim McKidde, from the ODOT project managers office for their acceptance and endorsement of the geogrid repair method. The Contractor was F. E. Ward of Vancouver, Washington. The authors also thank Ryan Berg (Ryan R. Berg & Assoc. Inc. of Minnesota) for coordinating and summarizing the technical review of this manuscript.

REFERENCES

Bell, J. R., Principles of Geotextiles with Applications to Transportation Engineering, Oregon State University, 1985.

Bishop, A. W., The Use of Slip Circle in the Stability Analysis of Slopes, Geotechnique, 5, 7-17, 1955.

Broms, B. B., Polyester Fabric As Reinforcements in Soil, 1st Int. Conf. Use of Fabrics, Paris, 1977.

Jewell, R. A., A Limit Equilibrium Design Method for Reinforced Embankments on Soft Foundations, 2nd Int. Conf. of Geotextiles, Las Vegas, 1982.

Koerner, R.M., Designing with Geosynthetics, 2nd Ed., Prentice Hall, 1990.

Tensar (in association with Henderson and Busby Partnership), Designing with Tensar: Techniques and Design Philosophy for Utilizing Tensar Grids in the Reinforcing of Soil Structures, 1982.

COMMERCIAL / INDUSTRIAL APPLICATIONS

Surcharge Embankments at Walt Disney World

Ian Kinnear
Jammal & Associates, Inc., USA
Frank Wood
Disney Development Company, USA

INTRODUCTION

Walt Disney World in Florida consists of some 28,000 acres of land primarily located in southwest Orange County. The property contains abundant swamp lands with ancient sinkholes that are in some instances infilled to considerable depths with organic soil. The Disney site is home to the Magic Kingdom, EPCOT Center and the Disney/MGM Studio Tour. Over the past few years, Disney Development Company has been responsible for the construction of several major road schemes and related infrastructure construction to support the three theme parks as well as new major hotel facilities that are being built on property. A generalized plan view of the Disney Center site is presented on Figure 1.

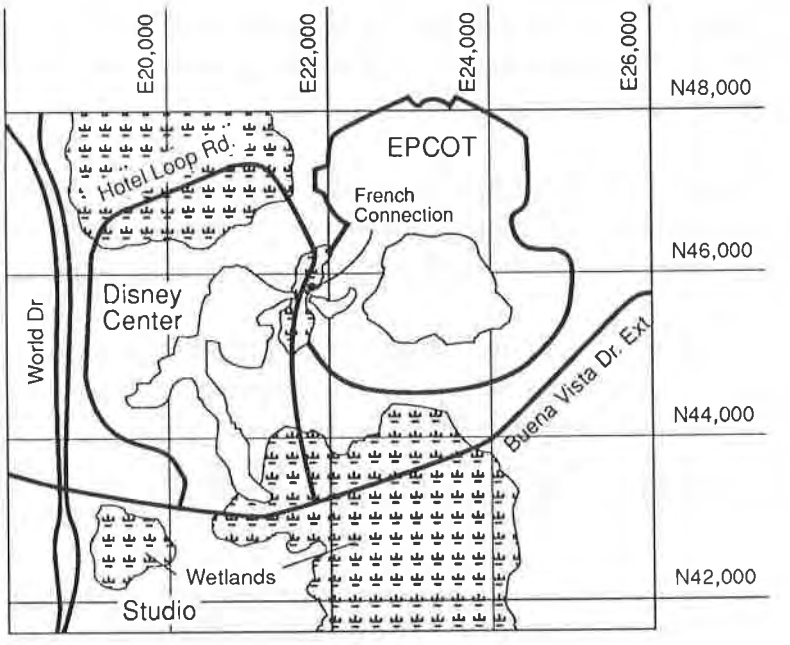

Figure:1 Disney Center site plan

Several of the new roadway alignments and utility corridors have crossed swamp areas that contain in excess of 100 feet of soft/highly compressible organic soils. The lateral extent and great depth of the soft deposits rendered conventional demucking and replacement filling virtually impossible and in any event extremely cost prohibitive. To facilitate embankment construction in such soft soil areas, reinforcing geogrids were utilized to enhance embankment slope stability.

This paper presents details on the construction techniques used in several of the major embankments that have recently been built over deep organic soils. Included are details on surcharging procedures, fill placement rates and performance data. Settlement monitoring has been an integral part of the construction projects and this data is also presented in the paper. In one surcharge embankment location a vertical movement in excess of 16 feet was measured. This particular area has been paved and is open to traffic. Settlement/performance monitoring is continuing and is discussed herein. Performance in embankment areas using geogrids is compared with areas where no geogrid was utilized.

OVERVIEW OF SUBSURFACE CONDITIONS

In the depth of influence of most major construction projects (i.e. upper 200 feet), the Walt Disney World property is underlain by materials deposited during four geologic eras. From the oldest to youngest, these include Eocene, Miocene, Pleistocene and Recent deposits.

The Eocene deposits consist of very porous sandy limestone that contains some large voids and caverns. The limestone prevails at typical depths in the range 80 to 120 feet below grade in areas that have not been subject to sinkhole collapse. In areas where collapse has occurred, the limestone may not be encountered until depths in excess of 250 feet. This limestone strata is the upper portion of the Floridan aquifer, which provides potable water to the area.

Overlying the limestone is the Hawthorn Formation which was deposited during the Miocene era. This layer consists of silty/clayey sands and clays that occasionally grade with shells and phosphate nodules. The Hawthorn Formation is on the order of 40 to 70 feet thick and forms an aquiclude to the underlying aquifer.

The soils from the top of the Hawthorn Formation to the ground surface consist of fine sands and silty fine sands of the Pleistocene era. These soils are typically 40 to 50 feet thick. In the swamp land areas are organic soils that consist of fibrous peat and organic silt. In geologic time, these organic soils are recent deposits. The organic soils vary from a few feet in thickness to in excess of 100 feet in some of the infilled relic sinkholes. On Figure 2 is a typical boring log from a high ground sandy area and one from a low ground swamp.

A generalized cross-section indicating subsurface conditions present within one of the development areas under consideration in this paper is presented on Figure 3. As may be seen from this cross-section, the organic soils exhibit significant thickness variations over short horizontal distances (2 horizontal to 1 vertical in extreme cases). Near the center of the relic sinkhole features which are typically circular, the Hawthorn Formation soils are relatively thin and the limestone is depressed.

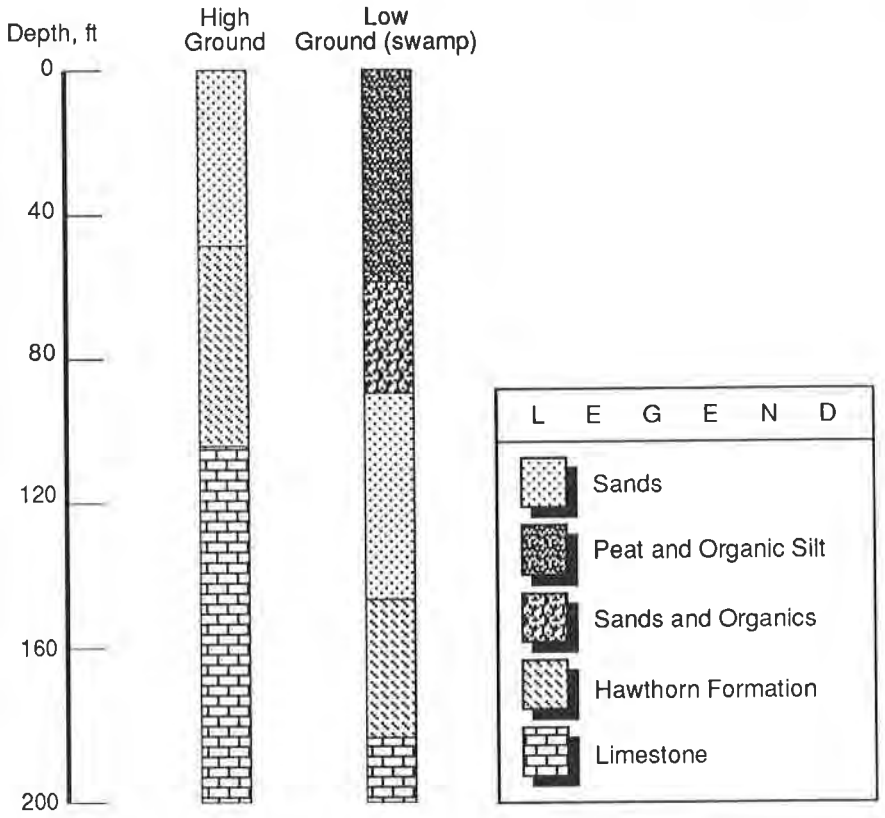

Figure:2 Typical boring logs

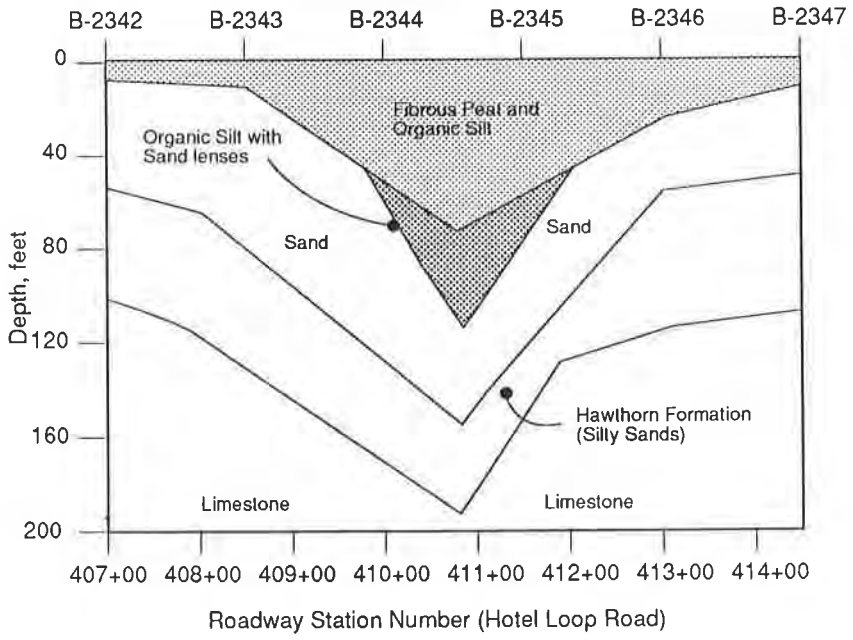

Figure:3 Cross section showing generalized subsurface conditions

ENGINEERING PROPERTIES OF ORGANIC SOILS

The organic soils at the Disney site grade from fibrous peat to organic silt. These materials characteristically have high natural moisture contents and low dry unit weights (natural moisture contents in the peat range from 150 to 1100 percent, while the organic silts have moisture contents in the range 80 to 250 percent). In-situ shear strengths are comparatively low and often do not exceed several hundred pounds per square foot. Typically, these soils are normally consolidated in-situ and exhibit a high degree of compressibility both from the standpoints of primary and secondary compression. In virgin compression, the peat has a compression ratio between 0.3 and 0.65 inch/inch and a coefficient of secondary compression ranging from 0.01 to 0.06. Coefficients of consolidation vary from 0.2 ft^2/day for the organic silts up to 3 ft^2/day for some of the more fibrous peats.

PROJECT CONSIDERATIONS

The Disney Center project included the construction of roadways and support infrastructure to service new hotels and entertainment facilities. The roadways were constructed on low fill embankments that increased in height at structure locations. The roadways were two, three or four lanes wide with an urban section consisting of curb and gutter. Buried utilities were installed within the road embankment fill which in addition to the storm sewer, included gas, water, electricity, sanitary sewer and communications. The utility lines comprised force mains as well as gravity lines.

The roadways traversed through high ground sandy areas as well as the swamp ground with the attendant variable organic soil deposits. About 2 miles of roadway traversed through organic soils. By conventional Department of Transportation computations, approximately 500,000 cubic yards of organic soils existed below the road pavements.

OPTIONS FOR DEALING WITH ORGANIC SOILS

Locally, the most common approach for dealing with organic soil deposits consists of excavation and replacement filling. Given the significant volumes of material that would have to be removed and replaced at this site, such an operation was considered extremely cost prohibitive (about $5M for the 500,000 cubic yards of organics). Additionally, mass excavation to such excessive depths would have a significant impact on the adjacent environmentally sensitive wetlands.

Other options considered for site preparation included partial demucking/backfilling and filling directly atop the organic soils following removal of the surface vegetation cover. A partial demucking scheme would remove the more compressible upper peats and leave the firmer/older organic soils. While long-term settlements are less than when fill is placed directly atop the full profile of organic soils, partial demucking requires substantial replacement fill volumes and has the attendant organic soil disposal problems and wetland impacts as total demucking.

The option with the highest technical risk but the least cost and environmental impact has been to fill directly over the organic soils in a controlled manner and to essentially undertake no demucking. This technique was utilized over the 2 miles of roadway on Buena Vista Drive extension and the Hotel Loop Road that are constructed over organic soils. Concerns that had to be addressed in constructing directly over the organics were:

1. Embankment stability
2. Long-term settlement
3. Lateral spreading, particularly in shoulder areas containing utilities

For areas where organic soils were less than 5 feet thick, a preload program was adopted. As the organic soils increased in thickness, geotextiles and geogrids were incorporated into the design to reduce the above concerns. Additionally, the deeper areas were surcharged to induce settlements prior to paving and utility installation. The height of the surcharge embankments varied from 3 to 10 feet, being highest where the organics were thickest.

DESIGN RATIONALE

In the past, a variety of earthfill structures have been placed atop organic soils of varying thicknesses without the use of geogrids or geotextile. Experience had indicated that while most embankments could be constructed over these soils at a slow controlled rate of filling, localized failures were being experienced on the larger projects. These failures were primarily wedge type and/or shallow circles with the slip plane being in the very soft organic soils that underlies the root mat at depths in the range 8 to 14 feet below grade. On this basis, embankment construction on organic soils was observed/judged to have a factor of safety close to one during construction. Because organic soils achieve appreciable strength gain as a result of consolidation, stability failures occur during or very shortly after construction or load application when pore pressures are high.

To enhance the factor of safety against stability failure during construction for the Disney Center project, we elected to utilize geogrid in the embankment fill. The number of layers selected was primarily based on typical profiles in a given area, ultimate embankment height and side slope geometry. A simple wedge failure calculation was carried out to determine if the number of layers of geogrid was adequate for the higher fill embankments.

Surcharge heights and time periods in given areas were selected such that the organic soils would be experiencing creep settlement at the end of the surcharge program rather than primary settlement. The purpose being to induce as much settlement as possible in the organic soils prior to constructing the road pavement section and installing utilities and storm sewers. For the deepest organic soils, the surcharge period was about 1 year. Drainage wicks were installed at one bridge approach embankment to speed up consolidation and permit construction access. Surcharge embankments were tappered in profile to make the settlement profile more uniform, particularly with regard to long-term differential settlement. Surcharge heights were proportioned relative to original organic soil thickness.

GEOTEXTILES AND GEOGRIDS

In constructing the road embankments over the organic soils, a geotextile was utilized for the full width of the fill. The purpose of the geotextile was to prevent the migration of fines from the fill into the root mat as a result of long-term vegetation decay. The geotextile was placed atop the levelling layer of fill. Specification requirements for the geotextile were as below:

Structure - Non-woven
Weight - 4.5 ounce/yard^2
Porosity - greater than 300 gal/min/ft^2
Effective Opening Size - 70 to 100 micron
Puncture ASTM D-751 - 60 lbs or more

As discussed earlier, geogrids were incorporated into the fill embankments where the organic soils were thickest and/or the embankments were relatively high (>10 feet). The embankment reinforcement ranged from single layers of biaxial geogrid to multiple layers of uniaxial geogrid. In areas the biaxial geogrid was placed full width across the embankment and in some instances in the shoulders only, below utility lines. A typical cross-section through a utility shoulder reinforced with geogrid is shown on Figure 4. In the deep organic pockets, up to 2 layers of uniaxial geogrid were used. A typical cross section for a two layer reinforced embankment system is presented on Figure 5. Specification requirements for the geogrid was as below.

Polymer Composition	Biaxial Grid Polypropylene	Uniaxial Grid High Density Polyethylene
Tensile Strength		
2% Strain	590 lbs	1465 lbs
5% Strain	950 lbs	3030 lbs
Ultimate	1170 lbs	5380 lbs

CONSTRUCTION PROCEDURES FOR TYPICAL EMBANKMENT

The general construction procedure for pioneering and building the road embankments in the heavily vegetated swamp areas was as follows. The sequence of operations listed is for the embankment shown on Figure 5.

1. The surface vegetation was clear cut as close to the existing ground surface as possible. Stumps were no more than 12 inches high and the root mat was left intact.

2. Cut vegetation was removed with care not to disturb the root mat. Limbs and small tree trunks less than 4 inches in diameter remained after clearing providing that they were distributed such that they did not lie on top of each other.

3. The first layer of fill placed on the root mat was about two feet thick and advanced in a uniform manner across the entire area. Lightweight equipment such as wide-track bulldozers with contact pressures of 4 pounds square inch or less were used to place the first layer.

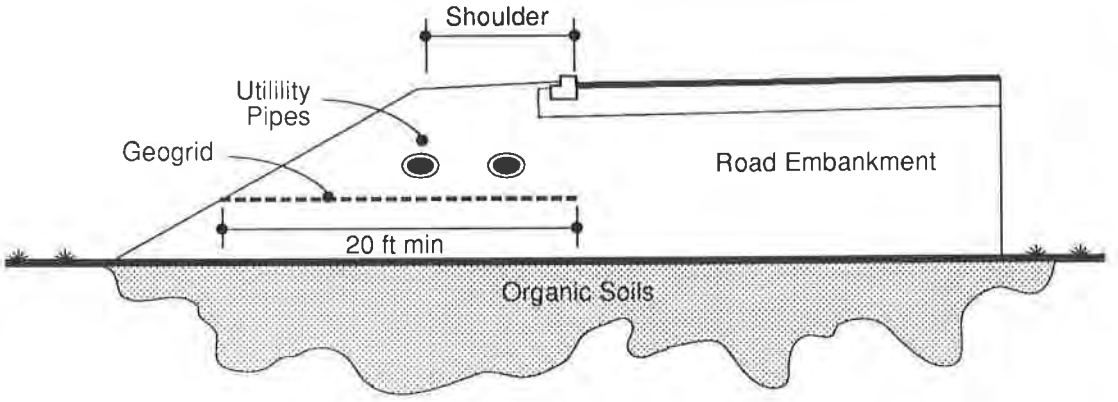

Figure:4 Typical cross-section through utility shoulder

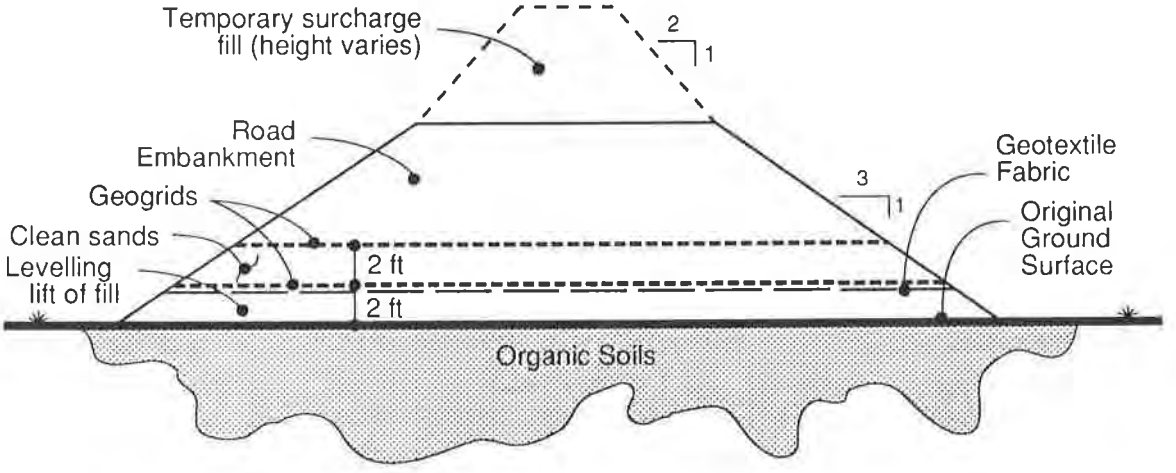

Figure:5 Typical cross-section for 2-layer reinforcement embankment system

4. Until the fill pad attained a minimum thickness of four feet, no heavy construction equipment was permitted on the pad, nor was fill material awaiting placement allowed to be stockpiled to heights greater than 3 feet.

5. Atop the first fill lift in the deep organic areas, a geotextile was placed followed by a geogrid. Geogrid consisted of Tensar SS 2 or SR 2 that was primarily rolled out perpendicular to the slope face. Adjoining rolls were overlapped about 6-9 inches.

6. Next, another two feet of sand was uniformly placed across the embankment. This layer was placed in a manner similar to the first layer.

7. The first 4 feet of fill constituted a drainage blanket and sand with less than 5 percent fines was used for this purpose. Elsewhere in the embankments, on site fills were used for construction. The on-site sand

fills had fines ranging from 10 to 18 percent by dry weight passing the U.S. Standard Number 200 sieve.

8. A second geogrid was placed at 4 feet for full width of the embankment in the areas of deep organic soils (e.g. Stations 409+00 to 413+00 as on Figure 3).

9. Subsequent fill was placed in one foot lifts and compacted to at least 95 percent of maximum laboratory dry density (ASTM D-1557).

10. Fill placement rates were controlled at 2 feet per week.

11. Surcharge fill was also placed at an approximate rate of 2 feet per week but it was uncompacted.

Within the embankment, settlement markers were established in the fill. The markers were typically set at the top of the geogrid and extended through the fill and surcharge as placement occurred. The settlement markers consisted of a steel base plate with threaded extension pipe. The extension pipe was sleeved within a pvc riser pipe to prevent friction on the marker as settlement occurred.

PERFORMANCE OVERVIEW

An integral part of the surcharge program was the settlement monitoring. Over 50 markers were established in the various fill embankments. The markers were read twice per week during filling and once per week thereafter. Figure 6 presents a plot of settlement versus time for two markers in one of the deep soil deposits. Marker 1 was at Station 411+00 and marker 2 at Station 412+00. Marker 1 recorded a total settlement of 16.1 feet from the embankment fill and temporary surcharge load over a period of 500 days. Marker 2 recorded a total vertical movement of 9.9 feet over a similar time period. Since paving the roadway in July of 1989 through July of 1990, the total measured settlement at the edge of curb in the area of Station 411+00 has been 1.4 inches and at Station 412+00 it has been 0.4 inches. In Table 1 is a summary of settlements during construction/surcharging and following paving in the embankment between section Stations 408+50 and 413+50. The approximate thickness of the organic soils at each of these data points is also given in the table.

Two interesting points from the table are one that the total movements were reasonably uniform given the vast variation in thickness (5 to 16 feet of settlement compared with 12 to 100 feet of thickness variations). The other point of interest is the movements that have been recorded in the past year. Again, these are relatively uniform and small given the movement that occurred during construction/surcharging.

In similar relic sinkhole areas where no grid has been used in construction, the settlement variations have been more comparable with that of the thickness variations in the organic soils and similarly the long-term differential settlements have been more pronounced. A case in point was on the nearby World Drive entrance road in which long-term differential settlements of 1 inch in 6 feet were noted over a 12 year period. At this particular location, the organic soils were on the order of 40 feet thick.

Table 1

Station	Thickness of Organics (Feet)	Settlement Movements During Construction (Feet)	Settlement Movements 7/89 to 7/90 (Inches)
408+50	12	4.7	0.4
409+00	25	5.3	0.6
409+50	30	7.7	0.5
410+00	60	9.8	0.6
410+50	90	11.1	0.8
411+00	110	16.5	1.4
411+50	90	14.7	1.0
412+00	60	9.9	0.4
412+50	35	6.5	0.2
413+00	25	5.8	0.2
413+50	20	4.7	0.2

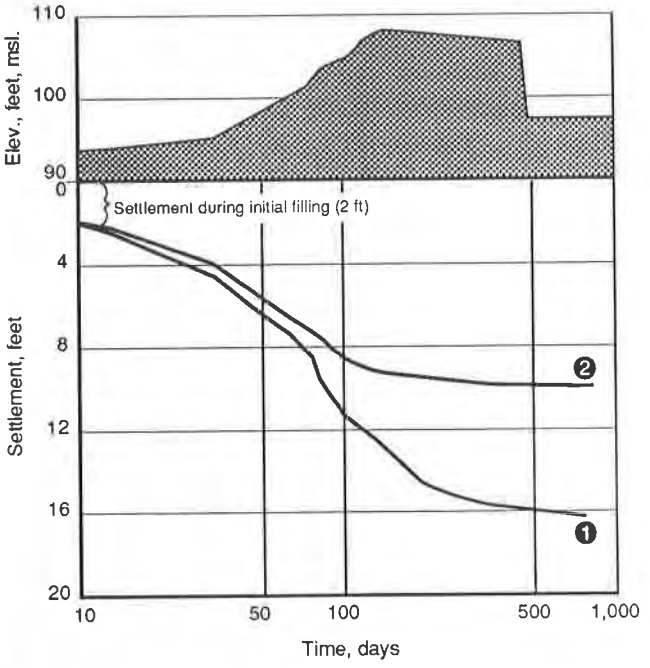

Figure:6 Settlement plot

In addition to the road embankments which were constructed on the organic soils, several large parking lots were built over similar soils. For these parking lots it was decided not to use fabrics or geogrids but rather to fill directly over the organic soils following selective clearing. This provided a means of comparison between geogrid and no geogrid in fill construction.

In one of the parking area slopes about 150 feet south of the deep muck pocket at roadway Station 411+00, a failure occurred. The failure was primarily thought to be due to placing fill too quickly coupled with the poor drainage characteristics of the on site silty sand fills. Restoration of the failed area included removing the slipped fill to original ground surface, using clean sand as the first three feet of backfill and placing geogrid back into the slope beyond the failure plane. Filling then proceeded in a manner similar to that discussed earlier. The restoration work was satisfactory, and no further slope failures took place on the project.

OTHER GEOGRID APPLICATIONS

Geogrids were utilized in other areas of the Disney Center project and two applications in particular are worthy of brief comment. The first application was for capping deep organic pockets in man-made lakes. These man-made lakes are typically excavated in the dry. To enhance water quality and to some degree stability, the bottom portions of the lake that contained organic soils received a layer of biaxial geogrid and fabric followed by two feet of clean sand. These capped features were stable enough to permit equipment to access areas for seawall and bridge construction. One such feature had 80+ feet of organics below the cap.

Another geogrid reinforcing application was along a lake edge which was also underlain to significant depths by organic soils. Additionally, the lake edge fill was to act as a buttress to a sensitive wetland area plus

provide access for tram traffic. This specific application included some selective demucking plus the placement of geogrid and fill in a controlled manner. A generalized cross-section through the buttressed lake edge fill is presented on Figure 7.

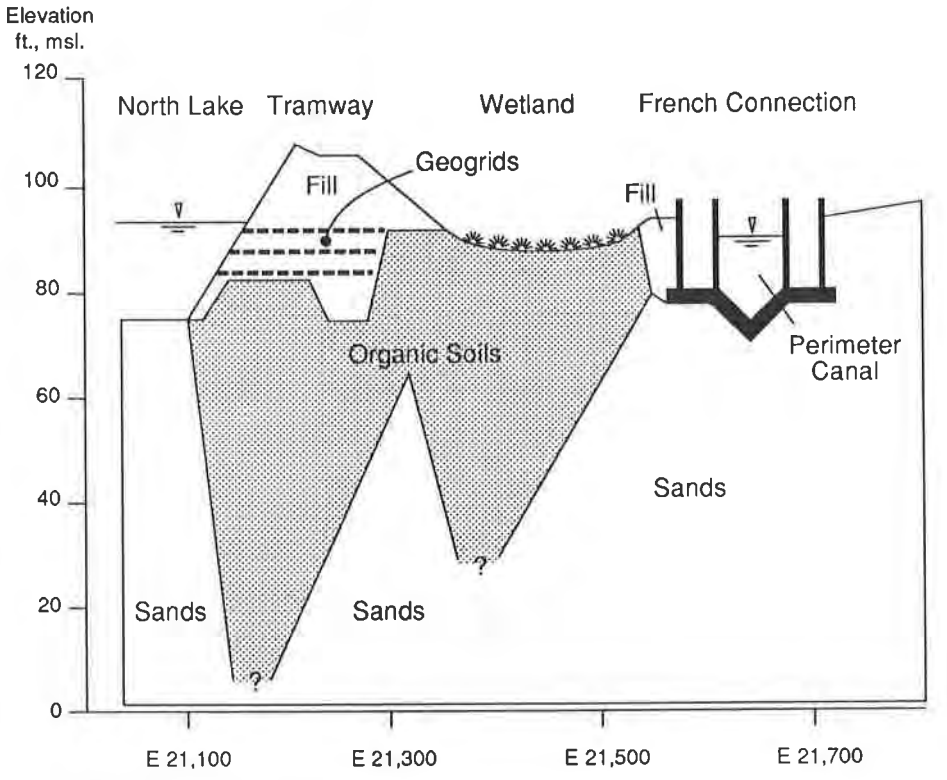

Figure:7 Typical cross-section through lake-edge fill

CONCLUSIONS

In working with geogrids on the Disney Center project, we have reached three main conclusions relative to their performance within earthfill embankments.

° Geogrids enhance the stability of slopes on soft organic soils. The benefits of this on the Disney projects were that one did not have to control fill rates too closely and that the on-site fills could be used for construction without too much concern for their drainage characteristics.

° Lateral spreading appears to be greatly reduced when geogrids are utilized along embankment shoulders. No problems have been experienced with buried utility lines which are sensitive to both vertical and lateral movements.

° Differential settlements that are being experienced in the reinforced embankments and fill slopes are less pronounced than in similar areas with no grid. This should prevent "birdbaths" from forming in the pavement plus reduce cracking in the curbs and asphalt.

ACKNOWLEDGEMENTS

Several individuals played an important part in this project related to constructing over organic soils. Project team members that the authors wish to particularly acknowledge are Hal McIntyre, Gary Ehrlich and Miller Andress. Organizations associated with the project were as follows:

Owner ..... Disney Development Company

Construction Manager ..... Mellon Stuart Company

Contractors ..... Hubbard Construction Company
..... Phillips & Jordan, Inc.

Civil Engineer ..... Greiner, Inc.

Geotechnical Engineer ..... Dames & Moore*

Construction Materials Testing ..... Jammal & Associates, Inc.

** Ian Kinnear was employed by Dames & Moore during the design phase of this project.*

Geogrid Reinforced Containment Dykes for Mountainside Oil Tank Farm in Seismic Zone

Thomas T. Heike
SNC Inc., Canada
Michael A. Patterson
SNC Inc., Canada
John R. Kerr
Tensar Earth Technologies, Canada

ABSTRACT

The need to expand its oil products storage facilities on the south slopes of Burnaby Mountain, caused Trans Mountain Pipe Line Company to consider several alternatives for design and construction of the associated containment dykes and also to upgrade their existing dykes to satisfy current industry regulations and engineering practice. The oil tank farm site is located downhill of Simon Fraser University campus and uphill of a residential area. The real estate restrictions and aesthetic considerations concomitant with this location, combined with the 20-25% natural ground slopes, the National Building Code of Canada's zone 4 seismic classification and limited available borrow material, placed some challenging demands on the design of the foundations and embankments.

These factors necessitated the use of geogrid reinforced earthfill embankments to provide the most economical dykes with adequate safety factors for containment of potential oil spills during an earthquake with peak horizontal ground acceleration of 0.21 g. The entire project required the installation of approximately 90,000 square meters of uniaxial and 95,000 square meters of biaxial polypropylene grids.

This paper describes the analysis, design and construction methods adopted for the dykes and includes the rationale for selection of the geogrid reinforced design in favour of other conventional and unconventional methods.

INTRODUCTION

In early 1988, Trans Mountain Pipe Line Company Ltd. embarked on a major expansion project which included the design and construction of three pumping stations at Darfield, B.C., Albreda, B.C. and Niton, Alberta and a 35% increase to their product storage capacity at their Burnaby Terminal. The capacity increase at Burnaby consisted of the installation of three new 150,000 bbl (23,860m^3) domed floating roof tanks at the west end of the terminal and their associated containment dyking. Design and construction of these dykes on the steep slopes of Burnaby Mountain, within the confines of the existing tank farm layout and property limits and to satisfy the National Building Code seismic zoning requirements, incorporated the use of approximately 69,000 square metres of synthetic geogrid reinforcement in 80,000 cubic metres of embankment.

In addition to the expansion program, TMPL requested a review of the factors of safety of the containment dykes surrounding the existing tanks. This review indicated that the factors of safety were not high enough to comply with current engineering practice when recent NBC seismic zone reclassification is considered. On the basis of these analyses a rehabilitation program for the existing dykes was considered and a decision made to reconstruct the dykes incorporating approximately 116,000 square metres of synthetic geogrid reinforcement in a total of 135,000 cubic metres of embankment.

This paper describes the analytical methods and results, design and construction methods adopted for the new and replacement dykes. A description of other alternatives considered and the rationale for selection of the geogrid reinforced design is briefly presented.

SITE DESCRIPTION

The site is located on the south facing slope of Burnaby Mountain in north-central Burnaby, British Columbia. It is situated downslope from Simon Fraser University campus and upslope from a residential subdivision in Burnaby. The area lies within the southwest coast climatic region of British Columbia and is characterized by a temperate inshore marine climate featuring cool summers and mild wet winters.

Average annual precipitation is 180-190 cms. (70-75 inches) and there is usually a significant soil moisture surplus, associated with the humid climate and a long frost-free season.

The tank farm is comprised of two rows of tanks constructed on terraces notched into the mountainside. The average ground slope varies from 15% to 25% generally being gentlest in the lower east section and steepest in the upper west section of the site. Access roadways run parallel to the contours above, below and between the two rows of tanks at approximately 20 metre elevation intervals. (See Figure 1)

The site is underlain by a variable thickness of sandy tills overlying Tertiary sedimentary rocks consisting of interbedded sandstones, conglomerates and shales of the Burrard and Kitsilano Formation (Roddick, 1979). In general, the thickness of surficial soils at the site varies from two metres at the eastern end of the property to 7.5 metres or more at the western end. The till formation locally has been divided into two units; an upper relatively loose silty sand layer identified as the Capilano sediments and a lower, dense, well graded granular till known as the Vashon Drift. The upper portion of the bedrock is moderately weathered and weak discontinuities sub-parallel to the bedding planes were identified. These discontinuities which dip at 3° to 5° south, were assumed to control the strength of the rock mass. Groundwater observations made during site investigations, indicated that in some areas, the phreatic line is within 0.5 metres of the ground surface.

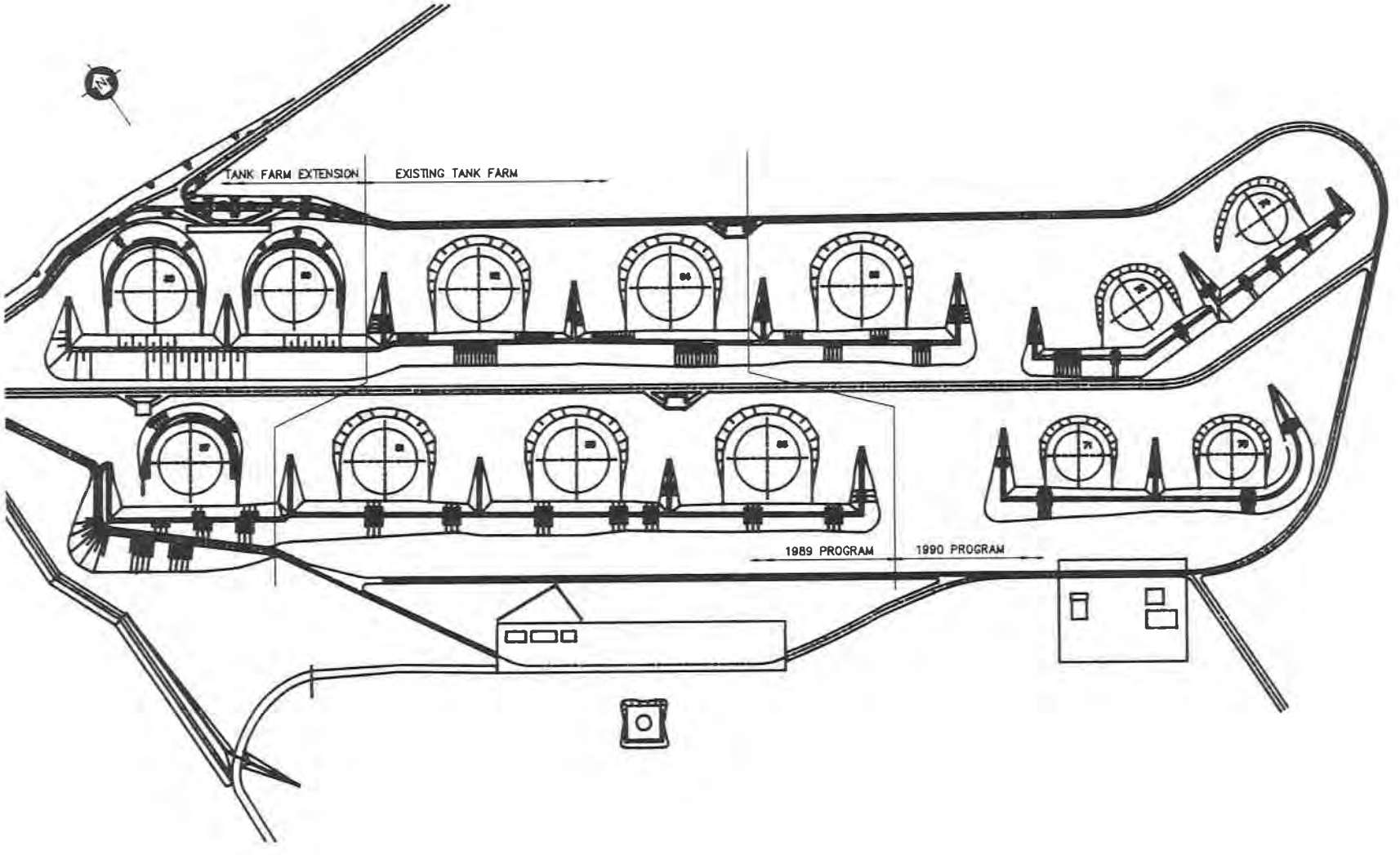

FIGURE 1: PLAN SHOWING LAYOUT OF EXISTING TANK FARM AND EXTENSION

0 50 100 200

GRAPHIC SCALE:

The project area lies within one of the most seismically active zones in Canada. In the generally accepted model of plate tectonics the British Columbia coast line is close to the North American plate which is moving over the Pacific Ocean plate. The relative movement of these plates has been postulated to be the source of several historically high magnitude earthquakes experienced in the region. The area lies within Seismic Zone 4 according to the National Building Code of Canada (1985).

PROJECT DESCRIPTION AND CONSTRAINTS

The construction and rehabilitation of the containment dykes formed part of a $20,000,000 expansion and upgrading program at Trans Mountain Pipe Line's Burnaby Terminal. The initial project scope required the addition of three new 150,000 bbl tanks (87,88 and 90) at the west end of the terminal (see Figure 2) along with the associated containment dyking. After an assessment of the existing dykes around the six 150,000 bbl tanks (81-86) and the four 100,000 bbl (71-74) it was decided to remove and replace them with structures engineered to current code requirements, design standards and engineering practice especially those affected by the latest NBC seismic zonation. The main objectives and criteria for design of the containment dykes were as follows:

- The dykes must be capable of impounding 110% of the tank's capacity. To maintain flexibility in product storage, combined containment of tank lots was not adopted.

- The minimum factors of safety for stability against shear under potential load combinations were as follows:

Normal Operating Condition	- 1.5
Abnormal Loads - Static (100%) oil spill)	- 1.3
Abnormal Loads - Seismic (NBC (1985) design earthquake)	- 1.0

- The containment structures must be aesthetically pleasing and visually blend in to its surroundings. This implied that grassed exterior slopes were preferable.

- The additional tanks and associated dyking had to be built within the existing property limits hence the existing infrastructure greatly influenced the location and configuration of the new structures.

- Initially, landscaped areas on the property were not to be disturbed hence local burrow material for dyke construction was severely limited. Material balances and cost/benefit evaluations developed during the project substantiated the value of exploiting materials on site and allowing for rehabilitation or enhancement of the existing landscape.

FIGURE 2. ELEVATION AND CROSS SECTION FOR NEW TANKS AND CONTAINMENT DYKING.

. The construction of the new dykes had to be done in one construction season to allow the new tanks to accept products in December, 1989.

. The scheduled movement of oil products was such that only two of the existing tank lots could be released for reconstruction of the dykes at any time.

DESIGN ALTERNATIVES

New Dykes. For the dykes to serve the three new tanks a conventional trapezoidal alternative was first considered since it would be similar in configuration to the existing dykes. The dyke location relative to each tank was selected to meet the requirements described above relating to containment capacity, space limitations and landscaping. The two options considered for the trapezoidal cross section were as follows:

1) Non-reinforced option which is similar to the existing dykes

2) Reinforced option which utilized geogrid earth reinforcing material

The ensuing study carried out on the first option concluded that this option was technically not acceptable. Factors leading to this decision were the indication of slope instability of the existing dykes (minor sloughing on some slopes), the increased regulatory requirements for containment capacity and the increased code requirements on seismic loading since the time that the existing dykes were constructed. It was therefore decided that a conventional trapezoid dyke would need to be reinforced and that geogrid reinforcing would be the most viable approach. The selection of geogrid was based upon its unique physical characteristics and proven performance in numerous slopes subjected to seismic loading similar to that anticipated on the Burnaby site. For reasons discussed later, only geogrid was considered for the report.

Due to the size of the trapezoid dykes and the initial areal limitations placed against on-site borrow sources for the required fill material, a large shortfall of fill material was identified. Importing the fill from an off-site borrow was ruled out due to cost and public nuisance of trucking. Therefore a hybrid dyke alternative was considered to minimize or eliminate the shortfall in fill. The hybrid dyke configuration was based on a vertical face at the uphill side and a sloping face on the downhill side.

The following options were considered for the vertical face portion of hybrid dyke alternative:

1. Reinforced concrete retaining wall
2. Concrete panels with steel reinforcing strips
3. Concrete panels with geogrid reinforcing
4. Others
   - Rollcrete
   - Soil-cement
   - Gabions

The first three options were investigated in sufficient detail to permit comparative cost estimating. The others were judged to be less desirable for this project from the point of view of availability of suitable construction materials at the site, degree of potential damage due to fire or level of permanence. The following descriptions of the first three options for the vertical face portion of the hybrid dykes are provided below:

1. Dyke with Reinforced Concrete Wall - This utilizes a traditional reinforced concrete wall which consists of a base section founded at a suitable soil bearing level and a vertical stem to retain the uphill side of a reinforced earth dyke and a sloping earth dyke on the downhill side.

2. Dyke with Concrete Panels and Steel Reinforcing strips - This consists of cruciform shaped precast concrete wall elements on the uphill side attached to galvanized horizontal steel reinforcing strips embedded in the compacted engineered fill in conjunction with a sloping earth dyke on the downhill side.

3. Dyke with geogrid reinforcing - This entails rectangular precast concrete panels on the uphill side attached to horizontal geogrids embedded in the compacted engineered fill in conjunction with a sloping earth dyke on the downhill side.

All three hybrid alternatives were eventually discarded for a trapezoidal dyke with geogrid reinforced slope faces on both sides. This alternative is shown in Figure 3 and is discussed in more detail in the following section.

Rehabilitated Dykes

a) **In-situ Strengthening Options**

Due to the volume of fill material in the existing dykes which serve ten operating tanks, in-situ strengthening options were initially considered. The following six options were studied:

1. Dynamic compaction of the existing dyke to densify the loose to medium silty sand fill material - This option was rejected since the shear strength of the underlying thin organic layer left at the original ground surface would not be improved and undesirable vibrational effects on buried piping, nearby computer facilities and neighbouring properties could occur.

2. Jet piling of the core of the dyke - This option is based on the use of high pressure fluid cement grout injection to improve the overall shear strength of the fill in the core zone This option was deemed inappropriate largely due to buried piping and impractical logistics to implement the jet piling technique on a narrow crested dyke.

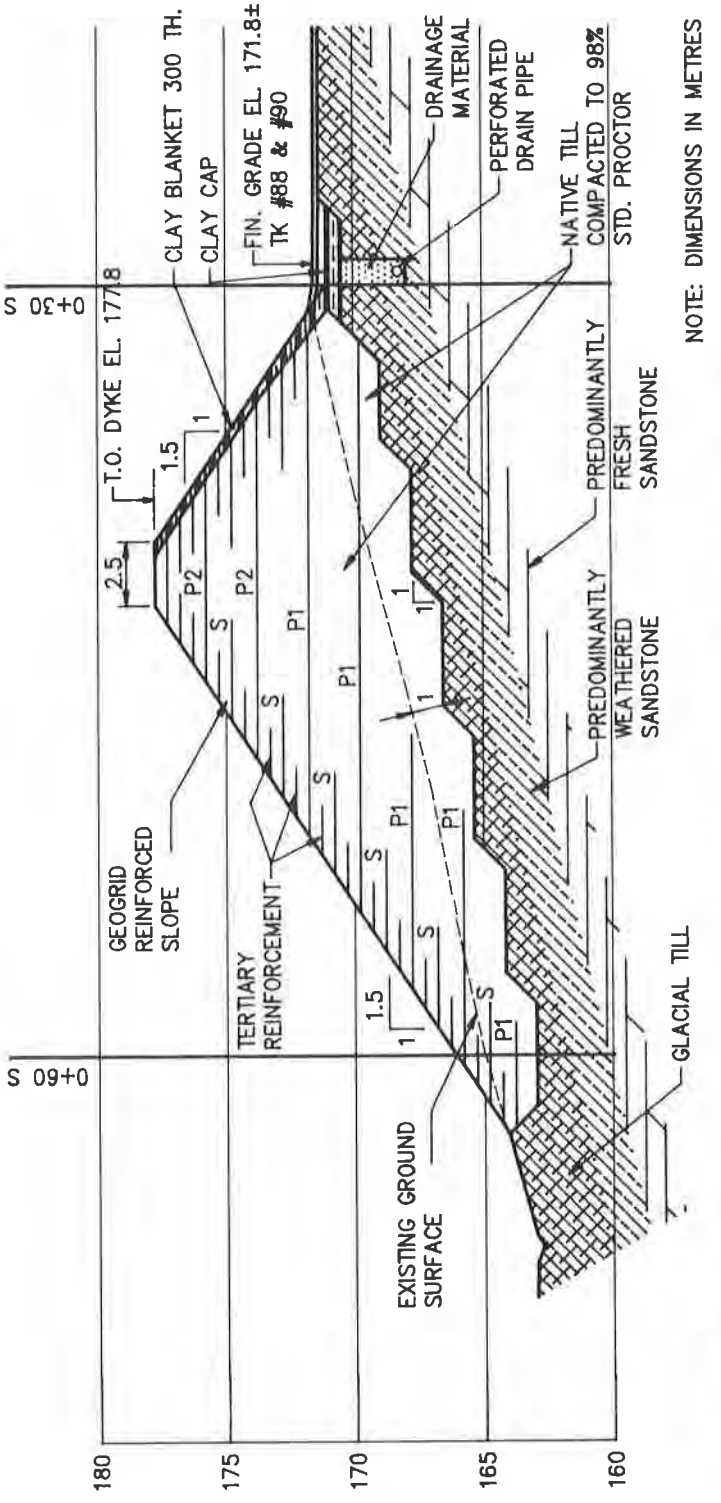

FIGURE 3. TYPICAL CROSS SECTION OF CONTAINMENT DYKES

3. Rib Drains and Outer Shell - This entails the placement of vertical drains perpendicular to the dyke axis which would reduce the porewater pressure and substituting the downhill slope surface with a coarse, granular material to improve the surficial stability. This option was rejected on the basis of impracticality.

4. Concrete Wall and Rock Anchors - This option consists of constructing a cast-in-place reinforced concrete toe wall keyed into bedrock with rock anchors placed near the top of the wall. This option was also rejected due to the inherent instability introduced by the deep excavation at the toe of the dyke required for the toe wall construction.

5. Concrete Slurry wall with Rock Anchors - This option has features similar to the previous option but replaces the cast-in-place reinforced concrete wall with a concrete slurry wall which is uphill of the dyke toe. In addition the downhill slope, to a thickness of one quarter of the dyke width, is geogrid reinforced to improve the internal slope stability of the dyke.

   This option was not adopted since it is technically and economically inferior to the "remove and replace" options described below.

6. Concrete Cantilever Wall - This option consists of constructing a reinforced concrete cantilever wall which lines up with the top of the uphill slope of the dyke and is founded on the till overburden. This installation would create a vertical uphill face of the dyke which is capable of withstanding the fluid pressure of contained oil. This option was rejected on the basis of cost.

b) **Remove and Replace Options**

Remove and replace options were investigated to compare costs and practicability with the aforementioned in-situ strengthening options.

The following four options were studied:

1. Trapezoidal dyke geogrid reinforced - This option consists of a traditionally shaped earth dyke which is reinforced with primary and secondary geogrid materials placed horizontally in compacted native till.

   This option, which was ultimately adopted for both new and rehabilitated dykes, is detailed in Figure 3 and presented in Figure 4 as Alt #1.

2. Trapezoidal dyke similar to Option 1 but with a 1.5 m wall on the dyke crest - The purpose of the 1.5 high wall is to maintain the required effective height of the dyke while reducing the fill quantity requirements. This option, shown as Alt #2 in Figure 4, was rejected on the basis of cost and undesirable schedule impact of required construction activities related to the 1.5m high wall.

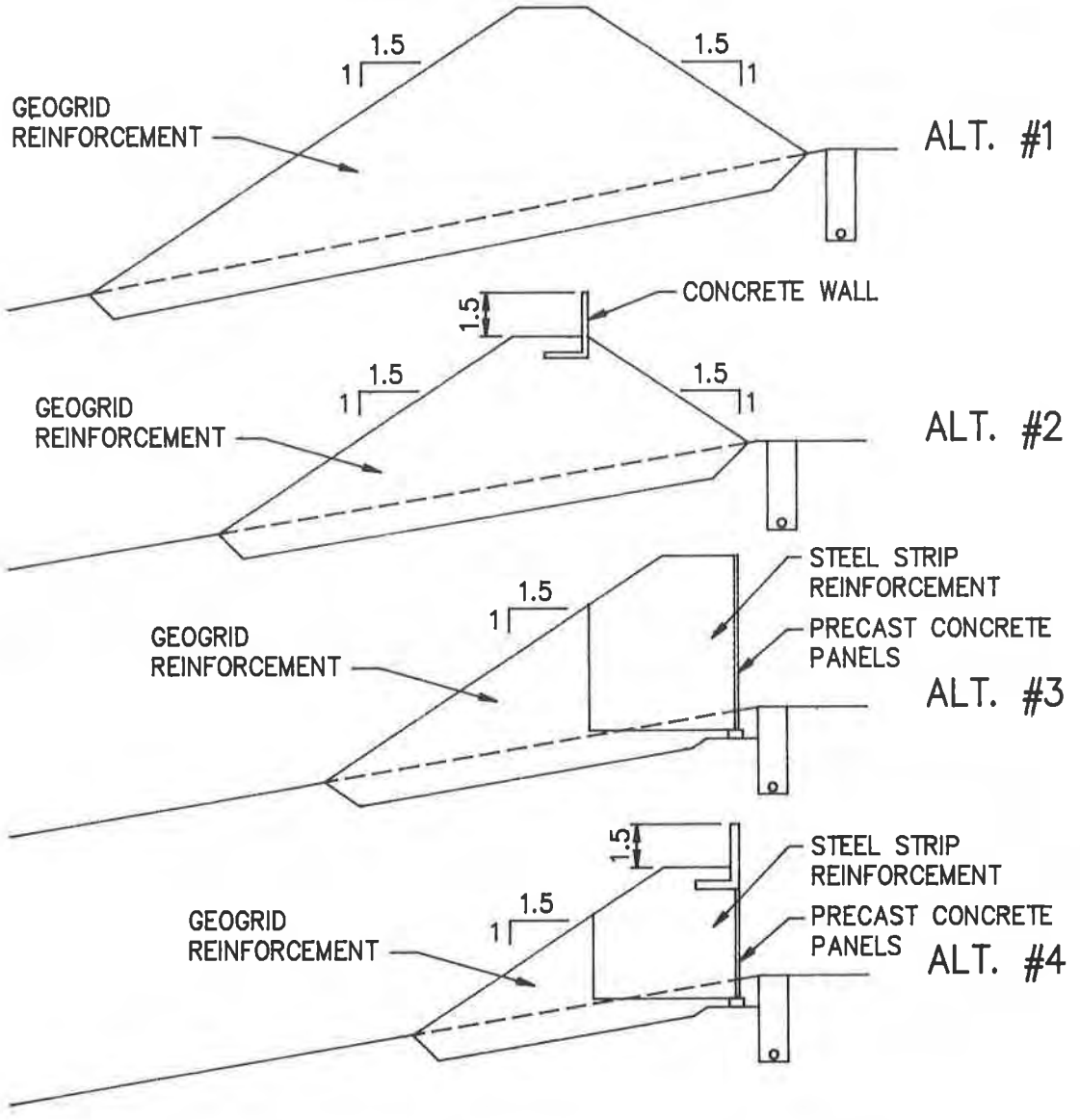

FIGURE 4. TYPICAL CROSS SECTIONS OF ALTERNATIVES FOR REHABILITATED DYKES

3. Hybrid dyke with concrete panels and steel reinforcing strips in the uphill portion and with geogrid reinforcing in the downhill portion - This option, which is shown as Alt. #3 in Figure 4, reduces the fill quantity requirement. However, it was found to be significantly more costly than the adopted scheme and therefore rejected.

4. Hybrid dyke similar to Option 3 but with a 1.5 m high wall on the dyke crest - The reason for this option is to reduce the fill quantities compared to Option 1 and the cost of reinforcing the dyke. This option, which is shown as Alt #4 in Figure 4, was found to be more costly than the adopted scheme and would incur undesirable schedule impacts associated with the 1.5 m high wall. Therefore this option was rejected.

RATIONALE FOR GEOGRID USE AND SELECTION

Geogrid reinforcement was selected for use on the project because of its use in conjunction with local materials proven performance history, ease of construction and economics. The use of earth reinforcing material was limited to geogrids to preclude concerns of interfacing dissimilar reinforcing materials and potential schedule conflicts. From the early stages of design, the objective was set to maximize the use of existing materials at site, mainly till, to build the new dykes and to rehabilitate the existing dykes. In this way capital costs, nuisance to neighbouring areas and schedules could be optimized. The adopted design of trapezoidal dykes required a large volume of till. The values for the geotechnical design parameters used in the analysis and design of the dykes were based on assumption that all required volumes of till for the construction of the dykes could be met with the till from required excavation or from borrow on site. The importing of materials was therefore limited to those materials required by the adopted design which are not present at the site.

Key reinforcement characteristics used in the design of the dykes included the following:

1. Proven long term allowable design strength.

2. Proven long term resistance to creep deformation under sustained load.

3. Tensile modulus high enough to provide strain compatibility with the soil being reinforced.

4. Sufficient durability to maintain reinforcement design characteristics for the life of the project.

5. Interaction coefficient high enough to provide adequate interaction/anchorage with the surrounding soil (minimum of 0.8 used for design).

6. High enough junction strength to prevent product deformation both during construction and in service. This was also a product specific requirement related to soil interaction.

Minimum physical properties for the reinforcement used are presented in Table 1.

Table 1. Minimum Physical Properties of Selected Geogrids

Type of Reinforcement	Ultimate Strength (kN/m)	Long Term Design Load (kN/m)	Tensile Modulus (kN/m)	Flexural Rigidity mg-cm
Primary 1	79	31.6	135.6	4,700,000
Primary 2	34	13.6	67.8	670,000
Secondary	31	12.4	25.1	750,000
Tertiary	21	8.4	19.0	250,000

The construction procedure was simple and expeditious with the laydown crew working just ahead of the fill placement and compaction operation.

Geogrid reinforcement enabled the dyke slopes to be steepened to 1V:1.5 H from an unreinforced angle of 1V:2H. Any flattening of the proposed dyke slope would have increased the area of the dyke footprint and therefore greatly increased the amount of fill required. Considerable savings were therefore achieved in overall cost and construction time. The construction time schedule was particularly important as, because of product storage commitments, the time required to build each tank dyke governed the critical path planning for the work.

The use of geogrid reinforcing permitted the optimum use of site materials which resulted in significant savings in the cost of constructing the adopted dyke design. The other design options would have incurred costly cast-in-place concrete or precast concrete panels, specialized construction techniques, or expensive off-site construction materials.

ANALYSIS AND DESIGN

In general, the internal (embankment) and external (overall) stability of the dykes was analyzed on computer using Bishop's Method applied to the Swedish method of Slices.

Pseudostatic analyses were carried out to evaluate the stability of the dykes under the design seismic conditions. In conformance with NBC, 1985, a value of 0.21g was used for the peak horizontal ground acceleration. A value of 0.85 was used for the seismic coefficient (K) as defined by Seed and Whitman (1970).

The strength parameters used for design analysis are presented in Table 2:

Table 2. Selected Design Parameters

Material	Unit Weight KN/m^3	ϕ' (deg)	c' MPa
Rockfill	20.0	45	0
Till Backfill	21.5	35	0
Engineered Fill (Composite)	21.5	38	0
Surficial silts and sands (Capilano Sediments)	20.5	33	0
In-situ Till (Vashon Drift)	21.0	38	0
Weathered Bedrock			
i. Across Bedding Planes	21.5	38	0
ii. Along Bedding Planes	18.0	34.5	0
Fresh Bedrock	-	-	5 (Total Strength)

The results of the analyses of internal and external stability are discussed below.

Internal Stability. The embankment material used for dyke construction consisted of sandy till and weathered bedrock available from the excavations for tank bases or borrowed from within the project area.

The till has at least 10% fines and when compacted to 98% Standard Proctor expected to have the design strength parameters. Typically, the crest of the dykes for the new tanks will be 14 m above ground elevation on the exterior side and 6.5 m above the finished grade on the interior side.

The replacement dykes are generally lower, varying from 12m to 5 m on the exterior side and 6-14 m on the interior side. The selected cross-section of the dykes is represented by a trapezoidal shape with a 2.5 m wide crest and 1.5 H to 1V slopes.

The tensile elements for reinforcing of the dyke slopes consisted of integrally formed polymer grid structure alternating vertically in three groups as shown in Fig. 3.

To provide optimum tensile strength in the transverse direction two grades of uniaxial elements were used in the primary reinforcement group. For the upper four metres of embankment, a geogrid with ultimate tensile strength of 34 KN/m was specified, while in lower positions, the specified geogrid had an ultimate uniaxial tensile strength of 79 KN/m. Secondary geogrid reinforcement with an ultimate tensile strength of 31 KN/m was specified to prevent shallower slip failures and a lighter weight biaxial tertiary group with ultimate tensile strength of 21 KN/m specified to enhance the behaviour of the slope face during a seismic event. The geogrid pattern and type was checked at each grid elevation. The resistance to the sliding mass is provided both by the strength of the backfill itself and the polymer geogrid woven within the backfill and extending beyond the theoretical incipient failure surface. A beneficial characteristic of the geogrid used is that the allowable tensile strength is dependent on the rate of loading. For seismic loading conditions, the allowable design strength of the geogrid was taken at 75% of the ultimate strength while 40% was used for the static case (Bonaparte et al, 1986). The results of the stability analyses show that the engineered embankment has a factor of safety of better than 1.5 for normal conditions and 1.15 under the design seismic loads. A summary of the factors of safety obtained under the various loading conditions is presented in Table 3.

External Stability. The results of preliminary stability analyses of the embankment and foundation led to the specification of two measures to enhance the structure's overall stability. Firstly, the relatively loose Capilano sediments were removed from the foundation to ensure that the embankment rests directly on the denser Vashon Drift materials. The excavation was terraced, as shown on Fig 3 to facilitate placing and compaction of the fill and geogrid in horizontal lifts. Secondly, a foundation drainage system was designed to control the uplift pressures under the downhill section of the dyke. The foundation drainage system consists of a nominal three metres deep trench close to the uphill toe of the dyke to intercept and lower the piezometric surface under the embankment. Perforated, filter-wrapped, PVC piping (200mm diam.) was placed at the bottom of the interceptor trench to collect the groundwater and transport it to catch basins or culverts in the site drainage system.

The trench was backfilled with granular drainage material and capped with clay to inhibit the percolation of surface water into the foundation drainage system.

The materials in the foundations were considered to be sufficiently dense and granular to exhibit dilatant behaviour under dynamic loading. This dilatant behaviour would result in pore water pressure reduction during a seismic event.

To take the dilatant characteristic of the foundation materials into account, the undrained shear strength for the materials was estimated using $\phi' = 38°$, Skempton's pore water pressure parameter, $A = 0$ and the at rest earth pressure coefficient $K_o = 1 - \sin \phi'$. The values calculated were then used in a total stress stability analysis for the seismic cases. Results of the stability analysis are shown in Table 3 below.

Table 3. Summary of Safety Factors

	No Spill No Earthquake	Oil Spill No Earthquake	No Spill with Earthquake
F.S. beneath dyke.	2.026	1.592	1.233
F.S. of slip plane passing through dyke into dyke foundation.	1.719	1.613	1.444
F.S. within the dyke.	1.529	1.529	1.227

The controlling case for design was taken as normal operating condition with the design earthquake but no oil spill. The scenario of combining a design earthquake with an oil spill is considered too remote to govern engineering design, however, a check of the dyke stability under these extreme loading conditions gave a factor of safety of 1.08 indicating that the dykes will withstand the loads imposed by a design earthquake even if the containment area is simultaneously flooded with an oil spill.

CONSTRUCTION

Prior to embankment construction, the area beneath the dyke was stripped of organic material and the relatively loose, sandy silt of the Capilano Formation removed to form a terraced foundation. The vertical trench for the foundation drainage system was excavated and the drainage pipes installed before backfilling of the trench with granular material and capping with clay.

At a location adjacent to the laydown area, geogrid layers were precut, colour coded and stored in advance.

The appropriate lengths of geogrids were placed horizontally in the fill at their specified elevations. The primary and secondary reinforcements were placed transverse to the dyke axis whereas the tertiary reinforcement was rolled out parallel to the dyke axis. The fill was placed and spread with tandem trucks and bulldozers. Maximum uncompacted lift thickness of 300mm was adequate to allow two lifts between each geogrid larger with minor grading and trimming required. No construction traffic was allowed to travel directly over the geogrids so a minimum cover of one lift of fill was required. The fill was compacted with vibrating rollers to 98% Standard Proctor density.

The final slope dressing specified was a 100 mm thick layer of topsoil on the exterior slopes followed by hydroseeding. On the interior slopes, a 300mm thick clay liner was specified to prevent any percolation of spilled petroleum product into the geogrid reinforced zone. A 100mm thick hydroseeded topsoil layer was specified to cover the clay on the interior slope. Heavy rains during the fall, before the grass growth was established caused surficial damage to the slope dressing and the dyke slope had to be protected with polyethylene cover during the winter. A remedial program involving the use of erosion control blankets for the slope was designed to be carried out in the following year's construction season. The learning curve for construction of the geogrid reinforced fill was short as within a week the contractor was placing 2000 cubic metres per day which was considered optimum for the equipment, work area and layout of the site. However, overall construction progress was slower than expected due mainly to poor weather, and repeated handling of material for moisture conditioning. Nevertheless, at the end of the 1989 construction season, 85% of the projected embankment volume was placed. The shortfall, along with the 1990 portion of the program was placed during the 1990 construction season.

CONCLUSIONS

From the experience in design and construction of the containment dykes for the TMPL, Burnaby tank farm, the following conclusions can be drawn.

- The incorporation of synthetic polymer geogrids into the design of the containment dykes enabled adequate factors of safety to be obtained with steep embankment slopes on a steep mountainside in a zone of high seismic activity.

- Compared to several other alternatives involving conventional and non-conventional techniques, the geogrid reinforced method was more economical.

- Construction procedures were not complicated and the learning curve for the placement crew was relatively short.

- Depending on the material used for embankment construction and the regional climate, adequate and immediate slope protection should be provided to protect against surface erosion caused by heavy rainfall on the relatively steep slopes.

ACKNOWLEDGEMENTS

This paper is presented with the permission of Mr. T.D. Doyle, Executive Vice President and Chief Operating Officer of Trans Mountain Pipe Line Company Ltd. Geotechnical assistance for design and analysis of the structures was provided by Hardy BBT Ltd. and Dr. N.R. Morgenstern of the University of Alberta. The authors wish to thank all of their colleagues involved in the design and construction of the project and all persons who assisted in preparation and review of this paper.

REFERENCES

NBC (1985) National Building Code of Code of Canada

Bonaparte, P., Schmertmann, G.R. and Williams, N.D. "Seismic Design of Slopes Reinforced With Geogrid and Geotextiles", Vol. 1, Vienna, Austria, April, 1986, pp 273-279.

Roddick, J.A. (1979) Vancouver North, Coquitlam and Pitt Lake Map Areas, British Columbia, "Memoir 335", Geological Survey of Canada

Seed H.B. and Whitman R.V. (1970) "Design of Earth Retaining Structures for Dynamic Loads" 4th PSC, ASCE, pp 103-147.

A Simplified Design Method For Silt Fences

Gregory N. Richardson
ENSCI, Corp., USA
Percy Middlebrooks
Georgia Department of Transportation, USA

INTRODUCTION

Many States are currently developing simplified design standards for silt fences. Such simplified guidelines are the result of use restrictions resulting from new and more rigorous State sedimentation control regulations, and of past silt fence failures. Past operational failures of silt fences are clear indicators that silt fence systems are not routinely engineered nor properly maintained. The simplified design method presented herein incorporates significant usage limitations on silt fence systems to greatly simplify traditional surface water runoff and erosion calculations. The resulting engineered silt fence designs are conservative in function, yet provide very economical sedimentation control structures owning to the inexpensive nature of geosynthetic silt fences.

APPLICATION RESTRICTIONS

The most common application of silt fences is to control sediment flow leaving new construction sites. As such, the simplified design method for silt fences developed here assumes that the design life of the silt fence is less than 6 months and that the ground surface tributary to the silt fence remains unvegetated during this time interval. Guidelines are also presented for silt fences having a longer design life but all nomographs included in this paper are intended for short-term, new construction applications.

Silt fences must also be limited to applications where the erosion occurs in the form of sheet erosion and where there is no concentration of water flowing to the barrier. To ensure such conditions, the flow velocity of the water reaching the silt fence must be less than 1 ft/sec. The flow velocity of surface water is a function of the slope steepness, slope length, and smoothness of the grounds surface. Making the conservative assumption that the ground surface is smooth, the flow velocity of surface water can be limited by reducing the allowable slope length as the inclination of the slope increases as given in Table 1.

TABLE 1

Slope Steepness vs. Slope Length

Slope Steepness	Maximum Slope Length, ft.
<2%	100 ft.
2-5%	75 ft.
5-10%	50 ft.
10-20%	25 ft.
>20%	15 ft.

This limits the drainage area for overland flow to a silt fence to less than 1/4 acre per 100 feet of fence. Greater slope lengths can be used if nonerosional outlets are provided as part of the silt fence barrier. Such outlets, however, indicate a sophistication of design not associated with the simple applications covered by this paper.

Additional limitations may be placed on the geometry of geosynthetic silt fences by State sediment control regulations. For instance, the height of the silt fence is limited to 18-inches in North Carolina and 36-inches in Georgia. Such height restrictions limit the sediment storage capacity behind the fence and result in the need for additional parallel rows of silt fencing.

ESTIMATING RUNOFF VOLUME

The silt fence system must be designed to provide a containment volume greater than the anticipated volume of runoff water. If this cannot be accomplished, then the silt fences must incorporate nonerosional outlets to allow controlled over topping of the fence. The calculation of runoff volumes for the small watershed areas appropriate for silt fence applications is best performed using the Rational Method given as follows:

$$Q = CiA \qquad \text{Eq. 1}$$

where Q = runoff, cubic feet per second
C = surface runoff coefficient
i = rainfall intensity, inch/hour
A = area, acres

While the English units of the variables do not appear to match, the conversion from acre-inch/hour to cubic feet per second is approximately unity and can be omitted. The silt fence system must be designed to have sufficient containment volume to hold the total runoff volume of the design storm.

The runoff coefficient C represents the land use of the drainage field. Under the assumption that the silt fence is being used at new construction sites, it is assumed that the runoff field is bare soils. For silt fences having a design life of less than 6 months this is appropriate. The value of C for bare packed soils ranges from 0.6 for a smooth surface to 0.2 for a rough surface. Thus, a conservative estimate of the weighted value of C is assumed to be 0.5. For longer design lives, this may be reduced if seeding is performed during the first 6 months.

Rainfall intensity, i, reflects both the regional rainfall history and the assumed return period of the design storm. The design return period of the storm is typically defined by State regulations and is commonly a 10-year storm. Figure 1 provides a map of 10-year rainfalls appropriate for use in designing silt fences. Note that the variation in rainfall intensity within many states is so small that a single rainfall intensity could be used, resulting in even more simplification of the design process. It should also be noted that, in the rigorous application of the Rational Method, the rainfall intensity is adjusted based on the time of concentration, T_c, for the drainage field. This is defined as the time it takes the farthest overland flow to reach the silt fence. For the small drainage fields associated with the silt fences, the value of T_c is small enough that the full rainfall intensity from Figure 1 must be assumed in design.

Making the above assumptions in Equation 1 results in the following expression for the total storage volume required of the silt fence:

$$\text{Volume (acre-inch)} = 0.5\ i\ A \qquad \text{Eq. 2}$$

Where i is the rainfall intensity in inches obtained from Figure 1 and A is the area of the drainage field in acres. This can also be express wholly in terms of feet as follows:

$$\text{Volume (cubic feet)} = 0.04\ i\ A \qquad \text{Eq. 3}$$

Where the drainage field area, A, is now expressed in square feet.

ESTIMATING SEDIMENT VOLUME

The volume of sediment removed by rainfall during the 6-month design life of the silt fences can be estimated using the Soil Conversation Service's Universal Soil Loss Equation (USLE) (Soil Conservation Service, 1977). The USLE is expressed as follows:

$$A = RKLSCP \qquad \text{Eq. 4}$$

Where
A = Soil Loss (Tons/Acre/Year)
R = Rainfall Erosion Index
K = Soil Erodibility Factor
LS = Slope length and steepness factor
C = Vegetative cover factor
P = Erosion control practice factor.

For new construction sites, this equation can be simplified by assuming no vegetative cover (C = 1) and minimal erosion control practices (P = 1).

The rainfall erosion index can be obtained from Figure 2. As with rainfall intensity, note that it would be possible to assign a single design value of R within many States. Additionally, the use of Figure 2 for those regions west of the 104° latitude is not recommended.

Due to the limited slope lengths and steepness factors applicable to silt fence applications, it is possible to greatly simplify the empirical solution for LS and at the same time integrate the soil erodibility factor, K. The resulting relationship is shown on Figure 3. Thus, it is possible to readily obtain the product KLS knowing only the average slope angle and general soil classification.

Solution of Equation 4 results in an estimate of the tons of sediment per acre of drainage field served per year. Use of this full estimated annual sediment tonnage for the 6 month slit fence provides a reasonable safety factor to prevent the sediment volume from exceeding the storage volume of the fence. The annual soil loss tonnage can be converted into a design volume by assuming that the sediments have a dry unit weight of 50 pounds per cubic foot.

CONSTRUCTION CONSIDERATIONS

The geotextile used in the construction of a silt fence must be sufficiently strong to resist bursting under the load applied by the pooled water and sediments. This minimum strength is a function of the height of impoundment and the spacing of the posts supporting the fence. Figure 4 shows the required geotextile tensile strength for a range of impoundment heights and post spacings. Generally, the use of geotextiles alone is restricted to

impoundment depths less than 24 inches and with post spacings less than 4 feet. Silt fences exceeding these limitations should incorporate a woven wire reinforcement (14 gauge, maximum 6-inch mesh spacing) to prevent burst failure of the geotextile. The physical demands on the fence posts also increase with increasing fence height and post spacing as shown on Figure 5. In general, post related problems are not encountered if the fence height is less than 24-inches, the post spacing is 4-feet, and the minimum post embedment depth is 16 inches.

General construction guidelines for silt fences are as follows:

1. Silt Fence Fabric: The geotextile shall meet the minimum specifications as defined by TF25 as follows:

Fabric Properties	Minimum	Test Method
Grab Tensile Strength (lb)	90	ASTM D1682
Elongation at Failure (%)	50	ASTM D1682
Mullen Burst Strength (PSi)	190	ASTM D3786
Puncture Strength (lb)	40	ASTM D751
Equivalent Opening Size	40-80	CW-02215
Ultraviolet Radiation Stability (%)	90	ASTM 9-26

2. Construct the filter fabric from a continuous roll cut to the length of the barrier to avoid joints.

3. Wood or steel posts are set on line at a spacing determined from Figure 5. In general, the spacing should be less than 3 times the height of the fence.

4. The upstream bottom of the filter fabric must be anchored in a soil or gravel trench as shown on Figure 6.

5. Do not install silt fences across streams, ditches, or waterways.

6. Tie the ends of the fences to the land contours in such a manner that flow around the ends of the fence is prevented.

7. If the fence may be overtopped, provide stabilized outlets to protect the fence system.

MAINTENANCE CONSIDERATIONS

A silt fence has a finite volume for collection of sediments. Regular inspection of the fence should be made after each storm to see if cleanout or replacement is required. Many State sediment control regulations now require replacement or cleanout of silt fences when the sediment depth exceeds half the fence height. If the silt fence is full, but the sediment cannot be removed, the sediments must be seeded and a new silt fence constructed down stream of the existing one.

DESIGN EXAMPLE

Design a silt fence profile for a site in Raleigh, North Carolina for a site having an average slope of 5% and consisting of silty clays.

(1) Maximum Slope Length: From the Table 1, the maximum, slope length is found to be 75 feet. The maximum spacing between parallel silt fences is therefore 75 feet.

(2) Runoff Volume:

Runoff Volume (cubic feet) = 0.04 i A Eq. 3

where i = 4 inches (Figure 1)
A = 1 x 75 = 75 sq. ft./ft. fence

Runoff Volume = 12 cubic ft./ft. fence

(3) Sediment Volume:

Soil loss, A (Tons/Acre/Year) = RKLS

where R = 250 (Figure 2)
KLS = 0.16 (Figure 3)

Soil Loss A = 40 Tons/Acre/Year
= 137 lbs./ft. fence/year
= 2.75 cu. ft./ft. fence/year

Design is controlled by Runoff Volume!

(4) Fence Height:

Try 18-inch fence, Volume = $1.5^2/.05$
= 45 cu. ft./ft. fence

Minimum 18-inch high fence is adequate!

(5) Posts/Spacing:

Try 3 x fence height = 4.5 feet
Figure 5, all typical posts work
Figure 4, all geotextiles work

Maximum 4.5 feet post spacing is adequate.

SUMMARY

The simplified silt fence design procedures presented here allows even silt fences on small sites to be rationally evaluated. Additionally, the procedure can be further simplified within those governmental regions where a singe value for rainfall and erosion related variables can be assumed. Such simplifications will provide significant user simplicity for major metropolitan areas.

REFERENCES

Erosion and Sediment Control Planning and Design Manual, North Carolina Department of Natural Resources and Community Development, 1988.

Richardson, G. N., and R. M. Koerner, Geosynthetic Design Primer, Industrial Fabrics Association International, St. Paul, MN, 1990.

Soil Conservation Service, National Engineering Handbook, Section 11 and 14, U.S. Department of Agriculture, Washington, DC, 1977.

Soil Conservation Service, Urban Hydrology for Small Watersheds, Technical Release No. 55, U.S. Department of Agriculture, Washington, DC 1986.

Mallard, P. and J. R. Bell, Use of Fabrics in Erosion Control, Transportation Research Report 81-4, Federal Highway Administration, Washington, DC, January, 1981.

Wyant, D. C., Evaluation of Filter Fabrics for Use as Silt Fences, Virginia Highway and Transportation Research Council, Charlottesville, VA 1980.

Hershfield, D. M., Rainfall Frequency Atlas of the United States, Technical Paper No. 40, U. S. Department of Commerce, Washington, D.C., 1961.

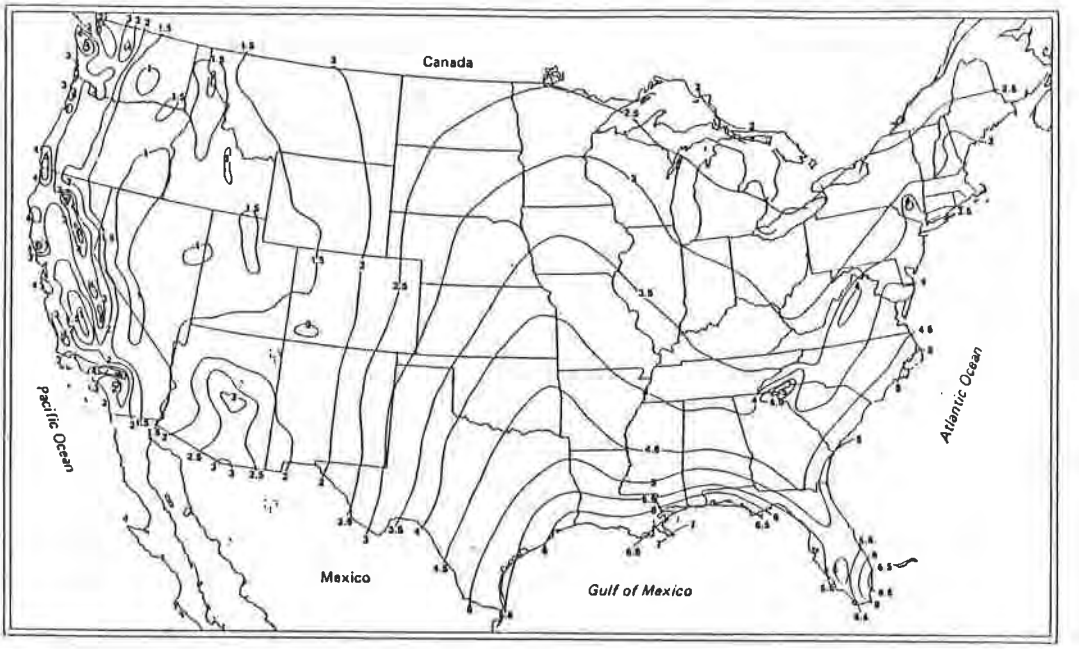

(HERSHFIELD, 1961)

Figure 1 10-Year Design Rainfall, inches

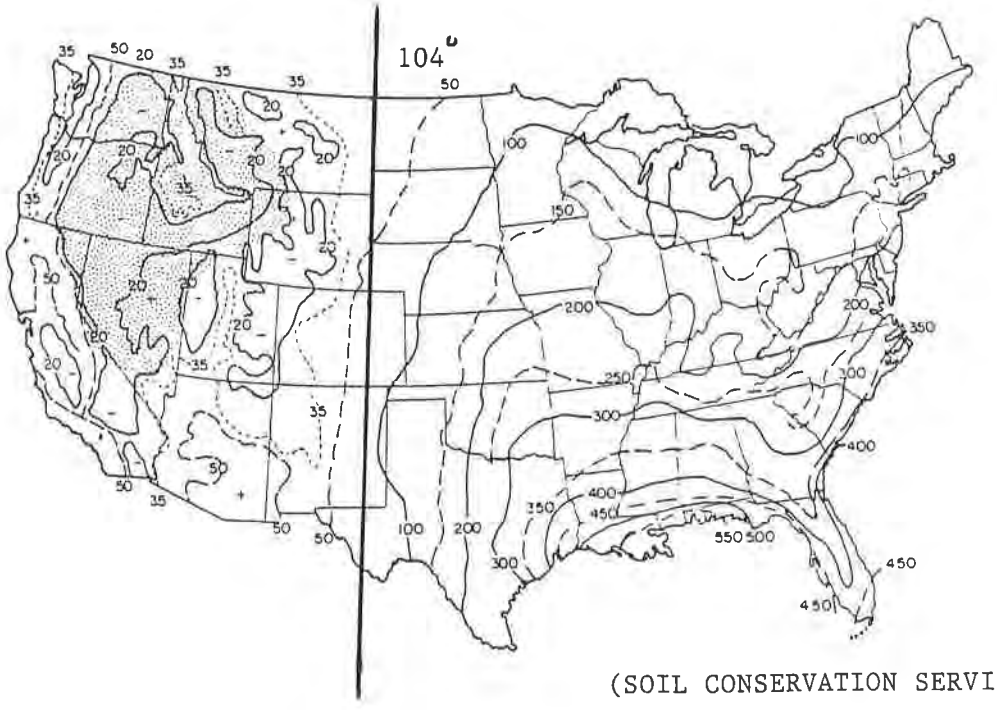

(SOIL CONSERVATION SERVICE, 1977)

Figure 2 Rainfall Erosion Index, R

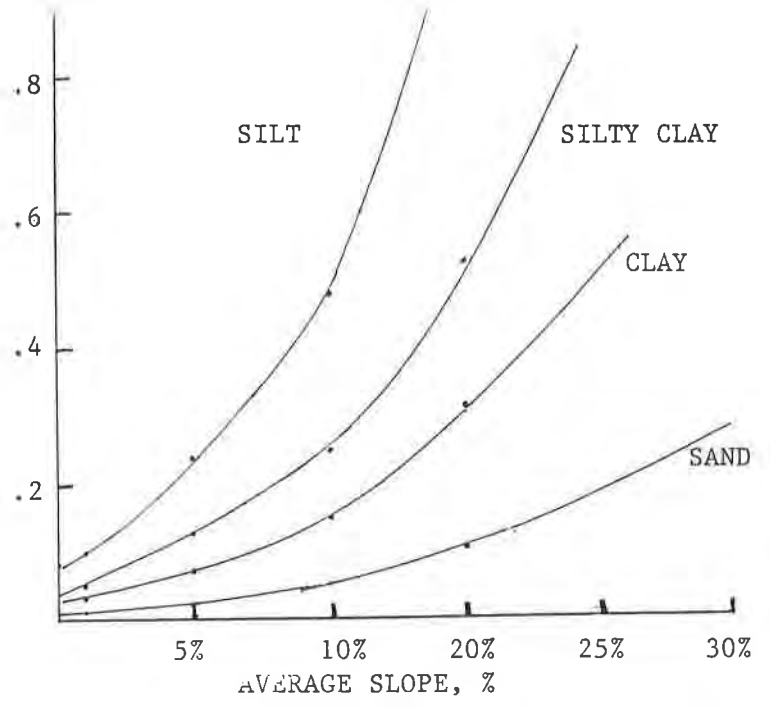

Figure 3 Universal Soil Loss KLS vs Slope

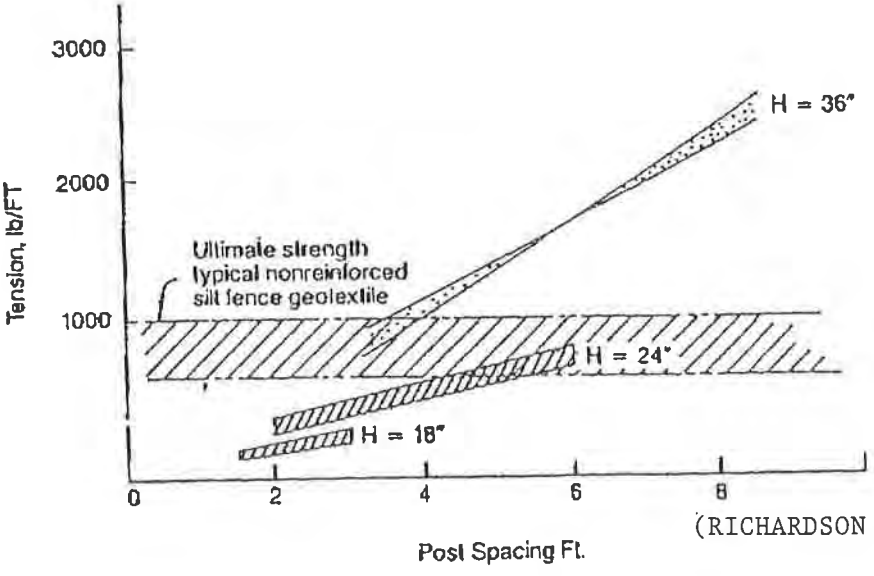

(RICHARDSON AND KOERNER, 1989)

Figure 4 Geotextile Strength vs Post Spacing

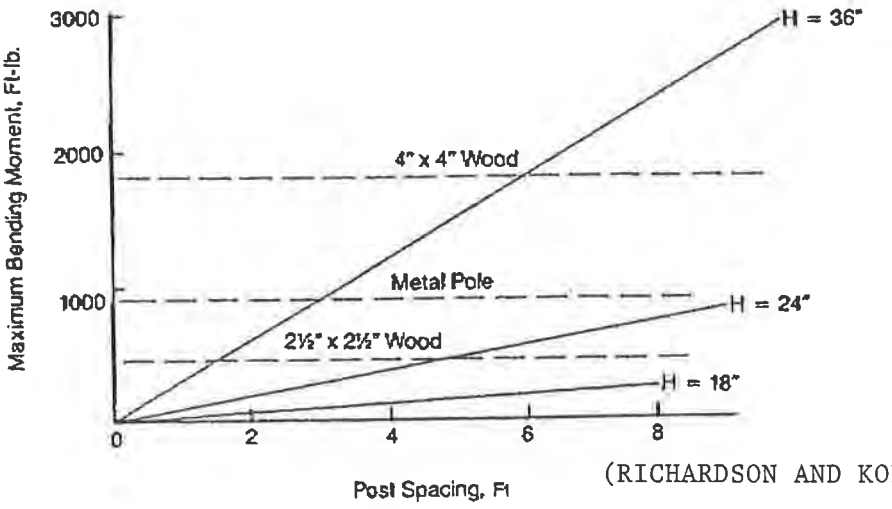

(RICHARDSON AND KOERNER, 1989)

Figure 5 Post Requirements vs Post Spacing

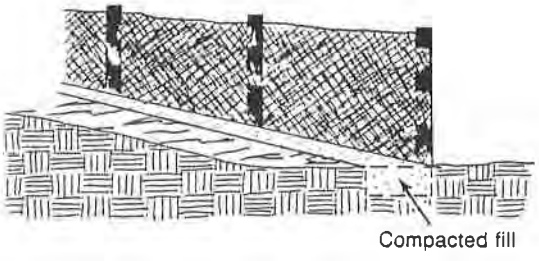

(RICHARDSON AND KOERNER, 1989)

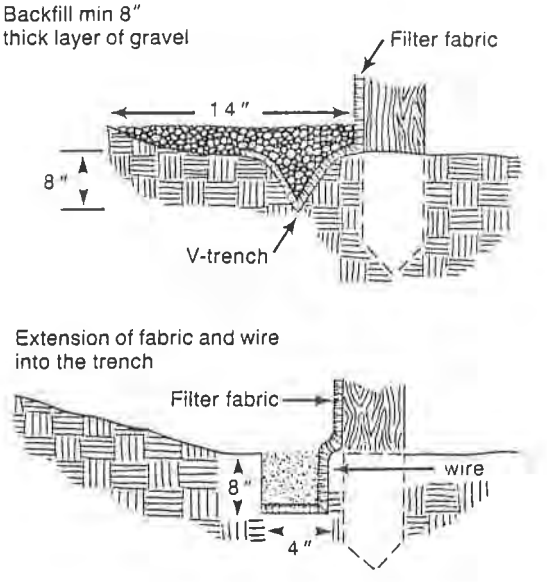

Figure 6 Anchorage of Silt Fence Base

Modular Block Faced Polymer Geogrid Reinforced Soil Walls U.S. Postal Service Combined Carrier Facility

Robert B. Anderson
Tensar Earth Technologies, Inc., USA
Fred N. Boyd
U. S. Postal Service, USA
Larry Shaw
Gifford Hill, USA

ABSTRACT

Polymer geogrids are seeing increased use as the reinforcing elements for reinforced soil retaining walls. The geogrids are typically placed horizontally between the lifts of compacted backfill. Many of the earlier walls used the geogrid material to also wrap the face of the structure. In later walls precast concrete panels, timber railroad ties, concrete block and brick masonry, and cast-in-place concrete has been used for the wall face material. Within the last three years, dry stacked masonry units have found wide spread use as facing elements in these reinforced soil structures.

The design and construction of two geogrid reinforced soil walls with masonry face units for a new postal facility is presented. One of the walls is up to 26 feet high and supports the building which is founded on spread footings. The other wall is as high as 40 feet and carries the parking lot. Where a section of the higher wall is buried behind a small cast-in-place concrete wall on adjacent property, the wall face is formed by the grid itself. All walls use common borrow classified as a silty sand with some clay. The ability of the wall system to use inexpensive fill provided an important economic advantage over conventional systems that use select granular, non-corrosive fill with their metallic reinforcing elements.

INTRODUCTION

The use of molded concrete modular block units to face geosynthetic reinforced soil wall structures gained wide acceptance during the late 1980's. This paper will discuss the design and construction of two major retaining walls for the new U. S. Postal Service Combined Northside Carrier Facility in Atlanta, Georgia.

The once residential section of North Atlanta known as Buckhead has experienced rapid commercial development. As shopping centers, office buildings, and apartment complexes were built the previously light residential mail flow changed to heavy commercial deliveries. To more efficiently respond to growing volume, the U. S. Postal Service needed a carrier facility within the geographical area. A carrier facility is used by the carriers to presort the mail prior to delivery and does not serve the public directly.

Sites for the facility were requested by advertisement. Of those offered, a site on Roswell Road was most desirable. The site had an irregular shape measuring about 183 feet north to south and 642 feet east to west. The plans for a building previously designed for a similar facility in Birmingham, Alabama were adopted to the geometry of the Atlanta property.

The building is a single story, concrete block and brick structure having a flat roof supported by steel trusses. It contains a large work area with adjoining offices. A loading dock is located on the west side of the building. Parking areas and driveways lie on all but the south side of the structure. The site plan is shown in Figure 1.

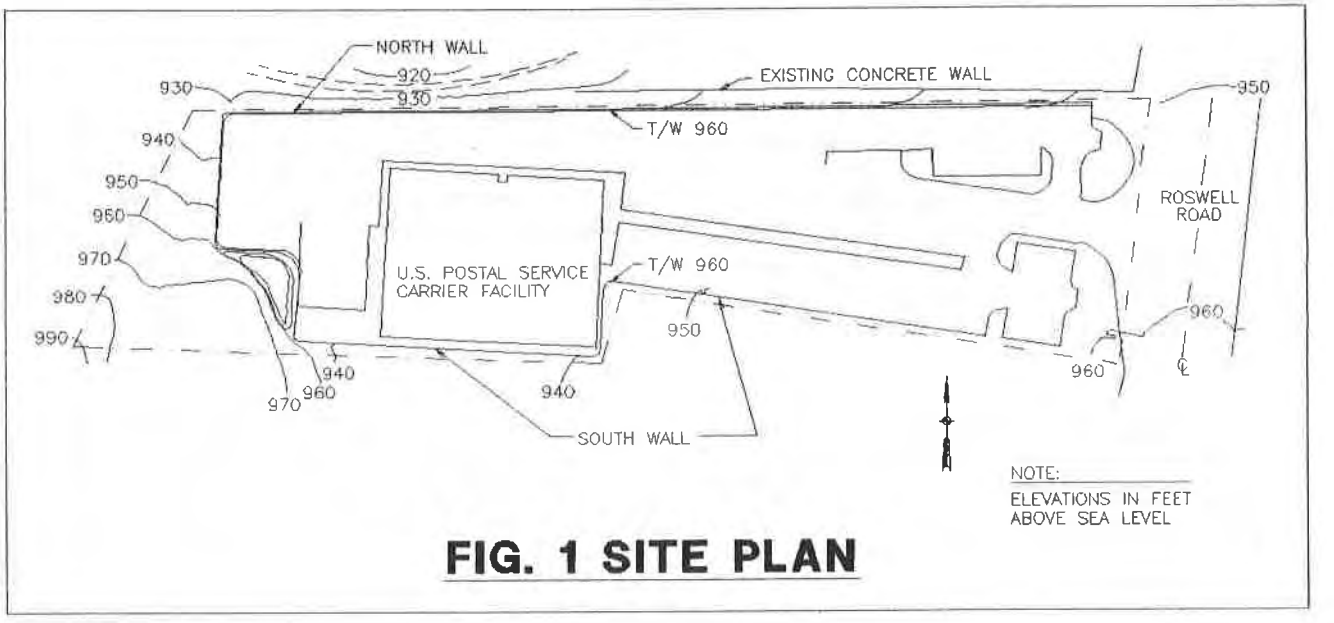

FIG. 1 SITE PLAN

SITE CONDITIONS

The site had been partially filled when a restaurant was constructed several years ago. The existing fill surface sloped down about 20 feet from Roswell Road on the East to the abandoned restaurant. A natural slope rose about 50 along the western end of the site. The fill sloped steeply downward along the entire length of the north property line. A concrete retaining wall as high as 12 feet separated the northern slope from the delivery road behind the adjacent shopping center. The wall extended about 280 feet west from Roswell Road. From the end of the wall the steep fill slope spilled down 10 to 15 feet onto the neighboring property.

Borings showed between 8 and 28 feet of random fill in the area of the future building. The fill was made up of fine sands and silts. Some borings found significant amounts of organics in the form of tree stumps and construction debris. Blow counts ranged from 6 to 20. The fill was underlain by residual soil and partially weathered rock having Standard Penetration Test values of 8 to 35 blows per foot.

SITE PROBLEMS

Up to 26 feet of additional imported fill was required to bring the site to final grade. If it were placed on the existing fill, the added load would cause significant settlement during construction. Furthermore, uneven subsidence due to decay of the organic debris could occur after construction was complete.

Both forms of settlement could damage the building, buried utilities, and the retaining walls that were to confine the high fill on the North and South sides of the site. Three approaches to the settlement problem were evaluated: remove and replace the existing fill with structural fill, support the structure on deep foundations, or surcharge the site to precompress the foundation fill and debris prior to constructing the building on shallow footings. The surcharge solution was selected as the most economical with the realization that long term subsidence was still a possibility and that it could result in some damage to the building and buried utilities. A 5 to 6 foot high surcharge was called for in the area of the future structure. A settlement monitoring program was recommended to determine when short term settlements were complete. The settlement preload period was estimated to be three months.

RETAINING WALL SELECTION

A reinforced soil wall system was determined to be well suited for the project. These systems had been found to be economical for the 10 to 30 foot wall heights required for this site. In addition, the systems were flexible. This was important because the surcharge approach that largely solved the settlement problem for the structure presented a problem for the retaining walls. Since the walls had to be constructed before the placement of the fill and surcharge material, they would be subjected to the full amount of both short term and long term settlement. The walls needed to tolerate the expected settlement without suffering structural damage. Several well proven reinforced soil wall systems were available that used steel tensile reinforcement and segmented, precast concrete panels that gave the wall face a similar tolerance for differential settlement. Geosynthetic soil reinforcement, a later development, had been also been used with success for reinforced soil walls.

The concept of steel reinforced soil walls was developed and pioneered by Henry Vidal. His system was introduced in the U.S. in the early 1970's and found widespread acceptance, particularly in highway construction. Vidal's Reinforced Earth™ wall system uses steel strips to reinforce the backfill. The friction between the strips and backfill imparts the horizontal strength into the backfill that is required to prevent a shear failure. The strips also connect the face elements, usually precast concrete panels, to the stabilize fill. The panels are separated from each other by a gap which permits differential movement between adjacent panels without developing stress concentrations that would crack or spall a rigid concrete wall. A free draining, granular backfill with a high friction angle is generally specified. The use of granular fill maximizes the efficiency of the frictional stress transfer between the tensile strips and the backfill and prevents pore water pressure development. Electro-chemical characteristics of the backfill are controlled to minimize corrosion rates of the galvanized steel reinforcement.

Some other available metallic reinforced systems use steel welded wire mesh for the tensile reinforcement elements. These interact with the backfill through a combination of friction on the tensile strands and passive resistance on the perpendicular strands. These systems also use precast concrete face panels and select granular backfill.

Geosynthetic reinforced soil using geotextiles had been successfully constructed in the late 1970's. Geogrids were used soon after their introduction in the early 1980's. The grids, like the welded wire reinforcement, developed soil stress transfer through friction and through passive resistance against their transverse elements. Many of the early walls used the geosynthetic to both reinforce the backfill and to wrap the face. Designs using precast and cast-in-place concrete facing soon followed (2). Masonry, timber, and gabion baskets were also used to face wall structures. However, usage of geosynthetics reinforcement for retaining walls was generally limited to value engineering situations, special conditions and test or demonstration projects. Proprietary wall systems based on geosynthetic reinforcement were not aggressively marketed until polymer geogrids were paired with modular block wall units in the mid 1980's.

Several modular block types were developed during the 1980's. Most share the characteristics of being molded of concrete, being small and light enough to be easily handled, and being dry stacked without mortar or cement. Size, shape, weight, color, and texture vary. Some systems use pins to connect and align courses. Others use cast-in lips or keys. Several have voids that are filled with crushed stone or sand to increase units' weight and the shear stress transfer between courses. The walls are often battered and the units can be articulated to allow curved as well as straight alignments.

The systems were originally developed for low walls such as those used in landscaping applications. They worked as simple gravity walls to resist the sliding and overturning loads of the backfill. Since the modular units were not cemented together and did not contain vertical tensile reinforcement, they did not have the bending resistance needed for higher walls. In general, the stable height of modular block walls was limited to between two and six feet depending upon the depth of the particular unit, backfill type, slope angle, and wall batter angle. When the modular systems were combined with a geogrid reinforcement the use of modular units was expanded. No longer were the modular systems limited by structural requirements. The soil and its geogrid reinforcement provided stability. The modular units became a non structural, architectural facade. The systems gained rapid acceptance, primarily in the commercial sector of the wall market, due to their economy, appearance, and structural competence (1).

Two reinforced soil wall systems were preapproved as alternates for the postal facility: the Reinforced Earth Company system and a Tensar geogrid/Keystone modular block system. The project was advertized using a line and grade approach. The bidders were given the geometrical requirements of the walls and specifications for the preapproved wall systems. Bidders were asked for a design and build proposal for both wall systems. The decision as to which system would be used was to be made by

the Postal Service based on cost and other factors. Final wall plans were to be submitted after system selection and award of the contract. This approach reduced prebid wall design and plan preparation costs to the Postal Service. It assured competition between the wall systems. It reduced the up front engineering costs to the competing wall system designers. Duplication of the significant costs of final plan preparation was avoided and was born in the end only by the selected wall system supplier/designer. It also required design and plan review of only one wall system by the Postal Service.

Bids were taken on the project in August 1989. The contract was awarded to Baggette Construction, Inc. of Decatur, Alabama. The Tensar/Keystone system was selected primarily for the $300,000, or 45%, cost savings it offered. Much of the savings was due to the cost of the select granular fill required for the metallic reinforcement system verses the cost of common borrow and on site fill material to be used in the geogrid reinforced soil system.

RETAINING WALL DESIGN

There were two principle walls as shown in the site plan in Figure 1. The South Wall is located along the property line and is about 525 feet long. It ranges in height from 2 to 26 feet. At each end the South Wall, cut walls not shown in the figure were added by change order to support the higher adjacent property to the south. The South Wall supports the building in its highest section and parking areas over other sections. Two 90 degree corners were required to follow the property line. The building is founded on spread footings five feet behind the wall and two feet below the top of the wall. The wall supporting the building is founded on 3 to 12 feet of level fill over residual soil. SPT blow counts of 3 were measured in the stratum of fill lying between 7 and 12 below the original fill surface. At shallower depths the blow counts ranged between 5 and 10. The fill material was described as fine sandy silt.

The North Wall separates the site from a shopping center that lies 20 to 40 feet below the Carrier Facility elevation. The previous fill provided 10 to 15 feet of the grade elevation difference. The North Wall was to emerge from the existing fill slope and extend the remaining 10 to 25 feet to final grade. The steep existing slope and the concrete retaining wall and slope combination that lies below the eastern half of the new wall created difficult foundation conditions for most of the North Wall.

The preliminary design of the modular block wall prepared for the bid was based on the use of on site and imported common fill material. Fill soil parameters based on available boring information and local experience were assumed. The proposal and quotation were conditioned upon availability of material that met the assumptions. Parameters used were a unit weight of 125 pounds per cubic foot and an angle of internal friction of 32 degrees. Subsequent tests verified the unit weight and measured a residual shear strength of 34 degrees. The walls were designed for temporary surcharge loads of 750 pounds per square foot, live loads of 250 psf and footing loads of 5000 pounds per linear foot. Design factors of safety were 1.50 for external sliding of the reinforced mass and for geogrid overstress and pullout and

2.00 for external overturning. The design bearing capacity of the foundation soil was as high as 6000 pounds per square foot for the highest wall sections.

Three geogrids were used in the design: Tensar UX1400, UX1500, and UX1600. They are long term design strengths of 1200, 2200, and 3000 pounds per linear foot respectively. The design strengths were determined from 10,000 hour, through-the-junction creep tests extrapolated two orders of magnitude using time-temperature superposition procedures. Partial Factors of Safety, as per Geosynthetic Research Institute Standard Practice GG4, (4) for chemical and biological degradation and for construction installation damage were taken as 1.0 (5, 3). Partial Factors of Safety for creep and junction strength were not applied because the method of testing for long term design strength accounted for both properties. A coefficient of interaction of 0.9 was estimated for pullout and sliding calculations.

Design was accomplished using the computer program Tenswal. The program is based on Mohr-Coulomb failure theory and the assumption that the reinforced and retained fill develop a Rankine active state of stress. The program uses the equations of static equilibrium to determine geogrid lengths required to prevent sliding or overturning of the reinforced mass and overstressing of the foundation. Geogrid spacing is based on the active earth pressure at the elevation of each grid. Anchorage lengths beyond potential failure planes are checked using the coefficient of interaction, shear strength of the fill and overburden pressure.

Typical sections of the South and North Walls are shown in Figures 2 and 3. In most sections of both walls, grid strength and spacing were varied throughout the wall section for efficiency. An exception was the area of the South Wall that supported the building. There the highest strength geogrid was used throughout because the upper grids had to carry the footing loads. Minimum grid spacing was 8 inches which was equal to the maximum lift thickness and the modular unit dimension. Maximum spacing was 3.33 feet. Grid length to wall height ratios were about 0.6 for the South Wall and between 0.45 and 0.5 for most of the North Wall. A prefabricated drainage composite consisting of a geotextiles bonded to both sides of a geonet was used behind the reinforced zone of the North Wall.

The Keystone modular units are 8 inches high, 18 inches wide and 24 inches deep and weigh about 95 pounds. Fiberglass pins fit into holes cast in the top and bottom of the units. The bottom holes are larger than the pins to allow articulation for corners and slight adjustments to wall batter. A split face finish was selected for its visual appeal.

The potential problem associated with the concrete retaining wall to the north was addressed by lowering the reinforced soil wall foundation elevation. This avoided any possibility of overloading the existing wall. To economize, the buried section of the wall used a wrapped face in lieu of the modular blocks.

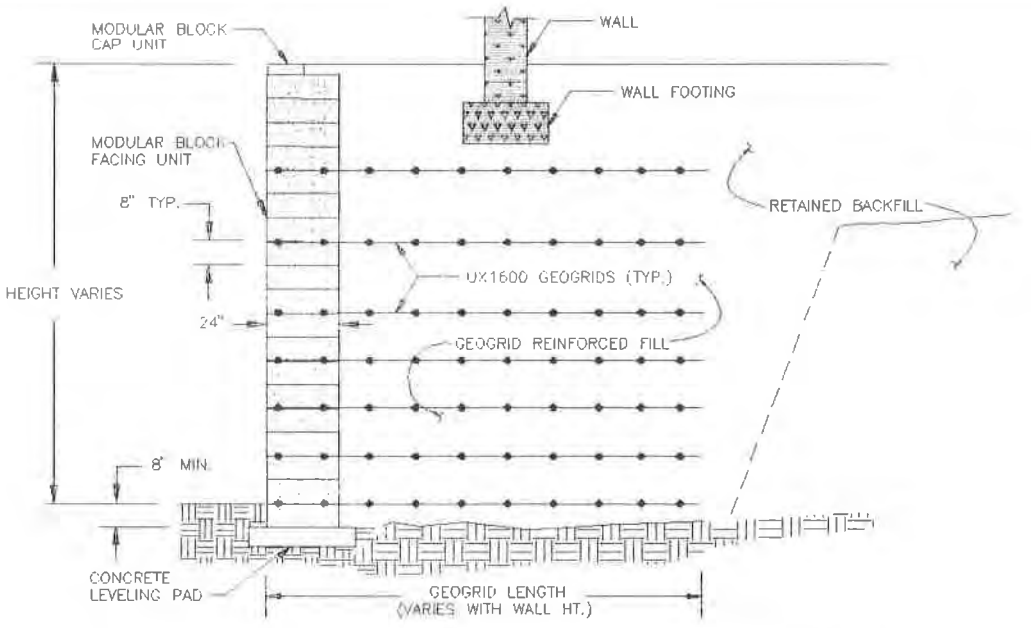

FIGURE 2. TYPICAL CROSS-SECTION SOUTH WALL
N.T.S.

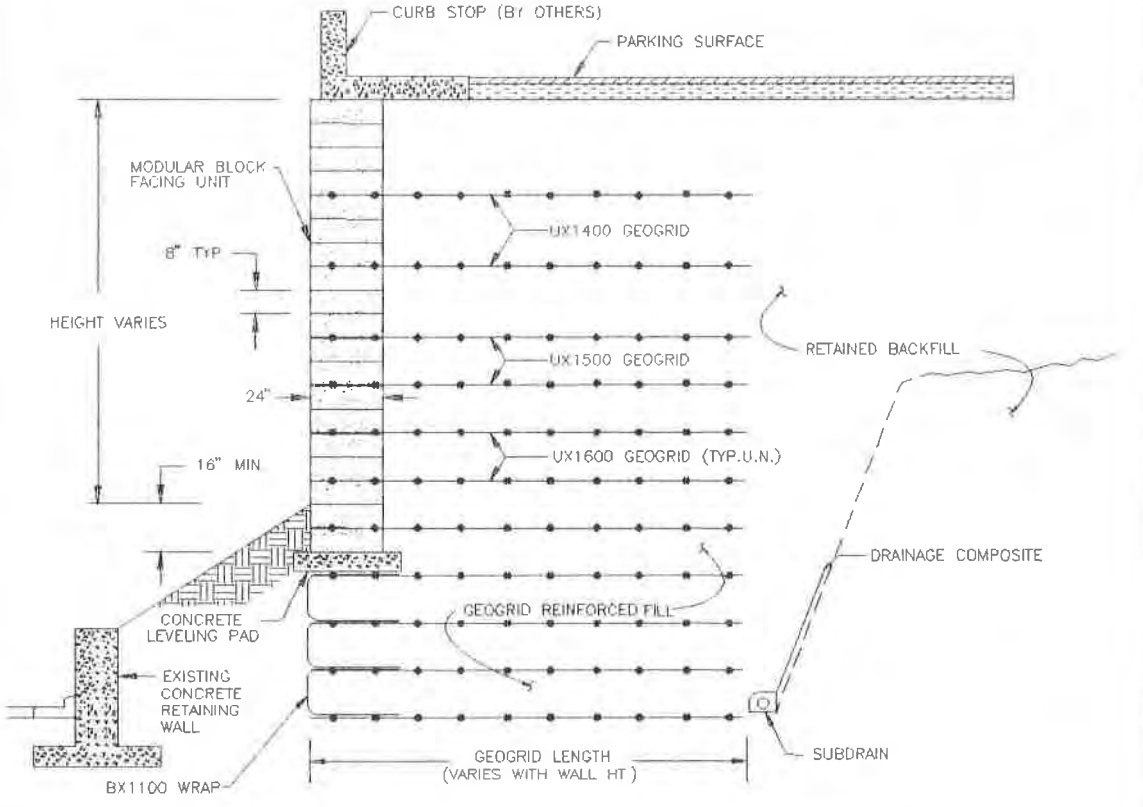

FIGURE 3. TYPICAL CROSS-SECTION NORTH WALL BEHIND C.I.P. WALL
N.T.S.

The potential problem regarding the steep fill slope to the west of the concrete wall was solved by the owners of the adjacent property. To the surprise of all, they excavated the slope to expand their parking area just before construction started on the Combined Facility! The design height of the section of wall suddenly went from 28 to 40 feet, making this the highest wall constructed to date with these materials. A change order was issued to cover the redesign and added construction costs.

WALL CONSTRUCTION

Construction of the South Wall began in October 1989. It was the first wall built to allow more time for foundation soil consolidation in the area of the building. The wall system foundation was prepared by removing the existing pavement and compacting the subgrade. A shallow trench was cut for the reinforced concrete leveling pad for the modular units. The first course of units were set in place and aligned. Crushed stone was placed in the voids in and between the modular blocks. The first lift of common fill was then placed and compacted. A hand operated tamper was used to compact the crushed stone and common fill within three feet of the wall face. A vibratory sheeps foot was used to compact the fill material behind this three foot zone to 95% Standard Proctor. Fiberglass alignment pins were inserted into the set of two holes in each unit that gave a vertical face rather than the normally used 1:32 batter. The units were broomed off. The first layer of geogrid, which had been precut to plan length at a staging area, was placed over the pins and pulled out over the fill perpendicular to the wall face. The geogrid roll widths were 4.25 feet. Adjacent grid strips were layed edge-to-edge with no mechanical connection. The next course of modular blocks and lift of fill were put on the geogrid and the procedure was repeated. The 90 degree changes in wall direction were curves rather than corners. Outside curves had a radius of curvature of 3.5 feet and were developed with three modular units. The geogrids layers overlapped into the backfill. Inside curves had a shorter radius of curvature and the grids fanned out into the fill. Construction details are shown in the photographs in Figures 4 and 5. The South Wall was completed in November.

Construction of the North Wall was then started but was soon delayed when a large pocket of organics and construction debris was discovered in the existing fill under and behind the highest section of the wall. The debris under the future reinforced soil zone was removed and replaced with crushed stone. As much as 15 feet was removed. The debris behind the reinforced zone was left in place. The fill behind the concrete wall was excavated to the pavement elevation in front of the wall. The first layer of uniaxial geogrid was placed on the subgrade. The synthetic drainage composite was positioned against the cut behind the grid and was fed into a geotextile wrapped french drain collector. Next a 4.4 foot wide strip of biaxial polypropolene geogrid was placed parallel to the future wall face. It overlapped the horizontal uniaxial grid about a foot. It was then bent 90^0 and was supported by the vertical face of the excavation. After placement and compaction of 18 inches of fill, the remaining two foot edge was folded back over the new fill and anchored with fill.

Figure 4
Detail of Modular Unit, Geogrid and Pin Connection Between Geogrid and Modular Units

Figure 5
South Wall With Spread Footing in Place

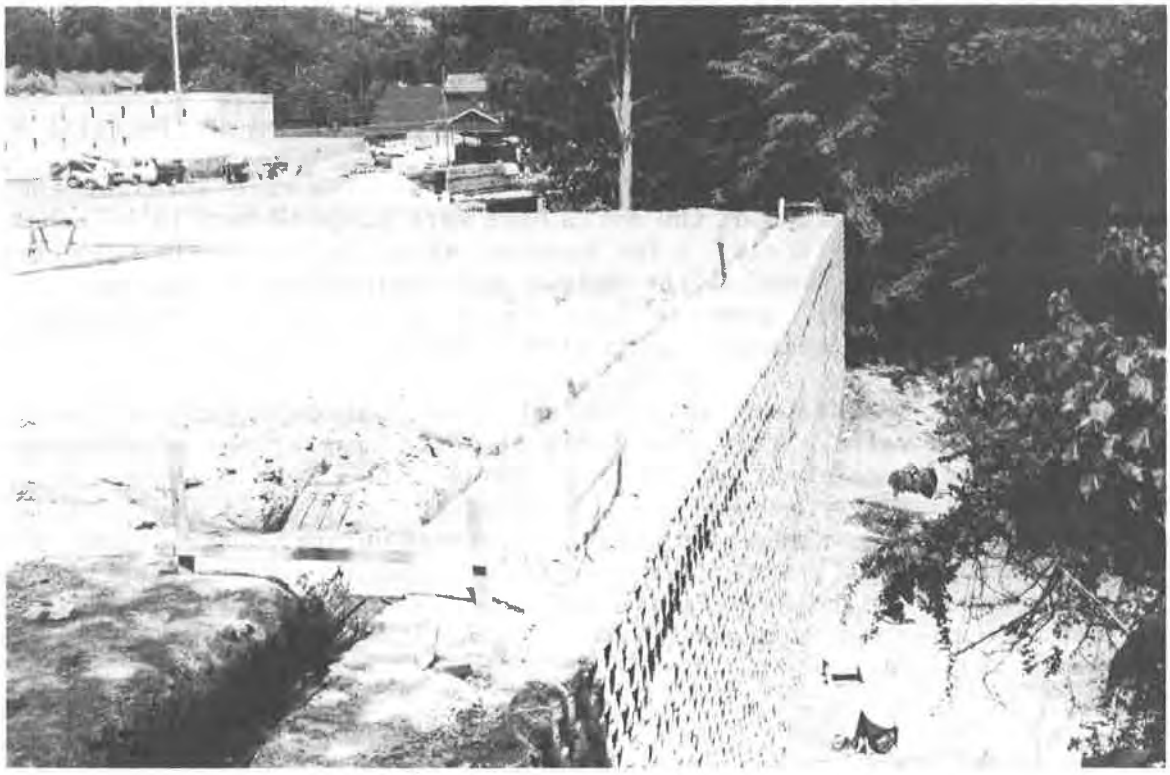

No leveling footing was used in the area behind the concrete wall until the buried section reached the elevation just below the level where the wall emerged from the slope. The remainder of the construction of the North wall was routine with the exception that a geonet was used as a cushion in the lower portions of the highest sections of the wall. The cushion was used to distribute the high compressive stress between courses that could cause localized flexural stress and cracking of the modular blocks. The nets were used in the lower 15 feet of the high sections of Wall A between every course where geogrid was not used. They were used in other areas where a grid layer elevation changed leaving only part of a unit supported on the edge of the underlying grid.

Construction of the North Wall was interrupted in December by wet weather. On site fill materials became saturated and could not be compacted to specified densities. Wall construction resumed in April and was completed in June. Cast-in-place concrete caps with an integral high curbs and light post piers were poured on top of the walls. A safety fence will eventually be placed on the curb. The spread footings were poured behind the South Wall in June and building construction followed. Figure 5 shows the South Wall during footing construction. Figure 6 is a ground level photo looking west along the North Wall. It shows the cast-in-place concrete wall in the foreground. Figure 7 is an aerial photo of the site looking southwest that shows the completed North Wall. Construction of the Combined Facility was then just underway.

POST CONSTRUCTION OBSERVATIONS

Settlement of the South Wall occurred as expected. It all took place during construction of the wall. When the wall was topped out the highest section was about 6 inches lower in the middle than at each end. This can be seen in Figure 5. The wall elevation was monitored by the contractor over the winter. No further post construction movements were observed. The settlement caused no apparent damage to the wall structure. No perceptible settlements were observed on the North Wall.

Alignment of the walls was variable. Some section were straight and plumb. Some sections were not. Areas of the North Wall were found to be 2 to 4 inches beyond or behind plumb in several areas. A few sections along the top to the wall were about 6 inches behind plumb. These slight bulges and undulations in the wall face were largely masked due to the irregular split faces of the units. The variations in alignment are much less noticeable than they would be in a smooth faced wall.

The alignment variations did not result from post construction movements but were built into the walls. They apparently resulted from slight misalignment while stacking the units or movement of the units while backfilling and compacting. Thus small variations grew over several courses before being noticed and corrected. The irregular split face also masked alignment variations during construction. Alignment corrections were generally made over several subsequent courses except in one area where new alignment pin holes were drilled to allow a corrective offset of about 2 inches between the two courses. The gradual correction approach was more aesthetically pleasing.

Figure 6
North Wall with Cast-in-Place Concrete Wall in Foreground

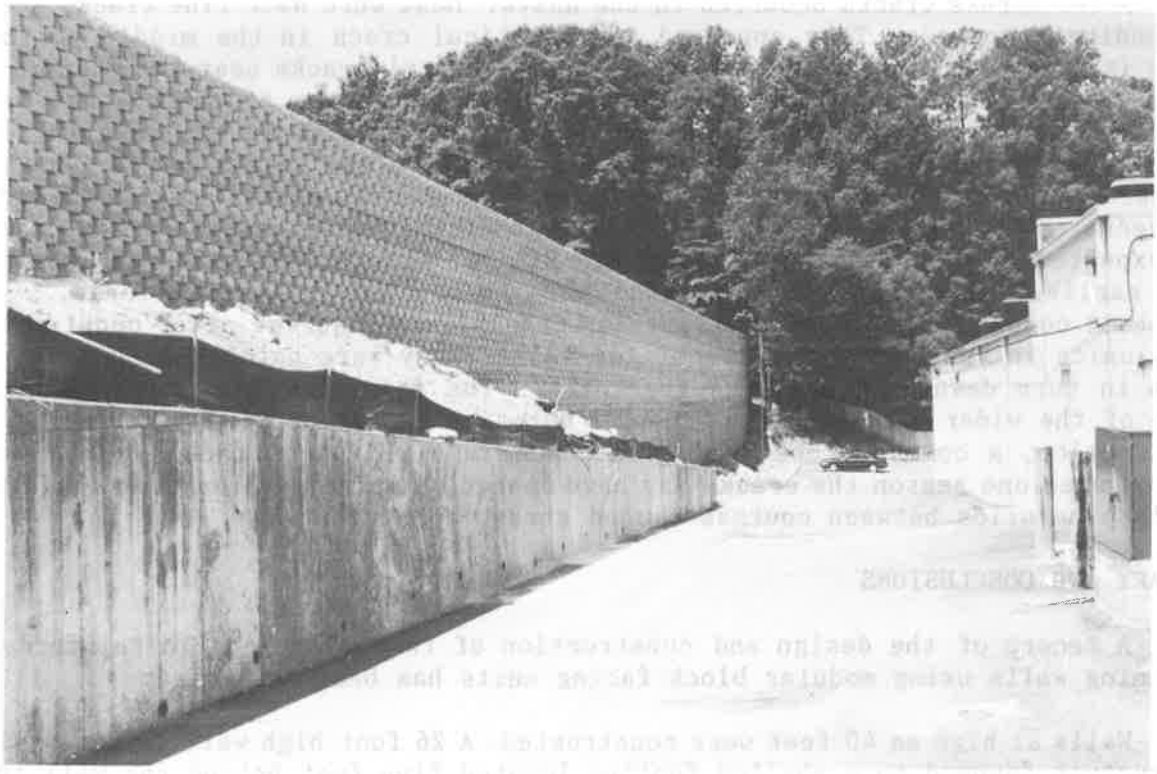

Figure 7
Site View Taken From Northeast

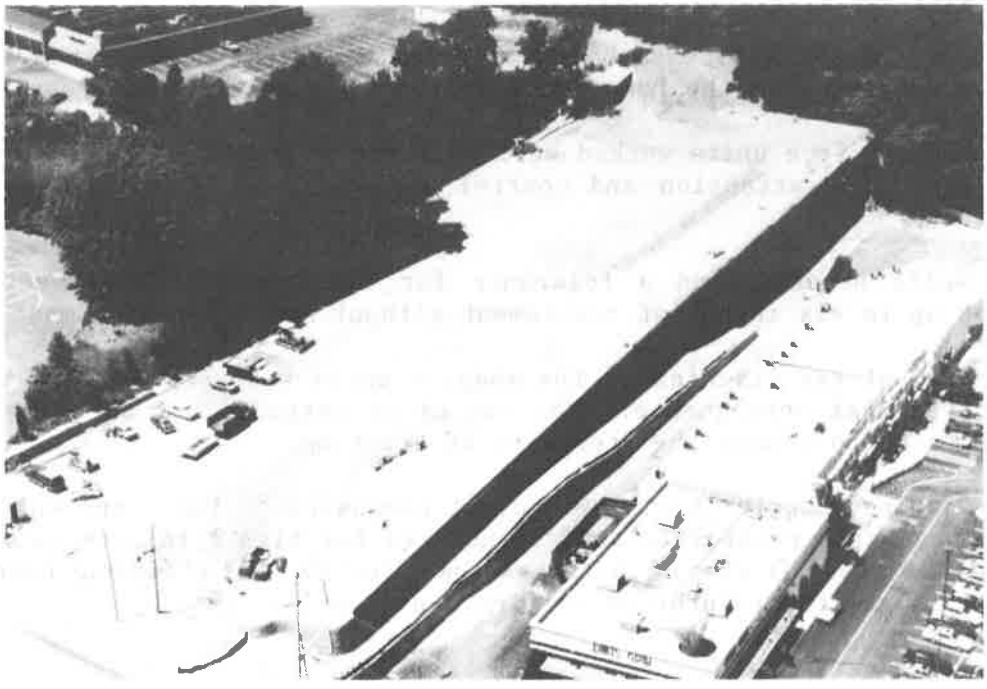

A few stress cracks occurred in the units. Most were hair line cracks generated by bending stresses. They appeared as a vertical crack in the middle of the unit where it straddled two underlying units or as diagonal cracks near the corners. With one exception these were confined to the lower few courses of the highest sections of wall. In the South Wall they occurred only over steps in the leveling footing which suggests those steps were not exactly equal to the height of the units. The few hairline cracks found in the over-35 foot high section of the North Wall indicated the geonet material was effective as a stress distributing cushion. The cracks are not expected to be a structural problem. Similar cracks that have been observed in some earlier walls have not effected performance of those structures. At the northeast corner of the North Wall, wider cracks were observed after construction in a few units in the curved section of the wall. They were patched with cement grout which in turn developed hairline fractures. The fractures have not widened. The cause of the wider cracks is not clear. Rotation of the perpendicular walls during construction, a commonly observed occurrence in rigid panel faced walls, has been suggested as one reason the cracks may have opened. Another explanation could be that overlapping grids between courses caused stress concentrations.

SUMMARY AND CONCLUSIONS

A record of the design and construction of two major geogrid reinforced soil retaining walls using modular block facing units has been presented.

Walls as high as 40 feet were constructed. A 26 foot high wall directly supports a structure founded on a shallow footing located five feet behind the wall face.

The long term durability characteristics of the high density polyethylene geogrids allowed use of the available silt and sand fill material instead of select granular fill.

The cost of the wall was about 45% below a conventional system. The savings was largely derived from the lower cost of the backfill material required.

The modular face units worked well with the geogrids. The system was easy to construct but close attention and control are required to avoid misalignment and uneven batter.

The walls demonstrated a tolerance for differential settlement. One wall experienced up to six inches of settlement without any apparent damage.

Flexural stress cracking of the modular units was very limited and was of no apparent structural consequence. The use of an extruded net as a cushion between courses appeared to reduce the frequency of cracking.

The Combined Carrier Facility project demonstrates the competence and economy of polymeric geogrid reinforced soil structures for high retaining walls supporting permanent buildings. It also illustrates the effective and efficient usage of modular blocks to face geogrid reinforced soil retaining walls.

A few stress cracks occurred in the units. Most were hair line cracks generated by bending stresses. They appeared as a vertical crack in the middle of the unit where it straddled two underlying units or as diagonal cracks near the corners. With one exception these were confined to the lower few courses of the highest sections of wall. In the South Wall they occurred only over steps in the leveling footing which suggests those steps were not exactly equal to the height of the units. The few hairline cracks found in the over-35 foot high section of the North Wall indicated the geonet material was effective as a stress distributing cushion. The cracks are not expected to be a structural problem. Similar cracks that have been observed in some earlier walls have not effected performance of those structures. At the northeast corner of the North Wall, wider cracks were observed after construction in a few units in the curved section of the wall. They were patched with cement grout which in turn developed hairline fractures. The fractures have not widened. The cause of the wider cracks is not clear. Rotation of the perpendicular walls during construction, a commonly observed occurrence in rigid panel faced walls, has been suggested as one reason the cracks may have opened. Another explanation could be that overlapping grids between courses caused stress concentrations.

SUMMARY AND CONCLUSIONS

A record of the design and construction of two major geogrid reinforced soil retaining walls using modular block facing units has been presented.

Walls as high as 40 feet were constructed. A 26 foot high wall directly supports a structure founded on a shallow footing located five feet behind the wall face.

The long term durability characteristics of the high density polyethylene geogrids allowed use of the available silt and sand fill material instead of select granular fill.

The cost of the wall was about 45% below a conventional system. The savings was largely derived from the lower cost of the backfill material required.

The modular face units worked well with the geogrids. The system was easy to construct but close attention and control are required to avoid misalignment and uneven batter.

The walls demonstrated a tolerance for differential settlement. One wall experienced up to six inches of settlement without any apparent damage.

Flexural stress cracking of the modular units was very limited and was of no apparent structural consequence. The use of an extruded net as a cushion between courses appeared to reduce the frequency of cracking.

The Combined Carrier Facility project demonstrates the competence and economy of polymeric geogrid reinforced soil structures for high retaining walls supporting permanent buildings. It also illustrates the effective and efficient usage of modular blocks to face geogrid reinforced soil retaining walls.

ACKNOWLEDGEMENTS

The Combined Carrier Facility was adapted to the site by the architectural firm of Charles H. McCauley Associates, Inc. of Birmingham, Alabama. The retaining walls were designed by Tensar Earth Technologies, Inc. of Morrow, Georgia. The general contractor was Baggette Construction, Inc from Decatur, Alabama. Geogrids, drainage composite, and geonet were manufactured by The Tensar Corporation of Morrow. The concrete modular units were provided by Keystone Retaining Wall Systems, Inc. of Edina, Minnesota who also constructed the walls.

REFERENCES

1. Anderson, R. B. and Blackwell, R. O., (1989) "Behind the Wall: Making More Efficient Use of Soil Reinforcement." Geotechnical Fabrics Report, St. Paul, MN, July/August, pp. 12-16.

2. Berg, R. R., Bonaparte, R., Anderson, R. P. and Chouery, V. E., (1986), "Design, Construction and Performance of Two Geogrid Reinforced Soil Retaining Walls." Proceedings, Third International Conference on Geotextiles, Vienna, Austria, pp. 401-406.

3. Bush, D. I. and Swan D. B. G., (1988), "An Assessment of the Resistance of Tensar SR2 to Physical Damage During the Construction and Testing of a Reinforced Soil Wall." The Applications of Polymeric Reinforcement in Soil Retaining Structures, Kulmer Academic Publishers, pp. 173-180.

4. Geosynthetic Research Institute (1990), "Standard Practice GG4: Determination of the Long-Term Design Strength of Stiff Geogrids." Drexel University, Philadelphia, PA.

5. Shelton, W. S. and Wrigley, N. E., 1987, "Long-Term Durability of Geosynthetics Soil Reinforcement." Proceedings, Geosynthetic '87 Conference, New Orleans, LA., pp. 442-445.

Design and Construction of an 18 Foot High Geogrid Stayed Concrete Block Wall "A Case History"

Douglas J. Yovaish
Michael D. Sims & Associates, USA
Stephen W. Berry
Michael D. Sims & Associates, USA

ABSTRACT

The Forest City Executive Center, located on State Road 436 in Seminole County, Florida, required approximately 20 feet of fill above the present grade in the near vicinity of Spring Lake, which forms a portion of the east site boundary. The area necessary to allow economical development of the site required the use of approximately 375 lineal feet of retaining wall, varying in height from 6 to 18 feet.

Michael D. Sims & Associates was retained to perform the geotechnical investigation required for input to the design of a retaining wall system. Prior to finalizing a design, an economical evaluation was conducted of conceptual retaining wall designs and are presented. A geogrid stayed concrete block wall was selected and its design finalized. Procedures for designing the geogrid stayed wall with respect to internal and global stability are presented as well as other design considerations consisting of structural elements and drainage requirements. Performance of the wall during and following construction are also presented.

The significance of this case study is that geogrid stayed retaining walls (a relatively new concept in 1986) provide an economical and attractive alternative to more conventional retaining wall systems.

INTRODUCTION

The Forest City Executive Center, located on State Road 436 in Seminole County, Florida (Plate 1, attached), required approximately 20 feet of fill above the present grade in the near vicinity of Spring Lake, which forms a portion of the east site boundary. The area necessary to allow economical development of the site required the use of approximately 375 lineal feet of retaining wall, varying in height from 6 to 18 feet. The approximate configuration of the retaining wall and adjacent Spring Lake is presented on Plate 2, attached.

Michael D. Sims and Associates, Inc., was retained to perform the geotechnical investigation required for input to the design of a retaining wall system. Prior to finalizing a design, an economic evaluation was conducted of conceptual retaining wall designs.

CONCEPTUAL DESIGNS

Based on the results of the field study and the proposed site grades, conceptual designs of four (4) types of retaining walls were determined as follows:

1. Reinforced Concrete Cantilever Wall
2. Concrete Panels Supported by King Piles
3. Tied-back Sheet Pile Wall
4. Geogrid Stayed Concrete Block Wall

From the conceptual designs, estimates for the construction cost for each alternative were prepared. The cost estimates were compared on a per square foot basis with the results presented in Table I.

TABLE 1

COST EVALUATION FOR CONCEPTUAL RETAINING WALL DESIGNS

WALL DESCRIPTION	ESTIMATED COST (PER SQ. FT.)
Reinforced Concrete Cantilever Wall	$25.00
Concrete Panels Supported by King Piles	$16.25
Tie-Back Sheet Pile Wall (Not Completely Priced)	Greater Than $25.00
Geogrid Stayed Concrete Block Wall	$10.50

In view of the estimated cost savings, the geogrid stayed concrete wall was selected for final design.

DESIGN OF GEOGRID STAYED WALL

General. The design consisted of selecting the type of geogrid reinforcement, followed by stability analyses. The internal stability, external stability, and the global stability of the wall were evaluated. The external stability analysis consisted of determining the minimum length of geogrid required to provide acceptable factors of safety against rotation and sliding as well as limiting the bearing pressure to an acceptable value (based on settlement performance). The internal stability analysis consisted of checking the embedment length beyond the theoretical failure wedge to ensure that the required tensile force can be developed. In addition, the required geogrid spacing and/or tensile strengths are checked as part of the internal stability analysis. Following the external stability analysis, a global stability analysis was performed to evaluate the factor of safety against a deep-seated arc failure surface below the wall.

Geogrid Selection. When selecting the type of geogrid material, the important engineering properties to consider are tensile strength, tensile modulus at low strain (less than 3 percent), and the ability of the material to resist creep under the application of service loads. For our design, Tensar SR-2 (manufactured by the Tensar Corporation, Morrow, Georgia) was selected. In addition to pertinent engineering properties, Tensar SR-2 material was selected based on the following:

- Experience and technical support provided by The Tensar Corporation Representatives.
- Past experience of the authors of this report with the use of Tensar materials to design and construct a 38 foot high reinforced earthen slope graded at 0.5 horizontal to 1 vertical.

The pertinent engineering properties of the Tensar SR-2 are provided in Table 2.

TABLE 2

MATERIAL PROPERTIES FOR TENSAR SR-2 CONSIDERED FOR DESIGN

ENGINEERING PROPERTY (Machine Direction)	VALUE (lb/ft)
Tensile Modulus	75,000
Long Term Allowable Load	2,000
Rupture Strength	5,400

The testing methods for determining the engineering properties presented in Table 2 were not standardized in 1986 when the wall was designed. However, they has since been standardized by ASTM and the Geosynthetic Research Institute. The manufacturers should identify their testing procedures in order to allow the design engineer to compare alternative reinforcing materials.

STABILITY ANALYSIS

General. The length, number, and spacing of geogrid layers were determined from the stability analysis. From a construction standpoint, a minimum geogrid length of 8 feet is recommended to allow access for men and equipment during the placement and pre-tensioning of the geogrids.

External Stability. The external stability analysis consisted of evaluating the wall as a gravity type retaining wall. The Rankine active earth pressure distribution and wedge type failure was assumed and may be represented by the free body diagram presented on Plate 3.

For our analysis, the minimum length of geogrid required to provide a factor of safety of 1.5 against sliding, 2.0 against overturning, and a maximum bearing pressure of 3,000 psf was determined. The analysis proceeded using the following equation (Tensar):

$$L_s = H \cdot \frac{FS_s \cdot K_b \cdot (H \cdot \gamma_b + 2q)}{2\, C_i \cdot \tan\phi_r (H \cdot \gamma_r + q)}$$

$$L_o = H \cdot \left[\frac{FS_o \cdot K_b \cdot (H \cdot \gamma_r + 3q)}{3\,(H \cdot \gamma_b + q)} \right]^{1/2}$$

$$L_b = H \cdot \left[\frac{K_b \cdot (H \cdot \gamma_b + 3q)}{\sigma_a - (H \cdot \gamma_r + q)} \right]^{1/2}$$

WHERE:

L_s, L_o, L_b = Minimum lengths of geogrid required to resist sliding, overturning and satisfy and the maximum allowable bearing pressure, respectively;

K_b = Active earth pressure coefficient for the backfill soils outside the reinforced zone;

γ_b, γ_r = Moist unit weight for backfill soils outside and within the reinforced zone, respectively;

σ_a = Maximum allowable bearing pressure;

q = Surcharge load;

ϕ_f = The lowest angle of internal friction between the reinforced backfill soil and the subgrade soils, whichever is lowest;

H = Height of wall;

C_i = Reduction factor for soil geogrid interaction (for Sand C_i ranges between 0.8 and 1.0);

FS_s, FS_o = Factors of safety against sliding and overturning, respectively.

The required lengths should be determined with and without the surcharge load. Because the geogrid length depends on the overturning moment and vertical stress at the bottom of the wall, the minimum length required may be longer when the surcharge is not in place. The eccentricity of the resultant normal force below the reinforced earth should be checked to ensure that the calculated length of geogrid is sufficient such that this eccentricity does not exceed 1/6th of the length of the geogrid.

Internal Stability. The internal stability analysis consisted of evaluating the maximum allowable geogrid spacing and the required embedment depth beyond the theoretical active failure wedge. In general, the geogrid spacing and/or specified geogrid strength can be varied over the height of the wall. For this design, however, the spacing was held constant and checked to be less than the maximum allowable spacing determined by the following equation:

$$V = \frac{T}{FS_v \cdot K_r[\,(\gamma_r \cdot Z_b + q) + K_b\,(\gamma_b \cdot Z_b + 3q)(Z_b/L)^2]}$$

WHERE:

V = Maximum allowable geogrid spacing

T = Allowable tensile load of geogrid

FS_v = Factor of safety for geogrid strength

Z_b = Depth below top of wall

K_r = Active earth pressure coefficient for the backfill soil within the reinforced zone

The tensile force developed within the geogrid (T_i will be dependent upon the soil confinement and geogrid spacing. The embedment length of geogrid outside the theoretical failure wedge (depicted on Plate 3) should be checked to ensure that the required tensile force may be developed in the specified length. Because the embedment length depends on the confining stress, the minimum length required may be longer when the surcharge is not in place. This is particularly true for the top few layers. Therefore, the minimum development length was determined using the following equation, both with and without the surcharge load included:

$$L_e = \frac{T_i \cdot FSp}{2 \cdot C_i \cdot \tan\phi_r \cdot (\gamma_r \cdot Z_b + q)}$$

WHERE:

L_e = Minimum length of geogrid required to develop tensile force (T_i)

FS_p = Factor of safety against pull out of geogrid

ϕ_r = Angle of internal friction of the backfill within the reinforced zone

For the geogrid stayed wall at the Forest City Executive Center, the minimum geogrid lengths for a typical spacing of 2 feet based on internal stability analysis are provided in Table 3.

TABLE 3

LENGTH OF GEOGRID REQUIRED BY THE INTERNAL STABILITY ANALYSIS

HEIGHT OF WALL (FEET)	LENGTH OF GEOGRID
6 to 11	8.0 (Minimum)
14 to 20	8.5 to 10.5

Global Stability. The global stability (i.e. general slope stability) of the wall must be analyzed to ensure against a general slope failure. Global stability of the retaining wall was checked using a computer solution of the Modified Bishop Methods of Slices. The computer code (STABGM) was based on an earlier code, modified by J.M. Duncan, et al., to include a force due to internal reinforcement. This computer code allows the tensile force due to the geogrid to be applied for the appropriate slice either horizontally or tangentially to the failure surface at that point. The tangential orientation was used in this analysis. Three cross-section locations were analyzed for this analysis. A cross-section through the wall at the most critical section showing soil strata and surcharge loads is provided on Plate 4.

With the exception of the portion of the wall located closest to Spring Lake, Global stability was satisfied by the geogrid configurations determined for the external and internal stability analyses. In the near vicinity of Spring Lake, however, the first three layers of geogrid were extended to lengths of 22 feet. In addition, an earthen berm was placed along the front of the wall approximately 5 feet wide, sloping into the lake at 4 horizontal to 1 vertical. The purpose of these modifications was to provide a minimum factor of safety of 1.5 against a deep-seated circular arc failure below the wall.

Structural Stability. The design of the structural elements was performed by others. The method of analysis consisted of modeling the concrete block wall as a continuous beam, supported at the geogrid layers, resisting an active earth pressure. The general shape of the assumed active earth pressure against the wall may be represented by the lateral pressure distribution depicted on the free body diagram on Plate 3.

From this analysis, a concrete block wall with vertical reinforcement of one (1), No. 5 bar at 16 inches on-center was recommended. In addition, the cells of each block were grouted with 3,000 psi concrete. Recommended horizontal reinforcement consisted of two (2) No. 4 bars, vertically spaced at 24 inches on-center. The wall was supported on a spread footing approximately 18 inches in width and 12 inches in thickness. Reinforcement within the spread footing consisted of two (2) No. 5 bars.

Drainage Requirements. Control of groundwater seepage must be considered during the design. The groundwater level at the Forest City site was equivalent to the elevation of Spring Lake (+85 feet MSL). The groundwater level fluctuations were estimated to be less than 2 feet and therefore the recommended drainage control was minor and was comprised of weep-holes spaced at 4 feet on-center, approximately 12 inches above the outside finished grade.

Construction. The first step in construction of the geogrid stayed wall consisted of removal of some organic soils below the highest portion of the wall and replacing them with clean compacted sand fill. Continuous dewatering was provided during this portion of the construction using a single stage well point system. The construction area was then leveled and compacted. The concrete foundation was formed and poured using normal construction procedures.

The general construction sequence for the block wall was to install the geogrids as the blocks were laid, grout the cells in the blocks, backfill and wall to the elevation of each geogrid, pre-tension the geogrid, backfill and compact the soil layer above the geogrid and continue in a similar manner to the top of the wall. However, numerous practical considerations were required. First, the wall was designed with a batter of 1 inch in 8 feet (1:96). Since rotation of the wall was anticipated during construction, this slight backward cant of the wall allowed this rotation to take place with the completed wall being near vertical. If this batter were not incorporated and the wall rotated slightly out of plumb, it would be stable, but now physically or aesthetically desirable. Pre-tensioning of the geogrid of individual geogrid layers was performed using a rake manufactured by the contractor for this purpose.

The construction of the block wall was actually performed in 4 foot height increments. The geogrid was placed over the vertical steel and through a minimum of 80% of the wall thickness. Once the wall was constructed to an elevation of 4 feet, the cells in the blocks were grouted. Since the geogrid partially obstructs the cell openings, this 4 foot height increment was chosen as a partial limit such that there was reasonable assurance that the cells in the concrete block has been filled. A minimum set time of 24 hours was allowed before backfilling adjacent to the completed portions of the construction.

At the appropriate level, the geogrid layers were pre-tensioned as discussed previously. While under tension, fill material was placed over the geogrid layers using a front-end loader. The fill material placed behind the retaining wall was relatively clean fine sand (less than 5% passing the U.S. No. 200 Sieve) and compacted by means of on-site construction equipment. Compaction of the fill material adjacent to the completed portions of the wall was performed using had operated vibratory plate compactors. Each fill lift was compacted to a minimum density equivalent to 95% of the soils Maximum Modified Proctor Density (ASTM D-1557). However, care was exercised not to over compact the soils immediately adjacent to the wall.

The construction process described above was then repeated for an additional 4 foot increment of the wall. Due to the length of the wall and the fact that the footing was stepped, the construction operation was essentially continuous with portions of the wall being backfilled while other portions were being constructed and/or grouted.

As shown on Plate 2, there were two bends in the wall, each with an internal angel of 135°. At these "corners" it is important that each portion of the wall be allowed to rotate prior to completing this rigid connection. For the wall at the Forest City Executive Center, this was done by placing form work on the interior and exterior faces of the wall with the required reinforcing steel extending through this section. These corners were poured after the wall had been constructed and backfilled to its final elevation.

Performance. The geogrid stayed, concrete block retaining wall at the Forest City Executive Center was completed in June, 1987 at the cost savings of more than $100,000 under the contract price of a cast in place reinforced concrete cantilever wall originally proposed for construction. At the time of this paper, the wall has performed satisfactorily in all aspects with no signs of cracking or other structural distress. For the most part, the batter of 1 inch in 8 feet remains. That is, during the backfill or loading process, the wall rotated less than anticipated. In our opinion, this is due to careful attention to pre-tensioning of the individual geogrid layers. Based upon our experience with both the design and construction of this type of retaining wall, we believe that the geogrid stayed concrete block retaining wall system provides an economically attractive alternative to more conventional retaining wall systems.

ACKNOWLEDGEMENTS

The developer of the project was Bob Hattaway Investment Corporation (Altamonte Springs, Florida). The Site Civil Engineer was Harling Locklin Associates (Orlando, Florida). The earthwork contractor (including wall construction) was Sunshine Building and Development (Cassleberry, Florida). The Geogrid Supplier was Contech Construction Products, Inc. (Longwood, Florida).

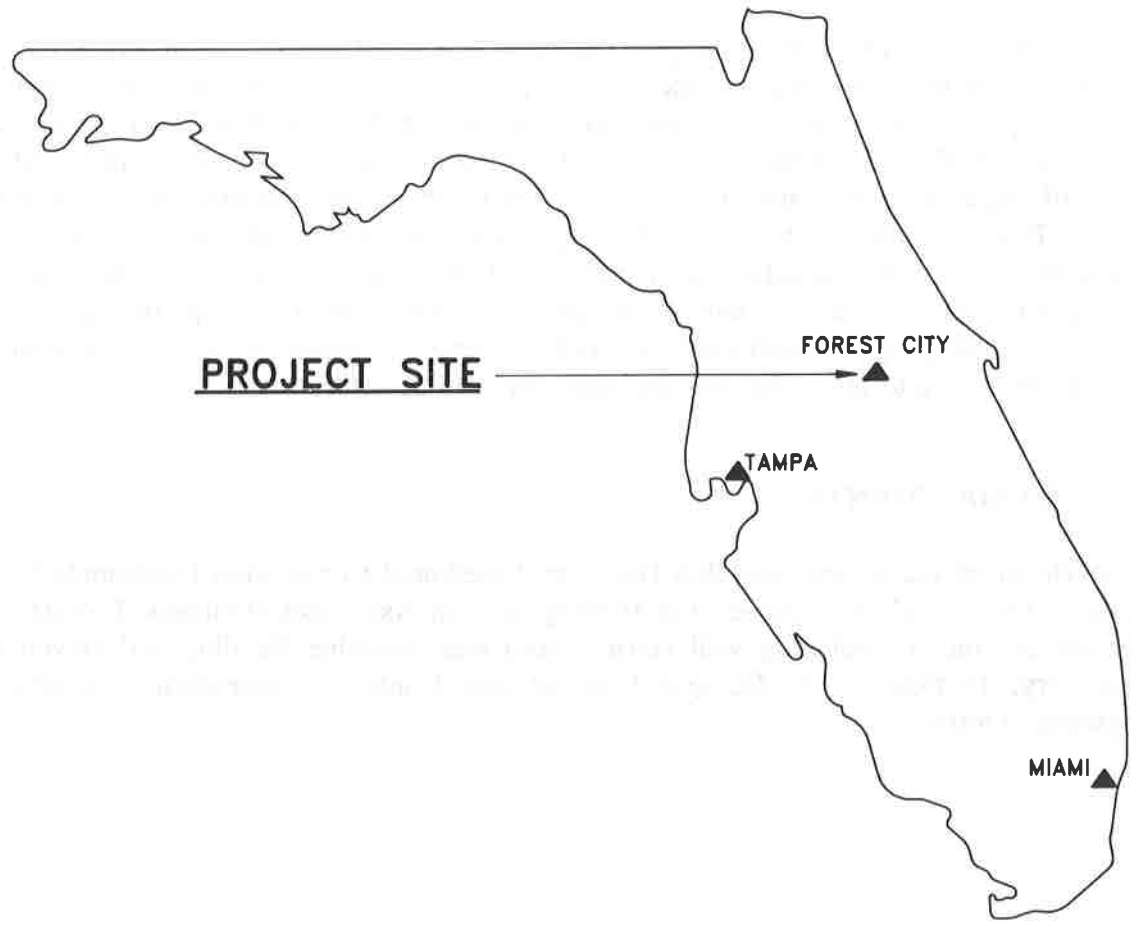

PLATE 1 : FOREST CITY EXECUTIVE LOCATION PLAN

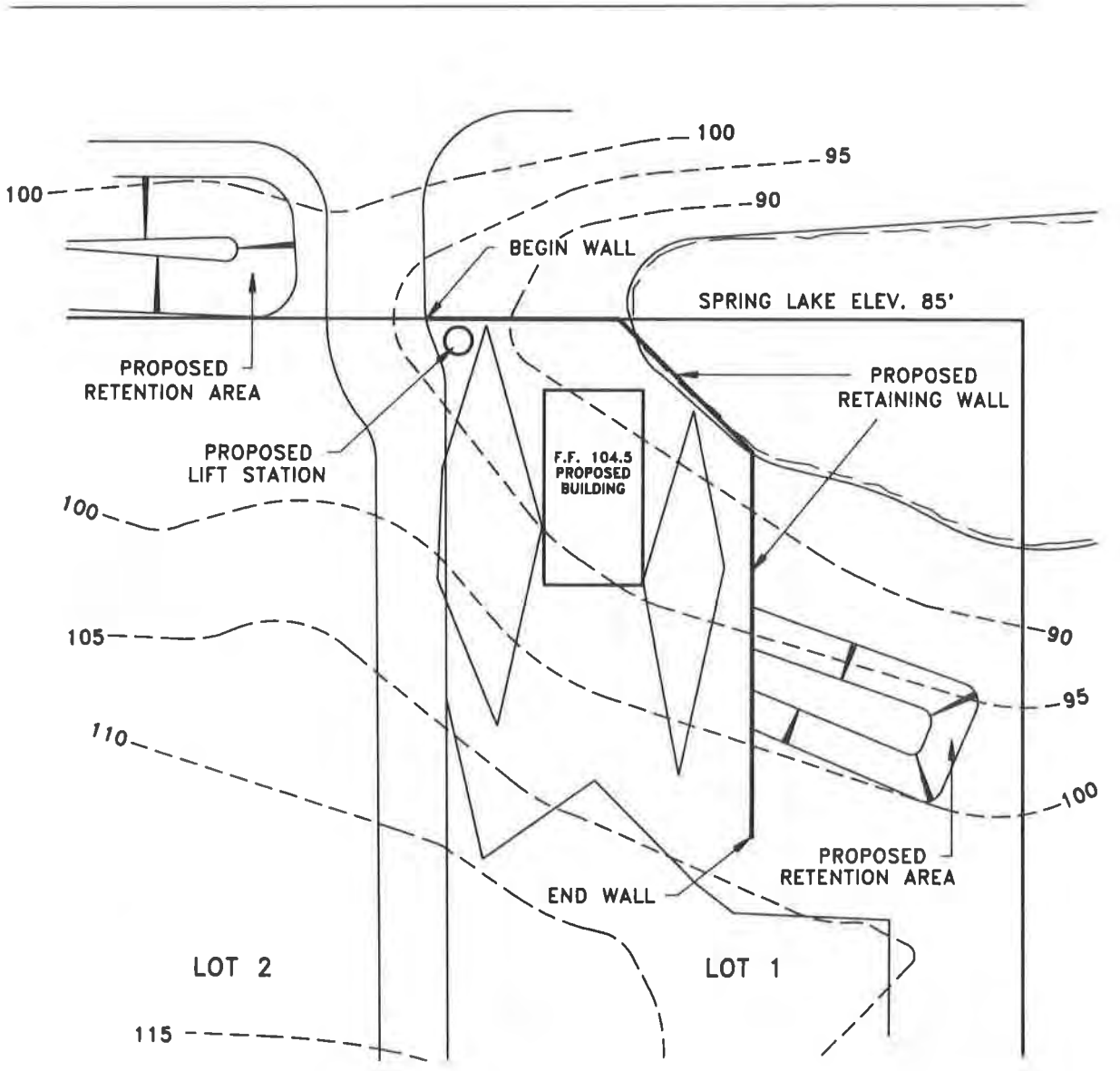

PLATE 2: FOREST CITY EXECUTIVE CENTER SITE DEVELOPMENT PLAN IN THE VICINITY OF SPRING LAKE

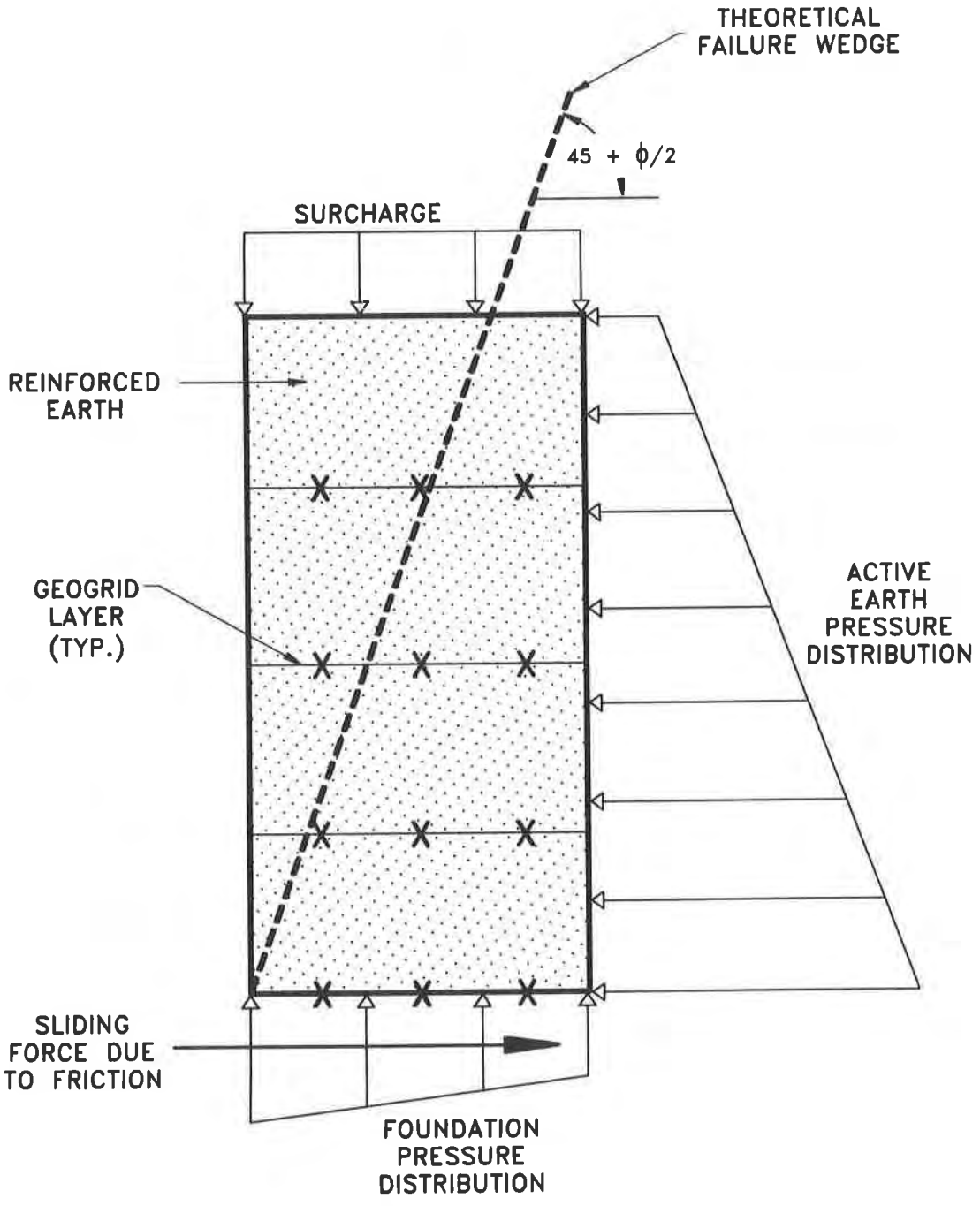

PLATE 3: FREE BODY DIAGRAM USED FOR THE EVALUATION OF EXTERNAL AND INTERNAL STABILITY

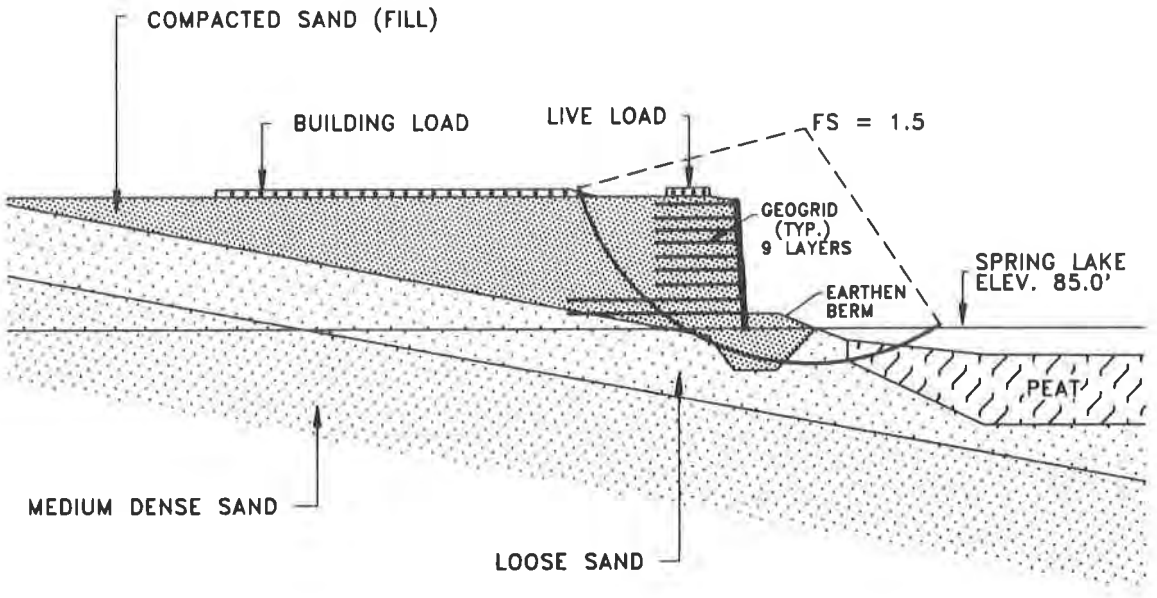

PLATE 4: MOST CRITICAL FAILURE SURFACE DETERMINED BY THE ANALYSIS FOR GLOBAL STABILITY

Geogrid Reinforced Soil-Cement Arch Over Accelerator Ring

John P. Gnaedinger
STS Consultants Ltd., USA
Safdar A. Gill
STS Consultants Ltd., USA

INTRODUCTION

The Brookhaven National Laboratory (BNL) undertook the task of increasing the energy in its accelerator. Such an increase in energy required a proportionate increase in the shielding above the tunnel in which the accelerator is installed. The original tunnel had been designed for approximately ten feet of sand fill, the shielding required for the original energy. However, the new energy level would require ultimately an additional twelve feet of shielding. The existing tunnel, therefore, was incapable of safely supporting the additional load.

The authors' firm was contacted by the Director of Facilities at the Brookhaven National Laboratory to review concepts proposed by others and, hopefully, to create additional options, hopefully, at a lower cost and with less damage to the existing facilities as well. All the work had to be constructed within the two months time available for construction, during summer close-down of operations.

The design alternative selected was a soil-cement arch that incorporated the use of geosynthetics as an integral part of the structure to safely achieve the required stress transfer away from the existing tunnel. The soil-cement arch, which was designed based on structural mechanics principles, consisted of an expanded polystyrene ('geoboard") base and soil-cement reinforced with geogrids. The 'geoboard' was used to control vertical arch deflection such that the arching action could occur and geogrids were used to restrain the arch laterally during construction and to increase the factor of safety against a tensile failure and arch collapse.

The first phase of the increased shielding was successfully constructed in the fall of 1989. This paper provides details of the design and construction process, along with a review of the performance as evaluated from an extensive instrumentation program.

ORIGINAL PROPOSALS

Several consultants had been and were retained by BNL for the purpose of designing the new facilities, construction of which could only be undertaken during the months of July, August, and early September of 1989. This resulted in the need not only for a decision on the work to be undertaken, but to contract the work within approximately thirty days, no easy task with three or four parties to be brought into agreement on the work to be undertaken.

The tunnel was approximately eighteen feet square, inner dimensions, with the wall approximately 12 to 15 inches thick and the roof 15 inches thick. The walls had continuous corbels at twelve feet height for support of crane rails. Figure 1 gives a cross-section through the tunnel.

An analysis of the stresses under the existing loads indicated that the design of the existing tunnel was just slightly stronger than enough to meet standard design criteria based on the existing loads, with no possibility of substantially increasing these loads as would be necessary.

There was little, if any, data available on the performance of the existing structure under the existing loads. There was, however, some information available on original soil conditions, but none with regard to the as-built soil conditions. Generally, the soils consisted of dense sand beneath the structure with backfill of undetermined quality surrounding the structure.

Originally proposed concepts involved placing a pile supported "bridge" across the structure, keeping the supporting piles approximately five feet or more away from the walls to avoid damage during pile driving. This bridge structure would prevent new shielding fill loads from acting on the existing tunnel structure. The bridge structure, however, would have substantial dimensions and cost, since it would be carrying twelve hundred pounds per square foot dead-load at approximately thirty feet span. Truss girders on the order of five feet or more would be required. Furthermore, the pile driving would tend to increase the density, and probably the lateral pressures against the sides of the walls.

THE NEW CONCEPTS

After discussion of the project with BNL engineers and the consultants involved, and further contemplation of the problem and possible solutions, the authors proposed

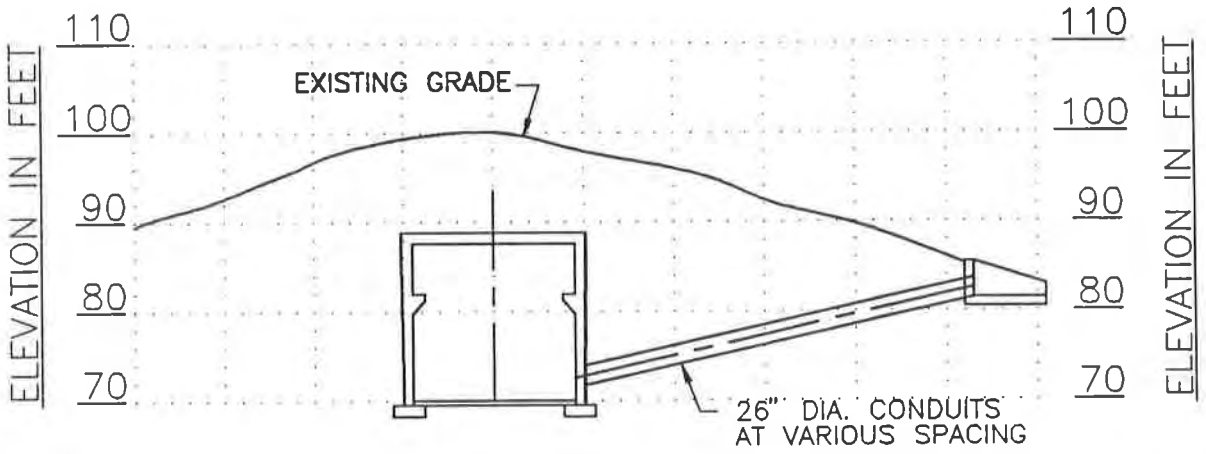

EXISTING TUNNEL PROFILE

SCALE: 1"=20'

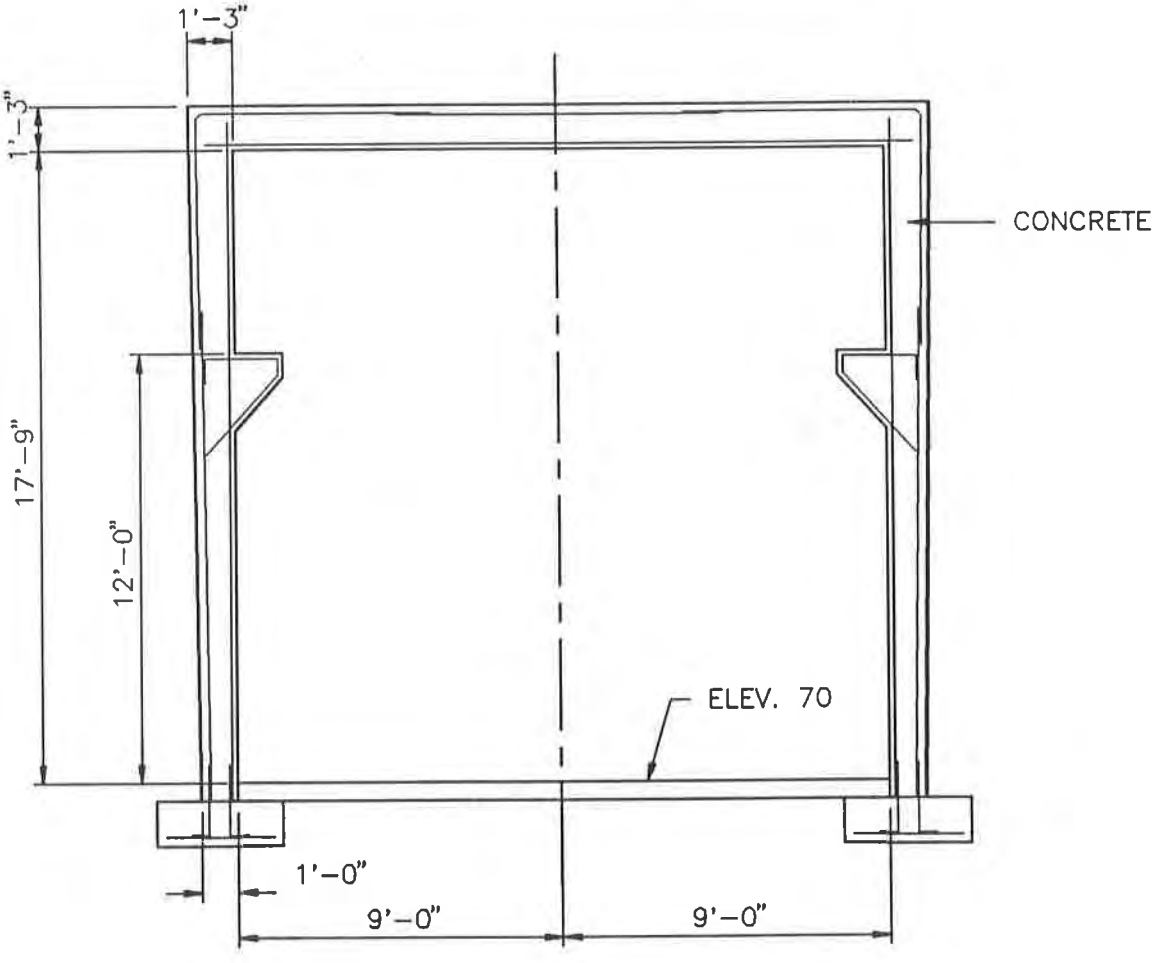

EXISTING TUNNEL REINFORCEMENT

SCALE: 1"=5'

FIGURE 1

C:\PEOPLE\SPIVEY\OFFICE1\DEPT3\SAC8690.DWG 1=20

the use of a soil-cement arch that would transmit new loads as well as the weight of the arch itself to sloping abutments of the arch. Figure 2 shows the final profile for the tunnel and soil/cement arch. The soil cement arch was designed based on structural mechanics principles for arch support. The haunches of the arch were angled away from the tunnel such that the stress distribution would be minimal at the tunnel walls, based on a Boussinesq distribution and effectively zero on the tunnel roof, provided adequate arch deflection could take place above the roof. The design was checked using a finite element method and the tunnel was instrumented, as shown in Figure 3, to confirm the design assumptions during the initial stages of loading as described later in this paper.

Since sand is the prevalent material at the site, it was proposed that this arch be constructed of sand-cement. However, as a further precaution, it was recommended that two layers of geogrid reinforcement be placed horizontally at points approximately 6 inches and 12 inches above the bottom of the new arch. The geogrid was required to restrain the arch laterally during construction and provide a factor of safety against tension cracks in the arch. Ultimately the geogrid was designed to support the arch should it crack. The structure did not rely on the geogrid alone as the arch was designed such that the geogrid was not required to function unless tension cracks developed in the bottom of the arch.

Low modulus 'geoboards' consisting of expanded polystyrene panels, were placed beneath the crown of the arch to allow for required arch deflection and minimize transference of load during arch deflection. The required deflection was determined statically from the estimated settlement of the arch plus the increase in deflection necessary to transfer all of the load to the haunches of the arch. It was also important that the materials support construction activity without collapsing or significantly strain hardening.

It was decided that there would be a six foot rise in the arch from the low points on the outside of the tunnel, and that the sloping abutment of the arch would be on a two to one slope, to permit compaction before placing the soil-cement. These dimensions were initially selected from geometric considerations and to avoid unnecessary over-excavation of the existing fill.

It was felt that the slope up and away from the structure at the abutments of the arch would result in only lateral movement away from the tunnel due to arch deflection and settlement components, so that it did not seem probably that any increase in lateral pressures against the wall would result.

One minor complication arose, but was not considered serious, in that the full twelve feet of additional fill was not to be placed in one increment, but in two increments. However, while this, of course, resulted in a short range lessening of the arch height, it also substantially reduced the load on the initial geogrid reinforced arch and on the polystyrene panels.

921 ℄ TYPICAL TUNNEL CENTERLINE
17' 17'
4' 4'
MIN. 12" EARTH COVER
EL. 110
EL. 110.5
EL. 110
12" EARTH COVER
18" EPS
FINAL GRADE
EL. 99
EL. 109.0
12" EARTH COVER
FINAL GRADE
TWO LAYERS OF GEOGRID
12" EPS
ELEVATION IN FEET
110
100
90
80
70
EL. 99.5 EL. 100
SOIL CEMENT
1.5
1
CLASS A BACKFILL
EL. 97.5
SOIL CEMENT
1.5
1
CLASS A BACKFILL
EL. 89
1/2
1/2
EL. 90.5
EL. 90.5
EXISTING GRADE
EXISTING GRADE
ARCH HAUNCH
℄ EXISTING 26"ø STEEL FOR ELECTRICAL CONDUITS
RANGE OF EXISTING STEAM LINE CROSSING
AGS
EL 70
10.5' 10'-3" 10'-3" 10.5'
ELEVATION IN FEET
110
100
90
80
70

FIGURE 2
TYPICAL CROSS SECTION OF SOIL/CEMENT ARCH
SCALE: 1"=20'

There existed an access tunnel at one point in the accelerator ring itself that was already designed for more than the original loads. Nevertheless, it was considered important that additional loads be minimized for transference to this tunnel as well as the main ring. Therefore, an arch above the tunnel, but parallel to the alignment of the tunnel (perpendicular to the circumference of the main ring), was designed so that arching across the access tunnel would be accomplished. Several other anomalies in the form of ventilation and other minor structures required special attention, which are not considered important for the purposes of this paper.

DESIGN OF GEOGRID REINFORCEMENT

The geogrid was designed to carry tensile stresses in the soil-cement arch spanning over the tunnel as a "reinforced concrete beam". In addition, the reinforcement necessary to restrain the lateral movement of the soil mass in the arch such that strains would be limited to 2% during construction of the first 6 foot high section based on the methods outlined by Christopher and Holtz, 1988. The 2% strain level was required to prevent cracking of the soil-cement. Finally, the reinforcement was designed as a catenary to support all of the load should the arch collapse during construction of the first 6 foot high section. These requirements would allow the arch to be safely constructed to a height of 6 feet and the soil-cement to adequately cure at that height before adding the remaining 6 feet of shielding material. Essentially, the geogrid served as a replacement for steel reinforcement.

The analysis indicated a required strength at 2% strain of 50 lbs/in to resist lateral movement and a required strength at 5% strain of 300 lbs/in to prevent total failure allowing for a design factor of safety of 2. The specified ultimate tensile strength was 625 lbs/in. Strength requirements were based on the wide width strip method as defined by ASTM D-4595. Although a safety factor of 3 would be used normally to include effects of creep and durability, the lower factor of 2 was considered adequate as the arch itself would normally remain in compression.

The geogrid actually used was TENSAR UX 1600 which was tested in our laboratory and had a strength of 360 lbs/in at 5% strain. Compressive strength tests on soil-cement specimens gave an average strength of 437 psi at 3% strain. The modulus values of the two provided closer strain compatibility than that for steel reinforcement and soil-cement. The selected HDPE geogrid would resist chemical degradation in the high alkaline environment of the cement stabilized soil and being inert would resist corrosion better than steel reinforcement in the prevailing environment of stray currents.

DESIGN OF GEOBOARD COMPRESSION PANELS

Based on the mechanical analysis and refined by the finite element model, the required deflection of a 6 inch thick geoboard was estimated to be on the order of 0.5

inches, requiring a modulus of 60 psi. The specified minimum compressibility was 10% at 5 psi stress. Expanded polystyrene panels conventionally used as construction insulation materials were selected as they were readily available in sizes that were conducive to construction, based on product literature they had the potential to meet design requirements, and they were cost effective. The boards consist of polystyrene spheres that are bonded together under pressure to produce a fairly deformable panel. Even so, initial testing indicated that conventional panels were too stiff. The manufacturer worked directly with the designers to specially produce panels to meet the design requirements based on laboratory test results. Laboratory compression tests indicated that strain at 5 psi stress was affected by the thickness of the sample. One inch thick samples had strains of 10.4 to 13.5%, while 6 inch thick samples showed smaller strains of 5.8 to 10.4%. The manufacturer modified the product so that compressibility exceeded 8% at 5 psi on a 6 inch thick sample.

FINITE ELEMENT ANALYSIS OF TUNNEL STRESSES

In order to estimate the stresses on the tunnel caused by the proposed increase in soil embankment height, and evaluate effectiveness of the proposed soil cement arch, a finite element method (FEM) analysis was performed. The FEM solution was obtained using an incremental finite element computer program for 2-dimensional plane strain analysis, FEADAM84, which was developed at the Virginia Polytechnic Institute and State University by J.M. Duncan, et al. (1984). This program calculates the stresses, strains, and displacements in embankments by simulating the actual sequence of construction operations and post-construction loading conditions. The program also approximates and accounts for non-linear and stress dependent stress-strain properties of the soils, according to a hyperbolic model (Duncan et al. 1980).

Several mesh configurations were actually constructed to "fine tune" the final model. A full model was constructed as it was found that the boundary conditions for a symmetrical half model were difficult to define at the arch. This resulted in a substantial increase in the amount of time required to run individual models and complete the analysis of the tunnel.

Very dense strata were assumed to be present at a depth of twenty feet below the tunnel. Therefore, the model was fixed by using hinges at that elevation. The model was extended twenty feet beyond the edges of the arch and roller joints, allowing for vertical movement but restraining horizontal deformation, were used at the boundary.

For the analysis, non-linear, elastic behavior were assumed for the various soil strata and the compressible layer of expanded polystyrene (EPS) panels placed below the soil-cement fill. Parameters for their behavior were estimated based on limited soil information provided by Brookhaven National Laboratories and comparing these soils with average values for similar soils reported by Duncan et al., 1980. The compressive EPS panel characteristics were modeled by actually constructing a simple finite element

model of a compression test and matching the values to those obtained in a laboratory compression test. The finite element analysis allowed a check of the strain compatibility of both materials with respect to the design assumptions.

Analyses were carried out for the following stages:

1) Construction of the existing soil conditions to the base of the arch at a height of nine feet above the tunnel.

2) Placement of the soil-cement to a height of sixteen feet above the tunnel crest (roof).

3) Placement of future fill to a height of twenty-two feet above the tunnel crest.

Each stage was constructed incrementally to simulate actual construction of the embankment. Due to time restrictions, the tunnel could not be modeled as a separate stiff unit. This would require an extensive evaluation of the structural support conditions. However, by simply modeling the tunnel as soil elements, the stress levels at the tunnel can be accurately evaluated and only the distribution of stresses across a particular section would be anticipated to vary due to this assumption. The benefit derived from the geogrid reinforcement and the provision of the compressible geosynthetic (EPS panels) was that they ensured continued performance of the arch concept, even if the soil-cement were to crack or the haunches were to settle.

RESULTS OF ANALYSIS

The results of the finite element analysis showed that the soil-cement acts effectively as an arch to substantially reduce the stress that would have been transferred to the tunnel crest and sidewalls due to embankment construction. Essentially, this increase simulates a height of fill of only 1.5 feet versus the actual 6 feet that will be placed in the first stage. After construction of the first arch section, an even more substantial reduction will be achieved for future construction.

The sidewall evaluation was a little more difficult to compare with existing conditions as the actual stress transferred to the tunnel wall, existing and future, would depend on the the stiffness of the tunnel. If the tunnel walls move freely, an active stress condition would exist such that the existing stress conditions would be similar to that obtained after construction of layer five corresponding to 6 feet additional fill. In this case, a 10% to 20% stress increase would be anticipated on the tunnel sidewalls. However, if the tunnel walls are relatively unyielding, an at rest condition would exist, such that the actual increase in stresses on the tunnel walls could be substantially different. In fact, the analysis indicates that the stress levels due to the arch could be less than the existing conditions.

The primary limitations of the model include the soil characteristics and the tunnel stiffness. The subsurface exploration provided very limited information upon which to base estimates of soil properties. While a decrease in soil stiffness in the area of the tunnel would not substantially affect the model, an increase in stiffness would have a significant effect in decreasing the stresses transferred to the tunnel walls. An increase in tunnel wall stiffness would have an effect in increasing the lateral stress from both the existing conditions and the increased shielding conditions.

INSTRUMENTATION

Since the existing tunnel structure was not capable of sustaining stress increases from the new embankment and the concept of shielding upgrade relied on the effectiveness of the soil-cement arch, it was considered essential that the tunnel be instrumented to monitor any stress increase. By instrumenting the tunnel and the corresponding effectiveness of the soil-cement arch, the construction could be controlled to avoid an over-stressed condition. This was done by installing strain gages on the tunnel roof and side walls at several locations within the construction area (Figure 3). Four stations along the length of the tunnel were instrumented. At each location, three bonded resistant strain gages were installed on the roof and three on the walls of the tunnel. The gages located on the tunnel roof were oriented in the transverse direction, perpendicular to the tunnel axis. The strain gages located on the tunnel wall were oriented vertically. At the same locations, tape extensometer bolts were installed on the walls and roof to monitor tunnel deflections.

Two inclinometers were installed to provide additional information on the change in stress on the tunnel due to the construction of the soil-cement arch. One inclinometer was installed approximately 4 feet from the tunnel to evaluate soil deformation towards or away from the tunnel during construction. The second inclinometer was installed 20 feet from the tunnel, outside the haunch of the soil-cement arch to evaluate the magnitude of deformation away from the tunnel at that location. Both inclinometers were installed at the same station.

Finally, three pressure cells were installed to directly monitor the change in stress in the soil caused by the addition of 6 feet of fill. Two earth pressure cells (Pc_2 and Pc_3) were installed at the haunch of the arch, in an attempt to monitor the increase in stress at the base of the arch (Figure 3). The third cell (Pc_1) was installed below the expanded polystyrene panels over the tunnel. This cell was located to monitor the change in stress in the soil directly below the crown of the arch.

More than the normal amount of instrumentation was considered necessary because of a difference of opinion among some of those involved as to the lateral pressures against the existing wall, which some felt would be substantially increased using only

FIGURE 3

INSTRUMENTATION LOCATION

SCALE: 1" = 20'

the vertical component of the vertical abutment pressure and based on distribution according to the Boussinesq theory.

ADDITIONAL INVESTIGATIONS

It was considered very important that the condition of the existing tunnel be evaluated, including inside measurements that would serve as a reference point for future measurements after completion of the arch, and to look for cracks that might evidence that the existing reinforcement was being stressed sufficiently to have caused tension cracks on the inside of the walls or the roof of the existing tunnel.

Measurements were taken at intervals along the alignment of the tunnel from the inside, both horizontally and vertically. Observations of evidence of cracking were undertaken. No significant cracks were determined to exist in the crown or the walls of the tunnel.

It should be pointed out that the walls of the tunnel were not poured integrally with a base slab as has been frequently undertaken in such structures, but footings were actually placed beneath the vertical walls of the tunnel, with a six inch slab between the walls. This increased the risk of additional settlement due to the additional load, though, again, because the abutment of the arch was expected to move outward rather than toward the tunnel, it was also expected that the effect of the new loads on the abutments would not significantly increase the lateral pressure against the walls, nor significantly increase the load on the existing footings.

RESULTS OF INSTRUMENT PROGRAM

Strain Gage Data - Tunnel Roof. Data from a typical roof strain gage is shown in Figure 4. At stations #1 and #2, the change in strain as measured with the strain gages was monitored before and after excavation from approximately elevation 98.0 to elevation 95.0 to evaluate the magnitude of stress relief due to the removal of the overburden soils. Since the amount of soil removed was known, this monitoring sequence allowed establishing a relationship between the change in vertical stress on the tunnel roof and the change in horizontal strain on the tunnel ceiling. This relationship was then used to interpret the changes in strain for stations 1 through 4.

During the excavation (unloading) phase of the construction of the soil-cement arch, the strain gages located on the roof of the tunnel reflected a negative strain. ranging from -40 to -80 micro inches per inch. The average change in strain with the removal of the 3 feet of soil was -60 micro inches per inch. Therefore, an average change in strain of 60 micro inches per inch corresponds to a change in vertical stress on the tunnel roof of approximately 0.165 tons per square foot (330 pounds per square foot).

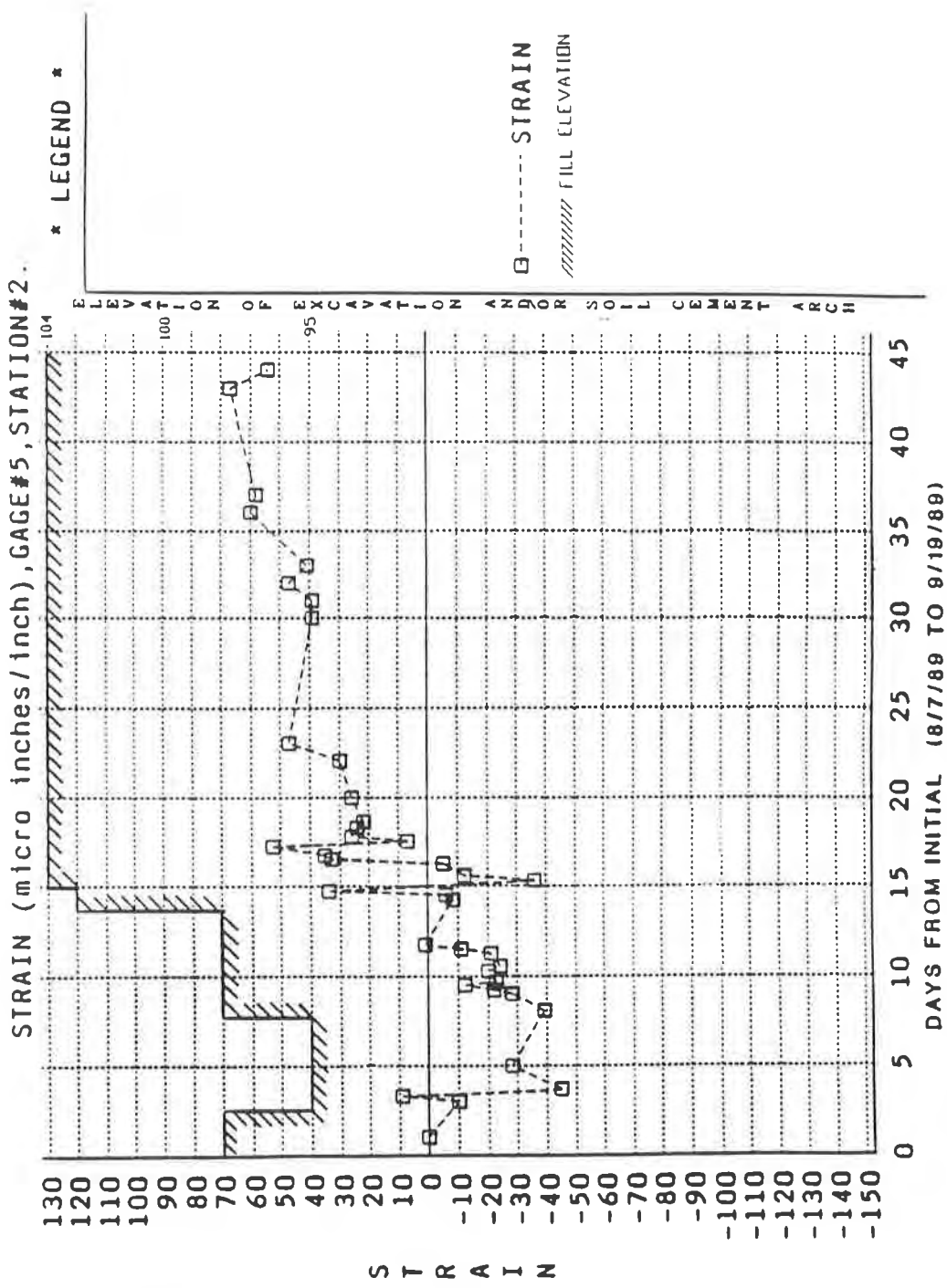

FIGURE 4

TYPICAL STRAIN GAGE DATA FOR ROOF GAGE

The final change in strain, as of September 19, 1989, along the tunnel roof after completion of the soil-cement arch, ranged from +15 to +90 micro inches per inch with an average increase in strain across the tunnel roof of +50 micro inches per inch. This corresponds to an average increase in stress on the tunnel roof of 0.138 tons per square foot, using the relationship established during the removal of overburden soil. The FEM analysis predicted an average increase in stress of 0.087 tons per square foot, equivalent to a height of fill of only 1.5 feet. The measured strains correspond to a fill height of 2.5 feet. The actual fill height was 6 feet.

Strain Gage Data - Tunnel Sidewalls. The sidewall evaluation is analytically more complex than the roof analysis because the actual stress transferred to the tunnel wall is dependent on the stiffness of the tunnel as described above in the finite element study.

Figure 3 shows the actual location of the strain gages along the tunnel sidewalls. Gage No. 1 was located 4.0 feet off the tunnel floor, Gage No. 2 was 8.5 feet off the tunnel floor, and Gage No. 3 was 3.0 feet below the tunnel ceiling.

Typical data for a wall strain gage is shown in Figure 5. The average total change in strain for Gage No. 1 at all four monitoring stations was 41 micro inches per inch, the correlating change in stress for Gage No. 1 was .115 tons per square foot. This represents an increase in lateral stress of approximately 20%.

The values of total change in strain for Gage No. 2 at all four stations ranged from -10 to +18 micro inches per inch with an average change in strain of +10 micro inches per inch. This correlates to a change in stress of 0.026 tons per square foot or a 6% increase in stress.

The average change in strain for Gage No. 3 at the end of construction was +14 micro inches per inch. There did, however, appear to be a wider range in readings at this location than anywhere else in the tunnel. The total change in strain ranged from -30 to +100 micro inches per inch. The average change in stress was 0.038 tons per square foot. This is a 14% increase in stress.

The change in strain and correlated change in stress, based on the relationship established during the removal of the overburden soil, appeared to indicate that the tunnel sidewalls are relatively flexible and that an active earth pressure condition exists. For this case, the finite element analysis predicted an increase in stress of 10% to 20%. The measured change in stress was 6% to 20%.

Convergence Tape Monitoring. Convergence tape bolts were installed in the tunnel floor, roof and sidewalls at the same monitoring stations as the strain gages. Deflections of the tunnel structure were monitored over the course of the construction

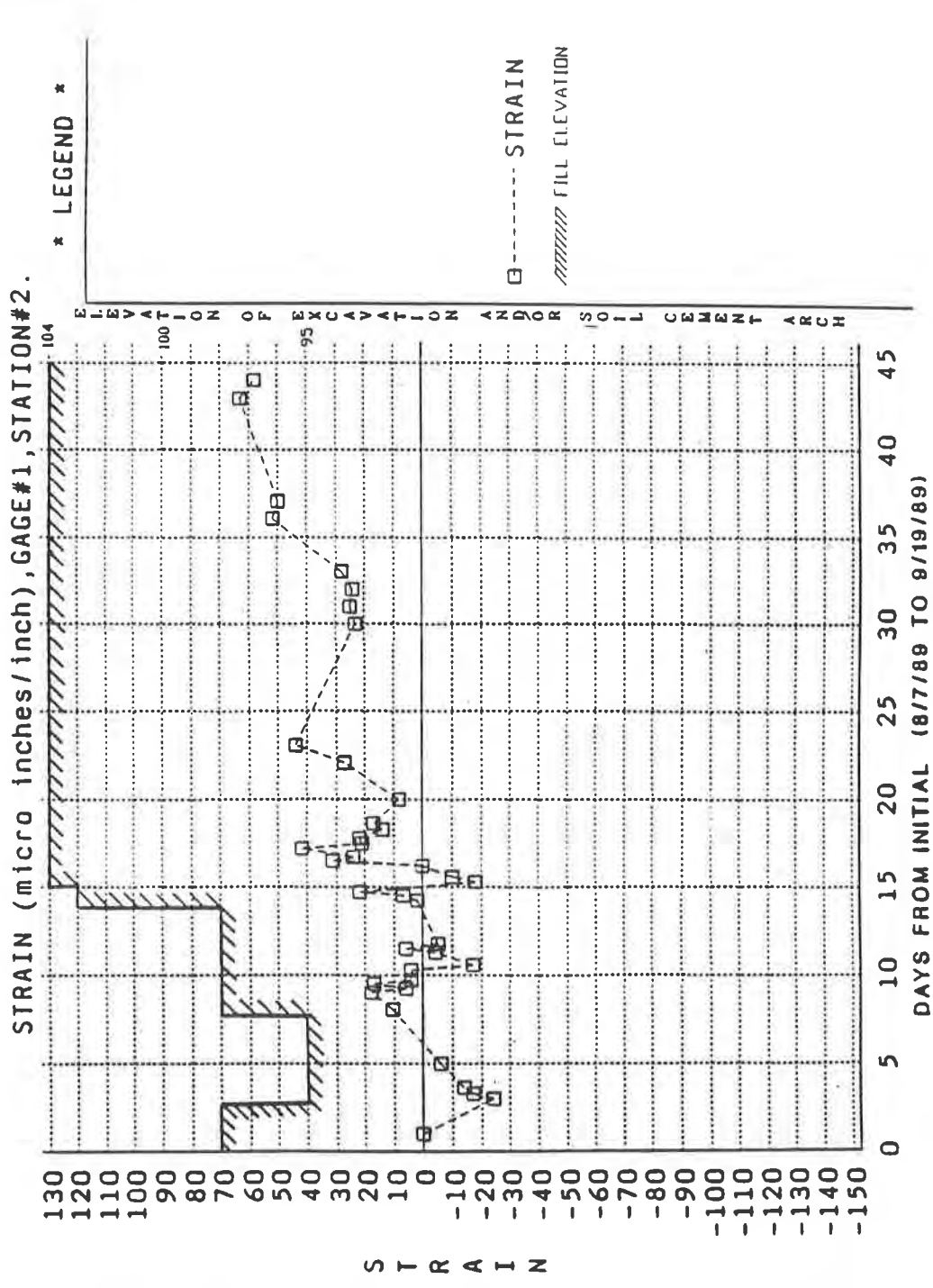

FIGURE 5

TYPICAL STRAIN GAGE DATA FOR WALL GAGE

of the soil-cement arch. Base line readings were established in early August (8/11/89) for all monitoring stations. The average change in deflection for all monitoring points, except for the horizontal deflection at Station No. 2, was less than 1 millimeter. The horizontal deflection at Station No. 2 showed a total of 11 millimeters change in deflection.

Pressure Cell Data. Three Glotzl pressure cells were installed to monitor the pressure exerted on the soil from the soil-cement arch. Pressure Cell No. 1 was located below the expanded polystyrene and was used to measure the stress exerted on the soil directly below the arch. Pressure Cells No. 2 and 3 were located at the interface between the soil-cement and the existing soil at the haunch of the arch (Figure 3).

The average pressure as measured by Pressure Cells No. 2 and 3 at the haunch of the arch was 1.34 tons per square foot (with a range between cells of 0.79 to 1.88 tons per square foot). The pressure measured by Cell No. 1 under the arch itself was 0.31 tons per square foot which was within 10% of the predicted stress from the FEM analysis.

Inclinometer Data. Two inclinometers were installed to provide additional indication of stress increase or decrease on the tunnel due to the construction of the soil-cement arch. The inclinometers were read on a daily basis during construction of the soil-cement arch at Monitoring Station No. 2 and once to twice a week for a period of approximately one month after construction of this segment of the arch was complete. The inclinometer data indicated no change in lateral displacement of soil below the arch, caused by the arch construction.

CONSTRUCTION

While it was recommended that a contractor most competent to do the work be selected based on qualifications, and a fair contract negotiated with the contractor and his subcontractor, federal requirements were for obtaining competitive bids.

Four bids were received. The dollar amount of the lowest bidder was substantially below the cost estimate for a traditional structural solution to the design that had been originally proposed. This permitted construction of a much greater length of surcharge than had been originally planned, because there was a fixed amount of money in the budget for the work.

The only controversy during construction resulted from the fact that the base material that was recommended for use with the soil-cement was overlain by a fine silt material, so that an extra had to be paid for stripping the unsuitable material to get access to the suitable material.

A continuous in place mixing process of the soil-cement was utilized. All material was placed in horizontal lifts, with the geogrids placed at the appropriate elevations. The geogrid sheets were 50 inches wide and came in 100 foot long rolls. The sheets were placed in full length across the tunnel, and overlapped 6 inches and tied together at the overlaps to prevent displacement during placement of soil-cement.

CONCLUSIONS

The soil-cement arch successfully minimized the additional stresses on the AGS tunnel caused by the addition of 6 feet of fill over the tunnel roof. The FEM analysis of the soil-cement arch predicted an increase in vertical stress on the tunnel roof of approximately 0.09 tons per square foot. The instrumentation and monitoring program measured the changes in stress and strain and were in general agreement with the FEM analysis, measuring a change in stress of 0.14 tons per square foot. The measured increase in stress on the tunnel roof corresponds to a fill height of 2.5 feet, the actual height of fill over the tunnel was 6 feet. The FEM analysis also predicted an increase in stress on the tunnel sidewalls of 10 to 20%. The measured stresses on the tunnel sidewalls were in agreement with the analysis. The convergence tape, inclinometer and pressure cell data all support the relatively small increase in stress experienced by the tunnel due to the fill placement.

The use of geosynthetics assisted the soil-cement arch in stress transfer over the existing tunnel. The geogrids resisted lateral stretching of the soil-cement arch and minimized its deflection which otherwise would have caused increase in vertical stress over the tunnel. Geogrid reinforcement provided a strain-compatible material for the arch reinforcement at the anticipated stress levels in the soil-cement. It provided a backup system of support for the fill, even if the soil-cement arch were to crack at its crown and cease to function as a compression arch. The geogrid also has better resistance to corrosion and degradation in the alkaline environment of cement stabilized soil. Expanded polystyrene filler at the arch crown assisted in load relief across the tunnel. Its deformation behavior was selected to match the anticipated settlement of the soil at the arch haunches so as to function in permanent relief of load over the tunnel.

ACKNOWLEDGMENTS

The work was undertaken under the general direction of E. Parke Rohrer and Bal Patel of the Brookhaven National Laboratory. General oversight of the work was performed by Louis P. Giacalone, Architect, and Ben Lavon, Structural Engineer. Barry Christopher and James Collin from STS Consultants, Ltd. were responsible for overall management, design of instrumentation, and construction monitoring of the project.

The geogrid was supplied by TENSAR Corporation. The manufacturer of the geoboard was Cellofoam/Southeastern of Conyers, Georgia.

REFERENCES

Christopher, B.R., and Holtz, R.D., (1985) "Geotextile Engineering Manual," STS Consultants, Ltd., Northbrook, Illinois; Report to Federal Highway Administration, No. FHWA-TS-86/203, 1044 pp..

Duncan, J.M., Seed, R.B., Wong, K.S. and Ozawa, S., (1984) FEADAM84: "A Computer Program for Finite Element Analysis of Dams"; Virginia Tech, Blackburg.

Duncan, J.M., et. al., (1980) "Strength, Stress-Strain and Bulk Modulus Parameters for Finite Element Analysis of Stresses and Movements in Soil Masses"; Dept. of Civil Eng., University of California, Berkeley.

Application of Geosynthetics to the W.H. Zimmer Generating Station Project

Rudolph Bonaparte
GeoSyntec Consultants, USA
Joseph E. Fluet
GeoSyntec Consultants, USA
Ronald D. Johnson
Tensar Earth Technologies, Inc., USA
Vicky Chouery-Curtis
Tensar Earth Technologies, Inc., USA

INTRODUCTION

The W.H. Zimmer Generating Station near Cincinnati, Ohio was largely constructed when a decision was made to convert the plant from nuclear power to coal-fired power generation. To provide a coal yard above the Ohio River floodplain in which the plant was located, fills as deep as 15 m were constructed. In the fall of 1987, as part of the conversion, a diversion channel was constructed for Little Indian Creek, which flowed through the site. The diversion channel bisects more than 600 m of fill before emptying into the Ohio River (Figure 1). To comply with space limitations along the channel alignment, the channel slopes were designed and constructed at 1H:1V (horizontal: vertical). Geogrid reinforcement was used to stabilize the steep channel slopes and provide an adequate factor of safety with respect to slope stability. This paper describes the design, construction, and performance of the Little Indian Creek diversion channel project. The project is especially interesting due to the large size of the channel's reinforced slopes, to lessons learned since construction, and, finally, to the way in which three different types of geosynthetics (geogrids, woven geotextiles, and nonwoven geotextiles) perform three different design functions.

CONCEPTUAL DESIGN

A plan view of the Little Indian Creek diversion channel is shown in Figure 1. The main features of the design include: (i) a 1H:1V slope up to 15 m high, constructed with sand fill, and stabilized with horizontal layers of high density polyethylene (HDPE) uniaxial primary geogrid reinforcement and polypropylene (PP) biaxial secondary geogrid reinforcement (Figure 2); (ii) a grout-filled, polyamide monofilament woven geotextile erosion control mattress placed on the face of the slope to prevent erosion of the sand fill (Figure 3); (iii) a PP needlepunched nonwoven geotextile on the slope face between the fill and the erosion control mattress to prevent migration of fine soil particles through filter points in the mattress in the event of seepage from the slope fill (Figure 3); and (iv) a masonry-block faced, geogrid-reinforced soil retaining wall on top of the slope (Figure 3).

The design of the Little Indian Creek diversion channel incorporates three different geosynthetics for three different functions: geogrids for soil reinforcement; monofilament woven geotextiles for containment (i.e., as a fabric formwork to contain fine aggregate grout); and needlepunched nonwoven geotextiles for filtration.

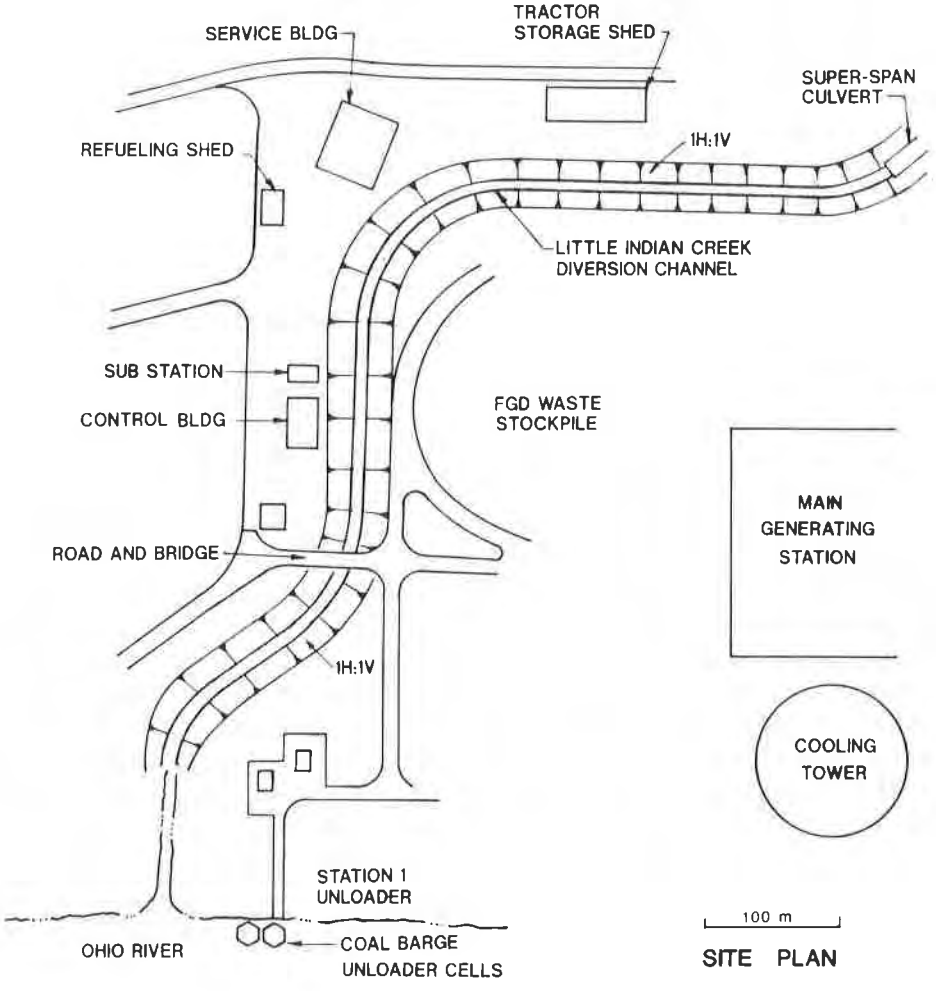

Figure 1. Site layout, Little Indian Creek diversion channel.

MATERIAL PROPERTIES

Soil. The sand used as embankment fill is a well-graded, brown and gray, fine to coarse sand with gravel that was dredged from the Ohio River. The sand is nonplastic with 2 to 10 percent fines (i.e., 2 to 10 percent passing a U.S. No. 200 sieve (74 μm)) and 5 to 30 percent gravel. The maximum gravel size is about 35 mm. Based on this fill type and the compaction requirements of the project specifications, the fill properties for design were conservatively estimated as follows: effective angle of internal friction, $\phi' = 35°$; total unit weight, $\gamma_m = 19.6$ kN/m^3.

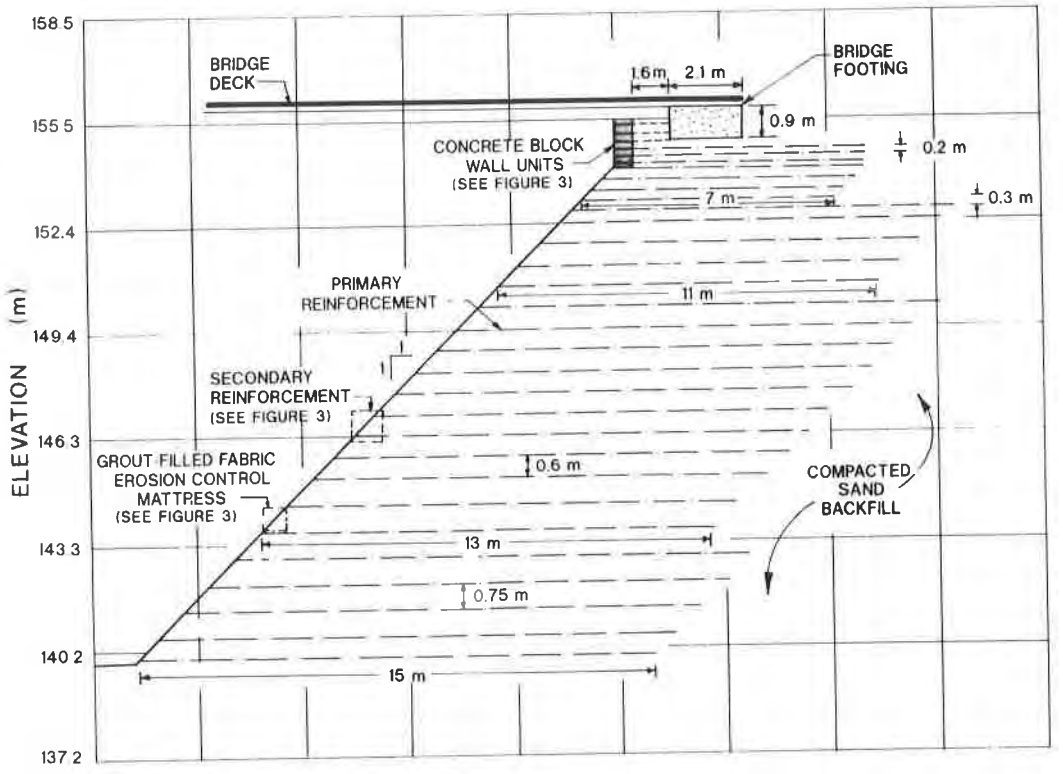

Figure 2. Cross section of the diversion channel slope at the location of the bridge crossing.

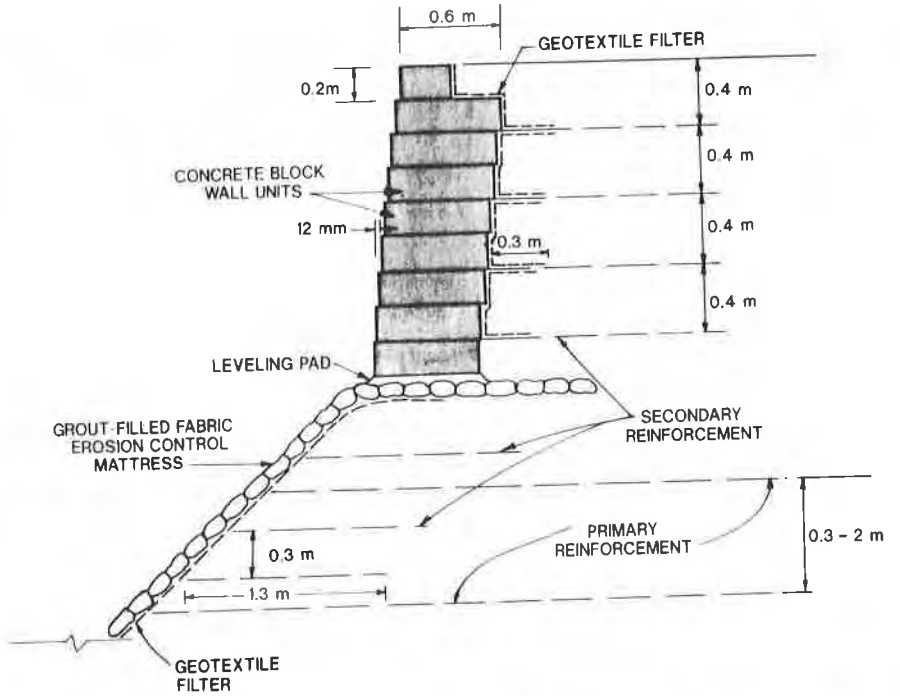

Figure 3. Detail showing the reinforced soil diversion channel slope and retaining wall, and the grout-filled fabric erosion control mattress.

The foundation soils at the project site consist primarily of well-graded brown and gray, fine to coarse sand and fine gravel. Standard penetration test (SPT) blowcounts in the sand (corrected to an effective overburden stress of 100 kPa) were generally in the range of 10 to 20, indicating a medium density. Along several sections of the channel, pockets of brown sandy clay up to 2 m thick were encountered. SPT blowcounts in this material generally ranged from 9 to 13, indicating a stiff consistency. To minimize the potential for slope failures due to shearing through the clay, it was excavated and replaced with compacted sand fill wherever it was encountered. Based on the results of stability analyses, the sand foundation was determined to be stable under the loads imposed by the diversion channel slopes.

Reinforcement. Due to the large radii of the channel's horizontal curves, the strain conditions in the channel slopes may be approximated as being plane strain; therefore, the use of uniaxial tensile reinforcement was adequate. Accordingly, the primary slope reinforcement was specified to be a HDPE uniaxial geogrid with a mass per unit area of approximately 900 g/m^2 (ASTM D-3776) and a uniaxial wide-strip tensile strength (i.e., a tensile strength in the geogrid's machine direction) of approximately 75 kN/m, based on tests at a strain rate of 10% per minute and 21°C (ASTM D-4595). The long-term allowable tension for design, α_t, for this reinforcement, derived from the results of constant-load creep tests, as described by McGown et al. [1984] and Bonaparte and Berg [1987], is 30 kN/m. The required design life of the primary geogrid reinforcement is 75 years; the suitability of the specified geogrid product for this design life was established using data in Shelton and Wrigley [1987] and Wrigley [1987].

The primary geogrid reinforcement was placed in layers in the diversion channel slopes with its machine direction aligned perpendicular to the slope face. The primary reinforcement is used to obtain an adequate factor of safety against slope instability. The primary reinforcement increases the factor of safety against failure along slip surfaces passing through the channel slopes and foundation. However, due to the relatively wide vertical spacing between layers of primary geogrid reinforcement (i.e., spacing ranged from 0.3 to 2 m, with 0.75 to 1.2 m being typical), surficial instability at the slope face is still a possibility. To address the potential for surficial instability, layers of PP biaxial geogrid were placed at 0.3 m vertical intervals at the slope face. This secondary reinforcement was placed with its cross-machine direction perpendicular to the slope face. The minimum width of the secondary reinforcement in the cross-machine direction is 1.3 m (Figure 3). The PP biaxial geogrid was specified to have a minimum mass per unit area of 200 g/m^2 and a minimum short-term initial tensile modulus of 1,000 kN/m (ASTM D-4595). Long-term allowable tension is not a design requirement for secondary reinforcement and thus was not specified.

Erosion Control Mattress. To prevent erosion of the channel slopes, a grout-filled fabric erosion control mattress was placed over the entire slope face. The cross section and details of the mattress, as designed, are shown in Figures 4 and 5. Figure 4 shows the slope face detail and Figure 5 shows the toe-of-slope detail. During construction of the diversion channel, a field change was made to the toe-of-slope detail. This change is discussed subsequently under "Construction". The mattress was specified to be about 90 mm thick and to have a weight per unit area of

about 2 kN/m^2. The mattress consisted of two polyamide monofilament woven geotextiles sewn together in such a manner so as to provide a formwork for placing a fine-aggregate concrete grout. During construction, grout was pumped into the fabric formwork in a controlled manner, filling the formwork from the bottom up. Care was taken while filling to prevent bursting of the formwork or pullout of the formwork from an anchor trench at the top of the slope. The manner in which the two layers of geotextile are sewn together results in a series of "filter points" in the formwork at 0.2 m centers. The filter points are intended to allow drainage of any ground-water seepage from the slope. Since the filter points do not meet strict filtration and retention criteria for the slope fill, a needlepunched nonwoven geotextile that did meet the criteria was placed between the fill and mattress.

The specified properties of the polyamide monofilament woven fabric formwork were as follows: mass per unit area (ASTM D-3776) $\geq$ 360 g/m^2; grab tensile strength (ASTM D-1682) $\geq$ 900 N; and grab tensile elongation (ASTM D-1682) $\leq$ 21 percent. The specified minimum grab tensile strength (ASTM D-1682) of all sewn seams was 900 N.

The specified properties of the PP needlepunched nonwoven geotextile were as follows: mass per unit area (ASTM D-3776) $\geq$ 140 g/m^2; grab tensile strength (ASTM D-1682) $\geq$ 600 N; grab tensile elongation (ASTM D-1682) $\geq$ 100 percent; apparent opening size (ASTM D-4751) $\geq$ 70; and permittivity (ASTM D-4491) $\geq$ 0.9 sec^{-1}.

The fine-aggregate concrete grout specifications included the following: Portland cement conforming to ASTM C-150, Type 1 or Type 2; fine aggregate conforming to ASTM C-33; a minimum 28 day compressive strength of 17 MPa when tested in accordance with ASTM C-31 and C-39; water reducers conforming to ASTM C-494 were allowed to reduce segregation, increase workability and pumpability, and increase water tightness; and air entraining agents conforming to ASTM C-260 were allowed to improve resistance to freezing and thawing and to reduce bleeding and permeability.

As shown in Figure 5, the design included a rip-rap filled trench at the bottom of the slope. The specifications for the rip-rap included: 100 percent finer than 0.6 m; not more than 40 percent finer than 0.4 m; not more than 20 percent finer than 0.2 m. As discussed below under "Construction", a field change to the toe-of-slope detail shown in Figure 5 was made during construction.

Retaining Wall. A reinforced-soil retaining wall up to 2 m high was constructed along a portion of the crest of the diversion channel, as shown in Figure 3. The facing elements for the wall consist of 0.2 m-high by 0.45-m deep by 0.6-m long partially-hollowed concrete blocks, each weighing about 0.4 kN. The blocks rest on an unreinforced concrete leveling pad. To provide added mass to the facing, the hollow in each of the blocks was filled with AASHTO No. 6 coarse aggregate. The sand fill behind the blocks was reinforced with biaxially-orientated PP geogrid reinforcement, as shown in Figure 3. The biaxially-orientated geogrid was specified to have a minimum mass per unit area of 300 g/m^2 (ASTM D-3776), a minimum short-term initial tensile modulus of about 1,300 kN/m (ASTM D-4595), and a minimum long-term allowable tension, α_t, of 5 kN/m. To prevent erosion of the fill through openings in the wall facing, a layer of PP needlepunched nonwoven geotextile was installed between the blocks and the sand fill, as shown in Figure 3.

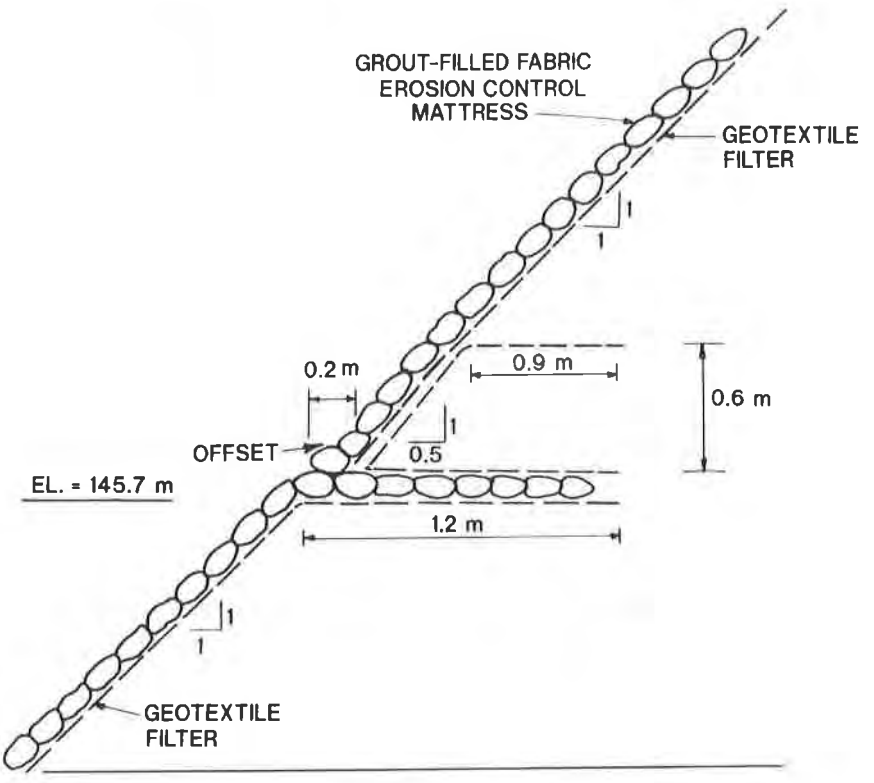

Figure 4. Detail of grout-filled fabric erosion control mattress.

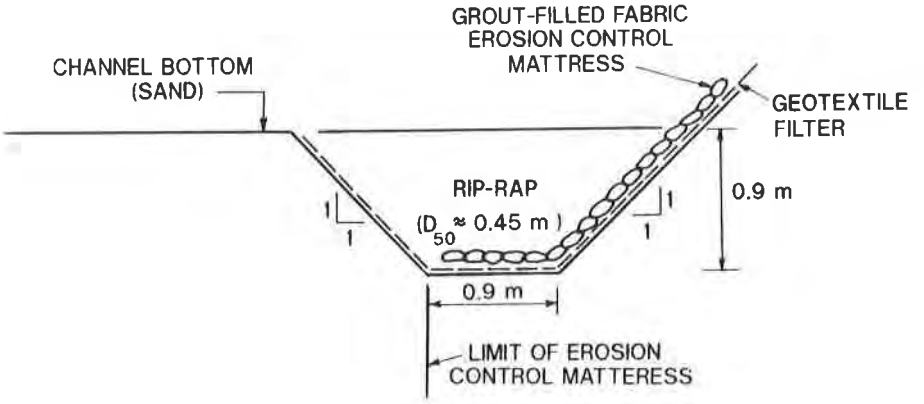

Figure 5. Detail of the toe of the diversion channel slope "as designed".

DESIGN

Overview. The design of the diversion channel included internal and external stability analyses of the channel slopes, stability analyses of the erosion control mattress on the slopes, stability analyses of the reinforced soil walls on top of the slopes, and an evaluation of the suitability of the needlepunched nonwoven geotextile to serve as a filter layer between the slope fill and the erosion control mattress.

Slope Stability. The stability of the diversion channel slopes was analyzed using Bishop's simplified method of slices [Bishop, 1955], modified to account for the presence of tensile reinforcement (e.g., as described in Bonaparte et al. [1987]). The minimum acceptable factor of safety under static loading conditions was specified to be 1.4. In the stability analyses, slip surfaces entirely within the reinforced soil zone were considered as were slip surfaces in the foundation soils and in the fill soils behind the reinforced zone. Typical slip surfaces analyzed using Bishop's simplified method are shown in Figure 6. For the analyses, the owner specified a design piezometric level in the sand fill at the elevation of the invert of the diversion channel. This level was chosen due to the fact that water levels in the channel and adjacent fill would respond almost simultaneously to changes in water level in the Ohio River. The owner expected that, except during flood stages in the Ohio River, the water level in the diversion channel would be very low (in fact, it was expected that the channel would often be dry).

The slope section shown in Figure 2 corresponds to the location where a bridge crosses the channel to allow the transport of coal from a stockpile area to the generating station. As shown in Figure 6, the bridge footing exerts a design stress (dead load plus live load) on top of the slope of 335 kPa. This footing surcharge had a significant effect on the required number of layers of reinforcement, as described subsequently. For the slope section shown in Figure 6, the critical slip surface (i.e., the slip surface with the lowest factor of safety) is behind and beneath the reinforced soil mass. The factors of safety of slip surfaces through the reinforced soil mass tended to be slightly higher. It can also be seen that four geogrid layers were needed immediately under the bridge footing to locally achieve the required factor of safety. The design of the slope below the bridge footing is conservative from two perspectives: (i) plane strain conditions were assumed, whereas three-dimensional effects at the ends of the footing increase stability in comparison to the plane strain case; and (ii) about 20 percent of the design load was due to live loads for which the allowable design strength of the geogrid (which has a viscoelastic tension-strain response) is higher than that assumed for design (i.e., higher than the allowable design strength under dead load conditions).

The stability analyses for the diversion channel project also considered noncircular slip surfaces that extended behind the reinforced soil zone then along a soil-geogrid interface to the slope face. Analyses of noncircular slip surfaces were evaluated using Janbu's simplified method of slices [Janbu, 1973] along with the assumption that the shearing resistance at the soil-geogrid interface is equal to 90 percent of the shear strength of the soil itself (based on direct shear test results by Sarsby [1985]). The noncircular failure surfaces were found to be non-critical.

Erosion Control Mattress Stability. The stability of the grout-filled erosion control mattress on the channel slopes was evaluated using simple sliding block analyses, such as those described by Giroud and Beech [1989] or Koerner [1990]. For design, it was conservatively assumed that the concrete grout had no strength and that the stability of the mattress resulted from shear stresses between the mattress and the underlying geotextile and fill and from tension in the fabric formwork. The critical slip surface was identified as being at the interface between the nonwoven and woven geotextiles. A friction angle of 20° was assumed along this interface. The selection of this interface friction angle was predicated on information from erosion control mattress fabricators that there would be some bleeding of the grout through the fabric formwork. Based on the fabricators' experience, the grout would create a weak bond between the fabric formwork and the underlying material. The maximum stable height of mattress along the interface (with a factor of safety of 1.25) was found to be 7.6 m. Since the maximum slope height was 15 m, the mattress had to be constructed in two stages, with the lower portion anchored at approximately the mid-height of the slope, as shown in Figure 4.

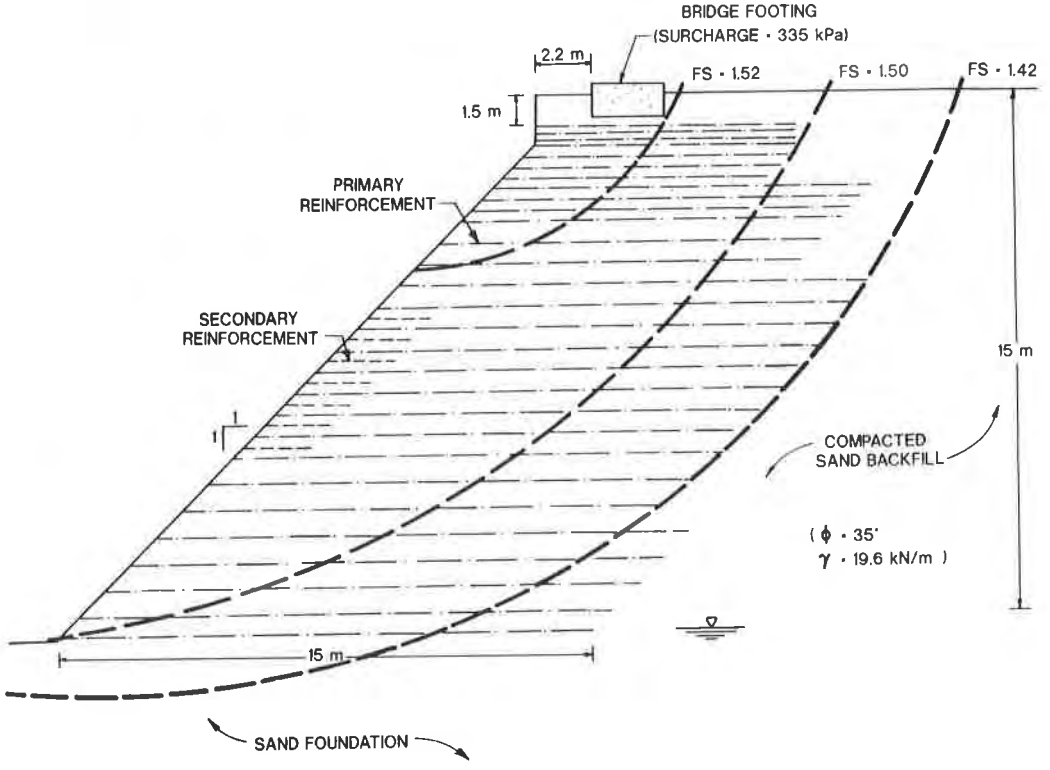

Figure 6. Typical circular slip surfaces analyzed at the location of the bridge crossing.

Reinforced Soil Wall Stability. The block-faced, reinforced soil wall at the top of the diversion channel was designed using the tie-back wedge method (e.g., as described in Bonaparte, Holtz and Giroud [1987] and Jones [1986]). Passive resistance from the blocks was neglected in the stability analyses.

Geotextile Filter Evaluation. The evaluation of the suitability of the needlepunched nonwoven geotextile to serve as a filter layer was based on criteria presented in Giroud [1987].

CONSTRUCTION

Channel construction was carried out by first overexcavating the channel foundation in areas containing pockets of clay, as previously described, and replacing the excavated clay with sand fill. The fill was placed in 0.3 m lifts using large scrapers and was spread using track-mounted dozers. If the fill was dry, it was moistened using a water truck. The fill was compacted using multiple passes of a large vibratory-drum roller. Primary geogrid reinforcement layers were placed at the design elevations as the fill height increased (Figure 7). Secondary geogrid reinforcement layers were placed at the edge of the slope at 0.3 m vertical intervals. At about the mid-height of the slope, the lower portion of the fabric formwork was installed, anchored at the top, and filled with grout. Fill and geogrid placement then continued until the elevation of the top of the channel was reached. The number of primary geogrid reinforcement layers varied with the height of the slope. For sections of the slope about 15 m high, the number of layers ranged from 17, at locations where there was only a nominal surcharge load on top of the slope, to 28, at the location of the bridge crossing. Once the final fill elevation was reached, the upper portion of the erosion control mattress was installed (Figure 8) and the block-faced, reinforced soil wall was constructed.

As previously noted, a field change was made during construction to the detail for the diversion channel toe of slope. The change was made to simplify construction. The "as-built" detail is shown in Figure 9. This detail can be compared to the "as-designed" detail in Figure 5. From Figure 9, it can be seen that the erosion control mattress was not embedded in the key trench at the toe of the slope, as called for in the original design. Also, the depth of the key trench was reduced from 0.9 m to 0.6 m and the trench was filled with AASHTO No. 1 stone (with a maximum particle size of 0.1 m) rather than rip-rap. The rip-rap that was placed on top of the key trench (at the location shown in Figure 9) had a mean size of about 0.25 m, rather than the specified mean size of about 0.45 m.

PERFORMANCE

The Little Indian Creek diversion channel structure has been in service from late 1987 to present, more than three and one-half years. The channel structure has endured the rigors of adjacent powerplant construction, winter weather (i.e., temperatures as low as -27°C), and high water levels in the Ohio River. The channel has been partially submerged by Ohio River floods on several occasions, with water levels in the channel exceeding an elevation of 146 m msl (mean sea level) (approximately 40 percent of the channel height) on ten occasions during the first three years of service. The maximum Ohio River flood event to date, on 18 February

1989, achieved a high water elevation in the channel of 151 m msl (approximately 70 percent of the channel height).

The channel has been inspected periodically since the time of construction by representatives of the American Electric Power Service Corporation (AEPSC) (i.e., the plant owner's engineer and construction manager for the powerplant conversion project) and by representatives of Tensar Earth Technologies, Inc. (the suppliers of the diversion channel design and geogrid reinforcement materials). The following observations have been made during the various inspections of the diversion channel.

Visual inspection of the geogrid-reinforced slopes has revealed no evidence of slope distress such as tension cracks at the crest of the slope, slumping at the surface of the slope, or cracking of the grout-filled fabric erosion control mattress.

The sections of reinforced slope supporting the channel bridge footings have performed well (Figure 10). No discernable settlement of the bridge approaches has been noted. The grout-filled fabric control erosion mattress on the sections of slope supporting the bridge footings shows no visible signs of distress or movement.

The reinforced-soil, concrete-block retaining wall at the crest of the slopes shows no evidence of lateral or vertical movements. No significant loss of the AASHTO No. 6 coarse aggregate fill placed in and between the concrete blocks, or of the reinforced sand fill behind the blocks, has been observed. The concrete blocks show no evidence of distress due to differential wall movements or climatic exposure.

Figure 7. Primary geogrid reinforcement installation.

Examination of the grout-filled fabric erosion control mattress revealed little evidence of deterioration of the fabric formwork. At times, seepage through the filter points has been observed near the bottom of the channel.

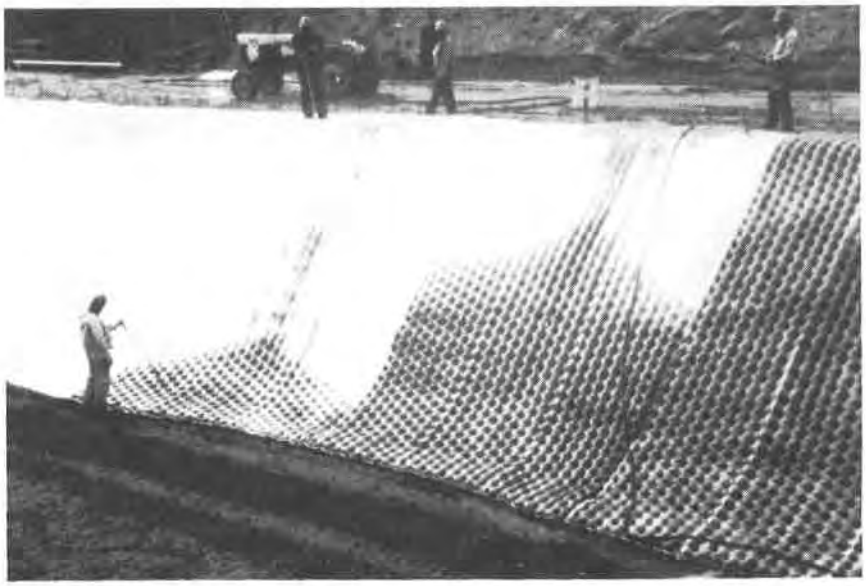

Figure 8. Grouting of fabric formwork to create the erosion control mattress.

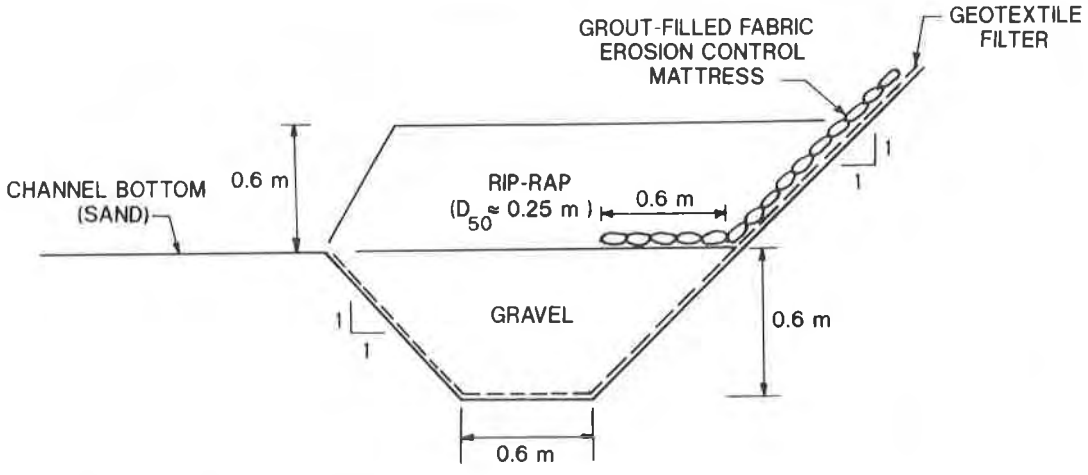

Figure 9: Detail of the toe of the diversion channel slope "as constructed".

Figure 10: Flow in the diversion channel at the bridge crossing.

On 23 April 1990, the project site experienced 73 mm of rain within 24 hours, with most of the rainfall occurring in only a few hours. The storm occurred at a time when the water level in the Ohio River was low so that there was very little tailwater in the channel. These conditions resulted in high flow velocities in the channel which caused erosion of the channel bottom, with isolated erosion pools up to 2 m deep, downstream transport of rip-rap, and undermining of a short section of the channel slope. Inspection of the channel after the storm revealed that scour had undercut the toe of the slope along the outside edge of the first curved section of the channel. At this location, the AASHTO No. 1 aggregate and rip-rap (see Figure 9) had been displaced and sand fill had been eroded from beneath the toe of the erosion control mattress. The erosion at the toe of the slope resulted in significant slumping and cracking of the erosion control mattress (Figure 11). The channel inspection revealed no areas of scour and undercutting other than that at the first curved section. However, subsequent storms and high flow conditions have caused minor amounts of scour and undermining in several other locations along the channel.

As previously noted, during design, the plant owner anticipated only relatively minor flow volumes and relatively low flow velocities in the channel. However, changes in drainage patterns within the Little Indian Creek watershed have increased flows in the channel above anticipated levels; this has resulted in higher than anticipated flow velocities. The toe-of-slope detail shown in Figure 9 was not sufficient to withstand the erosion forces associated with the high flow velocities in the channel. This "as built" detail utilized a smaller-size rip-rap and less embedment of the erosion control mattress than the "as designed" detail shown in

Figure 5. The "as-built" detail also resulted in a narrower width for the bottom of the channel and, hence, higher flow velocities. Neither detail called for placement of rip-rap across the entire bottom of the channel. Had the potential for high flow velocities been anticipated during design, placement of rip-rap across the entire bottom would have been appropriate.

To improve the resistance of the channel bottom to erosion, a remedial design was developed by AEPSC (Figure 12). Resistance to scour is improved by using rip-rap with a mean size of about 0.6 m and by extending the rip-rap across the entire channel bottom. As an additional remedial measure, a gravel toe drain has been installed at the toe-of-slope, as shown in Figure 12. The toe drain will be at least 0.9 m deep and will consist of AASHTO No. 57 stone wrapped in a needlepunched nonwoven geotextile filter layer. The purpose of the toe drain is to improve drainage of the slope fill in the vicinity of the toe and to provide a barrier to the piping of sand from behind the mattress.

The sections of the erosion control mattress that were undermined during the previous storm events will be repaired when remediation of the channel bottom is complete. Presently, AEPSC plans to pump grout behind the mattress to fill isolated undermined areas and to restore the mattress to its original position.

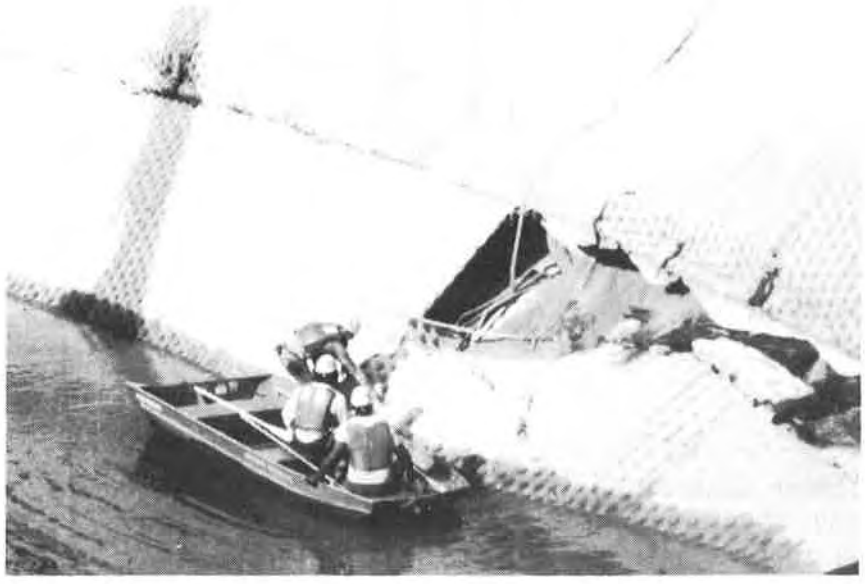

Figure 11. Damage to erosion control mattress due to scour at the toe of the channel slope.

CONCLUSIONS

The Little Indian Creek diversion channel project represents an interesting and successful application of three different types of geosynthetics at a major industrial site. The use of the different geosynthetics required development of several design details which were illustrated in the paper. The project demonstrates that problems can result when field changes are implemented without careful engineering review and that accurate design data, such as anticipated water levels and flow velocities in the channel, are critical to a successful design. Hopefully, the information in this paper will be useful to design engineers using geosynthetics for similar applications on future projects.

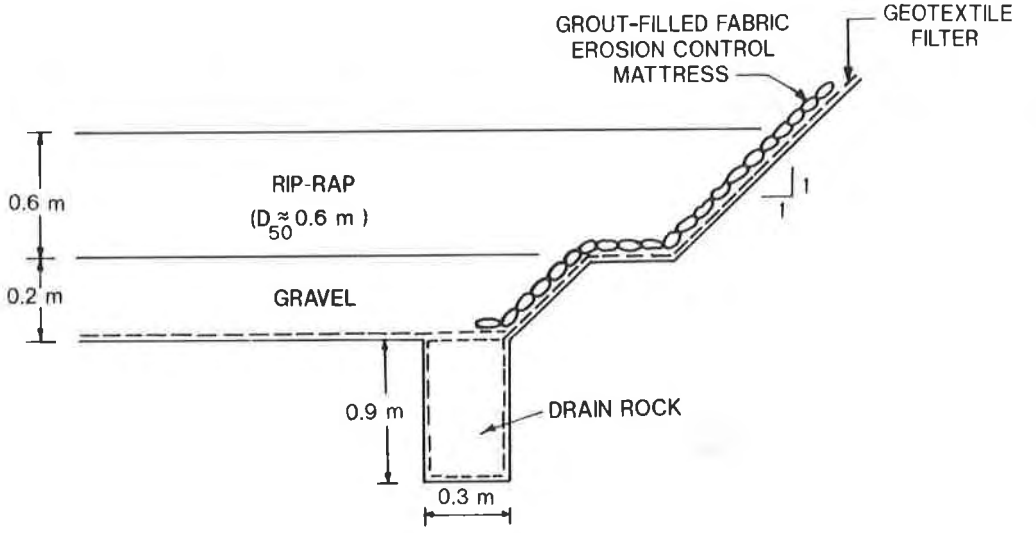

Figure 12. Detail of the toe of the diversion channel slope "as remediated".

ACKNOWLEDGEMENTS

The W.H. Zimmer Generating Station is jointly owned by the Cincinnati Gas and Electric Company, Southern Power Company, and Dayton Power and Light Company. Engineering and construction management for the powerplant conversion project was performed by the American Electric Power Service Corporation, of Columbus, Ohio. Messrs. Stephen A. Rossner and George A. Camporini from AEPSC contributed significantly to the design and successful construction of the Little Indian Creek diversion channel project. GeoSyntec Consultants (formerly GeoServices Inc. Consulting Engineers) performed the final diversion channel slope design under contract to The Tensar Corporation (Tensar), Morrow, Georgia. Tensar supplied the slope design and the geogrid reinforcement used for slope construction. Mr. Robert

Race, P.E. of Tensar Earth Technologies, Inc. provided much of the information in this paper on channel performance. The diversion channel contractor was Guepel Construction Company, Columbus, Ohio and the erosion control mattress was furnished and installed by Intrusion-Prepakt, Cleveland, Ohio.

REFERENCES

Bishop, A.W., "The Use of the Slip Circle in the Stability Analysis of Slopes", Geotechnique, 1955, pp. 7-17.

Bonaparte, R., and Berg, R.R., "Long-Term Allowable Tension for Geosynthetic Reinforcement", Proceedings of the Geosynthetics '87 Conference, Vol. 1, New Orleans, Feb 1987, pp. 181-192.

Bonaparte, R., Holtz, R.D., and Giroud, J.P., "Soil Reinforcement Design Using Geotextiles and Geogrids", Geotextile Testing and the Design Engineer, ASTM STP 952, J.E. Fluet, Jr., Ed., American Society for Testing and Materials, Philadelphia, 1987, pp. 69-116.

Giroud, J.P., "Tomorrow's Designs for Geotextile Applications, Geotextile Testing and the Design Engineer, ASTM STP 952, J.E. Fluet, Jr., Ed., American Society for Testing and Materials, Philadelphia, 1987, pp. 145-148.

Janbu, N., "Slope Stability Computations", Embankment Dam Engineering, John Wiley and Sons, 1973, pp. 47-76.

Jones, C.F.J.P., "Earth Reinforcement and Soil Structures", Butterworths Advanced Series in Geotechnical Engineering, 1985, 183 p.

Koerner, R.M., Designing with Geosynthetics, Second Edition Prentice Hall, Englewood Cliffs, NJ, 1990, 652 p.

McGown, A., Paine, N., and Dubois, D.D., "Use of Geogrid Properties in Limit Equilibrium Analysis", Proceedings of the Symposium on Polymer Grid Reinforcement in Civil Engineering, Institution of Civil Engineers, London, 1984, pp. 31-36.

Sarsby, R.W., "The Influence of Aperture Size/Particle Size on the Efficiency of Grid Reinforcement", Proceedings of the Second Canadian Symposium on Geotextiles and Geomembranes, Edmonton, 1985, pp. 7-12.

Shelton, W.S. and Wrigley, N.E., "Long-Term Durability of Geosynthetic Soil Reinforcement", Proceedings of the Geosynthetics '87 Conference, Vol. 2, New Orleans, Feb 1987, pp. 442-454.

Wrigley, N.E., "Durability and Long-Term Performance of Tensar Polymer Grids for Soil Reinforcement", Materials and Science Technology, Vol. 3, 1987, pp. 161-170.

Modular Concrete Retaining Wall and Geogrid Reinforcement Performance and Laboratory Modeling

John C. Kliethermes
Service Engineering, USA
Kenneth Buttry
University of Wisconsin-Platteville, USA
Earl McCullough
University of Wisconsin-Platteville, USA
Richard Wetzel
University of Wisconsin-Platteville, USA

INTRODUCTION

The project site is located in Bloomington, Minnesota in a townhouse development called Bluff Place Second Addition. The townhouses are two story residences with full basements and are valued in excess of $200,000. A three tiered retaining wall system was constructed in June of 1988 to support a 28 foot high embankment located behind the townhouses. A sidewalk and a road are located at the top of the embankment.

A tiered timber wall had been under construction at the site and had failed during a heavy rainstorm when it was about 18 feet high. This failed wall had not been designed and the city engineer subsequently required that the replacement wall be designed by a registered engineer. Five alternative wall systems were considered:

1. A timber wall,
2. A sheet pile wall,
3. A soldier pile wall,
4. A geogrid reinforced slope, and
5. A retaining wall system using modular concrete masonry units reinforced with geogrids.

The timber wall was rejected by the city engineer due to failure of the first wall. The sheet pile and soldier pile walls were rejected due to cost and aesthetic considerations. The reinforced slope system was estimated to have the least cost but was eventually rejected because of the design length of the geogrids required for stability and additional costs due to associated excavations. Estimated costs for each of the alternatives are presented in Table 1.

System	Cost per Square Foot
Timber Wall	$12
Sheet Pile Wall	$18
Soldier Pile Wall	$18
Reinforced Slope	$7
Reinforced Modular Wall System	$13

Table 1 Estimated Costs of Alternative Systems

The reinforced modular wall system was chosen due to aesthetic appeal, economics of construction, and the confidence of the designer in the system. A tiered wall system and a single height wall were considered and both were determined to provide the required stability and perform the required functions. The single height wall would have exceeded 16 feet in vertical height and was determined to be visually overpowering for the limited site space. The tiered wall provided some relief and was considered to provide a more pleasing solution.

Over 2,300 square feet of wall were installed by the developer's work force. The modular concrete units were delivered to the job site for $3.50 per square foot. Total cost for the geogrid was $15,000. Other costs including labor, excavation, backfilling, concrete footings, drain tile, and accessories were not available so the actual project cost is unknown; but was estimated to be $13 per square foot of wall. The developer and the city engineering department had no previous experience with the system.

DESCRIPTION OF RETAINING WALL SYSTEM

The retaining wall system was composed of two basic elements: modular masonry concrete block units, and geogrid reinforcement. No mortar is used in laying the block units as they are laid side by side and are stackable. Nominal dimensions of the concrete units are 8 inches high by 16 inches wide by 12 inches deep. A projecting lip, located at the front of each unit, serves to establish a 14° set-back angle for the wall and lock the units together from one course to the next. The block contains two through voids with a center rib. Two units are manufactured together face to face and then split in front of the projecting lips to create a broken rock face look. Each unit weighs approximately 50 pounds by itself and 80 pounds with crushed stone in the unit void spaces.

The geogrid was formed of high density polyethylene with apertures 5.4 inches long in the machine direction and 0.66 inches wide in the cross machine direction. The long term design strength provided by the manufacturer is 3,000 pounds/foot in the machine direction.

The retaining structure was constructed in three tiers as shown in Figure 1. The first course of modular units was positioned on a concrete footing and then the void spaces in the units were filled with crushed stone. Backfill was then placed behind the wall up to a level flush with the top. A second course of the units was then placed on top of the first in a running bond configuration, crushed stone placed in the voids, and the backfill placed. This procedure was repeated to bring the wall up to the desired elevation. The stone used was crushed limestone with a maximum size of 3/4 inches meeting ASTM C33 number 67 size designation.

Geogrid reinforcing was placed at the desired levels as the wall was being constructed. After a course of units was in position with the voids filled with crushed stone and the backfill placed; a layer of geogrid was placed on top of the units beginning directly behind the projecting lip and extending across the backfill. The next course of modular wall units were then placed on top of the geogrid and the voids filled with crushed stone. The geogrid was pulled taut before placing backfill on top. Thus, the geogrid is held in place by two mechanisms: friction between the grid and the modular concrete units, and

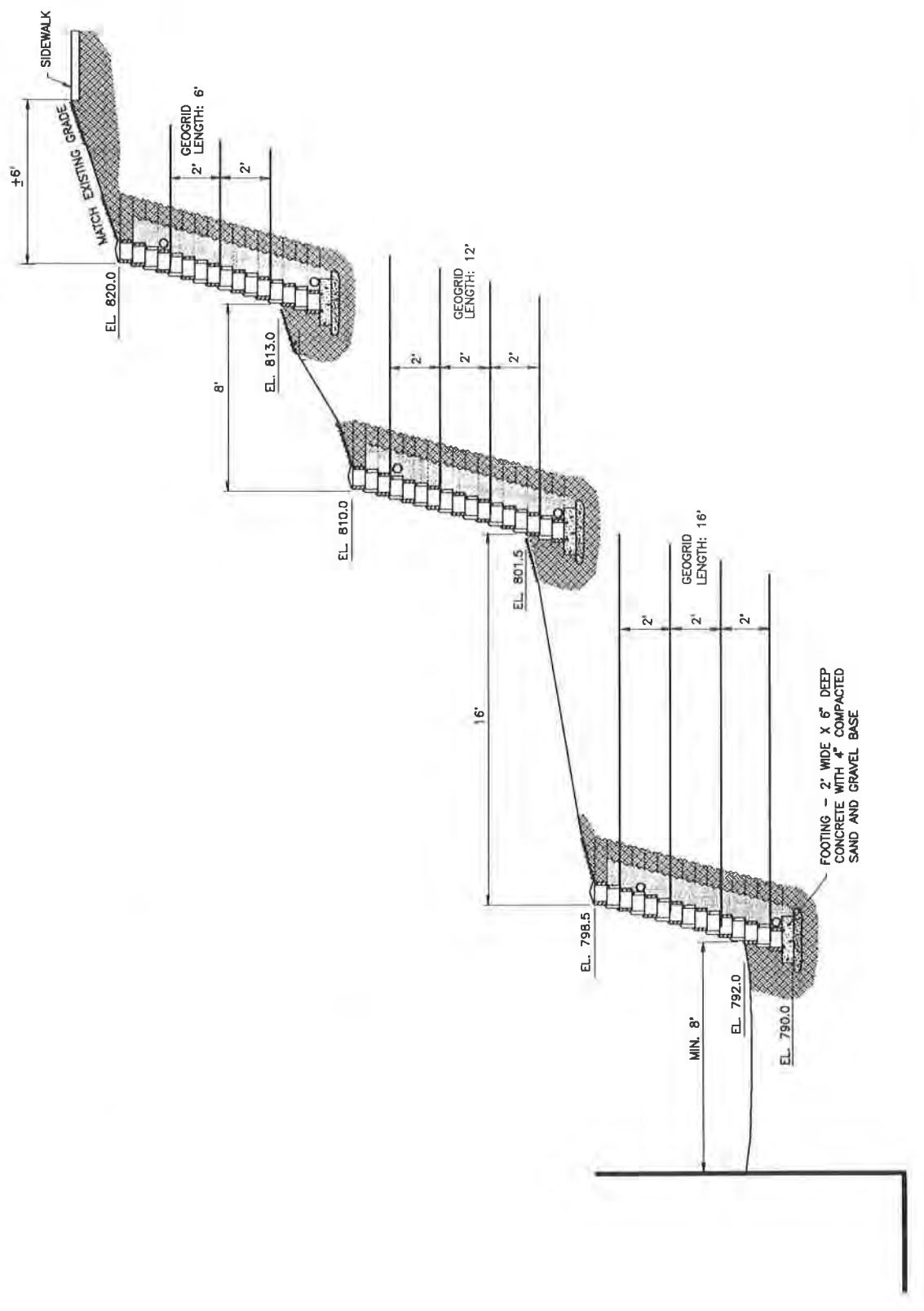

FIG. 1 MODULAR MASONRY RETAINING WALLS WITH GEOGRID REINFORCEMENT

interlocking between the grid and the crushed stone in the unit voids. There was no direct mechanical connection between the wall units and the geogrid.

DESIGN

Site Conditions. Soil borings were not available for the site; however, there was information from four borings taken approximately 350 feet away. These borings indicated alluvial sand underlain by glacial till which was classified as silty sand. The alluvium was loose at the surface becoming medium dense to dense at the base of the embankment. Standard Penetration Tests (SPT) indicated blowcounts of 4 blows/foot at the surface to 30 blows/foot at the base. On-site inspection revealed that the entire 30 foot high slope was generally a loose, poorly graded, fine sand and would be classified SP. The soil was considered to be cohesionless with a moist unit weight of 120 pounds/cubic foot and a friction angle of 32 degrees. These parameters were used in the stability analyses for both the in situ soil and reinforced fill section. Seepage problems were not anticipated as there were no ponding areas near the top of the slope.

Geometric Design. Geometric design of the system was governed by the location and grade of the townhouses at the base of the embankment and a sidewalk and road at the top. The sidewalk was located 30 feet above the townhouse grade and approximately 40 feet horizontally from the back of the townhouses. An offset of 8 feet from the townhouse wall to the base of the retaining system was required.

Design Concept. The basic design concept considers that the reinforced soil mass and the modular facing units act together as a gravity wall. External stability is concerned with the external forces acting on this mass. The length of the geogrid units which corresponds to the width of the reinforced mass is generally based on external stability. Internal stability is concerned with forces acting within the mass including the interactions between the geogrid, soil, and modular block units. Generally, the spacing of geogrid layers and forces in the geogrids are based on internal stability. The design followed procedures set forth in a Tensar Technical Note (1).

External Stability. The stability of each of the three tiers were evaluated as well as that of the entire system. Evaluations included sliding, overturning, bearing capacity, and global or slope stability.

The bottom tier was designed as a reinforced wall that was 8.5 feet high with a backfill slope of 16 feet horizontal to 3 feet vertical. A surcharge of 2,000 pounds/square foot was applied at the top of the backslope to account for the load applied by the middle and upper tiers. Required geogrid lengths were determined to provide factors of safety of 1.5 for sliding and 2.0 for overturning. Similar determinations for the middle and top tiers were made with the results presented in Table 2.

Geogrid Elevation feet	Length Required feet	Length Used feet	Maximum Force In Grid pounds/foot
Top Wall Tier			
817.5	6.1	6.0	555
815.5	6.1	6.0	672
813.5	6.1	6.0	1347
Middle Wall Tier			
808.5	9.4	10.0	876
806.5	9.4	10.0	876
804.5	9.4	10.0	1155
802.5	9.4	10.0	1195
Bottom Wall Tier			
796.0	12.7	16.0	1309
794.0	12.7	16.0	792
792.0	12.7	16.0	1097

Table 2 Geogrid Design Information

The ultimate bearing capacity was determined to be 7,500 pounds per square foot. An unreinforced footing with a width of 2 feet was selected to support the modular wall units providing a factor of safety of 3.

Slope stability analyses were conducted to evaluate the stability of the overall system. The facing units and geogrid reinforced soil sections were considered to be rigid units and assigned high shear strengths in order to utilize computer search routines that would not allow failure surfaces to cut through the reinforced soil mass. The desired factor of safety was 1.4. Slope stability was the controlling factor in design of the bottom tier and the geogrid length had to be increased to 16 feet to meet the required safety factor. The critical failure surfaces are shown in Figure 2.

Internal Stability. Internal stability of the reinforced soil mass included: geogrid spacing, tension analysis, wedge analysis, and embedment length. The long term strength of the geogrid including reductions for creep was 3,000 pounds per foot. Using a factor of safety of 1.5 the design strength was 2,000 pounds per foot.

While standard design procedures have been established for geogrid reinforced earth; the interaction of the geogrid with the units of the modular wall system is not well understood and rational design procedures have not been established. For example, the forces acting in the geogrid at the connection to the wall units are not known. Because of this uncertainty, a conservative approach was taken and a geogrid spacing of 2 feet was chosen. This spacing ensures that all modular wall units are in contact with a unit attached to a geogrid layer. The effect is to reduce the soil pressure acting on the back of the wall. The maximum forces estimated to be acting in each of the geogrid layers are presented in Table 2.

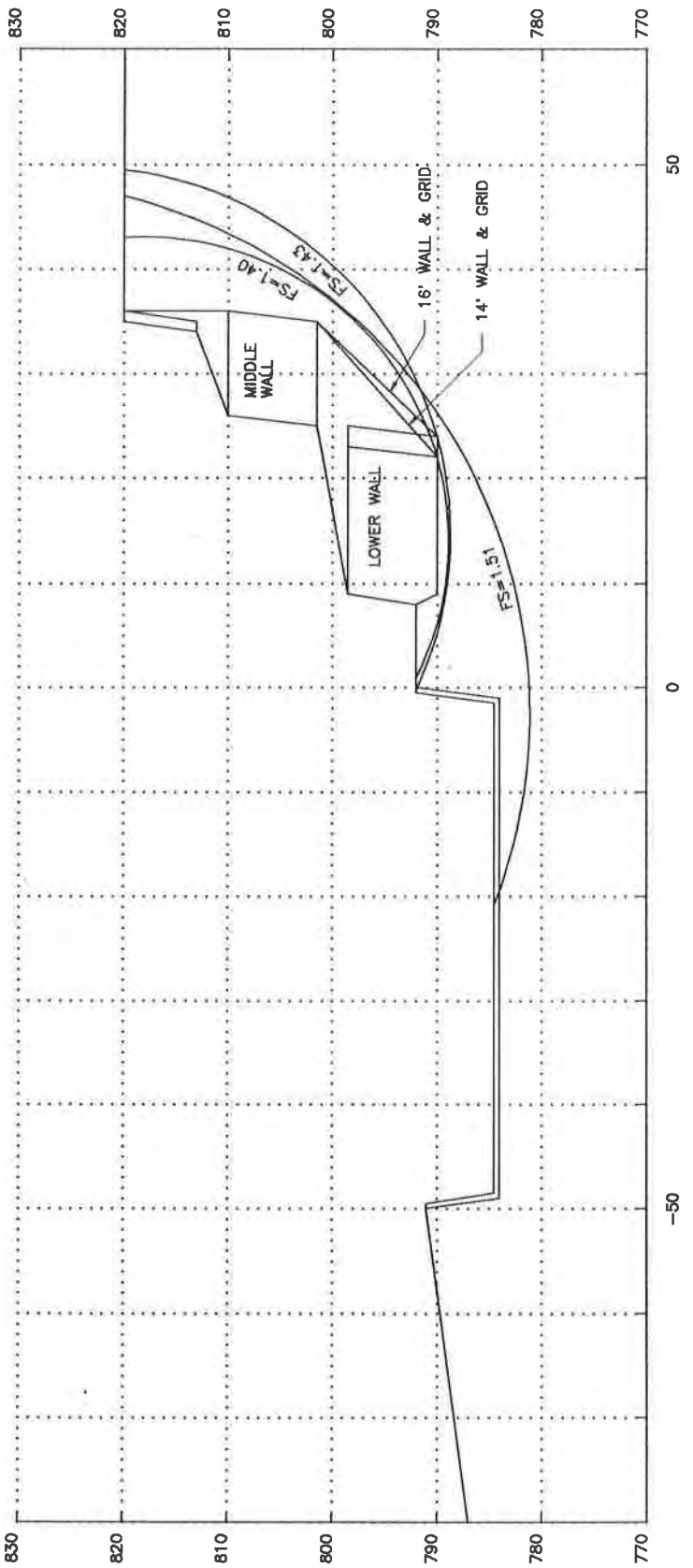

FIG. 2 CRITICAL FAILURE CIRCLES FOR SLOPE STABILITY

CONSTRUCTION

Photographs of the wall during construction and after completion are shown in Figures 3 and 4. Construction of the wall was accomplished in a very tight time frame and because of this the contractor chose not to use temporary shoring to support the slope during construction. This was done against the advice of the engineer. The failed timber retaining wall was removed and the bulk of the excavation was completed in two days. The length of the geogrid in the bottom tier required excavation to within 12 feet of the top of the embankment which resulted in a slope of 0.5 to 1 in the existing sand. During construction the slope face was exposed to the sun and as the moisture evaporated some sloughing of the sand occurred. A light misting of the slope face helped to control the problem, although constant attention was required to prevent overwatering.

Unreinforced concrete footings 2 feet wide by 6 inches thick were placed 2 feet below grade along the required alignment. The modular wall units were placed side by side on the footing one day after pouring. The units were filled with crushed stone and backfill placed and compacted prior to installation of succeeding courses. Units were placed with the front of the unit against the projection lip of the units in the previous course. Where geogrid was required, the grid was placed on the units and the succeeding course placed on top of the geogrid. Crushed stone was placed in the units and the geogrid pulled taut onto the compacted backfill. Backfill was placed over the geogrid prior to construction of the next course. The fine sand existing at the site was used for backfill and was compacted to 95 percent of Standard Proctor Density.

At the base of each of the three tiers a 6-inch drain tile was placed that extended the full length of the wall. This drain tile was surrounded by 12 inches of crushed stone placed behind the wall and extending the full height. This system along with the sandy soils at the site provided adequate drainage.

Periodic visits were made to the site by the design engineer to ensure compliance with design documents. Most of the workers were not experienced in retaining wall construction, but placement of the geogrid and modular units proceeded with little difficulty. During the final stages of construction it was discovered that some geogrid layers were placed using cut pieces from the ends of previous roles. To achieve a 6 foot embedment, three 2-foot sections were placed end to end. The engineer directed the contractor to correct this. It was also noted that the contractor sometimes filled the voids in the units with sand rather than the crushed stone that was specified.

LABORATORY TESTING PROGRAM

Three laboratory test series were conducted to aid in evaluating the integrity of the retaining wall system. In one series the shear resistance of the modular concrete wall units was determined. The second series was conducted to determine the pullout resistance of the geogrid from between the modular units. In the third series the sliding resistance between the bottom modular unit and a compacted granular base was determined.

Figure 3 Retaining Wall Under Construction

Figure 4 Completed Retaining Wall

Shear Resistance of Modular Concrete Wall Units. The wall is built up of modular concrete units stacked in a running bond configuration. The resistance of the system to horizontal shear forces has three components: friction between the modular units, the shear strength of the crushed stone placed in the voids of the units, and the shear strength of the concrete lip projections. This shear resistance was determined in the laboratory by applying a shear force to the top unit of a two-block stack while restraining the bottom unit as shown in Figure 5. A normal force was applied to the top unit by dead weights acting on a hanger arrangement. The shear force was applied using a closed-loop, electrohydraulic ram at a constant displacement rate of 0.5 inches/minute.

Results of fifty tests at normal loads ranging between 225 and 900 pounds/foot are presented in Figure 6. Forces are presented as pounds/foot which were calculated by dividing the total force or weight acting on a modular unit by the width of 16 inches or 1.33 feet. The mean shear strength of the units was 2,560 pounds/foot with a coefficient of variation of 15 percent. Shear strength of the concrete in the projection lip was determined to be the primary factor in the strength of the units and a displacement in excess of 0.4 inches was observed before the projection failed. As the block units have a split face the thickness of the projection varies from unit to unit depending on the manner in which the block splits. This is thought to be the reason behind the large variation in shear strengths measured. One unexpected result of the testing was that there was no apparent correlation between the shear strength and the applied normal load.

Frictional resistance between the concrete units was determined independently using the apparatus described except that there was a gap of about 3/8 inch between the projection on the lower unit and the front of the top unit. With this arrangement the force measured included only the friction between the block surfaces. Results indicated a friction angle of 33 degrees and that a displacement of 0.2 inches is required to develop the full frictional force.

Sliding of Base of Wall System. Frictional resistance of a modular unit resting on a granular foundation base was examined by placing a single unit on a compacted granular base and applying normal and shear forces. Testing was done using the apparatus shown in Figure 5 modified by replacing the bottom concrete block with a box containing the 3/4 inch maximum size crushed stone described previously. Behavior was evaluated with and without the cavities in the block filled with the same granular material. A friction angle of 41 degrees was measured with crushed stone in the block voids and 33 degrees with the voids empty. Displacements of 0.25 inches were required to develop the full resistance.

Geogrid Pullout Resistance. The purpose of this test series was to measure the pullout resistance of the geogrid from between the modular units. Testing apparatus is shown in Figure 7 and was designed to simulate field construction procedures as closely as possible. Two modular concrete units were placed side by side on the floor and the voids filled with crushed stone. A geogrid test specimen was then placed on top of the units with the front of the grid just behind the projecting lip as shown. The geogrid specimen was 16 inches wide by 26 inches long and positioned in the center of the bottom units. The 16 inch width of the geogrid matches the 16 inch width of the modular concrete unit. One concrete unit was then placed on top of the geogrid and the void filled with crushed stone. This configuration was used to simulate running bond construction.

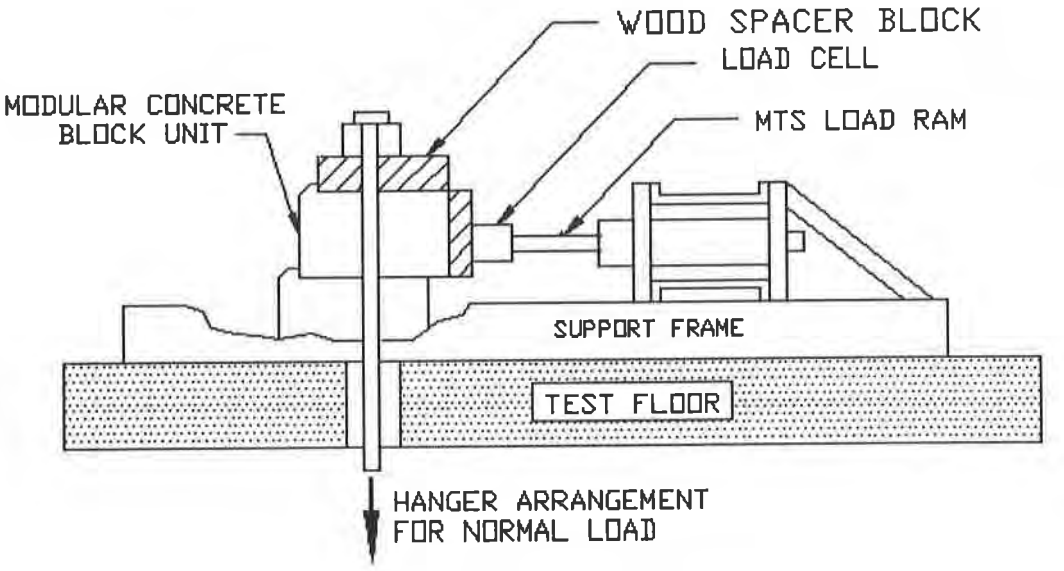

Figure 5 Shear Strength Testing Apparatus

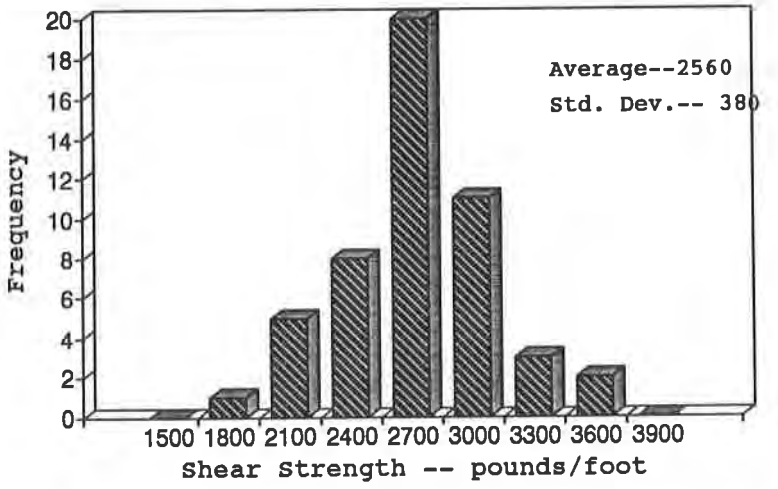

Figure 6 Shear Strength of Modular Concrete Units

Normal loads were applied as shown through a hanger system and dead weights. A clamping device was attached to the end of the geogrid and a pullout force applied at a constant displacement rate of 0.5 inch/minute The pullout force along with the movement of the clamping device was continuously monitored until the maximum force was reached. A rigid frame with a slot located at the back end of the modular units kept the units from moving. The geogrid was placed through the slot. Figure 8 shows the geogrid test specimen. The first 10 inches of the specimen was positioned between the concrete units and held in place by friction and interlock, the next 10 inches was a free length, and the last 6 inches was clamped to the pullout device.

Thirteen tests were conducted as described with the voids in the concrete units filled with crushed stone. Typical results indicated that the force increased at a uniform rate initially; after which it fluctuated up and down with a gradually increasing trend. The fluctuation is thought to be a result of alternate slipping and interlocking of the crushed stone and the geogrid. The maximum pullout resistance occurred at a displacement of 2 inches.

Twelve tests were also conducted in a similar manner except that the unit voids were left empty. Typical results from these tests showed that the force increased uniformly to a yield point and then remained relatively constant. These tests measured the friction between the geogrid and the contact surfaces of the modular concrete units.

Test results are summarized in Figure 9 which shows the measured geogrid pullout resistance plotted as a function of the normal load. For the tests with no stone in the voids the relationship is linear with a slope of 0.88.

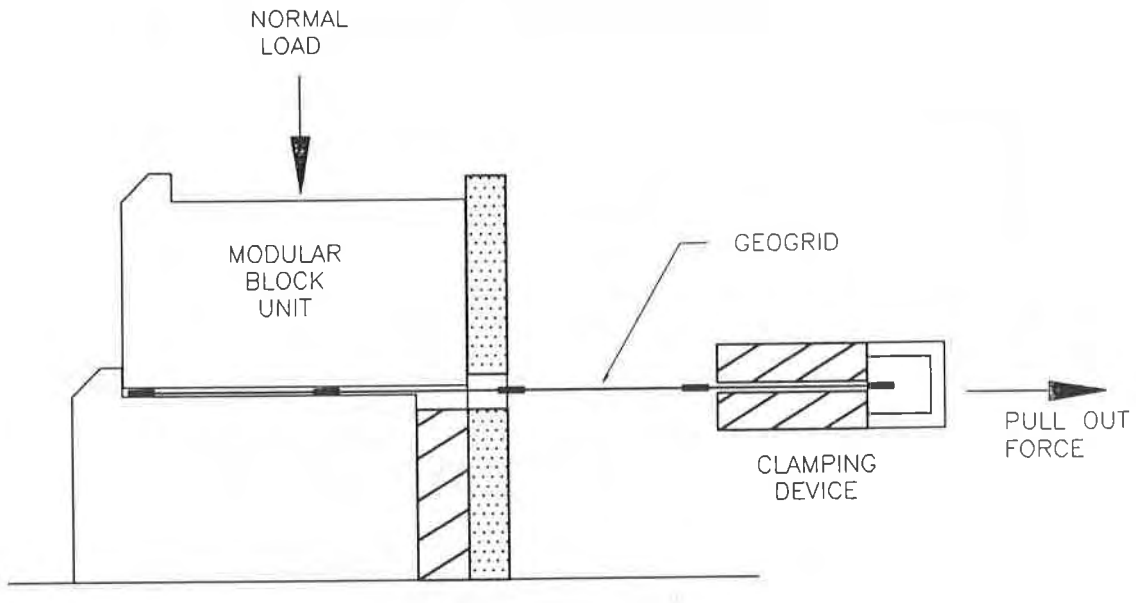

Figure 7 Apparatus for Determination of Geogrid Pullout Resistance

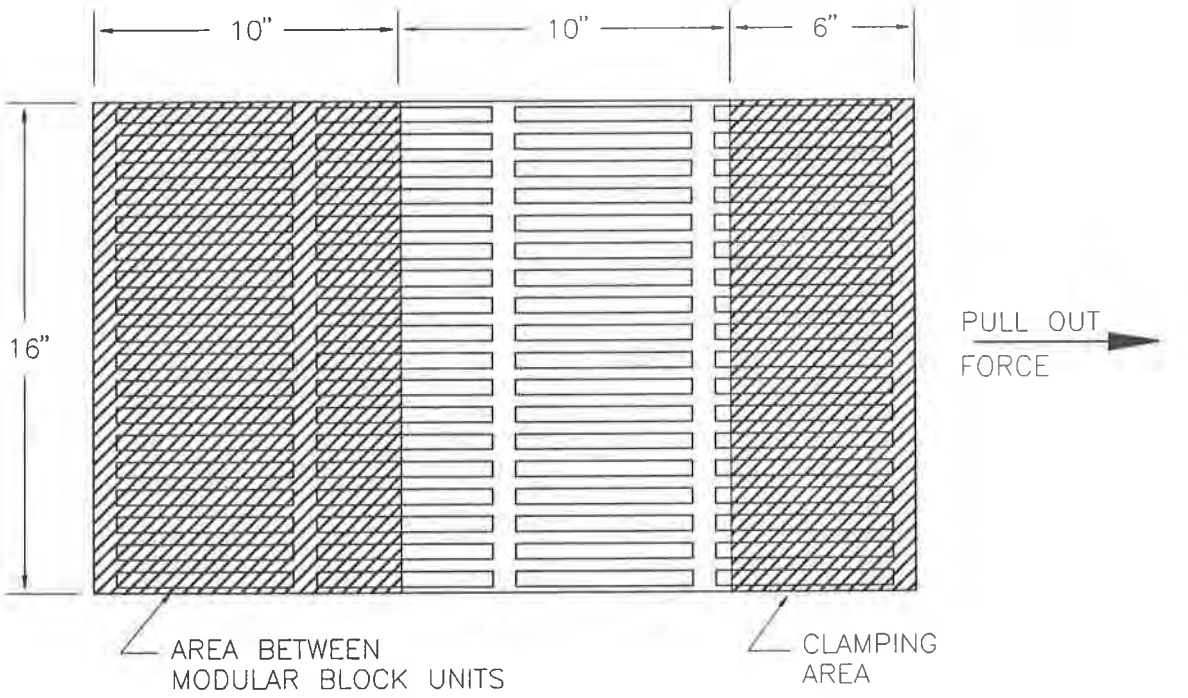

Figure 8 Geogrid Test Specimen

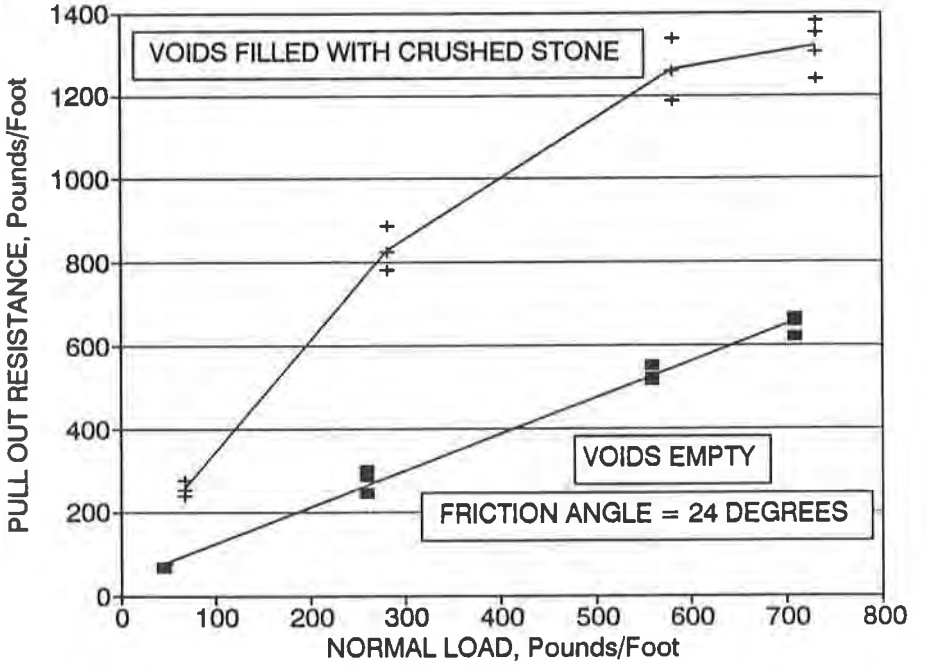

Figure 9 Geogrid Pullout Resistance

As there are two contact surfaces the corresponding coefficient of friction between the geogrid and the concrete units is 0.44 corresponding to a friction angle of 24 degrees. For the tests with the voids filled with crushed stone the relationship is nonlinear and appears to be approaching a maximum value. It is evident that the interlocking of the stone and the geogrid has a significant effect on the pullout resistance.

CORRELATION OF TEST RESULTS WITH DESIGN AND PERFORMANCE

Retaining Wall Performance. The wall has experienced frost action over two winters and has been exposed to significant rainfall. An inspection of the wall has been made on average every two months since construction. There has been no recognizable movement of the wall or evidence of settlement. The wall does not show any signs of settlement or slipping in the backfill. A minimal amount of settlement has occurred within the block voids. A small percentage of the wall units have cracks in the face. This is attributed to manufacturing flaws and not wall movements.

Connection Between Wall and Geogrid. A design standard published by AASHTO-AGC-ARTBA Task Force 27 (2) requires that the connection between the geogrid and modular wall units be designed to carry 100 percent of the maximum design tensile load in the geogrid at each level. The strengths of the connections were analyzed to check compliance with this design requirement and the results are shown in Table 3. Normal forces acting at each geogrid location were calculated and with this information the connection strengths were determined from Figure 9. The ratio of the strength of the connection to the design load is shown in the table. Values of one or greater indicate that the connection meets the proposed 100 percent criterion. It may be seen that connection strength meets the proposed criterion in seven of the ten geogrid layers.

Geogrid Elevation feet	Maximum Design Force Pounds/Ft	Connection Strength Pounds/Ft	Ratio Of Strength/ Max. Force
817.5	555	850	1.53
815.5	672	1200	1.79
813.5	1347	1300	.97
808.5	876	550	.63
806.5	876	1000	1.14
804.5	1155	1300	1.13
802.5	1195	1300	1.09
796.0	1309	850	.65
794.0	792	1200	1.52
792.0	1097	1300	1.19

Table 3 Strength of Geogrid Connections

The advent of modular masonry wall units used in conjunction with geosynthetic reinforcement may require a reevaluation of the design procedures established for reinforced soil walls. The design and fabrication of connections to carry 100 percent of the maximum geogrid design load may be done efficiently for paneled wall facing systems. On the other hand, it is sometimes difficult to

meet the 100 percent requirement for geogrid connections to modular wall systems. Some research studies have suggested that the maximum force in geogrid reinforcing elements occurs at some distance back from the face of the wall and that the force at the face is less than the maximum design load. It appears that more research is necessary to establish realistic design procedures for modular wall systems.

Shear Strength of Wall System. Shear forces in the wall were estimated by applying the geogrid design loads to the wall as point loads and assuming a uniform lateral soil pressure. With this method the maximum shear force was estimated to be 1250 pounds/foot. The mean shear strength of the wall system was determined to be 2560 pounds/foot from laboratory testing. This results in a factor of safety of 2.0 which is considered adequate.

SUMMARY

A modular masonry concrete retaining wall system was constructed in June 1988 at a townhouse development where a different type of wall had failed during construction. The modular wall system was selected over other alternatives because of aesthetic considerations and economy of construction. Design of the system was based on accepted industry procedures and the experience of the designer. Laboratory testing of the units verified that the shear strength of the modular wall system was adequate to support the loads with a safety factor of 2 or more. Results of testing the connections between the wall units and the geogrid reinforcement was not as conclusive. The connection strength exceeded the design requirement in seven of ten geogrid layers. In the other three the design strength was not met. The wall has performed well for two years and no significant problems have been observed. Further study is still required before realistic design standards can be established.

ACKNOWLEDGEMENTS

The writers wish to acknowledge and thank the Tensar Corporation for supplying the geogrid for the project and the Allan Block Company for supplying the modular block units. Service Engineering of St. Paul, Minnesota designed the system and the laboratory testing was conducted at the University of Wisconsin-Platteville. Funding for the laboratory testing was provided by the Allan Block Company and the University of Wisconsin-Platteville.

REFERENCE

1. "Guidelines For The Design Of Tensar Geogrid Reinforced Soil Retaining Walls", Tensar Technical Note TTN:RW1, August 1986.
2. "Guidelines For The Design Of Mechanically Stabilized Earth Walls", AASHTO-AGC-ARTBA Task Force 27 Report.

UNIT CONVERSIONS

1 foot	= 0.3048 m
1 square foot	= 0.0929 m^2
1 pound	= 4.448 N
1 pound/foot	= 14.59 N/m
1 pound/foot	= 0.01459 kN/m

BUILD YOUR GEOSYNTHETICS LIBRARY WITH THE LATEST INFORMATION ON GEOSYNTHETIC USAGE

with ***Geosynthetics '91*** Conference proceedings available **NOW** through the Industrial Fabrics Association International...

This two-volume set contains 68 technical papers presented at the ***Geosynthetics '91*** Conference, February 26-28, 1991, in Atlanta, GA, U.S.A.

Topics covered include: commercial/industrial applications, waste containment, interface stability, transportation applications, geosynthetic durability, technical advancements/testing & research, heavy construction applications and more.

Sample papers include:

"A Rational Design Method for Silt Fences"

"Geotextiles in Permanent Roads and Highways"

"Comparison of Design Methods for Geosynthetic-Reinforced Soil Walls"

"Underground Geomembrane Placement"

The cost is $55 plus postage *($5.00 U.S. & Mexico, $9.00 Canada, $19.00 Central America, $32.00 Europe & South America, $38.00 all other countries). To order, complete the form below and return it to IFAI, 345 Cedar St., Suite 800, St. Paul, MN 55101 U.S.A.; or fax your order to 612/222-8215.

Please send me the ***Geosynthetics '91*** Conference proceedings:

Cost: $55.00 per set _____

Number of sets desired _____

Subtotal _____

Postage* (see above) _____

Total _____

Payment enclosed _____ Bill my: _____

Visa/MasterCard ___ Am. Express ___

Credit card # _____

Signature _____

Exp. date _____

Member _____ Non-member _____

Name _____

Company _____

Address _____

City/State/Province _____

Zip/Postal Code _____

Telephone _____

Return to: Industrial Fabrics Association International, 345 Cedar St., Suite 800, St. Paul, MN 55101 U.S.A. Fax: 612/222-8215; Telephone: 612/222-2508.